

THE PHYSICAL REVIEW

PUBLISHED BY THE
AMERICAN INSTITUTE OF PHYSICS
INCORPORATED

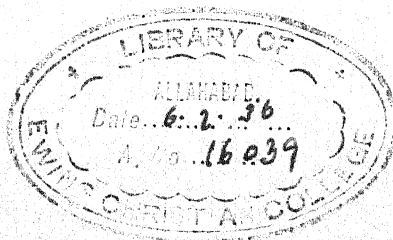
UNDER THE EDITORIAL SUPERVISION OF THE
AMERICAN PHYSICAL SOCIETY

BOARD OF EDITORS

Managing Editor, JOHN T. TATE, University of Minnesota, Minneapolis
Assistant Editor, J. W. BUCHTA, University of Minnesota, Minneapolis
K. F. HERZFELD, A. W. HULL, F. W. LOOMIS, A. J. DEMPSTER, DAVID M. DENNISON,
J. C. SLATER, R. C. GIBBS, E. O. LAWRENCE, J. H. VAN VLECK

VOLUME 42, SECOND SERIES
OCTOBER-DECEMBER, 1932

THE AMERICAN INSTITUTE OF PHYSICS, INCORPORATED
11 EAST 38th STREET, NEW YORK, N. Y.



Composed, Printed and Bound by
The Collegiate Press
George Banta Publishing Company
Menasha, Wisconsin

CONTENTS

OCTOBER 1, 1932

Isotopic Weight of H^2	- - - - -	KENNETH T. BAINBRIDGE	1
Ionization of Helium, Neon and Argon under Impact of their own Atoms and Positive Ions	- - - - -	CHARLES J. BRASEFIELD	11
Scattering of Slow Electrons. Part II	- - - - -	EUGENE FEENBERG	17
Analytic Atomic Wave Functions	- - - - -	J. C. SLATER	33
Nuclear Spin and Magnetic Moment of Li^7	- - - - -	L. P. GRANATH	44
Thermionic and Photoelectric Work Functions of Molybdenum	- - - - -	LEE A. DUBRIDGE AND W. W. ROEHR	52
Absorption Spectra of the Samarium Ion in Solids. I. Absorption by Large Single Crystals of $SmCl_3 \cdot 6H_2O$	- - - - -	FRANK H. SPEDDING AND RICHARD S. BEAR	58
Absorption Spectra of the Samarium Ion in Solids. II. Conglomerate Absorption of $SmCl_3 \cdot 6H_2O$ and a Partial Energy Level Diagram of the Sm^{+++} Ion as It Exists in Crystalline $SmCl_3 \cdot 6H_2O$	- - - - -	FRANK H. SPEDDING AND RICHARD S. BEAR	76
Luminescence of Solid Nitrogen	- - - - -	JOSEPH KAPLAN	86
Products of Dissociation in Nitrogen	- - - - -	JOSEPH KAPLAN	97
Momentum Relations in Crossed Fields	- - - - -	LEIGH PAGE	101
Effect of Strain on Magnetostriction and Magnetization in Nickel	- - - - -	C. W. HEAPS	108
Variation of Dielectric Constant with Temperature. II. Electric Moments of the Ethylene Halides	- - - - -	ERNEST W. GREENE AND JOHN WARREN WILLIAMS	119
Letters to the Editor	- - - - -		141
Probabilities of K-Electron Ionization of Silver by Cathode Rays	- - - - -	D. L. WEBSTER, W. W. HANSEN AND F. B. DUVENNECK	141
Concerning the Production of Secondaries by the Cosmic Radiation	- - - - -	J. C. STREET AND THOMAS H. JOHNSON	142
Structure of Atomic Nuclei. II	- - - - -	JAMES H. BARTLETT, JR.	145
Luminosity of Sodium Flames	- - - - -	C. D. CHILD	146
Gyromagnetic Ratios for Nickel and Cobalt	- - - - -	S. J. BARNETT	147
Angular Distribution of Electrons Scattered in Mercury Vapor	- - - - -	A. L. HUGHES	147
On the Radiation Originating from a Beam of Electrons in Mercury Vapor and the Mean Life of the 2^2S_1 State	- - - - -	LOUIS R. MAXWELL	148
Disintegration of Lithium by Swiftly-Moving Protons	- - - - -	ERNEST O. LAWRENCE, M. STANLEY LIVINGSTON AND MILTON G. WHITE	140
Book Reviews	- - - - -		152

OCTOBER 15, 1932

On the Scattering of Hard X-Rays by Solids	- - - - -	S. CHYLINSKI	153
Atomic Eigenfunctions and Energies	- - - - -	C. W. UFFORD AND G. H. SHORTLEY	167
Calculation of the Quantum Defect for Highly Excited S States of Para- and Orthohelium	- - - - -	LLOYD P. SMITH	176
Rotational Analysis of the First-Negative Bands of the CO^+ Molecule	- - - - -	R. F. SCHMID	182
Quantum Mechanics Treatment of the Water Molecule	- - - - -	ALBERT SPRAGUE COOLIDGE	189
On the Vibrations of Polyatomic Molecules	- - - - -	N. ROSEN AND PHILIP M. MORSE	210
Reflection of Atomic Beams from Sodium Chloride Crystals	- - - - -	R. M. ZABEL	218
Magnitudes of the L Absorption Discontinuities of Gold	- - - - -	FRED M. UBER AND C. G. PATTEN	229
First Spark Spectrum of Antimony	- - - - -	R. J. LANG AND E. H. VESTINE	233
Spectrum of Potassium Hydride	- - - - -	G. M. ALMY AND C. D. HAUSE	242
Far Infrared Spectra of Gases	- - - - -	JOHN STRONG AND S. C. WOO	267
Infrared Spectrum of H^2Cl	- - - - -	J. D. HARDY, E. F. BARKER AND D. M. DENNISON	279
Self-Recording Cosmic-Ray Electrometer and Depth-Ionization Curve	- - - - -	J. M. BENADE	290
High Voltage Direct Current Generator	- - - - -	RICHARD E. VOLLRATH	298
Magneto-Optic Rotation by Condenser Discharge	- - - - -	FRANCIS G. SLACK AND WILLIAM M. BREAZEALE	305
Errata	- - - - -		312
Evidence of Space Quantization of Atoms upon Impact	- - - - -	H. KUHN AND O. OLDENBERG	312
On the Relative Abundances of the Nitrogen and Oxygen Isotopes	- - - - -	GEORGE M. MURPHY AND HAROLD C. UREY	312
Letters to the Editor	- - - - -		313
On the Continuous Absorption Spectrum of Alkyl Iodides	- - - - -	Y. HUKUMOTO	313
Emission Probability for a Colliding Atom	- - - - -	R. W. DITCHBURN	314
Airplane Cosmic-Ray Intensity Measurements	- - - - -	L. M. MOTT-SMITH AND L. G. HOWELL	314
Unitary Theory, Pure Number Ratios and the Masses of Atomic Nuclei	- - - - -	ENOS E. WITMER	316
Solar Component of Cosmic Rays	- - - - -	J. C. STEARNS, WILCOX P. OVERBECK AND RALPH D. BENNETT	317
Book Reviews	- - - - -		319

NOVEMBER 1, 1932

Cosmic-Ray Ionization as a Function of Pressure, Temperature, and Dimensions of the Ionization Chamber	JAMES W. BRONXON	321
X-Ray Diffraction in Ethyl Ether near the Critical Point	F. H. WALDEMAR NOLL	336
Approximation of Geometric Optics as Applied to a Dirac Electron Moving in a Magnetic Field	OTTO LA PORTE	340
Isotope Displacement in Hyperfine Structure	-G. BREIT	348
Absorption Spectrum of Iodine Bromide	WELDON G. BROWN	355
On the Interpretation of the Rotational Structure of the CO ₂ Emission Bands	ROBERT S. MULLIKEN	364
On the Lifetime of the Metastable P ₂ Neon Atom	E. MATUYAMA	373
Molecular Scattering of Light from Ammonia Solutions. The Fine Structure of a Vibrational Raman Band	JOHN WARREN WILLIAMS AND ALEXANDER HOLLAENDER	379
Raman Spectra of a Series of Normal Alcohols and Other Compounds	R. W. WOOD AND GEORGE COLLINS	386
Magnetic Spectra of Secondary Electrons from Silver	S. CHYLINSKI	393
Experimental Establishment of the Relativity of Time	ROY J. KENNEDY AND EDWARD M. THORNDIKE	400
Propagation of Large Barkhausen Discontinuities. II	K. J. SIXTUS AND L. TONKS	419
Erratum		436
Supersonic Dispersion and Absorption in CO ₂	W. H. PIELEMEIER	436
Letters to the Editor		437
Raman Effect in Gase : CO and NO	S. BHAGAVANTAM	437
Note on the Electric Field in Paramagnetic Crystals	C. J. GORTER	437
Possibility of the Existence of the Chlorine Isotope Cl ³⁹	MURIEL F. ASHLEY AND F. A. JENKINS	438
Simple Amplifier for Geiger-Müller Counters	W. F. LIBBY	440
High-Speed Hydrogen Ions	M. STANLEY LIVINGSTON	441
Heisenberg Theory of Ferromagnetism	D. R. INGLIS	442
Note on the Term System of Ir I	WALTER ALLERTON	443
Isotope of Hydrogen in the Atomic Spectrum	DAVID H. RANK	446
Intensity of Cosmic-Ray Ionization in Western North America	R. D. BENNETT, J. L. DUNHAM, E. H. BRAMHALL, AND P. K. ALLEN	446
Dielectric Constant and Electric Polarization of Mixtures in the Neighborhood of the Critical Point	A. PIEKARA	448
Electric Moment of the Molecule of Nitrobenzene	A. PIEKARA	449
Book Reviews		451

NOVEMBER 15, 1932

Remarks on the Scattering of X-Rays by Gases and Crystals	G. E. M. JAUNCEY	453
Mass Ratio of the Boron Isotopes from the Spectrum of BO	F. A. JENKINS AND ANDREW MCKELLAR	464
Emission of Positive Ions from Heated Metals	LEROY L. BARNES	487
Temperature Variation of the Positive Ion Emission from Molybdenum	LEROY L. BARNES	492
Rotational Analysis of Ultraviolet Bands of Silicon Monoxide	PAUL G. SAPER	498
Zeeman Effect of Perturbed Terms in the CO Angstrom Bands	WILLIAM W. WATSON	509
Theory of Continuous Absorption of Oxygen at 1450A	E. C. G. STUECKELBERG	518
Photoelectric Quantum Counters for Visible and Ultraviolet Light. Part I	GORDON L. LOCHER	525
Non-Existence of Ion Mobility Spectrum in Air	ROBERT N. VARNEY	547
Vapor Pressure Constant of Methane	THEODORE E. STERNE	556
On the Origin of the Actinium Series of Radioactive Elements	A. V. GROSSE	565
Permeability of Iron at Ultra-Radio Frequencies	J. BARTON HOAG AND HAYDN JONES	571
Letters to the Editor		577
Velocities of Ions and Electrons in Pure Gases	C. M. FOCKEN	577
Variation of the Structure of Scattered Lines with the Frequency of the Primary Light	E. GROSS AND J. KHVOSTIKOV	579
Electron Lenses	C. J. DAVISSON AND C. J. CALBICK	580
On the Secondary Emission from Collectors in Neon Discharge	G. SPIWAK AND E. REICHRUEDEL	580
A Filter for the Study of the Raman Effect	A. H. PFUND	581
Note on Perturbation Theory of Molecules Formed from Two 2p Atoms	JOHN R. STEHN	582
Law of Force between Two He Atoms	W. G. PENNEY	585

Proceedings of the American Physical Society:

AMHERST MEETING OF THE NEW ENGLAND SECTION, October 8, 1932; Minutes and Abstracts 1-12, Author Index

DECEMBER 1, 1932

Relative Intensities of the $\Lambda\alpha_1$, β_1 , β_2 , and γ_1 Lines in Tantalum, Tungsten, Iridium, and Platinum	VICTOR J. ANDREW	591
Band Spectra of MgO, CaO and SrO	P. C. MAHANTI	609
Infrared Absorption Spectrum and the Molecular Structure of Ozone	SHERMAN L. GERHARD	622
Dispersion and Absorption of Helium	J. P. VINTI	632
Radiation from Slow Electrons	LEO NEDELSKY	641
Influence of Crystalline Fields on the Susceptibilities of Salts of Paramagnetic Ions. II. The Iron Group, Especially Ni, Cr and Co	ROBERT SCHLAPP AND WILLIAM G. PENNEY	666
Diamagnetism of Water at Different Temperatures	A. P. WILLS AND G. F. BOEKER	687
Some Properties of Homogeneously Distorted Cubic Ferromagnetic Lattices	FRANCIS BITTER	697
Hall e.m.f. and Intensity of Magnetization	E. M. PUGH AND T. W. LIPPERT	709
Mono-Crystal Barkhausen Effects in Rotating Fields	FRED J. BECK, JR. AND L. W. MCKEEHAN	714
Velocity of Sound in an Absorptive Gas	D. G. BOURGIN	721
Letters to the Editor		731
Tropism of Crystals	F. BITTER	731
X-Ray Reflections from a Quartz Piezoelectric Oscillator in a Bragg Spectrograph	M. Y. COLBY AND SIDON HARRIS	733
Determination of e/m for an Electron by a New Deflection Method	FRANK G. DUNNINGTON	734
Value of e/m	RAYMOND T. BIRGE	736
Errata, Structure of Atomic Nuclei	JAMES H. BARTLETT, JR.	737
Book Reviews		738

DECEMBER 15, 1932

Measurement of X-Ray Emission Wave-Lengths by Means of the Ruled Grating	R. B. WITMER AND J. M. CORK	743
Laue Patterns from Thick Crystals at Rest and Oscillating Piezoelectrically	J. M. CORK	749
Neutralization and Ionization of High-Velocity Ions of Neon, Argon and Krypton by Collision with Similar Atoms	HAROLD F. BATHO	753
Extension of the First Spark Spectrum of Caesium (Cs II)	J. OLTHOFF AND R. A. SAWYER	766
Infrared Absorption Spectrum of Hydrogen Cyanide	KYU NAM CHOI AND E. F. BARKER	777
Positive Ion Current at the Cathode in the Glow Discharge	A. KEITH BREWER AND R. R. MILLER	786
On the Nature of Active Nitrogen	J. OKUBO AND H. HAMADA	795
Origin of the Mercury Bands at 2480A	J. GIBSON WINANS	800
Auroral Spectrum	JOSEPH KAPLAN	807
Theory of Vibrational Isotope Effects in Polyatomic Molecules	E. O. SALANT AND JENNY E. ROSENTHAL	812
On Radiation Diffusion and the Rapidity of Escape of Resonance Radiation from a Gas	CARL KENTY	823
Note on the Equivalent Absorption Coefficient for Diffused Resonance Radiation	M. W. ZEMANSKY	843
Effect of Tension on the Electrical Resistance of Single Bismuth Crystals	MILDRED ALLEN	848
Effect of Homogeneous Mechanical Stress of the Electrical Resistance of Crystals	P. W. BRIDGMAN	858
Reflection of Metallic Atoms from Alkali Halide Crystals	ROBERT REX HANCOX	864
Theory of the Ferromagnetic Anisotropy of Single Crystals	RICHARD M. BOZORTH	882
Empirical Equation of State	HENRY S. FRANK AND FOO-SONG LEI	893
Proceedings of the American Physical Society:		900
CHICAGO MEETING, November 25-26, 1932; Minutes and Abstracts 1-55, Author Index		
Author Index to Volume 42		916
Analytic Subject Index to Volume 42		922

THE PHYSICAL REVIEW

The Isotopic Weight of H^2

By KENNETH T. BAINBRIDGE

Bartol Research Foundation of the Franklin Institute

(Received August 15, 1932)

The mass of neutral H^2 was measured on a mass-spectrograph as 2.01351 ± 0.00006 referred to He and 2.01351 ± 0.00018 referred to $O^{16} = 16$. The equivalent packing fraction of H^2 is 67.5 parts in 10,000. On the assumption that the nucleus is composed of two protons and one electron the energy of binding is approximately 2×10^6 electron-volts. If the H^2 nucleus is made up of one proton and one Chadwick neutron of mass 1.0067 then the binding energy of these two particles is 9.7×10^5 electron-volts. H_3^{1+} and He^+ provided the dispersion measurements for the spectra. The presence of $H^1 H^{2+}$ can only introduce in the mass determination a possible *maximum* error of 0.00003 mass units. Lines of mass 4.02852 on the spectra were attributed to $H_2^1 H^2$ ions because: (1) no lines of comparable intensity appeared in this position when commercial hydrogen of low H^2 content was used; (2) under the conditions existing in the discharge tube the abundance of H_2^{2+} was negligibly small compared to the abundance of $H_2^1 H^{2+}$; (3) the mass is less than the mass of H_4^{1+} by an amount outside of the limits of error. Two samples of enriched hydrogen were used which had been prepared by Brickwedde; both had been tested spectroscopically by Urey and Murphy, and one of them was identical with Bleakney's Sample III. From the value for the mass of H^2 , the energy balance is calculated for one process of noncapture disintegration of N^{14} by neutron impact, suggested by Feather, which would result in C^{12} and H^2 . It is concluded that this disintegration could not possibly occur under the conditions of his experiments.

INTRODUCTION

THE H^2 nucleus represents the simplest complex nucleus and as such may be more amenable to theoretical attack than other nuclei. Whether the nucleus is composed of two protons and one electron, or one proton and one neutron, an accurate determination of the mass of the H^2 nucleus is of interest not only in relation to the packing fractions of other nuclei but also as a clue to the possible structure of the H^2 nucleus itself. Also, the possibility exists that together with the electron, proton, neutron, and alpha-particle, H^2 may play a part in the structure of heavier nuclei.¹

In all calculations of the energy of binding of nuclear constituents it is essential to know the masses of the component parts. Bleakney² has placed a lower limit on the mass of the H^2 nucleus, but spectrographs of the Dempster

¹ N. Feather, Proc. Roy. Soc. 136, 726 (1932); J. Chadwick, *ibid.*, 706; N. S. Grace, J. Am. Chem. Soc. 54, 2562 (1932).

² W. Bleakney, Phys. Rev. 41, 32 (1932); 39, 536 (1932).

type such as Bleakney used are at present limited to a lower order of accuracy than mass-spectrographs which photograph mass-spectra and permit the reduction of observations from accurate mensuration of the photographic traces resulting from ionized atoms and molecules. In the future the ratio of the masses of H^1 to H^2 may possibly be obtained from band spectra with an error of only one part in 10^5 . The present paper is a report of the measurement³ of the mass of H^2 obtained with the mass-spectrograph recently described.⁴

The existence of an isotope of hydrogen of mass number two, predicted by Birge and Menzel,⁵ was demonstrated by Urey, Brickwedde, and Murphy.⁶ Their paper should be referred to for a bibliography of the subject and a review of previous work. Bleakney's work with his low-pressure spectrograph provided excellent confirmatory evidence of H^2 , and splendid measurements were secured of the relative abundance of H^2 in various samples of hydrogen. More recently Kallman and Lasareff⁷ were able to detect the presence of H^1H^2 in fractionated hydrogen.

CONDITIONS FOR THE MEASUREMENT OF THE MASS OF H^2

If the mass of H^2 should be close to that of H_2^1 then the resolving power of the apparatus might not permit the separation of the doublets H_2^{2+} , H_2^{1+} , and H_3^{1+} , H^1H^{2+} , and the mass of H^2 could not be compared with H^1 directly. The most accurate method of measurement of the mass of H^2 by a mass-spectrograph would be by comparison of the mass of $H_2^1H^{2+}$ with He^+ . Bleakney's value of a lower limit of the mass of H^2 showed clearly that $H_2^1H^{2+}$ if secured would be well separated from He^+ and the higher the mass of H^2 the greater the separation. From the suggested process of formation of triatomic hydrogen,⁸ $H_2^+ + H_2 \rightarrow H_3^+ + H$, it is clear that a high concentration of ions in the discharge tube would favor the production of H_3^{1+} and $H_2^1H^{2+}$. Brasefield⁹ has shown that under proper conditions of current density and pressure, an ion beam can be secured with a concentration of H_3^{1+} comparable to that of H_2^{1+} . Bleakney, and Kallman and Lasareff worked with very low pressures of hydrogen which would preclude secondary effects to a large extent and only permit measurements of ions produced by the primary process of electron impact. Relatively high current density and high gas pressure favor the formation of $H_2^1H^{2+}$.

EXPERIMENTAL PROCEDURE

Fortunately the conditions essential to the production of triatomic hydrogen can be achieved in the discharge tube of the mass-spectrograph.

³ K. Bainbridge, *Phys. Rev.* **41**, 115 (1932).

⁴ K. Bainbridge, *Phys. Rev.* **40**, 130 (1932). A detailed description of this apparatus will appear in the *Journal of the Franklin Institute*.

⁵ R. T. Birge and D. H. Menzel, *Phys. Rev.* **37**, 1669 (1931).

⁶ H. C. Urey, F. G. Brickwedde and G. M. Murphy, *Phys. Rev.* **40**, 1 (1932); **39**, 164 (1932).

⁷ H. Kallman and W. Lasareff, *Naturwiss.* **20**, 472 (1932).

⁸ H. D. Smyth, *Rev. Mod. Phys.* **3**, 370 (1931).

⁹ C. Brasefield, *Phys. Rev.* **31**, 52 (1928).

A cylindrical discharge tube was used, 8 cm in diameter, with a 2.5 cm diameter aluminum cathode of the shape described by Thomson.¹⁰ The top of the cathode was 2 cm above the surface of an iron plate which served as a magnetic shield for stray fields and also as a base for the discharge tube. The pressure of the gas in the discharge tube was in the range of 0.5 to 5 microns of mercury. The current was 75 ± 25 m.a. for different exposures at potentials from 7000 to 15,000 volts, which experience had shown produced $H_2^1H^{2+}$ with sufficient intensity.

Two Thordardson 1 K.V.A., 25,000 volt transformers, controlled by an induction voltage regulator, provided the current for the discharge. The combination of two kenetrons with two transformers gave full wave rectification. The output was not filtered in any way, as a wide range of energies in the discharge tube is essential to the proper functioning of the mass-spectrograph.

In addition to ordinary commercial tank hydrogen, two samples of enriched hydrogen were used which had been fractionated at the triple point by Dr. Brickwedde of the U. S. Bureau of Standards. These samples were placed at the disposal of the author through the kindness of Professor Urey, Dr. Brickwedde, Dr. Murphy, and Dr. Bleakney. One sample was from the same lot Bleakney used and designated *Sample III*. The other was fractionated later by Dr. Brickwedde and had been tested by Professor Urey and Dr. Murphy, who reported a greater concentration of H^2 than in *Sample III*.

The magnetic field and the potential across the velocity selector plates of the mass-spectrograph were adjusted to bring H_3^{1+} and He^+ within the first 8 cm of the recording plate. This region had been exposed for more than 15 spectra of C, CH_1 , CH_2 , CH_3 , CH_4 , and CH_5 , and also for the series O, OH_1 , OH_2 , OH_3 , and the mass scale had been found to be linear to within one part in 10,000.

The first 21 exposures showed that $H_2^1H^{2+}$, or possibly H_4^{1+} or H_2^{2+} , was present but in such small concentration that no measurements of the mass could be made to aid in determining the nature of the ion. In agreement with Thomson's results,¹¹ it was found that the presence of mercury vapor in the tube greatly weakens the triatomic hydrogen line. Subsequently, before photographing each series of spectra the discharge tube was cleaned out and baked by the energy of the discharge itself until no discharge could be run at voltages even as high as 25,000. The great amount of power dissipated in the discharge tube, about 500 watts, was sufficient to raise the walls of the tube to 200°C. At the same time the cathode and iron base were thoroughly cleaned by positive ion bombardment.

Ordinarily gases are admitted through a leak into the discharge tube and then are pumped out into the atmosphere. The valuable fractionated hydrogen, however, was not pumped out, but was circulated continuously by a diffusion pump. The gas was pumped out through the cathode slit, 0.005 cm \times 0.3 cm, and then was readmitted to the discharge through a hole under the side of the cathode. The gas passed through two liquid air traps, one on

¹⁰ J. J. Thomson, *Rays of Positive Electricity*, 2nd. ed., p. 30.

¹¹ Reference 10, p. 200.

typ
cur
the
tra
the
err
me
scr

by
Th
vie
pro
we
M
in

of
an
Th
sp
Bl
if
th
at
of
Br
pr

ge

ap

(19

each side of the circulating pump. In certain cases still further concentration of the H^2 in the enriched samples was achieved in the discharge tube itself

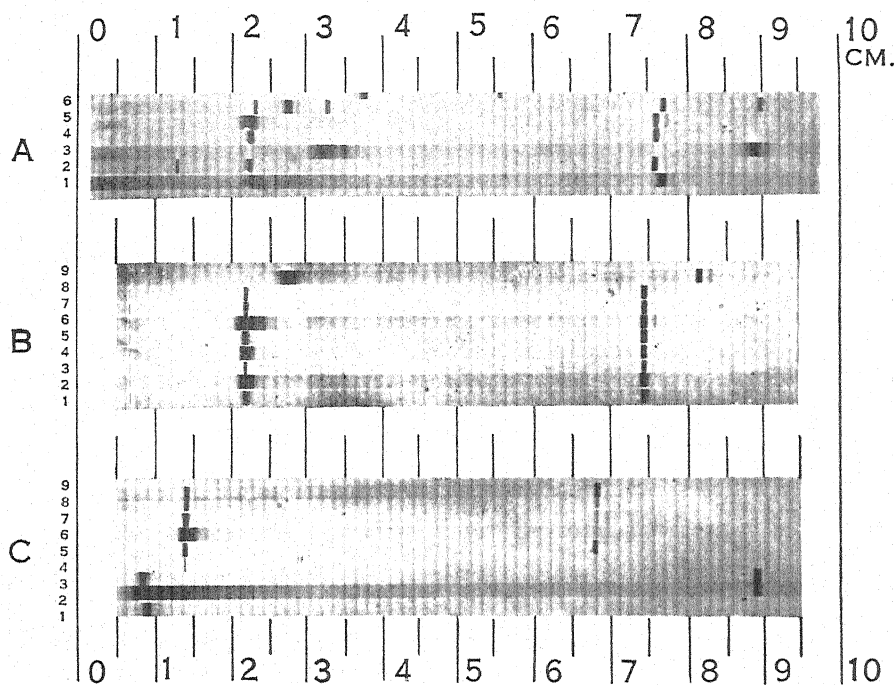


Fig. 1. Mass-spectra of hydrogen and helium ions. The descriptions of the spectra are given below in condensed form. The three samples of hydrogen used are designated: OH, for ordinary commercial tank hydrogen; BH, for Sample III Bleakney hydrogen; UH, for Urey-Brickwedde hydrogen. Spectra A June 10, Spectra B June 11, Spectra C June 14, 1932. Spectra are numbered in order as they were taken. T =exposure time in minutes. Description of ion is followed by number to nearest mm referring to attached cm scale as aid in locating specific lines. Lines which may not be or cannot be reproduced in half-tone are designated weak (w), or very weak (vw). Sharp lines on the left are fiducial lines to mark the plate position.

A1, BH, $T63$, H_2^1 2.3, He 7.7, $H_2^3H^2$ 7.8:
A2, BH, T 16 H_2^1 1.3; T 15, H_2^1 2.2, He 7.6,
 $H_2^3H^2$ 7.7 w:
A3, UH, H_2^1 3.5 premature exposure before
velocity selector potential and discharge
potential were set, $T60$ H_2^1 3.2, He 8.9,
 $H_2^3H^2$ 9.0:
A4, UH, T 16 H_2^1 2.3, He 7.6, $H_2^3H^2$ 7.7 vw
taken with 60 sec.⁻¹ pulsating current,
one transformer disconnected:
A5, UH, T 17.5, H_2^1 2.2, He 7.6, $H_2^3H^2$ 7.7:
A6, UH, three separate spectra, No. 175,
 H_2^1 2.3, He 7.7, $H_2^3H^2$ 7.8 w:
No. 2 $T12.5$, He 2.8, $H_2^3H^2$ 2.9 w, HeH 7.1:
No. 3 $T4$, H_2^1 3.3, He 9, $H_2^3H^2$ not reproduci-
ble on print.

B1, OH, $T16$, H_2^1 2.2, He 7.5:
B2, OH, $T30$, H_2^1 2.2, He 7.5:
B3, OH, $T3$, H_2^1 2.2, He 7.5:

B4, BH, $T15$, H_2^1 2.2, He 7.5, $H_2^3H^2$ 7.6 vw:
B5, BH, $T30$, H_2^1 2.2, He 7.5, $H_2^3H^2$ 7.6 w:
B6, UH, $T30$, H_2^1 2.2, He 7.5, $H_2^3H^2$ 7.6:
B7, UH, $T15$, H_2^1 2.2, He 7.5, $H_2^3H^2$ 7.6:
B8, UH, $T4$, H_2^1 2.2, He 7.5, $H_2^3H^2$ 7.6:
B9, UH, $T15$, H_2^1 2.7, He 8.15, $H_2^3H^2$ 8.3:

C1, UH, $T5$, H_2^1 .9, H_2^3 9 w, Hg present:
C2, UH, $T30$, H_2^1 .8, H_2^3 8.9:
C3, UH, $T1$, H_2^1 .8, H_2^3 8.9:
Pressure in discharge changed.
C4, UH, $T1$, H_2^1 1.4, He 6.8 w:
C5, UH, $T15$, H_2^1 1.4, He 6.8, $H_2^3H^2$ 6.9 vw:
C6, UH, $T30$, H_2^1 1.4, He 6.8, $H_2^3H^2$ vw:
Discharge voltage too low.
C7, UH, $T15$, H_2^1 1.4, He 6.8, $H_2^3H^2$ 7:
 H_2 content increased by separation by diffu-
sions.

C8, OH, $T15$, H_2^1 1.4, He 6.8, $H_2^3H^2$ 7 vw:
C9, OH, $T33$, H_2^1 1.4, He 6.8, $H_2^3H^2$ 7 vw.

by the method of differential diffusion. A dose of hydrogen was admitted and the excess gas pumped out through the slit while the discharge was running. When the gas pressure had been reduced to the right value for an exposure the process of circulation was started. Small but positive and useful increased concentrations of H^2 were obtained in this way.

Fig. 1 is a reproduction of contact prints of the spectra of hydrogen. A small amount of helium was added to the hydrogen to provide a reference mass.

IDENTIFICATION OF $H_2^1H^2$ ION

A line adjacent to and on the heavier mass side of He^+ might be due to H_4^1 , H_2^2 , or $H_2^1H^2$ ions. However, the following considerations demonstrate that the trace actually observed at that position on the plate could only be produced by $H_2^1H^2$ ions.

From Aston's data,¹² the mass of He is taken as 4.00216 ± 0.00013 , of H^1 as 1.00778 ± 0.00005 ,¹³ and of the electron as 0.000547 mass units, all referred to $O^{16} = 16$. The measurements of the separation of He^+ and the adjacent heavier ion gave 0.02691 ± 0.00006 mass units, as will be described later. This value added to the mass of the helium ion results in a mass of 4.02852 ± 0.00015 for the line adjacent to He^+ . H_4^{1+} is ruled out as a possibility since its mass, 4.03057 ± 0.00010 is quite outside of the limit of error of the measurements.

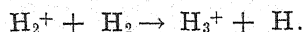
H_4^{1+} is also ruled out, because no lines adjacent to helium appeared when ordinary commercial hydrogen was used in the discharge tube. Spectra 1, 2 and 3B, Fig. 1 were taken with tank hydrogen in the spectrograph discharge tube and no lines appeared near the helium traces. The discharge tube was then evacuated and fractionated enriched hydrogen was admitted which produced lines corresponding to a mass of 4.02852 units on the immediately succeeding spectra 4, 5, 6, 7, 8, 9B. The lines are weak for spectra 4 and 5B as the electrodes and walls of the tube were still contaminated with ordinary hydrogen which reduced the concentration of H^2 in the first dose of fractionated hydrogen. The objection might be raised that the possible presence of mercury in the tube for the first few spectra so inhibited the appearance of a line at 4.0285 that such a line would have been absent in any case regardless of the source of the hydrogen. In order to disprove any such contention spectra 7, 8 and 9C were taken. Spectra 8 and 9C were photographed using commercial hydrogen in the discharge tube *after* successful runs had been made in which $H_2^1H^{2+}$ appeared. Faint lines did appear, but as may be seen in Fig. 1, they are weaker on 8C, a 15 minute exposure, and on 9C, a 33 minute exposure, than the $H_2^1H^2$ lines on spectrum 7C (15 minutes exposure). All three exposures were taken under conditions as nearly identical as possible. The faint traces of $H_2^1H^2$ on 8 and 9C were present owing to the practical impossibility of washing out the tube and cleaning the electrodes entirely free from the gas used in earlier exposures taken immediately before 8C and 9C. As the

¹² F. W. Aston, Proc. Roy. Soc. 115, 502 (1927).

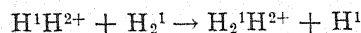
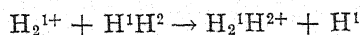
¹³ All succeeding calculations are made on the basis that Aston's limits of error are three times the probable error of his measurements.

line at 4.0285 only appeared in abundance when fractionated hydrogen was used, it was concluded that the ions responsible for that line contained H^2 and might be $H_2^1H^2$ or H_2^2 but could not be H_4^1 ions.

H_2^{2+} is eliminated as a possibility when the relative abundance of H_2^{2+} and $H_2^1H^{2+}$ is considered. From Bleakney's measurements the ratio H^1H^{2+}/H_2^{1+} is approximately 0.002. The atomic ratio of H^2/H^1 is 0.001 and the ratio H_2^{2+}/H_2^{1+} is 10^{-6} . The suggested mode of formation of triatomic hydrogen is



The production of $H_2^1H_2^{2+}$ is given by



and for each reaction of this type, assuming that H^1 and H^2 behave similarly, the probability is that three out of every four triatomic molecules will contain H^2 . If these reactions proceed in proportion to the product of the partial pressures of the constituents, the ratio $H_2^{2+}/H_2^1H^{2+}$ can be calculated. In the discharge tube the partial pressures for different molecules and ions are respectively: for H_2^1 , p ; for H_2^{1+} , ap ; for H^1H^2 , $0.002 p$; and for H^1H^{2+} , $0.002 ap$, where a is proportional to the amount of ionization extant. The amount of $H_2^1H^{2+}$ is $2 \times 3/4 \times 0.002 ap$ and the abundance of H_3^{1+} is ap . The ratio of $H_2^{2+}/H_2^1H^{2+}$ is equal to

$$H_2^{2+}/H_2^{1+} \times H_2^{1+}/H_3^{1+} \times H_3^{1+}/H_2^1H^{2+}$$

wherein all ratios are known except H_3^{1+}/H_3^{1+} which is a function of the conditions existing in the discharge tube. The value of H_2^{1+}/H_3^{1+} must be obtained experimentally. From Fig. 1, spectra 2, 3 and 4C, the ratio H_2^{1+}/H_3^{1+} was estimated at from 1 to 20 under varying conditions in the discharge tube. If the measured values of this ratio are substituted, the ratio of abundance of $H_2^{2+}/H_2^1H^{2+}$ is in the range 0.67×10^{-2} to 0.33×10^{-3} . The low abundance of H_2^{2+} precludes its appearance on the mass-spectra and the line of mass 4.02852 must be attributed to $H_2^1H^{2+}$.

Exactly the same relative abundance of $H_2^{2+}/H_2^1H^{2+}$ is obtained if the calculations are made without regard to the process of formation of triatomic hydrogen, on the basis of unweighted probability considerations alone.

DISPERSION MEASUREMENTS

The separation of H_3^{1+} and He^+ was measured by a comparator to secure the dispersion measurements for these spectra. The presence of H^1H^{2+} can only introduce a negligible correction to the mass scale measurements. If H^1H^{2+} were present to an abundance equal to that of H_3^{1+} then the dispersion figure would be in error by one part in 1100, equivalent to 0.00003 mass units in the value for the mass of H^2 . This possible systematic error is only one half of the probable error in the measurement of the isotopic weight of H^2 . As the ratio of abundance of H^1H^{2+}/H_3^{1+} could not be greater than 0.002×20 or

1/25, the effect of H^1H^2 ions was negligible and no correction to the dispersion measurements is necessary.

METHOD OF MEASUREMENT OF $He^+ H_2^1H^2+$ SEPARATION

The faintness of the $H_2^1H^2+$ lines in most cases prevented direct measurements by a comparator. The separations of the $H_2^1H^2+$ and He^+ lines on different spectra were measured by running the plates through a Goos-Koch microphotometer at a ratio of plate distance to record distance of approximately 1 to 40. For the first report³ of this work the densitometer records of 14 spectra had been measured and reduced to plate distances by a subsequent determination of the ratio of densitometer travel to plate travel. The microphotometer does not maintain the same multiplication ratio throughout its travel so that for this report, twelve spectra were remeasured with a glass reticle, (1/20 mm divisions), directly superimposed on the spectrum plates. The reticle was compared with one ruled on the Swarthmore College Observatory comparator and also measured directly on a Gaertner comparator. Two of the spectra measured for the first report of this work could not be measured by this method. The densitometer records were coated with a frosting coating and smooth curves were drawn in by pencil. Fig. 2 is a reproduction of some of the records of spectra used in the measurement of the mass of

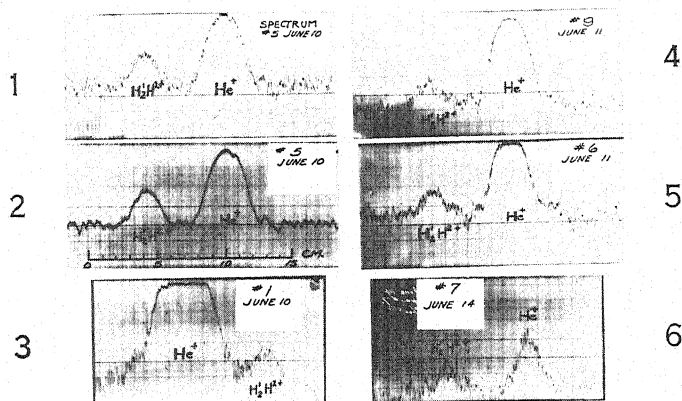


Fig. 2. Densitometer records of several $He^+ - (H_2^1H^2)^+$ doublets. Scale under record No. 2. Ratio of densitometer record distance to spectrum plate distance approximately 40 to 1. Micro-meter slit 0.002 cm wide.

$H_2^1H^2+$. These records, taken without the superposition of the reticle, illustrate the remarkable symmetry of the ion traces.¹⁴ Record No. 2 is of the

¹⁴ The symmetry of the spectral lines is a direct consequence of the design of the mass-spectrograph. Measurements of the separation of lines can be made referred to the centers of traces of unequal density, an advantage which can hardly be overestimated in cases in which it is impractical or impossible to obtain traces of equal density. The symmetry of the traces is a result of the fact that the ion beams are not brought to a focus at the surface of the recording plate. Any focussing action takes place in the circular path of the ions 90° from the ion source, or last slit of the velocity selector in the mass-spectrograph. The velocity selector introduces an essentially

same spectrum as No. 1 but it was made with a different adjustment of the densitometer to minimize the effect of the grain of the plate.

The separation of the traces was measured by superposition of the densitometer records on accurate millimeter cross-section paper and by direct scale measurement of the centers of the peaks. The probable error of a single observation, ± 0.00024 mass units, corresponds to an error of about ± 0.5 mm in a distance of 43 to 60 mm on the densitometer records of different spectra.

RESULTS

The results and their weight values for the mass difference between He^+ and $\text{H}_2^1\text{H}^{2+}$ are given in Table I.

TABLE I.

Fig. 1 spectrum	1A	2A	3A	4A	5A	6A
Mass difference	0.02749	0.02702	0.02688	0.02721	0.02688	0.02668
Weight	1	2	1	1	3	1
Fig. 1 spectrum	5B	6B	7B	8B	9B	7C
Mass difference	0.02627	0.02657	0.02742	0.02627	0.02714	0.02703
Weight	1	3	2	1	1	2

The averaged difference is 0.02691 ± 0.00006 . The probable error is a composite value of a probable error of one part in one thousand in measuring the reticle and the probable error of the above mass difference *per se*.

The mass of neutral H^2 is $M_{\text{He}} + 0.02691 - M_{\text{H}^1} = 2.01351 \pm 0.00006$ when referred directly to Aston's value for helium. The masses of He^+ and H_2^{1+} were compared directly by Aston with a probable error of only ± 0.000008 mass units in the determination of the mass of H^1 in terms of helium.¹⁵

The absolute value of H^2 is 2.01351 ± 0.00018 mass units referred to $0^{16} = 16$ and calculated on the basis that Aston's limits of error are equal to three times the probable error of his measurements. The equivalent packing fraction of H^2 is 67.5 parts in 10,000.

parallel beam of ions into the uniform magnetic field, or camera section of the spectrograph, so that the ions converge at 90° , then diverge, and at 180° from the source are again traveling in a parallel beam where the beam is normally incident on the surface of the recording plate. Spectrographs which deal with divergent nonparallel beams of ions bring the beams to a focus at the recording plate. A sharp edge (W. A. Wooster, Proc. Roy. Soc. **114**, 729 (1927)), or high density of ions at one position results, but the position of the edge of a trace shifts with changes in density and the separation of two adjacent traces of different density cannot be measured accurately (F. W. Aston, Proc. Roy. Soc. **115**, 496 (1927)). A complete discussion will appear in the Journal of the Franklin Institute.

¹⁵ Aston (Proc. Roy. Soc. **115**, 502 (1927)) gives three measured values for the difference in the packing fractions of helium and hydrogen, 73.7, 73.6 and 73.9. The correction for the mass of the electron gives a value of 72.4 for the excess of the packing fraction of hydrogen over that of helium. Ordinary error theory, of course, cannot be applied for the calculation of the probable error of only three measurements, but the theory of errors for small samples (W. A. Shewhart, Bell System Tech. J. **5**, 308 (1926)) may be applied and the error in Aston's measurements was calculated on that basis.

DISCUSSION

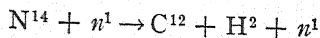
Nuclear structure of H^2

The energy of binding of the H^2 nucleus corresponds to 0.00205 mass units or approximately 2×10^6 electron-volts if the nucleus is composed of two protons and one electron. It is interesting to speculate that if the H^2 nucleus is composed of one proton and one Chadwick neutron,¹⁶ of mass 1.0067, then the binding energy would be 9.7×10^5 electron-volts. The energy of binding of the neutron itself has been given as 1 to 2×10^6 electron-volts. When more concentrated samples of H^2 are available, it may be possible to distinguish between the two suggested structures of the H^2 nucleus.

The possibility of H^2 as a nuclear structural unit

The binding energy of H^2 is small compared to the 35×10^6 electron-volts accorded helium nuclei. Grace¹ has suggested that the H^2 nucleus may be a constituent of other nuclei and suggests its inclusion in Li^6 and B^{10} . On this basis the binding energy of a Li^6 nucleus, composed of one H^2 nucleus and one helium nucleus, is 3.7×10^6 electron-volts. The binding energy of two helium nuclei and one H^2 nucleus combined as a B^{10} nucleus is 4.3×10^6 electron-volts. Such structures appear possible but the presence of H^2 in heavier nuclei, above mass 22, seems doubtful. While there is good evidence from various sources that α -particles retain their identity inside of nuclei, the small energy of binding of H^2 may not be sufficient to maintain the structure of that entity when it is subjected to the fields and perturbing forces of other particles in heavy complex nuclei.

Feather¹⁷ has suggested the process



for noncapture disintegration of nitrogen by neutron impact. When the known masses of the constituents are substituted the result is that at least 9×10^6 electron-volts energy must be supplied by the impacting neutron in order that this disintegration may proceed. The maximum energy of neutrons resulting from the disintegration of Be^9 is 5.7×10^6 electron-volts, entirely insufficient to promote the suggested noncapture disintegration of nitrogen. Feather decided on different grounds that H^2 does not result as a disintegration product of N^{14} but left the possibility open. Until positive evidence is obtained of the inclusion of H^2 in nuclei it is best not to complicate further the structure of nuclei by the addition of H^2 as a possible component, since what evidence is available militates against the addition of this unit.

The author is particularly indebted to Dr. Brickwedde who made this investigation possible by his preparation of the samples of enriched hydrogen at the U. S. Bureau of Standards, to Professor Urey and Dr. Murphy of Columbia University who placed a tested sample at the disposal of the author, to Br. Bramley and Dr. Bleakney for their interest and helpful discus-

¹⁶ J. Chadwick, Proc. Roy. Soc. 136, 270 (1932).

¹⁷ N. Feather, Proc. Roy. Soc. 136, 721, 726 (1932).

sions, and to Professor John A. Miller and the members of the Swarthmore College Observatory for their generous permission to use their measuring instruments.

Note added in proof: It has been the author's privilege to see the manuscript of a paper on the infrared spectrum of H^2Cl by J. D. Hardy, E. F. Barker, and D. M. Dennison. They have observed and measured the fundamental absorption bands due to H^2Cl^{36} and H^2Cl^{37} which lie in the neighborhood of 4.8μ . The value obtained for the mass of H^2 is 2.01367 ± 0.00010 if H^1 is 1.00778 as given by Aston. The details will be published shortly.

Professor R. T. Birge has pointed out to the writer that Aston's values for the mass of H^1 and He are probably too low. If the chemical value for the mass of H^1 is correct (R. T. Birge, Phys. Rev. Supplement 1, 1 (1929)), then the mass of H^1 is 1.00796 on the $\text{O}^{16}=16$ scale and Aston's value is too low by 1.8×10^{-4} units. The calculation of the mass of H^1 is made on the basis that the abundance of H^2 is 1 in 30,000 (W. Bleakney, Phys. Rev. 41, 32 (1932)) and that Mecke and Childs' value for the relative abundance of the oxygen isotopes is correct (Zeits. f. Physik 68, 362 (1931)).

If $\text{H}^1=1.00796$, then from the measurements of Hardy, Barker, and Dennison, the mass of $\text{H}^2=2.01403 \pm 0.00010$. The measurement of the mass of H^2 on the mass-spectrograph involves a knowledge of the mass of H^1 and of He also. Aston measured the ratio H/He and He/O . If the error 1.8×10^{-4} in H^1 is divided equally between H^1 and He then the mass of $\text{H}^1=1.00796$ and $\text{He}=4.00252$. On this basis my measurements give $\text{H}^2=2.01351 \pm 0.00018$ referred to O^{16} , a result identical with the value obtained before. The agreement between the band spectrum and mass-spectrograph values for the mass of H^2 , calculated on this new basis, can no longer be considered satisfactory.

Ionization of Helium, Neon and Argon under Impact of their own Atoms and Positive Ions¹

By CHARLES J. BRASEFIELD
Sloane Physics Laboratory, Yale University

(Received June 30, 1932)

The number of electrons liberated from neutral rare gas atoms under impact of their own atoms and positive ions was measured as a function of the kinetic energy of the impinging particles. When the impinging beam is composed mostly of neutral atoms, it is found that helium is ionized at about 60 equivalent volts, neon at about 50 volts and argon at about 40 volts. If the impinging beam is composed of atoms and positive ions in about equal proportions, additional ionization is found to set in in argon at around 330 volts. No ionization by positive ions was observed in either helium or neon up to 500 volts. Curves are shown which indicate the efficiency of ionization of the rare gases under impacts of their own atoms and positive ions.

INTRODUCTION

IONIZATION by positive ions has been considered one of the processes necessary for the maintenance of a gaseous discharge. Earlier attempts made to detect this effect directly were inconclusive due to the difficulty of distinguishing electrons produced by ionization of gas atoms from secondary electrons which are emitted from metal parts under impact of positive ions.² However, the experiments of Sutton, Beeck and Mouzon^{3,4} indicate quite conclusively that the rare gases are ionized under impact of the alkali positive ions, although the process is inefficient compared with ionization under electron impact. Beeck and Mouzon⁵ have found definite values of the minimum kinetic energy which an alkali ion must have in order to ionize a rare gas atom. More recently Wolf⁶ has reported that argon is ionized slightly by its own positive ions in the neighborhood of 300 equivalent volts. Still more recently, Beeck⁷ has reported preliminary experiments on the ionization of argon and neon by slow argon atoms.

Attempts to find a theoretical solution of the problem have been made, among others, by Franck,⁸ Joos and Kulenkampff,⁹ and Zwicky.¹⁰ About all

¹ This paper was presented before the American Physical Society at the New Haven meeting, June 23, 1932. The abstract printed in the program of this meeting should be disregarded.

² As a matter of fact, the skeptical may still claim with some justification that, even in the most recent experiments, the electrons are not products of ionization of gas atoms but are secondary electrons from the metal parts which are inherent in any experimental apparatus.

³ R. M. Sutton and J. C. Mouzon, *Phys. Rev.* **37**, 379 (1931).

⁴ O. Beeck and J. C. Mouzon, *Ann. d. Physik* **11**, 737 (1931).

⁵ O. Beeck and J. C. Mouzon, *Ann. d. Physik* **11**, 858 (1931).

⁶ F. Wolf, *Zeits. f. Physik* **74**, 575 (1932).

⁷ O. Beeck, *Proc. Nat. Acad. Sci.* **18**, 311 (1932).

⁸ J. Franck, *Zeits. f. Physik* **25**, 312 (1924).

⁹ G. Joos and H. Kulenkampff, *Phys. Zeits.* **25**, 257 (1924).

¹⁰ F. Zwicky, *Proc. Nat. Acad. Sci.* **18**, 314 (1932).

that can be said at present is that for central impacts between uncharged particles of the same mass, approximately one-half the kinetic energy of the impinging particle is available for ionization of the particle struck. Thus helium, neon and argon should be ionized under impacts of their own neutral atoms if the atoms have kinetic energy of approximately 49, 43 and 31 equivalent volts, respectively. Ionization of the rare gases under impact of their own positive ions might be expected at somewhat higher energies, for in this case the ejected electron escapes while in the field of force of two positive ions.

APPARATUS AND PROCEDURE

The apparatus used in this investigation is a modification of that used by Sutton and is shown drawn to scale in Fig. 1. The experimental tube was divided into two parts by a glass partition which separated the discharge chamber from the chamber in which ionization of the gas by the impinging

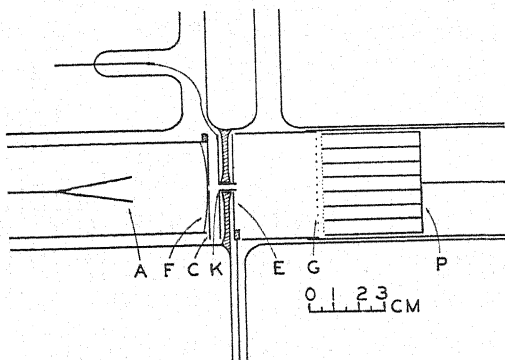


Fig. 1. Experimental tube.

particles was detected. A discharge was produced between the oxide-coated filament¹¹ *F* and the anode *A*. Positive ions of the gas are produced by electron impact and drift toward the filament. Since the voltage across the discharge, V_d , is concentrated at the filament, most of the positive ions that pass through the 2 mm hole in the virtual cathode *C* will have an energy of V_d equivalent volts. Between *C* and *K* they are further accelerated by an applied potential V_a so that most of the ions enter the canal *K* with an energy of $V_d + V_a$ equivalent volts. The canal is 7 mm long and 2 mm in diameter. Emerging from the canal, the particles in the beam (now a mixture of positive ions and neutral atoms) enter the ionization chamber where they are free to collide with the atoms of the gas. The ionization chamber is 3.3 cm long. Its walls are of sheet nickel and the far end is closed by a large mesh fine wire grid *G*, both of which are at the same potential as the plate *K*. At the near end of the ionization chamber is the electrode *E* to which a positive potential is applied to collect any electrons resulting from the impacts. In general 15 volts were found sufficient to saturate the electron current to *E*. The positive ions in the beam continue through the grid *G* and are collected by *P*. The

¹¹ Kindly supplied by Dr. M. J. Kelly of the Bell Telephone Laboratories.

face of P is covered by a wire grid to give a more uniform field between G and P . The distance from G to P is about 2 mm and P is kept at a positive potential with respect to G in order to prevent the escape of any secondary electrons resulting from the impact of positive ions upon P . We might expect secondary electrons with velocities as high as 16 volts in helium, 13 volts in neon and 7 volts in argon.¹² However, it was found that only a few volts were sufficient to stop most of the secondary electrons emitted from P , but to be on the safe side the potential between G and P was kept at 15 volts for helium and 12 volts for neon and argon. The metal parts of the tube were made of nickel and were outgassed by an induction furnace. The rare gases were obtained spectroscopically pure and were used without further purification. The tube was completely evacuated and a fresh supply of gas admitted before each run.

Keeping V_d and I_d (the discharge current) constant, the accelerating potential V_a was varied and readings were taken of the electron current to the plate E and the positive ion current collected by P . The same galvanometer was used to measure each of these currents. It had a sensitivity of 2324 megohms.

It has been assumed that the moving particles enter the ionization chamber with a velocity of $V_d + V_a$ equivalent volts. To check this, measurements were made of the positive ion current collected by P as the retarding potential between G and P was increased, for given values of V_d and V_a . It was found that the fastest ions reaching P did have a velocity of $V_d + V_a$ equivalent volts.

We are quite certain that all the particles leaving the neighborhood of the filament are positive ions. Knowing the distance the ions go from the filament until they reach the ionization chamber (1.1 cm) and also knowing the mean free path of the ions for neutralization, we can compute the fraction of ions and of atoms in the impinging beam as it enters the ionization chamber. The most reliable value of the mean free path for neutralization of A^+ in argon, obtained from the work of Wolf,⁶ is 1.6 cm at 0.01 mm pressure. For the mean free paths for neutralization of Ne^+ in neon and He^+ in helium we must make use of the more qualitative measurements of Kallman and Rosen¹³ which yield values of 2.5 cm at 0.01 mm pressure in each case.

RESULTS

If the discharge is operated at such a pressure that 95 percent of the particles entering the ionization chamber are neutral atoms, curves such as are shown in Fig. 2 are obtained. Here the electron current collected by the electrode E , I_e , is plotted against the energy of the impinging atoms in $(V_d + V_a)$ equivalent volts. It will be noticed that in all cases the initial electron current is not zero but has a definite constant value. It is thought that this is due to secondary electrons ejected from the canal K by the impinging positive ions, and of course it is impossible to eliminate such secondaries.

¹² See for example Rev. Mod. Phys. 2, 180 (1930) and references given there.

¹³ H. Kallman and B. Rosen, Zeits. f. Physik 61, 61 (1930).

When the impinging atoms have a certain minimum energy, ionization is observed to set in. This occurs in helium at about 60 volts, in neon at about 50 volts and in argon at about 40 volts. These values are in each case approximately 10 volts higher than we would expect theoretically. Further ionization also appears to take place in neon and argon at about 110 and 75 volts, respectively. Two possible explanations of these higher ionization potentials are suggested. They may represent the minimum energies which an atom must have in order to ionize successively two times. Or they may represent the minimum energy necessary to ionize one of the colliding particles and excite the other—a process which has been suggested in a recent paper by Weizel and Beek.¹⁴

In order to increase the proportion of positive ions in the impinging beam, the tube was now operated at as low a pressure as possible. The minimum pressure was determined in the case of helium and neon by the lowest pressure

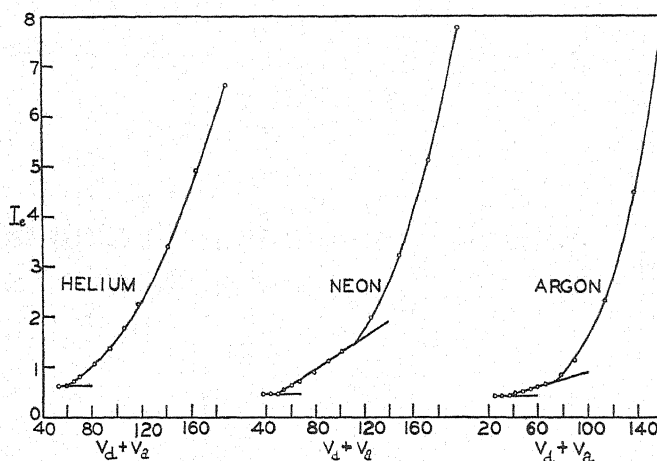


Fig. 2. Ionization of helium, neon and argon under impact of their own atoms. Helium: pressure=0.07 mm, $V_d=47$ v., $I_d=20$ m.a.; neon: pressure=0.07 mm, $V_d=31$ v., $I_d=20$ m.a.; argon: pressure=0.036 mm, $V_d=19$ v., $I_d=40$ m.a.

at which a discharge could be maintained; in argon by the lowest pressure at which there was an appreciable electron current collected by E . The results obtained under these conditions are shown in Fig. 3, where again the electron current collected by the electrode E , I_e , is plotted against the energy of the impinging particles in $(V_d + V_a)$ equivalent volts. The impinging beam in argon on entering the ionization chamber is composed of 60 percent A^+ and 40 percent A° (neutral atoms); in neon 55 percent Ne^+ and 45 percent Ne° ; and in helium 30 percent He^+ and 70 percent He° . As at the higher pressures, we again observe in neon and argon an increase in the ionization current (here at about 120 and 85 volts) due to successive impacts or to simultaneous ionization and excitation. No further abrupt increases in the ionization current are observed except in argon where further ionization seems to set in at about 330 volts. This is ascribed to ionization by argon ions and confirms

¹⁴ W. Weizel and O. Beek, *Zeits. f. Physik* 76, 250 (1932).

Wolf's observation⁶ that argon is ionized slightly by its own positive ions around 300 volts. If helium and neon are ionized by their own positive ions, the process must either be inefficient compared with the ionization of argon by its own positive ions, or it must take place at energies greater than 500 equivalent volts.

From the data used for Fig. 3 it is also possible to calculate roughly the efficiency of ionization of the rare gases under impact of their own atoms and positive ions. Knowing the number of positive ions collected by P ,¹⁵ the distance they have gone since entering the ionization chamber (3.5 cm) and also the mean free path of the ions, it is possible to calculate the number of initial positive ions entering the ionization chamber. Also, since the composition of

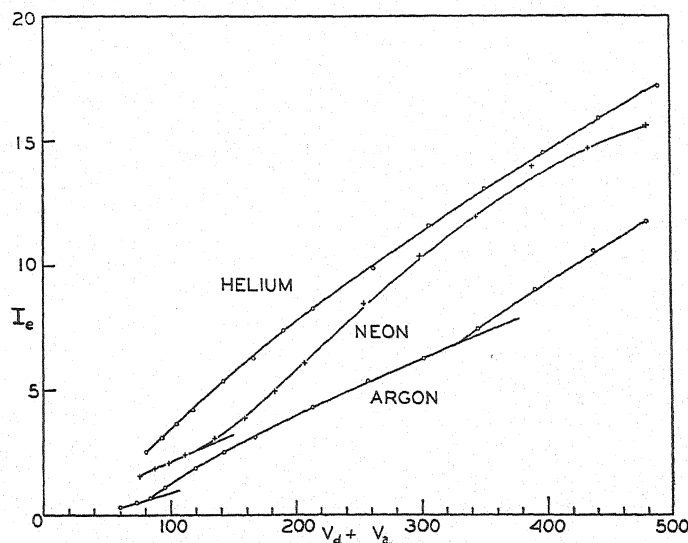


Fig. 3. Ionization of helium, neon and argon under impact of their own atoms and positive ions. Helium: pressure=0.028 mm, $V_d=70$ v., $I_d=10$ m.a.; neon: pressure=0.013 mm, $V_d=65$ v., $I_d=10$ m.a.; argon: pressure=0.0072 mm, $V_d=26$ v., $I_d=20$ m.a.

the beam on entering the ionization chamber is known, it is possible to calculate the number of atoms entering the ionization chamber. If now the ratio of the number of electrons produced (corrected for secondary electrons) to the number of initial atoms (or positive ions as the case may be) is divided by the gas pressure in mm and also by the length of the path of the particles in the ionization chamber (3.3 cm) we get N , the number of electrons produced per initial atom (ion) per cm path at 1 mm pressure. The variation of N with the kinetic energy of the impinging particles in $(V_d + V_e)$ equivalent volts is shown for helium, neon and argon in Fig. 4. These curves should only be con-

¹⁵ If any of the ions produced by collisions in the ionization chamber had succeeded in reaching P , we would expect to observe a marked increase in the positive ion current collected by P after ionization set in. No such increase was detected except when argon was ionized by A^+ . In calculating the efficiency of ionization of argon by A^+ , an attempt was made to correct for these additional positive ions by neglecting the increase in the positive ion current after ionization set in.

sidered as accurate as the measurements of the mean free path of the ions; in other words, only qualitatively correct.

If these curves are compared with similar curves of Sutton³ and Beeck¹⁶ for the efficiency of ionization of the rare gases under impact of the alkali positive ions, it can be seen that the rare gases are considerably more efficiently ionized

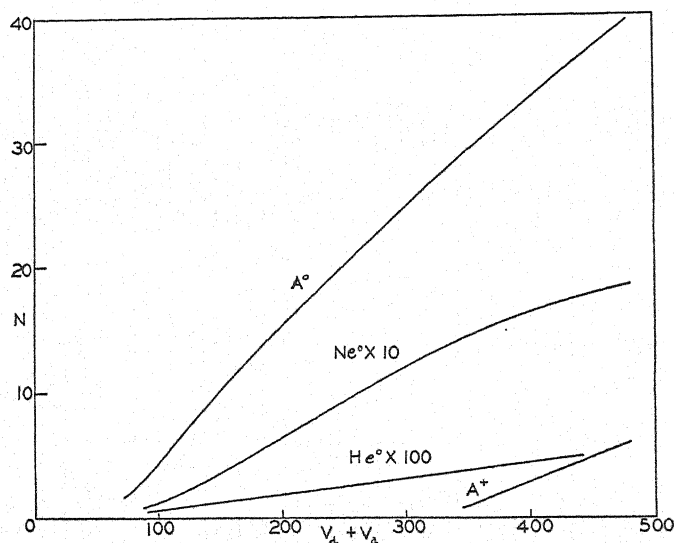


Fig. 4. Efficiency of ionization of helium, neon and argon under impacts of their own atoms (He^0 , Ne^0 , A^0) and positive ions (A^+). Ne^0 curve magnified 10 times; He^0 curve magnified 100 times.

by their own atoms (but less efficiently ionized by their own positive ions) than by alkali ions of approximately the same mass as the rare gas atom. As a matter of fact, in the case of argon and neon, the efficiency of ionization by their own atoms is comparable with the efficiency of ionization under electron impact.¹⁷

¹⁶ O. Beeck, Ann. d. Physik 6, 1018 (1930).

¹⁷ K. T. Compton and C. C. Van Voorhis, Phys. Rev. 27, 729 (1926).

The Scattering of Slow Electrons. Part II

By EUGENE FEENBERG
Harvard University

(Received June 9, 1932)

The scattering equations derived in an earlier paper are here found by a variation method, which is closely related to the Fock-Slater method of determining single electron functions for complex atoms. The equations for scattering in helium and the other inert gases are treated in detail and put into a form suitable for numerical integration. For scattering in helium excellent agreement with experiment is found in the neighborhood of the resonance potential; at 10.75 volts the agreement is poor. This discrepancy at low potentials is undoubtedly to be accounted for by atomic distortion which is neglected in the scattering equation.

IN AN earlier paper¹ the writer discussed the problem of electron scattering by an N electron atomic system from the standpoint of the $N+1$ Schrodinger equation for the scattering system and the external electron. The discussion is here extended.

We treat a simplified problem obtained by representing the atom as an outer electron shell in the potential field $V(r)$ of the core. N is then the number of electrons in the outer shell. Let $u(1, \dots, N)$ represent the normal state unperturbed atomic wave function and $v(1, \dots, N, x_0)$ the atomic wave function perturbed in an unspecified manner by the field of the external electron at x_0, y_0, z_0 . In particular v may be the unperturbed function u , independent of x_0, y_0, z_0 , or a solution of the wave equation for the atomic system in the field of a unit negative charge fixed at the point x_0, y_0, z_0 . We require of v that

$$\begin{aligned} \sum_{\text{spin}} \int \cdots \int v^*(1, \dots, N, x_0) v(1, \dots, N, x_0) d\tau \cdots d\tau_N &= 1, \\ \sum_{\text{spin}} \int \cdots \int v^*(1, \dots, N, x_0) \nabla_0 v(1, \dots, N, x_0) d\tau_1 \cdots d\tau_N &= 0, \\ \text{Limit}_{r_0 \rightarrow \infty} v(1, \dots, N, x_0) &= u(1, \dots, N). \end{aligned} \quad (1.1)$$

We write an approximate solution $\psi(0, 1, \dots, N)$ of the $N+1$ electron problem, antisymmetric in the space-spin coordinates $0, 1, \dots, N$, in the form

$$\psi(0, 1, \dots, N) = \sum_i \pm P_i v(1, \dots, N, x_0) f(0) s(0) \quad (1.2)$$

in which P_i is a permutation operator, $f(0)$ the scattering function, and $s(0)$ a spin function for the external electron. With W_1 the energy of the atomic system, W the kinetic energy of the external electron, and H the energy operator for the complete system,

¹ Feenberg, Phys. Rev. 40, 40 (1932); referred to in text as S.S.E.

$$H = -\frac{1}{2} \sum_0^N \nabla_i^2 - \left(\sum_0^N V(i) - \sum_0^N 1/r_{ii} \right), \quad (1.3)$$

we can briefly describe the method used in S.S.E.¹ to set up scattering equations as follows: Because ψ is only an approximation to the exact solution $(H - W - W_1)\psi$ does not vanish identically. We multiply $(H - W - W_1)\psi$ by the atomic wave function $v^*(1, \dots, N, x_0)$ and the external electron spin function $s(0)$, integrate over space coordinates $1, 2, \dots, N$ and sum over all spin coordinates and require that the resulting averaged value of $(H - W - W_1)\psi$ vanish identically. We find in this way an integral-differential equation for the scattering function f :

$$\sum_{\text{spin}} s(0) \int \cdots \int v^*(1, \dots, N, x_0) (H - W - W_1) \psi d\tau_1 \cdots d\tau_N = 0. \quad (1.4)$$

(1.4) is simplified by introducing the differential equation satisfied by v and the conditions (1.1).

I show that the function f determined by (1.4) gives the integral

$$K(f) = \sum_{\text{spin}} \int \cdots \int \psi^* (H - W - W_1) \psi d\tau_0 d\tau_1 \cdots d\tau_N \quad (1.5)$$

an extreme value. Some preliminary remarks are desirable before stating the variation problem. For large values of r the scattering function reduces to a plane wave plus a scattered wave: $f \sim e^{-ikz} + (1/r)e^{ikr}F(x/r, y/r, z/r)$. Thus neither $\int \cdots \int \psi^* H \psi d\tau_0 \cdots d\tau_N$ nor $\int \cdots \int \psi^* (W + W_1) \psi d\tau_0 \cdots d\tau_N$ exist. However it is possible to define a manifold of functions $R(x)$, $S(x)$ such that $K(f)$ is finite if f is a solution of an equation of the form $(\nabla^2 + 2W + R)f = S$. Eq. (1.4) provides a particular determination of the functions R and S . The condition for the conservation of charge is expressed by

$$\int \int_{\infty} (f^* \nabla f - f \nabla f^*) \cdot dS = 0, \quad (\text{S.S.E.},^1 \text{ section } 3), \quad (1.6)$$

which in turn implies that $K(f)$ is a real number. Finally

$$\begin{aligned} \delta K(f) &\equiv \sum_{\text{spin}} \int \cdots \int [\delta \psi^* (H - W - W_1) \psi + \psi^* (H - W - W_1) \delta \psi] d\tau_0 \cdots d\tau_N \\ &= \sum_{\text{spin}} \int \cdots \int [\delta \psi^* (H - W - W_1) \psi + \delta \psi (H - W - W_1) \psi^*] d\tau_0 \cdots d\tau_N \\ &\quad + C(N) \int \int_{\infty} (f^* \nabla \delta f - \delta f \nabla f^*) \cdot dS. \end{aligned}$$

With this introduction we are prepared to state the variation problem: Given a scattering function f satisfying (1.6) and a manifold of comparison functions $f + \delta f$ such that;

$$(a) \quad f + \delta f \sim e^{-ikz} + (1/r)e^{-ikr}(F(x/r, y/r, z/r) + \delta F)$$

for large values of r ,

(b) $K(f + \delta f)$ exists,

$$(c) \quad \iint_{\infty} (f^* \nabla \delta f - \delta f \nabla f^*) \cdot dS = 0,$$

(d) $\delta K(f) = 0$ for all comparison functions satisfying (a), (b), (c); to prove

(e) f a solution of (1.4).

The proof is simple. Subtracting from $\iint_{\infty} (f^* \nabla \delta f - \delta f \nabla f^*) \cdot dS$ its conjugate complex we find $\delta \iint_{\infty} (f^* \nabla f - f \nabla f^*) \cdot dS = 0$; or, neglecting terms in $\delta F \delta F^*$, the comparison functions satisfy the condition for the conservation of charge. Because of the symmetry properties of ψ we may write

$$\begin{aligned} \delta K(f) = C(N) \sum_{\text{spin}} \int \cdots \int & [v^*(1, \cdots, N, x_0) \delta f^*(0) s(0) (H - W - W_1) \psi \\ & + v(1, \cdots, N, x_0) \delta f(0) s(0) (H - W - W_1) \psi^*] d\tau_0 d\tau_1 \cdots d\tau_N. \end{aligned}$$

Then, seeing that the real and imaginary parts of δf are independently variable (except at infinity where they are connected by the relation (c)), (1.4) is an immediate consequence of (d).

It seems probable that (1.4) is the best scattering equation derivable from the assumption that the wave function has the form (1.2). The variation method of deriving (1.4) does not differ essentially from the Fock-Slater method of determining single electron functions for complex atoms. One point of difference may be noted: the atomic wave function, perturbed or unperturbed, is given; only the scattering function is varied.

SCATTERING BY THE INERT GASES

Using unperturbed atomic wave functions the solution is

$$\begin{aligned} \psi(0, 1, \cdots, N) = u(1, \cdots, N) f(0) s(0) + u(2, \cdots, N, 0) f(1) s(1) \\ + \cdots + u(0, 1, \cdots, N-1) f(N) s(N). \end{aligned} \quad (1.7)$$

The discussion applies to any atom with an even number of electrons in the outer shell, but in general there are several solutions and a corresponding number of scattering functions. With

$$V_1(0, 1, \cdots, N) = 2 \left(V(0) - \sum_1^N 1/r_{0i} \right),$$

$$U(0) = \sum_{\text{spin}} \int \cdots \int u^*(1, \cdots, N) V_1(0, 1, \cdots, N) u(1, \cdots, N) d\tau_1 \cdots d\tau_N,$$

$$V_2(0, 1, \cdots, N) = V_1(0, 1, \cdots, N) - U(0),$$

$$L(0, 1, \cdots, N) = \nabla_0^2 + 2W + V_1(0, 1, \cdots, N),$$

$$\begin{aligned} L(0) = \sum_{\text{spin}} \int \cdots \int u^*(1, \cdots, N) L(0, 1, \cdots, N) u(1, \cdots, N) d\tau_1 \cdots d\tau_N \\ = \nabla_0^2 + 2W + U(0) \end{aligned}$$

we have

$$\begin{aligned} -2(H - W - W_1)\psi &= u(1, \dots, N)s(0)L(0, 1, \dots, N)f(0) \\ &\quad + u(2, \dots, N, 0)s(1)L(1, \dots, N, 0)f(1) \\ &\quad \vdots \\ &\quad + u(0, 1, \dots, N-1)s(N)L(N, 0, 1, \dots, N-1)f(N) \end{aligned}$$

and (1.4) becomes

$$\begin{aligned} L(0)f(0) &= N \sum_{\text{spin}} s(0)s(1) \int \cdots \int u^*(1, \dots, N)u(0, 2, \dots, N) \\ &\quad \cdot L(1, 2, \dots, N, 0)f(1)d\tau_1 \cdots d\tau_N. \end{aligned} \quad (1.8)$$

Using (1.8) and the differential equation satisfied by u it is not difficult to verify the relation (1.6). If we attempt to solve (1.8) by the method of successive approximation the obvious and most suitable first approximation f_0 is the solution of the equation $Lf_0=0$ subject to the scattering problem boundary conditions: f_0 everywhere finite and $f_0 \sim e^{-ikz} + (1/r)e^{-ikr}F(z/r)$ for large values of r . With f_0 in the right hand member (1.8) reduces to

$$\begin{aligned} L(0)f(0) &= N \sum_{\text{spin}} s(0)s(1) \int \cdots \int u^*(1, \dots, N)u(0, 2, \dots, N) \\ &\quad \cdot V_2(1, 2, \dots, N, 0)f_0(1)d\tau_1 \cdots d\tau_N. \end{aligned} \quad (1.9)$$

Note that the potential function in the integrand is V_2 and not V_1 . The right-hand member of (1.9) is conveniently described as an exchange integral. It contributes a term to the scattering amplitude which may be interpreted as resulting from interchange of atomic and external electrons. (1.9) is certainly valid when the exchange term is so small that f does not differ appreciably from f_0 inside the region of high charge density. But it is neither a final nor very useful equation. To make further progress toward an understanding of (1.8) we must replace the exact atomic wave function by an approximate solution constructed from single electron functions:

$$u(1, \dots, N) \rightarrow (1/N!^{1/2}) |u_n(m)s_n(m)|, \quad n, m = 1, 2, \dots, N,$$

with $u_n = u_{n+N/2}$, $n \leq N/2$, $u_1, u_2, \dots, u_{N/2}$ normalized and mutually orthogonal,

$$s_1 = s_2 = \cdots = s_{N/2} = s, \quad s_{N/2+1} = \cdots = s_N = s',$$

$$\sum_{\text{spin}} s(1)s'(1) = 0, \quad \sum_{\text{spin}} s(1)s(1) = \sum_{\text{spin}} s'(1)s'(1) = 1.$$

With a suitable choice of single electron functions $u_1, \dots, u_{N/2}$ the error introduced by the substitution $u(1, \dots, N) \rightarrow (1/N!^{1/2}) |u_n(m)s_n(m)|$ is quite negligible. Arguments to support this statement will appear as the discussion develops.

HELIUM

$$u(1, 2) \rightarrow (1/2^{1/2})u(1)u(2)(s(1)s'(2) - s(2)s'(1)),$$

$$\begin{aligned} U(0) &= 2 \int \cdots \int u(1)u(2)u(1)u(2)(2/r_0 - 1/r_{01} - 1/r_{02})d\tau_1d\tau_2 \\ &= 4(1/r_0 - (1/r_0)) \text{ with } (1/r_0) = \iint u(1)u(1)(1/r_{01})d\tau_1, \end{aligned}$$

$$V_2(0, 1, 2) = 2(2(1/r_0) - 1/r_{01} - 1/r_{02}).$$

Eliminating the spin functions from (1.8) there remains

$$L(0)f(0) = u(0) \iiint u(1)[L(1) + 2((1/r_1) - 1/r_{01})]f(1)d\tau_1. \quad (2.1)$$

We write $f = \sum_0^\infty f_k$ with f_k defined by the system of equations

$$L(0)f_0(0) = 0,$$

$$L(0)f_{k+1}(0) = u(0) \iiint u(1)[L(1) + 2((1/r_1) - 1/r_{01})]f_k(1)d\tau_1.$$

We find then (S.S.E.,¹ section 2) that $\iiint uL f_k d\tau = 0$ and therefore $\iiint uL f d\tau = 0$. Thus the function f defined by the process of successive approximation outlined above is also a solution of the equation

$$L(0)f(0) = 2u(0) \iiint u(1)((1/r_1) - 1/r_{01})f(1)d\tau_1. \quad (2.2)$$

Now it is easily verified that (2.2) implies the relation $\iiint uL f d\tau = 0$. It is not true that every solution of (2.1) is a solution of (2.2). We shall see that for a particular choice of the one electron function u , (2.1) has an infinite number of distinct solutions, all satisfying the scattering problem boundary conditions and all yielding the *same scattering amplitude*. However the most practical procedure for accurately solving (2.1) is the method of successive approximation and this method leads directly to the orthogonality condition $\iiint uL f d\tau = 0$ and Eq. (2.2). The scattering amplitude is (S.S.E.,¹ section 2)

$$\begin{aligned} F(z/r) &= (-1/4\pi) \int \cdots \int u(1, 2)e^{ikr_0 \cos(r_0, r)} [V_1(0, 1, 2)u(1, 2)f(0) \\ &\quad - V_2(2, 1, 0)u(1, 0)f(2)]d\tau_0d\tau_1d\tau_2 \\ &= (-1/4\pi) \iiint e^{ikr_0 \cos(r_0, r)} [U(0)f(0) \\ &\quad - 2u(0) \iiint u(1)((1/r_1) - 1/r_{01})f(1)d\tau_1]d\tau_0. \end{aligned} \quad (2.3)$$

Since f is not known (2.3) is useful only for the qualitative survey afforded

when f is replaced by a simple approximation and the integrals then evaluated.

We assume now that the single electron function u is determined by a Hartree² equation:

$$(\nabla^2 + 2(E + 2/r - (1/r)))u = 0.$$

By Green's theorem $\iint u L f d\tau = \iint f L u d\tau$; (2.1) assumes the form

$$L(0)f(0) = 2u(0) \iint u(1)(W - E - 1/r_{01})f(1)d\tau_1. \quad (2.4)$$

Then

$$\begin{aligned} \iint_{\infty} (f^* \nabla f - f \nabla f^*) \cdot dS &= \iint \int (f^* L f - f L f^*) d\tau \\ &= 2 \int \cdots \int u(0)u(1)(W - E - 1/r_{01})(f^*(0)f(1) - f(0)f^*(1))d\tau_0 d\tau_1 = 0, \end{aligned}$$

a verification of (1.6). This is the first step in justifying the introduction of the approximate atomic wave function.

The Hartree equation may be written

$$\begin{aligned} (\nabla_0^2 + 2(W + 2/r_0 - 2(1/r_0)))u(0) &= 2(W - E - (1/r_0))u(0) \\ &= 2u(0) \iint \int u(1)(W - E - 1/r_{01})u(1)d\tau_1. \end{aligned}$$

We see that a solution of the Hartree equation is also a solution of (2.4). If f is a solution of (2.4) satisfying the scattering problem boundary conditions so also is $f + cu$ with c an arbitrary constant. With u determined by the Hartree equation, (2.1) has an infinite number of solutions and (2.2) presumably only one, but all satisfying the scattering problem boundary conditions and yielding the *same scattering amplitude*. (2.1) and (2.2) are thus equivalent physically, but not mathematically.

The freedom in the definition of f has this consequence: we are at liberty to impose practically arbitrary orthogonality conditions on f . Each such condition combined with (2.4) leads to a differential equation differing in form from (2.4), but having at least one solution in common with it. For example (2.2) is such an equation, imposing on its solutions the orthogonality condition $\iint \int u L f d\tau = 0$, having a solution in common with (2.1) for unrestricted single electron function u and a solution in common with (2.4) if u is the Hartree function. We try the condition $\iint \int u f d\tau = 0$; combined with (2.4) the equation

$$L(0)f(0) = -2u(0) \iint \int u(1)(1/r_{01})f(1)d\tau_1 \quad (2.5)$$

results. We verify that a necessary consequence of (2.5) and the Hartree equation

² Hartree, Proc. Cam. Phil. Soc., Jan. (1928).

tion for u is the orthogonality of u and f . For from (2.5) and the Hartree equation

$$\begin{aligned} \nabla_0 \cdot (u(0) \nabla_0 f(0) - f(0) \nabla_0 u(0)) + 2(W - E)u(0)f(0) \\ - 2(1/r_0)u(0)f(0) = - 2u(0)u(0) \iint u(1)(1/r_{01})f(1)d\tau_1. \end{aligned}$$

Integrated this yields

$$2(W - E) \iiint u f d\tau - 2 \iiint u(1/r) f d\tau = - 2 \iiint u(1/r) f d\tau$$

or $\iiint u f d\tau = 0$. For numerical integration by successive approximation (2.2) is far preferable to (2.5), in part because the derivation of (2.2) does not involve the assumption that u is a solution of the Hartree equation, but primarily because of the more rapid convergence brought about by the presence of the term $(1/r_1)$ in the exchange integral and because in (2.2) the orthogonality condition $\iiint u L f d\tau = 0$ is satisfied automatically by each successive approximation: thus $\iiint u L f_k d\tau = 0$.

There follows an argument that supplies an adequate justification of the substitution $u(1, 2) \rightarrow (1/2^{\frac{1}{2}})u(1)u(2)(s(1)s'(2) - s(2)s'(1))$ provided that the single electron function u is determined by the Hartree equation. Eq. (2.1) is derived by a method that proceeds as far as possible with the accurate atomic wave function before introducing an approximation. If now we begin with the approximate atomic wave function and evaluating (1.4) find an equation almost identical with (2.1) we must conclude that the substitution brings with it no serious error. Letting $u(1, 2)$ in (1.7) represent the approximate atomic wave function we have

$$\begin{aligned} & -2(H - W - W_1)\psi \\ & = u(1, 2) \left[\nabla_0^2 + 2(W + W_1 - 2E + 2/r_0 - 1/r_{01} - 1/r_{02} - 1/r_{12} \right. \\ & \quad \left. + (1/r_1) + (1/r_2)) \right] f(0)s(0) \\ & + u(0, 1) \left[\nabla_2^2 + 2(W + W_1 - 2E + 2/r_2 - 1/r_{01} - 1/r_{02} - 1/r_{12} \right. \\ & \quad \left. + (1/r_0) + (1/r_1)) \right] f(2)s(2) \\ & + u(2, 0) \left[\nabla_1^2 + 2(W + W_1 - 2E + 2/r_1 - 1/r_{01} - 1/r_{02} - 1/r_{12} \right. \\ & \quad \left. + (1/r_2) + (1/r_0)) \right] f(1)s(1) \end{aligned}$$

Combined with (2.4) this yields

$$(L(0) + 2(W_1 - W_1'))f(0) \tag{2.6}$$

$$= u(0) \iiint u(1)(L(1) + 2(W_1 - W_1') + 2(1/r_1 - 1/r_{01}))f(1)d\tau_1$$

in which W_1' is the value of the helium normal state energy given by the Hartree function: $W_1' = 2E - \int \dots \int u(1)u(1) (1/r_{12})u(2)u(2)d\tau_1 d\tau_2$ and $W_1' - W_1 = 0.8$ volts.³ (2.1) with kinetic energy W is identical with (2.6) with

³ Gaunt, Proc. Cam. Phil. Soc. 24, 328 (1928).

kinetic energy $W + W_1' - W_1$. We may conclude that the use of the Hartree atomic wave function to simplify (1.8) is certainly permitted for kinetic energies greater than 2 or 3 volts. It must be emphasized that (2.6) is not an alternative scattering equation; it is a check on the validity of a simplifying assumption.

For the numerical integration of (2.1), f_k is written as a sum of Legendre polynomials in the scattering angle with coefficients depending only on the distance from the scattering center:

$$f(x, y, z) = \sum_0^\infty f_k(x, y, z) = \sum_0^\infty \sum_0^\infty f_{kn}(r) P_n(\cos \theta). \quad (2.7)$$

Then

$$\begin{aligned} (L(0) - n(n+1)/r_0^2) f_{0n}(0) &= 0, \\ L(0) f_{k+1,0}(0) &= 8\pi u(0) \int_0^\infty u(1) ((1/r_1) - \gamma_0(0, 1)) f_{k0}(1) r_1^2 dr_1, \\ (L(0) - n(n+1)/r_0^2) f_{k+1,n}(0) \\ &= -8\pi/(2n+1) u(0) \int_0^\infty u(1) \gamma_n(0, 1) f_{kn}(1) r_1^2 dr_1, \quad n > 0, \\ \gamma_n(0, 1) &= r_0^n / r_1^{n+1}, \quad r_0 \leq r_1, \\ &= r_1^n / r_0^{n+1}, \quad r_0 > r_1. \end{aligned} \quad (2.8)$$

The convergence is quite rapid in both k and n .

NEON, ARGON, KRYPTON, XENON; $N=8$

As might be expected most of the results found for scattering in helium have their parallel here. The Fock⁴ equations for determining single electron functions are related to the N electron scattering problem as the Hartree equation to the helium scattering problem. But in the helium problem the Fock equation reduces to Hartree's. Thus the parallel is very close. With spin functions eliminated from the several defining equations

$$\begin{aligned} U(0) &= 2 \left(V(0) - \sum_1^N (1/r_0)_n \right), \\ V_2(0, 1, \dots, N) &= 2 \sum_1^N ((1/r_0)_n - 1/r_{0n}), \\ \text{and} \\ L(0) f(0) &= \sum_1^{N/2} u_n(0) \iiint u^*(1) (L(1) - 2/r_{01}) f(1) d\tau_1 \\ &\quad + 2 \sum_1^{N/2} u_n(0) \sum_1^{N/2} \iiint u_m^*(1) (1/r_1)_{nm} f(1) d\tau_1 \end{aligned} \quad (3.1)$$

⁴ Fock, *Zeits. f. Physik* **61**, 126 (1930).

in which

$$(1/r_0)_n = \iiint u_n^*(1)(1/r_{01})u_n(1)d\tau_1,$$

$$(1/r_0)_{nm} = \iiint u_n^*(1)(1/r_{01})u_m(1)d\tau_1.$$

The simpler equation

$$\begin{aligned} L(0)f(0) = & -2 \sum_1^{N/2} u_n(0) \iiint u_n^*(1)(1/r_{01})f(1)d\tau_1 \\ & + 2 \sum_1^{N/2} u_n(0) \sum_1^{N/2} \iiint u_m^*(1)(1/r_{11})_{nm}f(1)d\tau_1 \end{aligned} \quad (3.2)$$

imposes on its solutions the orthogonality condition $\iiint u_n^* Lf d\tau = 0$ and therefore has at least one solution in common with (3.1). This common solution is in fact found when (3.1) is solved by the method of successive approximation.

We assume for u_n the representation

$$u_1 = (1/4\pi)^{1/2} R_1(r), \quad u_2 = (3/4\pi)^{1/2} R_2(r) \cos \theta,$$

$$u_3 = u_4^* = (3/8\pi)^{1/2} R_2(r) e^{i\varphi} \sin \theta.$$

R_1 and R_2 are functions which give the energy integral for the atomic problem a minimum value. In terms of R_1 and R_2

$$\begin{aligned} \sum_1^N (1/r_0)_n &= 2 \int_0^\infty (R_1(r_1) + 3R_2(r_1)) \gamma_0(0, 1) r_1^2 dr_1, \\ u_2(0) \iiint u_2^*(1) + u_3(0) \iiint u_3^*(1) + u_4(0) \iiint u_4^*(1) \\ &= (3/4\pi) R_2(0) \iiint R_2(1) \cos(r_0, r_1), \\ \sum_1^{N/2} u_n(0) \iiint u_n^*(1)(1/r_{01})f(1)d\tau_1 &= \\ (1/4\pi) R_1(0) \iiint R_1(1)(1/r_{01})f(1)d\tau_1 \\ &+ (3/4\pi) R_2(0) \iiint R_2(1)(1/r_{01})f(1) \cos(r_0, r_1) d\tau_1, \\ u_1(0) \sum_1^{N/2} \iiint u_m^*(1)(1/r_{11})_{1m}f(1)d\tau_1 \\ (1/4\pi) R_1(0) \iiint R_1(1)(1/r_{11})_1 f(1) d\tau_1 &+ (1/3)(3/4\pi)^2 R_1(0) \iiint R_2(1)f(1) \end{aligned}$$

$$\begin{aligned}
& \cdot \int \int \int R_2(2)(1/r_{12})R_1(2) \cos(r_1, r_2) d\tau_2 d\tau_1, \\
& \sum_2^{N/2} u_n(0) \sum_1^{N/2} \int \int \int u_n^*(1)(1/r_1)_{nm} f(1) d\tau_1 \\
& (3/4\pi)^2 R_2(0) \int \int \int R_2(2) + (1/r_{12})f(1) \cos(r_0, r_2) (R_2(1)R_2(1) \cos(r_1, r_2) \\
& + (1/3)R_1(1)R_1(1)) d\tau_1 d\tau_2.
\end{aligned}$$

The angle functions combine into terms invariant under rotation of the axis of the atomic representation. It is convenient to take the axis in the direction of the incident electron beam. We expand f in a series of Legendre polynomials, $f = \sum f_n(r) P_n(\cos \theta)$, and find for the coefficients $f_n(r)$ the set of equations

$$\begin{aligned}
L(0)f_0(0) &= 2R_1(0) \int_0^\infty R_1(1)((1/r_1)_1 - \gamma_0(0, 1))f_0(1)r_1^2 dr_1 \\
&+ 2 \left[R_1(0) \int_0^\infty R_2(1) \left(\int_0^\infty R_2(2)\gamma_1(1, 2)R_1(2)r_2^2 dr_2 \right) f_0(1)r_1^2 dr_1 \right. \\
&\quad \left. - R_2(0) \int_0^\infty R_2(1)\gamma_1(0, 1)f(1)r_1^2 dr_1 \right]
\end{aligned} \quad (3.3)$$

$$\begin{aligned}
& (L(0) - 2/r_0^2)f_1(0) \\
&= 2R_2(0) \int_0^\infty R_2(1) \left(\int_0^\infty R_2(2)\gamma_0(1, 2)R_2(2)r_2^2 dr_2 - \gamma_0(0, 1) \right) f_1(1)r_1^2 dr_1 \\
&+ (4/5)R_2(0) \int_0^\infty R_2(1) \left(\int_0^\infty R_2(2)\gamma_2(1, 2)R_2(2)r_2^2 dr_2 - \gamma_2(0, 1) \right) f_1(1)r_1^2 dr_1 \\
&+ (2/3) \left[R_2(0) \int_0^\infty R_1(1) \left(\int_0^\infty R_2(2)\gamma_1(1, 2)R_1(2)r_2^2 dr_2 \right) f_1(1)r_1^2 dr_1 \right. \\
&\quad \left. - R_1(0) \int_0^\infty R_1(1)\gamma_1(0, 1)f_1(1)r_1^2 dr_1 \right]
\end{aligned}$$

$$\begin{aligned}
& (L(0) - n(n+1)/r_0^2)f_n(0) \\
&= -1/(2n+1) \left[R_1(0) \int_0^\infty R_1(1)\gamma_n(0, 1)i_n(1)r_1^2 dr_1 \right. \\
&\quad + 3R_2(0) \int_0^\infty R_2(1)(\gamma_{n-1}(0, 1)(n/(2n+1)) \\
&\quad \left. + \gamma_{n+1}(0, 1)(n+1)/(2n+3))f_n(1)r_1^2 dr_1 \right], \quad n \geq 2.
\end{aligned}$$

The writer must correct an error in the note added in proof to S.S.E.¹ There appears the statement "The scattering intensity does not tend toward

spherical symmetry with decreasing electron velocity." The statement is false. Each equation of the set (3.3) involves only one coefficient $f_n(r)$. $f_n(r)$ is roughly proportional to the coefficient of $P_n(\cos \theta)$ in the expansion of e^{ikz} in a series of Legendre polynomials. Thus $f_n(r)$ vanishes uniformly in r as $k \rightarrow 0$ and the scattered wave approaches spherical symmetry for sufficiently low velocities. If a generalization is permitted from results obtained for helium, the effect of exchange is to lower the limiting velocity below which scattering is sensibly spherically symmetric. There is apparently an effective cancellation of terms of opposite sign in the exchange integrals for f_0 and f_1 . Again if we generalize from results obtained for helium, this apparent cancellation is real. There arises the possibility that for quite low velocities the scattering amplitude proportional to $P_2(\cos \theta)$ is much larger than the scattering amplitude proportional to $P_1(\cos \theta)$. If this occurs in the neighborhood of the Ramsauer minimum cross section, the distribution in angle will depart strongly from spherical symmetry, but will retain more or less symmetry about the plane of right angle scattering. We have here a possible explanation of the distribution in angle in the inert gases found by Ramsauer and Kollath.⁵ The argument suffices to make the integration of (3.3) a problem of considerable interest. There is however one feature of the experimental distribution in angle at low velocities which is not reproduced by the exchange equations. The sharp rise in the krypton and xenon intensity curves below 30° may be explained by the reaction of the distorted atom on the incident wave. The effect of atomic distortion or polarization is to excite the partial scattering functions of high order; the partial scattering amplitudes then decrease slowly with increasing n and yield a large sum for small angles, but interfere effectively everywhere else.

In the remainder of the discussion the single electron functions u_n are solutions of the Fock equations

$$\left(\nabla^2 + 2(E_n + V(r) - \sum_{m \neq n}^N (1/r)_m) \right) u_n = -2 \sum_{m \neq n}^{N/2} (1/r)_{mn} u_m + \sum_{m \neq n}^{N/2} \lambda_{mn} u_m,$$

$$\lambda_{pn} = \iiint u_p^* \left(\nabla^2 + 2(E_n + V(r) - \sum_{m \neq n}^N (1/r)_m) \right) u_n d\tau$$

$$+ 2 \sum_{m \neq n}^{N/2} \iiint u_p^* (1/r)_{mn} u_m d\tau.$$

The condition $\lambda_{mn} = \lambda_{nm}^*$ implies the mutual orthogonality of the u 's. Using the Fock equations to simplify the exchange integral, (3.1) transforms into

$$L(0)f(0) = 2 \sum_1^{N/2} u_n(0) \iiint u_n^*(1) (W - E_n - 1/r_{01}) f(1) d\tau_1$$

$$\sum_1^{N/2} u_n(0) \sum_{m \neq n}^{N/2} \lambda_{nm} \iiint u_m^*(1) f(1) d\tau_1. \quad (3.4)$$

⁵ Ramsauer and Kollath, Ann. d. Physik, Feb. (1932), March (1932).

Then

$$\begin{aligned} \iint_{\infty} (f^* \nabla f - f \nabla f^*) \cdot dS \\ = \sum_{n=1}^{N/2} \sum_{m \neq n}^{N/2} \int \cdots \int \left(u_n(1) u_m^*(0) f^*(1) f(0) \lambda_{mn}^* \right. \\ \left. - u_n^*(1) u_m(0) f(1) f^*(0) \lambda_{mn} \right) d\tau_0 d\tau_1 = 0; \end{aligned}$$

the relation (1.6) is satisfied. We verify by substituting u_p for f that solutions of the Fock equations are also solutions of (3.4). If f is a solution of (3.4) satisfying the scattering problem boundary conditions so also is $f + \sum_1^{N/2} c_n u_n$. We fix f by the orthogonality conditions $\iint u_n^* f d\tau = 0$; (3.4) becomes

$$L(0)f(0) = -2 \sum_1^{N/2} u_n(0) \iiint u_n^*(1) (1/r_{01}) f(1) d\tau_1. \quad (3.5)$$

The orthogonality of u_n and f is a necessary consequence of (3.5) and the Fock equations. (3.5) is apparently much simpler than (3.2), but for numerical integration by the method of successive approximation (3.2) is preferable for reasons already discussed in connection with Eqs. (2.2) and (2.5).

If the atomic wave function $u(1, \dots, N)$ in (1.7) is replaced by $|u_n(m) s_n(m)|$, $\psi(0, 1, \dots, N)$ can be written as a determinant with $N+1$ rows and columns. But the determinant form of ψ discloses immediately that it is unchanged when f is replaced by $f + \sum_1^{N/2} c_n u_n s_n$. A scattering equation derived by a process which begins with the approximate atomic wave function constructed from single electron functions will have these functions as solutions. If now the single electron functions are solutions of the Fock equations, this scattering equation cannot differ essentially from (3.4) which also has as solutions the single electron functions. We conclude that the use of an approximate atomic wave function to simplify (1.8) is justified, particularly so when the approximate atomic wave function is constructed from solutions of the Fock equations.

TABLE I. $W = 21.5$ volts.

k	0	1	2
F_{k0}	0.243- i 0.711	-0.138- i 0.104	-0.064- i 0.001
F_{k1}	0.192- i 0.016	0.301- i 0.049	0.042- i 0.046
	FF^*	$\iint FF^* d\Omega$	$(2\pi i/k) (F(1) - F^*(1))^\dagger$
Without exchange	0.563+0.117 cos θ +0.039 cos ² θ	7.24	7.24
With exchange	0.668+0.225 cos θ +0.299 cos ² θ	9.65	9.25

[†] S.S.E.,¹ section 3. The relation $\iint FF^* d\Omega = (2\pi i/k) (F(\cos \theta) - F(\cos \theta))_{\cos \theta=1}$ is equivalent to (1.6). The calculation was carried through with the single electron function $u = (\alpha^3/\pi)^{1/2} e^{-\alpha r}$, $\alpha = 27/16$. The ratio 9.65-9.25/9.25 is a measure of the error introduced into the total cross section by the use of a single electron function different from the Hartree function.

TABLE II. $W=10.75$ volts (with the Hartree function).

k	0	1	2
F_{k0}	0.138- i 1.105	-0.124- i 0.025	-0.028+ i 0.010
F_{k1}	0.141- i 0.006	0.288- i 0.026	0.034- i 0.030
	FF^*	$\iint FF^* d\Omega$	$(2\pi i/k)(F(1)-F^*(1))$
Without exchange	1.239+0.052 $\cos \theta$ +0.020 $\cos^2 \theta$	15.66	15.66
With exchange	1.255+0.125 $\cos \theta$ +0.214 $\cos^2 \theta$	16.68	16.65

INTEGRATION OF 2.8. HELIUM

The partial waves f_{kn} yield partial scattering amplitudes $F_{kn}P_n(\cos \theta)$ which combine into the total scattering amplitude $F(\cos \theta) = \sum_0^\infty \sum_0^\infty F_{kn}P_n(\cos \theta)$.

Results of the numerical integration of (2.8) are found in Tables I and II.

For $n=2$ the partial scattering amplitudes are estimated from (2.3) with f replaced by e^{-ikz} :

$$F'(\cos \theta) = F_a(\cos \theta) + F_b(\cos \theta) \quad (4.1)$$

$$F_a(\cos \theta) = (1/4\pi) \iint \int e^{ik(r_1 \cos(r, r_1) - z_1)} U(r_1) d\tau_1$$

the Born first order scattering amplitude, and

$$F_b(\cos \theta) = (1/2\pi) \int \dots \int e^{ik(r_1 \cos(r, r_1) - z_2)} u(1)(1/r_{12} - (1/r_2))u(2)d\tau_1 d\tau_2,$$

$$U(r) = (4/r)e^{-2\alpha r}(1 + \alpha r), \quad u(r) = (\alpha^{3/2}/\pi^{1/2})e^{-\alpha r}, \quad \alpha = 27/16.$$

Letting $q=k/a$

$$\alpha^2 F_a(\cos \theta) = [1/(1 + q^2 \sin^2 \theta/2) + 1/(1 + q^2 \sin^2 \theta/2)^2].$$

We write

$$F_a(\cos \theta) = \sum_0^\infty F_{an}P_n(\cos \theta) \quad F_b(\cos \theta) = \sum_0^\infty F_{bn}P_n(\cos \theta)$$

and remembering that $\sin \theta d\theta = 2d(\sin^2 \theta/2)$ find

$$\alpha^2 F_{a0} = ((1/q^2) \log(1 + q^2) + 1/(1 + q^2))$$

$$\alpha^2 F_{a1} = 3[(1/q^2) \log(1 + q^2) - 1/(1 + q^2)].$$

The coefficients F_{bn} are taken from a recent paper by Massey and Mohr:⁶

$$\alpha^2 F_{b0} = -2/(1 + q^2)^2 [(3 - q^2)/(1 + q^2) - 8(15 + q^2)/(9 + q^2)^2]$$

$$\begin{aligned} \alpha^2 F_{b1} = & -4/(1 + q^2)^2 [1/q^2(1 - (1/q^2) \log(1 + q^2)) \\ & - (21/2 + (6/q^2) \log(1 + q^2) - (16/q) \tan^{-1} q) \\ & - q^2(3/2 - (3/q^2) \log(1 + q^2))] \end{aligned}$$

⁶ Massey and Mohr, Proc. Roy. Soc. A132, 605 (1931).

$$\alpha^2 F_{b2} = -4/(1+q^2)^3 [(6/q^4)((1/q^2) \log(1+q^2) - 1/(1+q^2) - 0.5q^2/(1+q^2)) \\ + (15/q^2)((1/q^2) \log(1+q^2) - 1/(1+q^2)) + ((48/q) \tan^{-1} q - 54.5/(1+q^2)) \\ + q^2((15/q^2) \log(1+q^2) - 45/(1+q^2) - 2.5q^3/(1+q^2))].$$

F_{b0} differs from the corresponding term computed by Massey and Mohr because we are using a different and more accurate form of the exchange integral. At 21.5 volts, $q^2=0.555$, $F_{b2}=0.040$,

$$\left. \begin{aligned} F_{a0} &= 0.505 \\ F_{00} &= 0.243 - i0.711 \\ F_{b0} &= -0.061 \\ F_{10} + F_{20} &= 0.202 - i0.105 \end{aligned} \right\} \quad \left. \begin{aligned} F_{a1} &= 0.160 \\ F_{01} &= 0.192 - i0.016 \\ F_{b1} &= 0.244 \\ F_{11} + F_{21} &= 0.343 - i0.095 \end{aligned} \right\}.$$

From the comparison we conclude that for $n \geq 2$ the partial amplitudes given by (4.1) agree well with the amplitudes found by numerical integration of (2.8). The complete scattering amplitude is then

$$F(\cos \theta) = \sum_0^2 (F_{k0} + F_{k1} \cos \theta) \\ + (F_a(\cos \theta) - F_{a0} - F_{a1} \cos \theta + F_{b2} P_2(\cos \theta)). \quad (4.2)$$

TABLE III. $W=21.5$ volts.

θ	$F_a(\cos \theta)$	$F_a(\cos \theta) - F_{a0} - F_{a1} \cos \theta$	$F_{b2} P_2(\cos \theta)$	$\sum_0^2 (F_{k0} + F_{k1} \cos \theta)$	FF^*
0	0.702	0.037	0.040	0.576-i0.927	1.29
20	0.682	0.027	0.033	0.544-i0.920	1.21
40	0.637	0.009	0.015	0.451-i0.901	1.04
60	0.578	-0.007	-0.005	0.309-i0.872	0.85
80	0.516	-0.017	-0.018	0.134-i0.835	0.71
100	0.465	-0.012	-0.018	-0.052-i0.797	0.64
120	0.422	-0.003	-0.005	-0.227-i0.761	0.63
140	0.392	0.010	0.015	-0.369-i0.731	0.65
160	0.374	0.019	0.033	-0.462-i0.712	0.68
180	0.370	0.025	0.040	-0.494-i0.705	0.68

Measurements in helium are not available at 21.5 volts. Ramsauer and Kollath⁵ give a series of intensity measurements over the energy range 1.8 to 19.2 volts.* The points labeled experimental in the 21.5 volt diagram are obtained from the 15.8 and 19.2 volt experimental points by a linear extrapolation. To change from the R. and K. units to atomic units the experimental intensity is multiplied by the factor $1/(0.532)^2 = 3.533$. The 15.8 volt curves for scattering with and without exchange are rough approximations found by averaging the calculated 10.75 and 21.5 volt amplitudes.

Except in the region below 30° the agreement at 21.5 volts is excellent. At 15.8 volts a discrepancy appears which becomes important at 10.75 volts. This discrepancy as well as the large difference below 30° is undoubtedly to

* The R. and K. intensities are absolute; those given by Bullard and Massey in an earlier paper (Proc. Roy. Soc. A133, 637 (1931)) are relative. To compare the two sets of measurements the B. and M. intensities are multiplied by a factor chosen for each velocity to make the fit as close as possible. Excellent agreement is found (see R. and K.).

be accounted for by atomic distortion which is neglected in deriving the exchange scattering equation. Considering the extreme difficulty of a calculation including atomic distortion it is disappointing to find the discrepancy at 10.75 volts so great.

The writer has had the privilege of many stimulating discussions with Dr. H. Bethe. He is indebted to Dr. R. Peierls for suggesting the derivation of scattering equations by a variation method and to Professor G. Wentzel and Professor E. C. Kemble for helpful criticism.

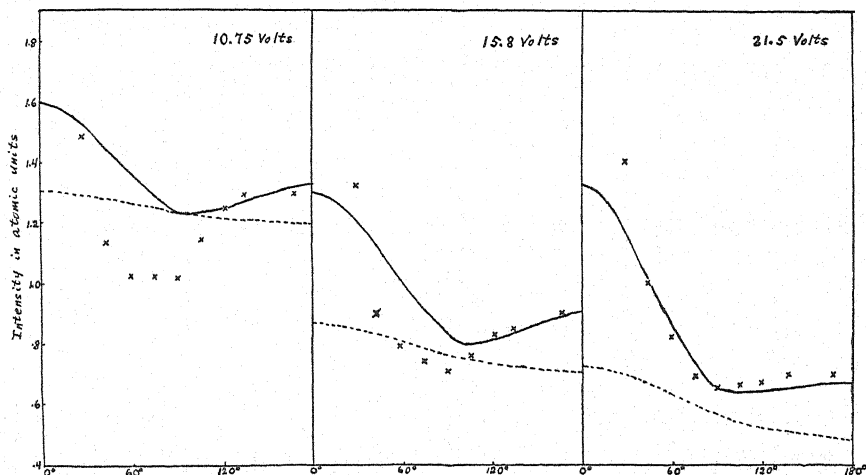


Fig. 1. Elastic scattering in helium. Crosses, experimental points from Ramsauer and Kollath.⁵ Full line, calculated intensity with exchange. Dotted line, calculated intensity without exchange.

Note added in proof: Massey and Mohr⁷ derive exchange scattering equations resembling only remotely the equations found by the writer. The discrepancy arises in M. and M.'s treatment from the introduction of unnecessarily crude approximations into an accurate equation. M. and M. write an exact solution of the two-electron problem (scattering in atomic hydrogen) in the form

$$\begin{aligned}\psi(1, 2) &= \sum_n u_n(1)f_n(2) + \int_E u_E(1)f_E(2)dE \\ &= \sum_n u_n(2)g_n(1) + \int_E u_E(2)g_E(1)dE\end{aligned}\quad (I)$$

in which $(\nabla^2 + 2(E_n + 1/r))u_n = 0$, $(\nabla^2 + 2(E + 1/r))u_E = 0$ and asymptotically $f_1 \sim e^{-ikz} + 1/r e^{-ikr} F(z/r)$, $g_1 \sim 1/r e^{-ikr} G(z/r)$. The solutions with correct symmetry and physical meaning are $\psi \pm (1, 2) = \psi(1, 2) \pm \psi(2, 1)$. The equations given by M. and M. for the determination of f_1 and g_1 are

$$\begin{aligned}(\nabla^2 + 2W)f_1(2) &= -2 \iint u_1(1) (1/r_2 - 1/r_{12}) \psi(1, 2) d\tau_1, \\ (\nabla^2 + 2W)g_1(2) &= -2 \iint u_1(1) (1/r_2 - 1/r_{12}) \psi(2, 1) d\tau_1.\end{aligned}\quad (II)$$

Orthogonality properties implicit in (I) are involved in the derivation of (II). In particular use is made of the relations

⁷ Massey and Mohr, Proc. Roy. Soc. A85, 289 (1932).

$$\begin{aligned}\iint u_1(1) (\psi(1, 2) - u_1(1)f_1(2))d\tau_1 &= 0, \\ \iint u_1(2) (\psi(1, 2) - u_1(2)g_1(1))d\tau_2 &= 0.\end{aligned}\tag{III}$$

It is thus clearly a dubious procedure to introduce into Eq. (II) an approximation for $\psi(1, 2)$ which is inconsistent with Eq. (III). The equations obtained by M. and M. following this procedure are at best of doubtful validity. For details the reader is referred to their paper. The reduction of (II) to the form given by the writer (S.S.E., section 2) is not difficult, but because the analysis is somewhat lengthy cannot be reproduced here.

Analytic Atomic Wave Functions

By J. C. SLATER

Massachusetts Institute of Technology

(Received July 26, 1932)

A method is suggested for setting up analytic atomic wave functions which form good approximations to Hartree's functions. These functions are of the form $\sum c r^n e^{-ar}$, where the exponent a as well as c and n vary from one term to another. The constants are determined for 1, 2, and 3-quantum electrons by fitting Hartree's values numerically for five selected atoms, and interpolation methods are presented for dealing with the intermediate atoms. A method is suggested for setting up exactly orthogonal functions, with no loss of accuracy. It is shown that the analytic wave functions are the solutions of central field problems in which the field is slightly different for different quantum numbers, on account of the inaccuracy in the function, but a table shows that the discrepancy between this and the correct field is small over the region where the wave function is large. Suggestions are made for future work, on the one hand in extending the tables, on the other in using the wave functions in investigating atomic energies, exchange integrals, etc.

FOR any detailed calculations dealing with atomic or molecular structure, good approximations to the atomic wave functions are essential. The most satisfactory method, in general, for building up such functions seems to be by the use of one-electron functions which are solutions of the problem of an electron moving in a central field, setting up sums of products of such functions, antisymmetric in the electrons. But no completely satisfactory set of one-electron functions has been developed. It is the purpose of this paper to suggest a considerable improvement in such functions.

The best one-electron functions which we have are those of Hartree.¹ It is to be regretted that these functions are not in more accessible form; but they have been computed, by Hartree or his collaborators, for the atoms He, Li⁺, Be⁺⁺, Be, B⁺⁺⁺, O⁺⁺⁺, O⁺⁺, O⁺, O, F⁻, Ne, Na⁺, Al⁺⁺⁺, Al⁺, Si⁺⁺, Cl⁻, A, K⁺, Ca⁺⁺, Cu⁺, Rb⁺, Cs⁺. It has been shown by the writer and by Fock² that these are the best one-electron functions which can be set up, if we neglect exchange terms, and it is to be presumed that the corrections made by introducing exchange would be small. We should state at the outset that the functions suggested in this paper are no improvement on Hartree's in the matter of accuracy; they are in fact somewhat inferior, but are much more convenient. For there are two important points in which Hartree's functions are far from satisfactory. First, and most important, they exist only as tables of values, and as such cannot be used for any analytical calculations. Second, the functions for different quantum numbers with the same atom are not exactly orthogonal to each other, and this introduces great complications when

¹ D. R. Hartree, Proc. Camb. Phil. Soc. 24, 89, 111 (1928) and later papers by Hartree and others. For Si⁺⁺, J. McDougall, Proc. Roy. Soc., to appear shortly. I am much indebted to Dr. Hartree for the list of atoms whose structure has been investigated, and for tables of values of wave functions.

² J. C. Slater, Phys. Rev. 35, 210 (1930); V. Fock, Zeits. f. Physik 61, 126 (1930).

calculations using antisymmetric combinations are made. Our present functions are analytical approximations to Hartree's functions, modified to make them orthogonal.

Among analytic wave functions, two types may be mentioned as extreme examples. First, Pauling³ has used hydrogen-like functions of the form $e^{-Zr/n}$ times polynomial in r , the coefficients of the polynomial being given as for a hydrogen problem with nuclear charge Z . He has set up a set of screening constants, giving Z for each electron of each atom. By comparison of one of Pauling's functions with the corresponding one of Hartree's (see Fig. 1), we see that the nodes in Pauling's functions lie at too large values of r . The reason is that the nodes get closer together for large Z . Now the nodes lie in any

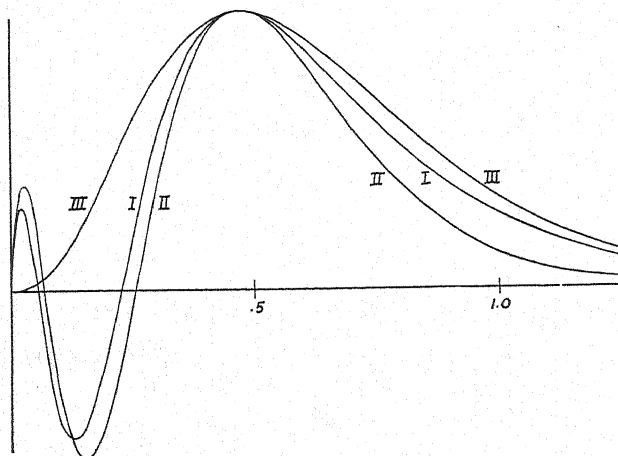


Fig. 1. Wave functions for $\text{Rb}^+ 3s$. I. Present wave function. On this scale, Hartree's curve departs from this by negligible amounts. II. Hydrogen-like curve. III. Single term $r^3 e^{-ar}$. Constants for II and III are chosen so as to make all curves coincide at the maximum, rather than to agree with the screening constants of Pauling and the writer, respectively.

case at smaller values of r than the principal, outer maximum of the function, and in an actual atom this region near the nucleus has a larger effective Z than the range around the maximum, compressing the nodes; while Pauling uses a constant Z all over the wave function. On account of this behavior of the nodes, Pauling's functions are rather badly in error.

The other extreme in the way of wave functions was suggested by the writer.⁴ These functions were of the form $r^{n-1} e^{Zr/n}$, without any nodes at all. It is plain that the correct wave functions, having nodes larger than in the writer's functions, but smaller than in Pauling's, lie between these two sets. In all these sets of functions, the maxima are so adjusted that they approximately agree in position.

ANALYTICAL EXPRESSION FOR WAVE FUNCTIONS

As a method of improving these functions, one may proceed according to the following line of thought. A $3s$ function for instance, has a wave function

³ L. Pauling, Proc. Roy. Soc. A114, 181 (1927).

[⁴ J. C. Slater, Phys. Rev. 36, 57 (1931).

in hydrogen (multiplied by r) of the form $e^{-Zr/3}(r^3 - ar^2 + br)$, where a and b are definitely determined. The three terms of this correspond roughly to the outer, middle, and inner maxima of the function: $e^{-Zr/3} r^3$ has its maximum at $9/Z$; the next term has its maximum at $6/Z$, and the inner one at $3/Z$. But now really the middle maximum lies in a range of larger Z than the outer one, and the inner maximum has still higher Z . Let us then use different Z 's for each maximum, taking a function of the form $r^3 e^{-Z_1 r/3} - a' r^2 e^{-Z_2 r/3} + b' r e^{-Z_3 r/3}$, where a' , b' are no longer the same as a and b . The maxima will then lie at $9/Z_1$, $6/Z_2$, $3/Z_3$, and if Z_2 , Z_3 are much larger than Z_1 , the inner maxima, and hence the nodes, will lie much further in than with the hydrogen-like function of Pauling. It is now actually found that functions of this form, as for example $c_1 r e^{-a_1 r} - c_2 r^2 e^{-a_2 r} + c_3 r^3 e^{-a_3 r}$, can form good representations of Hartree's functions, by proper choice of constants.

One further refinement of these functions proves to be necessary, if we are to get really satisfactory agreement with Hartree's functions. This can be seen most clearly from the $3d$ function, for which our method would give

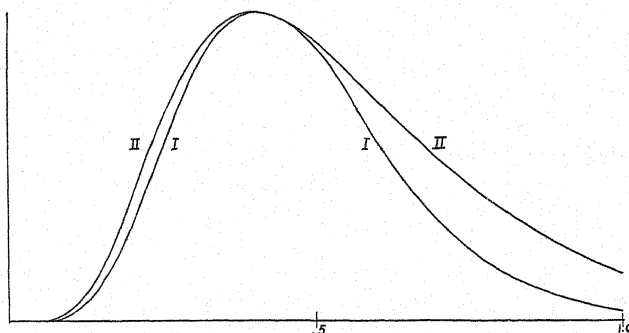


Fig. 2. Wave functions for $\text{Rb}^+ 3d$. I. Hydrogen-like curve. II. Present wave function, agreeing with Hartree's curve.

$r^3 e^{-ar}$. This has but one parameter, a , and if it is chosen to make the maximum agree with that of Hartree's curve, the general form of the curve is evidently wrong, as we may see from Fig. 2. Hartree's function falls off much more slowly for large r . The reason is clear; in the outer part of the orbit, the effective Z is smaller, resulting in a more gradual change of the function. This can be remedied by using two exponentials connected with the same power of r , as $r^3(c_1 e^{-a_1 r} + c_2 e^{-a_2 r})$, the smaller exponent giving the outer part of the function, the larger one the inner part. It is found that this gives a good representation, except for Cu^+ , where the $3d$ electrons lie at the outside of the atom. There the effect is so pronounced that three exponentials are necessary, and it was found that even as far along as Rb three exponentials improve the agreement, though they are not so necessary. Now the $3d$ is an extreme case, but for the other orbits as well it was found helpful to use two exponentials for the outer maximum, though not for the inner ones. The only wave functions represented sufficiently well without this were the $1s$ and $2s$. Thus for $3s$ we should use a function $c_1 r e^{-a_1 r} - c_2 r^2 e^{-a_2 r} + r^3(c_3 e^{-a_3 r} + c_4 e^{-a_4 r})$. Such a function

is capable of representing Hartree's solutions with very good accuracy. We give in Table I three examples of agreement between such analytical functions and Hartree's tables of values.

TABLE I. Comparison of analytic functions with Hartree's for 2s, 3s, and 3d electrons of Rb^+ .

r	2s		3s		3d	
	Hartree	Anal.	Hartree	Anal.	Hartree	Anal.
0.01	0.679	0.695	0.678	0.637	0.001	0.001
0.02	0.882	0.896	0.874	0.846	0.006	0.005
0.03	0.796	0.795	0.772	0.736	0.019	0.014
0.04	0.546	0.538	0.504	0.480	0.040	0.031
0.06	-0.138	-0.156	-0.211	-0.209	0.108	0.088
0.08	-0.795	-0.825	-0.867	-0.854	0.207	0.176
0.10	-1.290	-1.300	-1.308	-1.292	0.329	0.289
0.12	-1.601	-1.602	-1.492	-1.495	0.466	0.420
0.14	-1.752	-1.747	-1.476	-1.478	0.623	0.562
0.16	-1.777	-1.773	-1.276	-1.282	0.752	0.709
0.18	-1.715	-1.709	-0.954	-0.965	0.889	0.853
0.20	-1.597	-1.597	-0.557	-0.574	1.017	0.989
0.25		-1.213	0.540	0.519	1.284	1.278
0.30	-0.827	-0.842	1.508	1.496	1.462	1.468
0.35	-0.535	-0.546	2.198	2.199	1.556	1.575
0.40	-0.333	-0.340	2.600	2.611	1.583	1.601
0.45	-0.202	-0.205	2.763	2.786		1.570
0.5	-0.120	-0.121	2.750	2.778	1.505	1.498
0.6	-0.041	-0.039	2.416	2.441	1.335	1.316
0.7	-0.013	-0.012	1.927	1.950	1.138	1.107
0.8	-0.004	-0.004	1.449	1.472	0.944	0.915
0.9	-0.001	-0.001	1.052	1.070	0.767	0.748
1.0			0.742	0.762	0.614	0.606
1.2			0.350	0.364	0.382	0.386
1.4			0.160	0.165	0.230	0.235
1.6			0.072	0.071	0.137	0.139
1.8			0.032	0.030	0.080	0.079
2.0			0.014	0.012	0.047	0.045

METHOD OF DETERMINING CONSTANTS

After choosing a form of analytical wave function, at least two methods are available for determining the constants. One would be to construct a wave function for the whole atom from such functions, and determine the constants by the variation method, minimizing the whole energy. This would be a very interesting method, essentially that which Zener⁵ has used on the light atoms, except that Zener did not use our wave functions with the adjustable exponents. The second method, however, is simpler and more available, and that is to choose the functions to fit Hartree's curves as well as possible. This was the method adopted. Dr. Hartree very kindly supplied the complete tables of wave functions of the five atoms Si^{+4} , K^+ , Cu^+ , Rb^+ , Cs^+ , and these were fitted by numerical methods. The two schemes should, of course, arrive at substantially the same results. In the present paper, the coefficients and exponents are given for the 1, 2, and 3 quantum electrons of these atoms. They are tabulated in Table II, and plotted in Fig. 3.

⁵ C. Zener, Phys. Rev. 36, 51 (1930); Guillemin and Zener, Zeits. f. Physik 61, 199 (1930).

TABLE II. Exponents in analytic wave functions for five atoms.

Explanation: The wave function for a 1s electron (multiplied by r) is re^{-ar} , where a is tabulated. For a 2s, it is $re^{-ar} - cr^2e^{-br}$ where a and b are tabulated (for example, for Si^{+4} , $a=12.25$, $b=4.53$). For a 3s, it is $re^{-ar} - cr^2e^{-br} + r^3(de^{-fr} + ge^{-hr})$, where for example in K^+ , $a=15.35$, $b=5.89$, $f=3.27$, $h=2.30$. The coefficients are determined for orthogonal functions as follows: c in the 2s is determined to make 2s orthogonal to 1s; in 3s, d and g are related by the condition that $de^{-fr} = ge^{-hr}$ for $r=3/2.67$ (where 2.67 is in the column "3s intersection," and c , a and d , are determined to make the 3s orthogonal to 1s and 2s.

For a 2p, the function is $r^2(ae^{-br} + ce^{-dr})$, where the exponents are given by the entries "2p inner" and "2p outer," and the relation between coefficients is such that the terms are equal when $r=2/$ "2p intersection." For 3p, we have $r^2e^{-ar} - r^3(be^{-ar} + de^{-fr})$. For 3d, in Cu^+ and Rb^+ , the functions are $r^3(ae^{-br} + ce^{-dr} + fe^{-gr})$, where the exponents are tabulated, and also the values "3d inner intersection" and "3d outer intersection" from which the corresponding r 's are the values where the first two, or last two, exponentials are equal.

The curves are sufficiently straight so that linear interpolations between adjacent atoms should be fairly good. But extrapolations are dangerous, since the curves break at the completion of shells of electrons.

The constants as given do not suffice to describe the functions agreeing with Hartree's curves, but only the slightly different orthogonal functions.

Power of r	Orbit	Si^{+4}	K^+	Cu^+	Rb^+	Cs^+
r	1s	13.70	18.70	28.70	36.70	54.70
	2s	12.25	16.00		30.00	44.02
	3s		15.35	21.62	25.30	31.70
r^2	2s	4.53	6.67		14.80	23.03
	3s		5.89	10.35	13.40	19.92
	2p inner	6.00	8.98	14.69	18.80	27.95
	2p intersection	4.56	7.12	12.11	16.10	24.41
	2p outer	3.59	5.77	10.10	13.67	21.85
	3p		7.05	12.32	15.78	23.00
r^3	3s inner		3.27	6.62	9.17	15.76
	3s intersection		2.67	4.68	6.40	11.27
	3s outer		2.30	4.19	6.02	11.10
	3p inner		2.99	5.84	8.21	14.25
	3p intersection		1.72	3.55	5.43	10.66
	3p outer		1.72	3.57	5.54	10.60
	3d inner			6.29	9.20	15.46
	3d inner intersection			3.78	5.55	10.62
	3d middle			2.65	4.74	10.10
	3d outer intersection			1.15	1.12	
	3d outer			1.28	2.60	

The actual methods used for fitting Hartree's functions may be of interest. Suppose we wish to fit a 3s function, and that by interpolation or otherwise we can get first, rough estimates of the terms. Then first we subtract the estimated values of the terms in r and r^2 from Hartree's function, leaving approximately the term which should be represented by r^3 times the sum of two exponentials. We divide the difference by r^3 , take the logarithm to base two exponentials. We divide the difference by r^3 , take the logarithm to base 10, for convenience. The result would give a straight line if one exponential were enough. As it is, however, the line is likely to be bent sharply at small r 's, on account of inaccurate estimates of the terms in r and r^2 ; this can be disregarded. But more important, the line as a whole is curved, and must be represented, not by one term a^{-br} , but by two, in the form $\log_{10}(10^{a-br} + 10^{c-dr})$. The graph of this function has two asymptotes, the straight lines $a-br$ and $c-dr$; at the point where these lines cross, the graph lies a distance $\log_{10} 2$ above the intersection. We can make a further useful set of observa-

tions: where one line is, for example, 0.1 above the other, the graph lies a distance $\log_{10} (1 + 10^{-0.1}) = 0.2539$ above the upper straight line, and 0.3539 above the lower. Using a table constructed according to this model, making use of the positions of the asymptotes, and making a few trials, we may readily get the constants a, b, c, d . Then we compute the term $r^3(10^{a-br} + 10^{c-dr})$, subtract it and the approximate first term from Hartree's curve, and get the term which should be represented by $r^2 10^{e-fr}$. Dividing by r^2 and plotting the logarithm, we find a straight line, from which e and f are determined. Finally we subtract the difference of the correct second and third terms from

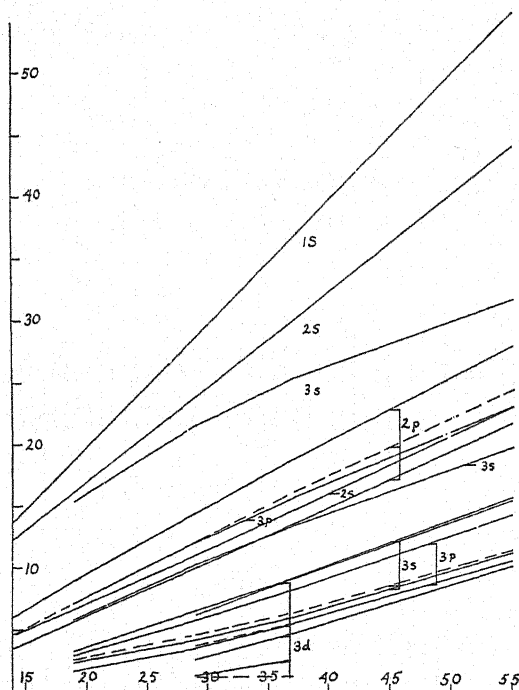


Fig. 3. Diagram of exponents and coefficients as function of atomic number. Drawn from the data of Table II, with linear interpolation. See Table II for explanation. The curves for intersections are drawn with dotted lines.

Hartree's function, divide by r and take the logarithm, and read off from this straight line the coefficient and exponent of the term in r . If the original estimates were far wrong, the process can be repeated, yielding good results fairly rapidly. The final straight lines turn out in all cases to be remarkably straight. The same method can be used on all the functions. It was found in many cases that the constants were by no means uniquely determined. It was possible to choose sets of constants varying over quite a wide range, giving equally good agreement with the curve. In these cases, constants were chosen to give smooth curves of exponents against atomic number, as described in the next section.

INTERPOLATION METHODS; ORTHOGONALITY OF WAVE FUNCTIONS

The wave functions for five isolated atoms would be of small value; the real use of the present method is that it provides a means of interpolation, by which wave functions of intermediate atoms can be found. The interpolation can be thrown into a form suggesting Moseley curves of x-ray term values. The reason is that the exponent Z/n , is of the same form as the square root of an x-ray term, which is plotted in those diagrams. In Fig. 3 we show the exponents as functions of atomic number, giving approximately straight lines, but breaking for the outer electrons when shells are completed, as in x-ray diagrams. Not only the exponents, but some of the coefficients as well, can be put in this form. Thus in an expression $r^n(ce^{-ar} + de^{-br})$, which we have in the outer parts of the wave functions, we may compute the value r_0 for which the two exponentials are equal: $ce^{-ar_0} = de^{-br_0}$. This point generally proves to be between the maxima of the two exponentials. Now these maxima come for $r = n/a$, and n/b , respectively. Thus we can define a quantity, analogous to a and b , equal to n/r_0 , which will lie generally between a and b , and will fall on the interpolation diagram just as the exponents themselves do. These quantities are plotted in Fig. 3. We discuss the other coefficients in the next paragraph.

The functions of Hartree, which we approximate, are not exactly orthogonal, as we mentioned above. Thus if we use our analytical expressions for Hartree's functions, we find that $(1s, 2s)$ (meaning by this the integral of the product of the functions) for Rb^+ is 0.0072, $(1s, 3s)$ is -0.0078, $(2s, 3s)$ is -0.0015, showing that the departure from orthogonality is of the order of a percent. Now when one constructs antisymmetric wave functions in the form of determinants, one has a certain freedom in choosing the one-electron functions entering into it. The reason is that the determinant has the same value, apart from a constant factor, if the elements of each row (or column) are replaced by arbitrary linear combinations of the corresponding elements of the other rows. For example, the determinant

$$\begin{vmatrix} 1s(1) & 1s(2) & 1s(3) \\ 2s(1) & 2s(2) & 2s(3) \\ 3s(1) & 3s(2) & 3s(3) \end{vmatrix}$$

has the same value as

$$\begin{vmatrix} 1s(1) & 1s(2) & 1s(3) \\ 2s(1) + a1s(1) & 2s(2) + a1s(2) & 2s(3) + a1s(3) \\ 3s(1) + b2s(1) + c1s(1) & 3s(2) + b2s(2) + c1s(2) & 3s(3) + b2s(3) + c1s(3) \end{vmatrix}$$

except for a constant factor which drops out on normalizing. As a result, we shall have the same wave function for an atom if, instead of using Hartree's one-electron wave functions, we use a set constructed after the following model: For 1s: Hartree's 1s; for 2s: Hartree's 2s + constant times his 1s; for 3s: Hartree's 3s + constant times 2s + constant times 1s, and so on. And here

the constants can be so chosen as to make the resulting functions orthogonal. Thus a set of orthogonal functions can be set up, similar to Hartree's, and giving just the same atomic wave function as Hartree's.

From our analytic functions, we can proceed in a very similar way to set up orthogonal functions. For the correct 2s, we should subtract some of our 1s from the 2s as determined from Hartree's function. But the 1s is so nearly the same as the inner term of the 2s, that we can subtract some of that instead. In other words, we merely change the coefficient of the term in r , to make the function orthogonal to 1s. Similarly, in the 3s function, we can change the coefficients of the terms in r , r^2 to get orthogonality with both 1s and 2s. It is easily seen that conditions of this sort give just enough equations to determine all the coefficients of our final orthogonal functions. We thus have the following rule: we use orthogonal wave functions of the form $c_1 r e^{-a_1 r} - c_2 r^2 e^{-a_2 r} + \dots$, where the coefficients are so chosen that the functions are all orthogonal (and of course normalized). The exponents are taken from our interpolation graph. In this process, the sum of exponentials occurring in the outer maximum is treated as a single term. Of course, this rule applies to the part of the wave function which is a function of r ; it is to be multiplied by the proper spherical harmonic of the angle.

As an example, let us choose the s states of Rb. For 1s the exponent from the graph is 36.70. Thus the function is $c r e^{-36.70r}$, and if we normalize to unity, we have $c^2 \int r^2 e^{-73.40r} dr = 1 = c^2 2! / (73.40)^3$, $c = 444.7$. Next, for the 2s, we have $c_1 r e^{-30.00r} - c_2 r^2 e^{-14.80r}$. For orthogonality, the integral of the product of this with $r e^{-36.70r}$ must be zero:

$$c_1 \int r^2 e^{-66.70r} dr - c_2 \int r^3 e^{-51.50r} dr = 0, \quad c_2/c_1 = (51.5)^4 / 3(66.7)^3 = 7.903.$$

Finally for normalization we have

$$c_1^2 \int r^2 e^{-60.0r} dr - 2c_1 c_2 \int r^3 e^{-44.8r} dr + c_2^2 \int r^4 e^{-29.6r} dr \\ = 1, \quad c_1^2 \{ 2 / (60.0)^3 - 2c_1 c_2 6 / (44.8)^4 + c_2^2 24 / (29.6)^5 \} = 1.$$

Solving these simultaneously gives $c_1 = 139.1$, $c_2 = 1099$. Lastly, for the 3s we have $c_1 r e^{-25.30r} - c_2 r^2 e^{-13.40r} + c_3 r^3 (c_3 e^{-8.97r} + c_4 e^{-6.02r})$. The value giving the intersection of the last two is 6.40, so that $c_3 e^{-8.97 \times 3 / 6.40} = c_4 e^{-6.02 \times 3 / 6.40}$, giving $c_4 = 0.2512 c_3$. Then applying the conditions of orthogonality with 1s and 2s, and normalizing, we find $c_1 = 49.65$, $c_2 = 534.8$, $c_3 = 572.5$, $c_4 = 143.8$, determining the function completely.

DIFFERENTIAL EQUATION SATISFIED BY THE WAVE FUNCTION

It is interesting to consider what differential equation is satisfied by our analytical wave functions. Let us write the function $u = \sum u_n = \sum c_n r^n e^{-a_n r}$, times function of angle, where we may have more than one term for a given exponent n . This can be written as the solution of an equation $Hu = Eu$, where $H = -\nabla^2 - 2Z(r)/r$, provided $Z(r)$ is properly chosen; for to get it we need

only set $Z(r) = -(r/2) (\nabla^2 u/u + E)$. Computing the derivatives, we have $\nabla^2 u = \Sigma([n(n-1) - l(l+1)]/r^2 - 2a_n n/r + a_n^2)u_n$, where l is the azimuthal quantum number, from which $Z(r)$ can be at once computed, if we assume a value of E . Since our functions are essentially the same as Hartree's, and since his are solutions of central field problems for which he has found the energy values, we take those values for E . We give in Table III for illustration

TABLE III. *Effective nuclear charge for 3-quantum electrons of Rb, compared with Hartree's value.***

r	Z Hartree	Z 3s	Z 3p	Z 3d
0.01	35.14	34.94		
0.02	33.56	32.97	31.49	
0.03	32.16	32.86		
0.04	30.89	32.75*	29.99	
0.06	28.65	23.47	28.38	
0.08	26.69	25.59	26.84	
0.10	24.92	24.56	25.34	22.40
0.15	21.41	21.57	22.09	
0.2	18.73	19.62*	— —*	18.59
0.3	14.64	14.44	14.56	15.04
0.4	11.66	11.70	11.60	11.95
0.5	9.55	9.63	9.54	9.53
0.6	8.06	8.12	8.10	7.78
0.7	7.05	7.22	7.05	6.64
0.8	6.29	6.30	6.26	5.97
0.9	5.66	5.80	5.68	5.68
1.0	5.12	5.38	5.16	5.32
1.2	4.25	4.71	4.35	4.77
1.4	3.60	4.07	3.61	4.00
1.6	3.12	3.27	2.84	3.15
1.8	2.77	2.23	1.93	2.34
2.0	2.52	1.34	0.96	1.71
2.5	2.19	-1.96	-2.00	1.60
3.0	2.07	-5.41	-5.26	4.09

** An electron moving in the field of potential $-2Z/r$, where Z has the tabulated value, would have just the analytic wave functions we have found. Asterisks mark the nodes, at which particularly large errors of Z are found.

the resulting values of $Z(r)$ for the 3-quantum orbits of Rb, computed for each wave function. We see that they are all different, as they naturally would be since we have not a real solution of a single central field problem. On the other hand, the curves agree with each other over wide ranges of variables, in fact over the whole range where the individual wave functions are large. Not only that, but they agree well with what we should expect from Hartree's calculations. We give also in Table III the values calculated from Hartree's field, representing the $Z(r)$ which, divided by r , gives the potential in which a 3-quantum electron moves (strictly different for 3s, 3p, 3d, but nearly enough the same so that we can use a sort of average).

On a graph of $Z(r)$ it is easily shown that a hydrogen-like curve, as used by Pauling, is represented by a straight line, and a single exponential term, as used by the writer, by a parabola-like curve opening downward. Obviously both of these are far less accurate than the functions of the present paper. The principal inaccuracies in our present values come at the nodes of the functions (where, since u appears in the denominator, a very small error in

the position of the node can result in a behavior of the Z curve resembling anomalous dispersion), and at large r 's, where the curves approach straight lines which generally are not horizontal, as they should be. Both these inaccuracies come in regions where the wave function is small, showing that at all points where it is large it satisfies rather accurately the differential equation which it should.

SUGGESTIONS REGARDING FURTHER WORK

It seems that the present wave functions are accurate enough to form good approximations, and at the same time are as simple as they could possibly be—they are scarcely more complicated than hydrogen wave functions. They should be useful, in the first place, in further calculations of atomic structure by Hartree's method. For by interpolation, a decidedly accurate approximation to the wave function can be obtained, to use as a starting point for the method of self-consistent fields. Of course, the curves of constants given in the present paper are far from satisfactory. No doubt they are not even the best approximations for the five atoms which have been computed. They cover only a few of the atoms for which calculations have been made, and not all the wave functions even of those. It is hoped that further work may improve and extend these curves, as the Moseley x-ray term diagrams have been continuously improved. In particular, attention is called to the fact that almost all the atoms which have been calculated by Hartree's method, except for a few light atoms, consist entirely of closed shells. If a few atoms were worked out containing uncompleted shells, as for instance in the iron group, it would be possible to extend the curves to the outer, optical electrons, adding greatly to their usefulness. Fairly reliable extrapolations can be easily made, though they are not indicated in this paper. The wave functions of the present paper should be useful, then, both in stimulating and in guiding further calculations by the method of self-consistent fields, and it is to be hoped that those who make such calculations will at the same time find analytical approximations to their results, so as to improve the curves.

The wave functions themselves are good enough so that a number of calculations become possible which could not be done before. These deal principally with applications of the perturbation theory to atomic structure; for here we have a really good set of orthogonal functions, which can be used as a starting point for perturbation calculations. It will be possible to compute the total energy of atoms, by integration of the energy operator over the orbits, as Zener has done for the light atoms. Further, the exchange integrals coming into the theory of atomic spectra can be calculated from these wave functions, if they are extended to the optical levels. Other interesting applications would be to the effect on the wave function of the perturbations produced by relativity in heavy atoms, and by exchange. The wave functions would be useful in the theory of hyperfine structure. Still another use, of course, is in forming atomic approximations to use with Heitler and London's method of treating molecular structure. Most of these applications demand

16,039

rather definitely the order of accuracy, as well as the analytical convenience, attained in the present wave functions, and which have been impossible before. In addition, there are other calculations which can be made better with these functions, but were possible before, as diamagnetism, polarizability, atomic diameters, etc., previously studied with less accurate analytic functions, and atomic scattering, etc., studied with Hartree's or the Thomas-Fermi functions. In conclusion, the writer wishes again to acknowledge his gratitude to Dr. Hartree for his kindness in providing the tables of wave functions, and for many useful suggestions.

The Nuclear Spin and Magnetic Moment of Li^7

By L. P. GRANATH

Department of Physics, New York University, University Heights

(Received July 25, 1932)

Measurements have been made on the hyperfine structure of the ${}^3P_0-{}^3S_1$ group of the $\lambda 5485$ line of $(\text{Li}^7)^+$ with a Fabry-Perot etalon crossed with a 21 ft. Paschen-mount concave grating. The method of using the etalon with an astigmatic grating is discussed. The results of the measurements on the Fabry-Perot patterns of the ${}^3P_0-{}^3S_1$ group indicates a nuclear spin of $3/2$ for Li^7 and a nuclear magnetic moment of 3.29 times the theoretical magnetic moment of the proton.

INTRODUCTION

THE hyperfine structure of the $1s2p\ {}^3P \rightarrow 1s2s\ {}^3S$ ($\lambda 5485$) line of Li^+ has been investigated with the object of determining the spin and the magnetic moment of the Li^7 nucleus. Schüler¹ was the first to observe the hyperfine structure of this line and in his original paper ascribed a spin of $\frac{1}{2}$ to the Li^7 nucleus, discarding as a ghost the third component of the group ${}^3P_0-{}^3S_1$. The author² found this group to be composed of three components thus removing the possibility of a spin of $\frac{1}{2}$ but the measurements were not of sufficient accuracy to decide between a value of 1, $3/2$ and 2.

There are three ways of determining the nuclear spin from the hyperfine structure of the $\lambda 5485$ line.

- (a) Agreement of the observed pattern with a theoretical calculated pattern for all of the hyperfine structure components.
- (b) Measurements of relative intensities of specially chosen hyperfine structure components such as 3, 2, 1 (${}^3P_0-{}^3S_1$).
- (c) Measurement of interval ratio of specially suitable components, in particular 3, 2 and 1.

The method (a) could be considered the best in theory provided the accuracy of the measurements were high enough. The difficulty of resolving closely spaced groups of lines such as Schüler's 4, 5, 6 group is however considerable and the theoretically expected difference between the appearance of the pattern as a whole for different spins is not very pronounced. This method has been used by Güttinger and Pauli³ and Goudsmit and Inglis.⁴ A precise determination of the nuclear magnetic moment is difficult by this method for reasons just mentioned.

Method (b) could be used provided intensity measurements could be made well enough. It is unnecessary to point out the pitfalls present in such measurements; even if the measurements could be made with sufficient cer-

¹ Schüler, *Zeits. f. Physik* **42**, 487 (1927); Schüler and Brück, *Zeits. f. Physik* **58**, 735 (1929).

² Granath, *Phys. Rev.* **36**, 1018 (1930).

³ Güttinger and Pauli, *Zeits. f. Physik* **67**, 743 (1931).

⁴ Goudsmit and Inglis, *Phys. Rev.* **37**, 328 (1931).

tainty only a few of the hyperfine structure components could be used without ambiguity on account of the large influence of the intermediate stages of coupling³ between the nuclear spin, the electron spin and the electronic total angular momentum.

For components 3, 2 and 1 the question of intermediate coupling does not arise and it may be possible to determine the spin from the relative intensities of these components.

Method (c) has the advantage of greater possible accuracy, it is unaffected by the intermediate coupling, it gives at the same time the spin and the effective nuclear magnetic moment.

The measurements given by Schüler on the position of components 1, 2 and 3 are not of sufficient accuracy to give quite definite information about the spin. In the present work the accuracy of the measurements of the relative position of 1 and 2 with respect to 3 has been increased in comparison with that of Schüler. It is believed that it is sufficiently high to establish the value of the spin as $3/2$, to show that the interval rule is obeyed, and to give the effective magnetic moment to at least 0.5 percent.

Working on the 3, 2, 1 ($^3P_0 - ^3S_1$) group the author² obtained an interval ratio of $\Delta\lambda_{32}/\Delta\lambda_{21} = 1.61(5) \pm 0.02(3)$ as against a value of 1.62 determined from Schüler's¹ data.*

The theoretical value of this interval ratio is, according to Goudsmit and Bacher,⁵

$$(i + 1)/i = 2, 5/3, 3/2 \text{ for } i = 1, 3/2, 2.$$

The value $1.61(5) \pm 0.02(3)$ indicated that the interval rule did not apply. This value was obtained from measurements on plates taken in the second order of a 21 ft. concave grating** and while the probable error was small on 100 measurements taken on 2 plates it was felt that not much weight could be attached to the ratio since the proximity of the components may have influenced each other. The problem then was to obtain photographs of the group with increased resolution and dispersion.

Photographs were obtained in the third order of the grating and measurements on these gave an unmistakable interval ratio of $\Delta\lambda_{32}/\Delta\lambda_{21}$ between 1.33 and 1.41 indicating a spin greater than $3/2$. Next an exposure was obtained in the fourth order of the grating. This gave an interval ratio of about 1.66 which agreed somewhat with the second order but definitely not with the value obtained from the third order plate taken during the same run. The intensity of the grating was low in this order and it was necessary to expose for 50 hours over a period of two weeks so only one exposure was taken. Moreover grating ghosts were present which tended to make the lines slightly blurred (due perhaps to nonperiodic irregularities in the ruling). Conse-

* The alleged inaccuracy in Schüler's conversion of the wave-length of component 3 was due to an oversight on my part of the position of the number 4 in Schüler's table.

⁵ Goudsmit and Bacher, *Phys. Rev.* **34**, 1501 (1929).

** The Anderson grating used at present in this mounting is the property of Townsend Harris Hall, College of the City of New York.

quently it was felt that the grating should be discarded in favor of the Lummer plate or Fabry-Perot interferometer.

A glass Lummer plate was then crossed with the second order of the grating by placing the Lummer plate behind the grating plate holder. (The mounting of this is identical with that for the Fabry-Perot which is described later.)

The results obtained with the Lummer plate are given in Table I, and a photograph of one of the patterns appears in Fig. 1.

TABLE I. Intervals and interval ratio as obtained with the Lummer plate.

Plate	$\Delta\lambda_{32}$	$\Delta\lambda_{21}$	
July 9 No. 2	0.2014	0.1189	0.4991 cm Lummer
July 9 No. 2	0.1965	0.1189	
July 19 No. 2	0.2007		
July 20	0.1954	0.1220	
July 20	0.1945	0.1231	
July 26	0.1950	0.1233	
July 27	0.1943	0.1199	0.4853 cm Lummer
March 24	0.1972	0.1172	
Average	0.1971	0.1204	$\Delta\lambda_{32}/\Delta\lambda_{21} = 1.637$

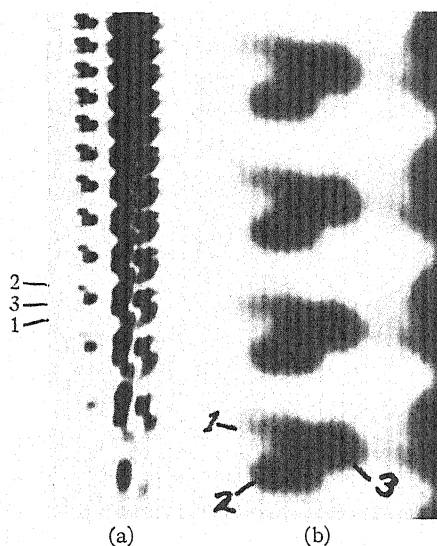


Fig. 1. Lummer plate crossed with second order of grating. (a) Complete pattern of $\lambda 5485$. (b) ${}^3P_0-{}^3S_1$ group of $\lambda 5485$.

These patterns were taken with a 17 cm camera on Cramer Isopresto plates with the exception of the plate of March 24 which was taken on an Eastman 3G plate which is of finer grain than the Cramer but considerably slower.

The agreement between the several values is fair but due to the overlapping of orders component 3 falls between components 1 and 2. This may have caused a consistent error in measuring the intervals. In addition to the over-

lapping of orders the dispersion was small and the grain of the plate not as fine as could be desired. The values obtained were not considered sufficiently accurate to decide the validity of the interval rule, consequently a method was sought which would give a greater dispersion with no overlapping of orders.

This was accomplished by using a Fabry-Perot interferometer with spacers of such thickness that there would be no overlapping of orders. The results thus obtained are believed to be the most reliable.

An attempt was also made to determine the intervals by so choosing the Fabry-Perot spacers as to obtain coincidence of 2 with 3 and the results thus obtained indicated that the ratio was 1.66 ± 5 percent.

APPARATUS AND METHOD

A Paschen-Schüler lamp excited by a 1500 volt d.c. motor generator was used as a source. Commercial helium, purified by chabazite kept at liquid air temperature was continually circulated through the tube. The 21 ft. concave grating (Paschen mounting) was used as a monochromator to single out the

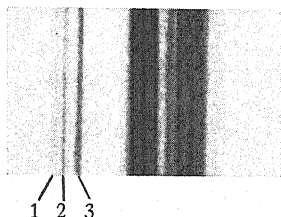


Fig. 2. Pattern of $\lambda 5485$ taken in 4th order of grating.

$\lambda 5485$ line of Li^+ , a slit being placed at the plate holder so that the $^3P_0 - ^3S_1$ group could be separated from the rest of the line, a photograph of which taken in the fourth order is shown in Fig. 2. A condensing lens of 28 cm focus (the collimating tube of a Hilger constant deviation spectrograph) rendered the light parallel which then went through a Fabry-Perot interferometer of 4 cm aperture. A camera of 35 cm focal length was used to photograph the pattern.

This method of using the Lummer plate or the Fabry-Perot interferometer with an astigmatic grating mount has several good features; it is fast, the exposure time necessary with the Fabry-Perot being not much more than that required for a straight grating exposure; the resolution and dispersion of the grating is sufficient to enable one to identify the order of the lines in the interference pattern immediately. The lines in the Fabry-Perot pattern taken with the grating also appeared much sharper than when the same Fabry-Perot plates were used with a Hilger E_2 spectrograph in the customary manner. The interference instrument is inside the grating room and therefore at constant temperature. It has the disadvantage however in that only one line may be photographed at a time.

The bull's-eye of the Fabry-Perot pattern was centered on the line by placing a mercury arc in front of the grating and then moving the interferometer until the pattern was centered. It is then centered for the line for which the pattern is desired. A diagram of the apparatus is given in Fig. 3.

The Fabry-Perot plates were coated with silver sublimed on them in a vacuum. The method is essentially that described by Ritschl,⁶ except that the films were not treated with acid. The spacers used were 1.78, 2.22 and 2.90 mm thick. Cramer Iso presto plates, the fastest that could be obtained for the green region of the spectrum, were used. These are excellent plates where speed in the green is required, but they must be used while fresh. The plates

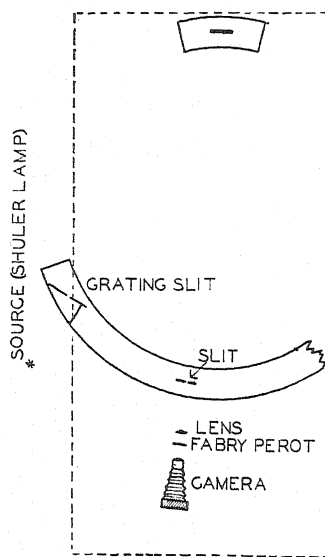


Fig. 3. Method of crossing Fabry-Perot etalon with astigmatic grating.

were developed for about twenty minutes in a fine grain boric acid developer. Exposure times were of the order of three to six hours.

RESULTS

Several patterns of the $^3P_0-^3S_1$ group are shown in Fig. 4. These were taken with a wide slit on the grating, with the rest of the pattern screened off by the slit at the grating plate holder. The spacers 1.78, 2.22, 2.90 mm yield a pattern with no overlapping of components of this group, the distance between orders being 0.519, 0.685, and 0.845A, respectively.

Microphotometer traces of the patterns were measured and from these measurements the wave-length intervals were calculated by the usual formula for the Fabry-Perot interferometer. The intervals were also calculated from measurements taken directly on the plates with a comparator. The results are given in Table II.

⁶ Ritschl, Zeits. f. Physik 69, 578 (1931).

In calculating the final value of $\Delta\lambda_{32}$ and $\Delta\lambda_{21}$ the intervals $\Delta\lambda_{32}$ for the spacer 1.78 have been discarded. It was found that perfect resolution was not obtained for components 2 and 3 due to the presence of the edge of component 5 of the $^3P_2-^3S_1$ group. This is a comparatively very intense component and it seems that some of the light from it was scattered by the slit and so appeared on one side of the pattern. This can be seen in Figs. 4c and 5c. It should be noted that practically all of the $\Delta\lambda_{32}$ intervals due to the 1.78 spacer

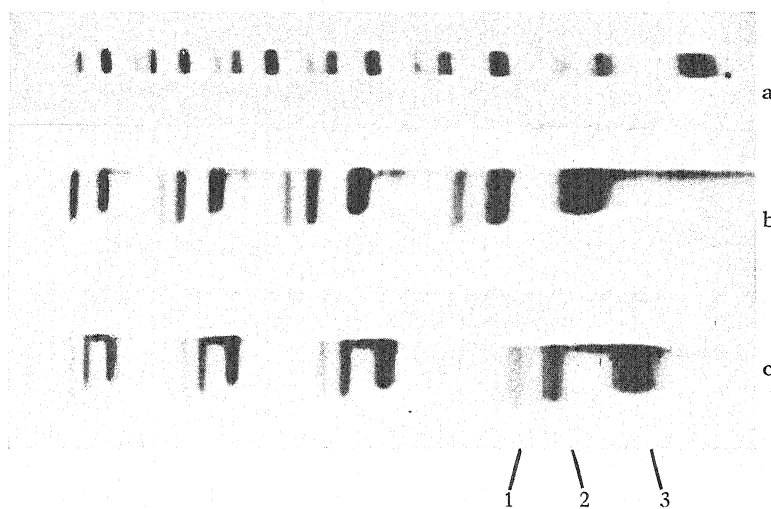


Fig. 4. Fabry-Perot pattern of the $^3P_0-^3S_1$ group. (a) 2.90 mm spacer plate April 28, No. 2. (b) 2.20 mm spacer plate May 16. (c) 1.78 mm spacer plate May 18.

TABLE II. Intervals and interval ratio as obtained with the Fabry-Perot interferometer.

Plate	Spacer (mm)	Intervals calculated from microphotometer traces						Intervals calculated from comparator measurements	
		A Calculated intervals		B Corrected intervals		C Chosen intervals			
		$\Delta\lambda_{32}$	$\Delta\lambda_{21}$	$\Delta\lambda_{32}$	$\Delta\lambda_{21}$	$\Delta\lambda_{32}$	$\Delta\lambda_{21}$	$\Delta\lambda_{32}$	$\Delta\lambda_{21}$
April 28 No. 1	2.90	0.2005	0.1183	0.2005	0.1200	0.2005		0.1976	0.1113
April 28 No. 2	2.90	0.1995	0.1175	0.1995	0.1190	0.1995		0.2017	0.1146
May 5	2.90	0.1983	0.1135	0.1983	0.1150	0.1983		0.2003	0.1123
May 6	2.90	0.1971		0.1971		0.1971			
May 16	2.20	0.2000	0.1179	0.2000	0.1179	0.2000	0.1179	0.2006	0.1154
May 16	2.20	0.2001	0.1183	0.2001	0.1183	0.2001	0.1183		
May 17	2.20	0.2003	0.1213	0.2003	0.1213	0.2003	0.1213	0.1997	0.1177
May 18	1.78	0.1967	0.1213	0.2000	0.1213		0.1213	0.2023	0.1202
May 19	1.78	0.1964	0.1179	0.2000	0.1179		0.1179	0.1970	0.1212
May 20	1.78	0.1948	0.1223	0.1990	0.1223		0.1223	0.1998	0.1202
June 7	1.78	0.1985		0.1985					
June 9	1.78	0.1961	0.1209	0.2000	0.1209		0.1209		
Ave. $\Delta\lambda_{32}/\Delta\lambda_{21}$		0.1982	0.1189	0.1994	0.1194	0.1994	0.1199	0.1999	0.1166
		1.666		1.670		1.663		1.714	

are smaller than the others except the trace of June 7 which has the best resolution of any of these for the 2-3 distance. A 2 percent change in the position of component 2 seems reasonable, based on calculations which will be described later.

The interval $\Delta\lambda_{21}$ is discarded for the 2.90 spacer since it was found that with this spacer the isotope component $^3P_0-^3S_1$ for Li^6 came midway between components 2 and 1. This would tend to decrease the distance between 1 and 2 and it is seen that they are somewhat smaller than those for the other spacers. Here again, judging from the resolution of 1 and 2, a 2 percent correction would seem reasonable. A microphotometer trace of one of the groups for this spacer is given in Fig. 5a (see also Fig. 4a).

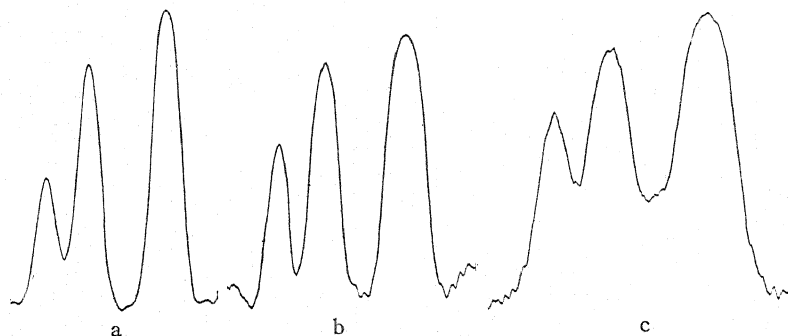


Fig. 5. Microphotometer traces of Fabry-Perot pattern. (a) 2.90 mm spacer plate April 28, No. 2. (b) 2.20 mm spacer plate May 16. (c) 1.78 mm spacer plate May 18.

The plates taken with the 2.90 and 2.20 spacers have the best resolution for the $\Delta\lambda_{32}$ interval. The second trace of the May 16 plate appears on the whole to be the best for both intervals. A reproduction of this trace appears in Fig. 5b (see also Fig. 4b).

The $\Delta\lambda_{21}$ interval for the 1.78 mm plates is assumed to be correct. Component 2 was undoubtedly shifted towards component 3 by about 2 percent and this would increase the $\Delta\lambda_{21}$ interval; consequently a correction to it was deemed unnecessary.

The correction to the intervals was estimated as follows: Immediately after obtaining a pattern the Fabry-Perot interferometer was removed and a mercury arc with a green filter was placed in front of the grating and different positions of the plate exposed to it for different times. Then by using the microphotometer a curve giving the relation between density and exposure was obtained for the plate containing the pattern. An intensity curve was plotted for component 3 and a Gauss error curve was then fitted to it thus giving the constant (a) in the equation $I = Ae^{-ax^2}$.

It was then supposed that the intensity due to components 1 and 2 was given by $I = A_1e^{-ax^2} + A_2e^{-a(x-x_0)^2}$ where A_2/A_1 should be approximately 2 (assuming the spin is 3/2). Knowing (a) it may then be calculated that the maximum of component 1 should be displaced by approximately 2 percent. A like correction was also deemed necessary on a few of the $\Delta\lambda_{23}$ distances as previously mentioned.

On account of absorption of lines in the cathode, 3 is likely to be somewhat wider than 2 and 1. Thus, by supposing the width of 1 and 2 to be the same as 3, one is likely to overestimate the correction. The mean value of the intervals $\Delta\lambda_{32}$ for the spacer 2.90 and 2.20 is 0.1994 and $\Delta\lambda_{21}$ for spacers 2.20 and 1.78 mm is 0.1200. (These are believed to be the most reliable values, those obtained by measuring the plates directly with the comparator being left out due to a possibility of a personal error in measurement. It will nevertheless be noted that the agreement between the comparator and microphotometer measurements is quite good.)

This yields an interval ratio $\Delta\lambda_{32}/\Delta\lambda_{21}=1.662$ which indicates a spin of $3/2$ and a fair agreement with the interval rule.

From the formulas of Goudsmit and Bacher⁵ with the correction factor $(1+\epsilon)=1.06$ of Breit and Doermann⁷ applied to these formulas one can calculate the magnetic moment of the Li^7 nucleus.

$$^3S_1 = (1 + \epsilon)0.228[g(i)/2](i, -1, -i - 1).$$

Solving for $g(i)$

$$g(i) = \frac{2 \times 0.1994 \times 10^{-8}}{5485^2 \times 10^{-16} \times 0.228 \times 1.06 \pm 5/2} = 2.19$$

and

$$1840\mu = ig(i)\mu_0 = 3.29\mu_0.$$

This indicates that the magnetic moment of the Li^7 nucleus is about $3 + \frac{1}{3}$ times the theoretical magnetic moment of the proton.

In conclusion the writer wishes to express his appreciation to Professor G. Breit for his generous interest and advice throughout the progress of the investigation, and to Dr. R. Garman and Mr. G. Shriver of the Department of Chemistry for their kindness in microphotometering the plates. Thanks are also due to Mr. H. Beck for construction of parts of the apparatus used. The lithium used in this investigation was obtained through the courtesy of the Maywood Chemical Works of Maywood, New Jersey.

⁷ Breit and Doermann, Phys. Rev. **36**, 1732 (1930).

The Thermionic and Photoelectric Work Functions of Molybdenum

By LEE A. DuBRIDGE* AND W. W. ROEHR
Washington University, St. Louis

(Received August 20, 1932)

The photoelectric and thermionic emission from pure molybdenum was studied during a prolonged process of outgassing by heat treatment at temperatures up to 2100°K. In a sealed-off tube an equilibrium condition was reached which was not changed by further treatment extending up to 1600 hours. Photoelectric curves taken at room temperature and at 940°K and analyzed by Fowler's method yielded a true work function for the outgassed Mo of 4.15 ± 0.02 volts. Thermionic data for the same specimen also yielded a work function of 4.15 volts, and a value of the constant A close to the theoretical value of 60 amp./cm² deg.².

THE present investigation was undertaken as a part of a program of examining the photoelectric and thermionic properties of metals after a prolonged heat treatment in the highest attainable vacuum. Its aim was two-fold: (1) to clear up if possible the discrepancies between the various published values for the surface work function of molybdenum, and (2) to obtain a further experimental test of Fowler's theory of photoelectric emission.

The thermionic work function of Mo has been determined under good vacuum conditions by Dushman and his co-workers¹ and by Zwikker.² The values obtained by these observers, 4.44 and 4.38 volts, respectively, are in good agreement with each other and undoubtedly represent the best values heretofore obtained for the outgassed metal. However, Dushman reported that great difficulty was encountered in eliminating the last traces of oxide from the molybdenum specimens so that completely consistent values of the thermionic emission were never obtained. The results of the present investigation indicate that it is possible to eliminate residual gas effects only by a very prolonged treatment and that the work function for the more thoroughly cleaned metal is slightly lower (4.15 volts) than the values obtained by the above observers.

Martin³ studied the photoelectric properties of Mo during outgassing treatment and found that after about 150 hours of heating at temperatures up to 1700°K the work function reached an apparently stable value of about 3.2 volts, while the value of the thermionic work function for the same specimen was 3.48 volts. While these two values are in fair agreement, the large discrepancy between these values and those obtained by Dushman and Zwikker led Dushman⁴ to suggest that the heat treatment had not been car-

* The work described in this paper was made possible by assistance to the first named author from a grant made by the Rockefeller Foundation to Washington University for research in science.

¹ Dushman, Rowe, Ewald and Kidner, *Phys. Rev.* **25**, 338 (1925).

² C. Zwikker, *Proc. Amst. Acad. Sci.* **29**, 792 (1926).

³ M. J. Martin, *Phys. Rev.* **33**, 991 (1929).

⁴ S. Dushman, *Rev. Mod. Phys.* **2**, 395 (1930).

ried out in this case at high enough temperatures to eliminate all impurities. In any case it appeared worth while to examine again the photoelectric and thermionic emission from Mo after a very prolonged treatment at the highest possible temperatures, to see whether a more gas-free condition could be reached than had hitherto been obtained.

APPARATUS AND PROCEDURE

With the few exceptions mentioned below the experimental technique was the same as that used by the authors in a recently reported study of palladium⁵ and need not be described again. The specimens, in the form of ribbons, were cut from a piece of very pure Mo foil about 0.01 mm thick. Temperatures were obtained from optical pyrometer readings, using the temperature scale determined by Worthing, and also from the resistance of the filament using Worthing's data.⁶

After a thorough baking of the tube, the outgassing of the filament was begun at a temperature in the neighborhood of 1750°K, since it was found that prolonged heating at higher temperatures during the early stages caused a failure of the filament before complete outgassing was attained. As the outgassing progressed the specimen was heated for long periods at 1900°K and for shorter periods up to 2100°K, at which temperature it soon burned out. It was found that if the tube was left sealed to the pumps it never reached a condition where consistent values of the photoelectric and thermionic emission could be obtained, even though the treatment was continued for 1000 hours. By sealing the tube from the pumps and allowing the residual gas to clean up by the getter action,⁷ it was found that a stable and apparently gas-free condition could be reached which was not changed by further heating. One specimen withstood continuous heating for about six weeks after being sealed from the pumps, during most of which time there was no change in the work function. Most of the data given below were obtained from this specimen, though other specimens which burned out more quickly showed a similar behavior.

The single-prism monochromator used in previous investigations was replaced by a Van Cittert double quartz-prism monochromator to obtain more nearly pure monochromatic light. The relative intensities of the spectral lines of the mercury arc source were measured with a Burt vacuum thermopile connected to a Zernicke galvanometer. A sodium-in-quartz photoelectric cell connected to an FP-54 tube amplifier⁸ was used for checking the intensities from time to time, and for determining the intensities of lines too weak to be measured with the thermopile. As before, the photoelectric currents were measured with a sensitive Cambridge Compton electrometer. The thermionic currents at the lower temperatures were measured with a Type R galvanom-

⁵ L. A. DuBridge and W. W. Roehr, *Phys. Rev.* **39**, 99 (1932).

⁶ A. G. Worthing, *Phys. Rev.* **28**, 190 (1926).

⁷ Aluminum was found to be a more satisfactory getter than magnesium since it did not distil throughout the tube during the baking process.

⁸ See L. A. DuBridge, *Phys. Rev.* **37**, 392 (1931).

eter and at the high temperatures with a potentiometer and standard 1-ohm resistance.

RESULTS

1. Photoelectric emission

During the early stages of the outgassing process both the photoelectric and thermionic readings showed great irregularities and large and irregular changes with temperature, typical of a metal which has not been freed of gas. The threshold shifted at first toward the red reaching a value in the neighborhood of 3500Å (3.5 volts). As the heating progressed the limit shifted again to the violet, to a minimum value near 2800Å (4.4 volts), and after still longer treatment, with the tube sealed from the pumps, the threshold finally reached a stable value of 2980Å (4.15 volts) as determined by the Fowler curves. This value could not be changed by further treatment at the highest temperatures.

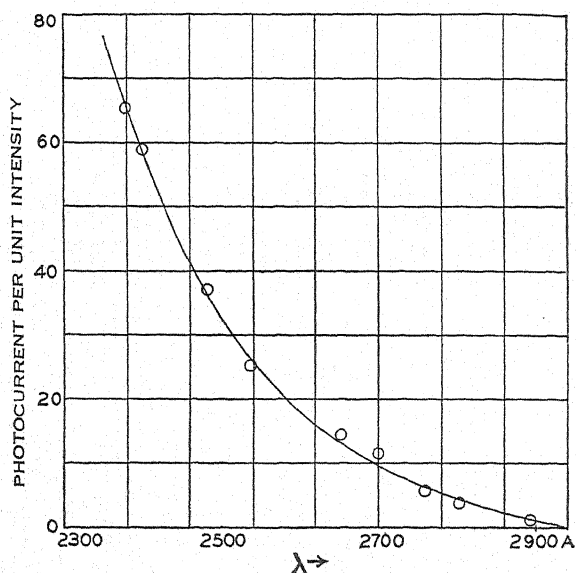


Fig. 1. Photoelectric threshold curve for outgassed Mo.

The ordinary threshold curve, taken at room temperature, for a specimen which had been outgassed for 1600 hours at temperatures up to 2100°K is shown in Fig. 1. This curve had remained practically unchanged by the last 800 hours of treatment, the tube having been sealed from the pumps after the first 400 hours. The pressure in the tube after sealing off, as read by an ionization gauge, was below 10^{-7} mm and showed a gradual decrease with time. During the last 800 hours of treatment both the photoelectric and thermionic measurements were entirely consistent and reproducible from day to day, indicating that the specimen was in a very gas-free state.

The Fowler curve for this specimen is shown in Fig. 2. The readings plotted were taken at room temperature (303°K) and at 940°K, the latter being

the temperature at which the thermionic currents just became appreciable. From the amount by which the observed points had to be shifted horizontally to fit the theoretical curve the following values of the threshold and work function were deduced:⁹

for $T = 303^\circ$, $\lambda_0 = 2992\text{\AA}$, $\phi = 4.14$ volts;

for $T = 940^\circ$, $\lambda_0 = 2983\text{\AA}$, $\phi = 4.16$ volts.

These values are in excellent agreement, and their average, 4.15 volts, may therefore be taken as the best value of the photoelectric work function for clean molybdenum. There is a possible error of the order of 0.5 percent involved in fitting the Fowler curves.

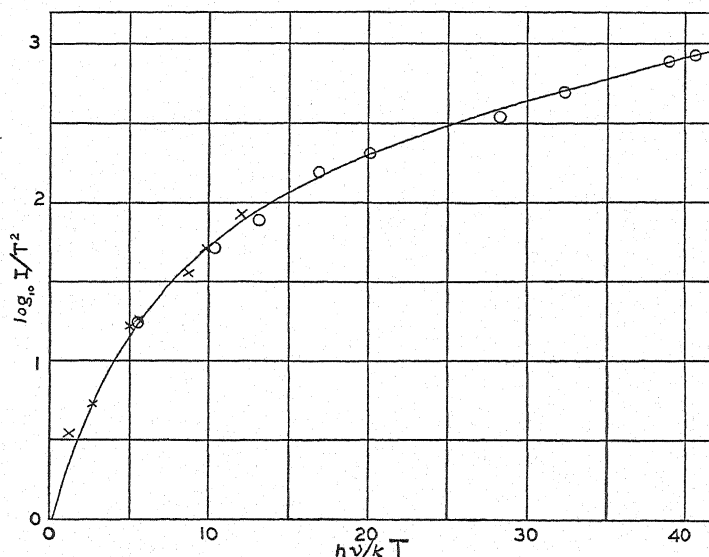


Fig. 2. Analysis of photoelectric data for Mo by Fowler's method.
Circles, $T = 303^\circ\text{K}$; crosses, $T = 940^\circ\text{K}$.

The agreement between the observed points and the theoretical curve shown in Fig. 2 is within the limits of error involved in measuring the currents and the relative intensities of the spectral lines. These data for Mo thus constitute a further experimental verification of Fowler's theory.

2. Thermionic emission

During the early stages of outgassing the thermionic data did not at all fit the Richardson equation. When the observations were plotted in the usual form of $\log I/T^2$ against $1/T$, a curve, usually concave toward the origin, instead of a straight line resulted. Hence no definite work function could be deduced. In general, however, the thermionic data ran parallel to the photoelectric data during the outgassing process. After equilibrium was reached

⁹ See R. H. Fowler, *Phys. Rev.* **38**, 45 (1931); L. A. DuBridge, *Phys. Rev.* **39**, 108 (1932) also reference 5. A discussion of Fowler's theory will also be found in Hughes and DuBridge, *Photoelectric Phenomena* pp. 241-248 (McGraw-Hill, 1932).

the thermionic emission showed a very consistent and reproducible behavior, again showing evidence that the specimen was quite gas-free. In Fig. 3 is shown a thermionic curve, taken after 1600 hours of treatment on the same specimen for which the photoelectric data of Figs. 1 and 2 were obtained. The value of the work function computed from the slope of this curve is 4.15 volts ($b=48,100$). Three other curves taken for this specimen at intervals over a period of about six weeks yielded the following values: 4.15, 4.17 and 4.14 volts. The average value is thus close to 4.15 volts and is in excellent agreement with the photoelectric value.

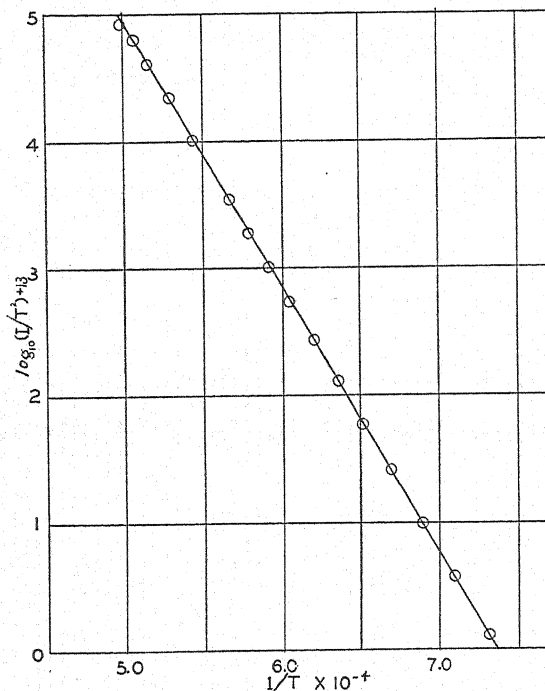


Fig. 3. Thermionic data for outgassed Mo. $\phi=4.15$ volts.

The average value of the thermionic constant A calculated from the data plotted in Fig. 3 is approximately 55 amp./cm² deg.², in good agreement with the theoretical value of 60.

DISCUSSION

The results of these experiments seem to confirm the suggestion that the low value of the work function for Mo reported by Martin is to be attributed to the fact that in his experiments the heat treatment was not carried out for a sufficiently long time or at sufficiently high temperatures to eliminate all impurities. Values of the same order as those reported by Martin were observed in the present investigation only during the early stages of heating. More prolonged heating at high temperatures always caused an increase in the work function. Our failure to check exactly the values of 4.38 and 4.44

volts reported by Zwikker and Dushman was somewhat more puzzling. Apparently the value 4.4 volts is characteristic of a specimen which has been given a reasonably thorough outgassing treatment, but a very prolonged treatment results in the slightly lower value of 4.15 volts. Many of our specimens did show work functions of the order of 4.4 volts during the treatment, but those which withstood the longer heating gave the lower value, which we believe to be characteristic of a very gas-free state. It is possible, of course, that the prolonged heating also causes a microscopic recrystallization of the surface which results in a slight reduction in the work function.

Absorption Spectra of the Samarium Ion in Solids. I. Absorption by Large Single Crystals of $\text{SmCl}_3 \cdot 6\text{H}_2\text{O}$

By FRANK H. SPEDDING¹ AND RICHARD S. BEAR
Chemical Laboratory, University of California

(Received July 22, 1932)

The visible and ultraviolet absorption of large single monoclinic crystals of $\text{SmCl}_3 \cdot 6\text{H}_2\text{O}$ has been studied at seven temperatures between 15° and 298°K. Measurements of the absorption lines and bands are given as they appear at four of these temperatures. The influence of temperature on the positions of lines and multiplets and on the width and intensity of lines is discussed. All phenomena are explained on the basis of three direct effects of temperature change on the crystal: Lattice contraction and expansion, temperature vibration of the lattice with consequent fluctuations in crystal fields, and Boltzmann distribution of the ions between excited lower levels about 160, 210 and 300 cm^{-1} above the basic level.

IN THE past few years the spectra of gaseous atoms and the simpler gaseous compounds have been fairly well interpreted, and many relations between the energy levels of the substances under investigation and their physical and chemical properties have been established. Since a large part of chemistry is concerned with solids and solutions, it would be very desirable if these relations could be extended to apply to them. Unfortunately, very little is known of the energy levels of solids. This paper is the first of a series covering observations on the absorption of the samarium ion in various solid compounds and aiming at the determination of the characteristics of energy levels in solids. These papers will thus deal with one phase of a systematic study of the energy levels of ions in solids and solutions that is being carried out in this laboratory. The rare earths, as has been demonstrated elsewhere,² offer the simplest field for such investigation.

Freed³ in his investigations of the magnetic susceptibility of $\text{Sm}_2(\text{SO}_4)_3 \cdot 8\text{H}_2\text{O}$ at various temperatures has predicted that the basic level of the samarium ion must have one or more levels lying near it. At higher temperatures a certain percentage of the ions, determined by the Boltzmann factor, would be distributed among these higher levels. Freed and Spedding⁴ have verified this prediction by means of photographs of the absorption of $\text{SmCl}_3 \cdot 6\text{H}_2\text{O}$ at various temperatures. They have reported that the multiplets observed can be divided into two classes: one group with intensities greatest at 20°K and another that is completely absent at 20°, making its appearance at 78° and increasing in intensity with the temperature. They attributed the former group to electronic transitions arising from the basic level and considered that the latter group arises from the excited levels.

¹ National Research Fellow in Chemistry.

² Freed and Spedding, *Nature* **123**, 525 (1929); *Phys. Rev.* **34**, 945 (1929); Spedding and Nutting, *J. Am. Chem. Soc.*, in press (1932).

³ Freed, *J. Am. Chem. Soc.* **52**, 2702 (1930).

⁴ Freed and Spedding, *Nature*, reference 2.

Because of the multiplicity of the lower levels of the Sm^{+++} ion it has been chosen for these investigations. The effects of temperature variation and of different crystal environments upon the lower levels are of course reflected in the spectra observed, and under such varying conditions the samarium ion should prove a powerful tool in the attempt to determine the nature of the energy levels of solids. To date we have photographed at several temperatures and under various conditions the absorption spectra of $\text{SmCl}_3 \cdot 6\text{H}_2\text{O}$, $\text{SmBr}_3 \cdot 6\text{H}_2\text{O}$, $\text{Sm}(\text{BrO}_3)_3 \cdot 9\text{H}_2\text{O}$, $\text{Sm}_2(\text{SO}_4)_3 \cdot 8\text{H}_2\text{O}$, $\text{Sm}(\text{C}_2\text{H}_5\text{SO}_4)_3 \cdot 9\text{H}_2\text{O}$, and $\text{Sm}(\text{ClO}_4)_3 \cdot x\text{H}_2\text{O}$. In this first paper we are considering only the absorption of single crystals of $\text{SmCl}_3 \cdot 6\text{H}_2\text{O}$, but in a second, which we are submitting at the same time, the conglomerate or so-called "reflection" spectrum of the chloride is described in detail. In the latter paper we give a partial energy level diagram for the samarium ion as it exists in the $\text{SmCl}_3 \cdot 6\text{H}_2\text{O}$.

The original plates made by Freed and Spedding were not suitable for this study in that they were taken with low dispersion which left most of the multiplets unresolved. We have for this reason taken new photographs at higher dispersion. This new work has been done also with conditions under better control and at several new temperatures.

EXPERIMENTAL PART

The photographs upon which this report is based were obtained from two large crystals and several smaller ones of $\text{SmCl}_3 \cdot 6\text{H}_2\text{O}$ which had been prepared from samarium material of exceptional purity purified by the late Professor C. James of New Hampshire College. Several such crystals have been examined by Dr. A. Pabst⁵ of this university, who has reported that their external symmetry is monoclinic. The large ones were obtained as transparent yellow tablets about 1.5 cm square and 4 mm thick. These were used to secure the visible spectra, for which a 3 m Wood grating with dispersion of about 5.5Å per mm in the first order was employed. A single photograph at liquid nitrogen temperature was taken with a 7 m grating but was too faint to be used for any but confirmation purposes. The larger grating proved unsatisfactory because of the long exposures required and the limited supply of liquid hydrogen available at any one time. At all other temperatures the smaller grating was found to be just as satisfactory, since the temperature blurring was larger than the resolving power of the instrument. The quartz extension of the Dewar used for the several ultraviolet photographs required smaller crystals about 5 mm wide and 1 mm thick. The ultraviolet spectra were obtained with a Hilger E 185 instrument with prisms so mounted as to give at one time about 3Å per mm, at another 2, in the $\lambda 3100$ region.

Most attention has been paid to the visible part of the spectrum, since most of the absorption occurs in that region and the effects of greatest interest are observed there. To facilitate work in the visible region over the temperature range employed, a special (Pyrex) Dewar was constructed and

⁵ A. Pabst, *Journal of Science* **22**, 426 (1931).

fitted out as shown in Fig. 1. The chief features are the triangular windows left in two sides; the crystal house with filter (for elimination of frozen solids from obstruction of the light path); the crystal holder of piston shape introduced through a metal tube, which enables exchange of crystals during a run without introduction of air (especially important with liquid hydrogen); and the liquefier used to produce the liquids ethylene, methane and nitrogen, at whose boiling points pictures were taken. The liquefier, which can be removed for runs at liquid hydrogen temperature, is essentially an air-tight can fitting within the top of the Dewar with independent openings to the outside. The liquefying agent, liquid air, was introduced into the can and the desired gas

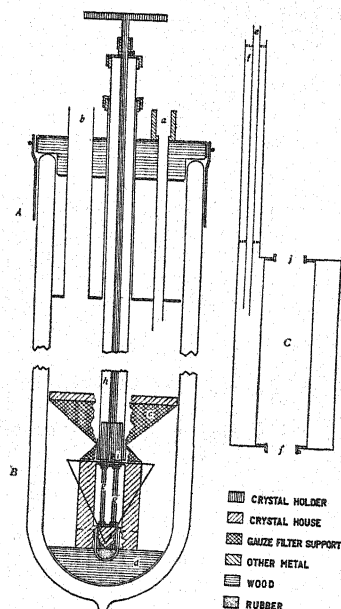


Fig. 1. Longitudinal cross section of Dewar for photography of visible absorption of solids at low temperatures, with *A*, top having inlet for liquid hydrogen, *a*, and outlet for gaseous hydrogen, *b*; *B*, crystal house with filter, *c*, and balsa "shock absorber," *d*; and *C*, liquefier for use with nitrogen, methane and ethylene having inlet for liquid air, *e*, and outlet for gaseous air, *f*. The triangular windows left in both sides of the silvered Dewar disclose the parts shown. The crystal is mounted between the two posts, *g* and *g'*, of the crystal holder, which can be introduced or withdrawn through the tube *h*. This tube is itself disconnectable from the crystal house at *i*, which permits insertion of the liquefier as follows. The liquefier when in position has the air outlet and inlet extending through and out of the hydrogen outlet of the top with the liquefier supports, *j* and *j'*, encircling the tube *h*. The inlet *a* is then used for entrance and exit of the gas to be liquefied. All of the above sets of concentric tubes and cylinders are made to fit snugly but not too tightly together, and the various metal parts, wherever possible, are constructed of German silver or Monel metal to avoid excessive conduction or corrosion. The dimensions of the Dewar are about 3 ft. by 4½ in. It was found possible to secure a charge of hydrogen lasting 15 hours.

condensed on the outside, from which it was allowed to drop to the bottom of the Dewar. To liquefy nitrogen the liquid air of the liquefier was evaporated under reduced pressure. Liquid hydrogen was transferred from the laboratory liquefier directly into the Dewar. In addition to room temperature and

those of liquid ethylene, methane, nitrogen and hydrogen, the temperatures of nitrogen and hydrogen boiling under reduced pressure, about 60° and 15°K , respectively, have been utilized.

The photographs were taken with "Speedway" and hypersensitive panchromatic plates with exposures of from two to four hours, depending on the temperature (see below). It was found that slightly overexposed plates gave the most reproducible results with respect to band edges and structure within wide intense bands. The plates were measured with a comparator us-

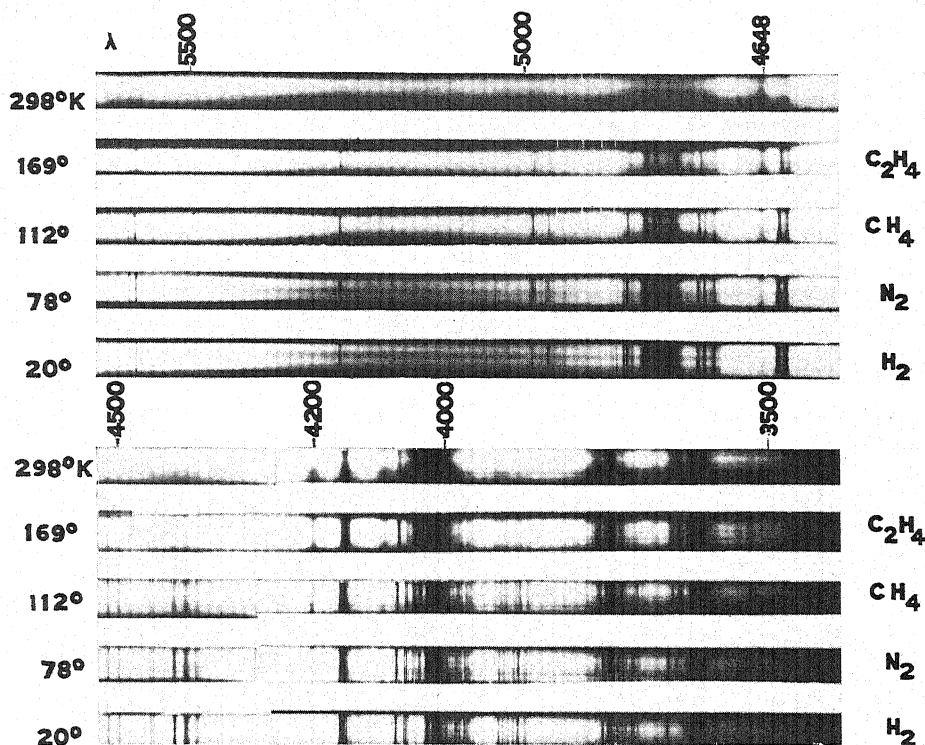


Fig. 2. Single-crystal absorption of $\text{SmCl}_3 \cdot 6\text{H}_2\text{O}$. The substances at whose boiling point the spectra were photographed are indicated on the right, the corresponding temperatures on the left. At $\lambda 4648$ and $\lambda 4200$ are the prominent high-temperature lines for which photometer curves are given in Fig. 3.

ing a low-power eye piece. The whole gave a magnification of five times, which somewhat limited the accuracy, but was necessary since many of the lines are faint and diffuse.

RESULTS

In Fig. 2 are shown reproductions of the $\text{SmCl}_3 \cdot 6\text{H}_2\text{O}$ visible absorption spectrum at five of the seven temperatures investigated. (The photographs taken at "reduced-pressure" temperatures were practically identical with those for which the nitrogen and hydrogen boiled at atmospheric pressure.) An effort was made to keep the exposures as nearly comparable in intensity

as possible. The pictures at room, liquid ethylene and liquid methane temperatures were taken under absolutely identical conditions as to crystal, position, exposure, etc., except for substitution of the proper liquid baths, but an increased transparency at lower temperatures made it necessary to shorten the exposure times when liquids nitrogen and hydrogen were used.

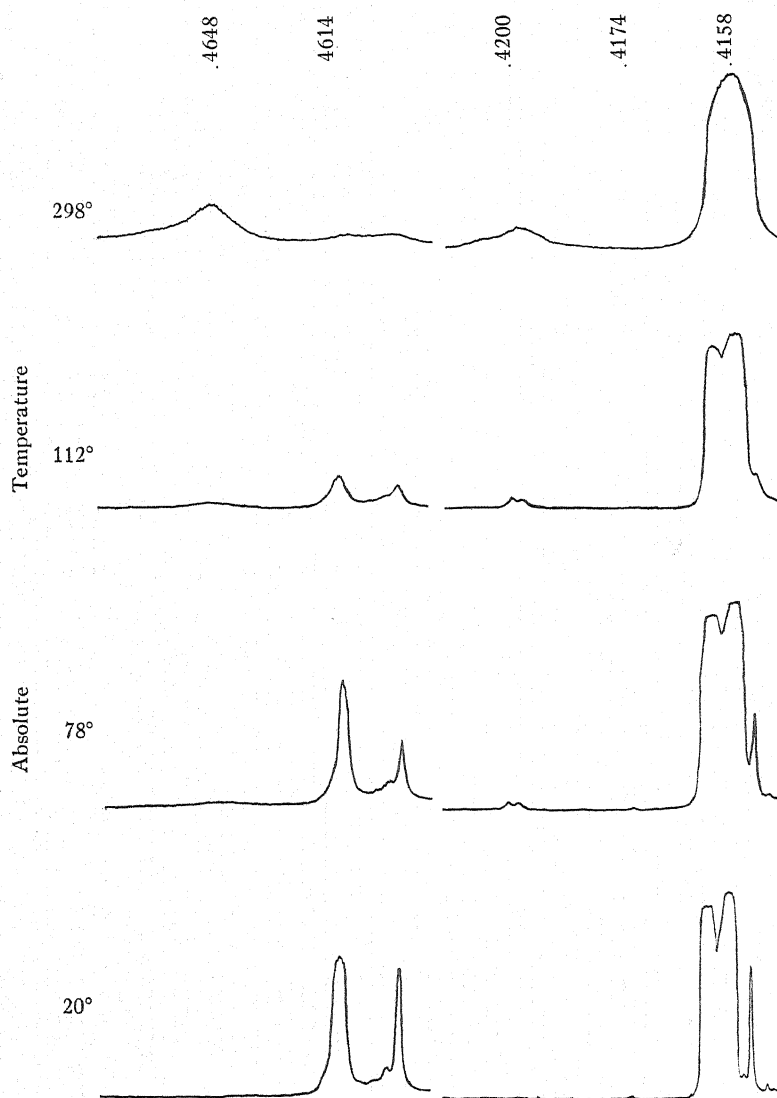


Fig. 3. Photometer curves.

Photometer curves of the two most outstanding multiplets of the visible region showing the decrease and increase of intensities are given in Fig. 3 for four temperatures. The ethylene curve is omitted because ethylene plates were found not to be comparable entirely in intensity under the high magni-

cation and sensitivity employed in photometering the plates. This is caused possibly by a slight absorption of the ethylene itself in these regions.

Table I gives measurements of the absorption lines and bands at four temperatures. Room and hydrogen temperatures are of interest as the extremes, nitrogen temperature because it is the lowest at which the "high-temperature" lines appear appreciably (offering their greatest sharpness), while ethylene measurements represent a temperature at which the high-temperature lines have greater intensity and still the increased definition of a low temperature. In fact the Boltzmann factor begins to cause rapid fading just below liquid ethylene temperature. Exact study of the methane-temperature absorption is of little interest because of the similarity to that occurring at nitrogen temperature.

TABLE I. *Single-crystal absorption lines and bands of $\text{SmCl}_3 \cdot 6\text{H}_2\text{O}$.*

H (Type) = high-temperature line; L (Type) = low-temperature line; HL (Type) = probably both types overlap; R.T., E.T., N.T., H.T. = columns of measurements for room, ethylene, nitrogen and hydrogen temperatures, respectively; Int. = columns of intensity, complete for hydrogen temperature but only occasionally filled for nitrogen temperature. Intensity is estimated roughly on a scale of 10, with very faint or doubtful lines given as 0; s, vs = degrees of increasing sharpness; d, vd = degrees of increasing diffuseness; b = broad line or band, most frequently found with bands; "2," "3" = possibly double or triple, respectively. Primed values represent band edges; c, centers.

Type	R.T. ν (cm^{-1})	E.T. ν (cm^{-1})	N.T. ν (cm^{-1})	Int.	$\lambda(\text{\AA})$	H.T. ν (cm^{-1})	Int.
L			17095		5848.1	17095	1d
L			17156.3		5827.20	17156.2	3s
L			17230		5802.2	17230	1d
L					5720.9	17475	1b
L		17877	17875.8		5592.65	17875.7	5s
L	{17905'}	17908	17908.0		5582.55	17908.0	7s
L	{17912'}		18103		5522.4	18103	1d
L			18124		5516.00	18124.1	1s
L	{18930'}	18929	18927.0		5282.05	18926.7	7s
L	{18939'}	18938	18937.4		5279.15	18937.2	7s
L			19032		5253.10	19031.2	2s
L					5221.4	19147	0
L	{20016'}	20026	20024.5		4992.55	20024.2	6s
L	{20050'}	20044	20042.5		4988.20	20041.8	4s
L		{20112'}	20115.5		4969.90	20115.5	7s
L		{20124'}	20123.6		4967.7	20124	2d "3"
L		{20170'}			4964.1	20139	1d "3"
L			20192		4951.1	20192	0
L		{20200'}	20204		{4949.1c 4947.5c}	{20200c 20207c}	1d
H	{20239'}	{20248'}					
	{20274'}	{20265'}					
L		20408	20404.5		4899.65	20404.0	2s
L			20520.2		4871.90	20520.1	3s
L		20547	20544.8		4866.05	20544.8	4s
L					4862.3	20560.7	0 "2"
L		{20577'}			4858.8	20574	0
L			20585.7		4856.40	20585.7	8s
L		{20592'}	20595		4854.3	20595	1d
L	{20605'}	{20601'}			{4852.3' 4851.5' 4849.5'}	{20603' 20607' 20615'}	{ 8d }
L		{20618'}	20611		4845.4	20633	2d
L			{20631'}		4843.5	20641	2d
L	{20642'}	{20645'}	{20648'}		4842.2	20646	2d
L					4839	20660	1d

TABLE I. (Continued)

Type	R.T.	E.T.	N.T.	Int.	H.T.	Int.				
L					4837.	20670	1d			
L					4832.	20690	1d			
L	{ 20698'	{ 20703'	{ 20706'		{ 4828.1'	{ 20706'				
L				{ 4827.2	20710	5d				
L				{ 4824.7	20721	9d				
L				{ 4822.3	20731	8d				
	{ 20739'	{ 20738'	{ 20736'		{ 4820.7'	20738'				
L					4817.8	20751	1d			
L					4816.0	20758	1d			
L		{ 20773'	{ 20770'		{ 4813.4'	{ 20769'				
L				{ 4812.8	20772	9d				
	{ 20784'			{ 20788'	20782'	{ 4811.3	20779	9d		
						20811'	{ 4810.5'	20782'		
L	{ 20819'	20819	20822'		{ 4804.3'	20810'	8d			
					20836'	{ 4803.1		20814		
						{ 4799.7'		20829'		
L		{ 20842'			4796.9	20841	7d			
L					20840					
L					4793.8	20855	5d			
L	{ 20895'	{ 20866'	{ 20864'		4791.9	20863	5d			
L				{ 20892'	{ 20893'		4787.4	20882	3d	
							{ 4784.9'	{ 20893'		
L							{ 4782.7	20903	10d	
				{ 4781.3'	20909'					
L	{ 20919'	{ 20922'	20927		{ 4778.4'	20922'				
					{ 20935'		{ 4775.3'	20935'	6d	
L							4772.1	20949	1d	
L							4766.0	20976	1d	
	{ 20992'	{ 20985'	{ 20980'		4763.4	20988	1d			
H	{ 21024'	{ 21024'	{ 21025'		4757.	21015	0			
		21069'	21069'		{ 4745.2'	21068'				
L			21074		4744.1	21073	8d			
		{ 21085'	21078'		{ 4743.0'	21078'				
L	{ 21104'	{ 21109'	{ 21108'		4735.9c	21110c	3d			
L				{ 21129'	{ 21118'		4734.3c	21117c	3d	
				{ 21154'	{ 21145'	21147'		4726.9'	21150'	
L										4726.1
			21161'		4725.1'	21158'				
		{ 21168'	21175'		4721.5'	21174'				
L			21178		4720.3	21179	4d			
	{ 21189'	{ 21183'	21182'		4718.8'	21186'				
				21205'	21209'		4713.9'	21208'		
L							4712.7	21213	2d	
					21225'	21224'		4711.6'	21218'	
		21302'	21301'		4693.0'	21302'	2d			
L	{ 21329'	21340'	21314'		4691.5'	21309'				
H	{ 21351'									
		{ 21397'								
H	{ 21423'	21426'								
H		{ 21489'	21480'	{ 21486'						
		{ 21526'	21510'	21504'						
L		21517	21515.1		4646.65	21515.0	1s			
					{ 4642.1'	21536'	0			
L			21548'		4640.2'	21545'				
			21607'		4626.2'	21610'				
L	{ 21629'	{ 21620'	{ 21620'				8b			
				{ 21646'	{ 21639'	{ 21639'		4620.1'	21639'	
L						21649'		4617.8	21649	3d
L						21661.8		4615.15	21661.8	4d
L			21675.4		4612.25	21675.4	5d			
	{ 21684'	{ 21674'								
				{ 21685'						
L				21691	21690	4609.1	21690	8b		
				{ 21701'	{ 21696'					
H	{ 22066'	22073								
	{ 22084'									

TABLE I. (Continued)

Type	R.T.	E.T.	N.T.	Int.	H.T.	Int.	
L	{22157' 22169'	22153	22151.8		4513.25	22150.8	6s
L	{22225' 22237'	22227	22221.6 22228.8		4498.90 4497.45	22221.5 22228.6	2s 5s
L			22423.6		4458.50	22422.8	2s
L	{22445' 22494'	22468 22488	22466.9 22487.9		4449.70 4445.55	22467.1 22488.2	6s 6s
L	{22511' 22556'	{22519' 22536'	22527.8 22543.1		4437.75 4434.8	22527.6 22543	3s 2d
L	{22643' 22675'	{22641' 22658'	{22645' 22656'		{4416.4' 4414.5' 4412.1' 4409.4 4405.1	{22637' 22646' 22659' 22672 22695	8b 0 0
L	{22733' 22762'	{22729' 22748' 22758' 22772'	{22726' 22739.6 22742' 22763.6		{4399.2' 4396.35 4391.70 4391.1' 4385.6	{22725' 22739.8 22763.8 22767' 22796	6d 4d 1d
L	{22813'	{22809' 22824' 22842' 22866'	22816.4 22838.1		4381.60 4377.50	22816.4 22837.6	4d 3d
L	{22874' 22922' 22942'	{22885' 22918' 22926 22933'	22876 22921.9		4370.4 4361.45	22875 22921.7	1d 2d
L	{22966' 22984'		22965		4353.7	22963	1d
L			22995		4347.6	22995	3d
L		{23017' 23033'	23023.8		4342.20	23023.4	2d
L		23057	23058		4335.8	23057	2d
L	Very faintly present	23086	23083		4331.1	23082	0
L	{23597' 23653'	{23118' 23131'	23123		4323.5	23123	2d
H							
H		23719					
H	{23737' 23753'	23738	23731.8	2s			
H			23778	1d			
H	{23783'	{23786' 23792	23789.2	4s			
H	{23802'	23806	23804.9	4s			
H	23824'	23811'	23840	0			
H		23857	23854	0			
H	{23879' 23902'	{23879' 23883 23901'	23881.5	1s			
H			23895.0	1s			
L			23912.3		4181.05	23910.8	1s
H			23928	1d			
L		{23951'	23949.8		4174.70	23947.0	2s
L		23973'	23973	1d	4174.30	23949.5	3s
H			23996	1d			
L					4165.30	24001.0	1d "2"
L					4162.85	24015.2	1d
L	{24030'	{24034' 24039	24036		{4159.4' 4156.1'	{24035' 24054'	10b
L			24051		4154.8'	24062'	
L	{24060'	{24067 24081	24066		{4152.7' 4152.7'	{24074' 24074'	10b
L			24081		4152.7'	24074'	10b
L	{24087'	24086'			4151.0'	24084'	

TABLE I. (Continued)

Type	R.T.	E.T.	N.T.	Int.	H.T.	Int.	
L					4149.65	24091.6	2s
L		24105	24102		4148.0	24101	6dw
L			24122.0		4144.45	24122.0	4s
L					4142.85	24131.1	2s
L		{24136'	24140.6		4141.25	24140.4	4sw"2"
L		{24152'	24152.1		4139.25	24152.2	2d"2"
L					4137.20	24164.2	1d
L		{24174'	24173		4135.5	24174	2d
L		{24190'	24189.8		4132.75	24190.3	2d
L		{24209'			{4129.4'	24210'}	2d
			24213		{4128.6'	24215'}	
L	{24223'	{24228'			4126.9	24225'}	
			24229		4125.9	24230	2d
					{4123.8'	24243'}	
			24255		{4122.4'	24251'}	2dw
L					4121.6	24256	
		{24266'	24266		{4120.9'	24260'}	
L		{24273	24273		4120.2'	24264'}	
					{4119.1'	24270'}	2d
L		{24282'			{4118.2'	24276'}	
					{4118.1'	24277'}	2d
	{24298'				{4117.4'	24280'}	
H			24310.1	2d			
L					4111.9	24316	2d
H	{24325'	24331	24324.2	1s			
LH	{24350'		24352.1	3d	4105.4	24351	2d
L					{4104.3'	24358'}	
					{4103.1'	24365'}	2d
H			24367.1	3d			
	{24377'	{24372'					
		24375					
HL		{24384	24381.7	3d	4100.2	24383	2d
H		{24388'	24395.5	1d			
HL	{24408'	24411	24408.6	3d	{4096.3'	24405'}	1d
					{4094.1'	24418'}	
HL	{24434'	24428	24424.7	3d	{4091.5'	24434'}	
H		24444	24440.7	3d	{4090.1'	24442'}	1d
H			24457.8	1d	{4087.8'	24456'}	
HL			24472.0	1d	{4086.1'	24467'}	1d
			{24489'				
H		24503	24499	1dw			
			{24508'				
			24514.0	1d			
L	{24541'	{24536'	24537.3		4074.30	24537.3	8sw
L	{24558'	{24552'	24544.5		4073.20	24543.8	8sw
L		24570	24568.6		4069.15	24568.1	4s
L		24589	24586.2		4066.20	24586.0	4s
L	{24613'	24619	24617.1		4061.10	24616.9	10sw
L		24637	24634.6		4058.15	24634.8	10sw
L	{24644'	24654	24652.8		4055.15	24653.0	10sw
					4054.85	24654.9	1s
	{24675'	{24681'	{24674'				
H		{24690'	24687	3d			
H			24699	4d	{4048.1'	24696'}	
H	{24709'		24717	1d"2"			
H			24732	1d"2"	{4043.1	24727}	0
					{4042.1'	24733'}	
H	{24740'	{24745'	24747	4d	4040.4	24742	0
H			24759	5d	4037.9	24758	0
?					4036.1	24769	0
?	{24768'	{24775'	{24772'		4034.6	24778	0
L					4031.50	24798	1d

TABLE I. (Continued)

Type	R.T.	E.T.	N.T.	Int.	H.T.	Int.	
L	{ { 24805	{ 24805'			4029.75	24808	1d
L	{ { { 24823'				{ 4027.8'	{ 24821'	
L	{ { { 24827				{ 4027.2	{ 24825	7d
L	{ { { 24846				{ 4023.8	{ 24845	7d
?	{ { { 24850'				{ 4022.9'	{ 24850'	
L	{ { { 24864.9						
L	{ { { 24876.7				4018.70	24876.7	5d
L	{ { { 24890'				{ 4016.9'	{ 24888'	
L	{ { { 24896				{ 4016.2	{ 24892	10b
L	{ { { 24950				{ 4007.2	{ 24948	
L	{ { { 24953'				{ 4006.5'	{ 24953'	
L	{ { { 24965				{ 4005.6'	{ 24958'	
L	{ { { 24975'	{ 24978'	24984		{ 4004.8	{ 24963	5d
L	{ { { 24996		24996		{ 4003.9'	{ 22469'	
L	{ { { 25000'		25007.6		4001.40	24984.1	3s
L	{ { { 25007.6		25018.3		3999.35	24996.9	2d
L	{ { { 25018.3		25024		3997.65	25007.8	4s
L	{ { { 25020'	{ 25026'	25033'		3995.90	25018.5	4s
L	{ { { 25033'		25047.9		3994.70	25026.1	3d
L	{ { { 25047.9		25067'		3993.7	25033	3d
L	{ { { 25068'		25074		3991.30	25047.6	3d
L	{ { { 25074		25079'		{ 3988.5'	{ 25065'	
L	{ { { 25080'		25097		{ 3987.45	{ 25071.7	3d
L	{ { { 25090'		25107		{ 3986.40	{ 25078.1	3d
L	{ { { 25101'		25114'		{ 3985.9'	{ 25081'	
L	{ { { 25107		25123'		3984.90	25087.8	2s
L	{ { { 25114'		25145.3		3983.35	25097.5	3d
L	{ { { 25120'	{ 25123'	25145.3		3981.70	25107.7	4d
L	{ { { 25123'		25145.3		{ 3980.8'	{ 25114'	
L	{ { { 25140'		25145.3		{ 3980.0	{ 25119	5d
L	{ { { 25145		25145.3		{ 3979.1'	{ 25125'	
L	{ { { 25153'		25145.3		3975.70	25145.7	5d
L	{ { { 25195'	{ 25191'	{ 25188'		3973.8	25158	2d
L	{ { { 25199		{ 25201'		{ 3969.1'	{ 25187'	
L	{ { { 25207'		{ 25221'		{ 3968.5	{ 25191	7d
L	{ { { 25219'		{ 25233'		{ 3966.6'	{ 25203'	
L	{ { { 25235'	{ 25229'	25250		{ 3963.8'	{ 25221'	
L	{ { { 25250		25275'		{ 3963.0'	{ 25226'	4d
L	{ { { 25275'		25284'		3962.1	25232	4d
L	{ { { 25326.8		25335		3959.1	25251	3d
L	{ { { 25335	25331	25360.6		{ 3955.4'	{ 25275'	
L	{ { { 25368'	{ 25368	25370		{ 3954.4	{ 25281	2d
L	{ { { 25380'	{ 25374'	25422'		{ 3953.2'	{ 25289'	
L	{ { { 25422'		25430'		3947.30	25326.6	2s
L	{ { { 25430'		25439'		3945.5	25338	1d
L	{ { { 25445'		25486	3d	3942.20	25359.4	2s
H	{ 25475'	{ 25479'	25501	3d	3940.2	25372	1d
H	{ 25500'	{ 25505'	25527.2				
L	{ 25520'	{ 25525'	25537.5		3932.50	25422.1	2s
L	{ 25548'	{ 25543'	25570'		3929.5	25441	1d
L	{ 25575'	{ 25567'	25580'				
L	{ 25600'	{ 25588'	25593'				
L					{ 3921.5'	{ 25493'	0
L					{ 3918.9'	{ 25510'	
L					3916.35	25526.7	5sw
L					3914.80	25537.0	4s
L					3912.3	25553	1d
L					{ 3909.6'	{ 25571'	
L					3909.1	25574	3d
L					{ 3906.2'	{ 25593'	

TABLE I. (Continued)

Type	R.T.	E.T.	N.T.	Int.	H.T.	Int.	
L	{25630' 25647'}	{25622' 25643'}	25626.2 25637		{3901.7' 3901.20 3899.1' 3897.90 3896.25 3894.35}	{25623' 25625.9 25640' 25647.4 25658.5 25671.0}	4d 1s 2s 5s
L			25658				
L	{25670'}	{25669' 25673 25686 25691' 25715'}	25671.2 25684.6		3892.30	25684.5	4s
L	{25692'}						
L	{25720'}	{25723 25733 25738' 25788'}	25719.5 25730.3		3887.00 3885.45	25719.4 25729.9	5d 5d
L	{25750' 25790'}						
L		{25791 25805 25810'}	25786.8 25799.8 25807		3877.00 3874.90 3874.00	25786.0 25799.8 25805.8	4s 4s 3d
L	{25825'}		25822.1		3871.65 3868.0 3865.0	25821.4 25846 25866	2d 0 0
H	{26310' 26342' 26395' 26430'}						
H		{26406' 26425'}	26394 26409	0 1d			
H			26423.3	2d	3783.60	26422.5	2s
H			26437	0			
H			26453	1d			
HL	{26457'}	26468	26467.8	2d	{3779.2' 3776.3'}	{26453' 26474'}	1wd"2"
H	{26490'}	26488	26482.9	2d			
H		26513	26510.5	3d			
H		26526	26524.8	3d			
HL		26544	26541.5	3d	{3767.7' 3765.0'}	{26534' 26553'}	1dw
H	{26553'}	26558	26556.3	3d			
H			26570	1d			
L	{26600'}	{26609' 26624' 26629}	{26608' 26611 26618 26620' 26627.1}		{3756.85' 3756.35' 3756.35' 3755.75'}	{26610.3' 26614.2' 26614.2' 26618.3'}	8s 8s
L	{26630'}						
L					3754.60	26626.5	9s
L	{26657'}	{26657' 26664 26670' 26682c}	{26659' 26670' 26680 26682' 26690.7 26700.9 26714.3 26727.6 26747 26768}		{3749.5' 3749.1 3747.4 3747.0' 3745.65 3744.20 3742.25 3740.55 3738.20 3735.25}	{26663' 26666 26678 26681' 26690.2 26700.4 26714.4 26726.4 26743.2 26764.3}	10d 10d
L	{26688'}						
L		26704	26700.9		3745.65 3744.20 3742.25 3740.55 3738.20 3735.25	26690.2 26700.4 26714.4 26726.4 26743.2 26764.3	5s 6s 5s 2d 3s 5s
L	{26725'}	26722"2"	26727.6				
L		26747	26744.0				
L		26768	26764.4				
L	{26775'}		{26775.2c 26780.9c}		3733.75 3733.00 3730.50	26775.2 26780.5 26798.3	5s 5s 1s
L	{26795'}	26782			3728.05 3725.10 3722.40	26816.2 26837.5 26856.7	2d 1d 2d
L	{26820'}	26815	26816.3		3720.80	26868.5	4s
L		26874	26869.4		3718.6 3717.4	26884 26893	0 0
L	{26856'}		26884				
L	{26877'}				3715.65	26905.6	4s
L		26907	26906				

TABLE I. (Continued)

Type	R.T.	E.T.	N.T.	Int.	H.T.	Int.
L			{26931'			
L			26933.4		3711.80	26933.6
L		{26935'	26937.7		3711.25	26937.4
		26939	26940'			4dw
		26944'				2d
	{26950'					
L		26957	26954.3		3708.90	26954.5
L			26967.9		3707.10	26967.8
L	{26980'				3705.55	26979.1
		{26993'				4s
L		27001	26999.1		3702.80	26998.9
	27012'	27010'				2d
L			27013.7		3700.6	27014.8
L					3698	27035
L					3695	27055
L			{27076'			0
			27092'		3691	27085
H	{27120'}	{27124'	27129'		3684	27135
	{27160'}	27141'			3679	27175
H	{27210'}		27203'		3673	27220
	{27262'}	{27256'	27261'			0
	{27295'}	27280'	27276'	1b	3665	27275
?			27303	0	3662	27300
L	{27340'}	{27334'	27333.2		3657.55	27332.9
L	{27362'}	{27348'	27344.8		3656.00	27344.4
L		27378	27374.1		3652.00	27374.4
H			27392	1s		3s
HL	{27410'}	27411	27412.8	4s	3646.80	27413.4
HL		{27432c	27431.1	4s	3644.1	27434
H	{27443'}	27450'	27445.9	4s		2s
H		27466'	27466.0	1d		1d
H		27487'	27480	1d		
		27511'	27519'		{3632.6'	27521'}
		27548			{3629.1'	27542'}
L	{27557'}	27556	27553		{3627.5'	27559'}
					{3626.8'	27565'}
L	{27585'}	27571	27569c		{3625.4'	27575'}
		27576'			3623.30	27591
L	{27610'}	27594	27591.4		3622.0'	27601'
		27608'	27606'		3621.4	27606
L					3620.3	27614
L		27614	27615		3618.2	27630
L		27634	27629		3617.6'	27635'
	{27638'}	27647'	27640'		3616.3	27645
L		27663'	27668'		3613.5'	27666'
					3612.8	27671
L	{27685'}	{27681'			3610.7	27688
		27688			3608.2	27707
L		27708				6d
	{27715'}	27714'				8d
L					3605.9	27724
			27726'		3605.6'	27727'
L		27748'	27743		3603.50	27742.9
L	{27765'}		27761'		3600.80	27763.8
L			27764		3599.60	27773.1
L		{27771'	27783		3598.25	27783.2
		27787'	27785'			3d
L			27795		3596.65	27795.8
L	{27795'}		27795		3594.8	27810
			27806			2s
		{27822'	27821'			1d
L			27826		3592.90	27824.7
L		{27840'}	27832'		3592.0	27832
L			27861		3588.2	27861
L			27881		3585.6	27881
L	{27895'}	{27890'}	27896'		{3583.0c	27902c}
L	{27910'}	{27912'}	27910'		{3582.1c	27909c}

TABLE I. (Continued)

Type	R.T.	E.T.	N.T.	Int.	H.T.	Int.	
L			27933		3578.95	27933.3	2d
L			27961		3575.2	27963	1d "2"
L					3571.6	27967	1d
H		28003					
L					3466.0	28034	0
H	{28045'	28043			3563.7	28053	0
	{28068'				3561.3	28072	0
H	{28100'	{28097'	{28094'				
	{28123'	{28118'	{28121'				
L	{28162'	28164	28161.3		3550.00	28160.8	3s
	{28183'						
L			28198		3545.3	28199	1d
L			{28236'		3541.0	28233	1d
L			{28246'		3539.8	28242	1d
L	{28250'	{28258'	28256.9		3538.05	28256.2	4s
L		{28264	28264.5		3537.05	28264.2	4s
L	{28278'	{28270'			3533.9	28290	0
					3532.2	28303	0
L	{28320'	{28319'					
L	{28340'	{28324	28322.2		3529.75	28322.5	5s
L		{28328'	28334.5		3528.45	28333.2	1s
L			28662.4		3487.93	28662.1	2vs
L		28669	28667.8		3487.34	28667.0	3vs
L					3485.9	28679	0s
L		28694	28691.3		3484.49	28690.4	3vs
L					3482.8	28704	0
L			28719.8		3481.05	28718.8	3vs
L		28732	28733.2		3479.34	28732.9	2vs
L			28745		3478.25	28742.0	1s
L			28760		3475.50	28764.7	1vs
L			28772.2		3474.58	38772.3	2vs
H	{28780'	{28768'					
		{28797'					
H	{28852'	{28827'	28833.9	0			
			28845	0			
L			28856.4		3464.55	28855.5	4s
			28877		3462.3	28874	0
L	{28882'	{28885'					
			28894.3		3460.00	28893.7	5s
L		28906'					
L		28928'	28926.9		3456.10	28926.2	4d
L	{28933'		{28939c		3454.6	28939	5d
			{28949c		3453.6	28947	5d
L	{28962'	28957'					
L		28990	28990		3448.50	28989.8	6d
					3446.7	29005	1d
L	{29027'	{29020'	{29023'		{3444.6'	{29023'	
L			{29027.7		{3444.05	{29027.3	6d
			{29040.8		{3442.50	{29040.4	6d
	{29053'	{29052'	{29048'		{3441.7'	{29047'	
L		29081	29078		3438.2	29076.7	6d
L			29102.1		3435	29104	0
L			29125.4		3432.45	29125.4	1d
L			29138		3430.9	29139	2d
L		29152	29151		3429.3	29152	3d
L	{29166'				3428.1	29162	2d
L	{29189'	29184	29186		3425.4	29186	2d
L			29206		3422.9	29207	1d
L	{29221'		29220.7		3421.30	29220.3	1d
L		{29239'	29237		3419.3	29237	1d
	{29248'		{29256'		{3417.2'	{29255'	
L					{3416.9	{29258	3d
L	{29264'				{3415.9	{29266	3d
	{29285'	{29272'	{29270'		{3915.6'	{29269'	
L					3412.0	29300	1d

TABLE I. (Continued)

Type	R.T.	E.T.	N.T.	Int.	H.T.	Int.	
L	{29324'	{29316'	{29316'		{3410.4'	29314'}	1b
	29349'	29342'	29356'		{3407.5'	29339'}	
L					{3406.4'	29348'}	
L					3402.4	29383	1d
L	{29654'	29655	29641.1		3372.85	29640.0	4s
	29674'		29656.3		3371.10	29655.5	3s
H	{29817'						
	29858'						
H	{29883'						
	29906'						
LH	29961'		29969.8		3335.90	29968.1	4s
	30000'						
L	30037'	{30038'	{30043'		3327.50	30044.2	7d
		30047	30048'				
L		{30058'	30055		3326.50	30052.9	5d
			30056'				
			30076'		3324.00	30075.8	7d
L	{30101'	30082	30081'				
L			30137'		3317.15	30137.9	3s
L			30153'		3316.25	30145.8	3s
L			30198'		3310.30	30200.1	4s
L		30203	30205'				
	{31138'		31141.7		3210.40	31139.8	6s
	31157'						
H	{31197'						
	31201'						
H	{31233'						
	31252'						
H	{31283'	Not					
	31301'	photo-					
L	{31346'	graphed	{31345'		{3189.5'	31344'}	10d
	31365'		31352'		{3189.0'	31349'}	
L			31377.3		3186.20	31376.1	8s
	{31389'		{31385'		{3185.4'	31384'}	
L			31386'		{3185.2'	31386'}	10d
	{31405'		31392'		{3185.0'	31388'}	
			31416'		{3182.3'	31415'}	
L	{31418'		31417.3		3182.10	31416.5	9s
L			31420.5		3181.90	31418.5	9s
	{31438'		31423'		3181.8'	31420'	
L			31444'		3179.30	31444.5	9d
L	{31449'		31445.5		3178.70	31450.3	9d "2"
L			31453.0				
	{31462'		31455'				
L			31479'		{3175.7'	31480'}	9d "2"
	31492'		31487'		{3175.3'	31484'}	
L			31549.6		3168.90	31547.5	5d
L			31564.4		3167.55	31561.0	4d
L			31576.7c		3165.85	31578.2	3d
			31581.2c				
L	{31592'		{31588'		{3164.8'	31588'}	
	31646'		31599'		{3133.7'	31599'}	10b
H	{32532'		31635'		{3160.9'	31627'}	
	32553'						
H	{32573'		32581.1				
H	32592'		32592.3				
L	{32696'		32698.0		3057.60	32696.1	10s
L	32713'		32739.6		3053.70	32737.5	5s
L	{32755'		{32752'		{3052.4'	32752'}	10b
	32774'		32767'		{3051.2'	32764'}	
H	{33503'						
	33512'						
					Not photographed		

Not photographed

TABLE I. (*Continued*)

Type	R.T.	E.T.	N.T.	Int.	H.T.	Int.
H	{33524'					
L	{33541'		33538.8			
L	{33695'		33700.8			
L	{34392'		34386.7			
	{34407'					
L	{34421'		34425.7			
	{34436'					
L	{34472'					
L	{34486'		34486			
L	{34510'		34513			
H	{35689'					
	{35719'					
L	{35782'		35790.3			
	{35805'					
L	{35846'		35853.1			
	{35868'					

From measurements of seven nitrogen and three hydrogen plates in a region where the lines are fairly sharp it has been found that because of the nature of the lines and the low magnification used in measuring them it is difficult to expect results to be accurate within less than 0.05Å. Band edges and more diffuse or faint lines cannot be given even to this accuracy. As a result of measurements of the best parts of two plates at each temperature, with confirmation by sharp lines of others, we have the figures as quoted in the table. Wave numbers are given, with wave-lengths for hydrogen temperature only. Figures are quoted to units or tenths of units (cm^{-1}) according to the accuracy thought possible. Intensities are estimated for hydrogen temperature only, except for an occasional nitrogen-temperature line which does not appear at hydrogen temperature, i.e., a high-temperature line. These intensities are very roughly determined on a scale of ten and represent the appearance of the lines on our plates. They are meant only for rough comparison and consequently are not to be used from one region of the spectrum to another. It will be noticed that only the most intense lines have appeared in the ultraviolet region. This is probably due to the fact that much thinner crystals were used in that part of the investigation.

DISCUSSION OF RESULTS

Effect of temperature on the positions of lines and multiplets

In general the centers of the multiplets shift to the red with decreasing temperature. At the same time the separations of the lines within the multiplet become greater, so that, although most of the lines are shifted to the red, occasionally one on the high-frequency side is shifted to shorter wave-lengths. The shift in either direction is small, rarely over 5 cm^{-1} , certainly not over 10 cm^{-1} , and takes place mostly above liquid nitrogen temperature. These results are in good accord with those already reported for gadolinium compounds.⁶ Such shifts are probably caused by effects discussed in the

⁶ Freed and Spedding, *Phys. Rev.*, reference 2.

previous report, briefly, the contraction of the crystal which brings the neighboring ions closer to the samarium ions and thus increases the field acting on them. This would result in a greater spreading of the levels, just as an increased external electric field would. The closer approach also would be expected to affect the higher excited levels more than the deeper basic level, so that the multiplets would be shifted to the red. This effect is again demonstrated by the fact that the red shift of the multiplets is greater for the high-energy levels which cause the ultraviolet lines, than it is for the levels that are responsible for the lower-energy multiplets to the red.

Width of lines

At liquid hydrogen temperature the lines can be divided into three classes: (1) broad sharp lines which are undoubtedly narrow multiplets with intense outer components; (2) fine sharp lines, relatively few in number, which are probably truly single; and (3) narrow diffuse bands which are also unresolved multiplets but whose edges are either faint or whose levels are not constant over the time of photographic exposure. (A similar effect of temperature is discussed for wider multiplets.) In the table these are designated respectively, by *s*, *vs* and *d*. In addition wide bands are indicated otherwise.

As the temperature is increased all these lines become broader and more diffuse at the edges. The higher the temperature the more pronounced the effect, with the result that at room temperature most of the multiplets have merged into broad diffuse bands. These facts are also in good accord with the theory that the multiplets are caused by the electric fields of the neighboring ions. At low temperatures the oscillating movement of the neighboring ions would be absent and the magnitudes of the fields fairly constant during the length of the photographic exposure. As the ions begin to move at higher temperatures the fields vary correspondingly, and at one instant the levels might be split but slightly, while at the next, a momentarily increased field would cause wider separations. The photograph registers the integrated effect over a large time interval, which appears as a blurring of lines.

Effect of temperature on the intensity of lines

The lines can be alternatively divided into three groups on the basis of their intensity changes with temperature.

(1) A large group, present on every plate, increase in intensity as the temperature is lowered. This group can be divided into two subgroups: in one the lines are located in the violet and ultraviolet and show very little intensity change, while in the other, which is situated between 6000 and 4320 Å, a marked intensity change with temperature is observed.

(2) Many fainter lines appear on the violet sides of the multiplets. These are weak at hydrogen temperature and rapidly fade out as the temperature is raised.

(3) A group of lines located on the red side of each multiplet are absent at 20°K but appear at all higher temperatures, usually increasing in intensity with the temperature. A few, however, pass through a maximum and then decrease in intensity as the temperature is raised, for reasons which shall appear later.

The first group, which we call a low-temperature group, consists of lines which originate from transitions between the basic level and excited higher ones.⁷ The lines of the second group are probably similar in origin to the first group but are fainter because of low transition probabilities.

The lines of the third group, which we term high-temperature lines, originate from transitions between several low-lying levels situated in groups separated from the basic level by about 160, 210 and 300 cm^{-1} , etc., and the same high excited levels that cause the low-temperature lines.

The intensities of both of these groups of lines will depend in part on the population in the lower levels, and this in turn will be governed by the Boltzmann factor. At hydrogen temperature the number of ions of energy corresponding to the excited lower levels will be extremely small, and consequently the lines originating from these should be absent. At liquid nitrogen temperature and higher these high-temperature lines are permitted by the Boltzmann factor and should increase in intensity. As the population in the excited lower levels increases, that of the basic level, and consequently the intensities of the lines arising therefrom, should decrease.

A factor which tends to mask the intensity changes of the low temperature lines is their great intensity. Certain strong lines and bands may be completely absorbed before the light has penetrated the whole path through the crystal. Consequently, a change in intensity would not be noticed.

The intensities of the lines depend also on the transition probabilities, which are not entirely independent of temperature in solids. In the case of the group of multiplets between 6000 and 4320Å this may be responsible for the great decrease in intensity, which is enough to make some of these multiplets almost disappear at room temperature.

Probably another factor aiding this abnormal decrease in intensity is the fluctuation of the crystal field at high temperatures previously mentioned. Under such conditions the coupling between the lattice and the orbits of the electrons or between the orbital and spin momenta of the electrons may be broken, especially in the final higher levels, and many of these levels may thus become potentially unstable, just as many similar levels do in the case of diatomic molecules. An electron jumping to one of these unstable levels would not be sharply quantized and would give rise to a continuous absorption. This

⁷ This basic level may be nondegenerate up to about 20 cm^{-1} , since it would be necessary for us to go to liquid helium temperature to detect the change in population between levels of this separation. It is possible to look for levels of this sort in the position of the lines themselves. However, since the separations of the sub-levels composing the "basic level" appear to be fairly small multiples of our error in measurement and because such separations frequently cause the lines to be wide or diffuse and are often unresolved, such levels would be very uncertain. Nevertheless, as we shall show in the paper on the conglomerate spectra, a degeneracy covering about five inverse centimeters is highly probable.

is observed to cause a continuous "general" absorption, which has already been mentioned to occur at high temperatures and which makes necessary at room temperature almost twice the exposure required at hydrogen temperature to secure the same blackening of the plate.

On the basis of the explanations given above for the intensity changes of the absorption lines it would appear possible to construct an energy level diagram for Sm IV . However, in the conglomerate spectra many additional lines appear or faint ones are intensified, with the result that more complete and convincing evidence is presented therein for the existence of the various lower levels we have postulated. Consequently a more complete and exact account of the various separations observed between the corresponding high- and low-temperature lines follows in the second paper of this series.

Absorption Spectra of the Samarium Ion in Solids. II.* Conglomerate Absorption of $\text{SmCl}_3 \cdot 6\text{H}_2\text{O}$ and a Partial Energy Level Diagram of the Sm^{+++} Ion as It Exists in Crystalline $\text{SmCl}_3 \cdot 6\text{H}_2\text{O}$

By FRANK H. SPEDDING¹ AND RICHARD S. BEAR
Chemical Laboratory, University of California

(Received July 22, 1932)

Additional lines of the $\text{SmCl}_3 \cdot 6\text{H}_2\text{O}$ absorption spectrum obtained from conglomerates of crystal fragments are reported for four temperatures between 20° and 300°K. These new lines, along with ones previously reported for single-crystal absorption, are used to establish the existence of excited lower levels situated at 145, 160, 204, 217, and roughly 300 cm^{-1} above the basic level. It is probable that there are other levels more than 400 cm^{-1} above the basic one. Two components of the 300 level, at 295 and 315 cm^{-1} , are thought to be present, and there are indications that the other levels, particularly the basic one, may be complex.

IT HAS been shown previously² that for rare earth salts the absorption or "reflection" spectra of conglomerates of small crystals are almost identical with the spectra obtained from single crystals. The chief difference is an enhancement of the fainter lines, many of which are consequently observed for the first time in the conglomerate absorption. This is brought about by the fact that the effective path length of the ray of light of frequency corresponding to that of the absorption is very much greater in the conglomerate case. The increased refractive index of the crystal fragments for such a wave-length causes the beam, once it has entered the solid, to be totally reflected, on the average, a great number of times before it strikes the surface at such an angle that it can emerge. As might be expected, the lines seem to be shifted slightly to the red. This shift is small, however, and is about of the order of our error in measurement. Comparison of Fig. 1 and the corresponding reproduction of the single-crystal spectrum in the first paper of this series³ shows that the conglomerate also causes quite an increase in intensity of *all* lines not already completely absorbed, which is in agreement with the above explanation.

Because of its enhancement of faint lines and disclosure of new ones, the conglomerate absorption is a very valuable addition to that of the single crystal and contributes much to the determination of the energy levels of the ion in the solid. Unfortunately the conglomerate spectra are not sufficient in themselves because of the excessive enhancement and consequent blurring of large regions of the spectrum.

* Contribution from the Chemical Laboratory of the University of California.

¹ National Research Fellow in Chemistry at the University of California.

² Spedding and Bear, *Phys. Rev.* **39**, 948 (1932).

³ Spedding and Bear, *Phys. Rev.* **41**, 58 (1932).

EXPERIMENTAL PART

The conglomerates employed were prepared from small single crystals and fragments by crushing these to a size of smallness sufficient to allow close packing in glass cells without reduction to a powder. The cells varied in thickness from 4 mm to 1 cm and were substituted for the single crystals in the apparatus described in the preceding paper. In general, the thicker layers composed of finer crystals brought out the greatest number of new lines, but this could not be continued indefinitely. Beyond certain limits the exposures required in photographing the spectra became of unreasonable and impossible length. A compromise between thickness of conglomerate and time of

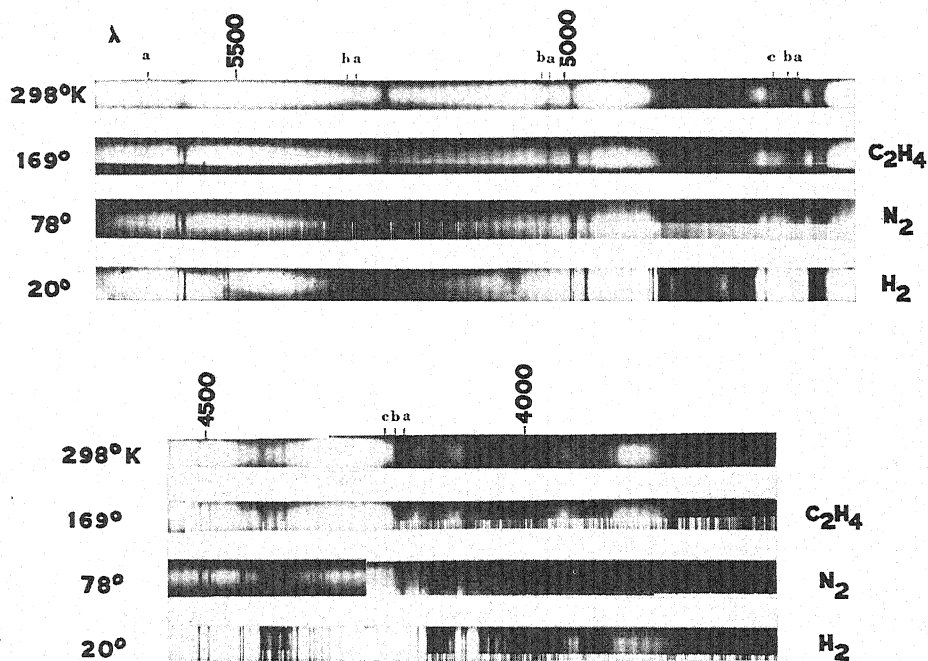


Fig. 1. Conglomerate absorption of $\text{SmCl}_3 \cdot 6\text{H}_2\text{O}$. The substances at whose boiling points the spectra were photographed are indicated on the right, the corresponding temperatures on the left. The small letters indicate various high-temperature lines of importance as explained in the text.

exposure had to be made. This varied with the region of the spectrum and the temperature, making it necessary to photograph conglomerates of several thicknesses and to use the parts of the plates which turned out to be most satisfactory.

In Table I we have given the positions of the new lines as they were observed to appear in the conglomerate absorption spectra at four temperatures. The large number of lines given in the preceding paper is not repeated here, as the wave-lengths in both types of spectrum are practically the same. Only for some of the sharp lines could differences be detected, in which cases

TABLE I. *New absorption lines of $\text{SmCl}_3 \cdot 6\text{H}_2\text{O}$ disclosed by conglomerates.*

H (Type)=high-temperature line; L (Type)=low-temperature line; HL (Type)=probably both types are present; R.T., E.T., N.T., H.T.=Columns of measurements for room, ethylene, nitrogen and hydrogen temperatures, respectively; f, vf, vvf=degrees of decreasing intensity; s, vs=degrees of increasing sharpness; d, vd=degrees of increasing diffuseness; b=broad, frequently used for bands; #=line or band appearing more distinctly in conglomerate than in single-crystal spectrum, hence repeated; incl.=the conglomerate band includes lines and bands formerly given and still approximately correct. Primed values indicate band edges; c, centers.

This table is chiefly a supplement to the single-crystal one. Lines or bands appearing only at one temperature may have been given in the former table for other temperatures. Lines with no intensity designation are quite distinct and have approximately the intensity 1 or 2 on the scale of the former table.

Type	R.T. $\nu(\text{cm}^{-1})$	E.T. $\nu(\text{cm}^{-1})$	N.T. $\nu(\text{cm}^{-1})$	Character	$\lambda(\text{\AA})$	H.T. $\nu(\text{cm}^{-1})$	Character
H	{16783' 16803'}						
L			17128.8	s	5837.0	17127	s
L		{17154' 17162'}					
L			17251.8	s	{5795' 5734'}	{17250' 17432'}	Many doubtful lines
L		{17469' 17480'}	17475	d	5720.9	17475	d
H			17659	vvf			
H			17672	vvf			
H			17692	vvf			
H			17703	vvf			
H	{17709'	{17712' 17723' 17732' 17744' 17768'}	17716.3	s			
H	{17727'		17730.6	s			
H			17748.6	s			
H			17763.1	s			
L			17848	d			
L	{17872' 17887' 17902' 17920'}						
L	#				5579.5	17918	f
L			17938	f	5572.4	17941	f
L			17954	f	5567.4	17957	f
L			17975	f	5561.4	17976	f
L			17991	f	5557.2	17990	f
L					5551.5	18008	vf
L					5546.2	18025	vf
L					5539.5	18047	vf
L					5536.7	18056	vf
L					5533.6	18066	vf
L					5530.2	18078	vf
L					5527.3	18087	vf
L					5520.1	18111	vf
L					5511.4	18139	vf
L			18197	fd	5495.5	18192	fd
L					5487.7	18218	vf
H	{18720' 18737' 18766' 18784'}	{18705' 18733' 18765' 18791'}	18768.0	f			
H			18780.4	f			
H			18792.2	f			
L			18971	fd	5269.5	18972	fd
L		18998	18994.9	fs	5263.35	18994.1	fvs
L					5262.05	18998.8	fvs
L	19005		19016.3	fvs	5257.45	19015.4	fv
L	19026	19023	19021.0	fvs	5255.90	19021.0	fvs
L		{19031' 19041'}					

Type	R.T.	E.T.	N.T.	Character	H.T.	Character	
L			19070	fd	5242.9	19068	f
L			19084	f	5238.5	19084	f
L			19097	fd	5235.0	19097	f
L					5232.0	19108	f
L			19146	vfd	5229.1	19118	f
H					5226.3	19129	f
H			19811	vfd			
H			19825	f			
H	{ 19837'	{ 19825'					
H	{ 19868'	{ 19834'					
H			19865.5	f			
H			19882.7	s			
H							
H	{ 19898'	{ 19881'					
H	{ 19915'	{ 19887'					
		{ 19897'	19897.0	s			
		{ 19805'					
			{ 19925'				
			{ 19945'	vf			
			{ 19956'	vfb			
HL		{ 19953'	{ 19981'				
HL		{ 19978'	{ 20070'	vfb	{ 4982.6c	20064c	vfb
			{ 20078'		{ 4975.9c	20091c	vfb
			{ 20088'		4972.1	20107	vfb
			{ 20097'	vfb			vfb
			20136	d			vfb
					{ 4960.0c	20156c	vfb
					{ 4954.8c	20177c	vfb
		# { 20194'					
		# { 20207'					
			20218	f	{ 4949.5'	20213'	vfb
			20230	f	{ 4940.5'	20235'	vfb
			20246	d			
		# { 20242'					
		# { 20253'					
		# { 20267'					
			20259	d			
			20280	vf			
			20299	vf			
			20328	vf			
	{ 20359'		20361	f			
			20386	f			
	{ 20432'		20421	fd			
		{ 20517'					
		{ 20527'					
			{ 21356'	fb	{ 4676.2'	21379'	fb
			{ 21393'		{ 4673.2'	21393'	
			{ 21474'		4654.1	21480	vfb
				db	4651.4	21493	vfb
			{ 21514'		4648.30	21507.2	s
			{ 21553'				
					# { 4613.2'	21671'	
					{ 4610.0'	21686'	
					{ 4606.1'	21704'	db
					4598.7'	21739'	
			{ 21773'	vfb	{ 4592.1'	21771'	
			{ 21789'		{ 4588.5'	21787'	vfb
			{ 21826'	vfb	{ 4580.5'	21825'	
			{ 21839'		{ 4577.8'	21839'	vfb
{ to next band							
{ 21843'							
			21887	vf	{ 4567.3'	21889'	vfb
			21898	vf	{ 4565.3'	21898'	vfb
			{ 21950'	vf	{ 4552.9'	21958'	vfb
			{ 21968'		{ 4550.4'	21970'	
{ 21991'			21994	d			
{ 22016'			22006	d			
			22069	d			
			22082	d			
			22172	vf			
			{ 22190'	vfb			
			{ 22203'				

TABLE I. (Continued)

Type	R.T.	E.T.	N.T.	Character	H.T.	Character	
L			{22248'	vf	4493.5	22248	vf
L			{22263'		4491.0	22260	vf
L					4488.4	22273	vf
L			22303	vfd	4482.4	22303	vf
H	{22309'		22327	vf			
H	{22337'		22341	vf			
H	{22374'		22384	vf			
H	{22402'		22399	vfd			
			{22567'	fd			
L			{22577'		4429.0	22572	d
L		{22599'	{22592'		4424.5	22595	d
L					4420.7	22615	d
		incl.	{22626'		{4418.6'	22625'	
L			# {22669'	# {4416.4'	22637'		b
			{22681'	to next band	{4411.5'	22662'}	
L					4400.85	22716.5	s
L		{22960'					
		{22979'					
L	{23126'				4327.6	23101	d
L	{23144'				4318.9	23148	d
H			23272	vf			
H			23282.9	s			
	{23352'						
	{23387'						
H	{23507'						
	{23535'						
H	# {23589'						
	{23612'						
H	# {23629'	{23621'					
	{23651'	{23647'					
H			23717	fd			
H			23750	fd			
H			23761	fd			
H			23823	fd			
H			#23840	f			
H			#23852	f			
L		{23907'					
		{23921'					
		{23948'					
L	{23943'	{23953					
	{23966'	{23957'					
		{24019'					
L		incl.					
	to next bd.	{24108'					
	{24160'						
L					4133.15	24187.8	s
L					4132.55	24191.3	s
L					4127.45	24221.2	s
L					4122.45	24250.7	s
L					4121.55	24256.0	s
L					4120.6	24262	d
L					4118.60	24273.2	s
L					4117.85	24277.6	s
L					4116.80	24283.8	s
L					4116.15	24287.7	s
L					4112.9	24307	d
L					4109.40	24327.7	s
					4108.30	24334.0	s
H		{24349'					
		incl.					
L					{4100.7'	24379'}	
					{4099.5'	24386'}	
					{4098.4'	24393'}	fb
		{24482'					

TABLE I. (Continued)

Type	R.T.	E.T.	N.T.	Character	H.T.	Character	
L					4071.40	24554.7	s
L					4070.90	24557.7	s
L					4070.30	24561.3	s
L					4067.60	24577.7	s
L		{ 24609'			{ 4061.8'	24613'	intense
L					# { 4061.35	24615.4	
L					{ 4060.65	24619.7	
L					{ 4060.3'	24622'	
L					4054.00	24660.1	s
L					4052.35	24670.2	s
L		incl.			4050.55	24680.9	s
L		{ 25163'					
L		{ 25419'					
L		{ 25448'					
L			25646.2	f			
L					3854.9	25934	fd
		{ 25960'			{ 3850.2'	25966'	fb
		{ 25994'			{ 3845.2'	25999'	
L			25992	bd	3839.5	26038	fd
L			26041	fd	3835.2	26067	fd
L			26070	vfd	3830.3	26100	d
L		{ 26104'	{ 26097'		3828.50	26112.4	s
			fd				
		26131'	{ 26120'				
H		26205'					
		26226'					
H		26263'					
		26274'					
H		26309'					
		26324'					
H		26391'					
		26424'					

the average shift was about 0.3 wave number to the red. This is about the error of measurement for sharp lines, and of course is even less important for diffuse or broad lines and bands.

In the violet, where the multiplets of greatest intensity are located, the conglomerates cause even greater absorption. The result is a blurring of the multiplets into wide bands which make it impossible to examine very accurately the absorption occurring beyond about 3700Å. (No ultraviolet investigation of the conglomerate absorption was undertaken, mainly because of the long exposures required.)

DISCUSSION OF RESULTS

Most of the new lines which are reported here belong unmistakably to one or the other of two classes. Some owe their low absorption coefficients to the small population in the lower levels producing them and are usually found on the red sides of the more intense multiplets. They thus resemble (and are) "high-temperature" lines (see the first paper of this series³), being similar to them in all ways. Lines of a second class have low absorption coefficients because of small transition probabilities for the electronic changes producing them. These occur on the violet sides of the multiplets and are identical with one type of "low-temperature" line discussed previously. The first class of the new conglomerate lines is valuable in determining the positions of the

lower levels lying near the basic one, while the others are useful in showing how the final excited levels are split in the crystal field and in locating levels which do not easily form electronic transitions with the basic level because of selection rules, etc.

The absorption lines at temperatures near the absolute zero can be considered as an energy-level diagram of the excited levels, since at these temperatures all lines must arise from a single basic level. As the temperature is raised the population in slightly higher levels increases as the Boltzmann factor dictates. As a consequence new lines appear which are separated from the more intense lines by amounts equal to the separation of the excited lower levels from the basic one.

At 15°K, the lowest temperature photographed by us, lines arising from levels more than 50 cm⁻¹ from the basic level would likely be distinguishable

TABLE II. Doublets of 160 cm⁻¹ separation (78°K).

Low-temperature line	High-temperature line	$\Delta\nu$ (cm ⁻¹)
17875.8	17716.3	159.5
17908.0	17748.6	159.4
18927.0	18768.0	159.0
20024.5	19865.5	159.0
20042.5	19882.7	159.8
20404.5	20246	158.5
20544.8	20386	158.8
20520.2	20361	159.2
22151.8	21994	157.8
22228.8	22069	159.8
22487.9	22327	160.9
22543.1	22384	159.1
23949.8	23789.2	160.6
24001	23840	161
24015	23854	161
25646.2	25486	160.2
26611	26453	158
26627.1	26467.8	159.3
26700.9	26541.5	159.4
27570	27412.8	157.2
27591.4	27431.1	160.3

TABLE III. Doublets of 145 cm⁻¹ separation (78°K).

Low-temperature line	High-temperature line	$\Delta\nu$ (cm ⁻¹)
17875.8	17730.6	145.2
17908.0	17763.1	144.9
18937.4	18792.2	145.2
20042.5	19897.0	145.5
20404.5	20259	145.5
22151.8	22006	145.8
22228.8	22082	146.8
22487.9	22341	146.9
22543.1	22399	144.1
23949.8	23804.9	144.9
25646.2	25501	145.2
26627.1	26482.9	144.2
26700.9	26556.3	144.6
26714.3	26570	144.3
27591.4	27445.9	145.5

in the photographs taken, and we should be able to detect lines resulting from levels 20 cm^{-1} or more distant from the lowest one. The first new lines to make their appearance, however, do so between 20° and 60°K and appear to originate from levels differing in energy from the basic level by about 145 and 160 cm^{-1} . In Tables II and III are given the frequencies of lines forming doublets of these separations; each doublet is composed of a high-temperature line and a low-temperature line. Only lines well separated from others are used for these tables, although in almost every multiplet evidence of these separations

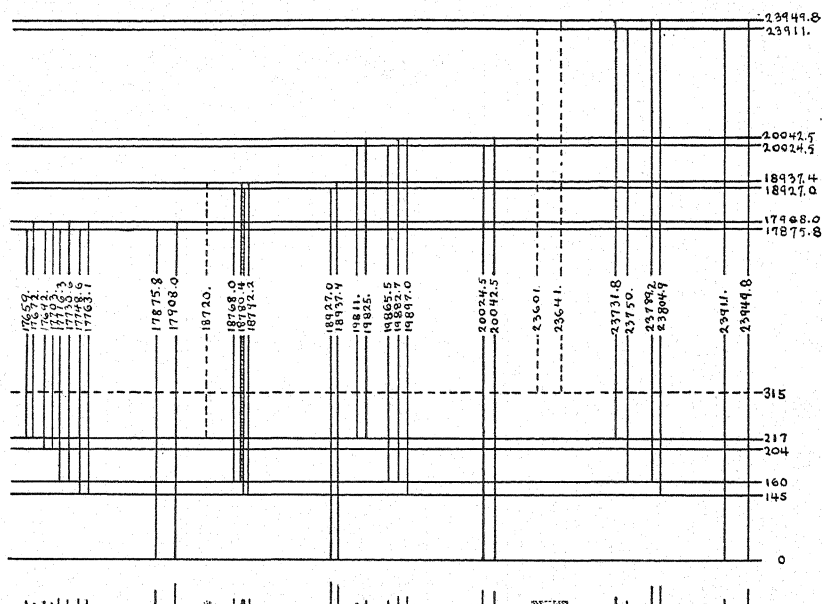


Fig. 2. Diagram of some of the multiplets of the $\text{SmCl}_3 \cdot 6\text{H}_2\text{O}$ absorption spectrum. Below the energy levels appears a representation of the lines as they appear on photographs, plotted however, within the multiplets, according to wave numbers. Relative intensities are indicated roughly by the heights of the lines used, though faint absorption is somewhat exaggerated. The solid lines in the levels or transitions indicate low-temperature values. The dotted lines show dependence on high-temperature measurements.

can be found. No other values for such differences are found to occur with nearly the same frequent repetition, and at liquid nitrogen temperature these two levels are sufficient to account for nearly all of the important, more intense high-temperature lines found in both the single-crystal and the conglomerate spectra. (See lines *a*, Fig. 1.)

At higher temperatures another group of lines which indicate two more levels at 204 and 217 cm^{-1} make their appearance (lines *b*). At liquid ethylene and room temperatures a third group resulting from one or more levels about 300 cm^{-1} (295 to 315 cm^{-1}) can be discerned (lines *c*). Finally, one or two bands found only at room temperature seem to require separations of more than 400 cm^{-1} , since they occur quite far from the nearest low-temperature lines.

In Fig. 2 is given a diagram of several multiplets that occur well apart from other lines and offer most clear and convincing proof of the existence of most of the levels described above. Except for the levels and transitions indicated by dotted lines, the values given are those at liquid nitrogen temperature. As a general rule the intensities of the lines arising from the 160 and 217 levels are a little greater than those of lines from the 145 and 204 levels, respectively. The lines from the 145 and 160 levels are, of course, much stronger than those from higher levels.

Each of the levels listed above not only has been established by from four to thirty measurements of lines whose temperature behavior supports the explanation given for them, but they also are consistent with many other lines that occur in complex regions of the spectra and cannot be determined with the same accuracy. The levels may very well be complex with a spread of from 2 to 30 cm^{-1} , but the accurate determination of this complexity is difficult for two reasons. In the first place the lines broaden as the temperature is increased with the result that at room temperature they are more than 10 cm^{-1} in width. Since the levels in many of the excited multiplets are separated by about this amount, it is impossible to tell whether the broad bands which make their first appearance at high temperatures are caused by transitions from one or more lower levels. The same is true for smaller separations in the lines appearing at lower temperatures. As a result we could not distinguish lines which might indicate 2 cm^{-1} separations in the 160 and 145 cm^{-1} levels or a 30 cm^{-1} separation in those at 300 cm^{-1} .

A second confusing factor is the fluctuating fields caused by the vibrations of the crystal, most important at higher temperatures. These probably cause partial uncoupling of the orbits or spins of the electrons with the field and produce instability in some of the upper levels. The multiplets then tend either to contract to a new center or else fade out entirely. While this latter effect is very pronounced in the case of $\text{PrCl}_3 \cdot 6\text{H}_2\text{O}$, which has been studied by one of us,⁴ for the samarium salt the fading is not very great until room temperature is reached.

It is rather interesting that the separations given in Tables II and III are spread over a range of 159 ± 2 and 145 ± 2 . This range is thought to be somewhat larger than the usual error would allow, though the combined errors of two lines might be that great. It is particularly noteworthy that the residuals, when plotted, instead of giving the ordinary Gaussian curve, seem to fall roughly into three groups. If this is true it would indicate that perhaps the

⁴ Spedding, unpublished work. Discussion of this will probably appear in Physical Review. Many lines which are strong at 80°K are faint at 195° and absent at 300°. $\text{PrCl}_3 \cdot 6\text{H}_2\text{O}$ also appears to have electronic isomers spread over some distance (105 cm^{-1} , etc.). In this case, however, these low levels are apparently affected at high temperatures in a manner similar to that indicated for the excited upper levels of the Sm^{+++} ion. As a consequence an increase in temperature results at first in an accompanying increase in the intensity of the lines arising from these levels, whose populations are governed by the Boltzmann factor. Finally, as the temperature becomes still higher, these lines fade because of the disappearance of the levels from which they originate. Similar phenomena have been observed by J. Becquerel (J. Becquerel, Gedenboek H. Kammerlingh Onnes, Leiden, 1922) in the case of Nd^{+++} .

basic level is split into three components, a very attractive result. The basic level of Sm IV as predicted by Hund⁵ is a $^6H_{5/2}$, and it would be expected to split into three doubly degenerate levels in a moderate electric field.⁶ However, without additional evidence it can only be mentioned as highly probable.

CONCLUSIONS

As a result of the above evidence it is safe to conclude that in $\text{SmCl}_3 \cdot 6\text{H}_2\text{O}$ the samarium ion has levels situated at 145, 160, 204, 217 and 300 cm^{-1} above the basic one. It is highly probable that these levels are complex, especially that the 300 level is double, with components at 295 and 315, and that other levels exist at 400 and greater wave-number separations from the lowest level. These levels are in good agreement with the predictions of one of us from magnetic data.⁷

⁵ Hund, *Zeits. f. Physik* **33**, 855 (1925).

⁶ Kramers, *Proc. Amst. Acad.* **32**, 1176 (1929). Bethe, *Ann. d. Physik* **3**, 133 (1929).

⁷ Spedding, *J. Am. Chem. Soc.* **54**, 2593 (1932). While these levels are for $\text{SmCl}_3 \cdot 6\text{H}_2\text{O}$ and the predictions are for $\text{Sm}_2(\text{SO}_4)_3 \cdot 8\text{H}_2\text{O}$, preliminary photographs and measurements show that the levels of the two salts are similar.

The Luminescence of Solid Nitrogen

By JOSEPH KAPLAN

University of California at Los Angeles

(Received August 18, 1932)

An explanation is proposed for nearly all of the radiations that have been observed by McLennan and his collaborators in the luminescence of solid nitrogen. The bands are associated with known bands of the second-, fourth- and first-positive groups of nitrogen; with hitherto unobserved second-positive bands; with a possible new system and with new modifications of the first-positive bands. These new modifications of the first-positive bands are related to the spectra of the aurora, night-sky and planetary absorption spectra. As a result of this correlation, it is now possible to see why Vegard identified the aurora spectrum as the spectrum of solid nitrogen and then proposed his theory of the upper atmosphere.

I. INTRODUCTION

THE purpose of the present paper is to discuss the identification of the spectrum of the brilliant luminescence which is observed when solid nitrogen is bombarded by cathode rays or canal rays.

The studies of the luminescence of solid nitrogen have been carried on mainly by Vegard¹ in the Cryogenic Laboratory in Leiden and by McLennan² and his collaborators in Toronto. It may be remembered that the work was originally an outgrowth of a hypothesis in which Vegard³ proposed that the green aurora line originated in the luminescence of solid nitrogen suspended in a state of fine division in the upper atmosphere. Further investigation by McLennan and Shrum² showed that the yellow-green band, which Vegard associated with the green aurora line, was broad and diffuse and consisted of three main components, none of which overlapped the green line. The work which has since followed^{4,5} has proved conclusively that the green line is a sharp narrow arc line of oxygen and its identification is now a matter of well-known record. Thus, Vegard's theory of the nature of the aurora and the upper atmosphere has not been confirmed.

It is interesting to mention at this point two other bands that Vegard and others have observed in the luminescence spectrum. These two bands, known as N_2 and N_4 and having wave-lengths of 5230A and 5945A, respectively, were associated by Vegard with two bands in the spectrum of the Aurora Borealis and hence were used as proof of the existence of solid nitrogen in the upper atmosphere. It will be shown in the present paper that it is now

¹ Commun. Phys. Lab. Univ. Leiden, No. 175; Ann. d. Physik **79**, 377 (1926).

² McLennan and Shrum, Proc. Roy. Soc. [A] **106**, 138 (1924). McLennan, Ireton and Thomson, Proc. Roy. Soc. [A] **116**, 1 (1927). McLennan, Ireton and Samson, Proc. Roy. Soc. **120**, 303 (1928).

³ Phil. Mag. **46**, 193 (1923).

⁴ Proc. Roy. Soc. [A] **108**, 501 (1925); *ibid.*, **114**, 766 (1927).

⁵ Babcock, Astrophysikal. J. **57**, 209 (1923).

possible to understand the agreement between some of the bands in the spectrum of solid nitrogen and those in the auroral spectrum, but it will also be shown that, while this agreement has a real significance, it is not a proof of the presence of solid nitrogen in the upper atmosphere. The explanation which is to be presented here is an outcome of the author's recent work on the auroral spectrum and on predissociation in nitrogen.⁶

II. THE LUMINESCENCE SPECTRUM

The data which are to be discussed here are taken from a paper by McLennan, Ireton and Samson,⁷ and since the only purpose of this paper is to analyze the data, the reader will be referred to that and other papers for the experimental details. A part of the luminescence spectrum was arranged by the above writers into two series of bands in the violet and ultraviolet and these series are given in Table I, which has been taken directly from McLennan, Samson and Ireton's paper. Series *B* consists of narrow bands and Series *C* of broad bands, both series degrading to the red. In Table II are given the wave-lengths of all of the bands which have been observed in the luminescence.

TABLE I.

<i>B</i> ₁	<i>B</i> ₂	<i>B</i> ₃	<i>B</i> ₄	<i>B</i> ₅	<i>B</i> ₆	<i>B</i> ₇	<i>B</i> ₈
2347	2479	2623	2781	2961	3158	3388	3644
<i>C</i> ₁	<i>C</i> ₂	<i>C</i> ₃	<i>C</i> ₄	<i>C</i> ₅	<i>C</i> ₆	<i>C</i> ₇	
3105	3285	3502	3732	3980	4255	4585	

TABLE II. Wave-length in angstroms of all bands observed in luminescence.

2347	2781	3055	3285	3732	4585	5552	} <i>N</i> ₁	6187
2479	2903	3105	3388	3980	4775	5616		6400 <i>N</i> ₃
2623	2961	3158	3502	4255	5230 <i>N</i> ₂	5659		6725
2765	3009	3234	3644	4493		5945		8535

In an earlier paper,² McLennan, Ireton and Thomson called attention to the fact that the violet and ultraviolet bands might be related to the second-positive bands of nitrogen, but the agreement was apparently not very convincing because the idea was not carried further. Vegard,⁸ on the other hand, had recognized the similarity between the luminescence spectrum and the auroral spectrum and he suggested that the same positive and negative bands were present in both spectra. A comparison of the auroral spectrum⁹ and Table II shows, however, that while some of the second-positive bands are common to the aurora and to the solid luminescence, most of the bands in Table II are not present in the auroral spectrum. Furthermore, none of the negative bands of nitrogen, which are by far the strongest bands in the auroral spectrum, are observed in the spectrum of the solid luminescence.

⁶ Kaplan, Phys. Rev. **38**, 582 (1931).

⁷ McLennan, Ireton and Samson, Proc. Roy Soc. **120**, 303 (1928).

⁸ Vegard, Nature **114**, 357 (1924).

⁹ Vegard, Phil. Mag. **46**, 193, 577 (1923).

As far as the writer knows, no further attempts have been made to correlate the spectra of solid nitrogen and gaseous nitrogen.¹⁰

In the following discussion it will be shown that not only are bands related to the second-positive group of nitrogen present in Table II, but that bands related to the fourth-positive, first-positive and to a hitherto undiscovered group of bands, are also present. The bands of the fourth-positive group are not very well known, appearing under very unusual excitation conditions only, hence the relationship between them and the bands in Table II are not at all obvious. Even more interesting will be the identification of two of the bands in Table II as second-positive bands which have never been observed in gaseous nitrogen, but whose wave-lengths can be predicted from the constants of the energy levels which are involved in the emission of the known bands of the system.

III. BANDS RELATED TO THE SECOND-POSITIVE GROUP

An examination of Tables II and III will show that many of the bands in the luminescence of solid nitrogen agree with bands of the second-positive group. Thus, for example, 2961 in the luminescence spectrum corresponds very well with 2962 in the second-positive group. Similarly, 3105 corresponds

TABLE III. *Nitrogen second-positive bands.*

$v' \backslash v''$	0	1	2	3	4	5	6	7	8	9	10	11
0	3371	3577	3805	4059	4344	4666						
1	3159	3339	3536	3755	3998	4269	4574	4917				
2	2977	3136	3309	3500	3710	3942	4201	4490	4814			
3	2820	2962	3116	3285	3469	3671	3894	4131	4416	4723		
4		2814	2953	3104	3267	3446	3642	3857	4094	4356	4648	4975

to 3104, 3158 with 3159, 3285 with 3285, 3502 with 3500, 3644 with 3642 and 4493 with 4490. The above-mentioned bands are the ones which are rather easily correlated with the second-positive bands. It is surprising that this remarkable agreement did not impress previous writers more than it has.

In a recent paper in this journal, the writer¹¹ discussed the sudden curtailment of the second-positive bands at $v'=4$. No one has ever observed bands which originate on $v'=5$, in spite of the fact that the total energy of the electronic level on which these bands originate is 15 volts and the energy in the $v'=4$ level is only 13.9 volts. The writer noticed, however, that 13.9 volts corresponds almost exactly to the energy necessary to dissociate a nitrogen molecule into two 2D metastable atoms and hence the idea was proposed that the absence of bands, which originate higher than $v'=4$, was due to an interaction between the higher vibrational states and the Heitler and London level which corresponds to the repulsive interaction of two 2D atoms. Thus if

¹⁰ In some recent papers Vegard has correlated gaseous and solid nitrogen spectra. The same criticism however that is presented here can be applied to Vegard's work. This will be done in detail in a later paper. *Zeits. f. Physik* 75, 30 (1932).

¹¹ Kaplan, *Phys. Rev.* 37, 1406 (1931).

any of the vibrational levels higher than $v'=4$ are excited, the molecule dissociates either by a radiationless transition to the repulsive energy level or perhaps by a transition in which radiation is emitted. At any rate, the corresponding second-positive bands are not emitted. The second-positive bands are but one of many similar cases of predissociation which were discussed by the writer in the above-mentioned paper, so that the explanation which was proposed had much evidence in its favor.

If it is assumed, therefore, that the absence of bands originating higher than $v'=4$ is accounted for by predissociation, it should be possible to calculate the wave-lengths of missing band-heads and under some circumstances to obtain these bands. That it is reasonable to expect conditions under which one might observe bands which are in general missing due to predissociation has been shown recently by the writer¹² in some work on the first-positive bands of nitrogen. With the well-known constants of the C and B levels, the predicted wave-lengths of the second-positive bands C_6-B_0 and C_7-B_2 are found to be 2479Å and 2621Å, respectively. A glance at Table II will show that there are two bands in the luminescence spectrum at 2479Å and 2623Å.

The agreement is quite remarkable and should remove any doubts that some relationship exists between the spectra of solid and gaseous nitrogen. It is worth while noting once more that in the luminescence spectrum we obtain for the first time second-positive bands which originate on levels higher than $v'=4$, thus substantiating the writer's notions regarding the absence of such bands in electrical discharges through gaseous nitrogen. Their presence in the luminescence spectrum indicates that one might find a consideration of Heitler and London levels profitable in the discussion of the spectrum of solid nitrogen. It will be seen in what follows that Heitler and London levels do play an important role in this problem.

A third band which agrees quite well with a predicted second-positive band is the band at 2765Å. The predicted C_9-B_4 band falls at 2761Å, the difference in frequencies being about 40 cm. The agreement is once again quite satisfactory.

The $\omega^*:v$ graph for the C level of N_2 is one which possesses such an enormous negative curvature that the resulting energy equation for the vibrational levels contains third and fourth degree terms with very large coefficients.¹³

$$E = 2018.67v' - 26.047v'^2 + 0.9873v'^3 - 0.546v'^4.$$

This equation was used to calculate the energies of the C_6 , C_7 and C_9 levels. The remarkable coincidence between the predicted bands and those observed in the luminescence is such, that the function given above for E , as calculated from known levels, must also give good values for the unobserved vibrational levels. This is very interesting when considered along with Birge's¹⁴ last discussion regarding the determination of heats of dissociation from band spectra. In that paper he discussed the failure of the linear extra-

¹² Kaplan, Phys. Rev. **38**, 373 (1931).

¹³ Birge and Spomer, Phys. Rev. **28**, 259 (1926).

¹⁴ Birge, Trans. Farad. Soc. **25**, 718 (1929).

polation method in determining heats of dissociation. It was shown that in general it is necessary to use two functions to represent the entire $\omega^v:v$ curve; one to represent the portion having negative curvature (or positive), the second function having positive (or negative) or zero curvature. Professor Birge had previously attempted to obtain a single analytical expression to represent the function $\omega^v = {}^0(v)$ in the cases of I_2 and O_2 , where the entire $\omega^v:v$ graphs are known and he found that in no case could he get a satisfactory fit. The function for E which is used here must therefore represent at least the vibrational levels $v'=0$ to $v'=9$ and no more, because the energy in $v'=9$ is 14.6 volts, which is the maximum of the function. Since the predicted total energy is 15.0 volts, the vibrational levels in the range from 14.6 to 15.0 volts must be calculated from a second function. It will be an interesting problem not only to attempt to obtain the bands 2479, 2623 and 2765 in electrical discharges in gases, but also to obtain bands which arise in the 14.6–15.0 volt range.

IV. BANDS RELATED TO THE FOURTH-POSITIVE GROUP

The fourth-positive bands of nitrogen arise in transitions between the D and the B levels. This group of bands was discovered in condensed discharges and it is almost never observed in uncondensed discharges, except under very unusual excitation conditions.^{15,16} In general these bands are much weaker than the second-positive bands and this is easily understood when one remembers that not only is the D level the highest known level in the molecule but that once more a repulsive level prevents the emission of bands which originate higher than $v'=0$.¹¹

In Table IV are given the wave-lengths of the known fourth-positive bands, each band consisting of five heads. A comparison with Table II shows

TABLE IV. Wave-lengths in the fourth-positive bands.

$v' \backslash v$	0	1	3	3	4	5	6
0	2260.8	2351.4	2448.0	2550.7	2660.5	2777.9	2903.9
	59.6	50.3	47.0	49.7	59.3	76.5	02.0
	58.4	49.0	45.6	48.4	57.9	75.1	00.3
	57.1	47.5	44.0	46.6	55.8	72.8	2898.1
	56	46.4	42.8	45.3	54.5	71.4	96.6

that the bands 2347, 2781 and 2903 agree quite well with the bands 2347.5 or 2346.4; 2777.9 and 2903.9 or 2902. The band 2765, which was identified as C_9-B_4 in the previous section, may be the fourth-positive band 2771.4. It is of some interest to note that only part of the fourth-positive group is present in Table II. This absence of part of the group was a characteristic of the second-positive bands as well. It will be shown later that this modification of the gaseous spectrum is not at all an unreasonable one when going from a gas to a solid.

¹⁵ Strutt, Proc. Roy. Soc. [A] 85, 377 (1917).

¹⁶ Kaplan, Phys. Rev. 33, 189 (1929).

V. BANDS RELATED TO THE FIRST-POSITIVE GROUP

The relationship between the luminescence spectrum and the first-positive bands of nitrogen is even more striking and interesting than the relationships discussed in the previous sections. We will consider first the luminescence band N_2 , which has eight components lying between 5204Å and 5240Å. The wave-lengths given by McLennan and his collaborators for these components are as follows:

(1)	(2)	(3)	(4)
5204.4	5210.4	5214.3	5220.1
(5)	(6)	(7)	(8)
5224.4	5228.8	5235.0	5240.0

This band was identified by Vegard with an aurora band, whose wave-lengths have been given by various observers as 5269, 5205, 5200, 5233, 5210, 5239, 5207, 5200, 5228, 5235, 5166, 5230. This identification was advanced by Vegard⁸ as proof that solid nitrogen existed in the upper atmosphere. It was criticized on the grounds that the 5230 band in the aurora is probably the fourth member of the first-negative band system of N_2 , the first three members of which are very strong in the aurora. This criticism was well based and undoubtedly the negative band 5227 does appear in the aurora, but the large variation in wave-lengths which have been reported in this region indicates that other bands also appear in the aurora. It will be shown that, not only is it possible to identify the N_2 band of the luminescence spectrum with some nitrogen bands, but that the same type of modification of the gaseous bands can account for both the N_2 band and the nitrogen bands in the aurora.

The first-positive bands of nitrogen are best known on account of their presence in the afterglow of active nitrogen. On a small dispersion spectrogram most of the individual bands of this system appear to consist of three strong and one weak head, while some of the bands consist of but one strong head. The recent rotational analysis of these bands by Naudé¹⁷ has shown that the three strong heads are in reality three groups of three strong branches which are P_1, Q_1, R_1 ; P_2, Q_2, R_2 and P_3, Q_3, R_3 branches belonging to the transitions ${}^3\Pi_{\text{low}} {}^3\Sigma$, ${}^3\Pi_{\text{medium}} {}^3\Sigma$ and ${}^3\Pi_{\text{high}} {}^3\Sigma$. In this paper we will continue to refer to these groups as heads.

A calculation of the positions of the first heads corresponding to the transitions $B_{17}-A_{12}$ and $B_{16}-A_{11}$, where A and B refer to the ${}^3\Sigma$ and ${}^3\Pi$ levels, respectively, shows that they have wave-lengths 5207 and 5240. These two wave-lengths approximately include the eight components of the N_2 luminescence band. The average separation of the components of the N_2 band is about 20 cm^{-1} , whereas the average separation of the first-positive band heads of any one band is about 22 cm^{-1} , thus giving us an additional reason for believing that the N_2 band is related to the first-positive bands 5207 and 5240. One objection to the attempt to compare the N_2 band with first-positive bands is that the luminescent band degrades to the red, whereas the first-positive bands degrade to the violet. This was also true, however,

¹⁷ Naudé, Phys. Rev. 38, 372 (1931).

for the second- and fourth-positive groups, yet the correlation in these cases was quite good.

The band N_1 in the solid luminescence spectrum consists of three diffuse components, the wave-lengths of which are 5556A, 5619A, and 5654A. There are no auroral radiations whose wave-lengths agree with these values, although Vegard attempted to correlate this band with the green auroral line. There are, however, three first-positive nitrogen bands, $B_{16}-A_{12}$, $B_{15}-A_{11}$, and $B_{14}-A_{10}$, which include the three components of the N_1 band. These bands are usually single-headed, with only the long wave-length head appearing, these heads having wave-lengths of about 5565A, 5617A, and 5665A, of which the 5617 head agrees very well with the second component of the N_1 band. It is to be noticed also that the B_{16} and B_{17} levels were involved in the identification of the N_2 band, while the B_{16} , B_{15} , and B_{14} levels are considered in connection with the N_1 band.

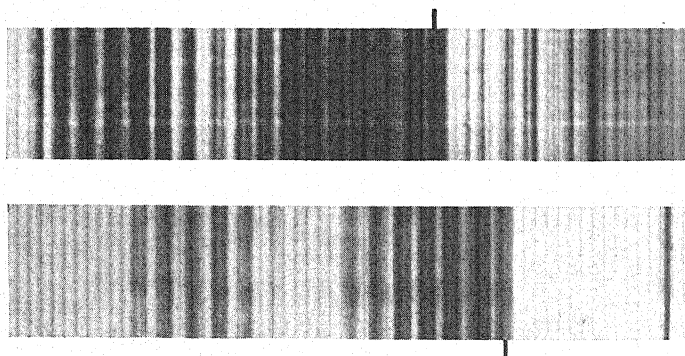


Fig. 1.

The band, the wave-length of which is given as 5552 in Table II and 5556 in McLennan, Ireton and Thomson's paper, probably corresponds to the second head of the $B_{16}-A_{12}$ band. This is in agreement with the results of a long series of experiments in nitrogen, and in nitrogen-oxygen mixtures, in which the writer has produced highly selective excitation of single heads of the first-positive group, and, what is even more interesting, single heads which correspond to radiations observed in the auroral spectrum and in the spectrum of the night-sky. Thus, it is possible for the first time to definitely identify certain auroral and night-sky radiations as nitrogen bands and also to show such marked variations in the appearance of this group of bands that the correlation of this group with the luminescence spectrum appears quite reasonable.

The band $B_{12}-A_8$, shown in Fig. 1, will illustrate the emission of single-heads in the writer's aurora experiments. It will be noted that the third head is very strong on one plate and almost missing on the other plate which was obtained from an ordinary discharge. This adds to other convincing demonstrations of the very striking variations that can be produced in the band spectrum of nitrogen.

The luminescence band N_4 at 5945A can be compared with an auroral band at 5945 and also with a first-positive band. Bands have been reported in the auroral spectrum¹⁸ at 5929A and 5945A, and various writers have suggested that these bands were first-positive bands. Since no evidence has existed until now, regarding the significance of single-headed excitation of these bands, no one was willing to be very definite regarding the identification of the so-called nitrogen bands in the aurora and perhaps in other astrophysical spectra, and such identifications have even been regarded as incorrect.¹⁹ The 5945A band in the luminescence is accompanied by two weak components at 5939A and 5932A, and these three wave-lengths correspond to within 1A to the second, third, and fourth heads of the 5959 band B_8-A_4 . It is really very nice once again to have the second head, the strongest head in the group, as was the case for the $B_{16}-A_{12}$, $B_{15}-A_{11}$ and the $B_{14}-A_{10}$ bands in the auroral experiments, and for the $B_{16}-A_{12}$ and the $B_{14}-A_{10}$ bands in the luminescence spectrum.

The luminescence band at 6187A can be identified either as the B_4-A_0 band at 6187 or the $B_{12}-A_8$ band at 6185. Since the $B_{12}-A_8$ band was used previously to show the enhancement of the weakest of the four heads, it is tempting to identify the 6187 bands as $B_{12}-A_8$. However the luminescence band 8535 corresponds very closely to the B_3-A_2 band 8541, and the luminescence band 6725 might quite readily be a part of the B_5-A_2 band at 6704. (Strong single heads are often excited on the long wave-length side of the first head.) Thus, for no other reason than to fill the gap, the 6187 band should be identified as B_4-A_0 . This procedure is especially tempting when one notes that Slipher²⁰ has obtained radiation in the light of the night-sky at 6870A, and this is without a doubt the band B_3-A_0 at 6875. He has also reported a band at 7270A which is very close to the B_6-A_4 band at 7273. It may be mentioned that Slipher has recently reported bands in the absorption spectra of the major planets at 6190, 7265 and 6467. Now 6468 is the first head of the B_8-A_5 band and the B_8-A_4 band is 5959, three heads and fourth of which make up the 5945 band in the solid luminescence, and the second heads of which appear in the aurora. To summarize briefly, the 6187 (or 6190) band appears in the first-positive group, the solid luminescence and in planetary absorption spectra. The 7265 (7270, 7273) band appears in the light of the night-sky, planetary absorption and first-positive group. The 6465 band appears in the same three spectra as the 6187 band. The meaning of these remarkable relationships between four such totally different phenomena will be discussed in other papers.

We come now to the band N_3 , which extends from 6360 to 6500, and has a maximum of intensity at 6400A. This range includes not only the 6465 band, which was discussed above, but also the 6394 band and part of the $B_{10}-A_7$ band at 6323. Now the 6323 band has been observed both in the aurora and in the light of the night-sky, so that the notion of correlating the

¹⁸ McLennan, Proc. Roy. Soc. 120, 334 (1928).

¹⁹ Sommer, Zeits. f. Physik 57, 582 (1929).

²⁰ Slipher, Ast. Soc. Pac. 41, 262 (1929).

6323 and the 6465 bands with the N_3 band is not at all unreasonable. McLennan, Ruedy and Anderson²¹ have shown that in the active nitrogen which is produced in a mixture of argon and nitrogen, containing only one-half percent nitrogen, the glow consists of the three bands 6394, 6469 and 6545 only. The normal afterglow in pure nitrogen does not include any of these bands except with very feeble intensity, so that the effect of argon must be a very violent one. Other writers have usually explained this effect by saying that the effect of the argon is to simply increase the population of the levels upon which the three bands originate. That this explanation is an insufficient one is seen readily when one considers that the 6394 band is B_9-A_6 , and that B_9-A_5 and other usually strong members of the progression which arise on B_9 are absent. This is an effect that cannot be explained merely as the result of a change in population in the B_9 level, and, as the writer has shown, it must be due to an enhanced interaction between the B_9 level and a new level in the molecule, for example, a Heitler and London level. The overlapping of N_3 and these three "ultimate" nitrogen bands, as well as the fact that the 5945 band, N_4 , has been correlated with the B_8-A_4 band 5959, can be presented therefore as evidence for the above identification.

Two of the luminescence bands N_2 and N_4 have appreciable periods of decay, whereas the band N_1 vanished the instant the source of excitation was cut off. The analogy here with the afterglow of active nitrogen is quite striking, especially so, since the same group of bands is present in both. Here, as well as in the nitrogen afterglow, two bands which originate on the same level can appear in the exciting discharge but not in the afterglow. Thus, for example, in the argon-nitrogen afterglow, the band B_8-A_5 was present, but B_8-A_4 was absent. In the solid luminescence, on the other hand, B_8-A_4 was present in the phosphorescence, whereas B_8-A_5 was absent. In both experiments, however, each one of these bands appeared in the exciting discharge. Further study will be needed in order to completely understand this rather interesting phenomenon.

VI. NEW NITROGEN BANDS

In addition to the bands which have been discussed, there are others for which no ready correlation with known nitrogen systems has been found. There are, however, other possibilities in nitrogen which may help to explain these bands. They may correspond to an intercombination system, in which case any attempts to explain them would be premature in view of the uncertainty regarding the absolute values of the energy levels of the triplet systems in nitrogen. In calling attention to the existence of these bands in the luminescence of solid nitrogen we wish at the same time to point out the fact that their existence indicates that there must be some undiscovered nitrogen bands in the visible and in the near ultraviolet. The relatively recent discovery by Hopfield of a system of bands in the ultraviolet gives us some hope that much more remains to be discovered in the spectrum of the nitrogen molecule.

²¹ Proc. Roy. Soc. 120, 334 (1928).

VII. DISCUSSION

A very interesting consequence of the method used in this paper to explain some of the second-positive bands, is a fairly good identification for two unknown radiations in the auroral spectrum. These two lines or bands have wave-lengths of 3208Å and 3432Å and are the only two unexplained radiations in the aurora which fall in that region of the spectrum. A simple calculation predicts that the C_8-B_7 band in the second-positive group should have a frequency of $31,153\text{ cm}^{-1}$, and that the C_5-B_6 transition should correspond to $29,160\text{ cm}^{-1}$. The two bands given above correspond to $31,166\text{ cm}^{-1}$ and $29,138\text{ cm}^{-1}$, respectively, thus giving some evidence in favor of the suggestion that the two aurora radiations are second-positive bands.

McLennan, Ireton and Samson² have discussed briefly the possibility that a small amount of hydrogen could be responsible for the luminescence spectrum attributed to solid nitrogen. Their supposition is based on the fact that a small quantity of a metal in solid solution in a diluting medium, is often responsible for the phosphorescent spectrum. A similar fact is true for gases; for example, in mixtures of argon and nitrogen or helium and nitrogen, in which only small amounts of nitrogen are present, the afterglow is a very strong and highly modified afterglow of nitrogen. Therefore, the doubt cast by McLennan and his collaborators, on the origin of the luminescence in solid nitrogen, is worth mentioning. It is, however, not a very serious one, in view of the striking correlation between the luminescence spectrum and the spectrum of gaseous nitrogen.

At this point it is worth while calling attention to another work of McLennan, Samson and Ireton²² in which they describe the results of irradiating solid argon with cathode rays. They found a great similarity between the spectrum of solid argon and that of solid nitrogen, which led them to the conclusion that hydrogen was responsible in both cases for the luminescence. It is more probable that the solid argon contained enough nitrogen so that it was a reproduction in the solid state, of the argon-nitrogen gas mixtures, which yield such beautiful and highly modified afterglows. In the case of the gaseous mixture the modifications which are introduced are so radical that it is not surprising to find that in the spectrum of solid argon, the nitrogen bands are slightly different from those in solid nitrogen. The experiments in solid argon should be repeated and it would also be of considerable interest to obtain the solid luminescence of known mixtures of argon and nitrogen.

It will be of some interest to recall briefly the Raman scattering experiments of McLennan and McLeod,²³ in which they obtained modified scattering from liquid oxygen, nitrogen and hydrogen, corresponding to vibrational and to rotational changes in those molecules. The magnitudes of the displacements agreed well with those that would be obtained from gases and the displaced lines were sharp. Since the intermolecular forces produce very small changes in the molecular energy levels, it is not surprising that there is such a clear relationship between the spectra of solid and gaseous nitrogen.

²² McLennan, Samson and Ireton, Roy. Soc. Canada Trans. **23**, 25 (1929).

²³ McLennan and McLeod, Nature **123**, 160 (1929).

The purpose of this paper has been to account in some way for the radiations emitted by solid nitrogen and this has been done. In closing, we wish to recall the many striking phenomena with which the first-positive bands of nitrogen have been connected, in this paper. These are, the spectrum of active nitrogen, the auroral spectrum, the light of the night-sky, planetary absorption spectra, and, finally, the spectrum of solid nitrogen. A general reason for the extreme modifications which this group of bands can undergo lies in the large number of Heitler and London (and possibly other) levels which lie in the energy range in which these bands arise. More will be said about this point in other communications.

Products of Dissociation in Nitrogen

By JOSEPH KAPLAN

University of California at Los Angeles

(Received August 17, 1932)

Use is made of four regions of predissociation in the triplet band systems of nitrogen in order to determine the products of dissociation from the known triplet states. Mulliken's proposal that the products of dissociation in the ${}^3\Sigma\mu^+$ level are two 4S atoms does not agree with the evidence which is presented here. This evidence proves that the products are a 4S and a 2D atom. The bearing of these results on the heat of dissociation of nitrogen is briefly discussed.

IT IS the purpose of this note to present experimental evidence showing that the ${}^3\Sigma$ level of nitrogen (lower level of the well-known first-positive bands) dissociates into a 4S atom and a 2D atom. These products of dissociation are not in agreement with the ones recently proposed by Mulliken,¹ according to whom the products of dissociation are two 4S atoms. We will also discuss the products of dissociation from the other triplet states of nitrogen.

Naudé's² recent analysis of the first-positive bands shows that the lower state of these bands must be a ${}^3\Sigma\mu^+$ state, and Mulliken has identified it as one of the states which can be obtained from two 4S atoms. The vibrational levels of the ${}^3\Sigma\mu^+$ state have been followed to 2.1 volts above $v=0$, so that the heat of dissociation into two unexcited atoms must be equal to or greater than 2.1 volts plus the energy of $v=0$ of ${}^3\Sigma\mu^+$ to which we will sometimes refer as A_0 . Recent experimental evidence has indicated that the heat of dissociation into normal atoms must be lower than the value of 9.1 volts, which has been proposed by Birge³ and others,^{4,5,6} probably as low as 8.2 volts. The ${}^3\Sigma\mu^+$ level must therefore be no higher than $9.1 - 2.1 = 7.0$ volts, and it may even be as low as $8.2 - 2.1 = 6.1$ volts, provided Mulliken's suggestion as to the products of dissociation is correct. The 6.1 volt value seems to be extremely low when compared with Sponer's 8.2 volt value for that energy.

We will now present the argument which will show that the products of dissociation of the ${}^3\Sigma\mu^+$ state are a 2D and a 4S atom. Elsewhere,⁷ we have called attention to the phenomenon of missing heads in the first-positive bands in nitrogen, and this was ascribed to predissociation of the molecule. The effect is beautifully shown in bands which originate on $v=13, 14, 15$ of the

¹ Mulliken, *Rev. Mod. Phys.* **4**, 53 (1932).

² S. M. Naudé, *Proc. Roy. Soc.* **136**, 114 (1932).

³ Birge, *T. Faraday Soc.* **25**, 713 (1929).

⁴ Kaplan, *Proc. Nat. Acad.* **15**, 226 (1929).

⁵ Tate and Lozier, *Phys. Rev.* **39**, 224 (1932).

⁶ Sutton, *Nature* **130**, 132 (1932).

⁷ Kaplan, *Phys. Rev.* **37**, 1406 (1931).

$^3\Pi_g$ upper state of the first-positive bands. The one head, which does appear with any appreciable intensity, is very weak compared with the intensity of the corresponding head of the normal neighboring bands. Now the energy of $v=13$ is about 3.6 volts higher than the energy of $v=0$ of $^3\Sigma\mu^+$ and since strong predissociation occurs at this energy, it is certainly equal to or greater than the energy required to dissociate the molecule into two atoms. It is of course impossible to give the exact value of D in terms of the energy of $^3\Sigma\mu^+$ and this 3.6 volt value, because we cannot say definitely what the setting in of predissociation at $v=13$ means. The energy of $v=13$ may correspond very closely to the energy required to dissociate N_2 into two particles and again it may be somewhat larger.

There is another region of predissociation, however, similar to the one at $v=13$, and this region of single-headed bands begins at $v=20$. The difference between $v=20$ and $v=13$ is about 1.1 volts, and the difference between the $^2P(3.56)$ and $^2D(2.37)$ metastable states of atomic nitrogen is about 1.2 volts. The agreement between the two values suggests that the first region of predissociation involves a 2D atom, and that the second region involves a 2P atom. The only reasonable interpretation of the above results is that the first region corresponds to dissociation into a 4S and a 2D atom, and that the second region corresponds to dissociation into a 4S and a 2P atom. Hence, if A_0 is the energy of $v=0$ of $^3\Sigma\mu^+$, then $D \leq A_0 + 3.6 - 2.37 = A_0 + 1.2$ volts.

The predissociation at $v=13$ can also be compared with the predissociation at $v=4$ in the initial $^3\Pi$ state of the second-positive bands. The bands which arise in $v=4$ are the last ones of a sequence; there are no bands originating on $v=5$ or higher. This sudden curtailment of the band system is ascribed to predissociation. The energy of $v=4$ is 5.76 volts higher than the energy A_0 , so that if $D \leq A_0 + 1.2$, the energy $A_0 + 5.76$ volts must correspond to dissociation into two 2D atoms, since that would require an energy of $D + 2(2.37)$ or $A_0 + 5.94$ volts. The agreement between the calculation and the experiment is quite good since in order to compare with the previously discussed predissociation we should use the energy of $v=5$ rather than that of $v=4$. The energy of $v=5$ is about $A_0 + 5.95$ volts, so the agreement in this case is almost perfect.

The energy of the $v=5$ level of the initial state of the second-positive bands is about $A_0 + 5.95$ volts, and the energy in $v=13$ is $A_0 + 3.6$ volts. The difference between these two is 2.35 volts, and the energy of 2D is 2.37 volts. This remarkable agreement certainly indicates that our arguments are consistent and probably correct.

The initial state of the fourth-positive group of nitrogen is the so-called D level, and only the $v=0$ level has ever been observed. The energy of the $v=1$ level is about $A_0 + 6.9$ volts, and the energy required for the production of a 2D and a 2P atom is equal to or less than $A_0 + 1.2 + 2.37 + 3.56$, i.e., $A_0 + 7.1$ volts. It seems reasonable once more to assign the non-appearance of higher vibrational levels to predissociation. It should be noted that we have made no use of an actual value for the energy of A_0 , since this energy is known only by electron impact measurements. A strong point in the present argument lies in the fact that we have made no use of this value.

We concluded from the first example of predissociation, namely, the one at $v=13$ in $^3\Pi_g$, that the heat of dissociation D was equal to or less than $A_0 + 1.2$ volts. Since the $A^3\Sigma\mu^+$ level has been followed to at least 2.1 volts of vibrational energy, it must be concluded that the products of dissociation are not two 4S atoms as Mulliken suggested, but that at least one excited atom is involved.

If we assume that D lies between 9.1 and 8.2 volts, then A_0 will lie between 7.9 and 7.0 volts, if the products of dissociation in $v=13$ are 4S and 2D . If we assume with Mulliken that the products of dissociation in $^3\Sigma\mu^+$ are two 4S atoms, then D cannot be equal to $A_0 + 1.2$ volts, since the vibrational levels have been followed to $A_0 + 2.1$ volts. We must conclude then that the predissociation at $v=13$ corresponds to dissociation into two 4S atoms, and D will be equal to or less than $A_0 + 3.6$. This would yield values for A_0 lying between 5.5 and 4.6 volts, and it is obvious that not even excitation potential measurements would account for the enormous difference between these values and the 8.2 volt value of Sponer. We must conclude that the products of dissociation from the $^3\Sigma\mu^+$ level are 4S and an excited atom, probably 2D . The triplet level due to two 4S atoms is therefore not known, and it will be an interesting problem to try to obtain evidence for its existence.

The predissociation phenomena which have been discussed in this note, enable us to suggest the identity of the products of dissociation from the several triplet states of N_2 . We have proved that the $^3\Sigma\mu^+$ level dissociates into an excited atom and a normal atom, and if we say that, in general, a linear extrapolation of the vibrational levels yields a value of the total energy which is too high, then there is no choice for the excited atom but the 2D metastable state. The linear extrapolation yields a value of 11.9 volts, and predissociation sets in at 11.8 volts, and this makes $D \leq 9.4$ volts. For the B level the linear extrapolation yields 14.62 volts, and if we use the 9.4 volt value for D the energy required to produce two 2D atoms is 14.2 volts, hence the identity of the products of dissociation as two 2D atoms is quite reasonable. For the C level, the products cannot be two 2D atoms because predissociation sets in at that energy in a manner which shows that higher vibrational levels exist. The linear extrapolation yields a value of 14.62 volts for the total energy, and 15.3 volts are required to produce one 2D and one 2P atom. This is therefore an exceptional case in which the linear extrapolation must be too low.

TABLE I.

Predissociating level	Energy based on $A_0=8.2$	Products of dissociation	Heat of dissociation
B_{13}	11.78	$^4S + ^2D$	9.4 or less
B_{20}	12.87	$^4S + ^2P$	9.3 " "
C_5	14.14	$^2D + ^2D$	9.4 " "
D_1	About 15.05	$^2D + ^2P$	9.1 " "

The results of this paper are summarized in Tables I and II. The derived values of D are obviously too high in most cases because predissociation sets in at an energy in general higher than that required to dissociate the molecule.

TABLE II.⁸

Birge	9.04 ± 0.2 volts
Kaplan	9.0 "
Tate and Lozier	8.4 ± 0.5 volts
(corrected by Sutton)	9.0 volts

This is in good agreement with Table II of recent values of D , taken from a letter by Sutton.⁸ The evidence indicates that D is probably slightly less than 9.0 volts because the data of Table I are based on Sponer's 8.2 volt value for A_0 , and all of these values will have to be lowered by the same amount as the 8.2 volt value is lowered. Even though no definite conclusion can be drawn regarding the value of the heat of dissociation of nitrogen it is clear from this paper that the upper limit is about 9.3 volts, and probably even lower, because the 8.2 value of Sponer is too high.

⁸ Sutton, Nature 130, 132 (1932).

Momentum Relations in Crossed Fields

By LEIGH PAGE

Sloane Physics Laboratory, Yale University

(Received July 9, 1932)

It is shown that the mechanical linear or angular momentum gained by ions moving in crossed electric and magnetic fields is at the expense of the electromagnetic linear or angular momentum already present. Hence Ross Gunn's theory of the acquisition of angular momentum by a star as the result of ion motions in its external electric and magnetic fields cannot be upheld.

Three cases are analyzed in detail: (a) Newtonian motion in uniform crossed fields, (b) Newtonian motion in the field of a uniformly magnetized charged sphere, (c) relativity motion in uniform crossed fields.

DURING the last three years Ross Gunn¹ has developed a promising theory of the formation of double stars and of planetary systems based on electromagnetic forces rather than on conventional gravitational attractions. While many of the features of his theory are undoubtedly significant, it will be shown that the mechanism which he invokes to account for the angular momentum of a star would not give rise to the effect which he anticipates. Gunn supposes that a star has combined electric and magnetic fields similar to those of the earth. Ions formed in its atmosphere acquire momentum in the direction of the vector $\mathbf{E} \times \mathbf{H}$, as shown in an earlier paper of the writer.² This momentum, which is in the same sense for ions of opposite signs, is transferred to the star as a consequence of collisions and gives rise to a continuing increase in the angular momentum of that body until finally fission occurs.

In a lecture some thirty years ago J. J. Thomson pointed out that outside a uniformly magnetized charged sphere there exists a Poynting flux everywhere in the direction of the parallels of latitude. This implies the presence of energy and momentum circulating around the axis of the sphere without ever departing from it. While this phenomenon leads to no predictions embarrassing to electromagnetic theory, no particular significance appears to have been attached to it. In the course of this paper it will be shown that this flux of momentum plays a very vital role in connection with the motion of ions in the atmosphere of a star.

While certain fundamental theorems of electrodynamics prove that the laws of conservation of both linear and angular momentum hold for an isolated electromagnetic system provided account is taken of both electromagnetic and mechanical momentum, and therefore that Gunn's argument

¹ Ross Gunn, *Phys. Rev.* **32**, 133 (1928); **33**, 614, 832 (1929); **34**, 335, 1621 (1929); **35**, 107, 635 (1930); **36**, 1251 (1930); **37**, 283, 983, 1129, 1573 (1931); **38**, 1052 (1931); **39**, 130, 311 (1932).

² Page, *Phys. Rev.* **33**, 553 (1929).

cannot be upheld, we shall investigate here the details of the process by which these laws are satisfied in some simple cases, including the case of a uniformly magnetized charged sphere in whose atmosphere ions are present.

A. UNIFORM CROSSED FIELDS

Consider a uniform electric field E in the direction of the y axis of a set of right-handed rectangular axes x, y, z combined with a uniform magnetic field H in the direction of the z axis. Then, as shown in an earlier paper,² ions of both signs progress in the x direction with a drift velocity cE/H which is independent of the charge or mass of the ion. The ion paths are cycloids, being prolate, common or curtate in accord with the magnitude and direction of the initial velocity. The cycloidal paths for the negative ions are obtained from those for the positive ions by rotating the latter through the angle π about the x axis. The integrated equations of motion are³

$$\begin{aligned} x - x_0 &= \frac{mc}{e} \left\{ \frac{v_{0y}}{H} \left(1 - \cos \frac{eH}{mc} t \right) + \left(\frac{v_{0x}}{H} - \frac{cE}{H^2} \right) \sin \frac{eH}{mc} t \right\} + \frac{cE}{H} t, \\ y - y_0 &= \frac{mc}{e} \left\{ - \left(\frac{v_{0x}}{H} - \frac{cE}{H^2} \right) \left(1 - \cos \frac{eH}{mc} t \right) + \frac{v_{0y}}{H} \sin \frac{eH}{mc} t \right\}, \\ z - z_0 &= v_{0z} t, \end{aligned}$$

where x_0, y_0, z_0 are the coordinates of the starting point and v_{0x}, v_{0y}, v_{0z} the components of the initial velocity.

Differentiating the first of these we find for the x component of the momentum

$$p_x = m \left\{ v_{0y} \sin \frac{eH}{mc} t + \left(v_{0x} - \frac{cE}{H} \right) \cos \frac{eH}{mc} t + \frac{cE}{H} \right\},$$

and comparing with the second

$$y - y_0 = (c/eH)(p_x - p_{0x}), \quad (1)$$

where $p_{0x} = mv_{0x}$ is the x component of the initial momentum.

This equation states that the displacement of the ion in the direction of the electric field is proportional to the gain of momentum in the direction at right angles to the two fields, that is, in the direction of the Poynting flux. Increase in momentum involves a displacement of positive ions in the same direction as the electric field, and of negative ions in the opposite direction.

Now suppose that at a certain instant n ion pairs per unit volume are formed. Under the action of the fields they separate, acquiring at the same time momentum in the direction at right angles to the two fields. Whether they make collisions with neutral particles and thereby transfer part of their momentum to the latter or not, the total mechanical momentum generated is proportional to the separation of the ions. If Δy denotes the mean separation of the positive from the negative ions, an effective electric moment

³ Page and Adams, *Principles of Electricity*, p. 289. In the present paper we are using Heaviside-Lorentz units.

$ne\Delta y$ is set up in the region under consideration. This gives rise to an electric field of the same magnitude in the direction opposite to that originally existing. Consequently the electromagnetic momentum g per unit volume increases in the amount $\Delta g = -(1/c)ne\Delta yH$.

However, if Δp is the increase in mechanical momentum per unit volume, it follows from (1) that

$$\Delta p = neH\Delta y/c$$

and consequently

$$\Delta p + \Delta g = 0. \quad (2)$$

So the increase in mechanical momentum of the ions is at the expense of the electromagnetic momentum already present. Production of ions acts as a mechanism for converting the latter into the former. When all the electromagnetic momentum has been transformed, the electric field is reduced to zero, and no more transverse momentum is acquired by the ions. Since electromagnetic momentum is consumed in the same region of space as that in which mechanical momentum is generated, Eq. (2) applies to angular momentum about any arbitrary axis as well as to the case of linear momentum for which it was derived. However, we shall discuss in the next section the specific angular momentum relations existing in the case of a uniformly magnetized sphere which has an electric charge.

B. UNIFORMLY MAGNETIZED CHARGED SPHERE

Take origin at the center of the sphere with polar axis in the direction of magnetization. The spherical coordinates consisting of the radius vector r , polar angle θ and azimuth ϕ are chosen so as to constitute a right-handed set in the order named. If Q is the charge on the sphere and M its magnetic moment, the nonvanishing field components are

$$E_r = \frac{Q}{4\pi r^2}, \quad H_r = \frac{2M}{4\pi r^3} \cos \theta, \quad H_\theta = \frac{M}{4\pi r^3} \sin \theta,$$

and the equation of motion of an ion with charge e and mass m is

$$mf = e\{E + (1/c)v \times H\},$$

which is equivalent to the three component equations

$$\begin{aligned} \ddot{r} - r\dot{\theta}^2 - r\sin^2\theta\dot{\phi}^2 &= \frac{e}{4\pi m} \left\{ \frac{Q}{r^2} - \frac{M}{cr^2} \sin^2\theta\dot{\phi} \right\}, \\ 2\dot{r}\dot{\theta} + r\ddot{\theta} - r\sin\theta\cos\theta\dot{\phi}^2 &= \frac{e}{4\pi m} \left\{ \frac{2M}{cr^2} \sin\theta\cos\theta\dot{\phi} \right\}, \\ 2\sin\theta\dot{r}\dot{\phi} + 2r\cos\theta\dot{\theta}\dot{\phi} + r\sin\theta\ddot{\phi} &= \frac{e}{4\pi m} \left\{ \frac{M}{cr^3} \sin\theta\dot{r} - \frac{2M}{cr^2} \cos\theta\dot{\theta} \right\}. \end{aligned}$$

The third equation is the significant one for our purposes. It can be written

$$\frac{d}{dt}(r^2 \sin^2 \theta \dot{\phi}) = -\frac{eM}{4\pi mc} \frac{d}{dt} \left(\frac{\sin^2 \theta}{r} \right),$$

or, if we put $p \equiv m r^2 \sin^2 \theta \dot{\phi}$ for the angular momentum of the ion about the axis of the sphere,

$$dp = - (eM/4\pi c) d(\sin^2 \theta / r). \quad (3)$$

Next we must calculate the change in electromagnetic angular momentum due to motion of the ion. To do this we shall first compute the electromagnetic angular momentum of an isolated system (Fig. 1) consisting of a point pole m and a point charge e . It is evident from symmetry that the resultant angular momentum is entirely about the line connecting m to e . As

$$E = e/4\pi\rho^2, \quad H = m/4\pi r^2,$$

the component of angular momentum parallel to this line is

$$g = - (me/16\pi^2 c r \rho^2) \sin \theta \sin \alpha$$

per unit volume. Therefore the total angular momentum can be written

$$G = - \frac{mea}{8\pi c} \int_0^\infty \int_0^{2\pi} \frac{r \sin^3 \theta}{\rho^3} d\theta dr$$

if we eliminate α by the relation $\rho \sin \alpha = a \sin \theta$. First we shall integrate with respect to θ , keeping r constant. In doing this it will be convenient to change

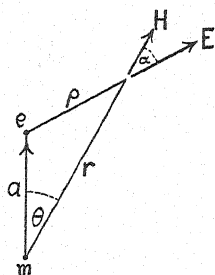


Fig. 1.

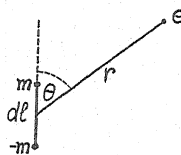


Fig. 2.

the variable of integration to ρ by means of the relation $\rho^2 = r^2 - 2ar \cos \theta + a^2$. We have then

$$\begin{aligned} ar \int \frac{\sin^3 \theta}{\rho^3} d\theta &= \int \left\{ 1 - \left(\frac{r^2 + a^2 - \rho^2}{2ar} \right)^2 \right\} \frac{d\rho}{\rho^2} \\ &= \left\{ \frac{(r^2 - a^2)^2}{4a^2 r^2} \frac{1}{\rho} + \frac{r^2 + a^2}{2a^2 r^2} \rho - \frac{1}{12a^2 r^2} \rho^3 \right\}. \end{aligned}$$

When $r < a$ the limits of ρ are $a - r$ and $a + r$, whereas when $r > a$ the limits are $r - a$ and $r + a$. For the first region

$$G_1 = - \frac{me}{6\pi a^2 c} \int_0^a r dr = - \frac{me}{12\pi c},$$

and for the second

$$G_2 = -\frac{mea}{6\pi c} \int_a^\infty \frac{dr}{r^2} = -\frac{me}{6\pi c}.$$

Adding, the total electromagnetic angular momentum is found to be

$$G = G_1 + G_2 = -me/4\pi c. \quad (4)$$

At first sight it seems strange that the angular momentum should be independent of the distance a between the charge and the pole. A little consideration, however, shows that this is to be expected. For if the charge is projected directly toward the pole the magnetic field exerts no force on it and its mechanical angular momentum along the line joining the two remains constant. So the electromagnetic angular momentum should be independent of a .

The magnetic field in which we are interested is that of a dipole. If the line joining the center of the dipole to the charge e (Fig. 2) has a length r and makes an angle θ with the axis of the dipole, the component of the electromagnetic angular momentum of the system along the axis of the dipole is

$$G = -\frac{me}{4\pi c} d(\cos \theta) = \frac{me}{4\pi c} \sin \theta d\theta.$$

Now if dl is the length of the dipole, $d\theta = dl \sin \theta/r$, and

$$G = (eM/4\pi c)(\sin^2 \theta/r), \quad (5)$$

where M is the magnetic moment mdl of the dipole. Comparing (5) with (3) we have

$$dp + dG = 0. \quad (6)$$

This equation shows that any gain in mechanical angular momentum by an ion is accompanied by an equal loss in electromagnetic angular momentum. Suppose that the uniformly magnetized sphere is initially uncharged electrically and that ions of one sign (electrons, for instance) are projected toward it from a great distance, the impinging ions having on the average no initial angular momentum about the axis of the sphere. When these ions strike the sphere they impart to it mechanical angular momentum in one sense while giving rise to an equal amount of electromagnetic angular momentum in the opposite sense. If, after the sphere has been charged by the impacting ions, ion pairs are formed in its atmosphere, the action of these ion pairs is to transform the electromagnetic angular momentum into mechanical angular momentum until finally the mechanical angular momentum imparted by the ions impinging from outside is just annulled. Therefore the electromagnetic process postulated by Gunn cannot lead to a continuing increase in mechanical angular momentum of the sphere.

If we replace the point pole by a finite sphere of magnetic charge in deducing (4) we are led to a different result, obtaining in addition to the term appearing on the right-hand side of that equation a second term containing

in the denominator the square of the distance a between the center of the sphere and the point charge. This additional term remains when we superpose two slightly displaced spheres of opposite sign so as to construct a uniformly magnetized sphere. Its presence is due to the fact that we erroneously employ H inside the magnetized sphere in calculating the electromagnetic momentum when we should in fact make use of B . The added term disappears when this error is corrected, and (5) is found to hold rigorously for a uniformly magnetized sphere as well as for a magnetic dipole. The analysis, which is somewhat laborious, will not be reproduced here.

C. RELATIVITY DYNAMICS

The preceding analysis is inapplicable to the case where the ions have velocities comparable with the velocity of light. In such an event the variation of mass with velocity must be taken into account. We shall develop the theory for the case of uniform crossed fields on the relativity dynamics.

As before we shall take E in the direction of the y axis and H in that of the z axis of a right-handed set of rectangular axes fixed in the observers' inertial system S . In addition we shall have occasion to refer to a set of parallel axes x', y', z' located in an inertial system S' moving in the x direction relative to S with the constant velocity $u = cE/H$. As shown in a previous paper² the electric field vanishes in S' and the ions describe helices around the lines of magnetic force with angular velocity

$$\omega' = -eH'/m_t c,$$

where m_t is the transverse mass. If v_0' is the initial velocity of an ion relative to S' , the components of velocity at any time t' are

$$v_x' = v_{0x}' \cos \omega' t' - v_{0y}' \sin \omega' t',$$

$$v_y' = v_{0x}' \sin \omega' t' + v_{0y}' \cos \omega' t',$$

$$v_z' = v_{0z}'.$$

Now the displacement of an ion along the electric field is

$$\begin{aligned} y - y_0 &= y' - y_0' = (1/\omega') \{v_{0x}'(1 - \cos \omega' t') + v_{0y}' \sin \omega' t'\} \\ &= -(1/\omega')(v_x' - v_{0x}'). \end{aligned}$$

Making use of the relativity transformations for the components of velocity,

$$y - y_0 = -\frac{1}{\omega'} \left\{ \frac{v_x - u}{1 - \beta \frac{v_x}{c}} - \frac{v_{0x} - u}{1 - \beta \frac{v_{0x}}{c}} \right\},$$

where $\beta \equiv u/c$ is the ratio of the relative velocity of the two inertial systems to the velocity of light. Now

$$v_x'^2 + v_y'^2 + v_z'^2 = v_{0x}'^2 + v_{0y}'^2 + v_{0z}'^2 \equiv v'^2$$

since the speed relative to S' does not change with the time. Transforming to system S we find

$$\frac{(1 - v^2/c^2)^{1/2}}{1 - \beta v_x/c} = \left(\frac{1 - v'^2/c^2}{1 - \beta^2} \right)^{1/2} \equiv \text{constant}.$$

Also

$$-\frac{1}{\omega'} = \frac{m_e c}{e H'} = \frac{m_0 c}{e H} \frac{1}{[(1 - \beta^2)(1 - v'^2/c^2)]^{1/2}},$$

where m_0 is the rest mass of the ion.

Therefore

$$\begin{aligned} y - y_0 &= \frac{m_0 c}{e H} \frac{1}{1 - \beta^2} \left\{ \frac{v_x - u}{(1 - v^2/c^2)^{1/2}} - \frac{v_{0x} - u}{(1 - v_0^2/c^2)^{1/2}} \right\} \\ &= \frac{c}{e H} \frac{1}{1 - \beta^2} \left\{ p_x - p_{0x} - \frac{u}{c^2} (T - T_0) \right\} \end{aligned}$$

where p_x is the momentum and T the kinetic energy of the ion. Now

$$(u/c^2)(T - T_0) = (\beta/c)eE(y - y_0) = (eH/c)\beta^2(y - y_0).$$

Solving for $y - y_0$, we find identically the same relation

$$y - y_0 = (c/eH)(p_x - p_{0x}) \quad (7)$$

between the displacement along the electric lines of force and the gain in momentum at right angles to the two fields as was obtained on the Newtonian dynamics. Therefore electromagnetic momentum is converted into mechanical momentum by ions produced in the atmosphere of a star or planet in precisely the same manner as in the cases previously discussed.

The Effect of Strain on Magnetostriction and Magnetization in Nickel

By C. W. HEAPS

Rice Institute, Houston, Texas

(Received June 20, 1932)

With a heterodyne beat method, magnetostrictive hysteresis loops have been obtained for a nickel wire under three different tensions. Magnetic hysteresis loops for the same wire and same tensions were also secured. The magnetostrictive contraction, dL/L , for the tensions 6.82 and 3.70 kg/mm² is given quite accurately by the one equation, $dL/L = -1.93 \times 10^{-10} I^2$, where I = intensity of magnetization. For a tension 0.72 kg/mm² the equation $dL/L = -1.30 \times 10^{-10} I^2$ holds somewhat less accurately. The effect of compression and of stretch on the residual magnetization of a nickel wire in a demagnetizing field is determined experimentally. From this experiment, and from the magnetostriction curves, it is shown that at certain field strengths the magnetism of a nickel wire, bent elastically into a circular arc, becomes unstable. Thus the large discontinuities in the magnetization curve observed by Forrer may be explained. It is suggested that the small Barkhausen jumps of magnetization may be due to similar magnetic instability produced in small regions by local strains.

THE phenomenon of hysteresis in magnetostriction has been observed by a number of investigators,¹ but a detailed study of the effect of strain on magnetostrictive hysteresis does not appear to have been made. The importance of strain, both in theories of magnetism and in experiments on particular phases of the subject, has recently been emphasized; for example, the very great influence which strains in the material may have on the Barkhausen effect or on the magnetic hysteresis loop.

The present paper reports experiments in which the magnetostrictive hysteresis loops and the magnetic hysteresis loops have been determined for a nickel wire under different tensions. Nickel was chosen for the experiments because the magnetostriction curves of a nickel crystal are not greatly affected by the orientation of the crystalline axis;² hence in a polycrystalline wire the effect of crystal size or crystal orientation should be of little importance in modifying magnetostriction. Furthermore, it is in nickel that very striking discontinuities of magnetization have been produced by strains in the material.³ The explanation of these discontinuities was one of the objects of the experiment.

THE EXPERIMENTAL METHOD

For observing magnetostriction the heterodyne beat method of measuring small capacity changes or small displacements was used. Two oscillating elec-

¹ H. Nagaoka, *Phil. Mag.* [5] 37, 131 (1894); L. W. McKeehan, *J. Franklin Inst.* 202, 737 (1926); A. Schulze, *Ann. d. Physik* [5] 11, 937 (1931); G. Dietsch, *Zeits. f. techn. Physik* 12, 380 (1931).

² Y. Masiyama, *Sci. Rep. Tohoku Imp. Univ.* [1] 17, 945 (1928).

³ R. Forrer, *J. de Physique* [6] 7, 109 (1926); 10, 247 (1929).

trical circuits have their beat note (of audiofrequency) picked up by a detector, amplified, and impressed upon an oscillograph. One plate of a condenser in one of the oscillating circuits is supported by the nickel wire under test. This wire is surrounded by a solenoid. If the field in the solenoid is varied the length of the nickel wire changes, thus changing the capacity of the oscillating circuit. The frequency of the heterodyne beat note is therefore altered by an amount which can be determined from the oscillograph record. From a knowledge of the calibration constant of the apparatus the change of length of the wire may thus be calculated. Details of the electric circuits have been described elsewhere.⁴

Fig. 1 shows the arrangement of the condenser, the capacity of which is changed by the magnetostriction of the nickel. This condenser is connected in parallel with an adjustable precision condenser which was set to have the same large capacity throughout the experiment. The upper plate *B* has a

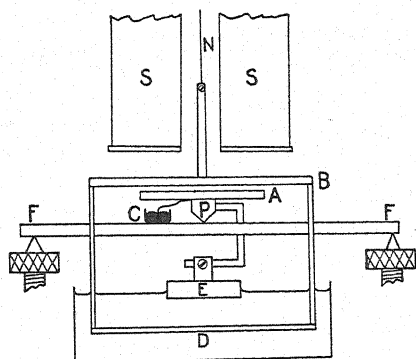


Fig. 1. Arrangement of condenser in the magnetostriction apparatus.

diameter 5 cm and is connected to earth through the nickel wire *N*. Three light, vertical rods, of which two are shown, are fixed to the edge of the upper plate and support a flat ring *D* of aluminum, immersed in oil to serve as a damping fluid. Plate *A*, of diameter 2 cm, is insulated by Bakelite from the point support *P* and counterbalance *E*. A wire from this plate dips into the mercury cup *C* by means of which connection is made to the oscillating circuit.

The micarta cross-bar *FF*, is supported on three leveling screws, of which two are shown. These screws are used to vary the capacity of the condenser. The plate *A* is carefully leveled by adjusting the counterweight *E*, which also serves as a damping plate. Weights may be placed on top of *B* to produce tension in the wire *N*. To level *B* accurately a small, easily movable weight was carefully adjusted on the top of the plate.

The solenoid, *SS*, of which only the lower part is shown, is 30.3 cm long and has 7195 turns. It is supported on a stand separate from that which supports the wire *N*. The nickel wire is 15 cm long and 0.018 cm in diameter. It is carefully centered in the solenoid so as to be in a uniform field. The current through the solenoid may be given a series of values by opening or closing a

⁴ A. B. Bryan, Phys. Rev. [2] 34, 615 (1929); C. W. Heaps and A. B. Bryan, Phys. Rev. [2] 36, 326 (1930).

series of switches which short circuit sections of a rheostat. These switches consisted of a series of metal contacts spaced equally along a vertical micarta bar which could be pushed down into a jar of mercury. With this device it was possible to put the nickel wire through the entire hysteresis loop in only a few seconds, the successive changes of length being indicated by frequency changes on a section of oscillograph film about 10 feet long. A condenser in series with a heavily damped vibration galvanometer was connected across the switching device, so that every time the solenoid current changed, the galvanometer received an impulse which was recorded on the oscillograph film.

The oscillograph consisted of a telephone receiver to the diaphragm of which a light mirror was connected. Records were obtained on positive motion picture film and developed by the contrast developer recommended by Town.⁵ The time scale was obtained by interrupting a beam of light by the cogs in the wheel of an electric clock running on 60-cycle current. Fig. 2

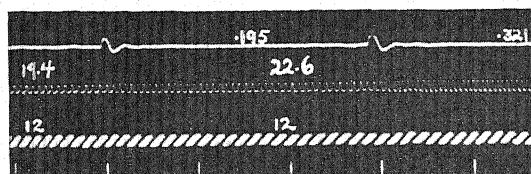


Fig. 2. Oscillograph record. Top trace = solenoid current; middle trace = heterodyne note; bottom trace = time scale.

shows a section of film. The topmost trace indicates changes of current in the solenoid, the middle trace is a record of the heterodyne beat note, the bottom trace is the time scale, each segment representing $1/60$ sec. The figure shows how the film was marked and how the frequency was determined for a given value of the magnetizing current.

To convert frequency changes into length changes it was necessary to calibrate the device. The following method was used. A leveling screw at *F* was adjusted till the heterodyne beat note emitted by the telephone receiver was in accurate tune with a tuning fork of pitch 1024. A micrometer microscope was then focussed on a fine scratch on plate *A*. By means of the leveling screw the plate *A* was now moved either up or down, so as to lower the pitch of the heterodyne note down through zero frequency and up to the frequency 1024 again. A total frequency change of 2048 was thus secured and the motion of *A* was large enough to be measured with considerable accuracy. For very small displacements of *A* (or *B*) such as were used in the experiment, it may be shown that the frequency change of the heterodyne note is proportional to the displacement. Thus the length change of the wire per cycle of frequency change is easily calculated. Throughout the experiments the value of this quantity was kept at 2.10×10^{-6} cm per cycle.

Magnetic hysteresis loops were secured by using a sensitive astatic magnetometer of the type described by Bozorth.⁶ The vertical component of the

⁵ G. R. Town, *Rev. Sci. Inst.* 1, 449 (1930).

⁶ R. M. Bozorth, *J.O.S.A. and R.S.I.* 10, 591 (1925).

earth's magnetic field was neutralized by means of Helmholtz coils, both in the magnetometer experiments and in the magnetostriction experiments. Demagnetization of the nickel could be effected by using liquid rheostats to decrease a 60-cycle alternating current through the magnetizing solenoid.

The nickel wire was cold drawn from Eimer and Amend's *pure sheet nickel*. After the drawing the wire was heated electrically to a bright red in an atmosphere of carbon dioxide, and cooled slowly by gradual decrease of the heating current. It was loaded and unloaded several times up to the limiting tension used in the experiment before any records were taken. The wire was very soft and experiments on a short sample indicated a definite yield at about 14 kg per mm². In order to keep well within the elastic limit stresses greater than 7 kg per mm² were not used during the experiment.

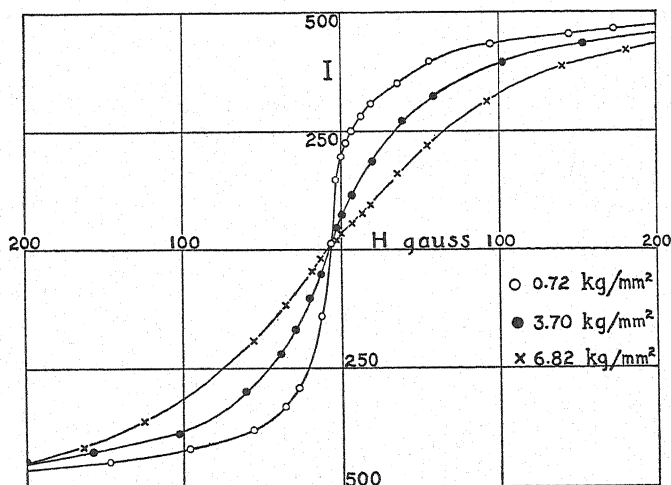


Fig. 3. The effect of tension on the descending branch of the hysteresis loop of nickel.

DISCUSSION OF RESULTS

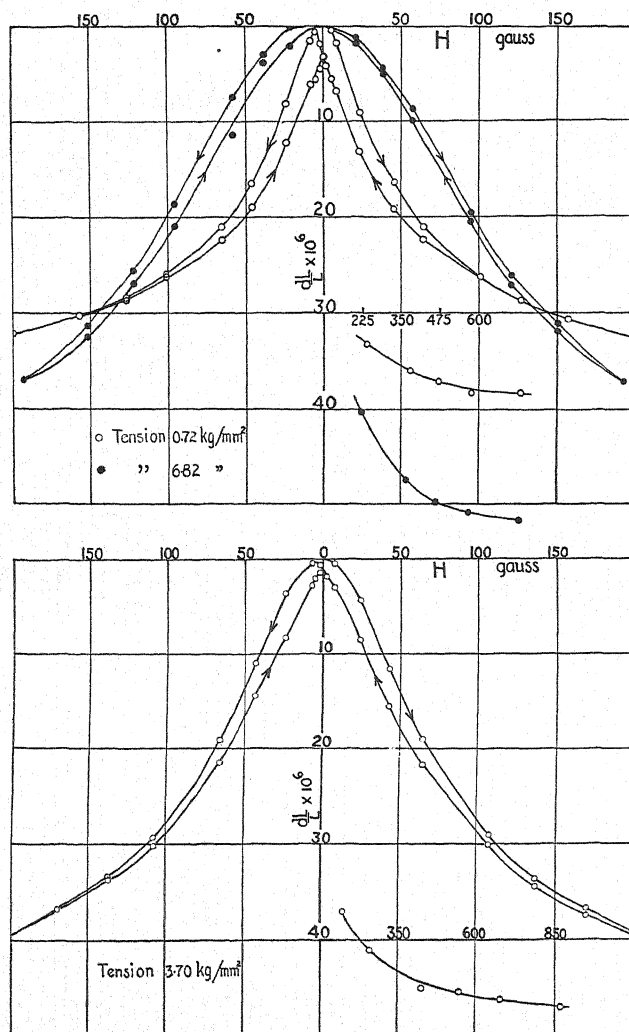
Fig. 3 shows how tension affects the magnetic hysteresis loop. These results agree, in general, with previous work.⁷ Figs. 4 and 5 show the effect of tension on magnetostriction. A point of interest here is the fact that the curves for different tensions cross at large values of the magnetic field, H . In other words, it appears that tension applied to a nickel wire will decrease the magnetostriction in small fields and increase it in large fields. Bidwell⁸ has observed a similar phenomenon. The explanation, as will appear later, lies in the way in which the intensity of magnetization varies with the field strength.

A second point of interest in connection with these curves is the effect of strain for very small fields. When the wire is loaded with 6.82 kg/mm² and saturated magnetically, the residual magnetostriction when the field is

⁷ M. Kersten, *Zeits. f. Physik* 71, 553 (1931).

⁸ S. Bidwell, *Proc. Roy. Soc.* 47, 469 (1890).

brought to zero is too small to be detected. Furthermore, a reverse field of at least 20 gauss must be applied before the magnetostriction becomes large enough to measure. The conditions are quite otherwise when the wire carries only 0.72 kg/mm². In this case the residual magnetostriction is quite large,



Figs. 4, 5. Fractional change of length, dL/L as a function of magnetic field, H .
The short segments are extensions to large fields.

and the reverse field, as it increases, causes the wire to elongate⁹ till a field of about 6 gauss is reached. At this point the residual magnetization is re-

⁹ This elongation, of course, is really a diminution of contraction produced by a decrease of residual magnetization. Deitsch (reference 1) appears to consider it as actual positive magnetostriction of nickel. There seems to be little doubt, however, but that it may be accounted for in the work of Dietsch by incomplete demagnetization of his specimen. In such a case the origin of the magnetostriction curve is improperly located.

duced to zero and for further increase of field the wire contracts. As will be noted later, this difference of behavior of stretched and unstretched nickel is of special significance in relation to discontinuities of magnetization.

In Fig. 6 the magnetostriction is represented as a function of the intensity of magnetization. The plotted points are values taken from the curves of Figs. 3, 4, and 5. The line drawn through the points and designated by *A* is the graph of the equation $dL/L = -1.93 \times 10^{-10} I^2$. It appears that for the two tensions, 3.70 and 6.82 kg/mm², the one curve *A* represents the experimental results with considerable accuracy. It is somewhat surprising that an increase of tension from 3.70 to 6.82, which produces such marked changes in the magnetic hysteresis loop and in the magnetostriction loop as plotted against the magnetic field *H*, should really have no effect on magnetostriction considered as a function of *I*.

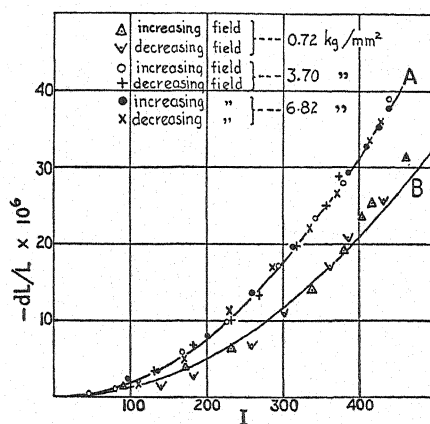


Fig. 6. Magnetostriction as a function of intensity of magnetization.

For the smallest tension the plotted points¹⁰ are somewhat irregularly distributed. The curve drawn through these points and designated by *B* is the graph of the equation $dL/L = -1.30 \times 10^{-10} I^2$. It represents to a fair approximation the experimental results. However, for small values of *I* the plotted points indicate the existence of appreciable hysteresis. The work of McKeehan and Cioffi, and of A. Schulze, seems to show that hysteresis is present in the $dL/L-I$ curves for unstrained nickel, in agreement with the present work. From Fig. 6, curve *A*, the additional conclusion may be drawn that the application of sufficiently large strains makes this hysteresis effect negligibly small.

Recently some important theoretical work has been done on the subject of magnetostriction. The theories of Akulov¹¹ and of Becker,¹² in which the energy of a strained dipole lattice is taken as the starting point, have been shown by Powell¹³ to be consistent with each other. Powell's equation for

¹⁰ The points for this curve are obtained on the assumption that $dL/L=0$ when $I=0$.

¹¹ N. Akulov, *Zeits. f. Physik* 52, 389 (1928); 59, 254 (1930); 64, 817 (1930); 69, 78 (1931).

¹² R. Becker, *Zeits. f. Physik* 62, 253 (1930); 64, 660 (1930).

¹³ F. C. Powell, *Proc. Camb. Phil. Soc.* 27, 561 (1931).

dL/L makes the effect proportional to I^2 . Powell states that his equation need not necessarily apply to values of dL/L determined experimentally because of the possibility of micromagnetization of crystals which as a whole are unmagnetized. In spite of this limitation it appears that where tension is applied to nickel the theoretical law of variation of dL/L is verified experimentally to a considerable degree of accuracy.

We may now consider why curve *A* of Fig. 6 represents equally well the data for the two large tensions. The obvious explanation is that either of the two large tensions is sufficient to produce a saturation effect. When tension is applied to nickel, current theories¹⁴ agree in supposing that the atomic magnets are orientated across the axis of tension, or that the magnetization vectors, I , of small microscopic blocks into which the nickel is divided, are so orientated. For a sufficiently large tension there is complete transverse orientation. A longitudinal magnetic field, in order to magnetize the wire to saturation, must orientate all these atomic magnets along the axis of the wire, thus causing maximum magnetostriction. When no tension is applied the atomic magnets may be initially orientated at random and the magnetic field, in lining them up, cannot produce such a large net length change because of the less favorable initial distribution of axes.

It appears from the curves of Fig. 6 that tensions of 3.70 and 6.82 kg/mm² are equally effective in producing complete transverse orientation of atomic magnets in nickel. This conclusion may be drawn because for both of these tensions we get the same magnetostriction produced by a given intensity of magnetization. On the other hand, for the tension 0.72 a considerably smaller magnetostriction is produced by this same intensity of magnetization. It is probable that the atomic magnets of the nickel under the tension 0.72 are distributed more or less at random. There will not be completely random orientation, however, even with this small tension. The quantitative working out of the theory indicates that the maximum magnetostriction under large strain should be 1.5 times the maximum magnetostriction under no strain. This ratio for tensions 6.82 and 0.72 is only 51.8/38.3, or 1.35. Apparently, therefore, the small strain has produced an appreciable transverse orientating of atomic magnets.

THE EFFECT OF STRAINS ON RESIDUAL MAGNETISM

The curves of Fig. 3 do not give a complete picture of the processes which may occur in the region of demagnetization. For example, from these curves, each obtained at constant tension, it might be concluded that compressing nickel in a demagnetizing field would increase the residual magnetism. However, since shock and vibration are known to facilitate demagnetization there might be some doubt about the correctness of this conclusion. In order to secure more detailed information regarding the region of demagnetization the following experiment was performed.

A wire of commercial nickel, 15 cm long and about 1 mm in diameter, was soldered to a strip of brass 15 cm long, 0.16 cm thick, and about 3 cm wide.

¹⁴ L. W. McKeehan, reference 1; R. Becker and M. Kersten, *Zeits. f. Physik* 64, 665 (1930).

The wire was soldered throughout its length to the brass and was parallel to the strip's long dimension. The brass strip was then suspended in a vertical solenoid beside the magnetometer, a second solenoid being arranged to balance the field of the first solenoid at the magnetometer. The effect of the magnetized nickel on the magnetometer could also be balanced by a third small solenoid. By bending the plate in one direction the nickel wire was stretched, by bending it in the opposite direction it was compressed. Furthermore, by clamping the strip with an initial bend, adjusting the demagnetizing field to the proper value, and then altering slightly the amount of bend, the effect of this small change of strain on the value of I could be determined by observing the direction of deflection of the magnetometer.

Fig. 7 gives qualitatively the results of the various experiments. Curve A is representative of compressed nickel, curve B of stretched nickel. The

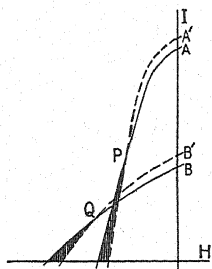


Fig. 7. The effect of strain on the intensity of magnetization of nickel in a demagnetizing field.

stretched wire has a smaller residual magnetism and a larger coercive force than the compressed nickel. The dotted curves associated with A and B indicate the effect of increasing the compression in each case.

The shaded areas represent regions where irreversible effects occur. In one case when the nickel was in a state of compression the point P was at about 8 gauss. For fields less than 8 gauss an increase of compression caused a reversible increase of residual magnetism. (However, as P was approached there was a decided tendency for irreversible decreases of magnetism to occur when the excess compression was removed.) For demagnetizing fields greater than that at P an increase of compression always caused an irreversible decrease of I . On the basis of these results the dotted curve A' was drawn as in Fig. 7.

It was found that in demagnetizing fields greater than that at P a decrease of compression produced an irreversible decrease of I . Hence the shaded area cannot be entered vertically starting from the dotted curve A' ; any attempt to enter in this way results in a drop downwards.

Very similar results were obtained with nickel when initially in a stretched condition, the curves B and B' being obtained. In one case the point Q was at about 10 gauss.

DISCONTINUITIES OF MAGNETIZATION

If a nickel wire is subjected to a bending torque its magnetization curve shows remarkably large discontinuities.¹⁵ For the production of these discontinuities it appears necessary that part of the wire be in a state of compression and part in a state of tension. If a wire with no internal strains is bent into the arc of a circle and the elastic limit not exceeded, we probably have the simplest conditions for producing these large discontinuities. In this case we may make a rough approximation and consider the wire as behaving like two wires fastened together laterally, one wire being stretched, the other compressed. The magnetic and magnetostrictive behavior of these separate wires is known from experiment, hence the behavior of the composite wire should be predictable.

Assume the composite wire magnetized to saturation in one direction and then subjected to a gradually increasing field in the opposite direction. For small values of this field we may assume from Fig. 4 that there is negligible magnetostriction of the stretched component. The compressed component of the composite wire will increase its length as the field increases. This increase of length of the compressed section tends to increase the degree of compression, since the wire will be assumed not to bend. Also, the tension of the stretched section is increased. The situation is similar to that found where a straight, bimetallic strip is used on a thermostat. As the temperature rises and the strip is not allowed to curve, one metal is increasingly compressed, the other increasingly stretched.

It is easy to show that the magnetization of such a composite wire will be stable for demagnetizing fields less than those corresponding to points *P* or *Q*, Fig. 7. In demagnetizing fields greater than these, however, there is instability. For, consider a small increase, ΔH , occurring in a shaded region of Fig. 7, and assume outside forces applied so as to keep the tensions in the two parts of the composite wire constant during this change. We then get decreases, ΔI_A , and ΔI_B , respectively, in the magnetizations of the compressed and stretched segments. However, from Figs. 3 and 7 we conclude¹⁶ that ΔI_B is much smaller than ΔI_A . Also from Fig. 4 we see that ΔH in this region produces negligible length change in the stretched segment *B*, as compared with that in the compressed segment *A*. Since the composite wire is not allowed to curve, the increase of length of *A* would produce a compressive stress in *A* and a tension in *B*, were it not for the external forces assumed to be applied. These forces are a pull on *A* and a compressive stress on *B*. Now remove these outside forces. From Fig. 7 it appears that decreases of magnetization, δI_A and δI_B , result, the value of δI_B being much less than δI_A . The effect of δI_A is to introduce magnetostrictive expansion of *A*, so that if the wire does not curve there results a compressive stress in *A* and a tensile stress in *B*. These new stresses now produce further increments of decrease of *I*.

¹⁵ R. Forrer, reference 3; M. Kersten, reference 7.

¹⁶ The curves for compressed nickel are not given in Figs. 3, 4, and 5. However, the differences between stretched and compressed nickel will be similar to the differences between stretched and unstretched nickel. The magnitude of the differences will, of course, be greater in the former case.

From the foregoing it is clear that conditions are such as to produce instability. The decrease of magnetization of the compressed segment, produced by a small increase of the demagnetizing field, introduces strains which tend to increase the magnetization change which produced them. Discontinuities of magnetization of the composite wire will thus appear for demagnetizing fields beyond the point P .

The large changes of magnetization produced by the above means would end when the strains produced by magnetostriction tend to inhibit the magnetization changes which produce them. It appears that this condition is met with as soon as all the residual magnetism is removed and I begins increasing in the direction of the field.¹⁷ In other words, a discontinuity of I , initiated above the H axis on the descending branch of the hysteresis loop, would not be expected to extend below the H axis.

It is a fact that the large Forrer discontinuities may be initiated in the demagnetization section of the hysteresis loop and that they frequently do not cross the H axis. On the other hand, there are instances where almost the entire left side of the hysteresis loop consists of a single discontinuity. It would appear, therefore, that conditions of instability must be present in many cases, even after all residual magnetization has disappeared and the I vector is increasing in the direction of the field.

Possibly it is not correct to assume, as we have done above, that nickel has its maximum length at the point where I passes through zero and begins increasing in the direction of the field. This assumption is not in agreement with the experimental work of Schulze, whose nickel begins to contract as soon as I is reduced below about 150. (It expands while I is being reduced from saturation to 150.) The curves of McKeehan and Cioffi, however, appear to indicate that $I=0$ when the slope of the dL/L curve is zero, in agreement with Fig. 6. Also from the standpoint of theories involving orientation of atomic magnets this assumption is the natural one to make. Schulze's curves, therefore, appear to require further experimental corroboration before they can be accepted.

The theory of the large discontinuities of magnetization given above may be applied to the much smaller Barkhausen discontinuities which usually require an amplifying device for their detection. Suppose that in a ferromagnetic substance there are small regions in a condition of strain similar to that assumed for the composite wire above. Then each of these small regions will contribute its own discontinuity to the magnetization curve. In this way the ordinary Barkhausen effect would be produced. The existence of these highly localized strains is not improbable. Recent experimental and theoretical work¹⁸ has demonstrated that a ferromagnetic crystal is made up of small

¹⁷ We assume that the contraction begins as soon as I begins increasing. In this case an increment, ΔH , causing an increment, ΔI_A , in the compressed segment, produces magnetostrictive strains which decrease the degree of compression of the compressed segment. A decrease of compression would produce a decrease of I . The strains produced by magnetostriction thus tend to inhibit the magnetization changes which produce the strains.

¹⁸ F. Zwicky, Phys. Rev. [2] 38, 1772 (1931); F. Bitter, Phys. Rev. [2] 37, 91 (1931); 38, 1903 (1931).

blocks which are more or less independent of each other in their magnetic behavior. These blocks will be the seat of local strains because of the differences in their magnetic condition. Webster's theory,¹⁹ which accounts for magnetostriction in unsaturated states, assumes that small regions are magnetized to saturation in various directions, the crystal as a whole not necessarily showing any resultant magnetization. The small regions are supposed to possess natural directions of easy magnetization.

A system of this kind would inevitably lead to a complicated pattern of internal strains associated with the blocks. An increasing magnetic field merely rotates the magnetization vector of each element without changing its magnitude. However, since each block expands transversely to its magnetization vector and contracts parallel thereto, it is evident that rotation of the separate vectors, either into or out of the condition of random orientation would set up strains of an elastic character between separate blocks. Whenever these strains produce magnetic instability a Barkhausen jump of magnetization occurs.

Experimental evidence has been obtained by Preisach²⁰ that the Barkhausen effect is fundamentally of the same nature as the large Forrer discontinuity. Stretching a wire of Fe-Ni alloy caused the small discontinuities to merge into a single large one; we may therefore suppose them to arise from the same underlying cause. Although the large discontinuities sometimes obtained in alloys may not be as simply explained as in the case of pure nickel, it appears evident that no theory of the effect can be satisfactory unless it considers strains as of fundamental importance in the whole phenomenon.

¹⁹ W. L. Webster, *Proc. Phys. Soc.* **42**, 431 (1930).

²⁰ F. Preisach, *Ann. d. Physik* [5] **3**, 737 (1929).

The Variation of Dielectric Constant with Temperature. II. Electric Moments of the Ethylene Halides

By ERNEST W. GREENE AND JOHN WARREN WILLIAMS
Laboratory of Physical Chemistry, University of Wisconsin

(Received August 15, 1932)

Both the free and hindered rotation of atoms or groups of atoms about single chemical linkages may be studied with the Debye relation between the molar polarization, P , and the reciprocal of the absolute temperature, $1/T$. The quantitative treatment by one of us for the simplest case of a free rotation has been compared with the more recent and more general expressions of Eyring and of Zahn. For the case in which the relation between P and $1/T$ is nonlinear the use of Meyer's equation has been suggested for the calculation of the electric moment of the molecule. An apparatus has been described for measuring the dielectric constant of a vapor as a function of temperature. This apparatus includes a comparatively cheap vapor condenser of Monel metal, a means of obtaining vapor at any desired pressure up to that characteristic of 100°C, and a method of measuring vapor pressure in an all-glass apparatus. An experimental procedure has been designed to minimize as far as possible the systematic errors due to simplifying assumptions in the capacity equations of the measuring circuit. The results of dielectric constant and density measurements on ethylene chloride and ethylene bromide have been recorded. The experimental values for the total polarizations of these compounds have been plotted against the reciprocals of the absolute temperature. These results have been utilized for the calculation of the several electric moments by the usual methods based on the linear equation of Debye and by the application of Meyer's equation. All of the methods for the calculation of electric moments were found to give results approaching each other at higher temperatures but tending to deviate more and more at lower temperatures. It has also been possible to calculate the characteristic moments of the C—Cl bond and the C—Br bond from the experimental data. The characteristic moments of the bonds were found to bear the same ratio to each other as the moments of the methyl compounds. It has been further shown that Meyer's equation is applicable to the results for vapors and for solutions now existent in the literature. The indications are that the difference between the experimental results for vapors and for solutions may be due to changes in internal structure produced in the molecule by the solvent.

INTRODUCTION

DURING the last two decades dielectric theory has played an important role in the development of ideas concerning the electrical constitution of matter. Quantum theory has clarified the view of intra-atomic matter, while the older kinetic and thermodynamic theories have been concerned with intermolecular action of comparatively large aggregates. In the field between, where the interest lies in the relative positions and interactions of atoms and groups of atoms within the molecule, dielectric theory has found important and unique application.

The interpretation of the temperature effect on the mean electric moment \bar{m} of a molecule in an external field F was presented by P. Debye in the year 1912 through the familiar equation:¹

¹ Debye, *Phys. Zeits.* 13, 97 (1912); See also *Polar Molecules*, Chemical Catalog Co., New York (1929).

$$\bar{m} = (\alpha_0 + \mu^2/3kT)F. \quad (1)$$

In this equation α_0 is the polarization due to deformation, μ is the permanent moment of the molecule, k is the Boltzmann constant (1.37×10^{-16}), and T is the absolute temperature.

The general formula for the polarizability is, therefore,

$$\alpha = \alpha_0 + \mu^2/3kT.$$

Experimental verification of this equation has followed its combination with the Clausius-Mosotti relation, written for the molar polarization P , as follows:

$$\frac{\epsilon - 1}{\epsilon + 2} \cdot \frac{M}{\rho} = P = \frac{4\pi N}{3} \alpha = \frac{4\pi N}{3} \left(\alpha_0 + \frac{\mu^2}{3kT} \right) \quad (2)$$

or

$$P = A + B/T. \quad (2')$$

Here ϵ is the dielectric constant, M is the molecular weight, ρ is the density, N is the Avagadro constant (6.06×10^{23}), $A = 4\pi N\alpha_0/3$ (molar polarization due to deformation), and $B = 4\pi N\mu^2/9k$ (molar polarization due to the permanent moment of the molecule). The experimental determination of ϵ and ρ for a compound over a series of temperatures permits the calculation of the relation between the total polarization P and $1/T$. This affords a direct check on the linearity of the Debye relationship. It also distinguishes between non-polar and polar molecules, and in the case of the latter, provides a means of calculating the permanent moment μ from the constant B . Such experimental studies have amply verified the fundamental correctness of the above equations.

From such results the electric moment μ has been obtained by one of the following methods:

- (1) The constant B , and thus μ , can be obtained from the slope of the linear plot of P vs. $1/T$.
- (2) Multiplying Eq. (2') through by T gives:

$$PT = AT + B. \quad (2'')$$

The quantity B can now be obtained from the intercept, at $T=0$, of the plot of PT vs. T . This method does not differ essentially from the first.

- (3) In Eq. (2') the deformation polarization A can be approximated from refractivity data. Ten percent may be added to the molecular refractivity in order to allow for the contribution of the atoms. The ratio B/T is then obtained as the difference between P and A . This method must be used when data at only one temperature are available. Its use, in conjunction with the value of B given above, depends as much upon the linear form of the Eq. (2') as does either of the other two methods.

INTRA-MOLECULAR ROTATION

The possibility of rotation about some valence bonds has long been suspected. We will confine our attention in this article to what are probably the

simplest molecules in which this phenomenon is exemplified, namely, the ethylene halides. In these compounds rotation about the C-C bond would be expected from the purely chemical evidence that it has been impossible to separate cis and trans isomers. The fact that these molecules have finite dipole moments has been established by numerous investigators. The most important results for ethylene chloride and ethylene bromide have been brought together in Table I. If the trans form alone were present there would result a zero moment. The finite moment found experimentally may be due to one of three possibilities: (1) Molecules of only the cis form may be present. (2) There may be a mixture of molecules of the cis and trans form. (3) The moment may represent an average of the moments of a number of molecules

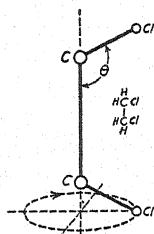


Fig. 1.

having effectively different dissymmetries due to the relative rotation of the two polar groups about the C-C linkage. The first of these is excluded because the cis form is the one having the higher potential energy (due to repulsion between like polar groups) and would thus hardly be formed in preference to the trans form. There is also evidence against this possibility in the fact that the moments in Table I are much lower than those of the corresponding cis forms of the acetylene dihalides. The second possibility, and indeed the first as well, would be at variance with all the evidence, both chemical and physical, for the rotation about such valence bonds. Evidence of a variation of moment with temperature further strengthens the supposition of such a rotation.

TABLE I. *Electric moments of ethylene chloride and ethylene bromide.*

Substance	benzene $\mu \times 10^{18}$	In solution in: hexane $\mu \times 10^{18}$	heptane $\mu \times 10^{18}$	As vapor $\mu \times 10^{18}$
Ethylene chloride	1.83 ² 1.86 ³ 1.75 ⁴	1.26-1.42 ²	1.16-1.42 ⁶	1.56 ⁷ 1.01 ⁸ 1.12-1.54 ⁹
Ethylene bromide	1.46-1.55 ⁵ 1.4 ⁴		0.79-1.05 ⁵	0.94-1.10 ¹⁰

² Meyer, *Zeits. f. phys. Chem.* **B8**, 27 (1930).³ Gross, *Phys. Zeits.* **30**, 504 (1929).⁴ Williams, *Zeits. f. phys. Chem.* **138**, 75 (1928).⁵ Smyth, *J. Am. Chem. Soc.* **53**, 2988 (1931).⁶ Smyth, *J. Am. Chem. Soc.* **53**, 4242 (1931).⁷ Ghosh, Mahanti and Sen Gupta, *Zeits. f. Physik* **54**, 711 (1929).⁸ Sanger, *Phys. Zeits.* **32**, 21 (1931).⁹ Zahn, *Phys. Rev.* **38**, 52 (1931).¹⁰ Zahn, *Phys. Rev.* **40**, 291 (1932).

In general there may be two types of rotation depending upon the energy state of the molecule. It will be recognized from the model in Fig. 1 that the cis configuration corresponds to a position of maximum potential energy of repulsion between the two moments, while the trans configuration corresponds to a position of minimum potential energy. In fact the resultant moment for the whole molecule would be largest for the cis form and zero for the trans form. This has been confirmed in the cis and trans forms of rigid double bond linkages. Calculations of Eucken and Meyer¹¹ have shown that free rotation occurs when the potential energy between the two halves of the molecule does not exceed $(1/10)kT$. However, if this potential energy exceeds $(1/10)kT$ there results a rotary oscillation about the position of minimum potential energy, which case we will call "hindered rotation" after the above authors. Obviously, in terms of the resultant moment of the molecule, there will be no sharp division between the two cases. When the rotation is hindered or oscillatory the amplitude of the oscillations will increase as the temperature is raised and the energy of the oscillations increases. The resultant moment of a molecule of this type will increase with the amplitude of the oscillations because the time average of the relative positions of the two polar groups will be further and further from the trans position. This is the theoretical basis for expecting the moment of the molecule to vary with temperature and thus produce a nonlinear relation between the total polarization and the reciprocal of temperature.

In the Debye theory the moment μ was assumed to be constant with respect to temperature. Consequently Eq. (2') cannot be applied to the general case of intra-molecular rotation. However, in the limiting case of free rotation the moment will be constant as the temperature varies as long as the rotation remains free and unhindered. This case has been treated vectorially by Williams.¹² The resultant mean moment for the molecule, which is the one that would be obtained experimentally from Eq. (2') if free rotation were actually the case, is given by:

$$\mu = 2^{1/2}\mu_1 \sin \theta \quad (3)$$

where μ_1 is the characteristic moment of the polar linkage and θ is the valence angle.

In applying Eq. (3) to the ethylene halides, using characteristic moments of 2.0 for C-Cl, 1.86 for C-Br, and 1.65 for C-I, Williams¹² found values of θ to be 38° for the chloride, 32° for the bromide, and 33° for the iodide. With tetrahedral carbon valences, the angle should be $180^\circ-110^\circ$ or 70° . We now know that the mutual repulsion of the two groups would not be likely to cause such a decrease in the angle, hence the natural conclusion is that the assumption of free rotation is not justified in these cases.

Eyring,¹³ using the matrix algebra, has developed a general equation for the average resultant moment of a molecule having free rotation about certain bonds in terms of the individual permanent moments, the angles between

¹¹ Eucken and Meyer, *Phys. Zeits.* 30, 397 (1929).

¹² Williams, *Zeits. f. phys. Chem. [A]* 138, 75 (1928).

¹³ Eyring, *Phys. Rev.* 39, 746 (1932).

the valence bonds, the rotation angles, and the energy. From this equation he has obtained several equations for simpler cases. Smyth,¹⁴ in conjunction with Eyring, has applied these equations to a number of organic compounds, comparing the calculated moments with the experimentally determined moments as a qualitative measure of the degree of freedom of the rotation. For the purpose of this discussion it will be sufficient to show that Eyring's equation reduces to the Williams equation above if applied to the simple case of free rotation about one single valence bond.

Eyring's equation for a paraffin chain of $n+1$ carbon atoms, with a free rotation about each C-C linkage, is:

$$\mu = \mu_1 [2n + 2(n-1) \cos \theta + 2(n-2) \cos^2 \theta + \dots + 2 \cos^{n-1} \theta]^{1/2} \quad (4)$$

where μ_1 is the characteristic moment of the C-X linkage and θ is the valence angle (110°). For the simplest molecules $n+1=2$, and the equation reduces to:

$$\mu = \mu_1 [2 - 2 \cos^2 \theta]^{1/2}. \quad (5)$$

Eq. (5) is identical with that used by Smyth for ethylene bromide and is also identical with the Williams Eq. (3), thus:

$$\begin{aligned} \mu &= \mu_1 2^{1/2} (1 - \cos^2 \theta)^{1/2} \\ &= \mu_1 2^{1/2} \sin \theta. \end{aligned} \quad (3)$$

Zahn¹⁵ has used similar methods in discussing a number of special cases.

It has been pointed out above that the resultant moment μ would be expected to vary with temperature for the case of hindered rotation, and that consequently the polarization would no longer be a linear function of $1/T$. The theoretical treatment of this case thus requires a new derivation of the relation between P , μ , and T , which takes the hindered rotation into consideration. Meyer² was the first to do this quantitatively from the classical theoretical standpoint. Meyer's equation is

$$\left. \begin{aligned} P &= 4\pi N/3 \{ \alpha_0 + [2(\mu_1 \sin \theta)^2/3kT](1 - X) \} \\ X &= \frac{\alpha/kT + \beta/(kT)^2 + \gamma/(kT)^3 + \dots}{m + n/kT + o/(kT)^2 + p/(kT)^3 + \dots} \end{aligned} \right\} \quad (6)$$

where N is the Avagadro constant, k is the Boltzmann constant, α_0 is the molecular deformation polarization, μ_1 is the characteristic moment of the C-X linkage, θ is the valence angle, T is the absolute temperature, and $\alpha, \beta, \gamma, m, n, o, p$ are constants associated with the structure of the molecule.

Eq. (6) expresses the nonlinear relationship between P and $1/T$ for the simple case of hindered rotation in the ethylene halides. Meyer pointed out that at high temperatures the term X becomes negligible and Eq. (6) reduces to

$$P = 4\pi N/3 \{ \alpha_0 + [2(\mu_1 \sin \theta)^2/3kT] \}. \quad (7)$$

¹⁴ Smyth, J. Am. Chem. Soc. **54**, 2261 (1932).

¹⁵ Zahn, Phys. Zeits. **33**, 400 (1932).

Comparing this with the Debye Eq. (2) it is seen that:

$$\mu = 2^{1/2}\mu_1 \sin \theta \quad (3)$$

which is the equation for free rotation previously developed.¹² Thus, at high temperatures Meyer's Eq. (6) is in accord with theory for the case of free rotation.

For the case of free rotation the resultant moment μ can be calculated from the experimental results by using the linear Debye equation in the three ways mentioned above. However, in order to calculate μ from experimental results when the rotation is hindered it is necessary to apply Eq. (6). This is a point which other experimenters either do not seem to have recognized or have thought unnecessary. At least we have been unable to find evidence of its use for the calculation in nonlinear cases.

On dividing the denominator of the function X of Eq. (6) into the numerator the function becomes:

$$\begin{aligned} X &= (\alpha/m)(kT)^{-1} + [(\beta m - \alpha n)/m^2](kT)^{-2} + \dots \\ &= C(1/T) + D(1/T)^2 + \dots \end{aligned} \quad (8)$$

where

$$C = \alpha/mk; D = (\beta m - \alpha n)/m^2k^2.$$

The expression for P in Eq. (6) then becomes:

$$\begin{aligned} P &= \frac{4\pi N}{3} \alpha_0 + \frac{4\pi N}{9k} 2(\mu_1 \sin \theta)^2 [(1/T) - C(1/T)^2 - D(1/T)^3 - \dots] \\ &= A + B' [(1/T) - C(1/T)^2 - D(1/T)^3 - \dots] \end{aligned} \quad (9)$$

where

$$A = (4\pi N/3)\alpha_0; B' = (4\pi N/9k)2(\mu_1 \sin \theta)^2.$$

In Eq. (9) the difference $P - A$ must be the polarization due to the resultant moment μ of the molecule at any temperature T . It is reasonable to suppose that the same relation holds between the resultant moment and the polarization caused by it as holds in the ordinary case where there is no intramolecular rotation. Then we can write from the ordinary Debye equation:

$$\begin{aligned} P &= A + (4\pi N/9kT)\mu^2 \\ \mu^2 &= (9kT/4\pi N)(P - A). \end{aligned} \quad (2)$$

Substituting for the value of $P - A$ in Eq. (9) we obtain the expression

$$\mu^2 = (9kT/4\pi N)B' [(1/T) - C(1/T)^2 - D(1/T)^3 - \dots].$$

Putting in the value of B' and simplifying we find

$$\mu^2 = 2(\mu_1 \sin \theta)^2 [1 - C(1/T) - D(1/T)^2 - \dots]. \quad (10)$$

For the actual calculation of μ it is more convenient to retain the constant B' , thus:

$$\mu^2 = (9k/4\pi N)B' [1 - C(1/T) - D(1/T)^2 - \dots]. \quad (10')$$

Now from the experimental plot of the total polarization P against $1/T$ the constants in Eq. (9) can be determined, and from these, substituted in Eq. (10'), the resultant moment μ can be calculated for any temperature.

EXPERIMENTAL

According to the results existent in the literature at the present time there is still some question as to whether or not ethylene chloride and ethylene bromide actually have nonlinear relationships between their total polarizations and the reciprocals of the temperature. Smyth,^{5,6} studying solutions in heptane, and Meyer,² working with solutions in hexane, obtain a curvature in their plots of P against $1/T$. However, the results of these investigators for the corresponding solutions in benzene are inconclusive. It should be emphasized that experiments with solutions alone can hardly be sufficient to decide a question of this sort because of ignorance of the effect of the solvent. The experiments of Zahn⁹ on the vapor of ethylene chloride show a nonlinear relationship while Ghosh and his associates⁷ obtain a linear relation, and Sanger's results⁸ are inconclusive.* Very recently Zahn¹⁰ has reported data for ethylene bromide vapor. It is difficult to draw any conclusion from these data of Zahn when his total polarizations are plotted against the reciprocals of temperature. In view of this situation it was decided to complete the work, begun early in 1930, with the ethylene chloride and ethylene bromide vapors.

The object of the experimental part was, therefore, to obtain values of the total polarization P over as wide a temperature range as possible. The apparatus and method were designed for vapors having an appreciable vapor pressure in the neighborhood of 100°C. The determination of ϵ requires capacity measurements on a condenser in a vacuum and in an atmosphere of the vapor. The density term in the Clausius-Mosotti relation requires a knowledge of the pressure of the vapor and the temperature. To satisfy these requirements the apparatus must contain: (a) A condenser in a chamber holding the vapor; (b) apparatus for admitting and exhausting the vapor; (c) a means of determining the pressure of the vapor in the chamber; (d) a means of controlling and measuring the temperature of the condenser chamber; (e) apparatus for measuring the capacity of the condenser.

(a) The condenser was of the concentric cylinder type. Four cylinders of Monel metal (cold drawn, seamless, annealed tubing) were polished inside and outside and mounted concentrically as shown in Fig. 2. Four mica spacers were used in each end to keep the cylinders in position. The dimensions and spacings are listed below the figure. In cutting the outside cylinder to length three lugs were left on each end. These were shaped as indicated in the figure and used to support the condenser in a vertical position in a large Pyrex tube. Part of the Pyrex chamber is shown by dashed lines in the figure. Alternate cylinders were electrically connected through short lugs left projecting from their ends when they were cut to length. These lugs were simply spot-welded together. Leads to the outside were small tungsten wires, spot-welded

* In a recent communication to us Sanger has stated that a redetermination of several of his experimental points has brought his results to a practical agreement with those of Zahn.

to the Monel lugs, passing out through gas tight Pyrex-tungsten seals. The lead from the outside and second inner cylinders was taken off at the bottom and grounded as indicated, while the lead from the first and third inner cylinders was taken off at the top and served to connect the condenser to the capacity measuring apparatus.

(b) The condenser and chamber were mounted vertically as shown in Fig. 3. The entrance tube was at the top and led out through the three-way stopcock marked *A*. One of the tubes from this stopcock led directly to the tube *D* containing the liquid under investigation. The third outlet from stopcock *A* led to the evacuating system through stopcocks *B* and *C*. Stopcock *B* led to a "Hi-Vac" oil pump and stopcock *C* led through the trap shown, and a calcium chloride tube, to a water aspirator.

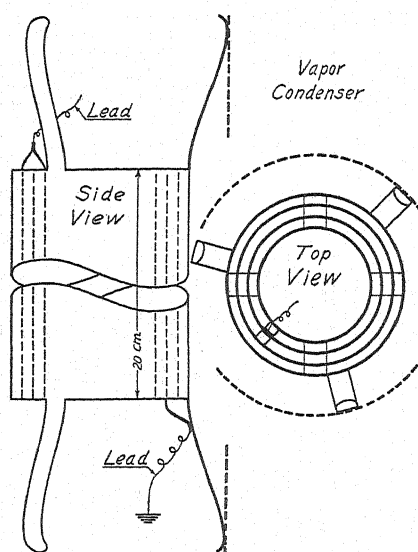


Fig. 2.	Cylinder	Outside Diam.	Spacing
	Outside	4.76 cm	
	1st inner	4.13	1.95 mm
	2nd inner	3.65	1.50
	3rd inner	3.18	1.50

Sufficient liquid for a whole series of determinations was placed in the tube *D* before it was sealed to the apparatus. The liquid was then cooled to a point where it solidified and the tube *D* was sealed to the apparatus through the small connecting tube. While the liquid was still frozen the stopcocks were turned so as to connect tube *D* through stopcock *B* to a source of carbon dioxide and the vacuum pump. In this way the space above the material was thoroughly flushed out several times with dry carbon dioxide, the carbon dioxide entering through stopcock *B* from auxiliary tubes not shown in the figure. Tube *D* was finally evacuated and then closed by means of stopcock *A*. By surrounding tube *D* with hot water contained in the vacuum flask the

liquid could be heated to give any desired vapor pressure up to that characteristic of 100°C.

In the meantime the rest of the apparatus was flushed out with dry carbon dioxide and evacuated. This was possible because the three-way stopcock *A* was mounted in such a way that the condenser chamber could be connected to the vacuum system while tube *D* was closed.

With the condenser chamber and connecting tubes evacuated stopcock *B* was closed and then stopcock *A* was turned to allow the vapor to flow from tube *D* into the condenser chamber until the desired pressure of vapor was obtained. Stopcock *A* was then set in an intermediate position so as to close both *D* and the condenser chamber. Condensation of vapor in the tube leading from stopcock *A* to the condenser chamber was prevented by means of the

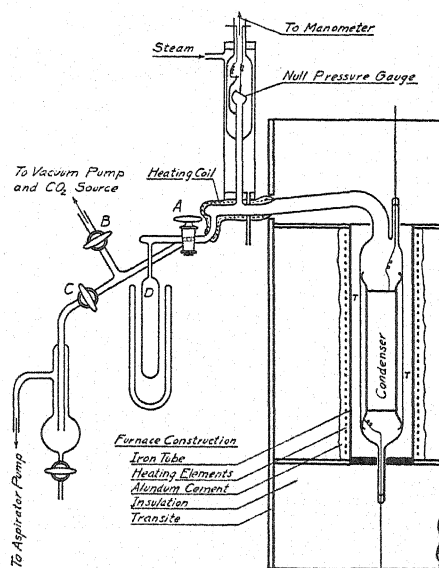


Fig. 3.

heating coil shown in the figure. Of course, the chamber itself was always kept at a temperature higher than that of the liquid in tube *D*.

After the measurements of temperature, pressure, and capacity (to be described later) the system was evacuated, keeping tube *D* closed as before. In evacuating the vapor, as much as possible was pulled out by the aspirator pump through stopcock *C*. Stopcock *C* was then closed and the system finally evacuated by the oil pump through stopcock *B*. In actual determinations the condenser chamber was flushed out several times with the vapor itself before it was finally admitted for the measurements. For the vapors of ethylene chloride and ethylene bromide stopcock *A* was lubricated with a paste made of P_2O_5 , SiO_2 , and phosphoric acid. Stopcocks *B* and *C* were lubricated with ordinary vacuum stopcock lubricant of the rubberized type.

(c) Pressure measurements were made by means of a null gauge of the

glass diaphragm type described by Daniels.¹⁶ This gauge, with the glass diaphragm and the platinum wires leading from it, is shown in Fig. 3. The vapor side of the gauge was connected directly with the large tube leading to the condenser chamber. Steam was passed around the gauge to prevent condensation of vapor inside. The other side of the gauge was connected to a mercury manometer for reading the pressure. A system of stopcocks leading both to the atmosphere and to the vacuum system allowed adjustment of the pressure to the null point.

A gauge of this type always has an additive correction factor which must be determined in order to convert manometer readings at the null point into actual pressures. This correction factor was obtained when there was no vapor in the apparatus by connecting the gauge and manometer system to the inside system through stopcock *B*, allowing carbon dioxide to flow into both systems to any desired pressure, (measured now on the manometer)

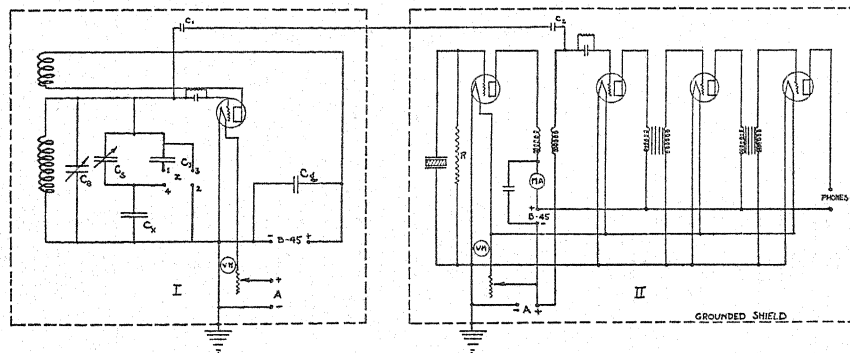


Fig. 4.

and then closing stopcock *B* and adjusting the pressure in the gauge and manometer system to the null point. The difference between the actual pressure and the pressure at the null point would then be the correction. The gauge was checked in this way after every two or three hours of operation. With a gauge of this type no vapors come into contact with the mercury manometer, the manometer can be operated at room temperature, and no mercury vapor enters the inside of the apparatus.

(d) The condenser chamber was mounted inside a vertical tube electric furnace. The furnace tube was of iron and was about four inches in diameter and sixteen inches long. It was closed at the top and bottom with metal ends and was grounded, thus serving as a shield for the condenser. The heating elements were nichrome wire wound non-inductively. There were about six or seven inches of insulation surrounding the tube. The heating current was drawn from a 220 volt a.c. circuit and was controlled by several *glow-coil* resistances and two slide wire rheostats. Temperature control was obtained by merely setting the resistance in the circuit and allowing the temperature to become constant.

¹⁶ Daniels, J. Am. Chem. Soc. 50, 1115 (1928).

Temperature measurements were made by means of two chromel-alumel thermocouples held against the outside of the condenser chamber at the points lettered *T* in Fig. 3. The cold junctions were kept in cracked ice and the voltage readings were made by means of a Leeds and Northrup Type-K potentiometer using a wall galvanometer.

(e) The dielectric constants were determined from capacity measurements made by the method of Pungs and Preuner.¹⁷ The electrical apparatus was the same as that used and described by Schwingel and Williams,¹⁸ and is shown in Fig. 4.

A rough control condenser C_s , a variable precision condenser C_y , a fixed mica condenser C_v of comparatively large capacity, and the vapor condenser C_x form the capacity of circuit *I*. The control condenser C_s is used to adjust the capacity to any desired point on precision condenser scale, and is left fixed for any series of determinations. The total series capacity of the part of the circuit containing the vapor condenser C_x is given by:

$$1/\text{total capacity} = 1/C_x + 1/(C_y + C_s). \quad (11)$$

Let ΔC_x represent the change in the capacity of the vapor condenser C_x on the admission of a vapor and let ΔC_s represent the change in the reading on the precision condenser required to bring the circuit back to the original total capacity. Then,

$$1/\text{total capacity with vapor} = 1/\text{total capacity evacuated}.$$

From Eq. (11):

$$\frac{1}{C_x + \Delta C_x} + \frac{1}{C_y + C_s + \Delta C_s} = \frac{1}{C_x} + \frac{1}{C_y + C_s}. \quad (12)$$

Solving for ΔC_x :

$$\Delta C_x = \frac{C_x^2 \cdot \Delta C_s}{(C_y + C_s)^2 + (C_y + C_s + C_x)\Delta C_s}. \quad (13)$$

In Eq. (13) any capacity in the leads from the vapor condenser will be included in C_x . As we shall consider C_x as the true capacity between the plates of the vapor condenser it will be necessary to replace C_x in (13) by $C = C_x + X$, where X is the lead capacity. Eq. (13) then becomes:

$$\Delta C_x = \frac{C^2 \Delta C_s}{(C_y + C_s)^2 + (C_y + C_s + C)\Delta C_s}. \quad (13')$$

Dielectric constant values can now be obtained from the equation

$$\epsilon - 1 = \Delta C_x / C_x. \quad (14)$$

Combining Eqs. (13') and (14):

$$\epsilon - 1 = \frac{C^2}{(C_y + C_s)^2 + (C_y + C_s + C)\Delta C_s} \cdot \frac{\Delta C_s}{C_x}. \quad (15)$$

¹⁷ Pungs and Preuner, *Phys. Zeits.* **20**, 543 (1919).

¹⁸ Schwingel and Williams, *Phys. Rev.* **35**, 855 (1930).

Assuming that $(C^2/C_x) = C$, and taking the reciprocal of both sides of Eq. (15):

$$\frac{1}{\epsilon - 1} = \frac{(C_v + C_s)^2}{C} \cdot \frac{1}{\Delta C_s} + \frac{(C_v + C_s)}{C} + 1.$$

Let the constant coefficient, $(C_v + C_s)^2/C = a^2$;
then

$$(C_v + C_s)/C = a/C^{1/2}.$$

Therefore,

$$1/(\epsilon - 1) = a^2(1/\Delta C_s) + a/C^{1/2} + 1, \quad (16)$$

where ϵ is the dielectric constant, a is a constant of the circuit, C is the capacity of the vapor condenser and the leads, and ΔC_s is the *difference* reading on the precision condenser.

Absolute values of $\epsilon - 1$ can be determined from Eq. (15) if values of the capacities C_x , X , C_v and C_s are known. In this work it was thought preferable to determine the constant a from calibrations with carbon dioxide, using Stuart's¹⁹ value of $\epsilon - 1$. Having determined a in this manner, $\epsilon - 1$ for a vapor is obtained directly from Eq. (16).

The vapor condenser has been described in part *a* of this section. Its capacity, including lead capacity, was found to be 530 mmf. The fixed condenser C_v was found to be 2834 mmf. In this work condenser C_v was mounted inside a vacuum flask in order to decrease fluctuations due to changes in room temperature and humidity.

The first step in the actual measurement of a dielectric constant is the determination of the constant a . As has already been mentioned, carbon dioxide is admirably suited for this purpose. Stuart's¹⁹ value of $(\epsilon - 1)10^6$ for carbon dioxide is 987 at 273°K and one atmosphere. This value was converted to that corresponding to the pressure and temperature of the experiment by multiplying it by the density ratio. We then have, according to Eq. (16):

$$1/(\rho/\rho_0)(987)10^{-6} = a^2(1/\Delta C_s) + a/C^{1/2} + 1,$$

where ρ is the density under experimental conditions and ρ_0 is the density under standard conditions. The quotient ρ/ρ_0 was calculated from Berthelot's equation.

The procedure followed was to make two or more determinations of the constant a in this manner at each temperature at which vapor determinations were made. After the whole temperature range of the apparatus had been covered all of the a values were averaged and the average was used to calculate the dielectric constants of the vapor at the several temperatures by Eq. (16). The vapors of the ethylene halides were run in a manner similar to carbon dioxide, readings being taken first with the apparatus evacuated, then with the vapor in the apparatus at a desired pressure, and finally after re-evacuation. In this manner the quantity ΔC_s could be determined for the several capacity balances.

¹⁹ Stuart, Phys. Zeits. 47, 457 (1928).

The molar polarization P is calculated from the equation

$$P = [(\epsilon - 1)/3](M/\rho).$$

The quantity (M/ρ) is obtained from Berthelot's equation,

$$M/\rho = C_1(T/p) + C_2 - C_3(1/T^2).$$

The constants of this equation are given below:

$$C_1 = 760R \text{ (if } p \text{ is in mm)} = 62370$$

	<i>Ethylene chloride</i>	<i>Ethylene bromide</i>
$C_2 = 9RT_c/128p_c =$	61.2	48.8
$C_3 = 54RT_c^3/128p_c =$	11.60×10^7	9.8×10^7
$R = 82.07 \text{ cc. atmos./deg.}$		
(Crit. temp.) $T_c^* =$	562.2°K	583.0°K
(Crit. press.) $p_c^* =$	53.06 atmos.	68.99 atmos.
*From	Nadejdine (1887)	Vespignani (1903)

SOURCES OF ERROR

Pressure

For carbon dioxide the pressures were read directly on the mercury manometer because it was not necessary to use the null gauge with a noncondensing gas. Using a reading glass the manometer reading was accurate to ± 0.2 mm. For vapor pressure readings the null gauge was necessary. However, as this could be set as closely as the manometer could be read, the accuracy here was also ± 0.2 mm. There should be no systematic errors in pressure readings because the null gauge was frequently checked. Of course, at both high and low temperature extremes such an error would develop, due to chemical change in the vapor in one case, and adsorption on the condenser cylinders in the other. In these cases the pressure would no longer be an indication of the amount of material between the condenser cylinders.

Temperature

Thermocouple readings on the potentiometer could be checked without difficulty to ± 0.002 millivolts. This corresponds to $\pm 0.05^\circ\text{K}$. The two thermocouples used were calibrated against a third chromel-alumel thermocouple which had just been calibrated in steam, tin, cadmium, and zinc. The calibration points were sharp and probably as accurate as the temperature values given for them in the literature. Temperatures were reported to the nearest degree because this is within the limit of accuracy of the capacity readings.

Capacity

The pertinent reading was ΔC_s , the difference between the precision condenser readings when the apparatus was evacuated and when it was filled with gas or vapor. The precision condenser could be read to ± 0.1 of a scale

division. As ΔC_s was reported in tenths of a scale division the reading accuracy was ± 1 . There are no systematic errors in $\epsilon - 1$ due to the method of calculation, because Eq. (16) does not involve any simplifying assumptions. Of course the practice of calibration with carbon dioxide depends upon the dielectric constant of this gas remaining constant over the temperature range used. This has been attested to by numerous investigators. It is further supported by the constancy of the a calculated from the determinations on carbon dioxide.

The accuracy of the total polarization P can be estimated by an analysis of the values of the constant a^2 obtained in a series of determinations on carbon dioxide. The least accurate of these series gave a mean absolute deviation of 2 percent.

PURIFICATION OF MATERIALS

Carbon dioxide was taken from a commercial cylinder and passed through concentrated sulphuric acid and a P_2O_5 tower.

TABLE II. Data on ethylene chloride. Run No. 1.

Temp. °K	$(1/T) \times 10^3$	Press. (mm)	ΔC_s	$(\epsilon - 1) \times 10^6$	P (cc)
297.5		52.7	314	473	55.5
297.6		55.3	337	507	56.6
297.6		57.5	348	523	56.1
297.6		54.8	331	498	56.1
297.7		49.4	292	440	55.0
297.9		47.0	287	432	56.7
297.9		49.6	302	456	56.8
297.9		52.4	319	488	57.6
297.8		48.3	293	449	57.5
Av. 298	3.36				57.0
345.8		54.2	264	399	52.8
345.9		61.3	301	454	53.1
345.5		112.6	558	830	52.9
345.6		106.4	529	787	53.0
Av. 346	2.89				53.0
395.3		332.4	1458	2070	50.8
395.2		327.6	1450	2060	51.2
395.4		329.2	1471	2080	51.4
393.0		423.1	1909	2650	50.6
393.0		324.5	1468	2080	52.0
393.3		318.2	1431	2030	51.7
Av. 394	2.54				51.3
447.8		112.2	424	635	52.7
447.9		109.1	400	600	51.0
448.3		158.0	581	863	50.6
448.4		157.9	576	855	50.2
Av. 448	2.23				51.1
495.5		80.3	264	399	51.1
495.7		89.5	294	444	50.9
Av. 496	2.02				51.0

TABLE III. Data on ethylene chloride. Run No. 2.

Temp. °K	$(1/T) \times 10^3$	Press. (mm)	ΔC_s	$(\epsilon-1) \times 10^6$	P (cc)
588.6	1.70	171.4	522	733	52.3
587.2		161.0	484	681	51.5
587.5		164.0	437	617	45.8
Av. 588					49.9
533.2	1.88	192.8	611	854	49.0
532.2		177.5	583	815	50.7
531.6		171.1	565	791	51.0
Av. 532					50.2
495.2	2.02	171.7	608	850	50.9
495.5		170.8	606	847	50.9
Av. 495					50.9
392.9	2.55	130.8	590	826	51.4
393.8		128.6	586	814	51.6
Av. 393					51.5

TABLE IV. Data on ethylene bromide. Run No. 1.

Temp. °K	$(1/T) \times 10^3$	Press. (mm)	ΔC_s	$(\epsilon-1) \times 10^6$	P (cc)
298.5	3.35	11.1	75	114	64
298.6		10.8	75	114	66
298.6		11.0	90	137	77
298.6		10.0	75	114	71
298.7		10.2	78	119	72
Av. 299					70
346.6	2.88	21.8	92	140	45.4
346.6		20.4	89	137	47.9
346.7		20.0	84	128	46.2
Av. 347					46.5
401.0	2.50	19.8	74	113	47.6
401.0		54.5	205	310	47.4
Av. 401					47.5
449.2	2.23	121.4	391	587	45.2
449.3		125.6	406	609	45.2
Av. 449					45.2
490.3	2.04	87.7	314	472	54.8
490.4		93.9	336	505	54.7
Av. 490					54.8

Ethylene chloride (from the Eastman Kodak Company) was washed twice with normal NaOH and three times with water. It was then dried over fused CaCl_2 for several days and fractionally distilled. The vapor of the distillate was kept in contact with P_2O_5 for several days. The liquid was then distilled directly into the apparatus as described above. B.P. 82.3–82.6°C.

Ethylene bromide (from the Eastman Kodak Company) was treated in the same way as the ethylene chloride except that the distillation was carried out under reduced pressure.

TABLE V. *Data on ethylene bromide. Run No. 2.*

Temp. °K	$(1/T) \times 10^3$	Press. (mm)	ΔC_s	$(\epsilon-1) \times 10^6$	P (cc)
611.9		130.1	324	510	49.8
613.2		103.6	254	400	49.2
Av. 612	1.64				49.5
562.2		89.4	410	642	84.0
562.2		61.7	283	447	84.6
Av. 562	1.78				84.3
494.5		109.3	481	750	70.5
494.9		89.8	391	613	70.2
Av. 495	2.02				70.4
454.0		87.0	285	449	47.3
454.2		80.1	268	422	49.8
Av. 454	2.21				48.6
425.5		80.5	265	419	45.9
425.2		71.8	238	376	46.3
425.2		65.2	224	354	47.9
Av. 425	2.36				46.7
392.3		67.1	249	392	47.6
392.0		67.4	248	391	47.3
Av. 392	2.55				47.5
363.5		45.4	196	311	51.7
363.4		46.5	202	320	51.9
Av. 363	2.76				51.8

CALCULATIONS WITH ETHYLENE CHLORIDE DATA

The Debye linear equation for the polarization as a function of the temperature is, $P = 23.9 + B/T$, where the value $A = 23.9$ for the deformation polarization is that obtained by Hitchcock²⁰ for the solid substance and is,

TABLE VI.

Temp. °K	P (cc)	B	$\mu \times 10^{18}$ e.s.u.
298	57.0	9,880	1.27
346	53.0	10,080	1.28
394	51.3	10,790	1.32
448	51.1	12,200	1.41
495	50.9	13,380	1.48
532	50.2	14,200	1.52
588	49.9	15,250	1.57

²⁰ Hitchcock, Quoted by Smyth, J. Am. Chem. Soc. **53**, 4242 (1931).

furthermore, in good agreement with estimates by the optical method. The constants B calculated from the experimental points, and the corresponding moments μ are given in Table VI.

The application of Meyer's equation will now be described, again taking the deformation polarization to be 23.9. Eq. (9) then becomes

$$P = 23.9 + B'(1/T) + B'C(1/T)^2.$$

The constants in this equation can be obtained from two experimental points. These points were selected so as to give the best approximation to all the experimental results.

Points selected.

$1/T$	$(1/T)^2$	P
2.02×10^{-3}	4.08×10^{-6}	51.0
2.55	6.50	51.5

The results of the calculation are $B' = 23.3 \times 10^3$ and $B'C = 4.89 \times 10^6$, so that the equation for the total polarization is

$$P = 23.9 + 23,300(1/T) - 4,890,000(1/T)^2.$$

The equation for the moment is,

$$\mu^2 = (9k/4\pi N) [23,300 - 4,890,000(1/T)].$$

From this equation the values of μ in Table VII are obtained. Assuming

TABLE VII.

T	$(1/T)10^3$	$\mu \times 10^{18}$ e.s.u.
298	3.36	1.05
346	2.89	1.22
394	2.54	1.33
448	2.32	1.42
495	2.02	1.48
532	1.88	1.52
588	1.70	1.56
(∞)	(0.00)	(1.94)—for free rotation

the valence angle θ to be 70° the characteristic moment μ_1 for $C-Cl$ can be obtained from:

$$B' = (4\pi N/9k)2(\mu_1 \sin \theta)^2,$$

with the result that

$$\mu_{C-Cl} = 1.46 \times 10^{-18} \text{ e.s.u.}$$

CALCULATIONS WITH ETHYLENE BROMIDE DATA

The Debye linear equation in this case is, $P = 29.7 + B(1/T)$, where the deformation polarization is 29.7.¹⁰ The individual experimental points, substituted in this equation give the results of Table VIII.

TABLE VIII.

Temp. °K	P (cc)	B	$\mu \times 10^{18}$ e.s.u.
347	46.5	5830	0.97
392	47.5	6980	1.05
401	47.5	7130	1.07
425	46.7	7220	1.08
449	45.2	6960	1.04

In applying Meyer's equation to the ethylene bromide data it was found that the points for the higher temperatures cannot fall on a parabola whose constant A has the value 29.7 and which represents the more reliable data at the lower temperatures. For this reason, the Meyer equation was applied only to the points corresponding to the lower temperatures in the case of ethylene bromide.

Points selected.

(1/T)	(1/T) ²	P
2.5×10^{-3}	6.25×10^{-6}	47.5
2.88	8.29	46.5

The equation for the total polarization is,

$$P = 29.7 + 15600(1/T) - 3,390,000(1/T)^2,$$

and the equation for the moment becomes,

$$\mu^2 = (9k/4\pi N)[15600 - 3,390,000(1/T)].$$

From this equation the values of (μ) in Table IX are obtained:

TABLE IX.

T	(1/T)10 ³	$\mu \times 10^{18}$ e.s.u.
357	2.8	0.99
385	2.6	1.05
417	2.4	1.10
455	2.2	1.15
(∞)	(0.0)	(1.59)—for free rotation.

Since $B' = 15600$ and $\theta = 70^\circ$,

$$\mu_{C-Br} = 1.20 \times 10^{-18} \text{ e.s.u.}$$

DISCUSSION OF RESULTS

The results of Zahn and Sanger for the vapors and the results of Smyth and Meyer for solutions are plotted, together with our results, in Fig. 5. The dashed curves represent the experimental curves of the various investigators while the full curves are the parabolas used in the calculation of our results. The circles represent results from vapor determinations and the

squares are results from solutions. The horizontal line separates the ethylene chloride points from those for ethylene bromide. Results for both compounds are plotted on the same axes and to the same scale. The low temperature values for the vapor and the high temperature values for the solutions are probably the least accurate.

For ethylene chloride our two points at the lowest temperatures undoubtedly are high due to adsorption of vapor on the condenser cylinders. This was confirmed by purposely coating the condenser cylinders with some thermal decomposition products of the vapors by admitting vapor to the condenser chamber at 400°C. With the adsorptive properties of the surface increased in this manner the P values obtained at the low temperatures were considerably higher than those shown on the graph. The range of temperature avail-

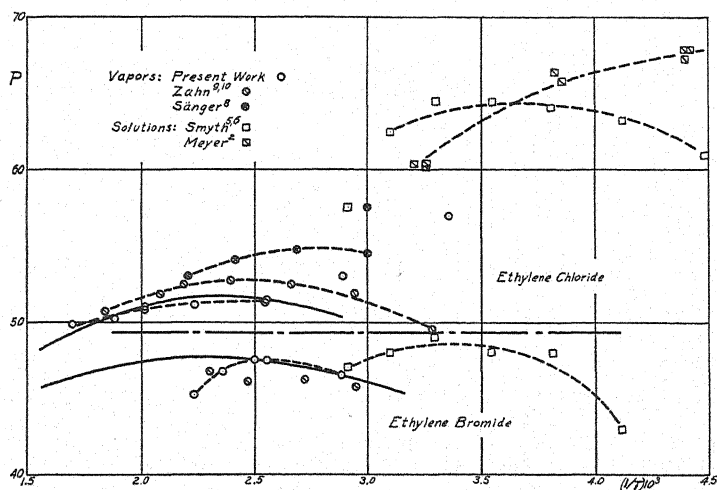


Fig. 5.

able for the investigation of ethylene bromide was much less than that for ethylene chloride. The erratic effects at high and low temperatures are indicated by the high values of the polarization P in Tables IV and V.

The dashed curves represent our interpretation of the experimental data reported by other investigators and by us. They support the theory that this type of compound should have a nonlinear relation between P and $1/T$.

For ethylene chloride the full curve on the graph, representing a parabolic relation between P and $1/T$ and calculated from our data, is a fair approximation to the experimental points. This theoretical curve has a greater curvature than the experimental curve and the maxima do not come at the same place. This is undoubtedly due to the particular selection of the deformation polarization in the calculation of the theoretical curve. A parabola could be drawn through three points on the experimental curve, and in this way the constant A in the equation could be evaluated directly from experiment. However, this procedure could hardly be expected to give an accurate measure of the deformation polarization.

The characteristic moment of (1.46×10^{-18}) for the $C-Cl$ bond, obtained from the constant B' , compares well with the value of (1.5×10^{-18}) , usually accepted. However, the figure (1.46×10^{-18}) is low compared to the experimental moment of methyl chloride, which is (1.86×10^{-18}) according to the tables of Smyth.²¹

Although our experimental points for ethylene bromide fall on a smooth curve it will be noticed that there is a rather sharp change in curvature at the peak. This, together with the large slope of the curve to the left of the peak, indicates that the two points for the higher temperatures may be too low. Even a straight line through these two points would give an intercept too small for the deformation polarization.

The constant B' for the parabola chosen as the representation of the data gives a characteristic moment for the $C-Br$ bond of (1.20×10^{-18}) . This seems low compared to the value of (1.5×10^{-18}) usually accepted. In this connection, however, the question arises as to why the bonds $C-Cl$ and $C-Br$ should both have characteristic moments of (1.5×10^{-18}) when the moments of the corresponding methyl compounds are (1.86×10^{-18}) and (1.45×10^{-18}) , respectively.²¹ It may be worth while to point out that the ratio of the characteristic moments obtained from ethylene chloride and ethylene bromide is very close to the ratio of the moments for the methyl compounds. Thus,

$$(\mu_1 \text{ for } C-Br)/(\mu_1 \text{ for } C-Cl) = 1.20/1.46 = 0.82$$

$$(\mu \text{ for } CH_3Br)/(\mu \text{ for } CH_3Cl) = 1.45/1.86 = 0.78.$$

The Table X contains a comparison of our moments for ethylene chloride calculated by the optical method and by the parabolic equation, with those reported by Zahn⁹ for the vapor. The moments of Zahn were obtained by graphical interpolation for the temperatures listed in our table. Zahn calculated his moments by means of Eq. (2''). Since his experimental curve for the polarization P agrees very well with ours his values for the moment can be used as a comparison of the method of calculation. The results of all three columns approach each other at the higher temperatures, while at lower temperatures the first and third columns deviate from the second and from each other. The optical method is definitely the least reliable.

TABLE X. Values of $\mu \times 10^{18}$. (Ethylene chloride.)

Temp. °K	Optical method	Parabolic equation	Zahn
298	1.27	1.05	1.10
346	1.28	1.22	1.25
394	1.32	1.33	1.36
448	1.41	1.42	1.44
495	1.48	1.48	1.49
532	1.52	1.52	1.53
588	1.57	1.56	
(∞)		(1.94)	

²¹ Smyth, *Dielectric Constant and Molecular Structure*, Chemical Catalog Co. (1931).

The comparison of μ values calculated for ethylene bromide vapor by the optical method, by the method of the parabola, and as reported by Zahn¹⁰ are given in Table XI. These results cannot be used for a study of the several methods of calculation because the different columns are not based upon the same experimental points. In view of this it is surprising how well they agree.

TABLE XI. Values of $\mu \times 10^{18}$. (Ethylene bromide.)

Temp. °K	Optical method	Parabolic equation	Zahn
357	0.99	0.99	0.98
385	1.04	1.05	1.01
417	1.08	1.10	1.05
455	1.02 ?	1.15	1.13 ?
(∞)		(1.59)	

The striking thing about the results for ethylene chloride, both in solution and as vapor, is that, with the exception of a few points in individual cases, they could all be represented as a family of parabolas having a common intercept. The parabola used by us would be a typical one for the family. The difference in the various parabolas is to be found in the heights and positions of the maxima. The same thing could probably be said for the data on ethylene bromide. The difference between the results for vapor and solution appears to be the same type of difference but of a larger order of magnitude. The horizontal position of the maximum is governed by the constant C in the equation. This can be seen at once by setting the derivative with respect to $1/T$ equal to zero. It has been pointed out that the constant C is a function of structural constants of the molecule. Consequently the difference between the curves for the vapor and for solutions may be due to some structural change within the molecule when it is dissolved. The difference between the results with the vapor and with solutions for ethylene bromide is much less than in the case of ethylene chloride. This might be expected on the above basis due to the heavier bromine atoms resisting structural changes more strongly than the chlorine atoms. It is not meant to suggest here that the discrepancies between different experiments with the vapor are due to structural changes since these differences are of the order of the absolute experimental error.

CONCLUSIONS

- (1) The results of the present experimental work are in accord with previous work which shows both ethylene chloride and ethylene bromide to give a nonlinear relationship between the total polarization P and the reciprocal of the absolute temperature ($1/T$).
- (2) At the lowest temperatures adsorption on the condenser cylinders tends to give high values of the total polarization and thus tends to decrease or even reverse the curvature of the P vs. $1/T$ relation.
- (3) At the highest temperatures ethylene bromide vapor gives abnormally high values for the total polarization, due, it is supposed, to the beginning of a thermal decomposition of the material.

(4) The relation between the total polarization P and the reciprocal of absolute temperature $1/T$ for the ethylene halides can be represented by an equation of the form

$$P = A + B'(1/T) - B'C(1/T)^2.$$

This equation should be applied to such systems in which the relationship between P and $1/T$ is nonlinear.

(5) The differences between the P vs. $1/T$ relationships for vapor and for solution can possibly be explained as due to changes in the internal structure of the molecule in question, due to the influence of the solvent.

(6) The theoretical ideas presented permit the calculation of the characteristic moments of the C-Cl and the C-Br bonds from the experimental data. In this computation it is assumed that the angle between the line joining the centers to the two carbon atoms and the direction of the carbon to halogen bond is that required by the normal undeformed tetrahedra used to represent the spatial configuration of the molecule.

LETTERS TO THE EDITOR

Prompt publication of brief reports of important discoveries in physics may be secured by addressing them to this department. Closing dates for this department are, for the first issue of the month, the twenty-eighth of the preceding month; for the second issue, the thirteenth of the month. The Board of Editors does not hold itself responsible for the opinions expressed by the correspondents.

Probabilities of *K*-Electron Ionization of Silver by Cathode Rays

The work reported here is an extension of a research described in previous papers¹ on the probabilities of *K*-electron ionization of silver by cathode rays, as measured by the intensities of the $K\alpha$ lines. To make it possible to have all collisions producing x-rays for any one measurement occur at the same cathode-ray speed, we are using constant potentials, of course, and also targets thin enough to avoid serious retardation of the cathode rays while they are in the silver.

The previous work extended only to 85 kv, or $3.3 V_K$ (where V_K is the *K*-series excitation voltage), but we are now working to $7V_K$. Because of the difficulty of exact absolute measurements of x-ray intensities, or even of the thicknesses of these very thin targets, we are reckoning all probabilities in terms of the most convenient arbitrary standard, the probability at $2V_K$. The ratio of the probability at any other voltage to this standard, we call $j(U)$, where $U = V/V_K$.

In these terms, $j(U)$ is of course zero up to $U=1$, and there it begins its rise abruptly, its graph starting upward from $U=1$ with a finite slope. The graph is concave downward, and reaches a very flat maximum, $j(U)$ remaining with 2 percent of 1.21 from $U=3.5$ to $U=7$. Aside from the standard, $j(2)=1.00$, some values at other points are as follows: $j(1.2)=0.39$, $j(1.5)=0.72$, $j(2.5)=1.11$, $j(3)=1.18$. All these values confirm the earlier work to within ± 0.01 , except at $U=3$, where the earlier value was lower by 0.025, probably because of gas in the tube. The values of j given here are all corrected for cathode-ray diffusion effects, as explained in the Physical Review paper cited above; but for the rediffusion constant of beryllium, the material on

which the silver was deposited, we are now using 0.025, a fair representative of the values found by Neher.² These new data are all based on one film, about 500A thick. We therefore plan to make further measurements, for greater accuracy and for certainty that there was nothing radically wrong with that film, before publishing the results in detail.

In the meantime, however, assuming for the present that they are at least a good first approximation, we can make some statements about their relation to various theories. The theories of Rosseland,³ Thomas,⁴ Ochiai,⁵ and Bethe⁶ are all based on the inverse-square law of repulsion between the cathode ray and the *K* electron, though with various differences in other assumptions. Rosseland and Thomas used classical quantum mechanics, and therefore were definite in their predictions. The theories of Ochiai and Bethe, on the other hand, are based on single-term approximations by Born's perturbation method, and are therefore restricted to values of $U \gg 1$. Whether this restriction keeps them from being applicable in the range $U \leq 7$ or not, we cannot say; nor can we be quite sure of what can be assumed, under conditions straining the above restriction, as to possible variations in some quantities treated as constants. But if we interpret them correctly, all these inverse-square-law theories agree in predicting a notable decline in the ionization probability in the region where we find our flat maximum.

² H. V. Neher, Phys. Rev. 37, 655 (Mar. 1, 1931). (Letter to the Editor.)

³ S. Rosseland, Phil. Mag. 45, 65 (1923).

⁴ L. H. Thomas, Proc. Camb. Phil. Soc. 23, 829 (1927).

⁵ K. Ochiai, Proc. Phys.-Math. Soc. of Japan 11, 43 (1929).

⁶ H. Bethe, Ann. d. Physik 5, 325 (1930).

¹ Phys. Rev. 37, 115 (Jan. 15, 1931) and Proc. Nat. Acad. Sci. 14, 769 (1928).

The only other quantum theory of x-ray line intensities that we have seen is the oldest of them all, that of Davis,⁷ who assumed the collisions to be equivalent to those of hard spheres. This theory predicted a deviation from our data in the direction opposite to that of the inverse-square theories.

To explain these deviations, several ideas present themselves. One is that the inverse-square law ought to be the best basic hypothesis, but that the deviations of these inverse-square theories from the data are caused by relativity effects, which might well be large at these voltages. Another idea is that the inverse-square law may fail between electrons at distances less than 10^{-11} cm, such as are demanded by these theories for the transfer of the large amounts of energy carried by our cathode rays. Still another idea is that the inverse-square law may fail for some other reason, connected with the dynamics of electrons within an atom, rather than with high energy. This last idea is the only one of these three, at least, that will explain observations on the inert gases by Hughes and Klein,⁸ Compton and Van Voorhis,⁹ and Smith.¹⁰ Their data cover argon, neon and helium, and in all cases show the same sort of departure from the inverse-square theories that we find here. Helium may perhaps be the best for comparison with our data, since it contains only K electrons; and Smith's data show most clearly a very flat maximum around $4.5 V_K$, remarkably like that given by our silver K electrons. Here at least, at 110 volts, there is no relativity or high energy problem.

⁷ B. Davis, Phys. Rev. 11, 433 (1918).

⁸ A. L. Hughes and E. Klein, Phys. Rev. 23, 450 (1924).

⁹ K. T. Compton and C. C. Van Voorhis, *ibid.* 26, 436 (1925) and 27, 724 (1926).

¹⁰ P. T. Smith, *ibid.* 36, 1293 (1930).

Concerning the Production of Groups of Secondaries by the Cosmic Radiation

The experiments with counters and cloud chambers have shown that the ionization attributed to the cosmic radiation is produced by ionizing corpuscular rays (capable of discharging a counter or of producing a cloud track) of energies ranging from 10^6 to 10^{10} electron volts. At least some of these corpuscular rays are secondaries originating within the surrounding matter, but whether the primary radiation which ejects these secondaries itself consists of ionizing corpuscles or is of a non-

To test the possibilities of laws other than the inverse-square, therefore, we have tried an interpolation between it and Davis's inverse-infinity power. For this purpose we made all other assumptions exactly like those of Rosseland's theory, the simplest of the inverse-square theories, but substituted an inverse-cube law for the inverse-square. The result is the equation

$$j(U) = \frac{6}{U \left\{ \left(\frac{\pi}{2 \cos^{-1} U^{-1/2}} \right)^2 - 1 \right\}}$$

This equation fits our present experimental values of $j(U)$ to within ± 0.01 for all values of U up to 3, though it is low by 0.04 at $U=5$ and by 0.08 at $U=7$. Altogether, it fits far better than any of the other theories, unless possibly the changes with U in the parameters of Bethe's theory may make it fit better than it appears to.

We must recognize, of course, that any theory such as this, based on the classical concept of force, with the introduction of quanta as extraneously imposed prohibitions, is at least antiquated. We must also remember that there is no basis for an inverse-cube hypothesis other than *ad hoc*. We therefore offer this hypothesis, not as one to be taken literally, but as a suggestion on the direction in which it may prove worth while to change the potential energy functions used in better theories.

D. L. WEBSTER

W. W. HANSEN

F. B. DUVEENCK

Stanford University,
California,

August 25, 1932.

ionizing gamma-ray or neutron character has been an unanswered question.

Experiments by Rossi¹ and by the writers² have shown that there are frequent groups consisting of two or more divergent ionizing rays which emerge simultaneously from a

¹ B. Rossi, Phys. Zeits. 33, 304 (1932); Rend. Lincei XV, 734 (1932).

² Johnson and Street, Phys. Rev. 40, 638 (1932).

block of lead, and a similar grouping phenomenon has been observed by those who have worked with cloud chambers. These observations could be explained by any one, or all of three postulates. I. The primary may be an ionizing ray which in passing through matter produces other ionizing rays by close collisions with electrons or nuclei. II. The primary may be a non-ionizing ray whose energy is at once transferred by a single nuclear collision to a group of secondary ionizing rays.

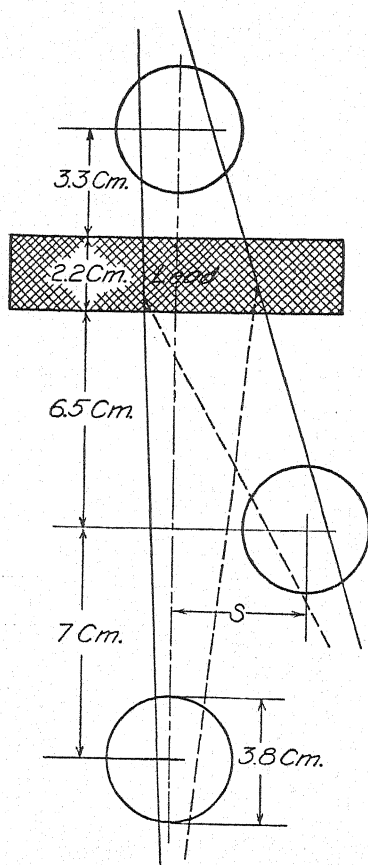


Fig. 1. Effective length of counter 9 cm.

III. The primary may be a non-ionizing ray whose energy is degraded by the formation of a succession of ionizing rays along an extended path.

To distinguish between these postulates we have made some experiments with the arrangement of three counters and the lead block shown in Fig. 1. If II is the correct hypothesis the presence of the lead block in the position indicated should have only an ab-

sorbing effect on the triple coincidence counting rate whereas an increase due to the lead should be noticed if I or III is right. The results in Table I show an increase due to the lead which is well above the statistical probable error, proving that at least a part of the grouping phenomenon must be accounted for either by postulate I or by III or perhaps by both.

To determine which of these two postulates applies, some experiments with the arrange-

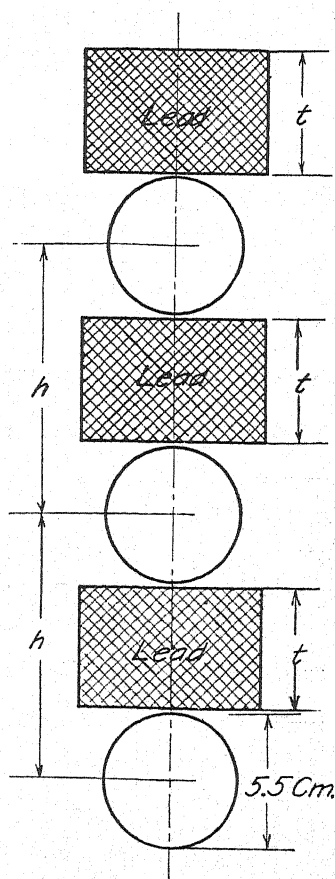


Fig. 2. Effective length of counter 12 cm.

ment of counters and lead blocks shown in Fig. 2 have been carried out. In this case the circuits were arranged for counting the double coincidences between counters 1 and 3 simultaneously with the triple coincidences. Counts were made both with the three lead blocks in position and with all of the lead removed. An explanation³ of the transition effects dis-

³ T. H. Johnson, Phys. Rev. 41, 545 (1932).

covered by Schindler⁴ and by Rossi¹ requires that, whether I or III is correct, the secondaries which enter any one of the lead blocks from above shall, for the most part, be absorbed in the thickness of lead used so that the probability that a primary be accompanied by a secondary below a lead block is inde-

chamber seldom contain more than two ionizing rays, and in the second place, a comparison of ionization measurements with counter data indicates an average of only two to three ionizing rays per group. These considerations necessitate the conclusion that if the primary is a non-ionizing ray it would be

TABLE I.

Distance <i>s</i>		Total counting period	Total counts	Counts per minute	Difference due to lead
4 cm	with lead	2484 min.	136	0.055 ± 0.003	0.015 ± 0.004
	without lead	3971	159	0.040 ± 0.002	
5 cm	with lead	3069	132	0.043 ± 0.002	0.014 ± 0.003
	without lead	2512	73	0.029 ± 0.002	
7 cm	with lead	5795	194	0.034 ± 0.002	0.018 ± 0.002
	without lead	3886	63	0.016 ± 0.001	

pendent of the condition above. However, most of the secondaries are sufficiently penetrating to pass through all three counters in the absence of the lead. If E is the efficiency of counter 2, the ratio T/D of triple to double counts without the lead is E whereas, with the lead in place, this ratio is EP , where P is the

unaccompanied by ionizing secondaries over such a large fraction of its path that P would be less than unity by an easily detectable amount. (If three were the average density of independently formed secondaries 20 percent of the path of the primary should be non-ionizing.) We are, therefore, left with the

TABLE II.

Spacing between counters (<i>h</i>)	Thickness of lead (<i>l</i>)	Total counting period	Total double counts (<i>D</i>)	Total triple counts (<i>T</i>)	<i>T/D</i>
13 cm	5 cm	1228 min.	2289	1913	0.84 ± 0.01 with lead
		1072	2389	1954	0.82 ± 0.01 without lead
18 cm	10 cm	1993	2074	1731	0.84 ± 0.01 with lead
		1497	2014	1615	0.81 ± 0.01 without lead

probability of any element of the path of the primary in lead being traversed by at least one ionizing ray (whether it be the primary itself or one of its secondaries). The results obtained are shown in Table II, from which it appears that there is no change in the ratio T/D due to the lead within the limits of error. Hence P is equal to unity. We must conclude, therefore, that the primary ray is either itself an ionizing ray or, if it is a non-ionizing ray, it is always accompanied by at least one of its secondary ionizing rays. This latter possibility must be excluded on other grounds. In the first place, the groups observed in the cloud

conclusion that all of the groups observed in the first experiment arise from an ionizing primary. This ray, of course, may itself have been produced by a non-ionizing gamma-ray or neutron and, furthermore, it is still possible that a part of the groups observed by other arrangements of counters or in the cloud chamber may arise according to postulate II.

We are indebted to Dr. E. C. Stevenson for his help in arranging the circuits and in recording the data.

J. C. STREET
THOMAS H. JOHNSON

The Bartol Research Foundation of The
Franklin Institute, Swarthmore, Pa.,
August 29, 1932.

⁴H. Schindler, *Zeits. f. Physik* **72**, 625 (1931).

Structure of Atomic Nuclei. II

It seems to be possible to regard the lighter nuclei as if their only constituents were protons and neutrons. The writer^{1,2} has suggested that closed shells exist, and that this may explain the presence of the "clusters" of nuclei discovered by Barton.³ The center of the cluster seems to lie about where the shells would be half-completed, provided that the closed shells correspond to the masses 36, 64, 100, 144, etc. On the simple model above, Zn 64 would have 30 protons and 34 neutrons, and it is hard to attach any particular significance to this arrangement. Also, one is rather at a loss to explain just what the constitution of Cl 37 is, unless it is admitted that after a closed shell has once become filled, stability conditions may favor the existence of holes in the closed shell for certain heavier isotopes.

To avoid these difficulties, one way is to adopt a tentative suggestion made to the writer by Prof. Dirac. This is that electrons may have a separate existence in certain nuclei, since β -type disintegrations exist. That is, that there are at least three types of primary particles, namely proton, neutron, and electron. The neutron is not to be thought of as a combination of proton and electron, but simply as a fundamental building-stone. Finally, the total angular momentum of the nucleus is integral or half-integral according as the total number of such independent particles is even or odd. This suggestion throws light on other phenomena and necessitates a revision of some earlier concepts.

In the central field of A 36, which has 18 protons and 18 neutrons, a neutron and an electron seem to be stabler than just a neutron. When they are added, Cl 37 is the result. One added proton gives A 38, and another proton K 39, where branching occurs. A neutron may be added, and an electron either added or taken away, resulting in the isobars A 40 and Ca 40, respectively. The existence of these isobars seems to support the hypothesis of nuclear electrons.

If to Ca 40 a neutron and electron be added, there is obtained the nucleus K 41, which emits β - and γ -rays. This nucleus contains 20 protons, 21 neutrons, and one electron. It

may be that the presence of this electron is partly responsible for the radioactivity of K 41, and that Sc 45 (and possibly Cl 37) will also have similar properties. Nuclei up to A 36 cannot disintegrate with emission of primary β -rays, owing to the absence of free electrons.

The isotopes thus far reported for the mass range $36 < M \leq 64$ are Cl 37, K 39, Ca 40, A 40, K 41, Ca 44, Sc 45, Ti 48, Cr 50, V 51, Cr 52, Cr 53, Cr 54, Fe 54, Mn 55, Fe 56, Ni 58, Co 59, Ni 60, Cu 63, and Zn 64. It has already been noted⁴ that "isotopes only become numerous for atomic numbers > 29 ." A glance at the distribution of isotopes seems to show one that a new regularity begins at $M=64$, and this we associate with the hypothesis that a closed shell has been formed. That is, Zn 64 is to consist of 32 protons, 32 neutrons, and two electrons. Though many points are missing in this mass range, still there are certain regularities apparent. For instance, the groupings Cr 50—V 51—Cr 52, Fe 54—Mn 55—Fe 56, and Ni 58—Co 59—Ni 60 are similar. It is probable that a fourth, Zn 62—Cu 63—Zn 64, exists. From Fe 54, Mn 55 may be formed by the addition of a neutron and an electron, and Fe 56 by the further addition of a proton. The total angular momentum of the Mn 55 nucleus is half-integral, so that it must contain an even number of electrons, namely two, as one would also expect for Fe 56. The nuclei Cr 50, Fe 54, Ni 58, and Zn 62 should, on the above basis, contain one electron and have half-integral spin values.

In addition to the isotopes A 38, Ca 42, Ti 46, K 43, and Sc 47 predicted by Beck,⁵ we would suggest V 49 or Ti 49, Fe 57 and 58, Ni 61 and 62, and Zn 62 as rather probable.

The isotopes which have been found for the mass range $64 < M \leq 100$ are Cu 65, Zn 66–68, and 70, Ga 69 and 71, Ge 70–77, As 75, Se 74, 76–78, 80, and 82, Br 79 and 81, Kr 78, 80, 82–84, and 86, Rb 85 and 87, Sr 86–88, Y 89, Zr 90, 92, and 94, Nb 93, Mo 92, 94–98, and 100, and Ru 96, 98–102, and 104. For most elements of even atomic number in this range, the isotopes have a mass range of about eight, as is exemplified by Zn 64–70, Ge 70–77, Se 74–82, Kr 78–86, Mo 92–100, and Ru 96–104. Accordingly, it might be expected

¹ J. H. Bartlett, Jr., *Nature* 130, 165 (1932).

² J. H. Bartlett, Jr., *Phys. Rev.* 41, 370 (1932).

³ H. A. Barton, *Phys. Rev.* 35, 408 (1930).

⁴ Rutherford, Chadwick, and Ellis, "Radioactive Substances," p. 524.

⁵ G. Beck, *Zeits. f. Physik* 47, 407 (1928).

that strontium has isotopes between 84 and 92, and zirconium isotopes between 88 and 96. We note the groupings Zn 64—Cu 65—Zn 66, Ge 70—Ga 71—Ge 72, Se 74—As 75—Se 76, Kr 78—Br 79—Kr 80, Mo 92—Nb 93—Mo 94, and Ru 96—(Ma 97)—Ru 98.

In the mass range $100 < M \leq 144$, the known isotopes are Ag 107 and 109, Cd 110–114, and 116, In 115, Sn 112, 114–122, and 124, Sb 121 and 123, Te 122–128 and 130, I 127, Xe 124, 126, 128–132, 134, and 136, Cs 133, and Ba 135–138. Since Sn and Xe have isotopes covering a mass range of twelve, this is probably true for other elements of even atomic number, and we should expect Te 118–130, Cd 106–118, Pd 100–112, and Ba 130–142.

Finally, a determination of the spin value for each isotope would be invaluable in deciding what the makeup of the nucleus is. For instance, Cl 35 has supposedly 17 protons

and 18 neutrons, so that the closed shell lacks one *d*-proton. The ground state should therefore be an inverted *D*-doublet, the lower level of which would have a total angular momentum $I=5/2$, which is the value actually observed.⁶ If Cl 37 does have an electron, then its spin should be either 2, 3, or 4. For this reason, it is not safe to assume, in unraveling a fine-structure pattern, that the nuclear spin for elements of odd atomic weight is capable of only half-integral values. At present, the information about nuclear spins is relatively meager, so that the rate of progress with nuclear stability questions is thereby limited.

JAMES H. BARTLETT, JR.

Quincy, Mass.,

August 30, 1932.

⁶ A. Elliott, Proc. Roy. Soc. 127, 638 (1930).

Luminosity of Sodium Flames

In a recent article by Bonner (Phys. Rev. 40, 105, 1932) on the luminosity of sodium flames attention was called to the fact that the greater part of the absorption of the sodium light by such flames occurs at their surfaces. It follows from this that a sodium flame which does not have any cool surface, such as was used by Bonner, must show less absorption than those with which other experimenters have worked. It is, therefore, surprising to find the opposite of this indicated by Bonner's data for concentrated solutions of NaCl.

That this difference is due neither to a difference in the apparatus used for measuring the light nor to the system of units employed is shown by the fact that Bonner found with dilute solutions less absorption than did either Locher (Phys. Rev. 31, 466, 1928) or myself (Phys. Rev. 38, 699, 1931). Similarly this difference can not be explained by any uncertainty in my measurements regarding the effective center of the flames, as was suggested by Bonner, since an error due to such a cause would have made my results different from his in the same way and to the same extent with both dilute and concentrated solutions and such was not the case.

Because Bonner's data was so different from what one might expect, I repeated his experiments as nearly as I could with the apparatus which I had previously used. I found, however, that it was impossible to make ac-

curate measurements of the length of the flame. Bonner had placed a non-luminous flame in front of the one into which salt was being sprayed, in order to keep the surface of the sodium flame hot. Due to diffusion of the sodium from one part into the other it was impossible to determine accurately the boundary between the two. If I measured the length of the sodium flame as if there were no diffusion from one part into the other, I obtained results which were much the same as those obtained by Bonner; but if I assumed that the sodium flame ended where it appeared to the eye to end, I obtained data similar to those which others have obtained. Bonner apparently assumed that it makes no difference how much diffusion there is from one part to the other. This would be entirely allowable, if it had been proven that a given amount of sodium gives the same amount of light irrespective of the number of flames into which it may be sprayed, but this is the assumption which Bonner is attempting to prove by his experiments and should not be assumed in the proof.

I believe, therefore, that one is justified in refusing to accept Bonner's experiments as definite proof of his conclusion.

C. D. CHILD

Colgate University,
Hamilton, New York,
September 8, 1932.

The Gyromagnetic Ratios for Nickel and Cobalt

In a paper recently published by the *American Academy of Arts and Sciences* (Proceedings, vol. 66, No. 8, pp. 273-348) I have given an account of an elaborate investigation of the rotation of permalloy and soft iron by magnetization. The gyromagnetic ratios for the two substances were found to be, respectively, $1.05 \times m/e$ and $1.04 \times m/e$, with errors probably less than $\frac{1}{2}$ percent.

Many successful observations have now been made on the less tractable substances nickel and cobalt. Preliminary values for the gyromagnetic ratios for these substances are, respectively, $1.06 \times m/e$ and $1.07 \times m/e$. The method, an alternating-current one, had to be modified to reduce the effects of certain sources of error, including magnetostriction, before any success was obtained with cobalt. Inasmuch as serious errors not suspected by other investigators have been eliminated in all of this work, the results obtained are far more reliable than those obtained by others, who have always obtained $1 \times m/e$ within the limits of their supposed experimental errors (with the exception of Einstein and de Haas,

who, in 1915, thought they had found $2 \times m/e$).

The gyromagnetic ratios obtained in this investigation agree with those published by L. J. H. Barnett and myself in 1925 (*Proceedings American Academy of Arts and Sciences*, vol. 60, No. 2) as the result of an elaborate investigation of the magnetization of many ferromagnetic substances by rotation, the mean for all these being $1.06 \times m/e$, with an error estimated as not greater than 2 percent. They also agree with the results obtained by me for iron when the effect was discovered in 1914, in view of the relatively large experimental error (some 10 or 15 percent) in these early observations. A complete account of this new work will be published later.

S. J. BARNETT

The University of California at Los Angeles,
and

The California Institute of Technology
September 12, 1932.

Angular Distribution of Electrons Scattered in Mercury Vapor

In a recent paper (Phys. Rev. 40, 731, 1932) describing an investigation on the scattering of electrons in mercury vapor, Tate and Palmer conclude that Mott's theory is quite inadequate to account for the angular distribution of the electrons which are scattered elastically. Mott's theory leads to a formula

$$I(\theta, v) = \left(\frac{e^2}{2mv^2} (Z - F) \operatorname{cosec}^2 \frac{\theta}{2} \right)^2$$

where $I(\theta, v)$ is the number of electrons having a velocity v and scattered through an angle θ , Z the atomic number of the scattering atom, and F the atomic structure factor. Their conclusion is based on the fact that the experimental curve representing the number of electrons scattered as a function of the angle is far less steep than the curve representing $\operatorname{cosec}^4 (\theta/2)$. This method of testing the formula implicitly assumes that F is independent of θ , an assumption which is not correct. F values are given by James and Brindley (Phil. Mag. 12, 81, 1931) for caesium ($Z=55$), together with a formula which en-

ables one to calculate the F values for any other heavy element from those listed for caesium. In this way a table of F values for mercury was constructed. On using these values in the formula given above, Mott's function $I(\theta, v)$ could be calculated. It was then found that there was a much better agreement between the theoretical curve and the experimental curve. The experimental curve is now somewhat steeper than the curve representing $(Z - F)^2 \operatorname{cosec}^4 (\theta/2)$, a result which is in accord with that obtained by Hughes, McMillen and Webb (Phys. Rev. 41, 154, 1932) for the scattering of electrons by helium atoms over the same range (0° to about 60°). They found that, when the experimental curves began to deviate from the Mott curves which is the case when electron energies less than about 400 volts are involved, the experimental curves are steeper than the theoretical curves.

The F values used for mercury are probably to be regarded only as a fairly close approximation. When such values are used to calculate a difference, $(Z - F)$, it is evident that we cannot at present expect to construct

a highly accurate theoretical curve. However the deviation between the theoretical curve and the experimental curve given by Tate and Palmer for 700 volt-electrons is probably real and not to be accounted for by the uncertainty in the F values. It would be interesting to see whether or not the theoretical, and ex-

perimental curves would coincide for mercury when higher electrons speeds are used.

A. L. HUGHES

Washington University,
St. Louis, Missouri,

September 14, 1932.

On the Radiation Originating from a Beam of Electrons in
Mercury Vapor and the Mean Life of the 2^3S_1 State

Previously the writer¹ has obtained photographs of the mercury spectrum produced by a beam of electrons in mercury vapor. The optical arrangement consisted of projecting the image of the electron beam on to the slit

recently been confirmed by Lees and Skinner.² The extension of the lines beyond the image of the electron beam is caused by the radiation of atoms lying outside of the boundaries of the beam. In Table I is included the most promi-

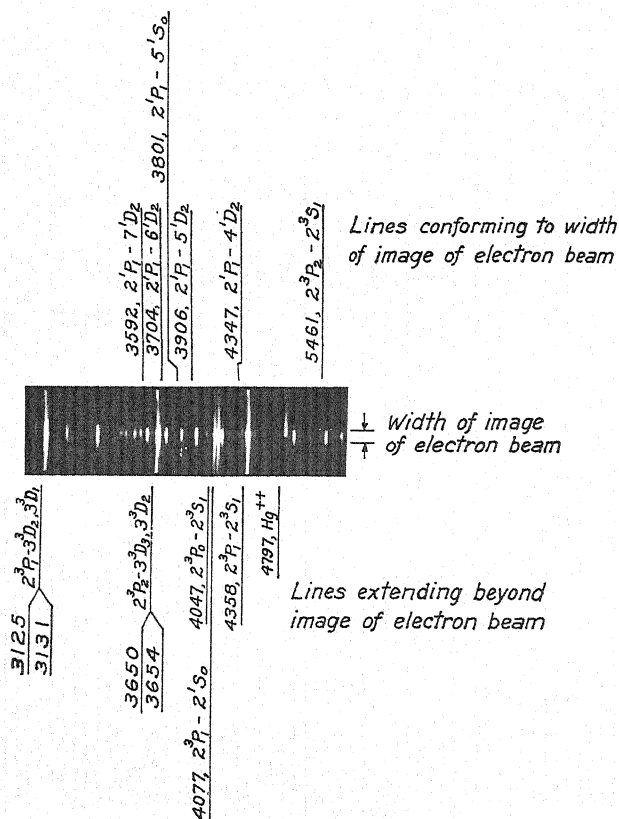


Fig. 1. A portion of the mercury spectrum illustrating the lengthening of lines beyond the image of electron beam.

of the spectrograph perpendicular to the length of the slit. It was found that some of the lines extended beyond the image of the electron beam, this being particularly true for the resonance line 2537A. This result has

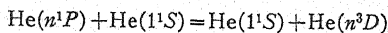
not been previously reported. The normal lines obtained which are classified into two groups; extended lines and normal lines. Fig. 1 illustrates a typical spectrogram obtained. In this particular case the electrons

¹ Maxwell, Phys. Rev. 32, 715 (1928).

² Lees, and Skinner, Proc. Roy. Soc. 137A, 186 (1932).

were accelerated to a velocity of 200 volts. A transverse electric field was applied for the purpose of drawing out the spark line 4797A as shown in Fig. 1. The shape of the lines was not particularly dependent upon the speed of the electrons. In general the lines having the levels 2^3P_0 , 2^3P_1 , 2^3P_2 , as the final state are lengthened, whereas the lines terminating in the 2^1P_1 state do not show spreading beyond the image of the electron beam. An exception to this rule, however, occurs for the line $2^3P_2 - 2^3S_1$ (5461A) which does not show any appreciable elongation. The lines of the series $2^1P - n^1S_0$ (4916A, 4108A) showed slight extension beyond the image of the electron beam, but the line 3801A, $2^1P_1 - 5^1S_0$ showed practically no spreading.

The lengthening of the resonance line (2537A) is obviously caused by absorption since it is very easily absorbed at the pressures of about 0.001 mm of Hg used in this case.



occurring outside the electron beam where the energy differences between the n^1P and n^3D states are of the order of the thermal energy. For mercury, similar atomic collisions resulting in a change from n^1P_1 to $n^3D_{1,2,3}$ states may be possible. Transitions of this kind to populate the 2^3S_1 state from any of the n^1P_1 levels will be very unlikely on account of the large energy differences involved.

Randall and Webb⁵ have measured the mean life of the 2^3S_1 state of mercury by using the lines $2^3P_2 - 2^3S_1$ (5461A), $2^3P_1 - 2^3S_1$ (4358A) and $2^3P_0 - 2^3S_1$ (4047A) and found that the lines 4358A and 4047A gave the mean life of 5.75×10^{-8} sec. while the line 5461A gave an entirely different value of 2.37×10^{-7} sec. In this connection it is very interesting to notice from Table I that the

TABLE I. Lines of the mercury arc spectrum.

Lines extending beyond image of the electron beam		Lines conforming to the width of image of electron beam	
$1^1S_0 - 2^3P_1$	2537	$2^1P_1 - 4^1D_2$	4347
$2^3P_0 - 2^3S_1$	4047	$2^1P_1 - 5^1D_2$	3906
$2^3P_0 - 3^3S_1$	2752	$2^1P_1 - 6^1D_2$	3704
$2^3P_0 - 3^3D_1$	2967	$2^1P_1 - 7^1D_2$	3592
$2^3P_1 - 2^3S_1$	4358	$2^1P_1 - 5^1S_0$	3801
$2^3P_1 - 3^3S_1$	2893	$2^3P_2 - 2^3S_1$	5461
$2^3P_1 - 4^3S_1$	2576		
$2^3P_1 - 2^1S_0$	4077		
$2^3P_1 - 3^3D_2, 3^3D_1$	3125, 3131		
$2^3P_1 - 4^3D_2, 4^3D_1$	2653		
$2^3P_1 - 5^3D_2, 5^3D_1$	2482		
$2^3P_2 - 3^3D_3$	3650		
$2^3P_2 - 3^3D_2$	3654		

It has been proposed³ that the lengthening of the other lines was caused by absorption of atoms in the 2^3P_0 , 2^3P_1 and 2^3P_2 state located in the vicinity of the electron beam.

Similar lengthening or spreading of spectrum lines has been found for helium⁴ and for the case of the lines $2^3P - n^3D$. Lees and Skinner suggested that it was caused by collisions of the type

³ Maxwell, Phys. Rev. **31**, 711 (1928); see also for instance, for absorption of excited states: Turner, and Compton, Phys. Rev. **25**, 606 (1925); Wood, Phil. Mag. **50**, 774 (1925); *ibid.* **4**, 466 (1927).

⁴ Lees, Proc. Roy. Soc. **137A**, 173 (1932); Lees and Skinner, reference 2; Maxwell, Early issue of Jour. Frank. Inst.

line 5461A which gave the greater mean life shows no lengthening while on the other hand the other two lines 4358A and 4047A have prominent spreading. This shows that outside of the electron beam there are atoms in the 2^3S_1 state which will give rise to transitions to the 2^3P_0 and 2^3P_1 levels but with practically the exclusion of transitions to the 2^3P_2 state. This undoubtedly means that the fine structure of the 2^3S_1 level plays an important part in the radiation phenomena, in support of the conclusion arrived at by Randall and Webb to account for the dis-

⁵ Randalls and Webb, Phys. Rev. **35**, 665, 1161 (1930); see also Richter, Ann. d. Physik, **7**, 293 (1930).

crepancies found for the mean life of this state.⁶

There exists the possibility that the photograph plate characteristics may vary for the triplet lines in such a manner as to weaken the spread of the line 5461A in comparison with the lines 4047A and 4358A, since the green line is nearer to the less sensitive portion of the plate. Exact intensity measure-

⁶ For further discussions see; Morozoroski, *Zeits. f. Physik* 68, 278 (1931); Frisch and Pringsheim, *Zeits. f. Physik* 67, 169 (1931).

ments were not obtained, however the difference in shape of the line 5461A in comparison with the other lines of this triplet appears too great to be accounted for by errors of this kind.

This work was done in the laboratory of the Bartol Research Foundation.

LOUIS R. MAXWELL

5336-42nd St., N.W.,

Washington, D.C.,

September 15, 1932.

The Disintegration of Lithium by Swiftly-Moving Protons

We have recently carried through preliminary experiments on the disintegration of lithium by swiftly-moving protons and have obtained results in confirmation of those of

the source of high-speed protons, we have bombarded a crystal of lithium fluoride with protons having energies of 360,000, 510,000, and 710,000 volts. Radiations emanating from

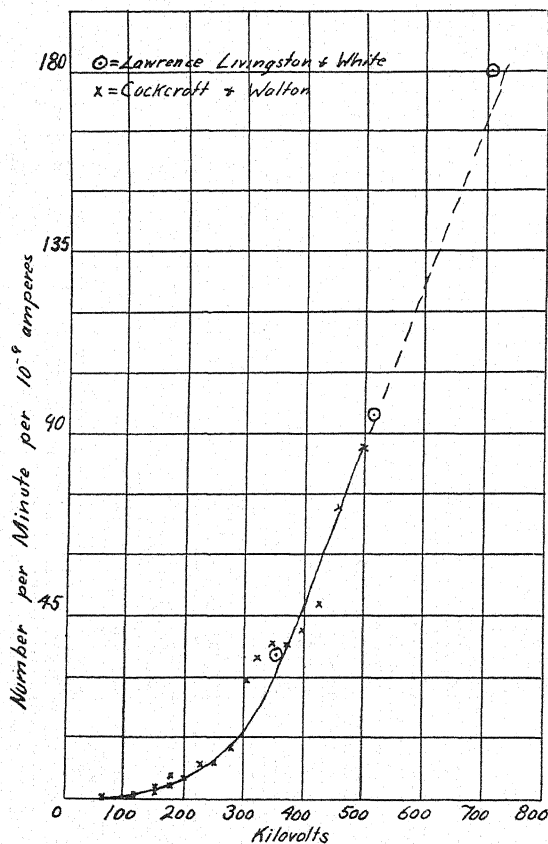


Fig. 1.

Cockcroft and Walton (*Proc. Roy. Soc. A* 137, 229-242, 1932).

Using the apparatus of Lawrence and Livingston (*Phys. Rev.* 40, 19-35, 1932) as

the crystal were detected by a Geiger point counter with a mica window (stopping power 2.2 cm of air) adjacent to the crystal, subtending a solid angle of $\pi/10$. Counts were ob-

tained proportional to the bombarding proton current (about 10^{-9} amp.), there being for 500,000 volt-protons about 95 counts per minute per milli-microampere. Fig. 1 is a plot of our observed number of counts per minute per milli-microampere for the three voltages and also the corresponding observations of Cockcroft and Walton adjusted to our curve at 500,000 volts. It is seen that our observed variation is in excellent agreement with theirs over the overlapping region and that our observation at 710,000 volts agrees with a linear extrapolation (dotted line) above their range of observation. In the above figure the two sets of data have been adjusted to agree at 500,000 volts. Actually there is an apparent disagreement in that when account is taken of geometrical considerations, our observed number of counts per unit current per unit solid angle is about five times that of one set of observations of Cockcroft and Walton (Fig. 4 of their paper) and about equal to that derived from another set of their observations (their Fig. 2)—while on the other hand, one would expect the observed rate of disintegration of lithium in a lithium fluoride crystal to be about one-fourth the rate for the pure metal.

There are numerous possible sources of this slight difference in observations. There is the possibility that our counter was registering counts in excess of the number of alpha-particles entering the counting chamber. The counter was operated with voltages above its gamma-ray threshold and therefore was sensitive to such radiations. However, some counts were obtained below the gamma-ray threshold showing that some of the counts certainly were due to alpha-particles. On the other hand, Cockcroft and Walton's values may be too low because of an appreciable lack of homogeneity of velocities of their bombarding protons or because of an appreciably rough lithium target which would diminish the number of alpha-particles escaping to the counter, i.e., at right angles to the proton beam.

At this early stage of the work we of course would not urge our absolute values as more

likely nearer the truth; but it is interesting to note that they are in excellent accord with the predictions of Gamow's theory. Professor J. R. Oppenheimer has kindly calculated for us, along the lines of Gamow's theory, the probability that an alpha-particle will be liberated by a proton striking a lithium fluoride crystal, taking account of the range and velocities of the proton within the crystal. His calculation for 500,000 volt-protons indicates that there should be from one to ten alpha-particles liberated for every 10^7 protons, while we observed six alpha-particles per 10^7 protons (assuming each count of the Geiger counter represents one disintegration alpha-particle). Dr. Oppenheimer also calculated the variation with energy of the proton of the probability of disintegration, obtaining the relative values of 1.0, 2.6 and 5.2 for the voltages 360,000, 510,000, and 710,000, respectively. These values, as may be seen from the above figure, are also in splendid agreement with our observations. Thus, these calculations, though still rough and schematic, show that the simple extension of Gamow's theory is fully able to account for the order of magnitude and voltage dependence given by observation.

These experiments were begun by Dr. James A. Brady who was joined later by Drs. Donald Cooksey and F. N. D. Kurie. They were successful in detecting radiations from the bombarded lithium fluoride but unfortunately because of insufficient available time had to abandon the experiments which we have carried on. We are much indebted to them for their participation in the earlier stage of the work as well as to Dr. Malcolm C. Henderson who has taken an active part in the work since their departure and is continuing with the experiments.

ERNEST O. LAWRENCE
M. STANLEY LIVINGSTON
MILTON G. WHITE

Radiation Laboratory,
Department of Physics,
University of California.
September 15, 1932.

BOOK REVIEWS

A History of Experimental Physics. C. T. CHASE. Pp. 195, Figs. 15. D. Van Nostrand Company, New York, 1932. Price \$2.25.

This book deserves the attention of all teachers and serious students of physics. The perspective to be gained by a study of the historical development of physics is valuable and leads to a better understanding of the subject. That the treatment is non-mathematical will appeal to some readers, but it seems to the reviewer that an essential part of physics is thereby omitted. It is striking that nearly half of the book deals with developments since 1895, an era of very rapid growth and of many new ideas. Since much of this material has not yet won its way into the usual general course in physics, this text makes an excellent supplement to such a course. The subject matter is very well selected and the style is clear and interesting. The few slips are not serious.

JOSEPH VALASEK
University of Minnesota

Vision and Colour Vision. R. A. HOUSTOUN. Pp. 238, Figs. 102. Longmans, Green and Company, New York, 1932. Price \$4.50.

When a physicist departs from a discussion of intensity and wave-length in connection with light, he is stepping over the boundary between physics and psychology. However, several of the great physicists have strayed in this way because of the many interesting phenomena involved in vision. The present volume will be an inducement to others to follow in their steps.

This volume gives, first of all, a resumé of existing knowledge on vision and color vision. It differs from the usual summary in that the author himself has performed many experiments in the field and has some pertinent criticisms and suggestions to offer. However, many readers will disagree with some of his conclusions. In particular, the association of the two reticular and nuclear layers of the retina with the red-green and yellow-blue processes of Hering will require further investigation. Can it be reconciled with the zonal color characteristics of the human eye? This particular phase of color vision is scarcely mentioned.

The author raises a mathematical objection to the Young-Helmholtz theory. It is not noticed that this will also apply to the author's theory for any stimulus which excites both processes. However it is not hard to make a plausible modifying assumption in either case.

It is to the credit of the author that he has devised experiments which make it possible to obtain a numerical measure of the normality or abnormality of color vision of an individual. As a result of such a measurement of color vision, it is found that there are no fixed types of color blindness, but that natural variation from the mean accounts for practically all of the abnormalities. The data in support of this are very impressive, but the reviewer thinks that at least the microscope experiment can be attacked on the ground that colors may be sensed by their darkness, i.e., that red may be detected as "the darker color" by the red blind. However, a wide circle of readers should find much food for thought and suggestions for further experiments in this interesting and stimulating book.

JOSEPH VALASEK
University of Minnesota

THE PHYSICAL REVIEW

On the Scattering of Hard X-Rays by Solids

By S. CHYLINSKI

Ryerson Physical Laboratory, University of Chicago

(Received August 8, 1932)

The distribution of the intensity of scattering for angles ranging from 10 to 105 degrees has been experimentally determined for various solids. For paraffin and aluminum the scattering occurred at an effective wave-length for the primary rays of 0.23A; for copper and lead the wave-length was 0.19A. These wave-lengths were determined from absorption measurements in aluminum. The scattering from paraffin and aluminum was from thin plates by the transmission method, while that from copper and lead was from thick plates by reflection. The ratios of intensities at any given angles to those at 90 degrees were corrected for the different ionization effects at those angles, on account of the change of wave-length due to the Compton effect. Comparison of the experimental results for paraffin with the predictions of the Breit-Dirac theory of scattering from free electrons shows distinct excess scattering. This part of the work has been performed with a precision of about 1 percent. In addition, the S -values (scattering per electron) were computed for the various materials from their experimental scattering functions, using the paraffin value at 90 degrees, as predicted by the Dirac theory, as the basic measure. The S -values from aluminum have a most probable error of less than 2 percent, while those from copper and lead, being based upon a not entirely satisfactory computation, are assigned less than 6 percent. Curves have been plotted of the S -values against $[\sin(\phi/2)]/\lambda$. The S -values show a large increase with the atomic number of the scatterer for the smaller values of $[\sin(\phi/2)]/\lambda$, while for the larger values they tend to come together.

I. INTRODUCTION

THE unit of scattering of x-rays by matter is the electron. J. J. Thomson¹ was the first to calculate, on the basis of the electromagnetic theory, the intensity scattering function for a free electron. His classical expression is

$$I_{\phi} = I_0(e^4/2m^2c^4r^2)(1 + \cos^2 \phi)$$

where I_{ϕ} represents the intensity of the scattered beam at an angle ϕ with the direction of the primary beam, at a distance r from the scattering electron, the mass of which is m and charge e in e.s.u. The primary beam is assumed to be unpolarized and its intensity is I_0 . c stands for the velocity of light. If we are dealing with an atom having Z orbital electrons, and if the distances between these electrons are so small as to be negligible in comparison with the wave-length of the incident x-rays, then we may suppose that all these electrons act as a unit in the scattering process. Thomson's formula shows

¹ J. J. Thomson, *Conduction of Electricity through Gases* p. 325, 2nd Ed.

that the scattering by the atom would then be Z^2 times the intensity due to a single free electron. If, on the other hand, the electrons in the atom are separated by distances large compared with the wave-length of the x-rays, we may suppose them to scatter independently, in which case the intensity should be only Z times that due to a single free electron. Depending, then, upon the concentration of the electrons in the atom, the intensity of the x-rays scattered from it will vary by a factor of Z . If the electrons are at distances comparable with the wave-length of the x-rays, interference, constructive as well as destructive, will take place between the x-rays scattered by the different electrons of the atom, and as a result the intensity scattered by the atom as a whole will then be between Z^2 and Z times that due to a single free electron. Compton,² Debye,³ Schott⁴ and others have calculated the intensity scattering function for various atomic models.

The intensity of x-rays scattered by a number of atoms depends not only upon the configuration of the electrons within each atom but also upon the configuration of the atoms in the molecules, as well as upon any special orientation of the molecules themselves. In the particular case, where the atoms are grouped in a crystal lattice, we have the so-called *Laue or Bragg Reflection* which, therefore, is only a special case of scattering. In the case of liquids or amorphous solids, the phenomenon known as "excess scattering" is probably the result of the cooperation of the three factors just mentioned. Debye⁵ has shown that the last two of these factors play no roll when perfect gases are used for scattering and hence excess scattering must in that case be ascribed solely to the configuration of the electrons within the atoms. On account of this simplification of the problem great progress has been made in the theories of scattering for monatomic gases. So far as the writer is aware, only Jauncey⁶ has made an attempt to solve the problem for amorphous solids.

The quantum theories predict a scattering function different from Thomson's formula. They are, however, based upon the assumption that for the limiting case of long wave-lengths, where the motion imparted to the scattering electron is negligible, the intensity of the scattered rays should approach that assigned to it by Thomson's classical formula. The older forms of the quantum theory were not successful in giving a unique solution for the scattering function. The newer forms do give such a solution and it is,

$$I_{\phi} = I_0 \frac{e^4}{2m^2r^2c^4} \frac{(1 + \cos^2 \phi)}{(1 + \alpha \text{ vers } \phi)^3}$$

where $\alpha \equiv h\nu/mc^2$, h being Planck's constant, ν the frequency of the x-rays, and the other symbols have the same significance as before.

² A. H. Compton, Washington University Studies 8, 99 (1921).

³ P. Debye, Ann. d. Physik 46, 809 (1915).

⁴ G. A. Schott, Proc. Roy. Soc. Lon. A96, 395 (1920).

⁵ P. Debye, Phys. Zeits. 28, 135 (1920).

⁶ G. E. M. Jauncey, Phys. Rev. 37, 1193 (1931).

Breit⁷ was the first to suggest this formula on empirical grounds and reasoning from the correspondence principle. Dirac⁸ derived it theoretically with the help of the quantum dynamics of Heisenberg and Born, and Waller⁹ as well as Gordon¹⁰ did the same on the principles of the de Broglie-Schrodinger wave theory. It is true, that more recently, Klein and Nishina,¹¹ on the hypothesis of the spinning electron using Dirac's relativistic quantum dynamics, have derived a scattering function which differs somewhat from the above. However, deviations of the two formulae are of the order of $(h\nu/mc^2)^2$, while the Breit-Dirac expression differs from the classical Thomson formula by quantities of the order of $h\nu/mc^2$. In the x-ray region, where $h\nu/mc^2$ is small the deviations between the two quantum expressions are virtually negligible. Even for an $\alpha=0.5$, which corresponds to a wave-length of 0.05A the deviation amounts to only about 10 percent.

The only experimental tests of the quantum formula for sufficiently hard rays, that have so far been published, are the indirect ones of Fricke and Glasser,¹² for effective wave-lengths of 0.18 and 0.115A, and those of Ishino,¹³ and Owen, Fleming and Fage,¹⁴ for the γ -rays from RaC. The first consisted in determining the ratios of the coefficients of photoelectric absorption to those of true absorption due to scattering in carbon, and in the latter two cases, in measuring the ratios for aluminum of the coefficients of true absorption due to scattering to the total scattering coefficients. A direct test, by comparing I_ϕ with the experimental values of scattered intensities, is attended by considerable difficulties. In the earlier technique of various authors,¹⁵ the wave-lengths used were too long to show appreciable deviations from the predictions of the classical theory. Where short wave-lengths were used the results are difficult to interpret on account of the comparatively large corrections that would have to be made in the ionization effects at different angles. This is due to the small absorption in the ionization chamber.

The work described in this paper was undertaken with a view of testing the scattering function given by the quantum theory. For hard x-rays and scattering materials of low atomic number, we may suppose, in view of the Compton effect, that the scattered rays are more or less completely modified. In that case the intensity of scattering should most nearly approximate that predicted by the quantum theory. Paraffin was selected as the light scatterer and in addition the scattering distribution curves were determined for aluminum, copper and lead.

⁷ G. Breit, Phys. Rev. 27, 362 (1926).

⁸ P. A. M. Dirac, Proc. Roy. Soc. Lond. A111, 422 (1926).

⁹ Ivar Waller, Phil. Mag. 4, 1228 (1927).

¹⁰ W. Gordon, Zeits. f. Physik 39, 117 (1926).

¹¹ Klein and Nishina, Zeits. f. Physik 52, 852 (1928).

¹² H. Fricke and O. Glasser, Zeits. f. Physik 29, 374 (1924).

¹³ M. Ishino, Phil. Mag. 33, 140 (1917).

¹⁴ E. A. Owen, N. Fleming, and W. E. Fage, Proc. Phys. Soc. 36, 355 (1924).

¹⁵ For a summary see Compton's *X-rays and Electrons* p. 306, D. Van Nostrand Co. N.Y.C. (1926).

II. APPARATUS AND EXPERIMENTAL PROCEDURE

A diagram of the apparatus is given in Fig. 1. A tungsten target x-ray tube was operated at 120 peak k.v. and 5 m.a. with half-wave rectification. The

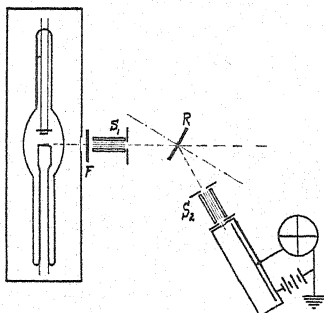


Fig. 1. Arrangement of apparatus.

tube was water cooled and immersed in oil in a heavy lead box. In the front of the box was fitted a heavy lead glass plate having a thin celluloid window. This arrangement permitted the tube to be brought very near to the spectrom-

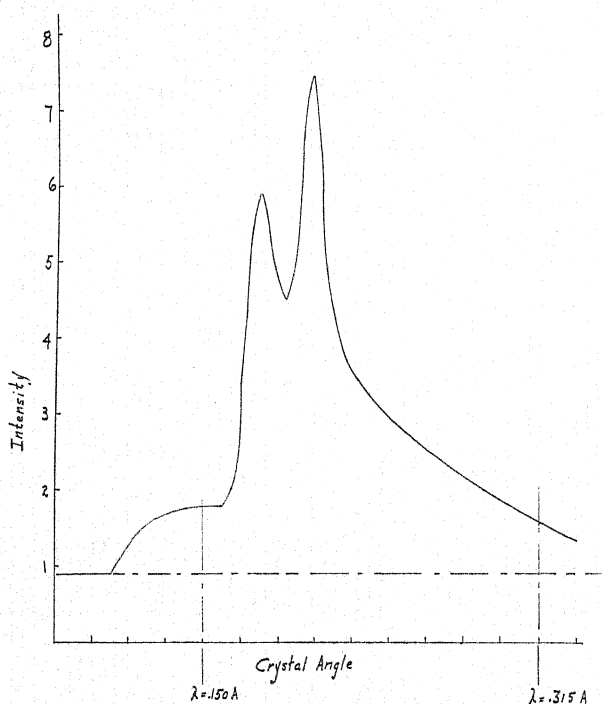


Fig. 2. Spectrum of radiation transmitted through tungsten filter.

eter with a consequent increase of intensity in spite of the absorption in the oil.

An effort was made to work with homogeneous radiation. It was hoped, that by designing all component parts of the apparatus for maximum effi-

ciency, it would be possible to use crystal-reflected rays. Unfortunately, however, the intensities obtained were too low for accurate measurements and the attempt had to be abandoned. Also, the balanced filter method could not be used as the two necessary elements for such filter, when using tungsten radiation, erbium and ytterbium, were not procurable anywhere in the United States. Finally, it was decided to use a tungsten filter, as shown at *F* in Fig. 1. The spectrum of the radiation transmitted through this filter, which consisted of two metallic tungsten foils each 0.065 mm thick, is given in Fig. 2. It is seen that the filtered band extends practically from about 0.15 to 0.315Å.

Soller collimators were used for both the primary and scattered beams. They are shown as *S*₁ and *S*₂ in Fig. 1. They were 10 cm long and the distance between adjacent lead spacers was 0.1 cm, so that a maximum angular divergence of a little over one degree was obtained in the horizontal plane. The width of the collimators could be varied by proper slits, the height of which was 1 cm. This made the scattering angle slightly larger than recorded on the spectrometer circle, but the corrections were too small to be taken account of.

R in Fig. 1. represents the scattering substance mounted in the center of the spectrometer. In the case of paraffin and aluminum thin plates of these materials were placed so that the normal to the plate always made an angle of $\phi/2$, where ϕ is the scattering angle. This so-called "Crowther position" has certain obvious advantages over other ways of mounting the scatterer. The copper and lead plates, for reasons of greater intensities, were mounted so that the angle between the face of the plate and the primary beam was always one half the scattering angle. These plates were thick enough to absorb all of the primary radiation.

The intensities were measured with a Compton electrometer, mounted over the axis of the spectrometer, having a sensitivity of 8900 divisions per volt on a scale 150 cm away. The ionization currents could be measured with a reproducibility of about 3 percent.

At first an ionization chamber 7 cm long filled with xenon at two atmospheres pressure was used. Due to the insufficient absorption in this chamber and the large fluorescent yield of xenon certain corrections had to be made which, considering the nature of the experiment, were felt to be too large. Accordingly, another high pressure ionization chamber was constructed and filled with argon at a pressure of 1000 lbs. per sq. in. It was made of cylindrical, seamless steel tubing, 40 cm long and 4.45 cm inside diameter. The window was of 0.7 mm celluloid. The absorption in the window for the wavelengths used was negligible and hence no corrections were made for it. The absorption in the chamber of a wave-length of 0.21Å is 90 percent and the fluorescent yield for argon is, according to Auger,¹⁶ only 0.07. The corrections are discussed in more detail below. The potential across the electrodes of the ionization chamber was 135 volts, which was about twice the value needed for saturation.

All parts of the apparatus were carefully shielded. The electrometer system, including the connections to the ionization chamber, was protected by

¹⁶ Auger, *Ann. de Physique* 6, 183 (1926).

large lead baffles. Other lead baffles, suitably disposed, prevented all stray radiation from reaching the ionization chamber.

The procedure consisted in a determination of the angular distribution of the intensities scattered from paraffin, aluminum, copper and lead. In the case of the last two, care was taken to exclude the characteristic radiations from entering the ionization chamber. This was accomplished by using an aluminum filter 0.65 mm thick for copper and one 1.3 mm thick for lead. Wave-lengths of the scattered rays at the different angles were determined by measuring the absorption in several sheets of aluminum. The final step was to make an accurate measurement of the scattered intensities at 90° from the different materials under experimental conditions as nearly alike as can be realized in actual practice.

The constants of the scattering materials are as follows: paraffin, 0.276 g per sq. cm; aluminum, 0.103 g per sq. cm; copper, 5.09 g per sq. cm; lead, 3.80 g per sq. cm.

The paraffin was from a block of commercial "Parowax." The aluminum and lead were from the usual rolled sheets of these materials. The copper was of electrolytic origin. An attempt to work with finely powdered aluminum failed because no good binding material was available.

III. EXPERIMENTAL RESULTS AND CALCULATIONS

The ratios of the ionization currents at any angle ϕ to those at 90° are given in the second column of Tables I to IV for each of the four materials.

TABLE I. *Paraffin at $\lambda 0.23A$.*

Angle ϕ	Exp. ratio of ionization $i\phi/i_{90}$	Ratio from Crowther's formula	Corrected ratio $P\phi/P_{90}$	Scattering per gram s/ρ	S
10	3.23	4.46	4.9	0.0432	1.84
20	2.50	3.42	3.72	0.0328	1.46
30	2.10	2.80	3.04	0.0268	1.28
40	1.75	2.28	2.46	0.0216	1.14
50	1.53	1.92	2.01	0.0177	1.03
60	1.33	1.59	1.67	0.0147	0.99
70	1.18	1.35	1.39	0.0122	0.92
80	1.06	1.15	1.16	0.0102	0.83
90	1.0	1.0	1.0	0.0088	0.74
105	1.15	1.26	1.24	0.0109	0.85

TABLE II. *Aluminum at $\lambda 0.23A$.*

Angle ϕ	Exp. ratio of ionization $i\phi/i_{90}$	Ratio from Crowther's formula	Corrected ratio $P\phi/P_{90}$	Scattering per gram s/ρ	S
10	9.50	12.60	13.80	0.1290	5.70
20	4.50	6.20	6.80	0.0636	2.95
30	3.00	4.05	4.40	0.0410	2.04
40	2.20	2.90	3.13	0.0293	1.61
50	1.60	2.03	2.15	0.0201	1.22
60	1.30	1.58	1.65	0.0154	1.08
70	1.20	1.39	1.43	0.0134	1.05
80	1.05	1.13	1.14	0.0106	0.905
90	1.0	1.0	1.0	0.0093	0.81
105	1.20	1.33	1.31	0.0122	1.0

TABLE III. *Copper at $\lambda 0.19\text{\AA}$.*

Angle ϕ	Exp. ratio of ionization	Scattering per gram	S
10	22	0.2340	11.0
20	7.95	0.0855	4.20
30	4.75	0.0510	2.69
40	3.25	0.0350	2.04
50	2.30	0.0247	1.59
60	1.70	0.0182	1.35
70	1.40	0.0150	1.19
80	1.15	0.0123	1.10
90	1.0	0.0107	0.99
105	1.07	0.0115	1.0

TABLE IV. *Lead at $\lambda 0.19\text{\AA}$.*

Angle ϕ	Exp. ratio of ionization	Scattering per gram	S
10	22.0	0.557	30.0
20	11.20	0.284	16.05
30	5.00	0.127	7.73
40	3.13	0.0792	5.30
50	2.15	0.0545	4.02
60	1.65	0.0418	3.56
70	1.35	0.0342	3.26
80	1.12	0.0284	2.94
90	1.0	0.0253	2.70
105	1.0	0.0253	2.53

These ratios were, of course, corrected for the leak in the electrometer system. The third column of Table I and II is derived from the second by evaluation from Crowther's formula.¹⁷ This formula for the intensity of x-rays scattered in a direction ϕ from a thin plate of material of thickness t is,

$$I_{\phi} = AIts/R^2 \cos(\phi/2) \quad (1)$$

where I_{ϕ} is the intensity scattered in a direction ϕ , I is the intensity of the primary rays *after* penetrating the plate in the Crowther position, s is linear scattering coefficient per unit solid angle in a direction ϕ , A is the area of the ionization chamber window, and R is the distance between the window and the plate. Also, I is given by

$$I \equiv I_0 e^{-\mu t / \cos(\phi/2)}$$

where I_0 is the intensity of the primary rays at the incident face of the scattering plate, and μ is the linear absorption coefficient of the primary rays in the plate.

From Eq. (1) an expression may be set up giving the ratio of the scattering per gram per unit solid angle in any direction ϕ relative to that at 90° with the primary beam, thus cancelling out I_0 .

Measurements of absorption in aluminum of the rays scattered from paraffin at 90° gave an absorption coefficient which by interpolation from the values given in Compton's table¹⁸ corresponded to a wave-length of 0.25\AA . At

¹⁷ J. A. Crowther, Proc. Roy. Soc. A86, 478 (1912).

¹⁸ Compton's *X-rays and Electrons*, p. 184.

30° the result was 0.23A. The values for aluminum were the same within the uncertainty of the measurement. Considering the hardness of these rays, the scattered radiation from paraffin may be assumed to be completely modified at 90° and that from aluminum is virtually so. Accordingly, for these two materials, the change in wave-length at the different scattering angles was computed from the formula for the Compton effect,

$$\Delta\lambda = (h/mc)(1 - \cos \phi)$$

where $\lambda = 0.25$ at 90° . The wave-lengths so obtained were used in the correction computations given below.

When x-rays of different wave-lengths enter an ionization chamber, the ionic saturation currents which one measures, are not in general proportional to the intensities in the beams. Allison and Andrew¹⁹ give an expression which enables one to calculate the true intensities. This expression is

$$I = cPFR \quad (2)$$

where I is the measured ionic saturation current, P is the power of the beam of x-rays entering the chamber, F is the fraction of the primary energy absorbed in the chamber, c is a constant for a given gas, which is inversely proportional to ϵ , where ϵ is the energy spent in producing a pair of ions, and R is given by

$$R = 1 - \frac{\tau_k}{\mu} \omega_k \lambda_i \sum_i \frac{f_i}{\lambda_i} e^{-\tau_i r} - \frac{\sigma_s}{\mu} e^{-\tau r} + \frac{\sigma_r}{\mu} \quad (3)$$

where τ_k is the absorption coefficient of the gas corresponding to frequency ν for the ejection of photoelectrons from the K -level, μ is the absorption coefficient of the gas for the wave-length of the primary beam, ω_k is the fluorescent yield for K -series as defined by Auger, f_i is the fractional part of the total number of quanta emitted, having the frequency ν_i of the i^{th} line of the K -series, τ_i is the fluorescent absorption coefficient of the gas for the i^{th} line of its own K -series, r is the effective path length of the radiation to the walls, σ_s is the true scattering coefficient, σ_r is the coefficient of absorption due to scattering or simply the recoil electron coefficient, and τ is the absorption coefficient for the scattered rays.

The last term of Eq. (3) has been added to Allison's original expression to take care of the Compton scattering. The σ_s is merely σ in Allison's expression, the usual scattering coefficient.

σ_s and σ_r were calculated from Compton's expressions,²⁰

$$\begin{aligned} \sigma_s &= \sigma_0(1 + \alpha)/(1 + 2\alpha)^2 \\ \sigma_r &= \sigma_0 \alpha/(1 + 2\alpha)^2 \end{aligned}$$

where σ_0 is the classical linear scattering coefficient, and α has the same significance as before.

¹⁹ S. K. Allison and V. J. Andrew, *Phys. Rev.* **38**, 1424 (1931).

²⁰ Compton's *X-rays and Electrons*, p. 312.

The second term of Eq. (3) is negligibly small, if we consider that the *K*-series of argon is around 4Å and hence strongly absorbed on its way to the walls; and also, that the fluorescent yield, as stated above, is only 0.07. It may be emphasized that the last term of Eq. (3) is based on the assumption that the recoil electrons are completely absorbed in their journey to the walls. This assumption is permissible as a short calculation from Whiddington's formula for the "reach" of a photoelectron will show.

The constant *c* in Eq. 2 may be eliminated by taking the ratio between the ionization due to a given wave-length as compared with that due to any other. In this manner the corrected ratios given in column 4 of Tables I and II were arrived at, using the wave-lengths at the different angles as determined from the formula for the Compton effect, with the experimental determination of wave-length at 90° serving as the basis.

With a thick scattering plate, in which there is complete absorption of the primary rays, which are incident on it at a glancing angle of $\phi/2$, it can easily be shown that the ratio of the scattering per gram per unit solid angle in any direction ϕ to that at 90° with the primary beam, is given by

$$(s/\rho)_\phi/(s/\rho)_{90} = I_\phi/I_{90} \quad (4)$$

where the symbols have the same significance as above. Hence in the case of copper and lead in Tables III and IV the experimental ratios are the true ratios, if, for the moment, we leave aside possible corrections for the wave-lengths at different angles.

The absorption measurements in aluminum of the scattered rays from copper and lead gave almost identical wave-lengths. There was no difference, within experimental error, between the wave-lengths at different scattering angles. The effective wave-length, determined as above from Compton's table, was 0.19Å.

It was thought desirable to place the ratios of the intensities of scattering upon an absolute basis by a comparison with paraffin, as Coven²¹ had done.

For unpolarized x-rays, the Breit-Dirac formula for the scattering per gram per unit solid angle in a direction ϕ , may be written,

$$\left(\frac{s}{\rho}\right)_\phi = N \frac{Z}{W} \frac{e^4}{2m^2c^4} \frac{(1 + \cos^2 \phi)}{(1 + \alpha \text{ vers } \phi)^3} \quad (5)$$

where *N* is Avogadro's constant, *Z* is the atomic number of the scatterer and *W* its atomic weight, and where the other symbols have the same significance as above.

This formula is, of course, strictly valid for free electrons only. But, considering the low effective atomic number of paraffin and the hardness of the primary rays in this experiment, we may assume as a first approximation that the value it gives for paraffin at 90° is the true value for paraffin. In that way we obtain a unit of measure. The average formula for paraffin is C₂₄H₅₀ which makes *Z/W* approximately equal to 0.5. Substituting this in Eq. (5),

²¹ A. W. Coven, Phys. Rev. **38**, 1424 (1931).

we get for σ/ρ at 90° the value of 0.0088, for a wave-length of 0.23A. With this basic value for paraffin at 90° and the corrected ratios for the other angles, the column in Table I giving the scattering per gram has been calculated.

Similar calculations for the other material were made by using the separately determined ratios at 90° . These were:

paraffin/aluminum	2.43	by transmission
copper/lead	1.12	by reflection.

Also, the scattering from a 2 mm plate of aluminum, arranged for reflection, was compared with that from copper and lead. The ratios were:

aluminum/copper	2.02	by reflection
aluminum/lead	2.26	by reflection.

Since the 2 mm aluminum plate did not absorb all of the primary radiation, the latter ratios had to be divided by $(1 - e^{-\mu l}) = 0.37$, where l is the maximum path of the x-rays in the aluminum plate.

Correcting all ratios for the different effects in the ionization chamber due to the different wave-lengths, we finally get the following relations:

$$(s/\rho)_{\text{Al } 0.23\text{A}} = 1.06(s/\rho)_{\text{Par. } 0.23\text{A}}$$

$$(s/\rho)_{\text{Cu } 0.19\text{A}} = 1.22(s/\rho)_{\text{Par. } 0.23\text{A}}$$

$$(s/\rho)_{\text{Pb } 0.19\text{A}} = 2.88(s/\rho)_{\text{Par. } 0.23\text{A}}.$$

The effective wave-length of the x-rays in the 2 mm aluminum plate was found to be 0.22A and in the above relations there is a small correction for the difference in the scattering power of aluminum at 0.23A and at 0.22A.

Using these relations at 90° and the corrected experimental ratios at the other scattering angles, the columns for the scattering per gram in Tables II, III and IV for aluminum, copper and lead, respectively, were calculated.

The S -columns in the tables give the scattering per electron relative to the classical scattering from a free electron. They were calculated on the assumption that the rays scattered from paraffin are completely modified, in which case we have from Eq. (5) that,

$$S = (1 + \alpha \text{ vers } \phi)^{-3}$$

which is then the actual value for paraffin. This value at 90° is 0.74. With the help of Eq. (5) and the experimentally determined values of (s/ρ) , the S -values at other angles and for the other materials were computed.

IV. DISCUSSION OF RESULTS

In Fig. 3 the dots represent the experimental values of the ratios of scattering from paraffin at a given angle compared with that at 90° . For convenience of comparison with Dirac's theory of scattering by free electrons, three curves have been drawn, evaluated from Eq. (5) for different values of α . Curve 1 corresponds to an α of 0.05A, curve 2 to an α of 0.1 and curve 3 to an α of 0.23A. The broken curve is plotted from Thomsons classical formula for the scattering from a free electron. It is interesting to note, although

the fact is probably entirely without significance, that the experimental values for angles between 30° and 90° lie almost exactly along curve 2, whereas, if the scattering from paraffin were equal to that from free electrons, we should expect these values to lie more nearly along curve 3, assuming Dirac's theory to hold for paraffin also. For angles below 30° there is a radical departure of the experimental values even from curve 2, but this circumstance can most probably be ascribed to line interferences, as, strictly speaking, none of the substances investigated can be entirely amorphous. In the backward direction also, there is excess scattering over what one would expect from the theory. Unfortunately, one could not go beyond 105° , as the lead box, containing the x-ray tube, was so close to the spectrometer, as to prevent its arm from swinging beyond that point.

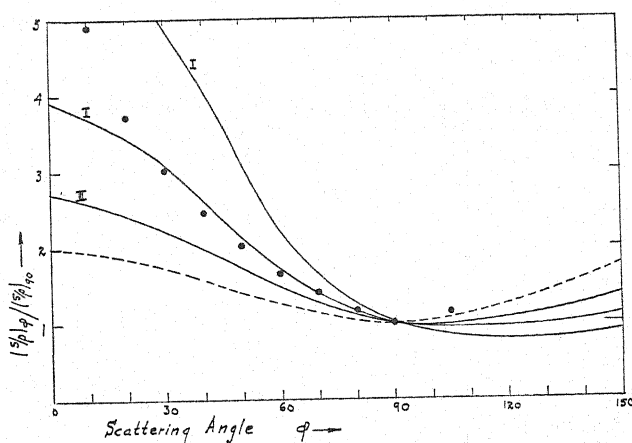


Fig. 3. Scattering from paraffin. Experimental values are represented by dots. Curves 1 and 2 are drawn from Dirac's formula for values of λ equal to 0.05, 0.1 and 0.23 Å respectively. The broken curve is from Thomson's classical formula.

But this value at 105° must be given some weight, for it, like all the other experimental values, represents the mean of the values obtained from three distribution curves for paraffin, each point on the latter being in turn the mean of four ionization measurements. It is estimated that the probable error of the dots in Fig. 3 is less than 1 percent.

There is some error introduced due to the use of Crowther's formula for the hard x-rays of this experiment. As Jauncey and Williams²² point out, Eq. (1) was derived by Crowther when the Compton effect was still unknown. The scattered rays should be divided into coherent and incoherent rays and the simple Crowther formula should be replaced by

$$I_\phi = [AIt/R^2 \cos(\phi/2)](s_1 + s_2 T) \quad (6)$$

where s_1 and s_2 are respectively the coherent and incoherent linear spatial scattering coefficients per unit solid angle in a direction ϕ , and where T is a complicated expression involving the absorption coefficients of the coherent

²² G. E. M. Jauncey and P. S. Williams, *Phys. Rev.* **41**, 127 (1932).

and incoherent scattered rays in the plate, in the air between the plate and the window of the ionization chamber.

Since we may consider the x-rays of wave-length 0.23\AA , scattered from paraffin at 90° , to be almost entirely modified and hence incoherent (unless, indeed, the modified ray is not entirely incoherent), s_1 in Eq. (6) becomes zero. A calculation for this particular case shows that the value of s_2 would be less than 1 percent larger than the value of s calculated from Eq. (1). This, therefore, places an upper limit upon the error from this source, as for the smaller angles the discrepancy would be smaller. The difference between the errors for 90° and 105° is trifling.

These results for paraffin are somewhat discordant with those obtained by Coven²¹ at an effective wave-length of 0.32\AA . He finds closer agreement with the Dirac theory for free electrons. There is, however, in his case a question as to the magnitude of the error in determining the effective wave-lengths. Also, no corrections were made for the different ionization effects at different angles. Jauncey and Harvey²³ report good agreement between the scattering from paraffin and the Dirac theory at an effective experimental wave-length of about 0.30\AA . They measured the ratios of the scattering at 97.5° and 120° as compared with that at 75° . Their corrections for the different ionization effects are more difficult than in this experiment. They used methyl iodide and ethyl bromide in their ionization chamber which require comparatively large corrections for the fluorescent yield.

It is difficult to see how the agreement with the theory from free electrons can be perfect, if we recall what has been said about interferences, unless, indeed, our conception of the mechanism of scattering should be modified.

In Fig. 4 are plotted the S -values against $[\sin(\phi/2)]/\lambda$ for the different scattering materials. These curves show very clearly how the scattering per electron increases with the atomic number of the scatterer. For paraffin at the larger angles, the scattering is practically that from free electrons, which condition seems to be approached also for the other materials as $[\sin(\phi/2)]/\lambda$ is increased.

The largest errors involved in measuring the scattering per electron are probably those of comparing the scattering from one material with that of another. The smallest of these is in the case of the comparison of the intensity of scattering from paraffin with that from aluminum. This is estimated to be of the order of 1 percent. Also, in the comparison of the intensity of scattering of lead to copper the error is of about the same magnitude. This is because in one case the transmission and in the other case the reflection method was used for the two materials in question. But when we come to compare the scattering from paraffin with that from copper or lead we have to use the scattering from aluminum by the reflection method as a sort of connecting link. A little thought on the calculation involved will show that it is not entirely satisfactory. This doubt is strengthened by the fact that an attempt to get the ratio of paraffin to copper, by scattering from a copper foil by the transmission method, gave a result which did not agree with the other within

²³ G. E. M. Jauncey and G. G. Harvey, *Phys. Rev.* **37**, 1203 (1931).

experimental uncertainty. There is a possibility that multiple scattering²⁴ may have some bearing on this, and this point will be investigated in the near future.

The possible error of method involved in determining the S -values for copper and lead is estimated, in view of the above, to be of the order of 5 per cent. On account of this large error it was thought inadvisable to attempt a

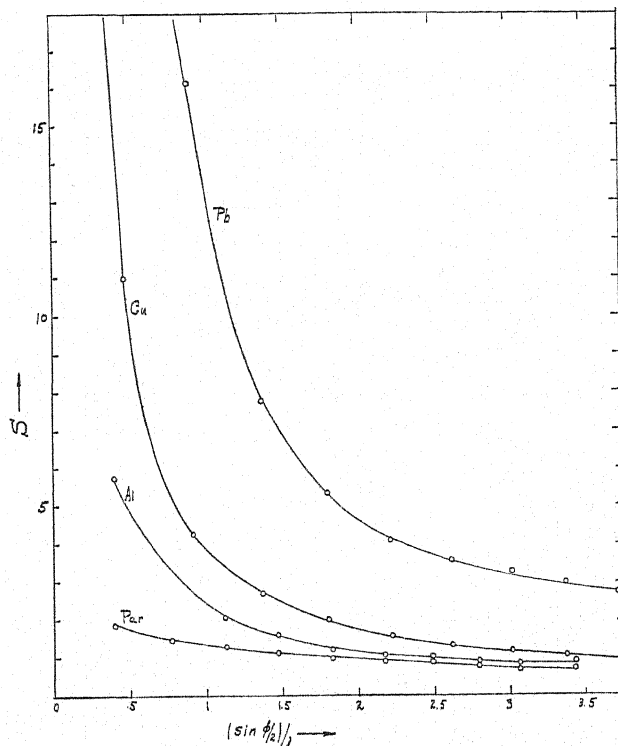


Fig. 4. Experimental values for the scattering per electron with the classical scattering from a free electron taken as a unit.

correction for the coherent and incoherent scattered radiations from copper and lead. Besides, this error is probably slight, as the radiation scattered from lead is almost entirely coherent and that from copper is mostly so.

Considering all sources of error, the most probable error for the S -values is estimated to be less than 2 percent for paraffin and aluminum, and less than 6 percent for copper and lead. Included in these calculations is the error involved in the determination of the effective wave-length. It must be emphasized that in experiments of this kind where one works with more or less heterogeneous radiation, the concept of "effective" wave-length is not a closely defined one, as one learns by reading the divergent opinions expressed by different authors.²⁵

²⁴ J. W. M. Dumond, *Phys. Rev.* **36**, 1685 (1930).

²⁵ See discussions under *X-Rays*, *International Critical Tables*, Vol. VI, 1928 Ed.

Jauncey,⁶ in his theory of diffuse scattering of x-rays by solids, arrives at an expression given by

$$S = 1 - (Z - 1)(f'^2/Z^2) + (F^2/ZN)X$$

where S is the scattered intensity per electron, relative to the scattered intensity from a single electron, Z is the atomic number, F is the atomic structure factor which includes the effect of thermal agitation, f' is related to f , the true atomic structure factor, N is the total number of atoms, and X is a complicated double summation.

So far, the double summation X has been evaluated only for a simple cubic crystal consisting of atoms of one kind.²⁶ It has not been determined for an amorphous solid and hence no comparison can as yet be made between Jauncey's theory and the present experimental results.

It is interesting, in connection with what has been said above about the excess scattering by paraffin at 105° , to note Chao's experimental result.²⁷ Working with γ -rays from ThC he finds at 135° an intensity of scattering by lead approximately three times that which one would expect from the formula of Klein-Nishina. This *anomalous* scattering he attributes to a cooperation of the nuclear electrons in the process of scattering.

In concluding, I wish to express my gratitude to Professor A. H. Compton for help in the course of this work.

²⁶ G. E. M. Jauncey and G. G. Harvey, Phys. Rev. **37**, 1203 (1931).

²⁷ C. Y. Chao, Phys. Rev. **36**, 1519 (1930).

Atomic Eigenfunctions and Energies

By C. W. UFFORD AND G. H. SHORTLEY
Palmer Physical Laboratory, Princeton University

(Received August 6, 1932)

In §1, the calculation of the nondiagonal elements of electrostatic interaction is sketched. In §2, attention is called to the fact that the matrix elements of L_x (the x -component of orbital angular momentum), as calculated between spherical harmonic eigenfunctions taken with positive phase, are negative when m_l is $+$ and positive when m_l is $-$. The calculation of eigenfunctions in LS coupling has always been done using only positive matrix elements of L_x . This amounts effectively to using a zero-order scheme in which one takes spherical harmonic eigenfunctions with negative phase for positive odd values of m_l , and positive phase for all other values. In §3 the calculation of first order energies for configurations which give more than one multiplet of a kind is considered, and explicit formulas given for the electrostatic energies and magnetic splitting of the two 2D 's of d^3 . The results are shown to compare satisfactorily with the observed data. The second 2D is predicted in general to be extremely high and inverted.

IN THIS paper we wish to calculate the separate energies and intervals of multiplets which occur more than once in a configuration. For this purpose we need the nondiagonal elements of the matrix of electrostatic interaction, which are given in §1. Since this matrix must be obtained algebraically, we discuss in §2 the interpretation, in terms of algebraic functions, of the eigenfunctions in LS coupling which have been found by various investigators. This consideration is necessary because of a question of phase to which attention has not hitherto been called. We then proceed in §3 to discuss the energy levels and separations, calculating in detail the two 2D 's of d^3 .

§1. MATRIX ELEMENTS OF ELECTROSTATIC INTERACTION¹

We shall first sketch the calculation of the matrix of the electrostatic interaction

$$G = \sum_{i>j=1}^N \frac{e^2}{r_{ij}} = \sum_{i>j=1}^N g(i, j) \quad (1.1)$$

in the zero-order scheme. In this scheme the eigenfunction belonging to the state $A = (a^1, a^2, \dots, a^N)$ will be the antisymmetric combination

$$\psi(A) = + (N!)^{-\frac{1}{2}} \sum_P (-1)^p P u_1(a^1) u_2(a^2) \dots u_N(a^N), \quad (1.2)$$

where P represents a permutation of quantum numbers relative to electron indices, and p has the parity of P . Here the symbol $u_i(a^i)$ indicates the one-

¹ The contents of this section are not original, although they have never been published in detail. The reduction of the nondiagonal elements to the form (1.5) and the calculation of the table of c 's were done over a year ago by Slater and his students at Harvard and M.I.T., and by Condon and the writers at Princeton. This fact is noted by Inglis, *Phys. Rev.* **38**, 862 (1931), footnote 7.

electron central field eigenfunction for electron i with the j^{th} set of quantum numbers $n^j l^j m_l^j m_s^j$:

$$u_i(a^j) = [R_i(n^j l^j)/r_i] \Theta_i(l^j m_l^j) \Phi_i(m_l^j) \delta(\sigma_i, m_s^j). \quad (1.3)$$

The angle factors are given by the formulas

$$\left. \begin{aligned} \Theta(l m_l) &= + \left[\frac{2l+1}{2} \frac{(l-|m_l|)!}{(l+|m_l|)!} \right]^{\frac{1}{2}} \sin^{|m_l|} \theta \frac{d^{|m_l|} P_l(\cos \theta)}{d(\cos \theta)^{|m_l|}} \\ \Phi(m_l) &= + (2\pi)^{-\frac{1}{2}} e^{i m_l \phi} \end{aligned} \right\} \quad (1.4)$$

These are given explicitly because their exact form will be essential in §2. The sign of the eigenfunction (1.2) is determined by the order of listing the quantum numbers, and we shall adopt for convenience the following standard order.² The individual sets will be listed first in increasing order of n values; sets with a particular n will be arranged in increasing order of l values; those with a particular nl will be listed in decreasing order of the m_l values; and the set with $m_s = +\frac{1}{2}$ will be listed before that with $m_s = -\frac{1}{2}$ in case the two sets agree in regard to n , l , and m_l .

In this scheme the diagonal elements of G have been given by Slater.³ The nondiagonal elements are easily obtained from formulas given by Condon.⁴ Since G is diagonal with respect to $M_L = \Sigma m_l$ and $M_S = \Sigma m_s$, there will be no component between two states of the same configuration which differ in regard to just one individual set. If the two states differ in regard to two sets, A having the sets a, b , while A' has the sets a', b' , this matrix element is given by

$$\begin{aligned} (A | G | A') &= \pm \left[\int \int \bar{u}_1(a) \bar{u}_2(b) g(1, 2) u_1(a') u_2(b') d\tau_1 d\tau_2 \right. \\ &\quad \left. - \int \int \bar{u}_1(a) \bar{u}_2(b) g(1, 2) u_1(b') u_2(a') d\tau_1 d\tau_2 \right], \end{aligned}$$

where the sign is to be chosen as in note 4. The general integral with four different quantum numbers which occurs here may be shown to be reducible to the form

$$\begin{aligned} &\int \int \bar{u}_1(a) \bar{u}_2(b) g(1, 2) u_1(c) u_2(d) d\tau_1 d\tau_2 \\ &= \delta(m_s^a, m_s^c) \delta(m_s^b, m_s^d) \delta(m_l^a + m_l^b, m_l^c + m_l^d) \\ &\quad \cdot \sum_k c^k(l^a m_l^a; l^c m_l^c) c^k(l^b m_l^b; l^d m_l^d) R^k(n^a l^a n^b l^b; n^c l^c n^d l^d) \end{aligned} \quad (1.5)$$

² Used by Shortley, Phys. Rev. 40, 185 (1932). See esp. pp. 194, 195.

³ Slater, Phys. Rev. 34, 1293 (1929).

⁴ Condon, Phys. Rev. 36, 1121 (1930). These formulas must be supplemented by a determination of sign given in reference 2. The rule is as follows: To the matrix component between two states, $\psi(A)$ and $\psi(A')$, differing in regard to one or two individual sets, one prefixes $+$ or $-$ according to the parity of the permutation which changes the set A' from its standard order to the order in which the equal elements in A and A' occupy the same places.

where

$$c^k(lm_i; l'm_i') = \left(\frac{2}{2k+1} \right)^{1/2} \int_0^\pi \Theta(k, m_i - m_i') \Theta(lm_i) \Theta(l'm_i') \sin \theta d\theta \quad (1.6)$$

$$R^k(n^a l^a n^b l^b; n^c l^c n^d l^d) = e^2 \int_0^\infty \int_0^\infty \frac{r_1^{<k}}{r_1^{k+1}} R_1(n^a l^a) R_2(n^b l^b) R_1(n^c l^c) R_2(n^d l^d) dr_1 dr_2. \quad (1.7)$$

Slater's a 's, b 's, F 's and G 's are special cases of these c 's and R 's, namely

$$\left. \begin{aligned} a^k(l^a m_l^a; l^b m_l^b) &= c^k(l^a m_l^a; l^a m_l^a) c^k(l^b m_l^b; l^b m_l^b) \\ b^k(l^a m_l^a; l^b m_l^b) &= [c^k(l^a m_l^a; l^b m_l^b)]^2 \end{aligned} \right\} \quad (1.8)$$

$$\left. \begin{aligned} F^k(n^a l^a; n^b l^b) &= R^k(n^a l^a n^b l^b; n^a l^a n^b l^b) \\ G^k(n^a l^a; n^b l^b) &= R^k(n^a l^a n^b l^b; n^b l^b n^a l^a). \end{aligned} \right\} \quad (1.9)$$

Hence the c 's may be obtained by taking the square roots of the b 's as given by Slater and Condon and Shortley⁵ except for sign.⁶ It is easily seen that the R 's which will be obtained within a configuration will always reduce to F 's and G 's.

§2. THE EIGENFUNCTIONS FOR LS COUPLING

The direct method of finding eigenfunctions in LS coupling is to proceed according to the definition of this scheme as one in which L^2 , S^2 , and either L_z , S_z , or J^2 , J_z are diagonal. This method, which has been discussed by Johnson,⁷ consists in finding the matrices of L^2 , S^2 (and $L \cdot S$) in the zero-order scheme and diagonalizing them simultaneously. Gray and Wills⁸ have given a method which depends essentially on the fact that the matrix of $J_x \pm iJ_y$, where J is any angular momentum, has but one component in each row or column, so that component connecting the state $\psi(j, m_j)$ with the state $\psi(j, m_j \mp 1)$. Wigner⁹ has given a general formula for the states which result

⁵ Condon and Shortley, Phys. Rev. **37**, 1025 (1931).

⁶ The signs are given by Inglis, Phys. Rev. **38**, 862 (1931), footnote 7, for s , p , and d electrons. These are repeated below, together with the signs for f electrons. To get c^k the square root of b^k is to be taken with the positive sign except for the following values of $(l^a m_l^a; l^b m_l^b; k)$, for which it is to be taken negative:

$(1 \pm 1; 2 \pm 2; 3)$	$(1 \pm 1; 2 \pm 1; 3)$	$(1 \pm 1; 2 \ 0; 1)$	$(2 \pm 2; 3 \pm 3; 3)$
$(2 \pm 2; 3 \pm 2; 3)$	$(2 \pm 2; 3 \pm 1; 1)$	$(2 \pm 2; 3 \pm 1; 5)$	$(2 \pm 2; 3 \ 0; 3)$
$(2 \pm 1; 3 \pm 3; 5)$	$(2 \pm 1; 3 \pm 2; 5)$	$(2 \pm 1; 3 \pm 1; 5)$	$(2 \pm 1; 3 \ 0; 1)$
$(2 \ 0; 3 \pm 3; 3)$	$(2 \pm 2; 3 \mp 1; 3)$	$(1 \pm 1; 1 \pm 1; 2)$	$(1 \pm 1; 3 \pm 3; 4)$
$(1 \pm 1; 3 \pm 2; 4)$	$(1 \pm 1; 3 \pm 1; 4)$	$(1 \pm 1; 3 \ 0; 2)$	$(1 \pm 1; 3 \mp 1; 2)$
$(2 \pm 2; 2 \pm 2; 2)$	$(2 \pm 2; 2 \pm 1; 4)$	$(2 \pm 2; 2 \ 0; 2)$	$(2 \pm 1; 2 \pm 1; 4)$
$(3 \pm 3; 3 \pm 3; 2)$	$(3 \pm 3; 3 \pm 3; 6)$	$(3 \pm 3; 3 \pm 2; 4)$	$(3 \pm 3; 3 \pm 1; 2)$
$(3 \pm 3; 3 \pm 1; 6)$	$(3 \pm 3; 3 \ 0; 4)$	$(3 \pm 2; 3 \pm 2; 4)$	$(3 \pm 2; 3 \pm 1; 6)$
$(3 \pm 2; 3 \ 0; 2)$	$(3 \pm 2; 3 \ 0; 4)$	$(3 \pm 1; 3 \pm 1; 6)$	$(3 \pm 3; 3 \mp 1; 4)$

⁷ M. H. Johnson, Phys. Rev. **39**, 197 (1932).

⁸ Gray and Wills, Phys. Rev. **38**, 248 (1931). The sign of the imaginary i as we use it is reversed from that in Gray and Wills, in accordance with the more usual convention.

⁹ Wigner, *Gruppentheorie*, p. 206.

from the addition of any two angular momentum vectors, and the determination of eigenfunctions using this formula has been discussed by Bartlett.¹⁰

All of these methods depend in the last analysis on the values of the matrices of L_x , L_y , L_z and S_x , S_y , S_z for one-electron eigenfunctions. If one calculates algebraically the matrix of L_x using the functions (1.3), one finds¹¹

$$\begin{aligned} \bar{u}(nlm_s)L_x u(nl, m_l - 1, m_s) \\ = \pm [(l + m_l)(l - m_l + 1)]^{1/2} \begin{cases} + & \text{for } m_l \leq 0. \\ - & \text{for } m_l > 0. \end{cases} \end{aligned} \quad (2.1)$$

Now ever since they were first calculated by Born, Heisenberg, and Jordan¹² all matrix elements of the x -component of an angular momentum vector have usually been taken as real and positive, in particular in references 7, 8, 9, 10. Of course, this is satisfactory as long as one uses matrix methods and is consistent in the determination of the matrices of other observables; but before one may calculate a matrix, such as that of the electrostatic interaction, purely algebraically, one must determine what this choice of positive sign implies in the phase of the eigenfunctions. Suppose we designate by $v(nlm_s)$ the system of one-electron eigenfunctions for which the matrix of L_x is given by

$$\bar{v}(nlm_s)L_x v(nl, m_l - 1, m_s) = + [(l + m_l)(l - m_l + 1)]^{1/2} \text{ for all } m_l. \quad (2.2)$$

Then the v 's will be related to the u 's by the scheme

$$\begin{aligned} v(nl, \dots 3, m_s) &= - u(nl, \dots 3, m_s) \\ v(nl, \dots 2, m_s) &= + u(nl, \dots 2, m_s) \\ v(nl, \dots 1, m_s) &= - u(nl, \dots 1, m_s) \\ v(nl, \dots 0, m_s) &= + u(nl, \dots 0, m_s) \\ v(nl, \dots -1, m_s) &= + u(nl, \dots -1, m_s) \end{aligned} \quad (2.3)$$

(or this same scheme with signs reversed). Here the signs alternate for positive values of m_l , but are all positive for negative values.

The matrix of L_y is given in terms of that of L_x , in any scheme by the relation

$$(m_l | L_y | m_l') = e^{i(\pi/2)(m_l' - m_l)} (m_l | L_x | m_l').$$

The matrices of S_x and S_y are the same in the u scheme and the v scheme since they are diagonal with respect to m_l . Hence the matrix of any function of L and S as calculated using positive angular momentum matrix components is correct for the v scheme.

This means that all eigenfunctions in LS coupling heretofore published have been in terms of zero-order functions in the v scheme and not in the more

¹⁰ Bartlett, Phys. Rev. **38**, 1623 (1931).

¹¹ See, for instance, Brillouin, Jour. de Physique **8**, 74 (1927).

¹² Born, Heisenberg, and Jordan, Zeits. f. Physik **35**, 557 (1925).

logical u scheme. This distinction is essential when one calculates the matrix of electrostatic interaction, for example; if one fails to note this one will obtain matrices of electrostatic interaction which are not at all diagonal in LS coupling.¹³

As an example we may take the case of p^3 , as calculated by Johnson using positive matrix components. If we use a notation m_l^\pm , in which we write $+$ for $m_s = +\frac{1}{2}$, $-$ for $m_s = -\frac{1}{2}$, the zero order states for $m_j = \frac{1}{2}$ are

$$\begin{array}{ll} \text{I } (1^0 0^0 -) & \text{III } (1^0 + - 1^-) \\ \text{II } (1^1 - - 1^-)^{14} & \text{IV } (1^0 - - 1^+) \\ & \text{V } (1^0 + - 1^+). \end{array}$$

In terms of these states the eigenfunction for ${}^2D_{5/2}$ ($M_J = \frac{1}{2}$) as given by Johnson is

$${}^2D_{5/2} = (1/5)^{1/2} \text{I} - (1/5)^{1/2} \text{II} + (1/10)^{1/2} \text{III} - (4/10)^{1/2} \text{IV} + (1/10)^{1/2} \text{V}.$$

This state must be interpreted, if we let \mathcal{A} represent the antisymmetrizing operator $+(N!)^{-1/2} \sum_P (-1)^P P$ which occurs in (1.2), as

$$\begin{aligned} {}^2D_{5/2} = & (1/5)^{1/2} \mathcal{A} v_1(1^-) v_2(0^+) v_3(0^-) - (1/5)^{1/2} \mathcal{A} v_1(1^+) v_2(1^-) v_3(-1^-) \\ & + (1/10)^{1/2} \mathcal{A} v_1(1^+) v_2(0^+) v_3(-1^-) - (4/10)^{1/2} \mathcal{A} v_1(1^+) v_2(0^-) v_3(-1^+) \\ & + (1/10)^{1/2} \mathcal{A} v_1(1^-) v_2(0^+) v_3(-1^+). \end{aligned}$$

In terms of the u scheme this becomes, according to (2.3)

$$\begin{aligned} {}^2D_{5/2} = & - (1/5)^{1/2} \mathcal{A} u_1(1^-) u_2(0^+) u_3(0^-) - (1/5)^{1/2} \mathcal{A} u_1(1^+) u_2(1^-) u_3(-1^-) \\ & - (1/10)^{1/2} \mathcal{A} u_1(1^+) u_2(0^+) u_3(-1^-) + (4/10)^{1/2} \mathcal{A} u_1(1^+) u_2(0^-) u_3(-1^+) \\ & - (1/10)^{1/2} \mathcal{A} u_1(1^-) u_2(0^+) u_3(-1^+). \end{aligned}$$

It is here, of course, not the sign of the whole expression, but the relative change of sign of the second term, which is significant. In the same way one must interpret all eigenfunctions which have been calculated using positive angular momentum matrices.

If one wishes to calculate eigenfunctions directly in the u scheme, one must substitute the values (2.1) instead of (2.2) in the formulas given by Johnson for the matrices of L^2 and $L \cdot S$. For the Gray-Wills' method one must use the formulas

$$\begin{aligned} (L_x - iL_y)u(lm_l) &= \pm [(l + m_l)(l - m_l + 1)]^{1/2} u(l, m_l - 1) \quad \begin{cases} + \text{ for } m_l \leq 0 \\ - \text{ for } m_l > 0 \end{cases} \\ (L_x + iL_y)u(lm_l) &= \pm [(l - m_l)(l + m_l + 1)]^{1/2} u(l, m_l + 1) \quad \begin{cases} + \text{ for } m_l < 0 \\ - \text{ for } m_l \geq 0 \end{cases} \end{aligned} \quad (2.4)$$

¹³ Failing to note this will in general affect the calculation of transition probabilities, but not in the particular case of transitions in which one electron jumps from p to s , as calculated by Ufford, Phys. Rev. 40, 974 (1932).

¹⁴ This state is the negative of Johnson's II because of the different order of listing the quantum numbers.

which have signs chosen in accordance with (2.1). When using Wigner's formula for the addition of an l electron to an ion of resultant orbital momentum l' , the sign of the coefficient¹⁵ $\langle l'l' L M_L | l'l m_l' m_l \rangle$ must be changed when $m_l = +1, +3, \dots$. This is because an electronic function which is different in the u and v schemes is combined with an ionic function which is equivalent in the two schemes in the sense of (2.3). In adding L and S to obtain eigenfunctions in the $LSJM_J$ scheme, Wigner's coefficients are used as given by his formula without change of sign, since the initial states are now independent of the scheme used in obtaining them. The changes given in this paragraph are required only when it is desired to calculate eigenfunctions directly using positive phases for all of the one-electron functions, the other alternative being the calculation using v 's throughout.

§3. FIRST-ORDER ENERGIES FOR CONFIGURATIONS WHICH GIVE MORE THAN ONE MULTIPLY OF A KIND

We shall now discuss the calculation of the first-order energies for configurations which give more than one multiplet characterized by the same values of L and S ; at the same time giving the detailed results for the configuration d^3 , which gives two 2D 's, and is the simplest and most completely analyzed configuration of this type.

The electrostatic energy of any multiplet occurring only once in a configuration may be obtained very simply by the diagonal sum method outlined by Slater,³ without having to calculate any eigenfunctions or to use nondiagonal elements of electrostatic interaction in the zero-order scheme. When several multiplets of a kind occur, however, this method gives only the sum of the energies. In order to separate the energies, one must solve a secular equation connecting a group of eigenfunctions representing the multiplets of one kind. This is most easily explained by an illustration: the case of the two 2D 's of d^3 . Consider the highest M_L and M_S values which belong to a 2D . These are $M_L = 2$, $M_S = \frac{1}{2}$. The zero-order states of d^3 , which are characterized by $M_L = 2$, $M_S = \frac{1}{2}$ are, in the notation of §2,

$$\begin{array}{ll} A & \mathcal{A}u_1(2^+)u_2(2^-)u_3(-2^+) & B & \mathcal{A}u_1(2^+)u_2(1^+)u_3(-1^-) \\ C & \mathcal{A}u_1(2^+)u_2(1^-)u_3(-1^+) & D & \mathcal{A}u_1(2^-)u_2(1^+)u_3(-1^+) \\ E & \mathcal{A}u_1(2^+)u_2(0^+)u_3(0^-) & F & \mathcal{A}u_1(1^+)u_2(1^-)u_3(0^+). \end{array}$$

In terms of these zero-order functions one must determine two orthogonal eigenfunctions for 2D , which will then be characterized by $M_L = 2$, $M_S = \frac{1}{2}$. A convenient way of doing this is to find by any of the methods of §2 the eigenfunctions for all the other multiplets which have states $M_L = 2$, $M_S = \frac{1}{2}$ (namely $^2H_{2,1/2}$, $^2G_{2,1/2}$, $^2F_{2,1/2}$, $^4F_{2,1/2}$) and then to choose two functions orthogonal to these and to each other. The following were obtained by this procedure:

¹⁵ This is Wigner's coefficient $s_{L m_l' m_l}^{(l'l)}$, formula (27) p. 206, *Gruppentheorie*. For example in Wigner's table, page 208, the signs in the column $\nu = 1$ should be changed, when $\mu = m_l'$, $\nu = m_l$.

$$\begin{aligned}
 {}^2D_{2,1/2}^a &= \frac{1}{2}[-A + B - C + E] \\
 {}^2D_{2,1/2}^b &= (84)^{-1/2}[-5A - 3B - C + 4D - 3E - 2(6)^{1/2}F].
 \end{aligned}
 \quad (3.2)$$

The matrix of electrostatic energy for these states becomes¹⁶

$$\begin{array}{cc}
 & \begin{array}{cc} a & b \end{array} \\
 \begin{array}{c} a \\ b \end{array} & \begin{vmatrix} 3F_0 + 7F_2 + 63F_4 & 3(21)^{1/2}(F_2 - 5F_4) \\ 3(21)^{1/2}(F_2 - 5F_4) & 3F_0 + 3F_2 - 57F_4 \end{vmatrix}
 \end{array}
 \quad (3.3)$$

which has for its eigenvalues the energies

$$\epsilon = 3F_0 + 5F_2 + 3F_4 \pm (193F_2^2 - 1650F_2F_4 + 8325F_4^2)^{1/2}. \quad (3.4)$$

This formula then gives the electrostatic energies of the two 2D multiplets. The eigenfunctions for these multiplets, for $M_L=2$, $M_S=\frac{1}{2}$, may now be obtained. If we write the eigenfunction for either of them as $\alpha^2 D_{2,1/2}^a + \beta^2 D_{2,1/2}^b$, we find

$$\begin{aligned}
 \alpha &= \left[\left(\frac{3F_0 + 7F_2 + 63F_4 - \epsilon}{3(21)^{1/2}(F_2 - 5F_4)} \right)^2 + 1 \right]^{-1/2} \\
 \beta &= -\frac{3F_0 + 7F_2 + 63F_4 - \epsilon}{3(21)^{1/2}(F_2 - 5F_4)} \alpha.
 \end{aligned}
 \quad (3.5)$$

Now since this is the only state with $M_J=5/2$, this state is identical with the state ${}^2D_{5/2}$, $M_J=5/2$. The eigenfunctions for the other values of J and M_J may be obtained from this by the Gray-Wills' procedure, and the whole matrix of magnetic interaction¹⁷ calculated. This procedure leads, however, only to secular equations which are too complicated to be solved. In all the analyzed d^3 configurations the magnetic interaction is very small compared to the electrostatic, so that one can consider it merely as a small perturbation on the electrostatic levels; hence it will suffice to calculate the diagonal elements of magnetic interaction in the $LSJM_J$ scheme. The use of the diagonal sum rule together with the Landé interval rule enables all of these elements to be readily calculated¹⁸ for multiplets which occur only once in a configuration; but for multiplets occurring more than once this method gives only the sums of the magnetic energies. For the state (3.5) one obtains by direct calculation the value

$$\begin{aligned}
 ({}^2D_{5/2}, 5/2 | V^1 | {}^2D_{5/2}, 5/2) &= [\alpha^2/2 - (21)^{1/2}\alpha\beta/3 - \beta^2/6]\zeta \\
 &= \frac{1}{6}[1 \mp (59F_2 - 435F_4)(193F_2^2 - 1650F_2F_4 + 8325F_4^2)^{-1/2}]\zeta,
 \end{aligned}
 \quad (3.6)$$

¹⁶ The notation is as in Condon and Shortley,⁵ $F_2 = (1/49)F^2(nd^2)$, $F_4 = (1/144)F^4(nd^2)$, where F^2 and F^4 are as in (1.9).

¹⁷ For the elements of this matrix see Johnson,⁷ p. 201, and Shortley,² §5. These elements are given with plus signs and must be so used only in the v scheme, as has been done by Johnson.

¹⁸ Pauling and Goudsmit, *Structure of Line Spectra*, §39. The a of this section is our ζ .

from (3.6) the lower 2D interval as 142 cm^{-1} , while the observed value is 129.4 . The interval for the higher 2D is calculated as -67.7 cm^{-1} .

In the $3d^3$ of V III White²⁰ has found all the multiplets except 2F and one 2D . The configuration d^3 has the peculiarity that the calculated electrostatic energies for 2H and 2P are equal. In this instance these energies are not at all equal so that we cannot depend much on 2H and 2P . However if we choose the F 's to make the other three multiplets, 4F , 4P , 2G fit exactly, the 2H energy is fairly good ($15,869\text{ cm}^{-1}$ calc., $16,906\text{ cm}^{-1}$ obs.) while that of the 2P is not ($11,327\text{ cm}^{-1}$ obs.). This is in accord with the observation of Condon and Shortley, who in two instances (Ti II and Zr II) found a reasonable fit for 2H , but not for 2P . The values of the constants which are obtained in this way are $F_2=1171$, $F_4=83$ ($3F_0=23,891$). These constants give for the values of the two 2D 's, $17,300$ and $42,700\text{ cm}^{-1}$. The first of these is agreeably close to the 2D found by White at $16,317\text{ cm}^{-1}$; the second is predicted $25,800\text{ cm}^{-1}$ higher than any other level of the configuration, which has a spread of only $16,900\text{ cm}^{-1}$ as analyzed! Hence it is not surprising that this second 2D was not found. The intervals as usual agree only roughly. White has remarked that 4F fits the interval rule fairly well, and if we use the ζ given by this level, (which is about an average ζ for the configuration), the calculated 2D intervals are 248 and -110 cm^{-1} ; the first of these is to be compared with the observed interval of 147 cm^{-1} .

For the $4d^3$ of Zr II, in which Kiess and Kiess²¹ report two 2D 's, Condon and Shortley obtain an approximate fit of all levels except 2P with $F_2=683$, $F_4=36$ ($3F_0=16,000$). With these values the calculated 2D 's lie at $11,750$ and $27,310\text{ cm}^{-1}$, with separations of 593 and -309 cm^{-1} , respectively. These separations are calculated using the 2H , which gives an average value for ζ , as standard. The observed 2D 's lie at $13,869$ and $14,559\text{ cm}^{-1}$ with separations of 734 and 435 cm^{-1} . Hence we must infer that, if these are correctly classified, one of them is very strongly perturbed.

These are all the instances of d^3 which are sufficiently analyzed for comparison with the theory. In general we have seen that the lower 2D corresponds well with the one usually observed; the second 2D is predicted extremely high and inverted.

²⁰ White, Phys. Rev. 33, 672 (1929).

²¹ Kiess and Kiess, Bur. Standards J. Research 5, 1210 (1930).

Calculation of the Quantum Defect for Highly Excited S States of Para- and Orthohelium

By LLOYD P. SMITH*

*Department of Physics, Cornell University***

(Received August 12, 1932)

Experimental term values for the S states of para- and orthohelium for the case when one electron is in the ground state and the other is in a highly excited S state can be represented by the formula $E = -R\hbar/(n - \Delta_{1,2})^2$; Δ_1 and Δ_2 being the quantum defects for the ortho and para systems, which have the respective numerical values, 0.298 and 0.140. The object of the present paper is to calculate the values of Δ_1 and Δ_2 by a convenient method quite different from that used by Hylleraas. Neglecting the polarization of the atom core, the results obtained for Δ_1 and Δ_2 are 0.289 and 0.160, respectively, in contrast to the corresponding values 0.230 and 0.122 obtained by Hylleraas before he corrected for polarization. This difference is due to the more accurate wave functions obtained here and indicates that the effect of polarization is not as great as it would appear from the calculations of Hylleraas.

HYLLERAAS¹ has already calculated the values of the quantum defects Δ_1 and Δ_2 for the highly excited S states of ortho- and parahelium assuming a solution of the wave equation in the form $\psi = \phi_1(r_1)\phi_n(r_2) \pm \phi_1(r_2)\phi_n(r_1)$, but in the differential equations determining the ϕ 's, certain assumptions were made as to the field in which each electron moves, of such a form that the equations could be solved. Since this procedure does not lead to the closest approximation to the solution of the helium equation compatible with the chosen form of ψ it seemed desirable to obtain a better solution based on Fock's² method for determining the approximate eigenfunctions for the many electron problem and to calculate Δ_1 and Δ_2 by a different method.

Fock assumes a solution of the wave equation for helium of the form

$$\Psi = \psi_1(x_1)\psi_2(x_2) \pm \psi_1(x_2)\psi_2(x_1) \quad (1)$$

where the plus and minus signs refer to para- and orthohelium and x_1 and x_2 refer to all the coordinates of electron 1 and 2, respectively. The solution (1) is substituted in the variational problem for which the wave equation for helium is just the Eulerian equation. In order to minimize the resulting integral it is found that ψ_1 and ψ_2 must satisfy the following simultaneous equations, when ψ_1 and ψ_2 are assumed normalized;

$$\begin{aligned} H\psi_1(x) + G_{22}(x)\psi_1(x) \pm G_{21}(x)\psi_2(x) \\ = (E - H_{22})\psi_1(x) \mp H_{21}\psi_2(x) \mp (H - E)\psi_2(x) \int \psi_1(x)\bar{\psi}_2(x)dx \end{aligned} \quad (2)$$

$$\begin{aligned} H\psi_2(x) + G_{11}(x)\psi_2(x) \pm G_{12}(x)\psi_1(x) \\ = (E - H_{11})\psi_2(x) \mp H_{12}\psi_1(x) \mp (H - E)\psi_1(x) \int \bar{\psi}_2(x)\psi_1(x)dx \end{aligned} \quad (3)$$

* National Research Fellow.

** Temporarily at Institut für Theoretische Physik, München.

¹ Zeits. f. Physik **66**, 453 (1930).

² Zeits. f. Physik **61**, 126 (1930).

where

$$\left. \begin{aligned} H &= -\frac{1}{2}\{\partial^2/\partial x^2 + \partial^2/\partial y^2 + \partial^2/\partial z^2\} - z/r \\ G_{ik} &= \int [\psi_i(x')\psi_k(x')/R_0]dx' \\ H_{ik} &= \int \psi_i(x)H\psi_k(x)dx \end{aligned} \right\} \quad (4)$$

and R_0 is the distance between the two electrons. The space coordinates are expressed in atomic units, i.e., of length $a_H = \hbar^2/4\pi^2me^2$ and the energy E is in units of $2Rh$; R being the Rydberg constant $R = 2\pi^2me^4/\hbar^3$. When ψ_1 and ψ_2 can be taken as orthogonal as well as normalized, the integral terms in Eqs. (2) and (3) drop out. The upper and lower signs refer to parahelium and orthohelium, respectively.

The method which will be used to compute the quantum defect for the case when electron 2, say, has a very small energy, requires a rather accurate determination of ψ_2 at large distances from the nucleus. An accurate solution for ψ_1 is not required except insofar as it is needed to determine ψ_2 . Due to the way in which ψ_1 enters in Eq. (3) it will be sufficient as a first approximation to assume ψ_1 to be the wave function associated with the helium ion in the ground state, i.e., a spherically symmetric function of the coordinates. By making this assumption, the possibility of taking polarization effects into account is precluded. Further, since we suppose that the energy of electron 2 is practically zero, the term $(E - H_{11})$ in Eq. (3) (which is nearly the energy of electron 2) will be replaced by the small term ϵ . As a result of these assumptions, Eqs. (2) and (3) reduce to

$$H\psi_1(x) = E\psi_1(x) \quad (2a)$$

$$H\psi_2(x) + G_{11}(x)\psi_2(x) = \mp \{G_{12}(x) + H_{12}\}\psi_1(x) + \epsilon\psi_2(x) \quad (3a)$$

the integral term in Eq. (3) dropping out because of Eq. (2a) assumed for ψ_1 . It is clearly seen that it is possible to find normalized solutions of Eq. (2a) and (3a).

The normalized solution of Eq. (2a) for the ground state of the helium ion is

$$\psi_1(r_1) = 2(2/\pi)^{1/2}e^{-2r_1}.$$

Substituting this expression for $\psi_1(r_1)$ in the expressions (4), we have;

$$\begin{aligned} G_{11}(r_2) &= \frac{8}{\pi} \int_0^\infty \int_0^\pi \int_0^{2\pi} \frac{e^{-4r_1r_1^2} \sin \theta_1 d\phi_1 d\theta_1 dr_1}{(r_1^2 + r_2^2 - 2r_1r_2 \cos \gamma)^{1/2}} \\ G_{12}(r_2) + H_{12} &= 2\left(\frac{2}{\pi}\right)^{1/2} \left[\int_0^\infty \int_0^\pi \int_0^{2\pi} \frac{e^{-2r_1}\psi_2(r_1)r_1^2 \sin \theta_1 d\phi_1 d\theta_1 dr_1}{(r_1^2 + r_2^2 - 2r_1r_2 \cos \gamma)^{1/2}} \right. \\ &\quad \left. - \int_0^\infty \int_0^\pi \int_0^{2\pi} e^{-2r_1} \left\{ \frac{1}{2} \frac{1}{r_1^2} \frac{\partial}{\partial r_1} \left(r_1^2 \frac{\partial \psi_2}{\partial r_1} \right) + \frac{2}{r_1} \psi_2 \right\} r_1^2 \sin \theta_1 d\phi_1 d\theta_1 dr_1 \right] \end{aligned}$$

where γ is the angle between the two electrons. The integrations over the angles can easily be carried out and in the case of $G_{11}(r_2)$ also the integration over r_1 . Carrying out these integrations and simplifying the notation by replacing the radius of the first electron r_1 by the integration variable s and replacing r_2 by r without subscript, the above expressions become,

$$G_{11}(r) = 1/r - e^{-4r}(1/r + 2)$$

$$G_{12}(r) + H_{12} = 8(2/\pi)^{1/2} \left[(1/r) \int_0^r e^{-2s} \psi_2(s) s^2 ds \right. \\ \left. + \int_r^\infty e^{-2s} \psi_2(s) s ds - 2 \int_0^\infty e^{-2s} \psi_2(s) s^2 ds \right].$$

Substituting these expressions in Eq. (3a) and at the same time writing $\xi = r\psi_2(r)$, Eq. (3a) becomes:

$$\xi_{\mp}'' + \{2/r + 2e^{-4r}(1/r + 2) + 2\epsilon\} \xi_{\mp} = \mp S(r) \quad (5)$$

where

$$S(r) = 64e^{-2r} \left[2r \int_0^\infty e^{-2s} \xi_{\mp}(s) s ds - \int_0^r e^{-2s} \xi_{\mp}(s) s ds - r \int_r^\infty e^{-2s} \xi_{\mp}(s) ds \right]$$

and ξ_- and ξ_+ denote the solution for para- and orthohelium, respectively. $S(r)$ contains only *Austausch* terms.

For large values of r and negligibly small values of ϵ , Eq. (5) reduces to

$$\xi_{\mp}'' + (2/r) \xi_{\mp} = 0 \quad (6)$$

whose general solution is

$$\xi_{\mp} = (\pi r)^{1/2} [A_{\mp} J_1 \{(8r)^{1/2}\} + B_{\mp} Y_1 \{(8r)^{1/2}\}] \quad (7)$$

where $J_1(z)$ and $Y_2(z)$ are the Bessel's functions of the first and second kind, respectively, of order 1. The solution of Eq. (5) for all values of r and negligibly small ϵ can be most conveniently obtained by solving it numerically by any of several well-known methods, over the domain from $r=0$ to a value of r such that Eq. (5) essentially reduces to Eq. (6), at which point the solution (7) is joined on, thus determining the arbitrary constants. Since only the ratio A/B will actually be required, it may be easily calculated by means of the expression

$$A/B = - (r^{1/2} \xi' Y_1 - 2^{1/2} \xi Y_0) / (r^{1/2} \xi' J_1 - 2^{1/2} \xi J_0)$$

where ξ and ξ' are the values of ξ and its first derivative at the point r and the argument of the Bessel's functions is $(8r)^{1/2}$ throughout. The domain over which the numerical integration must be carried out is not large, e.g., $0 \leq r \leq 4$. Since ψ_2 must be finite at $r=0$, ξ must be placed equal to zero at $r=0$, from which ξ' can be determined by means of the differential equation thus determining the solution uniquely. The first approximation is obtained by placing $S(r)=0$ and then obtaining a second approximation by substituting

the first approximation in $S(r)$. Three approximations will usually give a solution correct to four places. This method is not only convenient but is illuminating in that it shows very clearly the effect of the austausch terms on the

TABLE I. Numerical solutions of Eq. (5) for small r .

r	$S(r)=0$ ξ_0	Ortho ξ_+	Para ξ_-	r	$S(r)=0$ ξ_0	Ortho ξ_+	Para ξ_-
0	0	0	0	2.00	-0.1982	-0.1609	-0.2081
0.10	0.0819	0.0817	0.0822	2.10	-0.2203	-0.1734	
0.20	0.1339	0.1326	0.1359	2.20	-0.2402	-0.1839	-0.2667
0.30	0.1640	0.1604	0.1688	2.30	-0.2581	-0.1923	
0.40	0.1778	0.1706	0.1865	2.40	-0.2736	-0.1988	-0.3172
0.50	0.1794	0.1681	0.1928	2.50	-0.2870	-0.2034	
0.60	0.1721	0.1563	0.1901	2.60	-0.2982	-0.2062	-0.3583
0.70	0.1578	0.1379	0.1804	2.70	-0.3070	-0.2071	
0.80	0.1382	0.1153	0.1646	2.80	-0.3133	-0.2064	-0.3892
0.90	0.1149	0.0898	0.1439	2.90	-0.3175	-0.2041	
1.00	0.0885	0.0629	0.1193	3.00	-0.3195	-0.2003	-0.4097
1.10	0.0601	0.0354	0.0914	3.10	-0.3196	-0.1950	
1.20	0.0306	0.0081	0.0609	3.20	-0.3176	-0.1884	-0.4198
1.30	0.0004	-0.0185	0.0285	3.30	-0.3138	-0.1805	
1.40	-0.0299	-0.0440	-0.0052	3.40	-0.3080	-0.1715	-0.4198
1.50	-0.0609	-0.0680	-0.0397	3.50	-0.3007	-0.1614	
1.60	-0.0910	-0.0904	-0.0745	3.60	-0.2916	-0.1504	-0.4102
1.70	-0.1202	-0.1109	-0.1092	3.70	-0.2808	-0.1385	
1.80	-0.1479	-0.1296	-0.1432	3.80	-0.2687	-0.1258	-0.3917
1.90	-0.1740	-0.1462	-0.1763	3.90	-0.2551	-0.1124	
2.00	-0.1982	-0.1609	-0.2081	4.00	-0.2424	-0.0985	-0.3650
$A_+/B_+ = -0.779$				$A_-/B_- = -1.806$			

solution. The results of the numerical solutions for ξ_{\mp} together with the ratio A/B of the corresponding constants needed to continue the solution for large

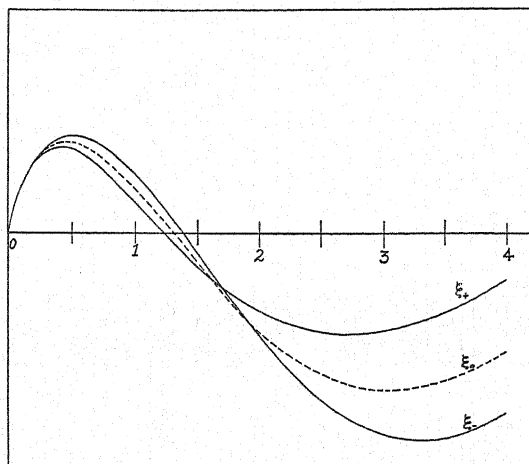


Fig. 1.

r by means of Eq. (7) are given in Table I. Graphs of these solutions together with the solution in which no austausch terms have been taken into account are shown in Fig. 1. It is of interest to note the appreciable phase shift in these

solutions due to the austausch effect. This phase shift is used to compute the quantum defect.

CALCULATION OF THE QUANTUM DEFECT

The method of calculating the quantum defects Δ_1 or Δ_2 consists of finding a solution of Eq. (5) for large values of r where the small but unknown energy term $2\epsilon\xi$ is retained and comparing this solution with that given by Eq. (7) already determined in the limit $\epsilon \rightarrow 0$. Retaining the term 2ϵ , Eq. (5) reduces, for large values of r to $\xi'' + (2\epsilon + 2/r)\xi = 0$. It is convenient to express the energy in units of Rh by writing $2\epsilon = -1/(n - \Delta)^2$, where n is a positive integer and Δ is the quantum defect which we seek, in which case the above equation becomes:

$$\xi'' + (2/r - 1/(n - \Delta)^2)\xi = 0. \quad (8)$$

Wentzel, Kramers, and Brillouin³ obtained approximate solutions of equations of this type. These solutions become invalid in the neighborhood of the point where the coefficient of ξ vanishes; the fundamental solution for the region where the coefficient of ξ is positive are oscillatory and go over into real exponentials when this coefficient is negative. It is important to know which oscillatory solution is the continuation of the increasing or decreasing exponential solution. These have been established by Kramers and Zwaan.⁴ For the case in hand it is necessary to use the oscillating solution which is a continuation of the exponential solution that decreases as r increases, in order that the solution of Eq. (8) will remain finite at $r = \infty$. The appropriate solution of Eq. (8) in the region where

$$2/r - 1/(n - \Delta)^2 > 0 \quad (9)$$

which remains finite at $r = \infty$ is

$$\xi = C \left\{ \frac{2}{r} - \frac{1}{(n - \Delta)^2} \right\}^{-1/4} \cos \left\{ \int_{2/(n - \Delta)^2}^r \left(\frac{2}{r} - \frac{1}{(n - \Delta)^2} \right)^{1/2} dr + \frac{\pi}{4} \right\}. \quad (10)$$

It is possible to use this solution for large r and still satisfy the condition (9) since we are at liberty to choose n as large as necessary. Upon performing the integration, Eq. (10) becomes;

$$\begin{aligned} \xi = C \left\{ \frac{2}{r} - \frac{1}{(n - \Delta)^2} \right\}^{-1/4} \cos & \left\{ \frac{2}{n - \Delta} \left[\frac{r}{2}(n - \Delta)^2 - \left(\frac{r}{2} \right)^2 \right]^{1/2} \right. \\ & \left. + 2(n - \Delta) \sin^{-1} \left[\frac{(r/2)^{1/2}}{(n - \Delta)} \right] - (n - \Delta)\pi + \frac{\pi}{4} \right\}. \end{aligned}$$

Since this expression will be needed only for the case where $r/(n - \Delta) \ll 1$, it can be simplified by omitting higher powers of $r/(n - \Delta)$ and can then be written as

$$\xi = C(r/2)^{1/4} \cos \{ (8r)^{1/2} - (n - \Delta)\pi + \pi/4 \}. \quad (11)$$

³ See for example; H. A. Kramers, *Zeits. f. Physik* 33, 828 (1926).

⁴ A. Zwaan, *Utrecht Dissertation*, 1929.

This solution can be most easily compared with that given by Eq. (7) in the domain where r is so large that the Bessel's functions appearing in Eq. (7) can be replaced by the first term in their asymptotic expansions, namely

$$\begin{aligned} J_1\{(8r)^{1/2}\} &= [1/\pi^{1/2}(2r)^{1/4}] \cos \{(8r)^{1/2} - \pi/2 - \pi/4\} + \dots \\ Y_1\{(8r)^{1/2}\} &= [1/\pi^{1/2}(2r)^{1/4}] \sin \{(8r)^{1/2} - \pi/2 - \pi/4\} + \dots \end{aligned}$$

Substituting these expressions in Eq. (7) it may be written,

$$\xi = C(r/2)^{1/4} \cos \{(8r)^{1/2} + 3\pi/4 + \delta\pi\} \quad (12)$$

where $\delta = \tan^{-1}A/B$. It is now evident that the two solutions (11) and (12) differ only in phase and since in the limit for large n the two solutions must be identical in phase, this serves to determine the unknown phase factor in Eq. (11). Equating the phases we have, $\Delta = n + \frac{1}{2} + \delta$. Since Δ denotes only the non-integer correction to n we may write $\Delta = \frac{1}{2} + \delta$, or remembering the two solutions for para- and orthohelium and also the relation for δ in terms of the constants A and B , we have,

ortho

$$\Delta_1 = \frac{1}{2} + (1/\pi) \tan^{-1} A_+/B_+$$

para

$$\Delta_2 = \frac{1}{2} + (1/\pi) \tan^{-1} A_-/B_- \quad (13)$$

The quantum defect may therefore be found by matching the phases of the two solutions (7) and (10) in the domain where they must be equal, namely for sufficiently large r and in the limit $n \rightarrow \infty$.

Making use of the numerical values of the coefficients A and B given in Table I, the following results are obtained for Δ_1 and Δ_2 , namely, $\Delta_1 = 0.289$, $\Delta_2 = 0.160$.

DISCUSSION OF RESULTS

The corresponding values of Δ_1 and Δ_2 calculated by Hylleraas; namely, for the case when the polarization of the atom core is neglected, are 0.230 and 0.122, respectively, while the values needed in order to yield the term values obtained experimentally are 0.298 and 0.140. The fact that the values obtained here are in better agreement with the values found experimentally is doubtless due to the more accurate wave functions obtained here. By attempting to take the polarization into account, Hylleraas obtained 0.29 and 0.15 for Δ_1 and Δ_2 which are in good agreement with the experimental results. However, in the light of the results obtained here, it does not seem likely that the polarization of the atom core plays as great a role, as regards the values of Δ_1 and Δ_2 , as that indicated by Hylleraas' calculations.

The writer is indebted to Dr. H. Bethe for suggesting this problem and for helpful discussions in connection with it, and to the National Research Council for the Fellowship under which this work was carried on.

Rotational Analysis of the First-Negative Bands of the CO^+ Molecule

By R. F. SCHMID

Ryerson Physical Laboratory, University of Chicago

(Received August 19, 1932)

By using the light of a graphite hollow cathode in a CO_2 atmosphere, the $^2\Sigma \rightarrow ^2\Sigma$ (first-negative) CO^+ bands at $\lambda\lambda 2299.7, 2325.2, 2419.4, 2445.8, 2474.2, 2504.5, 2577.7, 2607.2, 2638.7$ and 2672.3\AA have been photographed in the second and third order of a 21 foot Rowland grating. The analysis gives the rotational constants: $B_e' = 1.778 \text{ cm}^{-1}$, $\alpha' = 0.032 \text{ cm}^{-1}$ and $B_e'' = 1.954 \text{ cm}^{-1}$, $\alpha'' = 0.019 \text{ cm}^{-1}$. The ρ -type doubling of both of the upper and lower $^2\Sigma$ states seems to be very small. Only lines with high rotational quantum numbers show broadenings and sometimes measurable doublings. Definite perturbations could not be observed.

THE first attempt at a rotational analysis of the first-negative group of CO^+ was made by Blackburn.¹ He photographed the bands in the light of a helium discharge tube and measured mostly in the first order of a 21 foot grating. Since he did not publish his measurements and because the rotational constants given by him seem to be erroneous, new measurements seemed desirable. For that purpose a $1 \times 1 \times 1$ inch graphite block with a cylindrical hollow (3 mm width) was put in a bulb with a quartz window, and using a CO_2 atmosphere at 0.1 mm pressure a direct current of about 700 milliamperes was led through. A smaller piece of graphite served as anode. The cathode became red hot and the hollow gave a very bright blue colored light, which contained the whole CO^+ spectrum in considerable intensity and also some CO and CO_2 bands. In 50 hour exposures good second and third order pictures were obtained.

TABLE I. $\lambda = 2299.69\text{\AA}$ $0 \rightarrow 1$ band.

K	P	K	R	K	P	K	R
		1	43,456.0	19	43,319.0	25	43,434.4
1	43,445.6	2	458.6	20	309.1	26	429.3
2	441.2	3	461.7	21	298.6	27	423.8
3	436.6	4	464.0	22	287.9	28	418.0
4	431.7	5	465.8	23	276.6	29	412.1
5	426.5	6	467.4	24	265.1	30	405.5
6	421.0	7	468.5	25	253.2	31	398.3
7	415.1	—	—	26	241.2	32	391.1
8	409.0	14	468.5	27	228.7	33	383.6
9	402.5	15	466.9	28	216.0		
10	395.7	16	465.3	29	202.7	34	{375.5
11	388.5	17	463.2	30	189.4		{375.0
12	381.0	18	460.8	31	175.4		
13	373.1	19	457.8	32	161.6	35	{367.7
14	365.0	20	455.1	33	147.0		{366.8
15	356.6	21	451.6	34	131.9		
16	347.7	22	447.8			36	{359.3
17	338.5	23	443.7				{358.4
18	329.0	24	439.2			37	349.7?

¹ C. M. Blackburn, Proc. Nat. Acad. 11, 28 (1925).

TABLE II. $\lambda=2419.39A$ $0 \rightarrow 2$ band.

<i>K</i>	<i>P</i>	<i>K</i>	<i>R</i>	<i>K</i>	<i>P</i>	<i>K</i>	<i>R</i>
1	41,292.4	1	41,303.1	18	41,182.2	27	41,285.0
2	288.4	2	306.1	19	173.2	28	280.6
3	284.0	3	308.8	20	163.9	29	275.3
4	279.3	4	311.1	21	154.4	30	269.9
5	274.2	5	313.3	22	144.1	31	264.1
6	268.7	6	314.9	23	134.0	32	257.9
7	263.0	—	—	24	123.4	33	251.1
8	257.3	17	315.9	25	112.5		
9	251.1	18	314.2	26	101.3		
10	244.6	19	312.2	27	89.8		
11	237.9	20	309.8	28	78.4		
12	230.8	21	307.1	29	66.2		
13	223.3	22	304.2	30	53.8		
14	215.6	23	301.0	31	41.3		
15	207.9	24	297.5	32	28.3		
16	199.8	25	293.7	33	15.0		
17	191.2	26	289.4	34	1.4		

TABLE III. $\lambda=2325.17A$ $1 \rightarrow 2$ band.

<i>K</i>	<i>P</i>	<i>K</i>	<i>R</i>	<i>K</i>	<i>P</i>	<i>K</i>	<i>R</i>
4	42,956.9	12	42,993.4	21	42,820.5	29	42,925.9
5	952.3	13	992.3	22	809.4	30	918.9
6	946.8	14	990.8	23	797.7	31	911.0
7	940.8	15	989.0	24	785.7	32	903.0
8	934.5	16	986.9	25	773.5	33	894.5
9	927.7	17	984.3	26	760.6		
10	920.7	18	981.6	27	747.8	34	{885.7
11	913.4	19	978.3	28	734.5		{885.0
12	905.8	20	975.0	29	720.7		
13	897.6	21	971.2	30	706.7	35	{878.2
14	889.2	22	966.9				{876.3
15	880.4	23	961.9				
16	871.5	24	956.5			36	{868.0
17	861.8	25	951.0				{867.1
18	852.2	26	945.6				
19	841.9	27	939.3			37	{858.5
20	831.5	28	932.6				{875.6

TABLE IV. $\lambda=2445.84A$ $1 \rightarrow 3$ band.

<i>K</i>	<i>P</i>	<i>K</i>	<i>R</i>	<i>K</i>	<i>P</i>	<i>K</i>	<i>R</i>
1	40,848.4	0	40,856.3	16	40,754.0	23	40,849.4
2	844.3	1	859.3	17	744.9	24	845.3
3	839.6	2	862.1	18	735.8	25	840.8
4	835.0	3	864.6	19	726.2	26	836.0
5	829.8	4	866.8	20	716.4	27	830.8
6	824.8	5	868.7	21	706.5	28	825.5
7	819.0	—	—	22	696.2	29	819.8
8	812.9	15	870.5	23	685.1	30	813.3
9	806.7	16	869.2	24	674.2	31	806.9
10	799.9	17	867.5	25	663.2	32	800.1
11	792.9	18	865.4	26	651.3		
12	785.7	19	863.0	27	639.2		
13	778.1	20	859.9	28	626.6		
14	770.1	21	856.7	29	614.6		
15	762.1	22	853.1	30	602.3		

TABLE V. $\lambda=2577.68A$ 1 \rightarrow 4 band.

K	P	K	R	K	P	K	R
2	38,750.6	1	38,765.4	22	38,612.7	29	38,743.0
3	746.7	2	768.5	23	603.0	30	738.2
4	742.0	3	771.3	24	592.9	31	732.8
5	737.4	4	773.7	25	581.0	32	727.2
6	732.0	5	776.0	26	517.7	33	721.4
7	726.8	6	777.6	27	561.0	34	715.1
8	721.0	7	779.3	28	550.0	35	708.9
9	715.1	—	—	29	538.3	36	702.4
10	708.9	17	779.8	30	526.6	37	695.9
11	702.4	18	778.4	31	514.7	38	687.7
12	696.5	19	776.7	32	502.1	39	679.9
13	688.5	20	774.6	33	489.5	40	671.9
14	681.2	21	772.3	34	476.5		
15	673.6	22	769.5	35	463.6		
16	665.7	23	766.6	36	450.0		
17	657.7	24	763.5	37	436.1		
18	649.1	25	759.9	38	422.1		
19	640.5	26	756.1	39	407.8		
20	631.5	27	752.1	40	393.5		
21	622.2	28	747.6	41	378.1		
				42	362.7		

TABLE VI. $\lambda=2474.21A$ 2 \rightarrow 4 band.

K	P	K	R	K	P	K	R
2	40,377.2	1	40,391.5	25	40,190.3		
3	372.9	2	394.6	26	178.0	30	{40,336.3
4	368.0	3	397.1	27	165.4		335.3
5	362.9	4	399.1	28	152.6		
6	357.5	5	401.0	29	139.4	31	329.4
7	351.5	—	—	30	125.9		
8	345.5	13	403.0	31	111.9	32	{322.6
9	339.1	14	401.8	32	97.6		321.3
10	332.6	15	400.2	33	82.8	33	314.8
11	325.2	16	398.1				
12	317.7	17	395.8	34	{68.0	34	{307.0
13	310.0	18	393.3		{67.0		305.8
14	301.9	19	390.3				
15	293.6	20	386.9	35	{52.7		
16	284.7	21	383.3		{51.2		
17	275.7	22	379.2				
18	266.2	23	375.3	36	{37.0		
19	256.5	24	370.1		{34.4		
20	246.0	25	365.1				
21	235.6	26	359.7	37	{21.0		
22	224.8	27	353.7		{19.2		
23	213.5	28	347.7				
24	202.0	29	341.1	38	{6.2		
					{4.5		

TABLE VII. $\lambda=2607.16A$ 2 \rightarrow 5 band.

K	P	K	R	K	P	K	R
7	38,290.4			28	38,105.9	33	38,270.6
8	284.6	13	38,343.9	29	93.6	34	263.6
9	278.5	14	343.3	30	81.4	35	256.3
10	272.0	15	342.1	31	68.6	36	248.5
11	265.3	16	340.9	32	55.5	37	240.7
12	258.4	17	339.2	33	42.3	38	232.3
13	251.1	18	337.3	34	28.4	39	223.5
14	243.5	19	335.0	35	14.4	40	214.5
15	235.5	20	332.5	36	0.2	41	205.1
16	227.4	21	329.8	37	37,985.5	42	195.5
17	218.9	22	326.6	38	970.7		(double)
18	210.1	23	323.1	39	955.4		
19	201.1	24	319.1				
20	191.7	25	315.1	40	{939.7		
21	182.0	26	310.8		{938.8		
22	172.1	27	306.0				
23	161.7	28	301.0	41	{923.9		
24	151.4	29	295.6		{922.7		
25	140.4	30	289.9				
26	129.1	31	283.7	42	907.3		
27	117.8	32	277.3				
				43	{890.9		
					{889.2		

TABLE VIII. $\lambda=2504.48A$ 3 \rightarrow 5 band.

K	P	K	R	K	P	K	R
9	39,852.0	12	39,914.6	21	39,745.1		
10	845.1	13	913.5	22	733.9	24	{39,876.5
11	838.0	14	911.9				875.4
12	830.1	15	909.9				
13	822.2	16	907.5	23	{725.7		
14	813.8	17	904.8		{724.4	25	{870.7
15	805.2	18	901.6				{869.2
16	795.8	19	898.2			26	{865.1
17	786.7	20	894.3				{863.3
18	776.6	21	890.1				
19	766.5	22	885.7			27	{858.8
20	756.0	23	881.2				{857.0

TABLE IX. $\lambda=2638.72A$ 3 \rightarrow 6 band.

K	P	K	R	K	P	K	R
9	37,821.6	13	37,844.5	23	37,700.5	27	37,839.2
10	815.2	14	883.4	24	689.5	28	833.6
11	808.0	15	881.9	25	678.4	29	827.6
12	800.7	16	880.1	26	666.0	30	820.9
13	793.3	17	878.1	27	654.0	31	813.9
14	785.5	18	875.8	28	642.1	32	807.0
15	777.5	19	873.1	29	629.1	33	799.2
16	768.8	20	870.0	30	616.3	34	791.8
17	760.0	21	866.8	31	602.9	35	783.6
18	751.0	22	863.1	32	589.1	36	774.7
19	741.5	23	858.9	—	—	37	766.1
20	731.7	24	854.5	36 (?)	467.5		(double)
21	721.7	25	849.6				
22	711.4	26	844.6	37 (?)	{450.2		
					{449.2		

TABLE X. $\lambda=2672.31A$ 4 \rightarrow 7 band.

<i>K</i>	<i>P</i>	<i>K</i>	<i>R</i>	<i>K</i>	<i>P</i>	<i>K</i>	<i>R</i>
2	37,383.8	2	37,400.9	17	37,283.4	23	37,377.0
3	379.4	3	403.1	18	274.0	24	372.0
4	375.1	4	404.9	19	264.3	25	366.8
5	369.9	5	407.0	20	254.1	26	361.1
6	364.7	—	—	21	243.7	27	355.0
7	358.9	13	407.6	22	232.8	28	348.4
8	353.1	14	406.0	23	221.7	29	341.7
9	346.5	15	404.2	24	210.1	30	334.4
10	339.9	16	401.9	25	198.0	31	326.9
11	332.9	17	399.6	26	186.1	32	319.1
12	325.5	18	396.8	27	174.0	33	310.8
13	317.8	19	393.6	28	160.8		
14	309.7	20	389.9	29	147.4		
15	301.2	21	385.9	30	133.6		
16	292.3	22	381.5	31	119.9		

TABLE XI. Upper state combinations. $R(K) - P(K)$.

<i>v'</i>	0	0	1	1	1	2	2	3	3	4
<i>v''</i>	1	2	2	3	4	4	5	5	6	7
<i>K</i>										
1	10.4	10.7		10.9						17.1
2	17.4	17.7		17.8	17.9	17.4				23.7
3	25.0	24.8		25.1	24.6	24.2				29.9
4	32.3	31.8		31.7	31.6	31.1				37.2
5	39.3	39.1		38.9	38.6	38.1				
6	46.4	46.2			45.6					
7	53.4				52.5					
12			87.6					84.5		
13			94.7			93.0	92.8	91.3	91.2	89.8
14	103.6		101.6			99.8	99.8	98.1	97.8	96.4
15	110.3		108.6	108.4		106.6	106.6	104.6	104.4	103.0
16	117.6		115.4	115.1		113.3	113.5	111.7	111.3	109.6
17	124.7	124.7	122.5	122.6	122.1	120.1	120.2	118.1	118.1	116.1
18	131.8	131.9	129.4	129.6	129.3	127.1	127.2	125.0	124.8	122.8
19	138.7	139.0	136.5	136.8	136.2	133.7	134.0	131.7	131.6	129.3
20	145.9	145.9	143.5	143.5	143.1	140.9	140.8	138.4	138.3	135.8
21	153.1	152.7	150.6	150.2	150.1	147.8	147.8	145.0	145.2	142.2
22	160.0	160.0	157.5	156.9	156.8	154.5	154.5	151.9	151.6	148.7
23	167.1	167.0	164.2	164.3	163.6	161.8	161.3		158.5	155.4
24	174.0	174.2	170.8	171.2	170.6	168.1	167.7		165.0	161.8
25	181.2	181.2	177.5	177.6	178.9	174.8	174.7		171.2	168.7
26	188.2	188.1	185.0	184.7	184.4	181.6	181.7		178.6	175.0
27	195.0	195.2	191.6	191.6	191.0	188.3	188.2		185.1	181.0
28	202.0	202.2	198.1	198.9	197.6	195.1	195.1		191.5	187.6
29	209.4	209.1	205.2	205.2	204.8	201.7	202.0		198.5	194.3
30	216.1	216.2	212.3	211.0	211.6	209.5	208.5		204.6	200.7
31	222.8	222.8			218.1		215.1		211.1	207.1
32	229.6	229.6			225.1		221.8		217.9	
33	236.6	236.1			232.9		228.4			
34					239.6		235.2			
35					245.3		242.0			
36					252.4		248.3			
37					259.9		255.2			
38					265.7		262.6			
39					272.2		268.2			
40					278.4					

TABLE XII. Lower state combinations. $R(K-1)-P(K+1)$.

v'	0	0	1	1	1	2	2	3	3	4
v''	1	2	2	3	4	4	5	5	6	7
K										
1				12.0?						
2	19.4	19.0		19.7?	18.8	18.6				
3	26.8	26.8		27.1	26.5	26.6				25.9
4	35.1	34.6		34.8	33.8	34.2				33.2
5	43.0	42.4		42.0	41.7	41.6				40.2
6	50.7	50.3		49.7	49.2	49.6				48.2
7	58.4	57.6			56.6					
8	66.1				64.2					
13			104.1					100.8		
14			111.9			109.4	108.4	108.2	107.5	106.4
15	120.8		119.3			117.0	115.9	116.1	114.6	113.7
16	128.5		127.1	125.6		124.5	123.2	123.2	121.9	120.8
17	136.3		134.7	133.4		131.9	130.7	130.9	129.1	128.0
18	144.1	142.7	142.5	141.3	139.3	139.2	138.1	138.3	136.6	135.3
19	151.7	150.3	150.1	149.0	146.9	147.3	145.6	145.7	144.1	142.6
20	159.2	157.8	157.8	156.5	154.5	154.7	153.0	153.1	151.5	149.8
21	167.2	165.7	165.6	163.7	161.9	162.1	160.4	160.4	158.6	157.2
22	175.0	173.1	173.5	171.5	169.3	169.9	168.1		166.4	164.2
23	182.7	180.8	181.2	179.0	176.6	177.2	175.2		173.6	171.3
24	190.5	188.4	188.3	186.2	185.6	185.0	182.7		180.5	179.0
25	198.0	196.2	195.9	194.0	191.8	192.1	190.0		188.5	185.9
26	205.6	203.9	203.2	201.7	198.9	199.7	197.2		195.5	192.8
27	213.3	211.1	211.2	209.4	206.1	207.0	204.9		202.5	200.3
28	221.1	218.8	218.7	216.2	213.8	214.3	212.4		210.1	207.6
29	228.6	226.8	225.9	223.3	221.0	221.9	219.6		217.3	214.8
30	236.6	234.0			228.3	229.2	227.0		224.7	221.8
31	243.9	241.7			236.1		234.3		231.8	
32	251.3	249.2			243.3		241.4			
33	259.2	256.5			250.7		248.9			
34					257.8		256.3			
35					265.1		263.4			
36					272.8		270.8			
37					280.4		277.8			
38					288.2		285.3			
39					294.2					
40					301.9					
41					309.2					

The Tables I to X contain the measurements. The accuracy is $\pm 0.1 \text{ cm}^{-1}$. Most of the band lines appear single (the bands are composed of P and R branches as is usual for the case $^2\Sigma \rightarrow ^2\Sigma$). Only lines with high rotational quantum numbers show an increasing broadening and in some cases also splittings could be observed. Unfortunately (but naturally) the broadening or splitting causes a more rapid decrease of the intensity and so only a few doublets could be measured. Besides that, the dispersion and resolution of the grating used in the region of these bands allows one to observe doublets only when the separation is larger than 0.5 cm^{-1} (in the third order) or 1 cm^{-1} (in the second order). Considering these facts, not much can be said about the magnitude of the ρ -type doubling of the $^2\Sigma$ terms. It may be pointed out that while in most of the bands the doubling starts with rotational quantum numbers about 30 to 34, in the $1 \rightarrow 4$ band ($\lambda = 2577.7 \text{ \AA}$) no doublings were observed until rotational quantum numbers 40 to 42, while on the other hand

A Quantum Mechanics Treatment of the Water Molecule

By ALBERT SPRAGUE COOLIDGE
Harvard University

(Received August 8, 1932)

The perturbation method of Heitler and London has been applied to study the interaction of the atoms in the water molecule. For a preliminary calculation an arbitrary internuclear distance has been assumed, and no ionic wave function has been considered. The calculated binding energy, 3.5 volts, is too small, as was to be expected. An analysis of the sources of this energy in various types of resonance or electron interchange is developed, and the results compared with Slater's simplified model. Methods for the evaluation of electron reactions involving three centers are described, including a possible alternative for the customary Neumann method, applicable to two-center problems. Formulas for products of bi-axial surface harmonics and their integrals are given.

INTRODUCTION

THE present work was undertaken in order to investigate by an actual calculation the extent to which the chemical binding in a triatomic molecule can be referred to the overlapping of particular electron orbits, and to see to what degree the energy is affected by the reactions of atoms which are adjacent but not in chemical combination according to current doctrines of valence. The calculation of the reactions between electrons associated with three atomic centers proved very laborious. In order to reduce within practical limits the amount of computation, it has been necessary to confine the investigation to certain predetermined configurations of the nuclei. Assuming the oxygen atom at the center of a system of rectangular coordinates, the hydrogen atoms are supposed to lie in the XY plane, in approximately the directions of the X and Y axes respectively, and at equal distances from the center. This distance has been taken as $2 a_H$, in close agreement with Debye's¹ estimate, 1.07×10^{-8} cm. The method of computation permitted variation in the distance between the hydrogen atoms without excessive labor, and three distances have been computed: 2.5, 2.828, and $3 a_H$. The corresponding molecular angles (between the lines joining the oxygen to the two hydrogen nuclei) are $77^\circ 22'$, 90° , and $97^\circ 11'$. (It is assumed that these lines make equal angles with the X and Y axes respectively.) In defining wave functions we require, in addition to the rectangular coordinates, the radial distances r , s , t , measured respectively from the oxygen, the X hydrogen, and the Y hydrogen nucleus.

The oxygen atom has been represented as a nucleus of charge 6, surrounded by six electrons of the L shell, two in s orbits and four in p orbits. To each hydrogen atom a single electron has been assigned. Covalent bonds are supposed to result from the interaction of these electrons, in a manner depending

¹ Debye, *Polar Molecules*, p. 73.

upon the various possible methods of assigning spins. A general discussion of a similar but simpler model has been given by Slater.²

CHOICE OF WAVE FUNCTIONS

Four stages in the working-up of an approximate molecular wave function exist, and may well be defined at the outset. First, elementary functions for single electrons are selected. Second, products of these are combined in the manner of a determinant to form simple functions for all the electrons. Third, certain intermediate linear combinations of these simple functions are formed for the purpose of facilitating the solution of the secular equation. Fourth and last, a final function is constructed as another linear combination of the simple functions, with such coefficients as will give the minimum energy. This last step cannot, of course, be taken until the secular equation has been set up and solved so as to determine the coefficients. The minimum energy, obtained from the final function, will be already known, since it comes out of the secular equation; nevertheless, it will be instructive to find the final function and compute the energy over it, in order to see how the different electron reactions contribute to the total value.

Zener³ has given formulas for the best simple analytical elementary wave functions which can be used as a basis for a perturbation calculation of atomic energies. For 2s and 2p electrons, respectively, they may be written

$$r^{n^*-1}(1 - \alpha r^{-1})e^{-\delta r}S_0 \text{ and } r^{n^*-1}e^{-\delta r}S_1,$$

where S_0 and S_1 represent surface harmonics of order 0 and 1. For oxygen, the best value of n^* is 2, of δ , 2.24, while α is negligibly small. As has been shown by Pauling⁴ and by Slater^{2,5} it is advantageous in molecular problems to choose real surface harmonics, of which one has a maximum orientated along the line of each chemical bond. For the hydrogen electrons, the simple normal atomic orbits were assumed. The normalized elementary functions chosen for the computation are

$$\begin{aligned}\psi_0 &= (\delta^5/3\pi)^{1/2}re^{-\delta r}; & \psi_z &= (\delta^5/\pi)^{1/2}ze^{-\delta r}; \\ \psi_x &= (\delta^5/\pi)^{1/2}xe^{-\delta r}; & \psi_y &= (\delta^5/\pi)^{1/2}ye^{-\delta r}; \\ \psi_\xi &= (1/\pi)^{1/2}e^{-s}; & \psi_\eta &= (1/\pi)^{1/2}e^{-t}.\end{aligned}$$

It will be seen that they are all orthogonal except the following pairs: $o\xi$, $o\eta$, $x\xi$, $y\eta$, $\xi\eta$, $x\eta$, $y\xi$; the last two pairs approach orthogonality as the molecular angle approaches 90° . For δ , the round value $9/4$ was adopted.

Following Slater, we select six simple functions for all the electrons, which have the same unperturbed energy, and which cannot combine with any other functions of the same energy when the molecular angle is just 90° . With other angles, combinations with other functions become possible; but these

² J. C. Slater, Phys. Rev. **38**, 1109 (1931).

³ Clarence Zener, Phys. Rev. **36**, 51 (1930).

⁴ Linus Pauling, J. Am. Chem. Soc. **53**, 1367 (1931).

⁵ J. C. Slater, Phys. Rev. **37**, 481 (1931).

combinations become rapidly smaller as the angle approaches 90° , and are neglected here. Each simple function is the sum of $8!$ terms which may be derived by systematic permutations of the electrons among a definite set of orbits, and may be represented by the symbols characteristic of those orbits. The two possible spins may conveniently be designated by the presence or absence of an overline. Thus, we have

$$\begin{aligned}\psi_1 &= \bar{o} \bar{z} \bar{x} \bar{y} o z \xi \eta; & \psi_2 &= \bar{o} \bar{z} \bar{\xi} \bar{\eta} o z x y; \\ \psi_3 &= \bar{o} \bar{z} \bar{x} \bar{\xi} o z y \eta; & \psi_4 &= \bar{o} \bar{z} \bar{y} \bar{\eta} o z x \xi; \\ \psi_5 &= \bar{o} \bar{z} \bar{\xi} \bar{y} o z x \eta; & \psi_6 &= \bar{o} \bar{z} \bar{x} \bar{\eta} o z \xi y.\end{aligned}$$

Slater shows that the lowest energy is to be found from some combination of two intermediate functions: $A = \frac{1}{2}[\psi_1 + \psi_2 + \psi_5 + \psi_6]$; $C = \frac{1}{2}[\psi_3 + \psi_4]$. These do not combine with any of the other four possible independent linear combinations of the simple functions. The final function is $\psi_f = aA + cC$, where a and c are to be chosen with regard to normalization, and so as to satisfy simultaneously the equations

$$\begin{aligned}a(H_{AA} - \lambda\Delta_{AA}) + c(H_{AC} - \lambda\Delta_{AC}) &= 0, \\ a(H_{AC} - \lambda\Delta_{AC}) + c(H_{CC} - \lambda\Delta_{CC}) &= 0.\end{aligned}$$

Here H_{AA} , Δ_{AA} , etc., are the matrix components of the energy operator and of unity over the intermediate functions, and λ is the lower solution of the secular equation

$$\begin{vmatrix} H_{AA} - \lambda\Delta_{AA} & H_{AC} - \lambda\Delta_{AC} \\ H_{AC} - \lambda\Delta_{AC} & H_{CC} - \lambda\Delta_{CC} \end{vmatrix} = 0.$$

The values found for the quantities λ , a , and c , may be anticipated:

Molecular angle	$77^\circ 22'$	90°	$97^\circ 11'$
a	1.106	1.082	1.074
c	0.076	0.083	0.087
λ	-18.4976	-18.5133	-18.5150

The subsequent analysis may be somewhat clarified by adopting a different representation of the intermediate and final wave functions. Each of the $8!$ terms in a simple function can be expressed as the product of two factors, of which one contains only functions of space coordinates, and the other determines the spin. In every one of the other five simple functions may be found a term with the same space factor, but a different spin factor. Any linear combination of simple functions can therefore be made up in the form of $8!$ terms derivable by permutation from a typical term in which the space factor is of the same simple form as in the simple functions, but the spin is specified by a more complicated factor, involving in general non-integral coefficients.

MATRIX ELEMENTS

Let us examine the construction of the matrix elements of the total energy operator, or of unity, over a pair of functions (possibly identical) which may

be either simple, intermediate, or final. As is well known, it is sufficient to consider only the $8!$ terms obtained by selecting a single typical term from one of the pair of functions involved, applying the appropriate operator, and multiplying this in turn with each term of the other function. Since we do not consider the interaction between spin and orbital motion, we can separate each resulting term into a space factor and a spin factor.

The space factors will be the same in all classes of matrix elements, and will be characterized by the types of orbit exchange involved. Since the orbits to which the electrons are assigned are always selected from the same list (insofar as the space parts are concerned), the two assignments involved are related to each other by a certain scheme of permutation which we call an exchange. Thus, suppose that the typical term of one wave function has the space factor, $o_1z_2x_3\xi_4o_5z_6y_7\eta_8$, (the subscripts referring to definite electrons), and that in the other wave function occurs a term with the assignment $\xi_1z_2o_3x_4o_5z_6y_7\eta_8$. Then we may say that electrons 1, 4, and 3, respectively, make the transitions $o \rightarrow \xi$, $\xi \rightarrow x$, and $x \rightarrow o$, while the others are stationary; we shall represent this exchange by the symbol $[o\xi x]$. Similarly, an exchange system like $o \rightarrow z$, $z \rightarrow o$, $\xi \rightarrow \eta$, $\eta \rightarrow \xi$, will be denoted by $[oz:\xi\eta]$. The contribution from each exchange will be called an exchange element. The great majority of the $8!$ such elements in each matrix component will be found to vanish because of orthogonality between exchanging orbits, or for reasons of symmetry, and many of the surviving elements are equal in magnitude. Their computation will not be extensively discussed except in regard to certain features peculiar to the three-nucleus problem, to be taken up later.

The exchange elements of unity will be called exchange factors. Thus the exchange $[o\xi\eta]$ produces the factor $(o\xi)^2(\xi\eta)$, where $(o\xi) = \int dV \psi_o \psi_\xi$, $(\xi\eta) = \int dV \psi_\xi \psi_\eta$. These integrals are well known.

The exchange elements of the energy will be called exchange integrals, or gross exchange integrals when we wish to distinguish them from certain other quantities, to be discussed later, which arise from certain terms only in the operator, and correspond to what is ordinarily meant by the term exchange integral. In computing them, the total energy operator is used, including nuclear repulsions, kinetic energy of electrons, and reactions between each electron and all other electrons and nuclei. There will be in general 63 terms in each exchange integral, and the formulas are too cumbersome to warrant reproduction here.

We must now consider the part played by the spin factors in the matrix elements. This is simplest in the case of elements over the simple functions, where each orbit is associated with a definite spin. When the typical term of one function is combined with any particular term of the other, the resulting spin factor will be unity in case the spin of each electron is the same in both terms; otherwise it will be zero. Upon grouping together those exchange elements of identical value, we can represent the complete matrix element as a sum of typical exchange elements, each multiplied by an integral occurrence number, showing how many permutations produce an exchange of the given type with no changes of spin. (Of course, attention must be paid to the sign

with which each permutation occurs.) We shall see that it is convenient to represent the matrix elements over intermediate and final functions in a similar way, with the difference that the spin factors, and hence the occurrence numbers, attached to each of the exchange elements, will no longer be integral.

In order to determine the occurrence numbers for the simple functions, the following scheme was adopted. It depends upon the fact that all exchange elements vanish for exchanges involving more than two transitions between orthogonal orbits. First, a systematic list was made of all the permutations of each simple function which do not involve any electron in a change of spin as compared with a selected typical term. This list consists of 24 permutations among the 4 electrons of one spin, any one of which may be combined with any one of the 24 permutations among the other 4 electrons. In constructing the exchange list for a given matrix element involving this function with a second, a typical term was selected from the second function such that when it was combined with the typical term of the first function, no orthogonal transitions occurred. The 23 remaining permutations among one spin group of the first function were now compared with the typical term of the second, and the exchange types noted. The process was repeated for the other spin group. Many of the exchanges could be thrown out as involving more than two orthogonal transitions; while the number involving less than two was quite small. It was now easy to see which pairs of permutations, one from each spin group, could occur simultaneously without producing more than two orthogonal transitions, and the corresponding exchanges were added to the list. Finally a catalog of all exchange types was drawn up, and in it was entered the number of times that an exchange of each type was found to occur in each simple matrix element. These numbers are evidently the occurrence numbers of the preceding paragraph. The intermediate and final matrix elements are simple linear combinations of the simple elements. Upon making the corresponding linear combinations among the occurrence numbers for any particular exchange, we shall evidently get the occurrence number for that exchange in the intermediate or final matrix element. (Naturally, this cannot be done for the final function until the coefficients a and c are known.)

The above may be illustrated by reproducing a portion of the table showing the values of the exchange elements and occurrence numbers for certain combinations of functions. (The values are for 97° molecular angle.)

Exchange type	Exchange factor	Exchange integral	occurrence number in combinations of					
			$\psi_1\psi_1$	$\psi_1\psi_2$	$\psi_3\psi_3$	AA	AC	$\psi_f\psi_f$
[]	1.000	-17.7135	1	0	1	1	0.5	1.2554
[xy]	0	0.0475	-3	0	-2	-2.5	-2	-3.2791
[x ξ]	0.1072	-1.9876	0	0	-2	2	1	2.4878
[o $\xi\eta$]	0.0724	-1.3514	2	0	0	1	2	1.5368
[x ξ y η]	0.0001	-0.0009	0	-2	0	-1	-2	-1.5368

The products of the exchange factors or integrals with their occurrence numbers will be called exchange contributions to the given matrix element.

TOTAL AND BINDING ENERGY

The matrix of the total energy operator over the final function gives, of course, the energy of the molecule referred not to separated normal atoms, but to atoms stripped of all electrons except the two in the K shell of oxygen. It will be enormously greater (absolutely) than the molecular binding energy, and the unavoidable errors in its calculation will make it useless to try to get the binding energy by subtracting the true energy of the separate atoms. The question arises whether we can automatically separate out some sort of constant atomic energy, and construct a perturbation operator which will give the binding energy directly. In the case of the simple hydrogen molecule, this is readily accomplished. The total operator, as applied to a single permutation with electrons in designated orbits, can be represented as the sum of an atomic and a molecular part. Since the unperturbed functions are solutions of Schrödinger's equation, the effect of the atomic part of the operator is simply to multiply by a constant, the atomic energy. If the final function is normalized, the sum of the corresponding terms in the exchange contributions must be just the atomic energy. Therefore, to find the binding energy, these terms need not even be calculated. The remaining terms in the operator can be considered as a perturbation operator, and their matrix element over the final function will be the required energy.

In the present case, we are prevented from doing exactly this by two circumstances. One is that we have not started with accurate solutions of Schrödinger's equation, and the other is that not all the functions involved represent the normal state of the separated atoms. If we allow the nuclei to separate, we find that, of our original functions, ψ_1 and ψ_2 each produces one of the coincident levels of the lowest state of the oxygen atom, a 3P state. The remaining four do not remain separate, but $2^{-1/2}(\psi_3 + \psi_5)$ and $2^{-1/2}(\psi_4 + \psi_6)$ produce two more of the same levels, while $2^{-1/2}(\psi_3 - \psi_5)$ and $2^{-1/2}(\psi_4 - \psi_6)$ give levels of a higher 1D state. Even if we had accurate atomic functions for the different levels, the atomic terms in the operator would not produce a constant.

The difficulty can be partly overcome as follows. It will be readily seen that if we pay proper attention to normalization, we can find all the matrix elements equally well if, instead of choosing a single permutation of one of the functions with which to operate, we should choose any combination of permutations. Let us denote with ψ_m^n one single permutation from the function ψ_m , and with ψ_m^* the sum of all those permutations which assign, let us say, the first six electrons to one or another of the oxygen orbits, the 7th to the X hydrogen atom, and the 8th to the Y atom. Then a given matrix element can be found from $\sum_n \int dV \psi_a^n H \psi_b^*$. Now we can write $H = H_*^0 + H_*'$, where H_*^0 includes all the terms in the operator which connect the first six electrons with the oxygen nucleus or with each other, and the 7th and 8th, respectively, with the X and Y hydrogen nuclei. We may call this the atomic operator, and the remainder, H_*' , the molecular or perturbation operator. If now we may assume that the oxygen wave functions with which we started are true solutions of Schrödinger's equation, then the result of applying the atomic opera-

tor to these functions is just to multiply them by one of two constants which correspond to these two oxygen atom levels. Denoting with E^0 the ground energy, or mean of the two levels, plus the normal energy of two hydrogen atoms, and with ϵ the difference of either level from the mean, we may then write

$$\begin{aligned} H_*^0 \psi_1^* &= E^0 \psi_1^* + \epsilon \psi_1^* \\ H_*^0 \psi_2^* &= E^0 \psi_2^* + \epsilon \psi_2^* \\ H_*^0 (\psi_3^* + \psi_5^*) &= E^0 \psi_3^* + E^0 \psi_5^* + \epsilon \psi_3^* + \epsilon \psi_5^* \\ H_*^0 (\psi_4^* + \psi_6^*) &= E^0 \psi_4^* + E^0 \psi_6^* + \epsilon \psi_4^* + \epsilon \psi_6^* \\ H_*^0 (\psi_3^* - \psi_5^*) &= E^0 \psi_3^* - E^0 \psi_5^* - \epsilon \psi_3^* + \epsilon \psi_5^* \\ H_*^0 (\psi_4^* - \psi_6^*) &= E^0 \psi_4^* - E^0 \psi_6^* - \epsilon \psi_4^* + \epsilon \psi_6^* \end{aligned}$$

whence

$$\begin{aligned} H_*^0 \psi_3^* &= E^0 \psi_3^* + \epsilon \psi_5^* \\ H_*^0 \psi_4^* &= E^0 \psi_4^* + \epsilon \psi_6^* \\ H_*^0 \psi_5^* &= E^0 \psi_5^* + \epsilon \psi_3^* \\ H_*^0 \psi_6^* &= E^0 \psi_6^* + \epsilon \psi_4^* \end{aligned}$$

Upon adding these equations in suitable proportions to produce the final function, and applying the whole operator, we get

$$H\psi_f^* = E^0 \psi_f^* + H_*' \psi_f^* + \epsilon \psi_g^*,$$

where

$$\psi_g = \frac{1}{2}a(\psi_1 + \psi_2 + \psi_3 + \psi_4) + \frac{1}{2}c(\psi_1 + \psi_2 + \psi_5 + \psi_6) = aC + cA.$$

Hence

$$\int dV \psi_f^n H \psi_f^* - E^0 \int dV \psi_f^n \psi_f^* = \int dV \psi_f^n H_*' \psi_f^* + \epsilon \int dV \psi_f^n \psi_g^*.$$

The first integral on the right of this equation is the perturbation exchange integral corresponding to the group of exchanges represented by comparing the single permutation ψ^n with the group of permutations ψ^* ; they have all a single type of interatomic exchange, and differ only in permutations among the oxygen electrons.

Actually, we cannot expect the equation to hold exactly, because we have not accurate unperturbed wave functions. But if in place of the perturbation exchange integrals we introduce quantities which will satisfy the equation when the other integrals are actually calculated, then these quantities ought to be approximately equal to the perturbation exchange integrals: and upon adding the equations corresponding to all the permutations n , we see that the sum of these approximations must be equal to the difference between the molecular energy and the ground energy, except for the small term $\epsilon \Delta_{fg}$, which can be readily calculated. However, it is simpler and nearly as satisfactory to take simply the form $\int dV \psi_f^n H \psi_f^* - E^0 \int dV \psi_f^n \psi_f^*$ as the "net exchange integral," for these integrals must add directly to give $H_{ff} - E^0$, the

perturbation energy of the molecule with reference to the "ground state," or imaginary state characterized by the ground energy. To get the actual binding energy we must subtract ϵ , which we may regard as the perturbation energy of the free atoms referred to the same ground state.

Upon analysis, it turns out that E° is just H_{33} or H_{55} evaluated for the separated atoms, while ϵ is the negative of the exchange integral $[xy]$. The values are -18.3392 and -0.0475 . The resulting binding energy for 97° molecular angle is 0.1282 . It is very interesting to see how this is made up of contributions from the various exchanges. Table I shows both gross and net

TABLE I. Composition of molecular energy, 97° .

Exchange type	Gross contribution	Net contribution	Exchange type	Gross contribution	Net contribution
$[oz]$	-23.2995	-0.2772	$[o\xi\eta]$	-2.1540	-0.1112
$[xy]$			$[o\xi\eta:oz]$		
$[o\xi]$			$[o\xi\eta:xy]$		
$[o\xi:oz]$			$[z\xi\eta]$		
$[o\xi:xy]$			$[x\xi\eta]$		
$[x\xi]$	$+9.8696$	$+0.2937$	$[x\xi\eta:oz]$	-0.1257	-0.0178
$[x\xi:xy]$			$[x\xi\eta:yz]$		
$[x\xi:oz]$			$[o\xi o\eta]$		
$[x\xi:yz]$			etc.		
$[y\xi]$			$[o\xi ox\eta]$		
$[y\xi:oz]$	-5.1021	-0.2104	etc.	-0.0453	-0.0453
$[y\xi:xy]$			$[o\xi: o\eta]$	-0.4765	-0.0158
$[y\xi:yz]$			etc.	$+1.0867$	$+0.0693$
$[z\xi]$			$[x\xi: o\eta]$		
$[ox\xi]$			etc.		
$[oy\xi]$	-0.0681	-0.0755	$[x\xi: y\eta]$		
$[oz\xi]$			etc.		
$[xz\xi]$			miscellaneous	$+0.0086$	$+0.0102$
$[yz\xi]$			small terms		
$[xy\xi]$			Total		
$[oxo\xi]$			Atomic energy		
$[oyo\xi]$	$+0.1138$	$+0.1138$	" ϵ "		
$[\xi\eta]$			Binding energy	0.1283	0.1282
$[\xi\eta:oz]$					
$[\xi\eta:xy]$					
	$+1.7949$	$+0.0833$			

exchange contributions. In the interest of clarity, the number of entries is reduced by grouping together exchanges which involve the same interatomic transitions, differing only by transitions among the oxygen orbits; certain other exchanges producing small contributions are also grouped. We may try to correlate the net contributions with the familiar Coulomb and exchange integrals in Heitler and London's treatment of the H_2 molecule. The first value, -0.2772 , is to be regarded as the Coulomb contribution, for it involves no interatomic electron transitions. The second value, 0.2937 , which nearly cancels the first, is the repulsion due to the exchange between the hydrogen and the oxygen $2s$ electrons. The third, -0.2104 , which is roughly equal to the total molecular energy, because of cancellation among the other terms, is the expected binding energy between the hydrogen electrons and the $2p$ electrons of oxygen which are most favorably situated. The sixth term, 0.0833 , represents repulsion between the two hydrogen electrons, and is somewhat

more than offset by the next one, -0.1112 , arising from a cyclical exchange among three electrons. It is interesting that this term is by no means negligible. The remaining terms need not be discussed: they are small and cancel out extensively.

The fact that in order to produce the lowest molecular energy, we must take the simple functions in different proportions from those which give stable separated atoms, may be interpreted as indicating that the oxygen orbits are distorted on combination with hydrogen. It is interesting to see what increase in the internal energy of the oxygen atom accompanies this distortion. For this purpose we have only to compute the perturbation energy for infinite separation, using the simple functions in the proportions found for the molecular problem. This turns out to be just $\epsilon\Delta_{fg} = -0.0290$. The internal energy increase is, then, $\epsilon(\Delta_{fg} - 1) = 0.0185$. The difference is due entirely to the contributions from the $[xy]$ exchange, which (for separate atoms) enters with an occurrence number -0.6122 as against -1 in the most stable state.

DISCUSSION

Upon multiplying the calculated binding energy for 97° , 0.1282 , by the factor 27.08 , we obtain in volts the result 3.5 . The actual energy is about 10 volts, so that the result, while of the right order of magnitude, is much too small. A part of the error may be attributed to the failure to select the most favorable interatomic distance, but the greater portion is doubtless due to the omission of any wave functions of an ionic character. Pauling⁶ shows that the energy of the water molecule is considerably greater than that which would be expected to be produced by a nonpolar binding such as assumed in this calculation, so that the result is perhaps about what one would expect. It is hoped to attempt to improve the calculation by taking ionic states into account.

Note added in proof: This expectation has been realized. The ionic function used is $I = \frac{1}{2}(\psi_7 + \psi_8 + \psi_9 + \psi_{10})$, where

$$\begin{array}{ll} \psi_7 = \bar{o}\bar{z}\bar{x}\bar{y}ozx\eta & \psi_8 = \bar{o}\bar{z}\bar{x}\bar{\eta}ozxy \\ \psi_9 = \bar{o}\bar{z}\bar{x}\bar{y}oz\xi y & \psi_{10} = \bar{o}\bar{z}\bar{\xi}\bar{y}ozxy. \end{array}$$

This combines with the functions A and C , and with no other intermediate functions. For 97° molecular angle, the minimum energy is obtained from the final function (normalized) $0.7827A + 0.0773C + 0.3403I$, and is -18.5975 . The corresponding binding energy is 5.7 volts. The effect of varying the molecular angle is approximately the same as before.

A comparison of the results for the three angles indicates that, in agreement with the ideas of Slater, the hydrogen atoms are nearly at right angles, being forced slightly apart by mutual repulsion. The equilibrium angle is apparently about 95° .

It is interesting to compare the results of this calculation with Slater's analysis. The basis of comparison is rendered somewhat doubtful by his

⁶ Linus Pauling, Lectures at Massachusetts Institute of Technology (1932).

introduction of many simplifying assumptions. Slater neglects the presence of the o and z electrons entirely. We must therefore subtract out energy terms arising from their mutual influence, and must lump together their reactions on the hydrogen particles with those of the oxygen nucleus. This is taken care of in calculating the net exchange integrals by groups, as already explained. The next assumption is more difficult to deal with, for it seems in principle inconsistent. Slater assumes that all the elementary wave functions are orthogonal, so that normalization may be neglected, and the only exchange integrals surviving will be those involving just two electrons. He states that these integrals will be of the nature of that occurring in the hydrogen molecule problem, and will be independent of the presence of electrons not involved in the transition. Now, it is precisely because the wave functions are not orthogonal that molecular exchange integrals are negative, and lead to binding in the case of wave functions whose symmetry brings them in with positive occurrence numbers. When the functions are not orthogonal, there arise terms expressing the reaction of the exchanging electrons on the other electrons and nuclei, and while in any neutral molecule these tend to cancel out, the cancellation is by no means exact. Thus, the net exchange integral from the transition $[\xi\eta]$, calculated for two hydrogen atoms at the distance 2.8 in the absence of the oxygen atom, comes out -1.3 volts. When the oxygen atom is introduced the value increases to -3.1 volts. A comparison of the exchange integrals as calculated for 90° molecular angle with the values assumed by Slater follows.

Exchange	Slater	Coolidge
$[xy]$	1 volt	1.3 volts
$[x\xi]$	-5	-2.3
$[x\eta]$	-1	+0.6
$[\xi\eta]$	-0.8	-3.1

Slater's value for $[x\xi]$ was chosen essentially *ad hoc*, in order to get the right energy for the OH molecule, which is about half that of H_2O . Now, this energy also is probably largely ionic in character, so that it is not to be expected that a calculation of this kind should give more than a fraction of the observed value. Slater's estimate is therefore without doubt too high. It is certain that $[x\eta]$ should be positive, because of orthogonality. Finally, we may reasonably expect $[\xi\eta]$ to be larger than $[x\xi]$ because the wave functions overlap more, as is shown by the fact that the factor $(\xi\eta)$ is greater than that $(x\xi)$. This is due to partial cancellation between the parts of ψ_x which have opposite sign.

Slater predicts that the coefficient c will be much smaller than a , so that the wave function A alone will be a good approximation, and will give a better approximation for the energy. This prediction is seen to be verified. The energy over the normalized function A is -18.5133 .

METHOD OF COMPUTATION

In computing the matrix elements, the only novel problem was the evaluation of those terms involving orbits or nuclei of all three atoms. These may

express the electrostatic attraction between a nucleus and an electron which makes a transition between orbits of the other two atoms, or the repulsion between two transition electrons. These terms may be symbolized as ab/A and ab/cd , respectively, where small letters refer to orbits, capitals to nuclei, and the line / indicates electrostatic reaction. The case that a and b are ξ and η , and A the oxygen nucleus, was solved by setting up, with the aid of ellipsoidal harmonics, a general expression for the potential field of the $\xi\eta$ transition electron, and evaluating at the origin. In all other three-atom cases, it was necessary to express the orbits ξ and η in the form of series, each term being the product of a radial function and a surface harmonic, the center being the oxygen nucleus and the pole being the line of centers of the oxygen and the appropriate hydrogen nuclei. It was also found useful to have similar expansions for the products of the hydrogen orbits with the cosines of certain angles, namely, those which are characteristic of the $2p$ oxygen orbits.

Now, in the above symbolic representations, let a always be an oxygen orbit, while b , c , and d , may be any orbits. a may contain a surface harmonic factor of order 0 or 1, and the product ab may always be expressed as a radial function times a surface harmonic, or a series of such products. By means of the theory of harmonic potentials, the potential of this electric distribution may be calculated at any point, and will involve the same harmonic factor. The value at the position of the nucleus A gives at once the term ab/A , and to find ab/cd the potential of ab must be multiplied by cd and integrated. For this purpose cd can be expressed in terms each of which is a radial function multiplied by an angle factor which may be a harmonic or a product of two harmonics. Where b is also an oxygen orbit, it was found convenient to absorb the cosine factors (if any) which are found in the potential of ab , into the product cd before expansion, thus avoiding products of three harmonics.

Accordingly, the required terms are those giving the electrostatic action of two distributions of the form $F(r)S_n$ and $J(r)S_a'S_b''$. This is given by the expression $E_n(F, J) \times \int d\omega S_n S_a' S_b''$, where the integration is over all angles, and

$$E_n(F, J) = [4\pi/(2n+1)] \left[\int_0^\infty J r^{1-n} dr \int_0^r F r^{2+n} dr + \int_0^\infty J r^{2+n} dr \int_r^\infty F r^{1-n} dr \right].$$

The application of this formula is complicated by the fact that the radial factors occurring in the harmonic expansions have different analytical expressions over different ranges of r . Generally one of the harmonics can be reduced to unity.

It will be noted that the two-atom "Neumann" integrals which are so troublesome with unsymmetrical atoms may be evaluated by this method, and have been so done, since the radial functions required are the same as for the three-atom integrals. Thus, the integrals $\partial\xi/\partial\xi$ and $\partial\xi/\partial\eta$ differ only that in the former, we get products of coaxial harmonics, while in the latter the axes are different. In integrals of this class the series converges quite well.

Furry and Barlett⁷ report using this method with success, in connection with the beryllium molecule. With other classes of integrals convergence is less rapid. Here a valuable aid was furnished by the fact that when the two hydrogen nuclei coincide the integrals become easily calculable by ellipsoidal coordinates; the higher terms in the harmonic series can easily be estimated so that the result converges upon this known limit when the appropriate angle factors are introduced.

DEFINITE INTEGRALS

A number of definite integrals, which occur repeatedly in the course of the work, can well be defined and discussed together. In the following definitions, it is assumed that α and β are positive, and that R is positive except as otherwise noted. These restrictions are not always essential: they correspond to the cases actually occurring in the present work, and no attempt was made to find the most general conditions for the validity of the formulas used.

We define

$$G_n(R, \alpha) = \int_0^R \lambda^n e^{-\alpha\lambda} d\lambda, \quad (n \geq 0)$$

$$A_n(R, \alpha) = \int_R^\infty \lambda^n e^{-\alpha\lambda} d\lambda, \quad (\text{Either } n \text{ or } R, \text{ but not both, may be negative.})$$

$$B_n(R, \alpha) = \int_{-R}^{+R} \lambda^n e^{-\alpha\lambda} d\lambda, \quad (n \geq 0)$$

$$\begin{aligned} W_{nm}(R; \alpha, \beta) &= \int_0^R \lambda^n e^{-\alpha\lambda} G_m(\lambda, \beta) d\lambda, \quad (n \geq -1, m \geq 0, \alpha \text{ or } \beta \text{ may vanish.}) \\ &= \int_0^R \lambda^m e^{-\beta\lambda} [G_n(R, \alpha) - G_n(\lambda, \alpha)] d\lambda, \end{aligned}$$

$$U_{nm}(R; \alpha, \beta) = \int_0^R \lambda^n e^{-\alpha\lambda} A_m(\lambda, \beta) d\lambda = (m!/\beta^{m+1}) G_n(R, \alpha) - W_{nm}(R; \alpha, \beta),$$

$$\begin{aligned} V_{nm}(R; \alpha, \beta) &= \int_R^\infty \lambda^n e^{-\alpha\lambda} A_m(\lambda, \beta) d\lambda, \quad (-\infty < n < \infty, -\infty < m < \infty, R \text{ may} \\ &\hspace{15em} \text{vanish.}) \\ &= \int_R^\infty \lambda^m e^{-\beta\lambda} [A_n(R, \alpha) - A_n(\lambda, \alpha)] d\lambda \end{aligned}$$

$$T_{nm}(R; \alpha, \beta) = \int_R^\infty \lambda^n e^{-\alpha\lambda} G_m(\lambda, \beta) d\lambda = (m!/\beta^{m+1}) A_n(R, \alpha) - V_{nm}(R; \alpha, \beta).$$

The last four integrals represent $\iint x^n e^{-\alpha x} y^m e^{-\beta y} dx dy$ extended over various domains as indicated in Fig. 1.

⁷ W. H. Furry and J. H. Barlett, Jr., Phys. Rev. **38**, 210 (1932).

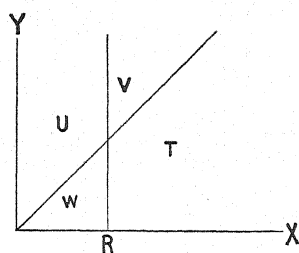


Fig. 1.

Recurrence relations are easily discovered by partial integration, and serve, with some special formulas, to calculate tables of the integrals.

$$G_n(R, \alpha) = \frac{1}{\alpha} [nG_{n-1}(R, \alpha) - R^n e^{-\alpha R}] \quad (n > 0) \quad (1)$$

$$= e^{-\alpha R} \sum_{\nu=0}^{\infty} \alpha^{\nu} R^{n+\nu+1} \sum_{\sigma=0}^{\nu} \frac{(-1)^{\sigma}}{(n+\sigma+1)\sigma!(\nu-\sigma)!}, \quad (1')$$

$$= [1/(n+1)] [\alpha G_{n+1}(R, \alpha) + R^{n+1} e^{-\alpha R}] \quad (1'')$$

$$G_0(R, \alpha) = \frac{1}{\alpha} [1 - e^{-\alpha R}] \quad (2)$$

$$A_n(R, \alpha) = \frac{1}{\alpha} [R^n e^{-\alpha R} + nA_{n-1}(R, \alpha)] \quad (3)$$

$$= \frac{1}{n+1} [\alpha A_{n+1}(R, \alpha) - R^{n+1} e^{-\alpha R}] \quad (3')$$

$$B_n(R, \alpha) = \frac{1}{\alpha} [R^n ((-1)^n e^{\alpha R} - e^{-\alpha R}) + nB_{n-1}(R, \alpha)] \quad (4)$$

$$W_{nm}(R; \alpha, \beta) = (1/\alpha) [G_{n+m}(R, \alpha + \beta) - R^n e^{-\alpha R} G_m(R, \beta) + nW_{n-1,m}(R; \alpha, \beta)] \quad (5)$$

$$= (1/\beta) [mW_{n,m-1}(R; \alpha, \beta) - G_{n+m}(R, \alpha + \beta)] \quad (m > 0) \quad (5')$$

$$W_{n0}(R; \alpha, \beta) = (1/\beta) [G_n(R, \alpha) - G_n(R, \alpha + \beta)] \quad (6)$$

$$W_{-1,0}(R; \alpha, \beta) = 1/\beta [\log(\alpha + \beta) - \log \alpha + E_i(-\alpha R) - E_i(-(\alpha + \beta)R)] \quad (7)$$

$$W_{nm}(R; 0, \beta) = [1/(n+1)] [R^{n+1} G_m(R, \beta) - G_{m+n+1}(R, \beta)] \quad (n \geq 0) \quad (8)$$

$$W_{-1,0}(R; 0, \beta) = (1/\beta) [\log R + \log \beta + C - E_i(-\beta R)] \quad (9)$$

$$V_{nm}(R; \alpha, \beta) = (1/\alpha) [R^n e^{-\alpha R} A_m(R, \beta) - A_{m+n}(R, \alpha + \beta) + nV_{n-1,m}(R; \alpha, \beta)] \quad (10)$$

$$= [1/(n+1)] [A_{m+n+1}(R, \alpha + \beta) - R^{n+1} e^{-\alpha R} A_m(R, \beta) + \alpha V_{n+1,m}(R; \alpha, \beta)] \quad (10')$$

$$= (1/\beta) [A_{n+m}(R, \alpha + \beta) + mV_{n,m-1}(R; \alpha, \beta)] \quad (10'')$$

$$= [-1/(m+1)] [A_{n+m+1}(R, \alpha + \beta) - \beta V_{n,m+1}(R; \alpha, \beta)]. \quad (10''')$$

To get (1'), we put $e^{-\alpha R} = e^{-\alpha R} \times e^{\alpha(R-\lambda)}$, and expand in powers of $R-\lambda$.

Formula (7) is obtained by writing

$$\begin{aligned}
 W_{-1,0}(R; \alpha, \beta) &= \lim (\sigma \rightarrow 0) \int_{\sigma}^R \lambda^{-1} e^{-\alpha \lambda} G_0(\lambda, \beta) d\lambda \\
 &= \lim (1/\beta) [E_i(-(\alpha+\beta)\sigma) - E_i(-\alpha\sigma) - E_i(-(\alpha+\beta)R) + E_i(-\alpha R)] \\
 E_i(-\alpha\sigma) &= C + \log |\alpha\sigma| - \alpha\sigma + \frac{1}{4}(\alpha\sigma)^2 - \dots \\
 C &= 0.57721.
 \end{aligned}$$

A similar reduction gives (9).

In calculating, we first prepared tables of G , taking the first values from (2) and applying (1) to advance n . Successive application of (1) leads at first to an increase in the number of significant figures in the result; but as n increases, the accuracy of the result degenerates, owing to increasing cancellation in the subtraction, and the higher values are unreliable. However, Eq. (1') converges rapidly for sufficiently large n , and when it has been used to calculate one value of G , (1'') can be used to compute successively lower values of n with increasing accuracy. From the G table, the W table can be readily prepared, noting the special formula (6) required when $m=0$.

The B table can be constructed directly from (4). For the A table, (3) works successfully for zero or positive n , and (3') for negative n when once the value for $n=-1$ is known. Now, $A_{-1}(R, \alpha) = -E_i(-\alpha R)$; but the series for the integral logarithm converges very slowly, the application of (3') for the first few negative values of n leads to serious degeneration of accuracy, and a sufficiently good value of $E_i(-\alpha R)$ is very laborious to compute. A more rapid and at the same time self-proving method is as follows: When the positive part of the table is computed and ratios of successive pairs of A 's compared, they are found to change slowly and regularly. It is therefore easy to make an extrapolation downwards and estimate the values of A for the first two or three negative n 's. From the estimates, (3') is used to continue down to the lowest n required, or to an n so low that the use of (3') for still lower n 's will not compromise the accuracy. When now the ratios are compared, it will generally be found that they no longer proceed regularly, but show fluctuations increasing in violence as the lowest n is approached. From the character of these fluctuations, it is simple to estimate the error in the lowest A , caused partly by the extrapolation and partly by the application of the recurrence relation. After a few trials, a value of the lowest A can be constructed such that when the table is built up from it by (3), (which gives increasing accuracy when used in this direction) the ratio differences are perfectly regular. These values may be confidently accepted, as the method is remarkably sensitive.

A similar method has been used in computing the V table. A value of V for the lowest required n and m was found by trial and error, aided by extrapolation, such that the rest of the table could be constructed by advancing n and m with the aid of (10) and (10''), with regularly increasing ratios in both cases. Evidently this provides a method of evaluating integrals of the form $\int \lambda^n E_i(-\alpha \lambda) e^{-\beta \lambda} d\lambda$ which are commonly found by graphical methods.

SURFACE HARMONICS

We need two systems of harmonics with their poles lying respectively in the directions of the two hydrogen atoms. We may define them in terms of the angles θ_x , ϕ_x , and θ_y , ϕ_y , associated with the two axes, θ as usual being the polar angle and ϕ the azimuth, its zero lying in the direction of the Z -axis in each case. Let

$$\begin{aligned} X_n^x &= P_n(\cos \theta_x), & Y_n^y &= P_n(\cos \theta_y), \\ X_n^y &= P_n^1(\cos \theta_x) \sin \phi_x, & Y_n^x &= -P_n^1(\cos \theta_y) \sin \phi_y, \\ X_n^z &= P_n^1(\cos \theta_x) \cos \phi_x, & Y_n^z &= P_n^1(\cos \theta_y) \cos \phi_y. \end{aligned}$$

We need to know the integral over all angles of certain products of two or three of these harmonics. With two harmonics the integral vanishes unless both are of the same order. In this case the only ones which do not vanish are

$$\int d\omega X_n^x X_n^x = \int d\omega Y_n^y Y_n^y = 4\pi/(2n+1) \quad (11)$$

$$\begin{aligned} \int d\omega X_n^y X_n^y &= \int d\omega X_n^z X_n^z = \int d\omega Y_n^x Y_n^x \\ &= \int d\omega Y_n^z Y_n^z = \frac{2n(n+1)\pi}{(2n+1)} \end{aligned} \quad (12)$$

$$\int d\omega X_n^x Y_n^y = [4\pi/(2n+1)]P_n(\alpha) \quad (13)$$

$$\int d\omega X_n^y Y_n^x = [4\pi/(2n+1)][(P_n''(\alpha) - \alpha(d/d\alpha)(\alpha P_n'(\alpha)))] \quad (14)$$

$$\int d\omega X_n^z Y_n^z = [4\pi/(2n+1)]P_n'(\alpha) \quad (15)$$

$$\int d\omega X_n^x Y_n^x = \int d\omega X_n^y Y_n^y = [4\pi/(2n+1)]P_n^1(\alpha). \quad (16)$$

Here α is the cosine of the molecular angle, γ . $P_n'(\alpha)$ and $P_n''(\alpha)$ are derivatives of $P_n(\alpha)$ with respect to α . These formulas may all be derived from the equation⁸

$$\bar{F} = (1/4\pi)\Sigma_m(2m+1) \int d\omega F P_m(\mu). \quad (17)$$

Here F is a function of position on the surface of unit sphere, μ is the cosine of polar angles with reference to an arbitrary pole, and \bar{F} is the average value of F taken around a small circle enclosing the pole, which will be equal to F at the pole if F is continuous there. If $F = S_n$, any surface har-

⁸ Jeans, *Electricity and Magnetism*, Ch. VIII Eq. (146).

monic of degree n , the summation reduces to the single term in n . Of the integral product formulas, (11) and (12) are well known, while (13) and (16) result directly from (17) on substituting Y_n^y or Y_n^z for F and taking the X -axis as pole. For (14) and (15), it is necessary to have an equation analogous to (17) involving the associated harmonics. This may be found by means of a partial integration thus:

$$\begin{aligned} \frac{2n+1}{4\pi} \int d\omega S_n P_n^1(\mu) \cos \phi &= \Sigma_m \frac{2m+1}{4\pi} \int d\omega S_n P_m^1(\mu) \cos \phi \\ &= \Sigma_m \frac{2m+1}{4\pi} \int d\omega S_n \cos \phi \sin \theta P_m'(\mu) \\ &= -\Sigma_m \frac{2m+1}{4\pi} \int d\omega \cos \phi P_m(\mu) \frac{\partial}{\partial \mu} (S_n \sin \theta) \\ &= -\overline{\cos \phi (\partial/\partial \mu) (S_n \sin \theta)} = \overline{\cos \phi (S_n/\theta + \partial S_n/\partial \theta)}, \end{aligned} \quad (18)$$

since in the neighborhood of the pole, $\cos \theta = 1$ and $\sin \theta = \theta$. We shall be able to express S_n near the pole in the form

$$S_n = A + B\theta \cos \phi. \quad (19)$$

Upon multiplication with $\cos \phi$ and averaging around a small circle, the constant term vanishes, and there remains

$$\overline{\cos \phi (S_n/\theta + \partial S_n/\partial \theta)} = B. \quad (20)$$

To derive (15), we take S_n equal to Y_n^z , select the X -axis as pole, and note that near the X -axis

$$Y_n^z = \cos \phi_x \sin \theta_x P_n'(\cos(\gamma - \theta_x \sin \phi_x)) = \cos \phi_x \theta_x P_n'(\alpha)$$

plus higher powers of θ_x . This in connection with (18) and (20) gives (15). To derive (14), we must replace $\cos \phi$ by $\sin \phi$ throughout (18), (19), and (20). It is convenient to take $S_n = Y_n^z = -\sin \phi_y \Sigma_m W_m \sin m\theta_y$. Near the X -axis this becomes equal to

$$\Sigma_m W_m \sin m(\gamma - \theta_x \sin \phi_x) = \Sigma_m W_m (\sin m\gamma - m\theta_x \sin \phi_x \cos m\gamma).$$

Application of (18) and (20) gives $[(2n+1)/4\pi] \int d\omega Y_n^z X_n^y = -\Sigma_m m W_m \cos m\gamma$. In order to show that this is identical with (14), it is only necessary to write $P_n'(\alpha) \equiv (1/\sin \gamma) \Sigma_m W_m \sin m\gamma$ and perform the indicated differentiations.

Where products of three harmonics must be integrated, two of the harmonics will necessarily have a common pole. The product of these two can always be expressed as a sum of single harmonics, and the preceding formulas then used to integrate the product of this sum with the third harmonic. Formulas for the products of two coaxial harmonics are given below. Their derivation is tedious but not difficult, and may be omitted.

$$P_1 P_n = [n/(2n+1)] P_{n-1} + [(n+1)/(2n+1)] P_{n+1}$$

$$P_2 P_n = \frac{3n(n-1)}{2(2n-1)(2n+1)} P_{n-2} + \frac{n(n+1)}{(2n-1)(2n+3)} P_n + \frac{3(n+1)(n+2)}{2(2n+1)(2n+3)} P_{n+2}$$

$$P_3 P_n = \frac{5(n-2)(n-1)n P_{n-3}}{2(2n-3)(2n-1)(2n+1)} + \frac{3(n-1)n(n+1) P_{n-1}}{2(2n-3)(2n+1)(2n+3)} \\ + \frac{3n(n+1)(n+2) P_{n+1}}{2(2n-1)(2n+1)(2n+5)} + \frac{5(n+1)(n+2)(n+3) P_{n+3}}{2(2n+1)(2n+3)(2n+5)}$$

$$P_4 P_n = \frac{35(n-3)(n-2)(n-1)n P_{n-4}}{8(2n-5)(2n-3)(2n-1)(2n+1)} + \frac{5(n-2)(n-1)n(n+1) P_{n-2}}{2(2n-5)(2n-1)(2n+1)(2n+3)} \\ + \frac{9(n-1)n(n+1)(n+2) P_n}{4(2n-3)(2n-1)(2n+3)(2n+5)} + \frac{5n(n+1)(n+2)(n+3) P_{n+2}}{2(2n-1)(2n+1)(2n+3)(2n+7)} \\ + \frac{35(n+1)(n+2)(n+3)(n+4) P_{n+4}}{8(2n+1)(2n+3)(2n+5)(2n+7)}$$

$$P_5 P_n = \frac{63(n-4)(n-3)(n-2)(n-1)n P_{n-5}}{8(2n-7)(2n-5)(2n-3)(2n-1)(2n+1)} \\ + \frac{35(n-3)(n-2)(n-1)n(n+1) P_{n-3}}{8(2n-7)(2n-3)(2n-1)(2n+1)(2n+3)} \\ + \frac{15(n-2)(n-1)n(n+1)(n+2) P_{n-1}}{4(2n-5)(2n-3)(2n+1)(2n+3)(2n+5)} \\ + \frac{15(n-1)n(n+1)(n+2)(n+3) P_{n+1}}{4(2n-3)(2n-1)(2n+1)(2n+5)(2n+7)} \\ + \frac{35n(n+1)(n+2)(n+3)(n+4) P_{n+3}}{8(2n-1)(2n+1)(2n+3)(2n+5)(2n+9)} \\ + \frac{63(n+1)(n+2)(n+3)(n+4)(n+5) P_{n+5}}{8(2n+1)(2n+3)(2n+5)(2n+7)(2n+9)}$$

$$P_1^1 P_n = P_{n+1}^1 / (2n+1) - P_{n-1}^1 / (2n+1)$$

$$P_2^1 P_n = \frac{3(n+1) P_{n+2}^1}{(2n+1)(2n+3)} + \frac{3 P_n^1}{(2n-1)(2n+3)} - \frac{3n P_{n-2}^1}{(2n-1)(2n+1)}$$

$$P_3^1 P_n = \frac{15(n+1)(n+2) P_{n+3}^1}{2(2n+1)(2n+3)(2n+5)} + \frac{3n(n+7) P_{n+1}^1}{2(2n-1)(2n+1)(2n+5)} \\ - \frac{3(n-6)(n+1) P_{n-1}^1}{2(2n-3)(2n+1)(2n+3)} - \frac{15(n-1)n P_{n-3}^1}{2(2n-3)(2n-1)(2n+1)}$$

$$P_4^1 P_n = \frac{35(n+1)(n+2)(n+3) P_{n+4}^1}{2(2n+1)(2n+3)(2n+5)(2n+7)} \\ + \frac{5n(n+1)(2n+13) P_{n+2}^1}{2(2n-1)(2n+1)(2n+3)(2n+7)}$$

$$\begin{aligned}
& + \frac{45(n-1)(n+2)P_n^1}{2(2n-3)(2n-1)(2n+3)(2n+5)} \\
& - \frac{5(2n-11)n(n+1)P_{n-2}^1}{2(2n-5)(2n-1)(2n+1)(2n+3)} \\
& - \frac{35(n-2)(n-1)nP_{n-4}^1}{2(2n-5)(2n-3)(2n-1)(2n+1)}.
\end{aligned}$$

Combinations of two coaxial associated harmonics are not needed.

Upon multiplying one of the preceding products by any other harmonic S_m , and integrating, the only term, if any, contributing to the result is that of order m . It will be seen that, in general, $\int d\omega S_n S_a S_b$ vanishes unless

$$|a - b| = n, n - 2, n - 4, \dots$$

HARMONIC EXPANSIONS OF HYDROGEN ORBITS

In working out the formulas for these expansions, a screening constant κ was introduced into the hydrogen wave function with the idea that it might later be wished to investigate the effects of varying this constant. In all the numerical work, κ was taken equal to unity.

We first seek a representation of $e^{-\kappa s}$ as a function of r and μ , where $\mu = \cos \theta_x = x/r$. Let

$$e^{-\kappa s} = \sum_n K_n(r) P_n(\mu).$$

Upon multiplying this equation by $[(2n+1)/2]P_n$ and integrating with respect to μ , we obtain

$$K_n(r) = [(2n+1)/2] \int_{-1}^{+1} e^{-\kappa s} P_n(\mu) d\mu.$$

Substitute $\kappa s = bv$, $b = \kappa(2Rr)^{1/2}$, $c = (R^2 + r^2)/2Rr$, $v = (c - \mu)^{1/2}$, $d\mu = -2vdv$. Further, let

$$T_\nu = \int_{(c-1)^{1/2}}^{(c+1)^{1/2}} v^\nu e^{-bv} dv = A_\nu((c-1)^{1/2}, b) - A_\nu((c+1)^{1/2}, b) \quad (\nu \text{ always odd}).$$

Then

$$\int_{-1}^{+1} \mu^n e^{-\kappa s} d\mu = 2[c^n T_1 - nc^{n-1} T_3 + [n(n-1)/2!] c^{n-2} T_5 - \dots].$$

Since the surface harmonics are power series in μ , we readily find

$$K_0 = T_1$$

$$K_1 = 3(cT_1 - T_3)$$

$$K_2 = (5/2)(3c^2T_1 - 6cT_3 + 3T_5 - T_1)$$

$$K_3 = (7/2)(5c^3T_1 - 15c^2T_3 + 15cT_5 - 5T_7 - 3cT_1 + 3T_3)$$

$$K_4 = (9/8)(35c^4T_1 - 140c^3T_3 + 210c^2T_5 - 140cT_7 + 35T_9 - 30c^2T_1 + 60cT_3 - 30T_5 + 3T_1)$$

$$K_5 = (11/8)(63c^5T_1 - 315c^4T_3 + 630c^3T_5 - 630c^2T_7 + 315cT_9 - 63T_{11} - 70c^3T_1 + 210c^2T_3 - 210cT_5 + 70T_7 + 15cT_1 - 15T_3).$$

When $r < R$ we find $b(c \pm 1)^{\frac{1}{2}} = \kappa(R \pm r)$,

$$T_\nu = \frac{e^{-\kappa R}}{(2\kappa^2 R r)^{(v+1)/2}} \sum_{\tau=0}^{\tau=v} R_{\tau\nu}(\kappa r)^\tau [(-1)^\tau e^{\kappa r} - e^{-\kappa r}]$$

with

$$R_{\tau\nu} = \sum_{\sigma=0}^{\nu-\tau} \frac{\nu!}{\tau! \sigma!} (\kappa R)^\sigma.$$

When these values are substituted we find expressions for $K_n(r)$, valid over the range $0 < r < R$, of the general form

$$K_n = (-1)^n e^{-\kappa R} \frac{2n+1}{(\kappa R)^{n+1}} [\Sigma(\nu \text{ even}) K_{\nu n} \sinh(\kappa r) (\kappa r)^{\nu-n-1} - \Sigma(\nu \text{ odd}) K_{\nu n} \cosh(\kappa r) (\kappa r)^{\nu-n-1}] \quad (21)$$

in which the $K_{\nu n}$ are constants, for which the general formulas were not developed. In the particular case that $R=2$, $\kappa=1$, their values were found by substituting the appropriate values for $R_{\tau\nu}$ to find T_ν numerically. The expressions proved awkward for computation, because they involve negative powers of r which become infinite at the origin, and while it can be shown that the differences always remain finite, the integrals required in the later stages of the calculation come out as small differences between huge numbers. It proved much more practicable to throw the K_n into the form of infinite series in positive powers of r , by expressing $\sinh r$ and $\cosh r$ in the ordinary power series, substituting in (21), and collecting the coefficients. All powers of r smaller than the n th were then found to cancel out, and also alternate powers above the n th, leaving

$$K_n(r) = (2n+1)e^{-R} \sum_{j=n}^{\infty} \kappa_j^n r^j, \quad (22)$$

where the κ_j^n exist only for even positive or zero values of $j-n$. As expressions of this type will repeatedly occur, it will be convenient to omit the expression of the limits of summation, and understand that it extends over all existing values of the coefficients. It should be noted that κ_j^n has no connection with the former screening constant κ , which has been dropped out, and that the superscript n is not the index of a power, but shows the order of the surface harmonic in whose coefficient it occurs. A table of the first few values found for κ_j^n will serve to show the rapidity of convergence:

j	$n=0$	$n=1$	$n=2$	$n=3$
0	1.000000			
1		0.333333		
2	0.000000		0.100000	
3		-0.016667		0.030952
4	-0.008333		-0.008333	
5		-0.002381		-0.003373
6	-0.000397		-0.000661	

For values of r greater than R , we must take $b(c \pm 1)^{\frac{1}{2}} = \kappa(r \pm R)$, giving

$$T_\nu = \frac{e^{-\kappa r}}{(2\kappa^2 R r)^{(\nu+1)/2}} \sum_{\tau=0}^{\nu} \rho_{\tau\nu} (\kappa r)^\tau$$

with

$$\rho_{\tau\nu} = \sum_{\sigma=0}^{\nu-\tau} \frac{\nu!}{\tau!(\nu-\tau-\sigma)!} (\kappa R)^{\nu-\tau-\sigma} [(-1)^{\nu-\tau-\sigma} e^{\kappa R} - e^{-\kappa R}].$$

Numerical values of $\rho_{\tau\nu}$ are readily found by observing that $\rho_{\tau\nu} = \binom{\nu}{\tau} (\kappa R)^{\nu-\tau+1} B_{\nu-\tau}(1, \kappa R)$, where $\binom{\nu}{\tau}$ represents a binomial coefficient. With the T_ν so evaluated, we obtain for $K_n(r)$ expressions, valid over the range $R < r < \infty$, of the form

$$K_n(r) = (2n+1)e^{-r} \sum k_j^n r^{-j} \quad (23)$$

where the coefficients k_j^n exist for all values of j between 0 and $n+1$. For $R=2$, $\kappa=1$, the following values were found:

j	$n=0$	$n=1$	$n=2$	$n=3$
0	1.81343	0.97438	0.35186	0.09474
1	-1.94876	-0.70371	0.16237	0.24371
2		-0.70371	-0.56845	0.04114
3			-0.56845	-0.60771
4				-0.60771

The factor $2n+1$ was left in explicitly, because it cancels out in most of the later integrations.

No special proof of the convergence of this representation of $e^{-\kappa s}$ as a series of harmonic terms was attempted. The electron reaction terms calculated by its use were compared, in certain two-nuclei cases, with the values obtained by ordinary methods, and found in complete agreement, which was regarded as sufficient proof of the validity of the method.

In addition to the fundamental expansion of $e^{-\kappa s}$, it was found useful to have similar expansions for $\cos \theta_x e^{-\kappa s}$ and $\sin \theta_x e^{-\kappa s}$. These were readily found as follows.

$$\text{Let} \quad \cos \theta_x e^{-\kappa s} = \sum_n L_n(r) P_n(\mu);$$

$$\text{then, as before,} \quad L_n = [(2n+1)/2] \int_{-1}^{+1} \mu e^{-\kappa s} P_n(\mu) d\mu;$$

now, $\mu P_n(\mu) = [1/(2n+1)](nP_{n-1}(\mu) + (n+1)P_{n+1}(\mu));$

hence, $L_n = [n/(2n-1)]K_{n-1} + [(n+1)/(2n+3)]K_{n+1}.$

By comparing coefficients of corresponding powers of r , we obtain

$$L_n(r) = (2n+1)e^{-R} \sum_j \lambda_j^n r^j \text{ for } 0 < r < R \text{ and}$$

$$L_n(r) = (2n+1)e^{-r} \sum_j l_j^n r^{-j} \text{ for } R < r < \infty, \text{ with}$$

$$(2n+1)\lambda_j^n = n\kappa_j^{n-1} + (n+1)\kappa_j^{n+1}; \quad (2n+1)l_j^n = nk_j^{n-1} + (n+1)k_j^{n+1}.$$

For $\sin \theta_x e^{-\kappa s}$ we get a simple expansion in terms of associated functions P_n^1 . Assume $\sin \theta_x e^{-\kappa s} = \sum_{n=1}^{\infty} M_n(r) P_n^1(\mu) d\mu$.

On multiplying by $P_n^1(\mu)$ and integrating, we find

$$M_n = [(2n+1)/2n(n+1)] \int_{-1}^{+1} (1-\mu^2)^{1/2} e^{-\kappa s} P_n^1(\mu) d\mu.$$

Substituting $(1-\mu)^{1/2} P_n^1(\mu) = (1-\mu^2)(d/d\mu)P_n(\mu) = n[P_{n-1}(\mu) - \mu P_n(\mu)]$, we obtain

$$M_n = \frac{1}{n+1} \left[\frac{2n+1}{2n-1} K_{n-1} - L_n \right] = \frac{1}{2n-1} K_{n-1} - \frac{1}{2n+3} K_{n+1}.$$

$$M_n(r) = (2n+1)e^{-R} \sum_j \mu_j^n r^j \text{ for } 0 < r < R \text{ and}$$

$$M_n(r) = (2n+1)e^{-r} \sum_j m_j^n r^{-j} \text{ for } R < r < \infty$$

$$(2n+1)\mu_j^n = \kappa_j^{n-1} - \kappa_j^{n+1}; \quad (2n+1)m_j^n = k_j^{n-1} - k_j^{n+1}.$$

The coefficients κ_j^n , k_j^n were computed for values of n up to 4, permitting the calculation of λ_j^n , l_j^n , and μ_j^n , m_j^n up to $n=3$.

I wish to express sincere thanks to Professors E. C. Kemble and J. C. Slater, under whose advice and encouragement this work was carried out, and to Mr. H. M. James for painstaking verification of formulas and computations.

On the Vibrations of Polyatomic Molecules

By N. ROSEN AND PHILIP M. MORSE
Massachusetts Institute of Technology

(Received August 17, 1932)

An exact solution of the wave equation is found for a form of one-dimensional potential energy which may be of use in discussing polyatomic molecular vibrational energies. An example of its use is given in an analysis of the vibration of the nitrogen in the ammonia molecule. The potential energy for this atom has two minima a distance $2x_m$ apart, separated by a "hill" of height H . The values of x_m and H are not known directly from band spectral data, and are needed for a full analysis of the spectrum. By joining two potential curves of the sort dealt with in the first part of this paper in a symmetric manner, a curve simulating that for the nitrogen atom in ammonia was formed. It was found that for certain values of the constants fixing this curve, the allowed vibrational energies were the same as the experimentally determined values for ammonia. The corresponding value of x_m was 0.38A, and that of H was $\frac{1}{4}$ electron-volt. These values are probably near the correct values of x_m and H for ammonia.

IN THE course of the study of polyatomic molecules one encounters potential functions of a form considerably different from those used in atomic or diatomic molecular problems. A perturbation method using any of the usual exact solutions of the Schrödinger equation would usually involve perturbation energies too large to give good results.

One method of obviating this difficulty is the use of the Wentzel-Kramers-Brillouin method. Another is to develop new exact solutions of the wave equation for potential fields more nearly like those usually encountered in polyatomic molecular problems.

One such exact solution, for a potential field with two minima,¹ has already been developed. Another solution, for a different form of potential field is described in this paper, and an example of its application to the vibrational states of NH_3 is given.

THE EXACT SOLUTION

The potential field² which is amenable of exact solution is

$$V(x) = B \tanh(x/d) - C \operatorname{sech}^2(x/d). \quad (1)$$

If $|B| < 2C$ this potential has a minimum value at $x_0 = -\tanh^{-1}(B/2C)$. The second derivative at this point is

$$(d^2V/dx^2)_{x=x_0} = (1/8d^2C^3)(4C^2 - B^2)^2 \quad (2)$$

and

$$V(x_0) = -(4C^2 + B^2)/4C.$$

¹ Morse and Stueckelberg, *Helv. Phys. Acta* **4**, 337 (1931).

² The continuous energy spectrum for a potential field somewhat like this has been discussed by Eckart, *Phys. Rev.* **35**, 1303 (1930).

The wave equation for such a potential is

$$d^2\psi/dz^2 + (-\epsilon - \beta \tanh z + \gamma \operatorname{sech}^2 z)\psi = 0 \quad (3)$$

where $z=x/d$, and $(\epsilon, \beta, \gamma) = (8\pi^2 M d^2/h^2)(-E, B, C)$. E is the allowed energy of the system. Now set $\psi = e^{az} \cdot \cosh^{-b} z \cdot F(z)$. The equation becomes

$$F'' + 2(a - b \tanh z)F' + [\gamma - b(b+1)] \operatorname{sech}^2 z \cdot F = 0$$

and ψ/F is finite in the range $-\infty \leq z \leq \infty$, if

$$a = -\frac{1}{2}[(\epsilon + \beta)^{1/2} - (\epsilon - \beta)^{1/2}] \text{ and } b = \frac{1}{2}[(\epsilon + \beta)^{1/2} + (\epsilon - \beta)^{1/2}] \quad (4)$$

where both square roots are taken as positive quantities.

Now let $u = \frac{1}{2}(1 + \tanh z)$. The equation for F in terms of u is

$$u(1-u)F'' + [a+b+1-2(b+1)u]F' + [\gamma - b(b+1)]F = 0. \quad (5)$$

The solution of this equation which remains finite at $u=0$ is the hypergeometric function

$$F = F\left([b + \frac{1}{2} - (\gamma + \frac{1}{4})^{1/2}, b + \frac{1}{2} + (\gamma + \frac{1}{4})^{1/2}; a + b + 1; u\right).$$

This series approaches infinity³ in the same manner as $\exp[2(b-a)z]$ as u approaches unity, unless $b + \frac{1}{2} - (\gamma + 1/4)^{1/2}$ is a negative integer. In this case the function is a Jacobi polynomial. Therefore ψ will not be finite everywhere unless

$$b = (\gamma + \frac{1}{4})^{1/2} - n - \frac{1}{2}. \quad (6a)$$

Referring to Eq. (4) we see that the other constant a becomes

$$a = -\beta/[(4\gamma + 1)^{1/2} - 2n - 1]. \quad (6b)$$

The allowed values of the energy E are

$$\begin{aligned} -E_n &= (h^2/8\pi^2 M d^2)(a^2 + b^2) \\ &= \frac{1}{4}[(4C + g^2)^{1/2} - g(2n+1)]^2 + B^2/[(4C + g^2)^{1/2} - g(2n+1)]^2. \end{aligned} \quad (6c)$$

The quantum number n can be zero or any positive integer less than or equal to $(\gamma + 1/4)^{1/2} - (\beta/2)^{1/2} - 1/2$. The constant $g^2 = h^2/8\pi^2 M d^2$.

Therefore the solution of the wave Eq. (2) is the wave function

$$\psi_n = N_n e^{ax/d} \cosh^{-b}(x/d) F\left(-n, (4\gamma + 1)^{1/2} - n; a + b + 1; \frac{1}{2}[1 + \tanh(x/d)]\right) \quad (7)$$

where the values of a and b are given in Eqs. (6a) and (6b). The normalizing factor is obtained from the following equation

$$N_n = 1/2^b [d \cdot G(a + b + 1, b - a - 1, 2(\gamma + \frac{1}{4})^{1/2}, a + b + 1; n)]^{1/2}$$

³ Whittaker and Watson, *Modern Analysis*, page 299.

where

$$\begin{aligned}
 G(k, \lambda, \mu, \nu; n) &= 2 \int_0^1 u^k (1-u)^\lambda [F(-n, \mu-n; \nu; u)]^2 du \\
 &= 2\Gamma(\lambda+1) \sum_{s=0}^{2n} (-1)^s [\Gamma(k+s+1)/\Gamma(k+\lambda+s+2)] \cdot \\
 &\quad \cdot \sum_t \frac{\Gamma(t+\mu-n)\Gamma(s-t+\mu-n)[\Gamma(\nu)n!]^2}{[\Gamma(\mu-n)]^2 \Gamma(t+\nu)\Gamma(s+\nu-t)(n-t)!(n+t-s)!t!(s-t)!}
 \end{aligned}$$

where the limits of the summation over t are fixed by the factorials.

The allowed energy levels for a typical form of Eq. (1) are given in Fig. 1.

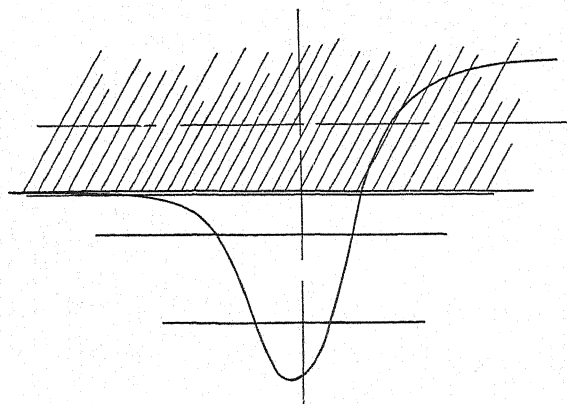


Fig. 1. Allowed energy levels for a potential function of form corresponding to Eq. (1).

When γ is much larger than unity then the allowed values of the energy become

$$E_n = V(x_m) + h\omega_0(n + \frac{1}{2}) - (h^2/8\pi^2 M d^2)(1 + 3B^2/8C^2)(n + \frac{1}{2})^2 + \dots \quad (8)$$

for small values of n . Here ω_0 is the classical frequency of oscillation about the minimum point, $x = x_m$.

$$\omega_0 = (4C^2 - B^2)/4\pi d(2MC^3)^{1/2}.$$

APPLICATION TO THE AMMONIA MOLECULE PROBLEM

An example of the use of these wave functions can be taken from the treatment of the vibrations of the ammonia molecule.

The equilibrium configuration of the ammonia molecule⁴ has a pyramidal structure with the three hydrogen atoms at the vertices of an equilateral triangle for the base, and the nitrogen atom along a perpendicular line through the center of the base. Due to the symmetry of the molecule there will be two equivalent positions of equilibrium for the nitrogen, at equal distances above and below the plane of the hydrogens. This equivalence of the

⁴ See the discussion and references given in the article of Dennison and Hardy, *Phys. Rev.* 39, 938 (1932).

two minima makes every vibrational level a doublet, a result which is found experimentally.

To analyze the vibrational behavior we first separate off the coordinates of the center of gravity of the molecule and the Eulerian angles fixing its orientation in space, and deal only with the coordinates fixing the relative positions of the atoms. One of these coordinates is x , the distance of the nitrogen atom from the plane of the hydrogens. The other five coordinates, z_1, z_2, z_3, z_4, z_5 , can be chosen that the positions of the two equilibrium configurations are at $z_1 = \dots = z_5 = 0, x = \pm x_m$. The potential function $V(x, z_1, z_2, z_3, z_4, z_5)$ therefore has its two minima at these two points.

Classically, the problem of small vibrations about either of these minima would be straightforward. The potential V near each minima has six mutually orthogonal principal axes, such that the kinetic energy becomes a sum of squares of velocities and the potential energy becomes a sum of squares of coordinates. These coordinates, which we can call y_0, \dots, y_5 , make up a so-called normal set of coordinates: by their means we can separate the problem and find the six fundamental modes of vibration. For ammonia, x almost coincides with one of the normal coordinate axes. Classically therefore x can be used as one of the normal coordinates with fair accuracy for small vibrations.

This analysis is valid for a classical consideration of small amplitude vibrations, but for large amplitudes the concept of normal coordinates is not valid; in general the energy equation cannot be separated. Quantum mechanically, the use of normal coordinates for the ammonia problem is never valid, for we can never have the equivalent of small vibrations (i.e., have the wave function all concentrated near one point) since there must be as much of the wave function about one minimum as about the other.

However, we can justify our use of x as a "normal" coordinate (i.e., our approximate splitting off from the general six-dimensional problem a one-dimensional problem in x alone) by the following method.

The general, vibrational equation, in six coordinates, will not be separable; but we can say a few things about the wave functions which satisfy it. From considerations of symmetry we know that all the wave functions will either be symmetric or antisymmetric about the nodal hypersurface $x = 0$. The function for the lowest state will be symmetric, having no nodes at all, and having two maxima near the two points $x = \pm x_m, z_1 = \dots = z_5 = 0$. The function for the next lowest state will be antisymmetric, its only nodal surface being the hypersurface $x = 0$. In fact all the wave functions can be separated into pairs, one function in each pair being similar to the other except for the addition of a nodal surface at $x = 0$.

The wave functions for the higher states will have other nodal surfaces as well. These surfaces will have quite complicated forms in general, and cannot be separated into clear-cut families of surfaces, as can be done in a separable problem. Nevertheless we will find that some of our wave functions will fall into an easily classified family. These functions will represent states where one type of oscillation is excited and the others are not; the nodal surfaces of

this family will be a one-parameter set of surfaces which will be orthogonal to the x axis. This family of wave functions is the set we wish to study. They will only be large near the x axis. Therefore, for these wave functions, we will not introduce much error if we consider their variation along the x axis to satisfy a one-dimensional wave equation, using for potential field $V(x, 0, 0, 0, 0, 0)$ (called hereafter $V(x)$ for short), and their corresponding energies to be given by the allowed energies of this one-dimensional problem.

Perhaps we could find other "normal coordinates" in a similar manner. In the other cases they might be curvilinear lines joining the two minimum points and they would each be tangent to one of the classical normal coordinates at these points. However, the reasoning is not as clear cut for these other cases, and since we do not need them for our problem, we will not digress further.

The problem of the vibrations along the x axis is clear cut and the behavior of the wave functions along the x axis and the corresponding energy values can be obtained by solving the wave equation

$$d^2\psi/dx^2 + (8\pi^2M/h^2)(W - V(x))\psi = 0. \quad (9)$$

From the discussion above we know that V must have two minima symmetrically placed at $x = \pm x_m$, separated by a potential "hill." As $|x|$ becomes large, V approaches some asymptotic value whose height above the minima gives the energy of dissociation of ammonia for this type of vibration.

In studying the behavior of ammonia it would be very useful to know the value of x_m , the height H of the hill between the minima and the general shape of the potential curve. The data for determining these quantities are obtained from the analysis of the molecule's infrared spectrum. Presumably by analyzing the rotational structure of the bands one could obtain values of the moments of inertia of the molecule about its major axes, and thence obtain the value of x_m . The moment of inertia about the x axis has been obtained⁴ in this manner, but this alone cannot give us any of the properties of $V(x)$. It seems that the best way to determine these properties is to assume a form of the potential field and then see whether the values of the vibrational energies computed for this field check with the experimentally determined levels. This method will not give us a unique answer, particularly since we know the values of only a few of the lowest vibrational energies. In general, a whole family of curves could be devised whose energy levels check with the observed levels. However, we are helped out of this difficulty by our knowledge of the general shape of V , and so we can rule out many potential forms as being unreasonable. From the results to appear later in this paper it seems probable that all those potential forms which appear reasonable and which check the data differ very little in their essential properties, and all give about the same value of x_m and H . If this is actually the case, then the values of x_m and H which are obtained in this paper are fairly close to the correct values.

A form of potential field which would satisfy our preconceptions of its form would be made by joining two potential fields $V(x)$ of the form given in Eq. (1) in a symmetric manner.

$$V(x) = \begin{cases} B \tanh(x/d - k) - C \operatorname{sech}^2(x/d - k), & x \geq 0 \\ -B \tanh(x/d + k) - C \operatorname{sech}^2(x/d + k), & x \leq 0. \end{cases} \quad (10)$$

This would make the half distance between minima, $x_m = kd - \tanh^{-1}(B/2C)$. The height of the intermediate hill, H , can also be found.

It can be shown¹ that as long as the energy level considered is below the top of the intermediate hill the difference between the level for the single minimum problem (such as for Eq. (1)), and that for the corresponding double minimum problem (such as for Eq. (10)), can be fairly accurately given by a perturbation calculation.

The wave functions for the double minimum problem become

$$\Psi_n^\pm(x) = K[\psi_n(x - dk) \pm \psi_n(-x - dk)] \quad (11a)$$

where the ψ 's are given in Eq. (7). The constant K is a normalization constant. The energies become

$$\begin{aligned} W_n^\pm = E_n + \int_0^\infty [\psi_n(x + dk)]^2 V(x) dx \\ \pm \int_0^\infty \psi_n(x - dk) V(x) \psi_n(-x - dk) dx. \end{aligned} \quad (11b)$$

This shows that for each level of the one minimum problem there is a pair of levels for the double minimum case.

The actual shift of the center of gravity of the levels, given by the first integral, is not particularly important, since its value is small compared to the distance between levels for different values of n . But the second integral is of importance since twice its value gives the separation between the levels in a pair. This separation is small compared to the energy difference between different pairs as long as the levels are below the top of the intermediate hill.

The integral

$$\Delta W_n = 2 \int \psi(x - dk) V(x) \psi(-x - dk) dx \quad (11c)$$

giving the inter-doublet separation can be computed since we know the functions ψ_n .

From Eq. (6c) the separation between the lower two pairs is

$$E_1 - E_0 = 2g(C + g^2/4)^{1/2} - 2g^2 - B^2/4 \frac{g(4C + g^2)^{1/2} - g^2}{C + g^2 - g(4C + g^2)^{1/2}}. \quad (12a)$$

The inter-pair separations turn out to be

$$\begin{aligned} \Delta W_0 &= \frac{4\Gamma(2b)e^{-2ak}}{\Gamma(b+a)\Gamma(b-a)(2\cosh k)^{2b}} \left[\frac{2C \tanh k}{b+1} - \frac{B}{b} \right] \\ \Delta W_1 &= \frac{2\Gamma(2b+2)}{\Gamma(b+a)\Gamma(b-a)(2\cosh k)^{2b}} \frac{e^{-2ak}}{[(2a^2+b)(b+1)^2 + a^2b(1+2b)]}. \end{aligned} \quad (12b)$$

$$\cdot \left\{ 2C \left[\left(\frac{a^2 - (b+1)^2}{b+1} + \frac{(b+1)^2}{b+2} \right) \tanh k + \frac{2a(b+1)}{b+2} \tanh^2 k \right. \right. \\ \left. \left. + \frac{(b+1)^2}{b+2} \tanh^3 k \right] \right. \\ \left. - B \left[\frac{a^2 - b - 1}{b} + 2a \tanh k + (b+1) \tanh^2 k \right] \right\} \quad (12c)$$

where from Eqs. (6a) and (6b) we have

$$b = (C/g^2 + \frac{1}{4})^{1/2} - n - \frac{1}{2}, \quad a = -B/2g^2b. \quad (12d)$$

The value of n for (12b) is zero and that for (12c) is unity.

The data by which we seek to obtain values for the constants in Eq. (10), representing a possible form for the potential field in ammonia are obtained from the paper by Dennison and Hardy.⁵ They are the separations between the two lowest pairs of levels, $E_1 - E_0 = 950 \text{ cm}^{-1}$ and the inter-pair separations $\Delta W_0 = 0.8 \text{ cm}^{-1}$, $\Delta W_1 = 33 \text{ cm}^{-1}$.

One difficulty is at once apparent, for there are four constants to determine in Eq. (10), B , C , d and k , and only three experimental values available

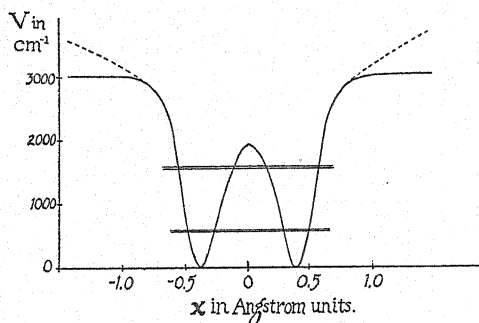


Fig. 2. Energy levels and potential function for the nitrogen atom in the ammonia molecule.

to make the fit. It would seem that even for this form of potential there would be a whole family of possible curves which would fit the data. This actually is true, a range of values of B , C , d and k was found which would fit. However this range of values is considerably curtailed if we require that V be reasonable in shape; that $|B|$ cannot be greater than $2C$, that the second level must be below the center hill, and that the hill should not be higher than the value of V at $x = \infty$.

These requirements limit the range of allowed values of C to between 2200 and 3000 cm^{-1} , that of B to between zero and 1000 cm^{-1} ; but that of d is between 0.16 and 0.185 Å and that of k is between 2.24 and 2.20. This means that the possible values of x_m lie between 0.365 and 0.390 Å, and those of H lie

⁵ Dennison and Uhlenbeck, Phys. Rev. 41, 313 (1932), obtain, by different methods, a result in exact agreement with this.

between 1950 and 2100 cm^{-1} . One of the potential curves for an intermediate set of values of the constants is shown in Fig. 2, with its corresponding energy levels.

The fact that all possible forms of potential of the form of Eq. (10) giving energy levels which fit the data give values of x_m and H which differ at most by eight percent, makes it seem probable that any form of V which would fit the data and have a reasonable form would give values of x_m near 0.38Å and of H near 2050 cm^{-1} (a quarter volt). This seems likely, for the value of $E_1 - E_0$ will more or less fix the curvature upward about the two minima, while the values of ΔW_0 and ΔW_1 will more or less fix the curvature downward about the central hill and the height of this hill, while the joining of the curves about the minima and the curve about the hill will more or less fix x_m .

The value of the dissociation energy $V(\infty) = V(x_m)$, however, is not closely fixed by our data, for it varies from 2200 to 4000 cm^{-1} . This is to be expected, since the energy levels we have used to fix our curves are very little effected by a change in the form of V for large values of x . In fact a potential curve of the form given by the dotted line in Fig. 2 would have very nearly the same values of allowed energies as the curve given by the solid line for Eq. (10). For this reason our analysis can tell us nothing about the value of the dissociation energy for this type of vibration (except that it cannot be less than 2200 cm^{-1} !).

However the value of x_m is the important value to be fixed, for a complete analysis of the ammonia spectrum requires a knowledge of its value. It seems likely that its value should be about 0.38Å, which makes the moment of inertia about the axis of symmetry $4.41 \cdot 10^{-40} \text{ gm-cm}^2$.⁵ The range of possible values of x_m introduces in this last result an uncertainty of only about 1 percent.

The Reflection of Atomic Beams from Sodium Chloride Crystals

By R. M. ZABEL

Physical Laboratory, State University of Iowa

(Received August 26, 1932)

The wave nature of helium, neon, and argon has been investigated by the reflection of beams of these gases from a freshly cleaved surface of sodium chloride. Evidence of diffraction was obtained in all cases, it being most pronounced in helium and least in argon. Both natural and laboratory grown crystals were used. The laboratory grown crystals were cleaved in moist air, dry air, and dry hydrogen. Laboratory grown crystals cleaved in dry air or dry hydrogen reflected a greater percentage of the incident molecules in the specular and diffracted beams than natural crystals or laboratory grown crystals exposed to moist air. The diffraction pattern obtained from crystals which had not been exposed to water vapor was produced by the spacing between rows of sodium and chlorine ions (1.99Å). Crystals which had been exposed to water vapor showed evidence of a spacing twice as long as those which had not been exposed.

INTRODUCTION

IT HAS been established for some time that quantum mechanics correctly describes the motion of free atoms and molecules. The recent experiments of Esterman and Stern^{1,2} with hydrogen molecules and helium atoms and of Johnson³ with hydrogen atoms have shown that both atoms and molecules exhibit properties of a wave motion of wave-length $\lambda = h/mv$ when reflected from the surface of a crystal.

The present investigation was undertaken first to study the effect of the treatment of the surface of the sodium chloride crystal upon the reflection obtained and second to study the reflection of neon and argon from sodium chloride.

APPARATUS

The beam system used in this experiment is similar to one previously described⁴ but it has been enlarged to permit greater pumping speed. Fig. 1 shows the arrangement of the crystal and detector in the beam system and the important dimensions. A special vertical slit 1×0.5 mm placed in the experimental chamber near the crystal greatly reduces the size of the penumbra of the beam.

The pressures in the various parts of the beam system are of the same order of magnitude as those previously described⁴ except that the pressure behind the first opening is necessarily somewhat higher because a channel is used where a hole in a thin wall had been used in the previous system. The pressure in this portion of the apparatus is normally about 6 mm of mercury for helium, 2.5 mm for argon and 1.5 mm for neon.

¹ Esterman and Stern, *Zeits. f. Physik* **61**, 95 (1930).

² Esterman, Frisch, and Stern, *Zeits. f. Physik* **73**, 348 (1931).

³ T. H. Johnson, *Phys. Rev.* **37**, 847 (1931).

⁴ A. Ellett and R. M. Zabel, *Phys. Rev.* **37**, 1112 (1931).

Fig. 2 shows two views of the apparatus which controls the position of the detector and crystal. The detector nozzle rotates about the crystal on a horizontal axis *A* perpendicular to the direction of the beam. Its position is indicated by the scale *B*. The crystal holder may be rotated about the beam as an axis. The method of producing this rotation is evident by a comparison of the two views since the one is taken with a considerably different setting than the other. Rotation of the crystal is also possible about the axis *CD* perpendicular to the beam so that the normal to the crystal may be pointed in any desired direction. The position of the crystal is indicated by the scales *E* and *F*. The combined motion of the crystal and gauge makes possible the complete study (except for the region between the incident beam and the

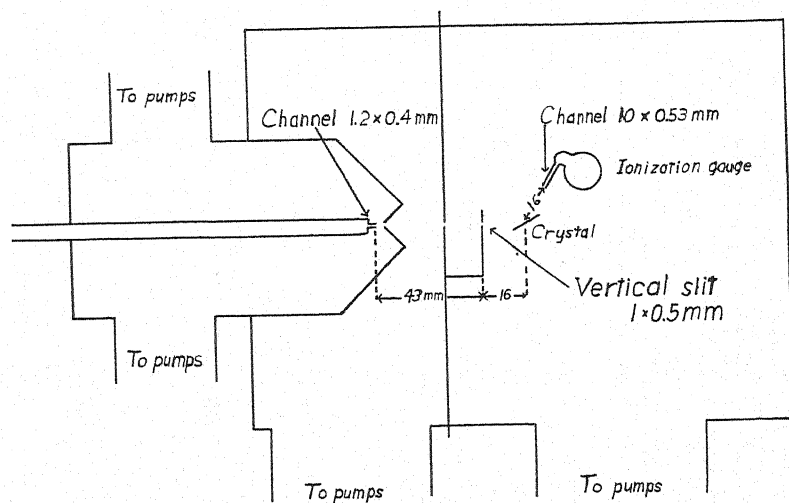


Fig. 1. The beam system.

crystal) of the reflection from a crystal with any desired angle of incidence. The crystal holder may also be lowered to permit measurement of the intensity of the incident beam. The four controls described above are operated magnetically by short bars on the end of four concentric tubes *G*.

An ionization gauge is used to detect the beam. A diagrammatic sketch of the gauge and its connections is shown in Fig. 3. In spite of the small size of the gauge, the plate is highly insulated by supporting it entirely from its tungsten lead. The Pyrex wall of the gauge is protected from evaporation of the filament by the plate itself. The grid is composed of the least number of turns which permit the gauge to be operated under normal conditions free from Barkhausen oscillations. The gauge is normally operated at 10 m.a. electron current as this value has been found experimentally to give the best balance between sensitivity and stability of the gauge. The sensitivity of the gauge is of the order of 5×10^{-10} mm of mercury per mm galvanometer deflection. The current due to the residual pressure in the experimental chamber is balanced out of the galvanometer by the simple circuit shown. The current under high-vacuum conditions is approximately 10^{-7} amperes

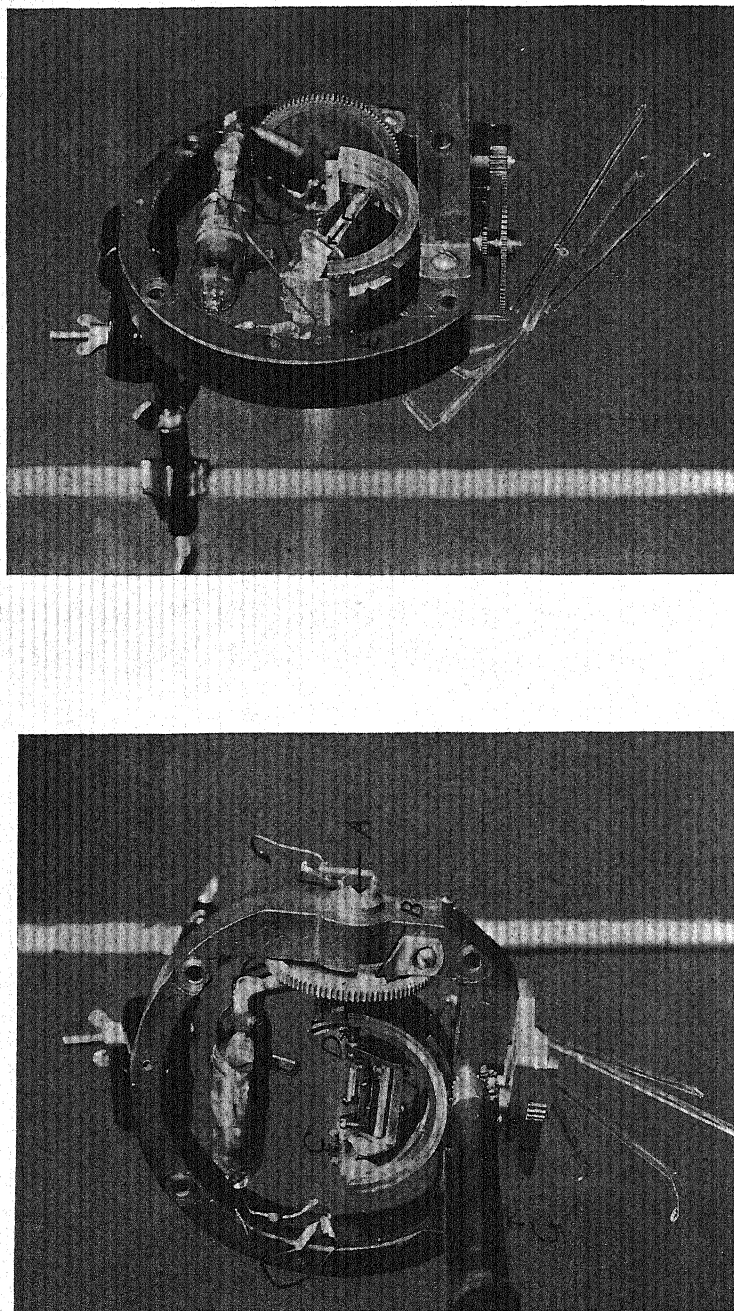


Fig. 2. Two views of detector and crystal rotating mechanism.

(corresponding to a pressure of the order of 10^{-6} mm of mercury) and is increased from 20 to 50 percent when the beam is in operation. The percentage increase in current due to the beam depends, of course, upon the kind of gas forming the beam and upon the beam intensity.

Since no attempt is made to compensate for general pressure changes in the experimental chamber one might expect considerable difficulty in maintaining a steady zero of the galvanometer. Such is not the case, however. The zero is checked before and after each reading and the two values normally agree within a few percent of the reading. The use of a compensating gauge might make the use of a more sensitive current measuring instrument feasible.

The gas used in forming the beam is exhausted by the various pumps operating directly on the beam system into a common chamber which is in turn pumped out by a set of special diffusion pumps capable of pumping

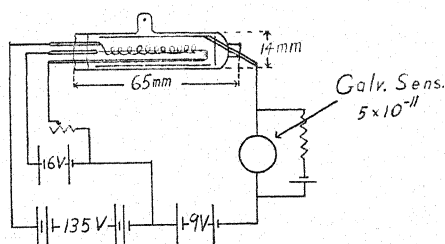


Fig. 3. The ionization gauge.

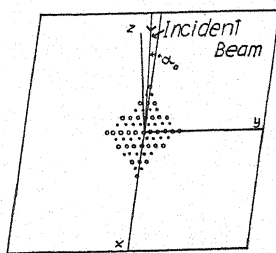


Fig. 4. Relative position of crystal and incident beam.

rapidly against high pressure. This set of pumps exhausts into another chamber which is connected to the first slit of the beam system so that the gas used in forming the beam may be continually circulated. The gas is purified as it circulates by passing it through a liquid air trap and a hot cathode misch metal arc. A hot cathode is used in the arc because the pressure is frequently too low for the satisfactory operation of an ordinary arc.

The crystals used in these reflection experiments were grown in this laboratory by Dr. R. Hancox and the author by the method recently developed by Strong.⁵

The treatment of the crystal surface after cleaving seems to have a very marked influence on the resulting reflection, hence it is discussed in some detail. The normal procedure in making a run is to evacuate the system for several days, fill it with dry hydrogen or dry air, cleave the crystal in an atmosphere of dry hydrogen, dry air, or moist air as desired and place it in the apparatus without exposure to any gas except that in which it was cleaved. When the crystal is cleaved in a dry atmosphere, the hydrogen or air used to fill the apparatus and the chamber in which the crystal is cleaved is passed through a long tube filled with P_2O_5 in order to dry it thoroughly. A continuous stream of this dry hydrogen or air flows through the cleaving chamber in order to carry away any moisture which might accumulate. The

⁵ John Strong, Phys. Rev. 36, 1663 (1930).

cleaving process is carried on in a large tin box with two holes in the sides to permit entrance of the hands and a third hole through which to place the crystal into the apparatus. These holes were made gas tight by the use of rubber sheeting. Perspiration from the operator's hands was avoided by covering them with rubber gloves during the cleaving process. After cleaving the crystal its thickness is measured, a metal sheet is chosen to place under the crystal to give the surface the proper height and the crystal and metal sheet are mounted on the crystal holder under molybdenum springs. The crystal holder is then placed in a beveled groove (see Fig. 2) in the apparatus through a ground joint by the aid of a long tweezer. The ground joint is sealed by glycolphthalic anhydride resin.⁶ An electric heater warms the joint so that it may be sealed merely by placing the parts together. Evacuation is started about thirty seconds after the crystal is cleaved and is complete in about fifteen minutes. The crystal is immediately heated to 350°C where it is maintained for several hours after which it is cooled to 100° or 150°C and is maintained at that temperature while readings are taken.

DIFFRACTION PATTERNS

Assuming that the ions in the surface layer of the crystal act as scattering points of a grating, the resulting diffraction pattern should be governed by the equations

$$\cos \alpha - \cos \alpha_0 = h_1 \lambda / d \quad (1)$$

$$\cos \beta - \cos \beta_0 = h_2 \lambda / d \quad (2)$$

where α and β are the angles measured from the principal axes (rows of like ions) in the crystal surface.

Fig. 4 shows the normal position of the crystal with respect to the beam, the plane of incidence being parallel and perpendicular to the principal axes of the crystal. Eq. (2) then reduces to

$$\cos \beta = h_2 \lambda / d. \quad (3)$$

The spectra investigated are given by (1) and (3) when $h_1 = \pm 1$ and $h_2 = 0$ and when $h_1 = 0$ and $h_2 = \pm 1$. The first type is found in the plane of incidence. The second is found by moving the detector along the intersection of the cone making a constant angle α_0 about the x axis (Fig. 4) and a cone making a variable angle β about the y axis or by moving the crystal and detector to obtain the same resultant motion.

In order to determine the position of the detector so that it will be on the diffraction cone and the relation between the angle β of Eq. (3) and the angle θ (taken from the apparatus) through which the crystal is rotated about the beam, consider Fig. 5. The axes x and y are parallel to the principal axes in the surface of the crystal and z is the crystal normal. The x' and x axes coincide, the y' axis coincides with the incident beam and the z' axis completes the primed system. With the crystal in this position the specular beam

⁶ Sager and Kennedy, *Physics* 1, 352 (1931).

($h_1 = h_2 = 0$) will be observed when the detector is raised $2\alpha_0$ above the negative y' axis. As the crystal is rotated through an angle θ about the incident beam (part I, Fig. 5) the x , y and z' axes take the positions denoted by x'' , y'' and z'' . The negative y'' axis will not be in the $y'z'$ plane defined by

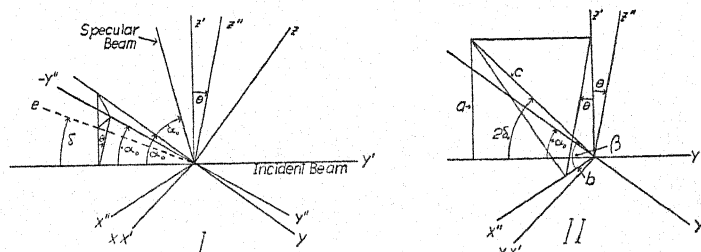


Fig. 5. Relations of angle taken from apparatus to β of Eq. (3).

the incident beam and the detector. Its projection in this plane is the line indicated as e . The angle which e makes with the negative y' axis is given by the equation

$$\delta = \tan^{-1} (\tan \alpha_0 \cos \theta). \quad (4)$$

Twice δ is then the angle, computed for any value of θ , above the negative y' axis at which the detector must be placed in order to be on the cone making an angle α_0 with the negative y'' axis. A relation between β and θ may be derived from part II of Fig. 5 as follows:

$$\cos \beta = b/c, \sin \theta = b/a, \sin 2\delta = a/c.$$

From the above equations $\cos \beta = \sin 2\delta \sin \theta$. For convenience the angle ϕ will be used hereafter where $\phi = 90 - \beta$. Hence

$$\phi = \sin^{-1} (\sin 2\delta \sin \theta). \quad (5)$$

DIFFRACTION IN HELIUM

Fig. 6 shows the results obtained in the reflection of helium from three distinct crystal surfaces. The curves have been plotted in terms of the angle ϕ where ϕ is determined from θ , the rotation of the crystal, by the aid of Eqs. (4) and (5). The crystals were cleaved in an atmosphere of dry hydrogen. There is an increase in the intensity of the specular and diffracted beam as well as a shift of the diffraction maxima to larger angles with each successive crystal. Crystal (1) was exposed to some water vapor as the operator's hands were not covered with rubber gloves during the cleaving of this crystal. Rubber gloves were used in cleaving crystal (2) but it had a poor surface which may account for its poor reflection. Crystal (3) was normal both in appearance and results.

The curves in Fig. 6 were taken with a wider set of slits than those specified in Fig. 1. All the following helium curves were, however, taken with the slits specified in Fig. 1, hence the following curves can not be compared with those in Fig. 6.

Fig. 7 shows the effect of water vapor on the surface of a crystal. Crystal (4) was cleaved in dry hydrogen and curve *a* was obtained. The crystal was then exposed to dry air at a pressure of 10 cm of mercury for several minutes after which curve *b* was obtained. There is no marked difference between the two curves. Crystal (5) was cleaved in dry air and its characteristics are as good as an ordinary crystal cleaved in dry hydrogen. Crystals (6) and (7) were cleaved in wet air (relative humidity 65 percent at 31°C) and both gave a very poor specular beam and diffraction pattern.

Crystal (8) of Fig. 7 was the most satisfactory surface which could be found in a large group of natural crystals as judged by the perfection of its

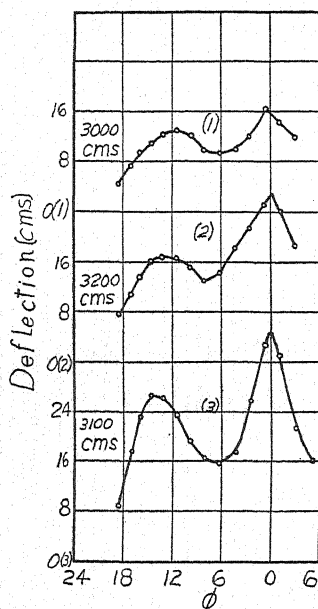


Fig. 6. Reflection of helium from sodium chloride crystals. Notations such as "3000 cm" etc., give the intensity of the incident beam. The numbers in parentheses identify individual crystals.

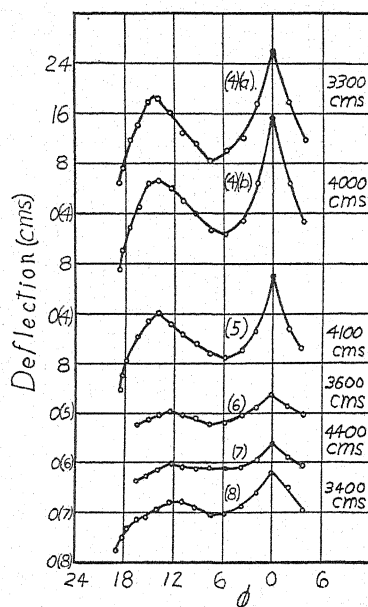


Fig. 7. Effect of water vapor on the "reflecting power" of a crystal surface.

optical reflection. Even this carefully selected crystal was, however, not as satisfactory as the laboratory grown crystals either in its reflection of light waves or particle waves.

The present status of the investigation indicates that there is a close correlation between the reflection of light waves and particle waves from the surface of a crystal. Crystals, either natural or laboratory grown, which give the most perfect optical reflection normally give the most intense specular beams and diffraction patterns.

With the slits specified in Fig. 1 the specular beam, if perfectly reflected, should reduce to zero at three degrees on either side of the peak. There is obviously some diffuseness in the reflection even in the most satisfactory crystals.

Fig. 8 shows the curve obtained by the same relative motion of gauge and crystal as previously described with the crystal turned 45° about its normal (Fig. 4) so that rows of like ions make an angle of 45° with the plane

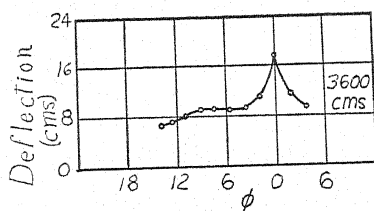


Fig. 8. Spectra from rows containing both sodium and chlorine ions.

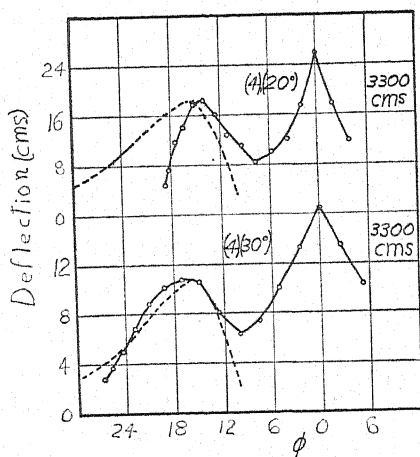


Fig. 9. Comparison of observed wave-length distribution with that calculated from Maxwell's distribution law for angles of incidence of 20 and 30 degrees.

of incidence. Any spectra found in this position would be due to rows which contain sodium and chlorine ions alternately. Obviously spectra do not arise from these rows.

WAVE-LENGTH DISTRIBUTION

The distribution in velocity of the molecules in the beam is given by Maxwell's law as

$$dI/dv = Ae^{-mv^2/2KT}v^3 \quad (6)$$

if the mean free path behind the first opening of the beam system is long compared to the diameter of the opening and if collisions along the path of the beam are negligible.

Assuming a wave-length $\lambda = h/mv$ associated with each particle of mass m and velocity v Eq. (6) may be written

$$dI/d\lambda = (A'e^{-\lambda_0^2/\lambda^2})/\lambda^5 \quad (7)$$

where

$$\lambda_0 = h/(2mKT)^{1/2}. \quad (8)$$

The diffraction curves are plotted in terms of ϕ where

$$\lambda = d \sin \phi. \quad (9)$$

Then

$$d\lambda/d\phi = d \cos \phi. \quad (10)$$

But

$$dI/d\phi = (dI/d\lambda)(d\lambda/d\phi). \quad (11)$$

Substituting from (7), (9) and (10) in (11) one obtains,

$$dI/d\phi = \frac{A'' \exp [-\lambda_0^2/d^2 \sin^2 \phi] \cos \phi}{\sin^5 \phi}. \quad (12)$$

Fig. 9 compares the intensity distribution obtained experimentally with that obtained from Eq. (12) for curves taken at angles of incidence of 20° and 30°. It will be noted that at 20° incidence the peak of the diffraction curve is at a smaller angle and the intensity of the diffracted beam falls off more rapidly with large values of ϕ than Eq. (12) predicts. This may be expected from geometrical consideration since the diffraction cones are nearing the angle (20°) where they will no longer intersect. In spite of this disadvantage 20° was used as the angle of incidence in almost all the curves because it gave a more intense specular beam and diffraction pattern than 30°.

The experimental and theoretical curves for 30° incidence are in satisfactory agreement in view of the fact that the first opening of the beam system was a channel and that the mean free path behind the channel was short compared to the diameter of the channel. Both the channel and the short mean free path might be expected to distort the wave-length distribution curve.

The grating spacing which produces the observed diffraction pattern may be determined by differentiating the right side of Eq. (12) setting the result equal to zero and solving for d which gives

$$d = \frac{2^{1/2}\lambda_0 \cos \phi_0}{\sin \phi_0} \frac{1}{(\sin^2 \phi_0 + 5 \cos^2 \phi_0)^{1/2}} \quad (13)$$

where ϕ_0 is the value of ϕ at the maximum of the diffraction curve and λ_0 is 0.888Å as determined from Eq. (8) when $T=300^\circ\text{K}$. Table I gives the spacings calculated from Eq. (13) for the various crystals used.

TABLE I. Spacings computed from the crystals investigated.

Crystal number	Note	Spacing in Å
1	Exposed to water vapor	2.80
2		2.54
3		2.28
4	Before exposure	2.22
4	After exposure	2.22
4	30° incidence	1.97
5	Cleaved in dry air	2.28
6	Cleaved in wet air	2.60
7	Cleaved in wet air	2.65
8	Natural crystal	2.80

The possible spacings are the distance between rows of like ions (3.98Å) or the distance between rows of unlike ions (1.99Å). It is evident from the

above table that the shorter spacing or second order spectra from the longer spacing is predominant in these crystals. The fact that the computed spacings at 20° incidence are longer than they should be has been explained in the previous discussion.

Table I shows that crystal surfaces which have been exposed to water vapor have a longer spacing than those which have not. Because of the width of the velocity distribution in the incident beam two peaks arising from spacings of 1.99Å and 3.98Å would not be resolved. Hence the change in spacing may be interpreted as being due to the fact that a portion of the crystal surface reflects with a spacing of 3.98Å after the crystal has been exposed to water vapor. This suggests that on the portion of the surface which acquires the new spacing one molecule of water may be collected by each sodium ion (union with sodium is assumed because of the affinity of sodium for water vapor) in such a way that the water molecules form a grating with a periodicity equal to the distance between rows of sodium ions. On the other hand, one may assume that heating the crystal removes the water vapor and that each molecule of water carries with it some of the ions in the crystal surface in a manner analogous to the removal of the surface when a salt crystal is dissolved in water. The gaps in the crystal surface caused by the removal of these ions would produce the observed increase in periodicity.

The latter hypothesis appears more reasonable than the first in view of the fact a crystal once exposed to water vapor can be heated to 700°C for some time without improving its "reflecting power." In either case the decreased intensity of the specular beam and diffraction pattern could be accounted for by the increased roughness of the surface.

The observed spacing of the natural crystal is also longer than the spacing of laboratory grown crystals. Since the best natural crystals which could be obtained still showed considerable evidence of strain it is possible that the strained condition causes the crystal to cleave imperfectly so that gaps are left in the surface. These gaps might give rise to a variety of spacings all longer than the fundamental spacing observed in the more perfect surfaces so that the tendency would be to shift the curve in the direction of longer spacings. This is in agreement with the results of experiment.

DIFFRACTION IN NEON AND ARGON

Fig. 10 shows the evidence of diffraction obtained in the case of neon and argon. It will be noted that the crystals used have been used previously with helium. The reflection is much more diffuse and the specular and diffracted beams much less pronounced than in the case of helium. The grating spacing corresponding to the maximum of the neon curve is 2.05Å and to the maximum of the argon curve 3Å. The diffraction peak of the argon curve has probably been moved toward smaller angles by the rapid decrease in intensity of the diffuse specular beam upon which the diffraction peak is superimposed.

As previously indicated the slits in the apparatus were changed between the study of crystal (3) and crystal (4) so that the argon and neon curves are

not comparable insofar as the relative intensity of the incident and specular beams is concerned.

SPECTRA IN THE PLANE OF INCIDENCE

Fig. 11 shows the reflection found in the plane of incidence. The angle (α of Eq. (1)) is measured from the plane of the crystal so that the specular beam should occur at 20° in each case. The maximum in the case of neon and argon is shifted by a considerable amount from the expected position of the specular beam. Conclusive evidence of diffraction appears only in the case of helium. There is probably, however, a very interesting relation between the fact that the diffraction peak in the helium curve appears only on

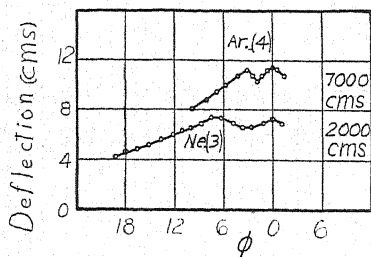


Fig. 10. Diffraction in neon and argon.

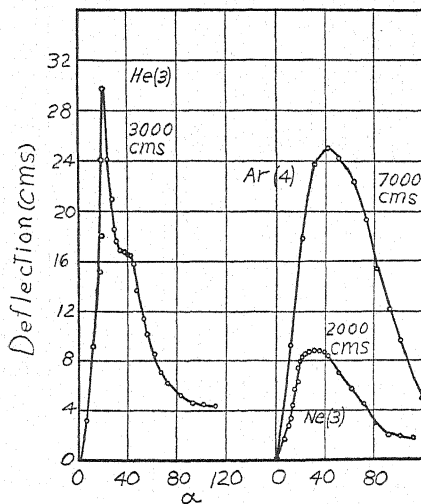


Fig. 11. Curves taken in the plane of incidence.

the large angle side of the specular beam and the fact that the argon and neon curves have a maximum at larger angles than the expected position of the specular beam.

Another point of interest in this connection is the similarity between the argon curve of Fig. 11 and curves obtained in the reflection of mercury from sodium chloride. Zahl and Ellett⁷ found in mercury a diffuse directed beam which for small angles of incidence has its maximum closer to the normal than the expected position of the specular beam. The similarity of the argon and mercury curves suggests that they have a common explanation.

In conclusion the writer wishes to express his appreciation to Professor A. Ellett for many helpful suggestions in connection with this investigation.

⁷ H. A. Zahl and A. Ellett, *Phys. Rev.* **38**, 977 (1931).

The Magnitudes of the L Absorption Discontinuities of Gold

By FRED M. UBER AND C. G. PATTEN
Department of Physics, University of California

(Received July 16, 1932)

Uniform evaporated films of gold have been used in obtaining values for the magnitudes of the L absorption discontinuities and the variations of the absorption coefficients with wave-length. The magnitudes of the discontinuities, where the scattering is considered as negligible, are $\delta_{L_I}=1.16$, $\delta_{L_{II}}=1.39$, $\delta_{L_{III}}=2.48$. These are in good agreement with the values obtained for mercury by one of the authors. Several comparisons are made with the data of other observers.

INTRODUCTION AND APPARATUS

THE results of recent measurements on the L absorption discontinuities of mercury by one of us¹ have suggested the advisability of carrying out similar measurements on gold. Improvements over the work of earlier investigators were sought in the uniformity of the absorbing screens and in the degree of homogeneity of the x-ray beam.

The absorbing screens were prepared by the evaporation of gold in the following manner. The gold was contained in a V-shaped trough of thin tungsten foil (0.005 cm thick) through which an electric current could be passed. Above this trough at a distance of 10 cm, and parallel with it, was a support which held several thin microscope cover glasses (22×22 mm). After the glasses were thoroughly cleaned, the whole ensemble was placed in a vessel to be evacuated. The vacuum was obtained with a diffusion pump and a liquid air trap. Gold films 0.001 mm thick could be made by this process in about two hours. They were free from imperfections and fogging. The glass was removed from the gold over an area of 4×15 mm by etching with hydrofluoric acid. The part of the gold film to be used as an absorbing screen, now without any glass backing, remained firmly supported and without wrinkles on its glass framework. Two such films were sufficient to absorb from one third to two thirds of the x-ray beam in the wave-length region investigated. The mechanical mounting was such as to allow the same part of the film to be reintroduced into the path of the beam as often as desired.

The slits (each 0.15×10 mm) defining the x-ray beam were placed at a separation of 35 cm, thus giving an angular width to the beam of 3' of arc. This corresponds to slightly more than 5 x.u. or to a wave-length spread of one half of one percent in the center of the group of wave-lengths measured. The position of the calcite crystal could be read to 10'' of arc. The ionization chamber, source of high potential, etc., are described in a previous paper.¹ The ionization currents were measured with a (FP 54 Pliotron) vacuum tube amplifier, using the rate of deflection method. As a source of radiation, a line-

¹ Fred M. Uber, *Phys. Rev.* **38**, 217 (1931).

focus metal x-ray tube with a tungsten target was employed. The operating voltages were below the excitation potentials of wave-lengths which would reflect in the second order. In making a few of the observations at long wave-lengths, tungsten L radiation was used.

METHOD AND RESULTS

Rates of deflection, alternately with and without the absorber, were measured several times for each position of the crystal. The averages of these gave values I_0 and I for each wave-length. The final values used for obtaining the points which are plotted in Fig. 1 are the averages for three different films.

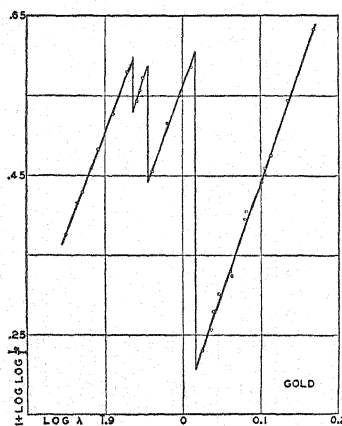


Fig. 1. The $\log \log I_0/I$, $\log \lambda$ curve for a given thickness of the absorber. From left to right the three discontinuities are L_I , L_{II} , and L_{III} .

The films were all made at the same time and no detectable difference in their thickness was found. A few of the points on the long wave-length side of the L_{III} discontinuity are for one film only.

From the two well-known equations for x-ray absorption, $\mu = A\lambda^c$ and $I = I_0 \exp(-\mu x)$, we obtain, where x is a constant, $\log \mu = \log (\log I_0/I) + \text{constant}$ and $\log \log I_0/I = \text{constant} + c \log \lambda$. Plotting $\log \log I_0/I$ against $\log \lambda$, we secure straight lines whose slopes give us the values for c . Following the customary nomenclature, we refer to that part of the curve which lies on the short wave-length side of the L_I discontinuity as the L_I branch. Similarly, the segment of the curve between the L_I and L_{II} discontinuities is designated as the L_{II} branch, the segment between the L_{II} and L_{III} discontinuities as the L_{III} branch, and the part of the curve on the long wave-length side of the L_{III} discontinuity as the M_I branch. The slopes of these branches are given in Table I along with some data of Backhurst² and Uber¹ for comparison. Due to the small wave-length separation between the L_I and L_{II} discontinuities, the slope of the L_{II} branch cannot be determined with the same precision as the others. We consider our value too high for this particular slope.

² Ivor Backhurst, Phil. Mag. (7) 7, 353 (1929).

TABLE I. Values of c for several elements.

Element	Branch of absorption curve				Observer
	L_I	L_{II}	L_{III}	M_I	
Platinum (78)	2.6	2.6	2.6	2.64	Backhurst ²
Gold (79)	2.91	2.91	2.64	2.61	"
	2.55	2.94	2.64	2.78	The authors
Mercury (80)	2.56	2.56	2.59	2.66	Uber ¹

The magnitude, δ , of an absorption discontinuity, where the scattered radiation is considered as negligible, is defined as the ratio of μ on the short and long wave-length sides of an absorption edge. Hence, since x is a constant, we have

$$\log \delta_L = \log (\log I_0/I)_{\lambda < \lambda_L} - \log (\log I_0/I)_{\lambda > \lambda_L}.$$

These values are readily taken from the figure by extrapolating the straight lines to the absorption edges. The wave-lengths for the L edges have been taken from Sandström.³ In this manner, we find

$$\begin{aligned} \log \delta_{L_I} &= 0.066 & \delta_{L_I} &= 1.164 \\ \log \delta_{L_{II}} &= 0.144 & \delta_{L_{II}} &= 1.393 \\ \log \delta_{L_{III}} &= 0.3945 & \delta_{L_{III}} &= 2.480 \\ \log \delta_L &= 0.6045 & \delta_L &= 4.02. \end{aligned}$$

In Table II, we compare these results with other published data. Our value of δ_{L_I} is definitely lower than that of Backhurst. The magnitudes accredited to Küstner have been interpolated from his graph, since no numerical data have been published as yet. His values for δ_{L_I} for a number of elements are practically the same.

TABLE II. Magnitudes of the L absorption discontinuities for several elements.

Element	δ_{L_I}	$\delta_{L_{II}}$	$\delta_{L_{III}}$	δ_L	Observer
Platinum	1.25	1.37	2.47	4.26	Backhurst ²
Gold	1.26	1.36	2.53	4.25	"
	1.24	1.39	2.48	4.20	Dauvillier ⁴
	1.16	1.39	2.48	4.02	The authors
	(1.15)	(1.35)	(2.45)	(3.85)	Küstner ⁵
Mercury	1.18	1.39	2.45	4.02	Uber ¹

Calculating the thickness of our absorption screen from the absorption coefficients of Backhurst² for gold, we found it to be 0.00024 cm. Proceeding with this value of x , we figured the increases in the mass absorption coefficient, μ/ρ , in crossing the absorption edges. They are compared with other data in Table III.

From our data, the absorption per L_I electron is seen to be slightly more than one half the absorption per L_{II} electron. This is in better agreement with

³ Arne Sandström, Zeits. f. Physik 65, 632 (1930).

TABLE III. *Increases in μ/ρ at each of the L absorption edges.*

Element	L_I	L_{II}	L_{III}	Observer
Platinum (78)	41.0	50.0	115.0	Backhurst ²
Gold (79)	41.6	48.2	118.7	"
	27.5	53.9	118.9	The authors
Mercury (80)	27.5	47.4	105.5	Uber ¹

the recent theoretical treatment of Stobbe,⁶ who finds the ratio of the true absorption coefficient of the L_I electrons to the sum of the true absorption coefficients of the L_{II} and L_{III} electrons to be 2/11 in the vicinity of the L absorption edges.

⁴ A. Dauvillier, C. R. 178, 476 (1924).

⁵ H. Küstner, Phys. Zeits. 33, 46 (1932).

⁶ M. Stobbe, Ann. d. Physik (5) 7, 661 (1930).

The First Spark Spectrum of Antimony

By R. J. LANG AND E. H. VESTINE
University of Alberta, Edmonton, Canada

(Received August 30, 1932)

The first spark spectrum of antimony has been analyzed by using the radiation from three sources, the hollow cathode in He and in Ne, and the vacuum spark. The spectrum extends from the infrared to the extreme ultraviolet with strong lines scattered throughout most of the entire range. Many important lines lie in the visible and near ultraviolet and the spectrum is weakest in the 2000Å region where the strong lines of the arc spectrum fall. The multiplets arising from the combination of the deepest terms (s^2p^3) $^3P'D'S$ with the next most important configuration (s^2ps) $^3P'P$ occur between $\lambda 1300$ and $\lambda 2000$. Two members of the singlet series ' $P-D$ ' and two members of the singlet series ' $P-S$ ' of the above configurations give an approximate value for the deepest term of $150,000\text{ cm}^{-1}$ and an ionization potential of about 18 volts. Some 50 energy levels are located based upon the classification of nearly 200 lines. Tables of term values and wave-lengths are given.

THE spectrum of antimony excited in various ways has been photographed and carefully measured from about 7000Å to about 600Å. The chief methods of excitation used were, the hollow cathode in an atmosphere of helium and sometimes of neon, the spark in hydrogen and the vacuum spark. In the case of the hollow cathode a cylinder of carbon was used to hold the metal in a thin layer around the inside wall of the tube. A current of from three to five milliamperes was used at a pressure of 800 or 1600 volts. In the use of neon as an atmosphere a stable condition was reached at a somewhat less current density but the metal lines were excited with much greater intensity than in the presence of helium. The tube containing the hollow cathode was made of fused quartz and was watercooled. For the investigation of the extreme ultraviolet the tube was connected directly to the vacuum spectrograph by means of a ground joint so that only the very narrow slit separated the hollow cathode tube from the main body of the spectrograph. In a few cases a fluorite window was placed over the slit. These photographs taken through fluorite served the very useful purpose of eliminating any second order lines from the list of wave-lengths. Two vacuum spectrographs were employed, one having a speculum grating of one meter radius and 15,000 lines per inch and the other two meters and 30,000 lines ruled on glass.

For the photography of the regions of longer wave-length several instruments have been employed. Much of the work was done on a concave grating of 1.5 meters radius having 15,000 lines per inch. Another grating which has the same type of ruling but a radius of 2 meters was used and some photographs which had been taken on prism spectrographs by Mr. Badami were very kindly loaned to one of us. Some very good photographs were also loaned to us by Mr. Smith of this laboratory.

Considerable time was spent in an effort to get a consistent set of meas-

urements of wave-length throughout the entire spectrum based upon the international standards of neon, helium and iron. The second order of the 1.5 meter grating at the Physikalisches-Technische Reichsanstalt at Berlin was employed for this purpose down as far as 2200Å, and below this we used the second order of the two-meter vacuum spectrograph at Edmonton employing a glass grating of 30,000 lines per inch at nearly normal incidence. Both of these gratings give very fine spectra; the latter especially gives very sharp lines and seems to be entirely free from ghosts.

The lines of neon and helium which occurred on the plates taken by using the hollow cathode were employed as standards to reduce the plates, using as far as possible the international values of these lines and supplementing these by the measurements of neon given by Paschen.¹ However, between $\lambda 2200$ and $\lambda 4000$ it was found that these standards were not nearly numerous enough for the purpose and it became necessary to supplement these plates with some taken of the spark in nitrogen or hydrogen on the two-meter grating in Edmonton, using one electrode of iron and one of antimony. In some cases the antimony lines came out diffuse and unsuitable for accurate measurement but enough standards were thus obtained to get fairly accurate measurements of the plates. In the region between $\lambda 2300$ and $\lambda 3000$ the interferometer measurements of iron made by Jackson² were employed in some cases.

The once-ionized antimony atom contains 50 electrons of which all but four are in completed groups and do not enter into the production of the spectrum discussed here. These four electrons give the configuration $(5s^2p^2)$ resulting in the set of deepest terms $^3P^1D^1S$. The next most important configuration is $(s^2p \cdot s)^3P^1P$ and these terms being odd will combine with the deepest (even) terms above. The resulting lines have been located extending from $\lambda 1300$ to about $\lambda 2000$. They are given in the upper right-hand section of Table I. Of the fourteen lines expected, thirteen have been found, and the missing intercombination line $^3P_2 - ^1P_1$ is much weaker than expected in Sn I³ and in As II⁴. The intensities of the lines given are taken from plates of the hollow cathode in helium. There seems little doubt but that these combinations are correctly assigned. The corresponding ones in Te III have also been found and an analysis of this spectrum now in progress will be reported upon separately.

The second members of the deepest terms together with the $^3D^3S^1P$ terms no longer excluded by the Pauli principle should combine with the $(s^2ps)^3P^1P$ terms giving lines in the visible region. It seems likely that we have discovered most of these combinations but it does not seem possible to identify the individual levels with the theoretical terms expected except in a tentative way. In the lower part of Table I on the right are shown the combinations between the $(s^2ps)^3P^1P$ terms and what appear to be the *S* and *D* terms

¹ Paschen, Ann. d. Physik 60, 405 (1919).

² Jackson, Proc. Roy. Soc. A130, 395 (1931).

³ Green and Loring, Phys. Rev. 30, 574 (1927).

⁴ A. S. Rao, Proc. Phy. Soc. London 243, 343 (1932).

of the $(s^2p \cdot p)$ configuration, while in the upper left the combinations of these latter terms with the $(sp^3)^3D$ terms are given. The assignment of the 3S and 3D terms were suggested to one of us by Mr. J. S. Badami on the basis of some fine structure measurements and the two terms 11 and 36 were discovered by him. Dr. J. B. Green also kindly sent us some preliminary results of the Zeeman effect for some of these lines. The correspondence between the assignment of terms as given in Table I and these measurements of fine structure and Zeeman effect is quite good. Some ten lines in the table were included in the Zeeman measurements and all of these except $\lambda 4140$ may be considered as supporting the scheme. The Zeeman effect for the above line suggests rather the combination $^3D_2 - ^3D_2'$. The nature of term number 40 could not be decided for certain. No Zeeman effect for $\lambda 6005$ was obtained but that for $\lambda 4344$ gives $\Delta j = 0$ which means that term 40 ought to have $j = 1$. The fine structure results give about the same result. The fact that $\lambda 6005$ is the strongest line in the spectrum surely fixes term 40 as a singlet. The only other singlet expected from the configuration (s^2pp) is a P term but there should be present, in that case, several more intercombination lines. It may be possible that the term is not real since it gives very few combinations; certainly far too few for a singlet P term.

It is possible to calculate approximate term values for term 48 is the second member of 8 and $48a$ is the second member of 10. The nature of term 8 (singlet D) is confirmed by the fine structure measurements so we may use the two lines whose wave numbers are 63,106.6 and 17,954.4 to calculate the value of the term $(s^2ps)^1P_1$. The approximate value obtained is $^1P_1 = 74,500$ giving for the deepest term $(s^2p^2)^3P_0$ a value of about 150,000. The ionization potential is therefore in the neighborhood of 18 volts. Since this term value rests upon but two members of a series it will be only very approximate and we have followed the usual custom of giving the deepest term zero value. We do not believe that this is the best method of fixing term values for even an approximate value enables anyone to estimate quickly the neighborhood in the spectrum in which higher members of any series will occur without having first to turn about all the term values. Giving the deepest term zero value casts undue weight upon a term value which after all may not be a real term at all. Its reality will often not be decided absolutely until series members *are* discovered in the spectrum.

We were not able to identify second members of the (s^2ps) configuration. In the spectrum of Sn I we find the perturbations of these terms upon each other are already pronounced as indicated by the inversion of both P and D terms. So that in Sb II, where the intermingling is still greater, due to wider separations, any assignment that might be made would probably not have much meaning. We may remark, however, that the P_1P_2 separation, which has the value 5738.5 in the first member should approach the doublet separation in Sb III, namely 6575. Terms 51 and 69 have a separation of 6439 and their combinations are fairly satisfactory so that they may represent P_1 and P_2 , respectively.

The intensity rules seem to be fairly well obeyed in the $^3P^3P$ and the $^3P^3D$

TABLE I. Multiplets in the spectrum of Sb II.

(s^2p^2)		3D_1 (9)	3D_2 (11)	3D_3 (13)	$(s^2p_3)^3P_0$ (17)	3P_1 (19)	3P_2 (31)	1P_1 (33)
0	2	66291	66501	67887	69134	69534	75273	75896
3055	3P_0	(66291)				1438.151(8) 69533.7 34		1317.56(6) 75897.8 96
	3P_1	1581.363(10) 63236.59 36	1576.114(10) 63447.2 46		1513.271(3) 66082.0 79	1504.230(7) 66479.2 79	1384.700(10) 72217.8 18	1372.843(2) 72841.5 41
5659	3P_2	1649.32(5) 60631.0 32	1643.57(5) 60843.1 42	1606.980(12) 62228.5 28		1565.554(10) 63875.2 75	1436.488(8) 69614.2 14	(70237)
	1D_2	1861.13(10) 53500 00	1861.81 53711.2 10			1762.312(6) 56743.6 43	1600.460(7) 62482.0 82	1584.622(10) 63106.6 05
23906	1S_0					2190.92(0) 45628.6 28		1923.388(5) 51991.6 90

TABLE I. (Continued).

(s^2p^3)		$^3D_1(9)$	$^3D_2(11)$	$^3D_3(13)$	$(s^2ps)^3P_0(17)$	$^3P_1(19)$	$^3P_2(31)$	$^1P_1(33)$
(s^2p^3)								
90353	26	66291	66501	67887	69134	69534	75273	75896
90645	30	4104.68(8) 24355.9 54	4140.54(15) 24144.65 44		4711.26(40) 21219.8 19	4802.01(20) 20818.9 19	6629.48(1) 15080.0 80	6915.58(4) 14456.1 57
91581	36		3985.98(8) 25080.86 80	4219.07(20) 23695.25 94	4647.32(30) 21511.79 11	4735.44(12) 21111.5 11	6503.26(6) 15372.6 72	6778.75(2) 14749.5 49
91716	38	3931.79(5) 25426.5 25	3964.75(10) 25215.2 15	4195.17(15) 23830.24 29	4427.25(3) 22581.1 82	4506.92(12) 22181.9 82	6079.80(30) 16443.4 43	6319.76(5) 15819.0 20
92543	40					4344.83(12) 23009.4 09		6005.21(100) 16647.6 47
92999	44		3772.78(4) 26498.15 98			4260.55(8) 23464.5 65	5639.75(30) 17726.4 26	5845.65(6) 17102.0 03
93851	48	3627.40(3) 27560.1 60	3655.26(2) 27350.07 50	3850.22(20) 25965.20 64		4111.24(4) 24316.7 17	5381.20(10) 18578.1 78	5568.13(15) 17954.4 55
95209	48a					3893.75(8) 25674.94 75		5176.55(15) 19312.52 13

multiplets shown in Table I. The intensity of the line $\lambda 3964$ in the 3DD multiplet may be misleading as it occurred always as a blend with a line of helium even when taken in neon since there was always a trace of helium in the neon. The presence of the antimony line was confirmed by the vacuum spark plates. The absence of the combination ${}^3P_0-{}^3D_1$ is not explained. It was thought that the term marked zero on this account could not be the deepest term (3P_0) and a determined effort was made to find another term but without success.

TABLE II. Term values in Sb II.

Even terms	Number	j value	Number of combinations	Odd terms	Number	j value	Number of combinations
0	2	0	7	58633	7	3	4
3055	4	1	17	66291	9	1	5
5659	6	2	15	66501	11	2	10
12791	8	2	14	67887	13	3	7
23906	10	0	7	68409	15	3	7
82221	12	1 or 2	5	69134	17	0	7
84814	14	1	4	69534	19	1	16
87830	16	1	4	70158	23	1 or 2	3
89560	20	2	8	72384	25	2	7
89626	22	2	7	73141	29	2	4
90353	26	1	4	75273	31	2	10
90607	28	1	5	75896	33	1	12
90645	30	1	16	76690	35	2	7
90893	32	1 or 2	4	77138	37	1	7
91581	36	3	7	78390	39	2	4
91716	38	2	19	90321	43	1	4
92543	40	0 or 1	4	91359	45	1	3
92935	42	1	2	97637	47	1	4
92999	44	1	14	104725	49	2	3
93851	48	2	12	105916	51	2 or 3	6
95209	48a	0	7	107463	53	1	6
95462	50	1	9	107829	55	2	3
105266	52	2 or 1	8	110852	59	1 or 2	4
				111578	61	1 or 2	5
				111624	63	1 or 2	6
				111668	65	1 or 2	5
				112355	69	2	9
				112402	71	1	7
				112730	73	2	5
				113201	75	1	7
				114048	77	0 or 1	4
				128514	79	1	6

In Table II the energy levels are given together with the numbers assigned and the j values of each, so far as these could be determined. The even terms have been assigned even numbers and the odd terms odd numbers. The fourth column gives the number of combinations on which each term value rests. It seems certain that while over fifty levels have been found these

do not represent a complete analysis of this spectrum because there are more terms for which $j=0$ and $j=3$ expected than have been found and because many more lines which appear to belong to Sb II remain unclassified. However, we are gratified that we were able to include so many of the very intense lines which occur in the visible and near ultraviolet in the scheme.

In Table III we give a list of the lines which are thought to belong to Sb II. In the columns headed a and b we give the intensities of the lines as measured in the hollow cathode in neon and helium, respectively. No measurements were made in helium beyond the fluorite limit. The results of the measurements made in the vacuum spark, while very useful in the analysis of the spectrum, are not included, following a suggestion of the editors. In the last column headed c we give the last two digits of the wave number calculated from the term values in Table II for comparison with the actual wave numbers of the lines. In very few cases above $\lambda 2000$ does the discrepancy exceed one unit and these have been indicated by an interrogation mark. Below $\lambda 2000$ somewhat greater tolerance is allowed but in nearly all cases the agreement is very good. There may be some arc lines still present in the table but we have omitted, we think, most of those which are known to belong to the arc spectrum.

TABLE III. Hollow cathode of antimony.

a	b	Wave-length (vac.)	Wave number	Classifica- tion	c	a	b	Wave-length (vac.)	Wave number	Classifica- tion	c
0		691.20	144676			8		1274.98	78432.6		
0		764.43	130816			0	3	1289.82	77530.2	8 ₂ -43 ₁	30
0		814.85	122722			3	6	1296.41	77136.1	2 ₀ -35 ₁	38
0		849.39	117731			0	6	1317.56	75897.9	2 ₀ -33 ₁	96
2		855.08	116948			8	10	1327.401	75335.2	4 ₁ -39 ₂	35
0		861.62	116060			1		1336.72	74809.9		
4		876.84	114045.8	2 ₀ -77 ₁	48	2	6	1349.834	74083.2	4 ₁ -37 ₁	83
0		888.44	112556.8			1		1356.289	73730.5	10 ₀ -47 ₁	31
1		896.75	111513.8			6	8	1358.039	73635.6	4 ₁ -35 ₁	35
1		907.36	110209.8			2	2	1372.843	72841.5	4 ₁ -33 ₁	41
2		914.91	109300.4	4 ₁ -69 ₂ (?)	04	2	5	1374.938	72730.5	6 ₂ -39 ₂	31
4		921.07	108569.3	4 ₁ -63 ₂	69	8	10	1384.700	72217.8	4 ₁ -31 ₁	18
0		922.60	108389.3	6 ₂ -77 ₁	89	2	2	1404.095	71220.2		
1		930.55	107463.3	2 ₀ -53 ₁	63	6	10	1407.827	71031.5	6 ₂ -35 ₁	31
3		932.32	107259.5			8	8	1436.488	69614.2	6 ₂ -31 ₂	14
2		937.17	106704.3	6 ₂ -69 ₂	06	4	8	1438.151	69533.7	2 ₀ -19 ₁	34
3		943.74	105961.4	6 ₂ -63 ₂ (?)	65	2	2	1467.75	68131.5		
2		950.91	105162.4			1		1482.539	67451.8	10 ₀ -45 ₁	53
2		957.78	104408.1	4 ₁ -53 ₁	08	2	7	1504.230	66479.2	4 ₁ -19 ₁	79
4		972.22	102857.4	4 ₁ -51 ₁ H?	60	1	5	1505.667	66415.7	10 ₀ -43 ₁	15
5		978.76	102170.1	6 ₂ -55 ₂	70	3	3	1513.271	66082.0	4 ₁ -17 ₀ (?)	79
6		983.57	101670.4	4 ₁ -49 ₂	70	2	7	1524.380	65600.4	8 ₂ -39 ₂	99
2		984.85	101538.3			1	6	1532.88	65236.7		
4		997.42	100258.6	6 ₂ -51 ₁	57	0	3	1543.87	64772.3		
6		1001.13	99887.1			3	8	1554.029	64348.9	8 ₂ -37 ₁	47
6		1009.43	99065.8	6 ₂ -49 ₂	66	6	10	1565.512	63876.8	6 ₂ -19 ₁	75
1		1015.38	98485.3			8	10	1576.114	63447.2	4 ₁ -11 ₂	46
4		1024.19	97638.1	2 ₀ -47 ₁	37	7	9	1581.363	63236.8	4 ₁ -9	36
4		1043.05	95872.7			4	10	1584.620	63106.6	8 ₂ -33 ₁	05
6		1052.21	95037.2	8 ₂ -55 ₂	38	2	7	1600.460	62482.0	8 ₂ -31 ₂	82
8		1056.27	94672.8	8 ₂ -53 ₁	72	10	12	1606.980	62228.5	6 ₂ -13 ₂	28
8		1057.32	94578.7	4 ₁ -47 ₁ (?)	82	5	5	1643.57	60843.1	6 ₂ -11 ₂	42
6		1073.81	93126.3	8 ₂ -51 ₁	25	5	5	1649.32	60631.1	6 ₂ -9 ₁	31
1		1076.85	92863.4			2	4	1655.54	60403.2		
5		1087.22	91977.7	6 ₂ -47 ₁ (?)	82	20	8	1657.036	60348.7	8 ₂ -29 ₁ (?)	50
3		1089.67	91770.9			5	4	1702.40	58740.6		
3		1094.63	91355.1			2	3	1725.298	57961.0		
1		1132.45	88304.1	4 ₁ -45 ₁	04	8	7	1736.43	57589.4		
0		1145.92	87266.1	4 ₁ -43 ₁	66	1	6	1762.312	56743.6	8 ₂ -19 ₁	43
1		1175.19	85092.6	2 ₀ -39 ₂ (?)	93	3	8	1788.46	55914.0		
1		1181.14	84663.9	6 ₂ -43 ₁	62	4	8	1810.60	55230.2	8 ₂ -13 ₂	96
0		1196.74	83560.3	10 ₀ -53 ₁ (?)	57	5	12	1814.971	55097.3		
1		1200.35	83308.9			1	3	1832.23	54578.3		
1		1218.96	82037.1			0	1	1836.48	54452.0		
6		1230.30	81280.9			2	4	1839.23	54370.6	8 ₂ -11 ₂	10
0	1	1272.75	78570.0	8 ₂ -45 ₁	68	3	10	1861.81	53711.2		

TABLE III (Continued)

a	b	Wave-length (vac.)	Wave number	Classifica- tion	c	a	b	Wave-length (vac.)	Wave number	Classifica- tion	c
5	10	1869.131	53500.8	8 ₁ -9 ₁	00	20	20	3850.22	25965.2	13 ₁ -48 ₂	64
2	2	1874.82	53338.4			8	8	3893.75	25674.94	19-48a	75
2	5	1878.538	53232.9	10 ₀ -37 ₁	32	5	2	3907.736	25583.0		
3	5	1891.27	52874.5	6 ₁ -7	74	4	8	3929.23	25443.1	15 ₁ -48 ₂	42
1	1	1923.388	51991.6	10 ₀ -33 ₁ (?)	90	5	8	3931.79	25426.5	9 ₁ -38 ₂	25
6	6	1956.47	51112.5			10	12	3960.53	25242.0	12 ₁ -53 ₁	42
		1990.60	50236.1			10	?	3964.75	25215.1	11 ₁ -38 ₂	15
		Wave-length (in air)				2	2	3980.98	25112.3	13 ₁ -44 ₁	12
3	2	2014.75	49617.8			8	9	3985.98	25080.9	11 ₁ -36 ₂	80
3	4	2024.06	49389.6			20	15	4033.56	24785.0		
5	2	2036.21	49095.0			2	12	4040.54	24742.2	15 ₁ -44 ₂	90
3	8	2063.34	48449.5			6	6	4065.32	24591.4	9 ₁ -30 ₁	54
3	3	2073.39	48214.7			8	10	4104.68	24355.9	19 ₁ -48 ₂	16
1	1	2117.35	47213.8			4	6	4111.24	24316.7		
10	15	2141.80	46674.9			20	15	4133.63	24185.0		
2	2	2159.09	46301.2			15	12	4140.54	24144.6	11 ₁ -30 ₁	44
6	12	2179.25	45872.9	10 ₀ -19 ₁	28	15	15	4195.17	23830.2	13 ₁ -38 ₂	29
	0	2190.92	45628.6			10	6	4200.49	23800.1	17 ₀ -42	01
5	7	2201.36	45412.2			20	5	4209.67	23748.2	6 ₁ -16 ₁	48
6	10	2208.50	45265.4			8	15	4219.07	23695.2	13 ₁ -36 ₂	94
6	7	2225.15	44926.8			10	6	4260.55	23464.6	19 ₁ -44 ₂	65
5	4	2288.97	43674.3			3	2	4271.54	23404.2	30 ₁ -77 ₁	03
0	1	2295.80	43544.4			6	6	4283.88	23336.8	9-22 ₁	35
1	1	2315.83	43167.8			6	5	4289.30	23307.3	15 ₁ -38 ₂	07
1	1	2360.98	42343.3			20	20	4304.12	23227.0		
0	4	2422.91	41260.2			3	0	4314.32	23172.1	15 ₁ -36 ₂	72
8	2	2480.46	40302.9			3	0	4332.64	23074.2	25 ₁ -50 ₁	74
15	15	2528.535	39536.7	16 ₁ -79 ₁	37	2	0	4335.34	23059.8	11 ₁ -20 ₂	59
10	8	2567.754	38932.8			12	12	4344.83	23009.4	19 ₁ -40	09
2	2	2578.91	38764.5	11 ₁ -52	65	12	3	4376.85	22841.1	20 ₂ -71 ₁	42
1	1	2619.681	38161.2	26 ₁ -79 ₁	61	12	10	4411.42	22662.1		
12	3	2656.55	37631.6			3	5	4427.25	22581.1	17 ₀ -38 ₂ (?)	82
4	7	2674.48	37379.4	13 ₁ -52 ₁	78	12	5	4431.87	22557.5	30 ₁ -75 ₁	56
2	1	2716.72	36798.2	38 ₂ -79 ₁	98	12	20	4446.48	22483.4	15 ₁ -32	84
8	5	2741.00	36472.3			15	9	4514.50	22181.9	19 ₁ -38 ₂	82
10	8	2764.62	36159.7			8	8	4526.04	22144.7		
7	7	2788.87	35846.3			8	8	4577.95	22088.2	32-73 ₂	37
10	8	2797.70	35786.6	85-36 ₂	86	8	8	4586.84	21837.7	28 ₁ -71 ₁	95
4	4	2818.98	35463.4	19 ₁ -52 ₂	34	4	4	4594.21	21795.4	17 ₀ -32	59
12	12	2847.13	35112.8			6	2	4594.93	21760.4	30 ₁ -71 ₁	57
8	4	2851.09	35064.0			30	20	4596.90	21757.0	28 ₁ -69 ₂	48
8	4	2858.03	34978.8			20	20	4599.09	21747.7	13 ₁ -22 ₂ (?)	39
10	10	2884.07	34663.3	48 ₂ -79 ₁	63	15	4	4604.77	21737.4	30 ₁ -69 ₂	10
5	3	2911.86	34577.4			10	3	4612.92	21710.5	13 ₁ -20 ₂	73
12	15	2966.10	34332.3			5	5	4617.92	21672.2	23-38 ₂	58
15	12	2980.962	34336.5			30	10	4647.316	21558.2	17 ₀ -30 ₁	11
8	8	3001.70	33304.8	48a-79 ₁	05	8	8	4647.919	21511.79	32-71 ₁	09
8	12	3021.89	33082.3	7-38 ₂	83	2	5	4653.32	21506.3	40-77 ₁	05
12	6	3034.01	32950.1	7-36 ₂ (?)	88	10	10	4656.35	21484.1	38 ₂ -75 ₁	85
12	20	3040.669	32877.96	25 ₂ -52 ₂	78	20	4	4657.95	21470.6	17 ₀ -28 ₁ (?)	73
6	12	3168.417	31552.40	12-77 ₁	27	3	3	4675.745	21462.7	25 ₂ -48 ₂	63
3	3	3171.45	31522.5			40	20	4694.95	21381.0		
8	3	3196.96	31270.7			12	12	4711.26	21293.5	20 ₂ -59	92
3	10	3210.113	31142.59			20	20	4735.44	21219.8	17 ₀ -26	19
15	15	3232.537	30926.56	7-20 ₂	27	12	12	4757.81	21111.5	19 ₁ -30 ₁	11
20	15	3241.280	30843.14			20	10	4757.81	21012.2	38 ₂ -73 ₂ (?)	14
3	6	3287.15	30412.9			20	10	4765.36	20978.9	30 ₁ -63	79
10	10	3303.90	30258.6			12	2	4766.91	20971.1	28 ₁ -61	71
8	8	3317.52	30134.3	12-69 ₂	34	30	15	4784.03	20897.2		
8	5	3333.20	29992.6	31 ₂ -52 ₂	93	20	10	4821.29	20818.9	19 ₁ -26 ₁	19
8	5	3336.88	29950.5			1	1	4832.82	20735.5	23-32	35
12	12	3366.84	29692.9			20	12	4838.27	20686.1	38-71 ₁	86
3	3	3383.09	29550.3			10	4	4843.74	20662.8	15 ₁ -20 ₂	63
3	12	3399.92	29404.0	12 ₁ -63 ₂	03	20	15	4850.50	20639.5	38 ₂ -69 ₂	39
2	2	3403.80	29370.5	33 ₁ -52 ₂	70	15	12	4877.24	20610.7	25 ₂ -44 ₂	11
4	8	3425.47	29184.7	12 ₁ -61	57	20	1	4880.01	20497.9	26 ₁ -59(?)	99
7	7	3459.26	28899.7			15	12	4947.40	20486.1	23-30 ₁	87
9	12	3473.50	28781.2			3	12	4948.52	20207.0	30 ₁ -59	07
15	15	3498.46	28575.9	35 ₁ -52 ₂	76	5	5	4975.71	20202.5	44 ₂ -75 ₁	02
12	5	3520.474	28397.2			1	10	4988.41	20092.1	19 ₁ -22 ₁	92
6	4	3559.24	28386.9	14 ₁ -75 ₁	87	5	5	4991.66	20040.9	65-36 ₁ (?)	43
10	20	3596.96	27793.3			10	7	5010.42	20027.8	19 ₁ -20 ₂	26
8	12	3629.92	27560.1	9 ₁ -48 ₂	60	4	4	5021.68	19952.8	38 ₁ -65	52
25	15	3637.80	27481.3	14 ₁ -69 ₂	41	6	7	5033.03	19908.1	38 ₂ -63	08
2	5	3655.26	27350.1	11 ₁ -48 ₂	50	15	10	5044.56	19863.2	38 ₂ -61	62
8	8	3683.27	27142.1			2	2	5066.99	19817.7		
8	8	3719.63	26876.8	39 ₂ -52 ₂	76	2	5	5109.71	19730.1	44 ₁ -73 ₂	31
20	8	3722.78	26854.0	14 ₁ -65	54	5	5	5132.30	19565.2	33 ₁ -50 ₁	66
4	2	3772.78	26498.1	11 ₁ -44 ₂	98	6	5	5164.72	19403.4	44 ₂ -71 ₁	03
4	2	3797.02	26328.9	15 ₂ -50 ₁ (?)	28	12	12	5166.32	19356.8	44 ₂ -69 ₂	56
						2	6	5172.46	19327.8	48 ₂ -75 ₁	50
						15	15	5176.55	19312.52	25 ₂ -38 ₁	28
						5	1	5208.80	19192.9	33-48a ₀	13
						20	8	5238.94	19082.5	40-63	81
						20	7	5354.24	18671.6	44 ₂ -65(?)	69

TABLE III. (Continued).

a	b	Wave-length (vac.)	Wave number	Classifica- tion	c	a	b	Wave-length (vac.)	Wave number	Classifica- tion	c
10	12	5381.20	18578.1	31-48 ₂	78	20	7	6154.945	16242.61		
15	15	5464.08	18296.3	19 ₁ -16 ₁	96	3		6186.00	16161.1	50 ₁ -63	62
	6	5471.95	18269.9	20 ₂ -55 ₂	69		12	6203.20	16116.2	50 ₁ -61	16
2	5	5475.77	18257.2	25 ₁ -30 ₁	57		2	6284.44	15908.0		
	1	5531.73	18072.5	37 ₁ -48a ₀	71	12	12	6302.764	15861.68	37 ₁ -44 ₂	61
1	1	5555.993	17993.6	48a ₀ -75 ₁	92	5	7	6319.76	15819.0	33 ₁ -38 ₂	20
15	20	5568.13	17954.4	33 ₁ -48 ₂	55	3	1	6376.11	15679.2	17 ₁ -14 ₁	80
				(Sb III?)		3		6396.21	15629.9		
3	1	5599.73	17853.1	44 ₂ -59	53	3		6406.08	15605.9		
10	2	5631.89	17751.1	29 ₂ -32	52	5		6474.43	15441.1	25 ₂ -16 ₁	42
10		5635.18	17740.7	50 ₁ -75 ₁	39	6	7	6503.26	15372.7	31 ₂ -30 ₁	72
30	15	5639.75	17726.4	31 ₂ -44 ₂	26	5	5	6511.13	15354.1		
4	3	5660.46	17661.5	31 ₂ -42	62	2	8	6529.88	15309.9	28 ₁ -51 ₂	09
	8	5705.50	17522.1	48a ₀ -73 ₂	21	1	3	6546.86	15270.3	30 ₁ -51 ₂	70
1	10	5789.52	17267.9	50 ₁ -73 ₂ (?)	68	2		6621.28	15098.6	22 ₂ -49 ₂	99
5	3	5825.50	17161.2	35-48 ₂	61		1	6629.48	15080.0	31 ₂ -26 ₁	80
6	8	5845.65	17102.0	33 ₁ -44 ₂	03	30		6647.44	15039.2		
15	?	5895.09	16958.6			15	3	6688.01	14948.0		
2		5901.20	16941.0	50 ₁ -71 ₁	40	3	4	6713.60	14891.0	35 ₂ -36 ₂	91
3		5917.77	16893.6	50 ₁ -69 ₂	93	2	6	6778.75	14749.5	33 ₁ -30 ₁	49
	8	5981.42	16713.8	37 ₁ -48 ₂	13	6	4	6806.67	14687.5	29 ₂ -16 ₁ (?)	89
100	100	6005.210	16647.60	33 ₁ -40	47	4	1	6812.98	14609.5		
	10	6006.105	16645.13			4		6815.58	14456.1	33 ₁ -26 ₁	57
20	20	6053.411	16515.05			4		6951.26	14178.0		
	1	6064.13	16485.9	29 ₂ -22 ₂	85	2		7075.11	14130.3		
	4	6073.932	16459.2	48a ₀ -65	59	2		7145.48	13990.3		
30	30	6079.797	16443.38	31 ₂ -38 ₂	43	2		7163.50	13955.8	35 ₂ -30 ₁	55
50	80	6130.043	16308.59	31 ₂ -36 ₂	08			7279.6	13731.	33 ₁ -22 ₂	30
	1	6137.30	16289.3	22 ₂ -51 ₂	90			7343.4	13613.	48 ₂ -53 ₁	12

(a), Intensity in hollow cathode in neon; (b), Intensity in hollow cathode in helium; (c), Wave numbers calculated from terms in Table II.

NOTE ON Sb III

While the work on Sb II was in progress occasion was taken to reinvestigate briefly the spectrum of Sb III using the more accurate wave-lengths in the vacuum spark now available. We find that the following terms which were previously given by one of us⁵ are real and satisfactorily identified: $(5p)^2P$, $(6p)^2P$, $(6s)^2S$, $(7s)^2S$, $(5d)^2D$, $(6d)^2D$, $(5f)^2F$, $(5g)^2G$, $(5p^2)^2D$, but that the terms called $(4f)^2F$, $(p^3)^4S$, $(p^2)^2P^4P$, and $(6g)^2G$ are not correct and should be discarded. It would appear that the states represented by quartet terms are not excited in the sources employed. There are several pairs of lines having exactly the separation of the deepest $5P$ terms throughout the extreme ultraviolet and doubtless some of them represent the so called PP combination. An attempt is now in progress to excite some more of these higher states in the arc spectrum of indium so that a consistent set of terms may be found in this isoelectronic sequence.

In conclusion we desire to state that a considerable part of the experimental work was done by one of us (R. J. L.) at the Physikalisch-Technische Reichsanstalt in Berlin and his appreciation and thanks are hereby tendered to Dr. Paschen for his kindly interest in the work and for the use of the facilities of his laboratory, and also to the members of his staff for their patient cooperation and courtesy. He wishes also to thank Dr. K. R. Rao and Mr. J. S. Badami for helpful discussions on this and allied spectra and especially the latter for the loan of very useful photographs of the spectrum of antimony. We wish also to thank Dr. Green for sending us the results of the Zeeman analysis prior to publication and Mr. Smith of this laboratory for the loan of some good plates of the vacuum spark spectrum. Finally we acknowledge a grant from the National Research Council of Canada which has enabled us to carry on this work.

⁵ R. J. Lang, Phys. Rev. 35, 445 (1930).

The Spectrum of Potassium Hydride

By G. M. ALMY AND C. D. HAUSE

University of Illinois

(Received August 17, 1932)

The $^1\Sigma \rightarrow ^1\Sigma$ molecular spectrum extending from 4100Å to 6600Å has been photographed with prism spectrographs with a d.c. potassium arc in hydrogen as source. In absorption spectrographs, also attempted, the bands were masked by alkali bands except in a short region, 4600Å to 4800Å. The spectrum is of the many-lined type. Analysis disclosed 29 bands falling into five v' progressions. Each band consists of P and R branches only. The rotational and vibrational constants (Table III), which fall into line with the corresponding values for LiH and NaH, are surprisingly different in the two states. B_v' and ω_v' show an anomaly, rising with increasing v' for low values of v' , then decreasing. Extrapolation of the vibrational levels indicates that the products of dissociation in the two states differ by the energy of the resonance lines of K (1.60 volts). Heats of dissociation of 1.25 and 2.06 volts are obtained for the excited and ground states, respectively. From potential energy curves a Franck-Condon diagram of intensity is drawn and is in good agreement with observed intensities.

THE molecular spectra of two of the diatomic hydrides have already been analyzed and reported; Nakamura¹ examined the spectrum of LiH as obtained in absorption while Hori² has made an extensive study of NaH in both absorption and emission. Most of the LiH spectrum falls between 3000Å and 4500Å, that of NaH between 3500Å and 5000Å. The two spectra, which are of the many-lined type, are much alike and have been assigned in each case to a $^1\Sigma \rightarrow ^1\Sigma$ transition. Extrapolation of the vibrational levels of the two states of an alkali hydride indicated as the products of dissociation a normal hydrogen atom and a normal alkali atom from the lower state and a normal hydrogen and an excited 2P alkali atom from the upper state. In this paper the analysis of the corresponding $^1\Sigma \rightarrow ^1\Sigma$ system of KH, obtained in emission and extending from 4100Å to 6600Å, is discussed.

A point of interest in the alkali hydrides is the anomalous behavior of ω_v' , the vibrational interval in the upper state. Instead of decreasing steadily with increasing v' in the usual way, it rises, attains a maximum at about $v'=9$, and then falls. This peculiar behavior is found in KH, as well as in LiH and NaH.

EXPERIMENTAL PROCEDURE

The source of the KH spectrum was a d.c. potassium arc operating in hydrogen. The arc was contained in a brass chamber, cooled by water circulating in a lead tube coiled about it. The electrodes, also water-cooled, were fixed into the removable top and bottom plates. The lower electrode was a hollow iron cylinder of about 1 cm internal diameter, with an iron cap having a 4 mm hole in its center. In the cylinder was a piston with a threaded shaft

¹ G. Nakamura, *Zeits. f. Physik* 59, 218 (1930); *Japanese Journal of Physics* 7, 31 (1931).

² T. Hori, *Zeits. f. Physik* 62, 352 (1930); 71, 478 (1931).

such that the piston could be advanced from outside the arc chamber. Thus potassium, contained in the cylinder, could be gradually extruded through the cap to keep a supply in the burning arc. A section of pressure tubing surrounded the piston shaft and its sleeve, soldered to the arc chamber, to prevent entrance of air. The shaft could be turned in the tubing. The upper electrode was of nickel or iron. Its shaft also entered the chamber through a sleeve, shaft and sleeve being surrounded by a section of tubing. The arc was struck by pressing the upper electrode against a coil spring.

Tank hydrogen was supplied continuously through a capillary tube. A pressure of about 20 cm of Hg was maintained, although the pressure did not seem to be a very critical factor in determining the intensity of the bands. Potential was supplied by a 500-volt d.c. generator and the current in the arc was held to about 3 amperes with series resistance. A single filling of potassium (about an ounce) could be made to last 3 or 4 hours. Exposures up to ten hours were taken.

Most of the analysis was made from photographs taken with an E-1 Hilger glass prism spectrograph. When the analysis was nearly completed a prism spectrograph fitted with a glass optical train (Hilger) consisting of a 60° prism, a 30° prism, and an achromatic lens of 3 meters focal length, in Littrow mounting, became available. This instrument was used to extend the spectrum above 5900Å where the dispersion of the E-1 was insufficient to give satisfactory measurements. The larger instrument had a dispersion of 10Å per mm at 6600Å, equal to the dispersion of the E-1 at 5000Å.

An attempt was made to photograph the KH spectrum in absorption. Potassium was heated, with hydrogen, in a length of iron tube, placed in a gas combustion furnace. The absorption spectrum was obtained but it was largely masked by other spectra. Below 4600Å the spectrum of K_2 was prominent. Above 4800Å the blue-green system of Na_2 (present as an impurity) extended up to the NaK bands falling just below the *D* lines of Na. Above the *D* lines the red system of Na_2 appeared. Between 4600Å and 4800Å, however, the spectrum of KH, corresponding exactly with the emission spectrum, could be observed.

ANALYSIS OF BAND SYSTEM

The KH spectrum is of the many-lined type; no heads or other regularities of structure are apparent on casual inspection. This is due to the fact that the heads of the bands almost coincide with the origins and to the overlapping of the bands. It is, therefore, not possible to make a vibrational analysis without first completing the rotational analysis, thus locating the band origins.

To carry out a rotational analysis, a beginning was made by picking out a branch of one of the stronger bands using the criterion that the second differences of the frequencies should be constant. This branch, being a strong one, could be followed through the origin and its character (*P* or *R*), as well as the rotational quantum numbers, determined. The combination differences,

$$\begin{aligned}\Delta_2 T' &= R(K'') - P(K'') \\ \Delta_2 T'' &= R(K'' - 1) - P(K'' + 1),\end{aligned}\quad (1)$$

were calculated for this band. Then bands in the same v' progression could be identified since they have the same value of $\Delta_2 T''$, while bands in the same v'' progression yielded identical values of $\Delta_2 T'$. Once the vibrational intervals were approximately determined the analysis proceeded rapidly. Often when the hunt for the correct combination differences did not give results promptly, a new start in the proper region with second differences disclosed the next band in a progression.

In this way 29 bands were located. The frequencies with quantum assignments are listed in Table VI at the end of this paper. Since about 85 percent of the lines appearing on the plates were assigned and since the remaining lines were mostly of very low intensity it is quite certain that the bands are of the simple two-branch type originating from a $^1\Sigma \rightarrow ^1\Sigma$ transition. The system thus corresponds to the similar systems found for NaH and LiH, assigned to $p\sigma^1\Sigma \rightarrow s\sigma^1\Sigma$ transitions.

CALCULATION OF MOLECULAR CONSTANTS

The next step was the calculation of the rotational constants and the band origins. The combination differences were tabulated (Tables IV and V) and mean values taken where more than one value was obtained for a particular pair of rotational levels. Since the rotational energy of a molecule in a $^1\Sigma$ state is

$$T = B_v K(K+1) + D_v K^2(K+1)^2 + F_v K^3(K+1)^3,$$

the combination differences can be expressed,

$$\begin{aligned}\Delta_2 T &= T(K+1) - T(K-1) \\ &= 4B_v(K + \tfrac{1}{2}) + 8D_v(K + \tfrac{1}{2})^3 + 12F_v(K + \tfrac{1}{2})^5\end{aligned}\quad (2)$$

where terms small in comparison with $F_v(K+1/2)^5$ are dropped. B_v depends upon v according to the relation,

$$B_v = B_e - \alpha_e(v + \tfrac{1}{2}) + \gamma_e(v + \tfrac{1}{2})^2 \quad (3)$$

in which $B_e (= h/8\pi^2 I_e c)$ is the extrapolated value corresponding to the non-vibrating molecule. Theoretically D_v and F_v also depend on v but the accuracy of the present data did not warrant the calculation of this variation. Hence D_v was set equal to D_e and F_v equal to F_e .

A method of successive approximation was used to obtain B_v . First, the D and F terms of Eq. (2), which are relatively small, were neglected and approximate values of B_v obtained, using the measured combination differences from Tables IV and V. Then approximate values of D_e and F_e were calculated from the theoretical relations,

$$\begin{aligned}D_e &= -4B_e^2/\omega_e^2 \\ F_e &= (D_e^2/B_e)(2 - \alpha_e\omega_e/6B_e^2).\end{aligned}\quad (4)$$

ω_e was approximately known from the separations of corresponding lines in successive bands in a progression. α_e was assumed to be zero in this ap-

proximation. These values of D_e and F_e were then used in Eq. (2) to obtain the second approximation for B_v , the mean for several values of K being taken. The origins of the bands were then calculated from the equation,

$$\nu = \nu_0 + (B_v' + B_v'')M + (B_v' - B_v'' + D_e' - D_e'')M^2$$

in which ν_0 is the origin. For the R branch $M = K'' + 1$, for the P branch $M = -K''$. Here the F_e terms are omitted because they are inappreciable for the values of M (< 15) used. From these calculated origins the vibrational intervals, ω_v , were determined and extrapolated to give ω_e . Then improved values of D_e and F_e were calculated from Eqs. (4) and the process described repeated to give a third approximation. This approximation was found to be sufficient, considering the accuracy of the data.

TABLE I. Band origins with values of ω_v interpolated.

$\nu'' \backslash \nu'$	0	1	2	3	4	Mean ω'_v
0				16386.0	868.3	15517.7
				259.5		259.5
1				16645.5	868.3	15777.2
				266.5		266.6
2			17809.5	897.5	16912.0	868.2
			272.7		271.8	
3		19009.9	927.7	18082.2	898.4	17183.8
		277.3		279.2		
4		19287.2	925.8	18361.4		
		283.3		282.1		
5	20527.4	956.9	19570.5	927.0	18643.5	
	287.8		288.9			
6	20815.2	955.8	19859.4			
	290.5	(293.8)				
7	21105.7	(952.5)	20153.2			
	291.5					
8	21397.2					
	293.8					
9	21691.0					
	293.0					
10	21984.0					
	292.8					
11	22276.8					
	291.6					
12	22568.4					
	290.0					
13	22858.4	955.1	21903.3			
			288.0			
14			22191.3			
			284.4			
15			22475.7			
			281.5			
16			22757.2			
Mean ω''_v	955.9		926.8	898.0	868.3	

In Table I the band origins are listed in square array with assignments of v' and v'' . The values of v'' are certainly correct but there is some doubt about v' . The correctness of the assignment of these quantum numbers will be discussed in the last section of the paper. The values of ω_v' and ω_v'' also appear in Table I. In Fig. 1, ω_v' is plotted against v' , together with corresponding graphs for NaH and LiH, showing the anomalous increase in ω_v' with v' for low v' . ω_v'' follows a normal course, decreasing linearly with increasing v'' . The values of ω_v' have been fitted with a power series in $(v+1/2)$

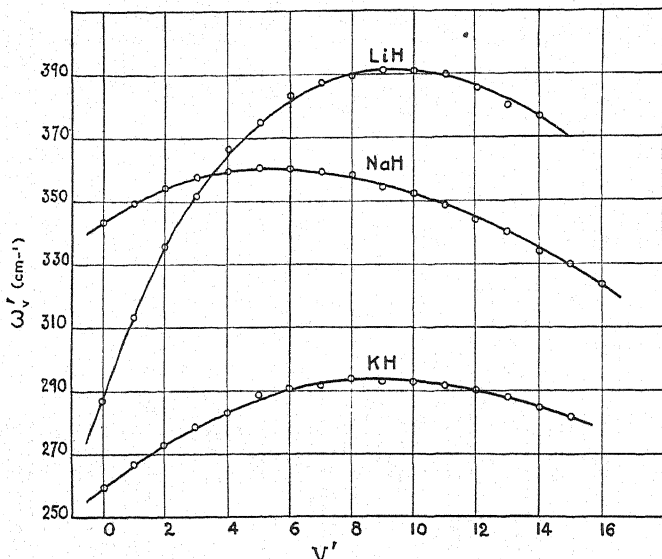


Fig. 1. Anomalous behavior of ω_v' in excited $^1\Sigma$ states of LiH, NaH, and KH.

by a least-squares calculation, with deviations, except one, less than 1 cm^{-1} . The result is incorporated in the following equation for the band origins,

$$\begin{aligned} \nu = & 19525.2 + [254.51(v' + \tfrac{1}{2}) + 3.26(v' + \tfrac{1}{2})^2 + 0.00725(v' + \tfrac{1}{2})^3 \\ & - 0.0105(v' + \tfrac{1}{2})^4 + 0.000273(v' + \tfrac{1}{2})^5] - [984.3(v'' + \tfrac{1}{2}) \\ & - 14.5(v'' + \tfrac{1}{2})^2]. \end{aligned}$$

The calculated values of B_v' and B_v'' are listed in Table II. B_v' parallels ω_v' in its anomalous behavior. It increases until $v'=6$ and then decreases.

TABLE II.

v	B_v'	B_v''	v	B_v'	B_v''	v	B_v'	B_v''
0	1.359	3.373	6	1.437		12	1.376	
1	1.385	3.292	7	1.432		13	1.360	
2	1.405	3.209	8	1.431		14	1.334	
3	1.422	3.122	9	1.416		15	1.323	
4	1.432	3.041	10	1.405		16	1.307	
5	1.438		11	1.391				

B_v'' decreases linearly with increasing v'' . The rotational and vibrational constants together with those of LiH and NaH, obtained respectively from Nakamura's and Hori's papers, are collected in Table III.

TABLE III. Principal rotation and vibration constants.

Constant	LiH	NaH	KH
I''_e	3.7×10^{-40}	5.65×10^{-40}	8.10×10^{-40} (g cm ²)
r''_e	1.6×10^{-8}	1.88×10^{-8}	2.24×10^{-8} (cm)
B''_e	7.38	4.896	3.415
α''_e	—	0.13	0.083
D''_e	—	-3.3×10^{-4}	-1.65×10^{-4}
F''_e	—	1.3×10^{-8}	1.5×10^{-8}
ω''_e	1395	1170.8	984.3
$x''\omega''_e$	22.7	18.9	14.5
I'_e	9.3×10^{-40}	14.66×10^{-40}	20.6×10^{-40} (g cm ²)
r'_e	2.5×10^{-8}	3.03×10^{-8}	3.58×10^{-8} (cm)
B'_e	3.00	1.887	1.344
α'_e	—	-0.028	-0.030
D'_e	—	-1.85×10^{-4}	-1.44×10^{-4}
F'_e	—	$\sim 0.8 \times 10^{-8}$	3.8×10^{-8}
ω'_e	272	335.24	254.5
$x'\omega'_e$	-9.61	-4.416	-3.26
Heat of { D' dissoc. { D''	1.14 2.56	1.47 2.24	1.25 (volts) 2.06 (volts)

A satisfactory explanation of the peculiar behavior of the upper state has not been given. Following Nakamura's account of it in LiH, Weizel³ attempted to explain the anomaly as due to an uncoupling, as the rotation increases, of the orbital angular momentum l of the $p\sigma$ electron of the excited molecule. Such an effect would result in a calculated value of B_v less than the "true" B_v , the depression being greater for slower vibrations. Such an explanation is inadequate to account for the behavior of ω_v' . The positions of the origins should be independent of rotational uncoupling effects. It might be argued that since the origins were calculated from rotational data, the calculated positions of the origins does depend upon the uncoupling. If, however, one uses for ω_v' the frequency intervals between corresponding lines of successive bands—lines for which K'' is so small, say 2, that the rotation could scarcely affect it—one obtains a series of values of ω_v' inappreciably different from those obtained from the calculated origins. That is to say, the anomaly, at least for ω_v' , seems to be independent of any rotational uncoupling that may be present.

³ W. Weizel, Zeits. f. Physik 60, 599 (1930).

POTENTIAL ENERGY CURVES AND HEAT OF DISSOCIATION

Potential energy curves, based on the Kratzer form, are shown in Fig. 2. In the form used, the potential energy does not involve coefficients in the vibrational energy beyond the second ($x\omega_e$) nor coefficients in the expression for B_v (Eq. (3)) beyond α_e . Though ordinarily positive $x\omega_e$ and α_e are negative in the upper state of KH. This change tends to steepen the potential energy curve for $r > r_e$ and flatten it for $r < r_e$. For the ground state the potential energy curve was obtained from the Kratzer expression for r near r_e , while in the neighborhood of dissociation the Morse form was used.

The heat of dissociation of the lower state was calculated from the expression $D = \omega_e^2 / (4x\omega_e)$ since the vibrational energy in this state is accurately represented by $T^v = w_e(v + \frac{1}{2}) - x\omega_e(v + \frac{1}{2})^2$ with $\omega_e = 984.3$ and $x\omega_e = 14.5$. D is thus 2.06 volts.

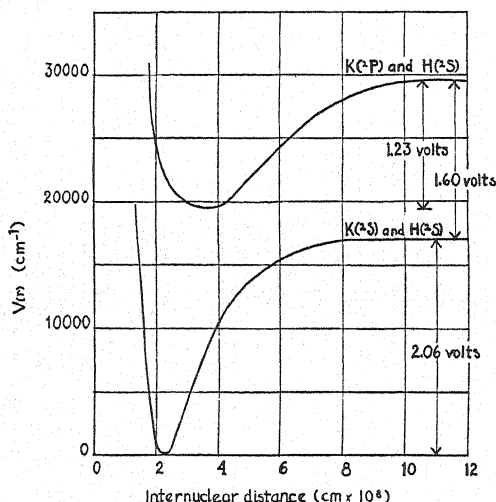


Fig. 2. Potential energy of normal and excited states of KH.

On account of the peculiar behavior of ω_v' the heat of dissociation of the upper state was determined by making use of the energy of the dissociated products. Rough extrapolation of the vibrational levels of the upper state indicated a heat of dissociation of about 1.5 volts. This requires that the atomic energy of the products of dissociation in the upper state be 1.8 volts greater than that of the products of the ground state. The resonance lines of potassium correspond to an excitation of 1.60 volts. Hence the products of dissociation in the upper state are normal hydrogen and potassium in the first excited state (2P). This atomic energy was added to D'' (2.06 volts) and the electronic energy of the excited molecular state (ν_0) subtracted from the sum to give 1.25 volts for D' , the heat of dissociation in the upper state.

From the potential energy curves the Franck-Condon intensity diagram in Fig. 3 was drawn, using the improved form suggested by Loomis and Nusbaum.⁴ The theoretical locus of maximum intensity is shown by the

curve, the observed bands by small circles. The discrepancy at high frequencies is not surprising since the steep, uncertain, part of the energy curve of the upper state is involved.

ASSIGNMENT OF v' AND v'' . ISOTOPE EFFECT

The assignment of v'' is certainly correct since a thorough search on emission and, more important, on absorption photographs disclosed no bands of a lower progression than the one for which v'' was set equal to zero. As to the upper state we suggested in a preliminary report⁵ that the bands now marked $v'=4$ belonged to the state for which $v'=0$. Improvements in technique enabled us to extend the spectrum to the red four vibrational intervals of the upper state. In the progression for which we now put $v'=0$, there are only two bands, (0, 3) and (0, 4). The evidence for the present assignment is

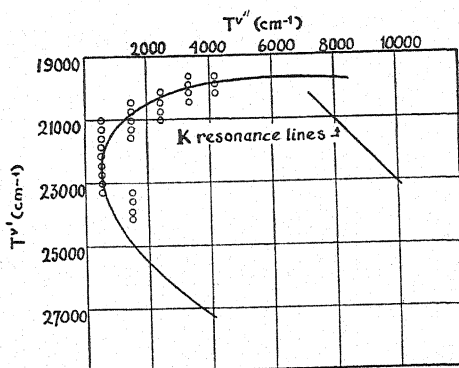


Fig. 3. Intensity diagram for KH. Circles are observed band origins. Curve is theoretical locus of maximum intensity.

first, that no bands assignable to a lower v' could be found even though the bands in this region (6100Å–6500Å) were well developed in the long exposures and, second, that the assignment fits well with the Franck-Condon curve, which is most reliable in this region. Additional evidence was sought through the isotope effect. The heavier isotope of potassium, of mass 41, is present in the ratio of about 1 to 20. No lines of $K^{41}H$ could be found in the emission photographs. In the absorption photographs, limited to the region 4600–4800Å, faint lines accompanied the intense lines in about the estimated positions. Measurements of the isotope shifts (about 1–2 cm⁻¹) made on two plates, were not sufficiently accurate to fix with certainty the v' assignment. Averages of calculated and measured values indicate that the assignment is about right, but may still be too high by one. Such a change would make little difference in any of the molecular constants listed.

⁴ F. W. Loomis and R. E. Nusbaum, Phys. Rev. **38**, 1447 (1931).

⁵ G. M. Almy and C. D. Hause, Phys. Rev. **39**, 178 (1932).

TABLE IV. (Continued). $R(K-1) - P(K+1) = T''(K+1) - T'''(K-1) = \Delta_2 T''(K)$.

K	$v' = 3$	$v' = 4$	$v' = 5$	$v' = 6$	$\begin{matrix} v'' = 1 \\ v'' = 7 \end{matrix}$	$v' = 13$	$v' = 14$	$v' = 15$	$v' = 16$	Mean
5	70.2	70.2	(68.5)	(74.2)	(67.7)	72.5		71.3	71.9	71.5
6	83.5	84.4	(82.3)	(81.1)	84.8	85.7	84.4	84.6	83.9	84.5
7	99.3	98.4	(95.5)	98.5	100.6	98.1	97.7	98.4	99.4	98.8
8	(113.5)	110.6	111.5	111.7	(114.4)	110.1	111.2	111.2	(109.9)	110.0
9	—	123.7	125.3	124.0	124.0	123.1	124.3	124.2	124.6	124.1
10	135.1	137.0	136.1	138.1	138.7	136.9	135.5	135.9	137.4	136.7
11	150.2	149.7	149.9	149.1	150.7	148.5	149.0	149.6	150.3	149.6
12	161.5	162.3	161.8	161.9	(165.6)	162.8	161.3	162.8	162.2	162.1
13	175.0	174.0	175.5	—	174.6	174.3	174.6	174.4	173.5	174.4
14	—	186.6	187.7	187.6	186.7	186.7	186.8	186.9	187.1	187.0
15	199.3	200.5	199.2	198.6	200.9	199.8	199.8	199.9	199.7	199.7
16	212.4	211.0	211.5	210.5	212.7	211.4	211.7	211.7	211.3	211.6
17	222.8	223.9	223.2	223.3	223.0	223.3	223.0	221.7	223.0	223.0
18	235.6	236.9	235.5	235.5	235.9	234.2	235.3	235.3	234.8	235.5
19	245.7	—	247.5	245.6	248.5	245.8	—	247.6	246.5	246.8
20	258.5	260.2	259.4	259.2	259.5	—	—	258.9	259.1	259.1
21	271.5	270.3	270.3	270.9	270.7	—	—	271.1	270.8	270.8
22	284.4	282.2	—	—	282.2	—	—	282.6	282.8	282.8
23	—	293.8	292.5	292.1	293.3	—	—	292.3	—	—
24	—	304.4	303.9	304.0	303.0	—	—	—	—	303.8
25	—	—	313.7	314.8	314.1	—	—	—	—	314.2
26	—	—	—	326.0	326.0	—	—	—	—	326.0
27	—	—	—	336.2	335.6	—	—	—	—	335.9
28	—	—	—	346.2	345.9	—	—	—	—	346.0
29	—	—	—	356.2	354.4	—	—	—	—	355.3
30	—	—	—	366.5	—	—	—	—	—	366.5

TABLE IV. (Continued). $R(K-1) - P(K+1) = T''(K+1) - T''(K-1) = \Delta_2 T''(K)$.

K	$v''=2$ $c'=4$			Mean			$v''=3$ $v'=2$			Mean			$v''=4$ $v'=1$ $v'=2$			Mean
	$v'=2$	$v'=3$	$v'=4$	$v'=5$	$v'=6$	$v'=7$	$v'=0$	$v'=1$	$v'=2$	$v'=3$	$v'=4$	$v'=5$	$v'=0$	$v'=1$	$v'=2$	
2														30.6		30.6
3														42.3		42.3
4														53.6		53.6
5														67.5		67.5
6														77.7		77.7
7														90.5		90.5
8														102.5		102.5
9														114.9		114.9
10														126.8		126.8
11														137.2		137.2
12														149.6		149.6
13														161.3		161.3
14														173.3		173.3
15														184.1		184.1
16														195.5		195.5
17														205.7		205.7
18														217.2		217.2
19														231.6		231.6
20														239.0		239.0
21														249.3		249.3
22														258.8		258.8
23														270.0		270.0
24														281.2		281.2
25														292.4		292.4
26														303.6		303.6
27														314.8		314.8

TABLE V. $R(K) - P(K) = T'(K) - T'(K-1) = \Delta_2 T'(K)$. (Values in parentheses omitted when taking mean.)

K	$v''=3$	$v'=0$ $v''=4$	Mean	$v''=3$	$v'=1$ $v''=4$	Mean	$v''=2$	$v'=2$ $v''=3$	$v''=4$	Mean	$v''=1$	$v'=2$ $v''=3$	$v'=3$ $v''=2$	Mean
2					13.0	13.0					19.3			19.3
3					19.4	19.4					24.1			24.1
4					24.6	24.6					30.4			30.4
5					29.8	29.8					37.5			37.5
6			26.1		36.7	36.7					43.1			43.1
7	35.7	34.1	34.9		41.8	41.8					46.0			46.0
8	(37.1)	41.3	41.3		47.5	47.5					53.6			53.6
9	(41.2)	45.5	45.5		52.8	52.8					58.4			58.4
10	49.8	50.4	50.1		57.1	57.1					61.7			61.7
11	55.9	54.5	55.2		61.6	61.6					69.6			69.6
12		61.1	61.1		66.5	66.5					75.2			75.2
13	(63.4)	66.4	66.4		71.7	71.7					80.4			80.4
14	(68.6)	70.0	70.0		76.7	76.7					88.9			88.9
15	75.5	75.5	75.5		82.0	82.0					94.2			94.2
16	84.6	79.5	79.5		86.3	86.3					97.6			97.6
17	(92.6)		84.6		89.4	89.4					102.6			102.6
18	(97.7)		84.6		95.8	95.8					107.1			107.1
19	(104.6)				100.5	100.5					113.6			113.6
20					105.8	105.8					120.9			120.9
21					107.7	107.7					125.8			125.8
22					114.2	114.2					129.0			129.0
23					118.7	118.7					133.3			133.3
24					120.7	120.7					136.9			136.9
25					118.7	118.7					139.8			139.8
26					120.7	120.7								
27					118.7	118.7								
28					120.7	120.7								

TABLE V. (Continued). $R(K) - P(K) = T'(K+1) - T'(K-1) = \Delta_2 T'(K)$.

K	$v'=0$	$v'=7$ $v''=1$	Mean	$v'=8$ $v''=0$	$v'=9$ $v''=0$	$v'=10$ $v''=0$	$v'=11$ $v''=0$	$v'=12$ $v''=0$	$v'=13$ $v''=0$	Mean
1				8.3	(10.0)	(10.2)	16.1	(7.3)	13.5	13.5
2	14.6		14.6	14.2	13.7	14.5	—	13.3	18.5	18.5
3	20.0		20.0	19.7	19.0	20.0	25.5	18.3	24.3	24.3
4	24.9		24.9	25.0	25.2	24.5	31.9	24.4	29.0	28.5
5	31.6		31.6	30.9	30.3	30.2	37.8	29.2	35.2	34.6
6	37.1	36.3	36.7	37.4	36.1	35.9	42.0	34.4	39.4	39.1
7	42.2	41.5	41.8	42.5	41.6	41.3	46.5	40.4	38.8	44.2
8	47.6	(50.3)	47.6	46.8	46.4	46.4	51.3	45.5	44.6	50.8
9	53.6	(57.7)	53.6	52.5	52.3	51.8	56.6	51.2	50.9	54.9
10	58.2	(56.9)	58.2	58.7	57.6	57.2	62.7	56.0	55.2	60.4
11	63.6	63.5	63.6	63.6	63.0	61.8	66.9	61.0	60.3	65.1
12	68.8	66.1	67.5	68.5	68.4	67.5	71.9	65.9	64.7	70.3
13	74.2	75.1	74.7	74.0	72.9	73.0	77.2	71.4	70.5	75.5
14	79.5	80.9	80.2	78.9	78.6	77.9	81.8	75.7	75.0	79.9
15	85.5	86.2	85.8	84.7	83.6	81.9	87.3	81.3	80.1	84.5
16	89.5	89.8	89.6	89.2	88.5	87.9	91.5	86.2	84.9	89.6
17	94.1	94.5	94.3	94.3	93.5	92.8	96.3	90.5	89.6	94.0
18	99.9	99.4	99.7	98.9	98.8	97.6	100.7	94.7	94.0	99.1
19	104.8	104.8	104.8	103.6	103.0	102.1	106.0	99.5	103.5	103.1
20	108.7	109.4	109.0	109.0	107.9	106.1	109.5	104.6	106.7	106.7
21	114.0	113.7	113.8	112.5	112.1	111.4	113.2	108.2	111.9	111.9
22	115.8	119.4	117.6	118.7	116.8	115.5	117.6	110.6	116.5	116.5
23	119.3	122.4	120.8	122.6	120.2	120.1	123.0	117.9	116.5	120.2
24		126.4	126.4	127.5	124.6	124.1	126.4	123.2	120.2	
25		130.7	130.7	132.7	128.4	129.5	128.5	126.4		
26		133.3	133.3		132.3	132.9	131.6	130.5		
27		138.4	138.4			138.4	132.5	(134.1)		
28		140.6	140.6					(136.6)		

TABLE V. (Continued). $R(K) - P(K) = T'(K+1) - T'(K-1) = \Delta_2 T'(K)$.

K	$v'=14$ $v''=1$	$v'=15$ $v''=1$	$v'=16$ $v''=1$
3		16.6	22.6
4		23.8	26.1
5		29.0	33.2
6	27.8	33.6	37.1
7	34.5	38.0	44.0
8	39.1	44.2	47.8
9	44.7	48.7	53.4
10	49.6	54.1	58.6
11	54.3	58.4	63.0
12	58.4	63.6	67.3
13	64.3	68.8	72.4
14	68.4	73.4	77.0
15	74.1	78.2	80.9
16	78.6	83.0	85.5
17		87.5	89.4
18		90.5	(93.9)
19		96.2	(98.6)
20		101.3	(101.3)
21		104.9	
22		108.3	

TABLE VI. Wave numbers and quantum numbers of all assigned lines. Vibrational quantum numbers are given in parentheses. Under intensity, d = diffuse; db = probably double; asterisk is assigned at least twice.

[illegible]

TABLE VI. (Continued).

K	(11, 0) (22, 276.80)			(12, 0) (22, 568.44)			(13, 0) (22, 858.44)		
	I	R	P	I	R	P	I	R	P
0				2	22,570.8*	22,563.5*	0	22,855.6	22,851.5
1	3	22,275.2*	22,259.1*	2	570.8*	553.0	1	846.3	842.1
2			243.4*	2	566.3*	538.0	0	833.1	827.7
3	1	250.3	224.8*	2	556.4*	518.6	1	815.0	808.8
4	1	233.1	201.2*	2	543.1	496.2	1	793.5	786.0
5	1	213.6	175.8	2	525.3*	469.4	1d	767.4	758.3
6	3	213.6	146.1*	1d	503.8	438.5	1	737.3	728.0
7	5	188.1*	112.4	2	479.0*	403.7*	2	704.1	692.8*
8	2	158.9	074.2*	2	449.2*	364.7	1	665.5	653.3
9	2	125.6*	031.8	3	415.9*	321.9	1	623.8	610.3
10	2	088.4	047.1*	3	377.9*	275.2*	1	577.6	563.5*
11	4	047.1*	002.2	2	336.2*	224.8*	2	527.7	512.9*
12	3	002.2	881.1*	2	290.7	170.1	2	473.7	457.2
13	3	002.2	823.0	2	241.6	112.4*	1	415.9*	398.6
14	3	900.3*	761.2*	2	188.1*	049.4	3d	354.6	336.2*
15	2	843.0	695.3	5	130.7	21,982.9*	1	289.0	269.7
16	2	782.6*	626.4*	2	069.1*	840.6*	1	219.5	199.3
17	4	718.0*	553.3*	3	004.3*	762.8*	3	146.1*	125.6*
18	2	649.6	476.6	3	21,935.3*	681.8	4	069.1*	047.1*
19	2	577.3	396.0*	3d	862.3*	597.1	2	21,987.9*	21,965.6*
20	3d	502.0*	311.5*	2d	786.4*	508.6	1	903.2	881.1*
21	4d	421.0*	223.7	3d	705.3*	416.8	2	815.4*	791.3
22	6	336.9*	132.6	3	619.2*	320.2*	2	722.7	698.9
23	6	250.3*	037.8	3	534.8	222.2	2	626.4*	602.5
24	2	160.9	039.5	1	443.4	119.7	3d	528.3*	502.0*
25	3d	066.0*	838.3*	3	348.6*	013.6	1	424.6	400.4*
26	1	20,966.8*	732.7	2	250.3*	20,905.5	4		292.9
27	2	864.3*	624.0*	2	147.7*		1		
28	2	756.6*		4d	042.0				

TABLE VI. (Continued).

[illegible]

TABLE VI. (Continued).

K	I	R	I	P	I	R	I	P	I	R	I	P
	(14, 1) (22, 191.26)				(15, 1) (22, 475.69)				(16, 1) (22, 757.19)			
3												
4												
5	2d	22, 147.9	0	22, 142.2	0	22, 461.8	1	22, 445.0	0	22, 731.5	0	22, 708.9
6	1	127.3	1d	119.7	3*	449.2	1	426.8	0	713.1	1	686.9
7	1	102.7	1	092.8	3d	432.7	2	403.7*	0	692.8*	0	659.6
8	3	074.2*	1	063.6	1	411.5	3	377.9*	2	666.3	0	629.1
9	1	041.0	1	029.5	2	386.4	2d	348.0	2	637.4	1d	593.4
10	3	004.3*	2	21, 991.4	2	357.3	1	313.1	2	604.2	2	556.4
11	0	21, 963.8	2	950.0	2	324.0	3d	275.3*	1	566.3	2	512.9*
12	2	919.5*	2	905.5	3d	287.2	1	233.1	2	525.3	1d	466.8
13	1	871.0	4	855.3*	2	246.5	4	188.1*	2	479.0	3d	415.9*
14	0	819.0	2d	802.6	2	201.2*	1	137.5	2	430.5	1	363.2
15	2	762.8*	1	744.9	2	152.5	2d	083.7	1	377.9*	1	305.5
16			2	684.2*	1	100.2	2	026.7	3	320.4	1	243.4
17			3d	619.2*	3d	043.8	2	21, 965.6*	1	259.1	3	178.2
18					2	21, 983.3*	3	900.3*	1	194.6	0	109.1
19					0	919.5*	2	832.0	0	125.6*	1	036.1
20					2	851.6	3	761.2*	3	053.7	1	21, 959.7*
21					2	780.4	2	684.2*	ld	21, 977.7*	1	879.1*
22					3d	705.3*	3	604.0	2d	896.6*	1	795.3
23					3	626.4*	2	521.5	3			
24						542.5*	1	434.2				
25							2	343.8				
							6	250.3*				
							4	155.8*				

TABLE VI. (Continued).

K	(5, 2) (18, 643.48)			(0, 3) (16, 386.0)			(1, 3) (16, 645.50)		
	I	R	P	I	R	P	I	R	P
2	2	18,566.9*					1d	16,646.0	16,631.8*
3	1	540.1					2d	637.3*	620.3*
4	1d	512.5					1d	625.1*	605.5
5	1	480.7					1d	608.9	585.6*
6	1	445.3					1	589.5*	556.7
7	1	404.2					2	569.7	527.1
8	1	361.5					2	544.2*	495.9
9	1d	314.6*					1d	516.7	464.2
10	1	263.8					2	484.0*	456.9
11	1	209.9*					2d	448.8	386.2
12	1	152.7					1d	409.0	342.8
13	2d	91.8*					2	366.8	295.1
14	3	314.6*					2d	320.6*	243.8*
15	1d	263.8					3	271.7	189.5*
16	4	209.9*					1	218.8	133.0
17	2	152.7					1	161.3	069.9*
18	2	91.8*					2	102.6	007.0
19	3d	027.8*					2	039.8	15,939.3*
20	3d	17,962.0*					1	15,973.1*	888.3
21	1	890.4					2	903.4*	795.7
22	3	816.1*					3d	830.8*	716.6
23	2	738.2					2	754.4*	635.8*
24	2	656.8*					1	673.6	552.9*
25	2	574.0					2	590.6*	
26	2	485.5					3	503.7	
27	3d	393.4*							

TABLE VI. (Continued).

[illegible]

Far Infrared Spectra of Gases

By JOHN STRONG* AND S. C. WOO
California Institute of Technology

(Received August 9, 1932)

The envelope of absorption in the far infrared is determined for 14 gases by the reststrahlen technique. The pure rotation envelopes of HCl and NH₃ are compared with the envelopes of the *R*-branch of their oscillation-rotation bands. The formula

$$\frac{I_i(\text{vib.} - \text{rot.})}{I_j(\text{rot.})} = \frac{\text{const.}}{\nu_r(1 - e^{-h\nu_r/kT})}$$

is used to modify the shape of the *R*-branch for comparison with the pure rotation envelopes. A thermopile is described for use when the receiver area is square. The novel feature of this thermopile lies in the use of only one receiver for four junctions. Also the cold junctions stay at the temperature of the receiver for all temperature fluctuations which require a time greater than one minute. Drifting is consequently greatly reduced. Absorption cells are described which are useful for wave-lengths greater than 20 μ . The windows for these cells are made from 1 μ lacquer films covered with a 50 μ layer of Kahlbaum paraffin. Interference effects are reduced to a minimum by the use of copper ribs across the windows, a device to prevent pressure changes in the cell so the windows will not bulge and mechanically accurate mounting of the cells. Interference effects are also reduced because the beam passing through the cells has a large angular divergence.

INTRODUCTION

MANY interesting characteristics of the band spectra of polyatomic molecules can be determined with spectroscopic equipment which is incapable of resolving the individual bands. We are indebted to Coblenz¹ for much of the pioneer work of this character for the near infrared bands. No systematic work of this character has been carried out, however, in the far infrared region where the pure rotation bands are found. Recently one of the authors² has applied the reststrahlen technique to spectroscopic studies in this region of the spectrum. The results obtained compare favorably, as regards the resolving power, with the prism studies of gases in the near infrared region. It is the purpose of this paper to report investigations of gases in this spectral region.

APPARATUS

The description of the reststrahlen apparatus can be found in earlier papers.² However, a new thermopile not previously described was developed for this apparatus by one of the authors.³ A description of this and of the absorption cells is presented below.

* National Research Fellow.

¹ W. W. Coblenz, *Investigations of Infrared Spectra*.

² John Strong, *Phys. Rev.* **37**, 1565 (1931).

³ John Strong.

New thermopile with one receiver

The image of radiation which the thermopile is to intercept for the reststrahlen apparatus is a square. A single receiver is less awkward to construct for this image than an array of separate receivers. For the thin rectangular image in a spectrometer this is not necessarily true. Fig. 1 shows the method of construction adopted for the reststrahlen thermopile. Each thermocouple consists of a pair of wires, each 1.5 mm long, soldered together at *P*. One wire, *T*, is a bismuth-tin alloy (95 percent Bi+5 percent Sn) and the other wire, *A*, is an antimony-bismuth alloy (97 percent Bi+3 percent Sb). The receiver, *R*, is made of silver foil and is 3 mm on an edge. One side is blackened (as described elsewhere⁴) with Welschbach mantle material. The other side is painted with a thinned lacquer. A scrap of high-melting paraffin attaches the hot junction to the receiver mechanically and thermally but not electrically because of the insulation afforded by the lacquer. Paraffin is better than other waxes for this purpose on account of its high heat conductivity. The cold junctions, *C*, are small pieces of No. 22 copper wire. These pieces take about

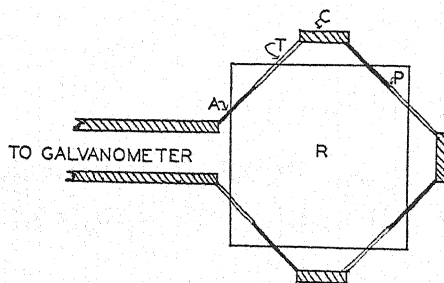


Fig. 1.

twelve times as long to heat up as the thermoelectric wires because of their larger mass and specific heat. As a consequence of its being connected thermally to the receiver and taking a time of about one minute to come to thermal equilibrium with the receiver, the thermopile is not sensitive to a difference in temperature of the surroundings and consequently much objectionable drifting is avoided. On the other hand, the cold junctions do not change their temperature materially during the time required to make an observation.

It is easy to show by calculation that the difficulty of making more than 4 couples is not justified by the increased deflection. The data given below are calculated for a square receiver 3 mm on an edge. Values are given of the deflection of a thermopile for various numbers of junctions. In each case the total resistance of the thermopile is taken as 25 ohms, the critical damping resistance of the galvanometer used. It will be noted that four junctions give 88 percent of the deflection given by six junctions.

For a description of how these calculations were made and for further remarks on the technique of making thermopiles, reference may be made to an article on this subject by one of the authors.⁴

⁴ John Strong, R.S.I. 3, 65 (1932).

TABLE I.

Number of junctions	1	2	3	4	5	6
Deflection with N junctions	0.28	0.52	0.72	0.88	0.95	1.00
Deflection with 6 junctions						

The absorption cells

The absorption cells were constructed from 4 inch thin walled brass tubing. There were four cells each 6 inches long. The cells could be successively placed in the radiation path so that the radiation from the Globar source passed twice through the cell, once as it passed upwards to a concave mirror and again as it was reflected downwards by this mirror to a focus on the entrance aperture of the reststrahlen apparatus. This apparatus has been described in an earlier paper.⁵ The mirror, source and entrance aperture were placed so close to the cell windows that the total length of radiation path for which the air was not dried with P_2O_5 was only about 3 inches. The four cells were soldered to a wheel which could be rotated about a vertical axis. By rotation of this wheel through 90° one cell could be removed from the radiation path and another moved into the path. The wheel was so mounted that the position taken by the cells in the radiation path was accurately reproducible.

A 1μ lacquer film was attached to each end of the absorption cells. The transmission of these films is great for wave-lengths greater than 20μ .⁶ After the lacquer windows were dry the window was brought in contact with hot molten paraffin (Kahlbaum $68-70^\circ C$, No. 3094). Kellner has found that this material is transparent for wave-lengths greater than 20μ .⁷ The transmission throughout the far infrared has also been measured by Barnes.⁶ When the paraffin coating on the lacquer film has cooled, the resulting window is uniform and of about 50μ thickness.

When these cells were filled with dry air and their transmission measured on successive nights the discrepancy in the measurements varied from 5 to 20 percent, particularly at wave-lengths greater than 80μ . It was thought that these variations might be due to interference effects because a cell placed in the radiation path showed some expansion of the windows due to heating of the gas in the cell. When this was avoided by putting two ribs across each window and closing the cell with a collapsed rubber toy balloon, these variations were materially reduced. These ribs were made from No. 22 bare copper wire. They were laid on the window and attached by a hot knife, wetted with paraffin. The knife was touched to the paraffin window over 2 or 3 inches of the length of the wire at a time, thus sealing the wire to the film in a neat manner without affecting the uniformity of the paraffin coat.

Measurements

The measurements of gas transmission were made as follows: The four

⁵ John Strong, Phys. Rev. **38**, 1818 (1931).

⁶ R. Bowling Barnes, Phys. Rev. **39**, 562 (1932).

⁷ L. Kellner, Geb. Sperling, Zeits. f. Physik **56**, 215 (1929).

cells were initially filled with dry air (P_2O_5 towers) and the reststrahlen energies transmitted by all these cells was measured. The Globar source was heated by a current from a 110 volt storage battery and an ammeter was used to test the constancy of this current. Two of the absorption cells were then filled with the gas to be studied. This gas was dry and prepared by a procedure which will be described later. Then the reststrahlen energies transmitted by the cells were again measured. The two cells containing dry air were used to free the results from dependence on the amount of moisture in the room air, from gradual decrease in emission of the source due to the batteries running down, and from possible variations in the reststrahlen apparatus which might arise from variations in the position of the crystal mirrors and filters. The ratio of the reststrahlen energy transmitted by the gas cell to that transmitted by the dry air cell was divided into the same ratio taken when both cells were filled with dry air to get the transmission of the gas alone. By using two gas cells the results could be checked as an insurance against mistake.

The materials used for this investigation were obtained as follows: acetylene, ethylene, propane, nitrous oxide, ammonia, sulphur dioxide, and hydrogen sulphide, all of high purity, were obtained from gas cylinders. Saturated vapors of water, chloroform, acetaldehyde and methyl iodide were obtained from the respective pure liquids by bubbling dry air through them. Hydrogen chloride was prepared from sulphuric acid and sodium chloride, cyanogen from copper sulphate and potassium cyanide, and nitrogen peroxide from copper and concentrated nitric acid. In the latter case, the gas was first condensed out in a tube immersed in a salt and ice bath and then evaporated into the absorption cell. Nitric oxide was prepared by the action of nitric acid upon arsenious oxide, the peroxide was frozen out with freezing mixture and the purified gas was then passed into the absorption cell. The air in the drying towers and absorption cells was displaced with nitrous oxide which was found to be transparent in the entire region we investigated. The gas thus obtained was still a little contaminated (a slightly yellowish tint) by the formation of nitrogen peroxide and trioxide with the traces of air in the apparatus.

All the gases except water and ammonia were dried through phosphorus pentoxide and concentrated sulphuric acid before they were introduced into the absorption cells.

EXPERIMENTAL RESULTS AND DISCUSSIONS

In this investigation, the absorption of fourteen gases has been studied. The results of twelve gases are represented in the following curves Figs. 2 to 11 where the percentages of absorption are plotted against wave number. The circles, crosses and solid dots, denote results of different experiments. It can be seen that the error in the observations is probably less than 5 percent, although in some cases it is greater as will be pointed out in the individual descriptions.

In this region of the spectrum the absorption bands are pure rotation, vibration, or possibly torsion-oscillation or rotation about a chemical bond.

In the case of symmetrical molecules, such as C_2H_2 , C_2H_4 , $(CN)_2$, there should be no pure rotation bands, because these molecules do not possess a permanent electric moment. But, on the other hand, they may have vibration bands in this region. The experimental results for each gas is discussed below.

Acetylene

The experiment on acetylene was carried out without the calibration of the empty cell. The results obtained were not plotted here but it is certain that acetylene does not have an absorption throughout this region more than 5 percent for a path length of 12 inches. This result is to be expected. The existence of a pure rotation band is excluded by its zero electric moment. The vibration bands have been investigated by Mecke.⁸ Although Mecke's designation does not seem to be quite correct,⁹ it is certain that all the active fundamental bands are in a region of wave-length shorter than 20μ .

Ethylene

Fig. 2 shows the absorption of ethylene. We can see that it has no absorption greater than 5 percent. Theoretically, ethylene is expected to have no pure rotation band, for it has no permanent electric moment. But on the

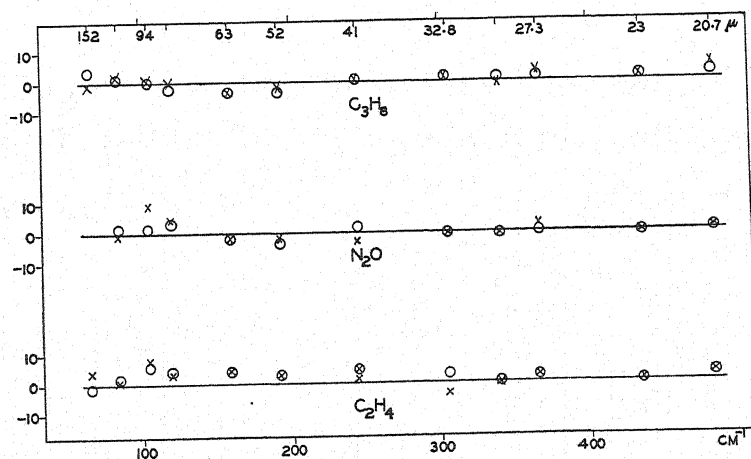


Fig. 2.

other hand, it is not possible to fit all of the twelve fundamental frequencies of the normal vibrations of ethylene to the already discovered spectral data.⁸ Consequently some active fundamental bands may possibly be in our region. It is possible, however, that these bands may be very weak or so narrow that they fall between our reststrahlen and hence escape detection. An example of how this may happen is seen in the case of the fundamental band of CS_2 ¹⁰ at 396.8 cm^{-1} , whose maxima lie at wave-lengths between those of the reststrahlen of CaF_2 (23μ) and calcite (27.3μ).

⁸ R. Mecke, *Zeits. f. Physik* **64**, 173 (1930).

⁹ Olson and Kramers, *J. Am. Chem. Soc.* **54**, 136 (1932).

¹⁰ D. M. Dennison and Wright, *Phys. Rev.* **38**, 2077 (1931).

Cyanogen

Fig. 3 gives the absorption of cyanogen. It possesses two maxima, one near 52μ and the other 94μ . The former band has been predicted by Woo and Badger¹¹ from investigations of the ultraviolet absorption and identified by

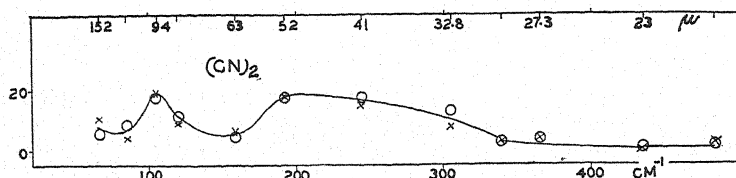


Fig. 3.

them as the fundamental band of the active deformation oscillation. The interpretation of the band at 94μ is unknown. The structure of cyanogen in the normal electronic state is probably linear and symmetrical and it has zero electric moment. These facts preclude the existence of pure rotation bands, but, on the other hand the vibration bands have all been located on the shorter wave side.¹¹

Nitrous oxide

The experimental results for nitrous oxide are given in Fig. 2. It has no absorption. Although the structure of this molecule is believed to be asymmetrical NNO,¹² its pure rotation band, if any, must be extremely weak on account of its exceedingly small electric moment. Even this weak absorption might, on account of the large moment of inertia of this molecule ($I = 65.95 \times 10^{-40} \text{ g cm}^2$ ¹³) appear at longer wave-lengths outside the region we investigated.

Propane

Propane (see Fig. 2) also does not show any absorption. The non-existence of pure rotation band is supported by its zero electric moment.

Hydrogen chloride

Our experimental results on the absorption of hydrogen chloride are given as circles in Fig. 4, where the crosses represent the data of Rubens and von Wartenberg.¹⁴ A is a smooth curve representing these results. It is the absorption of hydrogen chloride resulting from the pure rotation of the molecule. This band and also the vibration-rotation band of hydrogen chloride have been carefully investigated by other investigators. A very simple but definite relation between these two types of bands is derived from the following considerations. The intensity of the spectral line of frequency

$$\nu_j = \nu_0 + jh/4\pi^2A = \nu_0 + \nu_r; j = 1, 2, 3, \dots$$

¹¹ S. C. Woo and R. M. Badger, *Phys. Rev.* **39**, 932 (1932) and also paper to appear.

¹² E. K. Plyler and E. F. Barker, *Phys. Rev.* **38**, 1827 (1931).

¹³ The value of Plyler and Barker's paper was misprinted as 59.4×10^{-40} .

¹⁴ H. Rubens and H. von Wartenberg, *Verh. d. Phys. Ges.* **13**, 796 (1911).

in the *R*-branch of a vibration-rotation band of a diatomic molecule is

$$I_j(\text{vib.} - \text{rot.}) = \frac{8\pi^3 \nu_j N}{3ch \Sigma g_j e^{-W_j/kT}} V^2(v'', v') (1 - e^{-h\nu_j/kT}) \frac{j}{4} \exp \left[-\frac{h^2(j^2 - j)}{8\pi^2 I kT} \right]$$

where g_j and $V(v'', v')$ are respectively the quantum weight and the change of electric moment due to vibration. At a given temperature and for a given band we have

$$I_j(\text{vib.} - \text{rot.}) = \text{const.} \times j \exp \left[-\frac{h^2(j^2 - j)}{8\pi^2 A kT} \right].$$

The constant arises because of the fact that the frequency of the rotational line, ν_r , is negligible in comparison with the vibration frequency, ν_0 .

The intensity of the rotational line of frequency

$$\nu_j = \nu_r = jh/4\pi^2 A$$

in a pure rotation band is

$$\begin{aligned} I_j(\text{rot.}) &= \frac{8\pi^3 \nu_r N}{3ch \Sigma g_j e^{-W_j/kT}} (1 - e^{-h\nu_r/kT}) \frac{j}{4} \exp \left[\frac{-h^2(j^2 - j)}{8\pi^2 A kT} \right] \\ &= \text{const.} \times \nu_r (1 - e^{-h\nu_r/kT}) j \exp \left[\frac{-h^2(j^2 - j)}{8\pi^2 A kT} \right]. \end{aligned}$$

Now when we compare the intensities of the lines in the *R*-branch of a vibration band with those of the corresponding lines in the pure rotation band we obtain the following simple relation:

$$\frac{I_j(\text{vib.} - \text{rot.})}{I_j(\text{rot.})} = \frac{\text{const.}}{\nu_r (1 - e^{-h\nu_r/kT})}. \quad (1)$$

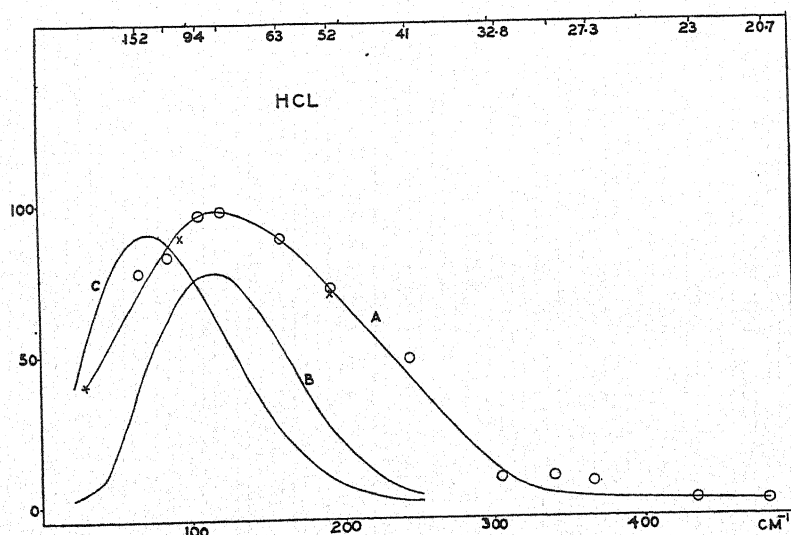


Fig. 4.

Consequently, the relative intensities of the rotational lines in the *R*-branch of a certain vibration band can be used to calculate the relative intensities of the pure rotation lines. We have carried out this calculation to get the shape of the pure rotation band for hydrogen chloride. In Fig. 4 curve *C* represents the intensity distribution plotted against the rotational frequency in the *R*-branch of the vibration band of hydrogen chloride. Curve *B* was calculated from curve *C* by the above simple relation. The agreement between *B* and our experimental curve *A* is very good.

Ammonia

The absorption of ammonia is given in Fig. 5. The strong absorption shows the pure rotation band whose fine structure has been carefully investigated by Badger and Cartwright.¹⁵ The results of intensity distribution among the rotational lines by those authors agree very well with the envelope we have obtained for the band; for example, the maximum of absorption in both cases

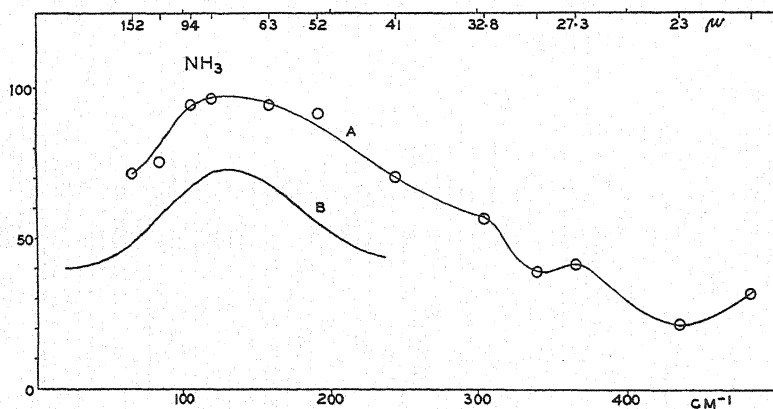


Fig. 5.

appears at $\nu_r = 125 \text{ cm}^{-1}$. Considerations, as in the case of hydrogen chloride, of the relation between the intensity distribution in the *R*-branch of a vibration band and that in the pure rotation band can be applied here with certain modifications. These modifications are necessary because the ammonia molecule has a more complicated structure. Ammonia can be regarded as a symmetrical top which possesses two different moments of inertia. Two types of vibration bands,¹⁶ parallel and perpendicular, can be distinguished depending upon whether the change of electric moment during the absorption of radiation is along or perpendicular to the axis of symmetry. The structure of the parallel bands alone would be similar to the pure rotation band because the permanent electric moment which gives rise to the pure rotation band is along the axis of symmetry. By applying the same formula developed above for hydrogen chloride, we can obtain the pure rotation absorption envelope from the *R*-branch of a parallel vibration band. In Fig. 5 *A*

¹⁵ R. M. Badger and C. H. Cartwright, *Phys. Rev.* 33, 692 (1929).

¹⁶ D. M. Dennison, *Rev. Mod. Phys.* 3, 280 (1931).

is our experimental curve and B represents the envelope of the R -branch of a parallel band modified by the above Eq. (1). We cannot say what interpretation is to be placed on the absorption between 23μ and 32.8μ .

Nitric oxide

In Fig. 6 are given the results of the absorption of NO. The circles, crosses and solid dots represent data of three separate series of experiments. On account of the difficulty of preparing pure nitric oxide absolutely free from traces of air in the absorption cells, the results of the three series of experi-

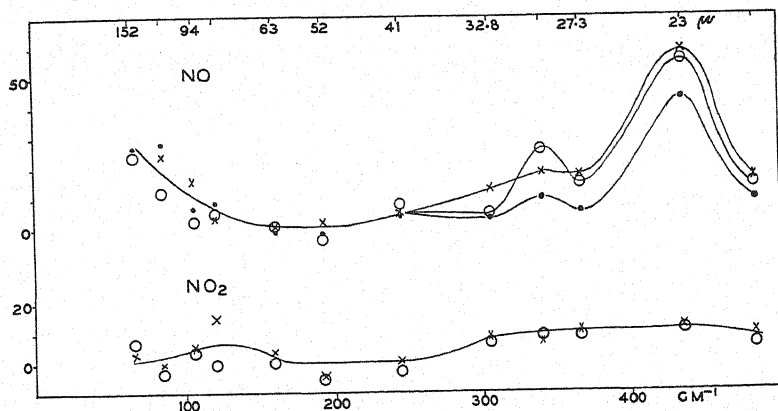


Fig. 6.

ments do not agree very well. The band beginning at 94μ , however, is certainly pure rotation band of nitric oxide and agrees very well with the calculated band with the maximum of absorption at about 50 cm^{-1} . The fundamental band of nitric oxide has been located at $5.30\mu^{17}$ and hence the bands at 29.4μ and at 23μ are probably bands of nitrogen trioxide or of other higher oxides of nitrogen.

Nitrogen peroxide

Nitrogen peroxide seems to show two maxima of absorption (see Fig. 6). Not so much is known about the structure of this molecule and, further, the matter is complicated by the presence of nitrogen tetroxide.

Methyl iodide

Within our experimental error, methyl iodide does not show any absorption in the region investigated. The molecule should have the structure of a symmetrical top, and hence a permanent electric moment lying along the axis of symmetry. The absence of absorption in our region indicates that the moment of inertia I_A of this molecule is so large that its pure rotation band lies entirely beyond 152μ or at least 117μ . The lower limit of I_A in order to show absorption at 152μ is about $25 \times 10^{-40}\text{ g cm}^2$, assuming that when $j=30$, the intensity of absorption becomes negligible.

¹⁷ Snow, Rawlins and Radeal, Proc. Roy. Soc. London [A] 124, 453 (1929).

Chloroform

This compound has absorption bands with maxima near 52μ and 94μ (Fig. 7). This band is probably one of the vibration bands of chloroform, be-

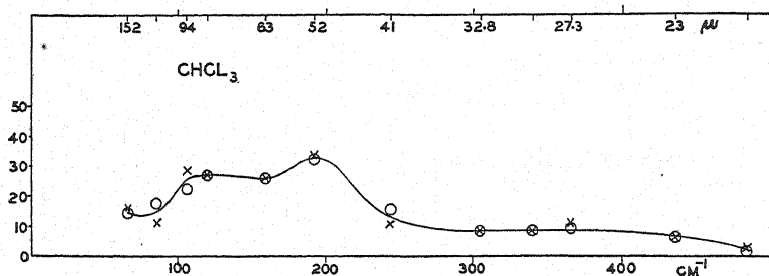


Fig. 7.

cause this compound should have the structure of a symmetrical top with so large a moment of inertia I_A that its pure rotation band would fall outside of the region we investigated.

Water

Fig. 8 gives the results of two series of experiments. There appear two maxima of absorption, one at 94μ and the other 52μ . In this case, the cells were filled with air saturated with water vapor at 19°C .

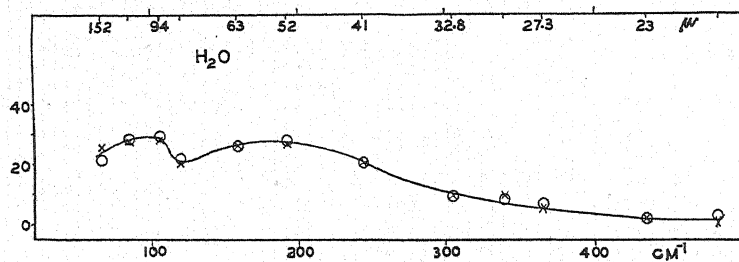


Fig. 8.

Hydrogen sulphide

The experiment with hydrogen sulphide was carried out without calibration of the empty cell (Fig. 9).

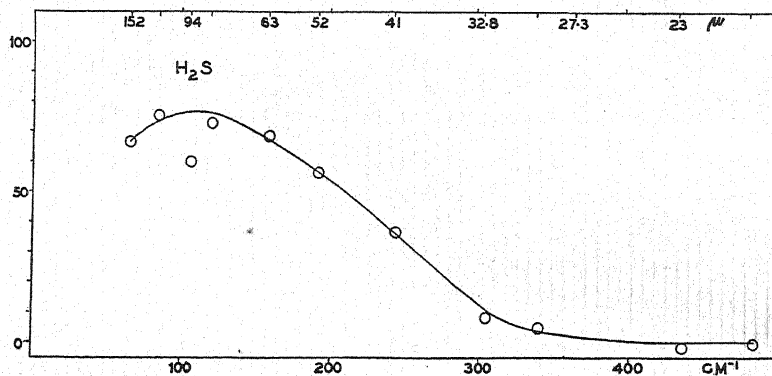


Fig. 9.

Sulphur dioxide

This compound has very strong absorption bands in the region of the spectrum investigated. In Fig. 10 the results of three series of experiments are shown. The circles represent the data obtained at the earlier period of our in-

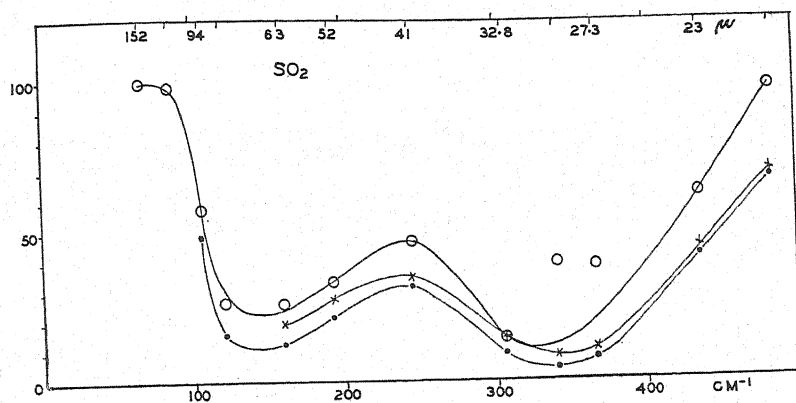


Fig. 10.

vestigation, when the empty cells were not calibrated, while the crosses and solid dots give the results of the experiments carried out with the calibration of the empty cells. Except for two points of the first series of experiments, all the data fall on the smooth curves which have the same positions of the

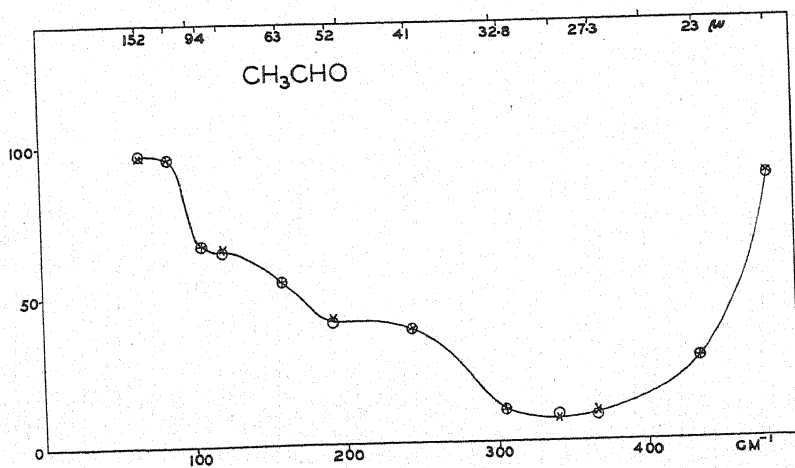


Fig. 11.

maxima and minima of absorption. The approximately parallel displacements of these curves show different values of the absolute percentage of absorption, which resulted from the different conditions obtained in the absorption cells.

DISCUSSION OF THE RESTSTRAHLEN TECHNIQUE

Fig. 12 gives the absorption of a cell filled with CS_2 vapor. This result is in agreement with a previous investigation for a 4-inch rather than a 12-inch radiation path. The absorption of CS_2 is given by the one point at 23μ . The absorption at other wave-lengths is due to the paraffin on the cell windows. This result, if we interpret the data as indicating a band for CS_2 at 23μ , is not in very good agreement with the grating data of Dennison and Wright.⁹ They find three maxima midway between the 23 and 27.3μ reststrahlen. Also their absorption is strong while that observed by the reststrahlen method is relatively weak.

This weakness of the reststrahlen technique, namely, that a band may occur between two of the points and be badly represented or possibly missed

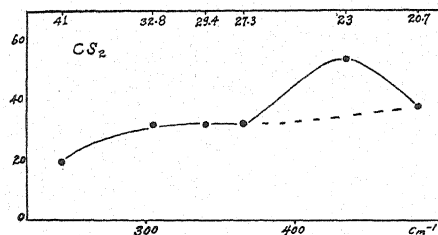


Fig. 12.

entirely, is only serious where the moment of inertia is large and consequently the absorption bands are narrow or where the spacing between the reststrahlen wave-lengths is large. Both conditions apply to CS_2 as it has a large moment of inertia and the gap between 23 and 27.3μ is the largest gap in the region investigated.

Because the prism technique (using KBr and KI prisms) may now be applied to 40μ , the usefulness of the reststrahlen technique will probably be confined to wave-lengths greater than 40μ . Between 40 and 152μ there are 20 reststrahlen bands available as compared with the 7 which were actually used in this investigation. When these are used together with the two bands at 218 and 343μ which are obtainable by the method of focal isolation, it can be said that the results are approaching the limit obtainable by other than the grating technique. There is, however, the possibility of applying the reflection characteristics of very rough surfaces to the isolation of wave-lengths greater than 343μ .

The Infrared Spectrum of H^2Cl

By J. D. HARDY,* E. F. BARKER AND D. M. DENNISON
University of Michigan

(Received August 29, 1932)

The fundamental absorption band due to HCl molecules involving the heavier isotope of hydrogen has been observed, using a cell 700 cm long with gas at atmospheric pressure. It lies in the region of 4.8μ . Both ordinary HCl and samples enriched in H^2 were examined. Nineteen lines have been measured in the band of H^2Cl^{36} , and seventeen in the band of H^2Cl^{37} . The estimated abundance of H^2 relative to H^1 is 1 to 35,000.

A satisfactory equation has been developed for the positions of these lines on the basis of measurements by Meyer and Levin upon the bands of H^1Cl , assuming identical dimensions and force fields for both molecules. The parameter ρ of this equation, representing the ratio of the reduced masses for H^2Cl and H^1Cl , has been adjusted to give the best agreement with the observed frequencies, and is found to be $\rho = 0.514430 \pm 0.000004$. Sources of error other than those involved in the observations are discussed, and an attempt is made to evaluate them. When these are taken into account, the values indicated for the mass of H^2 (on the scale $\text{H}^1 = 1.00778$ for the mass defect are: mass $\text{H}^2 = 2.01367 \pm 0.00010$, mass defect $= 0.00189 \pm 0.00010$. These values are compared with the results obtained by Bainbridge with the mass spectrograph.

§1

THE existence of a heavier isotope of hydrogen, recently discovered by Urey, Brickwedde and Murphy¹ suggests the search for band spectra due to molecules containing hydrogen nuclei, since the very large relative difference in mass between H^1 and H^2 must result in isotope displacements of correspondingly large frequency. Naturally the first substance to be chosen for such a study is HCl , both because of the simple character and accessible position of its fundamental band, and because its spectrum has already been investigated so thoroughly. A comparison of the bands due to H^1Cl and H^2Cl should yield a very reliable estimate of the relative abundance of the two species of hydrogen, and also provide a precise determination of the ratio between their masses.

§2

From the first reports of relative abundance it appeared that there should be little difficulty in locating the H^2Cl fundamental band without essential changes in the apparatus already in use. However, a careful examination of the region in which the band was expected, showed no trace of absorption lines in radiation which had traversed 30 cm of gas at atmospheric pressure. According to the data of Meyer and Levin this is more than 3000 times the minimum path length necessary for measurements upon the H^1Cl band at

* National Research Fellow.

¹ H. C. Urey, F. G. Brickwedde and G. M. Murphy, *Phys. Rev.* **40**, 1 (1932).

3.46 μ . The path length in HCl was then increased to seven meters, which would ensure the detection of the band even if H²Cl should be present only to the extent of one part in 10⁵ of H¹Cl. This was the maximum length which could be conveniently fitted into the room, and proved to be quite adequate for the purpose.

A plan of the optical system is shown in Fig. 1. The cell was constructed of galvanized iron tubing eight inches in diameter, and coated heavily inside with paraffin. The windows were of heavy mica, firmly cemented and clamped so as to withstand variations of pressure up to 40 mm of mercury. This was necessary to allow for changes of atmospheric pressure outside, and of gas pressure within the cell. Since it was not feasible to move this long cell into and out of the beam, measurements have been made only by comparing curves obtained with the cell filled with dry air and then with HCl. This procedure gives satisfactory results whenever the background is fairly clear, and fortunately the atmospheric absorption between 4.6 μ and 5.1 μ consists only of scattered narrow lines due to H₂O and possibly CO₂. The HCl gas was

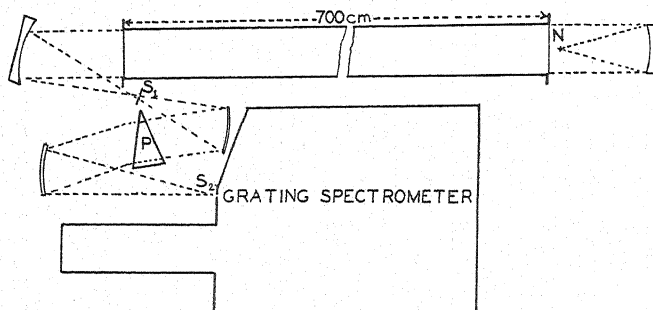


Fig. 1. Plan of spectrometer, fore prism and absorption cell.

at first obtained in the usual manner from sodium chloride and sulphuric acid, and allowed to flow directly from the generator into the cell, slowly displacing the air. In the samples thus prepared the first indications of a molecule of H²Cl were found. However the impurities in the salt developed a trace of CO which has a very strong absorption band in this same region, so that many of the H²Cl lines were completely hidden. This difficulty was eliminated by generating the HCl from distilled water which was dropped slowly upon pure phosphorus pentachloride. As the gas evolved it was frozen out in a large trap cooled in liquid air, and then slowly evaporated into the cell, a small residue being discarded so that moisture and other impurities were effectively avoided. The air displaced from the cell was passed through a second trap immersed in liquid air to prevent the escape of HCl. After some hours the contents of this trap were distilled back into the cell by transferring the liquid air to the first trap. A number of repetitions of this process made it possible to bring the concentration of HCl in the tube up to about 96 percent. The gas pressure inside the cell was kept about 10 mm above that of the atmosphere because HCl slowly disappears due to chlorinization of the paraffin. A test

for purity was made each day before taking observations. This consisted in the removal of a small amount of gas from the tube into a flask which had first been evacuated. The flask was then immersed in liquid air to freeze out the HCl , and the concentration determined from the resulting change in pressure.

Professor Urey suggested to us that a somewhat enriched source of the heavier hydrogen could be obtained from the electrolytic residue taken from cells in which commercial hydrogen is made. A sample of this residue was very kindly sent to us by Dr. Rohrer of the Ohio Chemical Company. It was distilled in order to eliminate the rather large amount of alkali contained in it, and then used to generate the gas with which most of our observations were made. The resulting increase in intensity of absorption made the measurements both easier and more precise.

The source of radiation for this experiment was a Nernst glower which was mounted directly in front of the cell window and exactly at the focal point of a concave mirror of 15 cm aperture and one meter radius. Placing the source in this position caused a minimum of distortion of the image and a minimum loss of energy due to divergence of the beam as it passed through the cell. At the spectrometer end of the tube the radiation fell upon a second concave mirror and was brought to a focus on the slit of the fore-prism spectrometer. From this slit it was collimated, sent through a large rocksalt prism, and finally brought to a focus upon the first slit of the grating instrument. The salt prism satisfactorily separated the first order of 4.8μ from the second order of 2.4μ . As a test of the separation, readings were made by adjusting the prism with the grating set at 4.8μ for maximum deflection and at 2.4μ for minimum deflection. These measurements showed the spectrum at 4.8μ to be contaminated with about 18 percent of second and third order impurity. The amount of impurity in the spectrum is of importance only in determining the intensities of the lines.

The grating spectrometer was built by one of us and has been described in previous papers. The grating had 4800 lines to the inch and a ruled surface of 4×5 inches, and was designed for concentration of the energy in the region around 5μ ; its figure was found to be good and the lines it produced were very sharp. The calibration was carried out by means of the helium line at $10,830.32\text{\AA}$, in the third, fourth and fifth orders. These lines were very strong and sharp and their positions could be determined to half a second of arc. The temperature of the room during the entire experiment was kept constant to within a degree centigrade and no correction was needed for change in grating constant due to temperature.

Slit widths varying from 0.15 mm to 0.25 mm were used, most of the measurements being made with 0.2 mm slits. The spectral range across the slit was then 9\AA or 0.4 cm^{-1} . The corresponding deflections were about 60 cm with the seven meter cell. The steadiness of the detecting system was such that readings could usually be repeated to within one percent. The detecting device consisted of a single junction thermocouple connected to a Leeds and Northrup H.S. galvanometer, which in turn actuated a Pfund amplifier, so

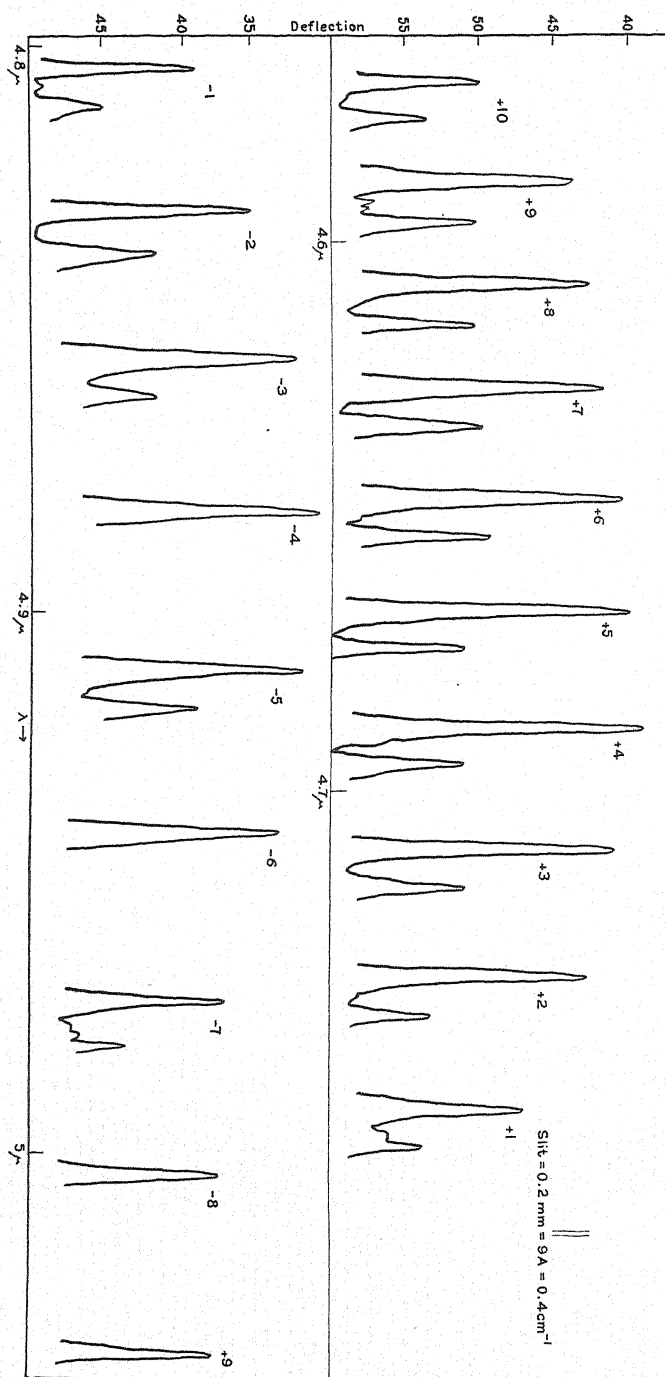


Fig. 2. The H_2Cl fundamental band. Positive branch above, negative branch below.

that the final deflections were about seven hundred times as large as would have been observed upon the first galvanometer at one meter.

In order to estimate the effectiveness of the instrument with the long cell, the lines of the band due to H^1Cl were observed as far out as possible on the negative branch. The faintest line that could be measured was the weaker component of -16 . The ratio between its intensity and that of the strongest line ($+3$) is approximately 1:270,000. The positions of the major components of lines -14 and -15 were determined carefully, and found to

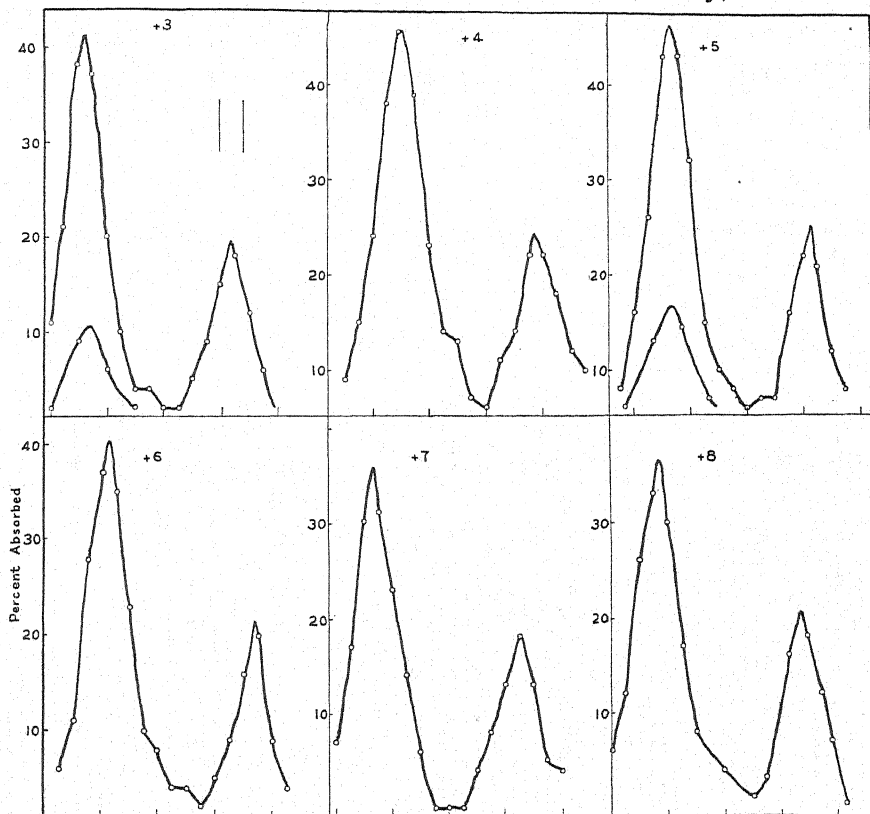


Fig. 3. Six lines of the positive branch in detail. Divisions on the horizontal scale are minutes, and correspond approximately to wave numbers.

be 2544.10 cm^{-1} and 2516.07 cm^{-1} respectively, while the corresponding values, computed by extrapolating the series of Meyer and Levin, are 2544.11 and 2516.03 . This agreement is particularly gratifying since their observations were made upon a different instrument, with a different grating, and calibrated in terms of the Hg line $\lambda 1.014$.

A survey of the background was made with dry air in the cell, to determine the positions and intensities of the atmospheric absorption lines, and this was followed by a similar set of observations upon HCl , other conditions being kept as nearly the same as possible. The absorption lines due to H^2Cl^{35} were unmistakable. Nineteen lines of easily measurable intensity were found

in which no serious distortion due to background appeared. In most cases the weaker component due to H^2Cl^{37} could also be observed. Fig. 2 is a plot of the entire band as measured with the seven meter cell filled with gas from the electrolytic residue. Galvanometer deflections are plotted against wavelengths, and atmospheric absorption lines have been omitted. A few of the weaker component lines on the negative side are absent because they were hidden or so badly distorted that their positions could not be determined satisfactorily.

After these lines had been located each one was remeasured with care, its contour being determined by at least five or six points taken at fifteen-second intervals on the circle. A few of the lines were measured several times as a test of consistency and it was found that their positions could be reproduced to within about two seconds of arc, which corresponds to $\pm 0.02 \text{ cm}^{-1}$. It seems safe to assume an experimental accuracy of about $\pm 0.05 \text{ cm}^{-1}$ across the whole band. In Fig. 3 are shown several lines of the positive branch plotted in detail. To arrive at an estimate of the percent absorption the undisturbed background was assumed to be completely transparent, and all the other readings on a line reduced to the same scale. Corrections were made for spectrum impurities due to slight overlapping of higher orders.

The absorption curves for the unenriched sample provide a means of determining the relative abundance of H^2 and H^1 . Since the absorption percentages are not very large, and the resolution is high, there is no considerable error in assuming that the area under any line is proportional to the integral of the absorption coefficient over the line. Thus the relative path lengths necessary for equal intensities of absorption may be determined for any pair of lines. The differences in transition probabilities must be taken into account, and also the differences in population of the various rotation states, since both the amplitude of vibration and the Boltzmann factor depend upon the reduced mass. Computations upon this basis indicate that H^2Cl is present in the ordinary gas in a concentration of about one part in 35,000 of H^1Cl and that the enriched sample has a concentration about ten times as great.

In determining the frequencies of the various lines it is necessary to correct for the index of refraction of air, the values of which were obtained from the work of M. Rusch.² His data indicate that $n-1 = 28.9 \times 10^{-5}$ is probably a satisfactory value for both the 3.5μ and 5μ regions. This correction is slightly different from the one used by Meyer and Levin, but the difference has been taken into account in comparing our results with theirs. Table I shows the observed frequencies reduced to vacuum for the nineteen lines in the H^2Cl^{35} band. These are compared with a set of computed values, and the differences, column 4, lie for the most part within the limit of observational error. Instead of listing the frequencies of the minor components due to absorption by H^2Cl^{37} , the table indicates in column 5 their displacements from the corresponding major components. These displacements have also been calculated, and the differences are shown in column 7. The formulae by which the calculated values were derived is discussed in §3. A few of the

² M. Rusch, Ann. d. Physik 70, 373 (1923).

TABLE I.

Line	Frequencies		Dif.	Isotope separations		Dif.
	Obs.	Calc.		Obs.	Calc.	
-9	1986.07	1986.11	+0.04	2.76	2.68	-0.08
-8	1998.53	1998.56	+0.03			
-7	2010.76	2010.82	+0.06	3.04	2.76	-0.28
-6	2022.85	2022.87	+0.02	2.91	2.79	-0.12
-5	2034.73	2034.72	-0.01	2.88	2.83	-0.05
-4	2046.38	2046.36	-0.02			
-3	2057.79	2057.78	-0.01	2.93	2.91	-0.02
-2	2068.95	2069.00	+0.05	3.13	2.94	-0.07
-1	2079.98	2080.00	+0.02	3.04	2.97	-0.07
+1	2101.28	2101.33	+0.05	3.04	3.03	-0.01
+2	2111.69	2111.65	-0.04	3.06	3.06	0.00
+3	2121.81	2121.75	-0.06	3.10	3.09	-0.01
+4	2131.62	2131.62	0.00	3.12	3.11	-0.01
+5	2141.29	2141.24	-0.05	3.15	3.15	0.00
+6	2150.64	2150.63	-0.01	3.19	3.17	-0.02
+7	2159.81	2159.78	-0.03	3.22	3.20	-0.02
+8	2168.66	2168.67	+0.01	3.29	3.22	-0.07
+9	2177.34	2177.32	-0.02	3.19	3.24	+0.05
+10	2185.74	2185.72	-0.02	3.24	3.26	+0.02

residuals in column 8 are larger than the error in observation, and these, as well as the larger ones in column 4, are probably due to displacements resulting from blends with weak atmospheric lines. The measurements on the minor components are probably also somewhat less accurate.

§3

The first step in comparing the infrared bands of H^1Cl and H^2Cl , and eventually in obtaining the ratio of the masses of H^1 and H^2 , is to assume that the force fields and dimensions of the two molecules are identical. This assumption appears to be fully justified both on theoretical and experimental grounds. From the theoretical side, the principal difference which might occur would be caused by a difference in the spins of the two hydrogen nuclei. The normal electronic state of HCl is a Σ state and consequently the nuclear spin of the hydrogen would be coupled with the nuclear spin of the chlorine and with the field produced by the rotation of the molecule. In either case the coupling energy is so extremely minute that the change in the energy states or in the force field would be quite too small to be measurable by spectroscopic means. From the experimental side the assumption is justified by the fact that all the band spectrum measurements on molecules containing isotope nuclei may be consistently correlated when the force fields in the molecules are taken to be identical.

The second step in the analysis is to show how the bands of H^1Cl and H^2Cl are to be related. To do this we use the equation developed by Fues³

³ E. Fues, Ann. d. Physik 80, 367 (1926).

for the energy levels of a rotating dipole. The frequencies of the lines of the fundamental band are given by the expression,

$$\begin{aligned} \nu = & (\nu_0 - hC/4\pi^2I - \nu_0B/4) \\ & + (h/4\pi^2I - 2\nu_0B - hk^2/8\pi^2I)J \\ & - \nu_0BJ^2 - hk^2J^3/2\pi^2I. \end{aligned} \quad (1)$$

The constant ν_0 varies as $\mu^{-1/2}$, I as μ^1 , k^2 as μ^{-1} and ν_0B as $\mu^{-3/2}$ where μ is the reduced mass of the system. The constant C is independent of μ .

These constants which determine the positions of the infrared lines have been very accurately deduced by Colby⁴ from the measurements by Meyer and Levin.⁵ Their values, slightly modified on account of the difference in the factor used for reduction of the wave-lengths to vacuum are as follows: $\nu_0 = 2989.24 \text{ cm}^{-1}$; $\nu_0B = 0.3030$; $h/4\pi^2I = 21.1678$, $hk^2/4\pi^2I = 0.00106$; $hC/4\pi^2I = 103.40$.

If the ratio of the reduced mass of H^1Cl to the reduced mass of H^2Cl is called ρ , the equation for the lines of the fundamental band of H^2Cl may be written,

$$\begin{aligned} \nu = & (2989.24\rho^{1/2} - 103.40\rho - 0.076\rho^{3/2}) \\ & + (21.1678\rho - 0.6060\rho^{3/2} - 0.0005\rho^2)J \\ & - 0.3030\rho^{3/2}J^2 - 0.0020\rho^2J^3. \end{aligned} \quad (2)$$

One of two courses may now be followed. The observed lines of H^2Cl may be expressed by means of an equation of the above type using a least squares solution, and the coefficients of J^0 , J , J^2 and J^3 equated to their corresponding theoretical values. Four independent values for ρ would thus be obtained, which should of course be consistent. However, the value determined from the constant term would be about ten times more accurate than that found from the coefficient of J , and the values obtained from the J^2 and J^3 terms would be still far less reliable.

A second procedure, and the one which was actually followed, is to choose a value of ρ and compute the corresponding positions of the lines. The positions so determined may then be compared with the frequencies of the nineteen observed lines. The differences between the observed and theoretical frequencies serve to fix a first order correction to ρ . Thus after a few approximations a value of ρ is obtained for which the sum of the residuals is zero. If all the residuals are within the experimental error and furthermore show no systematic trend, it is certain that a consistent method has been found for comparing the two bands.

The final equation (theoretical) which we obtain for the lines of the H^2Cl band is,

$$\nu = 2090.78 + 10.666J - 0.1118J^2 - 0.00056J^3. \quad (3)$$

This corresponds to a value of $\rho = 0.514430$.

The agreement between the observed and computed frequencies is shown in Table I and is very good indeed. The residuals are all very small,

⁴ W. F. Colby, Phys. Rev. **34**, 53 (1929).

⁵ C. F. Meyer and A. A. Levin, Phys. Rev. **34**, 44 (1929).

of the order of the experimental error and show no appreciable trend. The average value of these residuals divided by the square root of the number of observations is a measure of the probable error in fitting the theoretical equation. This again may be used to obtain the probable error in ρ . We find that $\rho = 0.514430 \pm 0.000004$.

The method of deriving the mass of the H^2 nucleus from ρ requires an additional assumption concerning the nature of the vibratory motion of the HCl molecule. (The validity of this assumption will be discussed in §4.) The reduced mass μ is in first approximation equal to $mM/(M+m)$ where m and M are the masses of the two nuclei. In higher order of approximation the motion of the electrons during the vibration must also be accounted for. μ might still be set equal to $mM/M+m$ where m and M now represent effective masses of the nuclei. The magnitude of the permanent electric moment of HCl shows that the electrons may be thought of as having a distribution such that the electronic charge about the H nucleus is on the average $\frac{4}{5}$ of an electron and that about the Cl nucleus is $17 + \frac{1}{5}$ electrons. The intensity of the fundamental band shows that the effective moving charge to be associated with the vibrating dipole is that of $\frac{1}{5}$ electron.⁶

From these two data it seems natural to assume that the effective masses m and M should be set equal to the mass of a hydrogen atom minus one-fifth of an electron and the mass of a chlorine atom plus one-fifth of an electron.

Let m_1 and m_2 be the effective moving masses of H^1 and H^2 respectively, and let M be the effective mass of Cl . Then

$$\rho = \mu_1/\mu_2 = [m_1M(m_2 + M)]/[(m_1 + M)m_2M]$$

or

$$m_2 = m_1/[\rho - (m_1/M)(1 - \rho)].$$

In mass units the mass of an H^1 atom is 1.00778 and that of an electron is 0.00055. Thus

$$m_1 = 1.00778 - 0.00011 = 1.00767$$

$$M = 34.983 + 0.00011 = 34.983.$$

On substituting these values, together with the observed value of ρ we obtain, $m_2 = 2.01356 \pm 0.00002$.

The mass of an H^2 atom referred to H^1 is therefore $m_2 + \frac{1}{5}$ electron or, $\text{H}^2 = 2.01367 \pm 0.00002$.

The mass of an H^2 nucleus is, $\text{H}^{2+} = 2.01312 \pm 0.00002$, and the mass defect is $\text{H}^{2+} - (\text{H}^1 + \text{H}^{1+}) = -0.00189 \pm 0.00002$.

Before proceeding to a discussion of the errors involved in our determination of the mass of the H^2 atom, it will be remarked that the satellite lines shown in Figs. 2 and 3 may be attributed to the molecule H^2Cl^{37} . The spacing of these satellites from the parent lines may be derived theoretically in a manner entirely similar to that used in finding the positions of the H^2Cl^{35} lines themselves. This difference may be expressed as a function of the line number J and has the following form (the contribution of the term cubic in J is here negligible), $(\text{H}^2\text{Cl}^{35}) - (\text{H}^2\text{Cl}^{37}) = 3.00 + 0.0311J - 0.00049J^2$.

⁶ D. M. Dennison, *Phys. Rev.* **31**, 503 (1928).

Table I contains a comparison of the measured and observed values of these displacements, and it is seen that the agreement is very satisfactory indeed. The residuals are somewhat larger than those of the lines of H^2Cl^{35} which is not surprising since the lines of H^2Cl^{37} are weaker and their positions are not as accurately determined.

§4

A probable error has been appended to the values for the mass of H^2 but this error represents merely the exactness of the agreement between the observed lines and positions computed from our formula. There are however other possible sources of error (systematic errors, errors in assumptions) which we will now discuss.

Our measurements are related to the constants derived by Colby from the data of Meyer and Levin. These observations were made on a different spectrometer using a different grating and the question of their accuracy becomes of great importance. Aside from the fact of the self-consistency of Meyer and Levin's data (i.e., the small residuals between the observed positions of the lines and the positions predicted by Colby's formula) we have one independent test of their accuracy. As mentioned earlier, two of the outer lines, -14 and -15, of the fundamental band of H^1Cl^{35} were measured on our spectrometer. These positions agree with the positions derived from Colby's equation to within the experimental error. This check insures that the calibration of both instruments was alike and furnishes a strong verification of the correctness of Colby's constants. The error which might be introduced from this source is therefore about equal to the probable error which we have given above.

A second possible source of error which must be investigated involves the range of validity of the Fues equation giving the energy of a rotating vibrator. An examination of this equation shows that the only term which might introduce an appreciable error is the constant term. The quantity ν_0 represents the zeroth order contribution to the frequency. The anharmonic part of the force function produces no effect in first approximation but in second approximation gives rise to the term $-\hbar C/4\pi^2 I$. It is to be expected that a fourth order perturbation would introduce a term, say $3D$, of which no account is taken in the Fues equation. Thus the energy of vibration could be written as a function of the vibrational quantum number v as follows;

$$W_v/\hbar = A + \nu_0 v - \hbar C v^2/8\pi^2 I + D v^3.$$

This new term would be important in the present investigation since, while ν_0 transforms as $\rho^{1/2}$ and $\hbar C/8\pi^2 I$ as ρ , D would transform as $\rho^{3/2}$. Since ν_0 is of the order 3000, and $\hbar C/8\pi^2 I$ of the order 50 we might expect D to be perhaps as large as 1. If this were the case the error in our determination of the mass of H^2 would be about 20 times as large as the probable error indicated. There are very good grounds for believing that this is not the case, however, and that D is much smaller than 1. In the first place the residuals shown in Table I are of the order of the experimental error and show no appreciable trend. This latter feature, the absence of trend, shows that the

constant and linear terms of Eq. (3) are consistent, or in other words that the constant and linear terms transform in the manner indicated in Eq. (2). Thus the general consistency of our results shows that D must be considerably smaller than 1.

It would be possible to determine the value of D if a sufficient number of the overtone bands of HCl were known experimentally. This is unfortunately not the case but such series are known for many diatomic molecules and it is found that D is always extremely small and in most cases may be set equal to zero. The success of the Morse⁷ potential function is largely due to this fact. In conclusion we estimate that the error introduced into the mass of H^2 from this cause cannot be of a larger order of magnitude than the probable error we have given.

Finally the assumption as to the magnitude of the effective moving masses m and M which enter the expression for μ must be considered. The effective inertia of the system depends not only upon the nuclear masses but also upon the masses of the electrons. The intensity of the fundamental band of HCl is consistent with the supposition that on the average $\frac{4}{5}$ of an electron moves with the H nucleus and $17\frac{1}{5}$ electrons move with the Cl nucleus. It seems reasonable therefore to assume that the effective moving mass m is equal to the mass of a hydrogen atom minus $\frac{1}{5}$ electron. In higher approximation this would be somewhat altered, perhaps by an amount of the order of $\frac{1}{5}$ the correction already introduced. This would mean that the error introduced would be about 0.00002 mass units, i.e., the same order as the probable error.

It has been shown that in addition to the probable error derived from the residuals of Table I, there are three independent sources of possible error, all of this same order of magnitude. These possible errors cannot be evaluated in detail but we estimate that their combined effect would be very liberally covered by a factor of ± 0.00010 .

Our final values for the mass of an H^2 atom and of the mass defect in mass units ($0=16$) are therefore,

$$\text{H}^2 = 2.01367 \pm 0.00010$$

$$\text{Mass defect} = 0.00189 \pm 0.00010.$$

These values agree quite satisfactorily with the results obtained by Bainbridge⁸ using the mass spectrograph. He gives $\text{H}^2 = 2.01353 \pm 0.00006$ and mass defect $= 0.00203 \pm 0.00006$.

Note added in proof, September 26, 1932: It should perhaps be remarked that we have expressed our results relative to the mass of $\text{H}^1 = 1.00778$. If this value is in error by an amount ϵ , our value for H^2 would be in error by 2ϵ . However, in first order the mass defect is independent of any small error in the mass of H^1 . In a similar manner the result obtained by Bainbridge for the mass of H^2 is given relative to the mass of H^1 . Dr. Bainbridge has informed us that his probable error of 0.00006 must be increased to 0.00018 if his value of H^2 is referred to $0=16$ rather than to $\text{H}^1 = 1.00778$.

⁷ P. Morse, Phys. Rev. **34**, 57 (1929).

⁸ K. T. Bainbridge, Phys. Rev. **41**, 115 (1932); **42**, 1 (1932).

A Self-Recording Cosmic-Ray Electrometer and Depth-Ionization Curve

By J. M. BENADE
Forman Christian College, Lahore, India

(Received August 30, 1932)

A self-contained automatic recording electrometer connected to a collecting rod in a thin steel-walled ionization chamber was used to measure intensity of cosmic rays at various depths in Konsar Nag, Kashmir. The lake is about 280 ft. deep. Its surface is about 11,600 ft. above sea-level and its water is practically free from radioactive matter. The electrometer consists of two short parallel phosphor-bronze ribbons attached at one end only. Their divergence is recorded photographically at eight minute intervals, and at the end of each hour the fibers are automatically recharged. The temperature, depth, and position of the instrument with respect to the vertical, are also recorded along with electrometer deflections. The curve obtained corresponds to those of Millikan and Cameron to a depth of 50 meters but at greater depths it more closely parallels that of Regener. The slopes of these curves at any particular depth seem to depend upon the type of ionization chamber as well as upon the intensity of the cosmic radiation at that depth.

INTRODUCTION

IN ANY ionization chamber used to determine the intensity of penetrating radiation, at considerable depths under water, a relatively large amount of ionization must take place when the instrument is near the surface while being lowered or raised. If the electrometer is of a type in which the deflections must be read directly while the instrument is at the surface of the water, a considerable correction will have to be made in order to obtain the actual rates of ionization at any particular depth. The relative magnitude of this correction is independent of the sensitivity of the electrometer, if the natural leak, be negligible. These corrections can of course be made but a considerable amount of labor is involved which can be avoided by using a self-recording instrument.

In 1928-29 a completely automatic self-recording electrometer was designed and constructed; but unfortunately before any useful data were obtained the instrument was lost at the bottom of a deep mountain lake in Kashmir. A new instrument was, however, constructed with which, in the summer of 1931, the data for the curves shown in Fig. 4 were obtained.

APPARATUS

Fig. 1, drawn approximately to scale, shows the construction of this instrument. The ionization chamber is at one end of a thin-walled steel cylinder of which the volume is 7330 cc. This chamber contained air at a pressure of 11.94 atmospheres when at a temperature of 0°C. Into the center of this chamber projects the collecting wire, supported by an amber insulator. This

collecting wire together with the electrometer ribbons has an electrical capacity of 1.86 e.s.u. On the end of this collecting wire are fixed by means of very small clamps two parallel pieces of phosphor-bronze ribbon each about 8 mm in length. When uncharged the free ends of these ribbons stand about 0.1 mm apart and when charged to 125 volts they separate to a distance of nearly 1 mm. This corresponds to distances between the shadows on the photographic film of from 3 to 20 mm. It may be noted incidentally that phosphor-bronze ribbon or other fine metallic ribbon serves very nicely the purposes of the ordinary gold leaf electroscope, especially when used with a projection lantern, or with a reading microscope in which case it may be made very small. Such an electroscope has several advantages. It is easily made, may have very small capacity (only a fraction of a cm), can be mounted in any position, is quite rugged, and is portable.

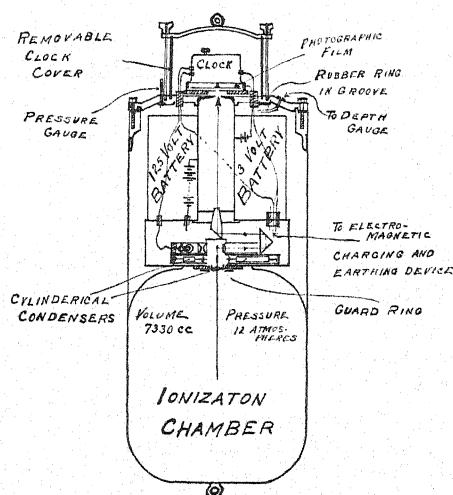


Fig. 1. Self-recording cosmic-ray electrometer. While in use the instrument floats under water with the ionization chamber upward.

On one side of the tips of the electrometer ribbons is mounted a small 2.5 volt lamp with condensing lenses and on the opposite side a $\frac{2}{3}$ in. microscope objective which together with two 90° prisms produces a well-defined shadow of the ribbons on a photographic film above. The film (6 cm in diameter) is mounted on a disk which in turn is mounted on a clock and makes one rotation in 12 hours. The photographic film rotates behind a narrow radial slit through which light enters for each exposure. By means of three separate circuits each controlled by the clock the electrometer is connected for an instant to a high potential battery through a protecting resistance at the beginning of every hour. The lamp lights up for about 2 seconds at eight minute intervals. At the end of an hour the electrometer is short circuited for a zero deflection record. The charging and discharging are done by means of electromagnetic devices mounted in a brass box which contains the electrometer ribbons and optical system as well as two large calcium chloride con-

tainers which open into the ionization chamber. In the next compartment are the batteries packed about a central brass tube through which the beam of light passes to the recording film. The upper end of the case is closed by a heavy steel plate bolted to a thick steel ring with a tongue and groove joint. To this ring is riveted the thin steel case. Above the cover plate are mounted the clock, pressure gauge, bimetallic thermometer, level and battery terminals. These are covered by a large cap which fits into a groove with a rubber gasket and is held in place by five bolts with knurled thumb-nuts. This cover is removed when an exposed film is to be removed and a fresh one inserted. There was never once any trace of leakage of water through this joint; and since the air pressure in the instrument was throughout much greater than the maximum water pressure outside there was no possibility of water leaking into the apparatus. In order to reduce the danger of insulation leakage a guard-ring was used with connecting wire leading into the clock chamber where it could be connected to the instrument case or to the H.T. battery at any one of three points so that it could be kept at zero potential, at 95 volts, 110 volts or 125 volts as desired. The charging device was so arranged that the collecting rod and electrometer fibers could be charged to any one of these three potentials, so that the guard-ring could if desired be kept at a potential higher than the initial potential on the electrometer. It was found that the rate of discharge of the electrometer at any particular depth was independent of the potential of the guard-ring indicating that the insulation leakage was negligible. The guard-ring was however normally kept at a potential of 110 volts. In order to measure the electrostatic capacity of the electrometer an adaptation of Millikan's method was used. For this purpose two cylindrical condensers exactly similar, except for length, were mounted symmetrically on opposite sides of the collecting wire near the insulator, so that by means of an external battery and the same electromagnetic devices used to charge and discharge the instrument, either one or the other of the condensers could be connected with the collecting rod. With a constant rate of ionization due to cosmic rays or a bit of radioactive material the time rates of discharge of the electrometer alone, and then when connected with the first condenser, and again when connected with the second condenser, enable one to calculate at once the capacity of the instrument provided of course the difference between the capacities of the condensers is known, and the connections are perfectly symmetrical. The capacity may be measured at any time without opening the case or in any way disturbing the instrument, the clock cover only being removed in order to connect the external battery to the terminals provided inside.

Fig. 2. shows typical films. At the outer end of each exposure will be seen the shadow of a small ball mounted on the end of a twisted piece of bronze ribbon and suspended so that while the instrument is in a vertical position the shadow will be in the center of a circular ring; whereas it falls to one side when the axis of the instrument is not vertical. The second film in Fig. 2. shows that a number of exposures were made while the instrument was not vertical. In about the middle of each exposure will be seen the two shadows

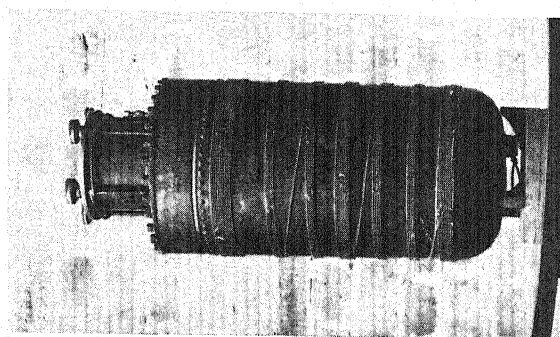
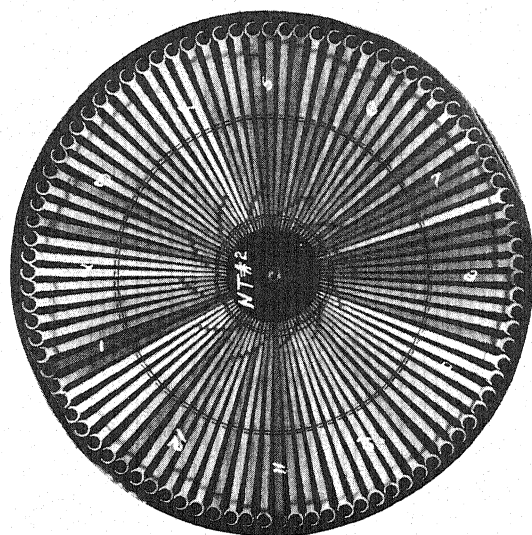
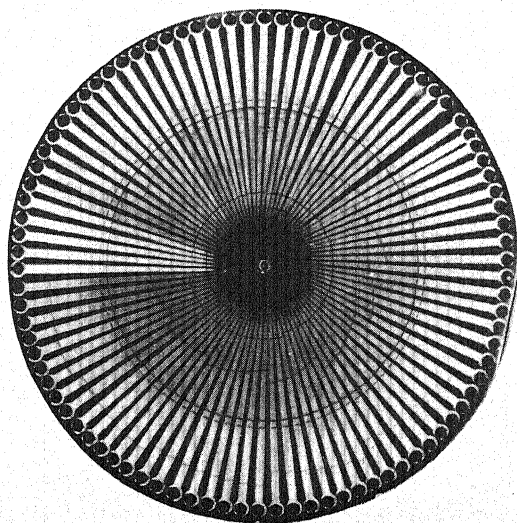


Fig. 2.



of the bimetallic thermometer, the distance between these shadows being a measure of the temperature. In Konsar Nag this thermometer was unnecessary for the temperature of the water was practically constant, there being large quantities of floating ice in the lake. In any case the temperature coefficient of the instrument used is known to be negligibly small. At the inner end of each exposure will be noticed two shadows, the separation between which is a measure of the depth of the instrument below the surface of water when the exposure was made. This proved to be very useful. The depth-gauge consists of the flattened curved tube of an ordinary steam-gauge mounted near the film so that a shadow of a thin wire attached to the free end of this tube falls on the photographic film. This tube communicates with the water (or air) outside the instrument and so as the instrument is submerged the increasing hydrostatic pressure causes the index-wire to move. Less distinct are the shadows of the electrometer ribbons; but they are sufficiently clear for accurate measurements of their separation by means of an especially mounted travelling microscope. All measurements of the developed films are made with this instrument. It was found in practice that small deviations of the axis of the instrument from the vertical do not introduce appreciable errors. However all records were obtained with the axis vertical, the ionization chamber being uppermost.

Calibration curves show that the electrometer deflections are very nearly proportional to the potential for a range of from 30 to 125 volts, the maximum used. As is to be expected the depth-gauge curve is also very nearly a straight line.

DATA

While in use the instrument was anchored to a sinker by a short bit of rope attached to the center of the clock cover. At the center of the other end was attached a small wooden float which helped to support the instrument in a vertical position with the ionization chamber uppermost at about 130 cm above the bottom of the lake. It was found that in one or two cases when the instrument was allowed to rest on the bottom of the lake the rate of ionization was appreciably increased presumably by gamma-radiation from the mud and rocks. Konsar Nag, the lake in which the instrument was used, is one of the larger high lakes of the Pir Panjal Range in Southern Kashmir. It is fed by snow and rain and has a number of large underground outlets so that it contains very little radioactive material. The lake is about one and a half miles long and about half as broad. Its bottom slopes steeply from the wider end to a depth of about 280 ft. As is usually found to be the case a large part of the bottom is nearly level. The maximum depth we found to be 285 ft. though the surface level varies considerably. During the ten days of our stay on its shore the level dropped about five feet and on the shore were clear indications that within the past few years the surface has risen to a level at least 25 ft. higher than that at the time of our visits in August 1929 and again in 1931.

In getting the desired data the electrometer was anchored at various depths ranging from a few inches to the maximum. A light wire chain,

marked off in ten-foot lengths, was attached to the sinker and served to give data for the calibration of the depth-gauge as well as to move the instrument from depth to depth and raise it to the boat in order to replace the exposed films. The electrometer was usually allowed to remain for three hours during the day-time in one position, and for longer periods during the cold nights for obvious reasons. This gave data for several curves at each depth, the mean of the slopes being taken as a measure of the rate of ionization for the corresponding depth. Since all ionization curves are plotted to the same scale, in order to get the number of ion pairs produced per cc of air at 0°C per atmosphere per second, it is only necessary to multiply the slope of the curve by a

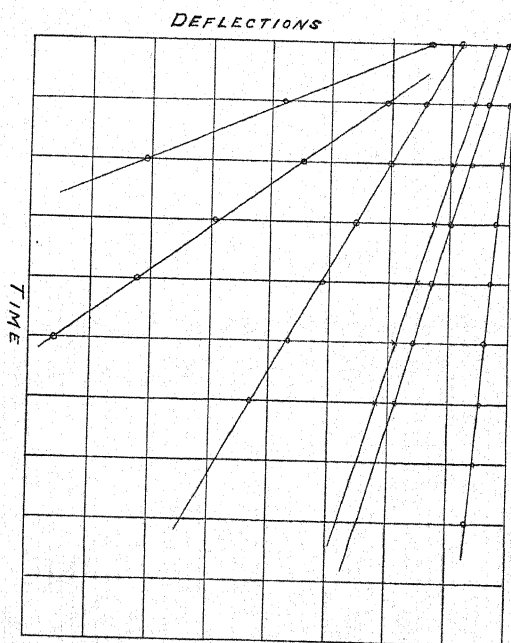


Fig. 3.

constant. This constant depends upon the electrostatic capacity of the collecting rod and electrometer fibers, sensitivity, quantity of air in the ionization chamber, the scale on which the curves are plotted and of course the charge on an ion.

It was feared that due to the rather large diameter of the ionization chamber and the low voltages to be used there might be a considerable amount of recombination. The fact that the ionization curves are for voltages higher than about 60 practically straight lines shows however that there is very little recombination taking place unless this occurs only immediately after ionization so that it is practically independent of the ionic drift velocities. If this be the case, as Millikan's results indicate that it is, then the fraction of ions lost by recombination should be independent of the number present

per cc at any instant. This is clearly indicated by the longer range curve obtained with the same instrument in other work to be reported later. Since all data used in the depth ionization curve correspond to electrometer potentials of 100 volts or more we can assume without appreciable error that we have complete saturation currents in the ionization chamber.

The residual ionization in the electrometer at a pressure of 11.94 atmospheres at 0°C is, as indicated by the lower end of the depth ionization curve, less than 0.18 ions per cc per second per atmosphere.

RESULTS

The result of the Konsar Nag work is shown in the heavy curve of Fig. 4 together with similar curves plotted to the same scale from data published by Regener and by Millikan and Cameron. It will be noticed that the curves are not exactly the same in form though they are similar in type. The data

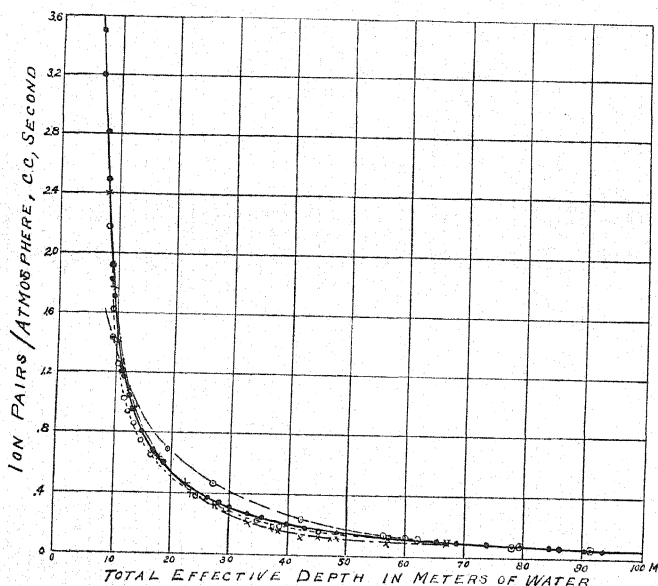


Fig. 4. Depth-ionization curve. Dashed curve with circles, Millikan and Cameron, 1931; dashed curve with crosses, Millikan and Cameron, 1928; dashed curve with dots in circles, Regener, 1930; curve with black dots, Benade, 1931.

for Millikan's and Cameron's two curves were obtained by electroscopes of similar type, the only difference being in the ionization chamber pressures. The ionization chamber used by the present writer has very much thinner steel walls (0.8 mm) but much larger volume and moderately low pressure (about 12 atmospheres of air). On the other hand Regener who used a larger heavy steel ionization chamber filled with CO_2 at a pressure of about 30 atmospheres, gets a curve with a very different slope in the upper portion. This seems to indicate that the exact form of the curve depends upon the

type of apparatus used in obtaining the data for the curve. This is not surprising in view of recent ideas about the cause of ionization in such instruments.

The Konsar Nag curve agrees very closely with that of the Regener at depths of sixty to ninety-three meters.

In conclusion the writer wishes gratefully to acknowledge a grant from the University of the Punjab to cover necessary travelling expenses to Konsar Nag and also the untiring assistance of his colleague Professor M. L. Joshi.

A High Voltage Direct Current Generator

By RICHARD E. VOLLRATH
University of Southern California, Los Angeles

(Received August 19, 1932)

When powdered materials are blown through metal tubes by means of compressed air considerable quantities of electricity are produced by contact electrification. It was found that 6×10^{-5} coulombs could be produced per gram of diatomaceous earth, a form of silica, blown through a short length of copper tube. A generator of extremely high voltage is proposed, and a small scale model of such a generator is described, by means of which currents of 8×10^{-5} amperes at 260 kilovolts were generated.

THIS work was undertaken to provide numerical data to serve as the basis for the design of a high voltage generator capable of generating a milli-ampere at voltages above a million.

THE PROPOSED GENERATOR

The discussion to follow will be simplified by a consideration of Fig. 1 which is a diagrammatic representation of the proposed high voltage generator. The small scale model constructed will be described later on.

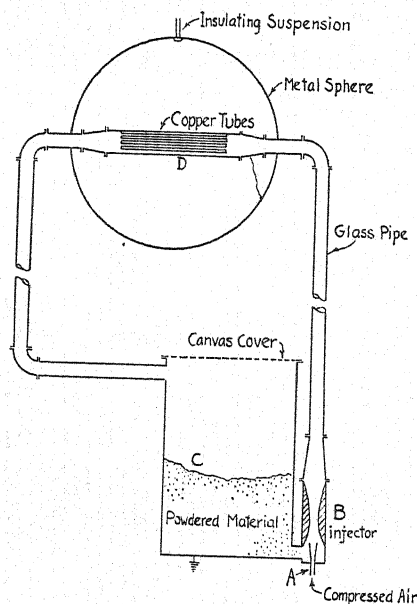


Fig. 1. Proposed high voltage generator.

A blast of compressed air is blown from a nozzle *A* into a suitably designed injector *B*. A powdered material *C* is sucked into the air stream by the action of the injector and carried along through glass or Bakelite pipe. The air laden

with the powdered material passes through a number of metal tubes *D* arranged in parallel within a large spherical conductor and electrically connected with it. The particles of powder become electrified by contact with the walls of the metal tubes. The charged particles are carried away from the sphere and returned to an earthed reservoir *C*. The potential of the sphere will rise until limited by corona discharge from its surface.

In order that one milliamperere can be drawn from the sphere, enough powder must be blown per second to produce a charge of 10^{-3} coulombs or 3×10^6 e.s.u. per second. It was the main purpose of this work to find out if such charges can be obtained from reasonably small quantities of powder. From an engineering standpoint quantities up to about 305 grams per second should be feasible since sand blast machines have been constructed capable of blowing this quantity of sand.

PREVIOUS WORK

It has been known for a long time that considerable charges are developed when particles of solids are blown over the surfaces of metals and other substances. Most of the work recorded in the literature gives no information as to the quantity of electricity produced in this manner by a given amount of material. However, the following brief resumé of the more pertinent articles showed that the charges obtainable were large enough to warrant further work along these lines.

According to Rudge¹ a few centigrams of flour blown into a large room produced a charged dust cloud whose potential as measured by a radium coated collector, or probe, was 200 volts. He pointed out that this and other results of a similar nature obtained by him accounted for potential gradients of 10,000 volts per meter observed during dust storms, and for lightening flashes occurring during the eruption of ashes from volcanoes.

Petri observed that a steel telegraph wire 5 kilometers long became electrically charged during a violent snowstorm. A continuous stream of sparks several millimeters long could be drawn from the wire; and Petri estimated the electrical power generated to be 1.2 horsepower. The effect has been attributed by Ebert and Hoffmann² to contact electrification of the snow blown over the wire by the wind.

A similar observation is recorded by Stäger³ who exposed a wire 9 meters in length to the driving snow during a snowstorm. There was a distinct corona discharge around the wire and a current of 17 to 20 milliamperes could be drawn from it. In this case the power generated was estimated to be 3 watts. Stäger in the same article gave the charge carried away by hoarfrost blown from a surface of ice. Under particularly favorable circumstances it amounted to 1000 e.s.u. per gram of hoarfrost. He also mentions the appearance of a corona discharge 10 cm long during the production of carbon dioxide snow by rapid evaporation of liquid carbon dioxide escaping from a tank.

¹ W. A. Douglas Rudge, Proc. Roy. Soc. London A90, 256 (1914).

² Ebert and Hoffman, Meteor. Zeits. 317 (1900).

³ A. Stäger, Ann. d. Physik 77, 230 (1925).

It is quite likely that the tremendous voltages produced in the Alps, and lately used in attempts to operate large x-ray tubes are generated by the electrification of snow blown over the ice covered peaks.

THEORETICAL LIMITATIONS

In pursuing this work the writer adopted the views of Helmholtz on frictional electricity. According to these, so-called frictional electricity is developed whenever two dissimilar surfaces are brought into contact and then separated. A double layer of charges, whose magnitude is determined by the contact difference of potential between the two surfaces, forms at the surface of contact—one charge residing on one surface and an opposite charge on the other. When the two surfaces are separated the charges of the double layer are torn apart, and a charge remains attached to one surface while the other carries with it a like charge but of opposite sign. A contact of very short duration of two insulators followed by their separation suffices to produce considerable charges, which indicates that the double layer does not penetrate very far into the body of the insulators in contact. The thickness of such double layers has been estimated to be of the order of 10^{-8} to 10^{-7} cm. From this it is evident that in order to produce large charges by contact electrification large surfaces of contact are the main consideration. This immediately suggests that at least one of the two substances brought into contact should be in a finely divided state so as to present a large surface. In this case the charges are produced by blowing the finely divided material over a metal surface; for example, the powder is blown through a metal tube. When the particles strike the metal surface and leave it they acquire a charge which they carry with them as they move along with the air stream. An opposite charge remains on the metal which, if insulated, rises in potential as long as the powdered material is blown over it.

Leaving out of consideration corona discharges from the conductor, the ultimate potential which can be reached depends upon the mobility, k , of the charged particles leaving the conductor and the potential gradient, X , at the point where they leave. The charged particles to escape must be impelled by the air stream with a velocity greater than kX . The electrical image force between the particle and the conductor is considered negligible owing to the smallness of the particles under consideration. It can easily be shown that the above requirement imposes no serious limitation upon the potentials attainable, even though the particles should have to overcome the maximum gradient possible in air, about 30,000 volts per cm.

A charged particle of radius r in air will have a maximum mobility when it is carrying the maximum charge q permitted by the limiting gradient at its surface, that is, $q/r^2 = 30,000$ or $q = 100 r^2$ e.s.u. For particles of radius 10^{-4} , $q = 10^{-6}$. Consider 1 cc of material broken into approximately spherical particles 10^{-4} in radius, each charged with the maximum 10^{-6} e.s.u. The total charge carried by all the particles is

$$Q = 10^{-6} / [(4/3)\pi r^3] = -10^6/4.$$

According to this only 12 cc of material would be necessary per second to carry a milliampere. The same calculation for particles of radius 10^{-5} cm gives $10^{-7}/4$ e.s.u. per cc. However, owing to the fact that air in very thin films has a higher breakdown strength, the gradient at the surface can be higher allowing it to carry a larger charge.

It now remains to show that a particle charged to the above calculated maximum can be driven against a gradient of 30,000 volts per cm. This can be done by making use of some data obtained by Deutsch⁴ on the motion of charged particles in electric fields in connection with a study of the Cottrell process of precipitating dust from gases.

He found that particles of radius $r = 10^{-4}$, after having picked up a charge of 376 electrons $= 1.8 \times 10^{-7}$ e.s.u. in a corona discharge moved with a velocity of 0.56 cm/sec. in a field of 300 volts/cm. Particles of $r = 10^{-5}$ cm picked up a charge of 5×10^{-9} and moved with a velocity of 0.42 cm/sec. in the same field. If we assume that the mobility varies linearly with the charge on a particle, we can use these results to determine the velocity of a particle of $r = 10^{-4}$ cm and carrying the maximum charge (10^{-6} e.s.u.) in a field of 300 volts/cm. The velocity will be $v = (0.56 \times 10^{-6}) / (1.8 \times 10^{-7}) = 3$ cm per sec. For the case of particles of radius 10^{-5} the velocity is less than 0.42 because the calculated maximum charge turns out to be less than that observed by Deutsch. With the above velocity of 3 cm/sec. in a field of 300 volts/cm, a particle of $r = 10^{-4}$, carrying a charge of 10^{-6} placed in a field of 30,000 volts/cm would move with a velocity of 300 cm/sec. Now a particle of this size can easily be blown with a velocity ten times as great. Apparently there is no difficulty to be expected in blowing the charged particles away from a highly charged conductor.

EXPERIMENTAL

The following experimental method was used to find the powder most suitable for the purpose in view. Fig. 2 shows the experimental arrangement.

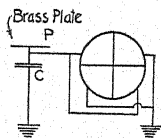


Fig. 2. Experimental arrangement for investigating powers for charges.

An insulated brass plate P was connected to one pair of quadrants of a Dolezalek electrometer and to a condenser c , as shown. One milligram of the powdered material to be investigated was placed on the brass plate, which was earthed and insulated before blowing off the powder with a puff of air. The magnitude of the charge produced was determined from the deflection of the electrometer and the capacity of the system. The powders were prepared by grinding various solids and sifting them through a 300-mesh sieve. This could not be done very well with metals which were used as obtained in the form of considerably coarser powders. The materials studied were mercuric

⁴ Deutsch, Ann. d. Physik 4, 824 (1930).

sulfide, mercuric iodide, sulfur, rosin, iron powder, antimony powder, clay, and diatomaceous earth, which is a form of silica occurring naturally in a very finely divided form.

The most promising materials were the metal powders and the diatomaceous earth. The metal powders could not be further investigated by the next method to be described because, owing to their great density, they could not readily be blown by the compressed air available. The diatomaceous earth turned out to be ideal for the purpose, not only because it gave such large

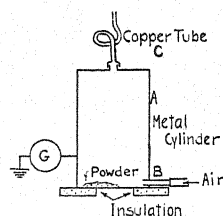


Fig. 3. Experimental arrangement for measuring charge obtainable from diatomaceous earth.

charges, but also because it is very light and easily blown. It consists of particles 10^{-4} cm in diameter and smaller, and it can be obtained commercially at 50 dollars a ton.

The diatomaceous earth was used in larger quantities in such a manner as to permit the charges produced to be measured on a galvanometer. It was placed in a metal cylinder *A*, Fig. 3, 12 cm diameter and 30 cm high from which it was blown by means of compressed air introduced tangentially at *B*. The air laden with the powder passed through a piece of copper tubing *C* having an inside diameter of 0.5 cm and a length of 20 cm. The cylinder, insulated by standing on blocks of paraffin, was connected to ground through a calibrated galvanometer which indicated the current flowing from the cylinder as the powder was being blown out. The measurements were made by placing 5

TABLE I. Charge obtained from 5 grams of diatomaceous earth blown by air flowing at rate of 1 liter/sec.

Time in min.	Current in amp. $\times 10^8$	Charge in coulombs $\times 10^8$	Time in min.	Current in amp. $\times 10^8$	Charge in coulombs $\times 10^8$
0.5	137.5	4125	8.0	16.5	495
1.0	96.3	2889	8.5	13.8	414
1.5	68.8	2064	9.0	10.5	315
2.0	55.0	1650	9.5	8.3	249
2.5	41.3	1239	10.0	5.5	165
3.0	41.3	1239	10.5	4.7	141
3.5	41.3	1239	11.0	3.9	117
4.0	57.8	1734	11.5	3.0	90
4.5	82.5	2475	12.0	2.8	84
5.0	82.5	2475	12.5	2.2	66
5.5	68.8	2064	13.0	1.9	57
6.0	63.3	1899	13.5	1.9	57
6.5	46.8	1404	14.0	1.4	42
7.0	35.8	1074	14.5	0.8	24
7.5	27.5	825			
			Total $30,696 \times 10^{-8}$ coulombs		
			or 6.1×10^{-5} coulombs/gram		

grams of the powder in the cylinder and blowing it out with air flowing at the rate of one liter per second. The current is read on the galvanometer until all the powder is gone. The current is a maximum at the beginning of a run and decreases gradually as the amount of powder blown out per second decreases during the progress of the run. Since the current fluctuated somewhat, an average current was estimated during each half minute interval. These averages are listed in the second column of Table I which gives the result of a typical run. It should be noted that the average current recorded for the first interval is really too low because the initial swinging of the galvanometer prevents the current from being read at all during the first 15 seconds, during which time the current is considerably higher. A small current could still be read after the air had passed for 15 minutes. This is due to the fact that a small amount of the powder clung to the inner surface of the cylinder from which it was gradually dislodged and blown out by the air. The charge obtained per gram of powder is for these reasons somewhat higher than that given at the end of the table. The total charge in coulombs obtained from 5 grams of powder was found by adding together the product of current in amperes and time in seconds for all the half minute intervals. The charge on the powder is negative.

The copper tube *C* in Fig. 3 was at first straight, and it was found that the total charge obtained increased about 25 percent by bending it as shown. This is probably caused by an increased number of particles striking the wall of the tube due to centrifugal force on them. No further charge was obtained by either lengthening or shortening the tube.

The charge given by 5 grams of powder reaches the surprising value of 3.07×10^{-4} coulombs or 6.14×10^{-5} coulombs per gram. According to this value only 16 grams would have to be blown per second to get a current of 1 milliampere. Altogether 20 such runs were made, giving results which deviated at the most 11 percent from those given in Table I. None of the vagaries, such as reversal of sign, usually associated with frictional electricity were ever observed. A few runs made with lower air velocities gave much lower results, ranging from 3.02×10^{-5} coulombs per gram for the lowest air velocity capable of carrying the dust out of the cylinder and up. This is believed to be due to the cohering of the particles of the powder. The individual particles are approximately 10^{-4} cm in diameter and smaller, but they cling together forming larger aggregates which are blown apart by the air stream, the more completely the higher the velocity. It seems likely that larger charges per gram might be obtained by using higher air velocities, but this point could not be proved because the air pressure available was limited to two atmospheres.

The diatomaceous earth used to obtain the above results contained 12 percent of adsorbed water. No difference resulted by using the powder dried at 300°C for 1 hour.

A small scale model of a high voltage generator using diatomaceous earth blown by air was constructed as shown in Fig. 4. In this figure, *A* represents an insulated sphere of spun copper 20 cm in diameter, within which 8 copper

tubes *B*, 0.5 cm inside diameter, were mounted. Compressed air introduced at *C* carried along with it diatomaceous earth introduced by a small screw conveyor *D* from a reservoir and blew it through the copper tubes. The charged powder left through a short length of glass tube and escaped into the air.

The potential of the sphere was estimated from the distance between it and a similar grounded sphere placed at such a distance from it that a thin spark jumped the air gap between them. The maximum potential reached

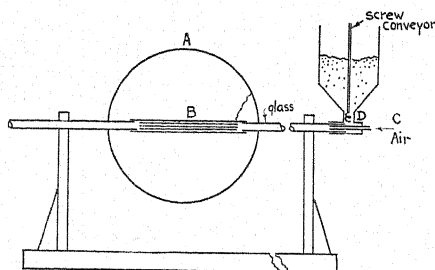


Fig. 4. Experimental high voltage generator.

seemed to be limited by a corona discharge from the sharp edges around the two openings in the sphere. The potential was estimated to be 260 kilovolts. A current of 8×10^{-5} amperes could be drawn from the sphere at this voltage by connecting it to ground through a glass tube filled with water and in series with a microammeter. The amount of powder introduced per second by the screw conveyor was 1.5 grams per sec.

In conclusion the writer wishes to thank Professor Millikan for very kindly placing the facilities of the California Institute of Technology at his disposal.

Magneto-Optic Rotation by Condenser Discharge¹

By FRANCIS G. SLACK AND WILLIAM M. BREAZEALE
Department of Physics, Vanderbilt University

(Received June 30, 1932)

The rotation of the plane of polarization of light produced by a condenser discharge across a spark gap has been measured when the condenser discharges through a coil surrounding various media of comparatively high Verdet constants. The set-up is similar to that used by Dr. Fred Allison except that a Lippich double field polarimeter replaces the crossed Nicols. The rotations have also been computed from the constants of the circuit, and curves show the agreement between calculated and experimental rotations to be good. Conclusions are drawn in regard to the relation of these measurements to the experiments of Allison.

THE recent experiments of Dr. Fred Allison and his collaborators² have attracted wide attention. The experiments here described were performed in an effort to throw more light on the physical phenomena involved in Allison's *Magneto-optic Method of Chemical Analysis*. The results to date appear to give some insight into the nature of the rotations involved. No attempt has been made to check the results reported by Allison, and except for some preliminary work in which definite "minima" were obtained for the "zero" reading of Allison's scale (CS_2 in both cells), the Nicol prisms were discarded in favor of a Lippich polarimeter in order that the net rotations caused by the alternating field might be observed in both magnitude and direction.

DESCRIPTION OF APPARATUS

Except for minor changes and the substitution of the half-shade polarimeter for the crossed Nicols the set-up is similar to that described by Allison.² Fig. 1 is a schematic diagram of connections. T is a Thordarson resonant spark transformer rated at 1 k.v.a., 25,000 volts maximum output at 110 volts primary. Current from the high side of this transformer is rectified by the G. E. Type KP-2 kenetron and charges the condenser C each sixtieth of a second. The condenser upon acquiring sufficient potential to break down the spark gap S , discharges through the coil L or L' and the resistance R and the inductance L'' . Light from the spark passes through the filter F and into the Lippich half-shade polarizer N_1N_2 , then traverses a path of about 10 cm in a material surrounded by the coil L , and thence to the analyzer N_3 . During such time as a current flows through the coil L a magnetic field is impressed on the material inside the coil and rotation of the plane of polarization of the light beam results (Faraday Effect). The average or net rotation may be measured

¹ F. G. Slack and W. M. Breazeale, Phys. Rev. 40, 1052A (1932).

² Fred Allison, Phys. Rev. 30, 66 (1927). Fred Allison and E. J. Murphy, J.A.C.S. 52, 3796 (1930). Fred Allison, Ind. and Eng. Chem. 4, 9 (1932). Fred Allison, Edna R. Bishop, Anna L. Sommer and J. H. Christensen, J.A.C.S. 54, 613 (1932). Fred Allison, Edna R. Bishop and Anna L. Sommer, J.A.C.S. 54, 616 (1932). Fred Allison, J. H. Christensen and George V. Waldo, Phys. Rev. 40, 1052A (1932).

by means of the analyzing Nicol N_3 . L' is a dummy coil provided to offer a path of equal impedance when L is cut out of the circuit for the purpose of taking zero settings on the polarimeter. L'' is ordinarily out of the circuit but is used when it is desired to obtain a variation in impedance by induc-

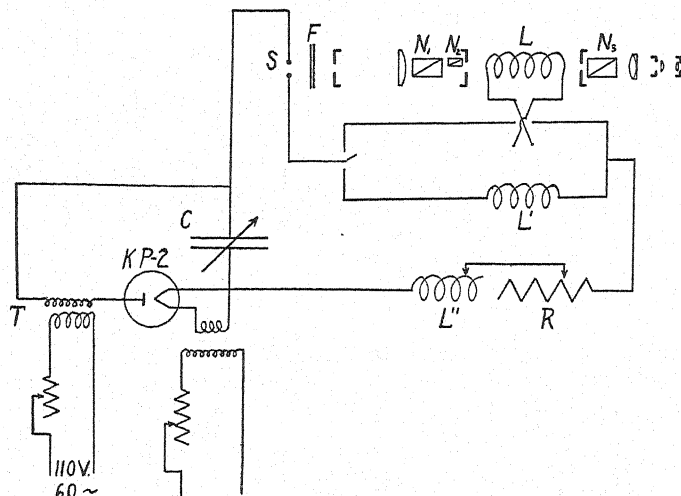


Fig. 1. Diagram of apparatus.

tance change. R is used to vary the resistance of the oscillating circuit and is also normally out of the circuit.

Occasionally it was desired to measure net rotations due to two coils operating in series or in parallel and with their fields acting on separate specimens to produce opposing or aiding rotations. Fig. 2 is a diagram of the par-

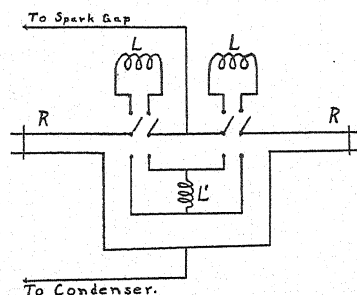


Fig. 2. Connections for two coils.

allel connections for this set-up. Two resistance trolleys R are then used, one in series with each coil. The rest of the apparatus is the same as shown in Fig. 1.

Some of the constants of the apparatus are as follows: For Fig. 1 the coils L and L' have 59 turns of No. 16 D.C.C. copper wire, are 12 cm long by 4.5 cm in diameter and measure 0.045 millihenries. The inductance coil L'' is wound with 325 turns of No. 18 D.C.C. wire and measures 0.66 mh. It is tapped at several points. The condenser C consists of 20 plates of glass 0.3 cm

thick covered with 25 cm squares of tin foil, giving a total capacity of 0.022 mfd. The capacity is varied by removal of the condenser plates. The resistance R consists of two straight wires stretched overhead and about 20 cm apart. The resistance is varied by a trolley which slides along on these wires. The wires are No. 25 chromel "C" ($6.85 \omega/\text{meter}$) and have a total length of about 16 meters, though somewhat longer ones have been used in obtaining some of the results reported herein. The material under test when a liquid (CS_2 normally) is contained in a glass cell 11.2 cm long and 2.5 cm in diameter, with thin cover glass ends sealed on with water glass. This cell is centered inside coil L . The spark gap, horizontally placed, has $\frac{1}{8}$ inch magnesium electrodes spaced from 0.25 to 0.30 cm apart. The filter F consists of Jena glass BG_4 plus GG_3 (each 2 mm) filters. These transmit principally the magnesium spark line 4481A and a small amount of the lines at 4703, 4391, and 3835A. Investigation by more complete filtering has shown that these faint lines do not affect the rotations. The polarimeter is a Schmidt and Haensch instrument with the Lippich half-shade polarizer giving a double field. The vernier may be read to 0.01 degree.

When the set-up in Fig. 2 is used it is necessary, due to the construction of the polarimeter, to use smaller coils and cells. In this case the active and dummy coils had 37 turns of No. 16 wire, measured 0.025 mh, and were 8 cm long by 4.5 cm in diameter. The glass cells used with these coils were 8 cm long and 2.5 cm in diameter. The rest of the apparatus was not changed.

In making all readings the procedure was first to make a zero setting on the polarimeter analyzer with the dummy coil L' in the circuit, then with coil L thrown into the circuit the oscillatory discharge of the condenser passes through the coil and produces a magnetic field which acts on the material in the cell. The plane of polarization of the light is rotated in accord with this field and a brightening of both polarimeter fields is observed, the brightening of one field being more pronounced. The analyzer is set to bring the two fields to equal brightness and the net rotation read from the scale. As recorded under "Results" such observations have been made for various circuit constants. The spark gap length and transformer primary voltage have been held approximately constant for the data given, the latter being about 60 volts, controlled by a series rheostat.

THEORY

Oscillations will normally exist in the discharge circuit, the frequency and damping depending on the constants of the circuit. Normally the oscillations are damped out after a few cycles. Examination of the spark in a rotating mirror, mounted on the shaft of a synchronous motor, shows that there are one or more trains of waves per cycle, the number depending on the primary voltage, the spark gap, and (to a lesser extent) on the circuit constants. Experiment shows the number of trains per cycle to have little or no effect on the rotations observed.

A relationship between the circuit constants and the rotations was derived as follows: First, the current-time curves for the oscillating circuit were plotted using the equation for damped sinusoidal oscillations;

$$i = [Ee^{-Rt/2L}/L(1/LC - R^2/4L^2)^{1/2}] \sin (1/LC - R^2/4L^2)^{1/2}t \quad (1)$$

where i is the current at any time t , and E is the initial voltage to which the condenser is charged. This assumes exponential damping which assumption was verified by cathode-ray oscilloscope observations.

The rotation was found to be proportional to the difference between the first and second current peaks (positive and negative, respectively). Fig. 3 shows the rotations due to the first peak, i_1 (positive), to the second peak i_2 (negative), and the net rotation, proportional to $i_1 - i_2$, obtained by subtracting the lower from the upper curve as the resistance R is varied. In calculating these curves the peak currents were computed assuming $E = 8000$ volts. A rheostat in the transformer primary reduced the secondary voltage to about this value, although the nature of the spark gap controls the breakdown potential.

The maximum value of the magnetic field is given by:

$$H = 0.4\pi ni \quad (2)$$

where n = No. turns per cm of the coil and i = peak current in amperes from Eq. (1). The rotation in degrees is equal to the field strength multiplied by Verdet's constant V and by the length of the cell, l : $\Theta = HVL = 0.4\pi nilV$.

Above about 90ω the circuit ceases to oscillate and hence the second peak does not exist. Here in calculating the currents Eq. (1) no longer holds and the following is used:

$$i = \frac{EC}{2} \left\{ \left[1 + \frac{R/2L}{(R^2/4L^2 - 1/LC)^{1/2}} \right] \left[-\frac{R}{2L} + \left(\frac{R^2}{4L^2} - \frac{1}{LC} \right)^{1/2} \right] e^{[-R/2L + (R^2/4L^2 - 1/LC)^{1/2}]t} + \left[1 - \frac{R/2L}{(R^2/4L^2 - 1/LC)^{1/2}} \right] \left[-\frac{R}{2L} - \left(\frac{R^2}{4L^2} - \frac{1}{LC} \right)^{1/2} \right] e^{[-R/2L - (R^2/4L^2 - 1/LC)^{1/2}]t} \right\}.$$

Since, in order to obtain agreement between calculated and observed curves of rotations as the resistance R is varied, it is necessary to shift the calculated curve approximately 2.5ω along the resistance axis, this value has been taken in all calculations as the resistance of the spark gap and circuit exclusive of the added resistance R .

The mechanical process causing the rotations appears to be as follows: Suppose the first half cycle of the current wave causes a clockwise rotation which causes a maximum brightness of the right-hand polarimeter field proportional to the first current peak. The second peak causes a counterclockwise rotation which brightens the left-hand field, but as the second peak is less than the first the increase in brightness of the left field is not so great as that of the right-hand field. Persistence of vision causes subsequent changes of the

field due to the rest of the wave train to pass unnoticed. This cycle repeats itself sixty times a second. Hence the first two peak currents determine the character of the observed fields. The net rotation is measured by setting the analyzer to bring the two fields to equal brightness.

RESULTS

Curves similar to the solid curve of Fig. 3 were computed for various circuit constants and compared with the experimentally-determined points. The experimental points are plotted as circles and Fig. 3 (curve 3) shows the agreement between calculated and measured rotations as R is varied. Fig. 4 shows the rotations as calculated (smooth curve) and as measured (plotted points) as a function of capacity change, R and L being held constant. Curves

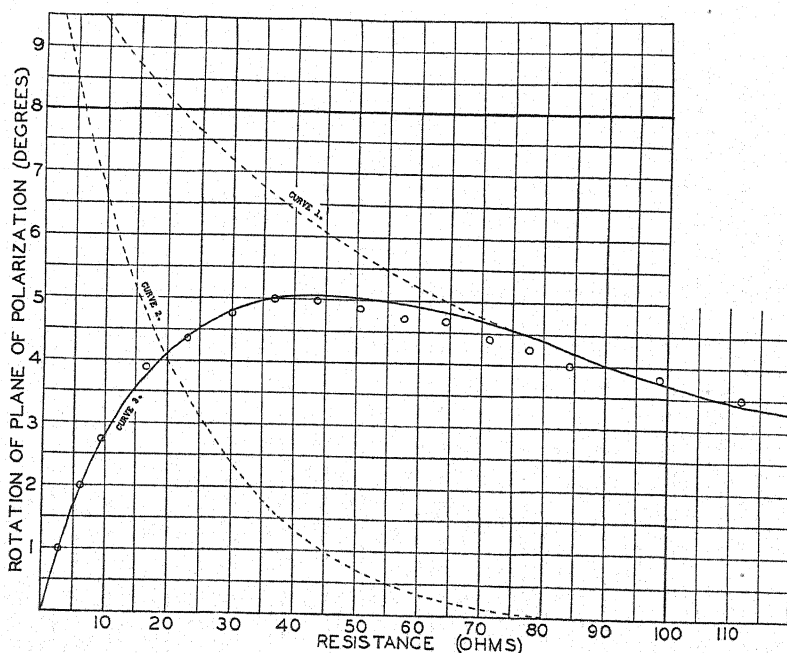


Fig. 3. Rotation-resistance curve. Curves 1 and 2, respectively, are calculated rotations due to first and second current peaks. Smooth curve 3 is difference between curve 1 and curve 2. 00000 experimental points. ($L=0.045$ mh; $C=0.022$ mfd.)

are shown for two different values of trolley resistance R , viz., $R=0$ and $R=7.5 \omega$. Fig. 5 shows the relations for these same values of R when C is held constant and L varied. The disagreement for the larger values of L in the curve for $R=0$ is probably due to a slight change in resistance of the spark gap at lower frequencies. It was necessary to correct for skin effect in the coil to obtain agreement at the high-frequency end of the curve. The agreement in the curve for $R=7.5 \omega$ is better since small changes in gap resistance do not have so much effect with a larger value of R .

As may be seen from the curves the experimental points show very fair agreement with the computed smooth curves. This indicates that the as-

sumption that the rotation is proportional to the difference between the first two peaks (positive and negative) is valid.

When two different materials are used in the two cells of Fig. 2 with opposite field directions cancellation of the rotation does not occur with equal

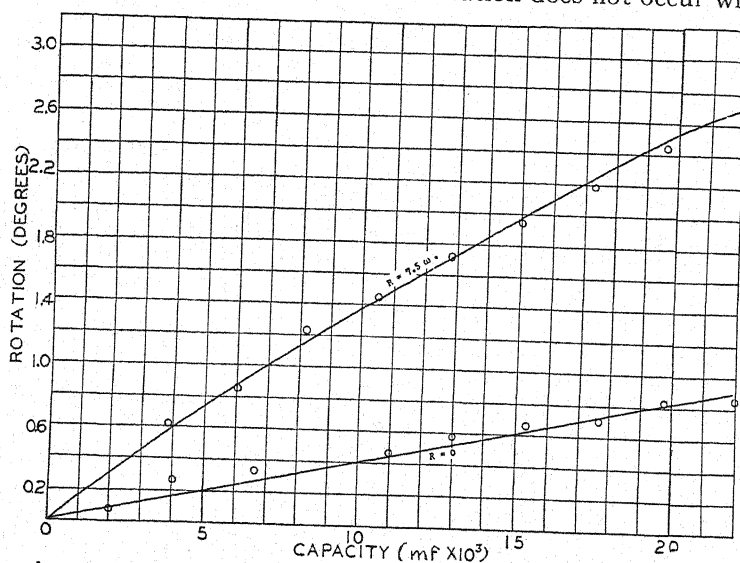


Fig. 4. Rotation-capacity curves. $L = 0.045$ mh; $R = 7.5\omega$ and $R = 0\omega$. Smooth curves calculated.

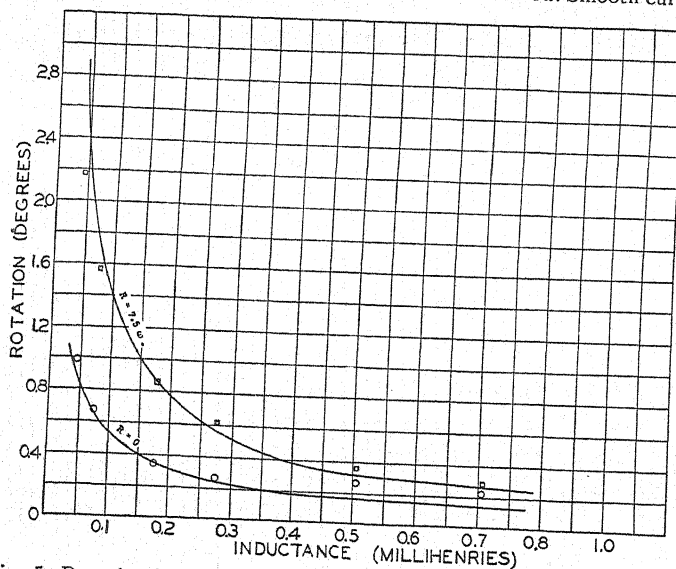


Fig. 5. Rotation-inductance curves. $C = 0.022$ mfd; $R = 7.5\omega$ and $R = 0\omega$. Smooth curves calculated.

resistances in each trolley. However, for any setting of one trolley a setting of the other may be found for which the net rotation is zero. This setting is independent of the direction of the fields of the two coils. It is different for different materials compared to the same standard. It is probable that calcu-

lation of the rotations as above, considering the parallel circuits and proper Verdet constants, would account for these readings and further work on this is contemplated.

No rotations could be observed when the light source was constant except when a synchronous rotating disk cut off the light while no discharge current was passing through the coil. Apparently the rotated part of the light was too small to be observable except in this case.

The cause of the asymmetrical rotations reported previously¹ has been found due to the unequal intensity of the two light beams after passage through the prisms of the Lippich polarizer. This difference does not affect readings when the rotation is constant but calculations show that it produces a difference of the order of magnitude of that found in the case of the oscillating rotations.³ The curves shown herein have not been corrected for this error since it would not appreciably affect the agreement between calculated and measured rotations.

CONCLUSION

The results of these experiments indicate that a polarimeter may be used to measure the magneto-optic rotations produced by a condenser discharge when the spark gap of the discharge circuit is used as light source. These rotations may also be calculated from the constants of the circuit so that fair agreement results.

In the case of different materials used in two cells zero readings were obtained by proper adjustment of trolley resistance. These readings could not be correlated with the time lags given by Allison² though this was hardly expected considering the high-resistance trolley here used. Change in length of a low-resistance trolley had no observable effect on the rotations measured. This leads to the conclusion that the polarimeter, in spite of its ability to measure the magnitude and direction of the rotations, is not so sensitive to time effects (change in length of wire path) as the crossed Nicols. With the Nicols any rotation of the plane of polarization of the light produces the same effect, that is a brightening of the single field. If two opposing fields are used it is thus necessary that they cancel each other at every instant in order to produce a minimum of light. For this to be the case the resultant time constants of the parallel paths of the discharge currents would need to be identical. These include the dielectric effect, Faraday effect time lag, Verdet constant, etc., for the materials. This would require the very sharp accurate settings for minima obtained by Allison, and as found by him would depend upon the properties of the material in the cells.

In conclusion, the authors wish to express thanks to Dr. Fred Allison for his kindness in demonstrating his apparatus upon several occasions and for supplying the details of his circuits. Thanks are also due to Mr. Wilson W. Woodcock, Jr. for assistance in the early stages of this work.

³ Thanks are due to Professor E. O. Lawrence and members of the Physics Department of the University of California for opportunity to check this work with a triple-field polarimeter resulting in the discovery of this difficulty. Especial thanks are due Dr. Harold Washburn for his assistance and suggestions.

ERRATA

Evidence of Space Quantization of Atoms upon Impact

By H. KUHN AND O. OLDENBERG

*Zweites Physikalisches Institut, Goettingen, and Physical
Research Laboratory, Harvard University*

(Phys. Rev. 41, 72, 1932)

Figs. 2, 3 and 4 in the above article are in the wrong order. The correct arrangement of these figures follows:

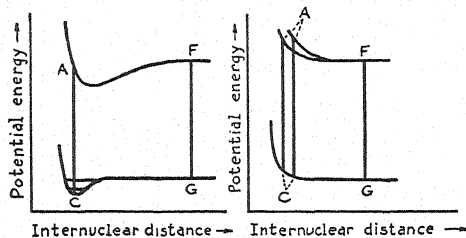


Fig. 2.

Fig. 3.

Fig. 2. Hypothetical band structure. *AC*, molecular band; *FG*, atomic line.

Fig. 3. Radiation during collision, *AC*; *FG*, atomic line.

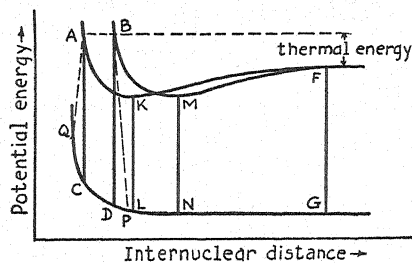


Fig. 4. Potential curves for the mercury and rare gas collision. *AC*, *BD*, diffuse maxima on the short wave-length side; *AQ*, *BP*, limits of the spectrum; *KL*, *MN*, band structure on the long wave-length side; *FG*, atomic line.

On the Relative Abundances of the Nitrogen and Oxygen Isotopes

By GEORGE M. MURPHY AND HAROLD C. UREY

Columbia University

(Phys. Rev. 41, 141, 1932)

On pages 141, 147 and 148 of the above paper on the relative abundances of the nitrogen and oxygen isotopes, the figures that we have given refer to the ratio $N^{14}O^{18}/N^{15}O^{16}$ and not to the inverse of this as we have stated.

LETTERS TO THE EDITOR

Prompt publication of brief reports of important discoveries in physics may be secured by addressing them to this department. Closing dates for this department are, for the first issue of the month, the twenty-eighth of the preceding month; for the second issue, the thirteenth of the month. The Board of Editors does not hold itself responsible for the opinions expressed by the correspondents.

On the Continuous Absorption Spectrum of Alkyl Iodides

A continuous absorption spectrum, without a neighboring band spectrum and a convergence limit, of a number (about forty) of alkyl halides was investigated in the region of the ultraviolet. The absorption spectra of these alkyl halides are entirely similar except that in the order chlorine, bromine and iodine compound the absorption regions are displaced towards the long wavelength side.

In the iodine compounds two or three absorption regions were found, in the other compounds only one region, undoubtedly for the reason that the analogous second or third

The long wave absorption of the iodine compounds corresponds to the decomposition into a normal alkyl residue and an iodine atom excited in the metastable state ($2^2P_{1/2}$). The second or third absorption region may correspond to the photochemical dissociation of the halides into a normal alkyl and a halogen atom excited higher than the metastable state, or into a slightly excited alkyl and an excited halogen atom ($2^2P_{1/2}$). Each difference $\nu_2(\text{max}) - \nu_1(\text{max})$ for various iodine compounds are given in the Table I. S. F. Evans¹ has recently analyzed the arc spectrum of iodine. According to the term scheme

TABLE I

	ν_1 (max) (cm^{-1})	ν_2 (max) (cm^{-1})	ν_3 (max) (cm^{-1})	ν_2 (max) - ν_1 (max) (cm^{-1})
$\text{C}_2\text{H}_5\text{I}$	34900	40600	45200	5700
$\text{C}_3\text{H}_7\text{I}$	37600	43500		5900
n- $\text{C}_4\text{H}_9\text{I}$	39800	45900		6100
iso- $\text{C}_4\text{H}_9\text{I}$	39700	47400		7700
n- $\text{C}_5\text{H}_{11}\text{I}$	39800	45400		5600
tert- $\text{C}_4\text{H}_9\text{I}$	37600	45400		7800
iso- $\text{C}_5\text{H}_{11}\text{I}$	39700	46900		7200
iso- $\text{C}_5\text{H}_{11}\text{I}$	39700	47200		7500

region were further in the ultraviolet than could be reached by the quartz spectrograph. Since the absorption regions shade off rather gradually on the long wave side and on the other side as well, where it can be observed, and since the apparent long wave limit shifts towards the red when the vapor pressure is increased, it is not possible to give any definite long wave absorption limit. So that, perforce, we must use in their stead either the observed limits of the pertinent absorption regions or, more conveniently in the present instance, the positions of the absorption maxima. The positions (ν) of the absorption maxima are given in Table I.

given by him, the possibility of states of excitation of the resultant iodine atoms higher than this metastable state may not be considered at the present moment. Therefore the excess energy may be ascribed to the alkyl residues. Details will be published in the Science Reports of the Tôhoku Imperial University, Japan, 21 (1932).

Y. HUKUMOTO

The Physical Institute,
Imperial University, Sendai, Japan,
September 7, 1932.

¹ S. F. Evans, Roy. Soc. Proc. A133, 417 (1931).

Emission Probability for a Colliding Atom

When mercury atoms are excited in the presence of a rare gas in addition to the resonance line a diffuse "band" with maxima is obtained in fluorescence. In order to explain the strong maxima it has been suggested^{1,2} that the collision process may lead to an "instantaneous" (i.e., short temporary) increase in the probability of emission. Now the probability of emission is connected with the line absorption by the equation $\int \alpha(\nu) d\nu = h\nu \cdot B_{12}/4\pi$ where B_{12} is the Einstein coefficient for emission and $\alpha(\nu)$ is the atomic absorption coefficient for radiation of frequency ν . The effect on the absorption of 2536 produced by argon has been investigated by Füchtbauer, Joos and Dinckelacker.³

¹ Kuhn and Oldenberg, Phys. Rev. 41, 72 (1932).

² Samson, Phys. Rev. 40, 957 (1932).

³ Füchtbauer, Joos and Dinckelacker, Ann. d. Physik 71, 204 (1923).

They find that $\int \alpha(\nu) d\nu$ is reduced slightly in the presence of the foreign gas (about 20 percent reduction for 50 atmospheres of argon). This means that the total probability of emission must also be reduced by collisions with the foreign gas.

This fact does not imply that an increase in the probability of emission at one stage of the collision process is impossible. It does require, however, that if such an increase exists there must be a larger decrease in the probability of emission at some other stage (or stages) of the collision process, so that the total probability for a colliding atom is less than for a completely free atom. The above rests, of course, on the assumption that the absorption experiments do really measure the complete $\int \alpha(\nu) d\nu$.

R. W. DITCHBURN

Trinity College, Dublin,
September 9, 1932.

Airplane Cosmic-Ray Intensity Measurements

The following is a preliminary report on certain cosmic-ray altitude-intensity measurements made with the use of airplanes. This work, begun in June of this year, was made possible through the cooperation of the United States Army Air Corps, and particularly through the kindness of Captain A. W. Stevens of this organization, who took an active interest in the project and assisted in making many of the observations. We are also greatly indebted to Lieutenants J. F. Phillips and C. D. McAllister who served as pilots on the various flights as well as to Major T. W. Blackburn of the Texas National Guard for the opportunity of making several preliminary flights here at Houston. The measurements were made at Wright Field, Dayton, Ohio, lat. 40° N, long. 84° W.

The airplane method was chosen on account of certain advantages over the customary methods. Over the balloon measurements it has the advantage that the altitude

can be maintained at a constant value while the measurement is being made. Over the mountain-top work it seems superior since troublesome corrections for local radiation do not have to be made. Not only can higher altitudes be reached but these can be attained much more quickly and conveniently than by scaling mountain peaks.

The measuring instrument is a Wulf-type closed electroscope patterned after those used by Millikan,¹ a type which seems best suited for use in airplanes. Its volume is 500 cc and it contains argon² at 75 atmospheres pressure. The case is made of steel and is about 1.3 cm in thickness. The volume was made small in order to allow lead shielding without excessive weight. Three shields were provided, the first two of thickness 1.3 cm each and a third outer shield of thickness 2.2 cm. It was found that over a suitable range of scale readings the rate of discharge was essentially linear with the time so that considerable gain in accuracy could be obtained by taking several (usually about eight) readings during one discharge. Most of the readings were taken visually though a few of the observations were made with a semi-automatic recording device.

The values which have been obtained up

¹ Millikan and Cameron, Phys. Rev. 37, 235 (1931).

² We are indebted to Professor A. H. Compton for the information that considerable gain in sensitivity can be obtained by the use of argon instead of air or nitrogen.

to the present are shown in Fig. 1. Curve 1 shows the rates of discharge with the electro-scope unshielded; curve 2, with 1.3 cm of lead shielding; curve 3, with 2.6 cm and curve 4 with 4.8 cm. The intensity has as yet only been obtained in arbitrary units on account of the difficulty of reducing our observed ionization in argon at 75 atmospheres to air at normal pressure. The intensity is

believed that the probable error of the individual points is about 3 percent. The values have been corrected for the "zero" of the electro-scope. This was obtained by measuring the rate of discharge with the various shieldings in a salt mine³ 700 feet underground. The "zero," or rate of discharge in absence of all radiation except that coming from the electro-scope itself, was thus found to be 3.5

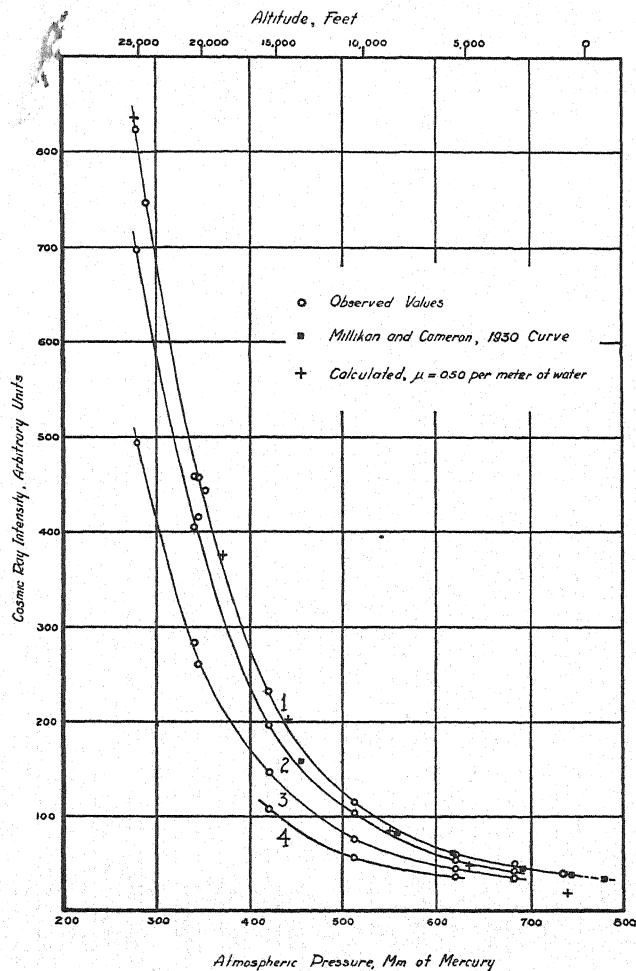


Fig. 1. Cosmic-ray altitude-intensity curve. Curve 1, electro-scope unshielded; curve 2, electro-scope inside 1.3 cm of lead; curve 3, with 2.6 cm lead; curve 4, with 4.8 cm lead.

referred to the rate of discharge produced by a small quantity of radium which could be accurately located at a distance of about 10 cm from the instrument. It was, however, found that the sensitivity remained practically the same for all the observations. It is

on the scale of the curves. In addition a cor-

³ We wish to thank Mr. J. E. Hanes, Superintendent of the Kler Mine of the Morton Salt Company at Grand Saline, Texas, for the opportunity of making these measurements.

rection of 1.2 has been made for the radioactivity of the airplane. That this correction is the above practically negligible value is due to the fact that all radioactive material (luminous paint) was carefully removed from the instruments. Had this not been done the necessary correction would have amounted to about 15 units and would have caused a serious loss of accuracy since we have found that it cannot be accurately determined.

For purpose of comparison the observations of Millikan and Cameron¹ have been indicated on the figure. Their values have been fitted to ours by putting one of their points (at 8.25 meters below the top of the atmosphere) on the curve. Our values are in good agreement with theirs taken in water below 8.25 meters but are somewhat above their values obtained with lead shielding the local radiation. This discrepancy may be due to difficulties involved in estimating the fraction of the cosmic rays getting through their shields. Evidence in favor of this view is obtained directly from the curves which show that our 4.8 cm shield, at the elevation of Millikan and Cameron's highest point, allowed the passage of 47 percent while for their 7.6 cm shield they found a transmission of 61 percent. This discrepancy seems to indicate that there are difficulties in making accurate measurements with the use of shields to correct for the local radiation. If one is satisfied with the value of the intensity inside the shields it seems possible to make

fairly reliable measurements since it is then not necessary to know accurately the fraction of the cosmic radiation removed by these shields.

By the use of Gold's⁴ table it is found that the upper part of the shielded curve is approximately fitted by assuming an absorption coefficient of 0.50 per meter of water. Extrapolating Millikan and Cameron's synthetic curve, which is dominated by a coefficient of 0.80 per meter of water at these elevations, it is found that it calls for a value of the intensity about double that found by us at 25,000 feet. This result may be accounted for by assuming that the radiation has not reached equilibrium with its secondaries at these elevations though the authors favor the view that the present results indicate that if a banded structure exists the values chosen for the constants of the components will have to be modified.

More complete discussion of these points will be given in a detailed account of this work to be published as soon as certain additional measurements now in progress are completed.

L. M. MOTT-SMITH
L. G. HOWELL*

The Rice Institute,
September 23, 1932.

⁴ E. Gold, Proc. Roy. Soc. A82, 43 (1908).

* Geophysics Department, Humble Oil and Refining Company.

Unitary Theory, Pure Number Ratios and the Masses of Atomic Nuclei

There are six universal dimensional physical constants: G , M , m , e , h and c . G is the gravitational constant, M the mass of the proton, and m the mass of the electron. All the other symbols are standard. The relations between these constants yield the three pure number ratios, α , β and γ , where

$$\alpha \equiv \frac{2\pi e^2}{hc}, \quad \beta \equiv \frac{M}{m}, \quad \gamma \equiv \frac{e^2}{GM^2}.$$

We will also introduce a quantity γ' , where

$$\gamma' \equiv \frac{e^2}{Gm^2}.$$

As L. L. Whyte¹ has pointed out, a unitary theory must provide a derivation of α , β and γ (or γ'). Conversely, if we can find significant

numerical formulas for α , β and γ , it may help us to construct this unitary theory just as the Balmer formula paved the way for Bohr.

The writer has found certain numerical formulas for α , β , γ and γ' , which are all of the same type, and represent these numbers to a remarkable degree of accuracy.

These formulas may or may not be significant, but they are, I think, interesting. They are:

$$\beta \equiv \frac{M}{m} = \left(\frac{7}{2}\right)^6 = 1838.266 = \left(42\frac{7}{8}\right)^2$$

(cf. E. E. Witmer, Nature 124, 180, 1929.)

$$\frac{1}{\alpha} \equiv \frac{hc}{2\pi e^2} = \frac{16}{5} \left(\frac{7}{2}\right)^3 = 137.2$$

$$\gamma^{1/2} \equiv \frac{e}{G^{1/2}m} = (7^2 + 2^2) \left(\frac{7}{2}\right)^{36} \\ = 2.04515 \times 10^{21}.$$

¹ L. L. Whyte, *Critique of Physics*, W. W. Norton & Co., 1931.

Furthermore

$$\gamma^{1/2} = \frac{e}{G^{1/2}M} = (7^2 + 2^2) \left(\frac{7}{2}\right)^{30}.$$

The values of these universal constants obtained from the values in Birge's paper² are:

$$\beta = M/m = 1838.26 \pm 1. \text{ (spectroscopic value)}$$

$$1/\alpha = 137.294 \pm 0.11$$

$$\gamma^{1/2} = \frac{e}{G^{1/2}m} = 2.0452 \times 10^{31}.$$

Comparison between the observed and computed values shows that the agreement in the cases of β and γ' is quite astounding, and in the case of $1/\alpha$ is good.

Another possibility for $1/\alpha$ is

$$\frac{1}{\alpha} = \frac{16}{5} \left[\left(\frac{7}{2}\right)^3 + \left(\frac{2}{7}\right)^3 \right] = 137.275.$$

Concerning the significance of these formulas, if any, it does not seem possible to do more than speculate at the present time. Nevertheless I would venture to suggest that the three-dimensional character of space should find expression in the formulas of a unitary theory. Our formulas are characterized by the universal appearance of the numbers 2 and 7, especially $7/2$, and most especially powers of $(7/2)^3$. We suggest the following interpretation of these formulas as a possibility.

Let $d=3$ =number of dimensions of space. Then $7=2d+1$, and

² R. T. Birge, Physical Review Supplement 1, 1 (1929).

$$\beta = M/m = (d + 1/2)^{2d}$$

$$\frac{1}{\alpha} = \frac{(d+1)^2}{d+2} (d+1/2)^d$$

$$\gamma^{1/2} = [(2d+1)^2 + 2^2] (d+1/2)^{(2d)}$$

$$\gamma^{1/2} = [(2d+1)^2 + 2^2] (d+1/2)^{2d(2d-1)}.$$

Having obtained these formulas the writer turned his attention to the masses of the atomic nuclei, using the data of Aston.³ This investigation led to the following formula for the masses. Let $W(A, Z)$ be mass of the nucleus of the atom with atomic mass A in the nearest integers and atomic number Z . Then

$$W(A, Z) = AM \left[1 - \frac{k}{2^{n+6}} \left(\frac{2}{7}\right)^3 \right]$$

where k and n are integers. It must be emphasized that the present data are not sufficiently accurate to test this formula adequately and that therefore the formula may be entirely wrong. We note that this formula is of the same type as those for α , β , γ and γ' .

For H^2 we take $k=2$ and $n=0$, obtaining for the mass of the H^2 nucleus 2.01356, if $M=1.00724$. The writer intends to publish a more extensive article on this subject in the near future.

ENOS E. WITMER

Randal Morgan Laboratory,
University of Pennsylvania,
Philadelphia, Pa.,
September 28, 1932.

³ F. W. Aston, Proc. Roy. Soc. A115, 487 (1927).

Solar Component of Cosmic Rays

The experimental results of some observers indicate a diurnal variation in cosmic-ray intensity of the order of 1 percent. As a possible explanation, it has been suggested that roughly 1 percent of the rays have their origin in the sun.

In this case it can be easily shown, on the assumption that the rays are photons, that the intensity of radiation from the part of the sky covered by the sun would be roughly 1000 times as great as the average over the remainder of the sky.

If we assume: (1) That the cosmic rays are photons; (2) that by Compton encounters they produce secondary electrons moving in the same direction as the primary rays (very nearly); (3) that these secondary electrons

are capable of actuating a Geiger-Müller counter; then we may test the relative intensity of the cosmic rays from the sun and other parts of the sky. We made the comparison by means of a pair of G.-M. counters arranged to record coincidental responses mounted on a telescope at Chamberlin Observatory, University of Denver. The distance between counters was adjusted, so that when their common axis intersected the center of the sun, only those rays from the sun would pass through both counters.

The telescope was then so oriented that this common axis pointed at the center of the sun continuously for two hours. Next, the tubes were aimed at an area slightly ahead of the sun by changing the right ascension but not

the declination of the telescope. These readings were continued for seven days. One day the instrument was trained on the sun from 10 to 12 A.M., and on a neighboring region

TABLE I. *Number of coincidences with counters aimed.*

Date	At the sun	Near the sun	At the zenith	At the horizon
Aug. 9	2	2	7	2
10	0	0	5	0
11	1	4	5	1
12	1	3	4	0
13	2	1	3	0
14	0	1	5	1
15	3	1	6	0
16	2	3	2	1
Total	11	15	37	5

from 12 to 2 P.M. The following day the procedure was reversed. To test the instrument, coincidences were taken with the telescope in

vertical and horizontal positions. The results are given in Table I. The test for adjustment with the tubes at 5 cm apart gave 92 and 86 coincidences in two hours on Aug. 8 and Aug. 17, respectively.

If the initial assumptions be allowed, it seems certain the sun does not contribute any appreciable amount of the total cosmic radiation. The above results indicate it may act as an absorber, but we do not believe the data justify this conclusion. Experiments on the moon are in progress to test this point. Funds granted by the Rumford Committee and American Association for the Advancement of Science were used to purchase the equipment.

J. C. STEARNS
WILCOX P. OVERBECK
University of Denver

RALPH D. BENNETT
Mass. Inst. of Tech.

September 30, 1932.

BOOK REVIEWS

Étalons Photométriques. PIERRE FLEURY. Volume 2 of the third Section de l'Encyclopédie Photométrique. Pp. 122+x, Figs. 41. Revue d'Optique, 1932. Price 25F.

At the present time, when the interest of physicists in the field of photometry is so strongly centered upon the need for a satisfactory reproducible standard of light to maintain the constancy of the present units as well as for the establishment of an accepted method of heterochromatic photometry, the appearance of this excellent treatise is most opportune.

A study of Professor Fleury's book makes one realize that perhaps in no other branch of physical measurements has the search for an adequate standard entailed a greater amount of effort or resulted in a greater variety of proposed standards than in the field of photometry. Slightly more than half the book is devoted to a very comprehensive account of this search. In describing the numerous devices that have at some time or other been adopted somewhere as standards of light as well as those devices which have been merely proposed as such, good judgment has been used in stressing the essential details.

Recognizing that some form of block-body radiator gives the greatest promise, at present, of providing a satisfactory reproducible light standard, the author devotes the last 40 percent of his book to a study of this question. His manner of treating the experimental work done and the problems involved reveals the touch of one who has been an active worker in this field.

The material in this book is very well selected and has been ably and interestingly presented. It will prove indispensable to all physicists working in the field of photometry and is recommended to all who are interested in the modern developments in this field.

H. T. WENSEL
Bureau of Standards

Kleiner Leitfaden der Praktischen Physik. FRIEDRICH KOHLRAUSCH. 5th edition revised by Friedrich Krüger. Pp. 498+xxviii, Figs. 379. B. G. Teubner, Leipzig and Berlin, 1932. Price 14 Mark 80.

This fifth edition of the "introduction" or "Kleiner Kohlrausch" is the first to appear under the editorship of Professor Krüger. It is, as he says in the preface, intended not only for the instruction of beginners in experimental work in physics, but also as a laboratory manual of physics for workers in neighboring fields, insofar as they need physical methods; therefore it does not describe methods of highest precision and does not attempt a complete enumeration, leaving these to the "Grosser Kohlrausch." Nevertheless, the book has grown considerably; it is two-thirds of the size of the larger book in the 11th edition of 1910.

The new edition has kept the main features inaugurated by Kohlrausch. Each chapter starts with a short statement of the principal laws governing the field treated, units, numerical constants and so on. Then follows an enumeration of the laboratory methods of measurement, the principle of each method, its particular advantage and accuracy are given, the place where instruments might be purchased (in Germany) is often mentioned, then there is often a remark concerning possible mistakes to be avoided or experimental tricks to be applied.

The book starts with a general introduction on measuring and units and a much needed discussion on accuracy of single measurements, their influence on complicated calculations, probable errors, methods of interpolation.

Then follows a description of general appliances (like pumps) and laboratory methods, the measurement of intervals of length and time, weighing.

The next five chapters are devoted to mechanics and mechanical properties, namely, the determination of density, of the constant of gravity, of static pressure, of velocity and pressure in the flow of fluids, and of elastic properties.

The chapter on acoustics has been greatly enlarged; after it surface tension, viscosity and heat measurements are treated.

Electricity and magnetism fill, with almost 200 pages, the longest chapter; it contains, among older methods, electrical oscillations and vacuum tubes, photoelectricity, medical applications and radioactivity.

The two last chapters treat electromagnetic radiation of all wave-lengths and even the experimental side of the wave properties of matter. This is followed by 41 tables.

The book is very well written and contains an enormous amount of information. Of course, most of the instruments referred to are of German make. My only objection is directed against some curious omissions, although that is clearly a matter of subjective judgment; e.g., in acoustics the methods of the ultrasonic interferometer are not mentioned, in calorimetric the electrical compensation of negative heats of reaction, in other parts the Compton electrometer and the Pointolite lamp.

At the University of Munich it was customary to recommend to candidates for the Ph.D. that they study the "Kohlrausch" for their oral. I still think that a very good idea, even more so with this new edition, and only wish that all our candidates would know (besides other things) its content.

KARL F. HERZFELD

Johns Hopkins University

THE PHYSICAL REVIEW

Cosmic-Ray Ionization as a Function of Pressure, Temperature, and Dimensions of the Ionization Chamber

By JAMES W. BROXON
University of Colorado

(Received August 15, 1932)

Experiments have been performed to test the adequacy of the writer's explanation of the dependence upon pressure of the cosmic-ray ionization in gases at high pressures in terms of subsidiary radiations emitted solely from the walls of the ionization chamber. The ionization in a 436 cc sphere of 33.32 g mass located at the center of the 660 lb. bomb of 13.8 liters capacity used in previous experiments, was found not to differ greatly from the average ionization in the large chamber at corresponding pressures up to 175 atmospheres. At the higher pressures gamma-ray ionization and cosmic-ray ionization were found to vary with the pressure in the same manner. These facts are considered to be incompatible with the explanation mentioned above. The temperature effect was found to amount to 0.19 percent increase in ionization per centigrade degree increase in temperature at a mean pressure of 23.3 atmospheres, and 0.27 percent per degree at 162.1 atmospheres, in qualitative but not entirely in quantitative agreement with the theory and observations of Compton, Bennett and Stearns. The cosmic-ray ionization at 205 atmospheres in the shielded bomb was found to agree within about one percent with the upper limit previously observed in the same chamber with similar shielding at pressures between 130 and 170 atmospheres. Certain transient effects associated with changes in pressure and temperature were observed.

CONTINUING the investigation of the residual ionization in gases at high pressures, the writer found that the ionization produced by the penetrating radiation in air¹ approached an upper limit at about 130 atmospheres in a spherical chamber of 11.72 inches internal diameter. No change in the ionization was observed as the pressure was increased to 170 atmospheres. A similar situation was observed in the case of nitrogen,² but in this gas the ionization was greater than that in air at corresponding pressures, and constant values were obtained only at a somewhat higher pressure. Earlier work³ had shown oxygen to resemble air, and carbon dioxide to resemble nitrogen, at pressures up to about 70 atmospheres.

Amplifying the hypothesis suggested by McLennan⁴ and later by Wilson⁵

¹ J. W. Broxon, *Phys. Rev.* **37**, 1320 (1931).

² J. W. Broxon, *Phys. Rev.* **38**, 1704 (1931).

³ J. W. Broxon, *Phys. Rev.* **27**, 542 (1926).

⁴ J. C. McLennan, *Phil. Mag.* **14**, 760 (1907).

⁵ W. Wilson, *Phil. Mag.* **17**, 216 (1909).

and Downey,⁶ the writer showed that the relation between ionization and pressure could be explained by assuming that the penetrating radiation produced no appreciable primary ionization, the immediate ionizing agent being secondary radiations excited only in the thick walls of the container. For two reasons the explanation appeared rather unsatisfactory. In order to explain the constant value of the ionization at sufficiently high pressures, it was necessary to assume that all the subsidiary radiations were emitted in directions normal to the inner surface of the chamber. Further, it appeared unlikely that secondary radiations should not be excited in the gas at the high pressures as well as in the vessel walls, inasmuch as altitude measurements indicate that the penetrating radiation is absorbed in air as in other materials.

Compton, Bennett and Stearns,⁷ and Millikan and Bowen⁸ have emphasized an alternative explanation. According to them the attainment of constant ionization values at the high pressures is due to a lack of saturation. This lack of saturation is due to a selective recombination, the recombination of the ion with the parent from which the electron was ejected, rather than to random recombination. On this account, the ordinary tests for saturation are found to be inadequate.

With this point of view, Compton, Bennett and Stearns were able to deduce an equation giving the proper variation of the ionization with pressure. They were further able to deduce a dependence upon temperature, insignificant in the neighborhood of atmospheric pressure, but considerable in the neighborhood of 100 atmospheres. The temperature effect was checked experimentally by measurements of the ionization produced in air and nitrogen by gamma-rays, greater ionization currents being observed at higher temperatures.

Bowen⁹ has also provided experimental evidence for the selective recombination hypothesis by showing that at pressures up to 93 atmospheres the ionization produced by gamma-rays increases with the potential gradient up to 1000 volts/cm, and that the dependence upon the gradient is nearly independent of the intensity of the ionization. This observation conflicts with the detailed theory of Compton, Bennett and Stearns, according to which a very much higher gradient would be required to increase the ionization current above the apparent saturation value.

The dependence of the ionization by gamma-rays in air and carbon dioxide upon pressure, temperature and potential gradient was carefully investigated by Professor Erikson¹⁰ in 1908. He found that as the pressure was varied from 1 to 400 atmospheres the ionization in air actually passed through a maximum, thereafter decreasing linearly with increase of pressure. The magnitude of this maximum and the pressure at which it occurred increased

⁶ K. M. Downey, *Phys. Rev.* **16**, 420 (1920); **20**, 186 (1922).

⁷ A. H. Compton, R. D. Bennett and J. C. Stearns, *Phys. Rev.* **39**, 873 (1932).

⁸ R. A. Millikan and I. S. Bowen, *Nature* **128**, 582 (1931).

⁹ I. S. Bowen, *Phys. Rev.* **41**, 24 (1932).

¹⁰ H. A. Erikson, *Phys. Rev.* **27**, 473 (1908).

with the potential gradient, the maximum gradients being provided by 2500 volts between gauze cylinders differing by 0.8 cm in radius. He found at a constant pressure that after an initial rapid increase the ionization continued to increase slightly with the potential gradient to the highest values used. At constant gas density, he found the ionization increased with temperature when high potential gradients were applied, whereas the ionization decreased with increasing temperature at low field intensities. The effects were explained by Professor Erikson in terms of the selective recombination with the parent atoms.

In addition to explaining the variation with pressure, an interesting feature of the secondary radiation hypothesis was that it led to correct values of the absorption coefficient of the primary penetrating radiation, upon assuming that the ranges of these radiations were represented by the diameter of the vessel at the lowest pressure at which the maximum ionization was attained, and the further assumption that they consisted of electrons scattered in such a manner that the Compton equation was applicable. That the application of this equation was quite unjustified was recognized, but the assumption that the secondary radiations consisted of protons ejected from the nucleus upon absorption of an incident quantum led to a similar conclusion. In this connection it is of interest that Millikan and Anderson¹¹ have found from expansion chamber observations in a magnetic field, that the secondary radiations are chiefly positive. Compton, Bennett and Stearns⁷ provide evidence in contradiction of this phase of the explanation. They have found the ratio of the ionization by a given intensity of gamma-radiation to that produced by the cosmic penetrating radiation in the same vessel at the same pressure, to be quite independent of the pressure within the range of their measurements. If the ionization in both cases were due almost entirely to secondary radiation from the walls, then a maximum ionization should be attained at a considerably lower pressure in the case of the gamma-radiation, in view of the much lower energy of the incident quanta in this case.

Sievert¹² and Tarrant¹³ have also observed a pressure effect in gamma-ray ionization corresponding to that observed by the writer with cosmic-ray ionization, and the former has obtained pressure-ionization curves with x-radiation which somewhat resemble Professor Erikson's high-pressure γ -ray ionization curves. They also consider the secondary radiation hypothesis unsatisfactory.

In an attempt to test further the adequacy of the suggested explanations of the characteristics of the ionization due to the penetrating radiation in gases at high pressures, the present investigation was undertaken.

IONIZATION IN THIN CENTRAL SPHERE

The assumption that the ionization in a gas by the cosmic penetrating radiation is due entirely to secondary radiations emitted normally from the

¹¹ R. A. Millikan and C. D. Anderson, *Phys. Rev.* **40**, 325 (1932). Also, see the conclusions of E. G. Steinke and H. Schindler, *Zeits. f. Physik* **75**, 115 (1932).

¹² R. M. Sievert, *Nature* **129**, 792 (1932).

¹³ G. T. P. Tarrant, *Proc. Roy. Soc. A* **135**, 223 (1932).

walls, would lead to the conclusion that the ionization in the central region of a spherical chamber should vary considerably from the average. At the lower pressures the ionization should be greater at the center whereas at high pressures it should be less, becoming negligible at sufficiently high pressures.

The difficulty with ascertaining the ionization in a given region is that solid material must be introduced in order to perform the measurement, and this material modifies the conditions. To approximate the desired conditions, an exceedingly thin vessel should be introduced into the central region.

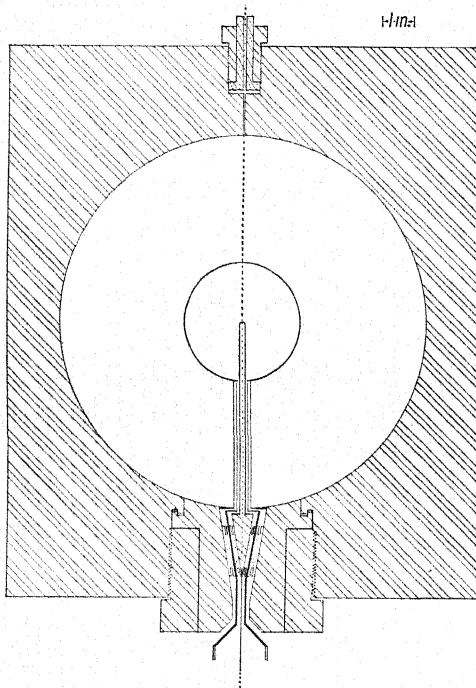


Fig. 1. Longitudinal section of ionization chamber.

Because it was highly desirable to know very definitely the region from which ions were drawn in the present instance, it was decided to construct a chamber with thin but continuous walls. Consequently, two thin steel hemispheres were spun, ground down to a still smaller thickness, and soldered together. This sphere was mounted at the center of the 11.72 in. bomb used in recent work,¹ as shown in Fig. 1.

The mass of the central sphere was 33.32 g. Its volume, as determined by filling and weighing with benzene whose density was carefully determined at the temperature of the experiment, was 436.7 cc, giving a mean internal diameter of 3.706 in. Division of the mass of the sphere by its area and the probable density of the steel gave an average wall thickness of about 0.006 in. Micrometer measurements showed the external diameter to vary between 3.712 and 3.746 in.

The large tube supporting the thin sphere had an outside diameter of 0.532 in., a wall thickness of 0.008 in., and weighed 7.40 g. The central tube, forming a continuation of the guard system, had an O.D. of 0.342 in., a wall thickness of 0.007 in., and weighed 4.09 g. The innermost tube, forming the collector, had an O.D. of 0.168 in., a wall thickness of 0.011 in., and weighed 3.90 g. The end of this tube was spun to an approximate hemisphere. The hole in the sphere through which this tube was admitted was $9/32$ in. in diameter. The volume of the tube inside the sphere was 0.67 cc, leaving a free volume of 436 cc inside the sphere.

The tubes and sphere were mounted on the plug¹⁴ of the large bomb, and when the latter was screwed into place the eccentricity of the central sphere relative to the interior of the bomb did not amount to more than $1/32$ in. The tubes were beneath the sphere. Twenty small holes were drilled in the outer tube to allow an equalization of pressure inside and outside the thin sphere. None were drilled within $\frac{1}{2}$ in. of the ends of the tube, however.

Because of the very much smaller volume, the ionization currents were correspondingly smaller than in the large sphere. However, for purposes of comparison, it was considered desirable to use precisely the same measuring equipment which had been used in the preceding high-pressure work. This equipment, the location, the method of measurement, etc., have been described fully.¹ The insertion of the small sphere constituted the only alteration; the same constant, modified by the volume ratio, yielding the number of pairs of ions per cc per sec. when multiplied by the number of volts/sec. applied to the compensating condenser. Because of the smaller currents, however, six or eight 15-minute readings or three or four 30-minute readings were made at each pressure, instead of the usual three 8-minute readings. Also, positive and negative ions were usually collected during alternate readings to insure that the smaller readings would not be affected by possible contact potentials or zero drift. That no appreciable deformation of the sphere occurred during the observations was shown by the fact that its induction coefficient relative to the central system varied linearly with the pressure, a situation which had been found to hold in the case of the rigid bomb.¹⁵

As in all previous work, the gas used throughout the present investigation was aged at least four weeks, often much longer, and was dried and freed from dust. With the bomb surrounded by the water shield only, observations of the ionization in the central sphere were made at various pressures between about 7 and 175 atmospheres. These are shown in Fig. 2, pressures again being reduced to 18°C. The dotted curve represents the average ionization measured in the large bomb under the same conditions; it is curve III of Fig. 5 of the paper of reference 1. The small square represents an observation of the

¹⁴ In order to eliminate a small leak, the main plug was redesigned to conform with the small one at the top of the bomb, so that the portion of the plug in contact with the gasket was not allowed to rotate as the plug was tightened. This design proved to be thoroughly satisfactory.

¹⁵ J. W. Broxon, *Phys. Rev.* **37**, 1338 (1931).

ionization in the small sphere with the lead shield only, and the cross represents the ionization measured with both the lead and water shields. The barometric pressures during the two series of observations with only the water shield did not differ by more than 0.05 in. It appears that the two observations designated by the square and the cross should be reduced by about 0.6 percent to conform to this barometric pressure.

The striking thing about the curve is its proximity to the dotted curve. The ionization in the central sphere seems to be definitely higher than the average in the large bomb at the lower pressures and a little lower at the highest pressures. However, constant values at high pressures are again attained,

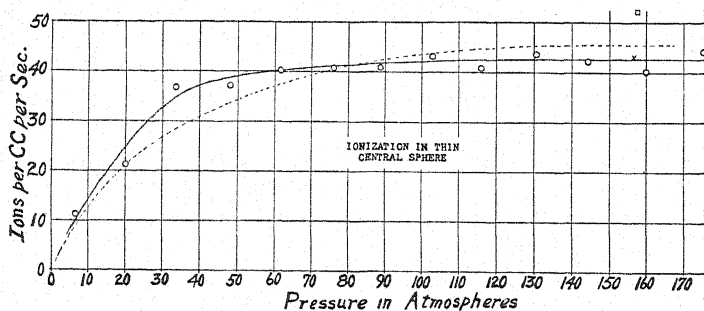


Fig. 2.

in this case at a lower pressure than in the large chamber. There are apparent differences between the curves, but not at all of the magnitude to be expected on the hypothesis of ionization due entirely to radiation from the walls. It is a striking observation that at the highest pressures the ionization in this small central sphere, weighing little more than an ounce, containing air weighing nearly three times as much, and surrounded by a blanket of air equivalent to a layer more than 50 ft. thick at atmospheric pressure, should be so nearly the same as the average ionization in the 660 pound bomb containing more than thirty times as much air.

IONIZATION BY GAMMA-RAYS

In order to compare the effects of cosmic rays and gamma-rays, about 2.85 mg of radium sulphate equivalent to 2 mg of Ra in Aug., 1923, sealed and enclosed in a container (apparently with 7.5 mm lead and 1.5 mm steel walls) was placed in a cabinet about two ft. outside the water tank surrounding the bomb. The radium was thus displaced horizontally about 9 ft. from the axis of the bomb, and about 21 in. below its center. The lead and water shields were removed from about the bomb, but the gamma-rays still had to penetrate the 9 mm lead-steel container, 2.5 in. of wood, 8.5 ft. of air, and the 1.7 to 6 in. steel walls of the bomb. With this arrangement, the gamma-ray ionization produced in the 13.8 liter chamber at the high pressures was about five times as great as that produced by the cosmic radiation with lead and water shields. Although the same potential, about 875 volts, which has been impressed across the ionization chamber throughout these investigations was

still used, it was perhaps not sufficient to produce saturation. At the highest pressure employed a decrease of 29 percent in the impressed voltage produced a decrease of about 1 percent in the ionization current.

The gamma-ray ionization is shown plotted against the pressure in Fig. 3. The values shown are not those actually observed. From the observed values were subtracted the residual ionization observed at corresponding pressures with no shields, curve I, Fig. 5, of the paper of reference 1. The differences,

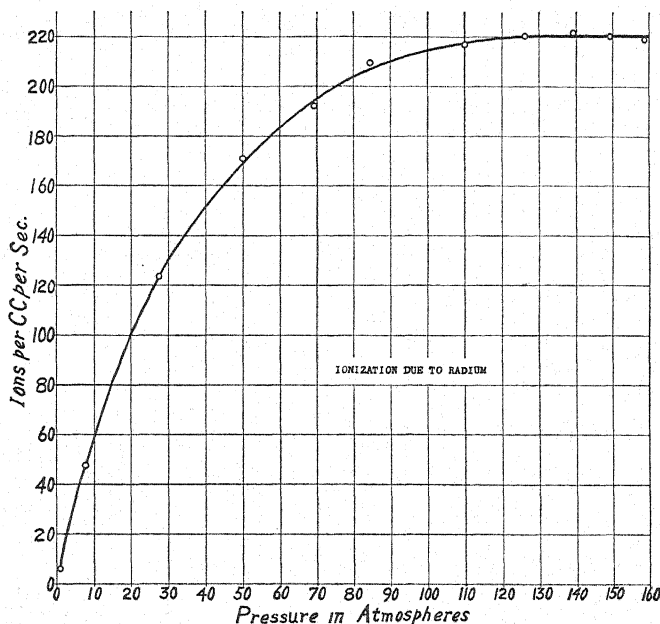


Fig. 3.

considered to represent the ionization actually produced by the gamma-radiation, are shown in Fig. 3.

The ratios of the gamma-ray ionization I_R to the cosmic-ray ionization I_C at corresponding pressures are shown in Table I. The cosmic-ray ionization values considered in this table are those obtained with both lead and water shields, represented by curve IV, Fig. 5, of the paper of reference 1. It is seen that the ratio is not quite constant, although it is nearly so at pressures above 60 atmospheres. This is not in full agreement with the observations of Comp-

TABLE I.

Atm. press.	0.82	10	20	30	40	50	60	70	80	90
I_R/I_C	4.21	4.90	4.97	5.07	5.07	5.13	5.17	5.20	5.20	5.17
Atm. press.	100	110	120	130	140	150	160			
I_R/I_C	5.16	5.16	5.17	5.17	5.18	5.18	5.18			

¹⁶ J. C. Stearns and W. Overback, Phys. Rev. 40, 636 (1932).

ton, Bennett and Stearns.⁷ Stearns and Overback¹⁶ have recently found the ratio to be constant for pressures between 5 and 70 atmospheres. The smaller ratios at low pressures in the present instance might possibly be explained in terms of a very minute contamination of the vessel with decreasing effectiveness at higher pressures, of the type described by Millikan.¹⁷ That such a contamination must necessarily be very small has been shown by the experiments with different shields at high and low pressures.¹ In any case, however, it is seen that the agreement between the gamma- and cosmic-ray ionization-pressure curves is entirely too good to permit of the explanation solely in terms of secondary radiations from the walls, in view of the conclusion that the ranges of these radiations should increase with the penetrability of the incident radiation.

TEMPERATURE EFFECT

To vary the temperature of the bomb, steam was passed from the University heating plant into the water surrounding the bomb and circulation was provided by a centrifugal pump which withdrew water from the bottom of the tank and returned it at the top. The lead shield was not used during

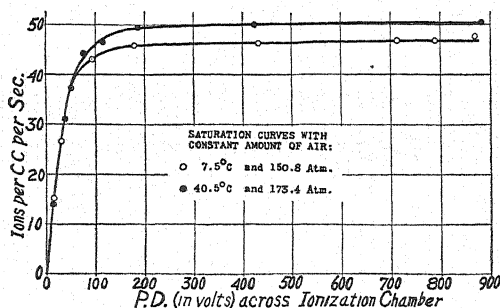


Fig. 4.

the temperature measurements. The water level was maintained constant during the temperature changes, this level being about $\frac{5}{8}$ in. lower than the top of the tank whereas previous experiments with the water shield were all made with the tank full. The steam was available only at a low pressure. In view of this fact it is apparent that changes in the temperature of the 660 lb. steel bomb, surrounded by an air space about 3 to 4.5 in. thick and then by more than 15,000 gallons of water, could be produced only very slowly.

Cold water was first passed rapidly into the tank through fire hoses. About 24 hours later ionization measurements were begun. In order to demonstrate the degree of saturation, observations were made with different applied potentials. The relation between the ionization and the potential drop across the ionization chamber, itself, is shown by the lower curve of Fig. 4. During these observations the average temperature of the bomb was 7.5°C, the average pressure of the gas was 150.8 atmospheres, and the barometric pressure, 24.55 in. The value of the ionization was considered to be

¹⁷ R. A. Millikan, *Phys. Rev.* 39, 397 (1932).

46.8 ions per cc per sec. The high potential observations were made first, and during the 10.5-hour period of the observations the temperature was decreasing at the rate of about 0.05°C per hour.

Steam was next passed into the water for several days. The steam was then shut off and another series of observations similar to those at the low temperature were made. During this period the average temperature was 40.5°C , the average pressure 173.4 atmospheres, and the barometric pressure, 24.87 in. The ionization under these conditions was considered to be 50.1 ions/cc sec. The temperature was again decreasing at the rate of about 0.05°C per hour. The ionization-potential relation under these conditions is shown by the upper curve of Fig. 4.

The air used during these observations was retained in the chamber at constant density for about a month, during which period a 15-day series of observations relative to the diurnal variation¹⁸ were made, the same air being used later for the γ -ray measurements described earlier in this paper. During this time no leak was observed. During the 15-day series of observations, the average ionization was 47.25 ions/cc sec., the average temperature, 17.42°C , and the average barometric pressure, 24.73 in.

After measurements at 205 atmospheres to be described later, the air was released to about 22.2 atmospheres. The ionization at this pressure is designated by the lower curve of Fig. 6. After apparent equilibrium had been attained the ionization was found to be 23.43 ions/cc sec. at a pressure of 22.2 atmospheres and a temperature of 14.45°C , the barometric pressure being 24.87 in. During these observations the temperature of the bomb was increasing at the rate of 0.12°C per hour.

Later the same air was heated in the manner described above. At an average temperature of 47.25°C and a pressure of 24.3 atmospheres, with the temperature decreasing at the rate of 0.13°C per hour, the average of 12 ionization readings was 25.48 ions/cc sec., the barometric pressure being 24.43 in. The dependence of the ionization upon impressed P.D. was not investigated at the lower pressures, the maximum P.D. employed at the high pressures being used as usual. It should be mentioned that all pressures given are pressures read directly from the gauge, plus the atmospheric pressure.

It is seen that at a mean pressure of 162.1 atmospheres, changing the temperature from 7.5°C to 40.5°C resulted in an increase of the ionization amounting to about 7 percent of the lower value. At a mean pressure of 23.3 atmospheres, changing the temperature from 14.45°C to 47.25°C resulted in an increase of 8.7 percent. These are the values given in a recent note.¹⁹ As stated there, these values had not been corrected for effects of variations in the density of the water shield with temperature, or for the effects of variations in barometric pressure. It appears that the alteration of the ionization due to change in the shielding provided by the water would amount to considerably less than 1 percent and may be neglected. A correction for barometric pressure appears to be necessary, however. When the 15-day series of

¹⁸ The results of this investigation will be presented in an early publication.

¹⁹ J. W. Broxon, *Phys. Rev.* 40, 1022 (1932).

observations was considered, it was found that an increase of about 0.187 in. in the barometric pressure appeared to result in a decrease of 1 percent in the ionization.

The variation of the ionization with barometric pressure as designated above was somewhat larger than had been expected. Moreover, it was found that an error had been made in recording the barometric pressure during the high pressure observations. When the readings are reduced to the average barometric pressure during the 15-day series, it is found that the variation with temperature at the high pressures is greater than that at the low pressures. Thus when the barometric correction is made, the temperature effect at 23.3 atmospheres amounts to 6.2 percent for 32.8°C change in temperature, or 0.19 percent per degree. At 162.1 atm. the increase is 8.9 percent for an increase of 33.0°C, or 0.27 percent per degree. When the three ionization values, measured at constant density but different temperatures at the high pressures, are plotted against the temperature, the ionization appears to increase slightly more rapidly with increase of temperature at the higher temperatures. With such a limited number of observations, however, this observation is probably of little consequence.

The temperature effect measured at the higher pressures is seen to agree rather well with that predicted by Compton, Bennett and Stearns.⁷ That observed at 23.3 atmospheres, however is considerably larger than that predicted by them, although the variation with pressure is in the right sense. The disagreement with their experimental observation with γ -ray ionization in nitrogen at 20 atmospheres is decided. The effect at 23.3 atmospheres is in good agreement with the 0.14 percent per centigrade degree observed by Wolff²⁰ for the γ -ray ionization in nitrogen at 21.5 atmospheres, however.

TRANSIENT EFFECTS

As mentioned in a former paper,¹ "If measurements were made immediately after filling, larger values were obtained than after the establishment of equilibrium conditions. Therefore, from two to six hours were allowed to elapse after filling the chamber before measurements of the ionization were begun." In view of the observed temperature effect, it was thought that the high values immediately after filling the ionization chamber might be explained by the very considerable increase of the temperature of the air upon compression. The effect is shown clearly by Fig. 5, representing the first complete set of observations made with the present apparatus March 29 and 30, 1930, with no shields. In Fig. 5 as in Fig. 6, the circles represent individual observations instead of the usual average of three or four observations. The curve shown in Fig. 5 is not drawn with reference to the observations therein designated. It is curve I of Fig. 5 of the paper of reference 1, obtained under the same conditions but with a new supply of air on April 26 and 27, 1930, time for equilibrium conditions being allowed in the latter case.

The values observed very soon after filling are seen to be nearly twice as great as the equilibrium value. Increase of temperature of the bomb showed

²⁰ K. Wolff, *Zeits. f. Physik* 75, 570 (1932).

the gas might have been heated some fifty degrees above the final temperature when compressed into the bomb. However, the temperature chart showed that the bomb had acquired a practically constant temperature before measurements were begun. Any change of temperature of the gas during the observations must have been rather small, although its temperature was probably still decreasing slightly.

In order to determine more carefully the relation between the ionization values and the time after filling, the bomb was filled with air to a pressure a

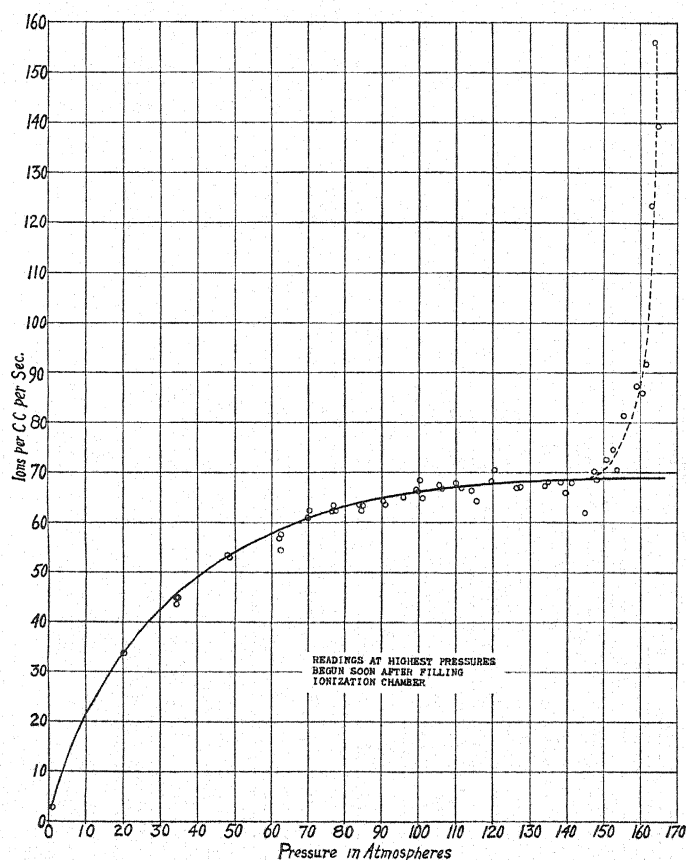


Fig. 5.

little above 205 atmospheres. The water shield with its surface $\frac{5}{8}$ in. below the top of the tank was used in this instance. The limit of the calibrated gauge used heretofore being 2500 lbs. per sq. in., the higher pressures were read on a second gauge which agreed with the first at pressures near its upper limit. After filling, the high potential was applied for a 15-minute interval before observations were begun. This has been the usual procedure. Single observations plotted against the time after filling the chamber are shown in the upper curve of Fig. 6.

The values obtained were again high at first, although as in the earlier

case the bomb appeared to have acquired an equilibrium temperature before readings were begun. That the effect was not an ordinary electrical one is indicated by the fact that when the air is allowed to remain in the bomb for several hours or even days, no initial high values are observed when readings are begun, the preliminary 15-minute application of the potential always being made, of course.

The lower curve of Fig. 6 represents the ionization as a function of the time after releasing the air rapidly from about 169 to about 22 atmospheres. The potential was applied almost constantly while the air was being released, so that observations could be begun very soon after closing the valve. A slight increase was again observed, but much smaller than that following compression. A brief reference to disturbances accompanying variations in pressure has been made by Steinke and Schindler.²¹

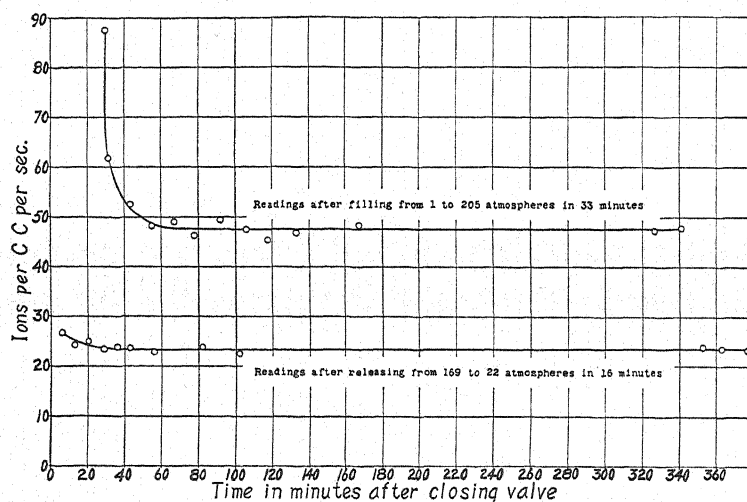


Fig. 6.

Another transient effect of some interest was observed during the temperature variations. Although changes in temperature were necessarily quite slow, the ionization at a particular density and temperature appeared to depend somewhat upon the rate of change of temperature. When the temperature was falling lower values were observed than when it was rising, so that during the investigation of the temperature effect the final steady values at a given temperature were anticipated somewhat.

The natural supposition is that these transient effects may at least to some extent be explained in terms of the characteristics of the measuring equipment. In view of the elaborate guard system and the null method employed, however, the explanation does not appear obvious to the writer.

Occasional sudden increases in the ionization current during a reading have been observed. These are quite infrequent and appear always to be well defined. Such readings have been discarded. It has been suggested that these

²¹ E. G. Steinke and H. Schindler, *Naturwiss.* 20, 15 (1932).

sudden increases might be due to nuclear disintegration in the gas by the cosmic rays. This possibility will receive attention in future work.

CONSTANCY OF IONIZATION AT HIGH PRESSURES

After making the observations at 205 atmospheres, the air was released to 172 atmospheres. When corrected for barometric pressure, the ionization values at these two pressures were found to be nearly identical. When further corrected for the slight difference in shielding, these observations at 205 and 172 atmospheres, made in May, 1932, are only about one percent greater than the values measured with the water shield in July, 1930, at pressures between 130 and 165 atmospheres. If one may assume that there is no variation with time, the variation of cosmic-ray ionization with pressure between 130 and 205 atmospheres may be considered to be only about one percent.

SATURATION

The degree of saturation attained is shown quite well in the curves of Fig. 4. Made with constant gas quantity, they represent the dependence of the current upon the applied P.D. at the pressures and temperatures shown.

Very nearly constant values appear to have been obtained in both cases. However, there is a possible increase in the ionization of one percent at the high potential end of the curves, due to doubling the applied P.D. Saturation appears much more nearly complete than in the curves of Professor Erikson's¹⁰ experiments with γ -rays at corresponding pressures, although he used much more intense fields. Of course, the ionization he employed was vastly more intense, but if all free ions were drawn out before recombination and the lack of saturation at the high gradients was entirely attributable to (initial) recombination with the parent atoms, one should expect the degree of saturation to be independent of ion density, as Bowen⁹ points out.

Bowen found that reducing the γ -ray ionization by a factor of about five at a pressure of 93 atmospheres produced very little change in the variation of the ionization current with potential gradient except at the lower gradients. It is rather surprising that the residual ionization, further reduced by a factor of about four, more nearly resembles the intense than it does the weaker γ -ray ionization in its dependence upon the gradient at that pressure, even at the lower gradients. It is these residual ionization currents which are more nearly comparable to those discussed in this paper. Throughout the range of gradients he investigated, Bowen found that at 93 atmospheres an increase of the gradient by a factor of about four produced an increase in the residual ionization current of from nearly 6 to a little more than 12 percent. This is possibly in conflict with the fact that in the present investigation the ionization in the small sphere was slightly less than that in the large one at 93 atmospheres (see Fig. 2). Since the central rods were of nearly the same size in the two cases, reduction of the radius of the surrounding vessel by a factor of more than three with the same applied P.D. of about 875 volts, should have increased the average gradient in the region of weak fields, in the neighborhood of the outer wall, by a factor probably greater than the radius ratio,

although the increase of the volume average may have been small. According to Bowen's observations, then, one might expect that an appreciably greater ionization should have been measured in the small sphere than in the large one at 93 atmospheres.

CONCLUSIONS

The experiments herein described constitute further evidence in favor of the contention that the explanation of the characteristics of cosmic-ray ionization at high pressures, entirely in terms of secondary radiations from the vessel walls, is quite inadequate. The experiments with the thin central sphere and with gamma-rays can not be reconciled with that explanation.

As has been mentioned, Bowen's⁹ observations of the dependence of the ionization upon potential gradient are in conflict with the details of the initial or selective recombination theory of Compton, Bennett and Stearns.⁷ The curves of Fig. 4 and the observations with the small sphere appear to agree rather better with their conclusions than with those of Bowen, although a small final slope persists in the "saturation" curves. The considerable temperature effect at 23.3 atmospheres is not in quantitative agreement with their conclusions, however.

In spite of the remarkable agreement between the ionization curves of Fig. 2, the excess of ionization in the small thin central sphere over that in the large bomb in the region from 30 to 50 atmospheres appears too great to be due to experimental error. This difference might be explained in terms of secondary radiations²² from the walls.

If, in view of the observed similarities in the characteristics of cosmic- and gamma-ray ionization at high pressures we may consider Professor Erikson's¹⁰ observations comparable with these, the ionization should have passed through a maximum within the pressure range of the present experiments. The constant values in the present instance appear to extend over a region of at least 75 atmospheres. No maxima of such breadth were observed by Professor Erikson. Also, the equation deduced by Compton, Bennett and Stearns to approximate the writer's experimental observations indicates that an increase of 2.8 percent should accompany an increase in pressure from 130 to 205 atmospheres, whereas no increase amounting to half this much was observed. The difference is too small to be conclusive, however.

One common characteristic of both the explanations of the pressure effect is their emphasis of the importance of ionization by secondary radiations. A primary electron or proton ejected by incident cosmic radiation could scarcely be expected to recombine with its parent atom. In view of the fact that the ionization is supposed to occur chiefly through the agency of subsidiary radiations, it seems to the writer that there is another possibility deserving of some consideration. Studies of the ionization produced by alpha-rays in different gases and of the ionization potentials of these gases have shown²³ that "for the diatomic gases examined, *viz.*, H₂, N₂, O₂, the difference

²² H. Geiger, *Nature* **127**, 785 (1931); H. Schindler, *Zeits. f. Physik* **72**, 625 (1931).

²³ Rutherford, Chadwick and Ellis, *Radiations from Radioactive Substances*, p. 81. R. W. Gurney, *Proc. Roy. Soc. A* **107**, 332 (1925).

between the energy spent and the minimum energy required to ionise the atom . . . is very marked. In fact only about half the energy spent is required to ionise the atom. This would indicate that a considerable part of the energy of the α -particle is used up in processes which do not involve ionisation, i.e., in excitation or dissociation of the molecules." The differences are found to be much smaller in the case of the monatomic gases, particularly helium.

If this explanation is correct, it seems that a considerable portion of the gamma- and cosmic-ray energies, through the agency of subsidiary radiations, might eventually be used otherwise than in the formation of ions. Should a portion of the energy finally be dissipated in some manner such as that suggested above, such molecular processes and consequently the efficiency of ionization might be expected to depend to a considerable extent upon temperature and pressure. If such a point of view is tenable, one might expect the effects to be less in the monatomic gases.

If, as Compton, Bennett and Stearns⁷ maintain, the differences between the values of the ionization measured in nitrogen and in air may be explained in terms of the selective or initial recombination hypothesis, then it should follow that complete saturation is very difficult to obtain even at atmospheric pressure. The writer has shown that the greater ionization in nitrogen persists even to atmospheric pressure.² In view of this and the considerable temperature effect in the neighborhood of 20 atmospheres, it seems that a careful scrutiny of ionization processes in different gases with especial regard to molecular structure should be of value. Further work of this nature is being carried on.

The writer is again indebted to Professor G. B. Williston, Mr. L. Strait and Mr. G. T. Merideth for assistance in recording observations, and to Professor S. L. Simmering and Mr. C. A. Wagner for compressing the air used in these experiments. The splendid work of Mr. M. M. Eaton, departmental mechanic, in constructing the ionization chamber and accessories is very much appreciated.

X-Ray Diffraction in Ethyl Ether near the Critical Point

By F. H. WALDEMAR NOLL
State University of Iowa

(Received September 16, 1932)

X-ray diffraction ionization curves were obtained for ethyl ether at 43.5 ± 0.7 kg/cm² pressure with temperatures in the range from 25°C to 210°C. The critical pressure and temperature of ether are 36.7 ± 0.2 kg/cm² and $194.6 \pm 0.3^\circ\text{C}$, respectively. In the region of the higher temperatures the ionization curves are a combination of the liquid and polyatomic gas types, falling rapidly near 0° with increasing angle, then rising to a distinct peak and again falling. Liquid semi-orderly "cybotactic" groups are in evidence from room temperature to 199°C but not for specific volumes greater than the critical specific volume. It seems reasonable to expect vanishing of these groups at the critical point. The influence of the polyatomic gas type begins to appear at the low temperatures and increases with temperature. The liquid type decreases almost linearly until 155°C where it begins to fall off very rapidly. The observations are in excellent accord with the "cybotactic" view of the interior of a liquid.

THERE are many experiments which are most readily interpreted by the view of Stewart¹ that there are, within a liquid, molecular aggregates of sufficient size and orderliness to give marked x-ray diffraction bands. These "cybotactic" groups are not permanent and do not retain the same constituent molecules. It is interesting to ascertain if this condition of semi-orderly groups exists near the critical point, and if so, how it varies with temperature.

APPARATUS AND METHOD

The x-ray spectrometer used, and the method of procuring diffraction curves, is essentially the same as the apparatus and procedure described by Stewart and Morrow.² The diffraction effects obtained are produced by Mo $K\alpha$ -radiation. The x-ray beam was made partially monochromatic by use of a zirconium oxide filter. The voltage applied was such as to produce a general radiation maximum at about 6° . Its influence is nevertheless noticed in the experiments, but does not interfere with the results and conclusions.

The liquid chosen was ethyl ether. The critical temperature³ is $194.6^\circ \pm 0.3^\circ\text{C}$ and the critical pressure is 36.7 ± 0.2 kg/cm². The pressure selected in this investigation, 43.5 ± 0.7 kg/cm², is not very near the critical pressure of 36.7 kg/cm². The higher pressure was necessary to prevent excessive density variations which could be produced by the slight unavoidable temperature fluctuations.

The liquid was contained in an aluminum tube with an external diameter of 1.0 cm and a wall thickness of 0.0176 cm. The optimum thickness of

¹ See articles by Stewart and co-workers, *Phys. Rev.*, 1927-1932. For review of literature, Good, *Helv. Physica Acta.* p. 205 (1930); Debye, *Ergebnisse der tech. Röntgenkunde* 2, 1 (1931).

² Stewart and Morrow, *Phys. Rev.* 30, 232 (1922).

³ Schroer, *Zeits. f. phys. Chem.* 140, 381 (1929).

ether under the selected pressure is 1.77 cm at 25°C and 6.3 cm at 210°C. The thickness of the ether column is thus always less than the optimum thickness. The aluminum tube was connected to a "U" tube, and thence to a Crosby dead weight gauge tester. The "U" tube was half filled with mercury, the gauge and connections were filled with oil, and the aluminum tube and connections were filled with ether. A special electric furnace with aluminum foil windows surrounded the aluminum tube. Temperature was measured with a constantan-copper thermocouple. All curves were corrected for scattering from the aluminum container, for decrease of density of the ether due to temperature increase, for cross fire slit penetration and for drift due to the penetrating radiation. No correction was made for the accentuation of general radiation by the aluminum container as this effect has no influence upon the conclusions.

EXPERIMENTAL RESULTS

X-ray diffraction ionization current curves, pressure constant at 43.5 ± 0.7 kg/cm², were obtained for the following temperatures, 25°C, 137°C, 155°C, 171°C, 186°C, 190°C,

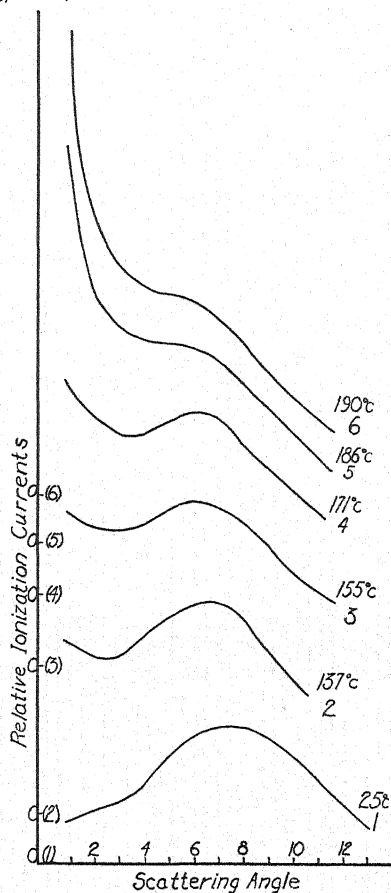


Fig. 1. Relative x-ray diffractions intensities of ethyl ether at a pressure of 43.5 ± 0.7 kg/cm².

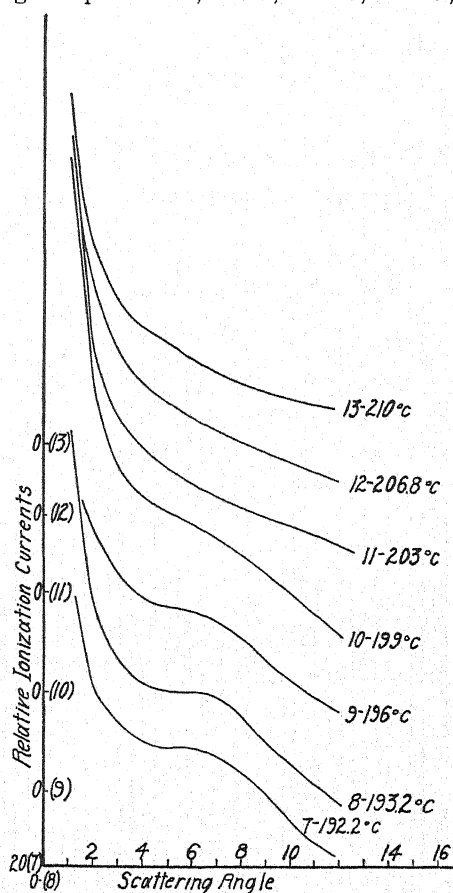


Fig. 2. Relative x-ray diffraction intensities of ethyl ether at a pressure of 43.5 ± 0.7 kg/cm².

171.4°C, 186°C, 190°C, 192.2°C, 193.2°C, 196°C, 199°C, 203°C, 206.8°C and 210°C. See Figs. 1 and 2.

A liquid type of curve is that obtained at 25°C.⁴ A polyatomic gas type⁵ is that obtained at 210°C. In the former case, there is a broad peak at 7.5° and 25°C with a decrease at both smaller and larger angles. In the gas type, the intensity is high near 0° but falls rapidly with increasing angle, the slope decreasing in magnitude. In point of fact, the 25°C curve shows an effect near zero that may be attributed to random molecules or molecules giving a gas type scattering. Indeed, the entire set of curves in Figs. 1 and 2 can be described by regarding the molecules as being either at random or in organized groups. Of course, this is not accurate, for there are conditions representing all gradations between these two extremes. If peak heights are plotted against temperature, Fig. 3 is obtained.

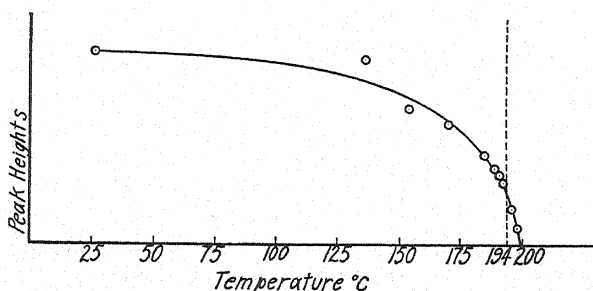


Fig. 3. Relative peak heights-temperature curve for ethyl ether.

The following results appear in the ionization curves as temperature is increased from 25° to 210°C, pressure being constant. (1) Peak heights decrease and finally disappear at about 5°C above the critical temperature. (2) Small angle scattering increases more and more rapidly as temperature increases. (3) Peaks become broader and the peak maximum shifts to smaller angles. However, the curves are too diffuse to obtain useful measurements on these two points. (4) In general, the curves may be described as changing from a liquid pattern to a gas pattern. (5) It is an interesting fact that no liquid peaks appear at a specific volume as great as the critical specific volume. A discussion of this point will appear in later publications from this laboratory.

Studies on the effect of temperature upon liquid x-ray diffraction have been made by Skinner,⁶ Stewart,⁷ Vaidyanathan,⁸ Ramasubramanyan,⁹ and Tanaka and Tsuji.¹⁰ Results stated here are either in agreement with or not

⁴ Similar curves can be found in the literature by Stewart mentioned in reference 1.

⁵ This type can be found in various reports, for example, see Debye, *Phys. Zeits.* **31**, 419 (1930) and Wollan, *Phys. Rev.* **37**, 862 (1931).

⁶ Skinner, *Phys. Rev.* **36**, 1025 (1930).

⁷ Stewart, *Phys. Rev.* **37**, 9 (1931).

⁸ Vaidyanathan, *Ind. Jour. Phys.* **3**, 391 (1929).

⁹ Ramasubramanyam, *Ind. Jour. Phys.* **3**, 137 (1928).

¹⁰ Tanaka and Tsuji, *Kyoto Coll. Sci. Mem.* **13**, 337 (1930).

contradictory to those obtained by the authors just mentioned. In respect to the increase of small angle scattering with increase of temperature, all observers are in agreement.

DISCUSSION

With temperature increase, under the stated pressure, one might generally expect, (a) decreased molecular attractive forces because of increased separation resulting from thermal expansion and (b) increased thermal agitation. These should decrease the conditions favorable for the existence of the cybotactic groups. With temperature increase one might then expect that the percent of grouped molecules and regularity of space array within groups at any instant would decrease and that the percentage of "more random" molecules should increase. The former causes the peak heights to decrease. Because of increased irregularity of array peaks would become broader. The intensity of scattering from the "more random" molecules would increase and this means an increased small angle scattering. Assuming that Bragg's law here applied measures the distance between approximate planes of scattering centers, then expansion should shift the maximum to smaller angles. With continued increase of temperature the conditions favorable for the existence of groups would ultimately vanish and the liquid diffraction pattern cease to exist. The above interpretations based on the cybotactic theory are in accord with the experimental results already described.

At the critical point the liquid and vapor phases merge into one phase. It seems reasonable to suppose that the characteristic of the liquid phase, which is the cybotactic group formation, would cease to exist at this point. According to this view, if the substance were at a less specific volume and higher pressure, since the molecules are in closer proximity, the groups might exist at a temperature above the critical one. This is the experimental fact.

The general conclusion from these experiments is that the cybotactic view is corroborated and that the molecules of ethyl ether in these experiments may be roughly regarded as existing either in semi-orderly groups, or as approximately random molecules.

The writer wishes to express his appreciation to the members of the Physics Department for their assistance and his thanks to Professor G. W. Stewart who proposed the problem and under whose direction this study was made.

The Approximation of Geometric Optics as Applied to a Dirac Electron Moving in a Magnetic Field

By OTTO LAPORTE
University of Michigan

(Received August 30, 1932)

The problem of a Dirac electron in a homogeneous magnetic field is integrated according to the recently published approximative method of Pauli. Homogeneous linear equations furnish, except for a multiplicative function, the eigenfunctions in zero approximation. An important condition of compatibility of the zero and first approximation determines these multiplicative functions. For the connection of the solution in the classically occupied regions with those that are classically not reached the Kramers connection formulae are used. The eigenvalue determination gives the result that the phase-integral is to be quantized not with half quantum numbers as is the case unrelativistically, but with whole quantum numbers, each level possessing a twofold degeneracy.

1.

THE advantages of the approximative method, due to Wentzel,¹ Brillouin² and Kramers³ of solving the Schrödinger equation are well known. In the limiting case of large quantum numbers this "W.K.B. method" allows the asymptotic calculation of eigenfunctions and eigenvalues.

In a recent paper⁴ W. Pauli has developed the corresponding approximative method for Dirac's relativistic wave equation of the electron. This problem differs from that of solving approximately the Schrödinger equation inasmuch as instead of one wave function ψ there are four $\psi_1 \cdots \psi_4$. If S is the classical relativistic action function of the problem, it is best to put

$$\psi_p = a_p e^{iS/\hbar} \quad \rho = 1 \cdots 4 \quad (1)$$

and to develop the amplitudes a_p into a power series in \hbar/i

$$a_p = a_p^{(0)} + (\hbar/i)a_p^{(1)} + \cdots \quad (2)$$

It is well known that the W.K.B. method is analogous to the transition from wave optics to geometric optics in isotropic media; the Hamilton-Jacobi partial differential equation appears then as the equation for the eiconal function. In the case of a non-scalar wave function the Eqs. (1) and (2) give in zero approximation, as is to be expected, the equations of relativistic mechanics, or optically spoken, of geometric optics with polarization. However, and this is essential, the spin of the electron or its optical analog, double refraction, does not appear until the next approximation at the same time

¹ G. Wentzel, *Zeits. f. Physik* **38**, 518 (1926).

² L. Brillouin, *C. R.*, July, 1926.

³ H. A. Kramers; *Zeits. f. Physik* **39**, 828 (1926); also Zwaan, *Diss. Utrecht*.

⁴ W. Pauli, *Helvetica Physica Acta* **5**, 180 (1932).

as diffraction effects make themselves felt, since the spin moment is proportional to the Planck constant.

We shall here apply Pauli's method to the case of an electron moving in a homogeneous magnetic field. Eigenfunctions are obtained and connected by means of the "Kramers connection formulae." The eigen-value determination shows that the phase integral should be quantized with whole numbers, but that a double degeneracy occurs.

2.

We write the Dirac equations:

$$\left(\frac{h}{i} \frac{\partial}{\partial x_0} - e\phi_0\right)\psi_\rho + \alpha_{\rho\sigma}^k \left(\frac{h}{i} \frac{\partial}{\partial x_k} + \frac{e}{c}\phi_k\right)\psi_\sigma + mc\beta_{\rho\sigma}\psi_\sigma = 0 \quad (3)$$

where $x_0 = ct$; $x_k = x, y, z$; ϕ_0 is the scalar, ϕ_k the vector potential of the external field. Roman indices run from 1 to 3, Greek ones from 1 to 4. Indices occurring twice are to be summed. The α^k and β are the well-known matrices which obey the usual conditions of anticommutability. Introducing (1) and (2) into (3) we obtain in zeroth and first approximation:

$$-\Pi_0 a_\rho^{(0)} + \Pi_k \alpha_{\rho\sigma}^k a_\sigma^{(0)} + mc\beta_{\rho\sigma} a_\sigma^{(0)} = 0 \quad (4)$$

$$-\Pi_0 a_\rho^{(1)} + \Pi_k \alpha_{\rho\sigma}^k a_\sigma^{(1)} + mc\beta_{\rho\sigma} a_\sigma^{(1)} = -\left(\frac{\partial a_\rho^{(0)}}{\partial x_0} + \alpha_{\rho\sigma}^k \frac{\partial a_\sigma^{(0)}}{\partial x_k}\right) \quad (5)$$

where

$$\Pi_0 = -\frac{\partial S}{\partial x_0} + \frac{e}{c}\phi_0; \quad \Pi_k = \frac{\partial S}{\partial x_k} + \frac{e}{c}\phi_k. \quad (6)$$

Corresponding equations hold for higher approximations. Condition for the solubility of the homogeneous system (4) for $a_\rho^{(0)}$ is that its determinant must vanish. This is equivalent with:

$$-\Pi_0^2 + \Sigma \Pi_k^2 + m^2 c^2 = 0 \quad (7)$$

which is the Hamilton-Jacobi partial differential equation. Let us assume that as far as its classical-mechanical aspects are concerned, the problem has been solved, so that we know Π_0, Π_k as functions of the coordinates. It is then seen that the system (4) has four solutions $a_{\rho\tau}^{(0)}$ ($\tau = 1 \dots 4$). They are, except for a multiplicative constant to be determined later,

$$a_{\rho\tau}^{(0)} = \Pi_0 \delta_{\rho\tau} + \alpha_{\rho\sigma}^k \Pi_k + mc\beta_{\rho\sigma} \tau. \quad (8)$$

It is easily seen by direct substitution that (8) satisfies (4) for any index τ . The above solutions are, however, not linearly independent, as there are the following four relations between them:

$$-a_{\rho\tau}^{(0)} \Pi_0 + a_{\rho\sigma}^{(0)} \alpha_{\sigma\tau}^k \Pi_k + a_{\rho\sigma}^{(0)} \beta_{\sigma\tau} mc = 0 \quad (9)$$

which form the adjoint system to (4). Each equation of this adjoint system connects three of the solutions (8); it is thus possible to express two of the

$a_{\rho\tau}^{(0)}$ by two others leaving only two linearly independent solutions (say $a_{\rho 1}^{(0)}$ and $a_{\rho 2}^{(0)}$) of (4). This is as it should be; the two independent solutions correspond to the two directions of the spin (or of the polarization). The general solution of (4) is then obtained by multiplying $a_{\rho 1}^{(0)}$ and $a_{\rho 2}^{(0)}$ with two as yet arbitrary functions C and C' of the coordinates and by adding:

$$a_{\rho}^{(0)} = C(x_0, x_k) a_{\rho 1}^{(0)} + C'(x_0, x_k) a_{\rho 2}^{(0)} \quad (10)$$

The determination of C and C' follows from (5), which is an inhomogeneous system whose homogeneous system has solutions. As is well known, the right-hand side of (5) and the solutions of the adjoint homogeneous system (9) have to be orthogonal, which condition can be put into the following form:

$$\bar{a}_{\rho\tau}^{(0)} \left(\frac{\partial a_{\rho}^{(0)}}{\partial x_0} + \alpha_{\rho\sigma k} \frac{\partial a_{\sigma}^{(0)}}{\partial x_k} \right) = 0; \quad \tau = 1, 2. \quad (11)$$

where we indicate by the bar, that the complex conjugate has to be taken (provided, as will be the case, that the Π themselves are real). Having determined C and C' by means of these differential equations,

$$a_{\rho}^{(0)} e^{iS/\hbar}$$

represents in first approximation the wave functions everywhere except in the vicinity of the turning points of the classical orbit, where certain of the Π_0, Π_k vanish, and the approximation of geometric optics breaks down. How to deal with these exceptional points, will be seen later.

3.

We put the magnetic field H parallel to the z axis of a cartesian coordinate system. The scalar potential ϕ_0 is zero; the vector potential is chosen to be:

$$\phi_1 = -Hy; \quad \phi_2 = 0; \quad \phi_3 = 0. \quad (12)$$

The Hamilton-Jacobi differential Eq. (7) becomes:

$$-\left(\frac{\partial S}{\partial x_0}\right)^2 + \left(\frac{\partial S}{\partial x} - \frac{eH}{c}y\right)^2 + \left(\frac{\partial S}{\partial y'}\right)^2 + \left(\frac{\partial S}{\partial z}\right)^2 + m^2c^2 = 0. \quad (13)$$

Since x_0, x and z are evidently cyclic, we put:

$$S = -\Pi_0 x_0 + p_x x + \Pi_3 z + \sigma(y) \quad (14)$$

where Π_0, Π_3 and $p_x = m\dot{x}$ are constant. We introduce for the sake of brevity

$$\Pi_r^2 = \Pi_1^2 + \Pi_2^2 = \Pi_0^2 - \Pi_3^2 - m^2c^2 \quad (15)$$

the constant momentum in the x, y plane. For $\sigma(y)$ we have:

$$\sigma = \int^y \Pi_2 dy = \int^y \left[\Pi_r^2 - \left(p_x - \frac{eH}{c}y \right)^2 \right]^{1/2} dy. \quad (16)$$

The radicand vanishes at the turning points $y_1 < y_2$.

$$(eH/c)y_{2,1} = p_x \pm \Pi_r.$$

It is seen that the orbits are circles with the radius $(c/eH)\Pi_r$, whose centers lie on a line parallel to the x axis and at a distance $(c/eH)p_x$ from it.

4.

It is now necessary to specialize the matrices α^k and β . We take the following well-known matrix system:

$$\begin{aligned} \beta &= \begin{pmatrix} 1 & 0 & 0 & 0 \\ 0 & 1 & 0 & 0 \\ 0 & 0 & -1 & 0 \\ 0 & 0 & 0 & -1 \end{pmatrix}; & \alpha^1 &= \begin{pmatrix} 0 & 0 & 0 & 1 \\ 0 & 0 & 1 & 0 \\ 0 & 1 & 0 & 0 \\ 1 & 0 & 0 & 0 \end{pmatrix}; \\ \alpha^2 &= \begin{pmatrix} 0 & 0 & 0 & -i \\ 0 & 0 & i & 0 \\ 0 & -i & 0 & 0 \\ i & 0 & 0 & 0 \end{pmatrix}; & \alpha^3 &= \begin{pmatrix} 0 & 0 & 1 & 0 \\ 0 & 0 & 0 & -1 \\ 1 & 0 & 0 & 0 \\ 0 & -1 & 0 & 0 \end{pmatrix}. \end{aligned} \quad (18)$$

Introducing these into (8) the $a_{p\tau}^{(0)}$ occurring in (10) are found to be:

$$\begin{aligned} a_{p1}^{(0)} &= (\Pi_0 + mc, \quad 0, \quad \Pi_3, \Pi_1 + i\Pi_2) \\ a_{p2}^{(0)} &= (0, \Pi_0 + mc, \Pi_1 - i\Pi_2, -\Pi_3). \end{aligned} \quad (19)$$

We then put (19) and (10) into (11) and get after a few elementary transformations:

$$\Pi_0 \frac{\partial C}{\partial x_0} + \Pi_1 \frac{\partial C}{\partial x} + \Pi_2 \frac{\partial C}{\partial y} + \Pi_3 \frac{\partial C}{\partial z} - \frac{1}{2} \left(\frac{\partial \Pi_2}{\partial y} - i \frac{\partial \Pi_1}{\partial y} \right) C = 0 \quad (20)$$

and the complex conjugate equation for C' .

It is most convenient to integrate these differential equations in the momentum space. We have

$$\partial C / \partial x_\sigma = (\partial C / \partial \Pi_\lambda) (\partial \Pi_\lambda / \partial x_\sigma)$$

which vanishes for $\sigma = 1, 2, 3$. Only the derivative with respect to y gives a contribution. Because of

$$\frac{d\Pi_1}{dy} = -\frac{eH}{c}; \text{ and } \frac{d\Pi_2}{dy} = \frac{eH}{c} \frac{\Pi_1}{\Pi_2} \quad (21)$$

one finds

$$\frac{\partial C}{\partial y} = \frac{eH}{c} \left(-\frac{\partial C}{\partial \Pi_1} + \frac{\Pi_1}{\Pi_2} \frac{\partial C}{\partial \Pi_2} \right).$$

By means of this formula and of (21) the differential Eq. (20) is readily transformed into:

$$-\Pi_2 \frac{\partial C}{\partial \Pi_1} + \Pi_1 \frac{\partial C}{\partial \Pi_2} + \frac{1}{2} \left(\frac{\Pi_1}{\Pi_2} + i \right) C = 0. \quad (22)$$

Introducing polar coordinates in the Π_1, Π_2 plane:

$$\Pi_1 = \Pi_r \sin \theta; \quad \Pi_2 = \Pi_r \cos \theta$$

we get:

$$-\frac{\partial C}{\partial \theta} + \frac{1}{2}(\operatorname{tg} \theta + i)C = 0.$$

Since Π_r does not occur in this differential equation C is seen to be a function of the quotient Π_1/Π_2 solely. Straightforward integration gives:

$$C = \frac{K}{(\cos \theta)^{1/2}} e^{i\theta/2} = \frac{K'}{\Pi_2^{1/2}} \exp \left[\frac{i}{2} \operatorname{arctg} \frac{\Pi_1}{\Pi_2} \right] \quad (23)$$

or

$$C = K'' \left(\frac{\Pi_1 - i\Pi_2}{\Pi_2} \right)^{1/2}. \quad (23')$$

The latter form is obtained using the well-known connection between the arctg and the \log . For C' the complex conjugate is found. Putting (23) and (19) into (10) we finally have:

$$\begin{aligned} a_p^{(0)} = \frac{K'}{\Pi_2^{1/2}} \bigg\{ & (\Pi_0 + mc) \exp \left[\frac{i}{2} \operatorname{arctg} \frac{\Pi_1}{\Pi_2} \right], \\ & (\Pi_0 + mc) e \exp \left[-\frac{i}{2} \operatorname{arctg} \frac{\Pi_1}{\Pi_2} \right], \\ & (\Pi_r + \Pi_3) \exp \left[\frac{i}{2} \operatorname{arctg} \frac{\Pi_1}{\Pi_2} \right], \\ & (\Pi_r - \Pi_3) \exp \left[-\frac{i}{2} \operatorname{arctg} \frac{\Pi_1}{\Pi_2} \right] \bigg\} \end{aligned} \quad (24)$$

or from (23'):

$$a_p^{(0)} = K''/\Pi_2^{1/2} \{ (\Pi_0 + mc)(\Pi_1 - i\Pi_2)^{1/2}, (\Pi_0 + mc)(\Pi_1 + i\Pi_2)^{1/2}, \\ (\Pi_r + \Pi_3)(\Pi_1 - i\Pi_2)^{1/2}, (\Pi_r - \Pi_3)(\Pi_1 + i\Pi_2)^{1/2} \}. \quad (24')$$

With these amplitudes the current and the density take the form

$$(s_x, s_y, s_z, \rho) = 4K''\Pi_r(\Pi_0 + mc) \frac{1}{\Pi_2} (\Pi_1, \Pi_2, \Pi_3, \Pi_0)$$

in agreement with the proportion:

$$s_k : \rho = \Pi_k : \Pi_0.$$

5.

The last problem will be the determination of the multiplicative constant K . It was pointed out before that, according to the sign of Π_2^2 we have to distinguish three regions (compare 17):

$$\begin{aligned}
 \text{(I)} \quad & y < y_1 & \Pi_2 &= \pm i(\Pi_1^2 - \Pi_r^2)^{1/2} \\
 \text{(II)} \quad & y_1 < y < y_2 & \Pi_2 &= \pm (\Pi_r^2 - \Pi_1^2)^{1/2} \\
 \text{(III)} \quad & y_2 < y & \Pi_2 &= \pm i(\Pi_1^2 - \Pi_r^2)^{1/2}.
 \end{aligned}$$

II is the classically occupied interval between the two turning points. Since in I and III the action function $\sigma = \int \Pi_2 dy$ becomes imaginary they represent classically unreached regions. The approximate expressions for the wave functions have, according to (1), (14) and (16), different analytical character in the three regions: in I and III they will be exponential functions with real exponents, and in II they will be oscillating functions. In the three regions one is at liberty to multiply the wave functions with constants, the relation between which remains undetermined by our approximate method. However, these constants are determined by the requirement that our approximate wave functions in the various regions be asymptotic expressions of one and the same physically admissible solution of the rigorous Dirac equations.

In the nonrelativistic theory where the same difficulty occurs, the Kramers connection formulae show how to link up the constants inside the two turning points with those outside. The Schrödinger equation may be written in the form:

$$\psi'' + \frac{f(y)}{h^2} \psi = 0 \quad (25)$$

where $f(y)$ is a continuous function with two roots y_1 and y_2 so that for $y_1 < y < y_2$ the function $f(y)$ is positive, otherwise negative. The requirement that ψ be real and vanish for $y = \pm \infty$ restricts the choice of asymptotic solutions to those that vanish exponentially outside and oscillate like trigonometric functions inside. Now the connection formulae of Kramers state, e.g., for the turning point y_1 , that for $y < y_1$, the function

$$K_I |f^{-1/4}| \exp \left\{ \frac{1}{h} \int_{y_1}^y (-f)^{1/2} dy \right\} \quad (26)$$

and for $y_1 < y < y_2$ the function

$$K_{II} |f^{-1/4}| \cos \left\{ \frac{1}{h} \int_{y_1}^y f^{1/2} dy + \epsilon \right\} \quad (27)$$

are then and only then, asymptotic representations of the same particular solution of the above differential equation if

$$K_{II} = 2K_I \text{ and } \epsilon = -\pi/4. \quad (28)$$

Similarly for the other turning point.

These considerations of Kramers can be applied to our case without change, because it is easily possible to bring our first order differential Eqs. (3) into the form of Eq. (25). For the second order Dirac equations

$$(-\Pi_0^2 + \Sigma \Pi_k^2 + m^2 c^2) \psi_\rho = - (eh/2ic) (\alpha^k \alpha^l)_{\rho\sigma} F_{kl} \psi_\sigma$$

are in our case no longer simultaneous equations. The field tensor F_{kl} has only one component $F_{12} = H_z$, and the matrix $\alpha^1 \alpha^2$ is diagonal, as is seen from (18). In order to get complete agreement with Kramers' form of the solutions we write the wave functions with the function C and C' in the form of (23). Then the Kramers amplitude is:

$$|f^{-1/4}| = |\Pi_2^{-1/2}| = |(\Pi_r^2 - \Pi_1^2)^{-1/4}| \quad (29)$$

and the phase is:

$$P_\rho = \frac{1}{h} \int_{y_1}^y \Pi_2 dy \pm \frac{1}{2} \left(\arctg \frac{\Pi_1}{\Pi_2} - \frac{\pi}{2} \right) \quad (30)$$

where according to (24) the upper sign is to be taken for $\rho = 1, 3$ and the lower sign for $\rho = 2, 4$. The phase constant was fixed so that P_ρ vanishes at y_1 in agreement with (26) and (27).

Since Π_2 is real within, and imaginary outside of, the interval $y_1 y_2$, the wave function $|\Pi_2^{-1/2}| \exp i P_\rho$ will indeed oscillate in region II and will be exponentially decreasing or increasing in I and III.

Now the requirement that ψ_ρ vanish for $y = -\infty$ leaves as only choice for region I:

$$\psi_\rho^I = K(\)_\rho |\Pi_2^{-1/2}| \exp(+P_\rho). \quad (31)$$

As is seen from (24) the bracket with the index ρ is either $\Pi_0 + mc$ for $\rho = 1, 2$ or $\Pi_r \pm \Pi_3$ for $\rho = 3, 4$. The unessential factor $\exp i(-\Pi_0 x_0 + p_x x + \Pi_3 z)$ was left off.

The Kramers connection requires that this wave function is continued in II as

$$\psi_\rho^{II} = 2K(\)_\rho |\Pi_2^{-1/2}| \cos(P_\rho - \pi/4). \quad (32)$$

The analogous connection must now be carried out at the other turning point y_2 . The phase Q_ρ which at y_2 plays the same rôle as P_ρ at y_1 , is

$$Q_\rho = \frac{1}{h} \int_{y_2}^y \Pi_2 dy \pm \frac{1}{2} \left(\arctg \frac{\Pi_1}{\Pi_2} + \frac{\pi}{2} \right). \quad (33)$$

Introducing the abbreviation

$$I = \frac{1}{h} \int_{y_1}^{y_2} \Pi_2 dy = \frac{1}{2h} \oint \Pi_2 dy = \frac{c\pi}{2ehH} \Pi_r^2 \quad (34)$$

one may write (32):

$$\left. \begin{aligned} \psi_\rho^{II} &= 2K(\)_\rho |\Pi_2^{-1/2}| \cos(Q_\rho - \pi/4 + I \pm \pi/2) \\ &= 2K(\)_\rho |\Pi_2^{-1/2}| \left\{ \cos\left(I \pm \frac{\pi}{2}\right) \cos\left(Q_\rho - \frac{\pi}{4}\right) \right. \\ &\quad \left. - \sin\left(I + \frac{\pi}{2}\right) \cos\left(Q_\rho + \frac{\pi}{4}\right) \right\} \end{aligned} \right\} \quad (35)$$

Applying the connection formulae again, the first term inside the parenthesis gives rise to an exponentially increasing function in III, the second term to the desired exponentially decreasing function. We must therefore require

$$\cos(I \pm \pi/2) = 0$$

which gives for ψ_p^{III} :

$$\psi_p^{\text{III}} = \pm K(\rho) |\Pi_2^{-1/2}| \exp(-Q_\rho). \quad (36)$$

The above condition leads to:

$$I = (n + \frac{1}{2} \pm \frac{1}{2})\pi$$

or using (34)

$$\oint \Pi_2 dy = (n + \frac{1}{2} \pm \frac{1}{2})h_0 \quad (37)$$

where $h_0 = 2\pi\hbar$ is the ordinary Planck constant. Eqs. (37), (34) and (15) determine the energy. Eqs. (31), (35) and (36) represent the eigenfunctions. Of course, they may also be written in a form analogous to (24').

Kramers obtained the result that the influence of wave mechanics upon phase-integral quantization meant replacing the integer quantization by half-integer quantization. As (36) shows, relativity and spin as embodied in the Dirac equations mean a return to whole number quantization but with each level possessing a twofold degeneracy. This result may be interpreted in the usual vector language that the spin moment $s = \frac{1}{2}$ is added in two directions to the orbital moment $l = n + \frac{1}{2}$. This used to be called the "branching-off principle."

The problem of an electron moving in a homogeneous magnetic field, was treated by various authors,⁵ according to the rigorous Dirac equations. It is interesting to note that our result for the energy agrees rigorously with the energy determination on the basis of the complete Dirac equations.

The author is greatly indebted to Professor W. Pauli for helpful discussions.

⁵ W. Alexandroff, *Zeits. f. Physik* **56**, 818 (1929); *Ann. d. Physik* **2**, 477 (1929). E. Fues and H. Hellmann, *Phys. Zeits.* **31**, 465 (1930). L. D. Huff, *Phys. Rev.* **38**, 501 (1931).

The Isotope Displacement in Hyperfine Structure

By G. BREIT

Department of Physics, New York University

(Received September 12, 1932)

With Goudsmit's extension of Landé's formula for $(1/r^3)$ it is possible to explain the order of magnitude of the isotope displacements in Hg, Tl, Pb arc and spark spectra on the hypothesis of small changes in nuclear radii. The nuclear radius is supposed to be proportional to the $1/3$ power of the atomic weight. The effective nuclear charge is supposed to be distributed with a roughly uniform density through the interior of the nucleus. The spectra Hg I, Hg II, Tl I, Tl II, Pb II, are in agreement with the above theory. The larger displacements are due to the addition or removal of a $6s$ or $7s$ electron to the electron configuration. The direction of the shift is in agreement with the supposition that the nuclear radius increases with atomic weight, the heavier isotope having the looser binding for the s and $p_{1/2}$ electrons. In order to explain the shifts of the $6p^2$, $6p7s$, $6p8s$, $d6p$, $6p8p$ configurations of PbI it is supposed that in this case the displacements are due principally to changes in the penetration to the nucleus of the $6s^2$ subgroup. These changes are presumably caused by differences in screening of the two $6s$ electrons from the nucleus as the valence electron is excited from the $6p$ state to the ionization limit.

THE elements Hg, Tl, Pb show in their hyperfine structure a number of components which are ascribed to the different isotopes of these elements. The observed displacements are considerably larger than would be expected according to the simple mass correction to the Rydberg formula given by the factor $(1 + m/M)^{-1}$. The suggestion has been made that these isotope displacements are due to deviations of the electric field of the nucleus from the inverse square law. Calculations by Racah¹ and also by Rosenthal and the writer² indicated however that on such a hypothesis the displacement would be expected to be several times larger than that observed. In addition, in the case of Tl, it appeared impossible³ to reconcile the observed direction of the displacement in the spark with that in the arc spectrum.

It has since been found possible to interpret the troublesome terms of Tl in such a way that the direction of the displacement in its arc and spark spectrum fits in with that observed in Hg and Pb. For these three elements, the large displacements can be attributed consistently to differences of binding of s electrons and particularly those of the deeply penetrating $6s$ electron. It was furthermore found that a simple formula used by Goudsmit³ in the calculation of hyperfine structure separations gives in these cases smaller values for the probability of finding an electron at the nucleus than the numerical calculations of Racah which have been used by Rosenthal and the writer as well. It appears possible that the numerical calculations may be sub-

¹ G. Racah, *Nature* **129**, 723 (1932).

² J. E. Rosenthal and G. Breit, *Phys. Rev.* **41**, 459 (1932).

³ Pauling and Goudsmit, *Structure of Line Spectra*. See also J. C. McLennan, A. B. McLay and M. F. Crawford *Proc. Roy. Soc. A* **133**, 652 (1931).

ject to cumulative errors and it is at all events of interest that Goudsmit's application of the Landé formula for $\langle 1/r^3 \rangle$ leads to a reasonable agreement of the expected and observed isotope displacements.

In order to obtain an expression for the square of the Shroedinger function at $r=0$ we use Landé's approximate formula

$$l(l+1) \left\langle \frac{1}{r^3} \right\rangle = \frac{R\alpha^2 Z_i Z_0^2}{\mu_0^2 (2l+1) n_0^2} \quad (1)$$

where l is the azimuthal quantum number, R the energy corresponding to the Rydberg constant, $\alpha = 2\pi e^2/hc$, μ_0 is the Bohr magneton, Z_i is the effective nuclear charge in the inner part of the orbit, Z_0 is the effective charge in the outer part of the orbit and n_0 is the effective quantum number defined by equating the term energy to $-R Z_0^2/n_0^2$. This formula has been derived by Landé by means of classical considerations with penetrating orbits. One may expect it, however, to be at least qualitatively correct also in quantum mechanics. For s terms the meaning of the left side of (1) is known to be⁴

$$\overline{l(l+1)r^{-3}} = 2\pi\psi^2(0) \quad (2)$$

so that

$$\psi^2(0) = \frac{Z_i Z_0^2}{\pi a_H^3 n_0^3} = 2.16 \times 10^{24} \frac{Z_i Z_0^2}{n_0^3} \text{ cm}^{-3} \quad (3)$$

where a_H is the Bohr radius. It will be noted that for *Coulomb fields* Eq. (3) is exact. The fact that for $l=0$ the left side of (2) is indeterminate does not concern us because in the relativistic theory of hyperfine structure this expression is replaced by one having a perfectly definite meaning. Also Eq. (3) may be interpreted along the lines of Landé's penetrating orbits by regarding $(Z_0/Z_i)^2/n_0^3$ as the factor by which the normalization constant in the region of effective nuclear charge Z_i is decreased on account of the presence of the region with effective nuclear charge Z_0 . Thus (3) is a reasonable approximation. We do not pretend, however, to regard it as exact and the ultimate test of its validity lies in comparing it with accurate numerical calculations. Computing $\psi^2(0)$ for the normal states of the alkalis by means of (3) we have the following comparison (Table I) with values of $\psi^2(0)$ obtained by means of numerical calculations of the eigenfunctions:

TABLE I.

Element:	Na	Cs	Rb
$\psi^2(0)$ by (3):	5.6×10^{24}	1.8×10^{25}	1.4×10^{25}
$\psi^2(0)$ according to Fermi ⁵ :	2.4×10^{24}	2.7×10^{25}	0.88×10^{25}
$\psi^2(0)$ according to Nile:		$1.7(5) \times 10^{25}$	

⁴ G. Breit, Phys. Rev. 37, 51 (1931).

⁵ E. Fermi, Zeits. f. Physik 60, 320 (1930).

For the lighter elements $\psi^2(0)$ is smaller when computed numerically. For Cs the very careful as yet unpublished calculations of Niele agree very well with (3) while Fermi's value is appreciably higher.

It will be seen that in the case of Tl the comparison of the magnitude of the hfs splitting of the 7s state is in much better agreement⁶ with that of the $6p_{1/2}$ using (3) than the numerical calculations of $\psi^2(0)$ for this state made by Racah. One may regard the hfs splitting as an empirical determination of $\psi^2(0)$ and it appears that this determination fits in with the magnitude of the isotope shift and with the value for $\psi^2(0)$ obtained by means of (3).

In mercury the isotope displacement has been observed both for the spark and the arc spectra. In the spark spectrum Schüller and Jones⁷ arrive at an interpretation according to which the largest displacement is that of the $^2D_{5/2}$ term belonging to the $5d^9 6s^2$ configuration. The other terms belong to the $5d^{10} 6s$, $5d^{10} 6p$, $5d^{10} 7s$ arrangements. The displacement between Hg²⁰⁴ and Hg²⁰² is 0.52 cm^{-1} and it is significant that the energy of Hg²⁰⁴ is higher than that of Hg²⁰². This shows that a change of an electron from the 5d to the 6s state produces a larger energy increase in Hg²⁰⁴ than in Hg²⁰². The 6s electron may be thus thought of as less tightly bound in Hg²⁰⁴ than in the lighter isotopes. Similarly in the arc spectrum⁸ of Hg the largest displacement is assigned to $6s^2 \ ^1S_0$, the shift between Hg²⁰⁴ and Hg²⁰² being 0.15 cm^{-1} while that between Hg²⁰¹ and Hg¹⁹⁹ is reported to be 0.21 cm^{-1} . The direction of the shift is again such that Hg²⁰⁴ has the highest energy. The 6s 7s configuration also shows a shift in the same direction but of a smaller magnitude, the displacement between Hg²⁰⁴ and Hg²⁰² being 0.03 cm^{-1} both in the 1S_0 and 3S_1 states.

It has been observed by Shenstone and Russell⁹ that the large displacement of the 1P terms of this spectrum finds a natural interpretation in a perturbation of these terms by the $5d^9 6s^2 6p$ configuration. In particular the $8 \ ^1P_1$ term⁹ shows an isotope displacement of practically the same amount as the $6s^2 \ ^1S_0$ term. The direction of the displacement is again the same and corresponds to a tighter binding of the 6s electron in the lighter isotope.

For Tl it appeared at first difficult² to interpret the displacement in terms of nuclear fields because the directions of the shift in the spark and arc spectrum did not agree. A further examination of the data¹⁰ showed that the terms with large displacements are the X_2 and the term previously designated as $6s 7p \ ^1P_1$. According to McLennan and Crawford¹¹ this designation is incorrect and it is therefore called by them 1_1^0 . In this term as well as in X_2 the lighter isotope Tl²⁰³ has a tighter binding between the electrons and the nucleus than Tl²⁰⁵. The analogy between this and Hg suggests that X_2 and 1_1^0

⁶ This has been observed first by Goudsmit who kindly informed the writer of the fact.

⁷ H. Schüller and E. G. Jones, *Zeits. f. Physik* **76**, 14 (1932), see Fig. 1, p. 17.

⁸ H. Schüller and J. E. Keyston, *Zeits. f. Physik* **72**, 423 (1931), see Fig. 16, p. 438. H. Schüller and E. G. Jones, *Zeits. f. Physik* **74**, 631 (1932).

⁹ A. G. Shenstone and H. N. Russell, *Phys. Rev.* **39**, 415 (1932), see p. 427. The " $8 \ ^1P_1$ " term practically belongs to the $5d^9 6s^2 6p$ configuration.

¹⁰ H. Schüller and J. E. Keyston, *Zeits. f. Physik* **70**, 1 (1931).

¹¹ J. C. McLennan and M. F. Crawford, *Proc. Roy. Soc. A* **132**, 10 (1931).

belong to a configuration involving two $6s$ electrons. Professor Goudsmit kindly examined the data on Tl II and Tl III, and it appears in fact quite logical to interpret the X_2 (McLennan and Crawford's 3_2^0) and the 1_1^0 terms of Tl II as belonging to the $5d^9 6s^2 6p$ configuration, the difference in term values of $5d^9 6s 6p^4 F^0$ and $5d^{10} 6s$ of Tl III being $\cong 124,000 \text{ cm}^{-1}$ while the difference in term values of 1_1^0 , X_2 from $5d^{10} 6s^2$ in Tl II is respectively $126,204$ and $125,437 \text{ cm}^{-1}$. With this interpretation, the observed senses of the displacements in Tl I and Tl II are in agreement provided one supposes that $5d^{10} 6s^2 6p^2 P_{3/2}$ of Tl I is undisplaced so that the largest displacement is to be assigned to $5d^{10} 6s^2 7s^2 S_{1/2}$ and a somewhat smaller displacement to $5d^{10} 6s^2 6p^2 P_{1/2}$. This view appears to be in disagreement with the reported fact that combinations of the higher 2P terms with $5d^{10} 6s^2 7s^2 P_{1/2}$ show no isotope shift. The experimental difficulties involved are apparently very high, however, as shown by the disagreement between Jackson and Schüller and Keyston on the isotope shift of $\lambda 3776$. Since the direction of the displacement in Tl II is the same as in Hg I, II and Pb I, II, it would be surprising if Tl I were different. [See discussion of Pb I below.]

The displacements in Pb II have been discussed previously.² The view that the large shifts are to be attributed to the $6s$ electrons is seen to be in agreement with the similar cases in Tl and Hg both with respect to the direction of the shift and its order of magnitude.

The isotope displacements in Pb I fit into the above theory only partly. Taking the $6p^2 \ ^1D_2$ level as having no displacement, and letting $\Delta W = W(\text{Pb}^{208}) - W(\text{Pb}^{206})$ we obtain, using the data of Kopfermann,¹² Rose and Granath,¹³ and of Schüller and Jones¹⁴ the following approximate values for ΔW in cm^{-1} : $6p^2 \ ^1S_0 + 0.01$; $6p^2 \ ^3P_{0,1,2} + 0.01$; $7s 6p \ ^3P_{0,1} + 0.09$; $d \ ^3D_{3,1} + 0.07$; $d \ ^3F_3 + 0.07$; $8s 6p \ ^3P_{1,2} + 0.09$; $7s 6p \ ^1P_1 + 0.07$; $6p 8p \ ^3P_1 + 0.08$; $6p 8p \ ^3P_0 + 0.07$. The fact that all levels of the $6p^2$ configuration have approximately the same isotope displacement indicates that ΔW for $6p_{1/2}$ is small and of the order of 0.01 cm^{-1} so that $\Delta W(6p_{3/2})$ can be neglected altogether. The relatively large displacement of the $d \ 6p$ terms is therefore rather puzzling. It may possibly be due to a perturbation by the $6p \ 7s$ configuration, and it may also be that there is as a consequence a perturbation with $6p \ 8s$. Such perturbations make it possible to explain why the displacements of $6p \ 7s$ and of $6p \ 8s$ are of the same order of magnitude. With the above mutual perturbations of $d \ 6p$ by $6p \ 7s$ and of $6p \ 8s$ by $d \ 6p$, the approximately equal shifts of the three configurations may be understood and should then be ascribed mainly to the influence of the $7s$ electron.

It is more difficult, however, to interpret the relatively large shifts of $6p 8p \ ^3P_{0,1}$ which follow from the observed structure¹⁴ of $\lambda\lambda 6059, 6012, 5896$. On the present theory we should expect the shifts to be of the same order as

¹² H. Kopfermann, *Zeits. f. Physik* **75**, 363 (1932); *Naturwiss.* **19**, 400 (1931); **19**, 675 (1931).

¹³ John L. Rose and L. P. Granath, *Phys. Rev.* **40**, 760 (1932). With the later data of Schüller and Jones $a' = 0.012$, $a'' = 0.372$ for $6p^2$.

¹⁴ H. Schüller and E. G. Jones, *Zeits. f. Physik* **75**, 563 (1932).

those of $6p^2\ ^3P_{1,2}$ while actually they are approximately the same as those of the $6p\ 7s$ configuration. It is not possible that the $6p\ 8p$ configuration could be perturbed by $6p\ 7s$ or $d\ 6p$ so that another explanation must be looked for.

It should be remembered in this connection that the subgroup $6s^2$ is present in all of the Pb I spectrum. A change in the screening constant of the two $6s$ electrons would lead to an isotope shift. It appears possible, although it is not certain, that the screening of the nucleus by $8p$ is sufficiently weaker than the screening by $6p$ to produce a larger penetration of $6s$ and a consequent isotope shift. The existences of such effects is also suggested by the apparent absence of isotope shifts in the lines $7s\ mp$ of Tl I which would otherwise be expected to show the full shift of the $7s$ electron. As has already been mentioned in connection with Tl I we do not feel very confident that a shift of the $7s\ mp$ lines could have been detected with certainty since there appears to be some contradiction between different observers of $\lambda 3776$. It appears nevertheless reasonable to suppose that in Pb I the $6s$ electrons have a smaller $\psi^2(0)$ when the valence electron is in a low energy state, because from the point of view of our theory this fits in with the presence of isotope shifts in all the higher terms in the Pb I spectrum. The mass effect considered by Hughes and Eckart for Li can hardly have much to do with the observed shifts in Pb I since there appears no reason why it should give the same shifts for the five ground levels and since it should give equal spacings between Pb^{206} , Pb^{207} , Pb^{208} which is not the case experimentally. It thus seems that changes in $\psi^2(0)$ of $6s$ and perhaps other underlying groups should be considered as mainly responsible for the isotope shifts in Pb I. In Pb II, however, we deal primarily with shifts due to the addition or subtraction of a $6s$ electron and we are thus not concerned with the smaller effects of differences in penetration.

Both the isotope shifts and the nuclear spin term splittings depend on the penetration of the electrons to the nucleus. We discuss, therefore, briefly the theoretical interpretation of the nuclear spin term splittings for Pb I in order to see whether it can be made consistently.

Using (jj) coupling and supposing that 3P_0 belongs to $6p_{1/2}\ 8p_{1/2}$ while 3P_1 belongs to $6p_{1/2}\ 8p_{3/2}$, we derive from the observed level splitting of -0.155 cm^{-1} the value¹⁵ $A = -0.103\text{ cm}^{-1}$ and $a''(6p) = A(6p_{1/2}) = 0.41\text{ cm}^{-1}$ which compares reasonably well with the value¹³ 0.37 cm^{-1} derived by means of the sum rule from the splittings of the $6p^2$ configuration. The interpretation of $6p\ 8p\ ^3P_1$ as $6p_{1/2}\ 8p_{3/2}$ appears to be a natural one in view of the fact that it falls into the same series with $6p^2\ ^3P_1$. Also the interpretation of $6p\ 7s\ ^3P_1$ and $6p\ 8s\ ^3P_1$ as $6p_{1/2}\ 7s\ (j=1)$ and $6p_{1/2}\ 8s\ (j=1)$ leads to reasonable values $a''(6p) + a(7s) = 0.586$, $a''(6p) + a(8s) = 0.386$ which gives on using $a''(6p) = 0.372$, $a(7s) = 0.214$ and $a(8s) = 0.014$. Using the observed¹⁴ splitting -0.060 cm^{-1} for $6p\ 7s\ ^1P_1$ and interpreting this term as $6p_{3/2}\ 7s\ (j=1)$, we obtain $A = -0.040\text{ cm}^{-1}$, $5a'(6p) - a(7s) = -0.160\text{ cm}^{-1}$. Using here $a(7s) = +0.214\text{ cm}^{-1}$ we get $a'(6p) = 0.011\text{ cm}^{-1}$ in good agreement with $a'(6p)$

¹⁵ S. Goudsmit, Phys. Rev. **37**, 663 (1931). For (jj) coupling

$$A = \{[j(j+1) + j_1(j_1+1) - j_2(j_2+1)]a(j_1) + [j(j+1) + j_2(j_2+1) - j_1(j_1+1)]a(j_2)\} / 2j(j+1).$$

$=0.007 \text{ cm}^{-1}$ which follows from the $6p^2$ configuration according to Rose and Granath's data¹³ and 0.012 cm^{-1} according to Kopfermann's¹² and the latest of Schüller and Jones.¹⁴ The 3F_3 level of the $d6p$ configuration must be interpreted as $d_{5/2} \cdot 6p_{1/2}$. For if the observed¹² splitting is 0.250 cm^{-1} , $A = 0.0714 \text{ cm}^{-1}$ and $a''(6p) = 0.43 \text{ cm}^{-1}$ again in fair agreement with 0.37 cm^{-1} from the $6p^2$ configuration. The hfs splittings do not call, therefore, for any change in the interpretation of the terms and we are thus unable to interpret the large displacements of the $6p \ 8p$ configuration^{16,17} *except as a change in the effective screenings of $6s^2$* . Experimental material on other levels of the $6p \ mp$ series would be of value in arriving at a definite explanation.

The comparison of the observed and theoretically expected shifts is given in Table II.

TABLE II.

Element and spectrum	Electron state	$\psi^2(0)10^{-26}$	Method of computation	Shift as multiple of $A\Delta y_0/y_0$	Fractional change in nuclear radius $\Delta y_0/y_0$	Expected shift in cm^{-1}	Observed shift in cm^{-1}
Tl I	$7s$	0.17	Goudsmit		$1/300$	0.07	0.06
"	"	0.49	Racah	360	"	0.2	"
"	$7p_{1/2}$			49	"	0.03	0.01 ± 0.005
Tl II	$6s$	<1.6	Goudsmit from Tl III		"	<0.8	0.23
"	"	2.8		2060	"	1.4	"
Pb I	$7s$				"		0.07
Pb II	$6s$		G. from Hg II		"	0.70	0.50
Hg I	$6s$				"		0.18
"	$7s$	0.30	G. from Hg II		"		0.03
Hg II	$6s$	1.45	G. from Hg II	1060	"	0.70	0.52

$$A = (n+1)/(2\rho+1) (2\rho+n+1) \sim 1/5 \text{ for } \rho=0.81.$$

It will be noted that in the one electron spectra of Tl I, Hg II the agreement with Goudsmit's formula for $\psi^2(0)$ is quite satisfactory. Only in such cases is the use of this formula safe because the screening is then the same in the calculation of the effective quantum number and in the calculation of

¹⁶ The *relative* values of the isotope shifts which should be expected for $7s$ and $6p_{1/2}$ of Pb I are approximately the same as in Tl I because for Pb I, $a(7s) \sim 0.22$, $a''(6p) \sim 0.37$ while for Tl I, $a(7s) \sim 0.40$, $a''(6p) \sim 0.71$ so that the ratio $a(7s)/a''(6p)$ is nearly the same for the two spectra.

¹⁷ The small disagreements which exist in the above comparison between theory and experiment for the hfs of Pb I can be easily explained by the influence of the penetration of the electrons on the coupling to the nucleus and by the fact that the coupling is intermediate between Russell-Saunders and jj . For the $6p^2$ configuration the Zeeman effect g values determine the 1D_2 term as $0.93 \ 6p_{3/2} \ 6p_{3/2} + 0.38 \ 6p_{3/2} \ 6p_{1/2}$ and 3P_2 as $0.93 \ 6p_{3/2} \ 6p_{1/2} - 0.38 \ 6p_{3/2} \ 6p_{3/2}$. The deviation from jj coupling measured by $(0.38)^2 = 0.14$ is quite large enough to account for the difference between $A(^1D_2) = 0.026$ and $a''(6p) = 0.012$. Neglecting matrix elements of the type $(p_{3/2}/H'/p_{1/2})$ we derive theoretically $A(^1D_2) = 0.024$, $A(^3P_2) = 0.089$ in excellent agreement with experiment. It is not quite certain that these matrix elements are sufficiently small to be neglected. Nevertheless it is clear that the deviations from jj coupling may easily account for the remaining discrepancies.

$\psi^2(0)$. With Goudsmit's value⁶ for $\psi^2(0)$ of 7s Tl I the hfs splitting of this term gives $\mu_0/\mu = (0.17/0.49)4050 = 1.4 \times 10^3$ which is in much better agreement with the value $\mu_0/\mu = 0.92 \times 10^3$ which follows according to Racah from the splitting of 6p_{1/2} Tl I than $\mu_0/\mu = 4.0 \times 10^3$. The isotope shift and the hfs splitting agree with Goudsmit's formula.

SUMMARY

It is seen from the above discussion that the theory of isotope shifts as due to changes in nuclear radii is substantially in agreement with the observed facts. The apparent objections^{1,2} to such a theory have been removed. The main changes with respect to previous work are: (1) changes in the probable values of $\psi^2(0)$; (2) the interpretation of electron configurations in Hg, Tl, Pb. The values of nuclear radii and their differences have a significance only so far as order of magnitude is concerned, on account of uncertainties in the values of $\psi^2(0)$.

The picture of the nucleus as having an approximately uniform charge density is expected to apply only to its action on extranuclear electrons and has presumably somewhat the same relation to reality as the Hartree central field has to the correct treatment of an atom in configuration space.

Absorption Spectrum of Iodine Bromide

By WELDON G. BROWN*

Ryerson Physical Laboratory, University of Chicago

(Received August 25, 1932)

It is shown by means of a vibrational analysis that the absorption spectrum of iodine bromide is analogous to that of iodine chloride and that an interpretation similar to that recently proposed by the writer and Gibson for ICl is applicable. The infrared bands of IBr discovered by Badger and Yost are classified as a ${}^3\Pi_1 \leftarrow {}^1\Sigma$ transition. The ${}^3\Pi_0+ \leftarrow {}^1\Sigma$ system is observed as a faint set of bands in the red, not hitherto reported, which exhibit the same type of predissociation as the corresponding bands of ICl. Transitions to a state which originates at the maximum of the ${}^3\Pi_0+$ state and which dissociates to yield normal iodine and excited bromine atoms are observed as a strong system of partially diffuse bands. Cordes' assignment of these bands to two systems is not confirmed. In the present work the vibrational quantum numbering for each system is deduced from measurements of the isotope effect due to bromine. The heat of dissociation of IBr is 1.808 ± 0.001 volts. For the four molecules I_2 , IBr, ICl, and Br_2 it is shown that the separation of the ${}^3\Pi_0+$ and ${}^3\Pi_1$ states is roughly equal to two-thirds of the mean 2P multiplet widths of the constituent atoms. The total ${}^3\Pi$ widths are then probably greater and the ${}^3\Pi_2$ state somewhat lower than has been supposed.

INTRODUCTION

THE close generic relationship between iodine bromide and iodine chloride furnishes good grounds for believing that their absorption spectra should be closely analogous. Thus, in accordance with the interpretation of the ICl spectrum recently proposed by the writer and G. E. Gibson,¹ one would expect to observe transitions from the normal ${}^1\Sigma$ state to ${}^3\Pi_1$ and ${}^3\Pi_0+$ states, the latter exhibiting predissociation. A system of bands in the infrared is known from the work of Badger and Yost² who have shown that the dissociation products of the upper state are normal atoms. In this respect the system is like the strong visible system of ICl and is therefore probably the ${}^3\Pi_1 \leftarrow {}^1\Sigma$ system. In the visible, according to Cordes,³ there are two systems of diffuse bands, the upper levels of which dissociate to give normal iodine plus excited bromine (a') and normal bromine plus excited iodine (a''). While one of these (a') may correspond to the peculiar 0^+ state of ICl, the other is quite unexpected, and transitions to the ${}^3\Pi_0+$ state were not observed.

In the hope of making a detailed study of the spectrum, photographs of the visible and infrared regions were made with high dispersion (21' Rowland grating). Lack of sufficient resolution has hindered the fine structure analysis,

* National Research Fellow in Chemistry.

¹ W. G. Brown and G. E. Gibson, *Phys. Rev.* **40**, 529 (1932). For the theory of the electronic states of the halogens, see R. S. Mulliken, *Phys. Rev.* **36**, 669, 1440 (1930); *Rev. Mod. Phys.* **4**, 17, 70 (1932).

² R. M. Badger and D. M. Yost, *Phys. Rev.* **37**, 1548 (1931).

³ H. Cordes, *Zeits. f. Physik* **74**, 34 (1932).

however, and the following results are based on a study of the vibrational levels.

The strongest absorption bands are the partially diffuse bands in the visible which were studied by Cordes. At longer wave-lengths, in the red, a faint system of double headed bands is to be observed. This occurs in several v' progressions each of which terminates abruptly with an apparently diffuse band, and is obviously the ${}^3\Pi_0+\leftarrow{}^1\Sigma$ system. The doublet nature of the heads is due to the equally abundant isotopes of bromine, 79 and 81. The infrared bands, as described by Badger and Yost, also appear in several v' progressions. A few members of the $v''=0$ and $v''=1$ progressions show the isotope effect sufficiently clearly for approximate measurement.

VIBRATIONAL ANALYSIS

Badger and Yost carried out a vibrational analysis of the infrared system but as a consequence of not having resolved the isotope effect their values of the vibrational constants for the normal state are only approximately correct and those for the upper state are without significance because of the arbitrary

TABLE I. *Infrared system.*

$v' \backslash v''$	0	1	2	3	4	$\Delta G'$
9				12,464		103
10				567		96
11				663		94
12			13,021	757	12,496	88
13			107	845	584	86
14		13,459	194	931	670	79
15		537	275	13,010		73
16		609	348	084		68
17		677	414	155		65
18		745	478	219		59
19		806	537	275		54
20		858	593	330		51
21		906	645	382		46
22		953	691	427		43
23		995	734			40
24		14,038	771			34
25		071	806			36
26	14,373	107	842			29
27	404	135	871			30
28	434	165				25
29	459					23
30	482					22
31	504					21
32	525					19
33	544					19
34	563					16
35	579					14
36	593					12
37	605					10
38	615					9
39	624					9
40	633					8
41	641					5
42	646					4
43	650					4
44	654					

v' numbering. As mentioned above, however, the isotope effect is observed only for a few members of the $v''=0$ and $v''=1$ progressions, and, because of the presence of a Q branch which tends to confuse the head formed by the R branch, it is not accurately measurable. Nevertheless, the data serve to determine the order of magnitude of the correction to be applied to the arbitrary v' numbering, and this turns out to be an increase of 9 ± 1 units.

Some uncertainty in the value of ω_e' is introduced by the long extrapolation from $v'=9$. In obtaining the value, $\omega_e'=140 \pm 5 \text{ cm}^{-1}$, we are guided to some extent by the assumption that the $\omega:v$ curve will have the same general shape as the corresponding curve for ICl which is known over its entire course. The heat of dissociation, on the other hand, can be determined with high precision, and the extrapolation gives for the convergence of the $v''=0$ progression the value $14,660 \pm 5 \text{ cm}^{-1}$, or $D''=1.808 \pm 0.001$ volts. This is somewhat higher than the Badger and Yost value, 1.801 ± 0.007 , but within their limit of error. The new value introduces a small discrepancy between the spectroscopic value for the heat of formation of IBr from I_2 and Br_2 and the thermal value determined by Yost and McMorris,⁴ but is nicely confirmed by the convergence of the system III bands.

The analysis of the infrared bands given in Table I, from low dispersion measurements, undoubtedly confirms that of Badger and Yost who have not yet published their data, and is given here for the sake of completeness. Table II contains the measurements of the isotope shifts, from photographs taken in the first order of the 21' grating.

TABLE II. Isotope shifts, infrared system.

v', v''	ν^*	$\delta\nu$ obs.	$\delta\nu$ calc.	v', v''	ν	$\delta\nu$ obs.	$\delta\nu$ calc.
26,1	14,106.8 103.2	3.6	3.7	29,0	14,459.2 454.0	5.2	4.8
27,1	137.8 134.2	3.6	3.5	30,0	482.3 477.5	4.8	4.5
28,1	165.2 162.4	2.8	3.2	31,0	503.9 499.9	4.0	4.3
26,0	373.3 367.6	5.7	5.7	32,0	525.1 521.6	3.5	4.1
27,0	404.4 398.3	6.1	5.5	33,0	544.3 540.0	4.3	4.0
28,0	433.6 427.0	6.6	5.2	34,0	563.4 560.2	3.2	3.8

* First given in each pair is the IBr⁷⁹ head.

More accurate data for the normal state are provided by the visible $^3\Pi_0+ \leftarrow ^1\Sigma$ bands, the analysis of which is given in Table III. The v'' numbering is fixed with reference to the infrared system and the v' numbering is that obtained from the isotope shifts in the usual way. Only bands with sharp heads

⁴ D. M. Yost and J. McMorris, J. Am. Chem. Soc. 53, 2625 (1931).

are included in the table; in addition, bands with $v' = 6$ have been observed in each progression. These bands are approximately 100 cm^{-1} distant from the corresponding $v' = 5$ bands, and like the $v' = 4$ bands of the corresponding ICl system, appear diffuse but with widely spaced series of lines superimposed.

TABLE III. ${}^3\Pi_{0+} \leftarrow {}^1\Sigma$ systems.

v'	v''	3	4	5	6	7
2				15,053.4 15,062.8 125.1 123.1		
3			15,438.7 260.2 15,444.4 258.5	15,178.5 257.0 15,185.9 256.5	14,921.5 14,929.4	
			116.8 116.3	116.5 116.1	115.1 116.1	
4		15,817.2 261.7 15,820.7 260.0	15,555.5 260.5 15,560.7 258.7	15,295.0 258.4 15,302.0 256.5	15,036.6 257.1 15,045.5 255.0	14,779.5 14,790.5
		108.6 108.4	108.3 107.6	108.4 108.0	107.7 107.1	106.7 107.1
5		15,925.8 262.0 15,929.1 260.8	15,663.8 260.4 15,668.3 258.3	15,403.4 259.1 15,410.0 257.4	15,144.3 258.1 15,152.6 255.0	14,886.2 14,897.6

Since the data provide only three values of ω_e' , which are not quite linear in v' , the extrapolation to $v' = -\frac{1}{2}$ is again somewhat uncertain, the value of ω_e' being $\sim 140 \text{ cm}^{-1}$. Thus, as nearly as can be determined, the ${}^3\Pi_{0+}$ and ${}^3\Pi_1$ states have the same value of ω_e . An extrapolation to the point of dissociation is much more uncertain but it is obvious that too low a value will be obtained. Even a linear extrapolation from the observed levels, which in most cases yields too high a value for the heat of dissociation, falls short of the limit I (${}^2P_{3/2}$) + Br (${}^2P_{1/2}$) by 1000 cm^{-1} . Clearly such an extrapolation is without significance except insofar as it shows the abnormality of the levels.

The remaining visible bands, which have their analogy in the system III bands of ICl, are remarkable not only for their intensity but also for the anomalous appearance of certain bands ($v' = 8$ and 11). These bands are assigned in the analysis (Table IV) in a way that may seem arbitrary, for, unlike all other bands in this system, they possess sharp heads showing the isotope effect clearly. Attempts were first made to consider them as members of an independent system, that is, as successive members in v' progressions instead of differing by three in quantum number. This possibility was rejected for two reasons, first, there are no additional bands of like character to support such an assignment, and secondly, the isotope shifts calculated on this basis do not agree with the observed values. Supporting their assignment in Table IV is the observation of the intervening levels, 9 and 10, although these bands are totally different in appearance and are so ill-defined that they are not measurable.

TABLE IV. System III, $0^+ \leftarrow 1^- \Sigma$.

v' \ v''	0	1	2	3	4
8		{16,947.8 265.1 16,947.3 263.5 54	{16,682.7 263.7 16,683.8 261.7 63	{16,419.0 262.0 16,422.1 260.5 66	{16,157.0 262.5 16,161.6 260.1 58
9		17,002* 256	16,746* 257	16,489* 271	16,218* 266
10		17,070* 264	16,806* 262	16,544* 260	16,284* 257
11		17,131 266	16,865.3 263.7	{16,601.6 262.5 16,603.1 260.1 60	{16,339.1 262.2 16,343.0 260.1 57
12		17,188* 263	16,925 263	16,662 259	
13		17,237 259	16,978 259	16,719* 264	
14		17,291 257	17,034 264	16,829	
15		17,358 265	17,093 264	16,829	
16		17,411 260	17,151 260		
17		17,462 269	17,237 269		
18		17,506 265	17,237 265		
19		17,556 265	17,291 265		
20		17,603 262	17,341 262		
21		17,645 261	17,384 261		
22	17,942 262	17,680 256	17,424 256		
23	17,983 257	17,726 264	17,462 264		
24	18,029 261	17,768 268	17,500 268		
25	18,068 267	17,801 268	17,533 268		
26	18,101 271	17,830 265	17,565 265		
27	18,130 267	17,863 264	17,599 264		
28	18,157 264	17,893 266	17,627 266		

v' \ v''	0	1
28	18,157 264	17,893 266
29	18,187 268	17,919 268
30	18,209 267	17,942 267
31	18,229 268	17,961 268
32	18,248 265	17,983 265
33	18,263 265	17,983 265
34	18,278 265	17,983 265
35	18,295 265	17,983 265
36	18,307 265	17,983 265
37	18,315 265	17,983 265

* Cordes' measurements.

Cordes has described the bands of this system as diffuse, but in reality they are only partially so. Fine structure appears throughout and in certain regions is remarkably sharp. It is true, however, that the heads are not sharp, except for those with $v' = 8$ and 11, and cannot be measured at all accurately as the combination differences of Table IV will show. The sharpness of the heads varies greatly, improving somewhat at high quantum numbers, and also, bands with $v' = 15$ and 20 are somewhat sharper than their neighbors.

No evidence has been obtained for the existence of a second band system in this region, as reported by Cordes. The bands assigned by Cordes to this second system fit, within the experimental error, in the v', v'' matrix of Table IV.

The dissociation products of the upper state are obviously normal iodine and excited bromine atoms, since, by a short extrapolation, we obtain the value, $18,345 \pm 15 \text{ cm}^{-1}$, for the convergence of the $v''=0$ progression. Subtracting the 2P separation of bromine, 3685 cm^{-1} , gives for the heat of dissociation $D''=14,660 \text{ cm}^{-1}$, in fortuitously good agreement with the value obtained from the infrared bands.

In attempting to determine the value of ν_e or of ω_e' we are again confronted with the uncertainty of a long extrapolation, as the lowest observed level is $v'=8$. There is some evidence for a maximum in the $\omega:v$ in this case

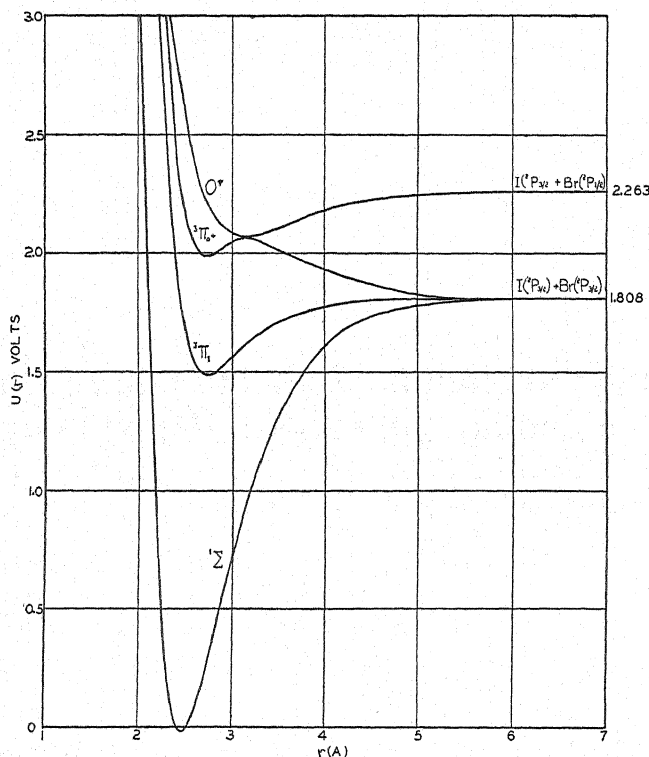


Fig. 1. Approximate potential energy curves for IBr. The r_e value for the normal state is assumed to lie midway between those for I_2 and Br_2 .

as well as in ICl. Assuming that ω does not change with v' up to $v'=8$, the origin of the upper state would lie approximately at the height of the $^3\Pi_0+v=5$ level, or perhaps 50 cm^{-1} higher if the $\omega:v$ curve actually has a maximum. The latter position is required by the interpretation. The fact that the upper state originates in the neighborhood of the last $^3\Pi_0$ level lends strong support to the interpretation, since it was not possible to prove this in the case of ICl.

It seems reasonable to suppose that the phenomena are essentially similar to those in iodine chloride, and that the upper state of system III arises in the same way, namely, by interaction of a repulsive O^+ state derived from

normal atoms and the $^3\Pi_0^+$ state with the resultant formation of a quantized set of levels at the intersection. This state being formed from two 0^+ states also has the 0^+ character, and leads to dissociation into normal iodine and excited bromine atoms. The situation is illustrated in Fig. 1 by means of approximate potential energy curves for the various states. To interpret the character of the bands and the irregular fine structure we must suppose a certain degree of communism between the new 0^+ state and the $^3\Pi_0^+$ state so that transitions only to certain limited ranges of rotational quantum numbers, varying from level to level, can give rise to sharp lines. In some cases, as for $v=8$ and 11, the range of quantum numbers will be so low that a sharp head will be formed. In others the range will be higher so that the band appears shifted to the red and the progression accordingly irregular. Thus it can be seen that the interpretation proposed to account for the structure of the ICl bands provides a qualitative explanation for the unusual appearance of this system of IBr. It is unfortunate that on account of the overlapping of bands, the large mass of molecule, and the equally abundant isotopes of bromine, a detailed study of the structure is a problem of extreme difficulty.

Likewise, the relative intensities of the transitions $^3\Pi_1 \leftarrow ^1\Sigma$ and $^3\Pi_0^+ \leftarrow ^1\Sigma$ are very much the same as in ICl when the Franck-Condon effects are taken into consideration. This involves the interpretation of the various regions of continuous absorption, and, because of the uncertainty as to the exact form of the potential energy curves, it is difficult to make an unambiguous assignment. The work of Cordes shows the existence of two regions of continuous absorption, with maxima at 4050Å and 4950Å, the latter being stronger. As drawn in Fig. 1 the potential energy curves indicate that transitions from the level $v''=0$ to the $^3\Pi_1$ state would be strongest in the region of the latter's discrete states but at high quantum numbers, while transitions to the $^3\Pi_0^+$ state would account for the strong maximum at 4950Å. (Since the energy of this radiation is slightly more than enough to give excited bromine atoms on dissociation, a decision as to which path the $^3\Pi_0^+$ state actually follows, that is, whether normal or excited bromine atoms are the result, cannot be made.) The maximum at 4050Å is then to be attributed to transitions to the 0^+ state, in harmony with the fact that iodine bromide does not exhibit a region of continuous absorption in the ultraviolet corresponding to that of iodine chloride.⁵ The continuous absorption associated with the infrared system is probably that underlying the $^3\Pi_0^+ \leftarrow ^1\Sigma$ bands. According to this interpretation the $^3\Pi_0^+ \leftarrow ^1\Sigma$ system is actually very much stronger than the $^3\Pi_1 \leftarrow ^1\Sigma$ transition, just as in ICl, although a comparison of transitions to discrete levels would yield an opposite conclusion.

VIBRATIONAL CONSTANTS

In obtaining the vibrational constants for the normal state, data from the three systems have been combined, the normal state being common, and selected to include only measurements of bands for which the isotope effect

⁵ H. Cordes and H. Spöner, *Zeits. f. Physik* **63**, 338 (1930).

has been measured. The theoretical relations between the constants for isotopic molecules have also been taken into consideration. Owing to the long extrapolations the ω values for the $^3\Pi$ states are too uncertain to differentiate between the isotopic species.

TABLE V. *Vibrational constants.*

State	ν^e	ω_e	$\omega_e x_e$	D_0 (volts)
$^1\Sigma$	0	$\begin{cases} 268.4 \\ 266.4 \end{cases}$	$\begin{cases} 0.78 \\ 0.77 \end{cases}$	1.808
$^3\Pi_1$	12,230	140		0.31
$^3\Pi_0^+$	16,240	140		
O^+	16,880	60		0.19

 $^3\Pi$ MULTIPLET WIDTHS

Unfortunately the $^3\Pi_2$ and $^3\Pi_0^-$ states cannot be observed in absorption since transitions to these states from the normal state are not allowed according to the selection rules,⁶ and, therefore, one cannot determine the total multiplet width from the absorption bands alone. However, Van Vleck⁷ has shown that the splitting of the 0^+ and 0^- levels at moderate values of r is small compared to the multiplet width, though not negligible. It may be assumed then that the separation of the 0^+ and 1 states gives an approximate measure of the half width of the multiplet and it is of some interest to consider how the values obtained in this way are related to the 2P atomic separations.

Data are available for the four molecules, I_2 , $I\text{Br}$, ICl , and Br_2 . The value for Br_2 is based on new measurements of the isotope effect in the infrared system according to which the arbitrary ν' numbering used by the writer⁸ is to be increased by 6 units. Unfortunately, the ν' numbering in the infrared system of iodine cannot be determined in this way as there are no isotopes of iodine. If one assumes that, as in $I\text{Br}$, ICl , and Br_2 , the $^3\Pi_0^+$ and $^3\Pi_1$ states of iodine have the same value of ω , a reasonable extrapolation can be made from the observed $^3\Pi_1$ levels,⁹ and a value for the separation obtained. The data are given in Table VI, together with the mean 2P widths in the atoms.

TABLE VI.

Molecule	Mean 2P width	$^3\Pi_0^+ - ^3\Pi_1$ obs.
I_2	0.94	0.68 ± 0.05
$I\text{Br}$	0.70	0.50
ICl	0.53	0.44
Br_2	0.46	0.27

⁶ R. Schlapp, Phys. Rev. 39, 806 (1932).

⁷ J. H. Van Vleck, Phys. Rev. 33, 484 (1929); 40, 544 (1932).

⁸ W. G. Brown, Phys. Rev. 38, 1179 (1931).

⁹ W. G. Brown, Phys. Rev. 38, 1187 (1931).

The proportionality is obvious, the 0^+ , 1 width being approximately two thirds the atomic multiplet width.

These results indicate that the total width of the $^3\Pi$ multiplets is greater by one-third than the mean 2P separations in the atoms, or approximately twice the width estimated by Mulliken.¹⁰ If true, this implies that the $^3\Pi_2$ state lies considerably lower than has been supposed. For I_2 this supposition of equal spacing of the components places the $^3\Pi_2$ component about 0.6 volts above the normal state. It would then be low enough to affect the dissociation equilibrium at high temperatures whereas Gibson and Heitler¹¹ have found very close agreement between the experimental values and those calculated by considering the normal state alone. It seems likely, therefore, that for the heavier halogens, at least, there is a considerable departure towards case c so that the spacing of the multiplet is no longer the usual equal spacing of molecular (case a) multiplets.¹²

¹⁰ R. S. Mulliken, *Phys. Rev.* **36**, 1413 (1931).

¹¹ G. E. Gibson and W. Heitler, *Zeits. f. Physik* **49**, 465 (1928).

¹² R. S. Mulliken, *Interpretation of Band Spectra, Part IIc*, *Rev. Mod. Phys.* **3**, 117 (1931).

On the Interpretation of the Rotational Structure of the CO_2 Emission Bands

By ROBERT S. MULLIKEN

Ryerson Physical Laboratory, University of Chicago

(Received September 17, 1932)

Schmid's analysis of the rotational structure of a number of the ultraviolet CO_2 emission bands is discussed, and it is pointed out that in spite of uncertainties, some definite conclusions can be drawn, notably that the molecule in equilibrium is nearly linear, or probably strictly linear, in both initial and final states, that B' is nearly equal to B'' , and that the values of both are approximately known (cf. Schmid). It is also shown that the bands are most probably of the type ${}^1\Pi \rightarrow {}^1\Pi$, but possibly ${}^1\Sigma \rightarrow {}^1\Sigma$ or (much less likely) ${}^2\Sigma \rightarrow {}^2\Sigma$ or some other type. If ${}^2\Sigma \rightarrow {}^2\Sigma$ the emitter must be CO_2^+ , otherwise CO_2 . It is proposed to designate by κ the quantum number corresponding to the angular momentum of rotation of the carbon atom relative to the O atoms around the O-C-O axis. It is pointed out that in electronic bands, one expects predominantly $\Delta\kappa=0$. This rule is then applied to possible interpretations of the band structures. Some suggestions are also made concerning the vibrational analysis. Evidence from the values of B and ν_1 is stated, which supports Smyth's interpretation of the a and c series as ν_1' progressions. It is suggested that the isolated bands $\lambda\lambda 2896, 2883$ may be the (0,0) band of a ${}^2\Pi \rightarrow {}^2\Pi$ transition of CO_2^+ with B' and B'' almost equal.

RECENT work by Schmid¹ in this laboratory on the rotational structure of a number of ultraviolet CO_2 emission bands has revealed an unexpectedly simple structure. Schmid's work indicates that the spectrum contains at least three band systems. The bands whose analysis he has published probably all belong to one system. They consist of P -form and R -form branches of about equal intensity, each showing staggering, i.e., being composed of doublets but with alternately the high- and low-frequency component of each doublet missing.

The observed structures are consistent with a molecular structure which when at rest is linear in both initial and final states. Small departures from linearity would apparently not affect the qualitative nature of the energy level scheme nor, for most practical purposes, the selection rules, but a large departure in either or both states would surely give rise to a less regular and simple band structure.²

For a symmetrical linear molecule, the electronic states can be classed as ${}^1\Sigma_g^+$, ${}^1\Sigma_g^-$, ${}^3\Pi_u$, etc., just as for a diatomic molecule, and the selection rules for electronic quantum numbers should be the same. The existence of three characteristic vibrations (quantum numbers ν_1 , ν_2 , and ν_3) does not affect in any essential way the structures of individual bands, although the fact that levels with given electronic and rotational quantum numbers change

¹ R. F. Schmid, Phys. Rev. **41**, 732 (1932).

² D. M. Dennison, Rev. Mod. Phys. **3**, 280 (1931) for the basis of these statements. Also Phys. Rev. **41**, 304 (1932).

from symmetrical in the nuclei to antisymmetrical, or *vice versa*, when v_3 changes from even to odd,² is essential in deciding which particular rotational levels and lines are present, which missing, in any given band.

The rotational energy is given for a diatomic molecule without electronic angular momentum by:

$$E_r/hc = \text{const.} + BK(K+1) + \dots$$

If $\Lambda > 0$ and $S > 0$ this is still essentially true, but every level is split up into a fine doublet (Λ -type doubling), the width of this increasing in general with K .³ If the molecule has two equal nuclei without spin, one component of each double level, alternately the upper and the lower, is missing. If $S > 0$, the case is more complicated, unless the spin is very loosely coupled. (This is usually true only for $\Lambda = 0$.) For a linear triatomic molecule like CO₂ there is an added complication in the existence² of a quantum number κ associated with, roughly speaking, the rotation of the C nucleus around the line joining the two O atoms.⁴ Λ and κ play similar roles. If $\Lambda = 0$, we expect κ -type doubling, with one component of each doublet missing, when $\kappa > 0$.² In analogy with Λ -type doubling, we might expect to find the doubling usually largest for $\kappa = 1$, much smaller for $\kappa = 2$, and so on. If $\Lambda > 0$ and $\kappa > 0$, the matter is more complicated (see below).

In general, Λ and κ are expected to obey the selection rules $\Delta\Lambda = 0, \pm 1$ and $\Delta\kappa = 0, \pm 1$. But since there is relatively little interaction, "coupling," between the nuclear motion connected with κ and the electron motions, one may expect in the case of an electronic band system to find practically only bands with $\Delta\kappa = 0$. This rule is similar to the rule $\Delta M_s = 0$ for atoms in the Paschen-Back effect and to the rule $\Delta\Sigma = 0$ for diatomic molecules in Hund's case *a*.³

With $\Delta\kappa = 0$, one expects band structures and intensity relations of exactly the same types as for diatomic molecules, except for some complications in the fine structure of $\kappa > 0, \Lambda > 0$. For instance, we can speak of cases, *a, b, c, d* of Hund.³ The bands analyzed by Schmid can hardly be case *a* bands, since these would show multiplet structure (e.g., heads all in pairs, or in triplets with approximately constant spacing), and in all probability would show noticeable Zeeman effects at high quantum numbers, contrary to Schmid's observations. Nor are they of the type with one state case *a*, the other case *b*.³

The bands must then be case *b*, with $S > 0$, or else be singlet bands ($S = 0$). Other cases (*c* and *d*) can safely be excluded for a molecule such as CO₂. The observed *P*-form and *R*-form branches are then surely actual *P* and *R* branches ($\Delta K = \pm 1$). Bands having *P* and *R* branches and no *Q* branches (or very weak *Q* branches) have $\Delta\Lambda = 0$, and an electric moment vibrating parallel

³ R. S. Mulliken, Rev. Mod. Phys. 3, 89 (1931).

⁴ The symbol κ has been chosen here after some consideration in preference to Dennison's *l*. Since it is likely to be of considerable importance, it seems desirable to have a unique symbol for this quantum number. The use of a Greek letter for a rotation around the figure axis of a molecule is in accordance with diatomic usage; the choice of κ suggests that, as with K , we are dealing with a nuclear rotation.

to the axis (here the O-C-O line). If $S > 0$, the band lines should almost certainly show evidence of fine structure if $\Lambda > 0$, and very probably even if $\Lambda = 0$. Only in the higher energy states of very light molecules (H_2 , He_2) is such fine structure so narrow as to escape observation (case b') for $\Lambda > 0$. For $\Lambda = 0$, $S = \frac{1}{2}$ ($^2\Sigma \rightarrow ^2\Sigma$ transition) there might possibly be an unobserved fine structure for CO_2 , since $^2\Sigma$ states of NO and CO^+ are known with separations that are barely detectable or not detectable. But it is much more likely that, if the bands were really $^2\Sigma \rightarrow ^2\Sigma$, some evidence of fine structure would have been found among the many bands and band-lines examined. Actually there is no evidence whatever of splitting or broadening of the lines in the absence of a magnetic field,—other than the staggered-doubling, which cannot possibly be a spin effect, since with spin doubling both components of a double line would be present or absent together.³ The possibility $^3\Sigma \rightarrow ^3\Sigma$ can be practically excluded, since in diatomic molecules (O_2 , NH , N_2 , etc.), except He_2 , this gives a fine structure too large to be missed.

One concludes then that very probably $S = 0$, but that possibly the bands are $^2\Sigma \rightarrow ^2\Sigma$. Of course if the emitter is CO_2 , as Smyth considers probable,⁵ the latter possibility is excluded. On the other hand, $S = 0$, is excluded if it is CO_2^+ .

The bands correspond, then, very probably to one of the types $^1\Sigma \rightarrow ^1\Sigma$, $^1\Pi \rightarrow ^1\Pi$, $^1\Delta \rightarrow ^1\Delta$, etc. Schmid's result that no Zeeman splitting or measurable broadening is observed even in strong fields¹ excludes all but $^1\Sigma \rightarrow ^1\Sigma$ and $^1\Pi \rightarrow ^1\Pi$. His definite observation that the low-numbered P lines are probably broadened (*apparently* weakened) agrees with what would be expected for the Zeeman effect of $^1\Pi \rightarrow ^1\Pi$. (The corresponding low-numbered R lines are obscured by other lines.) The fact that weak Q branches would be expected (just a few lines at low J values) for $^1\Pi \rightarrow ^1\Pi$, etc., but not for $^1\Sigma \rightarrow ^1\Sigma$, is no objection to the $^1\Pi \rightarrow ^1\Pi$ interpretation, since Schmid could not have detected these Q lines amid the strong and crowded R lines. A possible real objection, connected with the expected simultaneous occurrence of Λ and κ -type doubling, will be mentioned later. $^1\Sigma \rightarrow ^1\Sigma$ should show no Zeeman effect, or at most a slight broadening at *high* quantum numbers. The same is true of $^2\Sigma \rightarrow ^2\Sigma$ if, as we must suppose here in order to consider this case at all as a possibility, the spin is very loosely coupled, since then $\Delta M_S = 0$.

From the foregoing it would seem most probable that the bands are $^1\Pi \rightarrow ^1\Pi$, with $^1\Sigma \rightarrow ^1\Sigma$ as a second important possibility in case some unexpected explanation of the magnetic behavior of the low-numbered P lines can be found, and with $^2\Sigma \rightarrow ^2\Sigma$ as a rather remote possibility.

The bands analyzed by Schmid all show exactly the same type of structure, except for differences in the magnitude of the staggering. The strongest bands analyzed are three bands of the a progression of Smyth ($\lambda\lambda 3247$, 3370 and 3503) and three bands of Smyth's c progression ($\lambda\lambda 3254$, 3377 and 3511). The c bands show staggering, the a bands none within the experimental error,

⁵ H. D. Smyth, Phys. Rev. 38, 2000 (1931); 39, 380 (1932); cf. also H. J. Henning, Ann. d. Physik 13, 599 (1932).

but as Schmid shows, we may assume that a very small staggering is actually present.

Now as will be seen by reference to reproductions given by Smyth,⁵ and by Fox, Duffendack and Barker, each of the *a* bands above mentioned is the first, and also the strongest, member of a well-marked group of bands extending toward longer wave-lengths. No bands which could be associated with the group, except a few of much lower intensity, occur on the short wave-length side of the *a* band of each of these groups. Following each *a* band closely on its long wave-length side, and nearly as strong as the *a* band, is a *c* band. At longer wave-lengths in each group is a more or less irregular distribution of weaker bands (members of Smyth's series *b*, *d*, *n* and *j*). A few of these have been analyzed by Schmid; they include two examples with no observable staggering ($\lambda\lambda 3546$ and 3674), one with small staggering ($\lambda 3534$), and one with rather large staggering ($\lambda 3839$); one or two of these (especially $\lambda 3839$) may, however, perhaps not belong to the same system as the others.

The most natural interpretation of the above results consistent with the rule $\Delta\kappa=0$ and a ${}^1\Pi\rightarrow{}^1\Pi$ electronic transition is that the strong bands *a* and *c* correspond to low values, presumably 0 and 1, of κ and also of the related² quantum number $v_2(\kappa=v_2$ for $v_2=0, 1)$, the other bands to higher v_2 or κ values. Since $\kappa'=\kappa''$, the intensity distribution among different κ values would be determined by the initial (κ') distribution. The fact that each group starts suddenly with a strong band (*a*) is most easily understood if this band has $\kappa=0$, and $v_2=0$. With $\kappa=0$, we should have pure Λ -type doubling, with alternate components of each doublet missing, giving staggering. The fact that each branch (*P*, *R*) appears in the *a* bands to consist of a single series of lines without staggering is not unreasonable, since the Λ -type doublets might happen to be very narrow. (In the angstrom bands of CO, for instance the Λ -type doubling in the ${}^1\Pi$ states is too small to detect except for very high *J* values.) This is especially true (cf. Schmid's Fig. 2) since the observed band-line displacements depend on *differences* of displacements in the initial and final ${}^1\Pi$ states. With $\kappa=v_2=1$, assumed in the *c* bands, we might have κ -type doubling to explain the observed staggering; or the fact that $\kappa, v_2>0$ may increase the Λ -type doubling. [For a nonlinear molecule, a ${}^1\Pi$ state must split into two electronic states; and $\kappa>0$ or $v_2>0$, since it throws the C atom out of line with the O atoms, should induce such a splitting, giving Λ -type doubling even without rotation. Such a constant splitting might, however, escape observation.] With $\kappa=1, \Lambda=1$, there should be a quadrupling of each rotational level but with two components of each level missing; and unless they should more or less accidentally coincide, it would seem that each of the observed band-lines should be double (i.e., each line theoretically quadruple but with two components missing, alternately one pair and the other pair in adjacent lines; it can easily be shown theoretically that quadruple levels should give here quadruple lines, not more complex groups). The fact that only a staggered series of simple lines, not of doublets, is observed, tends to discredit the present interpretation. But until theoretical calcula-

tions have been made on the nature of combined κ - and Λ -type doubling, it seems worth considering. Another difficulty, however, is the fact that one would expect bands for which $\kappa=v_2$ has the values 0, 1, 2, \dots to form a nearly uniformly-spaced series, since the levels associated with v_2' and v_2'' should have approximately the uniform spacings characteristic of the harmonic oscillator; actually, the bands a , c , and so on, in each group are irregularly spaced.

An alternative interpretation may be attempted as follows. Disregarding as not quite conclusive the Zeeman effect evidence in favor of ${}^1\Pi \rightarrow {}^1\Pi$, suppose the bands are ${}^1\Sigma \rightarrow {}^1\Sigma$ (or ${}^2\Sigma \rightarrow {}^2\Sigma$). In this case there is no Λ -type doubling, only κ -type doubling, and if $\kappa > 0$ everything is consistent with the observed band structures. But for $\kappa = 0$, with $\Lambda = 0$, the rotational levels must be single, and now the requirement that every other level shall be missing means that for every other J value no level at all exists (with $\Lambda > 0$ or $\kappa > 0$, at least one level is present for every J value). This would give bands with alternate missing lines, i.e., with a spacing apparently twice as large as for bands with $\Lambda > 1$ or $\kappa > 1$. But the bands without appreciable staggering, to which we have tentatively assigned $\kappa = 0$, are in all other respects the same as the bands with staggering, so that the idea of alternate missing lines must be rejected (cf. also Schmid's evidence based on intensity measurements).¹ Hence if $\Lambda = 0$ for the a bands, we must rule out $\kappa = 0$. If $\kappa = 0$ does not apply to the a bands, then presumably there are other bands somewhere with $\kappa = 0$, since there is no theoretical reason why the transition $\kappa = 0 \rightarrow \kappa = 0$ should not occur. One might assume, for instance, $v_2 = 3$, $\kappa = 3$, for the a bands, $v_2 = 3$, $\kappa = 1$ for the c bands, and suppose that $v_2 = 2$, $\kappa = 2$; $v_2 = 2$, $\kappa = 0$; $v_2 = 1$, $\kappa = 1$; $v_2 = 0$, $\kappa = 0$ are among the weaker bands in the group. But this would require a rather surprising initial distribution (v_2' , κ'), as well as an improbable arrangement of the initial and final energy levels associated with v_2 and κ , such as to form a kind of band-group head just at the a band, with both lower and higher numbered bands at longer wave-lengths. Everything considered, the ${}^1\Pi \rightarrow {}^1\Pi$ interpretation seems more probable than a $\Sigma \rightarrow \Sigma$ interpretation, but both interpretations are tentative and far from satisfactory.

We may turn next to some other points connected with Schmid's analysis. Usually when a diatomic spectrum is analyzed, the correctness of the analysis is not considered as proved until conclusive combination agreements, i.e., agreeing sets of ΔT values, have been found for both initial and final electronic states. But when one is sure that the bands belong to a definite type, or to one of a few closely similar types, these requirements can be relaxed in some respects. In the case of Schmid's analysis of three of the c bands, combination agreements within experimental error are found for any of two or three different interpretations. According to these all the c bands may have a common initial state, or all may have a common final state in agreement with Smyth's vibrational analysis,⁵ or two may have a common initial, two a common final state. Corresponding statements hold for the three a bands analyzed by Schmid. One might think then that the analysis proves nothing, but this is far from being true. Schmid's results determine

within one or at most two units the correct rotational quantum numbers (K) of the band lines, and also determine the values of the rotational constants B' and B'' , and the moment of inertia and dimensions of the excited molecule, within a few percent. That is, we know that the correct values of B' and B'' must be chosen from just a few possible sets whose values do not differ much. Also, the difference $B' - B''$ is accurately known from the band structure, so that with the B values themselves approximately known, we can definitely conclude that B' and B'' are *nearly equal*. Further, Schmid's work shows definitely that neither B' nor B'' can be *exactly* the same in any of the a as in any of the c bands, but also that they are certainly very *nearly* the same in the a and c series. Schmid's work also indicates, but somewhat less conclusively, that the B' and B'' values are nearly the same in all the bands he has analyzed. These results are in agreement with the present interpretation according to which the a and c bands, since $\Delta\kappa = 0$, must differ in both initial and final states in respect to v_2 and κ at least. They do not support Smyth's assignment of a common final level to the a and c series but are not inconsistent with his formulation of the a and c series each as a v_1' progression.

Of the three or four possible combinations (ΔT sets), of which just one must be correct, indicated by Schmid's analysis for the series a and c , certain ones give almost exact integers for the effective rotational quantum numbers, the others almost exact half-integers.¹ The best agreement comes for one of the half-integral sets in each case. But the agreement is only slightly poorer for one of the integral sets. Since for a diatomic or linear polyatomic molecule the theory appears absolutely to demand integral K values for case b and for singlet transitions ($^1\Sigma \rightarrow ^1\Sigma$, $^2\Sigma \rightarrow ^2\Sigma$, $^1\Pi \rightarrow ^1\Pi$, or any other singlet or $\Sigma \rightarrow \Sigma$ transitions), it seems necessary to rule out the possible combinations which would give half-integral rotational quantum numbers. (In speaking of integral K values, we are using the formula $BK(K+1) + \dots$ for the rotational energy.) Half-integral values would be expected only for J values, in case a with S half-integral, but as has been mentioned above, the bands show no evidence of the multiple-headed structure necessary for this case, nor of the Zeeman effects probably to be expected (because of partial going-over to case b at high J values). Nevertheless, in view of the difficulties experienced in interpreting the bands as singlet or case b bands, it may be well not to exclude absolutely the possibility of case a bands. The most likely case a type, consistent with the observed P , R structure, would be $^2\Pi \rightarrow ^2\Pi$.

Ruling out half-integral numbers would restrict the possible combinations considerably. If one could be perfectly sure from the vibrational analysis that the a bands all have a common final state and constitute a v_1' progression, and the c bands likewise, as indicated by Smyth's tentative analysis, the correct combinations could be given with considerable confidence. New evidence in favor of the interpretation of the a and c bands as v_1' progressions, in spite of the difficulty in understanding an intensity distribution involving a range of v_1' values and only one v_1'' value, can be given as follows.

The well-known empirical relation that the quantity ω_e/B_e is very nearly

a constant for all states of a single diatomic molecule might reasonably be expected to be capable of extension to the linear CO_2 molecule, at least if we use ν_1/B , where ν_1 refers to the symmetrical vibration. Taking ν_1/B for the normal state of CO_2 ,⁶ one finds almost the same value as one obtains for the upper level of the ultraviolet emission bands using $\nu_1' = 1137$ (cf. Eq. (1) below) and using the most probable B' value of Schmid. No such good agreement is obtained if one uses Schmid's B'' and uses for ν_1 a value secured by reinterpreting the a or c series as ν_1'' progressions. Hence Smyth's interpretation of these ν_1' progressions receives strong support.

The reader may wonder why, in spite of his very accurate measurements, Schmid's analysis does not permit a decision between several different possible sets of combination differences. This is because of the fact, shown by Schmid's analysis, that if for instance we agree with Smyth that the a (or c) bands constitute a ν_1' progression, then the constant B' varies only very slightly with ν_1' . That is, if we write $B = B_0 - \alpha_1\nu_1 - \alpha_2\nu_2 - \alpha_3\nu_3 + \dots$ in analogy with the diatomic relation $B = B_0 - \alpha\nu + \dots$, we find that the ratio α_1'/B' is very much smaller than the usual values of α/B for diatomic molecules,—although it has the same sign as is usual in the diatomic case. The former fact causes several sets of possible combination differences to agree so closely that the differences between them cannot be certainly distinguished from experimental error.

If we should assume that the a (or c) bands have a common *upper* level and a set of lower levels differing by unit steps of ν_1'' , we would conclude that α_1''/B'' is very much smaller than α/B for diatomic molecules, so that the same difficulty as before would arise for the analysis. In this case α'' has the opposite sign to that usual in diatomic molecules, i.e., α in the above equation is negative.

With the assumption of a common lower level for the bands of the a (or c) series, the vibrational analysis⁵ gives an equation of the form

$$\nu = \text{const.} + 1136.85\nu' - 1.85\nu'^2. \quad (1)$$

Here the ratio x of the coefficients of ν'^2 and ν' is much smaller than in diatomic molecules, in agreement with the behavior of the ratio α/B . In diatomic molecules too the ratios x and α/B are closely related, and in the only two known diatomic cases where x has a negative sign, and only in these cases, α also has a negative sign. If, contrary to Smyth's analysis, and in spite of the evidence given above based on the value of ν_1/B , the a and c series should turn out to be ν_1'' progressions, x and α would have negative signs. Although this case is rare in diatomic, there is evidence that it is less so in polyatomic molecules. That the a and c series are *either* ν' progressions or ν'' progressions, and that the variable ν is ν_1 , seem to have been fairly well established.⁵

Since Schmid's analysis shows that B' and B'' are nearly equal, so that the dimensions of the molecule change very little in emitting the ultraviolet

⁶ Martin and Barker, Phys. Rev. **41**, 291 (1932). For ν_1 we may take the *average* of the two observed frequencies which result from the interaction of ν_1 and $2\nu_2$ ($\nu_2 = 2$, $\kappa = 0$).

bands, we can make by means of the Franck-Condon principle some predictions in regard to the intensities for various vibrational transitions. The most probable changes should be those conforming to $\Delta v_1 = 0$, $\Delta v_2 = 0$, $\Delta v_3 = 0$, except in case one or more of the v 's has a large initial value or large initial values. Apparently this is true of v_1 . The fact that the band system is not more complicated than it is suggests that perhaps $v_3' = 0$ mostly, and $\Delta v_3 = 0$, that v_2' (and κ') are confined mostly to a few small values, and that $\Delta v_2 = 0$ only (incidentally, $\Delta \kappa = 0$ requires $\Delta v_2 = \text{even}$, in view of the fact that κ is limited to the values $v_2, v_2 - 2, \dots, 0$ or 1).

An initial distribution involving one or several fairly large v_1' values can be understood if it is produced⁶ by electron impacts on unexcited molecules having mostly $v_1 = 0$, $v_3 = 0$, $v_2 = 0$ or 1 (the frequency ν_2 is the smallest of the three, and molecules with $v_2 > 0$ might be moderately abundant in the unexcited gas). Since the equilibrium dimensions of the molecule, which is linear in both states, are considerably different before and after electron impact in this case,^{1,6} the latter should tend mainly to excite v_1 , but v_3 not at all, and v_2 only indirectly through coupling of v_1 and v_2 .

Something further needs now to be said about the Λ -type or κ -type doubling found by Schmid. As Schmid has shown for the band $\lambda 3839$, the combination differences ΔT are surely of one of two classes. (Since $\lambda 3839$ has no state in common with any of the other bands analyzed, it is impossible to make tests of the possible combination differences by comparison with other bands; but by analogy considerations the numbering of the lines can be established within a few units;¹ all the possible combinations then fall into these two classes.) Corresponding remarks apply, Dr. Schmid has informed the writer, to the other bands measured by him but not belonging to the a and c series. In one of the two classes, the effective rotational quantum numbers are approximately integral (exactly so where the staggering is small), in the other approximately or exactly half-integral. If the analysis is carried through assuming integral quantum numbers, it shows that the Λ -type or κ -type doubling is moderately large, but if half-integral quantum numbers are assumed, it must be much smaller. In view of theoretical considerations presented above, showing that the rotational quantum numbers ought almost certainly to be integers, it appears necessary to accept one of the sets of possible combination differences which involve integral quantum numbers. But whether one of the integral or of the half-integral sets is adopted, Schmid's work shows perfectly definitely that the Λ -type or κ -type doublet-widths are not greatly different in the initial and final states, also that the departures of the positions of the two doublet components x and y from the positions given by $BK(K+1)$ are of the form $\text{const.} + a_x K + b_x K(K+1)$, with $a_x = -a_y$; and that b_x and b_y differ considerably, although only $b_x - b_y$ is determinable from the data. These details may prove of considerable value for the analysis of the system.

The definite fact, established by Schmid's work, that the doubling is nearly the same in the initial and final states suggests that the two states are closely similar in respect to the wave functions and energy levels dependent

on v_2 and κ , in agreement with conclusions stated above based on the near-equality of B' and B'' . A difficulty in the way of this conclusion, however, is the fact that there is a considerable interval (about 65 cm^{-1}) between each a band and the nearest c band. If v_2 is about 600 cm^{-1} , as in the infrared or Raman spectra of CO_2 , and if for the a bands $v_2 = \kappa = 0$ for both initial and final states while for the c bands $v_2 = \kappa = 1$, then v_2 must be about 10 percent different for the initial and final states, which is rather surprisingly large. Consideration of the bands in each group other than a and c increases this difficulty (cf. above).

In conclusion, it may be remarked that a great deal remains to be done before the problem of the structure of this system of CO_2 bands will be completely solved.

A rather casual suggestion concerning the interpretation of the two strong CO_2 bands near $\lambda 2896$ and 2883 may be worth making. The evidence of those who have worked on these bands shows rather clearly that they do not belong to the same system as those discussed above. Duncan's measurements,⁵ and those of Schmid, show probable P , Q and R branches, and Schmid's work shows also that all the band lines have pronounced Zeeman effects. The doublet structure ($\lambda 2896$, 2883) can be interpreted by a transition ${}^2\Pi \rightarrow {}^2\Pi$ (or possibly by some other transition between doublet states) in CO_2^+ . The doublet width has a reasonable value for a molecule like CO_2^+ . The fact that only a single isolated double band is found can be understood by the Franck-Condon principle if the constants of the molecule (assumed linear) are practically identical in initial and final states. The band is then to be interpreted as having $v_1' = v_2' = v_3' = 0 = v_1'' = v_2'' = v_3''$, probably with weaker bands superposed having one or more quantum numbers greater than zero. This interpretation is supported by the band structure, which is of a type expected when B' and B'' are very nearly equal. Several cases like this are known among diatomic band spectra, e.g., the NH band at $\lambda 3360$, which is a strong $(0,0)$ band with a $(1,1)$ and other weaker bands superposed.

On the Lifetime of the Metastable 3P_2 Neon Atom

By E. MATUYAMA

Physical Institute, Tohoku University, Sendai, Japan

(Received August 23, 1932)

To measure the lifetime of the metastable 3P_2 neon atom, the light from a Plücker tube was passed through the absorption tube which contained neon gas at various pressures ranging between 5.2 and 0.25 mm Hg. The gas was excited by external electrodes connected to the secondary coil of a high-frequency oscillator. By adopting the method of the rotating disk the percentage of absorption of the line $^3P_2-^3D_3$ at various stages after the interruption of the excitation of the gas in the absorption tube, was measured. The result obtained was that the life of the 3P_2 neon atom at a pressure of 5.2 mm Hg is about 0.005 sec., which is very near that already reported by Dorgelo, but several times longer than that obtained by Meissner and Graffunder. The effects of impurity and of temperature were also investigated.

THE most reliable experimental data up to date regarding the lifetime of the neon atom in the metastable 3P_2 and 3P_0 states have been reported in papers published by Meissner,¹ and Dorgelo² and Meissner and Graffunder,³ but there are still some discrepancies in their results.

Dorgelo, using the phosphorescopic method of a rotating disk, has measured the time elapsing after the interruption of the electrical excitation until the neon tube shows no measurable absorption. The results found by him for the lifetime of the 3P_2 state is 1/240 seconds, while that of the 3P_0 state is much shorter being about 1/2000 seconds. He has also verified his results by using the method of an alternate current. After rectification, one half-wave is sent through the discharge tube and the other half through the absorbing tube. Meissner and Graffunder used two coupled generators of equal period but of variable phase difference, one of them for the excitation of the Plücker tube and the other for the excitation of the absorbing tube. With any desired phase differences between them, they have measured the rate of decrease in the absorption of the lines above described for gas pressures ranging from 0.2 to 5.6 mm Hg and have found that the half period for 3P_2 is 7×10^{-4} sec., and that the lifetime of this state has a distinct maximum for pressures between 1.5 mm and 2 mm Hg.

The present writer has been working on the same subject using the method of exciting neon atoms with a high-frequency oscillatory current, and the results of the measurements on the rate of decrease of the absorption of the line $^3P_2-^3D_3$ (6402) will be here described.

The method used is also the same in principle as those of previous investigators which have been briefly described. An absorption tube contain-

¹ K. W. Meissner, *Ann. d. Physik* **76**, 124 (1925).

² H. B. Dorgelo, *Zeits. f. Physik* **34**, 766 (1925).

³ K. W. Meissner and W. Graffunder, *Ann. d. Physik* **84**, 1009 (1927).

ing neon is electrically excited for a time and the excitation is then cut off. After the lapse of any interval of time, the light from an emission neon tube is passed through the absorbing tube and the absorption of the line ${}^3P_2-{}^3D_3$ is measured quantitatively. The variations in the time intervals between the excitation of the absorption tube and the light flash from the emission tube were effected by means of a rotating disk with a small hole near the periphery of the disk and an electric contact, in a somewhat different manner from that used in Dorgelo's method. He varied the time intervals by altering the rotational velocity of the disk. However, this gives rise to alterations in the time intervals during which the light passes through the hole, and it will be very inconvenient for comparing the variations in the absorption due to the change of concentration of the metastable 3P_2 atom in the absorbing tube. It seems preferable to use the method of varying positions of electric contact without altering the rotational velocity of the disk. To ascertain whether the

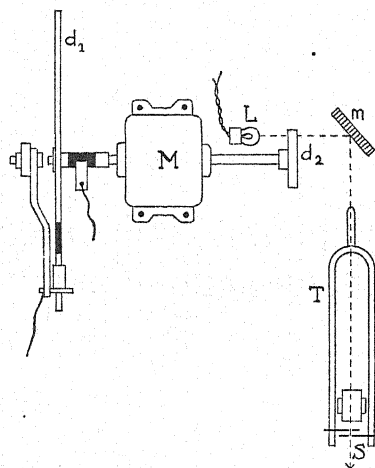


Fig. 1. Rotating disk and stroboscopic device.

disk d_1 while rotating always preserves a constant angular velocity, the following stroboscopic device was used as shown in Fig. 1. The light from an incandescent lamp L falls on the slit s after passing through a small hole in another disk d_2 which is attached to the axis of the motor M which carries disk d_1 , and is reflected by a mirror m . The slit s consists of two brass plates laying close to each other, each of which is attached firmly to each arm of an electrically-operated tuning fork T . By watching carefully the light from the lamp L through the slit s , the current to the motor M was so adjusted that the image of the light was always to be seen at rest. The rotational speed of the motor M was measured directly with a tachometer and was estimated as 1495 revolutions per minute. The rotating disk d_1 is made of a Bakelite plate 40 cm in diameter. A copper piece 6 cm in length, which serves as one of the terminals, is fixed along its periphery, and is connected electrically to a ring on the axis of the motor. The brush making contact with the disk d_1 is of copper, coated with a thin sheet of platinum to reduce the abrasion at

the contact. It is so placed as to be always able to turn around the same axis as that of the motor *M*. In addition to the precautions above described, the spring of the brush was made as strong as permissible and was adjusted to maintain the same condition of contact in every position of the brush.

The current for exciting the absorption tube was supplied by the secondary circuit of a high-frequency oscillator, which was constructed on the same principle as that of Gill and Donaldson. Its frequency was 3×10^7 cycles. The disk d_1 is inserted in series in the plate circuit of the oscillator and the current was kept at a constant value by slightly varying the filament current. The exciting duration was 0.0019 sec. per one revolution of the disk.

The optical system of the arrangement is shown in Fig. 2. The light from the emission tube *p*, which is fed with a high voltage d.c. generator, after passing through the lens l_1 and the absorbing tube *A*, focussed on the hole in the disk d_1 . It then passes through the lens l_3 , falls parallel on the six-stepped reducer *b* and is projected on the slit of the spectrograph by the lens l_4 . By

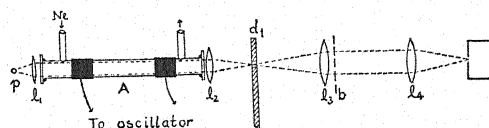


Fig. 2. Optical system for measuring absorptions quantitatively.

measuring the blackness of the plate before inserting the absorbing film it was proved that the illumination of the light falls uniformly on the stepped reducer. To maintain the constancy of the light intensity of the emission tube for the whole course of the experiment, a bulb of great capacity was attached to the emission tube. To prevent fluctuations of the light intensity which are liable to occur for a short time after the circuit has been made, the spectrogram was taken after a lapse of three hours from the beginning of excitation. In order to ensure the constancy of the light intensity of the emission tube, the other conditions being unchanged, the spectrogram, without exciting the absorbing tube, was taken on the same plate before and after the experiment. From this the blackness of the plate is corrected if necessary.

The neon gas used contained 1 percent of helium. It was circulated by means of a condensation pump through the absorbing tube, the tube filled with cocoanut charcoal immersed in liquid air, and the tube containing palladium black. The absorbing tube for the excited neon atom was of glass, 2.5 cm in inner diameter and 30 cm in length. The distance between the external electrodes was 15 cm. Since the light from this absorbing tube was very weak there were no appreciable error introduced into the spectrogram obtained.

The results obtained are diagrammatically shown in Fig. 3, in which the percentage absorption, reckoning the value at the instant of cutting off the excitation of the absorbing tube as 100, are plotted in logarithmic scale against the time which elapsed after the interruption of the excitation. The percentage absorption for the gas pressures 5.2, 1.2, 0.7 and 0.25 mm Hg at 13°C are represented by the curves 1, 2, 3, and 4, respectively, and for the

sake of comparison the results obtained by Meissner and Graffunder for the gas pressures 5.6, 1.42, and 0.50 mm Hg are also shown in the 1', 2', and 3' curves in the same diagram. It will be evident from the diagram that though Meissner and Graffunder have already found that the metastable atom in the 3P_2 state has a maximum life for a gas pressure of about 1.5 mm Hg, the lifetime obtained as the result of this experiment in all cases of pressure is markedly greater than the values found by these investigators. Indeed they seem much more nearly the same as those observed by Dorgelo. For instance, the half-life of the metastable atom for the pressure 1.2 mm Hg is 2.3×10^{-3} sec. from curve 2, while that from curve 2' which represents Meissner and Graffunder's measurement for the gas pressure 1.42 mm Hg gives 7×10^{-4} sec. which amounts only to one-third of the former. In addition, the whole lifetime, assuming this to be the time required to diminish the absorption to 3 percent of its initial value, is, in the case of a pressure 5.2 mm

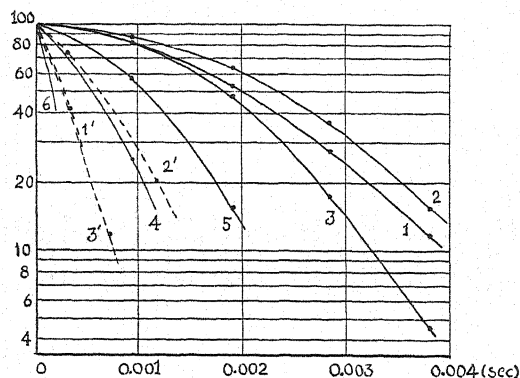


Fig. 3. Curves showing the decrease of the absorption. Curves 1, 2, 3 and 4 are for pressures 5.2, 1.2, 0.7, and 0.25 mm respectively at 13°C . Curve 5 is for neon mixed with hydrogen. Curve 6 is for neon heated at 216°C . Curves 1', 2', 3', are for pressures 5.6, 1.42, and 0.50 mm respectively, measured by Meissner and Graffunder and are plotted for the purpose of comparison.

Hg estimated as nearly $1/200$ sec. This fairly coincides with the value $1/240$ sec. observed by Dorgelo, at a pressure of 8 mm Hg, while the extrapolation of the curve 2' gives $1/500$ sec.

Next, the percentage absorption when hydrogen gas is present at a very low pressure in the absorbing tube was investigated. For this purpose the palladium tube was removed from the system and neon mixed with a small quantity of hydrogen was introduced. Under these conditions hydrogen is slowly adsorbed in the charcoal. The results obtained when a very small quantity of hydrogen is mixed with the neon at a pressure of 1.5 mm Hg are represented in curve 5. The curve shows that the rate of decrease of the absorption of the line $^3P_2 - ^3D_3$ is considerably increased in spite of the fact that the quantity of hydrogen mixed is so small that it was not possible to observe its secondary spectrum with a small direct vision spectroscope. L. Eckstein⁴ has already measured variations of the absorbing power of excited

⁴ L. Eckstein, Ann. d. Physik 87, 1003 (1928).

neon when the neon is mixed with various foreign gases as impurities. He found that the addition of helium in an increasing quantity causes only a slow decrease in the absorption while gases such as hydrogen, nitrogen and argon having lower excited levels than that of the 3P_2 and the 3P_0 neon states, produced the same effect but about 1000 times greater than helium. As one example in this investigation of the impurity effect, the addition of hydrogen at a pressure of 5.2×10^{-3} mm to the neon at 2.18 mm caused the reduction of the percentage absorptions of the line $^3P_2 - ^3D_3$ from 61.4 to 10 percent. This result is in good agreement with that shown in curve 4.

Thirdly, the effect of temperature was observed. It is already known that the energy difference between the 3P_2 and the 3P_1 neon atoms is 0.05 volts. The translational kinetic energy of the atom due to the heat motion at room temperature is estimated as 0.003 volts. To increase the mean kinetic energy of the neon atoms over 0.05 volts, the absorption tube was placed in the glass concentric cylinder, through the intervening space of which was circulated the vapor of diethyle aniline. The neon in the absorption tube was thus maintained at 216°C during the whole period of the experiment and the pressure was 5.6 mm Hg. It was observed that the absorption decreases so rapidly that no trace of it could be detected 0.001 sec. after the interruption of the excitation of the absorption tube.

The dependence of the decay of the metastable state on the gas pressure, on the diffusion of the metastable atoms, on the relative dimension of the absorption tube and the light flux through the tube, and on the collisions between the metastable atoms and other entities in the absorption tube have been fully considered by Meissner and Graffunder. Recently, Zemansky⁵ has again treated the problem with the data obtained by Meissner and Graffunder on the basis of several assumptions, and has calculated the radius of the excited neon atom. But his result, *viz.*, that the excited atom has a smaller radius than the normal one, conflicts with that expected from theory. Meissner and Graffunder have inquired why the lifetime they have obtained for neon can be several times smaller than that obtained by Dorgelo. The lifetime here obtained is, as already mentioned, much longer than Meissner and Graffunder's value, and falls very near that obtained by Dorgelo. Comparing the experimental conditions with those of Meissner and Graffunder, the absorption tube they used was a much wider and shorter one than that used here, and the light flux in both experiments filled the full section of the absorbing tube. But in the case of this experiment, before entering the spectrograph, some portions of the light are cut off by the aperture in the disk and the stepped reducer, therefore the effective light flux relative to the tube is unknown. From the dimensions of the absorbing tube used, it might be expected that the rate of decrease of absorption in the case of the narrow tube used would decrease more rapidly than in the wider tube, but in spite of this, contrary results were observed. In this experiment, the gas in the absorbing tube was excited with external electrodes and therefore was quite free from contaminations due to the sputtering of electrodes as well as to other gases

⁵ M. W. Zemansky, Phys. Rev. 34, 213 (1929).

occluded in these. By taking into consideration the percentage absorptions when only a trace of other gases are added, it seems very probable that the metastable neon atoms under these circumstances will have a lifetime longer than that in the case where the inner electrodes were used. There is also, in this case, some possibility that the recombination of ions must be considered. The reason the rise of temperature causes considerable increase in the rate of decrease of absorption may conceivably be that this increase is a simultaneous effect of increase of probability of transfer into the higher energy state 3P_1 , of increase in frequency of collisions between metastable and the normal atoms, and of increase in the coefficient of diffusion.

In conclusion, the writer wishes to express his indebtedness to Professor J. Okubo for advice given during the course of the experiment.

The Molecular Scattering of Light from Ammonia Solutions. The Fine Structure of a Vibrational Raman Band

By JOHN WARREN WILLIAMS AND ALEXANDER HOLLAENDER
Laboratory of Physical Chemistry, University of Wisconsin

(Received September 2, 1932)

The Raman band of the ammonia molecule corresponding to the infrared absorption at $3\ \mu$ has been partially resolved into its fine structure. The experiments have been made not with gaseous or liquid ammonia but with aqueous solutions of relatively high concentration. The lines have been assigned to Q , P , R , PP , and RR branches, corresponding to changes in rotational quantum number $\Delta k=0, \pm 1$, and ± 2 . The moment of inertia about a line normal to the axis of symmetry calculated from the spacing of the lines is $I=2.82 \times 10^{-40}$ g cm². As far as the present, somewhat incomplete results may be taken to indicate the structure of the NH_3 molecule is largely uninfluenced by the force fields of the solvent molecules.

A NUMBER of investigators have utilized the study of the Raman effect to indicate the changes taking place when an inorganic electrolyte is dissolved in water. The purpose of these studies has usually been to investigate the eventual possibility of obtaining a quantitative measure of the degree of dissociation of the dissolved electrolyte into ions. On the other hand the use of solvents to make it practical to work with simpler substances which do not dissociate upon solution has not met with general favor, it being assumed that perturbations arising from the mutual interaction of solvent and solute molecules will cause difficulties. Also in the case of pure liquids it has been stated¹ that similar interaction produces a lack of sharpness in the rotational states, so that rotational transitions give rise to continuous Raman spectra instead of sharply defined lines. In addition there are presented in this article data whose intent are to show a well-defined difference in the vibrational Raman shifts between gaseous and liquid ammonia.² Our experience with solutions in water has led us to believe such views to be unfortunate, at least in the case of the particular system we are about to describe, ammonia plus water. A very incomplete report of the work has already been published as a preliminary communication to the Editor of this Journal.³

The molecular scattering of light from gaseous ammonia has been studied by Wood,⁴ by Dickinson, Dillon and Rasetti¹ and, more recently and com-

¹ Dickinson, Dillon and Rasetti, *Phys. Rev.* **34**, 582 (1929).

² Experimental error cannot account for the difference in Raman shift in the case of the liquid, $\Delta\nu=3298$, and that for the gas, $\Delta\nu=3334$. However, the "somewhat weaker" shift reported for the liquid, $\Delta\nu=3215$, may be the strong vibration-rotation line, $\Delta\nu=3216$, in our Table I. If this is true, liquid ammonia and the aqueous solution give the same result in this case.

³ Hollaender and Williams, *Phys. Rev.* **37**, 1367 (1931).

⁴ Wood, *Phil. Mag.* **7**, 744 (1929).

pletely, by Amaldi and Placzek.⁵ There are here reported a vibrational line corresponding to $\Delta\nu = 3311$, and rotational lines which could be measured on both sides of the mercury exciting line $\lambda 2536$. The experiments with liquid ammonia^{6,7,1} have revealed the presence of the frequency differences $\Delta\nu = 3311$, $\Delta\nu = 1580$ and $\Delta\nu = 1070$, corresponding to three of the four fundamental frequencies of the pyramidal formula usually assumed for ammonia. Other weaker lines present in these spectra have either been described as having been caused by the association of single ammonia molecules to form double and triple molecules or have not been mentioned at all.

Carrelli, Pringsheim and Rosen⁸ were the first to study solutions of ammonia in water, reporting frequency shifts of $\Delta\nu = 3314$ and $\Delta\nu = 3385$. The next work, as far as we are aware, is contained in the preliminary note referred to above,³ in which it could be stated "that all the lines which have been reported from gaseous and liquid ammonia have now been found in the concentrated solution (16 normal) as well." There was also included here the microphotographic record of one of the plates which had been exposed in a small Steinheil glass spectrograph. This record shows not only the presence of the vibrational band corresponding to the infrared absorption at 3μ ⁹ but also unmistakable evidence of a fine structure due to its combination with the rotation spectrum of the ammonia molecule. The dispersion of the instrument was such that the position of the vibration-rotation lines could not be determined with a sufficient degree of accuracy to assign the proper rotational quantum numbers, so that further experiments with an instrument having a much greater dispersion were necessary. The work to be reported here was done with a Steinheil GH glass spectrograph. Satisfactory exposures were made with ammonia solutions varying in concentration from four normal to sixteen normal, but publication of the results had been postponed in the hope that exposures and microphotographic records suitable for reproduction might be included. It has just now come to our attention that in an article published last month Langseth,¹⁰ working with ammonia solutions of like concentration, has also been able to resolve the Raman band corresponding to the infrared absorption band at 3μ . The positions of the lines in the two researches agree very well with each other except that we have as yet been unable to find sufficient positive evidence for the combination frequency differences which would make possible the calculation of the moment of inertia characteristic of the rotation about the axis of symmetry. The moment of inertia calculated for the rotation about an axis at right angles to the line of symmetry is almost identical in the two experiments. Under these circumstances it is felt that immediate submission of our present results is advisable even though they are incomplete in certain respects.

⁵ Amaldi and Placzek, *Naturwiss.* 20, 521 (1932).

⁶ Daure, *Trans. Farad. Soc.* 25, 825 (1929).

⁷ Bhagavantam, *Ind. Jour. Phys.* 5, 35 (1930).

⁸ Carrelli, Pringsheim and Rosen, *Zeits. f. Physik* 51, 511 (1928).

⁹ Stinchcomb and Barker, *Phys. Rev.* 33, 305 (1929).

¹⁰ Langseth, *Zeits. f. Physik* 77, 60 (1932).

APPARATUS AND TECHNIC

The experimental arrangement was similar to that described by Kohlrausch¹¹ in his recent book. The ammonia gas, taken from a commercial cylinder, was thoroughly washed before it was passed into conductance water to form the solution. The solution to be investigated was placed in a long tube, illuminated along its length with a commercial mercury arc, and the spectrum of the scattered light which passed through a plane window in the end of the tube was recorded by using the spectrograph mentioned above. The tubes were cooled by means of a jacket through which a continuous stream of cold water was pumped. A comparison spectrum from a copper arc was recorded on each plate. The mercury lamps were cooled by an electric fan. The Raman lines reported were all excited by Hg 4047. The filter technic used was essentially that described by Wood. In the calculation of the frequency differences the frequency of this line was taken as $24,705\text{ cm}^{-1}$.

The plates were photometered with a Moll recording microphotometer. The frequencies of the Raman lines were obtained by interpolation on a calibration curve prepared from the microphotometric record of the copper spectrum. All lines reported were observed on several of the plates taken, with different concentrations of ammonia and different times of exposure. The intensity of the lines, while difficult to establish in any quantitative way, always became weaker as the concentration of the solution was decreased, indicating that the excitation of the water bands was not a source of difficulty and that the structure observed was actually characteristic of the ammonia molecule.

EXPERIMENTAL RESULTS

The results of the experimental determinations are summarized in Table I. The columns of this table give, from left to right; the frequency of the excited line in reciprocal centimeters, the corresponding frequency difference between exciting and excited line, the assignment of rotational quantum number for the transition $\Delta k \pm 1$, and the assignment of rotational quantum number for the transition $\Delta k = \pm 2$. In a number of cases the microphotometric record shows the head of the line to be somewhat broadened rather than sharp, therefore the exact positions of the weaker lines will be somewhat in doubt. Nevertheless, it is believed that most of them have been located to within $\pm 3\text{ cm}^{-1}$. It is interesting to note that the transitions $\Delta k = +1$ and $\Delta k = -1$ are required to account for the positions of some of the observed Raman lines. As Placzek¹² has pointed out this is to be expected in the case of a nonlinear molecule like ammonia. A graphical analysis of the k -structure assigned shows no irregularity or inconsistency.

In Table II there are compared the frequency differences of the several levels for ammonia found by Badger and Cartwright from their study of the infrared rotation bands, by Amaldi and Placzek from the Raman effect for

¹¹ Kohlrausch, *Der Smekal-Raman Effekt*, Springer, Berlin, 1931.

¹² Placzek, *Molekülstruktur*, Leipziger Vorträge, Hirzel, 1931; Amaldi and Placzek, *Naturwiss.* 20, 521 (1932).

TABLE I. Raman spectrum from aqueous ammonia solution showing fine structure of vibrational transition band corresponding to infrared absorption at 3μ .

ν in cm^{-1}	$\Delta\nu$ (4047A) in cm^{-1}	Transition $\Delta k = \pm 1$	Transition $\Delta k = \pm 2$
21096	3609	14 \rightarrow 15	6 \rightarrow 8
21125	3580	13 \rightarrow 14	
21161	3544	11 \rightarrow 12	
21215	3490	8 \rightarrow 9	3 \rightarrow 5
21230	3475	7 \rightarrow 8	
21254	3451	6 \rightarrow 7	2 \rightarrow 4
21280	3425	5 \rightarrow 6	
21296	3409	4 \rightarrow 5	1 \rightarrow 3
21315	3390	3 \rightarrow 4	
21332	3373	2 \rightarrow 3	0 \rightarrow 2
21356	3349	1 \rightarrow 2	
21394	3311	—	—
21430	3275	2 \rightarrow 1	
21450	3255	3 \rightarrow 2	2 \rightarrow 0
21469	3236	4 \rightarrow 3	
21489	3216	5 \rightarrow 4	3 \rightarrow 1
21510	3195	6 \rightarrow 5	
21532	3173	7 \rightarrow 6	4 \rightarrow 2
21567	3138	9 \rightarrow 8	5 \rightarrow 3
21586	3119	10 \rightarrow 9	
21607	3098	11 \rightarrow 10	6 \rightarrow 4
21631	3074	12 \rightarrow 11	
21656	3049	13 \rightarrow 12	7 \rightarrow 5
21685	3020	15 \rightarrow 14	8 \rightarrow 6
21709	2996	16 \rightarrow 15	
21743	2962	18 \rightarrow 17	

the gas, and by us from our work with aqueous solutions. The agreement, while it cannot be claimed to be excellent, is satisfactory when one considers the difficulties associated with the proper location of the lines and with a possible slight deformation of the ammonia molecule when dissolved to such high concentration.

TABLE II. Comparison between Raman and infrared spectrum of ammonia.

Concentrated water solution at 10°C Raman effect*			Gas under pressure Raman effect†		Rotation spectrum infrared absorption‡		
$\Delta k = \pm 2$	$\Delta k = \pm 1$	Frequency	$\Delta k = \pm 2$	$\Delta k = \pm 1$	Frequency	$\Delta k = \pm 1$	observed calculated
	1 \leftrightarrow 2	41		1 \leftrightarrow 2	—	1 \leftrightarrow 2	—
0 \leftrightarrow 2	2 \leftrightarrow 3	59	0 \leftrightarrow 2	2 \leftrightarrow 3	—	2 \leftrightarrow 3	—
	3 \leftrightarrow 4	77		3 \leftrightarrow 4	79.5	3 \leftrightarrow 4	79.8 79.5
1 \leftrightarrow 3	4 \leftrightarrow 5	97	1 \leftrightarrow 3	4 \leftrightarrow 5	99.5	4 \leftrightarrow 5	99.1 99.2
	5 \leftrightarrow 6	115		5 \leftrightarrow 6	119.5	5 \leftrightarrow 6	118.6 118.6
2 \leftrightarrow 4	6 \leftrightarrow 7	139	2 \leftrightarrow 4	6 \leftrightarrow 7	140.2	6 \leftrightarrow 7	— 138.0
	7 \leftrightarrow 8	164		7 \leftrightarrow 8	159.6	7 \leftrightarrow 8	156.8 157.1
3 \leftrightarrow 5	8 \leftrightarrow 9	176	3 \leftrightarrow 5	8 \leftrightarrow 9	179.0	8 \leftrightarrow 9	176.1 175.9
	9 \leftrightarrow 10	192		9 \leftrightarrow 10	199.0	9 \leftrightarrow 10	— 194.5
4 \leftrightarrow 6	10 \leftrightarrow 11	213	4 \leftrightarrow 6	10 \leftrightarrow 11	219.0	10 \leftrightarrow 11	—

* Present experiments.

† Amaldi and Placzek, Naturwiss. 20, 521 (1932).

‡ Badger and Cartwright, Phys. Rev. 33, 692 (1929).

In the microphotometric record mentioned above³ the fine structure corresponding to the *R* and *RR* branches was less distinct than that on the low wave-length side of the line corresponding to no change in rotation. There is

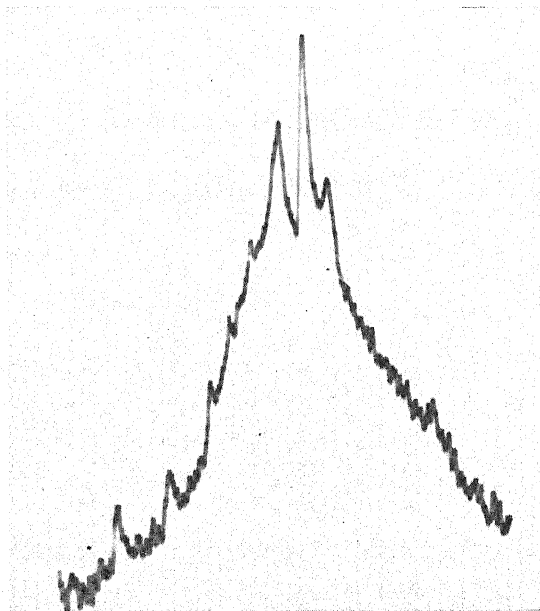


Fig. 1.

included as Fig. 1 a portion of a microphotograph which shows the resolution of the high wave-length side of the band to greater advantage. Another record, Fig. 2, taken from a plate for which a considerably higher dispersion was

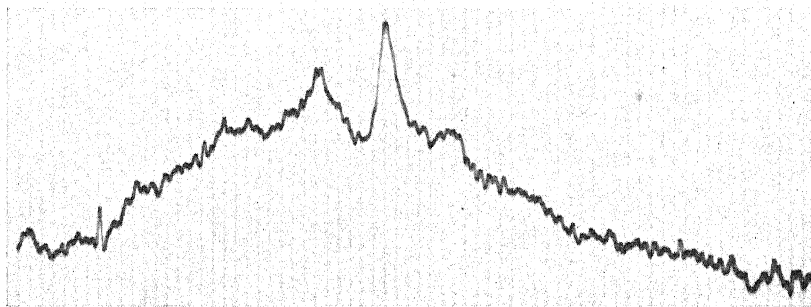


Fig. 2.

used, gives the general structure of the band and permits an estimate of the relative intensities of the lines to be made.

DISCUSSION

The structure of the ammonia molecule is now known to resemble a regular pyramid in form. This is definitely indicated both by potential energy

calculations¹³ and by observations of the molecular spectra. In neither case have the mathematical analyses and experimental results been sufficiently refined to enable the assignment of universally acceptable dimensions to the model. However, there is now agreement that the 3μ band in the near infrared is associated with a vibration of the electric moment parallel to the symmetry axis, and that it has been successfully resolved into one zero branch and a simple rotation series.⁹ From this band the moment of inertia of the molecule about a line normal to the symmetry axis has been obtained. Values lying between $I=2.77 \times 10^{-40}$ and $I=2.83 \times 10^{-40}$ have been reported by a number of investigators of the infrared spectra, so that the agreement here is excellent.

This absorption band has now been resolved by means of the Raman effect, the spacing of the lines corresponding well with that reported by Stinchcomb and Barker. From this spacing it is possible to calculate the moment of inertia.

As indicated in Table I the Raman lines have been assigned to an R branch, $\Delta k = +1$; to an RR branch, $\Delta k = +2$; to a P branch, $\Delta k = -1$; and to a PP branch, $\Delta k = -2$. The frequencies of the lines can be quite exactly expressed by means of the following formulae:

$$\begin{array}{lll} \Delta k = +1, & \nu = 3311 + 2B(k+1) & \text{where } 2B = 19.7 \text{ cm}^{-1}, \\ \Delta k = +2, & \nu = 3311 + 2B(2k+3) & \text{where } 2B = 19.8 \text{ cm}^{-1}, \\ \Delta k = -1, & \nu = 3311 - 2B(k) & \text{where } 2B = 19.4 \text{ cm}^{-1}, \\ \Delta k = -2, & \nu = 3311 - 2B(2k-1) & \text{where } 2B = 19.4 \text{ cm}^{-1}. \end{array}$$

The values for the constant $2B$ vary but little within each series, in addition the values determined for each series show only slight differences from each other. Taking 19.6 cm^{-1} as an average the moment of inertia may be calculated from the well-known formula, $B = h/8\pi^2 cI$, with the result that, $I = 2.82 \times 10^{-40} \text{ g cm}^2$. This value is almost identical with that given by Stinchcomb and Barker.⁹ It is evident that the dissolved ammonia molecules have not been deformed to any appreciable extent by the continual bombardment and electrical force fields of the solvent molecules otherwise the moment of inertia could have been expected to deviate somewhat from this value.

There has been much discussion with respect to a shift in the characteristic frequency differences given by an ion such as CO_3^- or SO_4^- when it is dissolved in water. Embirikos¹⁴ could detect shifts of approximately 10 cm^{-1} in sulphate solutions when the concentration was changed from one normal to two normal. Even larger shifts were observed by Woodward¹⁵ in the case of lines associated with the SO_4^- ion in his studies of sulphuric acid solutions. These systems differ from the type considered in this article because the scattering is caused by a doubly charged ion instead of by a neutral mole-

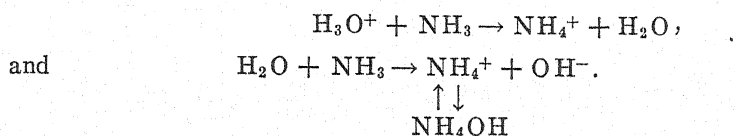
¹³ Debye, *Polar Molecules*, Chemical Catalog Co., New York, 1929.

¹⁴ Embirikos, *Zeits. f. Physik* 65, 266 (1930).

¹⁵ Woodward, *Phys. Zeits.* 32, 212 (1931).

cule. The ability of an ion to segregate and orient water molecules about it is well known.

Ammonia gas when dissolved in a large excess of water will first neutralize the acid H_3O^+ and then begin to remove protons from the water itself according to the reactions,



But as the concentration of the gas is increased greater and greater amounts of ammonia molecules which have not reacted in a chemical way must be present. In such cases the concentration of the ammonia molecules may become so great that observations of the light scattered by them may be made with relative ease. It might be well to mention that the concentration as determined by ordinary analytical methods includes both the NH_3 and the NH_4OH formed.

One might reasonably expect similar experiments in which hydrochloric acid gas was dissolved in water to be successful. Undissociated hydrochloric acid molecules are known to exist in aqueous solutions of concentration as low as one normal, and it is possible to obtain solutions containing more than ten times this amount of hydrochloric acid. However, Woodward¹⁸ and others have reported failure to find any Raman lines using a solution saturated with the gas. The concentration of the undissociated HCl molecules should be sufficient for the purpose. In spite of such experiences, it is to be hoped that there may be accomplished the resolution of the other bands of ammonia and the similar treatment of the spectra of many other simpler gaseous substances using the solution method to obtain a sufficient molecular concentration.

It is a pleasure to acknowledge the material assistance of Professor J. G. Winans of this University in connection with the interpretation of the results.

Raman Spectra of a Series of Normal Alcohols and Other Compounds

By R. W. WOOD AND GEORGE COLLINS
Rowland Hall, Johns Hopkins University

(Received September 14, 1932)

The Raman spectra of benzene, cyclohexane, cyclohexene, carbon disulfide, butyl bromide and the normal alcohols from CH_3OH to $\text{C}_{12}\text{H}_{25}\text{OH}$ were investigated. The technique recently developed by Wood was used in conjunction with a praseodymium filter. New lines were found in all cases and for some compounds the number was nearly doubled. Two new frequencies at 2660 and 2730 cm^{-1} were found in the spectra of essentially all the alcohols and butyl bromide. They appear to be characteristic of the saturated hydrocarbons. The lines which appear in the Raman spectra of the aliphatic hydrocarbons at 1450 and 1300 cm^{-1} have been attributed respectively to the transverse vibrations of the hydrogens of the CH_3 and CH_2 groups. The line appearing in the Raman spectra of the alcohols at 1270 cm^{-1} is attributed to the transverse vibrations of the hydrogens of the CH_2OH groups. It is pointed out that the Raman spectra of $\text{C}_{12}\text{H}_{25}\text{OH}$ is that of an infinitely long normal alcohol. The new lines of benzene reported by Weiler and Krishnamurti were verified with the exception of the 806 cm^{-1} frequency. In addition a new line at 1690 cm^{-1} was found. The two relatively strong lines of CS_2 at 650 and 800 cm^{-1} were each found to be doublet, thus completing the analogy with CO_2 . The separation of the components in each case was 10 cm^{-1} . The existence of a line at 391 cm^{-1} , originally reported by Bhagavantam, was verified.

THE Raman spectra of a number of organic compounds were investigated by an experimental arrangement recently developed by Wood.¹ New lines were found in all cases, and in some the number was nearly doubled. This emphasizes the importance of repeating much of the earlier work that was done before the technique of Raman spectra reached its present stage of development. Most of the recent improvements have been in the direction of improved methods of excitation, and it is perhaps well to call attention to the advantages of using spectroscopes of relatively high dispersion. This is shown by the present investigation in which a glass prism spectrograph with dispersion of 22A per mm in the blue was used. It was found that many of the bands reported in the literature actually possess structure. Likewise Langseth² using a one meter grating, found that the Raman lines of CCl_4 were double, and in some cases even triple. There is no doubt but that incomplete and inaccurate data have greatly retarded the interpretation of Raman spectra.

We have investigated the Raman spectra of a series of normal alcohols beginning with methyl (CH_3OH) and ending with dodecyl alcohol ($\text{C}_{12}\text{H}_{25}\text{OH}$). This series was loaned to us by Professor E. Emmet Reid of this University, and was complete up to $\text{C}_{17}\text{H}_{35}\text{OH}$. It proved to be unnecessary, however,

¹ R. W. Wood, *Phys. Rev.* **38**, 2168 (1931).

² Langseth, *Zeits. f. Physik* **72**, 350 (1931).

to investigate those above $C_{12}H_{25}OH$ as the higher members showed no differences in their Raman spectra. Benzene, cyclohexane and cyclohexene were taken since very pure samples of these were available. As they have already been rather extensively investigated, they served to indicate the efficiency of the apparatus. Carbon disulfide was investigated in order to verify the existence of a line at 390 cm^{-1} which is of vital importance in the analysis of the Raman and infrared spectra.

EXPERIMENTAL

All excitation was by Hg 4358. The experimental arrangement was essentially that described by Wood, modified in that two filters were employed in two Pyrex tubes placed one above the other over the mercury arc. The diameters of these tubes were 5 cm and 2.3 cm, the larger being placed below. With this arrangement a large part of the exciting light from the arc was concentrated into a narrow beam passing vertically through the Raman tube. In most cases a 30 percent aqueous solution of praseodymium ammonium

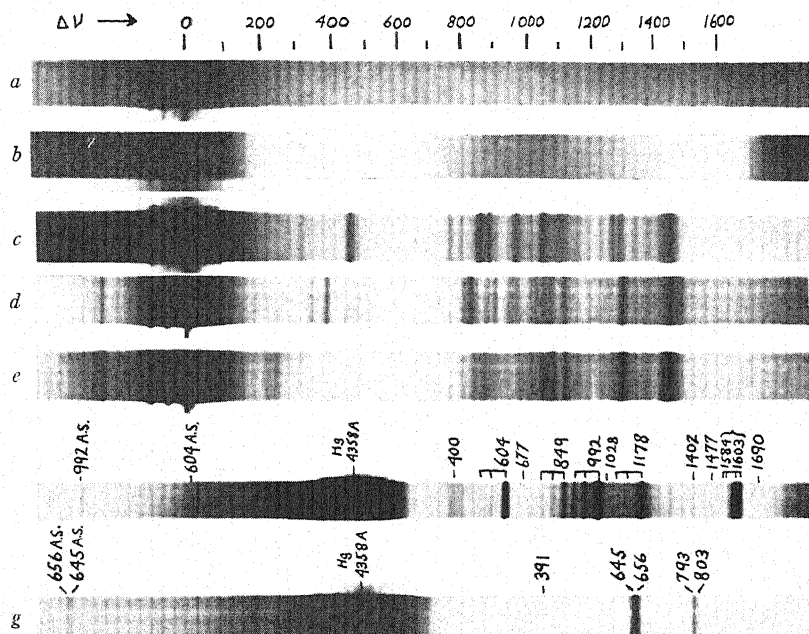


Fig. 1. a, Hg arc; b, Hg arc through praseodymium filter; c, C_3H_7OH (n); d, C_4H_7OH (n); e, $C_{10}H_{21}OH$ (n); f, benzene; g, carbon disulfide.

nitrate was placed in the smaller tube. Praseodymium has a strong and very sharp absorption band on the long wave-length side of, and very close to, Hg 4358, and when used as a filter absorbs the strong continuous spectrum of the mercury arc in this region, leaving a clear background for the Raman lines. Such a filter is particularly advantageous in obtaining Raman lines of low frequency when the excitation is by Hg 4358. Figs. 1a and 1b show the effect

tiveness with which this filter removes the background. This filter has the disadvantage of reducing the intensity of Hg 4358 to about one-half when used in the above concentration. A rather strong solution of crystal violet was substituted for the praseodymium when investigating Raman lines of frequency greater than 2000 cm^{-1} . The larger tube contained a quinine solution of sufficient concentration to absorb Hg 4047 and Hg 4077 and was protected against photochemical change by a sheet of noviol glass, as previously described. With this arrangement it was possible to make exposures of 70 hours or more before the general background appeared with appreciable intensity.

The wave-lengths of the Raman lines were determined by interpolation on a large dispersion curve obtained from the iron lines of the comparison spectrum. The frequencies given are accurate to about $\pm 3\text{ cm}^{-1}$ for moderately sharp lines.

The alcohols from $\text{C}_3\text{H}_7\text{OH}$ to $\text{C}_{12}\text{H}_{25}\text{OH}$ were prepared by Dr. Jane Meyers of this University. Those from CH_3OH to $\text{C}_7\text{H}_{15}\text{OH}$ were obtained from other reliable sources, and all were carefully purified by distillation. The benzene, cyclohexane, and cyclohexene were from samples especially purified for specific heat and melting point determinations. The remaining liquids investigated were from standard C. P. sources.

RAMAN SPECTRA OF ALCOHOLS

A chart of the Raman lines of the normal alcohols from CH_3OH to $\text{C}_{12}\text{H}_{25}\text{OH}$ is given in Fig. 2. The lines of frequency greater than 1500 cm^{-1} are not included, but may be found in the complete list of Table I. $\text{C}_{11}\text{H}_{23}\text{OH}$ is omitted from this series as it was not obtainable in sufficient quantities. Enlargements of some of the original plates may be found in Fig. 1.

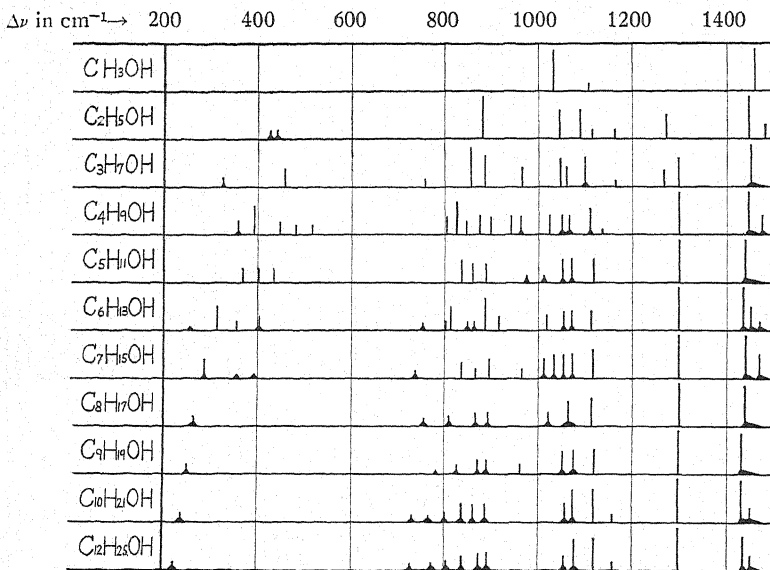


Fig. 2. Diagram of Raman frequencies of alcohols showing relative intensity and breadth of lines.

TABLE I. Raman frequencies in cm^{-1} .

CH_3OH	1028(10) 1107(2) 1457(10) 2729(1) 2831(10) 2942(10)
$\text{C}_2\text{H}_5\text{OH}$	426(5) 443(2) 883(20) 1047(10) 1091(10) 1115(1) (1162)(1) 1273(8) 1449(10) 1481(4) 2637(0) 2714(1) 2823(2) 2783(10) 2925(10) 2972(10)
$\text{C}_3\text{H}_7\text{OH}(\text{n})$	324(2) 458(4) 757(4) 856(10) 887(8) 967(4) 1049(5) 1064(4) 1100(6) 1268(4) 1296(6) 1451(10) 2663(1) 2731(2) 2873(15) 2905(10) 2931(10) 2963(10)
$\text{C}_4\text{H}_9\text{OH}$	350(3) 394(6) 448(3) 483(2) 514(2) 805(4) 825(8) 845(3) 877(4) 901(4) 944(4) 963(4) 1025(4) 1051(4) 1067(4) 1104(6) 1135(1) 1296(1) 1147(10) 1476(4) 2660(1) 2733(1) 2865(10) 2903(10) 2932(10) 2963(15)
$\text{C}_5\text{H}_{11}\text{OH}$	366(3) 401(3) 434(3) 835(3) 858(4) 889(4) 975(1) 1013(1) 1053(5) 1072(5) 1116(5) 1299(10) 1442(10) 2653(1) 2721(1) 2868(10) 2908(10) 2935(5) 2961(5)
$\text{C}_6\text{H}_{13}\text{OH}$	253(1) 311(5) 355(2) 402(3) 754(2) 802(2) 814(5) 850(2) 864(2) 888(8) 915(3) 1019(3) 1056(4) 1072(4) 1113(4) 1297(10) 1435(10) 1451(5) 1472(2) (Band 2842 to 2932 (10)) 2958(3)
$\text{C}_7\text{H}_{15}\text{OH}$	287(3) 357(1) 392(1) 735(2) 836(3) 866(2) 897(4) 966(2) 1012(4) 1035(5) 1054(5) 1074(5) 1116(6) 1297(10) 1442(10) 1471(5) (Band 2842 to 2952(10))
$\text{C}_8\text{H}_{17}\text{OH}$	263(2) 759(1) 809(2) 867(3) 894(3) 1023(3) 1066(5) 1120(6) 1300(10) 1442(10) (Band 2848 to 2941 (10))
$\text{C}_9\text{H}_{19}\text{OH}$	250(2) 784(1) 830(2) 872(3) 891(3) 963(2) 1055(5) 1078(5) 1118(5) 1297(10) 1432(10) (Band 2842 to 2932(10)) 2958(2)
$\text{C}_{10}\text{H}_{21}\text{OH}$	238(2) 727(1) 768(1) 801(2) 838(3) 863(3) 889(4) 1059(4) 1076(7) 1116(7) 1159(2) 1295(10) 1430(10) 1449(3) 2643(1) 2719(1) (Band 2836 to 2929(10)) 2954(2)
$\text{C}_{12}\text{H}_{25}\text{OH}$	224(2) 722(1) 771(1) 805(2) 838(4) 874(4) 893(4) 1056(4) 1079(7) 1119(7) 1159(2) 1297(10) 1433(10) 1449(10) 2847(10) 2887(10) 2925(8) 2958(3)
Benzene	400(2) 604(10) 677(1) 849(5) 982(2)* 992(20)* 1028(0) 1178(10) 1402(2) 1477(2) 1584(10) 1603(5) 1690(1) 2291(0) 2452(1) 2542(1) 2618(2) 2920(0) 2948(3) 3051(5)* 3065(5)* 3163(2)* 3186(2)*
Cyclohexane	380(2) 422(3) 801(10) 1026(8) 1154(4) 1264(8) 1342(2) 1442(10) 2626(0) 2661(1) 2693(0) 2750(0) 2849(10) 2880(1) 2920(10) 2934(10)
Cyclohexene	171(2) 282(3) 390(5) 445(1) 487(2) 635(1) 715(3) 821(10) 873(2) 904(3) 963(3) 1034(3) 1062(5) 1134(1) 1218(10) 1238(2) 1263(4) 1426(10) 1443(3) 1650(10) 2634(9) 2660(1) 2833(10) 2856(10) 2873(10) 2908(10) 2934(10) 3020(10)
Carbon disulfide	391(1) 645(10) 656(20) 793(8) 803(3)
Butyl bromide	218(3) 235(3) 276(5) 345(1) 387(2) 411(2) 457(5) 559(20) 640(10) 736(5) 796(6) 833(0) 865(5) 893(4) 909(2) 967(1) 993(2) 1011(2) 1048(8) 1097(8) 1214(5) 1260(4) 1294(5) 1441(10) 2660(0) 2733(1) 2833(2) 2868(10) 2902(5) 2934(10) 2963(10) 3008(3)

* Weiler's values.

Two new Raman lines, hitherto unreported, were found in the spectra of $\text{C}_2\text{H}_5\text{OH}$, $\text{C}_3\text{H}_7\text{OH}$, $\text{C}_4\text{H}_9\text{OH}$, $\text{C}_5\text{H}_{11}\text{OH}$ and $\text{C}_{10}\text{H}_{21}\text{OH}$. They lie at about 2660 and 2730 cm^{-1} . CH_3OH shows only the one at 2730 cm^{-1} . To determine whether these frequencies are associated with the OH groups, the Raman spec-

tra of C_4H_9Br were taken. The position of these new lines was found to be the same in C_4H_9Br and C_4H_9OH showing that they are independent of the radical attached to the end of the molecule. This, combined with the fact that these frequencies appear in so many of the alcohols, makes it seem likely that they are characteristic of the saturated hydrocarbons. New lines, in addition to those discussed above, are now considered.

In methyl alcohol a new frequency was found at 1107 cm^{-1} .

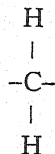
In ethyl alcohol the 426 cm^{-1} frequency as reported in Kohlrausch³ was resolved into two components, 426 and 443 cm^{-1} , and an additional line was discovered at 1115 cm^{-1} .

In normal propyl alcohol new lines were found at 324 , 757 , 1064 , 1165 and 1268 cm^{-1} . The frequency 1364 cm^{-1} reported by Duare⁴ and by Gameson and Venkateswaran⁵ was not verified. Trumpy likewise failed to find this line.

Six new lines were found in the spectrum of normal butyl alcohol (C_4H_9OH) and six lines previously considered single were resolved into two components. The Raman spectra of normal alcohols above butyl have not been investigated previously.

Lines whose frequencies remain unchanged, or which change in a systematic way from molecule to molecule, are of course the easiest to interpret. Attention is called to five of this type which occur in the spectrum of the alcohols. There is the broad, often unresolved, line at 1450 cm^{-1} , the strong lines at about 1300 and 1120 cm^{-1} , the double line at 1055 and 1075 cm^{-1} (unresolved in $C_8H_{17}OH$), and the group of lines below 500 cm^{-1} . Something may be said in regard to these frequencies.

Kohlrausch³ and Trumpy⁶ have attributed the 1450 cm^{-1} frequency to vibrations of the hydrogens of the



groups (referred to in the future as CH_2 groups). They have at the same time attributed the 1300 cm^{-1} frequency to vibrations of the end CH_3 groups against the remainder of the molecule. This assignment appears unlikely, since, if the line at 1300 cm^{-1} were due to vibrations of the CH_3 group against the remainder of the molecule, its frequency should diminish with increasing mass of the molecule. Fig. 2 shows clearly that this is not the case, and another explanation must be looked for. Andrews has pointed out that the line at 1450 cm^{-1} appears whenever a CH_3 group is present in a molecule, and that the line at 1300 cm^{-1} is usually associated with the presence of CH_2 groups. These two lines presumably arise from a transverse or bending motion

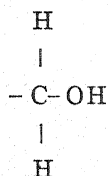
³ Kohlrausch, *Der Smekal Raman Effekt*, p. 309.

⁴ Duare, *Ann. d. Physik* **12**, 375 (1929).

⁵ Gameson and Venkateswaran, *Ind. Jour. Phys.* **4**, 196 (1929).

⁶ Trumpy, *Zeits. f. Physik* **62**, 806 (1930).

of the hydrogen atoms with respect to the carbons. The fact that these frequencies are so constant would indicate that the influence of the hydrogen bending motions does not extend to adjacent atoms. The 1270 cm^{-1} line which appears in the spectrum of ethyl and propyl alcohol is then explained as arising from transverse vibrations of the hydrogens of the



groups (referred to as a CH_2OH group). The hydrogens of this group would be expected to have a different frequency from those of the CH_2 group as their bond strength should be changed by the presence of the OH radical. In support of this contention, attention may be called to the following.

Methyl alcohol (H_3COH) and isopropyl alcohol³ ($\text{H}_3\text{C}\cdot\text{HC}\cdot\text{OH}$) CH_3 contain no CH_2OH or CH_2 groups, and do not show the 1270 and 1300 cm^{-1} frequencies. Ethyl alcohol ($\text{H}_3\text{C}\cdot\text{H}_2\text{COH}$) contains a CH_2OH group, and no CH_2 group, and shows only the 1272 cm^{-1} frequency. Normal propyl alcohol ($\text{H}_3\text{C}\cdot\text{H}_2\text{C}\cdot\text{H}_2\text{OH}$) contains a CH_2OH group and shows both the 1270 and the 1300 cm^{-1} frequencies. Butyl ($\text{H}_3\text{C}\cdot\text{H}_2\text{C}\cdot\text{H}_2\text{C}\cdot\text{H}_2\text{COH}$) and the higher alcohols, however, have both CH_2OH and CH_2 groups, and show only the 1300 cm^{-1} frequency, indicating a possible discrepancy. The explanation may be, however, that the 1270 cm^{-1} frequency exists in the higher alcohols, and is simply too weak to be recorded. The decreased number of CH_2OH groups with respect to the CH_2 groups in the higher alcohols makes this explanation plausible.

The double frequency at 1055 and 1070 cm^{-1} probably arises from a side-wise compressional motion of the carbon chain suggested by Collins.⁷ These values are close to the calculated one of 1075 cm^{-1} . In calculating this frequency the influence of the hydrogen atoms attached to the carbons was neglected. Their influence may produce two frequencies instead of one, resulting from the hydrogens vibrating with or against the carbon atoms. A compressional vibration of the type considered is optically inactive, and would account for the high intensity of these lines. It is to be noted that the Raman spectra of $\text{C}_{10}\text{H}_{21}\text{OH}$ and $\text{C}_{12}\text{H}_{25}\text{OH}$ are identical and these two spectra differ but slightly from that of $\text{C}_9\text{H}_{19}\text{OH}$. A further increase in the length of the carbon chain above that of $\text{C}_{12}\text{H}_{25}\text{OH}$ should then produce no change in the Raman spectra. This being the case the Raman spectra of $\text{C}_{12}\text{H}_{25}\text{OH}$ may be considered that of an infinitely long hydrocarbon chain with an OH group at one end.

RAMAN SPECTRUM OF BENZENE

The Raman spectrum of benzene has been examined recently by Weiler⁸

⁷ Collins, *Phys. Rev.* **40**, 829 (1932).

⁸ Weiler, *Zeits. f. Physik* **69**, 586 (1931).

and Krishnamurti,⁹ who have reported new frequencies at 687, 806, 1407 and 1477 cm^{-1} . The existence of all these frequencies with the exception of 806 cm^{-1} was verified. The position of the latter frequency when excited by Hg 4358 coincides closely with that of the strong 848 cm^{-1} Raman line excited by a weaker line of the mercury triplet (Hg 4347.5), and it was found impossible to distinguish between the two. Inasmuch as Krishnamurti used Hg 4358 as the exciting line, the existence of 806 cm^{-1} is perhaps doubtful. A hitherto unreported frequency was found at 1690 cm^{-1} . This Raman line falls within one of the praseodymium absorption bands, and otherwise would probably be masked by the continuous background of the arc. An enlargement of one of the benzene plates is given in Fig. 1b with the Raman frequencies, both stokes and antistokes marked. The effect of the praseodymium filter in reducing the continuous background is very noticeable.

RAMAN SPECTRA OF CYCLOHEXANE AND CYCLOHEXENE

The samples of cyclohexane and cyclohexene were of extreme purity, and benzene-free. There was no evidence of the cyclohexane line at 992 cm^{-1} reported by Krishnamurti, and since this frequency corresponds to the strong est benzene line, the inference is obvious. The existence of the new lines in cyclohexane reported by Krishnamurti at 2630, 2662, 2889 and 2963 cm^{-1} was verified, with small discrepancies in their exact frequencies.

Cyclohexene, due no doubt to its unsymmetrical ring structure, shows many more Raman lines than either benzene or cyclohexane. In addition to those already reported by Weiler,⁸ new lines were found at 445, 715, 1134, 1238, 2634, and 2660 cm^{-1} ; the latter not appearing in benzene and having perhaps the same origin as the lines of similar frequency which occur in the Raman spectra of the alcohols.

RAMAN SPECTRUM OF CARBON DISULFIDE

A special effort was made to obtain the complete spectrum of CS_2 . The lines at 645 and 793 cm^{-1} were resolved into two components, the separation in both cases being 10 cm^{-1} . An enlargement of one of the plates is shown in Fig. 1g. From this it can be seen that the weaker component of the 800 cm^{-1} line is on the long wave-length side while the weaker component of the 650 cm^{-1} line is on the short wave-length side. As is to be expected, this condition is reversed in the antistokes member of the 650 cm^{-1} line. Of the three lines reported by Bhagavantam¹⁰ at 412, 1229 and 1577 cm^{-1} only the first was verified. The observation of 793–803 as a doublet is of especial interest. It has been previously reported single but a doublet is required to make the analogy with the spectrum of CO_2 complete.

⁹ P. Krishnamurti, *Ind. Jour. Phys.* **4**, 543 (1931).

¹⁰ Bhagavantam, *Nature* **126**, 995 (1930).

Magnetic Spectra of Secondary Electrons from Silver

By S. CHYLINSKI

Ryerson Physical Laboratory, University of Chicago

(Received August 29, 1932)

By means of a magnetic analyzer and electrometer, the spectra of secondary electrons from silver, when bombarded with cathode rays of energies in the range of 2.1 to 30 equivalent k.v., were determined. Each of the kinetic energy distribution curves shows one prominent peak the location of which varies somewhat with the primary voltage. For voltages up to about 10 k.v. it is located between 0.6 and $0.7 eV_0$, where eV_0 is the primary energy; for voltages between 15 and 30 k.v. it is located between 0.7 and $0.8 eV_0$. The slopes of the curves on the high energy side of the peaks increase with increasing primary voltages, becoming discontinuous at a point which, within experimental error, corresponds to the primary energy. On the low energy end the peaks decrease less rapidly, reaching half maximum values around $0.3 eV_0$ for voltages up to 10 k.v. and around $0.5 eV_0$ for the higher primary voltages. The curves have a shape similar to that of the continuous x-ray spectrum curves.

I. INTRODUCTION

WHEN x-rays strike a substance they give rise, among other phenomena, to an electronic radiation. This so-called x-ray photoelectric effect, has been placed upon a secure basis by the experiments of M. de Broglie.¹ His work established the fact, that when a monochromatic beam of x-rays of frequency ν is incident on a substance, a number of groups of secondary electrons are expelled, the energies of which are given by Einstein's equation,

$$\frac{1}{2}mv^2 = h\nu - h\nu_0 \quad (1)$$

where $h\nu_0$ stands for the quantities $h\nu_K$, $h\nu_{L_1}$, $h\nu_{L_2}$, \dots , the work of extraction for the corresponding levels K , L_1 , L_2 , etc., of the atom. Knowing v , the velocity of each group of electrons, the several values of $h\nu_0$ and from them the absorption limits ν_K , ν_{L_1} , ν_{L_2} , \dots , can thus be obtained. The different groups of electrons were isolated by the magnetic spectrograph.

de Broglie's experiment and other similar experiments provided an almost direct method of proving that electrons exist at various energy levels and that there are one K level, three L levels, five M levels, etc.

It is also known, since the work of Lenard² and his collaborators, that electrons striking a metal surface cause an emission of secondary electrons.² The early work in this field is full of contradictory statements. Since ionization, characteristic radiations etc., are produced by electron bombardment as well as by x-rays, one might expect to find magnetic spectra of secondary electrons such as those observed by de Broglie in the case of the x-ray photoelectrons. Such spectra have actually been observed in the case of certain

¹ M. de Broglie, *Comptes Rendus* 1, 274, 527, 746 and 806 (1921).

² P. Lenard, *Quantitatives über Kathodenstrahlen*, 1925 Ed. The name "secondary" electrons is used by Lenard and his school in a very restricted sense. In this article we mean by secondary all those electrons that issue from a target when it is bombarded by primary electrons.

gases, for instance, by Dymond,³ Harnwell⁴ and others for helium, and by Eldridge⁵ for mercury vapor. In the case of solids no such clear-cut results have been obtained. One might think the reason for this to be partly due to the use of the electric counterfield method of analysis, which was used by the early investigators in this field. This method gives essentially integrated results and hence the existence of any special groups of electrons should be indicated merely by bends or inflections of the velocity distribution curves. The author⁶ applied the magnetic analyzer method which is described in detail below. Lorenz⁷ made an indirect study of secondary electrons from a tungsten target by comparing the spectra of the focal spot and the so-called stem radiations. The stem radiation is supposed to be produced by the electrons which leave the target and fall back on it due to the negative field of the glass walls and the positive field of the target. The two spectra are similar but that of the stem radiation is displaced towards longer wave-lengths. The difference between the short wave-length limits of the two types of radiation Lorenz identifies as corresponding to the work of extraction of the electrons from definite levels within the atom. Reasoning in this manner he concluded that the secondary electrons were electrons that had been knocked out from the different atomic levels by the primary electrons. Wagner⁸ criticized these conclusions and by a photographic magnetic spectrum analysis showed that no such groups of electrons as Lorenz had found, actually existed. He studied the magnetic spectra of high-speed secondary electrons emitted by gold, silver and aluminum targets when bombarded with cathode rays of 16 to 40 k.v. He found the velocity distribution curves to be everywhere continuous except possibly at the high velocity end; also that most of the secondary electrons had speeds close to those of the primary electrons, as the author⁶ had found for silver in the range of 5 to 20 k.v. These electrons were evidently of the type that in Lenard's old terminology were named "re-diffused," that is, those electrons which issue from the solid after undergoing deflections by a penetration of relatively few atomic layers.

The present work was undertaken with a view of settling the question of whether or not energy relations exist between the primary and secondary electrons analogous to those that de Broglie found in the case of x-rays and photoelectrons. It was decided to study the electronic emission proceeding in a definite direction from a silver target bombarded with electrons of speeds in the range of 2 to 30 k.v., which region contains all of the critical potentials necessary to excite the various x-ray spectra of silver. It is well known that a certain minimum potential is necessary to excite the *K*-series spectrum of an element. An increase in the primary potential beyond that minimum might be supposed to detach a *K*-electron which should then issue with an

³ E. G. Dymond, Phys. Rev. **29**, 433 (1927).

⁴ G. P. Harnwell, Phys. Rev. **33**, 559 (1929).

⁵ J. A. Eldridge and H. F. Olson, Phys. Rev. **28**, 1151 (1926).

⁶ S. Chylinski, Phys. Rev. **28**, 429 (1926).

⁷ E. Lorenz, Zeits. f. Physik **51**, 71 (1928).

⁸ P. B. Wagner, Phys. Rev. **35**, 98 (1930).

energy equal to the difference between the energy of the primary electron and that required for *K*-ionization, the thermionic work function being negligible. The same should be true for the other levels. For instance, with a primary potential of 2 k.v. all of the *N* and *M* levels of silver should be excited and we might expect groups of secondary electrons given by the following relations:

$$P - W_{N7} = 2000 - 106, P - W_{M5} = 2000 - 723, \text{ etc.}$$

where *P* stands for the primary potential and the *W*'s represent the energy in electron-volts corresponding to the different absorption limits. In addition to the removal of these electrons by inelastic collisions, one might expect photoelectrons to be released from higher levels, due to the x-rays originating in the deeper levels of the same atom or other atoms. Thus, if the analysis is correct, there should appear on the velocity distribution curves distinct peaks, some of which, namely those due to electron impact, should shift their position towards the high velocity end with increasing primary potentials, while those due to x-ray photoelectrons should remain fixed. After a primary potential of about 4 k.v. is reached new peaks should appear, since the *L* absorption limits of silver correspond to about 3.8 k.v. The *K*-excitation would not be reached until a voltage of 25.5 k.v. was passed. The intensity of x-ray lines is known to vary approximately as $(V_0 - V)^2$, where V_0 is the primary voltage and *V* is the minimum voltage required to excite a given series. Hence one might expect the *N*, *M* and *L* electrons to be continuously more numerous as the *K*-voltage is approached.

Webster,⁹ in his studies of the production of characteristic x-rays from silver concludes that they are largely of direct origin, that is produced by the ejection of *K*-electrons from atoms by the impact of the primary electrons on those atoms, rather than of indirect origin, which may be ascribed to the ejection of *K*-electrons by the photoelectric effect of continuous x-rays excited by cathode rays in other atoms. The ratio of direct to indirect rays he finds equal to about 2 at 50 k.v. for silver.

Certain considerations are rather discouraging as far as the expectation of the appearance of definite groups of secondary electrons is concerned. Chief among them is the very low line-emission efficiency of cathode rays. This amounts to only a fraction of one percent. Also, as Wagner⁸ has pointed out, most of the atoms from which, for example, the *L* electrons are ejected are not at the surface of the target, and hence there are energy losses along the paths of both the primary and secondary electrons; and that the probability of a cathode ray transferring all of its energy to a given orbital electron is small.

II. APPARATUS

The principal parts of the apparatus are shown diagrammatically in Fig. 1. *B* is a brass cylinder two inches long and of eight inches outside diameter. The cover is fitted to it by means of a ground joint. A little sealing wax around the outside edge makes it air tight. Soldered to the cover is a

⁹ D. L. Webster, Proc. Nat. Acad. Sci. 14, 330, 339 (1928).

small brass pipe having a ground taper into which is fitted the glass cone which supports the cathode. The bottom of *B* consists of a brass plate which is permanently soldered to it. This plate holds the water-cooled silver target *T*, an amber plug through which passes the connection to the Faraday cylinder *F* and a brass pipe leading to the vacuum pumps.

Electrons from the hot cathode pass through a small circular hole in the cover and strike the target. The silver is 2 cm in diameter and 2 mm thick. The target surface is located at 45 degrees with the plane of the drawing, the normal to the surface making an angle of 45 degrees with the primary beam. Electrons escaping from the target at right angles to the primary beam and

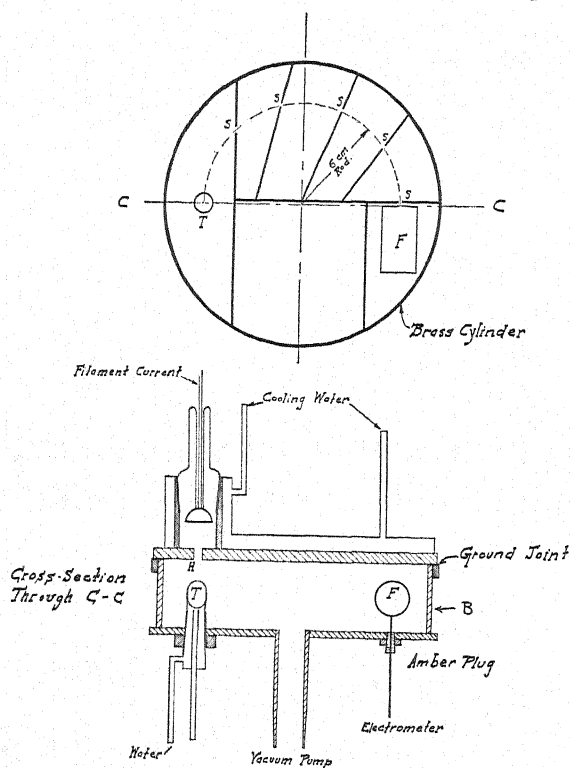


Fig. 1. Diagram of apparatus.

the normal to the target are bent into a semi-circle by means of a uniform magnetic field, which is parallel to the primary rays. The circle has a radius of 6 cm. The beam that enters the Faraday cylinder is reduced by a series of five slits *S* to a cross section much less than 1 mm².

The distance between cathode and cover was 3 cm and that between cover and target was 2 cm. The accelerating potentials were applied between cathode and cover, which, together with the rest of the brass cylinder and the target, was at ground potential. The target is thus located in a space that is practically free from electrostatic disturbances, especially so since the electron current was small, not greater in most instances than 1 m.a. Measure-

ments were made by means of a Dolezalek electrometer, having a sensitivity of 500 divisions per volt. To reduce stray (tertiary) electrons, the walls of the brass chamber were covered with a layer of soot.

The vacuum was obtained by mercury diffusion pumps. These were in continuous operation during the progress of the work. The vacuum was at all times less than 10^{-5} mm of mercury. Preliminary experiments showed no evidence of any ionizing effects due to residual gas. Before use, the apparatus was strongly heated to drive out all occluded gases; the target was heated by electron bombardment lasting several days. To insure steady conditions the apparatus was in operation for about four hours before any measurements were taken.

The magnetic field was supplied by a solenoid which slipped over the vacuum chamber, the latter being mounted on a wooden pedestal. The solenoid was 36 inches long, having about 2700 turns of insulated copper wire. In the middle of the solenoid, where the vacuum chamber was located, the field was found to be very uniform. It was calibrated by means of the usual search-coil ballistic galvanometer method. For any given magnetic intensity H , the voltages equivalent to kinetic energies of the electrons entering the Faraday cylinder could then be computed from the relation

$$V = \frac{1}{2}e/mr^2H^2 \quad (2)$$

where the symbols have the usual signification. The solenoid current was supplied by a large storage battery.

A diagram of the principal electrical connections is given in Fig. 2. The 60-cycle alternating current was rectified by the two kenotrons K and smoothed out by the condenser C , which had a capacity of 0.32 microfarads. The high potential was measured by means of a specially constructed electrostatic voltmeter. This was calibrated against a spark gap. The cathode filament was heated by a current from the secondary of a 110 volt 60-cycle transformer. Throughout each run the current to the target, as measured by a milliammeter, was kept constant by a rheostat. In the case of the 2.1 k.v. run the potential was supplied by a storage battery.

III. EXPERIMENTAL PROCEDURE AND RESULTS

The procedure consisted in applying a definite potential to the cathode and obtaining readings on the electrometer for different values of the solenoid current, everything else being kept constant. From these data curves were plotted, of which that shown in Fig. 3 is a typical example. The crosses represent experimental points for a primary voltage of 5 k.v. The electrometer readings are plotted as ordinates, against abscissas that are proportional to the magnetic field intensities and consequently to the square root of the energy. From these, by an application of relation (2) another set of curves was constructed, the abscissas now being proportional to voltages equivalent to kinetic energies. To get the velocity distribution or kinetic energy distribution curves, such as those shown in Figs. 4 and 5, each ordinate of the intermediate curve was divided by the corresponding value of V . This had to be

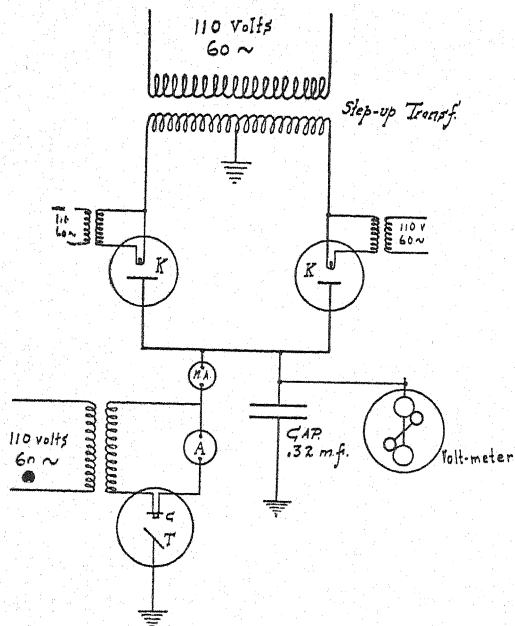


Fig. 2. Diagram of connections.

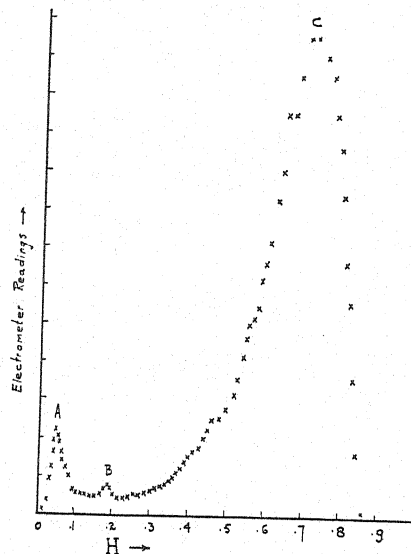
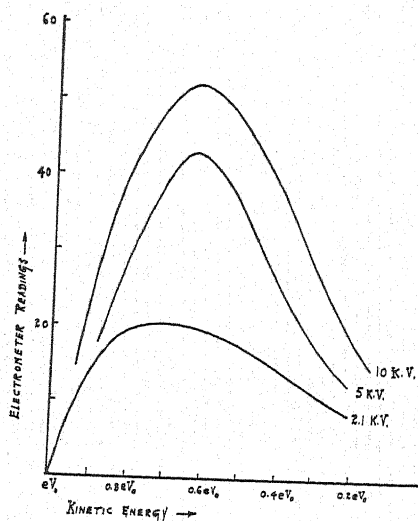
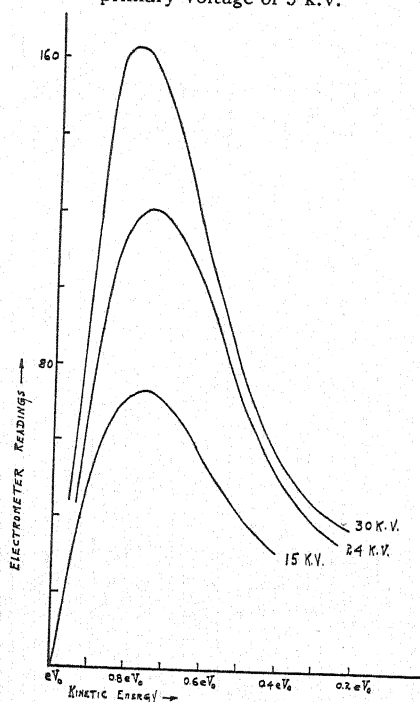


Fig. 3. Experimental curve for primary voltage of 5 k.v.

Fig. 4. Velocity distribution of secondary electrons for primary voltages V_0 of 2.1, 5 and 10 k.v.Fig. 5. Velocity distribution curves for primary voltages V_0 of 15, 24 and 30 k.v.

done in view of the change of resolving power of the magnetic analyzer from one part of the scale to another. For any given value of H the electrons entering the collector have values of V in the range of $V \pm \Delta V$, and ΔV is not a constant, but proportional to V .

In this manner the kinetic energy distributions of secondary electrons for primary potentials ranging from 2.1 to 30 k.v. have been investigated. This was done in steps of about 2.5 k.v., but only six representative distributions are shown in Figs. 4 and 5, the rest having exactly similar characteristics.

IV. DISCUSSION

An examination of the curves in Figs. 4 and 5 reveals no such discontinuities as might have been expected if there had been energy relations between the primary and the secondary electrons of the type discussed in the introduction. For voltages up to about 10 k.v. there appear two small peaks, A and B in Fig. 3, which grow less prominent with increasing primary voltages, until at 12.5 k.v. they can no longer be detected. They appear at practically the same places in all curves, A at 8 volts and B at 220 volts. Little if any importance should be attached to the peak at 8 volts. The method of analysis is unreliable for values of V near zero. The low speed electrons do not get away from the target because of the space charge field, or if they do get away they are dispersed by their mutual repulsions and fail to reach the collector. It is not clear what the meaning of the B peak is.

All curves are characterized by the prominent peak at C . For primary voltages up to 10 kilovolts the location of this peak is, in terms of kinetic energy of the primary beam eV_0 , between 0.6 and 0.7 eV_0 ; for voltages between 15 and 30 kilovolts it is located between 0.7 and 0.8 eV_0 . The slopes of the curves on the high energy side of the peaks increase with increasing primary voltages, seemingly becoming discontinuous at a point which, within experimental error, corresponds to the primary energy eV_0 . On the low energy end the peaks decrease less rapidly, reaching half maximum values around 0.3 eV_0 for the set shown in Fig. 4 and around 0.5 eV_0 for those in Fig. 5. The curves show plainly that most of the secondary electrons have very high speeds.

In conclusion one may say that, while undoubtedly some of the secondary electrons must have come from the inner orbits, their number must also be relatively so small as to be of no detectable influence upon the shape of the velocity distribution curves. The general shape of these curves merits perhaps a remark. They are of the same form as the continuous x-ray spectrum curves. It is not clear, however, what significance, if any, should be attached to this similarity.

It is a pleasure to express my appreciation of the kind interest and help extended to me by Professor Arthur H. Compton during the course of this work.

Experimental Establishment of the Relativity of Time

By ROY J. KENNEDY AND EDWARD M. THORNDIKE
University of Washington and Polytechnic Institute of Brooklyn

(Received July 9, 1932)

None of the fundamental experiments on which the restricted principle of relativity is based requires for their explanation that the classical concept of absolute time be modified; the present experiment was devised to test directly whether time satisfies the requirements of relativity. It depends on the fact that if a pencil of homogeneous light is split into two components which are made to interfere after traversing paths of different length, their relative phases will depend on the translational velocity of the optical system unless the Lorentz-Einstein transformation equations are valid. Hence, such a system at a point on the earth should give rise to an interference pattern which varies periodically as the velocity of the point changes in consequence of the rotation and revolution of the earth. The effect to be expected for a small velocity is so very small that it has been necessary to devise a special source of light, an interferometer of great stability and a refinement of the technic of measuring displacements in the interference pattern. With the apparatus finally employed, we have shown that there is no effect corresponding to absolute time unless the velocity of the solar system in space is no more than about half that of the earth in its orbit. Using this null result and that of the Michelson-Morley experiment we derive the Lorentz-Einstein transformations, which are tantamount to the relativity principle.

AMONG the several classical experiments which suggested the restricted principle of relativity there appears to be none in which any question as to the nature of time is involved. That is, in any of them, time as indicated by an ideal clock moving with the earth might be related in any way to that indicated by a hypothetical fixed clock without at all affecting their results, at least insofar as can be inferred from such theories of the experiments as we are at present able to construct. In experiments such as those of Rayleigh and Brace, of Trouton and Noble, and of Fizeau, all of which yielded null results, there is present the theoretical difficulty that unknown properties of matter are involved. The Michelson-Gale experiment gives a positive result, which is consistent with the concepts of either relative time or absolute time. In fact, it seems that the only experiment heretofore reported that permits of any definite interpretation is that of Michelson and Morley; and the null result of this experiment is completely explained if we suppose that space dimensions in the direction of motion are contracted by an amount depending upon a suitable function of velocity; so here, too, no question as to time is raised. Hence, although such experiments have suggested the relativity theory, they do not form a sufficient basis for the logical derivation of it.

It appears, then, that the theory has needed confirmation, particularly in its most revolutionary aspect; i.e., its denial of a significance for absolute time. Such confirmation has been obtained in the work reported in this paper, and by combining our results with those of the Michelson-Morley experiment, we derive the Lorentz-Einstein transformations which are well known to embrace the whole theory.

The principle on which this experiment is based is the simple proposition that if a beam of homogeneous light is split at a half-reflecting surface into two beams which after traversing paths of different lengths are brought together again, then the relative phases of the superposed beams will depend upon the velocity of the apparatus unless the frequency of the light depends upon the velocity in the way required by relativity. Furthermore, the phase-difference can be made to determine the positions of fringes in an interference pattern, so that by measuring these positions for various velocities of the system, the question whether the frequency follows the relativity requirement can be decided. The variation of the velocity of the system comes about because of the motions of rotation and revolution of the earth.

The theory of this experiment requires the following two assumptions:

- (a) There exists at least one coordinate system in which Huyghen's principle is valid and the velocity of light is the same in all directions. This assumption is unobjectionable from the standpoint either of relativity or of any plausible hypothesis involving an ether; for relativity, it is true for all uniformly moving systems, and in the latter case for any system at rest in the ether.
- (b) The Michelson-Morley experiment indicates that a system moving with uniform velocity v with respect to such a system has dimensions in the direction of motion contracted in the ratio $[1 - v^2/c^2]^{1/2}$ as compared to dimensions in the fixed system, while dimensions perpendicular to this direction are unchanged. This is in part assumption, for although there can be little doubt that the experiment yields a strictly null result, nevertheless it actually shows only that dimensions in the direction of and perpendicular to the motion are in the ratio mentioned; either of these dimensions might be any function of the velocity so long as that ratio is preserved.

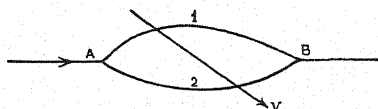


Fig. 1.

Let us consider one such system S' , and suppose that a system S (attached, for instance, to the surface of the earth) moves practically uniformly with velocity v with respect to it. In S is set up an arrangement for producing interference; i.e., one in which a pencil of homogeneous light is divided as mentioned above into two pencils which are recombined after traversing paths of different lengths. We can simplify the discussion by treating the general case instead of the particular arrangement used in the experiment, and by adopting a rule regarding expressions for the distances, angles and times in system S that will be of interest; i.e., the magnitudes of these quantities will be expressed by unprimed letters when they are referred to standards moving with S , and by the same letters primed when referred to standards fixed in S' .

The path of a typical ray with respect to S can be represented schematically as in Fig. 1 where the ray coming from the left is divided at A into rays 1 and 2 which recombine at B . The courses of the same rays with respect to

S' are evidently determined by the requirement that to each element ds' of a ray is to be added an elementary vector $v dt'$ where dt' is time required for light to traverse the element, and c is the velocity of light with respect to S' . The length of the resulting element is evidently $c dt'$; hence $c^2(dt')^2 = (ds')^2 + v^2(dt')^2 + 2v ds' dt' \cos \theta'$. Hence,

$$dt' = \frac{ds'}{c(1 - \beta^2)} [\beta \cos \theta' + (1 - \beta^2 \sin^2 \theta')^{1/2}] \quad (1)$$

where $\beta = v/c$ and θ' the angle between v and the element ds' .

If for the moment we consider a set of rectangular coordinates in S and S' with corresponding axes parallel and x -axes parallel to velocity v , we have from assumption (b)

$$\begin{aligned} ds' &= [(dx')^2 + (dy')^2 + (dz')^2]^{1/2} = [(dx)^2(1 - \beta^2) + (dy)^2 + (dz)^2]^{1/2} \\ &= ds \left[1 - \beta^2 \left(\frac{dx}{ds} \right)^2 \right]^{1/2} = ds(1 - \beta^2 \cos^2 \theta)^{1/2} \\ \cos \theta' &= \frac{dx'}{ds'} = \frac{dx(1 - \beta^2)^{1/2}}{ds(1 - \beta^2 \cos^2 \theta)^{1/2}} = \cos \theta \left(\frac{1 - \beta^2}{1 - \beta^2 \cos^2 \theta} \right)^{1/2} \\ \sin^2 \theta' &= \sin^2 \theta / (1 - \beta^2 \cos^2 \theta). \end{aligned}$$

When these expressions are substituted in Eq. (1), it reduces to

$$dt' = [ds/c(1 - \beta^2)^{1/2}] (1 + \beta \cos \theta), \quad (2)$$

the right side of which equation involves only quantities referred to standards moving with S . The time for light to traverse the whole ray AB along path 1 is therefore

$$t_1' = \int_1 dt' = 1/c(1 - \beta^2)^{1/2} \int_1 (1 + \beta \cos \theta) ds$$

and a similar expression holds for path 2. Hence difference of time for the two paths is

$$t_1' - t_2' = 1/c(1 - \beta^2)^{1/2} \left\{ \int_1 ds - \int_2 ds + \beta \left[\int_1 \cos \theta ds - \int_2 \cos \theta ds \right] \right\}.$$

The term in brackets multiplied by β vanishes, since in order to interfere the rays must intersect, and therefore their projections on the line joining A and B are equal; these projections are the integrals in brackets. Hence

$$t_1' - t_2' = (s_1 - s_2)/c(1 - \beta^2)^{1/2} = \Delta s/c(1 - \beta^2)^{1/2}, \text{ say,}$$

and the number of waves corresponding to this difference of time is

$$n = \nu'(t_1' - t_2') = \nu' \Delta s/c(1 - \beta^2)^{1/2} \quad (4)$$

where ν' is the frequency of the light employed as measured by an observer in S' . This number n is seen to be independent of orientations, lengths and

dispositions of paths, but to depend upon difference of path-lengths, the relative velocity of S and S' (through β) and the frequency.

The foregoing treatment is strictly valid only if the moving system is regarded as not subjected to forces, but is undoubtedly sufficient for the purpose in the small constant field of gravitation and acceleration at the surface of the earth. Moreover, although the rotation of the apparatus with the earth involves a slight effect on the time difference computed above (whether regarded from the standpoint of relativity or classical theory), it turns out to be altogether negligible in amount. This effect is a function of rotational velocity, not of orientation of apparatus.

We have now to consider the effect of a change in the velocity v on the number n expressed by Eq. (4). In that equation c is evidently a constant, while the difference Δs , because it is referred to standards moving with the system, is constant unless the courses of the rays between the points of separation and recombination are dependent on the velocity; that this is not the case can be shown by Huyghens' principle. A direct consequence of this principle is that the course of the ray is determined by the condition that the time required for traversing the path is a minimum compared with the time for any neighboring path. Now, Eq. (3) expresses the time in terms of coordinates moving with S , and if minimized in the usual way would yield the equations of the paths. For the present purpose, however, it is unnecessary to carry out this operation. Rewriting (3) we have

$$t' = 1/c(1 - \beta^2)^{1/2} \left\{ \int_A^B ds + \beta \int_A^B \cos \theta ds \right\}.$$

It will be observed that although the expression involves the velocity of the moving system, nevertheless the course of the ray is quite independent of it. That this is so is evident from the following considerations: the second integral is equal to the projection of the path on the line joining A and B , and being the same therefore for all paths, cannot contribute to the determination of the minimizing path. The first integral is expressed in terms of distances referred to standards moving with the system and so is independent of the velocity. Hence the actual courses of the rays, which are got by minimizing integrals of this form, are independent of the velocity, and Δs is a constant. This proof is essentially that of Lorentz extended by the inclusion of the contraction hypothesis.

The quantity ν' in Eq. (4) is the only one whose possible variability with velocity remains to be considered. From the standpoint of relativity, $\nu' = \nu(1 - \beta^2)^{1/2}$ where ν is the constant value of the frequency which would be determined with standards moving with S ; this value of ν' would evidently make n a constant. Furthermore, it will be shown later that insofar as the atom is to be regarded as a typical clock, the Lorentz-Einstein transformations can be derived from this relationship and assumption (b). If, on the other hand, $\nu' \neq \nu(1 - \beta^2)^{1/2}$ these transformations do not apply and it turns out that there exists but one system S' satisfying assumption (a); this unique system would be the absolute reference frame postulated in the classical

ether theory. In this case n is evidently a function of the velocity of S with respect to the absolute reference frame. Evidently, then, the relativity hypothesis can be tested by determining whether n is constant as v changes in consequence of the motions of rotation and revolution of the earth.

For the present purpose the total velocity of the apparatus can be got by adding vectorially a presumably constant velocity v_0 of the sun, the orbital velocity v_1 of the earth and the circumferential velocity v_2 due to the rotation of the earth (taking account of latitude). Its square can be reduced to

$$v^2 = v_0^2 + v_1^2 + v_2^2 + 2v_\alpha v_1 \sin(\theta_1 - \omega_1) + 2v_\beta v_2 \sin(\theta_2 - \omega_2) + 2v_1 v_2 \cos(\theta_1 - \theta_2),$$

where v_α is the projection of v_0 on the orbital plane, v_β is projection of v_0 on the equatorial plane, ω_1 and ω_2 are constants related to the direction of v_0 , and θ_1 and θ_2 are angles expressing the position of the earth in its orbit and its orientation on its axis with respect to the fixed-stars.¹ This procedure assumes only that the fixed-star system has no great angular velocity with respect to the fundamental system S' ; there is an unimportant approximation in the last term.

In order to get an idea of the magnitude of the effect that might be expected, let us assume that $v' = v$ and replace v by c/λ ; then (4) becomes $n = \Delta s/\lambda(1 - \beta^2)^{1/2}$. Expanding this, ignoring terms in β above second degree, substituting for the velocity from the expression above, and gathering constant terms into one,

$$\begin{aligned} n &= (\Delta s/\lambda)(1 + \frac{1}{2}(v^2/c^2) + \dots) \\ &= (\Delta s/\lambda c^2)[v_\alpha v_1 \sin(\theta_1 - \omega_1) + v_\beta v_2 \sin(\theta_2 - \omega_2)] + \text{a constant} \\ &= \delta n + n_0. \end{aligned} \tag{5}$$

Here the variable part of n is represented by δn and the constant by n_0 and we assume v_α and v_β to be large compared with the orbital and circumferential velocities v_1 and v_2 . Hence δn should be proportional to the sum of a term with a period of a year and one with a period of a sidereal day.

In performing the experiment, we wish, of course, to make δn as large as possible. The only factor that can be controlled is the ratio $\Delta s/\lambda$, the largest feasible magnitude of which is a measure of the homogeneity of the light. For various reasons the most suitable light seems to be the mercury line of wave-length 5461. With this, sufficiently clear interference fringes could be got when Δs was as large as 318 mm (the value finally used) and on substituting this in the expression for n it turns out that the rotation of the earth would produce a daily variation of a thousandths of a fringe for 200 km per

¹ More specifically, θ_1 is the angle between the projection of v_0 on the orbital plane and a direction in that plane determined by the angle ω_1 which depends on the position of the earth in its orbit or the time of year at which θ_1 is taken as zero. Similarly, θ_2 is the angle between the projection of v_0 on the equatorial plane and a direction in that plane determined by the angle ω_2 which depends on the time of day at which θ_2 is taken as zero. In the reduction of the data, the θ 's are taken as zero at the beginning of each run, so the ω 's depend on the times of starting runs. In the comparison and final summary of data, the θ 's are of course referred to the same sidereal time.

second, while the orbital motion would produce the same variation in six months for 3 km per second.

Because of the probable minuteness of these effects it was necessary to contrive new ways of detecting them. In the rather complicated method first proposed² the phase variation would show itself in the rotation of the plane of polarization of a beam resulting from the superposition of two oppositely circularly polarized beams. This scheme, although theoretically capable of great precision, was abandoned in favor of the much simpler one finally employed. In the latter, ordinary interference rings were formed and photographed, and the problem became one of measuring very small changes in the diameters of the rings. It was satisfactorily solved by devising a special comparator which will be discussed later.

Evidently, it was necessary to take every precaution to keep the experimental conditions constant; we were able, in fact, to reduce the average daily periodic error in $\Delta s/\lambda$ to about two parts in 10^{10} . This great stability was attained mainly by using interference apparatus made almost entirely of fused quartz and kept in a vacuum at a temperature constant to within about a thousandth of a degree. The apparatus was furthermore (partly accidentally) compensated for temperature to such an extent that one degree change produced a shift of only about a hundredth of a fringe. The vacuum was employed as simplest way to eliminate variations in pressure, which would have caused variations in index of refraction of optical paths, and, by mechanical action, variations in lengths of paths.

Several disturbing factors producing spurious effects had to be dealt with. Perhaps the most troublesome was the variability in density of the photographs due (in the earlier green-sensitive plates) to rapid aging which affected the emulsions in varying degrees. Since the photographic effect of light is not proportional to its intensity, it follows that a spurious displacement of an interference pattern of the type used is to be expected if the density of the photographs is not constant. The methods adopted to eliminate this and other difficulties are discussed elsewhere in the paper.

APPARATUS AND EXPERIMENTAL PROCEDURE

The general arrangement of the experimental apparatus is sketched in Fig. 2. Light from source S passes through a small circular opening in screen S_1 , is rendered approximately plane-parallel by lens L_1 is dispersed in direct vision prism P and the green ($\lambda 5461$) image of first opening is focused over a second one in screen S_2 by lens L_2 . The water-cell C is to absorb stray heat radiation. The green light from second opening is polarized by nicol prism N so that the electric vector is horizontal, and then enters the vacuum chamber V through a window and is concentrated by lens L_3 to the extent required to produce the greatest intensity in interference pattern. The light is then split into two pencils at the half-reflecting mirror M_1 which is inclined at such an angle (Brewster's angle) that reflection of the polarized light occurs only at its platinized face; the faces of the compensating plate M_4 are equally

² Kennedy, *Phys. Rev.* 20, 26 (1922).

inclined. Hence no stray (non-interfering) light can be superposed at these faces on the two pencils from M_1 ; these pencils are reflected by mirrors M_2 and M_3 back to M_1 , at which one is partially transmitted and the other partially reflected through lenses L_4 and L_5 which focus the light as a system of interference rings on a wide horizontal slit just in front of a photographic plate in the holder H . The slit is 5 or 6 mm wide, so the plate receives a symmetrical central section of the interference pattern of that width. The plate is held by a spring in the holder lightly against the metal tube T which is sealed against the window W of the vacuum chamber. Most of the length of the tube as well as the vacuum chamber is within the tank V containing

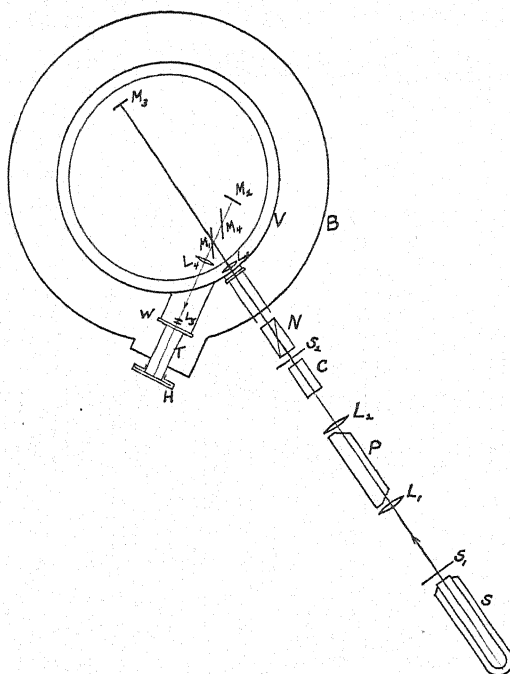


Fig. 2.

water at a temperature constant to within less than 0.001°C ; hence slight variations in room temperature cannot affect focusing and thereby diameters of rings. The plate holder, which is kept from contact with the vacuum chamber in order to preclude the possibility of jarring the latter when the holder is operated, is arranged to let the plate slip down two slit-widths automatically every half hour. On each plate six photographs are taken consecutively in this way, and twelve hours after the start of the first series six more are taken in the spaces left vacant during first exposure of the plate; hence the developed plate will contain a series of photographs alternately taken twelve hours apart. The purposes served by this procedure will be explained later. Four such plates are taken during a day's run.

The temperature of water-bath was easily kept nearly constant for many weeks in succession. The temperature was chosen only slightly above that of

room, the water was circulated continuously and the mercury-toluene thermostat was arranged to control the potential of the grid of a vacuum tube which actuated the relay in the heating circuit—in this way only a minute current is broken at the mercury surface and it does not become contaminated with a film of oxide. The optical part of the apparatus was enclosed in a small dark room within a larger one. The temperature of the inner room was kept constant to within a few hundredths of a degree, that of outer room to within about a tenth.

The interference apparatus consisted essentially of a set of four interferometer plates of the best quality obtainable, mounted on a circular fused quartz base 28.5 cm in diameter by 3.8 cm thick. The method of mounting the plates is perhaps worth describing: the support of each plate was cut from a flat plate of fused quartz, and fused to a tapered plug of the same material which, after being ground to fit a tapered hole in the base, was etched away

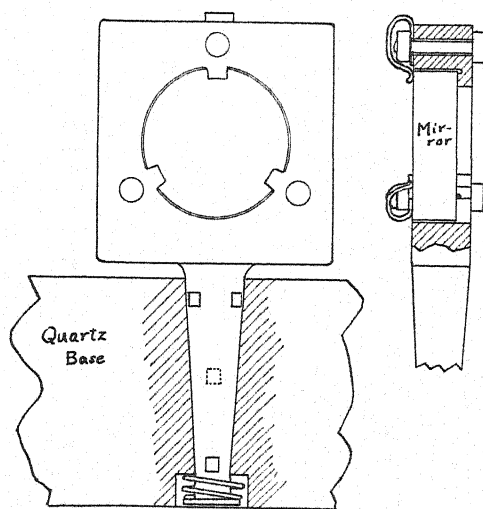


Fig. 3.

over the whole conical surface except in four spots of two or three square millimeters area, which were therefore the sole points of contact of the plug with the base. This procedure was necessary to insure a definite fixed position of plug, since if it were merely ground into the plate it would probably fit the hole only in a region near its middle. The positions of the bearing spots are indicated by the small squares in Fig. 3, the dotted one being on the opposite side of plug from the others. The plugs were held down by light springs as shown in the figure. The end mirrors were circular etalon plates 25 mm in diameter. Their supporting frames were fashioned so as to provide three projections of quartz against which the mirror was held by a light spring opposite each projection. The faces of the projections were ground flat and so as to be very nearly in a vertical plane when the frame is in place on the base. Final adjustment of mirrors was made by rotating them about their horizontal axes; it will be evident that in this way (because of slight in-

clination to each other of the faces of the mirror) a very fine adjustment can be made. It was sufficient simply to rotate the mirrors with the unaided fingers, to correct for the departure from the vertical, while viewing the interference rings with a telescope. The reflecting surfaces were of platinum applied by cathode deposition. It was impossible to use silver for the purpose because traces of mercury vapor in the vacuum chamber would quickly dissolve it. The light lens system which formed the rings on the photographic plate was attached to the base by means of invar plugs similar to those described above.

The quartz base rested on a piece of uniform velour, the back side of which was cemented to a heavy flat brass plate which was supported in an accurately horizontal position at three points. Each fiber of the nap of the velour thus served as a tiny spring so that the weight of the quartz plate was evenly distributed; this is important, since a fused material of this sort is essentially only semi-solid. The friction between the velour and the rough bottom face of the base sufficed to hold the latter accurately in position.

In order to produce interference under the existing condition of large difference of paths of the two beams, the image in the half-reflecting mirror of the face of either end-mirror must be nearly parallel to the face of the other end-mirror; it will be shown that such an adjustment of the mirrors gives rise to a pattern consisting of a series of concentric circular rings. In order that the effective diameter of each ring may be sensibly independent of accidental variations in distribution of light intensity over the faces of mirrors and with respect to direction in the beam, it is necessary to make this parallelism very accurate. The accuracy of adjustment could be tested by the simple procedure of moving a broad slit in various directions across the pencil incident on the half-reflector while the rings were observed in a telescope or photographed; when the diameters of rings were constant for all positions of slit the adjustment was the best obtainable.

The particular spectral line employed in the experiment was chosen on basis of several requirements. As has been pointed out, it must be capable of producing interference with large path-difference; it must also be entirely controllable as to intensity, the intensity must be fairly large, and the line must be easily separable from adjacent ones. On the whole, these conditions seemed best satisfied by the line $\lambda 5461$ of mercury. The homogeneity of any light is roughly proportional to the inverse square root of absolute temperature of source; hence the first source employed was a water-cooled mercury arc. This produced excellent interference rings, but it was soon noticed that their diameters depended on the part of the arc from which the light was taken; this suggests a Doppler effect due to motions of evaporating molecules from the hot liquid surface where the arc was brightest. Such an effect due to velocities variable by only a few centimeters per second would evidently be objectionable in view of the stability required.

The source finally used was an electrodeless discharge in unsaturated mercury vapor. The tube is sketched in Fig. 4. The inner tube in which the discharge took place was connected to a continuously operating pumping

system through a capillary tube (heated to prevent condensation in it) of such length and diameter as to keep the pressure of the vapor just below that of saturated vapor at the existing temperature. The vapor was supplied by the mercury well at the rear of tube, and the small amount escaping through the capillary would condense and return by way of the other vertical tube. The temperature of the source, and thereby the pressure of vapor, were kept constant by means of carbon-tetrachloride in the jacket surrounding the inner tube; the liquid was maintained at its boiling-point by heat from the discharge, and its vapor was condensed and returned by the water-cooled condenser connected to top of jacket. It will be evident that with the discharge occurring at some distance from the mercury well, first-order Doppler effects would be eliminated since no mercury condenses in the forward part

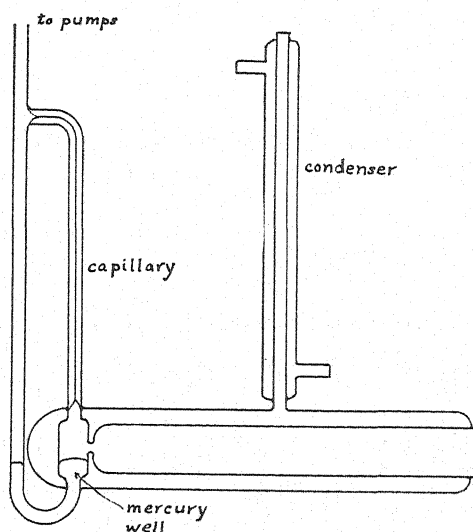


Fig. 4.

of the tube and therefore velocities of vapor molecules are on average same in all directions. Electrical energy was supplied by a coil of some thirty turns of wire around the outside of the jacket, in which oscillations of 20 meters wave-length were produced by a 75-watt transmitting tube. This discharge produced a uniform steady glow over nearly the whole diameter of the inner tube, and the interference rings were completely free from the fluctuations in brightness and diameter which were visible with the ordinary arc. During a run, and for some time in advance of it, the tube was kept in continuous operation in order that all conditions should be steady. It was found that the frequency of the light depended on the temperature of the cooling liquid and the voltage applied to oscillator, so these factors had to be closely controlled. These effects probably arise from the complicated structure of the green line; its "frequency," as inferred from the interference pattern, is of course a sort of mean of the frequencies of its components, weighted according to their intensities. It is to be mentioned that each of several attempts to

use sealed-off tubes failed; after a few minutes of operation with such tubes the rings would disappear, presumably because the oscillatory discharge readily excited a green band in traces of oxygen which probably remain in tube.

In view of the theorem of Lorentz previously discussed, the usual theory of interference for stationary systems can be applied directly to the present situation. In Fig. 5, A represents the surface of one end-mirror and B the

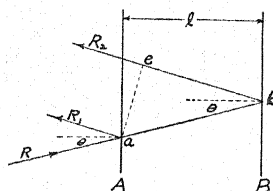


Fig. 5.

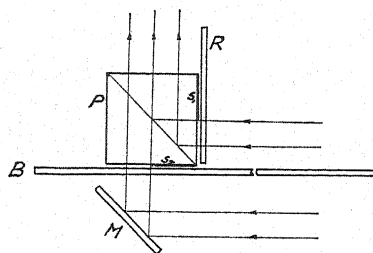


Fig. 6.

image of the other at distance l from A . Since A and B are parallel, the ray R impinging on both at angle θ produces on reflection the two parallel rays R_1 and R_2 . If these are brought to a focus, the difference between the lengths of their paths will evidently be $ab + be$. Now

$$ab = l/\cos \theta, \quad be = ab \cos 2\theta. \quad ab + be = (l/\cos \theta)(1 + \cos 2\theta) = 2l \cos \theta.$$

For constructive interference, this path-difference must contain an integral number of waves; hence the cones of rays for which $2l \cos \theta_i (i=1, 2, 3, \dots)$ equals a series of consecutive integers³ can be brought to a focus as a series of concentric rings of radii $r_i = (\sin \theta_i)/k_1$, where k_1 is a constant depending on magnification of lens system producing the interference pattern. Now $ab + be$ is the quantity Δs in Eq. (4); hence $\Delta s_i = 2l \cos \theta_i = 2l(1 - k_1^2 r_i^2)^{1/2}$ and $n = 2\nu' l(1 - k_1^2 r_i^2)^{1/2}/c(1 - \beta^2)^{1/2}$. It is convenient to consider only the central ray, and to express its phase in terms of the radii of the rings. For this ray $r=0$, so

$$n = 2\nu' l/c(1 - \beta^2)^{1/2} = n_0 + \rho \quad (6)$$

where n_0 is an integer and ρ a fraction. In general, for constructive interference $n = n_0 - i$. Then

$$\begin{aligned} n_0 - i &= [2\nu' l/c(1 - \beta^2)^{1/2}](1 - k_1^2 r_i^2)^{1/2} = (n_0 + \rho)(1 - k_1^2 r_i^2)^{1/2}. \\ \therefore \quad \rho &= (n_0 - i)/(1 - k_1^2 r_i^2)^{1/2} - n_0 = n_0 - i + \frac{1}{2}(n_0 - i)k_1^2 r_i^2 - n_0 \dots \\ &= (k/2)r_i^2 - i, \end{aligned} \quad (7)$$

approximately; here k is a new constant. The approximations are justified since n is of order $10^5 \times i$ and $k_1 r_i$ has a maximum value of about 10^{-2} for the rings measured. From Eq. (7) we find on differentiating

³ When the distances are expressed in wave-lengths.

$$\delta\rho = kr_i\delta r_i = kr_j\delta r_j = \dots \quad (8)$$

If measurements $\overline{\delta r_i}$ of the values of the variations in r_i are made for each of a number of rings of orders m to p , the mean value of $\delta\rho$ computed from them is

$$\delta\rho = \frac{k}{p - m + 1} \sum_m^p r_i \overline{\delta r_i}. \quad (9)$$

It will be convenient to have $\delta\rho$ in another form. In the final summary of data there are many values of $\delta\rho$ to be averaged for each value of the hypothetical velocity. It is clear, then, that the final average will be unaffected if we replace the variations δr_i in (8) by their individual measured values $\overline{\delta r_i}$, so that $r_i\overline{\delta r_i} = r_j\overline{\delta r_j}$. Multiplying and dividing the right side of Eq. (9) by $\sum_m^p 1/r_i$ it becomes

$$\delta\rho = \frac{k}{\sum (1/r_i)} \sum \overline{\delta r_i} \quad (10)$$

when the expressions $(r_i/r_j)\overline{\delta r_i}$ that appear in the product are replaced by $\overline{\delta r_j}$. Since we are dealing with extremely small variations in the radii, the radii can be measured and $\sum 1/r_i$ computed once for all for a given adjustment of apparatus; then the variations $\delta\rho$ are simply proportional to the sums of the variations in the several radii. This possibility greatly expedites the labor of measurement of plates; the way in which it was employed is discussed in connection with the description of the comparator designed for the purpose. It should be remarked that in this procedure insufficient weight is given to the somewhat greater precision of measurements on the larger, sharper, rings; however the final weighting of data is based on mean deviations of the computed values of $\delta\rho$, and the conclusions as to precision are not vitiated by this approximation.

The principle of the comparator is as follows:

A diametral section of each photograph to be measured is made to appear juxtaposed with a similar section of a nearly identical photograph which is used as a standard of reference for the whole series. In this way very small differences between reference and measured plates reveal themselves. The juxtaposition is along a diameter of each of the systems of concentric rings, and the comparison is made by moving the standard until one side of a ring on one plate appears to be continuous with the corresponding ring on the other plate, and then noting the distance along the line of demarcation which the standard must be moved in order to make the other sides of same rings coalesce similarly. This distance is evidently the difference between the diameters of the two rings. On the shaft of a fine micrometer screw which moves the reference plate, and concentric with it, is mounted a graduated slip-ring arranged so as to be held stationary when the portions of interference rings on one side of center are matched, and to rotate with the screw when the matching is done on the other side of center; the angle through which slip-ring is rotated during settings on a number of rings is thus evidently

proportional to the sum of the differences of their diameters from those on corresponding rings on reference plate. Hence in view of Eq. (10) a single reading (of this angle) summarizes the measurement of the whole exposure. Nine or ten rings, alternately dark and light, and near the center, were usually measured.

The device is diagrammed in Fig. 6; there P is a pair of similar right-angled prisms cemented together on their diagonal faces (one of which is half-silvered) and mounted on a carriage which can be moved by the micrometer screw on ways perpendicular to the section represented. The heavy lines s_1 and s_2 represent thin metal strips covering half the right and bottom faces of the prism combination; the lower edge of s_1 and left edge of s_2 are ground accurately straight and the strips are cemented to the prisms in such a way that the image of the former edge in the diagonal mirror exactly coincides with the latter. After traversing a water-cell a beam of light from right of figure passes through the reference plate R , which is mounted on the carriage and has its emulsion side in contact with screen s_1 along a diameter of the ring system; another beam, by way of mirror M , illuminates a similar part of the photograph on the plate B which is to be measured, and both parts are viewed from above through a lens system magnifying about four times. The latter plate is held by springs against stops which fix position of the emulsion side regardless of thickness of plate and of course at such a distance as to eliminate parallax. The exposures can be compared in turn by sliding the plate to right or left of diagram (toward or away from operator). Since the ring system may not be exactly circular and also in order to expedite placing the plates in position for comparison, a sharp notch was cut in each end of the slit behind which the plate is held during exposure; this leaves a sharp point at each end of the photograph which serves for setting accurately along the same diameter. It is to be noted that the comparator is automatically compensated for temperature (both reference and measured photographs being on same material); this compensation was not particularly important for the present purpose because the scheme of interleaving photographs taken twelve hours apart secured the same result.

So accurately and quickly can the settings be made that the measurement of a photograph can be made after some practice with a probable error of a thousandth of a fringe (i.e., a thousandth of the shift that would be produced by changing path-difference by one wave-length) in about five minutes. The labor of comparing the 48 exposures comprising a day's run is thus not great. It was particularly desirable to be able to make rapid measurements during the numerous preliminary adjustments of apparatus, tests of effects of varying the several experimental conditions, etc.

Two precautions were taken in order to keep the operator from being influenced in making settings on the comparator. The slip-ring, on which could be read the average differences of the diameters at any stage of comparison of a particular exposure, was kept covered until the final setting was made, thus preventing unconscious corrections during the later settings. Also, the plates were marked in such a way that the operator was in com-

plete ignorance of times of day at which they were exposed; not until a full day's readings were finished were they arranged in chronological order for computation.

DATA AND RESULTS FOR DAILY EFFECT

It was intended when the experiment was proposed to look chiefly for an effect of a change of velocity due to the orbital rather than the rotational motion of the earth. However with the first apparatus constructed, in which the mirrors were mounted in invar frames, it was found impossible to eliminate a slow, rather irregular variation in the interference pattern which would have masked the effect sought; hence it was decided to concentrate on the possible rotational effect. Three series of data were taken with this apparatus (in April and October, 1929 and January, 1930); after an interruption of over a year, during which the apparatus was rebuilt in its final form, three more series were taken in May, July and August 1931. The same form of light source was used in all six series. A large amount of data previously obtained with the water-cooled arc and under less carefully controlled conditions are ignored in the summary because of necessity of applying doubtful corrections to it. No corrections have been applied to the data here presented. Where results of the several series are combined, they are weighted in accordance with the usual theory of errors in terms of probable errors computed from the mean deviations.

Each of the series extended over a period of only a few days; during such a time we may regard $\sin(\theta_1 - \omega_1)$ in Eq. (5) as virtually constant. From this equation and Eq. (6), $\delta n = \delta\rho + a$ constant. Since θ_1 is proportional to θ_2 we have from Eq. (5)

$$\delta\rho = a \sin(\theta_2 - \omega_2) + b\theta_2 + k'$$

where a , b and k' are constants, the last two including any slow uniform variation such as might result from stresses in the apparatus. Letting computed values $\delta\rho_i$ correspond to angles θ_i , we have according to the principle of least squares the condition that the most probable values of a and ω_2 are those for which

$$\sum(\delta\rho - \delta\rho_i)^2 = \sum[a \sin(\theta_i - \omega_2) + b\theta_i - \delta\rho_i]^2$$

is a minimum. When account is taken of the fact that the data are distributed uniformly over the day, we infer from this condition that

$$a = (2/m) \sum_1^m \delta\rho_i \sin(\theta_i - \omega_2) + 2b \cos \omega_2$$

$$\tan \omega_2 = - \sum \delta\rho_i \cos \theta_i / (\sum \delta\rho_i \sin \theta_i + mb).$$

The constant b can be computed by comparing mean values of $\delta\rho$ on successive days; m is a number of exposures per day, usually 48.

Incidentally, the last two equations show the importance of the procedure of interleaving the exposures so that adjacent ones on any plate are made twelve hours apart. For it is known that the photographic emulsion

is subject to shrinkage which varies from plate to plate, the plates may be slightly curved, and there are probably variable stresses in the apparatus due to different weights of plates; there is also a slight effect on measured diameters due to varying densities of photograph such as would result from different treatment and sensitiveness of plates. All of these errors are evidently automatically eliminated in the process of computing, however, since each is multiplied into a sine or cosine term in θ_i and then added to a similar product into a term of opposite sign. Compensation is made also for the greater shrinkage of emulsion near ends of plates, because the plates were started alternately one and two slit-widths from the end.

TABLE I.

				A	B	C	D
(1)	2.0	(25)	2.2	-2.1	-0.26	1.7	1.70
	2.4		1.6	-0.1	0.03	1.5	1.49
	2.0		2.2	0.7	0.27	-1.1	-1.06
(4)	0.7	(28)	1.1	0.9	0.45	-1.7	-1.67
	0.2		1.1	-1.8	-1.10	0.0	0.00
	2.1		2.1	-1.3	-0.92	1.3	1.03
	3.2		1.4	0.8	0.63	2.8	1.98
(8)	0.9	(32)	0.6	0.0	0.00	0.6	0.37
	3.4		2.2	1.8	1.56	0.6	0.30
	2.0		0.0	1.6	1.48	2.4	0.92
	1.0		0.9	1.9	1.83	-1.7	-0.44
(12)	1.4	(36)	1.0	-0.4	-0.40	1.2	0.16
	1.3		2.1				
	2.0		0.2	$\Sigma u_i \sin \theta_i = 3.57$		$\Sigma u_i \cos \theta_i = 4.78$	
	1.7		2.1				
(16)	1.0	(40)	0.4	$\tan \omega_2 = -4.78/3.57, \omega_2 = 207^\circ$			
	0.8		1.1				
	0.3		1.3	$\sin \omega_2 = -80, \cos \omega_2 = +0.60$			
	1.2		2.5				
(20)	-0.2	(44)	0.7	$a = (2/48) (0.60 \times 3.57 + 0.80 \times 4.78) = 0.26$			
	1.6		0.3				
	1.5		0.6				
	1.7		2.4				
(24)	0.8	(48)	2.7				

A sample of data for a period of three days and the computations for the resultant amplitude and phase of the sine curve to which it most closely conforms is given in Table I. The numbers in the two columns at the left are means of the three values of $\delta\rho$ at the same hour of each day, arranged in chronological order. Column A contains sums and differences of the four terms in the previous columns for which the sines of the corresponding phase angles are equal or opposite.⁴ Column B contains products of the terms of

⁴ The summation in the formula above for the amplitude can evidently be expanded as follows:

$$\begin{aligned} \sum_1^m \delta\rho_i \sin(\theta_i - \omega_2) &= \cos \omega_2 \sum_1^{48} \delta\rho_i \sin \theta_i - \sin \omega_2 \sum_1^{48} \delta\rho_i \cos \theta_i \\ &= \cos \omega_2 \sum_1^{12} (\delta\rho_i + \delta\rho_{25-i} - \delta\rho_{24+i} - \delta\rho_{49-i}) \sin \theta_i \end{aligned}$$

column A into the sines of the corresponding phase angles. Columns C and D contain the corresponding quantities to A and B, using the cosine instead of the sine.

The results for the daily effect are summarized in Table II. The column headed ω contains the phase angles corresponding to the sidereal time of the maximum value of δn . The amplitudes are expressed in thousandths of a fringe.

TABLE II.

Time of year	Weighted amplitude	ω
January	0.16	89°
April	0.27	273
May	0.18	18
July	0.14	43
August	0.30	128
October	0.22	183

Since the total velocity of the earth could vary during the year by no more than twice the orbital velocity it is probably as well to average these results without reference to the first term in Eq. (5) that is, by simply adding them vectorially. When that is done, the amplitude of the resulting sine curve is 0.06 ± 0.05 . Substituting in (5) this is found to correspond to a velocity $V_\beta = 24 \pm 19$ kilometers per second.⁵

SEARCH FOR LONG PERIOD EFFECT

Because the apparatus in its final form appeared to be permanently in adjustment and the average values of the ring diameters proved to be nearly constant, it became feasible to test whether an effect exists due to orbital motion, i.e., to determine the coefficient V_α in first term bracketed in Eq. (5). The direct way of doing this would evidently be like that for daily effects which has just been discussed, i.e., to determine δn for a large part of a year and fit the data to a curve of the required form. Instead, a modification of this procedure was adopted in order to make it unnecessary to keep all the experimental conditions the same for long times. It is based on the assump-

$$- \sin \omega_2 \sum_{i=1}^{12} (\delta \rho_i - \delta \rho_{25-i} - \delta \rho_{24+i} + \delta \rho_{49-i}) \cos \theta_i.$$

The terms in parentheses in the last two summations are the quantities in the columns A and C, respectively.

⁵ There is a superficial appearance that this result conflicts with the assumption introduced in Eq. (5), i.e., that v_1 and v_2 are negligible in comparison with v_α and v_β , since the value just determined for v_β is even less than the orbital velocity v_1 . The contradiction is merely apparent however; it arises from the adoption of a corresponding velocity as a means of expressing the accuracy of the result, as has been customary in discussions of the Michelson-Morley experiment. From that experiment it is not inferred that the velocity of the earth is but a few kilometers per second, but rather that the dimensions of the apparatus vary very nearly as required by relativity. From the present experiment we similarly infer that the frequency of light varies conformably to the theory.

tion that the most probable rate of variation of δn (computed from measured values of $\delta\rho$ over short times) is equal to the derivative of the most probable first term in Eq. (5). Each of three series of data, taken for periods varying from eight days to a month, and at intervals of three months, was used to compute the daily rate of change of $\rho\delta$ at those times of year. This rate was found by averaging arithmetically the readings of each day of a given series and determining by the method of least squares the slope of the most probable straight line represented by them. Similarly the most probable sine curve corresponding to these three derivatives is computed. Some 300 exposures comprised the three series.

The three computed rates of change were 0.050 ± 0.020 , 0.007 ± 0.013 and -0.015 ± 0.021 , all expressed in thousandths of a fringe per day. The computed sine curve has an amplitude of 2.96 thousandths and this corresponds to a velocity $V_\alpha = 15 \pm 4$ km per sec. Since the relatively small probable error is based only on the internal consistency of the data and is therefore not to be taken very seriously, this result can scarcely be regarded as indicating a real velocity. Furthermore the direction of the computed velocity is 123° away from that computed above.

As we have used only 300 exposures in the application of this method, it is evident that the accuracy could be increased by a large factor if data were taken steadily for a few months. The proverbial brevity of life, however, argues against laboring the point.

If the last result and that for the rotational effect are given the same weight and combined vectorially (ignoring difference of direction of V_α and V_β)⁶ their resultant is 10 ± 10 km per sec. In view of relative velocities amounting to thousands of kilometers per second known to exist among the nebulae, this can scarcely be regarded as other than a clear null result; it is of the same order of precision as that of the Michelson-Morley experiment. It is perhaps best expressed as at present in terms of a velocity, although of course the conclusion to be drawn is that the frequency of a spectral line varies in the way required by relativity.⁷ This appears to be the only investigation in which a quantum phenomenon is shown to conform to Einstein's theory.

Insofar as the radiating atom may be regarded as a typical clock, the result of this experiment can be combined with assumption (b) to derive the Lorentz-Einstein transformations. Throughout the foregoing discussion we have dealt with time regarded as measured only at a fixed place in the moving system S ; in order to specify unambiguously the time at another point of S it is necessary to specify the operations which define it. Perhaps the most natural meaning to attach to the concept is that the time at any point is the indication of a clock which has been moved with infinitesimal velocity to the

⁶ The two results can be combined only by making some approximation.

⁷ It is of course altogether possible that there is a real (inherently observable) velocity which is so nearly perpendicular to the orbital and equatorial planes as to have components in them small enough to have escaped observation, but the probability seems small in view of the nebular velocities mentioned above.

point, and from the same location as an identical clock with which it was originally in agreement; it turns out that this definition is equivalent to that of synchronizing by means of light signals.

We have shown that the frequency ν' of an atom moving with velocity v bears the relation $\nu' = (1 - v^2/c^2)^{1/2} \nu$ to that of a fixed atom. Let us assume that the indications of clocks under similar conditions bear the same ratio. Suppose that at time $t = t' = 0$, the origins of parallel coordinates in S and S' (previously defined) coincide, and that the S -clock passes through the origin with a small velocity with respect to S . Because of this motion, the velocity of the clock with respect to S' will have components, say, $v + u_x, u_y, u_z$; hence the times t' and t indicated by a clock in S' and the clock in S will thereafter stand in the relation

$$t = t' \left[1 - \frac{(v + u_x)^2 + u_y^2 + u_z^2}{c^2} \right]^{1/2} = \left[t'^2 \left(-\frac{v^2}{c^2} \right) - \frac{2t' u_x v}{c^2} - t'^2 u^2 \right]^{1/2}.$$

Now $u_x t'$ is equal to S' -measure of distance x traversed in S by the clock; hence $u_x t' = (1 - v^2/c^2)^{1/2} x$. If this is substituted in the second term of the right side of the above equation and u is made to approach zero,

$$t = \left[t'^2 \left(1 - \frac{v^2}{c^2} \right) - \frac{2v x t'}{c^2} \left(1 - \frac{v^2}{c^2} \right)^{1/2} \right]^{1/2}$$

and so

$$t' = \frac{1}{(1 - v^2/c^2)^{1/2}} \left[\frac{v x}{c^2} + t \left(1 + \frac{v^2}{c^2} \frac{x^2}{t^2} \right)^{1/2} \right].$$

Here x/t is the velocity of clock with respect to S , and it approaches zero with u ; hence the coefficient of t in the last expression is unity, and

$$t' = [1/(1 - v^2/c^2)^{1/2}] [t + (v/c^2)x]. \quad (11)$$

The statement that the systems are in uniform relative velocity, together with fact that t' is independent of y and z implies

$$x' = x'(x + vt) ; \text{ hence } \partial x'/\partial x = (1/v)(\partial x'/\partial t). \quad (12)$$

The measurement in S' of the length of an interval δs in S is obtained by observing the distance $\delta s'$ between points in S' with which the ends of the interval coincide at same S' -time. For measurement along x' axes we have, because of Lorentz-Fitzgerald contraction

$$\delta x' \equiv \frac{\partial x'}{\partial x} \delta x + \frac{\partial x'}{\partial t} \delta t = \left(1 - \frac{v^2}{c^2} \right)^{1/2} \delta x$$

when

$$\delta t' \equiv \frac{1}{(1 - v^2/c^2)^{1/2}} \left(\delta t + \frac{v}{c^2} \delta x \right) = 0, \text{ i.e.,}$$

when $\delta t = -(v/c^2)\delta x$. Hence

$$\frac{\partial x'}{\partial x} \delta x - \frac{v}{c^2} \frac{\partial x}{\partial t} \delta x = \left(1 - \frac{v^2}{c^2}\right)^{1/2} \delta x.$$

From this and (12)

$$\frac{\partial x'}{\partial x} = \frac{1}{(1 - v^2/c^2)^{1/2}} \quad \text{and} \quad \frac{\partial x'}{\partial t} = \frac{v}{(1 - v^2/c^2)^{1/2}}.$$

Hence

$$x' = (1 - v^2/c^2)^{-1/2}(x + vt).$$

This equation and (11) together with $y' = y$, $z' = z$, are the Lorentz-Einstein transformations; because they are known to possess the group property, the system S' which has been used as a tentative standard of reference evidently loses all trace of uniqueness.

The research set forth in this paper has been carried on over a period of several years, during which many obligations have been incurred. Preliminary work on it served as basis for the senior author's doctoral thesis at Johns Hopkins University. The main work was done at the California Institute of Technology with the aid of fellowships granted by the National Research Council, the Guggenheim Memorial Foundation and the Institute; it was completed during leave of absence granted by the University of Washington. Particularly acknowledgment is made to Professors E. T. Bell, R. C. Tolman and R. A. Millikan, whose interest and encouragement have made the work possible, and to Mr. Julius Pearson to whom several essential refinements of the apparatus are due.

Propagation of Large Barkhausen Discontinuities. II

By K. J. SIXTUS AND L. TONKS
General Electric Company, Schenectady, New York

(Received September 9, 1932)

A new formula for the penetration time of large Barkhausen discontinuities is given which is based on definite assumptions regarding the condition for magnetic reversal. In order to bring this formula into agreement with experimental results, it must be modified by the introduction of a length of 0.035 cm of unknown origin. The modified formula agrees well with the results observed for wires of various diameters, a strip, for various impressed fields, tensions and torsions, and for variations of jump magnitude and electrical resistivity. The behavior of the discontinuity in a 15 percent NiFe wire relative to heat treatment was investigated. Changes in critical (minimum propagating) and coercive fields were indicative of the internal state of strain in the wire. The presence of cold-work strains appears to be necessary for the occurrence of the jump but the addition of strains arising from cooling through the γ - α transformation reduces the tendency to form the large discontinuity. Propagation was observed at temperatures up to 350°C. With increasing temperature the slope A of the v - H curves increased. At the same time the range between the critical field and the field at which propagation starts spontaneously at some point in the wire decreased. Etching the surface of a wire also increased A and decreased propagation range. Cracks appearing in the wire surface indicated that the release of surface strains may well have been responsible. It was established that neither the removal of material nor the absorption of hydrogen were the cause.

I. INTRODUCTION

THE earlier work which has already been reported upon under the same title and in two additional notices^{2,3} has been continued and extended. Some phases of the new material will be discussed in the present paper and additional results will be published shortly.

As a considerable number of symbols denoting various magnetic fields are required we list them here: H , longitudinal main field impressed on the wire; H_0 , critical field, minimum longitudinal field for propagation; $\Delta H = H - H_0$, excess field; H_s , starting field, minimum value of H which initiates propagation in the wire; H_e , eddy current field; H_p , field arising from the magnetic pole distribution; H_m , total field at a point; and H_c , coercive force, used in place of H_0 when the large discontinuity is absent.

II. REVISED FORMULA FOR THE PENETRATION TIME

1. Old formula

In I we have shown that one has to distinguish between the propagation in two different directions: A propagation into the wire, which depends on

¹ K. J. Sixtus and L. Tonks, *Phys. Rev.* **37**, 930 (1931). This paper will be referred to as I in the text. On page 932 a was erroneously defined as the wire diameter. Throughout I and here also a is the radius of the wire.

² K. J. Sixtus and L. Tonks, *Phys. Rev.* **39**, 357 (1932).

³ I. Langmuir and K. J. Sixtus, *Phys. Rev.* **38**, 2072 (1931).

eddy currents arising in the material, and a propagation in the longitudinal direction, depending, we believed, on conditions in the surface of the wire. The propagation into the wire requires a time interval δt which we have called the penetration time. The approximate calculation made in I gave values one-fourth of those found experimentally in a 0.038 cm diameter wire. We shall here give the derivation of Eq. (8A)² previously stated without proof. In the interim an independent derivation⁴ has appeared which is, however, less satisfactory for our purpose.

2. Basic assumptions

Any exact calculation of this time must take the actual manner of penetration into consideration. The hypothesis adopted is that stated in I, p. 947, with the additional assumption, already implicit in I, Eq. (7), that magnetization reverses when the total field H_m at a point in the discontinuity exceeds the critical field H_0 , and that it reverses so rapidly that the eddy currents generated reduce H_m to H_0 at every instant. This, in turn, implies that the discontinuity is of infinitesimal thickness, but the results of the calculation will be valid to the extent that this thickness is small compared to the diameter of the wire.

For clarity, we shall call the portion of the wire already traversed by the discontinuity, and which has therefore changed magnetization, the *saturated phase*, the unchanged portion, the *antisaturated phase*. Thus the moving discontinuity can be looked upon as a propagating phase boundary.

3. Calculation of eddy current field

Denoting distance along the wire and in the direction of propagation by x , and representing the shape of the phase boundary by the unknown function, $R=R(x)$, our first problem is to set up this function.

The change in flux in a cross section of the wire during the time dt is $2\pi R dR \cdot 4\pi \Delta I$, where $4\pi \Delta I$ is the change in induction between the two phases. The line integral of e.m.f., E , around the wire at a radial distance $r > R$ is thus

$$2\pi r E = (8\pi^2 R \Delta I / c) dR / dt \quad (1)$$

(of course, for $r < R$, $E=0$). By introducing the longitudinal velocity of propagation $v(=dx/dt)$ and using R' for dR/dx this becomes

$$E = 4\pi v R R' \Delta I / rc. \quad (2)$$

Since the current density I is E/ρ , the total circular current per cm length of wire is

$$\int_R^a E dr / \rho = (4\pi v R R' \Delta I / \rho c) \ln(a/R) \quad (3)$$

where a is the radius of the wire.

⁴ W. Wolman and H. Kaden, Zeits. f. techn. Physik 13, 330 (1932).

This eddy current, in turn, gives rise to a magnetic field H_e at R which is given by

$$H_e = - (16\pi^2 v \Delta I / \rho c^2) R R' \ln(a/R) \quad (4)$$

the negative sign indicating that H_e is in opposition to H , the impressed field.

4. Field relations and shape of phase boundary

It is readily seen that H , H_e , and the field H_p arising from the magnetic poles created in the reversal all contribute to H_m , so that

$$H_m = H + H_e + H_p. \quad (5)$$

It will be shown later that in the propagating wave it is justifiable to neglect H_p , because the poles are distributed over such a great length of the wire. The application in Eq. (5) of the fundamental assumption that $H_m = H_0$ leads to the appearance of the quantity $H - H_0$ in the equation, a quantity which will be called the "excess field" and will be denoted by ΔH . Then eliminating H_e with Eq. (4) gives

$$R R' \ln(a/R) = (\Delta H \rho c^2) / (16\pi^2 v \Delta I) \quad (6)$$

as the differential equation of the boundary. Integration gives

$$R^2 [\ln(a^2/R^2) + 1] = (\Delta H \rho c^2 x) / (4\pi^2 v \Delta I) \quad (7)$$

the integration constant being chosen so that the discontinuity intersects the axis at $x=0$. The length, λ , of the discontinuity is then the value of x when $R=a$.

5. Penetration time

Noting that

$$\lambda/v = \delta t \quad (8)$$

Eq. (7) gives

$$\begin{aligned} \delta t &= 4\pi^2 a^2 \Delta I / \rho c^2 \Delta H \\ &= 3.94 \times 10^{-8} a^2 \Delta I / \rho \Delta H \end{aligned} \quad (9)$$

in practical units. Thus the exact definition of the discontinuity under our assumptions doubles the numerical factor in I, Eq. (8), thereby reducing the discrepancy between $\delta t_{\text{exp.}}$ and $\delta t_{\text{calc.}}$ which is noted in I, Table I, column 7, from the factor 4 to the factor 2. In the case of a strip the corresponding formula is

$$\delta t_{\text{strip}} = 7.88 \times 10^{-8} b^2 \Delta I / \rho \Delta H \quad (10)$$

where b is the half-thickness.

The derivation of these equations was based on the assumption that the surface of magnetic discontinuity makes only a small angle with the axis, but a plot of Eq. (7), as given in Fig. 1, shows that the discontinuity is perpendicular to the axis both at the axis and at the surface of the wire. Other considerations must apply in these two regions. At most, however, the ex-

ceptional districts include less than one percent of the discontinuity, so that Eqs. (9) and (10) may reasonably be expected to be valid.

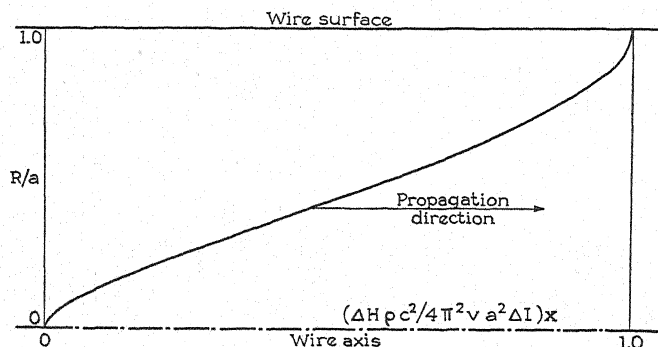


Fig. 1. Theoretical shape of the boundary in a wire.

6. Test of formula and empirical modification

For the further testing of these formulas a new series of oscillograms were taken covering variations in a , ΔI , and ρ . The procedure is described in I, page 944. It immediately appeared that δt was proportional to a rather than a^2 , the missing power of a being replaced by an empirical constant which in an earlier note² was given as 0.031 cm. A more complete and critical examination of the data leads, however, to the present slightly higher value, 0.035 cm. Accordingly, Eq. (9) was changed to

$$\delta t_{\text{wire}} = 3.94 \times 10^{-8} \times 0.035 a \Delta I / \rho \Delta H. \quad (11)$$

The results of applying this modified equation to a series of 15 percent NiFe wires under both tension and torsion are shown in Table I. No systematic variation of $\delta t_{\text{calc.}} / \delta t_{\text{exp.}}$ is evident. Only the torsion case, subdivision 3, shows a marked general deviation from unity. It is remarkable and doubtless significant that the empirical length of 0.035 cm determined by tension experiments should apply even this well to a case where the strains are so different. The fact that the jump is only 50 percent of the double saturation value appears, in the light of later results,^{4,5} to arise from a transverse component in the reversal as well as from a probable absence of reversal near the axis where the shearing strain approaches zero. The former case is covered by the theoretical formula, but in the latter the necessary correction would reduce the calculated time, thus making the discrepancy worse. This case certainly demonstrates, however, that three- to four-fold changes in ΔI are accompanied by only a 20 percent difference between formula and experiment.

The theoretical formula for a strip was modified in exactly the same way as the wire formula, that is, to

$$\delta t_{\text{strip}} = 7.88 \times 10^{-8} \times 0.035 b \Delta I / \rho \Delta H. \quad (12)$$

^{4,5} See also R. M. Bozorth and J. F. Dillinger, Phys. Rev. **41**, 345 (1932).

Subdivision 6 shows that this semi-empirical formula applies. In addition it should be noted that this is an extreme case in that b is less by half than the smallest wire radius.

TABLE I. *Experimental and calculated times of penetration in 15 percent NiFe wire and ribbon under tension or torsion. Wire No. 37; resistivity, $\rho = 31 \times 10^{-6} \omega \text{ cm}$.*

Osc. No.	ΔH oersted	ΔI e.m.u.	v cm/sec.	δt , millisec. exp.	calc.	$\frac{\delta t_{\text{calc.}}}{\delta t_{\text{exp.}}}$	λ cm
1. Diameter, $2a = 0.0533 \text{ cm}$; tension, 71 kg mm^{-2} ; $H_0 = 1.40$ oersted							
124	0.21	2960	2500	18.5	16.7	0.90	47
123	0.44	3040	6000	8.0	8.2	1.02	48
122	0.67	3060	10000	5.0	5.5	1.10	50
2. Diameter, $2a = 0.038 \text{ cm}$; tension, 77 kg mm^{-2} ; $H_0 = 2.07$ oersted							
109	0.11	2320	2100	11.4	18.0	1.57	24
118	0.47	3170	8800	6.2	5.7	0.92	59
111	0.69	3210	13800	3.8	3.9	1.02	52
107	1.04	3260	21600	2.3	2.6	1.14	50
3. Diameter, $2a = 0.038 \text{ cm}$; torsion, 4 turns/80 cm ; $H_0 = 2.49$ oersted							
120	0.16	830	3000	5.6	4.4	0.78	17
119	0.39	1030	8000	2.9	2.3	0.79	23
4. Diameter, $2a = 0.026 \text{ cm}$; tension, 85 kg mm^{-2} ; $H_0 = 3.49$ oersted							
104	0.31	3170	6500	6.2	6.0	0.96	41
105	0.66	3280	15000	2.8	2.9	1.03	42
5. Diameter, $2a = 0.013 \text{ cm}$; tension, 158 kg mm^{-2} ; $H_0 = 5.93$ oersted							
133	0.39	1600	7400	1.6	1.20	0.75	12
134	0.63	3150	11600	2.1	1.45	0.69	24
132	0.87	3320	15800	1.2	1.10	0.92	19
135	0.97	3320	17800	0.9	0.97	1.08	16
131	1.21	3320	22000	0.75	0.78	1.04	17
6. Strip, 0.0071×0.0685 ; tension, 85 kg mm^{-2} ; $H_0 = 3.80$ oersted							
127 ^b	0.35	2450	4600	3.0	2.20	0.73	14
127 ^a	0.47	2920	5800	2.4	1.95	0.81	14
126	0.81	3130	9800	1.5	1.24	0.83	15
125	1.39	3130	19600	(1.2)*	0.70	(0.58)	(24)

* Uncertain because of the shortness of the time interval.

7. Further tests of formula

Table I, as remarked, covers experiments in which ΔI shows some variation from one test to the next. A greater range was embraced by using wires of different compositions. These wires showed, in addition, marked differences in resistivity, the 39 percent Ni-Fe having $71 \times 10^{-6} \omega \text{ cm}$ and the 90 percent Ni-Fe having $13.5 \times 10^{-6} \omega \text{ cm}$. The 39 percent alloy lies in a range where it is difficult to obtain large discontinuities. After quite a number of trials it was found that combined torsion and tension were required to give large enough jumps to work with. The 90 percent alloy lies in a range where tension reduces the size of discontinuities. Accordingly torsion alone was used in this case.

The results are exhibited in Tables II and III. Although there are deviations from unity in column 7 of each table, these show no correlation with

TABLE II. *Experimental and calculated times of penetration in 39 percent NiFe wire under combined tension and torsion.* Wire No. 26; resistivity, $\rho = 71 \times 10^{-6} \omega \text{ cm}$; diameter, $2a = 0.0388 \text{ cm}$; torsion, 15 turns; tension 30.5 kg/mm^2 ; $H_0 = 8.36$ oersted.

Osc. No.	ΔH oersted	ΔI e.m.u.	v cm/sec.	δt , millisec. exp.	δt , millisec. calc.	$\frac{\delta t_{\text{calc.}}}{\delta t_{\text{exp.}}}$	λ cm
255	0.24	690	4300	1.40	1.08	0.77	6.0
254	0.36	728	6400	0.80	0.76	0.95	5.1
253	0.48	765	8700	0.75	0.60	0.80	6.5
252	0.61	803	11400	0.60	0.50	0.83	6.8
256	0.74	820	14000	0.50	0.42	0.84	7.0

A vibrator with natural frequency 5000 cycles/sec. was used for these oscillograms.

TABLE III. *Experimental and calculated times of penetration in a 90 percent NiFe wire under torsion.* Wire No. 6a; resistivity $\rho = 13.5 \times 10^{-6} \omega \text{ cm}$; diameter, $2a = 0.0386 \text{ cm}$; torsion, 5 turns; $H_0 = 4.02$ oersted.

Osc. No.	ΔH oersted	ΔI e.m.u.	v cm/sec.	δt , millisec. exp.	δt , millisec. calc.	$\frac{\delta t_{\text{calc.}}}{\delta t_{\text{exp.}}}$	λ cm
209	0.46	460	1000	1.82	1.97	1.08	1.8
206	0.58	500	1300	1.96	1.70	0.87	2.5
213							
214							
202	0.80	520	1900	1.60	1.28	0.80	3.0
205							
208							
211							
215	1.04	550	2800	1.21	1.04	0.86	3.4
204	1.15	550	3400	1.28	0.94	0.74	4.4
210							

variations in any of the listed quantities. In this connection it must also be borne in mind that there is some indefiniteness in interpreting the oscillograms of the discontinuity which yield the values of δt , particularly in the lower velocity cases. The general shape of the trace is that of an isosceles triangle with the sides curving into the zero line. The time occupied by the curved portion in relation to the velocity of propagation represents roughly the distance along the wire that one should expect the effects of an advancing (and receding) magnetic change to reach ahead (and persist behind) when the actual size of the search coil is taken into account. Thus the search coil had an outer radius of 1 cm and an axial thickness of 0.6 cm and the distances found from the oscillograms were about 1 cm.

8. Significance of empirical constant

It is interesting to observe that the special constant, 0.035 cm, appearing in Eqs. (10) and (11), lies in the neighborhood of the radius above which propagation does not occur. For example, as mentioned in I in connection with Fig. 9, the 0.071 cm diameter wire showed propagation but only with

decreasing jump magnitude, and other tests on larger wires have also failed to show propagation without decrement. What significance, if any, is to be attached to this coincidence is not known.

III. ANNEALED WIRES

1. Introduction

It was thought that the effect on the magnetic properties of the material of annealing at different temperatures might give more information regarding the influence of various factors, such as inhomogeneous strains and crystal orientation. Such tests have already been reported by Preisach.⁵ Practically all of the measurements in this and the following section were made on 15 percent NiFe (Ingot No. 37) so that unless otherwise stated all results and conclusions apply to this alone. The exact percentage composition of this wire by weight as determined by chemical analysis was: Ni, 14.75; Mn, 0.11; C, 0.02; P, 0.02; S, 0.016; Si, trace; Fe, remainder.

Although many different heat treatments have been tried, we shall only describe the results obtained on a series of wires heated for 10 hours in hydrogen at 400°, 600°, 800° and 1250°C, since these exhibit the important phenomena very clearly. Using the equilibrium diagram and with the help of x-ray spectrograms and photomicrographs we shall attempt to explain these observations. The transformation points for the alloy of 15 percent Ni-Fe were taken from the extensive report of Peschard⁶ which furnished the main basis for the diagram published in the National Metals Handbook (p. 608). In a 15 percent alloy with very pure constituents the transformation from α - to γ -phase occurs between 570° and 670° in heating, whereas in cooling the change from γ to α structure occurs between 300° and 140°C. In a rough test it was found that the α - γ transformation in the present wire began as low as 450°C. The difference between this value and the one found by Peschard can be ascribed to impurities.

The original wire had undergone a severe cold working as it had been drawn cold from 0.080 to 0.038 cm diameter and had, accordingly, a fibrous structure with very fine crystal grains whose boundaries, even with a magnification of 1500, could not be recognized. X-ray spectrograms showed the well-known orienting effect of cold working. In the center portion of the wire one could observe a preferred crystal orientation of the (110) axis parallel to the wire axis; but near the surface to a depth of about $\frac{2}{3}$ of the radius there was random crystal orientation.

2. Properties of annealed wires

The changes in the magnetic properties of the wire after annealing are given in Figs. 2 and 3. Annealing at 400°C, below the transformation range, caused a marked reduction of coercive force and critical field for all tensions, and the large discontinuity appeared at a lower tension than before. The x-ray pattern did not differ from the one obtained with the original wire.

⁵ F. Preisach, *Ann. d. Physik* **3**, 737 (1929).

⁶ Peschard, *Rev. de Met.* **22**, 490 (1925).

Obviously, the only effect of annealing in this case was the release of internal strains, a result well known in connection with the reduction of coercive force of ferromagnetic materials.

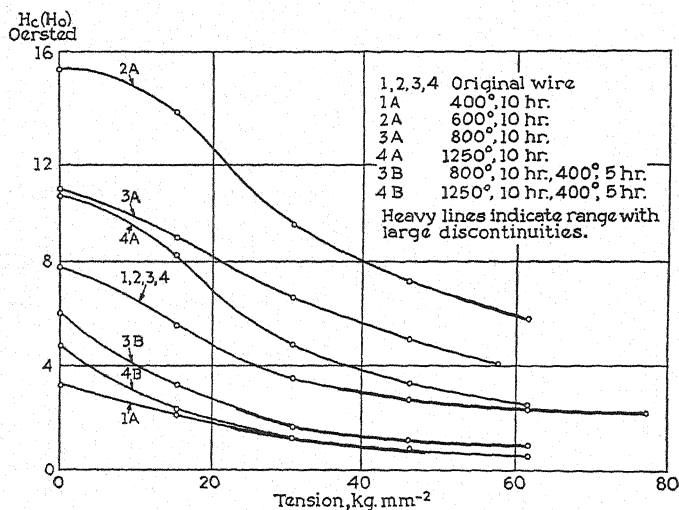


Fig. 2. Effect of annealing on coercive force H_c or critical field H_0 .

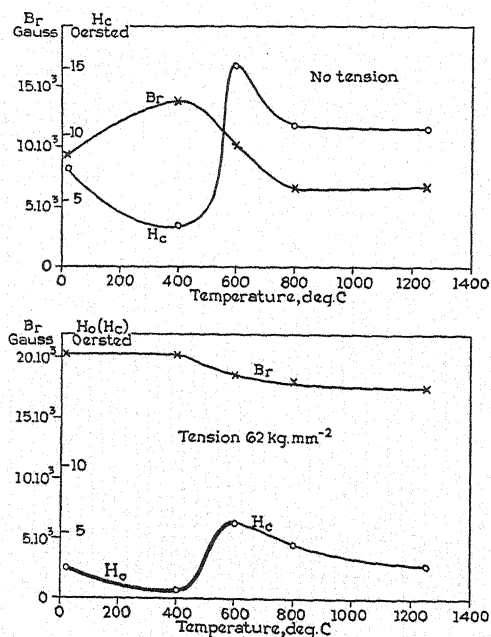


Fig. 3. Remanence and coercive force (or critical field).

After the anneal at 600°C, where the wire had at least partly undergone the α - γ transformation, H_0 and H_c had been increased many fold, and a discontinuity could only be obtained with very high tension. At the same time

the remanence had decreased. Again the x-ray analysis showed no change in crystal orientation, and besides gave no indication of the presence of the γ -phase.

We therefore have to conclude that the increase in H_0 or H_c , as the case may be, is not due to a variation in crystal orientation nor to the presence of the γ -phase. Presumably the wire shows persisting effects of the transformation between γ - and α -phase, even though the sample was cooled slowly with the furnace. These observations are consistent with the view that large inhomogeneous strains are present whose suppression to an extent sufficient to align the preferred directions of the elementary districts requires large applied tension.

The 800° wire showed increased H_c , and photomicrographs revealed a certain grain growth of the crystals, while there was no apparent change in crystal orientation as seen from the x-ray spectrograms. No large discontinuities could be obtained in this wire. In a wire with only 2 hours anneal a 50 percent discontinuity was observed for high tension (72 kg mm^{-2}).

The 1250° wire, having high H_c and no discontinuities, had lost its fibrous structure entirely. It had recrystallized and new crystals of 0.01 to 0.05 cm linear dimensions had formed. In the center portion preferred crystal orientation was still noticeable, although it was less pronounced than before.

Both the 800° and the 1250° wire were tempered for 5 hours at 400°C. This treatment reduced their H_c (see Fig. 2) nearly to the value of the original 400° wire, but only in the 800° wire was the discontinuity restored. The effect on H_c is consistent with the view, expressed above, that intense strains were set up during the γ - α transformation which were relieved by subsequent tempering below the transformation temperature. The recrystallization of the 1250° wire, i.e., the formation of large crystals with new orientations in this case, is accompanied by the complete disappearance of the jump, and the release of strains by tempering cannot bring it back.

In all the wires tested the slope A of the v - H curves was only slightly affected by the heat treatment with no apparent tendency to either increase or decrease. The variations which were found were no larger than those already observed in unannealed wires (I, Fig. 9), lying for different wires under various tensions between 19,000 and 32,000 cm sec.⁻¹ oersted⁻¹.

3. Theory

It is difficult to formulate any approximately complete explanation of these effects. One conclusion does seem possible, however, and that is that uniform crystal orientation is not necessary for the occurrence of the jump. Too small a fraction of the wire cross section shows partial orientation compared to the complete reversal of the whole wire which is often observed. Secondly, experiments have been made⁷ which show that the preferred direction dominating the discontinuity can be in the surface layers where no uniform crystal orientation exists, and this direction coincides with a principal strain axis which can make any angle up to 45° with the wire axis.

The following not quite satisfactory hypothesis for the response of the

NiFe wire to heat treatment is offered in the absence of complete and convincing data: The type of strain distribution introduced by cold working is necessary for the occurrence of the jump. A possible explanation for the relationship between strain and critical field is offered by the ideas of Bloch.⁸ On his view it is the presence of local variations in strain which establishes magnetic barriers and thereby leads to Barkhausen discontinuities. Annealing at 400°C reduces the strains, with a consequent decrease in H_c (H_0). Annealing at 800°C does not eliminate them completely even though the α - γ transformation range has been traversed, but on the return from this temperature the γ - α change introduces widely dispersed strains of a different type which tend to obliterate the jump. When this treatment is carried on for 10 hours, the jump is actually eliminated. Subsequent heating at 400° has no additional effect on the cold-work strains, but does decrease the transformation strains so that the jump reappears. Finally, a 10-hour 1250° anneal does eliminate the cold-work strains to such a degree that no jump can be found subsequently.

4. Special experiments

A few special cases remain which should be mentioned. The wire, which apparently had the smallest internal strains as judged by its decreased hardness and the fact that it had the smallest H_c (H_0) observed so far for any

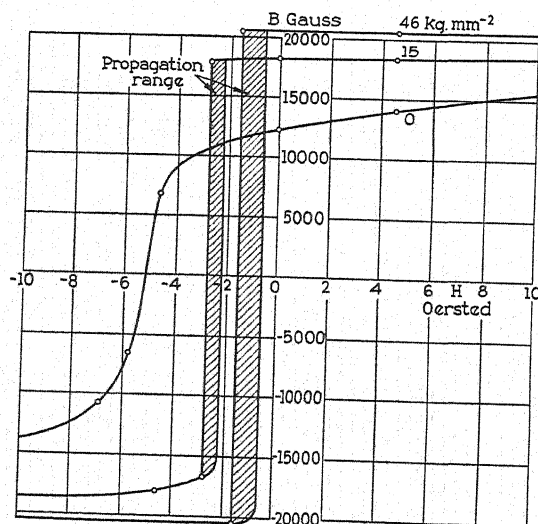


Fig. 4. Hysteresis loops under different tensions for wire annealed at 800° for 1 hr., then at 400° for 6 hrs.

given tension, had been heated for 1 hour at 800°C and subsequently for 6 hours at 400°. Besides it gave a large discontinuity with an extremely low applied tension (approximately 10 kg mm⁻²). The hysteresis loops for various tensions are given in Fig. 4.

⁷ L. Tonks and K. J. Sixtus, Phys. Rev. **41**, 539 (1932).

⁸ F. Bloch, Zeits. f. Physik **74**, 332 (1932).

All the wires so far mentioned were annealed without tension. In one experiment a wire was annealed under a tension of 82 kg mm^{-2} for one hour at 300°C . It showed very nearly the same variation of H_0 with tension as a wire given the same heat treatment without tension.

A soft permalloy wire (78.5 percent NiFe, annealed for 1 hour at 900°) gave no jump when tension was applied, but after it had been stretched plastically by about 1 percent of its length, the same tension produced a large discontinuity in its hysteresis loop. Both the soft and the deformed wire had a slight preferred crystal orientation at the center and to about the same degree. The theory formulated above is consistent with this behavior if we assume that the strains introduced by stretching are of the same nature as those caused by drawing or rolling.

A 35 Ni, 20 Fe, 45 Ni perminvar wire showed an anomalous behavior for which no explanation can at present be offered. This wire had been annealed at 1000°C for 1 hour and was extremely soft. It is known⁹ that under these conditions a large jump occurs with no applied tension. Its v - H curves were taken over a considerable range of H and their slopes were found to be nearly equal to those of Ni under torsion. When tension or torsion was applied, the discontinuity diminished, and if these stresses were sufficiently large, the phenomenon disappeared completely. An x-ray spectrogram showed the crystal structure to be of the face-centered cubic type.

IV. PROPAGATION AT ELEVATED TEMPERATURES

1. Experimental procedure

In order to extend the propagation measurements to higher temperatures, the set-up comprising the wire, the main coil, the two search coils and the adding coil had to be placed into a furnace. This was accomplished in the following way:

On the middle part of a Nonex capillary tube (120 cm in length, 0.15 cm in inside, and 0.5 cm in outside diameter) two search coils (each 0.6 cm long with 500 turns of 0.0075 cm diameter enameled copper wire) were wound at a distance of 20 cm from each other. Beyond one of them and 15 cm away, 10 turns of enameled copper wire (of 0.05 cm diameter) were wound to serve as an adding coil. The glass tube and coils fitted into an alundum tube (of 1.6 cm outside diameter) on which the coil to give the main field was directly wound. This coil consisted of 1200 turns of 0.05 cm diameter enameled copper wire in a single layer occupying a length of 67 cm, thus having a constant of 22.5 oersteds/amp. All the coils and leads were covered by a cement of water-glass and flint, which protected the copper from too rapid oxidation in the temperature range used.

Both tubes were placed in an electric furnace which had an equal temperature zone about 70 cm long. A copper-copric thermocouple in the furnace was used to determine this temperature. The wire was inserted in the capillary tube and put under tension by an arrangement similar to the one used before.

⁹ H. Kühlewein, *Wiss. Veröff. Siemens-konz.*, 10 (2), 72 (1931).

The leads to the different coils were brought out at both ends of the furnace. During the measurements the heating current was turned off in order to avoid any possible influence of its magnetic field. In that interval the temperature of the furnace fell at most 20° . This comparatively small change did not affect the results.

All supports, etc., were made of brass as it had been noticed that iron parts, even if only slightly magnetized, disturbed the homogeneity of the field sufficiently to result in low starting fields. The velocity measurements were taken in as short a time as possible to avoid large changes in temperature. Since the tension was maintained by a spring, the flow occurring at the higher temperatures reduced this stress and constant readjustment was necessary to keep it constant. These measurements have led to several general observations.

2. Variation in H_0

Figs. 5 and 6 show a typical family of v - H curves for a fresh wire when heated to 300°C and cooled to room temperature again. One feature is that the critical field decreased markedly as the wire was heated for the first time, but with decreasing temperature H_0 remained practically constant at a value

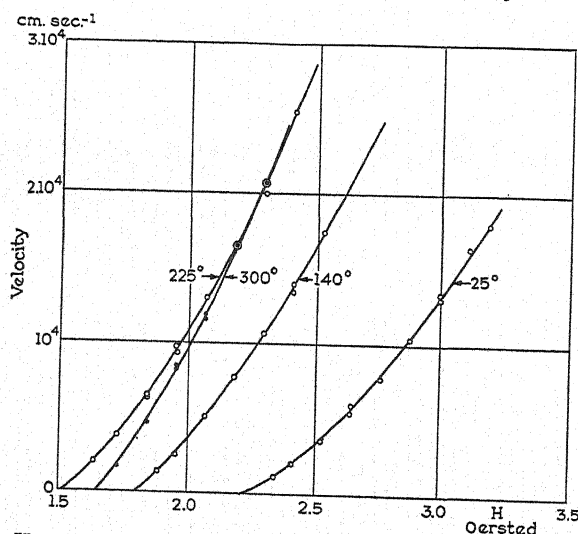


Fig. 5. v - H curves for increasing temperature with a tension of 77 kg mm^{-2} .

somewhat above the minimum reached during the heating. Fig. 7 shows this behavior for a wire at two different tensions. Subsequent heat cycles in which the maximum original temperature was not exceeded only retraced the first cooling curve. The explanation given in the present section III applies here. The permanent, if partial, relief of internal strains leads one to expect that the only effect of subsequent heating and cooling would be of the same character as the usual change in coercive force with temperature. A rough estimate from the curve for annealed Fe^{10} puts the expected reduction in the

¹⁰ *Handbuch der Physik*, 15, p. 194.

neighborhood of 25 percent for a 300-degree rise in temperature, while actually almost no change with temperature was observed. We were, of course,

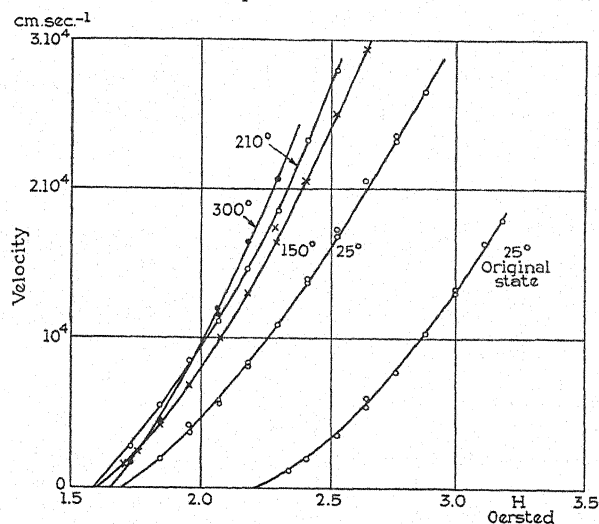


Fig. 6. v - H curves for decreasing temperature with a tension of 77 kg mm^{-2} .

dealing with a wire still having high internal strains and these, together with the uniform applied tension, may easily cause this very different behavior.

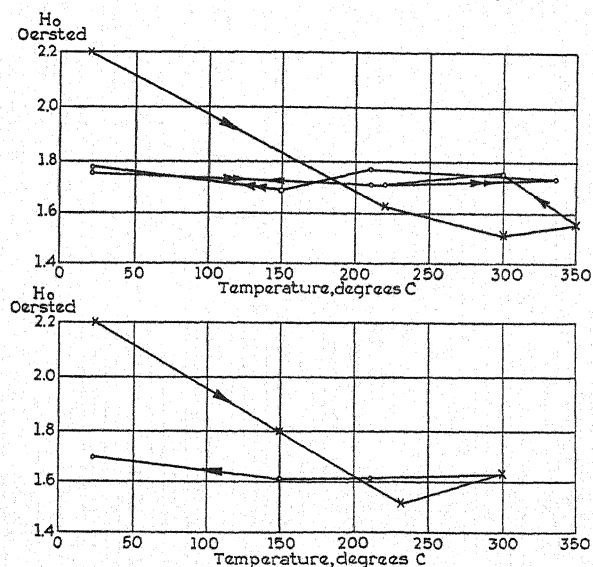


Fig. 7. Effect of temperature on H_0 . Tension: 62 kg mm^{-2} for upper curve, 77 kg mm^{-2} for lower curve.

3. Variation in H_s

Comparing Fig. 5 with Fig. 6 we observe that the propagation range, $H_s - H_0$, was greater at any temperature for a wire heated previously to a

higher temperature than for a fresh wire. The same result was found in section III at room temperature for wires annealed at 400°C. This indicates that the strain irregularities which gave rise to the weaker starting nuclei were eliminated by this low temperature heat treatment.

We further observe that $H_s - H_0$ decreased with increasing temperature. This probably arose from the increase in thermal energy which enhances the chance for the spontaneous formation of a nucleus at a particular field strength.

Above 350°C a new effect appeared. The starting field became so erratic that velocity measurements could not be made. The discontinuity frequently broke up into several part jumps in the same way that can occur at room temperature at small excess fields. The latter action is probably caused by local variations in H_0 which, at small values of ΔH , are comparable with or even exceed it, so that H does not exceed H_0 for every point in the wire. Thus portions of the wire are left unreversed until a larger main field is applied. In the present case, however, it is not possible to assign a reasonable cause for increased variability of H_0 . The α - γ transformation does not change the saturation intensity appreciably below 450°C. It might still be supposed that highly localized portions of the alloy had transformed at 350°C, but, if the local forces were such as to cause the change 100° below the general transition, one should expect this γ -phase to persist even below the main γ - α transformation which begins at 300°. Actually, the wire when cooled to 300°C had regained in full its ability to propagate, so that this explanation is not convincing.

4. Variation of A

If Fig. 8 the variation with temperature of the slope A of the v - H curve is plotted. These results are taken from Figs. 5 and 6, from experiments with

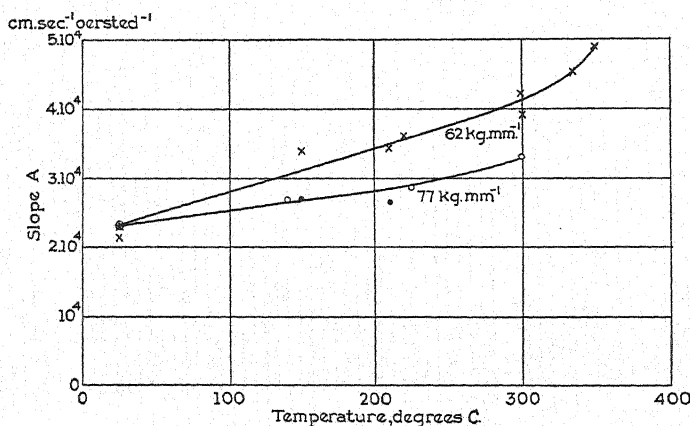


Fig. 8. Effect of temperature on slope A of v - H curves.

a wire under 77 kg/mm² tension, and from tests on a wire of different composition, namely 25 percent Ni, under a tension of 92 kg/mm². In those cases where the v - H curves were not straight lines, a tangent to these curves at

$v = 10^4$ cm sec.⁻¹ represented approximately the average slope of the curve and gave the value of A used in the diagram.

The increase in A shown by the figure might easily be caused by the increase in resistivity of the wire which amounts to about 90 percent from room temperature to 320°C for the 25 percent Ni wire. The factors, aside from the excess field, which determine v are not definitely known so that it is possible that resistance changes may affect it. On the other hand, we have noted in I, section II, that measurements at room temperature on wires of different compositions and hence of different resistivities gave values of A which showed no correlation with resistivity.

Another feature of the curves of Figs. 5 and 6 holds more hope for an explanation of the increase in A . It is the accompanying decrease in propagation range. Similar behavior was remarked in earlier experiments² where the point to point properties of a cold wire were investigated with the result that greater values of A were found at those places where the reversal could be started by the smaller adding fields. The minimum adding field is the least field which will start a reversal at a particular point. The starting field for the wire is the field which will just reverse the magnetization at that point where the minimum adding field is the least. Accordingly, it is permissible to assume that H_s is a rough measure of the average minimum adding field for the whole wire. The result is that both present and earlier observations record the same relation between slope and propagation range whether the variable factor is temperature or the local state of the wire.

The possibility of developing a theory relating slope to average minimum adding field seems very hopeful and the attempt to do this will be made in a later paper.

V. ETCHED WIRES

1. Effect of etching

In our picture of the discontinuity, the velocity of propagation depends upon conditions at the wave front and hence at the surface of the wire. On this view it was expected that changes in the surface, such as caused by etching of the wires, would affect the propagation.

Wires of 15 percent NiFe (No. 37), 0.038 cm diameter were etched to various smaller diameters in a 15 percent solution of hydrochloric acid. This decreased the critical field for constant tension per unit area, an effect which presumably arises from the release of internal strains accompanying the removal of the outer layers of the wire.

In all cases the etching resulted in a marked increase in the v - H slope A amounting to 50 percent on the average. Even a reduction in diameter of as little as 5×10^{-4} cm had this effect. Fig. 9 shows a typical case. Subsequent polishing of etched wires with emery paper had erratic results, usually decreasing but sometimes increasing A . In the single case in which the etched and polished wire (0.0360 cm dia.) was drawn through a die (0.0355 cm dia.) there was a complete restoration of the original slope. Since the same stress was applied to the etched wires as to the unetched, the tension being ad-

justed to the reduction in cross section, the increase in A is not to be attributed to a change in applied stress. Besides, in unetched wires A is practically constant for wide variation in tension. Neither does the increase in A arise from the reduction in wire size, for it has been found that A is independent of diameter in unetched wires.

Etching has a marked effect on the starting field. A wire having a propagation range of 1.07 oersteds before etching would, after a slight removal of

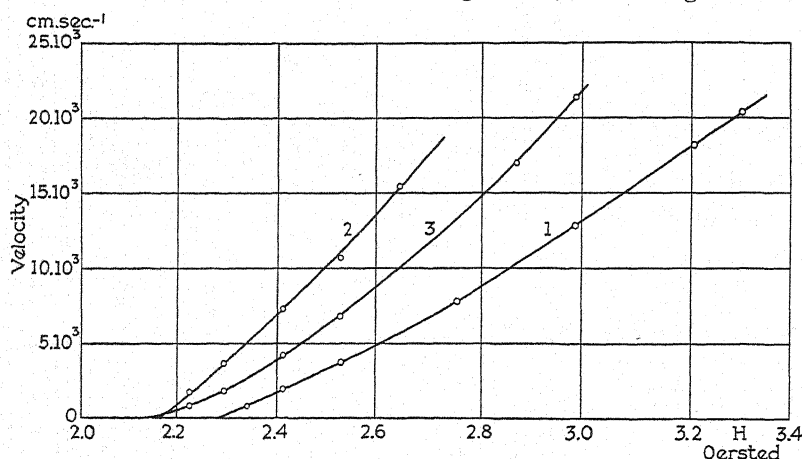


Fig. 9. v - H curves after etching and polishing of a wire. (1) Original wire; 0.0380 cm dia., tension of 77 kg mm⁻². (2) Wire after etching; 0.0375 cm, 75 kg mm⁻². (3) Etched wire after polishing; 0.0350 cm, 65 kg mm⁻².

surface material, show a reduction to 0.55 oersteds. If the wire was then polished, the range again increased with decreasing v - H slope to 0.85 oersteds (see Fig. 9). Here again we have the same relation between propagation range and A which has been noted twice before. When the etching experiments were in progress neither this behavior nor its probable significance had been recognized. Still, the following conclusions reached in a rather exhaustive search in other directions furnish data which are fundamental to any complete explanation.

2. Surface effects and propagation

The etching changes the surface in several respects. They are absorption of hydrogen, roughening of the surface, and formation of cracks. It is well known that in etching iron or steel in HCl or H₂SO₄, large amounts of atomic hydrogen are taken up by the metal. But two experiments showed that this cannot be the explanation. First, heating the wire to 200°C for several hours to remove the hydrogen did not reduce the slope; second, etching in HNO₃ where no hydrogen is produced had the same effect on the slope as etching in HCl or H₂SO₄. On the other hand, there was no change in slope when the wire was used as cathode in the electrolysis of NaOH, where, presumably, large amounts of hydrogen were absorbed but the surface of the wire was not attacked. All these observations provided ample evidence that hydrogen was not responsible for the effects.

Under the microscope the surface of the wire looked smooth before the etching but appeared coarse afterwards. It was thought that roughening of the surface of a fresh wire with coarse emery paper would give the same magnetic effect, but the resulting variation from the normal value of A was within the normal range of variation.

One possibility of explanation remains. According to metallurgical references,¹¹ acid attacks the different crystal faces with different rapidity, and in some cases it dissolves the intergranular substance more quickly than the grains. This is especially true of materials with internal strains. This latter action may cause the formation of cracks in the material if high stresses across the notches formed by the acid are present.

Such fissures parallel in general to the wire axis were actually observed under the microscope on all the etched wires. Sometimes as many as five were found around the circumference at a given point along the wire. They were of several mm in length and of various widths averaging, as well as could be judged, 10^{-3} cm. It must be admitted that it is hard to understand how a crack of this width can open up as the result of the removal of only 2.5×10^{-4} cm of material. If these fissures had been the cavities which the photomicrographs show in the wire, they should also have been seen after polishing, but this was not the case. If the cracks arise from intense stresses, one should be able to prevent their formation by a preliminary annealing of the wire which is not so complete as to destroy the discontinuity. The attempt was made by heating a wire at 400°C for 10 hours. Its stiffness showed that it still contained internal strains, so that the appearance of etching cracks was not surprising. Even so, some annealing had occurred, for the heat treatment had reduced the coercive force from 7.8 to 3.3 oersteds. It may well be the release of surface strains made evident by the formation of cracks which reduces the starting field and increases A . Subsequent polishing would, on the other hand, reintroduce strains with contrary consequences.

3. Strips

A length of No. 37 wire of 0.024 cm diameter was cold rolled down to a strip 0.0076 cm thick and 0.071 cm wide. A portion cut from this was etched and it, like the wires, showed an increase in slope and a decrease in propagation range. The increase in A was, however, only 30 percent, which is considerably smaller than that found for wires. Under the microscope the etched strip showed no cracks but only a general roughness.

Two other samples cut from the same length of strip were reduced in thickness by polishing with emery paper. Erratic increases in slope up to 100 percent resulted but there was no correlation with propagation range apparent.

The taking and interpretation of the x-ray spectrograms used in studying the effect of heat treatment was done by Dr. W. P. Jesse of this laboratory to whom we express our thanks. Dr. I. Langmuir has, with his continued interest and suggestions, contributed essentially to this paper and also to the other papers on this same subject which are now in preparation.

¹¹ G. Tammann, *Lehrbuch der Metallographie*, 1920; Z. Jeffries and R. S. Archer, *The Science of Metals*, 1924.

ERRATUM

Supersonic Dispersion and Absorption in CO_2

By W. H. PIELEMEIER
Pennsylvania State College

(Phys. Rev. **41**, 833, 1932)

The third sentence in the footnote on page 837 should read, "The value of τ computed from Grossmann's maximum A is approximately $9(10)^{-7}$."

LETTERS TO THE EDITOR

Prompt publication of brief reports of important discoveries in physics may be secured by addressing them to this department. Closing dates for this department are, for the first issue of the month, the twenty-eighth of the preceding month; for the second issue, the thirteenth of the month. The Board of Editors does not hold itself responsible for the opinions expressed by the correspondents.

Raman Effect in Gases: CO and NO

With the high pressure apparatus described by the author in earlier communications,¹ the Raman spectra of gaseous carbon monoxide at a pressure of about 35 atmospheres and of gaseous nitric oxide at a pressure of about 20 atmospheres have been obtained. Besides unresolved rotational wings in the close proximity of the Rayleigh lines, Raman lines corresponding to vibrational transitions have been recorded in both cases. The frequency shifts are compared, in the table, with the respective vibration frequencies of these molecules in the ground state as deduced from absorption spectra (infrared for CO and ultraviolet for NO).² The agreement between the two sets of values is very satisfactory. It may be noted that the values

from that given in the table. The vibration frequency of nitric oxide from Raman spectra is reported here for the first time.

The two gases used in the above investigation are generated under pressure by permitting the necessary chemicals to react with each other in closed and evacuated steel cylinders. In the case of CO, formic and concentrated sulphuric acids are used and the gas obtained appears to be very pure. Potassium ferrocyanide, potassium nitrite and acetic acid are used for generating NO, and it appears from the Raman spectrum of the resulting gas that it contains, besides nitric oxide, large proportions of nitrogen, nitrous oxide and carbon dioxide.

S. BHAGAVANTAM

210, Bowbazar Street,
Calcutta, India,
September 14, 1932.

Gas	Raman frequency	Absorption frequency
CO	2139	2138
NO	1877	1878

2155 and 2142 reported earlier by Rasetti³ for carbon monoxide differ to some extent

¹ Bhagavantam, Ind. Jour. Phys. 6, 319 (1931).

² Int. Crit. Tab. 5, 412 and 415.

³ Rasetti, Nature 123, 205 (1929) and Nuovo Cim. 6, 356 (1929).

Note on the Electric Field in Paramagnetic Crystals

The work¹ of Kramers, Bethe, and especially of Van Vleck and his collaborators has created the possibility of drawing conclusions from magnetic data about the electric fields in paramagnetic crystals and hence about the spatial arrangement of atoms and molecules in the crystal.

In his recent paper Van Vleck¹ has shown that it is possible to account for the different magnetic behavior of crystals of hydrated Co and Ni compounds by assuming that to a first approximation the electric fields possess cubic symmetry around the magnetic ion, but that in the second approximation a

rhombic term must be added. Quantitative calculations amplifying the theory are to be

¹ H. A. Kramers, Comm. Leiden 60; Proc. Amsterdam Acad. 33, 959 (1930); H. Bethe, Ann. d. Physik 3, 133 (1929); Zeits. f. Physik 60, 218 (1930); J. H. Van Vleck, *The Theory of Electric and Magnetic Susceptibilities*, Oxford University Press; Phys. Rev. 41, 208 (1932); O. M. Jordahl, W. G. Penney and R. Schlapp, Phys. Rev. 40, 637 (1932); W. G. Penney and R. Schlapp, Phys. Rev. 41, 194 (1932); Schlapp and Penney, Phys. Rev. (in press).

published shortly by Schlapp and Penney in this journal.

If the potential energy of an electron in the lattice can be developed as a power series in the displacement from the center of the magnetic ion, the terms which give rise to a decomposition of the energy levels are

$$\Phi = \Sigma_i \{ Ax_i^2 + By_i^2 + Cz_i^2 + D(x_i^4 + y_i^4 + z_i^4) \}.$$

Van Vleck concludes that D must be positive to account for the experimental data on hydrated salts of the iron group. The purpose of the present note is to consider what atomic groupings will lead to a positive D .

Since the contribution to D due to the different charges in the neighborhood of the central ion is proportional to R^{-5} (where R is the distance from the central ion), it is evident that only the immediate neighbors will give a noticeable contribution to the value of D .

If the metal ion is surrounded by 6 oxygen ions or water-dipoles² in an octahedral arrangement, D will be positive.³ If on the contrary the ion is surrounded by 8 or 4 negative charges in a cubic or tetrahedral arrangement, D will be negative. This leads to the conclusion that in the hydrated salts of the iron group the metal ion is surrounded by six molecules of crystal water.

Dr. C. A. Beevers of the University of Liverpool kindly expressed to me his opinion

² The dipoles will orient themselves in the field of the positive ion with the negative charge inside. With the octahedral arrangement the negative charges are at the face centers of a cube embracing the positive ion.

Possibility of the Existence of the Chlorine Isotope Cl^{39}

Hardy and Sutherland¹ in a recent paper found no evidence for the existence of a third isotope of chlorine, Cl^{39} , in the absorption spectrum of HCl . They made a careful search for lines due to HCl^{39} in the 1.7μ absorption band, but failed to confirm the maxima reported by Hettner and Böhme,² even with much greater path lengths than used by the German investigators. A year ago, the writers³ studied the ultraviolet absorption spectrum of AgCl vapor⁴ at high vapor densities expressly to test the assertions of Becker⁵ as to the existence of this isotope. Our results were entirely negative, a contradiction made more

that, from the result of x-ray researches, the arrangement indicated above may be regarded as probable, though not proved for the alums and the hepta- and hexa-hydrated sulphates. It seems probable to me that also in solutions the metal ions will be surrounded by six water molecules.

Penney and Schlapp have performed calculations on rare earth salts, and have shown that it is possible to explain the temperature variation of the susceptibilities of the octahydrates of Pr and Nd sulphates, assuming a cubic field again with a positive value of D . Consequently, here also, the octahedral grouping of the oxygen atoms is suggested. This demands six oxygen neighbors for the metal ion, but in the substances so far investigated there are only four water molecules to each such ion. Hence it is necessary to suppose either that oxygen atoms belonging to the SO_4 -group figure among the immediate neighbors, or else that a water molecule may be shared by two metal ions. Both assumptions could give rise to deviations from cubic symmetry, which can perhaps account for any magnetic anisotropy which may be disclosed when measurements, on the principal susceptibilities of single crystals of rare earth salts become available.

A quantitative discussion of the arrangements proposed above will be able to decide whether the picture corresponds to reality.

C. J. GORTER

Natuurk. Laborat. v. Teylers Stichting,
Haarlem, Holland,
September 15, 1932.

³ Cf., for instance, H. Bethe, *Ann. d. Physik* **3**, 196 (1929).

striking by the subsequent confirmation of Becker's conclusions by Hettner and Böhme. The latter authors refrained from commenting on our results, pending more complete publi-

¹ J. D. Hardy and G. B. B. M. Sutherland, *Phys. Rev.* **41**, 471 (1932).

² G. Hettner and J. Böhme, *Zeits. f. Physik* **72**, 95 (1931).

³ M. Ashley and F. A. Jenkins, *Phys. Rev.* **37**, 1712 (1931).

⁴ B. A. Brice, *Phys. Rev.* **35**, 960 (1930).

⁵ H. Becker, *Zeits. f. Physik* **59**, 583 and 601 (1930).

cation of these. However, most of the essential data, including an estimate of an upper limit for the abundance of Cl^{39} , were included in our abstract.³

The question of the existence of this isotope is of considerable interest for the systematics of nuclei, for if it were actually present it would make Cl the only known element, outside of the radioactive families, of odd atomic number having more than two isotopes. Such a violation of one of the few generalizations we have about the stability of nuclear types should certainly be critically examined. Furthermore, according to the theories of Urey⁶ and of Bartlett,⁷ Cl^{39} lies in the very interest-

continuous spectrum was a high-current hydrogen discharge.⁸ The two observed heads of AgCl^{35} and AgCl^{37} are indicated in the figure, as well as the expected position of the AgCl^{39} head. It is seen that the region where the latter head should appear remains clear of structure from the 0,0 sequence up to a density corresponding to 800°C and that no trace of the head is visible. The microphotometer trace (upper curve), at the left, is from the 800° spectrogram, and also fails to show the head in question. At 850° the background begins to interfere; the lower curve is from a plate taken at this temperature. Here the absorption of even the AgCl^{37} head is com-

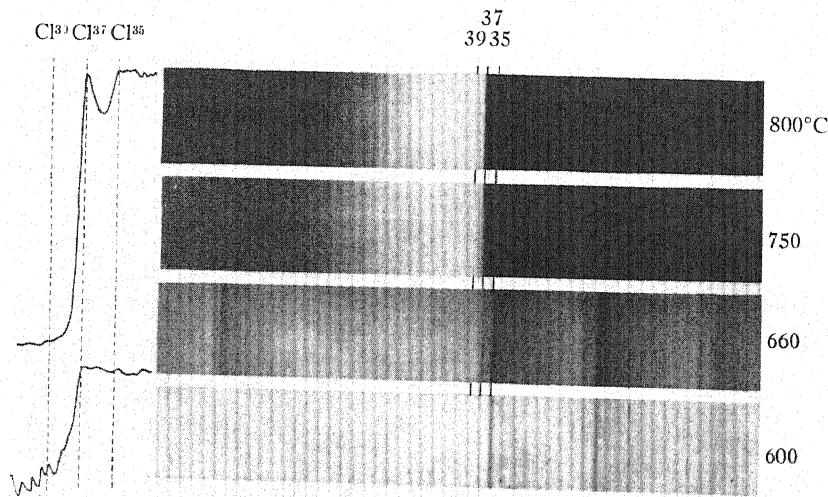


Fig. 1.

ing region immediately following the completion of the "closed shell" of nuclear protons and neutrons at A^{36} . Hence we wish to give here a somewhat more complete account of the evidence we obtained from the AgCl spectrum.

The accompanying reproduction shows the absorption of AgCl vapor in the region of the 0,1 band at various densities of the vapor, as photographed in the first order of a 21-foot grating. The vapor was contained in a quartz tube without windows, the heated portion being about 80 cm long and 2 cm in diameter. Temperatures along the tube were determined by a thermocouple. The source of the

plete, but no evidence for an AgCl^{39} head appears. The gradual rise of the curves in the neighborhood of the black edge is probably to be ascribed to the Eberhard effect.

Our estimate for the upper limit for the abundance of Cl^{39} was obtained as follows. On a plate taken at 550°C the AgCl^{37} head was just visible, and easily detectable by the microphotometer. From the equation given in I.C.T. Vol. 3, p. 214 for the vapor pressure of AgCl , with a considerable extrapolation to low pressures, one finds the values 2.6×10^{-4} and 3.6×10^{-1} mm at 550° and 850°, respectively. The vapor densities are then approximately in the ratio 1:1400 at these two temperatures, so that if Cl^{39} were present in this

⁶ H. C. Urey, J. Am. Chem. Soc. 53, 2872 (1931).

⁷ J. H. Bartlett, Jr., Nature 130, 165 (1932).

⁸ E. O. Lawrence and N. E. Edlerson, Rev. Sci. Inst. 1, 45 (1930).

proportion relative to Cl^{37} , it should be detected on the 850° plate. Now Cl^{35} is 3.15 times as abundant as Cl^{37} , so the maximum value possible for the ratio $\text{Cl}^{39}:\text{Cl}^{35}$ is 1:4400. The limit obtained in the infrared work of Hardy and Sutherland, using a path of seven meters, was 1:1600. It is apparent from the practically complete absorption of the AgCl^{37} head that our sensitivity is somewhat greater than that of the infrared work, where even the strongest HCl^{37} lines gave an appreciable deflection. It is to be regretted that neither Becker nor

Hettner and Böhme have given any estimate of the relative abundance of Cl^{39} , but it is obvious from their absorption curves that if the HCl^{39} maxima are real, the abundance must be much greater than either of the above limits.

MURIEL F. ASHLEY
F. A. JENKINS

University of California,
The Physical Institute, Utrecht,
September 20, 1932.

Simple Amplifier for Geiger-Müller Counters

The numerous uses to which Geiger-Müller counters have been put and their general effectiveness seem to warrant the publication of a simple amplifying and recording device which has been used in this laboratory during the last several months.

100 cm^2 , of lengths from 1 to 10 cm, and made of copper, nickel, zinc, and aluminum with wires of steel, tungsten, or aluminum have been used. Counting rates from 10 per minute to 400 per minute have been observed with the various counters and various exciting

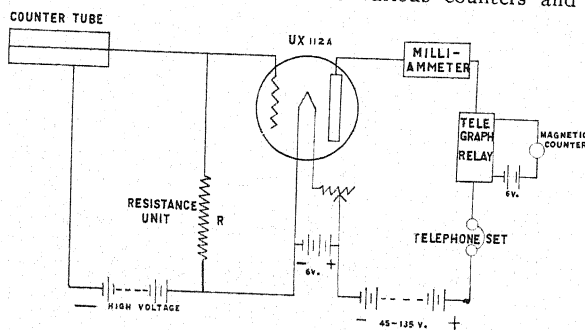


Fig. 1. Circuit diagram.

The circuit follows. The crucial part of the circuit is the resistance R . There is a definite value for this resistance which for each set of characteristics of the counter, the counting rate, and the voltage applied to the counter, gives the greatest amplification. The impulses

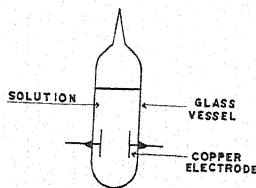


Fig. 2. Resistance unit.

are recorded as momentary diminutions of the normal filament plate current which are sufficient to actuate the ordinary telegraph relay with contact reversed so the magnetic counter circuit will be closed by each current diminution. Counters of surface area from 5 cm^2 to

sources and the appropriate resistances, R .

The resistances consist of solutions of isopropyl alcohol in pentane of the proper compositions sealed in glass vessels with sealed-in electrodes, as shown in Fig. 2.

The solutions must be nearly pure pentane of compositions ranging up to approximately 7 volume percent of alcohol.

The resistance determines both the time of recovery of the system after each impulse and the size of each "kick" so that the product of the two is approximately constant if other conditions are not changed. As a result, it is possible to obtain "kicks" which completely repress the filament-plate current, (normally about 5 m.a.) if the counting rate is not higher than about 40 per minute, for this type of "kick" can be obtained with a minimum period of about a 0.5 second with a counter of about 75 cm^2 area and 25 cm length. For a rate as high as 300 or 400 per minute the kicks cannot be much greater than 1/10 of the

TABLE I.

Speed of count (min. ⁻¹)	Size of kick (percent of filament-plate current)	Approximate volume percent of isopropyl alcohol
200	5-10	6
40	80-100	1

filament plate current. The counter characteristics affect the composition of the best solution very little. The following table contains the compositions and "kick" size for counters approximately the same as that

described immediately above.

The amplifying tube can be any radio tube which will give a filament plate current of 3 or more milliamperes. The relay is an ordinary 680 ohms telegraph relay.

Argon gas at about 5 cm of Hg pressure is generally used in the counter, and the applied voltage is generally between 600 and 1500 volts.

W. F. LIBBY

Department of Chemistry,
University of California,
September 28, 1932.

High-Speed Hydrogen Ions

In a paper on the production of high speed light ions without the use of high voltages¹ a method and apparatus were described in detail for producing 1,220,000 volt-protons. The value of such high-speed protons for studies of the atomic nucleus has been shown recently by Cockcroft and Walton.² Using the above mentioned apparatus, their results have lately been checked and somewhat extended in this laboratory by disintegration of the lithium nucleus.³ It is obvious that for further nuclear studies ions of still higher energies will be exceedingly valuable and an apparatus of larger dimensions has now been developed which produces hydrogen ions with energies equivalent to 3,600,000 volt-electrons.

An essential part of the apparatus is an electromagnet which gives uniform fields over considerable areas; indeed, the maximum producible ion energies are proportional to the area of the useful region of the magnet's field.

Although the magnet now being used has an iron coil 45 inches in diameter, for this first step the pole face diameter has been reduced to 27.5 inches, giving fields in excess of 15,000 gauss over a gap of 3.5 inches. Actually only a region of 20 inches diameter in the center of the poles has been used in the present experiments. The chamber between the poles was evacuated by means of a high-speed pumping system which kept the pressure of heavy gases and vapors down to the order of 10^{-6} mm of mercury and a pressure of hydrogen of ap-

proximately 10^{-5} mm of mercury was maintained by a suitable capillary leak. The ions were produced in this hydrogen gas by an electron beam from a filament near the center of the chamber which could be moved to the proper position, i.e., such that the ions started from a point away from the geometrical center of the apparatus by a distance equal to the radius of their first circle in the magnetic field. The high-frequency fields were applied across the diametral gap between two large hollow semi-circular electrodes, (one of which was at ground potential) by means of a "tuned plate—tuned grid" oscillator circuit, using a Federal Telegraph 20 kilowatt water-cooled tube. Wave-lengths down to 25.8 meters were used and voltages applied on the electrodes of approximately 15,000 volts or less. At the edge of the 20 inch circle the ions passed through an electrostatic deflecting system which bent them out of the beam (and at the same time measured their energies) into a collector connected to a suitable electrometer. From the electrostatic voltages applied on the deflecting plates the energies were calculated, and were found to check closely in each case with those expected.

Using a 28.5 meter wave-length, and a magnetic field of 14,000 gauss, hydrogen molecule ions were produced with energies of 3,000,000 volt-electrons and with a current of approximately 10^{-8} amperes. Using 25.8 meters and 15,250 gauss, 3,600,000 volt ions were produced. Due to the efficient focussing action of the high-frequency electrodes, the ion currents remain approximately the same throughout the range from 1 to 3.6 million volts. These H_2^+ ions with energies of 3,600,000 volt-electrons are, for nuclear purposes, essentially equivalent to protons of energies

¹ Ernest O. Lawrence and M. Stanley Livingston, *Phys. Rev.* **40**, 19 (1932).

² Cockcroft and Walton, *Proc. Roy. Soc. A* **137**, 229-242 (1932).

³ Lawrence, Livingston and White, *Phys. Rev.* **42**, 150 (1932).

LIS

s and
Sny-
it to

of 1,800,000 volt-electrons. Hydrogen molecule ions rather than protons were accelerated in the present experiments because protons require a much lower wave-length (for the same magnetic field), which is difficult to obtain due to the large capacity in the oscillating circuit.

It appears now entirely practicable to go to much higher energies by using a still larger chamber. However, it seems more desirable to hesitate awhile on the road to higher voltages and use these 1,800,000 volt protons for some nuclear studies. This we intend to do.

I wish to express my deepest gratitude to

Prof. Ernest O. Lawrence for his constant help and guidance in this development, and to Commander T. Lucci for his invaluable assistance. These experiments have been made possible through the help of the Federal Telegraph Company, the Research Corporation and The Chemical Foundation.

M. STANLEY LIVINGSTON

Radiation Laboratory,
Department of Physics,
University of California,
Berkeley, California,
October 3, 1932.

The Heisenberg Theory of Ferromagnetism

The theory of the existence of ferromagnetism, due to Heisenberg,¹ disagrees in some of its consequences with experiment. It is here shown to be not quite as unphysical as has been supposed. Heisenberg's principal result is contained in the well-known simultaneous equations:

$$\text{I. } y = \tanh x$$

$$\text{II. } x = \frac{1}{2}(\beta - \beta^2/z)y + \beta^2 y^3/4z \quad (1)$$

$\beta = zJ/kT$ = (number of nearest neighbors of atom in crystal) \times (e.s. exchange integral)/ kT .

neglected). I_0 is the intensity of absolute saturation. The atomic spin is that of one electron.

The prevalent interpretation of these equations has been based on a graphical solution similar to that of the Weiss theory, neglecting the fact that II does not give a straight line

the graphical manner of solving (1), but must bear in mind that the equations do not hold for zero external field, when the magnetization may change in direction. The part of the

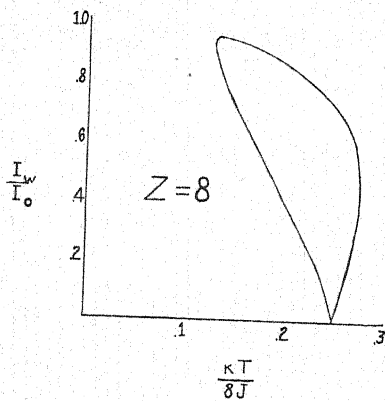


Fig. 1.

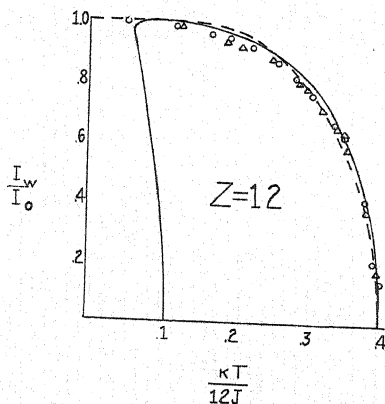


Fig. 2.

$y = I_w/I_0$. I_w is the magnetization in a field only strong enough to orient the large crystal spin (if extant) and to overcome the small magnetic interactions² of the electrons (here

¹ W. Heisenberg, *Zeits. f. Physik* 49, 619 (1928).

² The magnetic interactions are largely responsible for direction effects, remanence, hysteresis, and demagnetizing forces, which may not be expected of the Heisenberg model, unmodified. One might expect hysteresis from

magnetization curve treated by (1) when the term $\mu H/kT$ is added to x is, of course, only that beyond the usual experimental saturation. In that region Kapitza has measured that with 240,000 gauss the magnetization of Fe and Ni at room temperature increases not more than 1 percent. After simplifying (1) by taking II linear (see footnote 3), calculation shows that the increase for Ni should be 1 percent and for Fe less than one-tenth as much. The corresponding increase for Ni at 330°C should be about 10 percent.

(Heisenberg's Fig. 1), that is, neglecting y^3 . One obtains ($z \geq 8$) only the axis-intercepts of Figs. 1 and 2, two positive critical temperatures (coincident for $z=8$) between which ferromagnetism should exist.

Numerical solution of (1) is simpler in the following form of the equations:

$$\beta = \frac{z}{2-y^2} \left\{ 1 \pm \left[1 - \frac{2(2-y^2)}{zy} \log \frac{1+y}{1-y} \right] \right\} \quad (2)$$

Solutions are plotted in Figs. 1 and 2 for $z=8$ (Fe) and $z=12$ (Ni, Co). The first is an extreme case, where the results are very sensitive to small changes in the assumptions, and have very little semblance to physics. In the second, the higher-temperature branch of the curve is theoretically, as well as experimentally, preferred. Its intercept is taken as the Curie temperature. Data from the experiments of O. Bloch,³ e.g., for Ni (circles) and Co (triangles) lie very close to the curve.

The lower-temperature branch of each curve is a mathematical ghost of which the origin may be explained as follows. The theory in the approximation used seeks only the spin with an extreme value of the probability, presumably a maximum. At a high temperature very low spins of the crystal are most probable. Higher spins have lower energies, and with decreasing temperature become more probable, giving the higher-temperature branch of the curve. In reckoning this effect, the distribution-in-energy of states of each value of spin is approximated with the central part of a Gaussian distribution. The distant parts of this distribution are small and neglected. Unfortunately they extend to infinity, whereas the corresponding physical distribution has definite and fairly narrow limits. At very low temperatures only the very few states of high spin have a high probability, but, due to the Gaussian distribution, the tremendously nu-

merous states of low spin have each a finite (mathematical) probability, so the total probability may be greater for low spins. As the temperature decreases below the Curie point, a probability peak may thus develop at zero spin. Between this and the maximum giving the higher-temperature branch of the curve is a minimum, corresponding to the lower branch. (This identification of the curves has been verified by reckoning second derivatives.) The lower branch is thus non-magnetic. As the temperature further decreases, the low-spin states overwhelm the others, and the two extrema merge.

Thus we see that the higher branch of the curve alone gives the magnetization resulting from the assumption of a Gaussian distribution. It differs very little, so far as it goes uninterrupted, from the curve obtained by assuming an infinitely sharp distribution³—i.e., that states with the same spin have the same energy—if we determine the constant J from the Curie point in each case. (The latter curve is drawn with dots in Fig. 2 to a different scale of abscissae than that shown, its axis intercept being $kT/12J' = \frac{1}{2}$.) We conclude that the numerical results of the theory are fairly insensitive to variation of the distribution assumed. Because of this insensitivity, we may be satisfied that the simple assumption of an infinitely sharp distribution gives a fairly good approximation to the result that would be obtained from the actual, incalculable distribution.

This justifies, as an approximation, a simplified form of the theory having quite satisfactory consequences, and lends weight to the usual conclusion that the Heisenberg concept of ferromagnetism is physically correct.

Note added October 17, Zurich. For small z the Gaussian "spread" is relatively broader and there appears no extremum of probability, except that at zero spin. The condition that z be at least 8 for ferromagnetism is thus also a consequence of the mythical, low-spin, low-energy states to which Heisenberg⁴ ascribed the second critical temperature.

D. R. INGLIS

Landheim Pulvermühle,
Dusslingen bei Tübingen,
October 4, 1932.

Note on the Term System of Ir I

The first regularities in the spectrum of Ir I were found by Mr. C. P. Snyder about 1900. He discovered a constant difference wave

number array consisting of 12 columns and 54 rows, the array containing 240 lines. Snyder never published his work but sent it to

³ See a paper by Bitter, *Phys. Rev.* 39, 340 (1932). A similar comparison made by Tyler, *Phil. Mag.* 11, 596 (1931), shows the "theoretical" curve (which also appears in Van Vleck's book) bulging not enough towards its ends. The equations there used, (1) lacking terms in β^2 , may be very simply derived by modifying Heisenberg's theory to the extent of endowing all states having a given spin with the same energy.

Professor H. A. Rowland, who turned the array over to Dr. N. E. Dorsey, his assistant, who later turned it over to Dr. W. F. Meggers. The author obtained the loan of the original array through the courtesy of Dr. Meggers.

The underwater spark spectrum of Ir has been photographed by Meggers and Laporte.¹ With the results obtained they were able to determine the ground state and fix the relative energy values for the 12 columns in Snyder's array. They also noted all the lines ap-

of Exner and Haschek³ for the region 4500 to 2200Å.

The present array consists of 16 low even terms and 77 middle and high terms. It contains 566 lines, including nearly all the strong lines of the spectrum.

The J values of the terms have been deduced from a study of the intensities and combinations, and a knowledge of the theoretical number of times each value of J for the low even terms should occur. The two ground

TABLE I.

λ air	I	comb.	λ air	I	comb.
5894.06-6		{N-7°	3334.19-6		38°-K
5625.56-8		{7°-M	3266.45-10		16°-D
5449.50-10		9°-M	3241.52-6		12°-C
5364.32-8			3220.79-15 (R.U.)		9°-B
4938.09-6		5°-I	3219.53-6		
4778.16-7		9°-J	3168.88-6		20°-E
4728.86-6		13°-L	3133.31-8		22°-E
4616.37-6		9°-I	3100.42-15		{13°-B
4548.50-6		1-3°	2951.23-8		{24°-E
3800.10-10		1°-A	2943.17-10		9°-A
3636.22-8		25°-H	2936.71-8		29°-E
3628.69-10		9°-E	2934.63-8		{63°-M
3617.23-8		19°-G	2924.81-10		{30°-E
3609.78-8		3°-B	2849.74-8		10°-A
3573.74-10		{4°-B			13°-A
3559.01-8		{13°-F	2839.18-6		71°-K
3522.05-10		9°-D	2824.44-6		22°-B
3515.96-10		5°-C	2797.72-5		24°-B
3513.67-15 (R.U.)		2°-A	2694.22-5		{53°-G
3448.99-10		7°-C	2664.77-5		{28°-B
3437.05-10		15°-E	2661.98-5		19°-A
3368.50-10		6°-B			30°-B

pearing in the underwater spark which were involved with the interval of the two ground states, 2835.0 cm⁻¹. Meggers and Laporte tentatively called the two ground states ²D_{2½} and ²D_{1½}, but mentioned that they might be ⁴F_{4½} and ⁴F_{3½}.

The above results have been extended by the writer, using the wave-length data of Meggers² for the region 8426 to 4500Å and

¹ Meggers and Laporte, Phys. Rev. **23**, 660 (1926).

² Meggers, Sci. Papers Bur. of Standards, No. 499. Bull. Bur. of Standards **20**, p. 19 (1925).

³ Exner and Haschek, Spektren der Elemente bei normalem Druck, **II**.

states have the same J value of 4½, and are most probably ⁴F terms. The rare ultimate is given by a combination of the second lowest odd term with the ground state. This term has a J value of 5½ and is possibly ⁴G_{6½}.

At present, further progress is hindered because of the incompleteness of the data. The region from 4500 to 1900Å is particularly incomplete. This region is to be photographed in a search for new lines and for better wave-length determinations of the old lines. An attempt will also be made to obtain the Zeeman patterns of the strongest lines.

It has been thought worth while to publish a list of the strongest combinations and terms, since they have not been published before.

TABLE II.

Term symbol	J	Term value cm^{-1}	Term symbol	J	Term value cm^{-1}
<i>Even terms</i>					
A ⁴ F	$4\frac{1}{2}$	0.0 (S)	L	$4\frac{1}{2}$	13939.8 (A)
B ⁴ F	$4\frac{1}{2}$	2835.0 (S)	M	$2\frac{1}{2}$	16103.4 (S)
C	$1\frac{1}{2}$	4079.1 (A)	N	$3\frac{1}{2}$	17779.3 (A)
D	$2\frac{1}{2}$	5784.9 (S)	O	$1\frac{1}{2}$	18547.0 (A)
E ⁴ F?	$3\frac{1}{2}$	6323.9 (S)	P	$2\frac{1}{2}$	19060.5 (S)
F ⁴ F?	$3\frac{1}{2}$	7106.7 (S)	1	$4\frac{1}{2}$	52508.9 (A)
G	$2\frac{1}{2}$	9877.8 (S)	2	$4\frac{1}{2}, 3\frac{1}{2}$	54892.6 (A)
H	$1\frac{1}{2}$	11831.1 (S)	3	$3\frac{1}{2}$	55381.9 (A)
I	$2\frac{1}{2}$	12218.5 (S)	4	$4\frac{1}{2}, 3\frac{1}{2}$	56416.1 (A)
J	$2\frac{1}{2}$	12951.6 (S)	5	$3\frac{1}{2}$	56792.7 (A)
K	$3\frac{1}{2}$	13087.8 (S)	6	$4\frac{1}{2}, 3\frac{1}{2}$	59878.0 (A)
<i>Odd terms</i>					
1° ⁴ F??	$4\frac{1}{2}$	26307.6 (A)	13°	$4\frac{1}{2}$	35080.6 (M)
2° ⁴ G??	$5\frac{1}{2}$	28452.3 (A)	15°	$3\frac{1}{2}$	35410.7 (S)
3°	$3\frac{1}{2}$	30529.7 (A)	16°	$1\frac{1}{2}$	36390.1 (A)
5°	$1\frac{1}{2}$	32463.5 (S)	18°	$2\frac{1}{2}$	37446.3 (S)
6°	$4\frac{1}{2}$	32513.4 (A)	19°	$3\frac{1}{2}$	37515.4 (S)
7°	$2\frac{1}{2}$	33064.8 (S)	20°	$4\frac{1}{2}$	37871.7 (M)
9°	$3\frac{1}{2}$	33874.3 (S)	21°	$3\frac{1}{2}$	38158.3 (A)
10°	$5\frac{1}{2}$	34180.4 (M)	22°	$4\frac{1}{2}$	38229.9 (S)
12°	$2\frac{1}{2}$	34919.9 (S)	23°	$2\frac{1}{2}$	38358.0 (A)
24°	$3\frac{1}{2}$	38567.9 (S)	49°	$3\frac{1}{2}$	45896.3 (S)
25°	$2\frac{1}{2}$	39324.4 (S)	50°	$2\frac{1}{2}$	46093.7 (S)
27°	$2\frac{1}{2}, 3\frac{1}{2}$	39806.0 (S)	51°	$4\frac{1}{2}$	46220.7 (M)
28°	$3\frac{1}{2}, 4\frac{1}{2}$	39940.4 (M)	52°	$3\frac{1}{2}$	46979.6 (M)
29°	$3\frac{1}{2}$	40291.3 (S)	53°	$1\frac{1}{2}$	46983.3 (S)
30°	$4\frac{1}{2}$	40389.9 (S)	54°	$2\frac{1}{2}$	47165.1 (S)
31°	$1\frac{1}{2}$	40524.6 (S)	55°	$2\frac{1}{2}$	47537.5 (S)
32°	$3\frac{1}{2}$	40710.7 (S)	56°		47548.7 (S)
33°	$4\frac{1}{2}$	41118.7 (M)	58°	$2\frac{1}{2}$	48206.5 (S)
34°	$2\frac{1}{2}$	41522.5 (S)	71°	$4\frac{1}{2}$	48299.1 (M)
36°	$1\frac{1}{2}$	42268.2 (S)	59°	$3\frac{1}{2}$	48448.8 (S)
38°	$2\frac{1}{2}$	43071.7 (S)	60°	$1\frac{1}{2}$	48802.1 (S)
39°	$3\frac{1}{2}$	43176.2 (S)	61°	$2\frac{1}{2}$	49146.6 (S)
40°	$1\frac{1}{2}$	43200.9 (S)	62°		49621.4 (S)
41°	$3\frac{1}{2}$	43592.2 (S)	64°		51814.6 (S)
42°	$2\frac{1}{2}$	44596.8 (S)	65°		51852.3 (S)
43°	$3\frac{1}{2}$	44642.6 (S)	66°		52051.7 (S)
44°	$4\frac{1}{2}$	44652.6 (M)	67°		52134.2 (S)
45°	$1\frac{1}{2}$	44785.5 (S)	68°		52224.4 (S)
46°	$2\frac{1}{2}$	45111.7 (S)	70°		52806.6 (S)
47°	$2\frac{1}{2}$	45186.0 (S)			

Table I contains a list of all lines of intensity 6 or greater as estimated by Exner and Haschek on an intensity scale of 15 for the strongest lines and 1 for the weakest. Column one gives the wave lengths in Å.; column two, the estimated intensity; column three, the combination giving the line.

Table II contains a list of the most certain terms. Column one gives the term symbol; column two, the J value; column three, the

term value expressed in cm^{-1} . A term value followed by (S) indicates the term as in Snyder's array; (M) indicates the term was first noted by Meggers and Laporte; (A) indicates the term was noted by the author.

WALTER ALBERTSON

Massachusetts Institute of Technology,
Cambridge, Massachusetts,
October 6, 1932.

The Isotope of Hydrogen in the Atomic Spectrum

Urey, Brickwedde and Murphy¹ have shown the existence of H^2 by photographing the lines due to H^2 in the atomic spectrum with a 21-ft. grating. Professor Urey has informed the author that Professor Shenstone at Princeton has succeeded in getting some indication of the H^2 lines but his photographs were complicated by very bad ghosts from his grating (see also²).

Using a long discharge tube of the type described by Wood³ the $H^2\gamma$ line was photographed with a glass prism spectrograph. The tube used was 220 cm long and 8 mm diameter and was observed end on through about 40 cm of the central portion of the tube. The tube was supplied with moist electrolytically prepared hydrogen which was admitted by means of a long fine capillary. This tube operated in a very black stage and the spectra was excited by a transformer which could deliver a maximum current of about 310 m.a.

The spectrograph was a six prism glass instrument used as a littrow which makes it effectively twelve prisms and gave a dispersion in the $H\gamma$ region of about 1.09 angstroms per mm. The author expects to publish a full description of this instrument as well as a

photograph showing the $H^2\gamma$ line in J.O.S.A. in the near future.

On passing a current of 190 m.a. through the tube a 2.5 hour exposure did not record the presence of the $H^2\gamma$ line although a 1 sec. exposure recorded $H^1\gamma$ with about five times the intensity necessary to make it visible on the plate. Upon increasing the current to 310 m.a. the $H^2\gamma$ line appeared with a 35 minute exposure. This type of behavior has been observed and explained by (U., B. and M.⁴). Since the transformer used could only deliver 310 m.a. a further enhancement of $H^2\gamma$ with respect to $H^1\gamma$ could not be produced. From these results it might be concluded that the ratio of H^2 to H^1 is not more than 1 part in 80,000 in ordinary H_2 if the reciprocity law held for the photographic plate. Due to failure of this law for low intensities Bleakney's² value of 1 part in 30,000 is probably much more reliable. Measurements of the plates gave for the wave-length of $H^2\gamma$ 4339.256 Å or $\Delta\lambda = 1.211$ in substantial agreement with U., B. and M.'s value of 1.206 for ordinary hydrogen.

DAVID H. RANK

Physics Laboratory,
Pennsylvania State College,
State College, Pennsylvania,
October 10, 1932.

¹ Urey, Brickwedde and Murphy, Phys. Rev. 39, 164 (1932); 40, 1 (1932).

² Walker Bleakney, Phys. Rev. 41, 32 (1932).

³ R. W. Wood, Proc. Roy. Soc. 97, 455 (1920).

⁴ Urey, Brickwedde and Murphy, Phys. Rev. 40, 464 (1932).

Intensity of Cosmic-Ray Ionization in Western North America

This letter is a preliminary report of one of the ten cosmic-ray expeditions organized and supplied with apparatus by Professor A. H. Compton and supported in part by the Carnegie Institution of Washington. Measurements of ionization intensities due to penetrating radiation were made by this expedition in Alaska, California and Colorado.

The apparatus was a duplicate of that already described in this journal,^{1,2} and the method of making measurements was also essentially the same. It might be mentioned that the effect of high humidity made it

necessary to discard some of the earlier observations. This difficulty was overcome by maintaining a fairly constant high temperature in the observation tent by means of a stove.

Table I gives the time, place, elevation, mean barometer, and duration of observations at each place where measurements were made. One observation (column 7) involved a radium comparison test, a ground radiation test and a cosmic-ray test, and required about 3 hours. Thus a six-hour shift consisted of (1) four electrometer drifts in each direction with the radium at 1 meter; (2) four cosmic-ray drifts in each direction with the radium distant; (3) three cosmic-ray drifts in each direction with the radium distant and the outer of the three shields removed; (4) a repetition of

¹ A. H. Compton, Phys. Rev. 41, 111 (1932).

² A. H. Compton, Phys. Rev. 41, 681 (1932).

TABLE I. *Relative cosmic-ray intensities.*

Place	Dates	Lat. N	Long. W	Elev. meters	Mean bar cm	No. of obs.	Mean C_{123}	Mean dev. % δ	$\delta/n^{1/2}\%$
Ft. Yukon	6/24-7/2	67°	145°	129	75.1	61	0.170	2.8	0.4
Kennecott	7/9-7/19	62°	143°	1840	61.2	75	0.254	2.8	0.3
Berkeley	7/30-8/2	38°	122°	116	75.1	18	0.166	5.2	1.2
Tioga Pass	8/4-8/15	38°	119°	3040	53.0	80	0.363	3.9	0.4
Pasadena	8/17-8/21	34°	118°	259	73.6	30	0.174	3.8	0.7
Denver	8/26-8/29	40°	105°	1616	62.3	23	0.240	4.4	0.9
Summit Lake	8/30-9/9	40°	105°	3900	48.3	80	0.492	3.7	0.4

(1); (5) a repetition of (2). The single set of measurements (3) served to make the small ground radiation correction for both cosmic-ray measurements. The electrometer sensitivity was adjusted at each elevation to such a value that a single cosmic-ray drift required about ten minutes. Observations at each place were made continuously, the shortest series being 54 hours and the longest 240 hours.

The value C_{123} is a net ratio of cosmic-ray ionization current to gamma-ray ionization

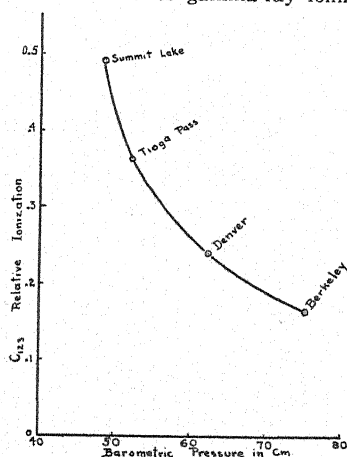


Fig. 1. Variation of ionization with barometric pressure at lat. 40°N.

current, corrected for ground radiation. Therefore these values are only relative.

Because of possible systematic errors we feel that the values of $\delta/n^{1/2}$ give an unduly optimistic indication of the probable error of these measurements. It may be as large as one or two percent even in the longer series of observations.

The values obtained at Berkeley, Tioga Pass, Denver and Summit Lake represent intensities at nearly the same latitude. These four sets of observations give the curve of ionization against barometric pressure shown in Fig. 1.

This curve agrees fairly well with those obtained by Millikan and Cameron³ and Compton.¹ Using this curve to reduce the values at Pasadena, Berkeley and Ft. Yukon to sea level, we get the lower curve of variation with latitude for this region, shown in Fig. 2. The

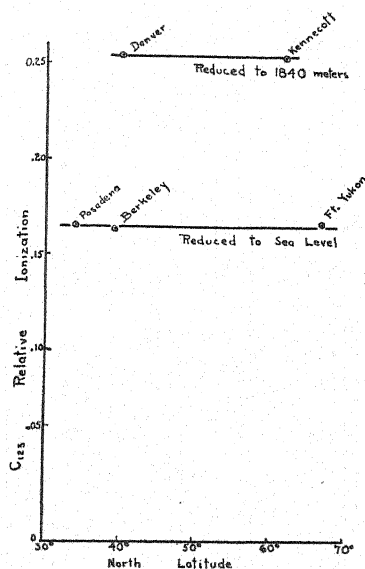


Fig. 2. Variation of ionization with latitude.

upper curve of this figure shows the relative values at Denver and Kennecott both reduced in the same manner to 1840 meters.

These results indicate no significant variation of intensity of ionization due to penetrating radiation (when measured by this method) in the region covered.

R. D. BENNETT, Mass. Institute of Tech.

J. L. DUNHAM, Harvard University

E. H. BRAMHALL, Mass. Institute of Tech.

P. K. ALLEN, Yale University

October 14, 1932.

³ Millikan and Cameron, Phys. Rev. 37, 242 (1931).

The Dielectric Constant and Electric Polarization of Mixtures in the Neighborhood of the Critical Point

There exist many mixtures of liquids, chiefly organic liquids, which disclose critical phenomena in the system liquid-liquid. As a result of a long series of experiments, I am able to state that the most suitable medium for dielectric tests is the pair of liquids: hexane-nitrobenzene, the critical temperature of dissolution of which is 16.9° , and the critical concentration 51.4%. The object of the present work was to test the behavior of the dielectric constant ϵ , the density d , the gram

and the dilatometer were placed in a specially constructed thermostat enabling the maintenance of any constant temperature between -4° and $+60^\circ\text{C}$.

The results obtained for the mixture having the critical concentration are shown in Fig. 1. With the fall from higher temperatures to the critical temperature, the dielectric constant increases, but at a decreasing rate; the corresponding curve is bent downwards, which does not occur at other concentrations. The

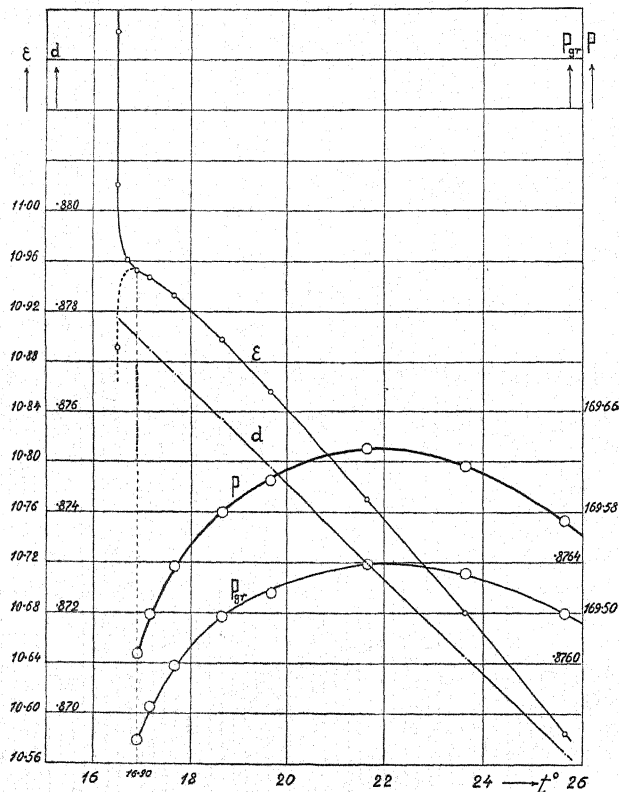


Fig. 1.

polarization of the mixture P_{gr} , and the molecular polarization P of the dissolved nitrobenzene, when approaching the critical point where, as is well known, considerable fluctuations of density take place, manifesting themselves by the critical opalescence.

The measurements of the dielectric constant were conducted as in the recently published research A. Piekara, *Nature* 130, 93 (1932). The measurements of the density were carried out in the dilatometer. The condenser

molecular polarization of nitrobenzene at first increases, but from 22° it decreases more and more rapidly. It is obvious that the density fluctuations are responsible for such a considerable decrease of the polarization of nitrobenzene. The critical opalescence begins at 18.7° . It is interesting that even above 18.7° , where no opalescence can be detected, the fluctuations of density, although very feeble, cause the decrease of polarization.

At the temperature of 16.9° the separation

of phases occurs. The dielectric constant increases rapidly, in connection with the production of the emulsion hexane-nitrobenzene.

Mixtures were also tested having concentrations lower, and higher, than the critical concentration, especially in the neighborhood of the point at which the separation of phases takes place. The dielectric constant undergoes a rapid fall if the emulsion nitrobenzene-hexane is formed, or a rapid increase if the

emulsion hexane-nitrobenzene is produced.

The detailed results of these investigations will be published later in the Bull. Acad. Polonaise (Cracovie).

A. PIEKARA

Physical Laboratory,
Sulkowski Gymnasium,
Rydzyňa, Poland,
September 12, 1932.

The Electric Moment of the Molecule of Nitrobenzene

Recently there have been published a number of investigations establishing the fact that in the neighborhood of 9.6° nitrobenzene undergoes some, as yet not clearly understood, modification (M. Wolfke and J. Mazur, Zeits. f. Physik 74, 110, 1932; G. W. Stewart, Phys. Rev. 39, 176, 1932; H. Trotter, Phys. Rev. 40, 1052, 1932). At the same time, however, there

the temperature point of 9.6°. Already the first measurements have been shown that such change does not occur. Now I am able to give more accurate data concerning this matter.

I experimented with dilute solutions of nitrobenzene in hexane. Both substances have been carefully purified and dried. Fig. 1 shows the

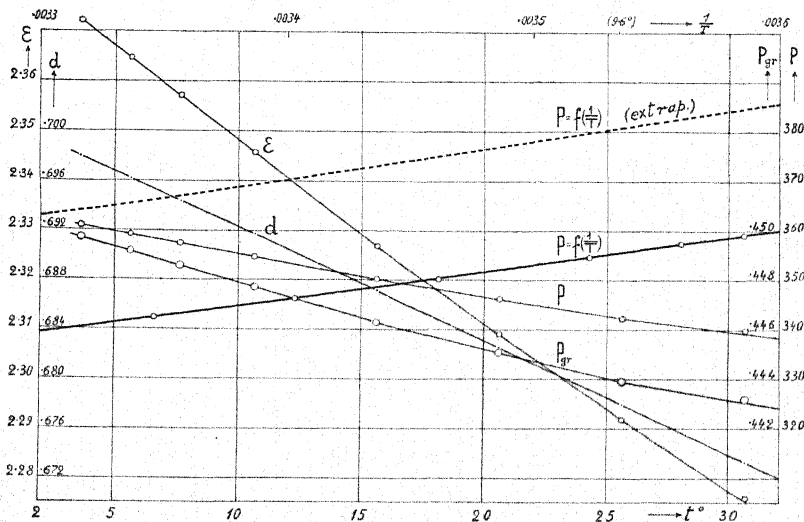


Fig. 1.

appeared publications denying the existence of these allotropic forms of liquid nitrobenzene (M. Wolfke and S. Ziemecki, Acta Phys. Polonica 1, 271, 1932; Massy, Warren and Wolfenden, Nature 129, 441, 1932; J. N. Friend, Nature 129, 471, 1932; A. Piekara, Nature 130, 93, 1932). Studying the problem of the critical point of dissolution—chiefly on the mixtures of nitrobenzene and hexane—I resolved to derive profit from the occasion and to examine if the electric moment μ and the polarizing ability γ of the molecule of nitrobenzene undergo any change when passing

graphs of the dielectric constant ϵ , density d , gram polarization

$$P_{gr} = \frac{\epsilon - 1}{\epsilon + 2} \frac{1}{d},$$

and the molecular polarization of nitrobenzene P , for one of the solutions tested, having a concentration (by weight) $c=0.04034$. P is to be computed from the formula

$$P = \frac{M}{c} [P_{gr} - (1 - c)P_{gr}']$$

where P_{gr}' is the gram polarization of the pure solvent, and M is the molecular weight of

nitrobenzene. According to the theory of Debye, P is composed of two parts, a "dielectric" one P_d , and a "paraelectric" one P_p , and, if the association does not exist, can be expressed:

$$P = P_d + P_p = \frac{4\pi}{3} N\gamma + \frac{4\pi N\mu^2}{9KT}$$

The relation between P and $1/T$ is visible from the straight line in Fig. 1. The dotted line refers to the polarization value, extrapolated for the concentration $c=0$. The value of angular coefficient of this line gives us: $\mu = 3.54 \times 10^{-18}$. The accuracy of this value is too small to attribute to it any greater importance, since the association of the molecules of nitrobenzene makes an accurate extrapolation impossible.

For calculating the μ value, another frequently employed method may be used, according to which it is supposed that $P_d = R_\infty$ (molecular refractivity, extrapolated for infinitely long waves). According to J. W. Williams (Phys. Zeits. 29, 174, 1928) we have: $P_d = 32.0$ cc. Since (for 25°) $P = 366.7$ cc, we find $P_p = 334.7$ cc, and $\mu = 4.03 \times 10^{-18}$. A third method may also be used which is based on the supposition that P_d is equal to the molecular polarization of solid nitrobenzene.

My measurements (l. c.) give the following results (0°): $\epsilon = 3.44$, $d = 1.342$, hence $P_d = 41.1$ cc. Consequently $P_p = 325.6$ cc (at 25°), and $\mu = 3.97 \times 10^{-18}$.

As a result of the application of the two last methods, we may assume:

$$\mu = 4.00 \times 10^{-18};$$

the error involved in this value is less than ± 1 percent. This μ value is a little greater than the one (3.90×10^{-18}) found by J. W. Williams (l. c.).

Since the polarization, reciprocal of temperature ($1/T$) graph on Fig. 1 is a straight line, it is obvious that neither the electric moment μ nor the polarizability γ of the molecule of nitrobenzene undergo any change (cf.: L. Meyer, Zeits. f. Physik 75, 421, 1932). Consequently the structure of the molecule of nitrobenzene does not undergo any change.

The full report of these investigations will appear in the Bull. Acad. Polonaise (Cra-covie).

A. PIEKARA

Physical Laboratory,
Sulkowski Gymnasium,
Rydzya, Poland,
September 12, 1932.

BOOK REVIEWS

Tables of Cubic Crystal Structure of Elements and Compounds. I. E. KNAGGS AND B. KARLIK. With a section on alloys by C. F. Elam. Pp. 90. Adam Hilger, Ltd., London, 1932. Price 11/6d.

This little book will be of great aid to the crystal-structure worker when dealing with cubic substances. Table I lists all investigated inorganic substances in alphabetical order with chemical formulas and complete references. Table Ia contains the relatively few cubic organic compounds. Table II enumerates the 513 cubic substances in the order of increasing length of the edge of the unit cell.

Tables III and IV are corresponding tabulations of alloys. Bibliographies of about 1000 references complete this excellent up-to-date catalogue. The printing and binding are of high quality.

J. W. GRUNER
University of Minnesota

Electrons and Waves. H. STANLEY ALLEN. Pp. 316+vii, Figs. 60. MacMillan and Co., Ltd., London. 1931. Price \$2.50.

This account of modern physics follows a middle course. The discourse is of an essentially popular nature suited to the intelligent layman; yet there is preserved some degree of rigor in the exposition of the newer physical theories and therefore the book should be of interest to some physicists, particularly those that have only a slight familiarity with modern developments. The historical sketches given are especially noteworthy both from the point of view of the expert and the layman. But this account of recent progress will be appreciated more by the reader who has not specialized in physics. The book is well written and contains many good figures that illustrate modern physical phenomena, such as electron and x-ray diffraction pictures and Wilson cloud-chamber photographs.

E. O. LAWRENCE
University of California

Gmelins Handbuch der anorganischen Chemie, 8 Auflage. Herausgegeben von der Deutschen Chemischen Gesellschaft; Verlag Chemie, Berlin, 1932. System Nummer 59 Eisen, Teil B. Lieferung 5; page 294 + xviii + xxxviii*, Figs. 62; 53.50 R.M. System Nummer 58 Kobalt; Teil A. Lieferung 2, page 282 + xviii + xvi, Figs. 33; 48 R.M.

With the fourth continuation on iron and the first on cobalt, both volumes have reached completion. An extensive table of contents accompanies each issue, thus facilitating looking up special subjects in these exhaustive monographs on iron and cobalt. In previous announcements of sections of Gmelins 8th edition, the work has been warmly praised and the present additions uphold the high scientific standing of the preceding volumes. According to the reviewer's knowledge, Gmelins Handbuch offers the most complete, exhaustive and modern compilation of the physical and chemical properties of the elements and their compounds.

I. M. KOLTHOFF
University of Minnesota

CURRENT LITERATURE OF PHYSICS

Extracts from the Tables of Contents of Some
of our Contemporaries

NATURE

VOL. 130, No. 3283

OCTOBER 1, 1932

Magnetism and Quantum Mechanics. By E. C. S.	490
Measurements of Solar Radiation. By S. Chapman	497

Letters to the Editor:

Selective Transmission of γ -Radiation by Lead. By F. L. Hopwood, T. E. Banks and T. A. Chalmers	506
Magnetic Moment and the Chemical Bond in Alloys. By J. Dorfman	506
Expanding Universe. By D. D. Kosambi and E. A. Milne	507
Electron Oscillations. By Antonio Rostagni	509

NATURE

VOL. 130, No. 3284

OCTOBER 8, 1932

Letters to the Editor:

Has Physics Discarded Mechanism? By J. E. Turner	544
Change of Paramagnetic Susceptibility due to Absorption of Light. By D. M. Bose and P. K. Raha	544
Causes of Ionization in the Upper Atmosphere. By Ivo Ranzi	545

ZEITSCHRIFT FÜR PHYSIK

VOL. 78, Nos. 3 AND 4

SEPTEMBER 21, 1932

Double Band of Solid Hydrogen Chloride. By G. Hettner	141
Structure of Atomic Nuclei. By W. Heisenberg	156
Liberation of Neutrons from Beryllium. By F. Rasetti	165
Absorption Measurements on Balmer Lines in a Neon-Hydrogen Mixture with Condensed Discharges. By T. Takamine, L. S. Ornstein and J. M. W. Milatz	169
Flexible Electron Beams. By E. Brüche	177
New Investigations on the Electrolytic Rectifying Action. By A. Güntherschulze and Hans Betz	196
Wood's Method for Separating the D-Lines. By E. Gaviola and Peter Pringsheim	211
Relation between Infrared Characteristic Frequencies and Dielectric Losses. By M. Czerny and W. Schottky	220
Magneto-Elastic Phenomena in Vibrating Wires and Rods in a Magnetic Field. By O. v. Auwers	230
Influence of the Superposition of High Frequencies on the Corona Current. By A. Gemant	240
Accurate and Absolute Measurement of Small Capacities. By J. Clay	250
Most Dense High-Order Packing of Spheres. By E. K. Broch	257
Variation with Pressure of the Ionization by Cosmic Rays. By Bernhard Gross	271
Wave Mechanical-Classical Picture of the Neutron. By Hans K. Kudar	279

DIE NATURWISSENSCHAFTEN

VOL. 20, No. 40

SEPTEMBER 30, 1932

Oxide Cathodes. By A. Gehrts	732
<i>Short Original Communications:</i>	
Method of Multiplying Canal-Ray Energies and its Application to Atomic Disintegration. By Chr. Gerthsen	743

THE PHYSICAL REVIEW

Remarks on the Scattering of X-Rays by Gases and Crystals

By G. E. M. JAUNCEY
Washington University, St. Louis, Missouri

(Received September 9, 1932)

§§1 and 2: Woo's most recent formulas for the separation of the diffusely scattered radiation from polyatomic gases and simple crystals into coherent and incoherent radiation are discussed. It is shown that Woo's formulas for the total scattered radiation reduces to the author's respective classical formulas when $\alpha (=h/mc\lambda)$ is made zero. This removes the objection made by the author in a previous note. It is shown that the incoherent scattered radiation depends upon the root mean square of the E 's while the coherent radiation depends upon the arithmetic mean of the E 's, thus giving a mathematical distinction between the incoherent and coherent radiation even in the classical theory. §3: Evidence is presented in favor of the true atom form factor f of an atom in a crystal (sylvine) being a function of the temperature of the crystal. The average electron distribution about the center of an atom in a crystal must be a function of the violence of the thermal agitation of the atom. At 0°K the electron distribution in an atom of sylvine is more diffuse than in an atom of argon. As the temperature rises above 0°K the electron distribution becomes less diffuse and finally becomes like that of argon at about room temperature. §4: It is shown that the $S_p = (S + F^2/Z)_c$ relation can be replaced by a relation between experimental quantities alone—otherwise, an empirical relation. §5: A digression on the philosophy of physics in which it is noted that the empirical relation of §4 contains no vestige of the Thomson or any other theory of x-rays. This supports the view that physical laws express relations between pointer readings. §6: The classical theory for the diffuse scattering of x-rays by a crystal consisting of atoms of several kinds is worked out and a formula obtained. By the use of Woo's method, the formulas for the coherent and incoherent radiation are also obtained. The restrictions upon these formulas are discussed.

§1. POLYATOMIC GASES

THE following papers on the scattering of x-rays by gases and crystals have appeared in the Physical Review during recent months: Paper I by Jauncey,¹ Paper II by Woo,² Paper III by Jauncey³ and Paper IV by Woo.⁴ In this section the author wishes to comment on Paper IV by Woo. In Paper I, Jauncey discusses the classical theory of the scattering of x-rays from polyatomic gases whose molecules consist of n atoms of one kind and arrives at the formula⁵

¹ G. E. M. Jauncey, *Phys. Rev.* **38**, 194 (1931).

² Y. H. Woo, *Phys. Rev.* **39**, 555 (1932).

³ G. E. M. Jauncey, *Phys. Rev.* **39**, 561 (1932).

⁴ Y. H. Woo, *Phys. Rev.* **41**, 21 (1932).

⁵ For definition of S see, G. E. M. Jauncey and P. S. Williams, *Phys. Rev.* **41**, 127 (1932).

$$S_{\text{class}} = 1 + (Z + 1)f'^2/Z^2 + (f^2/nZ) \sum_{r=1}^n \sum_{s=1}^n (\sin kl_{rs})/kl_{rs} \quad (1)$$

where

$$k = (4\pi \sin \frac{1}{2}\phi)/\lambda \quad (2)$$

and

$$f'^2 = f^2 - \left(Z \sum_{r=1}^Z E_r^2 - f^2 \right) / (Z - 1). \quad (3)$$

In Eqs. (1) and (3) f is the true atom form factor for each atom in the molecule of the gas and l_{rs} is the distance between the r th and s th atoms of a molecule. The quantities E_r are defined in a paper by Jauncey⁶ on the diffuse scattering of x-rays by solids. In Paper II Woo takes account of the Compton effect and separates the scattered radiation into coherent and incoherent parts. The result of Woo's separation is to replace Eq. (1) above by

$$S = S_{\text{incoh.}} / (1 + \alpha \text{ vers } \phi)^3 + S_{\text{coh.}} \quad (4)$$

where α is the Compton quantity $h/mc\lambda$. In Paper II Woo gives

$$S_{\text{incoh.}} = 1 - f'^2/Z^2 \quad (5)$$

and

$$S_{\text{coh.}} = (f'^2/nZ) \sum_{r=1}^n \sum_{s=1}^n (\sin kl_{rs})/kl_{rs} \quad (6)$$

for polyatomic gases whose molecules consist of n atoms of one kind. In Paper III the author objected to Woo's formula for $S_{\text{coh.}}$ because the author believes that a formula which takes account of the separation into coherent and incoherent scattered radiation must reduce to the classical formula when α is put equal to zero. In other words, the right side of Eq. (1) must equal $S_{\text{incoh.}} + S_{\text{coh.}}$, or, as we may write it,

$$S_{\text{class.}} = S_{\text{incoh.}} + S_{\text{coh.}} \quad (7)$$

This is not the case when Woo's formulas as given in Eqs. (5) and (6) are used.

Before considering Woo's Paper IV, the author wishes to introduce a new symbol f'' . The true atom form factor f is defined by⁶

$$f = \sum_{r=1}^Z E_r \quad (8)$$

or, in other words, f/Z is the arithmetic mean of the E 's. The new quantity f'' is to be defined by

$$f''^2 = Z \sum_{r=1}^Z E_r^2 \quad (9)$$

⁶ G. E. M. Jauncey, Phys. Rev. 37, 1193 (1931).

or, in other words, f''/Z is the root mean square of the E 's. Eq. (3) now becomes

$$(Z - 1)f'^2 = Zf^2 - f''^2 \quad (10)$$

and Eq. (1) may be written in the form

$$S_{\text{class.}} = 1 - f''^2/Z^2 + (f^2/Z) \left\{ 1 + (1/n) \sum_{r=1}^n \sum_{s=1}^n (\sin kl_{rs})/kl_{rs} \right\}. \quad (11)$$

From the point of view of the classical theory the author has no preference as between Eq. (1) and Eq. (11). The only difference is one of symbols.

In Paper IV Woo replies to the objections raised by the author in Paper III and arrives at Eq. (4) together with the defining equations

$$S_{\text{incoh.}} = 1 - f''^2/Z^2 \quad (12)$$

and

$$S_{\text{coh.}} = (f^2/Z) \left\{ 1 + (1/n) \sum_{r=1}^n \sum_{s=1}^n (\sin kl_{rs})/kl_{rs} \right\} \quad (13)$$

which replace Eqs. (5) and (6). It is seen that these formulas for $S_{\text{incoh.}}$ and $S_{\text{coh.}}$ satisfy Eq. (7) and so the author's objections are removed. Eq. (13) takes the special forms

$$S_{\text{coh.}} = (f^2/Z) \{ 1 + (\sin kl)/kl \} \quad (14)$$

for a diatomic gas and

$$S_{\text{coh.}} = (f^2/Z) \{ 1 + (3 \sin kl)/kl \} \quad (15)$$

for a gas each of whose molecules consist of similar atoms with their centers at the corners of a regular tetrahedron. The quantity l is the distance between two atoms in the same molecule. If there are thermal vibrations of the atoms in the molecules of a gas, then, comparing with the author's Paper I, it is seen that $(\sin kl)/kl$ in Eqs. (14) and (15) is replaced by

$$\{ (\sin kl_0)/kl_0 \} \exp(-ky^2/4)$$

where y is the most probable change in the separation of any pair of atoms in a molecule from the mean separation l_0 .

§2. SIMPLE CRYSTALS

The classical theory of the diffuse scattering of x-rays by simple cubic crystals consisting of atoms of one kind has been worked out by Jauncey and Harvey.⁷ This theory leads to the formula

$$S_{\text{class.}} = 1 - f''^2/Z^2 + (f^2 - F^2)/Z \quad (16)$$

in virtue of Eq. (10). The quantity F is the atom form factor as referred to a lattice point, but not to the center of the atom. In Paper IV Woo separates

⁷ G. E. M. Jauncey and G. G. Harvey, *Phys. Rev.* **37**, 1203 (1931).

the diffusely scattered radiation from a crystal into two parts according to Eq. (4), where $S_{\text{incoh.}}$ is given by Eq. (12) and

$$S_{\text{coh.}} = (f^2 - F^2)/Z. \quad (17)$$

It is seen that the right sides of Eqs. (12), (16), and (17) satisfy Eq. (7).

From Eqs. (12), (13), (16), it is seen that through f the coherent portion of the scattered radiation depends upon the arithmetic mean of the E 's and that through f'' the incoherent portion depends upon the root mean square of the E 's. This seems to give a mathematical distinction between the coherent and incoherent radiation even in the classical theory because the distinction between f'' and f remains even if $\alpha (=h/mc\lambda)$ is zero.

§3. TEMPERATURE AND THE TRUE ATOM FORM FACTOR

In his formulas for the scattering of x-rays by crystals, the author has preferred to write F for the atom form factor as referred to a lattice point, but not to the atom center, instead of in the manner fe^{-M} , where f is the true atom form factor (which is due to the electron distribution relative to the center of the atom) and e^{-M} is the Debye⁸ or Waller⁹ temperature factor. In the derivation of the classical formulas for the scattering of x-rays by a solid and by a crystal, Jauncey^{6,7} notes two different orders of velocity—the velocity of an electron in an atom relative to the center of the atom and the velocity of thermal agitation of the center of an atom about the lattice point with which the atom is associated. The atom may be likened to a planet with an electron atmosphere. The electrons of the atmosphere will pass through all their configurations many times while the atom as a whole is performing one vibration about its lattice point. The effective atom form factor F of an atom in a crystal is made up of two factors— f the true atom form factor and H the temperature factor. The second factor H is due to the changing configurations of the centers of the atoms relative to their respective lattice points, caused by the thermal motions of the atoms in the crystal. The author has made no special assumptions⁶ concerning the form of H . Since values of $F(=fH)$ are determined experimentally by measurements of the integrated reflection from crystals, it is only necessary for Eqs. (16) and (17) to include F but not to include the form of H . The form of H is not as yet accurately known. According to James and Brindley,¹⁰ H is fairly well given for sylvine by Waller's formula⁹ at low temperatures but is not given by this formula at high temperatures.

In the Debye-Waller formula

$$F = fe^{-M} \quad (18)$$

it is postulated that the true atom form factor f is not affected by the heat motions of the atoms, or, in other words, that the electron distribution in an atom is independent of the violence of the thermal agitation of the atom

⁸ P. Debye, Ann. d. Physik **43**, 49 (1914).

⁹ I. Waller, Zeits. f. Physik **17**, 398 (1923).

¹⁰ R. W. James and G. W. Brindley, Proc. Roy. Soc. A**121**, 155 (1928).

amongst the surrounding atoms. If we think of an atom in a crystal as being held to a lattice point by a quasi-elastic force, the atom will be acted upon by no force when at a lattice point and may be considered when at this point as being undistorted. However, if the atom is displaced from its lattice point, some amount of distortion in the electron distribution of the atom will occur. The f value for the atom will be the result of an average electron distribution for the electron configurations of the atom about its own center taken over many (comparatively slow) thermal vibrations of the atom about its lattice point. As the temperature rises the average electron distribution will become more and more distorted, if we measure the distortion as a departure from the electron distribution when the atoms are all at rest at their lattice points. There is no actual attractive force on a given atom towards its lattice point, but this apparent force is due to the forces of the neighboring atoms upon the given atom. As the thermal vibrations of the atoms become more violent, the atoms approach each other more closely and the electron atmospheres of the atoms become more distorted. It seems therefore that the average electron distribution about the center of an atom in a lattice should be a function of the temperature. Accordingly, the true atom form factor f should be a function of the temperature. The situation is somewhat the same as the case in the kinetic theory of gases where the quantity b in van der Waal's equation has been found to be a function of the temperature.¹¹ As the temperature rises and the impacts between molecules become more violent, the molecules penetrate each other more and more and so the distortion of the molecules due to impacts increases with the temperature.

Jauncey and Harvey¹² have shown that the relation

$$S_{\text{gas}} = (S + F^2/Z)_{\text{cryst.}} \quad (19)$$

holds very well for argon and sylvine at room temperature. On the other hand Jauncey and Williams⁵ have found that the $(S + F^2/Z)$ values for sodium fluoride at room temperatures are consistently lower than the S values for neon. Now from Eqs. (4), (12), and (17) it follows that for a crystal

$$S + F^2/Z = (1 - f''^2/Z^3)/(1 + \alpha \text{ vers } \phi)^3 + f^2/Z \quad (20)$$

so that, if f and f'' are not functions of the temperature, $(S + F^2/Z)$ should be independent of the temperature. Jauncey and Harvey¹³ have measured the S values for sylvine at temperatures of 90°K and 300°K and, using James and Brindley's F values¹⁰ for sylvine at these two temperatures, have found that the $(S + F^2/Z)$ values at 90°K are distinctly less than those at 300°K. According to Eq. (20) the implication of this is that either or both f and f'' are functions of the temperature. If for simplicity we for the present assume $f'' = f$ (as is the case if all the E 's are equal¹⁴), then, since $(S + F^2/Z)$ is less at

¹¹ See K. F. Herzfeld, *Handb. d. Physik.* XXII, p. 399.

¹² G. E. M. Jauncey and G. G. Harvey, *Phys. Rev.* **38**, 1071 (1931).

¹³ G. E. M. Jauncey and G. G. Harvey, *Phys. Rev.* **38**, 1925 (1931).

¹⁴ G. E. M. Jauncey, *Phys. Rev.* **38**, 1 (1931).

90°K than at 300°K, f is less at 90°K than at 300°K. This means that the average electron distribution in an atom of sylvine departs more and more from the electron distribution in an argon atom as the temperature falls below room temperature. It is just a matter of good fortune that at room temperature the average electron distribution in an atom of sylvine is the same as that in an atom of argon. In the case of sodium fluoride it is probable that room temperature is too low a temperature for the electron distribution in an atom of this crystal to be the same as that for neon. It therefore appears that at temperatures approaching absolute zero, the f values for a crystal (such as KCl or NaF) are less than those for the corresponding gas (argon or neon). Consequently, the electron distribution in an atom of a crystal at absolute zero is more diffuse than in the atom of the corresponding gas. As the temperature rises above absolute zero, the atoms of the crystal vibrate amongst one another with increasing violence with the result that the average electron distribution about the center of each atom becomes less diffuse and finally at high temperatures becomes like the average electron distribution about the center of an atom of the corresponding gas.

It should be remembered that the atoms in crystals like NaF and KCl are ionized. It might be expected that on this account the electron distributions in the atoms of the respective crystals at absolute zero would differ from the electron distributions in the atoms of the corresponding gases.

§4. AN EMPIRICAL RELATION

In a recent report Wollan¹⁵ quotes the author as stating that the relation

$$S_{\text{gas}} = (S + F^2/Z)_{\text{cryst.}} \quad (21)$$

represents a relation which could have been established empirically without the aid of theory. As Dr. Wollan learned of this in private conversation with the author it seems worth while to discuss the statement in greater detail.

For simplicity we shall assume that the scattering occurs without change of wave-length as is pretty nearly the case for argon and sylvine. Crowther's formula¹⁶ for the intensity of x-rays scattered in a direction ϕ from a slab of material whose thickness is t is

$$I_{\phi} = (At/R^2 \cos \frac{1}{2}\phi) \cdot s \quad (22)$$

where I is the intensity per unit area of the rays transmitted through the slab when held in the Crowther position, A is the area of the ionization chamber window, R is the distance of the window from the slab, and s is the linear spatial scattering coefficient per unit solid angle in the direction ϕ . The quantity s in Eq. (22) is thus measured and defined in terms of experimental quantities and may therefore itself be considered an experimental quantity. Having found s by means of Eq. (22) we divide by ρ the density of the scattering material and obtain s/ρ which we shall call the mass spatial scattering

¹⁵ E. O. Wollan, Rev. Mod. Phys. 4, 205 (1932).

¹⁶ J. A. Crowther, Proc. Roy. Soc. A86, 478 (1912).

coefficient per unit solid angle in the direction ϕ . The quantity s/ρ has been determined for argon by Wollan¹⁷ and for sylvine by Harvey.¹⁸ Referring to the paper by Jauncey and Williams,⁵ we see that the relation between S the scattering factor per electron and s/ρ the mass spatial scattering coefficient is

$$S = \frac{s/\rho}{(NZ/W) \cdot (e^4/m^2c^4) \cdot (1 + \cos^2 \phi)/2} \quad (23)$$

where N is Avogadro's number, Z is the number of electrons in an atom of the scatterer, W is its atomic weight, and e , m and c have their usual significance.

We shall now introduce the quantities r the linear reflection coefficient and r/ρ the mass reflection coefficient of a crystal for x-rays. The mass reflection coefficient is given in terms of experimental quantities by

$$r/\rho = (i_\phi \omega \cos \frac{1}{2}\phi) / \rho I t \quad (24)$$

where ω is the angular speed at which the crystal is turned through the Bragg reflection position, i_ϕ is the total energy of the reflected x-rays entering the ionization chamber, I is the energy per unit time per unit area penetrating the crystal, and t is the thickness of the slab of crystal.¹⁹ According to the classical theory of reflection of x-rays from a mosaic crystal¹⁹

$$r/\rho = \frac{1}{2} \cdot \frac{\rho N^2}{W^2} \cdot \lambda^3 F^2 \cdot \frac{e^4}{m^2 c^4} \cdot \frac{1 + \cos^2 \phi}{\sin \phi \cos \frac{1}{2}\phi} \quad (25)$$

From Eq. (25) we may obtain an expression for F^2/Z . Upon substituting this expression for F^2/Z , and also the right side of Eq. (23) for S_{gas} and for $S_{\text{cryst.}}$ in Eq. (21), we note that the expression $(NZ/W) \cdot (e^4/m^2c^4) \cdot (1 + \cos^2 \phi)/2$ factors out, leaving us with

$$(s/\rho)_{\text{gas}} = (s/\rho)_{\text{cryst.}} + \frac{W \sin \phi \cos \frac{1}{2}\phi}{\lambda^3 \rho N} \cdot (r/\rho)_{\text{cryst.}} \quad (26)$$

Now in a simple cubic crystal the principal grating space d is given by

$$d^3 = W/\rho N. \quad (27)$$

This equation together with Bragg's law

$$n\lambda = 2d \sin \frac{1}{2}\phi \quad (28)$$

gives

$$\lambda^3 \rho N / W = (8 \sin^3 \frac{1}{2}\phi) / n^3 \quad (29)$$

so that Eq. (26) reduces to

$$(s/\rho)_{\text{gas}} = (s/\rho)_{\text{cryst.}} + (n^3/4) \cdot \cot^2 \frac{1}{2}\phi \cdot (r/\rho)_{\text{cryst.}} \quad (30)$$

¹⁷ E. O. Wollan, Phys. Rev. **37**, 862 (1931).

¹⁸ G. G. Harvey, Phys. Rev. **38**, 593 (1931).

¹⁹ See A. H. Compton, *X-Rays and Electrons*, pp. 125-127.

This relation contains only experimental quantities. It contains no such quantities as Avogadro's number, the atomic weight and number of the scatterer, the charge and mass of the electron, or the wave-length of the x-rays. In this present paper we have derived Eq. (30) by means of an extension of Thomson's classical theory of the scattering of x-rays. We have made use of such theoretical concepts as the charge and mass of the electron and the wave-length of x-rays, yet in the final equation all quantities connected with these concepts have cancelled out and we are left with a relation between experimental magnitudes such as angles, densities, thickness, distances, electrometer deflections, and speed of rotation of the crystal. Without any knowledge of the theory of the scattering or reflection of x-rays the relation expressed by Eq. (30) could have been established by means of experimental measurements on the diffuse scattering of x-rays from (say) argon and sylvine together with measurements on the reflecting power of the crystal for x-rays. The quantity n of Eq. (30) may be considered as a pure number obtained experimentally by counting. Hence the relation expressed by Eq. (30) may be called an empirical relation. Of course it is understood that the experimenter would use x-rays of the same hardness (perhaps Barkla's characteristic rays from a metal like copper or molybdenum) for the crystal as for the gas.

§5. DIGRESSION ON PHILOSOPHY

For convenience we shall for the moment speak of Eq. (21) as a theoretical relation because the numerical values of each of the S 's and of the F are obtained by dividing an experimental quantity by quantities which are introduced by the Thomson theory as for instance in Eq. (23). We have shown how the theoretical relation Eq. (21) may be replaced by the empirical relation Eq. (30) which contains no vestige of the Thomson theory. In his physical philosophy, the author inclines to the operational viewpoint of Bridgman.²⁰ Further, the author supports the view that physical laws express relations between pointer readings made on gross (macroscopic) instruments. Eq. (30) is such a relation. The literature of physics abounds in theoretical relations of the type of Eq. (21). Just as it has been possible to replace the theoretical Eq. (21) by the empirical Eq. (30), so the author believes it is possible to replace other theoretical relations of physics by empirical relations among gross physical magnitudes. The author believes that one purpose of theoretical physics is to facilitate the discovery of empirical relations among gross physical magnitudes. Concepts such as the charge and mass of an electron and the wave-length of x-rays are very useful but the author doubts that they represent reality in the world.²¹

§6. COMPLICATED CRYSTALS

The author has discussed the classical theory of the diffuse scattering of x-rays by solids⁶ in a paper to be referred to as Paper V. In a second paper

²⁰ P. Bridgman, *Logic of Modern Physics*.

²¹ G. E. M. Jauncey, *Modern Physics*, pp. 538-540.

the author together with Harvey has applied the theory to the diffuse scattering by simple cubic crystals consisting of atoms of one kind.⁷ We shall refer to this second paper as Paper VI.

Following the argument of Paper V we arrive at Eq. (13) of that paper. Up to this point in Paper V the electrons are not aggregated into atoms. If, instead of aggregating the electrons into atoms of one kind as was done in Paper I, we aggregate them into atoms of two kinds, which we shall distinguish by the subscripts 1 and 2, we obtain, in place of Eq. (22) of Paper V,

$$S = 1 + \frac{\nu_1(Z_1 - 1)f_1'^2/Z_1 + \nu_2(Z_2 - 1)f_2'^2/Z_2}{\nu_1Z_1 + \nu_2Z_2} \quad (31)$$

$$+ \{1/n(\nu_1Z_1 + \nu_2Z_2)\} \sum'' \sum'' \iint p_r p_s \cos k(z_r - z_s) dz_r dz_s$$

where ν_1 and ν_2 are the respective numbers of the atoms of kinds 1 and 2 in a molecule of the solid and n is the number of molecules in the scattering speck. Now, distinguishing between the rapidity of the orbital motions of the electrons in the atoms and the comparative slowness of the heat motions of the atoms about their equilibrium centers as is done on pages 1200 and 1201 of Paper V, we obtain, in place of Eq. (31) of Paper V,

$$S = 1 + \frac{\nu_1(Z_1 - 1)f_1'^2/Z_1 + \nu_2(Z_2 - 1)f_2'^2/Z_2}{\nu_1Z_1 + \nu_2Z_2} \quad (32)$$

$$+ \{1/n(\nu_1Z_1 + \nu_2Z_2)\} \cdot \{F_1^2X_{11} + F_1F_2X_{12} + F_2^2X_{22}\}$$

where the X 's are double summations of cosines. The problem is now to determine the X 's for a crystal.

Following the argument of Paper VI, Eq. (4) of that paper is replaced by

$$I = \{Z_1 \sum \sum \sum \cos kw_{pqr} + Z_2 \sum \sum \sum \cos kw_{pqr}\}^2 \quad (33)$$

$$+ \{Z_1 \sum \sum \sum \sin kw_{pqr} + Z_2 \sum \sum \sum \sin kw_{pqr}\}^2$$

where the first triple summation in each set of braces $\{ \}$ refers to atoms of kind 1 and the second triple summation to atoms of kind 2. Let us consider one of the single summations, say, $\sum \cos kw_{pqr}$ where the summation is with respect to p , so that we may write it as $\sum \cos kw_p$. The quantity w_p is the perpendicular from a point on a lattice line of the crystal upon the reference plane.^{6,7} The lattice points on the line are either such that consecutive points are at equal distances from each other or can be separated into sets of points such that in each set consecutive points are at equal distances from each other. One of these alternatives is true even when the axes of the crystal are not rectangular and when the consecutive atoms along a lattice line are not equally spaced. Hence either $\sum \cos kw_p$ has a value given by Eq. (7) of Paper VI or can be broken up into a small number of summations each of which has a value given by this equation. Proceeding to the summations with respect to

q and r we arrive at a result similar to Eq. (11) of Paper VI. Now, except for particular values of $k \{ = (4\pi \sin \frac{1}{2}\phi)/\lambda \}$, the right side of Eq. (11) of Paper VI is of the order unity. As in Paper VI, we divide by the total number of atoms in the speck of scattering matter and find S to be of the order of 10^{-17} if we are dealing with a speck of crystal of linear dimensions, say, 0.1 mm. The order 10^{-17} may be called zero, so that $S=0$ for a speck of crystal consisting of point atoms located exactly and permanently at the lattice points of the crystal. Now, referred to Eq. (32), S must become zero for point atoms located at lattice points—that is, for $f_1' = F_1 = Z_1$ and $f_2' = F_2 = Z_2$. Hence, substituting these values in the right side of Eq. (32) and rearranging, we obtain

$$(n\nu_1 + X_{11})Z_1^2 + X_{12}Z_1Z_2 + (n\nu_2 + X_{22})Z_2^2 = 0. \quad (34)$$

Since X_{11} , X_{12} , and X_{22} are constants determined only by the geometrical make-up of the crystal and do not depend on Z_1 and Z_2 and since also Eq. (34) holds for any values of Z_1 and Z_2 , this equation is an identity. Hence

$$X_{11} = -n\nu_1, \quad X_{12} = 0, \quad \text{and} \quad X_{22} = -n\nu_2. \quad (35)$$

Substituting in Eq. (32) and eliminating f' by means of Eq. (10), we obtain

$$S_{\text{class.}} = \left\{ 1 - \frac{\nu_1 f_1'^2/Z_1 + \nu_2 f_2'^2/Z_2}{\nu_1 Z_1 + \nu_2 Z_2} \right\} + \left\{ \frac{\nu_1 (f_1^2 - F_1^2) + \nu_2 (f_2^2 - F_2^2)}{\nu_1 Z_1 + \nu_2 Z_2} \right\}. \quad (36)$$

The extension of this formula to the scattering by crystals consisting of more than two kinds of atoms is obvious. Woo's method of taking account of the Compton effect gives Eq. (4) together with

$$S_{\text{incoh.}} = 1 - \left(\sum_r \nu_r f_r'^2/Z_r \right) / \sum_r \nu_r Z_r \quad (37)$$

and

$$S_{\text{coh.}} = \left(\sum_r \nu_r (f_r^2 - F_r^2) \right) / \sum_r \nu_r Z_r \quad (38)$$

where the subscript r refers to the r th type of atom in a molecule of the crystal.

In conclusion it should be noted that the validity of Eq. (36) and also of Eqs. (37) and (38) for the diffuse scattering from a complicated crystal rests upon the validity of the same simplifying assumptions as were made in Paper V in the derivation of Eq. (16) of the present paper for a simple cubic crystal consisting of atoms of one kind. The first simplifying assumption is that expressed by Eq. (14) of Paper V in which it is assumed that the probability function for each electron is symmetrical about a reference plane (see Paper V) through the nucleus. This may not be the case in certain types of crystals. This assumption of symmetry is back of Eq. (26) of Paper V. Then, again, the assumption of symmetry in the thermal vibrations of the atoms of the crystal about their respective lattice points is back of Eq. (29)

of Paper V. In section 3 of the present paper we have seen that the electron distribution about the center of an atom of a crystal is probably a function of the temperature. At absolute zero the probability of an electron in an atom of sylvine being in a volume element dv is not only a function of the distance r of dv from the nucleus but also of the direction of the line joining dv and the nucleus with respect to the axes of the crystal. This will affect the f values for the atoms of the crystal. Above absolute zero it seems from the evidence given in §3 that the function of the direction approaches a constant as the temperature increases, so that at high temperatures the electron distribution about the nucleus of an atom of sylvine is a function of the distance r alone as is the case in an atom of argon.

Mass Ratio of the Boron Isotopes from the Spectrum of BO

By F. A. JENKINS* AND ANDREW MCKELLAR
Department of Physics, University of California

(Received September 20, 1932)

Wave number data. New measurements are made of the rotational structure of the α bands of BO, and the wave numbers of the lines in the ${}^2\Pi_{1/2}$, ${}^2\Sigma$ component up to about $J=20$ are tabulated for the (0, 0), (0, 1), (0, 2), (1, 0), (1, 1), (1, 2), (2, 0), (3, 0), and (4, 0) bands of both the $B^{11}O$ and $B^{10}O$ systems. The ${}^2\Pi_{1/2}$, ${}^2\Sigma$ component of (5, 0) is also measured for $B^{11}O$ and the ${}^2\Pi_{3/2}$, ${}^2\Sigma$ component of (1, 0) for $B^{11}O$ and $B^{10}O$.

Vibrational isotope effect. Values of ΔG_v are computed by least-squares methods, and from the ratio $\Delta G_v^i/\Delta G_v^e$, the isotopic mass coefficient $\rho = (\mu/\mu^i)^{1/2}$ is found to be 1.02908 ± 0.00003 , from the data on the ${}^2\Sigma$ state, and 1.02913 ± 0.00004 , from that on ${}^2\Pi_{1/2}$. The latter figure is less trustworthy than the former, because of the presence of perturbations in the upper state. The mass-spectrograph measurements of Aston give $\rho = 1.02908 \pm 0.00003$. The relation $\rho = x_e^i/x_e$ is verified to within the probable error, one part in 500. Improved values are obtained for the vibrational constants of the ${}^2\Sigma$ state, while for the ${}^2\Pi_{1/2}$ state, the equations $\Delta G_v = 1260.415 - 21.870(v' + \frac{1}{2})$ and $\Delta G_v^i = 1297.130 - 23.228(v' + \frac{1}{2})$ are considered to give the constants least influenced by perturbation effects.

Rotational isotope effect. From the rotational term-differences, the constants B_v and α are computed, also by least squares. The equations $B_v'' = 1.7803 - 0.01648(v'' + \frac{1}{2})$, $B_v'^i = 1.8850 - 0.01772(v'' + \frac{1}{2})$, $B_{v-1/2}^i = 1.4277 - 0.0196(v' + \frac{1}{2})$, and $B_{v-1/2}^e = 1.5115 - 0.0211(v' + \frac{1}{2})$ give values of $\rho^2 = B_v^i/B_v$ and $\rho^2 = \alpha_e^i/\alpha_e$ which yield values of ρ equal to those obtained from the vibrational constants to within the probable error, one part in 4000 for the B_v 's and one in 100 for the α_e 's. A perturbation is found in the rotational levels of ${}^2\Pi_{1/2}^{(4)}$, which reaches its maximum at $J' = 13\frac{1}{2}$. It is caused by the crossing of these levels by those of ${}^2\Sigma^{(17)}$, and affects only one component of the Λ -doublets, as expected. The Λ -doubling is investigated, and its constants computed.

Electronic isotope effect The spin coupling constant, A , is evaluated by the 1, 0 band, and found to be the same for $B^{11}O$ and $B^{10}O$, having the value 122.36 ± 0.03 cm^{-1} . The origins of the two isotopic band systems, ${}^2\Pi_{1/2}$, ${}^2\Sigma$, are found to be $\nu_2^e = 23,958.85 \pm 0.05$, $\nu_2^e = 23,959.18 \pm 0.06$, giving an electronic shift of 0.33 ± 0.08 cm^{-1} , the $B^{10}O$ origin being displaced toward the violet.

INTRODUCTION

MANY verifications of the theory of the isotope effect in band spectra¹ have established the fundamental correctness of the theory. They have also led to the discovery of new isotopes of low abundance. The frequencies of the band lines of a suspected isotopic molecule can be predicted with great certainty. The possibility of reversing the usual procedure, and of computing accurately the relative masses of isotopic atoms from the observed frequen-

* Fellow of the John Simon Guggenheim Memorial Foundation, at present in the Physical Institute, Utrecht.

¹ F. W. Loomis, Bull. Nat. Res. Council 57, 250 (1926). R. Mecke, Geiger and Scheel's Handbuch der Physik 21, 565-573 (1929).

cies was first explicitly mentioned by Giauque,² although of course it was implied in Mulliken's original work.³ Thus far the only case in which data of sufficient accuracy and completeness were available has been the atmospheric bands of oxygen, from which the mass ratio $O^{18}:O^{16}$ has now been found by Babcock and Birge⁴ with an apparent accuracy of one part in 100,000. Since the oxygen isotopes have not yet been observed with the mass-spectrograph,^{4a} the band-spectrum method is the only one at present available for determining the atomic weights of O^{18} and O^{17} .

It therefore appears highly desirable to apply this method to an element for which the isotopic masses have already been found by Aston's precision mass-spectrograph. This would allow us to decide whether the theory of the isotope effect is sufficiently correct in its finer details to be reliable in such an exacting application. For this purpose the most accurate results are obtained in the case of a light element where the proportional difference in mass of the isotopes is large. Boron and lithium are especially suitable, and in the present work it will be shown that the spectrum of BO gives satisfactory agreement with Aston's values for the mass-ratio $B^{11}:B^{10}$. Work on the $Li^7:Li^6$ ratio from the Li_2 bands is now in progress.

The BO spectrum excited in active nitrogen was used by Mulliken in his first and most accurate test of the isotope effect.⁵ Of the three band systems in this spectrum, the α system is the most favorable for precise work, because it occurs at longer wave-lengths where an advantageous ratio of wave-length interval to frequency interval exists. The rotational structure of these bands was first shown by one of us⁶ to be that of a $^2\Pi, ^2\Sigma$ transition, in which the $^2\Pi$ level is inverted and constitutes a good example of the case *a* type of spin coupling. The complete experimental material was not given in this article, because further measurements, particularly of the bands of the less abundant isotopic molecule $B^{10}O$, were anticipated. In the meantime Scheib⁷ has published extensive measurements of four bands of the α system as developed in the arc. Because of the higher temperature, many more rotational lines of each band are observed than in active nitrogen. All of Scheib's measurements concern the bands of the more abundant isotope, $B^{11}O$, since none of the $B^{10}O$ bands were identified in his work. Furthermore, the data given by Scheib for the (0,1), (0,2), (0,3) and (0,4) bands, while they suffice for the determination of the molecular constants of the lower, $^2\Sigma$ state, do not

² W. F. Giauque, *Nature* **124**, 127 (1929).

³ R. S. Mulliken, *Phys. Rev.* **25**, 119 (1925).

⁴ H. D. Babcock and R. T. Birge, *Phys. Rev.* **37**, 233A (1931). See also the preliminary account and discussion given by Birge in *Trans. Farad. Soc.* **25**, 718 (1929). In the work of Mecke and Wurm, *Zeits. f. Physik* **61**, 37 (1930), the data were insufficient, and the methods not sufficiently rigorous, to yield a result of much significance.

^{4a} F. W. Aston, *Nature* **130**, 21, July 2 (1932). Here is recorded the observation of the oxygen isotopes O^{17} and O^{18} by the mass-spectrograph and their abundance is estimated but no accurate mass determinations are made.

⁵ R. S. Mulliken, *Phys. Rev.* **25**, 259 (1925).

⁶ F. A. Jenkins, *Proc. Nat. Acad. Sci.* **13**, 496 (1927).

⁷ W. Scheib, *Zeits. f. Physik* **60**, 74 (1930).

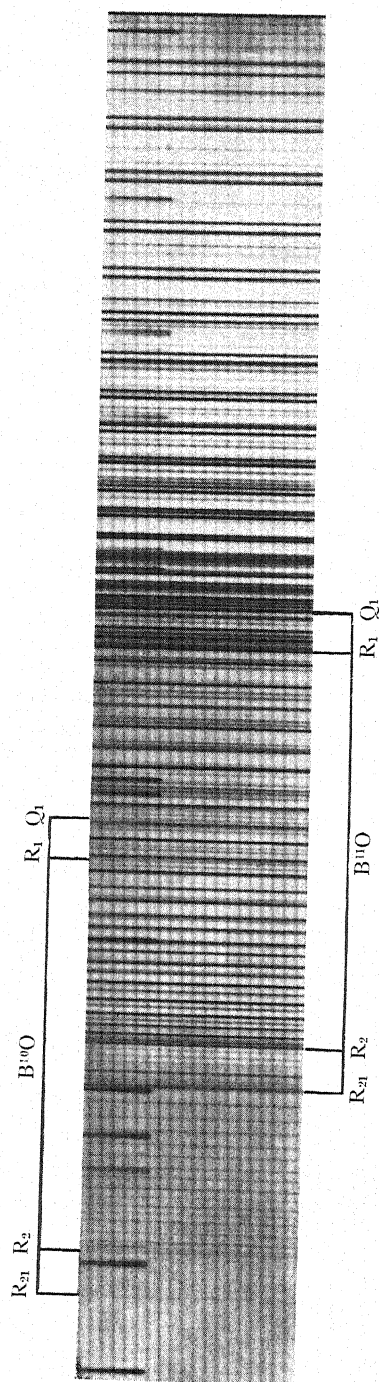


Fig. 1. The 2, 0 band of the α system of BO. First order of the 21-foot grating. The origin of the fainter, $B^{10}O$, band lies 8.876 Å further to the violet (i.e., to the left) in this case, and its rotational structure is seen to be almost an exact replica of that in the $B^{10}O$ band, but on a slightly larger scale.

yield all the constants of the $^2\Pi$ state, because these bands involve only $v' = 0$. Hence the present article, besides giving the first measurements on the $B^{10}O$ system, also supplements Scheib's data for the upper state of the $B^{10}O$ system.

EXPERIMENTAL DATA

The spectrograms used in our analyses have already been briefly described in connection with the preliminary work mentioned above.⁶ For a source, BCl_3 vapor was mixed with a stream of flowing active nitrogen containing traces of oxygen. The spectrum was photographed in the first and second orders of the Harvard 21-foot grating of 120,000 lines, which is mounted on the Paschen system. Double exposures of the iron arc spectrum were used to insure correct placing of the standards.

These plates have been completely remeasured with a Société Gènevoise comparator. Independent measurements of the same band gave results differing on the average by less than 0.01 cm^{-1} . For the purpose in hand, it was not necessary or desirable to measure all the lines of each band, since an analysis of the $^2\Pi_{1/2}$, $^2\Sigma$ component only will give the required data. Also this sub-band is much freer from blends than the other, particularly for the fainter

TABLE I. 1, 0 band.

K''	R_{21} $\lambda 4014.962$	R_2 $\lambda 4017.087$	R_2^i $\lambda 4012.781$	Q_2	Q_2^i	P_2	P_2^i
0					24,911.64		
1	24,894.06	14,886.66	24,913.36	24,882.42			
2	896.66	886.66	913.36	879.51	905.90		
3	898.36	885.72	912.46	875.88	901.98		
4	899.48	884.14	910.75	871.47	897.30	24,861.83	
5	899.84	881.83	908.27	866.33	891.88	853.80	
6	899.84	878.71	905.04	860.44	885.72	845.16	24,869.41
7	898.36	874.92	900.94	853.80	878.71	835.81	859.47
8	896.66	870.35	896.15	846.38	870.77	825.60	848.77
9	894.06	865.02	890.50	838.24	862.14	814.71	837.00
10	890.75	858.94	884.14	829.34	852.67	803.07	824.87
11	886.66	852.10	876.79	819.70	842.50	790.66	811.64
12	881.83	844.50	868.78	809.31	831.51	777.47	797.93
13	876.26	836.15	859.92	798.16	819.70	763.54	783.06
14	870.25	827.05	850.27	786.30	807.10	748.84	767.42
15		817.19	839.83	773.61	793.75	733.52	750.99
16		806.57	828.61	760.15	779.34	717.32	733.52
17		795.24	816.55	745.98	764.48	700.31	715.99
18		783.06	803.54	731.15	748.84	682.77	
19		770.16	790.09	715.45	732.18	664.33	
20		756.58	775.56	698.99	714.75	645.16	
21		742.08		681.85	696.36	625.26	
22		726.99		663.91		604.59	
23		710.75		645.16		583.07	
24		694.28		625.71		560.91	
25		676.82		605.54		537.97	
26		658.43		584.54		514.25	
27		639.47		562.82		489.74	
28		619.77		540.24		464.59	
29		599.14		517.01			
30				492.68			
31				467.79			
32				442.10			

TABLE I. (Continued). 1, 0 band

K''	R_1 $\lambda 4035.467$	R_1^i $\lambda 4031.039$	Q_1 $\lambda 4037.415$	Q_1^i $\lambda 4033.112$	P_1	P_1^i	P_{12}
0	24,764.96						
1	768.27		24,761.36	24,787.78			
2	770.94		761.19	787.78	24,754.45	24,780.54	
3	772.50	24,799.63	760.15	786.62	750.53	776.54	
4	773.31	800.52	758.23	784.55	745.98	771.52	
5	773.31	800.52	755.55	781.74	740.50	765.77	24,728.19
6	772.50	799.63	752.07	778.02	734.22	759.14	719.38
7	770.94	798.16	747.75	773.31	727.27	751.49	709.54
8	768.63	795.24	742.65	767.97	719.38	743.31	698.96
9	765.43	792.05	736.72	761.63	710.75	734.22	687.60
10	761.36	787.78	730.01	754.45	701.31	724.15	675.38
11	756.58	782.63	722.45	746.48	691.03	713.10	662.34
12	750.99	776.54	714.10	737.58	679.95	701.31	648.55
13	744.54	769.82	704.96	727.87	668.04	688.93	633.97
14	737.30	762.00	695.02	717.32	655.39	675.38	618.57
15	729.27	753.55	684.23	705.88	641.90	661.02	602.44
16	720.40	744.03	672.67	693.55	627.61	645.85	585.34
17	710.75	733.52	660.29	680.41	612.53	629.88	567.50
18	700.31	722.45	647.14	666.36	596.59	612.92	548.89
19	688.93	710.75	633.12	651.53	579.87	595.21	529.45
20	676.82	697.61	618.34	635.76	562.37	576.48	509.24
21	663.91	684.23	602.74	619.18	544.03	557.10	488.23
22	650.18	669.28	586.32	601.74	524.86	536.83	466.44
23	635.76		569.06	583.48	504.97	515.70	443.79
24	620.32		551.07		484.24		
25	604.32		532.23		462.68		
26	587.13		512.62		440.37		
27	569.49		492.18		417.24		
28	551.07		470.90		393.25		
29			448.90				
30			426.06				
31			402.37				
32			377.92				

TABLE I. (Continued). 1, 1 band.

K''	R_{21} $\lambda 4339.369$	R_2 $\lambda 4341.931$	R_2^i $\lambda 4346.957$	Q_2	Q_2^i	P_2
0				23,024.05	22,997.43	
1	23,031.71	23,024.78	22,998.16	020.45	993.48	
2	034.49	024.78	998.16	017.55	990.50	
3	036.50	024.05	997.43	014.12	986.73	23,007.27
4	037.86	022.57	995.80	009.91	982.18	000.20
5	038.37	020.45	993.48	004.92	977.23	22,992.34
6	038.37	017.55	990.50	22,999.23	971.08	983.96
7	037.46	013.96	986.73	992.83	964.29	974.80
8	035.93	009.61	982.18	985.65	956.78	964.89
9	033.66	004.56	976.81	977.82	948.48	954.27
10	030.67	22,998.82	970.70	969.25	939.31	942.95
11	026.96	992.34	963.83	959.97	929.60	930.89
12	022.57	985.13	956.24	949.99	919.04	918.17
13	017.55	977.23	947.92	939.31		
14	011.50	968.62	938.77	927.84		
15	004.92	959.25	928.88	915.70		
16	22,997.43	949.16	918.17			
17	989.42	938.33				
18	980.64	926.81				
19	971.08	914.55				
20	960.89					
21	949.99					
22	938.33					

TABLE I. (Continued). 1, 2 band.

K''	R_{21} $\lambda 4715.525$	R_2 $\lambda 4718.660$	R_2^i $\lambda 4736.250$	Q_2	Q_2^i	P_2
0				21,185.85	21,107.19	
1	21,193.24	21,186.55	21,107.87	182.20	103.85	
2	196.20	186.55	107.87	179.47		21,175.35
3	198.39	185.85	107.19	175.96	096.63	168.95
4	199.40	184.56	105.75	171.87	092.28	162.29
5	200.64	182.51	103.85	167.02	087.28	154.61
6	200.64	179.86	100.84	161.52	081.28	146.37
7	199.99	176.51	097.30	155.33	074.94	137.33
8	198.82	172.46	092.97	148.49	067.59	127.71
9	196.84	167.73	088.05	140.95		117.40
10	194.11	162.29	082.38	132.70		106.38
11	190.81	156.18	075.88	123.80		094.70
12	186.55	149.38		114.21		082.38
13	182.20	141.91		103.85		068.97
14	176.51	133.72		092.97		
15	170.42	124.87		081.28		
16	163.61	115.26				
17	156.18	105.04				
18		094.07				
19		082.38				

TABLE I. (Continued). 0,0 band.

K''	R_{21}	R_2 $\lambda 4227.480$	R_2^i	Q_2	Q_2^i	P_2
0				23,646.02	23,637.42	
1		23,648.13		643.86	634.99	
2		648.13		641.02	632.03	
3		647.40	23,638.71	637.42	628.20	
4		646.02	637.42	633.19	623.77	
5	<i>not observed</i>	643.86	634.99	628.20	618.43	23,615.57
6		641.02	632.03	622.50	612.45	606.98
7		637.42	628.20	616.09	605.66	
8		633.19	623.77	609.00	598.13	587.84
9		628.20	618.43	601.12	589.93	577.27
10		622.50	612.45	592.60	580.81	565.87
11		616.09	605.66	583.31	571.02	553.85
12		609.00	598.13	573.35	560.47	540.93
13		601.12	589.93	562.67		527.62
14		592.60	580.81	551.23	537.20	
15		583.31	571.02	539.14	524.27	
16		573.35	560.47	526.33		
17		562.67				
18		551.23	537.20			
19		539.14	524.27			
20		526.33				

TABLE I. (Continued). 0,1 band.

K''	R_{21} $\lambda 4585.702$	R_2 $\lambda 4588.759$	R_2^i $\lambda 4601.883$	Q_2	Q_2^i	P_2
0	21,789.96			21,783.90		
1	793.32	21,786.30	21,724.17	781.94	21,719.77	21,775.06
2	796.15	786.30	724.33	779.22	716.84	768.70
3	798.41	785.73	723.64	775.75		761.73
4	799.89	784.45	722.40	771.59	708.64	754.11
5	800.83	782.50	720.35	766.76	703.80	745.83
6	800.83	779.84	717.50	761.27	697.84	736.86
7	800.42	776.54	714.06	755.08	691.33	727.23
8	799.17	772.52	709.86	748.26	684.09	716.84
9	797.31	767.83	704.90	740.74	676.22	705.83
10	794.76	762.51	699.28	732.52		694.20
11	791.48	756.44	692.89	723.64		681.78
12	787.56	749.71	685.78	714.06		
13		742.31	678.04	703.80		
14		734.21		692.89		
15		725.45		681.29		
16		715.94				
17		705.83				
18		694.99				
19		683.45				

TABLE I. (Continued). 0,2 band.

K''	R_{21} $\lambda 5007.846$	R_2 $\lambda 5011.650$	R_2^i $\lambda 5040.468$	Q_2	Q_2^i	P_2
0		19,947.96	19,833.91	19,943.72	19,829.65	19,936.67
1		947.96	833.91	940.82		
2	19,958.11	947.55	833.35	937.49		
3	960.39	946.48	832.34	933.46		923.60
4	961.93	944.61	830.45	928.90		916.22
5	962.84	942.16	827.85	923.60		908.17
6	963.12	938.94	824.61	917.66	802.01	899.35
7	962.84	935.34		911.05	794.98	889.94
8	961.93	930.97		903.81	787.37	879.99
9	960.39	925.93	810.87	895.96	779.07	869.29
10	958.11	920.24	804.89	887.44		857.97
11	955.26	913.91	798.19	878.25		845.90
12	951.69	906.92	790.86	868.43	749.96	833.35
13		899.35	782.81	857.97		
14		891.05	774.06	846.84		
15		882.09	764.69	835.09		
16		872.48	754.55			
17		862.18				
18		851.33				
19						

TABLE I. (Continued). 2,0 band.

K''	R_{21} $\lambda 3828.047$	R_2 $\lambda 3829.857$	R_2^i $\lambda 3820.962$	Q_2	Q_2^i	P_2
0				26,101.49		
1		26,103.26	26,164.03	099.18	26,159.69	
2	26,112.75	103.26	164.03	096.22	156.58	
3	114.48	102.18	162.84	092.45	152.56	26,085.55
4	115.61	100.38	161.06	087.91	147.78	078.34
5	115.61	097.91	158.36	082.61	142.09	070.30
6	115.13	094.56	154.79	076.51	135.68	061.47
7	113.73	090.45	150.43	069.60	128.39	051.82
8	111.40	085.55	145.23	061.96	120.26	041.42
9	108.57	079.88	139.25	053.45	111.40	030.19
10	104.81	073.38	132.38	044.23	101.49	018.25
11	100.38	066.13	124.64	034.16	090.86	005.47
12		058.10	116.14	023.43	079.41	25,991.96
13		049.22	106.77	011.75	067.10	977.63
14		039.58	096.51	25,999.35	053.95	
15		029.14	085.55	986.19	039.94	
16		017.91	073.38		025.08	
17		005.91	060.65		009.26	
18		25,993.03	047.15		25,992.42	
19		979.45	032.79			
20			017.53			
21			001.43			

TABLE I. (Continued). 3,0 band.

K''	R_{21} $\lambda 3660.631$	R_2 $\lambda 3662.205$	R_2^i $\lambda 3649.691$	Q_2	Q_2^i	P_2
0						
1	27,304.88	27,298.22	27,391.80	27,294.37	27,387.41	
2	307.45	298.22	391.80	291.30	384.25	
3	309.14	297.12	390.50	287.44	380.23	27,280.77
4	309.95	295.14	388.37	282.77	375.31	273.25
5	309.95	292.38	385.56	277.29	369.60	265.18
6	309.14	288.85	381.78	271.00	362.97	255.95
7	307.45	284.46	377.79	263.88	355.33	246.46
8	304.52	279.21	371.59	255.95	346.98	235.70
9	301.52	273.25	365.16	247.14	337.64	224.22
10	297.12	266.28	357.87	237.54	327.44	211.91
11	292.38	258.70	349.67	227.13	316.36	198.88
12		250.13	340.61	215.89	304.52	184.89
13		240.76	330.65	203.79	291.44	
14		230.63	319.96	190.90	277.84	
15		219.57	308.20	177.03	263.42	
16		207.74			247.76	
17		195.06			231.57	
18		181.60	267.95		214.43	
19			252.58		196.40	
20			236.45			
21			219.57			
22			201.64			
23			183.44			

TABLE I. (Continued).
4,0 band 5,0 band

K''	R_2 $\lambda 3511.222$	R_2^i $\lambda 3495.848$	Q_2	Q_2^i	R_2	Q_2
0						29,621.18
1	28,472.01	28,597.22				617.95
2	472.01	97.22	28,465.22	28,590.06	29,624.75	613.87
3	470.71	95.65	461.25	85.58	623.49	608.93
4	468.66	93.40	456.45	80.41	621.18	603.11
5	465.71	90.41	450.80	74.50	617.95	596.43
6	461.90	86.15	444.31	67.61	613.87	588.87
7	457.20	81.38	436.91	59.80	608.93	580.29
8	451.70	75.39	428.70	51.01	603.11	570.89
9	445.31	68.60	419.62	41.45	596.43	560.61
10	438.05	60.86	409.61	30.76	588.87	549.41
11	430.00	52.21	398.80	19.33	580.29	537.36
12	421.08	42.77	387.16	06.98	570.89	524.31
13	411.75	32.20	374.61	28,493.69	560.61	
14	400.10	20.83	361.18		549.41	
15	388.60	08.58			537.36	
16	376.20				524.31	
17	362.98					

isotopic system. This will be evident from the enlargement, Fig. 1. All the four branches of the ${}^2\Pi_{1/2}$, ${}^2\Sigma$ sub-band, which are designated in order R_{21} , R_2 , Q_2 , and P_2 , could be accurately measured in most cases for the stronger system, $B^{11}O$, but the R_{21} branch (and sometimes the P_2) of $B^{10}O$ was too faint to measure. To get the constants of the lower state, the two progressions $v'=0$ and $v'=1$ were measured from $v''=0$ to 2, while for the upper state four additional bands of the strong $v''=0$ progression, (2,0), (3,0), (4,0) and (5,0), were investigated. Of these ten bands, only 0,1 and 0,2 had been measured by Scheib. Our results are systematically lower by 0.21 cm^{-1} in the former band, and by 0.16 cm^{-1} in the latter. The possibility of a constant error of this magnitude in our measurements was eliminated by checking against the lines of the 0,9 β -band of NO and the boron doublet, $\lambda\lambda 2496.778$, 2497.733 (in the second order), which were present in the band source.

In Table I will be found the wave numbers in vacuum of all of the measured lines assigned to the various branches in these bands, with the wavelength in I.A. of the observed heads at the top of the appropriate columns. The column headings for the less intense system, that of $B^{10}O$, carry the superscript i . For 1,0 the low-frequency sub-band ${}^2\Pi_{1/2}$, ${}^2\Sigma$ was also measured and analyzed in order to find the constants of the ${}^2\Pi_{1/2}$ state and the electronic coupling coefficient, A . The 0,0 band was unsatisfactory for this purpose because it is fainter, and confused with the 3,2 band.

VIBRATIONAL ISOTOPE EFFECT

The vibrational terms of the two isotopic molecules may be represented⁸ by the following equation:

$$\begin{aligned}
 B^{11}O\ G &= \omega_e(v + \tfrac{1}{2}) - x_e\omega_e(v + \tfrac{1}{2})^2 + y_e\omega_e(v + \tfrac{1}{2})^3 + \dots \\
 B^{10}O\ G^i &= \omega_e^i(v + \tfrac{1}{2}) - x_e^i\omega_e^i(v + \tfrac{1}{2})^2 + y_e^i\omega_e^i(v + \tfrac{1}{2})^3 + \dots \\
 &= \rho\omega_e(v + \tfrac{1}{2}) - \rho^2x_e\omega_e(v + \tfrac{1}{2})^2 + \rho^3y_e\omega_e(v + \tfrac{1}{2})^3 + \dots,
 \end{aligned} \tag{1}$$

⁸ R. S. Mulliken, Phys. Rev. **25**, 125 (1925).

in which ρ^2 is the ratio of the reduced masses μ/μ^i . We shall use the superscript i to distinguish quantities pertaining to the less abundant molecule $B^{10}O$. The problem of finding the relative masses thus becomes one of evaluating as accurately as possible the constant ρ from the relation

$$\omega_e^i/\omega_e = \rho. \quad (2)$$

Other values of this constant, though much less accurate, can be found from the higher power term; since

$$x_e^i/x_e = \rho, \quad y_e^i/y_e = \rho^2. \quad (3)$$

From the spectrum we can evaluate the term-differences

$$\Delta G_v = \omega_e - 2x_e\omega_e(v + \frac{1}{2}) + 3y_e\omega_e[(v + \frac{1}{2})^2 + 1/12] + \dots \quad (4)$$

by finding the separation of the origins of two adjacent bands in a progression. This separation is best determined by a study of the combination differences of the type

$$\begin{aligned} R_2^{(0,0)}(K) - R_2^{(0,1)}(K) &= Q_2^{(0,0)}(K) - Q_2^{(0,1)}(K) = P_2^{(0,0)}(K) - P_2^{(0,1)}(K) \\ &= \Delta G_{1/2}'' - (B_0'' - B_1'')(K + \frac{1}{2})^2 + \dots \\ &= \Delta G_{1/2}'' - \alpha''(K + \frac{1}{2})^2 + \dots \end{aligned} \quad (5a)$$

$$\begin{aligned} R_2^{(1,0)}(K) - R_2^{(0,0)}(K) &= Q_2^{(1,0)}(K+1) - Q_2^{(0,0)}(K+1) \\ &= P_2^{(1,0)}(K+2) - P_2^{(0,0)}(K+2) \\ &= \Delta G'_{1/2} - (B'_{0,-1/2} - B'_{1,-1/2})(K + \frac{1}{2})^2 + \dots \\ &= \Delta G'_{1/2} - \alpha'(K + \frac{1}{2})^2 + \dots \end{aligned} \quad (5b)$$

in which the higher power terms can be shown to be negligible for all practical purposes. $B_{v,-1/2}$ represents the effective B_v for the component ${}^2\Pi_{1/2}$ of the upper state. These term-differences, which we shall refer to as ΔT , are fitted by least squares to a parabola having its vertex at $K = -\frac{1}{2}$. The constant term in this solution yields the best value of the vibrational term-difference ΔG , which is required. Fig. 2c shows by diagrams the relation of pairs of lines, connected by arrows, whose wave-number difference gives a single value of ΔT (and of ΔT^i) for the lower state. This will be clear from the term diagram in Fig. 2b.

The first step in the computation is obviously to prove from the experimental data that the vertex of the $\Delta T:K$ parabola actually does occur at $K = -\frac{1}{2}$ to within the error of the measurements. Fig. 2d shows the data from the R_2 branches of the 1,0 and 1,1 bands and their least squares solution in the form of Eq. (5a). By carrying through the solution, admitting a linear term in $(K + \frac{1}{2})$, a value of the constant term was obtained which differed from the first value by less than its probable error. This justifies the assumption that the vertex occurs at $K = -\frac{1}{2}$, an assumption made in obtaining all of the results discussed below. To show the extent to which Eq. (5a) is capable of representing the data, we give in Table II the results of the solution for $Q_2^{(0,0)}(K) - Q_2^{(0,1)}(K)$. This is a typical example from the

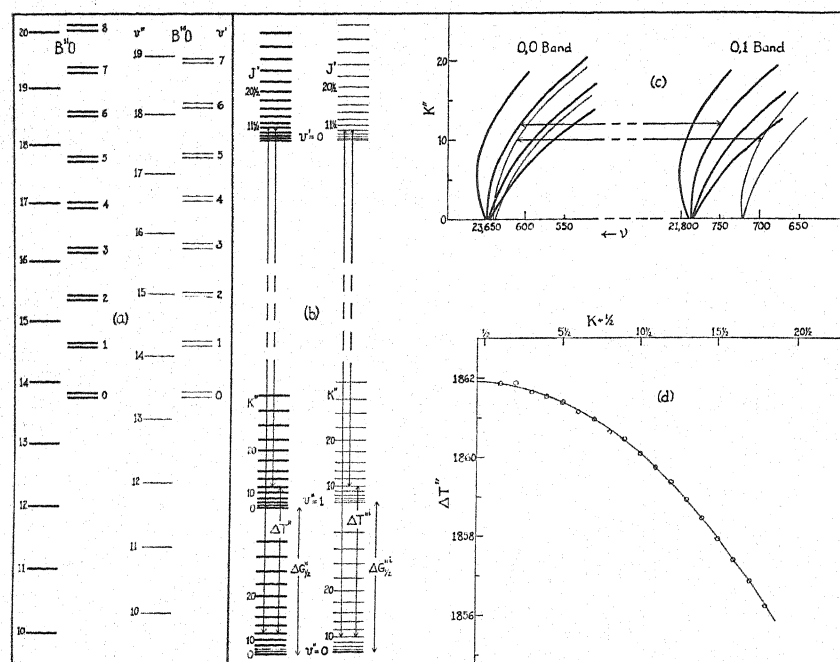


Fig. 2. (a) Some vibrational levels of the two isotopic molecules drawn to scale. The single levels on the left belong to the lower, $^2\Sigma$ state, and the double levels are $^2\Pi$. For $B^{18}O$, the $v''=17$ level of $^2\Sigma$ lies very close to $v'=4$ of $^2\Pi_{1/2}$, the upper component. This explains the observed perturbation in the $v'=4$ rotational levels (cf. Fig. 3 and text, p. 478). (b) Alternate rotational levels associated with $v''=0$ and 1 of $^2\Sigma$ and with $v'=0$ of $^2\Pi_{1/2}$. The difference in frequency of the two lines whose transitions are indicated by the long vertical arrows, $R_2^{(0,0)}$ (12) and $R_2^{(0,1)}$ (12), gives the term-difference $\Delta T''$ (12) in the lower state. As explained in the text, the various values of $\Delta T''$ and $\Delta T''_i$ are extrapolated to $\Delta T''(-\frac{1}{2})$, giving accurate values of the vibrational term-differences $\Delta G''$ and $\Delta G''_i$. (c) Fortrat diagrams of the $^2\Pi_{1/2}$, $^2\Sigma$ components of the 0, 0 and 0, 1 bands. Heavy curves represent branches of the $B^{18}O$ bands, and light curves those measured for $B^{16}O$. The arrows indicate the differences $\Delta T''$ (12) and $\Delta T''_i$ (10). (d) A typical $\Delta T'' : K + \frac{1}{2}$ parabola, derived from the R_2 branches of the 1, 0 and 1, 1 bands. Circles are observed values, while the curve is the least squares solution, which intersects the axis, $K + \frac{1}{2} = 0$, at the value of $\Delta G_{1/2}''$.

TABLE II. $\Delta T'' = \Delta G_{1/2}'' - (B_0'' - B_1'')(K + 1/2)^2 = 1861.937 - 0.01698(K + 1/2)^2$.

K''	$\Delta T''$ (Obs.)	$\Delta T''$ (Calc.)	O - C
1	1861.92	1861.899	+0.021
2	1861.80	1861.831	-0.031
3	1861.67	1861.729	-0.059
4	1861.60	1861.593	+0.007
5	1861.44	1861.423	+0.017
6	1861.23	1861.220	+0.010
7	1861.01	1860.982	+0.028
8	1860.74	1860.710	+0.030
9	1860.38	1860.404	-0.024
10	1860.08	1860.065	+0.015
11	1859.67	1859.691	-0.021
12	1859.29	1859.284	+0.006
13	1858.87	1858.842	+0.028
14	1858.34	1858.367	-0.027
15	1857.85	1857.857	-0.007

42 least squares solutions carried out in evaluating the various values of $\Delta G_v''$ and $\Delta G_v'$.

TABLE III. *Vibrational constants of the $^2\Sigma$ state.*

$B^{11}O$	Branch	Bands	$\Delta G_v''$	α''	Wt.
	R_2	0,0-0,1	1861.86 \pm 0.01	0.0164	19
	Q_2	0,0-0,1	1861.94 \pm 0.01	0.0170	15
	P_2	0,0-0,1	1861.92 \pm 0.04	0.0171	6
			Av. 1861.896 \pm 0.018		
	R_2	0,1-0,2	1838.37 \pm 0.01	0.0164	18
	Q_2	0,1-0,2	1838.37 \pm 0.01	0.0164	14
	P_2	0,1-0,2	1838.38 \pm 0.03	0.0162	8
			Av. 1838.375 \pm 0.002	Av. 0.01656 \pm 0.00013	
$B^{10}O$	R_2^i	0,0-0,1	1915.28 \pm 0.02	0.0189	11
	Q_2^i	0,0-0,1	1915.29 \pm 0.01	0.0173	6
			1915.286 \pm 0.003		
	R_2^i	0,1-0,2	1890.41 \pm 0.02	0.0179	11
	Q_2^i	0,1-0,2	1890.10 \pm 0.02	0.0138	3
			1890.343 \pm 0.078	0.01774 \pm 0.00082	
			$\omega_e = 1885.417 \pm 0.037$	$\omega_e^i = 1940.229 \pm 0.078$	$\rho = 1.02907$
			$x_e = 0.006238$	$x_e^i = 0.006428$	± 0.00004
					$\rho = 1.030$
$B^{11}O$	Branch	Bands	$\Delta G_v''$	α''	Wt.
	R_2	1,0-1,1	1861.90 \pm 0.01	0.0164	18
	Q_2	1,0-1,1	1861.94 \pm 0.01	0.0169	14
	P_2	1,0-1,1	1861.86 \pm 0.02	0.0160	9
			1861.903 \pm 0.015		
	R_2	1,1-1,2	1838.34 \pm 0.01	0.0164	19
	Q_2	1,1-1,2	1838.36 \pm 0.01	0.0164	14
	P_2	1,1-1,2	1838.33 \pm 0.03	0.0167	10
			1838.348 \pm 0.005	0.01641 \pm 0.00007	
$B^{10}O$	R_2^i	1,0-1,1	1915.27 \pm 0.02	0.0177	15
	Q_2^i	1,0-1,1	1915.40 \pm 0.06	0.0189	9
			1915.318 \pm 0.044		
	R_2^i	1,1-1,2	1890.36 \pm 0.03	0.0179	11
	Q_2^i	1,1-1,2	1890.29 \pm 0.04	0.0154	6
			1890.336 \pm 0.025	0.01770 \pm 0.00040	
			$\omega_e = 1885.458 \pm 0.031$	$\omega_e^i = 1940.300 \pm 0.092$	$\rho = 1.02909$
			$x_e = 0.006246 \pm 0.000006$	$x_e^i = 0.006438 \pm 0.000013$	± 0.00005
					$\rho = 1.031$
					± 0.002

Lower state

The $^2\Sigma$ state is the easiest and most satisfactory to deal with because it does not involve complicated interactions of electronic and rotational mo-

tions. That the spin doubling is negligible, even for large rotation, is shown by an examination of Scheib's results.⁹ Further advantages of the $^2\Sigma$ state over the $^2\Pi$ for the precise determination of ρ lie in the greater magnitude of ω_e , as well as in the fact that this is the normal state, and therefore should be free from perturbations.

Table III contains the results of the various solutions for $\Delta G_v''$, with the probable error of each computed from the residuals by the accepted least squares formulas.¹⁰ It will be noticed that the faint R_{21} branch has not been used at all, nor the P_2 branch in the case of $B^{10}O$. The mean values have been taken separately for the progressions $v'=0$ and $v'=1$, so that two independent evaluations of the vibrational constants are obtained. Computation of the probable errors of the mean $\Delta G_v''$ values based on their internal consistency¹⁰ (on the probable errors of the individual determinations of ΔG_v) showed that these are considerably smaller than the probable errors found from external consistency (determined from the deviation of the individual determinations from their mean). Therefore, following the recommendation of Birge,¹⁰ we have adopted the probable errors from external consistency even though these are based on such a small number of items. The items are then logically weighted according to the number of observations, or values of ΔT , used in the evaluation of each, rather than inversely as the squares of their probable errors. In this way the most consistent set of values of a given vibrational term-difference is obtained, as well as a conservative estimate of the probable error of the mean.

Following each set of results in Table III are given the ω_e and x_e calculated by Eq. (4). The data, involving as they do only $v''=0, 1$, and 2 , are not sufficient to determine the term $y_e\omega_e(v+\frac{1}{2})^3$ or higher powers. But these terms are usually negligibly small for the ground states of stable molecules, and in fact Mulliken's data on band heads shows no departure from a linear dependence of ΔG_v on v up to $v''=8$. Hence we obtain the constants on the assumption that these terms are zero. Our best values of ρ , from the ratio ω_e^4/ω_e , are listed in Table III. The values from x_e^4/x_e are much less accurate but agree to well within the probable error.

Upper state

In the determination of the vibrational constants for the $^2\Pi$ state, there are several complications not present in the $^2\Sigma$ state. In the first place, since the spin lies coupled to the figure axis by the field of the orbit, the electronic level is two-fold with a separation of about 122 cm^{-1} . Assuming no interaction of the spin with the molecular rotation, we could work exclusively with the one component, $^2\Pi_{1/2}$, $^2\Sigma$, as a separate band system. This procedure is largely justified, as will be shown below in the discussion of the rotational energy function. However, there are unknown additive constants,¹¹ such as

⁹ Cf. R. S. Mulliken and A. Christy, *Phys. Rev.* **38**, 87 (1931). We have also reexamined the data and find no evidence of an appreciable spin doubling.

¹⁰ R. T. Birge, *Phys. Rev.* **40**, 207 (1932).

¹¹ R. S. Mulliken, *Rev. Mod. Phys.* **2**, 114 (1930).

\overline{G}^2 and C_2 , in the energy function which, though small, cannot be corrected for in obtaining the true ΔG values. Finally, the most serious difficulty is the possibility of perturbations, which may affect the vibrational, as well as the rotational terms. These are known in the analogous band system of CN,¹² and are also found here, though to a lesser degree. Because of these draw-

TABLE IV. *Vibrational constants of the $^2\Pi$ state.*

$B^{10}O$	Branch	Bands	$\Delta G_v'$	α'	Wt.
$B^{11}O$	R_2	1,0-0,0	1238.58	0.0196	18
	Q_2	1,0-0,0	1238.53	0.0193	14
	P_2	1,0-0,0	1238.49	0.0181	7
			Av. 1238.545 \pm 0.016		
	R_2	2,0-1,0	1216.65	0.0196	18
	Q_2	2,0-1,0	1216.70	0.0200	15
	P_2	2,0-1,0	1216.67	0.0204	9
			1216.675 \pm 0.010		
	R_2	3,0-2,0	1195.08	0.0193	18
	Q_2	3,0-2,0	1195.10	0.0196	13
	P_2	3,0-2,0	1195.11	0.0195	8
			1195.095		
	R_2	4,0-3,0	1173.87	0.0194	11
	Q_2	4,0-3,0	1173.92	0.0200	13
			1173.896		
	R_2	5,0-4,0	1152.88	0.0195	10
	Q_2	5,0-4,0	1152.73	0.0193	11
			1152.799	0.01959	
$B^{10}O$	R_2^i	1,0-0,0	1273.93	0.0213	15
	Q_2^i	1,0-0,0	1273.87	0.0214	13
			1273.902 \pm 0.021		
	R_2^i	2,0-1,0	1250.66	0.0209	18
	Q_2^i	2,0-1,0	1250.69	0.0211	14
			1250.674 \pm 0.008		
	R_2^i	3,0-2,0	1227.83	0.0210	17
	Q_2^i	3,0-2,0	1227.81	0.0206	14
			1227.823		
	R_2^i	4,0-3,0	1205.426	0.0214	14
	Q_2^i	4,0-3,0	1205.329	0.0210	11
			1205.383	0.02111	
With only $\Delta G'_{1/2}$ and $\Delta G'_{11/2}$:					
$\omega_e = 1260.415 \pm 0.033$			$\omega_e^i = 1297.130 \pm 0.048$	$\rho = 1.02913$	
$x_e = 0.008676$			$x_e^i = 0.008954$	± 0.00004	
				$\rho = 1.032$	

¹² F. A. Jenkins, Y. K. Roots and R. S. Mulliken, Phys. Rev. 39, 16 (1932).

backs the resulting values of ρ are of little importance in bettering those already obtained. However, the analysis has been done since it gives fairly reliable values of the vibrational constants, and affords a check on the ρ already found from the lower state.

Our measurements include bands of the $v''=0$ progression up to $v'=5$ for $B^{11}O$, and $v'=4$ for $B^{10}O$. All of the values were computed from the ΔT parabolas of the type of Eq. (5b), using least squares in exactly the same way as for the lower state. The results are shown in Table IV. The probable errors of the individual ΔG_v 's have not been calculated because internal consistency is of little value in getting the probable error of the mean, as explained above. But the residuals were always examined, and where a trend was noted, the worst value or values were discarded, and a new solution made. In the solutions for $\Delta G'_{3\frac{1}{2}}$ and $\Delta G'_{4\frac{1}{2}}$ from the R_2 branch, the residuals

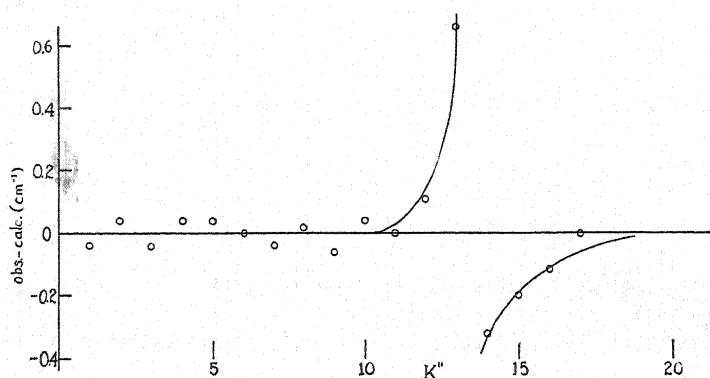


Fig. 3. Residuals of the ΔT parabola $R_2^{(4,0)} - R_2^{(3,0)}$ from the solution adopted. The large discontinuity in the curve at $K=13$ represents a perturbation in the rotational terms of the upper state.

grew suddenly large above $K=11$, showing the presence of a large perturbation in the R_2 branch of the 4,0 band. The Q_2 branch is perfectly regular. The perturbation reaches its maximum (0.66 cm^{-1}) at $J'=13\frac{1}{2}$ of the ${}^2\Pi_{1/2}$ state. Fig. 3 is a plot of the residuals from the final, adopted solution for $\Delta G'_{3\frac{1}{2}}$ (R_2 branch), and shows the usual form characteristic of a large perturbation.

This perturbation is obviously analogous to one of those occurring in the $v'=6$ levels of the ${}^2\Pi$ state in CN.¹² It results from the near equality of energy levels with the same J in the ${}^2\Pi$ and the lower ${}^2\Sigma$ states. When we computed the terms in these two states from the data already established, it was found that by far the closest approach of any two terms is ${}^2\Sigma^{(17)}$ to ${}^2\Pi_{1/2}^{(4)}$. The levels are drawn to scale in Fig. 2a, and one sees that the lowest ${}^2\Pi_{1/2}$ terms are far removed from the ${}^2\Sigma$ terms, and hence not likely to be seriously perturbed. But for the vibrational states near $v'=4$, we expect irregularities in the ΔG values, such as were found in CN. Actually, anomalies are present, the ΔG curve departing greatly from a straight line, and showing a large

"positive" curvature (positive γ_e).¹³ It does not seem of value to attempt an analytical representation of all the observed vibrational terms of the upper state.

For the determination of ρ , the states $v'=0, 1$, and 2 only have been used, to avoid as far as possible the effect of the perturbations. The resulting values, shown in Table IV, agree surprisingly well with those from the normal state, considering the difficulties and approximations in their evaluation.

ROTATIONAL ISOTOPE EFFECT

Although the rotational effect is capable of yielding values of ρ which are only about one-tenth as accurate as those from the vibrational effect, we have studied it to obtain the best possible values of the rotational constants for both "main" ($B^{11}O$) and "isotopic" ($B^{10}O$) systems. This is essential if conclusions are to be drawn about the electronic effect, as will be done below. The principal constant, B_v , which occurs in the expressions for the rotational energy, differs for the two isotopic molecules according to the following equations.⁸

$$B^{11}O:B_v = B_e - \alpha_e(v + \frac{1}{2}) + \gamma_e(v + \frac{1}{2})^2 + \dots \quad (6a)$$

$$B^{10}O:B_v^i = B_e^i - \alpha_e^i(v + \frac{1}{2}) + \gamma_e^i(v + \frac{1}{2})^2 + \dots \quad (6b)$$

$$= \rho^2 B_e - \rho^2 \alpha_e(v + \frac{1}{2}) + \rho^4 \gamma_e(v + \frac{1}{2})^2 + \dots$$

Here the only value of ρ which is at all accurate is found from

$$B_e^i/B_e = \rho^2,$$

the constants α_e and γ_e being too small to permit much precision.

Lower state

For the main system, values of B_v'' could be calculated directly by least squares from the combination differences

$$\Delta_2 F_2''(K) = R_2(K-1) - P_2(K+1) = 4B_v''(K + \frac{1}{2}) + 8D_v''(K + \frac{1}{2})^3 + \dots \quad (7)$$

after eliminating the cubic term as usual¹⁴ by preliminary calculation of D_v from the theoretical relation with B_e and ω_e . We have used $D_e'' = -6.29 \times 10^{-6}$, $\beta'' = 0$, $D_e''^i = \rho^4 D_e'' = 7.05 \times 10^{-6}$. For the isotopic system, however, where the P_2 branch was not available, we must use the quantities

$$\begin{aligned} \Delta_1 F''(K) &= R_2(K - \frac{1}{2}) - Q_2(K + \frac{1}{2}) - \Delta\nu_{dc} \dots \\ &= 2B_v''(K + \frac{1}{2}) + 4D_v''(K + \frac{1}{2})^3 - \Delta\nu_{dc} \dots \end{aligned} \quad (8)$$

The term $\Delta\nu_{dc}$ represents the Λ -doubling in the upper state from which the two lines come. It can easily be corrected for, as we shall show later, and we have proved by tests on the main system that the resulting B_v 's agree exactly

¹³ Although it is commonly said that a negative curvature is the normal one (Birge and Spomer), it appears that in the few cases where extensive and accurate measures of band origins are available (NO β , SiN) a positive curvature for the upper state is most common. However, perhaps perturbing effects are also at work in these cases.

¹⁴ Reference 1, p. 174.

with those from Eq. (7). The chief results of these calculations are collected in Table V. No values are quoted for $v''=2$, since the data from the isotopic system for this state are too fragmentary to be of value here.

The data of Table V were derived from the analysis of the rotational term-differences alone, and thus furnish a valuable independent check on the results from the vibrational analyses contained in Tables III and IV. It is

TABLE V. Rotational constants of the $^2\Sigma$ state.

B^{11}O			B^{10}O		
B_{v}''			$B_{\text{v}}''^i$		
0,0	1.7715	0,1	1.7569	0,0	1.8738
1,0	1.7720	1,1	1.7545	1,0	1.8763
2,0	1.7725		1.7557 ± 0.0008	2,0	1.8768
3,0	1.7719			3,0	1.8753
Av. 1.7720 ± 0.0001			1.8758 ± 0.0006		
$B_{\text{e}}'' = 1.78015 \pm 0.0004$			$B_{\text{e}}''^i = 1.88465 \pm 0.0008$		
$\alpha_{\text{e}}'' = 0.0163 \pm 0.0008$			$\alpha_{\text{e}}''^i = 0.0171 \pm 0.0011$		
$\rho^2 = B_{\text{e}}''^i/B_{\text{e}}'' = 1.0587 \pm 0.0005$			$\rho = 1.0289 \pm 0.00025$		
$\rho^3 = \alpha_{\text{e}}''^i/\alpha_{\text{e}}'' = 1.05$			$\rho = 1.02$		

possible to improve somewhat the accuracy of the value of ρ from rotational constants, by assuming the more accurate values of α_e obtained in connection with the vibrational analysis. Thus, if we fix $\alpha_e'' = 0.01648 \pm 0.00008$, $\alpha_e'' = 0.01772 \pm 0.00042$ and use the B_v'' values of Table V, we find:

$$B_e = 1.7803 \pm 0.0004$$

$$B_e^i = 1.8850 \pm 0.0005$$

$$\rho^2 = 1.0588 \pm 0.0004$$

$$\rho = 1.0290 \pm 0.0002$$

$$\rho^3 = \alpha_e''^i/\alpha_e'' = 1.075 \pm 0.024$$

$$\rho = 1.024 \pm 0.008$$

Upper state

As stated above, the initial state of these bands is an inverted $^2\Pi$. Because of the large multiplet separation, it is obviously very near to case *a* type of spin coupling, at least for small rotation. The form of the rotational energy function is in general complicated in such a state, because of the spin uncoupling which occurs as the rotation increases. In the present instance, however, the departure toward case *b* should be inappreciable at small rotational quantum numbers. This was found to be true, by investigating graphically the combination differences

$$\begin{aligned}\Delta_2 F_2'(K) &= R_2(K) - P_2(K) = 4B'_{v,-1/2}(K + \tfrac{1}{2}) + 8D'_{v,-1/2}(K + \tfrac{1}{2})^3 + \dots \\ \Delta_2 F_1'(K) &= R_1(K) - P_1(K) = 4B'_{v,+1/2}(K + \tfrac{1}{2}) + 8D'_{v,+1/2}(K + \tfrac{1}{2})^3 + \dots\end{aligned}\quad (7)$$

using the very complete data for the 1,0 band. The quantities $B'_{v,-1/2}$ and $B'_{v,+1/2}$, although not equal, were found to be practically constant below $J \sim 30$. Hence, if lines of low J are used, the spin uncoupling need not be considered. Probably this $^2\Pi$ state departs more toward case *c*, where the two

components can be considered as separate electronic levels (each with its own constants) than toward case *b*. Fortunately, this makes it possible to apply the usual least squares methods for the evaluation of B_v , and in doing so we have confined ourselves to lines having rotational quantum numbers below 15.

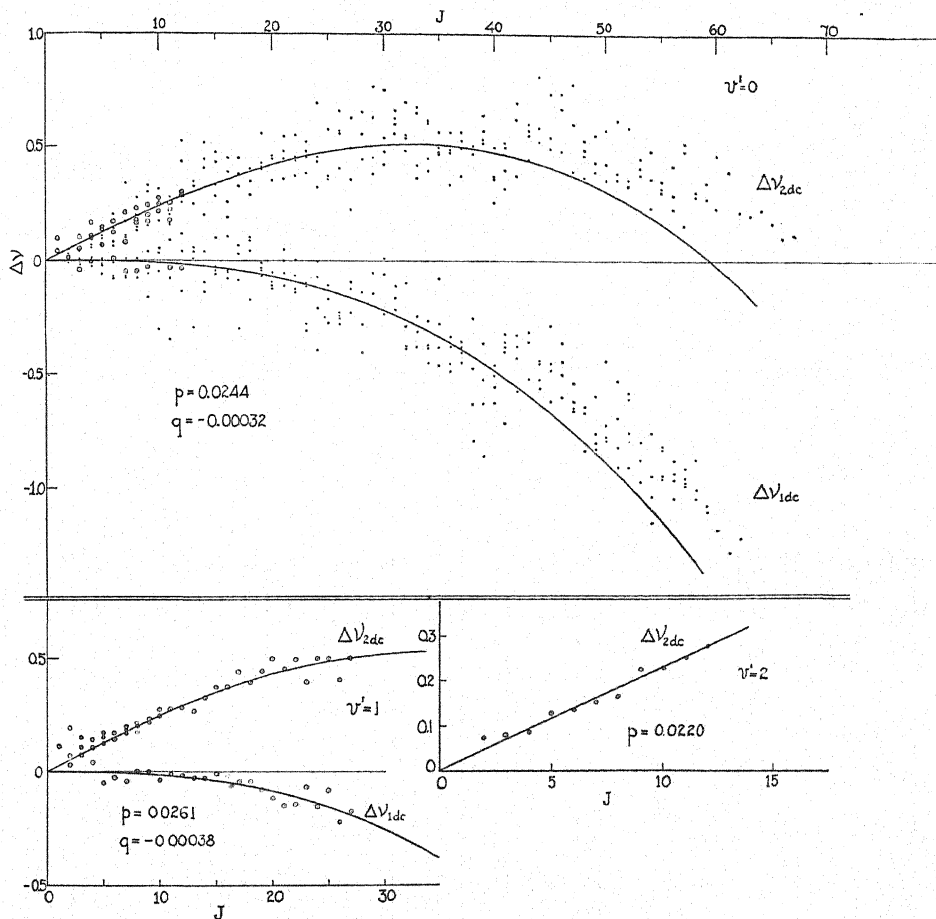


Fig. 4. Λ -doubling in the upper states $v' = 0, 1$ and 2 . Values indicated by circles are from our data, and the small dots are from the measurements of Scheib.⁷ The curves are the theoretical ones, drawn according to the constants indicated.

Another factor which must be considered is the Λ -doubling, which splits all the $^2\Pi$ rotational states into two. Particularly, this must be corrected for in the $B^{10}O$ combination differences, where only R_2 and Q_2 branches are available. For the main system, the Λ -doubling could be evaluated directly as the combination defect:

$$2\Delta\nu_{dc}(J + \frac{1}{2}) = [R(J) - Q(J)] - [Q(J + 1) - P(J + 1)]. \quad (8)$$

Fig. 4 shows graphically the course of $\Delta\nu_{2dc}$ (in $^2\Pi_{1/2}$) and $\Delta\nu_{1dc}$ (in $^2\Pi_{1/2}$)

for the lowest three vibrational levels. Below about $J=15$, they may be well represented by the equation¹⁵ of Van Vleck for inverted case a states:

$$\begin{aligned}\Delta\nu_{2dc} &= p(J + \tfrac{1}{2}) \\ \Delta\nu_{1dc} &= -(p/Y^2 + 2q/Y)(J - \tfrac{1}{2})(J + \tfrac{1}{2})(J + 1\tfrac{1}{2}).\end{aligned}\quad (9)$$

Y stands for A/B_v , A being the spin coupling constant, while p and q are small constants. Their values, as found graphically, are given in Table VI.

TABLE VI. Constants of the Λ -doubling.

$B^{11}O$	v'	p	q	$B^{10}O$	p (calc.)
	0	0.0244	-0.00032		0.0257
	1	0.0261	-0.00038		0.0277
	2	0.0220			0.0233
	3	0.0244			0.0258
	4	0.0188			0.0199

For $v'=0$ and 1, we have used the more general expression given by Mulliken and Christy,⁹ for states intermediate between cases a and b . The curves in Fig. 4 for these states are the theoretical ones, based on these equations. For $B^{10}O$, not enough branches are observed to permit the direct determination of $\Delta\nu_{dc}$. However, an examination of the theoretical expression,⁹ for these constants shows that the magnitude of p depends on B_v and of q on B_v^2 . In connection with Eqs. (9), this requires that $\Delta\nu_{2dc}$ be greater for $B^{10}O$ than for $B^{11}O$ by the factor ρ^2 , and $\Delta\nu_{1dc}$ greater by ρ^6 . Thus we obtain the values in the last column of Table VI. The determination of $B_{v,2}$ was then made by correcting the combination difference, so that

$$\begin{aligned}R_2(K) - Q_2(K) - \Delta\nu_{2dc}(K + \tfrac{1}{2}) &= \Delta_1 F_2'(K + \tfrac{1}{2}) \\ &= 2B_{v,-1/2}(J + \tfrac{1}{2}) + 4D_v(J + \tfrac{1}{2})^3 \\ R_1(K) - Q_1(K) - \Delta\nu_{1dc}(K + \tfrac{1}{2}) &= \Delta_1 F_1'(K + \tfrac{1}{2}) \\ &= 2B_{v,+1/2}(J + \tfrac{1}{2}) + 4D_v(J + \tfrac{1}{2})^3.\end{aligned}$$

The cubic term was first eliminated, with

$$D_v = -7.09 \times 10^{-6} + 5.08 \times 10^{-8}(v' + \tfrac{1}{2})$$

$$D_v^i = -7.92 \times 10^{-6} + 5.86 \times 10^{-8}(v' + \tfrac{1}{2}).$$

The resulting values of $B_{v,2}$ are collected in Table VII. As before, a considerably better ρ is obtained if we use the more accurate α_e 's from the ΔT parabolas. Adopting these, and solving by least squares the values of $B_{v,-1/2}$ from $v'=0$ to 3, we find

$$B_{e,-1/2} = 1.4277 \pm 0.0005 \quad B_{e^i,-1/2} = 1.5115 \pm 0.0006$$

$$\rho^2 = 1.0587 \pm 0.0006 \quad \rho = 1.0289 \pm 0.0003$$

$$\alpha_e = 0.0196 \quad \alpha_e^i = 0.0211$$

$$\rho^3 = 1.078 \pm 0.008 \quad \rho = 1.025 \pm 0.003.$$

¹⁵ R. S. Mulliken, Rev. Mod. Phys. 2, 109 (1930).

TABLE VII. Rotational constants of the $^2\Pi$ state.

$B^{11}O$	B_e	From bands			$B^{10}O$	B_e^i
$B_{0,-1/2}$	1.4172	0,0	0,1	0,2	$B_{0,-1/2}^i$	1.4991
$B_{1,-1/2}$	1.3969	1,0	1,1	1,2	$B_{1,-1/2}^i$	1.4793
$B_{1,+1/2}$	1.3679		1,0		$B_{1,+1/2}^i$	1.4488
$B_{2,-1/2}$	1.3789		2,0		$B_{2,-1/2}^i$	1.4605
$B_{3,-1/2}$	1.3609		3,0		$B_{3,-1/2}^i$	1.4382
$B_{4,-1/2}$	1.3450		4,0		$B_{4,-1/2}^i$	1.4243
$B_{5,-1/2}$	1.3346		5,0			

With only data for $v'=0, 1, 2$, and 3
 $B_{e,-1/2}=1.4266$
 $\alpha_e=0.0188$

$B_{e,-1/2}^i=1.5092$
 $\rho=1.0286$
 $\alpha_e^i=0.0203$
 $\rho=1.03$

In computing ρ , the values of $B_{e,-1/2}$ have been used rather than the "true" B_e , which the theory of case *a* states shows to be the mean of $B_{v,-1/2}$ and $B_{v,+1/2}$. This was done because it appeared that the difference between $B_{1,-1/2}$ and $B_{1,+1/2}$ was less than the theoretical value, $2B_1^2/A$ by from 5 to 10 per cent and it was therefore uncertain how well the state approximates the theoretical case *a*.

ELECTRONIC ISOTOPE EFFECT

It is important to note that the above results, because they are derived from analyses of the vibrational and rotational term-differences, involve no assumption as to the presence or absence of differences in the electronic terms of the two molecules. It is only when one is concerned with the frequency differences between corresponding bands of the two molecules, the "isotope shift," that the electronic effect enters. Since we have now fixed the relative position of all the terms of each type of molecule, within a given electronic state, it remains to find the separations of the terms of the $^2\Pi$ state from those of $^2\Sigma$. This requires the determination of the origin of one band, and we have chosen to do it for 1,0. The lines of the R_2 and Q_2 branches are given by the differences:

$$\begin{aligned} R_2(J) &= [T_{2e}' + G_1' + F_2'(J+1)] - [T_e'' + G_0'' + F''(J)] \\ Q_2(J) &= [T_{2e}' + G_1' + F_2'(J)] - [T_e'' + G_0'' + F''(J)]. \end{aligned} \quad (11)$$

Hence, the band origin may be expressed:

$$\begin{aligned} \nu_2^{(1,0)} &= (T_{2e}' - T_e'' + G_1' - G_0'') = R_2(J) - F_2'(J+1) + F''(J) \\ &= Q_2(J) - F_2'(J) + F''(J). \end{aligned} \quad (12)$$

In the lower state, we have

$$F''(J) = B_0''(K + \frac{1}{2})^2 = B_0''(J+1)^2. \quad (13)$$

In the upper state, we can use the expansion of the Hill and Van Vleck equation for large negative values of $Y=A/B_e$. Neglecting the small, unknown constants, this reduces to

$$F'(J) = B_{v,-1/2}(J + \frac{1}{2})^2 + B_v/Y \pm \frac{1}{2}p(J + \frac{1}{2}) + \dots \quad (14)$$

The positive sign applies to R_2 , and the negative to Q_2 . Y has the value -88.51 , as shown ahead. From the first eight lines of these two branches, sixteen values of the origins were computed for both main and isotope bands. The results are

$$\nu_2^{(1,0)} = 24,885.09 \pm 0.01 \text{ cm}^{-1} \quad \nu_2^{(1,0)i} = 24,911.73 \pm 0.01 \text{ cm}^{-1}.$$

The two system-origins are then readily obtained from the relation

$$\nu_{2e} = \nu_2^{(1,0)} - [\omega_e'(1\frac{1}{2}) - 2x_e'\omega_e'(1\frac{1}{2})^2] + [\omega_e''(\frac{1}{2}) - 2x_e''\omega_e''(\frac{1}{2})^2]. \quad (15)$$

We find

$$\text{B}^{11}\text{O}:\nu_{2e} = 23,958.85 \pm 0.05 \quad \text{B}^{10}\text{O}:\nu_{2e}^i = 23,959.18 \pm 0.06.$$

Thus there remains a discrepancy of $0.33 \pm 0.08 \text{ cm}^{-1}$ which in all probability represents an electronic isotope effect. It agrees in sign and order of magnitude with the value 0.47 cm^{-1} obtained by one of us⁶ in 1927 from measurements on the main and isotope Q_2 head of the 0,0 bands, a less accurate method. Although it is commonly supposed that electronic isotope effects are smaller than the above, recent work both experimental and theoretical on the atomic spectrum of lithium¹⁶ have yielded shifts even greater than this. Our result appears to be the first evidence of any sort of an electronic isotope effect in molecular spectra.

In the above, we have treated the ${}^2\Pi_{1/2}$ component as a separate band system. This is justified if the value of the coupling coefficient, A , is the same for B^{11}O and B^{10}O in different vibrational levels of the ${}^2\Pi$ state. The data are insufficient for testing this point except in the case of the 1,0 band. Here the values of A have been calculated separately for main and isotope systems. The term-formula for ${}^2\Pi_{1/2}$, corresponding to Eq. (14) is

$$F_1'(J) = B_{v,+1/2}(J + \frac{1}{2})^2 - B(2 - 1/Y), \quad (16)$$

omitting the Λ -doubling, which is negligible for small J . The separation of pairs of terms of the same J in the two components may thus be expressed as follows:

$$\begin{aligned} T_2(J) - T_1(J) &= (T_{2e} - T_{1e}) + (B_{1,-1/2} - B_{1,+1/2})(J + \frac{1}{2})^2 \\ &\quad + 2B_1(1 + 1/Y) \pm \frac{1}{2}p(J + \frac{1}{2})^2 \\ &= -A - [2B_1/\alpha](J + \frac{1}{2})^2 + 2B_1(1 + 1/Y) \pm \frac{1}{2}p(J + \frac{1}{2})^2. \end{aligned} \quad (17)$$

This separation was evaluated from the combination differences

$$R_2(J - 1) - Q_1(J) \text{ and } Q_2(J) - P_1(J + 1),$$

the positive sign in the final term of Eq. (17) being applicable in the former, and the negative in the latter case. The A computed in this way was constant below about $J = 10$, and the mean values adopted are

¹⁶ D. S. Hughes and C. Eckart, Phys. Rev. **36**, 694 (1930); D. S. Hughes, Phys. Rev. **38**, 857 (1931).

$$A = -122.36 \pm 0.03 \text{ cm}^{-1} \quad A^i = -122.36 \pm 0.05 \text{ cm}^{-1}.$$

Hence $Y = A/B_v = -88.51$, from the mean value of B_1 . It is not surprising to find the spin coupling coefficients equal for the two isotopic molecules, since they should be practically uninfluenced by the nuclear masses.

DISCUSSION OF RESULTS

The different determinations of the coefficient ρ are summarized in Table VIII. It will be seen that the accuracy in this quantity obtainable from the four important constants decreases in the order of their size; thus in the order ω_e , B_e , x_e and α_e . For these the probable error is roughly one part in 20,000, 4000, 500 and 100, respectively. The agreement between the several values is always of the order of magnitude of their probable errors, and more often closer than the computed errors would indicate. This shows that the latter represent conservative estimates. We note a slight tendency of the x_e to give too high a value of ρ , while α_e gives values too low. Considering the probable errors, however, it seems that little significance can be attached to these trends.

TABLE VIII. Results from analysis of vibrational structure.

Constants used	Bands used			ρ	Probable error
ω_e''	0,0	0,1	0,2	1.02907	± 0.00004
ω_e''	1,0	1,1	1,2	1.02909	± 0.00005
x_e''	0,0	0,1	0,2	1.030	—
x_e''	1,0	1,1	1,2	1.031	± 0.002
α_e''	0,0	0,1	0,2	1.023	± 0.018
α_e''	1,0	1,1	1,2	1.026	± 0.009
ω_e'	0,0	1,0	2,0	1.02913	± 0.00004
x_e'	0,0	1,0	2,0	1.032	—
α_e'	0,0	1,0	2,0	1.025	± 0.003
	3,0	4,0			

Results from analysis of rotational structure.					
B_e''	0,0	1,0	2,0	1.0289	± 0.00025
	3,0	1,1	0,1	1.0290*	± 0.0002
α_e''	0,0	1,0	2,0	1.02	—
	3,0	1,1	0,1		
B_e'	0,0	1,0	2,0	1.0286	—
	3,0	1,1	0,1	1.0289*	± 0.0003
α_e'	0,0	to	5,0	1.03	—
	0,1	1,1			

* These values obtained if the more accurate α_e from the vibrational analysis is used.

Aston¹⁷ has measured the masses of the boron isotopes with the precision mass-spectrograph, and found the following results:

$$B^{10}: 10.0135 \quad \text{Limit of error } 0.0015$$

$$B^{11}: 11.0110 \quad \text{" " " } 0.0016.$$

¹⁷ F. W. Aston, Proc. Roy. Soc. 115A, 509 (1927).

The masses are based on $O^{16} = 16$. From these we find

$$\begin{aligned}(\mu/\mu^i)^{1/2} = \rho &= 1.02908. \quad \text{Limit of error } 0.00009 \\ &= 1.02908 \pm 0.00003\end{aligned}$$

assuming the probable error to be one-third of the assigned limit of error. This agrees strikingly well with the best results in Table VIII. Thus the mean of the two determinations from ω_e'' is exactly the above value, with the same probable error. The value from ω_e' is untrustworthy for reasons given above, while those from the B_e 's should be given negligible weight, because of the magnitude of their probable errors. Hence the agreement with Aston's result is complete, and constitutes the first independent check on the accuracy of his relative masses.

Since it is ρ , the square root of the ratio of the reduced masses, which is obtained from the band spectrum, one must assume one of the absolute masses to evaluate their ratio. This is because the ratio of the vibration frequencies is dependent not only on the ratio of the masses of the molecules, but also on their absolute values. If we let m_{11} and m_{10} be the respective atomic weights, we have

$$m_{11}/m_{10} = 16\rho^2/[m_{10}(1 - \rho^2) + 16] = [m_{11}(\rho^2 - 1) + 16\rho^2]/16$$

Assuming Aston's value, $m_{10} = 10.0135$, our mean value of ρ gives for the mass ratio

$$m_{11}/m_{10} = 1.09961 \pm 0.00006$$

and from Aston's two masses, directly

$$\begin{aligned}m_{11}/m_{10} &= 1.09962. \quad \text{Limit of error } 0.00032 \\ &= 1.09962 \pm 0.00011.\end{aligned}$$

We have therefore verified the value of the slope of the packing fraction curve of Aston, assuming the absolute value of the packing fraction, at atomic weight 10.

In closing, we wish to acknowledge the kind assistance of Professor R. T. Birge on the methods of treating the data. Most of the above methods have already been applied by him in his very accurate computation of the masses of the oxygen isotopes.

The Emission of Positive Ions from Heated Metals

By LEROY L. BARNES

Department of Physics, Cornell University

(Received September 27, 1932)

The positive ion emission from iron, nickel, copper, rhodium, columbium, platinum, uranium and thorium has been studied. In addition to the emission of singly charged atoms of the alkalies, reported by others, it is found that iron, nickel, copper, rhodium and columbium emit singly charged atoms of their own metals. The results from rhodium and columbium are in agreement with those already reported by H. B. Wahlin.

INTRODUCTION

FOR many years it has been known that positive electricity will leak away from a metal when the metal is heated to a visible red. This leakage has been found, in some cases at least, to be due to two types of ion emission (1) to positive ions of impurities^{1,2,3} in the metal (2) to positive ions of the metal^{4,5} itself. Mass-spectrographic studies indicate that the first type of emission, from a given sample of metal, can be reduced to zero by sufficient heating and aging of the sample. In this paper we shall be primarily interested in the second type of positive ion emission.

That a well-aged tungsten filament emitted positive ions when heated to a high temperature, was first discovered by Jenkins⁶ and independently by L. P. Smith.⁷

By means of a Dempster type mass-spectrograph, Smith⁴ made an analysis of the positive ion emission from both tungsten and molybdenum. In addition to the ions of the alkalies, which were emitted at relatively low temperatures, he found that, when the temperatures of the respective metals were sufficiently high to produce fairly rapid vaporization, ions corresponding to singly charged atoms of the metals were emitted.

While Smith's work was in progress, H. B. Wahlin⁸ was making similar investigations and reported that tungsten, molybdenum, tantalum and rhodium each emitted singly charged atoms of its own metal. Later Wahlin⁵ reported similar results for chromium, columbium and ruthenium.

The author has made a mass-spectrographic examination of the positive ion emission from iron, nickel, copper, rhodium, columbium, platinum,

¹ O. W. Richardson, *Emission of Electricity from Hot Bodies*.

² J. J. Thomson, *Conduction of Electricity through Gases*.

³ Barton, Harnwell and Kunsman, *Phys. Rev.* **27**, 739 (1926).

⁴ L. P. Smith, *Phys. Rev.* **35**, 381 (1930).

⁵ H. B. Wahlin, *Phys. Rev.* **37**, 467 (1931).

⁶ Jenkins, *Phil. Mag.* **47**, 1025 (1924).

⁷ Smith, *Phys. Rev.* **33**, 279 (1929).

⁸ Wahlin, *Phys. Rev.* **34**, 164 (1929).

uranium and thorium. The mass-spectrograph used was essentially the same as that used by Smith.⁴ The positive ion currents from the mass-spectrograph were measured by means of an FP-54 Pliotron and a high sensitivity galvanometer, the maximum current sensitivity being of the order of 10^{-16} amperes.

EXPERIMENTAL WORK AND RESULTS

In addition to the sodium and potassium emission observed by others,^{1,2,3,4,5} the author has found that when platinum is first heated to a dull red, a relatively weak emission of rubidium and caesium ions is obtained. The purpose of the investigation, however, was to find out, in the case of each metal tried, whether or not positively charged atoms of the metal itself would be emitted when the metal was heated.

IRON AND NICKEL

Filaments of iron and nickel, when heated to temperatures just below their respective melting points, were found to emit singly charged atoms of these metals, but the filaments lasted only a few seconds because of the high temperature required to get the emission. This made it impossible to obtain data on the positive ion currents. In order to obtain an emission which would last long enough to make possible a more accurate recording of the location of the ions on the mass scale, a source of the following type was tried.

A wire of the metal to be investigated, was rolled out into a uniform strip from two to three thousandths of an inch thick. One end of the strip was then made pointed so that it could enter a small wire die. A piece of nickel wire about 0.02 inch in diameter was placed in contact with the strip and the two were drawn through the die. This left the strip in the shape of a trough and

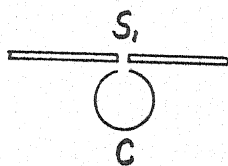


Fig. 1.

with continued drawing of the trough alone, through successively smaller dies, it took on the shape of a cylindrical shell with a slit down the side. The ends of this cylindrical shell were then spot welded to the filament leads of the mass-spectrograph and it was placed in front of the slit S_1 as shown in Fig. 1. Fig. 1 is an end view of the slit S_1 (the first slit of the mass-spectrograph) and the cylindrical shell C . The shell was heated by means of an electric current.

Because of radiation the outside of such a source is cooler than the inside. Thus the shell may be cool enough on the outside to support its own weight, while on the inside it is hot enough to vaporize quite rapidly and give a measurable emission of positive ions.

From one nickel source of this type an emission of positive ions of nickel was maintained for more than an hour before the cylinder melted. Data taken

with this source are shown by the first curve in Fig. 2. The currents were very small, of the order of 10^{-16} to 10^{-15} amperes, and in this case not very steady, as is shown by the roughness of the curve. The mass scale was checked by the potassium peak from the same source, and as is shown the two peaks fall quite close to atomic weights 58 and 60, the mass numbers of the two isotopes of nickel.

A large number of iron sources, of the type described above, were tried but the emission of positive ions of iron was never maintained for more than three or four minutes before the cylinder melted. This did not allow sufficient

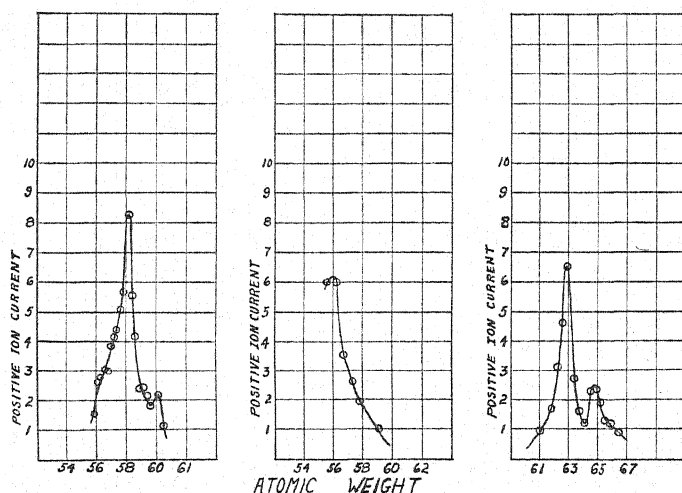


Fig. 2.

time for data to be taken on a complete peak. The second curve of Fig. 2 shows that part of the curve due to iron ions which it was possible to obtain before the cylinder melted.

It may be of interest to note that the melting point of iron is nearly 100° higher than that of nickel and that the rate of vaporization⁹ of iron, just below its melting point, is a little higher than for nickel just below its melting point. The above results show, however, that nickel gives the stronger ion emission. The ionization potentials for iron and nickel¹⁰ are 7.83 volts and 7.63 volts respectively. One might raise the question whether or not the difference in the emission in the two cases could be due to this small difference in ionization potentials.

COPPER

The author has previously reported¹¹ that positive ions of copper were obtained when the copper was supported and heated by a tungsten filament. In that case, due precaution was not taken to avoid the possibility of obtain-

⁹ Jones, Langmuir and MacKay, *Phys. Rev.* 30, 201 (1927).

¹⁰ Ruark and Urey, *Atoms, Molecules and Quanta*.

¹¹ L. L. Barnes, *Phys. Rev.* 37, 218 (1931).

ing copper ions produced by thermal ionization of the copper vapor striking the hot tungsten filament. The production of copper ions by this method has been described by Kingdon.¹²

To make certain that no mistake had been made in saying that the copper ions were emitted by the copper itself, a thin strip of copper was bent into the shape of a trough and placed over the straight tungsten filament and then closed on the under side of the filament. This source was placed at right angles to the slit of the mass-spectrograph so that no part of the tungsten was exposed to the slit. With such an arrangement all ions entering the slit must come from the copper surface. With this source the third curve in Fig. 2 was obtained, showing the two isotopes of copper at atomic weights 63 and 65.

Wahlin¹³ has recently reported that he has obtained positive ions of copper at a temperature just below and at the melting point of the metal.

RHODIUM

The two peaks shown in Fig. 3 were obtained from a rhodium filament at a temperature of about 1800°C. The smaller peak falling at atomic weight 103 corresponds to singly charged atoms of rhodium and the larger peak at 137 to singly charged atoms of barium. A recent communication from the company from which the rhodium was purchased, states that they have detected,

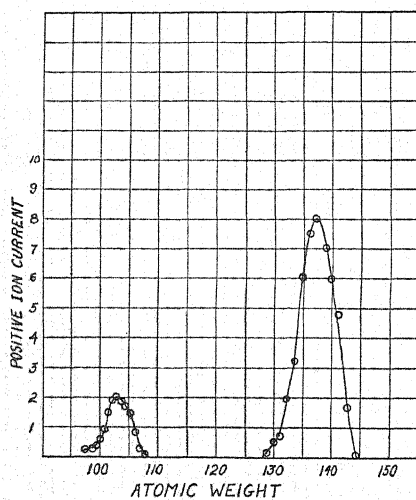


Fig. 3.

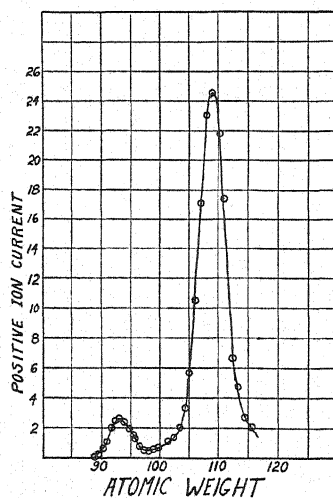


Fig. 4.

by spectroscopic analysis, a trace of barium in all of the samples of rhodium which they have tested. The fact that the barium ion current is larger than the rhodium ion current may be explained by the fact that the ionization potential for barium is so much lower than that for rhodium. One would expect that with both metals at the same temperature, a much greater percentage of the vaporized barium would be ionized than of the vaporized rhodium.

¹² Kingdon, *Phys. Rev.* **23**, 778 (1924).

¹³ Wahlin, *Phys. Rev.* **38**, 1074 (1931).

The peak due to rhodium ions is a confirmation of results already reported by Wahlin.⁵

COLUMBIUM OR NIOBIUM

Fig. 4 shows two peaks due to positive ions from a columbium filament at a temperature of about 1800°C. The smaller peak at atomic weight 93 corresponds to singly charged atoms of columbium (also reported by Wahlin).⁵ The larger peak at 109 is just 16 mass units greater than that due to columbium ions. It has been demonstrated by Wahlin¹⁴ that uranium oxide ions and thorium oxide ions may be obtained from heated tungsten filaments containing these oxides. It would not be surprising if the columbium used here contained some of its own oxide, near the surface at least, and, in view of Wahlin's results, that some of the evaporating oxide comes off as CbO^+ (mass 109).

PLATINUM

Several attempts to obtain positive ions of platinum have resulted in nothing more than a rush of current at the time that the filament burned out. This rush of current accompanying the burning out of the filament came only if the accelerating potential, for the ions in the mass-spectrograph, happened to be set at approximately the correct value for platinum ions to be recorded. To be sure that it was not due to an electrical disturbance accompanying the burning out of the filament, a platinum filament was burned out with the accelerating potential set well off the value for platinum ions and no rush of ion current was observed. Both filaments and cylindrical shells, of the type used in the case of iron and nickel, were tried in an attempt to get an emission of platinum ions which could be recorded, but none was obtained.

Both Smith and Wahlin were unsuccessful in obtaining platinum ions by this method. Murawkin¹⁵ reports that from a heated platinum foil alone he obtained no platinum ions but with an electrolytic layer of copper on a platinum foil he obtained a surprisingly large emission of platinum ions. The positive ion currents which he has recorded for platinum ions are some 10,000 times larger than the smallest current detectable in the author's experiments. If the ions which he obtains in this way are positive ions of platinum, it is, indeed, an interesting fact in view of its analogy to the enhanced electron emission from tungsten when covered with a layer of thorium.

URANIUM AND THORIUM

Strips of uranium and thorium, very kindly provided by Professor Wahlin, were heated in the mass-spectrograph and a careful search for positive ions of these metals was made but none were found. This is in agreement with Wahlin's report.⁵

The author wishes to express his appreciation to Dr. L. P. Smith who was responsible for his first acquaintance with this field of research, and to Professors R. C. Gibbs and C. C. Murdock for their helpful suggestions and criticisms during the course of the work reported here.

¹⁴ Wahlin, *Phys. Rev.* **39**, 183 (1932).

¹⁵ Murawkin, *Ann. d. Physik* **8**, 385 (1931).

The Temperature Variation of the Positive Ion Emission from Molybdenum

By LEROY L. BARNES

Department of Physics, Cornell University

(Received September 27, 1932)

The temperature variation of the positive ion emission from aged molybdenum filaments was studied with two different types of tube. The values for the positive ion work function and for the reflection coefficient for molybdenum ions are found to be in better agreement with the theory of positive ion emission presented by L. P. Smith than were his experimental results on molybdenum ions.

INTRODUCTION

L. P. SMITH¹ has made a study of the temperature variation of the positive ion emission from tungsten and molybdenum. Following, in a general way, the work of Bridgman² he has developed an expression for the rate of evaporation of positive ions as a function of the temperature. From this work the particular expression for molybdenum is,

$$\log_{10} I + 0.453 \log_{10} T + 2.70 \times 10^{-4} T = - \Phi_{+0} e / 2.303 k T + \frac{1}{2.303 k} \int_0^T \frac{dT}{T^2} \int_0^T C_{p,p} dT + \frac{S}{2.303 k} + \log_{10} (1 - r) + 12.76 \quad (1)$$

where I is the positive ion current per cm^2 of the emitting surface at the temperature T degrees absolute, Φ_{+0} is the positive ion work function at $T=0$, e the electronic charge, k the Boltzmann constant, r the reflection coefficient for the positive ions, $C_{p,p}$ the heat capacity associated with the surface heat of charging produced by the evaporation of one ion, and S_p the entropy associated with the surface heat of charging at $T=0$. By a separate calculation it was shown that no serious error should be introduced by neglecting the terms containing $C_{p,p}$ and S_p . Thus Eq. (1) becomes

$$\log_{10} I + 0.453 \log_{10} T + 2.70 \times 10^{-4} T = - \Phi_{+0} e / 2.303 k T + \log_{10} (1 - r) + 12.76. \quad (2)$$

Plotting values of the left side of this equation against corresponding values of $1/T$ gave a straight line, the slope of which gave, for molybdenum, $\Phi_{+0} = 6.09$ volts, and the constant term obtained from the intercept was 6.90.

At this point two difficulties were encountered. First, it was pointed out that if one computes the value for r from the equation $\log_{10}(1-r) + 12.76 = 6.90$ it is found to be so large that only one ion out of about 100,000 striking a surface would be condensed. Secondly, the value obtained for Φ_{+0} was found

¹ L. P. Smith, *Phys. Rev.* **35**, 381 (1930).

² Bridgman, *Phys. Rev.* **27**, 173 (1926).

to be too small to close the following energy cycle. Starting with an inclosure in which molybdenum is in equilibrium with its radiation at a given temperature T , we remove an electron and a positive ion from the metal thus requiring an amount of work $\Phi_{-T} + \Phi_{+T}$, where Φ_{-T} and Φ_{+T} are the respective work functions at the temperature T . Then allow the electron and positive ion to combine to form a neutral atom, yielding an amount of energy corresponding to its ionization potential V . The cycle is believed to be completed when the atom has been allowed to condense back on the metal, yielding a amount of energy equal to the heat of condensation U_T . If this is a reversible cycle we should have,

$$\Phi_{+T} + \Phi_{-T} = V + U_T. \quad (3)$$

Putting in the accepted values for the different terms along with the above value for Φ_{+0} we have

$$V + U_0 = 7.35 + 6.33 = 13.68$$

$$\Phi_{+0} + \Phi_{-0} = 6.09 + 4.42 = 10.51$$

and we see that the cycle fails to close by 3.17 volts.

The results from tungsten gave rise to the same difficulties and Smith was thus led to conclude that "unlike the evaporation of electrons and neutral atoms, the evaporation of ions is not strictly represented by an equation based upon thermodynamical arguments under equilibrium conditions." He suggests the possibility that tungsten and molybdenum may slowly recrystallize in an irreversible manner, when raised to high temperatures, thus yielding the necessary energy to close the above cycle.

Considering the previous success of the type of thermodynamical argument used here by Smith, in explaining similar phenomena, and knowing the very marked differences in experimental results obtained by different observers investigating the thermionic properties of metals, the author was led to make a further study of the temperature variation of the positive ion emission from molybdenum. Molybdenum was chosen rather than tungsten because Smith had found that its emission decayed much less with time than did the emission from tungsten.

EXPERIMENTAL WORK AND RESULTS

The first tube used was of the type shown in Fig. 1, a type used by many observers in the study of the thermionic properties of metals. The molybdenum filament was held in place along the axis of the three nickel cylinders by means of a weak molybdenum spring. The two end cylinders were kept at the same potential as the center cylinder but only the positive ion current to the center cylinder was measured.

A temperature scale for the central portion of the filament was obtained by the method described by Smith,¹ from Worthing's² data on the total radiation, in watts per cm², from molybdenum.

² Worthing, Phys. Rev. 28, 190 (1926).

The tube was baked at a temperature of about 470°C before and after the first outgassing of the metal parts. The metal parts were first heated with an induction furnace and then the cylinders were brought to a higher temperature by electron bombardment. Then with the three cylinders made negative with respect to the filament, the filament was aged at a temperature of 2000°K for 20 hours before any readings were taken. During the time the aging was going on the filament was flashed occasionally, for a few seconds, at a temperature of about 2600°K . Even after this aging process was completed it was found that the filament had to be taken over the temperature range to be used several times before the rate of decay of the emission became small.

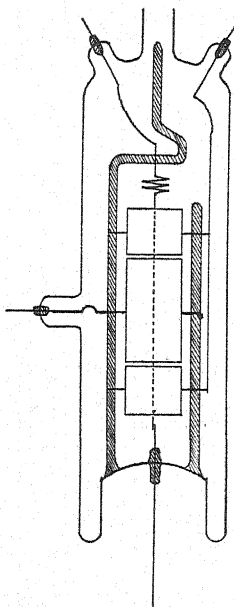


Fig. 1.

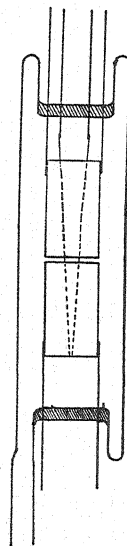


Fig. 2.

A sample of the data taken with this tube is shown in Fig. 3. From the slope of this line the value of Φ_{+0} is 8.15 volts and from the intercept the constant term is 11.96.

Since these values are so much higher than those obtained by Smith it was decided that a more exact duplicate of his experiments might lead to an explanation of the difference in the results. For this purpose a tube of the type he used was built. A diagram of this tube is shown in Fig. 2. The two cylinders were kept at the same potential but only the current to the lower cylinder was measured. The hairpin filament used in this tube had been shaped by heating it, while under tension, in a vacuum. Smith's filaments were shaped by heating them, under tension, in hydrogen. (This difference in procedure does not seem to lead to any serious difference in results as will be shown later.)

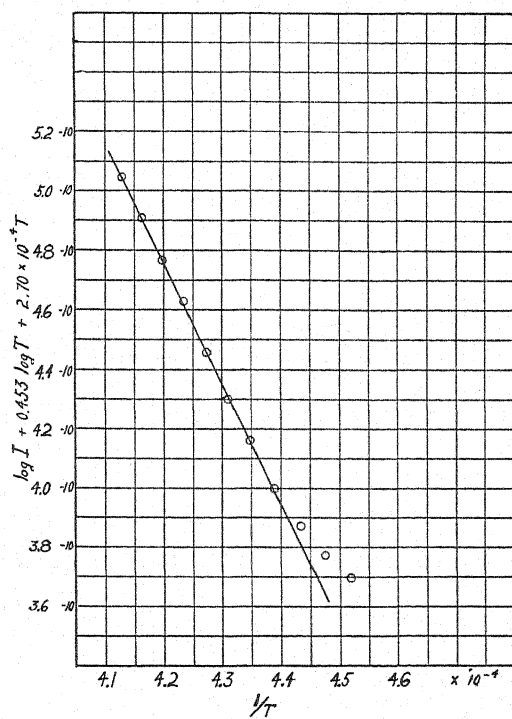


Fig. 3.

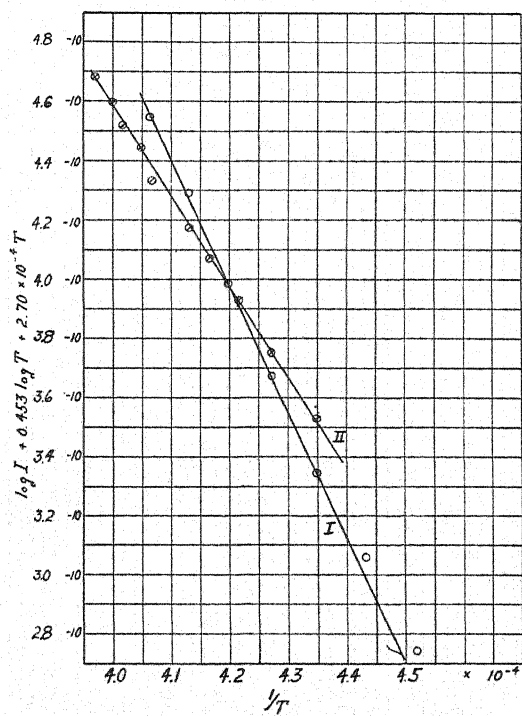


Fig. 4.

Curve I of Fig. 4 is a plot of representative data obtained from this tube. From this curve $\Phi_{+0} = 8.5$ volts and the constant term is 11.8. Curve II of Fig. 4 is a plot of the data for molybdenum given in Smith's paper. Quite obviously the slopes are different, and the results obtained by the author are in fair agreement with those obtained from the other type of tube.

After all of the data to be discussed later had been taken, hydrogen was admitted to the tube to a pressure of 6 mm Hg and the filament glowed for 15 minutes at a temperature of about 1800°K. The hydrogen was then pumped out and the filament kept at a temperature of 1900°K for one hour. Then after taking the filament slowly over the temperature range to be used, the

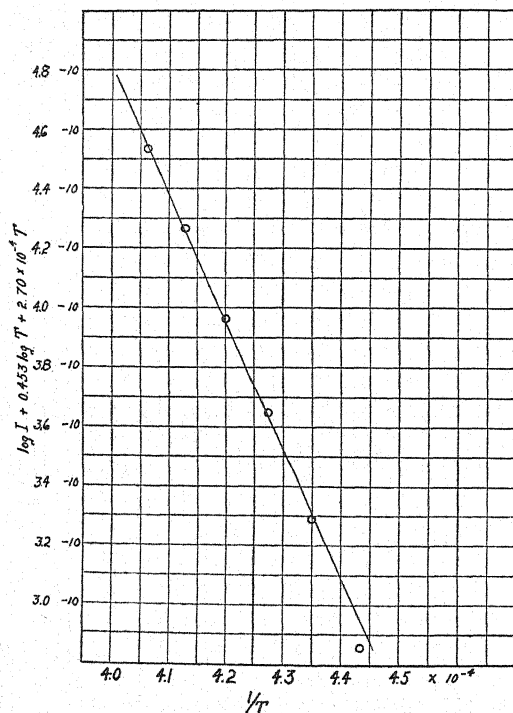


Fig. 5.

data shown by the curve of Fig. 5 were taken. From this curve $\Phi_{+0} = 8.65$ volts and the constant term is 12.2. Whether or not the small increase in these values, over the previous values obtained, is to be attributed to the use of the hydrogen is a matter to be decided by more detailed experiment, but these results obviously do not serve to explain the difference between the results obtained by Smith and those obtained by the author.

In Table I the values of the constant term and of Φ_{+0} are given for four separate runs taken with each tube.

The variations in the values of Φ_{+0} and of the constant term which appear here, do not seem to follow any definite order as regards aging of the filaments, and, within the limits of error of the experiments, no variation of

TABLE I. Values of the constant and of Φ_+ .

Straight filament		Hairpin filament	
Φ_{+0} (volts)	Constant term	Φ_{+0} (volts)	Constant term
8.12	11.8	8.15	11.0
8.23	11.9	8.20	11.3
8.06	11.7	8.00	11.0
8.15	12.0	8.50	11.8
8.14	11.8	8.20	11.3 Average

these values with the applied voltage, over the range of 100 to 400 volts, could be detected.

It should be noted that the lower points on the curves of Figs. 3 and 4, fall above the straight line which fits the other points reasonably well. This was true of all of the curves obtained with the exception of the one taken after the hydrogen was used. A study of the positive ion emission in this lower temperature range, with higher current sensitivity than that used here might prove to be interesting.

The average of the work function values, given in Table I, comes within about one volt of closing the energy cycle, and the average of the constant term values gives a value for r of about 0.9. This would mean that one ion out of about 10 striking a surface would be condensed. This result seems more reasonable than that obtained by Smith but in comparison with the values of reflection coefficients for neutral atoms and electrons it seems large.

At this point due respect should be paid the suggestion that a gradual irreversible recrystallization of the metal might account for the necessary energy to close the cycle (3). E. A. Hazlewood⁴ has found that such a recrystallization does take place for tungsten and molybdenum at high temperatures. The results, however, are of such a qualitative nature that no quantitative comparison with the positive ion emission data can be made.

The experimental results presented in this paper indicate that the theory of positive ion emission developed by Smith may be better than his experimental results led him to believe, and that the amount of energy called for from the recrystallization process may not be as great as he supposed.

⁴ E. A. Hazlewood, *Crystal Growth in Molybdenum and Tungsten Filaments at High Temperatures*. A thesis, Cornell University Library.

Rotational Analysis of Ultraviolet Bands of Silicon Monoxide

By PAUL G. SAPER

Ryerson Physical Laboratory, University of Chicago

(Received September 6, 1932)

From measurements on silicon arc spectrograms a rotational analysis has been made of the (0,1), (0,2), (0,3), (0,4) and (1,4) bands of the ultraviolet band system of silicon monoxide (SiO). The bands were found to be due to a ${}^1\Pi \rightarrow {}^1\Sigma$ transition as was expected by analogy with the fourth positive bands of CO. Among the constants obtained from the analysis are

$$\begin{array}{lll} B_0' = 0.6270 & r_e' = 1.62 \times 10^{-8} \text{ cm} & \alpha' = 0.00657 \\ B_0'' = 0.7238 & r_e'' = 1.51 \times 10^{-8} \text{ cm} & \alpha'' = 0.00494 \end{array}$$

A number of perturbations of the Q branch lines were observed. Some conclusions were reached as to the nature of the perturbing levels. From measurements of band heads of this system made by Jevons and the results of the present analysis the following equation was obtained for the band origins:

$$\begin{aligned} \nu_0 = & 42835.3 + 851.51(v' + 1/2) - 6.143(v' + 1/2)^2 + \\ & 0.0437(v' + 1/2)^3 - 1242.03(v'' + 1/2) + \\ & 6.047(v'' + 1/2)^2 - 0.00329(v'' + 1/2)^3. \end{aligned}$$

INTRODUCTION

THE ultraviolet band system of silicon monoxide (SiO) has heads, as listed by Jevons,¹ extending from 2176.6Å to 2925.3Å. The bands are shaded toward longer wave-lengths. According to Cameron,² these bands might be the analog of the fourth positive bands of CO. If so, they must be of the type ${}^1\Pi \rightarrow {}^1\Sigma$.

The writer has now made a rotational analysis of the (0,1), (0,2), (0,3), (0,4) and (1,4) bands. The analysis confirms the idea that they are ${}^1\Pi \rightarrow {}^1\Sigma$. Each band was found to consist of one P , one Q and one R branch.

SPECTROGRAMS

Using as a source a carbon arc with SiO₂ placed in the lower (positive) carbon, the writer photographed these bands in the first and second orders of a twenty-one foot concave grating. The iron arc was used as a comparison spectrum. Measurements of the (0,1) and some other bands were made from the spectrograms thus obtained in the second order, and the (0,1) band was partly analyzed. Then measurements were made of the (0,1), (0,2), (0,3), (0,4) and (1,4) bands from plates of silicon arc spectrograms, which Professor R. S. Mulliken received through the kindness of Professor W. F. C. Ferguson of New York University. The exposures were made by Professor Ferguson with the new, very large Hilger quartz spectrograph at the Bureau of Standards. The iron arc served as a comparison spectrum on these plates. The

¹ W. Jevons, Proc. Roy. Soc. London **106**, 174 (1924).

² W. H. B. Cameron, Phil. Mag. (7) **3**, 110 (1927).

iron arc wave-lengths which were used were from those measured by K. Burns and F. M. Walters, Jr.³ The quartz spectrograph plates just mentioned showed a dispersion, at 2500Å, of about 0.874Å/mm, as compared with about 1.24Å/mm for the grating second order plates, and also showed a greater resolution than the grating plates. From measurements on these quartz spectrograph plates the five bands mentioned above were analyzed.

ROTATIONAL ANALYSIS

As the bands were excited at high temperature the series were long, and there was some overlapping of series lines from one band to another. Many of the observed lines were blends, and there were a number of atomic lines in the spectrum. The (0,1) band was analyzed first. The *Q* branch lines could be distinguished from the other series lines because of their greater intensity. The *R* branch lines near the origin were considerably stronger than the *P* branch lines in this region. Members of the *P*, *Q* and *R* series with common values of the rotational quantum number of the lower energy state were selected from these series with the aid of the relation

$$R(J) - Q(J) \cong Q(J+1) - P(J+1). \quad (1)$$

According to the quantum theory of band spectra, there is Λ -type doubling in a ${}^1\Pi$ state; each rotational level of this electronic state is double (*c* and *d* sets of sub-levels⁴). The *Q* lines are due to transitions from a different set of sub-levels of the ${}^1\Pi$ state than those from which the *P* and *R* lines originate. As a result there is a "combination defect" equal to $[R(J) - Q(J)] - [Q(J+1) - P(J+1)]$. In the case of these SiO bands this defect was found to be relatively small compared to the quantities $[R(J) - Q(J)]$ or $[Q(J+1) - P(J+1)]$ themselves.

In order to assign correctly the absolute J'' values the following relations were used:

$$\Delta_2 T'(J) = R(J) - P(J) = 4B'(J + \frac{1}{2}) + 8D'(J + \frac{1}{2})^3 + \dots \quad (2)$$

$$\begin{aligned} \Delta_2 T''(J) &= R(J-1) - P(J+1) \\ &= 4B''(J + \frac{1}{2}) + 8D''(J + \frac{1}{2})^3 + \dots \end{aligned} \quad (3)$$

These relations were also used to calculate the constants B' and B'' . The values of $[R(J) - P(J)]$ were plotted against successive integers. For relatively small values of J'' these points lay very approximately on a straight line and then with increasing J'' they began to deviate slightly from the line. A straight line was drawn through the points up to where they began to deviate. The slope of this line gave a good approximation to the value of $4B'$. Similarly, by plotting the values of $[R(J-1) - P(J+1)]$ against successive integers a good approximation to $4B''$ was obtained. Then D' and D'' were calculated with the aid of the theoretical relation

$$D_e = -4B_e^3/\omega_e^2, \quad (4)$$

³ K. Burns and F. M. Walters, Jr., Publications of the Allegheny Observatory of the University of Pittsburgh, Vol. VIII, No. 4.

⁴ R. S. Mulliken, Rev. Mod. Phys. **3**, 89 (1931).

neglecting the difference between D_e and D_v . The values of ω_e' and ω_e'' were obtained from the vibrational analysis of SiO made by Jevons,¹ from measurements on the heads of the bands. It was found that when the quantity $[R(J) - P(J) - 8D'(J+1/2)^2]$ was plotted against successive integers, the points now all lay very approximately on a straight line, showing that there was no need of considering terms of higher power than the third to represent $\Delta_2 T'(J)$. A similar statement holds for $\Delta_2 T''(J)$. Thus by successive approximations and least squares the values of B' and B'' were obtained for the five bands analyzed. The values of B_0' as thus obtained from the analysis of the (0,1), (0,2), (0,3) and (0,4) bands agreed to within one-tenth of one percent or less. The values of B_1'' , B_2'' , B_3'' and B_4'' showed a very approximately linear variation according to the formula

$$B_v = B_0 - \alpha v. \quad (5)$$

The wave numbers of the P , Q and R lines, together with the rotational quantum numbers assigned to them, are listed in Table I. There are a number of perturbations of the Q branch lines. Their significance will be considered in a later section.

TABLE I.

The first six numbers give the wave number of the line considered. The seventh number, in bold-face type, expresses the estimated relative intensity of the line. Blends of two or more lines are indicated by an asterisk (*). The letter A indicates that a heavy atomic line is superposed on a band line.

P	(0,1) band Q	R	J''	P	(0,2) band Q	R
	41392.74		14		40174.56	
	89.74		15		71.98*	
	86.66		16		68.94	
	83.04		17		66.16	
	79.36*		18		62.96	
	75.76*		19		59.79*	
	71.96*		20		56.26	
	67.98*		21	40126.44	52.6A*	
	63.96		22	21.54	48.86	
	59.76*		23	15.84	44.96	
	55.46*		24	10.44	40.56	
	50.76*		25	04.64	36.06*	40167.53
	45.86*		26	40099.15	31.38*	64.62
	40.98*		27	92.93	26.76*	61.64
41300.46*	35.76*	41371.96*	28	86.74	22.16*	58.06
41293.86*	30.56*	67.98*	29	80.33	17.08*	54.14
87.13	24.86*	63.54	30	73.85	11.88*	50.34
80.33	19.06*	58.78*	31	67.24	06.08*	46.04
73.22	13.06*	54.14	32	60.69*	00.48*	41.54
65.73	06.86*	49.04	33	53.34	40094.48*	36.06*
57.93	00.46*	43.96	34	46.19*	88.89*	31.88*
50.03	41293.86*	38.36	35	38.89*	82.58	26.76*
42.13	88.06	33.74	36	31.28*	76.88	22.16*
34.83	80.76	28.14	37	24.28*	70.06	17.08*
26.13	73.66	22.24	38	15.58*	63.16	11.88*
17.53	66.26	15.84	39	07.56*	56.46	06.08*
08.83	58.66	09.64	40	39999.26*	49.16	00.48*
00.13	51.16	03.24	41	90.78*	42.06	40094.48*
41191.03	43.26	41296.54	42	82.16*	34.56	87.99*
81.53	35.26	89.74	43	72.86*	26.96	81.84

TABLE I. (Continued).

P	(0, 1) band		R	J''	P	(0, 2) band		R
	Q					Q		
72.03	27.06		82.84	44	64.64	19.26		75.04
62.43	18.66		75.74	45	55.16	11.36		68.34
52.63	09.96		68.44	46	45.64	03.16		61.39*
42.63	01.26		60.64	47	36.14	39994.66		53.94
32.43	41192.28*		52.64	48	26.24	86.16		46.19*
22.03	82.86		44.64	49	16.34	77.56		38.89*
11.53	73.68*		36.54	50	06.34	68.66		31.28*
00.66*	63.98*		27.94	51	39896.04	59.56		24.28*
41089.56*	54.18*		19.64	52	85.84	50.36		15.58*
78.36*	44.08*		10.84	53	75.2A*	40.86		07.56*
66.76*	34.06		01.54	54	63.94	31.16	39999.26*	
54.96*	23.66	41192.28*		55	53.04	21.26		90.78*
43.23	13.06	84.04		56	41.84	11.36		82.16*
31.53	02.36	73.68*		57	30.28*	01.06		72.86*
20.04	41091.26	63.98*		58	19.52	39890.65		63.34
06.94	80.06	54.18*		59	07.34	80.1A*		54.04
40994.24	41068.76	41144.08*		60	39795.14	39869.35	39944.24	
81.44	56.66	33.34		61	82.64	58.15		34.44
68.64	45.86	22.54		62		47.65		24.54
55.54	33.46	11.74		63		36.05		14.14
42.04	21.26	00.66*		64		24.25		03.94
28.35	08.86	41089.56*		65		12.64	39893.24	
14.7A*	40996.16	78.36*		66		00.85		82.94
00.25	83.26	66.76*		67		39788.75		71.94
40886.74	70.16	54.96*		68				61.96*
72.24	57.16	42.84		69				49.34
57.54	43.66	30.44		70				37.63
42.57*	29.96	18.06		71				26.04
27.84	16.36	05.36		72				
12.63	02.16	40991.7A*		73				
40797.13	40887.96	79.26		74				
81.73	73.46	66.05		75				
65.83	58.55	52.55		76				
49.63	42.57*	38.65		77				
33.55*	29.65	24.95		78				
16.83	13.95	10.64		79				
00.45*	40798.15	40896.34		80				
40683.35*	82.35	81.64		81				
66.15*	66.44	66.83		82				
48.75*	50.04	51.53		83				
30.95*	33.55*	37.53		84				
13.15*		21.03		85				
		05.63		86				
		40789.53		87				
		73.33		88				
		57.13		89				
		40.33		90				
		23.53		91				

TABLE I. (Continued).

P	(0,3) band		R	J''	P	(1,4) band		R
	Q					Q		
	38980.56*			7				
	79.54*			8				
	78.54*			9				
	77.04*			10				
	75.99*			11				
	74.08*			12				

TABLE I. (Continued).

<i>P</i>	(0, 3) band <i>Q</i>	<i>R</i>	<i>J''</i>	<i>P</i>	(1, 4) band <i>Q</i>	<i>R</i>
	71.59*		13		38617.22	
	69.44*		14		15.11	
	67.04*		15		12.53	
	64.54*		16		10.04*	
	61.48*		17		07.36*	
	58.76*		18		03.94*	
	55.79*		19		00.96*	38625.34
	52.29*		20		38597.63	23.23
	48.79*	38974.08*	21		93.95	21.22
	45.29*	72.19*	22		90.24	18.64
	41.56*	69.44*	23	38558.33	86.44	16.01
	37.56	67.04*	24	52.83	82.53	13.23
	33.36	64.54*	25	47.26*	78.43	10.04*
	29.19*	62.44	26	41.51	73.93	07.36*
38890.88*	24.56	59.44	27	35.72	69.23	03.94*
85.06*	19.99*	56.39*	28	30.04*	64.54	00.36*
78.97*	15.24	52.29*	29	23.82	59.86	38596.62
72.56*	10.39*	48.79*	30	17.42	54.74	92.82
66.16*	05.06	45.29*	31	11.14*	49.43	88.83
59.56*	38899.86	40.94	32	04.41	43.82	84.73
52.86*	94.38	36.25	33	38497.84	38.66*	80.42
46.14	88.56	31.75	34	90.64*	32.76*	75.43
38.94	83.85	28.04	35	83.64*	26.83	70.72
31.64	77.56	23.14	36	76.14*	20.72	66.03
25.15*	71.16	18.79*	37	68.53	14.59*	61.24*
17.06*	64.66	13.09*	38	60.93	07.94*	55.83
09.44	58.16	07.78*	39	53.44	01.26*	50.56*
01.36*	51.46	02.39*	40	45.13	38494.64*	45.24
38793.54	44.76	38896.69*	41	37.04	87.54*	39.06*
85.34	37.56	90.88*	42	29.04	80.34*	33.26*
76.94	30.56	85.06*	43	19.84	73.03*	27.82
68.14	23.26*	78.97*	44	11.63	66.13	21.42
59.44	15.69*	72.56*	45	03.14*	58.69*	14.59*
50.54	07.96*	66.16*	46	38393.93	50.53	07.94*
41.44	38799.99*	59.56*	47	84.43	42.86	01.26*
32.04	92.06*	52.86*	48	75.04*	33.53	38494.64*
22.75	83.86	45.44	49	65.38*	25.34	87.54*
13.14	75.36	38.34	50	55.53	17.84	80.34*
03.44	66.86	31.14	51	45.93	08.94	73.03*
38693.24	58.16	23.26*	52	36.74*	00.86*	65.64
83.15	49.16	15.69*	53	26.14*	38391.23	57.92
72.95	40.06	07.96*	54	15.64*	81.86*	48.54
38662.44	38730.76	38799.99*	55	38304.63*	38371.76	38440.13
51.74	21.26	92.06*	56	38293.64*	62.26	31.73
40.85*	11.66	83.04	57	82.66*	52.26	22.94
	01.86	74.44	58		42.25	14.03
	38691.86	65.74	59		32.06	05.23
	81.46	56.64	60		21.76	38396.34
	70.96	47.64	61		10.96	86.44
		38.24	62		00.25	77.04
		28.55	63		38289.46	67.63
		19.05	64			57.13
		08.65	65			47.13
		38699.15	66			36.74*
		88.65	67			26.14*
		78.22	68			15.64*
		67.35	69			04.63*
		56.64	70			38293.64*
		45.64	71			82.66*

TABLE I. (Continued).

J''	P	(0,4) band Q	R	J''	P	(0,4) band Q	R
11		37782.53		43	37592.03	45.74	00.44*
12		80.83		44	83.93	38.94	37694.75*
13		78.73		45	75.72	31.74	89.14*
14		76.62		46	67.23	24.74	82.94*
15		74.34		47	58.73	17.24	76.62
16		71.83*		48	49.64*	09.64	70.23
17		69.14*		49	40.93	01.94	63.64
18		66.36*		50	31.93	37594.36	57.03
19		63.53		51	22.63	86.05	50.13
20		60.66*		52	13.13	77.75	43.44*
21		57.26*		53	03.53	69.45	36.63
22		53.73		54	37493.83	60.85	28.83
23		50.13		55	83.73	52.04	21.03
24		46.53		56	73.83*	43.14	14.12
25		42.54		57	37463.43	37534.24	37605.63
26		38.44	37771.83*	58		25.04	37597.63
27	37700.44*	34.23	69.14*	59		15.54	89.43
28	37694.75*	30.14*	66.36*	60		05.94	81.43
29	89.14*	25.43	63.01	61		37496.04	72.44
30	82.94*	20.83	59.44*	62		86.65	63.63
31	77.23	15.94*	55.83	63		76.43	54.63
32	70.82	11.04*	52.02	64		66.14	45.63
33	64.52	05.94*	48.13	65		56.09*	36.03
34	57.93	00.44*	43.93	66		45.16*	27.23
35	51.22	37694.75*	39.43	67		34.16*	17.74*
36	44.33*	89.94	35.63	68		23.46*	07.73
37	38.13	84.14	31.04	69			37497.73
38	30.43	77.94	26.33	70			87.43
39	23.13	71.84	21.33	71			77.32
40	15.63	65.63	16.44*	72			66.94
41	07.93	59.14	11.04*	73			56.09*
42	00.22	52.54	05.94*				

In Tables IIA and IIB, there are listed agreements in the combination differences.

TABLE IIA. Agreements in the combination differences.

Note (1): $R(J) - Q(J+1)$ should not necessarily be exactly the same for the (0,4) and (1,4) bands, since the Δ -type doublet widths are not necessarily the same, for given J values, for $v'=0$ and $v'=1$.

Note (2): In some of the bands, additional combination differences are available, but are omitted from the table because of the absence of comparison data from other bands.

J	$R(J) - Q(J) = T'(J+1) - T'(J) + \Delta\nu_{dc}'(J)$				$R(J) - Q(J+1) = T''(J+1) - T''(J) + \Delta\nu_{dc}''(J+1)$	
	(0,1)	(0,2)	(0,3)	(0,4)	(0,4)	(1,4)
25		31.5	31.2			
26		33.3	33.3	33.4	37.6	38.1
27		34.9	34.9	34.9	39.0	39.4
28	36.2	35.9	36.4	36.2	40.9	40.5
29	37.4	37.1	37.0	37.6	42.2	41.9
30	38.7	38.5	38.4	38.6	43.5	43.4
31	39.7	40.0	40.2	39.9	44.8	45.0
32	41.1	41.1	41.1	41.0	46.1	46.1
33	42.2	41.6	41.9	42.2	47.7	47.7
34	43.5	43.0	43.2	43.5	49.2	48.6
35	44.5	44.2	44.2	44.7	49.5	50.0
36	45.7	45.3	45.6	45.7	51.5	51.5

TABLE IIA. (Continued)

J	$R(J) - Q(J) = T'(J+1) - T'(J) + \Delta\nu_{dc}'(J)$				$R(J) - Q(J+1) = T''(J+1) - T''(J) + \Delta\nu_{dc}''(J+1)$	
	(0,1)	(0,2)	(0,3)	(0,4)	(0,4)	(1,4)
37	47.4	47.0	47.6	46.9	53.1	53.3
38	48.6	48.7	48.4	48.4	54.5	54.6
39	49.6	49.6	49.6	49.5	55.7	55.9
40	51.0	51.3	50.9	50.8	57.3	57.7
41	52.1	52.4	51.9	51.9	58.5	58.7
42	53.3	53.4	53.3	53.4	60.2	60.2
43	54.5	54.9	54.5	54.7	61.5	61.7
44	55.8	55.8	55.7	55.8	63.0	62.8
45	57.1	57.0	56.9	57.4	64.4	64.0
46	58.5	58.2	58.2	58.2	65.7	65.1
47	59.4	59.3	59.6	59.4	67.0	67.7
48	60.4	60.0	60.8	60.6	68.3	69.3
49	61.8	61.3	61.6	61.7	69.3	69.7
50	62.9	62.6	63.0	62.7	71.0	71.4
51	64.0	64.7	64.3	64.1	72.4	72.2
52	65.5	65.2	65.1	65.7	74.0	74.4
53	66.8	66.7	66.5	67.2	75.8	76.1
54	67.5	68.1	67.9	68.0	76.8	76.8
55	68.6	69.5	69.2	69.0	77.9	77.9
56	71.0	70.8	70.8	71.0	79.9	79.5
57	71.3	71.8	71.4	71.4	80.6	80.7
58	72.7	72.7	72.6	72.6	82.1	82.0
59	74.1	73.9	73.9	73.9	83.5	83.5
60	75.3	74.9	75.2	75.5	85.4	85.4
61	76.7	76.3	76.7	76.4	85.8	86.2
62	76.7	76.9		77.0	87.2	87.6
63	78.3	78.1		78.2		
64	79.4	79.7		79.5		
65	80.7	80.6		80.0		
66	82.2	82.1		82.1		
67	83.5	83.2		83.6		
68	84.8			84.3		

TABLE IIB. Agreements in the combination differences.

J	$R(J) - P(J) = \Delta_2 T'(J)$				$R(J-1) - P(J+1) = \Delta_2 T''(J)$	
	(0,1)	(0,2)	(0,3)	(0,4)	(0,4)	(1,4)
27		68.7	68.6	68.7	77.1	77.3
28	71.5	71.3	71.3	71.6	80.0	80.1
29	74.1	73.8	73.3	73.9	83.4	82.9
30	76.4	76.5	76.2	76.5	85.8	85.5
31	78.4	78.8	79.1	78.6	88.6	88.4
32	80.9	80.9	81.4	81.2	91.3	91.0
33	83.3	82.7	83.4	83.6	94.1	94.1
34	86.0	85.7	85.6	86.0	96.9	96.8
35	88.3	87.9	89.1	88.2	99.6	99.3
36	91.6	90.9	91.5	91.3	101.3	102.2
37	93.3	92.8	93.6	92.9	105.2	105.1
38	96.1	96.3	96.0	95.9	107.9	107.8
39	98.3	98.5	98.3	98.2	110.7	110.7
40	100.8	101.2	101.0	100.8	113.4	113.5
41	103.1	103.7	103.1	103.1	116.2	116.2
42	105.5	105.8	105.5	105.7	119.0	119.2
43	108.2	109.0	108.1	108.4	122.0	121.6
44	110.8	110.4	110.8	110.8	124.7	124.7
45	113.3	113.2	113.1	113.4	127.5	127.5
46	115.8	115.7	115.6	115.7	130.4	130.1

TABLE IIB. (Continued).

<i>J</i>	<i>R(J) - P(J) = Δ₂T'(J)</i>				<i>R(J-1) - P(J+1) = Δ₂T''(J)</i>	
	(0,1)	(0,2)	(0,3)	(0,4)	(0,4)	(1,4)
47	118.0	117.8	118.1	117.9	133.3	132.9
48	120.2	119.9	120.8	120.6	135.7	135.9
49	122.6	122.5	122.7	122.7	138.3	139.1
50	125.0	124.9	125.2	125.1	141.0	141.6
51	127.3	128.2	127.7	127.5	143.9	143.6
52	130.1	129.7	130.0	130.3	146.6	146.9
53	132.5	132.3	132.5	133.1	149.6	150.0
54	134.8	135.3	135.0	135.0	152.9	153.3
55	137.3	137.7	137.5	137.3	155.0	154.9
56	140.8	140.3	140.3	140.3	157.6	157.5
57	142.1	142.6	142.2	142.2		
58	143.9	143.8				
59	147.2	146.7				
60	149.8	149.1				
61	151.9	151.8				

Λ-TYPE DOUBLING

The combination defects in the (0,1), (0,2), (0,3) and (0,4) bands were computed for each value of *J* and, where possible, averaged over the different bands. The definition of $\Delta\nu$ (in cm^{-1}) for Λ -type doubling,⁵ which will be used here is

$$\Delta\nu_{dc}(J) = T_d(J) - T_c(J). \quad (6)$$

For a ${}^1\Pi$ state,⁵ according to Van Vleck, one expects theoretically

$$T_d(J) = T_0 + B_v J(J+1) - 2C + (C + C_1)J(J+1) + \dots; \quad (7)$$

$$T_c(J) = T_0 + B_v J(J+1) - 2C + (C + C_2)J(J+1) + \dots$$

$$\Delta\nu_{dc}(J) = qJ(J+1), \text{ where } q = C_1 - C_2, \quad (8)$$

$$= (B_d - B_c)J(J+1).$$

The combination defect is:⁵

$$\begin{aligned} [R(J) - Q(J)] - [Q(J+1) - P(J+1)] \\ = \Delta\nu_{dc}(J) + \Delta\nu_{dc}(J+1) \\ \cong 2\Delta\nu_{dc}(J + \tfrac{1}{2}) \\ \cong 2q(J + \tfrac{1}{2})(J + 3/2) \\ \cong 2q(J+1)^2. \end{aligned} \quad (9)$$

From the numerical values of the combination defect corresponding to the various quantum numbers *J*, the value of *q* was computed by least squares. It was found that $q = B_d - B_c = -6.7 \times 10^{-5}$. In Fig. 1, the observed combination defects are plotted in comparison with a curve given by $-13.4 \times 10^{-5} (J+1)^2$.

⁵ R. S. Mulliken and A. Christy, Phys. Rev. **38**, 87 (1931).

If the almost certainly correct assumption⁵ is made that the $^1\Sigma$ lower electronic state of the observed bands is $^1\Sigma^+$, then the Q series lines originate from c levels.⁴

As mentioned before, there are a number of perturbations of the Q lines. This suggests the presence of other electronic energy levels near the $^1\Pi$ level. Since there are a number of perturbations of the Q lines, but not of the P and R lines, apparently the c levels are perturbed much more than the d

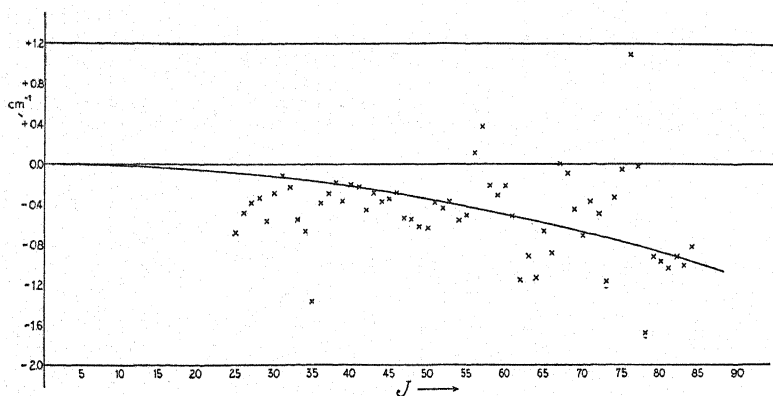


Fig. 1. The observed combination defects (cf. Eq. (9)) are shown by crosses. Each point indicated is, where possible, the average for the (0,1), (0,2), (0,3) and (0,4) bands. The curve is that given by $-13.4 \times 10^{-6}(J+1)^2$. Most of the small deviations between the experimental points and the curve may be due to experimental error, but most of the large ones are due to the perturbations of the Q lines.

levels and it seems likely that even for the unperturbed lines, it is the c levels rather than the d levels which are mainly responsible for the Λ -type splitting. If so (cf. Eqs. (7, 8)), $|C_2| \gg |C_1|$. Then since experimentally $(C_1 - C_2)$ is negative, C_2 would be positive. The expressions for the coefficients C_1 and C_2 are⁶

$$\begin{aligned} C_1 &= 8 \sum (\text{all } v \text{ values of all } ^1\Sigma^+ \text{ states}) |BL_v(\Pi, \Sigma^+)|^2 / \nu(\Pi, \Sigma^+), \\ C_2 &= 8 \sum (\text{all } v \text{ values of all } ^1\Sigma^- \text{ states}) |BL_v(\Pi, \Sigma^-)|^2 / \nu(\Pi, \Sigma^-). \end{aligned} \quad (10)$$

The quantities BL_v are approximate constants for any pair of electronic states, Π, Σ . $\nu(\Pi, \Sigma^+)$ is the wave number (cm^{-1}) corresponding to the energy difference between the $^1\Pi$ state and v value considered and any $^1\Sigma^+$ state and v value. If the $^1\Pi$ level is above the $^1\Sigma^+$ level it is taken as positive, if it is below the $^1\Sigma^+$ level it is taken as negative. $\nu(\Pi, \Sigma^-)$ has a similar meaning. Hence, from the argument above, that $|C_2| \gg |C_1|$ and $C_2 > 0$, it would follow that $\nu(\Pi, \Sigma^-) > 0$. This would indicate the presence relatively close to and below the given $^1\Pi$ state of one or more $^1\Sigma^-$ levels, which cause perturbations of the c levels of the $^1\Pi$ state.

BAND ORIGINS

From the relation

$$\begin{aligned} \nu = \nu_0 + B_v'J'(J' + 1) + D_v'J'^2(J' + 1)^2 \\ - B_v''J''(J'' + 1) - D_v''J''^2(J'' + 1)^2 \end{aligned} \quad (11)$$

as the equation of a band line for a ${}^1\Pi \rightarrow {}^1\Sigma$ transition, the value of ν_0 , for a given band, was taken as the definition of the band origin. With the observed wave numbers of twelve *P*, twelve *R* and ten *Q* lines of relatively small rotational quantum numbers, thirty-four values of ν_0 were calculated for the band under consideration. The average of these values was taken as the origin of the band. This was done for each of the five bands analyzed. Then a parabola was fitted by least squares to the values of ν_0 for the (0,1), (0,2), (0,3) and (0,4) bands, and by this means the values of ν_0 for the (0,0) and (0,5) bands were calculated. Then with aid of the values of B_v' and B_v'' the interval $(\nu_{\text{head}} - \nu_0)$ was calculated for most of the bands (other than those here analyzed) whose heads were measured by Jevons,¹ and with the wave numbers of the heads as listed by him, values of ν_0 were obtained. From the aggregate of the values of ν_0 calculations were made for ω_e' , ω_e'' , $x_e'\omega_e'$ and $x_e''\omega_e''$, giving greatest weight to the ν_0 data obtained directly by the present measurements, and the following equation was obtained for the origins of this band system:

$$\begin{aligned} \nu_0 = 42835.3 + 851.51(v' + \tfrac{1}{2}) - 6.143(v' + \tfrac{1}{2})^2 \\ + 0.0437(v' + \tfrac{1}{2})^3 - 1242.03(v'' + \tfrac{1}{2}) + 6.047(v'' + \tfrac{1}{2})^2 \\ - 0.00329(v'' + \tfrac{1}{2})^3. \end{aligned} \quad (12)$$

MOLECULAR CONSTANTS

In Table III there are listed the values of all the molecular constants obtained in the present work. The values of β' and β'' corresponding to the relation

$$D_v = D_e + \beta(v + \tfrac{1}{2}) = D_0 + \beta v \quad (13)$$

were calculated from the theoretical formula⁶

$$\beta = \frac{\alpha^2}{6\omega_e} + \frac{20\alpha B_e^2 - 32x_e B_e^3}{\omega_e^2}. \quad (14)$$

A check on the correctness of the analysis was afforded by a rule, due to R. T. Birge. According to this rule the quantity $2x_e B_e / \alpha_e$ is approximately equal to 1.4. For these bands substitution of the proper values showed that

$$2x_e' B_e' / \alpha' = 1.38$$

$$2x_e'' B_e'' / \alpha'' = 1.43.$$

An additional check is given by the approximate relation⁷ that for molecules composed of two atoms of nearly equal mass, the quantity $r_e^3 \omega_e$ is approximately equal to $3000 \times 10^{-24} \text{ cm}^2$. For these bands

⁶ E. C. Kemble, Jour. Opt. Soc. Am. 12, 1 (1926).

⁷ P. M. Morse, Phys. Rev. 34, 57 (1929).

$$r_e'^3 \omega_e' = 3620 \times 10^{-24}$$

$$r_e''^3 \omega_e'' = 4276 \times 10^{-24}.$$

TABLE III. Values of the molecular constants.

Upper state $^1\Pi$	Lower state $^1\Sigma$
$B_e' = 0.6303$	$B_e'' = 0.7263$
$B_0' = 0.6270$	$B_0'' = 0.7238$
$B_1' = 0.6205$	$B_1'' = 0.7189$
$\alpha' = 0.00657$	$B_2'' = 0.7138$
$D_e' = -1.382 \times 10^{-6}$ (calc.)	$B_3'' = 0.7091$
$\beta' = 2.88 \times 10^{-3}$ (calc.)	$B_4'' = 0.7041$
$I_e' = 43.95 \times 10^{-40}$ g cm ²	$\alpha'' = 0.00494$
r_e' (for Si ₂₈ O ₁₆) = 1.62×10^{-8} cm	$D_e'' = -0.993 \times 10^{-6}$ (calc.)
$q = B_d - B_e = -6.7 \times 10^{-5}$	$\beta'' = -1.55 \times 10^{-3}$ (calc.)
$\omega_e' = 851.5$	$I_e'' = 38.14 \times 10^{-40}$ g cm ²
$x_e' \omega_e' = 6.14$	r_e'' (for Si ₂₈ O ₁₆) = 1.51×10^{-8} cm
$y_e' \omega_e' = 0.0437$	$\omega_e'' = 1242.0$
	$x_e'' \omega_e'' = 6.05$
	$y_e'' \omega_e'' = 0.00329$

It is to be expected that for SiO the values of $r_e'^3 \omega_e'$ and $r_e''^3 \omega_e''$ will be greater than 3000×10^{-24} , since the masses of the two atoms are rather unequal.

The writer wishes to express his thanks to Professor R. S. Mulliken for proposing this problem and for his valuable advice and suggestions; also to Professor W. F. C. Ferguson of New York University for the spectrograms taken by him with the large quartz spectrograph, and to Dr. W. F. Meggers of the Bureau of Standards for the use of the latter.

Zeeman Effect of Perturbed Terms in the CO Angstrom Bands

By WILLIAM W. WATSON

Sloane Physics Laboratory, Yale University

(Received September 29, 1932)

The Zeeman effect of the perturbed lines in the CO angstrom bands ($^1\Sigma \rightarrow ^1\Pi$) is described. The perturbations are multiple, occur in the $^1\Pi$ state, and contain excess, much-displaced lines. New lines extending the "resonance" curves of Rosenthal and Jenkins are found. The perturbed lines show large, irregular Zeeman patterns, whereas the neighboring band lines with these intermediate and high J values are apparently insensitive to the magnetic field. Always the greater the displacement of the perturbed line, the larger its Zeeman effect. The patterns differ at each perturbation point: they are either broad, asymmetrical doublets; very broad, uniform blocks; sharp, narrow doublets; or just a shift, increasing the amount of the perturbation. An explanation is offered, assuming the perturbing state to be case a $^3\Pi$.

INTRODUCTION

THE details of the perturbations in a number of band spectra have been examined by Rosenthal and Jenkins,¹ Dieke² and others. These observations are in general in good agreement with the requirements of the theory as set up by Kronig³ and by Ittmann.⁴ Briefly, perturbations should occur whenever two energy levels for the molecule having the same J value approach closely to one another, the two levels having the same symmetry characteristics, Λ values the same or differing by at most 1 unit, the same multiplicity, and about the same internuclear distance. The perturbed energy levels do not cross, but rather separate from each other, so that the curves showing the departures of the perturbed band lines from the regular course of the branches to which they belong are of the "resonance" type.

Especially violent perturbations occur in the CO angstrom bands¹ ($^1\Sigma \rightarrow ^1\Pi$), particularly in the 0, 0 band at 4511Å. Rosenthal and Jenkins were the first to give a correct quantum analysis of this band, basing their assignments on the necessity of obtaining smooth deviation curves for the perturbed lines, agreement with known $\Delta_2 F'(J)$ combination differences, and the abandonment of the notion that the Λ -doubling in the $^1\Pi$ state should remain small and regular. This work showed that the perturbations are in the lower $^1\Pi$ state and that they are multiple, coming in this 0, 0 band at $J=9, 16, 17$ and >30 in the P and R branches and at $J=12, 29$ and >35 in the Q branch. From the fact that these perturbations are multiple and from an examination of the nature of the near-lying levels of CO, it was concluded that the perturbing state is probably a $^3\Pi$ state, in violation of the Kronig rule that the

¹ J. E. Rosenthal and F. A. Jenkins, Proc. Nat. Acad. **15**, 381 and 896 (1929).

² G. H. Dieke, Phys. Rev. **38**, 646 (1931).

³ R. de L. Kronig, Zeits. f. Physik **50**, 347 (1928).

⁴ G. P. Ittmann, Zeits. f. Physik **71**, 616 (1931).

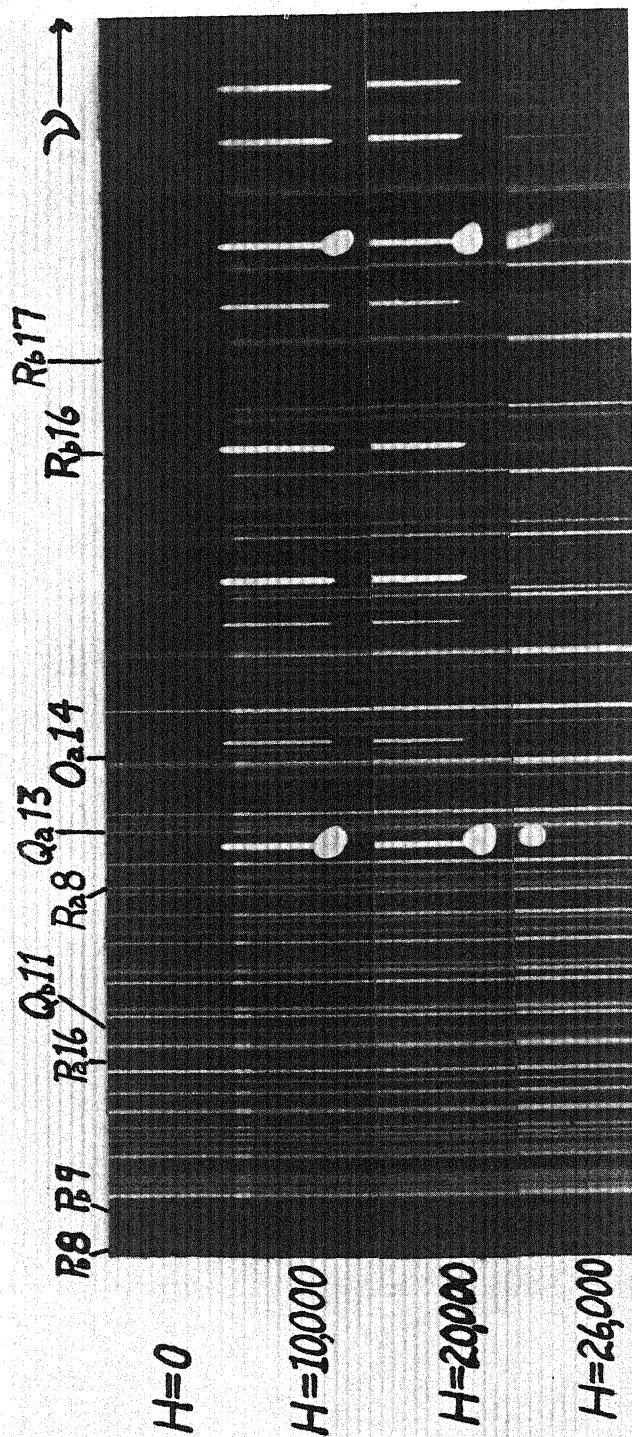


Fig. 1. The (0, 0) CO angstrom band at 4511 Å with magnetic field strengths up to 26,000 gauss. Several of the more violently perturbed lines are indicated, others being of too low intensity to show in the reproduction. Fe comparison lines.

perturbing terms should have the same multiplicity. We shall return to this point below.

In his work on the regular Zeeman effect in these CO bands, Crawford⁵ noted the existence of large, irregular Zeeman effects for certain of the band lines which are involved in these perturbations. In the present investigation the details of these peculiar Zeeman patterns have been examined, and possible explanations are presented in connection with the facts about the perturbations and the probable nature of the interacting levels.

EXPERIMENTAL PROCEDURE

Spectrograms of the 0, 0 and 0, 1 bands of the CO angstrom system were obtained in the second order of the 21-foot concave grating in a stigmatic mounting, the dispersion being approximately 2.42Å per mm. The magnetic field strengths varied from 10,000 gauss to 26,700 gauss. On each plate was placed in addition to the field exposure a no-field comparison spectrum and the spectrum of the Fe arc for wave-length determinations. The source was a 15,000 volt a.c. discharge between small copper disks 3 to 4 mm apart, mounted in the gap space of a large Weiss electromagnet. These electrodes were attached to the electrode holders of a modified Back chamber, and were insulated from the pole faces with mica. CO₂ gas from a commercial cylinder was pumped slowly through the discharge chamber at a pressure of about 5 mm, in some cases directly from the cylinder, while in other cases the gas was first passed through a hot copper oxide tube and a tube filled with P₂O₅. The time of exposure was of the order of 12 hours each for the Zeeman effect spectrogram and for the no-field comparison.

This source is of course weak, but because of the increased intensity of the spectra with the grating in the stigmatic mounting, the exposure times were not excessive. Disturbing discharge in regions outside that of uniform field was effectually reduced by having copper disk electrodes but 4 mm in diameter as against a pole face diameter of 20 mm, and by taking care to see that the gas pressure never became too low. A faint background of impurity lines increasing in intensity towards the violet is present on all the spectrograms. It was found, however, that by allowing a slight leak of air into the CO₂, this unwanted spectrum was reduced in intensity to the point where it caused but little trouble in the measuring of the spectrograms. The N₂⁺ bands thus introduced could be tolerated because they do not overlap the interesting perturbation points in the CO bands.⁶ In Fig. 1 are to be seen Zeeman patterns of some of the perturbed lines in the (0, 0) 4511Å band at the several field strengths.

ADDITIONAL LINES AT PERTURBATION POINTS IN 0, 0 BAND

A marked feature of the quantum analysis of the (0, 0) band as made by Rosenthal and Jenkins¹ is the occurrence of two lines for each of one or more

⁵ F. H. Crawford, Phys. Rev. 33, 341 (1929).

⁶ These ²Σ→²Σ bands of N₂⁺ also display interesting Zeeman patterns for lines involved in their perturbations. These perturbations are very similar to those in the corresponding band system of the isoelectronic molecule CN, and will be the object of further study.

J values at the center of a perturbation. Furthermore, they reported the sum of the intensities of the two lines to be always about that calculated by interpolation for an unperturbed line of that J value. Also, the greater the displacement of the line the less is its intensity. According to the theory this appearance of extra lines is to be expected, for around the perturbation points the wave functions of the molecule for the two electronic states concerned become "mixed," losing their separate identity, with the result that transitions from the upper $^1\Sigma$ state to the perturbing state ($^3\Pi$?) are possible.

There are in fact more of these extra lines than are given in Table I of reference 1. The assignments of these additional lines are given in Table I,

TABLE I. Quantum assignments of lines of intermediate J value in the (0, 0) CO angstrom band.

J''	P		Q		R	
	a	b	a	b	a	b
7	22,164.60		22,191.30		22,222.99	
8	167.25	150.90*	197.10		233.45	217.08*
9	172.10	159.48	203.84		246.09	233.45
10	180.96	166.32	211.55	185.00*	d	248.11
11		171.65	220.63	200.73		261.16
12		176.87	231.85	214.38		274.08
13		182.54	246.09	227.05		287.59
14		188.97	263.48	238.77		301.79
15	179.86*	196.47		250.26	d	317.02
16	193.44	205.92		261.92	321.80	334.21
17	205.41	219.03*		274.08	341.39	355.32*
18	215.59			286.77	359.43	

where the new lines are indicated by a *. The line $P_b(8)$ lies some 12 cm^{-1} beyond the head of the band, and there is even an indication of a line $P_b(7)$ still further to the red. The new lines are all displaced many cm^{-1} from the unperturbed points for the particular J values, and are all consequently of low intensity. The correctness of the assignments is attested however by the existence of exactly the required $\Delta_2 F'(J)$ combination differences, and by the fact that they are all much affected by the magnetic field, being even broadened slightly in the no-field comparison spectrum by the field due to the residual magnetism in the magnet. Strong lines of other branches lie in the positions indicated for $R_a(10)$ and $R_a(15)$, making their observation impossible. The perturbations in the region of higher J values have not been examined in detail.

OBSERVED ZEEMAN PATTERNS

All of the band lines in the immediate neighborhood of the perturbations exhibit large, irregular Zeeman patterns, whereas the regular Zeeman effect for lines with these intermediate and high J values for a $^1\Sigma \rightarrow ^1\Pi$ transition is so small as to leave the unperturbed lines totally unaffected by the magnetic field. There is a different type of Zeeman effect at each of the perturbations in the (0, 0) band, and always the perturbed lines having the greatest displacements are magnetically the most sensitive. A brief tabulation of some of the details of these patterns at three different field strengths is given in

Table II. Measurement on some of the perturbed lines is prevented either by their nearness to or fusion with other lines in the band, or by their low inten-

TABLE II. Zeeman patterns of perturbed band lines in the (0, 0) CO angstrom band at 4511 Å cm⁻¹ units. + indicates a shift to the high-frequency side, - to the low-frequency side of the no-field band line.

	10,000 gauss	20,000 gauss	26,000 gauss
a. P, R branch perturbation at J=9.			
P _b (8)	Broadened +0.80 to -0.84 Min. intens. in center + side stronger	Broad doub. -0.75 to -1.35 and (stronger) +0.62 to +1.34	Broad doublet
P _b (9)	Broadened +0.31 to -0.49	Broadened (stronger) -0.83 to -0.36 and weaker to +1.07	Broadened, - stronger
R _a (7)	No effect	Slight sym. broadening	Broadened +0.38 to -0.63
R _a (8)	Slight sym. broadening	Broadened +0.42 to -0.38	Broadened +0.43 to -0.56
R _b (9)			
R _b (8)	Broadened +0.72 to -0.83 Min. in center, + side stronger	Broad doub. + stronger +0.48 to +1.25. -block block fuses into P _a (18)	Stronger +0.38 to +1.10 - block weaker
R _b (10)	No effect	Broadened +0.33 to -0.26	Broadened +0.40 to -0.45
b. Q branch perturbation at J=12.			
Q _a (10)	No effect	No effect	
Q _a (11)	No effect	Shift of +0.06. Sharp	Slight + shift
Q _a (12)	No effect	Shift of +0.13. Sharp	Shift of +0.15. Sharp
Q _a (13)	No effect	Shift of +0.51. Sharp	Shift of +0.67. Slight broadening
Q _a (14)	No effect	Shift of +0.89. Slight broadening	Shift of +1.06. Slight broadening
Q _b (11)	No effect	Shift of -0.32. Sharp	Shift of -0.58. Slight broadening
Q _b (12)	No effect	Slight—shift	Definite—shift
Q _b (13)	No effect	No effect	Shift of -0.12
Q _b (14)	No effect	No effect	Shift of -0.06
c. P, R branch perturbation at J=16.			
P _a (16)	Broadened +0.55 to -0.56	Broad block +1.09 to -1.03	Very broad and diffuse
R _b (15)	No effect	Slight sym. broadening	Broadened +0.49 to -0.27.
R _b (16)	Broadened +0.25 to -0.26	Broadened +0.62 to -0.66	Broadened +0.79 to -0.73
R _b (17)	Slight broadening	Broad doub. +0.38 to +1.14 and -0.39 to -	Broad doub +0.24 to +1.28 - block weaker
R _a (16)	Broad block 1.13 wide	Strong -block	Stronger at -1.04
R _a (17)	Broadened +0.27 to -0.26	Broadened +0.36 to -0.26	Sym. broadened
R _a (18)	No effect	Slight broadening	Slight broadening
d. Q branch perturbation at J=29.			
Q(30)			Sharp doub. +0.30 and (weaker) -0.20.

sity. A sufficient number of observations can be made at each perturbation, however, to enable one to say definitely the kind of pattern that is developed.

Several points about these Zeeman patterns should be emphasized. The doublets which the field produces for some of the most perturbed lines are never quite symmetrically placed with respect to the original line, the asymmetry increasing with increasing field strength. Also when a line which at low field strength is just uniformly broadened splits in stronger fields into two blocks of radiation, the two are never of the same intensity, the block on the side of increased perturbation energy being in some instances the stronger, while for other lines the reverse is true. In the Q branch around $J=12$ the displaced lines are not noticeably affected by a field of 10,000 gauss, although the perturbation is just as violent as the first two P and R branch perturbations, i.e., the two sets of interacting levels must come just as close to each other. The effect of the higher field strengths on these Q lines is merely to increase slightly the magnitude of their displacement in the perturbation, the Q_a lines being shifted to higher frequencies, the Q_b lines to lower frequencies. The most perturbed lines experience the greatest shift, and are but slightly broader than the corresponding no-field lines. A similar Zeeman effect has been observed for one of the perturbations in the $(0, 1)$ band, but has not been worked out in detail.

The lines at the center of the P and R branch perturbation around $J=16$ mostly undergo a uniform symmetrical broadening as the field increases, but the line R_b (17) which has the largest displacement in the perturbation does become a broad doublet at the higher field strengths. And the widths of these patterns is just as large as those in the first P, R perturbation, despite the fact that the overall spread of the $2J+1$ component levels due to the field in the ${}^1\Pi$ state is but one half as great (varies as $1/J$), while the perturbations are of about the same degree. This would indicate that the interacting levels of the other electronic state are here more affected by the field, for instance that they are ${}^3\Pi_2$ levels, while for the first perturbation ${}^3\Pi_0$ levels are responsible. We shall mention this again in the discussion below.

Finally the character of the Q (30) line pattern at the high field strength should be mentioned. This is a narrow, sharp, but not symmetrical doublet, and the same is true of the pattern for the line Q (29) at the second Q -branch perturbation in the $(0, 1)$ band. One would expect narrower Zeeman patterns with sharper components, other things being equal, from these perturbed lines of high J values because of the decreased width of the group of Zeeman sublevels if J is large. And for the same reason only the one or two most displaced lines at these perturbations of high rotational levels should be appreciably affected by the magnetic field. Our observations show this to be the case.

DISCUSSION

As Rosenthal and Jenkins have shown,¹ the $a^3\Pi$ state of CO could be the state that interacts with the ${}^1\Pi$ levels to produce these perturbations, for extrapolation of the known vibrational levels of the a state indicates that its $v=10$ level approaches closely ${}^1\Pi^{(0)}$ with nearly the same ω values. Or it may be that the $d({}^3\Pi?)$ level which lies below and very close to the ${}^1\Pi$

state is responsible for the perturbations. There is definitely no singlet level in this energy range. Also the fact that the perturbations are multiple would indicate that the perturbing terms do not belong to a singlet state. And in addition the finding of a very different type of Zeeman effect at each of the principal perturbations in the (0, 0) band seems to require different interacting levels at each of the points, in order that some variations in the arrangement of the magnetic sublevels exist. It is true that $^3\Pi$ and $^1\Pi$ levels perturbing each other constitutes a violation of the Kronig rule that the two perturbing states must have the same multiplicity. However, this rule need not be expected to hold here, for singlet-triplet transitions of fair intensity do occur in CO. And from such a $^1\Pi$, $^3\Pi$ interaction as many as six perturbations could be produced in one of the $^1\Sigma \rightarrow ^1\Pi$ bands, since all Π terms are doubled (Λ -doubling).

It is reasonable to assume that the $^3\Pi$ state is fairly close to case *a*, for the separation⁷ of the P_1 and P_3 branches near the origins of the $^3\Sigma \rightarrow ^3\Pi$ third positive CO bands is some 50 to 60 cm^{-1} . This spacing is almost entirely due to the multiplet intervals in the $^3\Pi$ level, since Dieke and Mauchly report that the triplet separation of the $^3\Sigma$ state is unnoticeable near the origin.⁸ In the range of rotational energy levels in which we are interested, then, this spacing of the $^3\Pi$ levels is still probably considerably greater than the splitting produced by the magnetic field. The partial transition towards case *b* with increasing rotational energy would only tend to make the group of magnetic sublevels slightly asymmetrical with respect to the no-field level.

In case *a* states of diatomic molecules the additional energy of the component levels due to the magnetic field is given by the well-known formula⁹

$$W_{\text{mag.}} = \frac{\Lambda(\Lambda + 2\Sigma)M}{J(J + 1)} \frac{eh}{4\pi mc} |H| \quad (1)$$

where all the symbols have their usual significance. For $^1\Pi$ levels this reduces to

$$W_{\text{mag.}} = \frac{+M}{J(J + 1)} \left(\frac{eh}{4\pi mc} |H| \right) \quad (1a)$$

while for the $^3\Pi_0$, $^3\Pi_1$ and $^3\Pi_2$ levels with $\Sigma = -1, 0$ and $+1$, respectively, we have

$$^3\Pi_0: W_{\text{mag.}} = [-M/J(J + 1)] (\Delta v_{\text{norm}}) \quad (1b)$$

$$^3\Pi_1: W_{\text{mag.}} = [+M/J(J + 1)] (\Delta v_{\text{norm}}) \quad (1c)$$

$$^3\Pi_2: W_{\text{mag.}} = [+3M/J(J + 1)] (\Delta v_{\text{norm}}). \quad (1d)$$

⁷ R. K. Asundi, Proc. Roy. Soc. A124, 277 (1929).

⁸ G. H. Dieke and J. W. Mauchly, Phys. Rev. 40, 123 A(1932).

⁹ Cf. for instance, R. de L. Kronig, *Band Spectra and Molecular Structure*, p. 37.

The $^3\Pi_1$ levels have exactly the same Zeeman splitting, then, as $^1\Pi$ levels of the same J value, while for $^3\Pi_0$ the splitting is of exactly the same amount but with the level $+M$ lowest and the level $-M$ highest. In $^3\Pi_2$ the overall width of the group of sublevels is three times that in the $^3\Pi_0$ and $^3\Pi_1$ levels.

As an aid in discussing the effect of the magnetic field on the perturbed levels, the possible arrangements of these levels at the intersection points is sketched in Fig. 2, only the extreme values of $M = \pm J$ being shown. If the $^3\Pi$ level lies just below the $^1\Pi$, the explanation is the same with the substitution of $-M$ for $+M$ and $+M$ for $-M$ throughout. Now the matrix elements of the perturbation energy will be different from zero only if diagonal in M as well as J ; i.e., only levels of the same M will perturb each other. With a normal $^3\Pi$ the first close approach of levels with the same J will involve the $^3\Pi_0$ levels (Fig. 2a). In this case the levels with $+M$'s are thrown closer to levels of the same $+M$ value in the other group, and are thus perturbed more,

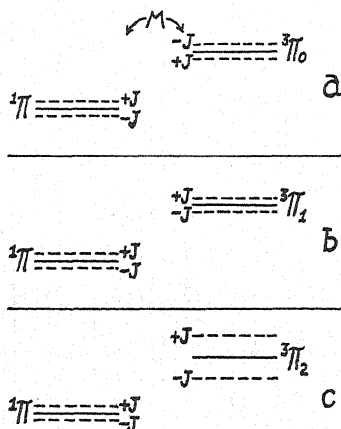


Fig. 2. Rough sketch showing the relative placing of the magnetic sublevels and widths of level patterns in case a $^1\Pi$ and $^3\Pi$ levels of the same J value. Only the no-field levels (solid lines) and the levels with extreme values of $M = \pm J$ are drawn. The other $2J-1$ sublevels will be spaced fairly uniformly between the two extreme levels in each case. The separation of the $^1\Pi$ and $^3\Pi$ levels and the scale of the splitting is quite arbitrary.

say into or beyond the normal region of $-M$ levels. The latter at the same time are forced farther apart from the $-M$ levels of the same value in the other state, and so are perturbed less than before, being thrust through or beyond the region where normally the group of $+M$ levels would be found. This effect would just tend to invert and spread out the whole pattern of magnetic sublevels in each group. The sensitiveness of the perturbation energy to slight change in the interval between the interacting levels is evidenced by the magnification of the Zeeman patterns of the lines (P_b (8) pattern spread 1.64 cm^{-1} at 10,000 gauss as compared to the regular $2\Delta\nu_{\text{norm}}/J \cong 0.11 \text{ cm}^{-1}$). The occurrence of a region of zero intensity at the center of the Zeeman pattern for a much displaced line such as P_b (8) at the higher field strengths must be attributed to this sensitiveness of the perturbation energy to the size of the interval between the perturbing levels, and to the fact that in

the $^3\Pi$ groups the level $M=0$ will probably be of not exactly the same energy as the original level owing to a slight tendency to spin uncoupling by the field.

If the crossing-over occurs between the $^1\Pi$ and $^3\Pi_1$ levels (Fig. 2b), no effect of the magnetic field on the perturbed band lines should be observed if the $^3\Pi_1$ is strictly case *a*, for the field splitting in the two sets of levels is identical. But a small asymmetry with respect to the no-field levels of the block of magnetic sublevels, due to spin-field coupling, could have the effect of increasing or decreasing slightly the energy interval between the two levels having the same J value. And because this energy interval is already small (perturbation very large), the perturbation energy is appreciably increased or decreased. The type of Zeeman effect observed at the Q -branch perturbation at $J=12$ could originate in this kind of interaction.

When the levels concerned are $^1\Pi$ and $^3\Pi_2$ (Fig. 2c), the situation is somewhat like that for the $^1\Pi$, $^3\Pi_0$ interaction. Because the splitting due to the field in the $^3\Pi_2$ level is about three times that in the $^1\Pi$ level of the same J value, the $-M$ levels are forced closer together, with resulting increased perturbation, while each $+M$ level is separated further from the corresponding $+M$ level of the other group with consequent decrease in the perturbation energy. The result should be a much-broadened, solid Zeeman pattern for the perturbed band line, with perhaps a narrow minimum of intensity in the center at the highest field strengths. This is the type of pattern observed for the lines of the P , R perturbation at $J=16$.

The narrow, sharp doublets observed in the field for the $J=29$ Q -branch perturbation could originate in the $^1\Pi$, $^3\Pi_0$ type of interaction described above, the comparative narrowness being caused by the decrease in the splitting of the levels the higher the J , and the sharp doublet character originating in an asymmetry in the $^3\Pi_0$ group of Zeeman levels, caused by the ever closer approach to case *b* as J increases.

Theory of Continuous Absorption of Oxygen at 1450A

By E. C. G. STUECKELBERG

Palmer Physical Laboratory, Princeton University

(Received September 6, 1932)

The continuous absorption of O_2 has lately been measured by Ladenburg, Van Voorhis and Boyce. Their suggested explanation in the term diagram of the molecule is compared to the corresponding matrix elements.

PART I. THEORY OF CONTINUOUS ABSORPTION IN DIATOMIC MOLECULES

CONTINUOUS absorption and emission in diatomic molecules have been explained as transitions between electronic states with discrete vibrational energy and electronic states with continuous energy.

Condon¹ gave in his paper a qualitative way of obtaining the relative intensities of the observed continua. This has been applied to the continuous emission of H_2 by Winans and Stueckelberg² and by Finkelburg and Weizel.³ Other applications have been made by Kuhn.⁴

The present paper gives a quantitative explanation of the continuous absorption of O_2 as measured by Ladenburg, Van Voorhis and Boyce.⁵ The probability (number of transitions per second) of a transition from the discrete state k to the energy continuum W is:

$$\Gamma_{kW} = (\pi^2/\hbar) |H_{kW}|^2 (dQ_W/dW).$$

H_{kW} is the matrix element of the perturbing energy H , and dQ_W/dW is the number of states per region dW . In our case we have $H = ME$ where M is the electric moment of the system, and $E = E_0 \cos 2\pi\nu t$ the electric field strength of the incoming light wave. One obtains $|H_{kW}|^2 = |M_{kW}|^2 E_0^2/3$. The factor $\frac{1}{3}$ is due to the averaging over the angle between E_0 and M . Let N_k be the number of molecules in the state k per cm^3 , and let n be the number of incident light quanta per cm^2 and sec. The number of quanta absorbed in the thin layer Δl per sec. is

$$\Delta l dN_k/dt = \Delta n = - \sum_k \Gamma_{kW} N_k \Delta l.$$

Between n and E_0^2 we have the relation: $cE_0^2/8\pi = nh\nu = I_\nu$. This leads to the following expression for the absorption coefficient:

$$\alpha_\nu = - \frac{\Delta n}{n \Delta l} = \frac{8\pi^2}{3} \sum_k \frac{N_k}{h} |M_{kW}|^2 \frac{\nu}{c} \frac{dQ}{d\nu}; I_{\nu,t} = I_{\nu,0} e^{-\alpha_\nu l}. \quad (1)$$

¹ E. U. Condon, Phys. Rev. **32**, 858 (1928).

² J. G. Winans and E. C. G. Stueckelberg, Proc. Nat. Acad. Amer. **14**, 867 (1928).

³ W. Finkelburg and W. Weizel, Zeits. f. Physik **68**, 577 (1931).

⁴ H. Kuhn, Zeits. f. Physik **63**, 558 (1930).

⁵ R. Ladenburg, C. C. Van Voorhis and J. C. Boyce, Phys. Rev. **40**, 1018 (1932); referred to as L.V.a.B.

The electric moment $M(\epsilon, r\theta\phi)$ depends on the coordinates ϵ of all the electrons and on the usual coordinates $r\theta\phi$ of the two heavy nuclei. We assume, that the wave function $\Psi_k(\epsilon, r\theta\phi)$ can be decomposed into

$$\psi_k(\epsilon, r\theta\phi) = \phi_n(\epsilon, r)\Theta_{JM}(\theta\phi)\psi_{nv}(r).$$

The matrix element $M(n''J''M''v'', n'J'M'v')$ can be written, after integrating over $\epsilon, \theta\phi$,⁶ (if $J \gg 1$ and $\Lambda' = \Lambda'' = 0$, and if there is no external magnetic field) as:

$$|M(n''J''v'', n'J'v')| = |M_{k''w'}| = (2J)^{1/2} \int dr \cdot M_{n''n'}(r) \psi_{n''v''}(r) \psi_{n'v'}(r). \quad (2)$$

$M_{n''n'}(r) = M(r)$ is the electric moment associated with an electron jump from state $n' \rightarrow n''$, if the nuclei are held fixed at the distance r . We assume for the vibrational states v'' the states of a harmonic oscillator i.e.:

$$\psi_{n''v''}(r) = e^{(-1/2)(r-r_0'')^2/a''^2} \times \text{Polynomial in } (r - r_0'') \quad (3)$$

$$\psi_{n''v''=0}(r) = \psi_0 = a^{-1/2} \pi^{-1/4} e^{(-1/2)(r-r_0'')^2/a''^2}, \quad (3b)$$

where a'' (in cm) is defined by the molecular constants ω_0'' and μ :

$$a''^2 = a^2 = (\hbar^2/8\pi^2\mu)(1/\hbar c\omega_0''/2);$$

$$1/\mu = 1/M_I + 1/M_{II} \quad W'' = \hbar c\omega_0''(v'' + \frac{1}{2})$$

and where r_0'' is the equilibrium separation. The functions (3a) and (3b) are different from zero only in the immediate neighborhood of r_0'' . We expand:

$$M(r) = M(r_0'') + (r - r_0'')M'(r_0'') + \dots \quad (4)$$

(2) will be of a similar form:

$$M_{k''w'} = g[M(r_0'') + \beta \cdot M'(r_0'') + \dots]. \quad (5)$$

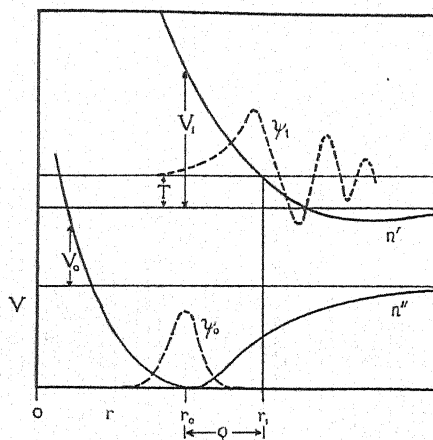


Fig. 1. Potential energy functions $V(r)$ and nuclear wave functions: $\psi_1(r)$ for a non-quantized level of the electronic state n' , $\psi_0(r)$ for the lowest vibrational level of the electronic state n'' .

⁶ W. Weizel, Bandenspectren Hb.d. Exp. Phys. Ergänzungsband I, p. 164.

We are left with the determination of the wave function $\psi_{n', W'}$ representing an oscillation between a finite $r=r_1$ and infinity ($r=R$, $\lim R=\infty$) (see Fig. 1). r_1 is the separation at which the potential energy V_1 equals the kinetic energy at infinity T . We make use of the method by Kramers⁷ in order to obtain an expression for $\psi_{n', W'} = \psi_1$. His solution is, if $p^2 = 8\pi^2\mu(T - V_1)/h^2$: and if $\gamma = (8\pi^2\mu)/h^2 \cdot \partial/\partial r \cdot V_1(r)$; $\rho = r_1 - r_0''$; $\xi = r - r_1$; $p_\infty^2 = 8\pi^2\mu T/h^2$:

$$\begin{aligned} \xi \gg 0; \quad T - V_1 \gg 0: \psi_1 = \psi_{1>} &= R^{-1/2} \left(\frac{2p_\infty}{p} \right)^{1/2} \cos \left[\int_0^\xi p d\xi - \frac{\pi}{4} \right] \\ \xi \cong 0; \quad T - V_1 \cong 0: \psi_1 = \psi_{10} &= R^{-1/2} \left(\frac{2p_\infty}{\gamma^{1/3}} \right)^{1/2} \omega(\gamma^{1/3}\xi) \end{aligned} \quad (6)$$

$$\xi \ll 0; \quad T - V_1 \ll 0: \psi_1 = \psi_{1<} = R^{-1/2} \text{ neg. real. exp.}$$

Condon² has shown in a qualitative way, that the part where $T - V_1 \cong 0$, i.e., the region near r_1 , is the most important in evaluating (2). We assume therefore that the part of the integrand in the neighborhood of r_1 only (i.e., the function ψ_{10}) is of importance. This is certainly true, if the slope of the potential energy curve γ of the state n' is constant over the range where ψ_0 is different from zero, and if $\gamma a^3 \ll 1$.

(2) becomes:

$$M_{n', W'} \cong g M(r_0) \cong M(r_0) \left\{ \frac{4}{\pi^{1/2}} \frac{J p_\infty}{\gamma^{1/3} a R} \right\}^{1/2} \int_{-\infty}^{+\infty} d\xi e^{-\xi^2/2a^2} \omega(\gamma^{1/3}\xi).$$

The function $\omega(z)$ is tabulated by Kramers⁷ and can be expressed by a complex integral (Airy's Integral):⁸

$$\omega(z) = \frac{-i}{2\pi^{1/2}} \int_{(P)} dt e^{z t + t^3/3} \quad (\text{for the path } P \text{ see Kramers}).^7$$

Then one has for g .

$$\begin{aligned} g &= \left[\frac{4}{\pi^{1/2} R \gamma^{1/3} a} \right]^{1/2} \frac{-i}{2\pi^{1/2}} \int_{(P)} dt \\ &\quad \int_{-\infty}^{+\infty} d\xi e^{-[(\xi + \rho - a^2 \gamma^{1/3} t)^2/2a^2]} e^{(t^3/3) + (1/2) a^2 \gamma^{2/3} t^2 - \gamma^{1/3} \rho \cdot t}. \end{aligned}$$

If the substitutions $\xi' = \xi + \rho - a^2 \gamma^{1/3} t$; $\tau = t + b$; $b = \frac{1}{2} \gamma^{2/3} a^2$; and $x = \gamma^{1/3} \rho$ are made, the integration over $d\xi'$ can be carried out:

$$g = \left[\frac{8\pi^{1/2} J p_\infty a}{R \gamma^{1/3}} \right]^{1/2} e^{bx + (2/3)b^3} \omega(-(x+b)) = \left[\frac{4\pi^{1/2} J p_\infty}{R \gamma a} \right]^{1/2} f^{1/2}. \quad (8)$$

We abbreviate

$$f = 4b\omega^2(-(x+b)) e^{2b + (4/3)b^3}. \quad (9a)$$

⁷ A. H. Kramers, Zeits. f. Physik 828 (1926).

⁸ G. N. Watson, Theory of Functions, p. 188, Cambridge, 1922.

If the argument of $\omega(z)$ takes large negative values ($-z > 2$), a good approximation is

$$2\omega(z) = (-z)^{-1/4} e^{-(2/3)(-z)^{3/2}}$$

we make a further substitution: $y = x/b^2 = (\rho/a)(4/\gamma a^3)$ and have for $-(x+c) \gg 2$:

$$\begin{aligned} f &= (1+y)^{-1/2} \exp \left[-\frac{4b^3}{3} \left\{ (1+y)^{3/2} - (1+(3/2)y) \right\} \right] \\ &= \left(1 + 4\frac{\rho}{a} \frac{1}{\gamma a^3} \right)^{-1/2} e^{-(\rho^2/a^2) - \dots} \end{aligned} \quad (9b)$$

If $\gamma a^3 \gg 1$, this is practically the same result as one obtains if one "reflects" the function ψ_0^2 on the potential energy curve of the repulsive state $v/c = (v/c)(\rho)$.

If the argument of the function ω is positive, i.e., if $(x+b^2)$ is negative the expression for M_0 oscillates. This was also predicted from the qualitative picture of Condon.² The conditions for oscillations are

$$\begin{aligned} -(x+c^2) &= -\gamma(\frac{1}{4}\gamma a^3(a+\rho)) \gg 0 \quad (\text{order of } 1) \\ -\rho/a &\gg \frac{1}{4}\gamma a^3 + 1/(\gamma a^3)^{1/3}. \end{aligned}$$

The next step is to justify the application of ψ_{10} in (7) in the whole region ξ between $-\infty$ and $+\infty$.

The function $M(r)$ depends on r . The final result involves an average value of $M(r)$, say $M(r_i)$. If r_i coincides with r_1 , we can conclude, that the region around $r=r_1$ is the most important one. Taking the expansion (4) and (5) this means $\beta = r_1 - r_0 = \rho$.

In the integral:

$$g\beta M'(r_0) = M'(r_0) \int_{-\infty}^{+\infty} d\xi (\rho + \xi) \psi_0(r) \psi_1(r) \quad (10)$$

we make the same substitutions and notice, that

$$\int_{-\infty}^{+\infty} dt \gamma^{1/3} t e^{(t^3/3) + (1/2)\gamma^{2/3} a^2 t^2 - \gamma^{1/3} t \rho} = -\frac{\partial}{\partial \rho} \int_{-\infty}^{+\infty} dt e^{(t^3/3) + \dots}$$

This gives:

$$\beta = -(a^2/4)(1/f)(\partial/\partial \rho)f. \quad (10a)$$

As long as $y < 1$, we have roughly:

$$\beta = \rho + a[1/(\gamma a^3)^{1/3}] \cong (r_1 - r_0), \text{ if } \gamma a^3 > 1.$$

The application of ψ_{10} is therefore justified. The parts of the integrand due to $\psi_{1<}$ and $\psi_{1>}$ are negligible to the same extent as the far away parts of ψ_{10} , which, even if taken into account, do not change appreciably the final result, as long as

$$\gamma a^3 \gg 1 \text{ or } a^3(\partial/\partial r)V_1 \gg \hbar^2/(8\pi^2\mu). \quad (11)$$

The evaluation of matrix elements for which $v'' \neq 0$ can be carried out in the same way as (10) and (10a).

The number of energy levels dQ/dp_∞ in the unstable part of state n' per region dp_∞ goes to infinity as the radius R becomes infinite: $dQ = (R/\pi)dp_\infty$. Going from p to $\hbar\nu$, we have for the number of levels per $d\nu$

$$dQ/d\nu = 4\pi\mu R/\hbar p_\infty. \quad (12)$$

If $\omega_0'' \gg kT/\hbar c$, practically all the molecules are in the level $v'' = 0$. The expression for the absorption coefficient is, making use of (1), (7), (8) and (12):

$$\alpha_\nu = \frac{128\pi^{9/8}}{3} \frac{\mu}{\hbar^2\gamma a} \sum_J \left(\frac{\nu}{c}\right) M^2(r_1) f J N_J.$$

We have to average over the different rotational levels J . (ν/c), M^2 and f can be considered as independent of J : $\sum_J J \cdot N_J \cong (3\pi^{1/2}/2) N (kT'/\hbar c \cdot B_0)^{1/2}$ (see Weizel⁶ p. 167).

$$\alpha_\nu = 64\pi^5 \cdot \frac{N\mu(kT/\hbar c \cdot B_0)^{1/2}}{\hbar^2 \cdot \gamma a} \left(\frac{\nu}{c}\right) M^2(r_1) f \cdot \text{cm}^{-1}. \quad (13)$$

PART II. THE CONTINUOUS ABSORPTION OF OXYGEN

The continuous absorption of oxygen, extending from 1750Å to 1300Å, has been measured by L.V.a.B.⁵ They explain this absorption as a transition from the normal $^3\Sigma$ state of the molecules to the upper $^3\Sigma$ state. The Frank-Condon principle applied to the potential energy curves, calculated by Morse⁹ and Stueckelberg,¹⁰ gives the right order of magnitude for ν/c . We have $\omega_0'' \gg kT/\hbar c$ and $\Lambda' = \Lambda'' = 0$ for $\Sigma \rightarrow \Sigma$ transitions. Therefore a comparison between the experimental curve $\alpha_\nu = \alpha_\nu(\nu/c)$ by L.V.a.B.⁵ and the theoretical expression (13) can be carried out in the following way. We plot

$$\text{const.} - \log [\alpha_\nu/(\nu/c)] = -\log f = (4b^3/3) [(1+y)^{3/2} - (1 + (3/2)y)] + \frac{1}{2} \log [1+y]$$

as a function of y (Fig. 2). To do this we had to assume a value for $b = b_0$. As a is a known quantity ($\omega_0'' = 1566 \text{ cm}^{-1}$; $a = 5.16 \times 10^{-10} \text{ cm}$) this fixes the value of $\gamma = \gamma_0$.

The comparison between $-\log f$ and the experimental curve of $-\log (\alpha_\nu/(\nu/c))$ gives ν/c as a function of y . This relation is also plotted in Fig. 2. Instead of marking the individual points, an area was drawn. According to the theory $\nu/c = (\nu/c)(y)$ ought to be a straight line, if M and γ are constants over the region. This seems to be true within the limits of error. We obtain a value for $d(\nu/c)/dy$. The definition of y and γ leads to the relation

⁹ P. M. Morse, Phys. Rev. **34**, 57 (1929).

¹⁰ E. C. G. Stueckelberg, Phys. Rev. **34**, 65 (1929).

$$\gamma^2 = [32\pi^2 \cdot \mu c / ha^4] [d(\nu/c)/dy].$$

This newly determined value of $\gamma = \gamma_1$, gives a new value for $b = b_1$. The procedure is repeated until $\gamma_m = \gamma_{m-1}$. This is the case in Fig. 2. The probable

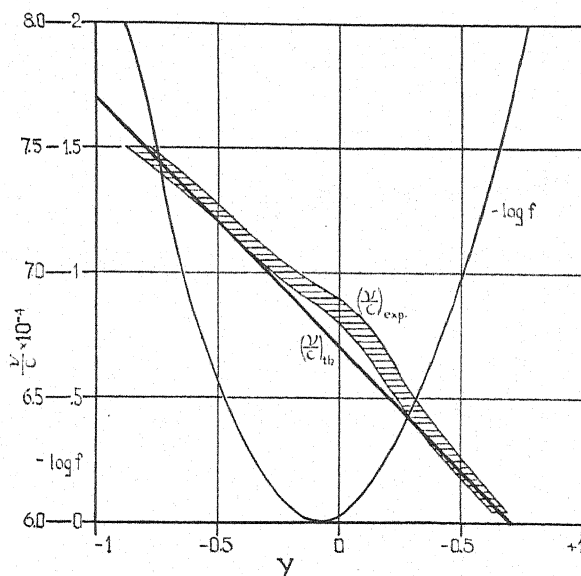


Fig. 2. $-\log f = -\log (\alpha_\nu/(\nu/c))$ and wave number (ν/c) as functions of the parameter $y = 4\rho/\gamma a^4$. The experimental points (L.V. and B.) are plotted as a broad stripe. The black line has been chosen to determine curve A in Fig. 3.

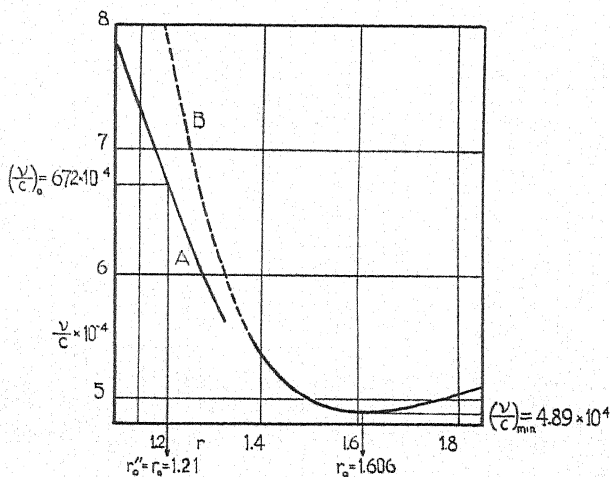


Fig. 3. Potential energy curves for the upper ${}^3\Sigma$ -state of the O_2 molecule. The ordinates are the energy in wave numbers (ν/c) , measured from the lowest vibrational level of the normal ${}^3\Sigma$ -state. $r_0'' = r_0$ is the equilibrium separation of the normal ${}^3\Sigma$ -state. (r in 10^{-8} cm^{-1} .)

error in γ is about 2 percent. The value of ν/c for $y = \rho = 0$ determines the height of the potential energy curve over the equilibrium separation r_0'' .

The value of γ determines the inclination of the potential energy curve at this point.

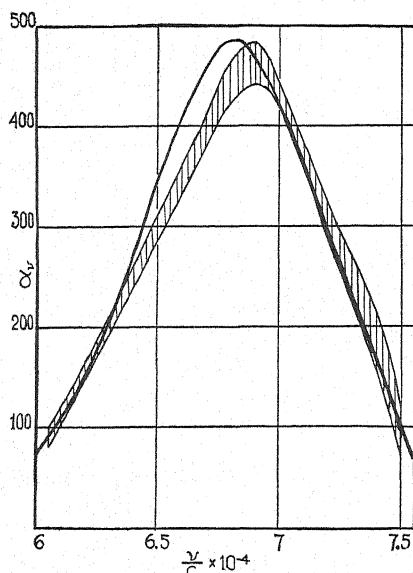


Fig. 4. Absorption coefficient of O_2 as a function of (ν/c) . The broad stripe represents the experimental result of L.V. and B., while the black line shows the theoretical absorption coefficient α_ν based upon the potential energy curve A in Fig. 3.

The results are:

$$(\nu/c)_{r=r_0} = (6.72 \pm 0.05) \times 10^4 \text{ cm}^{-1}$$

$$\gamma = (0.51 \pm 0.01) \times 10^{29} \text{ cm}^{-3}$$

$$(d(\nu/c)/dr)_{r=r_0} = (10.8 \pm 0.2)(10^4 \text{ cm}^{-1}/10^{-8} \text{ cm}).$$

Fig. 3 is a comparison between the so defined curve A and the curve calculated by Morse⁹ and Stueckelberg,¹⁰ B . One sees that the extrapolation of their calculation (dotted line B in Fig. 3) is too steep. However the curve A seems to point in the right direction. Fig. 4 compares the theoretical absorption coefficient (based upon A) with the experimental values of L.V.a.B. Like in Fig. 2, an area is plotted instead of marking their individual points.

Eq. (13) permits a determination of $M(r_0)$ under the assumption of room temperature ($T=290^\circ\text{K}$) and with $B_0=1.44 \text{ cm}^{-1}$.⁶

$$M(r_0) = (4.77 \times 10^{-10} g^{1/2} \text{ cm}^{3/2} \text{ sec.}^{-1/2}) \times (0.65 \times 10^{-8} \text{ cm}).$$

This is a reasonable result.

Photoelectric Quantum Counters for Visible and Ultraviolet Light. Part I

By GORDON L. LOCHER¹
The Rice Institute

(Received September 28, 1932)

Extremely sensitive instruments for measuring faint light, from 900A to 7500A, have been made by combining the essential features of photoelectric cells and Geiger-Müller tube counters, so that the photoelectrons ejected by the radiation are individually counted. With some of the tubes described, photocurrents of 0.05 electrons per second can be measured. Photoelectric surfaces of Sn, Cd, Zn, Cu, brass, Ag, Hg, Mg, I₂, and Se, were used for measuring ultraviolet light. Visible-sensitive surfaces were made by coating Cu cathodes with fused NaCN, and with amalgams of Na, K, Cs, Sr, and Na-K, and subsequently directing intense H⁺ bombardment against them, in a hydrogen atmosphere. In this manner, thin films of hydrides of the respective metals were formed by reduction. The KH-on-Hg cathodes were the most sensitive to visible light, while the most sensitive one for ultraviolet light was a thin layer of I₂ on Se. Very thin films of about 30 aniline dyes and photographic sensitizers were successively coated on the zinc cathode of a counter. The dye usually shifted the photoelectric threshold toward the ultraviolet, but increased the total sensitivity of the surface. Similar effects were obtained by reversing the direction of field in the counting tube and introducing traces of certain organic liquids into the vicinity of the tungsten wire, which was then the cathode. Thus diethyl-aniline increased the sensitivity by a factor of about 25. Different gases were also tried in the counting tubes; it was found best to use a gas with a high minimum ionization potential, when possible. A counter was used for comparing the total ultraviolet luminosities of several light sources. Thus a particular quartz mercury arc, using about 120 watts, gave 6×10^6 times as much ultraviolet as did a 1000-watt incandescent lamp. Amplifying and recording apparatus is described which is suitable for counting as many as 100 electrons per second, arriving at random times. The paper also discusses criteria for determining the useful electron-counting sensitivity of a counter, the factors limiting its counting speed, an explanation of its mode of operation, and evidence for the existence of other ionic emissions, besides electrons, from counter cathodes. Some possible applications of the counters are mentioned.

I. INTRODUCTION

THE devices described here are combined photoelectric cells and Geiger-Müller tube counters. Photoelectrons liberated from the sensitive surfaces cause small individual discharges between the electrodes, which are amplified and made to operate an impulse recorder or oscillograph. The number of photoelectrons liberated, hence the number of impulses, in unit time, is a measure of the intensity of the incident light.

The main advantage of these counters over other kinds of light detectors lies in their enormous sensitivity for measuring photocurrents. This is shown by comparison of the counters with a Hoffmann electrometer and photoelectric cell. About 1000 electrons per second are required to give a detectable

¹ Later, National Research Fellow, Bartol Research Foundation of The Franklin Institute.

current in the electrometer, even when adjusted to very high sensitivity, whereas some of the counters described here will readily detect a "current" of 0.05 electrons per second, or about 1/20,000 as much. Other desirable features of the counters include simplicity of construction and use, portability while operating, and cheapness of construction. Certain limitations inherent in them will be discussed in a later section of this paper.

In counting individual photoelectrons, occasionally liberated, one seems to approach the limit of sensitivity of a photocurrent measuring device. So the problem of measuring the faintest light becomes one of preparing stable photoelectric surfaces of high quantum efficiency, that have the most suitable spectral distribution of response for the light to be measured.

The work reported here is of a preliminary nature. It includes details of construction of the counters, their general behavior while in use, methods of amplifying and recording impulses, and most especially, methods of preparing numerous photoelectric surfaces that respond to light from the far ultraviolet to the infrared.² The writer believes that these counters will find useful application in numerous problems requiring the detection and measurement of faint radiation, and that by their high sensitivity they will make possible the performance of others hitherto very difficult, or impossible. One may especially cite astronomical photometry, spectroscopy, and physical optics, as fields where advantageous application is expected.

B. Rajewski³ has shown that the usual type of Geiger-Müller⁴ tube counters can be modified to respond to ultraviolet light, by adding quartz windows and coating the interior of the metal tubes with cadmium or zinc. He believes one of these to be sensitive enough to detect 12 quanta of 2650Å light per sq. cm per second, and further reports the detection of the "mitogenetic rays," supposed by some biologists to be emitted by rapidly dividing plant cells and certain animal tissues. Rajewski's counters were sufficiently large to give a rather high rate of spontaneous counting, in darkness. This is due to radioactivity, cosmic rays, and other spurious causes. By surrounding the counters with a heavy iron shield, the accidental rate was reduced to 20 or 30 impulses per minute.

Rapid spontaneous counting is objectionable for two reasons. In the first place, the accidental count is subject to statistical variation, and in the second, it forms a background on which the true count is superposed, thereby raising the minimum detectable light intensity. In this respect, the use of counters exactly parallels that of vacuum photoelectric cells. Statistical variation in their dark currents becomes troublesome when very feeble light is to be measured; and the superposition of the fluctuating dark current on the true photocurrent diminishes the useful sensitivity of the cell. By the *useful*

² The important matter of measuring the quantum efficiencies and sensitivities of particular counters, expressed as the least number of quanta that can be detected in a given time, has not yet been done.

³ B. Rajewski, *Phys. Zeits.* 32, 121 (1931).

⁴ H. Geiger and W. Müller, *Phys. Zeits.* 29, 839 (1928); *Phys. Zeits.* 30, 489 (1929); *Phys. Zeits.* 30, 523 (1929).

sensitivity of a cell or counter, one means the best sensitivity for which the results may be *reproduced*, within arbitrarily assigned limits of error, under identical experimental conditions.

The problem in hand is one of measuring light that can be concentrated by lenses and mirrors. This offers a means of reducing the accidental count inherent in large tubes, by using small ones and focusing the light on the photoelectric surfaces. However, the resistance between electrodes must be at least 10^{10} ohms,⁵ so a modified form of counter construction is necessary in order to get the required insulation. The use of alkali photoelectric surfaces lowers the resistance and greatly accentuates the difficulty of maintaining good insulation.

The tube described in the next section had a minimum path between electrodes of about 25 cm, over Pyrex glass. Its resistance is estimated at 10^{18} to 10^{16} ohms. The rate of accidental counting, in darkness, depended on the electrodes. Thus the average for cathodes of copper, zinc, cadmium, tin, and mercury was about 1.5 per minute. Similar electrodes bearing alkali metals gave accidental counts ranging from about 3 per second to 6 per minute. Several iodine-coated silver and copper ones showed very high sensitivity to ultraviolet light, with rates as low as 0.7 per minute, in darkness. No shield was used for stopping penetrating radiation; the count due to stray γ -rays and cosmic rays should be 0.5 to 0.9 per minute, with counters of the size used.

II. DESCRIPTION OF THE COUNTERS

Fig. 1 is a sectional diagram of the counting tube. Essential parts are the axial electrodes E_1 and E_2 , the Pyrex tube A , and the quartz window B , which is attached with wax. E_2 is a three-fourths-cylindrical cathode, carrying the photoelectric surface on its concave side. The tube is filled with a gas at 6 to 8 cm pressure. E_2 is maintained at a high negative potential with respect to E_1 , so that photoelectrons set free by the impinging light will be drawn to E_1 with sufficient velocity to start "bursts" of ionization by collision. These cause minute current-impulses that are amplified and automatically counted. By means of the ground joint C , the part-cylindrical electrode may be removed for replacement or treatment. The wire electrode is also removable. It is attached to the lead wires L_1 , by hooks, and is kept under a slight tension by a small steel spring.

This design has been found very convenient for experimentation with photoelectric surfaces, and for studying the operating characteristics of the tube. The counter used by the writer has been assembled and dismantled some hundreds of times during the course of various tests.

The cylindrical electrodes had an average length of 11 mm, and were about 7 mm in internal diameter. Longitudinal slots about 4.5 mm wide were sawed in them to admit the light. The wire electrodes were usually of polished platinum or tungsten, from 0.038 mm to 0.11 mm in diameter.

⁵ Otherwise, fluctuations in the leakage current across the insulators are amplified and recorded as impulses. This spurious count becomes more numerous as the insulator resistance diminishes. The writer found a metal-ebonite G.-M. tube, 1 cm in diameter, to be very unsatisfactory for that reason.

It has been found desirable to use especial care in centering the electrodes, and in making the anode surface smooth. If the wire does not lie nearly along the axis of the cylinder, or if there are major irregularities on the latter, the field may be so distorted as to render much of the photoelectric surface feeble or inoperative. Photoelectrons released with very low velocities in small pits in the metal probably fail to get into the field, and are not counted. It

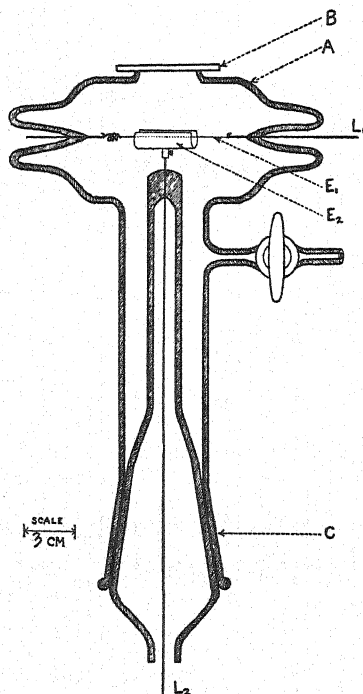


Fig. 1. Cross section of the counting tube. E_1 , wire electrode; E_2 , cylinder electrode, carrying the photoelectric surface; B , quartz window; A , glass body of tube; C , ground joint; L_1 and L_2 , leads to amplifier and high-potential source, respectively.

was shown that cathodes differing appreciably from cylindrical form were completely unsatisfactory. Sharp points on the wires are even more objectionable than those on the cylinders, because of the tendency to discharging action. Hence it is good practice to polish the wire with rouge paper before introducing it into the counter. The use of oxide and other coatings on the wires will be discussed in the section dealing with the preparation of electrodes.

III. AMPLIFIERS AND IMPULSE RECORDERS

Numerous good amplifiers for use with Geiger-Müller counters have been described elsewhere.⁶ But the requirements of the present work are rather

⁶ For example: J. A. Van den Akker and E. C. Watson, *Phys. Rev.* **37**, 1631 (1931); B. Rajewski, reference 3; R. Jaeger and J. Kluge, *Zeits. für Inst.* **52**, 229 (1932); N. A. de Bruyne and H. C. Webster, *Cambridge Phil. Soc. Proc.* **27**, 113 (1931).

more stringent than for other counters, because the tube electrodes are much nearer together and less ions are produced by collision at each impulse. The impulse current must also be kept sufficiently small that no *light* will be emitted by the discharge. Even when this light is far below the limit of visual sensitivity, its photoelectric action will generally cause extended impulses, instead of sharp ones. It is little more than a fortunate accident that one can get impulses that are strong enough to amplify and record, but too weak to generate light in the counters, especially when alkali metals are present. These remarks apply as well to Geiger-Müller counters for cosmic rays, γ -rays, and x-rays. On the basis of the behavior of photoelectric counters with many different cathodes, filled with different gases, and on comparison of their behavior with that of ordinary tube counters, the writer has become of the opinion that the extension (i.e., "drawling") of impulses observed when the operating potential across the tube is slightly too high, results chiefly from this secondary photoelectric action of the light generated by the discharges themselves.

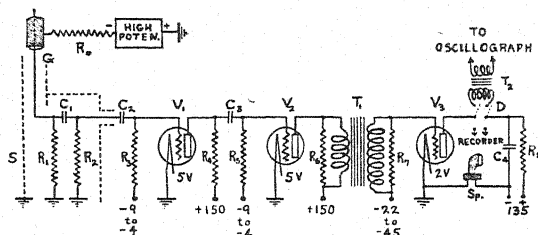


Fig. 2. Amplifying and recording circuit. The resistances, R , are in megohms; capacities, C , are in microfarads.

$R_0 = 1000$. (xylene)	$R_7 = 2$. to ∞	V_1 , UX 240
$R_1 = 30$. (xylene)	$R_8 = 0.1$ (variable)	V_2 , UX 240
$R_2 = 0.5$	$C_1 = 0.01^*$ to 0.0005	V_3 , W.E. 269-A (thyatron)
$R_3 = 10$.	$C_2 = 0.01$	G , counting tube
$R_4 = 5$.	$C_3 = 0.01$	Sp , loud speaker
$R_5 = 1$.	$C_4 = 1$.	S , grounded shield
$R_6 = 0.5$ to ∞	$T_1 = 1$ to 3	D , d.p.d.t. switch

Another feature of obvious importance is that the amplifier and recorder be capable of accurate and very fast counting when relatively high light intensities are being handled. Several high-gain amplifiers were tried and discarded before a rather satisfactory one was developed. The circuit diagram of this one is shown in Fig. 2. The use of a thyatron as a relay tube is a great convenience; it gives uniform impulses and eliminates the relatively slow-moving mechanical parts of a relay, yet allows enormous gain in amplification. The arrangement for stopping the thyatron discharges is patterned after that of Jaeger and Kluge;⁷ the condenser C_4 is charged through the resistance R_8 ; when an impulse causes an arc to strike in the thyatron, C_4

* The 0.01 mfd condenser used was of rather low resistance, so that R_1C_1 did not represent the true constant for the discharge of C_1 . In this case, C_2 was added in order to better isolate the grid of V_1 from the high-potential source.

⁷ R. Jaeger and J. Kluge, *Zeits. für Inst.* **52**, 229 (1932).

discharges through the tube and recording device, after which the arc stops. R_s is made just large enough to keep the arc from being maintained directly from the battery. Fig. 3 shows some typical impulses recorded on an overdamped string oscillograph. It will be observed that they normally last for about 0.01 second. With oscillographic recording, the thyatron recovers quickly enough to record about 100 random-spaced impulses per second. Considerable gain in the time resolving-power of the apparatus is effected by recording the impulses on an oscillograph so that the wave form of the amplifier output can be examined.

R_0 and R_1 are liquid resistors each consisting of an appropriate mixture of pure xylene and absolute alcohol, sealed in a small glass T-tube provided with platinum electrodes.⁸ The resistance is adjusted by altering the proportions of the two liquid components, while filling the tube. The magnitude of

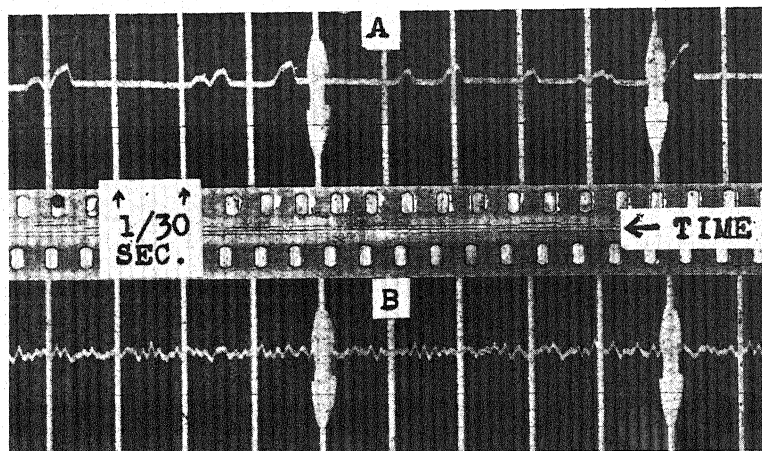


Fig. 3. Oscillograms showing rapid counting: A, about 30 per second; B, about 225 per second.

the resistance is not critical, but should be constant, for good operation. R_0 limits the current that can flow during each impulse, in order to prevent the discharges from being luminous. The resistance of the counting tube, itself, becomes relatively small while the discharge is taking place, hence it cannot be used to limit the current.

A convenient recorder for low-speed impulses has been made by replacing the balance wheel of an Ingersoll watch with an electromagnetic escapement. The energy required to operate the recorder is about 0.03 watt, and its maximum counting speed for regularly spaced impulses is about 40 per second. But for impulses spaced at random, the safe counting rate is only about 10 per

⁸ Similar to that of N. Campbell, *Phil. Mag.* **22**, 301 (1911), and **23**, 668 (1912). Other constant high-resistance units have been described by J. A. Van den Akker, reference 6., H. C. Rentschler and D. E. Henry, *Rev. Sci. Inst.* **3**, 91 (1932), and by H. L. White and E. A. Van Atta, *Rev. Sci. Inst.* **3**, 235 (1932). The writer is indebted to Dr. L. M. Mott-Smith for the loan of a shielded xylene resistor and condenser used in the preliminary part of this work.

second. The characteristics of this device seem to be similar to those of a recorder used by Van den Akker⁹ for counting x-ray photoelectrons.

Wynn-Williams¹⁰ has recently described an elegant arrangement for counting electric impulses at high rates. This might be used to a great advantage with any kind of Geiger counter, to increase the range of intensity of the phenomenon being measured. Instead of recording every impulse, each second, or fourth, or eighth, etc., is recorded, depending on the number of reducing units put in the circuit. A time resolving-power of about 1/1400 second is reported, so that the circuit should be capable of accurately counting *several hundred random impulses per second*. The limiting factor is the de-ionization time of the thyatron tubes used, not the inertia of any mechanical system. Corresponding to a count-reducing factor F , there is an uncertainty in the number of impulses, $\pm F/2$. But since F would rarely be made greater than 16, the error thus introduced is negligible, except for short or slow counts.

IV. THE FIELD IN THE COUNTER

For supplying the potential across the counters, a high-voltage battery is considered preferable to a rectifier, in all respects except economy. A simple rectifier, similar to that of Van den Akker and Watson,⁶ was used in most of the experimental work reported here. It consisted of a 1 mfd condenser charged by a small transformer and kenotron tube; voltage variation was obtained by altering the primary voltage of the transformer. However, a rectifier that draws its energy from a fluctuating source of power is very apt to have slow but troublesome fluctuations in its output potential. There is also some difficulty in accurately adjusting this potential, because the "soakage current" into the condenser makes the voltage drift slowly upward to its maximum value.

The voltage suitable for operating a counter depends on the shape, material, and state of the cathode surface, and on the kind and pressure of the gas in the tube. In the present work, the voltages ranged from 600 to 2000; they were usually 1000 to 1200 volts. The correct value for a given counter may be ascertained by causing faint light or γ -radiation to strike the cathode, while slowly raising the applied voltage until it crosses the threshold value. The threshold is the same for light, x-rays, and radioactive radiations.

It is important to determine and maintain the correct operating potential. The low-voltage edge of the threshold is quite sharp, but above this there is usually a *voltage plateau*, any part of which may be used. Impulses will be feeble or absent on the low-voltage side of the plateau; on the high-voltage side they become extended (mushy), and spontaneous discharges develop with increasing rapidity and finally merge into a steady discharge. The width of the plateau may be 10 to 100 volts; this depends on the gas, and on the counter cathode.

The range just described is one in which the counter *must* be operated,

⁹ J. A. Van den Akker, Rev. Sci. Inst. 1, 672 (1930).

¹⁰ C. E. Wynn-Williams, Proc. Roy. Soc. A136, 312 (1932).

if its results are to have any significance. But the characteristics of operation are not constant within this range. In particular, the sensitivity of the counter usually increases as the applied potential increases toward the high-voltage side of the plateau, a gain as high as 100 percent sometimes being observed. The augmented count is believed to be a *bona fide* effect, if the potential is not too near the edge of the range. The explanation of this is not yet clear. Since the increase in field strength never exceeded 10 percent of its initial value, it is impossible to account for any large added sensitivity by merely supposing that the photoelectric work function of the surface was diminished by the increase of field, although this effect undoubtedly takes place to a certain extent in counters.¹¹ So if the quantum efficiency (ratio of the number of photoelectrons to the number of incident quanta) remains about the same across the voltage plateau, while the sensitivity of the counter increases, it is reasonable to suppose that the efficiency of the tube *for counting the photoelectrons liberated* is improved by the use of a more intense field. Two possible explanations of this appear. The first and more favorable one supposes that under normal conditions, a few of the photoelectrons cross the inter-electrode space without producing enough ionization by collision to give impulses, but that on accelerating them more strongly, a larger fraction will be counted. The second possibility is that higher fields may extend more deeply into the microscopic crevices in the cathode surface, thereby removing and counting photoelectrons that were liberated with almost zero velocity in them. In photoelectric counters we have a problem not met in other counters, or in vacuum photoelectric cells, namely the difficulty of collecting the very slow photoelectrons that are set free by light just shorter than the threshold wave-length; if these electrons are in a weak field, many will be turned back into the metal by collisions with gas molecules. In practice, it seems safest to use a potential slightly higher than the threshold value. The voltage plateau of the best visible-sensitive counters is so narrow that there is little choice, anyhow.

V. PREPARATION AND CHARACTERISTICS OF ELECTRODES

Photoelectric quantum-counters have characteristics of behavior not less distinctive than those of photoelectric cells. The sensitivity, spectral distribution of response, and wave-length threshold of a counter depend not only on the material of its cathode, but on its previous history, its physical state, the presence of traces of foreign substances, and amount of previous ionic bombardment. The use of outgassed surfaces, or of surfaces in vacuum, is precluded by the principle of operation of the counters. Further, the success of those with alkali metal surfaces, or any other, is contingent upon the maintenance of very high resistance between electrodes.

Cathodes sensitive to ultraviolet light only

Experiments were first done with cathodes of zinc, cadmium, tin, copper, brass, silver, mercury, and magnesium. Under normal conditions, the sensi-

¹¹ On the basis of effects found by Lawrence and Linford, Ives, Schurmann, and Nottingham (see Hughes and DuBridge, *Photoelectric Phenomena*, p. 110).

tivities and dark-rates of these counters were very constant with time; the photoelectric thresholds, which were about the same that the metals show in ordinary photoelectric cells, were in the ultraviolet, except in the case of magnesium. Silver, mercury, magnesium, and tin electrodes were more sensitive within their ranges of response than were the others. Also, the average rate of spontaneous counting in darkness, or *dark-rate*, for the entire group was about 1.5 per minute, while cathodes of magnesium and very pure silver had dark-rates consistently less than 1 per minute. This fact, and the discovery that the dark-rate of copper could be reduced to a similarly low value by covering the entire electrode with a molecularly-thick coat of iodine, leads to the conclusion that the higher rates of uncoated copper, cadmium, tin, etc., are largely due to the emission of α -particles by the metals themselves.

Following the interesting work of Olpin,¹² concerning the effect of dyes on the photoelectric properties of alkali metals, many tests were made with counters having cadmium and zinc cathodes coated with extremely thin films of aniline dyes and photographic sensitizers.¹³ The relation of the sensitivity to the film thickness makes it appear that the photoelectrons were mainly liberated from the metal and drawn through the film. The *sensitivity* of zinc electrodes was markedly increased by the addition of certain thicknesses of dyes, but the photoelectric threshold was always displaced toward the ultraviolet. This displacement is the reverse of that found by Olpin, in alkali photoelectric cells. Furthermore, the thickness and texture of the coating on the cathode seems to have more to do with the increase of sensitivity than did the color or composition of the dye. An explanation tentatively suggested is that the dye merely served as an insulating layer, which allowed the potential to be raised above the normal operating value, with a resulting increase in the sensitivity. Reasons for the rise of sensitivity with voltage have already been discussed. On this theory, one would account for the shift of photoelectric threshold by assuming that the slowest photoelectrons failed to penetrate the film. A similar effect was remarked in the case of thin oxide films on magnesium and copper: the sensitivity increased, but the threshold moved toward the ultraviolet. Fig. 4 shows the response of a slightly oxidized magnesium cathode to light from a carbon arc. Cadmium was found less sensitive to the effects of dyes than was zinc. Much additional work will be required to determine with certainty what the action of dyes on counter electrodes may be. In view of Olpin's results, it would be especially interesting to try dyed alkali metal cathodes.

The total sensitivity of a thin cathode in an air-filled counter was found to decay almost exponentially with time, falling to half its original value in 12 hours. The air was at 6 cm pressure. This decay is due to the formation of a film of oxide of increasing thickness. There was also a decrease in the dark-rate during the same period (28 hr.), but it was by a smaller percentage. How-

¹² A. R. Olpin, *Phys. Rev.* **36**, 251 (1930).

¹³ Including: aesculin, alizarine, aniline black, anthracene, China-blue, Congo-red, cyanin, eosine, fluorescein, litmus, methylaniline violet, orthochromblau, picric acid, pinacyanol, pinaverdol, pinachromviolet, salicylic acid, uranin, and others.

ever, the sensitivity and dark-rate of a clean tin cathode, in nitrogen, were not perceptibly altered by standing $5\frac{1}{2}$ months.

If either electrode is coated with an insulating film of oil, grease or lacquer, the applied voltage can be raised far above the normal maximum, without starting a discharge. But once a discharge is started by the action of light or other radiation, it continues until the potential is removed. The break will then "heal" in an interval that varies from a small fraction of a second, in the case of a light oil, to nearly a minute, for a viscous grease. Under some conditions, the disruptions may begin and stop spontaneously; they then take place rythmically with a frequency that rises with the applied voltage, often to several hundred per second. This action superficially re-

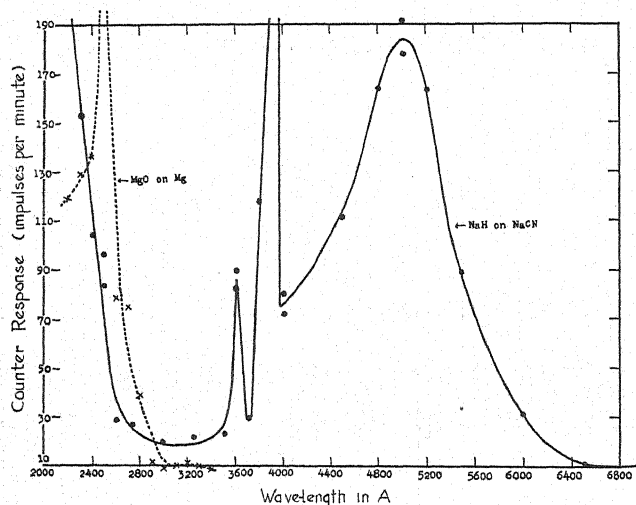


Fig. 4. Response of two counter electrodes to light from a carbon arc.

sembles that of an electrolytic interrupter. Fast rythmic discharges may sometimes take place only when light falls on the cathode. Under such conditions they might be mistaken for normal response; but their regularity shows that this is not the case.

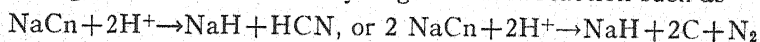
A curious displacement of the photoelectric threshold of a tin electrode was accidentally brought about by strongly bombarding the surface with ionic nitrogen, in a nitrogen atmosphere. The counter showed greatly increased sensitivity and responded to light well into the visible region, for several minutes after treatment of the surface; it then returned to its initial state. This effect could be repeated an indefinitely large number of times. It is likely that the shift is due to the partial dislodgment of a compact gaseous layer from the electrode, in spite of the high pressure of the surrounding gas (7 cm). Another possibility is that a photosensitive but unstable compound is formed. Unfortunately, no other gases have yet been tried for the effect with tin, nor has nitrogen bombardment been tried on cathodes of other metals. The thresholds of silver and copper did not show any appreciable shift after strong and extended bombardment with ionic hydrogen, in a

hydrogen atmosphere. The large *permanent* shift of the threshold toward the red, effected by bombardment of some salts with hydrogen, is the subject of part of the next section.

Alkali metal cathodes

The advantages of alkali metal cathodes, arising from their high sensitivity and response to long wave-lengths, more than compensates for the difficulties met in preparing them. Even if it were possible to move the photoelectric thresholds of other metals into the visible region by means of dyes, it seems certain that the quantum efficiencies of such surfaces would be much inferior to those of alkali metals. The chief obstacle encountered is in finding a good way to introduce the latter into the tube as a deposit on the cathode. If sent in by distillation, the metal tends to spread over the interior surface of the glass. This results in diminished resistance that is fatal to the successful operation of the counter. A possible alternative is to coat the photoelectric material on the demountable cathode, while *outside* the counter, and then seal it into the counting tube. Naturally the air and moisture must be kept away from the surface during all processes, and this is not easy to do. However, two modifications of this second method have been devised and carried out by the writer, with very gratifying results.

The first process *consists in the formation of a hydride of the desired metal on the cathode, by reducing a salt with atomic hydrogen.* For example, a copper cathode, coated with a thick layer of fused sodium cyanide, was introduced into the counter; the tube was then exhausted and filled with dry hydrogen at a pressure of 7 centimeters of mercury. Next, a discharge of 15 to 100 microamperes was passed through the gas for 30 minutes, so that the cyanide was under strong bombardment with hydrogen ions. A reaction such as



is believed to have taken place on the surface; the sensitivity of the counter was greatly increased, and its photoelectric threshold was permanently shifted from the ultraviolet to about 6400Å. Choice of the cyanide for this purpose, in preference to another salt, was made on the basis of its low heat of formation; it seemed likely that such a salt could be most easily reduced. Fig. 4 shows the approximate distribution of the response of this counter to the light from a carbon arc. The curve was made with a quartz monochromator, and is uncorrected for the stray light that gets through the instrument. One may observe that the peak at 5000Å does not coincide with any shown by sodium metal in an ordinary photoelectric cell. The question may justly be raised as to whether the response is really from sodium metal. The answer seems affirmative, for the high sensitivity and response to red light appear only after the ionic bombardment, and immediately vanish with the admission of any air into the tube. It is also well known that the spectral distribution of response of thin films depends greatly on the nature of the underlying surface, and on the previous ionic bombardment.¹⁴ The dark-rate of

¹⁴ See: A. L. Hughes and L. A. DuBridge, *Photoelectric Phenomena* (McGraw-Hill Book Co., Inc., 1932).

this counter subsided from 86 impulses per minute, just after preparation, to 2.95 per minute, a few hours later. (The results shown in Fig. 4 were obtained about a day after forming the surface.) The peaks at 3600Å and 3900Å are due to groups of lines in the spectrum of the arc used. Three other similar surfaces were prepared from sodium cyanide; the kind of surface on which the salt was used was found to be immaterial.

It should be mentioned that during the discharge used for sensitizing the cathode, an irregular film was always deposited on the wire anode. These films can, and must, be removed by electrically heating the wire to a bright glow for a few seconds.

Several attempts were made to produce potassium hydride surfaces from the cyanide by a process like that just described. These met with little success and were abandoned when it was found that excellent surfaces could be prepared from amalgams of the alkali metals.

The second process consists in the *formation of alkali hydrides by bombardment of amalgams with atomic hydrogen*. Two surfaces of this type were prepared with sodium, three with potassium, one with sodium-potassium, and one with caesium. The sodium counters made by this process were several times as sensitive as those previously prepared from the cyanide; but their sensitivity was far exceeded by the potassium ones. The latter were, in fact, the most sensitive counters for visible light that the writer has been able to prepare.

The technique for forming them was much like that with the cyanide. The demountable cathode, of heavy copper, was lightly coated with clean mercury and dipped into the amalgam, which was preserved under xylene.¹⁵ While still coated with a protecting film of xylene, the electrode was sealed into the counting tube, from which the air was immediately swept out with dry hydrogen. Long pumping removed the xylene, after which fresh hydrogen was introduced to the proper pressure. A discharge was then passed between the electrodes, and the coating was evaporated from the wire, as before. The copper acted as an absorbent for excess mercury, which presently disappeared into the cathode. At the same time, the physical appearance of the surface changed: sodium and potassium ones became dull gray, while caesium took on a light golden luster. It is not known whether or not this was accompanied by the expected concentration of the alkali metal on the surface. The question hinges on determining whether the light metal sinks into the copper along with the mercury, or is filtered out at the surface. The final step was to evaporate the film that was incidentally deposited on the wire during the discharge. The counter was then ready for use.¹⁶

¹⁵ Amalgams were prepared by electrolysis of salt solutions, using mercury cathodes. They were then washed with water and xylene. See: J. W. Mellor, *A Comprehensive Treatise on Inorganic and Theoretical Chemistry*, 4, 1010 (Longmans and Co., London).

¹⁶ While preparing this paper, it has occurred to the writer that the use of mercury is superfluous. The technique suggested is to immerse the counter cathode in clean alkali metal, melted under an inert but volatile liquid, and make the transfer to the counter while a film of the liquid remains as a protective coating.

The photoelectric thresholds of the amalgam counters were found by means of filters to be roughly the same as for the alkali metals in photoelectric cells. Thus for sodium, the threshold was around 6000Å, for potassium, 6500Å, and for caesium, >7500Å.¹⁷ Sodium-potassium mainly showed the response properties of sodium, which predominated in the mixture used. Amalgams of potassium and sodium became granular at fairly high concentrations of the light metals, while the mixed amalgam remained fluid at similar concentrations. The latter was thus easier to apply to the electrode than that of the single metal.

Minimum rates of accidental counting for the several cathodes were as follows: sodium, 4.7 per minute; caesium, 5.8 per minute;¹⁸ potassium, 2.3 *per second*. It is not known what part of the potassium count is due to β -particles from its radioactivity. This might, of course, be approximately calculated by measuring the amount of metal, thickness of film, and coefficient of absorption of the particles by the film. The writer believes that the major part of the count is due to other spurious causes, such as the evaporation of charged molecules, or a chemical change involving the emission of electrons or light. In support of this view, it may be mentioned that various other electrodes that were presumedly devoid of radioactive material showed high rates of accidental counting for short periods after their introduction into the counter, or after strong ionic bombardment. The duration of this high count could sometimes be controlled by the length or manner of treatment of the surface, and usually subsided within a period that varied from a few seconds to several hours after treatment.

Several cathodes coated with ammonium amalgam were also tried in the counter. But the ammonium always decomposed before it could be used, in spite of the fact that the time between its preparation and exposure as a photoelectric surface was less than two minutes.

A strontium amalgam counter was also prepared by a process like that used with the alkali metals. Its response was good for $\lambda < 4600\text{Å}$, and could be detected at $\lambda \sim 7000\text{Å}$. The sensitivity to light from an incandescent lamp was estimated to be about one-sixth that of the sodium counters. The sensitivity was neither improved, nor was the spectral distribution altered, by directing a stream of hydrogen ions against the cathode. Several barium amalgam surfaces were also tried, but were not successful. The concentration of barium metal was initially small, so it was probably destroyed by combination before it could be tried in the counter.

Non-metallic cathodes

Thin films of numerous non-metallic substances have been tried on counter electrodes, in addition to the dyes previously mentioned. Both liquids and solids were used; the latter were usually more easily handled and more constant in behavior. A few of the surfaces that seemed especially in-

¹⁷ Found with filters. See: A. L. Hughes and L. A. DuBridge, reference 14, p. 457-9.

¹⁸ The electrodes of the Cs counter were not well centered, so the sensitivity and dark-rate are not comparable with those of other counters.

teresting will be mentioned here. Generally speaking, if the film is exceedingly thin, the photoelectric behavior is that of the underlying surface; if it is thick, the characteristics are those of the material of the film itself; intermediate thicknesses lead to a variety of effects.

Iodine was deposited from solution on cathodes of copper, silver, and selenium. (The size of crystals and thickness of the deposit can be reduced at will by heating the electrode in a flame.) The photoelectric threshold of a molecularly thick deposit was between 2300 and 3000Å, in air or hydrogen, which were the only gases used. It was observed that the deposition of a thick film on a particular copper electrode reduced the dark-rate from about 1.5 to 0.9 per minute; also, that the behavior of the counter was the same after bombardment of the iodine with atomic hydrogen, provided that the anode wire was subsequently cleaned by heating. The distinctive feature of the iodine counters was their extremely good sensitivity. For example, the response to light from a flame was about twice as high from iodine-coated copper as from clean copper, in spite of the fact that the latter responds to longer wave-lengths. After strong heating in contact with iodine, a copper electrode became coated with a thin film of light-green material, presumed to be an iodide. The dark-rate of the counter then increased to 90 per minute, and remained practically constant even after extended bombardment with atomic hydrogen!

Selenium, deposited as a thick coat on copper, by evaporation, also had a threshold between 2300 and 3000Å; its dark-rate was 57 per minute. The threshold was shifted to about 4100Å by hydrogen bombardment, but returned to its former value when air was admitted to the tube, about 15 minutes later. The operating potential was also made more critical by the discharge. The reason for the change of threshold is not known, but it seems reasonable to suppose that the hydrogen bombardment produced a surface film of a compound whose photoelectric threshold was nearer the red.

The counter having the highest sensitivity to ultraviolet light of any yet prepared, had a non-metallic cathode. It was made by coating copper with a thick film of selenium, depositing on this a very thin film of iodine, subjecting the composite surface to strong bombardment with atomic hydrogen, and removing the film from the anode wire by heating. The photoelectric threshold was again between 2300 and 3000Å, and the dark-rate was about 1 per second. Light from a small constant flame, which increased the count from a good tin cathode by 29 impulses per minute, increased that from the Se-I one by 460 per minute. So the sensitivity of the Se-I was about 15 times that of tin, to the source of light used! A possibility that should not be overlooked in the case of this and similar electrodes, is that *the emission of photoelectrons may merely be an electrical by-product of a photochemical change*. One seems obliged to look for the explanation of the high rates of spontaneous counting, sometimes got from electrodes in the relative absence of light, or of radioactive material, by finding out whether physical or chemical changes are taking place that are accompanied by the ejection of charged particles or the emission of photoelectrically active light.

No substance that was coated on the cathode of the counter, and that could be retained there without disturbing the necessary electrical characteristics of the device, failed to show photoelectric response. Thus barium chloride, deposited from solution, responded in the ultraviolet, but also showed very weak response to wave-lengths as long as 7200Å. After bombardment, the sensitivity to the red was somewhat improved. Similar behavior was shown by a film of red cuprous oxide on copper; it showed strong response to the ultraviolet and very weak response to $\lambda \sim 7200\text{Å}$. The absence of this red-response was found a convenient means of testing the "photoelectric cleanness" of the copper surface.

The wire anodes

The anode wires should be very smooth. For successful operation of any counter, a high symmetrical field must be maintained between electrodes, and this is more disturbed by microscopic irregularities on the anodes than by much larger ones on the cathodes. In other kinds of tube counters, some investigators^{3,4} have used oxide-coated tungsten wires, while others^{9,19} used bare ones. The oxide serves as a partial insulator which allows the operating potential across the tube to be raised above its normal value. The writer has found that the oxide film is, in general, more troublesome than desirable, because of its tendency to become disrupted in spots; even one such break is fatal to the success of the counter. Moreover, in visible-sensitive counters, and some others, it is necessary to remove other kinds of films from the wires by heating them to incandescence (usually in hydrogen), and this excludes the use of the oxide. Platinum and tungsten wires were found most convenient; they may be heated to high temperatures, and will withstand the corrosive action of bombardment with alkali-metal ions. The size of the wire determines the operating potential,²⁰ but any small diameter seems to serve equally well.

VI. TESTS AND MEASUREMENTS MADE

Inverse square law

Reliable measurements of light intensity cannot be made with any device, unless the rates of its response to a given source obey the inverse square law of variation with distance. To test this, a small alcohol lamp that burned at a constant rate was set at 250 and 500 cm from a tin-cathode counter; resulting increases in the rate were respectively 68.4 and 17.4 impulses per minute. The deviation of these results from the inverse square relation, (1.8 percent), is within the limits of statistical error and fluctuation of the lamp. Pending tests with a better source, we may conclude that the inverse square law is applicable, at least to a good approximation. Incidentally, the maximum permissible counting rate for any counter and recorder may be taken as that at which the departure from the inverse square relation, due to

¹⁹ H. Kniekamp, *Phys. Zeits.* 30, 237 (1929), and L. F. Curtiss, *Bur. Stds. Jour. Res.* 4, 601 (1930).

²⁰ D. Cooksey and M. C. Henderson, *Bull. Amer. Phys. Soc.*, June 9, 1932, give an empirical formula relating field, applied voltage, and radii of the electrodes.

coincidence of successive impulses, becomes as large as the greatest permissible error. This rate is the reciprocal of the time resolving-power and can easily be found by experiment.

Ultraviolet light from different sources

Application of the photoelectric counter to intensity measurements is illustrated in Table I, which gives the relative total response of a tin-cathode counter to ultraviolet light from four sources of widely different intensities. The wave-lengths actuating the device lie approximately between 1950 and 3500Å. The dark-rate, 1.7 per minute, was deducted from the rates recorded. Values in the last column were reduced to a comparable basis by use of the inverse square law, and are proportional to the ultraviolet luminosities of the several sources. The extreme feebleness of the ultraviolet from all but the quartz mercury lamp is made evident by these data.

TABLE I. *Ultraviolet light intensity from various sources.*

Source	Distance (meters)	Cathode area exposed	Counting rate (No. per minute)	Computed rates for source at 1 meter and electrode area of 1 cm ² , per min.
Mercury arc ^a	47.0	0.000855 cm ²	48.0	120,000,000.
Bunsen flame ^b	4.0	0.63 "	73.9	188.
Alcohol lamp ^c	4.0	0.63 "	18.7	47.5
Electric lamp ^d	4.0	0.63 "	7.5	19.

^a Cooper-Hewitt quartz lamp; 4 amp., 30 volts, d.c.

^b Meeker burner; 0.024 cu. ft. methane per minute, mixed with air.

^c Burned 9.3 g of denatured ethyl alcohol per hour.

^d 1000-watt projection lamp; 8.8 amp., 115 volts, d.c.

The ultraviolet from the slow oxidation of a small piece of white phosphorus was easily detected; but no "mitogenetic rays" were found from any root-tips or bacteria cultures, nor was any radiation that was capable of operating the counter detected from the slow oxidation of iron or aluminum, or from mechanically distorted crystals or other materials.

Different gases

Air, hydrogen, oxygen, nitrogen, and methane were used successfully in a counter with a tin cathode. For a given pressure, the operating potential was found to be higher for gases with high ionization potentials, than for others. Operation was most successful with the gas of highest ionization potential used, namely nitrogen; the voltage plateau was widest, so that the potential was least critical of adjustment. In this connection, one recalls the very satisfactory use of helium in other tube counters, by Bearden and Haines,²¹ who also found the gamma-ray sensitivity of these to be somewhat greater than that of similar air-filled counters. Their observations seem significantly related to the fact that helium has the highest (minimum) ionization potential of any ordinary gas.

²¹ J. A. Bearden and C. L. Haines, Bull. Amer. Phys. Soc., April 12, 1932.

The question has been raised: Why does the discharge of a Geiger-Müller counter *stop*, once it has been set going by an ion? The explanation proposed here is this: Before the discharge begins, there is a large field between the counter electrodes; this is sufficient to give the initial ion enough velocity to ionize the gas, hence to start a general discharge in the tube. During the course of the discharge, the voltage across the tube falls below the critical value for the gas used, and no new ions are generated. The discharge then declines and the residual ions are swept out of the field with sufficient quickness that none remain when the full potential has become reestablished across the tube. The fall of voltage during the discharge is Ri , where R is the external resistance, and i is the maximum current that flows through the tube. A possible inference from the work with different gases is that the use of a gas with a high ionization potential is desirable because it assists in quenching the discharges.

Cellophane window

The short wave-length limit of response of photoelectric counters is determined by the material of their windows; the cut-off of the counters used in most of the work described here was about 1950Å. In order to get transparency to shorter wave-lengths, the quartz was replaced with a sheet of cellophane, 0.02 mm thick, supported on a thin metal plate that was drilled to half its area with 0.68 mm holes. The limit for this window should be about 900Å, but the air between it and the source probably raised the limit to about 1450Å.²² In work requiring the measurement of light as short as 900Å, the source might be mounted in a vacuum chamber of which the thin counter window formed one side.

VII. MODIFIED COUNTERS FOR OTHER USES

The success of the photoelectric counters has led to their use for other purposes. Three slightly modified types will be briefly described here. The first is a convenient counter for α -particles, especially intended for measuring the strengths of sources; the second is a counter for detecting and measuring faint x-rays and γ -rays; the third is a reversed-field counter which may be useful for measuring intensities of spectral lines.

Alpha-particle counter

This adaptation was made by replacing the quartz window with one of very thin mica, 1.05 mm in diameter. The mica reduced the range of the α -particles from polonium by 1.73 cm, in air, so that its thickness must have been approximately 0.007 mm. In order to have a low spontaneous count and to avoid response to visible light, an iodine-coated copper cathode was used; its dark-rate, 0.7 per minute, was negligibly small.

Fig. 5, A, and B, illustrates the use of the counter with a polonium source about 0.0086 cm² in area; C was made with a source 2 cm² in area. The polonium was electrolytically deposited on platinum foil; different parts of the deposit were found to be of similar activity. Distances shown on the

²² A. L. Hughes and L. A. DuBridge, *Photoelectric Phenomena*, p. 458.

curves are subject to a lateral displacement of about 0.5 mm, due to the uncertainty of the initial position of the micrometer frame that carried the source.

Other tests with the α -ray counter led to favorable results. The first showed that the voltage plateau was wider than those of most photoelectric counters, so that small fluctuations of the potential applied to the tube did not alter the count from a constant source. A second test showed that variation of the gas pressure in the counting tube had no detectable effect on the

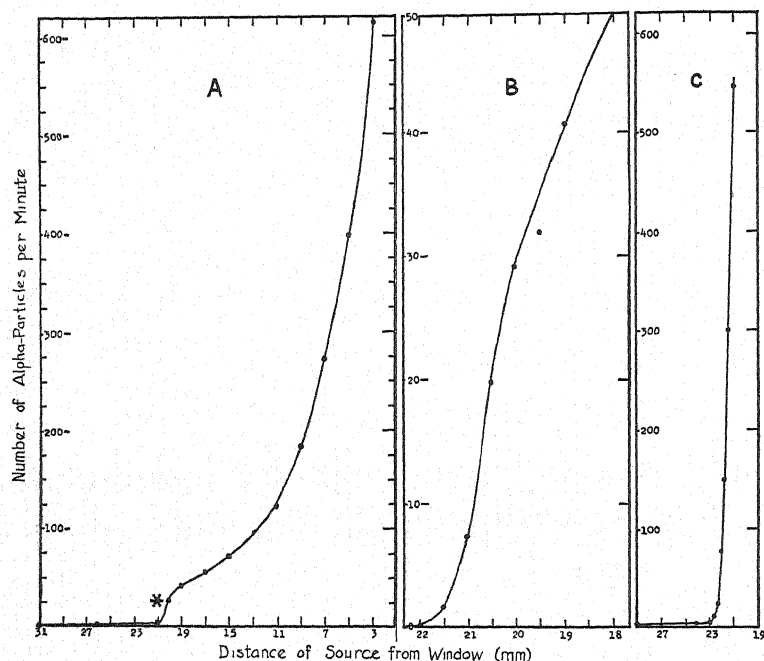


Fig. 5. Curves illustrating use of the α -particle counter with a polonium source: A, count from a plane source of small area; B, starred portion of A, on a larger scale; C, count from a plane source of large area.

range of the α -particles, as determined with the counter. It seems that if the particle gets through the window, it is almost certain to produce enough ions to start an impulse. A third test indicated the order of accuracy to be expected with short observations. Table II contains the data of this test.

TABLE II. *Experiments with alpha-rays.*

Time in minutes	Total number of α -particles	Number per minute	Percent deviation from the mean rate
10	1431	143.1	-0.56
10	1441	144.1	+0.14
10	1450	145.0	+1.10
10	1403	140.3	-2.50
10	1475	147.5	+2.50
10	1436	143.6	-0.21
		Mean: 143.9	

The statistical error of the average count (1.77 percent) is larger than the mean of the absolute values of the observed deviations from the mean rate (1.17 percent).

X-ray and gamma-ray counters

Photoelectric counters may be used for detecting and measuring faint x-rays and γ -rays, without modification of form. A series of experiments, described in a previous note,²³ were done with a tin-cathode counter used in that capacity. The sensitivity of the apparatus was calculated for each arrangement, in terms of the minimum amount of radium, in equilibrium with its decay products, that could be detected by its γ -ray emission.

Shielding against stray radiation is facilitated by the smallness of the electrodes; the small external dimensions of the detector also allow it to be brought close to the source. It is, of course, very desirable to use a cathode with a low dark-rate, such as that used in the α -particle counter. Selection of the material and aperture of the window depends on the purpose for which the counter is to be employed.

Wire-cathode counters

The wire electrode may be used as the photoelectric element of the counter by reversing the direction of the electric field. Some interesting results were obtained with a cathode of tungsten wire, in the presence of vapors of certain organic liquids. These were coated on the cylinder electrode, or thinly on the wire itself. Ethyl chloride, ethyl alcohol, ether, methyl alcohol, and especially nitrobenzene, increased the sensitivity for ultraviolet light by a factor of 1.5 to 3. The effect seems to be due to the presence of *vapor* of the substance in the vicinity of the wire, or on its surface. Sensitizing agents did not appreciably increase the sensitivity of the counter for γ -rays, so their action appears to be a reduction of the photoelectric work function of the surface.

Diethyl-aniline vapor caused an unusually great increase, estimated to be 25 times the original sensitivity! This occurred when the liquid was coated on either electrode, only a trace being required for the purpose. This counter maintained its high sensitivity and low dark-rate for 10 hours; at that time it was dismantled. After treatment, the photoelectric threshold was roughly 3000A, but the matter of a shift due to introduction of the vapor was not examined. It was found that this sensitizer also extended the range of air pressures at which the tube could be operated successfully. The characteristics were about the same at 14 cm as at 0.5 cm, with suitable voltage adjustment.

Water vapor increased the photoelectric sensitivity of the wire nearly as much as diethyl-aniline did. But the water had to be introduced in a much larger quantity, so that it presently spread over the interior of the tube, decreasing the resistance and greatly increasing the rate of spurious counting.

These incomplete experiments with reversed fields were among the first tried with photoelectric counters, so that good technique and auxiliary ap-

²³ G. L. Locher, Phys. Rev. 40, 884 (1932).

paratus were not yet developed. But the results suffice to show that very high sensitivity may be reached with counters having sensitized wire cathodes. Obvious extensions of the work would include the use of thoriated tungsten and oxide-coated wires, and quantitative tests of the sensitizing effects of many other substances, both with these counters and normal photoelectric ones. Organic liquids have not yet been tried on the cathodes of the latter.

Since the wire-cathode counters have active surfaces that are very narrow, they might easily be applied to the measurement of faint spectral lines.

VIII. DISCUSSION

Sensitivity for counting electrons

We may establish certain criteria for determining the useful electron-counting sensitivity of a photoelectric counter, without knowing the magnitude of the quantum efficiency of its photoelectric surface. The total useful sensitivity is taken as the intensity of light that causes the smallest increment in the counting rate that can be detected with certainty. An increment is regarded as "detected with certainty" when it exceeds the statistical error of the count by a pre-determined amount. It is further stipulated that the results be capable of reproduction, within pre-assigned limits of error, under identical experimental conditions.

The useful sensitivity evidently improves with extension of the time of the observation, for the relative statistical error of the count diminishes as the number of electrons recorded increases. It will also be best for a counter with a small dark-rate, for reasons set forth in section I of this paper.

Considerations of the limiting sensitivity are only important when the count is small, either due to shortness of the interval over which the observation is made, or to extreme feebleness of the radiation measured. But since the most important applications of photoelectric counters are apt to be for measurement of faint radiation, it is desirable to consider the factors that limit their sensitivity for counting electrons, in addition to the limitation imposed by the quantum efficiency of the photoelectric surface.

As an illustrative example, consider a typical counter for which the dark-rate is 1.50 ± 0.106 per minute, as determined by a one-hour observation. When exposed to a particular faint source of light for an hour, suppose the total count is 120. Of these impulses, 90 ± 6.36 are due to accidental causes, while 30 ± 3.67 result from the light. Under such conditions, it is evidently possible to detect less than one-half photoelectron per minute, with certainty. But if the same apparatus is run for only 5 minutes, and if the total count is 10, the corresponding distribution would be 7.5 ± 1.84 due to accidental causes, and 2.5 ± 1.06 due to the light. And if we take the minus sign with the latter rate, the increment due to the light is smaller than the statistical fluctuation of the dark-rate, so the light could not be detected with certainty, in 5 minutes. Similarly, if the counter had a dark-rate of 60 ± 0.67 per minute (instead of 1.50 ± 0.106), an increase of 30 ± 3.67 impulses per hour could not be detected by means of a 1-hour observation.

The foregoing discussion applies as well to counters for measuring other feeble ionic emissions, as to photoelectric ones. Moreover, S. Smith²⁴ has pointed out that very similar conditions obtain in the measurement of very faint light with a photoelectric cell and electrometer, when the dark-current of the cell, (>30 electrons per second) is comparable with the additional current due to the light.

In cases where the light to be measured can be concentrated on the counter cathode, the total useful sensitivity increases as the size of the cathode diminishes. But if the light cannot be conveniently concentrated, an important question arises: Does the useful sensitivity increase with the size of the cathode, and if so, within what limits? To answer this, one must recall that both the accidental count and the number of desirable photoelectrons increase with the area of the electrode, and that there is an upper limit to the speed of counting, imposed by the time required by the counter and recording apparatus to recover from each previous impulse (i.e., by the time resolving-power). The matter can probably be best settled by experiment.

Limitations of photoelectric counters

The following are believed to be the four chief limitations of photoelectric counters, which affect their use for quantitative measurement. The relative significance of each obviously depends on the specific application of the counter.

(a) The maximum intensity of light that can be measured is restricted by the speed at which the photoelectrons can be counted. Pending further developments of impulse recorders, the safe counting speed can hardly exceed 300 or 400 electrons per second; yet photocurrents of such low orders (5×10^{-17} ampere) are measurable only with great difficulty in other types of instrument. Higher intensities can, of course, be measured with the counters by using smaller cathodes, or by diminishing the area exposed, until the rate comes within the permissible limit.

(b) A very constant source of high potential is required. Otherwise, the sensitivity is apt to vary as the potential moves across the voltage plateau. The permissible variation depends on the requirements of the work, and on the width and slope of the plateau of the counter used.

(c) Accurate measurements of very small intensities require extended observations. This characteristic is shared in common with all other devices for measuring phenomena that are subject to statistical fluctuations.

(d) The spectral distribution of response may change as the counter is used. The existence and magnitude of this effect depend on the kind of gas used, the kind of cathode surface, and the intensity of ionic bombardment of the cathode. Gas-filled photoelectric cells sometimes show similar changes.²⁵

It is believed that photoelectric counters will not only provide powerful means of measuring faint radiation, but also of studying a variety of photoelectric phenomena, such as the photoelectric properties of non-metals,

²⁴ S. Smith, manuscript not yet published.

²⁵ N. R. Campbell and D. Ritchie, *Photoelectric Cells* (Sir Isaac Pitman and Sons, 1929).

gases, and compounds, the feeble electron emission of substances illuminated with light of very long wave-lengths, and the effects of sensitizers on photo-electric surfaces. They should also make possible investigations of ionic and light emissions accompanying physical and chemical changes and biological processes.²⁶

The author wishes to thank Dr. Sinclair Smith for his valuable assistance in the early development of the counters, and for making available the facilities of the Mt. Wilson Observatory Laboratories, where the preliminary work was done. Later development was carried out at the Rice Institute, through the kindness of Professor H. A. Wilson, whose council is gratefully acknowledged. Dr. W. F. G. Swann has very kindly read the manuscript of this paper, and has made helpful suggestions concerning its contents.

²⁶ One form of the apparatus described in this paper was exhibited at the A.A.A.S. meeting, Dec. 28-31, 1931.

Non-Existence of Ion Mobility Spectrum in Air

By ROBERT N. VARNEY
University of California, Berkeley

(Received July 19, 1932)

A modified form of the Rutherford a.c. method of measuring ion speeds, as suggested by Loeb and Bradbury, has been used to investigate the range of speeds with which negative ions in air travel. It differs in that the ions are produced only during a small fraction of the a.c. period, this being accomplished by interrupting the ultraviolet light beam with a rotating shutter. The theoretical curves of $d(i/i_0)/dV$ against V assuming both the presence and the absence of an ion spectrum are given. The experimental curves for ions 0.03 to 0.006 sec. old agree closely with the theoretical curves for a spectrum, but it is shown that on application of a diffusion correction the spectrum in clean dry air reduces to negligible width; the presence of ozone in considerable amounts, however, produces a spectrum extending 10 to 12 percent on each side of the mean mobility.

INTRODUCTION

THE question of whether normal ions in air travel with a unique speed or with speeds spread over a range or spectrum of values has been completely discussed and all experimental evidence to date on both sides has been analyzed in a recent paper by Loeb and Bradbury.¹ They suggested that, if in the Rutherford a.c. method of measuring mobilities a shutter in conjunction with the commutator which produced the square-wave a.c. were used to interrupt periodically the ultraviolet light beam, a higher resolving power might be obtained for the a.c. method. The principle has been used by Fontell² and by Bradbury,³ both, however, using x-ray ionization, and by Hamshere⁴ using α -ray ionization. The suggested photoelectric method promised to be an improvement over the first of these because the exact distance travelled by the ions could be more exactly determined; and over the second, because it was hoped that ultraviolet light would produce less active substances in the air than either x-rays or α -rays.

APPARATUS

The apparatus consisted of a metal ionization chamber provided with plane plates, the upper being brass and the lower speculum metal. A quartz window permitted the light from a quartz-mercury arc to fall on the lower plate. The beam of light passed first, however, through a window of the rotating shutter. The air from the room was slowly passed over P_2O_5 and $CaCl_2$, and through a double trap immersed in liquid air.

¹ L. B. Loeb and N. E. Bradbury, *Phys. Rev.* **38**, 1716 (1931).

² N. Fontell, *Commen. Physico Mathematicae Soc. Scientiarum Fennica* **23**, 7 (1931).

³ N. E. Bradbury, *Phys. Rev.* **40**, 508 (1932).

⁴ J. L. Hamshere, *Proc. Camb. Phil. Soc.* **25**, 205 (1929); *Proc. Roy. Soc. A* **127**, 298 (1930).

The shutter served at the same time as a commutator to provide a square-wave, alternating potential on the lower plate. The shutter, which was variable in size, allowed the speculum plate to be illuminated from the time the negative potential was applied up to any desired time before that at which the potential reversed. Ions thus produced during the negative part of the cycle travelled upward either until they reached the upper plate or until the potential was reversed, when they were drawn back again to the bottom plate. (A slight positive bias insured complete sweeping out of the ions from the field; see Fig. 1).

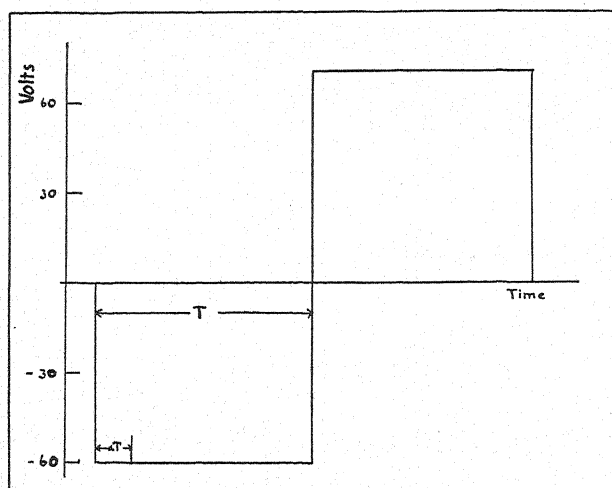


Fig. 1. Diagram showing the characteristics of the square-wave a.c. with the positive bias and the relative magnitudes of T and αT indicated.

PROCEDURE

The following method was used to take and to reduce the results. (1) Electrometer deflections for various voltages applied to the lower plate were taken with the shutter-commutator moving. These deflections are called i . The electrometer could be read to about 0.2 percent of its average deflection, and average reading could be repeated to ± 0.2 percent. The voltmeter could be read to a little better than ± 0.10 volts.

When a smooth curve of i against V was drawn, the curve usually passed directly through all but one or two points. If more than two points deviated noticeably in any one curve, the whole curve was discarded as erratic.

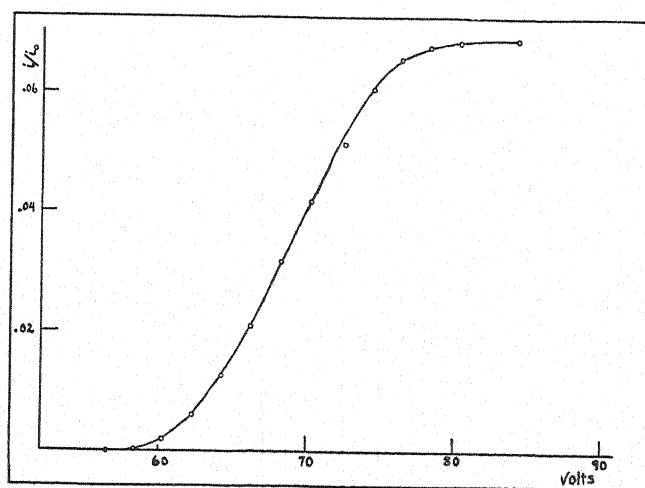
(2) Similar deflections were obtained but with the shutter-commutator stationary, giving the i_0 readings. These gave greater difficulty because of the relatively short time necessary to produce the deflection. A straight line was drawn through the data points and the values of i_0 taken from it. From the work of Bradbury⁵ on the photoelectric current in gases, it appears that over ranges of 30 volts or less the use of a straight line is permissible. The probable error on this line was around one-half percent.

⁵ N. E. Bradbury, Phys. Rev. 40, 980 (1932).

(3) The ratio of i to i_0 was then plotted against voltage. Note that i values have not been smoothed. Table I shows a typical set of data. The probable error of points on this curve with respect to the curve lies between ± 0.05 volts and ± 0.02 volts (see Fig. 2).

TABLE I. Typical set of data for i/i_0 .

V (volts)	i/i_0	V (volts)	i/i_0	V (volts)	i/i_0	V (volts)	i/i_0
150	0.0407	134.5	0.0290	124.84	0.0054	114.9	0.0000
146.75	0.0406	132.2	0.0230	122.8	0.0029	112.9	0.0000
142.75	0.0399	130.5	0.01865	120.8	0.00136		
138.33	0.0363	128.5	0.0128	128.8	0.00039		
136.0	0.0325	126.67	0.00855	116.9	0		

Fig. 2. Experimental curve of i/i_0 .

(4) It was desired to plot $d(i/i_0)/dV$ against V , i.e., to plot the derivative curve. It is a well-known fact that integration smooths out while differentiation accentuates discontinuities and irregularities in a curve. In this case, theoretical considerations given below led the writer to believe that the actual discontinuities occurred in the second derivative curve. If so, they would be shown much more sharply in the first derivative curve than in the original curve, a break in the slope appearing in the former case with only an inflexion or hardly noticeable increase in the rate of curvature in the latter case.

Differentiation was performed by taking the slope at various points with a straight edge. An important check was made by placing the straight edge successively through every two adjacent data points and using this for the slope at the mean of the two, i.e., finite differences were used. As a final check, the i/i_0 curve was completely redrawn and redifferentiated in several cases to check against possible personal errors. The deviations were well within the limits claimed for the method.

The probable error in determining the derivative curve is between ± 0.07 volts and ± 0.10 volts. Adding to this the probable errors in reading all instruments, the resulting probable error is between ± 0.15 volts and ± 0.20 volts. The effect of this on the mobilities found is discussed in the conclusion.

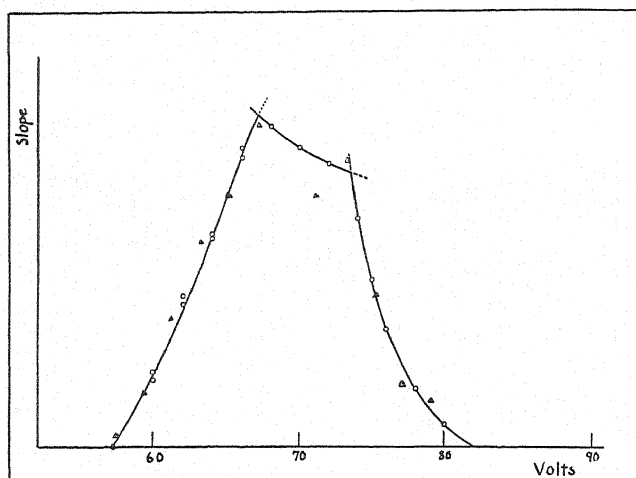


Fig. 3. Curve showing slope of each point of the i/i_0 curve in Fig. 2. This is an experimental result of plotting $d(i/i_0)/dV$ against V and shows the two zeros and the two break points distinctly. The triangles are finite difference points, and the double set of circles come from two different drawings of the i/i_0 curve.

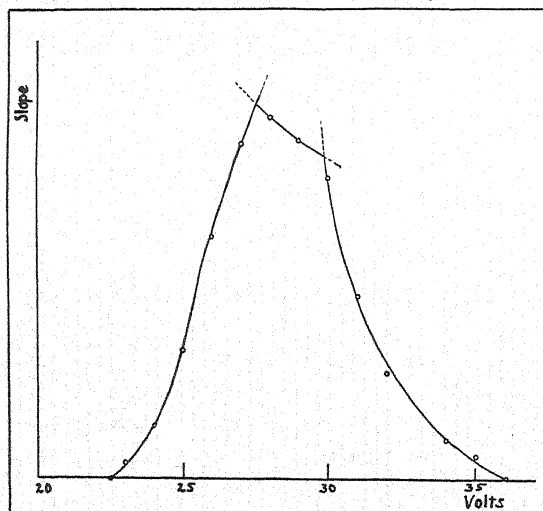


Fig. 4. Another experimental curve of $d(i/i_0)/dV$ against V similar to Fig. 3 but taken with a slower shutter speed.

It is important to notice that while an inflexion point in a curve may only be found by attempting to discover the point at which the curve crosses its tangent, the same point in the first derivative curve may be found as the intersection of two smooth curves, that is, in this case, by the use of five or

more ordinary points instead of a single critical point. Since theory indicates a break point and since experiment gives two curves approaching each other at a sharp angle and showing an apparent point of intersection to an accuracy of ± 0.20 volts at worst, the question of whether or not such a single point actually exists in the data becomes of no interest. Just what its disappearance would mean is unknown, but it certainly would not affect the discussion of the existence or non-existence of an ion mobility spectrum.

Two break points were found in each curve, but only the sharper one, occurring at an inflexion point in the i/i_0 curve, was used (see Figs. 3 and 4).

(5) The determination of the limits of the spectrum from the derivative curves and the corrections for diffusion are discussed at a later point.

SIGNIFICANCE OF THE RESULTS

Loeb and Bradbury¹ have worked out the essentials of the theory of the method. What happens when the shutter closes and what the derivative curve would be, was not considered by them.

Taking k_1 and k_2 as the highest and lowest mobilities, respectively, in an assumed ion spectrum; V as the field strength; d as the plate separation; T the half period of the a.c.; and αT the length of time the shutter is open; their work gives directly

$$i/i_0 = [1/V(k_1 - k_2)T](Vk_1T - d - d \log(k_1VT/d)) \quad (1)$$

holding over the region $V=d/k_1T$ to $V=d/k_2T$ and

$$i/i_0 = 1 - [d/V(k_1 - k_2)T] \log(k_1/k_2) \quad (2)$$

holding from $V=d/k_2T$ on indefinitely.

When the shutter is used, it can be shown that Eq. (2) ceases to hold at $V=[d/k_1(T-\alpha T)]$ and that a new equation

$$\frac{i}{i_0} = 1 - \frac{k_1(T - \alpha T)}{(k_1 - k_2)T} + \frac{d}{V(k_1 - k_2)T} \left(1 + \log \frac{Vk_2[T - \alpha T]}{d} \right) \quad (3)$$

holds over the region $V=d/[k_1(T-\alpha T)]$ to $V=d/[k_2(T-\alpha T)]$.

On differentiating Eqs. (1), (2), and (3) with respect to V , the required result is obtained;

$$\frac{d(i/i_0)}{dV} = \frac{d}{V^2(k_1 - k_2)T} \log \frac{k_1VT}{d} \quad (4)$$

$$\frac{d(i/i_0)}{dV} = \frac{d}{V^2(k_1 - k_2)T} \log \frac{k_1}{k_2} \quad (5)$$

$$\frac{d(i/i_0)}{dV} = -\frac{d}{V^2(k_1 - k_2)T} \log \frac{Vk_2(T - \alpha T)}{d}. \quad (6)$$

Eqs. (4), (5), and (6) hold respectively over the same regions as Eqs. (1), (2), and (3). Fig. 5 represents a theoretical curve for a spectrum of negative ions having mobilities between 1.6 and 2.2 cm/sec. per volt/cm, neglecting any effect of diffusion.

The shape of the curves is not of so much interest as the voltages of the zeros and break points. As the shutter begins to open, the lower zero point at a voltage $V_0 = d/k_1 T$, and the first break point at $V_1 = d/k_2 T$, are obtained. Similarly, when the shutter closes, the second break point at $V_2 = d/k_1(T - \alpha T)$ and the upper zero at $V_3 = d/k_2(T - \alpha T)$ appear.

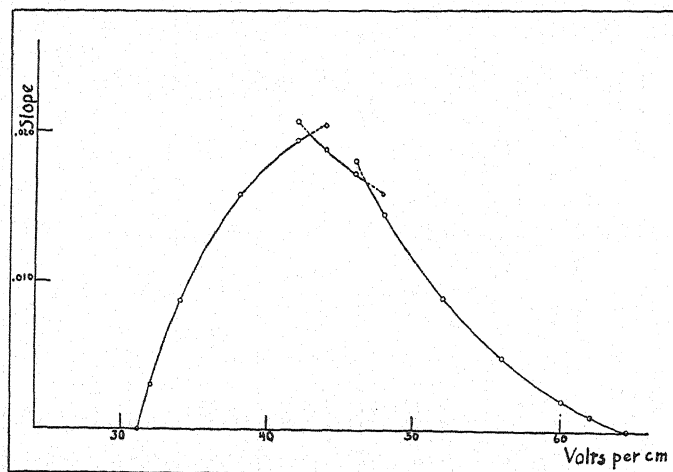


Fig. 5. Graph of the theoretical values of $d(i/i_0)$ with the following assumptions: $k_1 = 2.2$, $k_2 = 1.6$, shutter size, $\alpha T = T/3$, $T = 0.0292$ sec., no diffusion. This is a graph of Eqs. (4), (5), and (6).

In obtaining Eqs. (1), (2), and (3), it was assumed that the mobilities were spread uniformly over the region bounded by k_1 and k_2 . The spread in any case would undoubtedly not be uniform, but this would only change the shape of the curves without altering either the positions of the break points or of the zero points. Furthermore, it would alter the equation of the middle curve only by changing its constant coefficient.

Two things are apparent from the curve: (1) If there is a unique mobility, i.e., *no spectrum at all*, the lower break point will occur at the same voltage as the lower zero, and the upper break point will occur at the same voltage as the upper zero. The curves represented by Eqs. (4) and (6) will then become vertical straight lines, (see Fig. 6). This corresponds to saying that the i/i_0 curve will have no asymptotic feet. (2) At any constant speed the smaller the shutter is made the closer together will the two break points lie. Care must be taken not to make the shutter too small for it is possible to eliminate completely the middle curve, represented by Eq. (5), thus giving only one break point which has no significance with respect to the limits of the mobility spectrum.

One further point of great importance is the diffusion of the ions. The effect of diffusion on the curve will be to yield an apparent mobility spectrum, i.e., asymptotic feet on the i/i_0 curve and therefore a derivative curve like Fig. 5 rather than Fig. 6.

The chance that a molecule will move by diffusion in a time t from its position to any point between two parallel planes dx apart and at a normal distance x away, is given by^{6,7}

$$[1/(4\pi Dt)^{1/2}]e^{-x^2/4Dt}dx$$

where D is the coefficient of diffusion and is given by $D = 0.0236k$.⁸

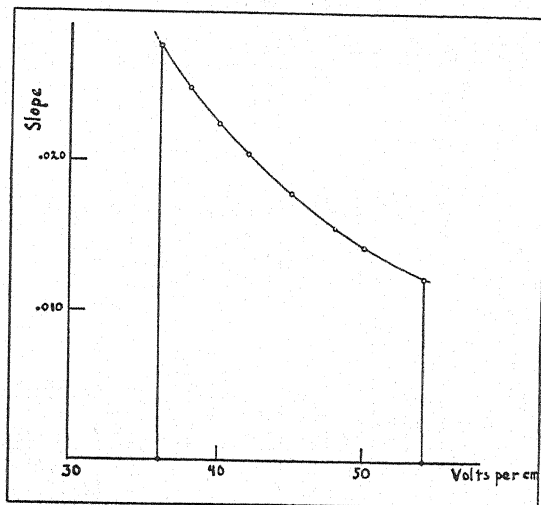


Fig. 6. This curve is represented by the equation $d(i/i_0)/dV = V_0/V^2$, and it is computed on the assumption that there is no mobility spectrum and no diffusion. The other conditions are the same as for Fig. 5.

In order, therefore, to get the number of ions which will diffuse from their non-diffused positions in a band of width αTVk to a distance equal to or greater than the remaining plate distance, the given probability must be integrated with respect to x between the limits $d - Vkt$ and infinity, and with respect to t from $T - \alpha T$ to T . This result must be multiplied by N_0 and divided by the elapsed time αT .

$$N = \frac{N_0}{\alpha T} \int_{T-\alpha T}^T \int_{d-Vkt}^{\infty} \frac{1}{(4\pi Dt)^{1/2}} e^{-x^2/4Dt} dx dt.$$

The integrations were performed with the aid of a table of values of the probability integral and by a standard method of approximation (Simpson's rule).

⁶ J. Zeleny, Phys. Rev. 34, 310 (1929).

⁷ A. Einstein, Ann. d. Physik 17, 558 (1905).

⁸ L. B. Loeb, *The Kinetic Theory of Gases*, p. 451. McGraw-Hill, N. Y., 1927.

The minimum value of N/N_0 , that could be detected by the apparatus was measured, and the value of x , where x is the distance of the upper edge of the undiffused band of ions from the upper plate, was calculated for this N/N_0 . In other words, the distance was found to which the minimum detectable number of ions would diffuse. Now ions moved by diffusion as well as by electric forces may be regarded in exactly the same light as ions moving with an extended mobility spectrum. The fastest ions travel a distance $d+x$ while the slowest ions travel a distance $d-x$ under the same voltage. By applying the same method as was used in obtaining the theoretical mobility spectrum curve, it is apparent that under the force of the voltage V_0 the fastest and most diffused ions will travel a distance d , while the undiffused ions of greatest speed will travel a distance $d-x$; likewise, under the voltage V_1 , the ions which have been diffusing backward with the greatest speed will have travelled a distance d (forward while the slowest undiffused ions travelled a distance $d+x$).

Therefore, $d-x = V_0 k_1 T$, and $d+x = V_1 k_2 T$ where k_1 and k_2 apply as previously defined to the undiffused ions. Thus k_1 and k_2 may be calculated from the voltages of the zeros and the break points (see Figs. 3 and 4).⁹

On applying the diffusion correction the results given in Table II were obtained (results A applying to ions in clean air, and B to ions in old and heavily irradiated air; k_1 and k_2 are in units of cm/sec. per volt/cm).

TABLE II. Values of highest and lowest mobilities, after correcting for diffusion.

	k_1	k_2	T	α	$k_1 - k_2$
A	2.22	2.14	0.00580	7/60	0.08
	2.23	2.20	0.00586	7/60	0.03
	2.23	2.13	0.01150	1/6	0.10
	2.22	2.18	0.01150	7/60	0.04
	2.22	2.22	0.0117	7/60	0.00
	2.25	2.20	0.0280	1/6	0.05
	2.27	2.20	0.01148	1/6	0.07
B	2.4	2.0	0.0292	7/30	0.4
	2.4	1.86	0.0292	7/30	0.54

CONCLUSIONS

It is interesting to note that when the air is allowed to remain in the chamber for several sets of readings, a mobility spectrum appears as shown by the results in B above. The spectrum did not appear when air was left in the chamber for several days without exposure to ultraviolet light from the quartz-mercury arc. It was thus shown that ozone and the nitric oxides, which are formed in air in considerable quantity by the light from such an arc, cause a mobility spectrum. The very small residual spectrum that was found in A might be attributed to the inevitable presence of traces of these

⁹ A consideration similar to the above applies to the case of the second break point and zero respectively, but these are not used because of the inaccurate knowledge of the exact time at which the shutter closes.

impurities, but it is much more likely due, in large part, to small instrumental irregularities in the measurements.

It is therefore safe to conclude that there was no mobility spectrum in air over the intervals studied, in terms of the magnitude of the spectrum asserted to exist by some writers,^{4,10} if the air was relatively clean. An appreciable spectrum did appear after prolonged radiation. The resolving power of the method is excellent and is capable of greater refinement if needed. At the slowest shutter speed, a shift of one volt in the position of one of the critical points shifts the mobility by 0.085 cm/sec. per volt/cm while at the highest speed the mobility is only altered by 0.017 cm/sec. per volt/cm. The probable error in determining the derivative curve is between ± 0.15 volts and ± 0.20 volts, a small figure in consideration of the high resolving power. Whether greater refinement is desirable remains an open question because of the difficulties of accurately correcting for diffusion.

In conclusion, the writer wishes to express his indebtedness to Professor L. B. Loeb under whose direction and continual guidance the experiment was carried out, and to Mr. P. L. Porterfield, who assisted throughout the work. The writer is also grateful to Professor R. T. Birge for his instructions on the method of determining the probable errors and for his critical examination of the work of reduction of the observations.

¹⁰ M. I. a Porte, *Ann. de Physique* 8, 466, 711 (1927).

The Vapor Pressure Constant of Methane

By THEODORE E. STERNE*

Harvard University and The Massachusetts Institute of Technology

(Received September 12, 1932)

§1. It can be shown by statistical quantum mechanics that the vapor pressure constant of a molecule whose principal moments of inertia are all equal to A is

$$i = \log (64\pi^5 k^4 m^{3/2} A^{3/2} / h^6) + \sum_r D_r \log (G_r / r \omega_0)$$

at ordinary temperatures; where m is the mass, k is Boltzmann's constant, h is Planck's constant, the D_r 's are the gram molecular fractions of the two varieties, and where the G_r 's and $r\omega_0$'s are constants.

§2. It is found that G_1 for methane is 5/12, G_2 is 9/12 and G_3 is 2/12.

§3 and §4. It is shown by quantum mechanics that ${}_1\omega_0$ for methane is 5, ${}_2\omega_0$ is 9, and ${}_3\omega_0$ is 2; if the spins of the hydrogen nuclei are taken into consideration but the spin of the carbon nucleus neglected, which is permissible.

§5. With the value $A = 5.17 \times 10^{-40}$ c.g.s. units, it is found that the vapor pressure constant in atmospheres and common logarithms of methane at ordinary temperatures should be -1.94 . The experimental result given by Eucken, -1.97 ± 0.05 , agrees with this.

INTRODUCTION

IN RECENT papers^{1,2,3,4} the author has studied the vapor pressures of diatomic vapors. The work was an extension of that of R. H. Fowler,⁵ who first investigated, theoretically, the vapor pressure of hydrogen made up of the two non-combining varieties para-hydrogen and ortho-hydrogen. In a subsequent paper⁶ the author investigated the vapor pressure constant of a polyatomic vapor, ammonia. It was shown that the vapor pressure constant i of a molecule such as ammonia, two of the principal moments of inertia of which, A and B , were equal with the third C differing from A and B , should be given by

$$i = \log \frac{64\pi^5 m^{3/2} k^4 A C^{1/2}}{h^6} + \sum_r D_r \log \frac{G_r}{r \omega_0}$$

at ordinary temperatures for which the constant part of the specific heat of the vapor at constant pressure was equal to $4R$ per gram molecule. There R was the gas constant; m was the mass of the molecule; k was Boltzmann's constant; h was Planck's constant; the D_r 's were the gram molecular fractions of the different sorts r of molecules present (there were two varieties of ammonia molecules); G_r was the numerical factor by which the expres-

* National Research Fellow.

¹ T. E. Sterne, Proc. Roy. Soc. A130, 367 (1931).

² T. E. Sterne, Proc. Roy. Soc. A130, 551 (1931).

³ T. E. Sterne, Proc. Roy. Soc. A131, 339 (1931).

⁴ T. E. Sterne, Proc. Roy. Soc. A133, 303 (1931).

⁵ R. H. Fowler, Proc. Roy. Soc. A118, 52 (1928).

⁶ T. E. Sterne, Phys. Rev. 39, 993 (1932).

sion $16(2^{\frac{1}{2}})\pi^{7/2}AC^{1/2}k^{3/2}T^{3/2}/h^3$ must be multiplied in order to obtain the rotational partition function R_r for the gas molecule of type r ; and $r\omega_0$ was the statistical weight of the lowest quantum state of a molecule of ammonia in the crystalline phase "at the absolute zero."

This theory yielded a value for the vapor pressure constant of ammonia in satisfactory agreement with experiment. It therefore becomes interesting to investigate next the vapor pressures of substances for which all three principal moments of inertia of the polyatomic vapor molecules, A , B and C , are equal to each other. We shall therefore in this paper consider the vapor pressure constant of methane, CH_4 . The methane molecule appears to consist of four hydrogen nuclei placed at the vertices of a regular tetrahedron, together with a carbon nucleus at the centroid of the tetrahedron; and the three principal moments of inertia appear to be equal. The Raman spectrum has been studied by Dickinson and others.⁷

§1. THE VAPOR PRESSURE OF METHANE

There should be three varieties of methane molecules, which should retain their separate identities over fairly long periods at ordinary and low temperatures. If we use the notation of the article on ammonia, we say that the first variety is characterized by wave functions which are completely symmetrical $S(4)$ in the spins of the four hydrogen nuclei; the second variety is characterized by wave functions $S(3+1)$ in the spins of the four hydrogen nuclei; and the third variety is characterized by wave functions $S(2+2)$ in the spins of the four hydrogen nuclei. A simpler notation is to follow Dirac's procedure⁸ by introducing the observable s , which describes the magnitude of the total proton spin angular momentum, $\frac{1}{2}\Sigma_r\delta_r$, in units of $h/2\pi$, through the formula

$$s^2 - \frac{1}{4} = (\frac{1}{2}\Sigma_r\delta_r, \frac{1}{2}\Sigma_r\delta_r)$$

where the scalar product is meant. Then the first variety corresponds to the eigenvalue $s' = 5/2$, the second variety to $s' = 3/2$, and the third variety to $s' = \frac{1}{2}$. By methods similar to those employed in the article on ammonia,⁶ §1, it is easy to show that the vapor pressure constant i of a polyatomic vapor, for which the three principal moments of inertia of the molecules are equal to A , is given by

$$i = \log (64\pi^5 k^4 m^{3/2} A^{3/2} / h^6) + \Sigma_r D_r \log (G_r / r\omega_0). \quad (1.0)$$

Here the symbols have the same meanings as in the INTRODUCTION to this paper. Number G_r is here the factor by which the expression $16(2^{\frac{1}{2}})\pi^{7/2}A^{3/2}k^{3/2}T^{3/2}/h^3$ must be multiplied in order to obtain the rotational partition function R^s for a gas molecule of the r th sort. The derivation of the Eq. (1.0) above proceeds in the same fashion as the derivation of Eq. (1.92) in the author's paper on ammonia, except that since a number of selector variables has to be used equal to one more than the number of non-combining groups of terms, we are obliged to use four selector variables in the case of methane although

⁷ Dickinson, Dillon, and Rasetti, *Phys. Rev.* **34**, 582 (1929).

⁸ Dirac, *Principles of Quantum Mechanics*, first edition, Chap. XI.

three were sufficient in the case of ammonia. A quadruple integral must occur in the case of methane in the equation analogous to the Eq. (1.1) of the article on ammonia. To find the G_r 's, we shall have to determine the rotational partition functions R_1 , R_2 and R_3 for the three sorts of methane molecules, respectively.

§2. THE ROTATIONAL PARTITION FUNCTIONS OF FREE METHANE MOLECULES

The rotational energy levels are given by⁹

$$W = (h^2/8\pi^2A)j(j+1) \quad (2.0)$$

where j can take on positive integral values. There is another quantum number K , which can take on the values 0, 1, 2, 3, \dots , j for each value of j . The weights of the levels are given by Villars and Schultze,¹⁰ and are taken from the work of Elert.¹¹ The rotational partition functions R_1 , R_2 and R_3 for the three sorts of methane molecules, respectively appear to have been calculated correctly by Villars and Schultze, at least insofar as the asymptotic expressions

$$R_1 \sim (5/12)\Omega, \quad R_2 \sim (9/12)\Omega, \quad R_3 \sim (2/12)\Omega \quad (2.1)$$

where

$$\Omega = 16(2\pi)^{7/2}A^{3/2}k^{3/2}T^{3/2}/h^3,$$

are concerned. In deriving Eqs. (2.1) we may use methods similar to those used for obtaining the corresponding expressions in the case of ammonia, given in considerable detail in the paper⁶ on ammonia.

It appears, therefore, that

$$G_1 = 5/12, G_2 = 9/12, G_3 = 2/12. \quad (2.2)$$

In this paper the spin of the carbon nucleus is neglected, since the vapor pressure constant of methane could not depend upon its value in any case, and since further the spin is zero.

We must now determine the values of ${}_1\omega_0$, ${}_2\omega_0$ and ${}_3\omega_0$.

§3. THE SPHERICAL OSCILLATORY MOTION OF METHANE MOLECULES IN CRYSTALLINE METHANE

It appears from the considerations advanced by L. Pauling¹² that at very low temperatures, and *a fortiori* at the absolute zero, molecules of methane are not rotating in crystalline methane, but on the contrary are oscillating about orientations of minimum potential energy in the crystal lattice. It will be necessary for us to consider the nature of these motions in some detail in order to be able eventually to evaluate the ω_0 's for methane.

It is not necessary, however, to solve in detail in this paper the quantum mechanical problem which is involved. Taking into account the geometrical symmetry of the methane molecule, we can generalize at once the results

⁹ Dennison, Rev. Mod. Phys. **3**, 280 (1931)

¹⁰ Villars and Schultze, Phys. Rev. **38**, 998 (1931).

¹¹ Elert, Zeits. f. Physik **51**, 6 (1928).

¹² L. Pauling, Phys. Rev. **36**, 430 (1930).

obtained in the case of the ammonia-type molecule considered in the paper on the vapor pressure of ammonia.⁶ We take the origin, O , at the mass center of the molecule; and fixed orthogonal axes OX, OY, OZ such that the orientation of minimum potential energy for the methane molecule corresponds to the presence of the hydrogen nuclei 1, 2, 3, 4 at the points $(0, 0, 6^{1/2}a/2)$, $(-2 \cdot 3^{1/2}a/3, 0, -6^{1/2}a/6)$, $(3^{1/2}a/3, -a, -6^{1/2}a/6)$ and $(3^{1/2}a/3, a, 6^{1/2}a/6)$ respectively; the carbon nucleus being of course at O . Let us investigate the forms of the potential and kinetic energies of the molecule, regarded as rigid, for small displacements of the molecule from this orientation of minimum potential energy. As in the case of ammonia, we specify a displacement by the small rotations x, y and z of the molecule about the axes OX, OY and OZ respectively. The Hamiltonian for the methane molecule is similar to the Hamiltonian for the ammonia molecule, but its form is simpler than the latter because of the higher degree of symmetry of the methane molecule. We see therefore as in the case of the ammonia-type molecule that the lowest energy level of the methane-type molecule, when the arrangement of the hydrogen nuclei is that specified above, can be represented by only a single linearly independent wave function describing its spherical oscillatory motion.

In order to find the values of the ω_0 's, we must now study the symmetry properties of the complete wave functions of the methane molecule, taking into account the spins of the hydrogen nuclei and the various possible distributions of the hydrogen nuclei among the neighborhoods of the four points whose coordinates are specified above.

§4. THE VALUES OF ${}_1\omega_0$, ${}_2\omega_0$ AND ${}_3\omega_0$

The discussion of the symmetry properties of the spherical oscillatory wave functions of a methane molecule in crystalline methane is somewhat more involved than the discussion of the case of an ammonia molecule in crystalline ammonia, because a methane molecule contains one more hydrogen nucleus than an ammonia molecule. There are 24 possible permutations of the protons in a methane molecule as compared with the 6 which are possible in the case of ammonia. For the sake of simplicity and elegance we shall therefore use the methods described by Dirac¹³ in order to consider the symmetry properties of the wave functions of methane. Dirac's procedure can be followed as easily for protons as for electrons, because both protons and electrons have one-half quantum spins. We shall accordingly depart here from the methods which we used for considering ammonia, and in what follows we shall assume that the reader is already familiar with Dirac's theory of the permutation observables.

We must take account of the spins of the hydrogen nuclei and also of the spherical vibrational factors in the wave functions. In dealing with the vibrational factors we must now take account of the different arrangements of the hydrogen nuclei which are possible among the four mean positions, a, b, c and d , say, which we specified in §3. If the vibrational factor in a wave func-

¹³ Dirac, *Principles of Quantum Mechanics*, first edition, §66.

tion for the lowest vibrational level with which we are concerned is denoted by f , then $f(1, 2, 3, 4)$ would refer to a state in which nucleus 1 was in the vicinity of position a , 2 in the vicinity of position b , 3 in the vicinity of position c , 4 in the vicinity of position d ; with analogous meanings for the other 23 f 's which are possible. In accordance with §66 of Dirac's book, let us denote the z -component σ_z of the spin vector σ of the i 'th hydrogen nucleus by σ_i , so that the representative of a state will be $(x_1, x_2, x_3, x_4, \sigma_1, \sigma_2, \sigma_3, \sigma_4 |)$; the single variable x being written instead of x, y, z and the suffix z being dropped from the σ_z 's that occur in representatives. Then in accordance with Dirac's equation (32) it is sufficient to study the permutations P^σ which operate only on the σ 's, and this results in a considerable simplification since it allows us to ignore the x 's. There are five types of permutations of four particles, namely: the types 4, 3+1, 2+2, 2+1+1 and 1+1+1+1. There are thus five independent commuting observables χ^σ which are constants of the motion:

$$\begin{aligned}\chi_1^\sigma &= (1/6)\Sigma P^\sigma_4 \\ \chi_2^\sigma &= (1/8)\Sigma P^\sigma_{3+1} \\ \chi_3^\sigma &= (1/3)\Sigma P^\sigma_{2+2} \\ \chi_4^\sigma &= (1/6)\Sigma P^\sigma_{2+1+1} \\ \chi_5^\sigma &= \Sigma P^\sigma_{1+1+1+1} \equiv 1.\end{aligned}$$

Here, for instance, ΣP^σ_{2+2} is the sum of all permutations which operate on the spin variables σ , of type 2+2. We shall find it easier to study the χ^σ 's than the χ 's. There are 15 simultaneous equations like Dirac's Eq. (22) involving the χ^σ 's; if we notice that $\chi_5^\sigma \equiv 1$ we have merely the 10 equations

$$\begin{aligned}(\chi_1^\sigma)^2 &= \frac{2}{3}\chi_2^\sigma + \frac{1}{6}\chi_3^\sigma + \frac{1}{6} & (\chi_1^\sigma\chi_3^\sigma) &= \frac{1}{3}\chi_1^\sigma + \frac{2}{3}\chi_4^\sigma \\ (\chi_2^\sigma)^2 &= \frac{1}{2}\chi_2^\sigma + \frac{1}{3}\chi_3^\sigma + \frac{1}{6} & (\chi_1^\sigma\chi_4^\sigma) &= \frac{2}{3}\chi_2^\sigma + \frac{1}{3}\chi_3^\sigma \\ (\chi_3^\sigma)^2 &= \frac{2}{3}\chi_3^\sigma + \frac{1}{3} & (\chi_2^\sigma\chi_3^\sigma) &= \chi_2^\sigma \\ (\chi_4^\sigma)^2 &= \frac{2}{3}\chi_2^\sigma + \frac{1}{6}\chi_3^\sigma + \frac{1}{6} & (\chi_2^\sigma\chi_4^\sigma) &= \frac{1}{2}\chi_1^\sigma + \frac{1}{2}\chi_4^\sigma \\ (\chi_1^\sigma\chi_2^\sigma) &= \frac{1}{2}\chi_1^\sigma + \frac{1}{2}\chi_4^\sigma & (\chi_3^\sigma\chi_4^\sigma) &= \frac{2}{3}\chi_1^\sigma + \frac{1}{3}\chi_4^\sigma\end{aligned}$$

and when we solve them for the sets of simultaneous eigenvalues $\chi^{\sigma'}$ of the observables χ^σ we obtain the values given in Table I, where the sets are denoted by s, α, β, γ .

If we introduce the observable s , which we defined in §1, to describe the magnitude of the total spin angular momentum we find by the methods of §66 in Dirac's book that

$$\begin{aligned}\chi_1^\sigma &= [1/192][(4s^2 - 13)^3 + 8(4s^2 - 13) - 48] \\ \chi_2^\sigma &= (1/16)(4s^2 - 9) \\ \chi_3^\sigma &= [1/96][(4s^2 - 13)^2 - 48] \\ \chi_4^\sigma &= (1/24)(4s^2 - 1) \\ \chi_5^\sigma &= 1.\end{aligned}$$

There is therefore one set of numerical values $\chi^{\sigma'}$ for the χ^{σ} 's, and thus one exclusive set of states, for each eigenvalue s' of s . The eigenvalues of s are $5/2$, $3/2$, and $1/2$; we readily find that corresponding to these eigenvalues of s the exclusive sets of states are those which we have denoted by s , β and T respectively. There are no other sets possible; the sets α and A being impossible in the case of a set of four protons. The relationship between s' and the $\chi^{\sigma'}$'s is shown in Table I.

TABLE I.

Exclusive sets of states.	S	α	β	A	γ
Eigenvalues					
s'	5/2	—	3/2	—	1/2
$\chi_1^{\sigma'}$	1	1/3	-1/3	-1	0
$\chi_2^{\sigma'}$	1	0	0	1	-1/2
$\chi_3^{\sigma'}$	1	-1/3	-1/3	1	1
$\chi_4^{\sigma'}$	1	-1/3	1/3	-1	0
$\chi_5^{\sigma'}$	1	1	1	1	1

The three sets, however, may be degenerate; and in fact they are degenerate. Corresponding to any s' there are $2s'$ possible values for the z -component of total spin angular momentum $\sum_{r=1}^4 \sigma_r$, which we may denote by s_z . Thus for the exclusive set of states S , s_z' may be 4, 2, 0, -2 or -4. Similarly for the set β , s_z' may be 2, 0 or -2. For the set γ , s_z' must be 0. Each of the states so defined may itself be degenerate, and some of them are in fact degenerate. These latter degeneracies are essential and cannot be removed by perturbations which are symmetrical between the particles; but we must study them in order to enumerate our representatives correctly and thus obtain our ω_0 's.

Let us choose a representation whose fundamental states are the eigenstates of the z -components σ of the spin vectors of the hydrogen nuclei, corresponding to the simultaneous eigenvalues of all four σ 's. There will of course be $2^4 = 16$ fundamental states, since the eigenvalues of the σ 's are independent and can each be $+1$ or -1 . We wish to find the number of linearly independent eigenstates corresponding to each choice of simultaneous eigenvalues for s_z and s ; that is, we wish to find the number of linearly independent wave functions or representatives capable of representing each of these eigenstates of s_z' and s' in the σ representation. Denoting states by ψ 's, we have

$$\psi(s_z', s') = \sum \psi(\sigma')(\sigma' | s_z', s')$$

and also

$$(s'^2 - \frac{1}{4})(\sigma' | s_z', s') = \sum (\sigma' | s^2 - \frac{1}{4} | \sigma'')(\sigma'' | s_z', s'). \quad (4.1)$$

To calculate the matrix elements $(\sigma' | s^2 - \frac{1}{4} | \sigma'')$ we use the relation

$$s^2 - \frac{1}{4} = 6\chi_4^{\sigma}; \quad (4.2)$$

to calculate the matrix elements $(\sigma' | \chi_4^{\sigma} | \sigma'')$ we allow the observable χ_4^{σ} to operate on the various $\psi(\sigma')$'s in turn and we write down the matrix elements by comparison with the equation

$$\chi_4 \psi(\sigma'') = \sum \psi(\sigma') (\sigma' | \chi_4 \sigma' | \sigma''). \quad (4.3)$$

If we write down the set of simultaneous Eqs. (4.1) for any set of eigenvalues S_z' and s' and solve it, we shall find thereby a linear relation or linear relations obeyed by the representative $(\sigma' | s_z', s')$ and from this we can find the number of linearly independent eigenfunctions $(\sigma' |)$ which are possible; or in other words, the number of independent $\psi(s_z', s')$'s. The following calculations should make this clear.

Case 1,

$s' = 5/2$, $s_z' = 4$. The only $\psi(\sigma')$ which can be concerned is $\psi(1, 1, 1, 1)$ and there is thus only one eigenfunction possible: $(\sigma'_1, \sigma'_2, \sigma'_3, \sigma'_4 | 4, 5/2)$ is a constant when all the σ' 's are 1, and vanishes for all other values of the σ' 's.

Case 2,

$s' = 5/2$, $s_z' = 2$. The only fundamental $\psi(\sigma')$'s which can be concerned when $s_z' = 2$ are those which $\sum \sigma' = 2$; they are $\psi(1, 1, 1, -1)$, $\psi(1, 1, -1, 1)$, $\psi(1, -1, 1, 1)$ and $\psi(-1, 1, 1, 1)$. We shall denote these states by $\psi(1)$, $\psi(2)$, $\psi(3)$ and $\psi(4)$, respectively, for brevity. We find easily from Eqs. (4.2) and (4.3) that the matrix representing $s^2 - \frac{1}{4}$ is

	1	2	3	4
1	3	1	1	1
2	1	3	1	1
3	1	1	3	1
4	1	1	1	3

(4.4)

The set of Eqs. (4.1) in this case becomes

$$\begin{aligned} -3(1 |) + (2 |) + (3 |) + (4 |) &= 0 \\ (1 |) - 3(2 |) + (3 |) + (4 |) &= 0 \\ (1 |) + (2 |) - 3(3 |) + (4 |) &= 0 \\ (1 |) + (2 |) + (3 |) - 3(4 |) &= 0 \end{aligned}$$

and hence

$$(1 |) = (2 |) = (3 |) = (4 |)$$

so that only one linearly independent eigenfunction exists, given by $(r | 2, 5/2) = \text{const.}$, $r = 1, 2, 3, 4$.

Case 3,

$s' = 5/2$, $s_z' = 0$. The $\psi(\sigma')$'s concerned when $s_z' = 0$ are $\psi(1, 1, -1, -1)$, $\psi(1, -1, 1, -1)$, $\psi(-1, 1, 1, -1)$, $\psi(1, -1, -1, 1)$, $\psi(-1, 1, -1, 1)$ and $\psi(-1, -1, 1, 1)$; denoted by $\psi(1)$, $\psi(2)$, $\psi(3)$, $\psi(4)$, $\psi(5)$ and $\psi(6)$ respectively. The other $\psi(\sigma')$'s can be ignored. The matrix representing $s^2 - 1/4$ is

	1	2	3	4	5	6
1	2	1	1	1	1	0
2	1	2	1	1	0	1
3	1	1	2	0	1	1
4	1	1	0	2	1	1
5	1	0	1	1	2	1
6	0	1	1	1	1	2

(4.5)

and we find after solving the Eqs. (4.1) in this case that $(r|0, 5/2) = \text{const.}$; $r = 1, 2, 3, 4, 5, 6$. This is the only eigenfunction possible.

Cases 4 and 5,

for $s' = 5/2$, $s_z' = -2, -4$ respectively, are similar to cases 1 and 2 and in each case only one eigenfunction exists.

Case 6,

$s' = 3/2$, $s_z' = 2$. When we solve the set of Eqs. (4.1) in this case, using the matrix for $s^2 - 1/4$ given by (4.4), we find that

$$(1|2, 3/2) + (2|2, 3/2) + (3|2, 3/2) + (4|2, 3/2) = 0. \quad (4.6)$$

We can choose three and only three linearly independent eigenfunctions obeying Eq. (4.6). All other possible eigenfunctions obeying (4.6) can be expressed as linear combinations of these three. Thus we might choose the 3 eigenfunctions $(r|)_1, (r|)_2, (r|)_3$ defined by the following table:

r	1	2	3	4
$(r)_1$	1	-1	0	0
$(r)_2$	1	0	-1	0
$(r)_3$	1	0	0	-1

Any fourth function $(r|)_4$ obeying (4.6) would be in the form

r	1	2	3	4
$(r)_4$	a	b	c	$-a-b-c$

and we should have

$$(r|)_4 = -b(r|)_1 - c(r|)_2 + (a+b+c)(r|)_3$$

so that it would not be linearly independent.

Case 7,

$s' = 3/2$, $s_z' = 0$. Using the matrix (4.5) we find eventually that $(1|) = -(6|)$; $(2|) = -(5|)$; $(3|) = -(4|)$. There are three and only three linearly independent eigenfunctions.

Case 8,

$s' = 3/2$, $s_z' = -2$. This is similar to case 6, and there are three linearly independent eigenfunctions.

Case 9,

$s' = 1/2$, $s_z' = 0$. Using the matrix (4.5) we find that

$$(1|) = (6|); (2|) = (5|); (3|) = (4|); (1|) + (2|) + (3|) = 0.$$

There are two and only two linearly independent eigenfunctions possible, which might be for instance the functions $(r|)_1$ and $(r|)_2$ given by

r	1	2	3	4	5	6
$(r)_1$	1	-1	0	0	-1	1
$(r)_2$	1	0	-1	-1	0	1

Recapitulating, we can prepare Table II showing the numbers ω_0 of eigenfunctions which are possible in the different cases:

TABLE II.

s'	s_z'	ω_0	Totals
$5/2$	4	1	5
	2	1	
	0	1	
	-2	1	
	-4	1	
$3/2$	2	3	9
	0	3	
	-2	3	
$1/2$	0	2	2

and we see therefore that ${}_1\omega_0 = 5$; ${}_2\omega_0 = 9$; ${}_3\omega_0 = 2$.

§5. THE VAPOR PRESSURE CONSTANT OF METHANE

From the results of §2, we have at once that $D^1 = 5/16$, $D^2 = 9/16$, $D_3 = 2/16$. Hence it follows from the results of the last section and §2 that the last term in Eq. (1.0) is $\log 1/12$. We are now in a position to calculate the vapor pressure constant of methane. Taking the molecular weight with sufficient accuracy to the 16.04 and the moment of inertia A to be 5.17×10^{-40} c.g.s. units, we find that the vapor pressure constant i' at ordinary temperatures, in atmospheres and common logarithms,¹⁴ is $i' = -1.94$. This is in good agreement with the experimental value given by Eucken¹⁵ $i' = -1.97 \pm .05$.

The writer wishes to thank the National Research Council for a grant which enabled these investigations to be carried out.

¹⁴ We merely use Eq. (1.0) with common logarithms instead of natural logarithms, and subtract the quantity 6.006 from the right-hand member.

¹⁵ Eucken, Phys. Zeits. 31, 361 (1930).

On the Origin of the Actinium Series of Radioactive Elements

By A. v. GROSSE

Kent Chemical Laboratory, University of Chicago

(Received September 13, 1932)

Data on the actinium series gathered from carefully selected material have been correlated. It can be definitely concluded from these data that the actinium series is independent and the decay much more rapid than in the uranium-radium series. The significance of this fact for geology (age determinations, heat evolution) is pointed out.

THE experimental material on the actinium series and its theoretical interpretation has been so far extremely conflicting.¹ This is chiefly due to the fact that the determinations of the chemical composition, geologic age, activity ratio of the actinium to the uranium-radium series, the chemical atomic weights of uranium leads and lately the isotopic constitution of these leads have never been determined with the same material for all investigations.

Thanks to the help and cooperation of Mme. Pierre Curie, Mme. Irene Joliot-Curie and Drs. G. Baxter, K. Fajans, O. Hönigschmid, A. C. Lane and H. Schlundt we were able to gather and to investigate a valuable collection of uranium-minerals and preparations from uranium-lead atomic weight determinations.

F. W. Aston had the great kindness to investigate in his mass-spectrograph some lead preparations from these sources, and it is to him that the credit for clearing the problem is due.²

We laid special stress on the determination of the so-called "branching ratio" or as we may better call it now "activity ratio." The older determination of O. Hahn and L. Meitner³ (3 percent), and newer ones of J. Wildish⁴ (1.5–5 percent) and E. Gleditsch and co-workers⁵ (2.7–3.3 percent) are all based on the separation of protactinium with tantalum and seem to us un-

¹ For older literature see St. Meyer and E. v. Schweidler, *Radiaktivität*, 1927, p. 490. J. Wildish, Jour. Amer. Chem. Soc. **52**, 163 (1930). E. Gleditsch and E. Foyn, Comptes Rendus **194**, 1571 (1932). E. Gleditsch and S. Klementsén, Comptes Rendus **194**, 1731 (1932). G. Kirsch, *Geologie und Radiaktivität*, p. 184, 1928. F. W. Aston, Nature **123**, 313 (1929). Lord Rutherford, Nature **123**, 313 (1929). A. Holmes, Nature **126**, 348 (1930). A. F. Kovarik, Science **72**, 122 (1930). G. B. Baxter and A. D. Bliss, Jour. Amer. Chem. Soc. **52**, 4850 (1930). For summaries on the actinium problem see: M. C. Neuburger, Sammlung chem. und chem.-techn. Vorträge **26**, No. 10/11 (1921). G. Elsen, Zeits. f. anorg. Chem. **180**, 304 (1929). G. Elsen, Chemisch Weekblad **25**, 517 (1928); **28**, 1, 7, 714 (1931). G. Elsen, Rec. des Trav. chim. Pays-Bas **51**, 284 (1932).

² F. W. Aston, Nature **129**, 649 (1932).

³ O. Hahn and L. Meitner, Phys. Zeits. **20**, 529 (1919); Zeits. f. Physik **8**, 202 (1922).

⁴ Reference 1.

⁵ Reference 1.

reliable since it could be shown through the isolation of element 91⁶ that its chemical properties widely differ from those of tantalum,⁷ just as those of its neighbors uranium and thorium differ from their lower homologues, tungsten and hafnium.

Our determination of the Pa:U ratio was carried out, in collaboration with Dr. I. D. Kurbatov, at the Chemical Institute of the Technische Hochschule in Berlin-Charlottenburg.⁸

TABLE I.

		1	2	3	4	5
1 Mineral		Carnotite ^a	Kolm ^b	Pitchblende ^c	Pitchblende ^d	Pitchblende ^e
Geographical origin		Colorado, U.S.A.	Gullhogen, Westergotland, Sweden	Katanga, Belg. Congo, Africa	Morogoro, East Africa	Wilberforce, Canada
3 Chemical analysis	U %	19.09	0.43 ^g ; 0.41	72.26	70.45	53.52 ¹¹ ; 52.71
	Th %	0	0.0	0.01 ¹⁰	ab. 0.2	10.37 ¹¹
	Pb %	trace	0.026 ^g	6.68	8.30	9.26 ¹¹
4 Isotopic constitution of Pb	Pb 206%		93.3 ¹²			85.9 ¹²
	207%		6.7 ^f			8.3 ^g
	208%		0.0			5.8
	others		0.0			0.0
Percentage of	RaG		93.3 ¹²			85.9
	AcD		6.7			8.3
	ThD		0.0			5.8 ¹⁴
6 Chem. atomic weight of Pb			206.013 ¹⁵ ± 0.008	206.048 ¹⁶		206.195 ¹⁷
7 Phys. atomic weight of Pb			206.058 ± 0.01	206.067 ¹⁸		206.20 ¹⁸
8 Pb:U ratio		very small	0.061	0.0924	0.1178	0.1730
9 RaG:U ratio		very small	0.058	0.086	0.1093	0.1486
10 Geological age in years		< 70.10 ⁶	404.10 ⁶	591.10 ⁶	748.10 ⁶	987.10 ⁶
11 Pa-α activity in mg. U ₂ O ₅ for every 1 g U in the mineral		28.0	27.9	27.8	27.6	28.2
12 Number of disintegrating Pa-atoms for 100 decaying U-atoms			4.0 ± 0.1, mean value, calculated from row 11			
13 Number of AcD atoms for 100 atoms RaG in U-Pb			4.8 ± 1.8 ¹⁹	7.2 ± 0.3		9.7 ± 0.3 -1.0

^a Obtained from H. Schlundt; from the same lot used by J. Wildish (reference 4) for which he obtained Pa:U = 5.16:100.

^b Obtained from A. C. Lane, from the same general lot used for G. P. Baxter's kolm lead atomic weight determination.

^c Obtained from Mme. Pierre Curie and Mme. Irene Joliot-Curie.

^d Obtained from F. Kranz, Bonn, Germany.

^e Obtained from A. C. Lane and G. P. Baxter, from the same lot used for the Wilberforce lead atomic weight determination.

^f The lead tetramethyl used by F. W. Aston was prepared from the original PbCl₄ used by O. Hönigschmid. According to private information from Dr. Aston the lead from Mme. Curie's sample had an identical isotopic constitution.

^g The material used by F. W. Aston was prepared from G. P. Baxter's original atomic weight preparation.

⁶ A. v. Grosse, Naturwiss. 15, 766 (1927); Nature 120, 621 (1927); Ber. d. Deut. Chem. Ges. 61, 233 (1928).

⁷ A. v. Grosse, Jour. Amer. Chem. Soc. 52, 1742 (1930).

⁸ Part of these results were reported at the meeting of the Chicago Section of the Amer. Chem. Society on September 25, 1931; see also G. Elsen, Chem. Weekblad 28, 714 (1931).

⁹ R. C. Wells and R. E. Stevens, Jour. Washington Acad. of Science 21, 412 (1931).

¹⁰ The Th was separated with UX₁, added as indicator, concentrated and the Th-content determined with W. Noddack's x-ray spectrograph at the Physikalisch-Technische Reichsanstalt, Berlin-Charlottenburg.

¹¹ R. C. Wells, Jour. Amer. Chem. Soc. 52, 4852 (1930).

¹² F. W. Aston, Nature 129, 649 (1932).

¹³ Since the mineral contains practically no Th, and therefore no ThD, the absence of Pb²⁰⁸ indicates the absence of ordinary lead, the latter containing 49.55 percent Pb²⁰⁸ (see Aston, reference 12).

¹⁴ From the Th-content and age we calculate, using Th = 6, 1.10⁻¹¹a⁻¹, the percent of ThD = 6, 0 indicating the absence of ordinary lead.

Our method consisted in precipitating the Pa from a strongly acid (HNO_3 , HCl) solution of the U-mineral together with added Zr (in the proportion of 20–50 mg ZrO_2 , in the form of oxychloride or nitrate, to 1 g U) by an excess of H_3PO_4 , and freeing the filtered $\text{Pa-ZrP}_2\text{O}_7$ precipitate from adsorbed radioactive impurities (especially Io, Ra, and Po) through the addition and subsequent separation (repeated if necessary) of minute quantities (2–10 mg) of Th, Ba, Bi (and Te), Pb and La salts. The method was tested with radioactively pure Pa preparations in different concentrations and found to separate 98–99 percent of the available Pa in a radioactively pure state. The activity of the Pa preparation was compared with that of pure U_3O_8 , both in extremely thin layers, in an ordinary Rutherford α -electroscope and expressed in mg U_3O_8 .

The results of all determinations and investigations with our material are correlated in Table I.

These data all support A. Piccard's²⁰ and especially Lord Rutherford's²¹ ideas about the actinium series. The following conclusions can be drawn:

1. The actinium series is independent of the U-Ra series. It is derived from a U-isotope, the actino-uranium (Ac-U), which occurs in all U-minerals in a constant ratio to UI, independent of the geological age, geographic origin, thorium content and uranium concentration. 4.0 atoms Ac-U, or of any other member of the Ac-family, decay for every 100 UI-atoms disintegrating, i.e., the activity ratio of the Ac to the U-Ra series is 4:100. Our determinations completely support the older results of Stefan Meyer, V. F. Hess and G. Kirsch.^{22,23,24}

2. AcD, the end product of the actinium series, has an atomic weight of 207 (or more exactly 207.010 ± 0.01), therefore $\text{Ac} = 227$ and $\text{Pa} = 231$.

3. The AcD content of uranium lead (and therefore also its atomic weight) increases with the geological age of the mineral. From the AcD content in U-Pb of minerals of definite age and the activity ratio the half period of Ac-U can be calculated (see formula 2 below); the best value is $T_{(\text{AcU})} = 4.0 \times 10^8$ years, $\lambda_{(\text{AcU})} = 5.5 \times 10^{-17} \text{ sec.}^{-1}$.

Fig. 1 shows the increase of AcD content in uranium lead with the age of the mineral. The theoretical curve is calculated for $T_{(\text{AcU})} = 4.0 \times 10^8$ years.

The values of AcD content, derived from chemical atomic weight determinations of uranium leads of different ages, including kolm²⁵ and also oldest pitchblendes, for instance, from Black Hills, South Dakota²⁶ (at. wt. = 206.07₁

¹⁶ G. P. Baxter and A. D. Bliss, Jour. Amer. Chem. Soc. **52**, 4848 (1930).

¹⁷ O. Hönigschmid and L. Birkenbach, Ber. Deut. Chem. Ges. **56**, 1837 (1923).

¹⁸ G. P. Baxter and A. D. Bliss, Jour. Amer. Chem. Soc. **52**, 4851 (1930).

¹⁹ F. W. Aston, reference 12.

²⁰ Value tentatively calculated from the chem. atomic weight of kolm lead.

²¹ A. Piccard, Arch. sciences phys. and natur. **44**, 161 (1917); A. Piccard and E. Stahel, same journal (5) **3**, 541 (1921).

²² Lord Rutherford, Nature **123**, 313 (1929).

²³ St. Meyer and V. F. Hess, Wiener Ber. (Akad. d. Wiss.) **128**, 909 (1919).

²⁴ St. Meyer, Wiener Ber. (Akad. d. Wiss.) **129**, 483 (1920).

²⁵ G. Kirsch, Wiener Ber. (Akad. d. Wiss.) **129**, 309 (1920).

corrected age = about $1300 \cdot 10^6$ years) are, within experimental errors, in agreement with this theoretical curve.

4. The AcU content of the element uranium, independent of source, equals at present 0.4 percent by weight. It was much larger in former geological epochs, i.e., over 4 percent about 1600×10^6 years ago; it will diminish in the future, for instance in about $1600 \cdot 10^6$ years the content will be only 0.03 percent. Similarly the activity and heat evolution due to the actinium series and their importance for geology were much larger in past times, equalling about half the value of the uranium series in the earliest part of the earth's history. (The determination of the AcU/UI or Pa/UI ratio affords a method of measuring the "age of uranium" in meteorites as compared with our uranium on earth.)

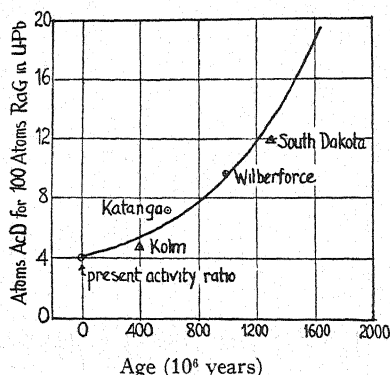


Fig. 1. Theoretical curve for $T(\text{AcU}) = 4.0 \times 10^8$ years. Triangles with dots are calculated from chemical atomic weight determinations.

5. Owing to the more rapid decay of AcU it is necessary to make corrections in geological age calculations.²⁷

The exact age (t) is

$$t = 1/\lambda_{(\text{UI})} \cdot \log_e \left(1 + \frac{238 \text{ U} - \text{Pb}}{206 \text{ UI}(1 + r)} \right) \quad (1)$$

where r is the ratio of AcD to RaG in U-Pb (see Fig. 1) and

$$r = R \cdot \frac{\lambda_{(\text{UI})}(e^{\lambda_{(\text{AcU})}t} - 1)}{\lambda_{(\text{AcU})}(e^{\lambda_{(\text{UI})}t} - 1)} \quad (2)$$

when R is the activity ratio of Ac to U-Ra series, i.e., 0.040.

²⁵ Compare G. P. Baxter and A. D. Bliss, *Jour. Amer. Chem. Soc.* **52**, 4850-51 (1930).

²⁶ T. W. Richards and L. P. Hall, *Jour. Amer. Chem. Soc.* **48**, 706 (1926).

²⁷ A. Holme's objections (*Nature* **126**, 348 (1930)) to Lord Rutherford's conclusions (*Nature* **123**, 313 (1929)) are only correct so far as Aston's first value for the AcD content in U-Pb was too high, owing to the so-called "hydride effect," i.e., coincidence of the Pb^{207} line with the $\text{Pb}^{206} \text{ H}^1$ line. With the help of a nearly pure ThD (94.1 percent Pb^{208}) which we owe to the kindness of Professor K. Fajans (for its source and at wt., see K. Fajans, *Sitzungsber. Heidelberg. Akad. d. Wiss.* 1918 A, Abh. 3, 0. Hönigsmid, *Zeit. f. Elektrochemie* **25**, 91 (1919)), Aston was able to measure this effect and correct for it in his subsequent determinations.

Since t occurs also in the correction factor it is easier to calculate the RaG:UI and U-Pb:U ratios for set values of t and derive the age from the Table II ($T_{\text{AcU}} = 4.0 \times 10^8$ years).

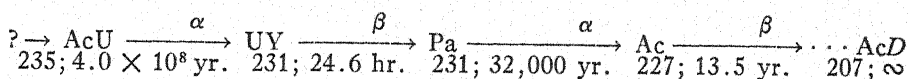
TABLE II.

Age, t (years)	RaG: UI ratio or g RaG for 1g UI	U-Pb: U ratio or g U-Pb for 1g U
0×10^6	0.0000	0.0000
100	0.0139	0.0145
200	0.0280	0.0293
300	0.0423	0.0445
400	0.0569	0.0600
500	0.0718	0.0760
600	0.0868	0.0924
700	0.1022	0.1094
800	0.1177	0.1269
900	0.1335	0.1450
1000	0.1495	0.1638
1100	0.1658	0.1835
1200	0.1824	0.2040
1300	0.1992	0.2258
1400	0.2164	0.2492
1500	0.2337	0.2733

6. 1 g U contains in equilibrium $2.7_3 \times 10^{-7}$ g Pa, since $T_{\text{(Pa)}} = 32,000$ years.²⁸ 1 g Ra is associated with 0.8_1 g Pa at the present geological time; in the past it was more common than radium (1600×10^6 years ago about 10 g Pa occurred for every g of Ra) and in the future it will become rapidly rarer (in 1600×10^6 years the Pa:Ra-ratio will be only 0.06).

7. The pleochroic haloes discovered by S. Iimori and Y. Yoshimura²⁹ cannot be due to the Ac-series, since these have always occurred together with the U-Ra-series on earth.

8. The transformation scheme for the actinium series is as follows (atomic weight, period):³⁰



The only fact not in harmony with the other data on the actinium series presented here is the presently accepted value for the atomic weight of uranium (238.14, $O = 16$). The atomic weights of all members of the three series can be calculated with precision, if the atomic weight of their corresponding end product is known, by adding to it, step by step, the well-known masses of particles and energies emitted during each disintegration.

From Aston's recent measurements³¹ we have for the physical atomic weight of $\text{Pb}^{206} = 206.01 \pm 0.01$ or 205.96 ± 0.02 on the chemical scale, using

²⁸ A. v. Grosse, *Naturwiss.* 27, 505 (1932).

²⁹ S. Iimori and Y. Yoshimura, *Scient. pap. Inst. Tokyo* 5, 11 (1926).

³⁰ "?" indicates that there still is a possibility for the existence of a second actino-uranium, see also A. v. Grosse, reference 28.

³¹ F. W. Aston, *Nature* 129, 649 (1932).

R. Mecke's³² conversion factor (1.00022). From this starting point the calculated values for the following members of the U-Ra-series are:³³

Radio element	Phys. at. wt., $O^{16} = 16$	Chem. at. wt., $O = 16$
RaF (Po)	210.02	209.97
Ra-Em	222.05	222.00
Ra	226.06	226.01
UI	238.08	238.03

± 0.02

$\pm \text{ab. } 0.02$

This atomic weight of UI and Aston's observation³⁴ that it constitutes at least 97 percent of the element uranium indicate that the value 238.14 for the latter is too high.

The author wishes to express his gratitude to the *Notgemeinschaft der Deutschen Wissenschaft* in Berlin and to Mr. H. J. Halle of New York City for financial support in this investigation.

³² R. Mecke and W. H. J. Childs, *Zeits. f. Physik.* **68**, 362 (1931).

³³ Our complete data were published in F. G. Houterman's report—*Ergebnisse der exakten Naturwissenschaften*, p. 199, 1930.

³⁴ F. W. Aston, *Nature* **128**, 725 (1931).

Permeability of Iron at Ultra-Radio Frequencies

By J. BARTON HOAG AND HAYDN JONES
Ryerson Physical Laboratory, University of Chicago

(Received September 12, 1932)

Measurements have been made by the self-inductance method at ultra-radio frequencies of the "initial" magnetic permeability of iron wire by use of the new frequency determination method of Hoag. The following values have been obtained: 30.31, 22.10, 18.69 and 9.65 at frequencies of 469.8, 589.8, 829.8 and 1350 megacycles, respectively, corresponding to wave-lengths of 63.81, 50.83, 36.13 and 22.21 cm. These values of permeability are appreciably lower than those of Arkadiew in this region but show a similar decrease with increase of frequency.

INTRODUCTION

THE study of permeability of iron at very high radio frequencies is of great interest in connection with theories of magnetism. Anomalies in the measured values of permeabilities at frequencies from 10^8 to 10^6 cycles per second (3 to 300 meters wave-length) were observed by Kartschagin¹ and by Wwendensky and Theodortschik² and discussed by Arkadiew³ and Page.⁴ However, the more recent experiments of Sokolow,⁵ Michels,⁶ Strutt,⁷ Wait,⁸ Laville,⁹ and Wait, Brickwedde and Hall¹⁰ do not show these peculiarities of the permeability values in this range.

Two fundamental procedures employing the skin-effect equations derived by Maxwell, Heaviside, Rayleigh, Kelvin and others, have been used to determine permeabilities at high frequencies. The first is based upon a measurement of the damping or high-frequency resistance in two parallel (Lecher) wires while the second depends on the measurement of their high-frequency inductance. It is found in all cases that the values of permeability μ_k obtained by the resistance method are greater than those μ_n obtained by the inductance method. The possible accuracy of measurement by the former method is much greater than by the latter. For example, values given by Michels for μ_k in the wave-length range from four to thirteen meters are accurate to 3 percent while μ_n values are in error by 4-13 percent. The present work was undertaken with a view to increasing the accuracy and high frequency range of the inductance method.

¹ W. Kartschagin, *Ann. d. Physik* **67**, 325 (1922).

² B. Wwendensky and K. Theodortschik, *Phys. Zeits.* **24**, 216 (1923). *Ann. d. Physik* **68**, 463 (1922).

³ W. Arkadiew, *Zeits. f. Physik* **28**, 11 (1921).

⁴ L. Page, *Phys. Rev.* **21**, 456 (1923).

⁵ L. Sokolow, *Ann. d. Physik* **83**, 1136 (1927).

⁶ R. Michels, *Ann. d. Physik* **8**, 877 (1931).

⁷ M. J. O. Strutt, *Zeits. f. Physik* **68**, 632 (1931).

⁸ G. R. Wait, *Phys. Rev.* **29**, 566 (1927).

⁹ M. G. Laville, *Comptes Rendus* **176**, 573-986 (1923).

¹⁰ G. R. Wait, F. G. Brickwedde and E. L. Hall, *Phys. Rev.* **32**, 967 (1928).

Fig. 1 gives a résumé of typical values of the measured permeabilities of iron in the range from 1 cm to 500 m. The letters refer to the workers listed above and the $H-J$ values are those presented in this paper. The anomalies of Kartschagin (K), Wwendensky and Theodortschik (W and T), suggestive of natural resonance phenomena, are shown, while the constancy of the more recent work of the others (excluding Arkadiew) is apparent. The work of Hagens and Rubens with long heat waves reflected from metallic mirrors, indicated that the value of permeability at these frequencies was unity. It is seen in Fig. 1 that the values obtained by Arkadiew with damped waves, as well as our values with undamped waves, show a gradual transition as the region of heat waves is approached. The intensity of the magnetic fields in all cases is less than 0.5 gauss. Variation with field intensity has not been detected.

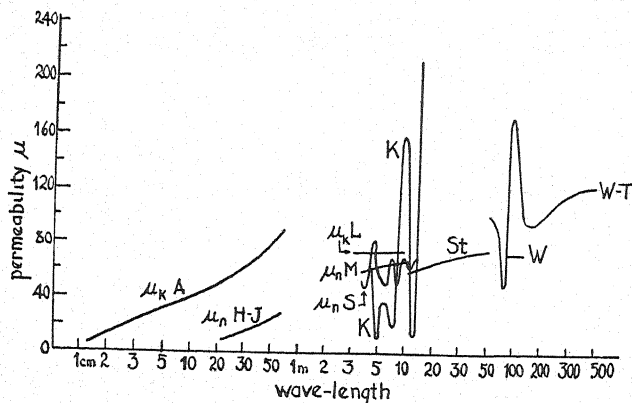


Fig. 1. Permeability of iron at high frequencies.

THEORY OF μ_n DETERMINATION

The J. W. Nicholson¹¹ form of the equation for the inductance of two parallel wires whose magnetic permeability at high frequencies is μ_n is given by the following equation

$$L = 4 \log_e \frac{d}{r} + \frac{4\mu_n}{x} \frac{\text{ber } x \cdot \text{ber}' x + \text{bei } x \cdot \text{bei}' x}{(\text{ber}' x)^2 + (\text{bei}' x)^2} \quad (1)$$

where L is the high-frequency inductance per centimeter of the double wire system; d is the separation of the wires in cm; r is the radius of one wire in cm;

$$x = 2r(\pi\omega\mu_n/\rho)^{1/2} \quad (2)$$

in which $\omega = 2\pi \times \text{frequency} = 2\pi V/\lambda$; V is the velocity of waves in the lecher wires; λ is the wave-length in cm; ρ is the specific resistance of one wire; also

$$\text{ber } x = 1 - \frac{x^4}{2^2 4^2} + \frac{x^8}{2^2 4^2 6^2 8^2} - \dots \quad (3)$$

¹¹ J. W. Nicholson, Phil. Mag. 17, 255 (1909).

and

$$\text{bei } x = \frac{x^2}{2^2} - \frac{x^6}{2^4 2^6 2^2} + \frac{x^{10}}{2^4 2^6 2^8 2^{10}} - \dots \quad (4)$$

The primed values ($\text{ber}'x$, $\text{bei}'x$) are the first derivatives with respect to x .

For extremely high frequencies this equation reduces to

$$L = 4 \log_e d/r + [(2\mu_n R \times 10^9)/\omega]^{1/2} = L_a + 2L_i \quad (5)$$

where R = ohms resistance of a one cm length of a single wire, and $L_a (= 4 \log_e d/r)$ is the inductance per cm of the double wire at low frequencies. The second term, which is equal to $2L_i$, represents that part of the inductance which varies with the frequency. This variation is due to the fact that as the frequency increases the currents are more and more confined to the surface of the wire, leaving a larger inner region filled with material of permeability μ_n . This inductance, L_i , is often referred to as the inner self-inductance. Therefore, solving Eq. (5) for the permeability, we obtain

$$\mu_n = \omega(2L_i)^2/(2R \times 10^9). \quad (6)$$

From the usual cable theory, the velocity of propagation of current waves along the parallel wires is given by $V = 1/(LC)^{1/2}$, which, for our case of high frequencies, becomes

$$V = [(L_a + 2L_i)C]^{-1/2}. \quad (7)$$

This velocity is appreciably smaller than the velocity of light c unless L_i is negligible. Further, we have $c = f\lambda_B$ and $V = f\lambda_F$, where f is the frequency of the generator, λ_F is the wave-length in the magnetizable wires and λ_B is the wave-length in non-magnetizable wires. Combining these equations, we obtain

$$2L_i = 2L_a(\lambda_B - \lambda_F)/\lambda_F \quad (8)$$

where $L_a = 4 \log_e d/r$ from Eq. (5). Substituting this value of the inner self-inductance in Eq. (8) gives the following working equation,

$$\mu_n = (1920\pi/R)(\log_e d/r)^2(\lambda_B - \lambda_F)^2/\lambda_B\lambda_F^2 \quad (9)$$

where R is the d.c. resistance in ohms per cm of a single magnetizable wire. It is to be noticed that the accuracy with which μ_n may be determined depends on the precision of the wave-length measurements.

APPARATUS

Fig. 2 shows the apparatus used for determining the permeability by the self-inductance or wave-length method. An electron oscillator of the magnetron type was used as a generator of the ultra-radio frequencies. The elements of this vacuum tube consisted of a 4 mil tungsten filament surrounded coaxially by a molybdenum cylinder whose inside diameter was 1 cm. This vacuum tube was placed in a magnetic field so that the filament was parallel to the lines of force. The cylinder was raised to a positive potential of 100–1200 volts. Oscillations were produced by slowly increasing the magnetic field

to a value at which the anode current, indicated by the milliammeter (*A*), suddenly decreased. The frequencies which were produced with this tube ranged from 1.36×10^9 to 0.47×10^9 cycles per second (22 cm–64 cm). These ultra radio frequency oscillations were fed through two 0.01 mfd condensers (*c*) into a lecher wire system (*WW*). These wires were 0.318 cm in diameter and 150 cm long and were suspended 1.90 cm apart.

The double short circuiting bridge similar to that described by L. Tonks¹² (*B* in Fig. 2) consisted of two short-circuiting bars separated by approximately one-fourth of the wave-length in use. This served effectively to reduce the dead-end effect of the portion of the wires to the right of (*B*).

A small pick-up coil (*e*) of copper wire was mounted near the coupling condensers as indicated in the figure. Currents induced in this side circuit were rectified by the crystal (*d*). The a.c. components were by-passed by a small condenser, while the d.c. component served to deflect the galvanometer (*G*).

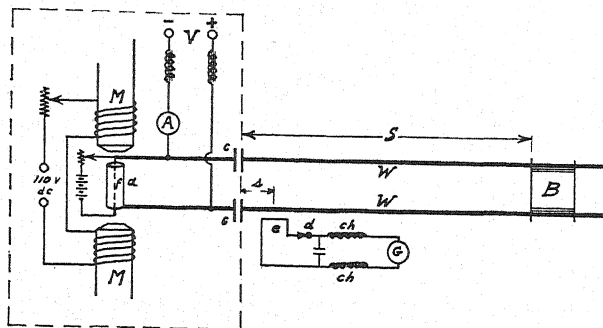


Fig. 2. Circuit used to measure high-frequency permeabilities.

Calculations for this apparatus showed that the impedance of the generator was approximately equal to the characteristic line impedance of the lecher wires.

MEASUREMENT OF THE WAVE-LENGTH

The usual cable theory has been applied by Hoag to the present apparatus. This gives the following equation for the galvanometer current i_g in terms of the position S of the bridge (see Fig. 2),

$$i_g = I_0 \cos^2 [360(S - s)/\lambda] \quad (10)$$

Fig. 3 shows experimental values for a 64 cm wave. That the equation of this curve is correctly expressed by Eq. (10) may be seen by solving the equation for the bridge position. Thus

$$S = s + (\lambda/360) \cos^{-1} (i_g/I_0)^{1/2}. \quad (11)$$

If we replot the data of Fig. 3 using values of S as ordinates and $\cos^{-1}(i_g/I_0)^{1/2}$ as abscissae, the points fall along the straight line shown in Fig. 4. The y

¹² L. Tonks, *Physics* 2, 1 (1932)

intercept gives the value of the distance s , thus eliminating all difficulty in determining the end corrections of the lecher wire system. The slope of the line is equal to $\lambda/360$. In order to obtain the wave-length λ with greater pre-

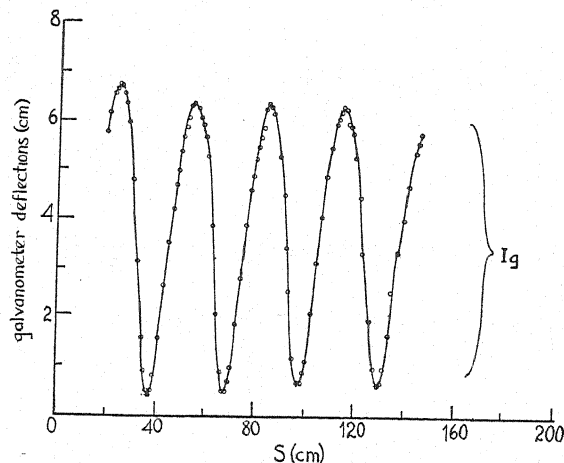


Fig. 3. Galvanometer deflections for various bridge positions.

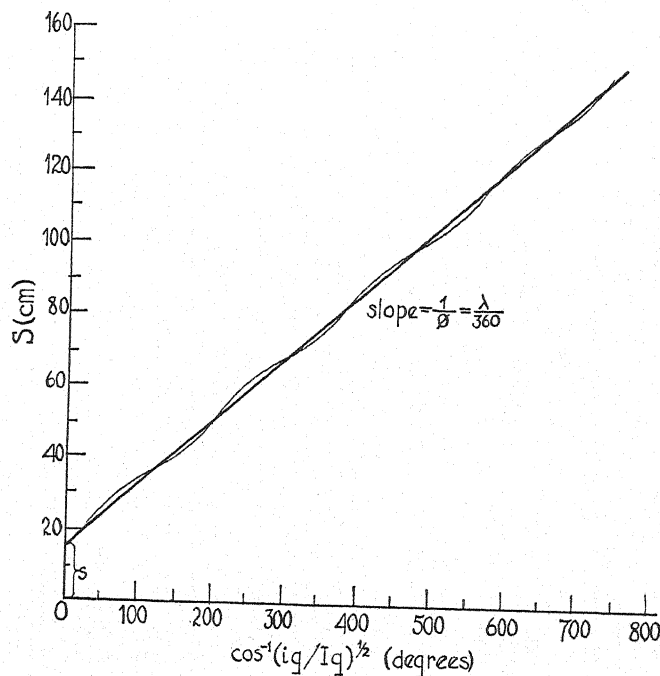


Fig. 4. Measurement of the wave-length.

cision, an average for symmetrical points on the experimental wavy line of Fig. 4 was determined. Wave-lengths measured by this method are accurate to three significant figures throughout the range investigated.

In order to stabilize the frequency and strength of the oscillations, the various currents used to operate the magnetron were continuously maintained at fixed values during the time necessary to obtain the data for both iron and brass lecher wires. In this way, values of λ_F and λ_B for a definitely fixed frequency were obtained. Approximate values of the wave-length were obtained by doubling the distance between successive peaks in Fig. 3.

RESULTS

The wave-lengths measured by this method and the permeabilities calculated from Eq. (9) are given in Table I. The d.c. resistance R was equal to 0.00032 ohms per cm length of a single iron wire. The separation of the lecher

TABLE I.

Approx λ cm	λ_F cm	λ_B cm	μ_n	f megacycles
64	63.55	63.81	30.31	469.8
51	50.68	50.83	22.10	589.8
36	36.04	36.13	18.69	829.8
22	22.18	22.21	9.65	1350.

wires (d) was 1.90 cm and each wire had a radius r of 0.159 cm. It is to be noted that the μ_n values are appreciably lower than those of Arkadiew. They gradually diminish at shorter wave-lengths, as is to be expected in this transition region.

LETTERS TO THE EDITOR

Prompt publication of brief reports of important discoveries in physics may be secured by addressing them to this department. Closing dates for this department are, for the first issue of the month, the twenty-eighth of the preceding month; for the second issue, the thirteenth of the month. The Board of Editors does not hold itself responsible for the opinions expressed by the correspondents.

Velocities of Ions and Electrons in Pure Gases

In a review on "Electrical Discharges in Gases," K. T. Compton (*Rev. Mod. Phys.* 2, 123 (1930)) arrives at a general mobility equation which should apply to ions and electrons. No test of the equation was made by comparison with experimental results of the mobilities of positive ions, because at that time no determinations had been made in which the nature of the ions was sufficiently well established.

In a paper read before the New Zealand Institute, I used Compton's equation to calculate the mobilities of certain positive ions moving in pure gases. These mobilities had been experimentally measured with accuracy by Tyndall and Powell (*Proc. Roy. Soc. A* 134, 125 (1931) and 136, 145 (1932); *Nature* 127, 592 (1931)). My calculations for the mobility of helium ions in helium showed that Compton's equation yields values several times greater than 21.4 cm/sec. per volt/cm, the value obtained by Tyndall and Powell. Further, for values of X/p ranging from 0.3 to 4.2 volt/cm per mm of mercury, the mobilities calculated from the equation change rapidly, contrary to the experimental values. Hassé's calculations (*Phil. Mag.* 1, 139 (1926) and 12, 554 (1931)) from Langevin's general equation are in much closer agreement with the best experimental values or positive ions in the case of helium and in the other cases I considered, and, in addition, this equation leads to the well-established law connecting mobility and pressure and to the fact that the mobility is independent of the electric field for small to moderate fields.

In obtaining his equation Compton neglects the effect of the attractive forces between ions and molecules. The reasons given for this procedure (*R.M.P.* 2, 209 (1930)) justify it in the consideration of electrical discharges through

gases, but the simplification is only a rough approximation under the conditions existing during mobility measurements. The expression there quoted for the force between an ion and a neutral molecule is only half the correct form. Assuming that this is a typographical error, there still seems to be a numerical error in Compton's estimates of the effect of attraction, which may have influenced his judgment of the relative unimportance of the attractive forces. These forces depend on the ratio (R) of the energy of dissociation of an elementary cluster to the average kinetic energy of the ions and molecules. From Hassé's calculations I estimated that the effect of the attractive forces for values of R up to 1.6 is greater than indicated by Compton's figures. This emphasizes the vagueness of his conclusion that "the ion free path is not appreciably diminished by the fact of its charge unless the mutual kinetic energy is of the order of the cluster dissociation energy, or less." The mobility of the ions will be much reduced by the attractive forces when the cluster dissociation energy is considerable compared with the average kinetic energy of a molecule. This is the condition that clusters of charged and uncharged molecules should be formed. Although Tyndall and Powell found no evidence of ionic clusters in their work on pure helium, even in this case the effect of the attractive forces is to reduce the calculated mobility by about 50 percent. It is not possible yet to make a much closer approximation to the forces between ions and molecules in close proximity than the inverse fifth power law of attraction.

There appears to be no adequate reason to extend the concept of mobility to the case of electrons where the velocity in the direction of the electric field (W) is not in general pro-

portional to the field strength (X) (*vide* V. A. Bailey, *Phil. Mag.* **46**, 213 (1923)). Compton's equation for the mobility of electrons can be considered as an equation for the velocity of electrons under standard conditions of temperature and pressure (W_0), and it appears to be as accurate as any equation yet proposed which neglects the large variations of mean free path with velocity of agitation. In my paper I suggested a method whereby the agreement between velocities predicted from Compton's equation and the

have been measured at 15°C and p mm pressure. λ is the mean free path of the electron at 0°C and 1 mm pressure and has been assumed equal to the usual kinetic theory value. The results in the case of oxygen are shown in Fig. 1. Curve I shows the experimental velocities obtained by Brose (*Phil. Mag.* **1**, 536 (1925)), which are believed to be the best available for the range of X/p considered. Curve II shows the values calculated from Compton's equation, and Curve III shows the values calculated from Eq. (1)

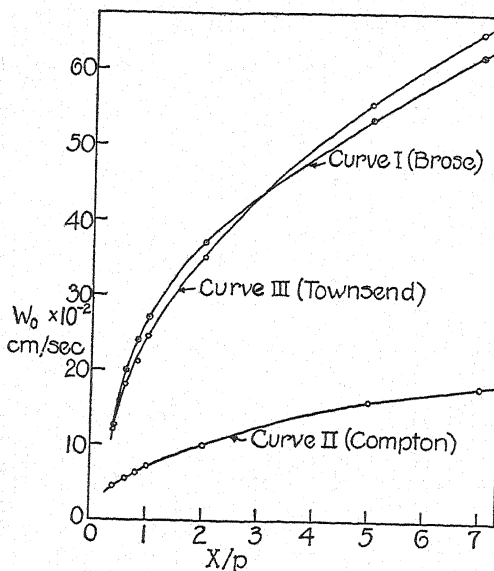


Fig. 1. Drift velocities of electrons in oxygen.

best experimental results could be improved in the case of typical gases like oxygen, nitrogen and helium. The suggestion was to adopt Townsend's expression for the average fractional energy loss at an encounter between an electron and a molecule, i.e., $f = 2.46 W^2/C^2$, where C is the velocity of agitation of the electrons, instead of assuming that the collisions are like those between perfectly elastic spheres, in which case $f = 2.66 m/M$ approximately, where M is the mass of the molecule. For the purpose of rapid calculation I wrote Compton's equation for electrons (R.M.P. **2**, 234 (1930)) in the form

$$W_0 = 41,600(p\lambda X)^{1/2} \times f^{1/4} \quad (1)$$

where it is assumed that the drift velocities

by using Townsend's expression for f and Brose's values for W and C . The improved agreement with the experimental value in this gas by using the method suggested is much more marked than in the case of monatomic gases, where for small values of X/p the collisions are nearly elastic. The agreement thus obtained in the cases of the gases considered is as close as can be expected from any theory which neglects the variation of mean free path of the electrons with their velocity of agitation.

C. M. FOCKEN

Department of Physics,
Otago University,
Dunedin, New Zealand.
October 1, 1932.

Variation of the Structure of Scattered Lines with the Frequency of the Primary Light

In a communication by one of us on a new type of modified radiation¹ mention was made of experiments in which the variation in structure of scattered lines with the variation of the frequency of the primary light was examined. These experiments gave some interesting results which have not yet been published.

The modification of wave-length when the radiation 4047A of the mercury arc was used as the primary light has been studied by means of an echelon grating and compared with that of 4358A. In order to obtain greater accuracy the experiments were carried out with benzene under scattering angle $\theta = 135^\circ$.

a considerable difference in the displacements of the modified lines. We have undertaken therefore similar experiments with another primary line under another scattering angle.

The yellow radiation 5791A of the mercury arc was chosen as the primary light. The scattering was examined in benzene under the angle $\theta = 90^\circ$. In consequence of the smaller sensitivity of the photographic plates in the yellow region of spectrum and the decrease of the intensity of scattered light (according to Rayleigh's law) a very long exposure (80 hours) was required.

The results of the measurements for the yellow line 5791A and those for the blue line

TABLE I.

λ A	$\Delta\lambda$ (obs.) A	$\Delta\lambda$ (calc.) A	$\frac{\Delta\lambda(4358)}{\Delta\lambda(4047)}$ (obs.)	$\frac{\Delta\lambda(4358)}{\Delta\lambda(4047)}$ (calc.) = $\frac{4358 \cdot n(4358)}{4047 \cdot n(4047)}$
4358	0.063	0.050	1.13	1.07
4047	0.056	0.047		

The displacement of the lines modified by elastic heat waves ought to vary with the primary wave-length according to the equation

$$\Delta\lambda = \pm 2\lambda_0 n(v/c) \sin(\theta/2) \quad (1)$$

where λ_0 is the primary wave-length, v is the velocity of sound in the medium, n is the refractive index of the medium, c is the velocity of light in vacuum and θ is the scattering angle.

The observed and calculated values of $\Delta\lambda$ for 4358A and 4047A as well as their ratios, observed and calculated, are given in Table I.

These results confirm the existence of the

4358A obtained earlier by one of us¹ are compared in Table II. The observed values agree with the calculated ones satisfactorily within the experimental errors.

The variation of $\Delta\lambda$ with the wave-length of the primary light according to the Eq. (1) (as well as with the scattering angle and velocity of sound in the medium)¹ proves again that the observed modification of the wave-length is produced by elastic heat oscillations in the scattering medium and is not the Raman effect due to the frequencies of the rotation spectrum of molecules of liquids.

TABLE II.

λ A	λ (obs.) A	$\Delta\lambda$ (calc.) A	$\frac{\Delta\lambda(5791)}{\Delta\lambda(4358)}$ (obs.)	$\frac{\Delta\lambda(5791)}{\Delta\lambda(4358)}$ (calc.) = $\frac{5791 \cdot n(5791)}{4358 \cdot n(4358)}$
5791	0.055	0.047	1.17	1.31
4358	0.047	0.036		

connection between $\Delta\lambda$ and λ_0 given by Eq. (2).

The difference between the wave-lengths of the lines 4358A and 4047A is not great enough to produce in the experiments just described

¹ E. Gross, Nature **126**, 201 (1930).

E. GROSS
J. KHVOSTIKOV

Optical Institute,
Leningrad,
October 5, 1932.

Electron Lenses

We wish to amend a statement which appears over our names in an abstract in the *Physical Review* for August 1, 1931.¹ It is there stated, as a result of calculation, that the distorted electrostatic field about a circular hole in a charged conducting plate (a vacuum tube electrode) has for electrons, or other charged particles, the properties of a spherical lens of focal length $f = 2V/(G_2 - G_1)$, where V represents the kinetic energy of the particles in equivalent volts, and $(G_2 - G_1)$ represents the difference between the potential gradients on the emergence and incidence sides of the plate. The part of this statement which requires amendment is the formula for the focal length, which should read: $f = 4V/(G_2 - G_1)$.

The original formula, with 2 as the numerical factor, is correct for the other case men-

tioned in the abstract, that of a rectangular slit. The field about such a slit acts as a cylindrical lens; it was with lenses of this type only that tests had been made at the time the abstract was written. More recently we have made observations on the lens action of the fields about circular holes, and have obtained results in agreement with the corrected formula given above. We hope to have a report of these investigations ready for publication within the next few months.

C. J. DAVISSON

C. J. CALBICK

Bell Telephone Laboratories,
New York City,
October 13, 1932.

¹ Davissan and Calbick, *Phys. Rev.* (2) **38**, 585 (1931).

On the Secondary Emission from Collectors in Neon Discharge

There are known some deviations from Langmuir's theory for currents to a collector in a neon discharge.¹ In order to investigate the causes of such deviations a number of experiments was carried out by us in 1931-32. The experiments were made with cylindrical tubes of different diameters from 3 to 5 cm (pressure $p = 1-2$ mm) with movable collectors of various geometrical shapes. These tubes were made with heated as well as with cold cathodes. The collectors were made of iron, nickel and molybdenum. Before filling the tubes neon was purified in the usual way. The discharge tube could be illuminated by an outside neon source. This illumination caused a corresponding change of the collector current.

When collector potentials approached the anode potential the volt-ampere curves obtained with probe electrode placed in the positive column differ somewhat from those given by Found and Langmuir.²

The shifting of the movable collector across the tube permitted the study of the secondary emission from the probe electrode on the axis of the discharge and also its changes when the collector approached the wall of the tube. Close to the wall the shape of the collector's characteristic in the ion part approached the shape of ordinary curves (e.g., mercury vapor) in absence of secondary emission from the collector. Again when the electrode was

placed on the axis of the positive column or beyond it at high negative potentials the curves had a shape analogous to that given by Found and Langmuir. It is known that a considerable increase of the ion current can be explained by the ionization in the sheath by electrons escaping from the probe electrode. It should be noted that the conditions in some of our measurements were such that only a slight part of the positive column radiation could pass the anode and reach the collector behind it. In other cases in order to study the influence of the radiation on the secondary emission, special tubes with a "transparent" anode (grid-anode) were used. With the increase of illumination intensity, from the emission tube the corresponding decrease of ion current to the collector in the discharge tube was observed. At probe electrode potentials near the space potential the collector current depends only slightly on the intensity of illumination. Ion currents to the collector placed near the wall do not depend on the magnitude of the discharge current up to certain limits. Thus the changes of the collector current due to illumination also do not depend on the discharge current. When the

¹ W. Uytterhoeven, *Proc. Nat. Acad. Sci.* **15**, 32 (1929).

² C. G. Found and I. Langmuir, *Phys. Rev.* **39**, 237 (1932), (Fig. 9.)

same collector was shifted towards the axis of the tube not only the collector current changed with the change of the discharge current but the influence of illumination from the outside source as well. Metastable atoms in a neon discharge may firstly, ionize the impurities (volume effect) and secondly, liberate electrons from surfaces (surface effect). The collector current at high negative potentials according to Foud and Langmuir depends on the sheath conditions. We believe that our experiments lead to the conclusion that the secondary emission is mainly influenced by the metastable atoms.

Pike's³ calculations which have led him to the conclusion that the efficiency of metastable atoms is small compared with the photoeffect of the radiation hardly may be applied in our and other authors' experimental conditions. Pike bases his calculations on Penning's curves⁴ for spark potential referring to high neon pressures (18–20 mm). It is well known however that the changes in the emission from the cold cathode affect the spark potential only at low pressures. At high pressures the volume effect plays the main role.⁵ This explains the small value got by Pike for the efficiency of metastable atoms in liberating the electrons from the collector. Measurements with a plane collector placed beyond the column which could be oriented perpendicular and parallel with the axis of the tube showed that for the perpendicular position of the electrode the ion currents were somewhat greater than for the parallel one. Kenty⁶ assumes that this increase of the current is

one of the evidences of the direct photoeffect from the collector. But in our experiments this difference in the current existed even when the main discharge was switched off. Thus in our experiments the cause of this effect was not the radiation diffusing from the positive column, but the change of the configuration of the gap between the collector and the anode. In the discharge tube with a transparent anode and a collector placed at the axis of the tube beyond the anode and directly affected by radiation from the positive column the ion currents to the collector decreased sharply when a glass wall was approached by the collector from the side opposite to radiation. When the collector was screened from the positive column with various screens the ion current decreased. But this decrease was almost independent of the optical properties of the screens. All these experiments point out the existence of a surface effect under the action of metastable atoms and a comparatively small direct influence of the photoeffect on the secondary emission.

G. SPIWAK

E. REICHRUDEL

Research Physical Institute of
the Moskow State University.

October 14, 1932.

³ E. W. Pike, *Phys. Rev.* **40**, 314 (1932).

⁴ F. M. Penning, *Zeits. f. Physik* **46**, 335 (1928); **57**, 723 (1929), (Fig. 4).

⁵ L. I. Neuman, *Proc. Nat. Acad. Sci.* **15**, 259 (1929), (Fig. 3).

⁶ C. Kenty, *Phys. Rev.* **38**, 377 (1931).

A Filter for the Study of the Raman Effect

To excite Raman spectra¹ by means of the 4358 mercury line, it is current practice to eliminate the 4047 groups by means of a quinine sulphate solution. Since this solution turns brown upon prolonged exposure, recourse is had to the use of a preliminary filter of pale Noviol glass which absorbs the 3650 line as well as lines of shorter wave-lengths—and which, hence, prolongs the useful life of the quinine solution.

Recently, in developing a series of filters transmitting, respectively, only the ultra-violet, the visible, and the infrared, it was found that a solution of sodium nitrite NaNO_2 has a short wave-length transmission limit at about 4050. The behavior of a saturated solution of sodium nitrite in a cell 12 mm

thick is shown in the accompanying photographs. Actual measurements, carried out with a quartz monochromator and a Weston

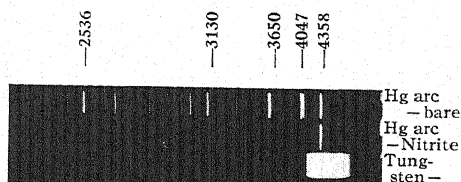


Fig. 1.

Photronic Cell show that while the transmission of the nitrite filter for the 4358 line is

¹ R. W. Wood, *Phys. Rev.* **38**, 2168 (1931).

65 percent, the transmission for the 4047 line is less than 1 percent. The transmission of the Noviol glass was 56 percent for the 4358 line. This indicated that the sodium nitrite solution would be at least as effective as the quinine sulphate-Noviol combination and possess, in addition, the advantage of permanence. Prolonged exposures to the intense radiation of a quartz mercury arc have failed to show any noticeable effects upon the transmission of the nitrite solution.

A freshly prepared solution of sodium nitrite in water shows turbidity which is not removed by filtering. If the solution be allowed to stand for several days, the suspended matter settles out and leaves the solution

quite clear. For most cases a saturated solution in a 12 mm layer will suffice. For use in Wood's system of filters, it is suggested that 2 parts of water be added to 1 part of the saturated nitrite solution and that the mixture be used to fill the glass tube of 3.6 cm internal diameter.

Actual Raman spectrograms taken by Professor Wood showed that the necessary time of exposure with the nitrite filter was no greater than that required by the quinine-Noviol filter and that the nitrite filter did not change its color.

A. H. PFUND

The Johns Hopkins University,
October 22, 1932.

Note on Perturbation Theory of Molecules Formed from Two $2p$ Atoms

The various methods which can be used to estimate (either quantitatively or qualitatively) the energy levels of diatomic molecules do not always give concordant results for the ordering of the levels. Professor Van Vleck has suggested that a comparison of these methods might yield information of some value; this note gives the results of such a comparison in a particular instance. The case chosen is that of a molecule formed from two similar atoms, each containing a single $2p$ electron (plus perhaps non-bonding closed inner shells). We shall neglect the "hybridization" of the $2s$, $2p$ levels; for, though important in hydrogenic atoms because of degeneracy, it is usually less important in heavier atoms. The various schemes of calculation include the following:

1. The Heitler-London perturbation method, inclusive of the electron repulsion term, e^2/r_{12} , in the potential energy. This has been done, to the first order approximation, by Bartlett;¹ his results, corrected as suggested in a later paper,² are shown in Fig. 1. This is the method leading to the concept of "electron pairs."

2. The Heitler-London perturbation method, exclusive of the electron repulsion term. The results, readily calculated from Bartlett's tables, are indicated in Fig. 2.

3. The "two-center" or "molecular orbital" method, also exclusive of detailed electronic interaction. This is the method used extensively in the "Aufbauprinzip" of Hund and Mulliken. It consists essentially of adding the attractive energies of the separate electrons,

each calculated as for the one-electron two-center problem, to the repulsive energy of the nuclei. It will be necessary for us to distinguish the two following ways of applying (3):

(3a) First order perturbation theory, neglecting electronic repulsion, with unperturbed wave functions of the type $[a_i(1) \pm b_i(1)] \times [a_j(2) \pm b_j(2)]$. The choice of sign for each electron's orbital determines whether it is *gerade* or *ungerade*. (Notation: $a_i(1)$ refers to the wave function of electron 1 on nucleus a in the state $m_l = i$, etc.) This method, like (1) and (2), has the disadvantage that it is applicable only for large internuclear distances. It has been worked out by Lennard-Jones;³ the results for our two-electron case are given in Fig. 3.

(3b) Semi-empirical methods of Hund⁴ and Mulliken,⁵ which are guided by correlation of the configurations and levels of known molecules with those of the united atoms and

¹ J. H. Bartlett, Jr., Phys. Rev. **37**, 507 (1931).

² W. H. Furry and J. H. Bartlett, Jr., Phys. Rev. **39**, 211 (1932).

³ J. E. Lennard-Jones, Trans. Faraday Soc. **25**, 668 (1929). As a check, the same results have been found with the aid of Bartlett's tables.

⁴ F. Hund, Zeits. f. Physik **73**, 577 (1932).

⁵ R. S. Mulliken, Rev. Mod. Phys. **4**, 1 (1932); particularly Fig. 43, which is here taken as a standard by which to judge the accuracy of the perturbation methods.

thereby give at least the correct ordering of energy levels. The results by this method, for the one-electron two-center problem, are roughly the same as those by (3a), shown in Fig. 4, save that the dashed σ_u curve should be replaced by the dotted one. (This discrepancy is the reason for dashing this and other curves affected by it.) The σ_g curve should also be somewhat higher for the smaller values of R .

A study of these figures yields the following information:

(a) Figs. 1 and 2 show that the electronic repulsion term raises the triplet levels less than the singlet ones. This is due to the fact that the triplet wave functions are antisymmetric in their orbital part and therefore become zero whenever both electrons occupy the same position, which is just where $1/r_{12}$ becomes infinite. (The same effect is well known in atomic spectra.)

(b) Methods (2) and (3a) differ only in their choice of unperturbed wave functions. (3a) includes "polar" terms, like a_i (1) a_i (2), which allow the possibility of both electrons being on the same nucleus at once and which keep the u or g property of the individual electronic orbitals; this method should be the better one when inter-electronic action is neglected. (2) excludes polar terms and thus keeps an electron on each nucleus at the cost of spoiling the symmetry properties of the individual electronic orbitals; this method may be preferable whenever the inclusion of electron repulsion tends to prevent the two electrons from accumulating on the same nucleus. The best wave function would probably be a linear combination of that of (2) and that of (3a), as Mulliken⁶ has emphasized in the case of $1s$ electrons. The two *ungerade* states made up of equivalent electron configurations, $\sigma_u\sigma_g\Sigma_u$ and $\pi_u\pi_g\Sigma_u$, Δ_u , are the same in both sets of curves. This, as pointed out by Hund,⁷ is due to the fact that the polar terms for such equivalent states cancel when one "antisymmetrizes" the product wave function of (3a) to form the triplet wave function, so that the final functions are the same in either method.

(c) The disagreement between methods (3a) and (3b) shown in Fig. 4 tells us that,

for $R < 8$, the first order perturbation theory (3a) will give not even qualitatively correct results for states involving a σ_u electron—the dashed curves of Fig. 3. This indicates that probably no perturbation calculation for such values of R is reliable. The increase in the discrepancy, as R becomes less than 8, is accompanied by the change in sign of certain integrals in the expression for the energy. This change of sign would, if taken too naively, indicate a weakness in the criterion that the amount of "overlapping" of wave functions is a measure of bonding power; for it was upon assumptions as to the definite sign and magnitude of such integrals that the criterion was first built up. Here, after the change in sign, the overlapping would seem a drawback, rather than an asset, to bonding power. However, the criterion still agrees with the empirical results (3b), even for small R . Furthermore, as Professor Mulliken has kindly pointed out, the question is of little practical significance; for in actual molecules ZR (the analogue to R in hydrogen—see caption to figures) is seldom less than 8.

(d) Neglecting electronic interaction, method (3) has the $\sigma_g\sigma_g^1\Sigma_g$ state lowest; including that interaction, it might instead place in that position the lowest triplet state, $\sigma_g\pi_u^3\Pi_u$. Either of these possibilities, however, disagrees with method (1)'s choice of $(\sigma\sigma)^3\Sigma_u$ as the most stable state. Observations (b) and (c) combine to explain this discrepancy. According to (b), the $\sigma_g\sigma_u\Sigma_u$ state is one of those for which both the Heitler-London and the two-center perturbation methods yield the same results; according to (c), it is one of those states for which the two-center perturbation method gives definitely wrong results. Therefore the Heitler-London method also gives incorrect results for this state; that is why its curve is dashed in Figs. 1 and 2 as well as in Fig. 3.

J. R. STEHN

Department of Physics,
University of Wisconsin,
October 26, 1932.

⁶ R. S. Mulliken, Phys. Rev. **41**, 65–71 (1932).

⁷ F. Hund, Zeits. f. Physik **73**, 11 (1931).

Law of Force between Two He Atoms

During the last few years a number of papers¹ have appeared dealing with the energy of interaction of two He atoms as they are brought closer and closer together. The purpose of the present Letter is to point out that the law of force obtained by the most recent quantum theoretical considerations agrees surprisingly well with that found by Lennard-Jones² from classical considerations on the viscosity and equation of state of helium gas. Classically it is found that for fairly large internuclear distances a force of attraction prevails, but that at distance of 2.5 angstroms or less, a very strong repulsive force dominates the situation. These two types of force receive their interpretation in the quantum theory as electrostatic polar attraction, and repulsion due mostly to electron exchange. The polar attraction has been calculated by Slater and Kirkwood¹ taking account only of the dipole-dipole interaction. This calculation was

action as calculated by Slater and Kirkwood is obtained.

Lennard-Jones² has found that in order to fit the experimental data on the variation of viscosity of He with temperature and on the equation of state

$$V(\rho) = 1.78 \times 10^{-6}/\rho^{13} - 6.21 \times 10^{-13}/\rho^4 \text{ ergs.}$$

The figure shows the variation of $V(\rho)$ with ρ for the three laws. It is surprising how closely the curves follow each other. The agreement is not good at large internuclear distances and it is in this region that the quantum theoretical calculations are most accurate, and are therefore to be preferred. At smaller internuclear separations, however, the reverse situation may very well apply, since the influence of the higher poles increases very rapidly as ρ decreases and these have been taken into account only approximately. Moreover, in this region the valence term may not be accurate although it is probably fairly near the truth.

There have been several attempts to estimate the second virial coefficient of He. Although it is not difficult to make approximate calculations which agree well with the experimental values, an exact theoretical treatment is lacking. The method used up to the present is a semi-classical one in which classical statistics are assumed for the translational energies of the atoms but for the internal motions quantum statistics are employed. Calculations along these lines have given good agreement with experiment as far as the second virial coefficient is concerned. One can use a similar procedure to obtain the coefficient of viscosity. For this calculation the weak attractive field of He is not of much importance. Since the quantum theoretical law of force agrees well with that of Lennard-Jones at those values of ρ where $V(\rho)$ is about equal to the mean thermal energy of the molecules, it must also give a good value for the viscosity. The detailed calculations are rather laborious and it hardly seems worth while to make them until the law of interaction is known with greater accuracy.

W. G. PENNEY

Department of Physics,
University of Wisconsin,
November 1, 1932.

¹ J. C. Slater, *Phys. Rev.* **32**, 349 (1928); J. C. Slater and J. G. Kirkwood *ibid.* **37**, 682 (1931); H. Margenau, *ibid.* **38**, 747 (1931).

² J. E. Jones, *Proc. Roy. Soc.* **107**, 157 (1925).

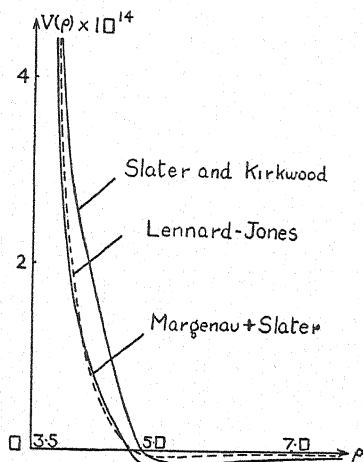


Fig. 1.

improved by Margenau,¹ who introduced the correction for the dipole-quadrupole and quadrupole-quadrupole interactions. The modification engendered by these other terms is considerable. The force of repulsion, or valence force, is known from the work of Slater.¹ Combining the results of Margenau and Slater, the mutual potential energy of two He atoms, distance ρ apart, is

$$V(\rho) = [7.7e^{-2.43\rho} - 0.68(1 + 7.9/\rho^2 + 30/\rho^4)/\rho^6] \times 10^{-10} \text{ ergs,}$$

ρ being measured in terms of a_0 , the radius of the first Bohr orbit for H. If the terms in $1/\rho^8$ and $1/\rho^{10}$ are omitted, the energy of inter-

PROCEEDINGS OF
THE NEW ENGLAND SECTION
OF THE AMERICAN PHYSICAL SOCIETY

ORGANIZATION OF THE SECTION

The New England Section has been organized with the approval of the Council of the American Physical Society, and is under the general supervision of this Council.

Only members or fellows of the American Physical Society are eligible for membership in the section.

The officers of the section are a chairman, vice-chairman, secretary-treasurer, and a program committee, consisting of these three officers and two other elected members.

There will be two meetings of the section a year, one about the middle of October and the other about the end of January. The programs of these meetings will include, not only the usual ten-minute papers, but also invited papers on subjects of interest to physicists in general.

MINUTES OF THE AMHERST MEETING, OCTOBER 8, 1932

The first regular meeting of the New England Section was held in Amherst, Massachusetts, on Saturday, October 8, 1932. The presiding officers were Professor E. C. Kemble, chairman of the section, and Professor Louise S. McDowell. All sessions were held in the Fayerweather Physics Laboratory, Amherst College.

About 80 were present at the morning sessions and about 120 at the afternoon sessions.

The morning session was devoted in part to the reading of contributed papers, and in part to a business meeting.

At the business meeting the organization committee, consisting of Professors E. C. Kemble, S. R. Williams, Louise S. McDowell, G. F. Hull, and P. M. Morse, made its report, outlining the steps which had been taken in organizing the section.

The constitution of the section, which had been approved by the Council of the American Physical Society at its meeting in Washington, April 28, 1932, was adopted by the section.

The secretary of the organization committee reported that 101 members had joined and paid their yearly dues.

The election of officers for the section for the calendar year 1933, then took place. The officers elected were:

Professor E. C. Kemble, Chairman
Professor S. R. Williams, Vice-Chairman
Professor P. M. Morse, Secretary-Treasurer
Professors Louise S. McDowell and G. F. Hull,
members of the Program Committee

Professor W. G. Cady of Wesleyan University kindly invited the section to meet at Middletown, Conn., for its October 1933 meeting. This invitation was later accepted by the program committee.

A vote of thanks was extended to the members of the Physics Department at Amherst for their efforts, which had made the meeting such a success.

The session had its luncheon at the Morrow Cafeteria, Amherst College.

The afternoon session was devoted to invited papers. The first two constituted a colloquium on "Magnetism" and were on *Mechanical Hardness as Measured by Magnetostrictive Effects* by Professor S. R. Williams of Amherst College, and on *Recent Developments in the Theory of Magnetism* by Professor J. C. Slater of Massachusetts Institute of Technology. The third invited paper was a lecture and demonstration of *High-Frequency Sound Effects* given by Professor G. W. Pierce of Harvard University.

The program of the section consisted of 12 papers, the abstracts for which are given below. An author index will be found at the end.

PHILIP M. MORSE, *Secretary-Treasurer*

ABSTRACTS

1. **Anomalous rotational temperature of mercury hydride.** FOSTER F. RIEKE, *Harvard University*.—Gaviola and Wood obtained the spectrum of mercury hydride by sensitized fluorescence, using the mercury resonance line for excitation. The observations were made that with the mixture hydrogen, nitrogen, and mercury the intensity distribution showed predominance of high rotational quanta, while with water vapor plus mercury, low quanta. An attempt has been made to explain the former observation by a sequence of elementary processes involving the persistence of abnormal rotation through thousands of collisions. The author has obtained the rotational temperature of a band emitted by the mercury plus water mixture; even this has proved to be anomalously high (a few thousand degrees) and cannot be explained by the hypothesis mentioned. It seems to be more compatible with a theory of the transfer of rotational energy in which estimates of probabilities of transfer are based on the laws of impact.

2. **Temperature variation of viscosity and of the piezoelectric constant of quartz.** K. S. VAN DYKE, *Wesleyan University*.—From measurements of the decrement of the longitudinal vibrations of a quartz resonator at various external circuit loads the decrement under short circuit is found by extrapolation. This decrement measures the inherent viscous losses in the quartz itself when the damping effects of suspension, silver-plated electrodes and surrounding gas have been eliminated. Decrement determinations at different temperatures (same resonator, 67.5 k.c. mode, and method as in *Phys. Rev.* 40, 1026 (1932)) show the value of viscosity of quartz (defined as the ratio of logarithmic decrement to Young's modulus) to increase from 0.7×10^{-17} at -80°C to 2.4×10^{-17} at 40°C , the increase being about twice as rapid at the upper temperature as at the lower. At room temperatures the variation is of the order of one percent per degree centigrade. The piezoelectric constant of quartz (11) also obtained from these decrement determinations decreases from 5.57×10^4 absolute e.s.u. at -80°C to 5.27×10^4 at 40°C . This variation is also more rapid for the higher temperatures, being ten times as large at 40° as at -80° . At room temperature the variation is about one-tenth of one percent per degree centigrade.

3. **The effect of pressure on the electrical resistance of fifteen metals down to liquid oxygen temperatures.** P. W. BRIDGMAN, *Harvard University*.—Measurements made 15 years ago on the pressure coefficient of a number of metals between 0° and 100°C have been extended to -78° (solid CO_2) and -183° (liquid oxygen). In order to avoid freezing of the transmitting medium pressure must be transmitted with gaseous helium. This introduces a number of difficulties of technique, which have been so far overcome that routine measurements have

been made to 7000 kg/cm² at -183° . Over this range no very striking results have been found. Resistance decreases nearly linearly with pressure, perhaps even more nearly linearly than at room temperatures. There is in almost all cases a numerical increase in the coefficient at low temperatures, but the increase is usually not large, the largest effect being a doubling of the coefficient of Al, and there is no simple correlation with other properties of the metal.

4. Momentum transfer to cathode surfaces by impacting positive ions in a helium arc. K. T. COMPTON AND E. S. LAMAR, *Massachusetts Institute of Technology*.—The momentum transfer to an auxiliary cathode has been studied in the positive column of a low voltage helium arc. The auxiliary cathode was a flat molybdenum plate insulated on one side by glass and suspended in such a way that its deflection gave a measure of the pressure against it. The measured pressure on the cathode is believed to be due to two phenomena. The first is the recoil of those ions which retain some of their kinetic energy after neutralization. The second is a radiometer effect due to the heating of the cathode by positive ion bombardment. On the basis of these assumptions it was possible to calculate from the experimental data an accommodation coefficient for helium positive ions and the fraction of the measured current carried by electrons. Although the accuracy of the experiment is not high, the values of the accommodation coefficient, ranging from 0.37 to 0.53, are in qualitative agreement with those obtained by Compton and Van Voorhees. The fraction of the current carried by electrons, ranging from 0.54 to 0.62, agrees fairly well with the results of Harrington.

5. Electron diffraction by a silver film on a gold crystal. H. E. FARNSWORTH, *Brown University*.—A thin film of silver (not visible) was deposited on the (100) face of a gold crystal by evaporation in a vacuum. The silver formed in a lattice structure having the same orientation as that of the underlying gold crystal. The diffraction beams obtained for the thin silver film have the same characteristic fine structure, which varies with the angle of incidence, as that previously found for a more massive silver crystal, (Phys. Rev. **40**, 684 (1932)), except that the relative intensities of the components of one of the lowest voltage beams for the silver film are reversed. As previously observed (Phys. Rev. **40**, 1049 (1932)) the fine structure of the diffraction beams for a gold crystal differs from that of the corresponding beams of a silver crystal. Deviations from the plane grating formula for normal incidence are the same for the beams from the thin film as for those from a more massive silver crystal. These results substantiate the previous evidence (Phys. Rev. **40**, 684 and 1049 (1932)) that the fine structure characteristics are at least partly determined by the nature of the atoms composing the crystal rather than by the lattice itself.

6. The continuous electron affinity spectrum of hydrogen. C. K. JEN, *Harvard University*.—A wave-mechanical calculation has been made of the intensity distribution in the continuous emission spectrum due to the capture of electrons by normal hydrogen atoms and in the corresponding absorption spectrum due to the dissociation of negative hydrogen ions. Approximate wave functions for the continuous range of upper energy levels have been combined with the discrete state wave function for H^{-} given by Hylleraas to give the matrix elements for the desired transitions. The computed results for the emission (assuming uniform distribution of electrons against velocity) or absorption spectrum show that the emitted or absorbed intensity starts with a small value from the edge, determined by the theoretical value of electron affinity, and steadily increases toward the short wave-length side. Due to the low intensity at the edge, the experimental determination of the electron affinity by means of its spectrum becomes quite difficult. If this simple picture holds approximately for the more complicated halogen atoms, the diffusion of the continuous spectrum limit may partially account for the repeated experimental failure to find the electron affinity spectrum of these elements.

7. The effect of exchange on elastic cross sections. PHILIP M. MORSE AND W. P. ALLIS, *Massachusetts Institute of Technology*.—An exact solution has been obtained for the separable type of wave functions for elastic scattering from hydrogen- and helium-like atoms, by using a simplified form of potential field and of atomic electron wave function. Exchange has a considerable effect on the angle distribution of the antisymmetric type function (which is re-

sponsible for all of the cross section for helium-like and for three quarters of that for hydrogen-like atoms). The alteration is greatest for light atoms and for low velocities. The effect on the symmetric wave function is small. The usual approximation methods are shown to be unsatisfactory for light atoms and low velocities.

8. **Differential analyzer solution for the wave functions of the *K*-shell.** S. CALDWELL, *Massachusetts Institute of Technology*.—With the differential analyzer (see Bush, *Jour. Franklin Inst.* 212, 447–488 (1931)), for the solution of the wave equation of helium-like atoms it is possible to consolidate the steps of the Hartree method and to secure self-consistent solutions directly from the machine. Procedures have been established to obtain solutions which also satisfy the requirements of finiteness and normality. The work with the machine has been completed for atoms of atomic numbers $Z=2$ to $Z=8$, inclusive, and also for $Z=32$. Energy values are obtained, and analytic approximations to the wave functions can be gotten.

9. **On the possibility of deriving work from statistical fluctuations.** V. GUILLEMIN, JR., *Massachusetts Institute of Technology*.—It has been repeatedly suggested that the statistical fluctuations occurring within a system in equilibrium might be used, through the intelligent intervention of an animate being, to obtain useful work from the heat energy of a reservoir at the lowest available temperature. Maxwell put forth such a suggestion quite seriously (the Maxwell demon). His justification is of a very general nature, namely, that all classical laws are independent of the absolute scale of the system. Therefore, a system which obviously works on a large scale will also work on the scale of molecular dimensions. Perhaps the most profound difference between classical and modern (relativity, quantum) laws is that the latter are *not* independent of absolute scale. Making no assumption about the process of perception other than that it requires the existence at the demon, of a vector quantity which is a function of the coordinates of the molecule to be perceived, it can be shown that the energy which must necessarily be dissipated into heat every time the trapdoor is opened or closed is much greater than the energy of the captured molecule. Similar results are obtained for the case of Brownian particles and for fluctuations in general.

10. **Mechanical hardness as measured by magnetostrictive effects.** S. R. WILLIAMS, *Amherst College*.

11. **Recent developments in the theory of magnetism.** J. C. SLATER, *Massachusetts Institute of Technology*.

12. **Some applications of high-frequency sound effects.** G. W. PIERCE, *Harvard University*.

AUTHOR INDEX TO ABSTRACTS OF THE AMHERST MEETING OF THE NEW ENGLAND SECTION

Allis, W. P.—see Morse

Bridgman, P. W.—No. 3

Caldwell, S.—No. 8

Compton, K. T. and E. S. Lamar—No. 4

Farnsworth, H. E.—No. 5

Guillemin, V., Jr.—No. 9

Jen, C. K.—No. 6

Lamar, E. S.—see Compton

Morse, Philip M. and W. P. Allis—No. 7

Pierce, G. W.—No. 12

Rieke, Foster. F.—No. 1

Slater, J. C.—No. 11

Van Dyke, K. S.—No. 2

Williams, S. R.—No. 2

THE PHYSICAL REVIEW

The Relative Intensities of the $L\alpha_1$, β_1 , β_2 , and γ_1 Lines in Tantalum, Tungsten, Iridium, and Platinum

By VICTOR J. ANDREW

Ryerson Physical Laboratory, University of Chicago

(Received October 10, 1932)

The relative intensities of the $L\alpha_1$, β_1 , β_2 , and γ_1 lines in tantalum, tungsten, iridium, and platinum were measured and corrections were applied for the partial absorption of the beam along its path and within the ionization chamber, for the partial reflection by the crystal, for the effects of voltage and absorption within the target, and for interference from adjacent lines. To verify the method of making the target correction, an experiment was performed which consisted of measuring the relative intensities of $L\alpha_1$, β_1 , and γ_1 of platinum at different angles from the face of the target. The following relative intensities were measured at 30 k.v. without correction for reflection by the crystal or absorption within the target:

	α_1	β_1	β_2	γ_1
Tantalum	100	49.5	18.8	9.0
Tungsten	100	49.4	20.2	10.0
Iridium	100	48.0	21.2	10.2
Platinum	100	46.1	21.0	9.7

INTRODUCTION

THE relative intensities of x-ray lines have been investigated with considerable precision where the lines are only slightly separated in wavelength. Where a considerable separation is present, all the corrections to observed intensities become more important. Two of them offer some difficulty. The correction for the fraction of the beam reflected by the crystal can be made only when the dependence of the coefficient of reflection on wavelength has been determined by using the same crystal in a double crystal spectrometer. The correction for the absorption within the target requires a knowledge of the depth distribution of emission of x-rays and is involved with the correction for the tube voltage.

The intensities of the lines in the L series of tantalum, tungsten, and platinum have been measured by Jönsson,¹ Hicks,² and Allison and Andrew.³

Measurements of the relative intensities were made on the elements tantalum (73), tungsten (74), iridium (77), and platinum (78). The lines α_1 , β_1 ,

¹ Axel Jönsson, *Zeits. f. Physik* **36**, 426 (1926).

² Victor Hicks, *Phys. Rev.* **36**, 1273 (1930); **38**, 572 (1931).

³ Allison and Andrew, *Phys. Rev.* **38**, 441 (1931).

β_2 , and γ_1 were chosen because they are widely separated and distributed over a rather broad wave-length range. Particular attention was given to the two more difficult corrections referred to above.

APPARATUS AND PROCEDURE

The design and adjustment of the apparatus which was used for these experiments has been described by Allison and Andrew.³ It is a single crystal spectrometer with an ionization chamber. The slits were 25.4 cm apart and 0.013 cm wide. The ionization chamber was filled with methyl bromide to a pressure of 76 cm. The x-ray tube was of a type described by Allison.⁴ The target was mounted at 45° to the electron beam, and the x-rays were observed at 45° to its face. The various targets were polished in the vicinity of the focal spot so that they gave a clear mirror-like reflection, and only the slightest scratches were visible to the unaided eye, in order that surface irregularities would produce negligible uncertainty in the thickness of the layer in which the rays were absorbed before leaving the target. The electron current was kept low enough (usually one milliampere) so that the polish was not damaged. The targets were repolished whenever they became seriously coated with tungsten from the filament. Such coating occurred only when the tube was operated without a sufficiently high vacuum.⁵ No readings were used in which the intensity of tungsten $L\alpha_1$ was as great as 1 (relative to 100 for the $L\alpha_1$ line of the element being studied), and in most cases it was not measurable (less than 0.3). When it reached 7, the change in intensity of the other lines being studied was approximately 2.

The electrometer sensitivity was about 3 meters per volt. Adjustments were made so that it was found experimentally that the rate of deflection was proportional to the current (with a possible constant correction), and that the rate of deflection for constant current was the same on all parts of the

TABLE I. *Tantalum* (73).

Trial	Line	i	i_b	$i-i_b$	I_λ	Weight
1	α_1	22.46	0.64	21.82		1
	β_1	16.96	0.64	16.32	74.3	
	β_2	7.70	0.64	7.06	32.1	
	γ_1	4.26	0.64	3.62	16.5	
2	α_1	21.72	0.69	21.03		2
	β_1	14.92	0.69	14.23	67.8	
	β_2	6.45	0.69	5.76	27.6	
	γ_1	3.57	0.69	2.88	13.9	
3	α_1	17.16	0.65	16.51		3
	β_1	12.20	0.65	11.55	69.7	
	β_2	5.76	0.65	5.11	30.9	
	γ_1	3.41	0.65	2.76	16.7	
Weighted averages:						
$I(\beta_1)=69.8$		$I(\beta_2)=30.0$		$I(\gamma_1)=15.7$		

⁴ S. K. Allison, Phys. Rev. 30, 245 (1927) (Fig. 1).

⁵ S. K. Allison, Phys. Rev. 34, 7 (1929).

TABLE II. Tungsten (74).

Trial	Line	i	i_b	$i-i_b$	I_λ	Weight
1	α_1	17.54	0.80	16.74		2
	β_1	11.90	0.80	11.10	68.7	
	β_2	6.80	0.80	6.00	34.4	
	γ_1	4.22	0.80	3.42	19.5	
2	α_1	22.73	0.84	21.89		3
	β_1	15.62	0.84	14.78	67.5	
	β_2	7.30	0.84	6.46	29.5	
	γ_1	4.10	0.84	3.26	14.9	
3	α_1	24.10	0.83	23.27		2
	β_1	16.67	0.83	15.84	68.0	
	β_2	7.87	0.83	7.04	30.2	
	γ_1	4.38	0.83	3.55	15.2	
4	α_1	22.85	0.70	22.15		3
	β_1	15.74	0.70	15.04	67.9	
	β_2	7.49	0.70	6.79	30.7	
	γ_1	4.28	0.70	3.58	16.2	
Weighted averages:						
$I(\beta_1)=67.9$		$I(\beta_2)=31.0$		$I(\gamma_1)=16.3$		

TABLE III. Iridium (77).

Trial	Line	i	i_b	$i-i_b$	I_λ	Weight
1	α_1	25.15	0.75	24.40		2
	β_1	15.73	0.75	14.98	60.7	
	β_2	8.00	0.75	7.25	29.7	
	γ_1	4.18	0.75	3.43	14.1	
2	α_1	25.15	0.76	24.39		3
	β_1	15.38	0.76	14.62	59.9	
	β_2	7.90	0.76	7.14	29.3	
	γ_1	4.07	0.76	3.31	13.6	
3	α_1	23.40	0.69	22.71		2
	β_1	14.56	0.69	13.87	61.2	
	β_2	7.22	0.69	6.53	28.7	
	γ_1	3.81	0.69	3.12	13.7	
Weighted averages:						
		$I(\beta_2)=29.3$		$I(\gamma_1)=13.7$		

scale. The latter condition may be quite different from that of having the deflection proportional to the voltage, and must not be confused with it.⁶

Tables I, II, III, and IV give the experimental data obtained on tantalum, tungsten, iridium, and platinum, respectively. i is the uncorrected electrometer current in mm per second observed at the peak of the line. The tabulated values are not individual readings, but each one is a peak measured on a curve drawn through a group of points (usually five) at intervals of $\frac{1}{4}$ minute of arc, in the vicinity of the peak. i_b , the base line intensity, was observed at angles sufficiently distant from all lines due to the target material or tungsten contamination. The base did not vary perceptibly over the range of the lines

⁶ This is due to the charge induced on the quadrant by the moving needle. See J. B. Hoag, *Electron Physics*, p. 142.

involved, and so the same value was used for all of the lines in one trial. Care was taken to measure a value as accurately as possible near the γ_1 line, since this line was the weakest, and therefore required the most accurate base line correction.

TABLE IV. *Platinum (78).*

TABLE IV. <i>Fulcrum</i> (78).						
Trial	Line	i	i_b	$i-i_b$	I_λ	Weight
1	α_1	20.00	0.68	19.32		2
	β_1	11.80	0.68	11.12	57.5	
	β_2	6.80	0.68	6.12	31.7	
	γ_1	3.08	0.68	2.40	12.4	
2	α_1	18.77	0.64	18.13		2
	β_1	10.73	0.64	11.09	55.7	
	β_2	6.22	0.64	5.58	30.8	
	γ_1	2.91	0.64	2.27	12.5	
3	α_1	17.40	0.65	16.75		2
	β_1	10.13	0.65	9.48	56.6	
	β_2	5.83	0.65	5.18	30.9	
	γ_1	2.73	0.65	7.08	12.4	
Weighted averages:						
$I(\beta_1)=56.6$		$I(\beta_2)=31.1$		$I(\gamma_1)=12.4$		

$$I_\lambda = 100 \frac{(i - i_b)_\lambda}{(i - i_b)_\alpha}$$

is the intensity of the line λ (representing β_1 , β_2 , or γ_1) with the base correction, but without the corrections for absorption, etc., relative to the α_1 line as 100. The weights of the different trials were determined by the stability of the x-ray tube during the measurements.

CORRECTIONS TO OBSERVED INTENSITIES

In Table V are shown the observed intensities, the necessary corrections, and the resultant transition probabilities. The corrections for partial absorption in the mica x-ray tube window, in the air, and in the aluminum ionization chamber window are denoted respectively by $F_m = \exp [(\mu_{m\lambda} - \mu_{m\alpha})d_m]$, $F_a = \exp [(\mu_{a\lambda} - \mu_{a\alpha})d_a]$ and $F_w = \exp [(\mu_{w\lambda} - \mu_{w\alpha})d_w]$. μ denotes a linear absorption coefficient and d a thickness in cm. The subscripts m , a , and w refer respectively to mica, air, and aluminum, and the subscripts λ and α , respectively, to the wave-length of the line in question and of the $L\alpha_1$ line.

$$F_i = (1 - e^{-\mu_{i\alpha} d_i}) / (1 - e^{-\mu_{i\lambda} d_i})$$

is the correction for the fraction of each wave-length absorbed in the ionization chamber. The subscript i refers to the methyl bromide in the chamber. In the work of Allison and Andrew³ it was shown that the relative intensities of certain lines were within experimental error the same when the ionization chamber was filled with air, sulphur dioxide, methyl bromide, methyl iodide, argon, or krypton, and so it is reasonable to suppose that when the proper corrections are made, the relative intensities of any lines are independent of

TABLE V. Corrections and results.

Line element at. no.	β_1			β_2			γ_1		
	Ta 73	W 74	Ir 77	Pt 78	Ta 73	W 74	Ir 77	Pt 78	Ta 73
I_A	69.8	67.9	60.5	56.6	30.0	31.0	29.3	31.1	15.7
I					1.7	1.8	1.9	4.0	
I_A'					28.3	29.2	27.4	27.1	
$\log I_A'$	1.844	1.832	1.782	1.753	1.452	1.465	1.438	1.433	1.196
$\log F_m$	-0.050	-0.046	-0.036	-0.033	-0.059	-0.053	-0.040	-0.036	-0.084
$\log F_a$	-0.070	-0.066	-0.054	-0.050	-0.082	-0.077	-0.059	-0.055	-0.120
$\log F_w$	-0.032	-0.030	-0.025	-0.023	-0.038	-0.035	-0.027	-0.025	-0.055
$\log F_t$	0.003	0.004	0.014	0.017	0.004	0.006	0.017	0.020	0.018
$\log F_e$	0.040	0.040	0.042	0.044	0.049	0.049	0.049	0.050	0.082
$\log F_{tR}$	0.110	0.110	0.136	0.141	-0.010	-0.020	-0.017	-0.018	0.133
$\log F_{tW}$	0.022	0.022	0.042	0.047	-0.018	-0.030	-0.018	-0.010	0.043
$\log P'$	1.695	1.694	1.681	1.664	1.274	1.305	1.326	1.322	0.955
$\log P_R$	1.845	1.844	1.859	1.849	1.313	1.334	1.358	1.354	1.170
$\log P_W$	1.757	1.756	1.765	1.755	1.305	1.324	1.357	1.362	1.080
P'	49.5	49.4	48.0	46.1	18.9	20.2	21.3	21.7	9.0
P_R	69.9	69.8	72.2	70.6	20.7	21.6	23.0	23.4	14.8
P_W	57.1	57.0	58.2	56.9	20.3	21.1	22.9	23.8	12.0
P^1_1	51.	47.4		45.0	20.	20.2			10.
P^2_2		50.6							8.3
P^3_3									10.5

¹ Jonsson, reference 1.² Hicks, reference 2.³ Allison and Andrew, reference 3.

the gas in the ionization chamber. The wave-lengths measured were all long enough so that no bromine K fluorescent radiation was excited, and all other fluorescent radiation was so soft that it was practically all absorbed before it reached the walls of the ionization chamber. The dimensions of the ionization chamber and the gas pressure within it were such that practically all of the β -rays came to the end of their ionizing range within it. F_c is the ratio of the coefficient of reflection of the calcite crystal for α_1 and for λ . As pointed out by Allison,⁷ the coefficient of reflection of a single crystal cannot be measured experimentally. However, the coefficient of reflection defined as the area under the rocking curve of crystal B of a double-crystal spectrometer is approximately proportional to the coefficient of reflection from a single crystal, and, since we use only ratios of the coefficient of reflection, the proportionality constant will drop out. The values of F_c are derived from graphical interpolation of data obtained by Professor Allison on a double-crystal spectrometer, when using the same crystal, which is numbered $V-B$ in his paper. F_t is the correction for the effects of the tube voltage and the absorption within the target. The derivation of this correction is discussed in the next section.

In Table VI are shown the various constants used in the calculation of the corrections. The absorption coefficients of mica, air, and methyl bromide were taken from Allison and Andrew.³ Those of aluminum were taken from Comp-

TABLE VI. Constants.

Element	Line	$\lambda(A)$	μ_m	μ_a	μ_w	μ_i	$V_0(k.v.)$
Ta	α_1	1.519	136.4	0.0109	132.6	0.266	9.87
	β_1	1.324	86.0	0.0072	88.0	0.174	11.11
	β_2	1.282	77.4	0.00655	80.0	0.160	9.87
	γ_1	1.136	52.6	0.00455	56.3	0.112	11.11
W	α_1	1.473	123.0	0.0100	121.2	0.201	10.18
	β_1	1.279	76.8	0.0065	79.4	0.158	11.52
	β_2	1.242	69.8	0.00595	72.7	0.144	10.18
	γ_1	1.096	47.0	0.0041	50.8	0.102	11.52
Ir	α_1	1.348	91.7	0.00765	93.6	0.185	11.17
	β_1	1.155	55.4	0.0048	59.2	0.116	12.80
	β_2	1.133	52.2	0.0045	55.7	0.110	11.17
	γ_1	0.989	34.0	0.0030	37.0	0.072	12.80
Pt	α_1	1.310	83.2	0.0070	85.4	0.171	11.53
	β_1	1.118	50.1	0.00435	53.8	0.108	13.24
	β_2	1.100	47.5	0.0041	51.4	0.105	11.53
	γ_1	0.956	30.6	0.0027	29.6	0.067	13.24
$d_m=0.0023$		$d_a=43.5$	$d_w=0.00165$	$d_i=28.1$	$V=30$		
μ_a and μ_i were calculated for 76 cm pressure and 20°C.							

ton.⁸ For mica, air, aluminum, and methyl bromide, curves were drawn for μ versus λ^3 , which were nearly linear, and then μ was read from the curves for the desired wave-lengths. For the four target materials, the absorption coefficients were calculated from the equation⁹

⁷ S. K. Allison, Phys. Rev. **41**, 1 (1932).

⁸ A. H. Compton, *X-Rays and Electrons*, p. 180.

⁹ Ivor Backhurst, Phil. Mag. **7**, 353 (1929).

$$\log \mu/\rho = C + m \log \lambda + 4 \log Z.$$

From the experimental measurements of μ by Allen¹⁰ for tungsten, platinum, gold, and lead, by Kellström¹¹ for silver, by Backhurst⁹ for platinum and gold, and by Uber¹² for mercury, average values of the constants were chosen as $C = -5.750$ and $m = 2.63$ for the lines α_1 , β_1 , and β_2 (above the L_{III} absorption limit), and $C = -5.356$ and $m = 2.61$ for the line γ_1 (between the L_{II} and the L_{III} absorption limits). The constant b/ρ of the Thomson-Whiddington equation does not vary rapidly with Z . The value 4.55×10^5 for all of the elements used as targets was chosen by interpolation between values obtained for various elements by Terrill.¹³ ρ appears in both the factor μ/ρ and the factor b/ρ , but it cancels out in the calculations.

In several instances the lines measured lie close to other lines. In all such cases, the amount of error in the observed intensity of the principal line was calculated, and when it exceeded 0.2 a correction was made. Table VII shows the derivation of such corrections. $\delta\lambda$ and $\delta\theta$ are the separation between the principal line and the interfering line, in angstroms and in minutes of arc,

TABLE VII. *Interfering lines.*

Element	Line	Interfering line	$\delta\lambda^{14}$	$\delta\theta$	f	I_i'	I_λ'	I_i
Ta	β_2	β_{15}	0.0016	0.92	0.6	0.1 ¹⁵	28.3	1.7
W	β_2	β_{15}	0.0016	0.92	0.6	0.1 ¹⁵	29.2	1.8
Ir	β_2	β_{15}	0.0016	0.92	0.6	0.1 ¹⁵	27.4	1.6
Ir	β_2	β_3	0.0055	3.2	0.04	0.23 ¹⁶	27.4	0.3
Pt	β_2	β_{15}	0.0016	0.92	0.6	0.1 ¹⁵	27.1	1.6
Pt	β_2	β_3	0.0019	1.1	0.44	0.20 ¹⁶	27.1	2.4

respectively. Since the peak of intensity *vs.* angle which is found experimentally is approximately identical with the peak of the principal line, and is in general considerably off the peak of the interfering line, a factor f is introduced by which the intensity of the interfering line must be multiplied to de-

¹⁰ S. J. M. Allen, *Phys. Rev.* **28**, 907 (1926).

¹¹ G. Kellström, *Zeits. f. Physik* **44**, 269 (1927).

¹² F. M. Uber, *Phys. Rev.* **38**, 217 (1931).

¹³ H. M. Terrill, *Phys. Rev.* **22**, 107 (1923).

¹⁴ From S. K. Allison, *Phys. Rev.* **34**, 176 (1929) and Manne Siegbahn, *Spektroskopie der Röntgenstrahlen*, Ed. II, p. 208.

¹⁵ S. K. Allison, *Phys. Rev.* **34**, 176 (1929).

¹⁶ The following sources of data were used for the relative intensities of β_2 and β_3 . All of the data were taken at, or corrected to, 30 k.v. Since the lines are very close together, all corrections other than for the tube voltage disappear. A curve for I_i' *vs.* Z was drawn from these data, and the values used above were read from the curve.

I_i'	Element	Source
0.34	Ta	Victor Hicks, <i>Phys. Rev.</i> 38 , 572 (1931).
0.33	W	Allison and Armstrong, <i>Phys. Rev.</i> 26 , 714 (1925).
0.26	Os	S. K. Allison, <i>Phys. Rev.</i> 34 , 7 (1929).
0.35	W	Axel Jönsson, <i>Zeits. f. Physik</i> 36 , 426 (1926).
0.23	Ir	Fig. 2 of this paper.

termine the amount of interference present at the peak of the principal line. f varies from unity to zero with increasing $\delta\theta$. It is assumed that the apparent shape of all lines is the same (and is due to the width of the slits). Fig. 1 shows an experimental curve of the iridium β_2 and β_3 lines. The values of f were measured on the left side of the curve. I_i' is the ratio of the intensity of the interfering line to the intensity I_λ' of the principal line. The final correction for interference $I_i = fI_i'I_\lambda'$ is subtracted from the intensity I_λ in Table V to obtain the intensity I_λ' of the principal line alone.

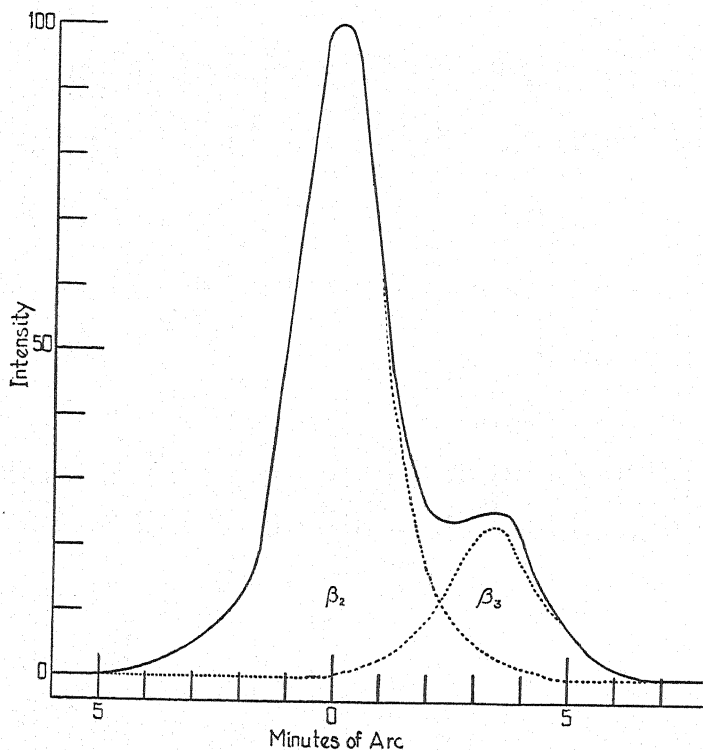


Fig. 1. Separation of the $L\beta_2$ and β_3 lines in iridium.

THEORY OF THE CORRECTION WITHIN THE TARGET

In most intensity measurements heretofore the effect of absorption within the target has been neglected. Kulenkampff¹⁷ and Wisshak¹⁸ have used such a correction, but it was based on the assumption that electrons falling on the target maintain their initial velocity until they are suddenly stopped, rather than losing velocity according to the now accepted Thomson-Whiddington law, and that the number of electrons decreases exponentially with depth within the target. It has been customary to express intensities extrapolated to infinite voltage. The expression for transition probability developed here-

¹⁷ H. Kulenkampff, Ann. d. Physik 69, 548 (1922).

¹⁸ F. Wisshak, Ann. d. Physik 5, 507 (1930).

after does not agree with this convention. It follows an expression developed by Jönsson.¹⁹ An experiment was then performed to test certain aspects of the calculations.

The intensity dJ_λ of a given spectrum line λ , due to the increment of depth dx within the target is

$$dJ_\lambda = c_\lambda F(x) dx e^{-\mu_\lambda x / \sin \theta}. \quad (1)$$

c_λ is a constant which includes the geometry of the spectrometer, the power into the x-ray tube, etc., and of particular interest, the probability of a transition which will produce the line λ after an electron has been removed from the proper inner shell. $F(x)$ is the ionization function or the probability of ejection of an electron from a particular shell by an incident electron with the velocity which it retains after penetrating the target to the depth x . $e^{-\mu_\lambda x / \sin \theta}$ is the correction for the absorption of the x-rays between the depth x of their emission and the surface of the target, when they are measured at an angle θ with the surface. μ_λ is the absorption coefficient of the target material.

The total intensity J_λ observed for the line is the integral of Eq. (1) from the surface of the target to the depth x_0 where the velocity of the impinging electrons has been reduced so much that they are no longer able to remove electrons from the proper inner shells.

$$J_\lambda = c_\lambda \int_0^{x_0} F(x) e^{-\mu_\lambda x / \sin \theta} dx. \quad (2)$$

It is more convenient to use as the variable V_x , the velocity of electrons in electron kilovolts at the depth x . The relation between V_x and x is taken from the Thomson-Whiddington equation $V_x^2 = V^2 - bx$ or $x = (V^2 - V_x^2)/b$. Eq. (2) now becomes

$$J_\lambda = \frac{2c_\lambda}{b} e^{-\mu_\lambda V^2 / b \sin \theta} \int_{V_0}^V F(x) e^{\mu_\lambda V_x^2 / b \sin \theta} V_x dV_x. \quad (3)$$

The integration is between the limits V , which is the velocity of the impinging electrons at the surface of the target, or the voltage across the x-ray tube, and V_0 , which is the critical excitation voltage for the line λ .

Before Eq. (3) can be integrated, an expression for $F(x)$ must be found. Rosseland²⁰ has found from theoretical considerations

$$F_R(x) = k_\lambda (1/V_x) (1/V_0 - 1/V_x). \quad (4_R)$$

Webster, Clark, Yeatman, and Hansen²¹ have an empirical

$$F_W(x) = k_\lambda (1 - V_0/V_x) / (3 + V_x/V_0). \quad (4_W)$$

which they find fits experimental curves of intensity *vs.* tube voltage with a thin target better than Rosseland's expression does. k_λ in Eq. (4) represents

¹⁹ Axel Jönsson, *Zeits. f. Physik* **43**, 845 (1927).

²⁰ S. Rosseland, *Phil. Mag.* **45**, 65 (1923).

²¹ Webster, Clark, Yeatman, and Hansen, *Proc. Nat. Acad. Sci.* **14**, 679 (1928).

the relative probability of a particular inner shell being ionized, and the remainder of the equation gives the variation of this probability with the velocity of the impinging electrons. The subscripts R and W are used to denote the results dependent on each of the two preceding expressions.

Inserting Eq. (4) in Eq. (3), we obtain

$$J_{\lambda R} = \frac{2c_{\lambda}k_{\lambda}}{b} e^{-\mu_{\lambda}V^2/b\sin\theta} A_{\lambda R}$$

$$J_{\lambda W} = \frac{2c_{\lambda}k_{\lambda}}{b} V_0 e^{-\mu_{\lambda}V^2/b\sin\theta} A_{\lambda W}$$

where

$$A_{\lambda R} = \int_{V_0}^V \left(\frac{1}{V_0} - \frac{1}{V_x} \right) e^{\mu_{\lambda}V_x^2/b\sin\theta} dV_x \quad (5_R)$$

$$A_{\lambda W} = \int_{V_0}^V \frac{V - V_0 + V_x}{3V_0 + V_x} e^{\mu_{\lambda}V_x^2/b\sin\theta} dV_x. \quad (5_W)$$

Taking the ratio J_{λ}/J_{α} which was defined as I_{λ}' in the preceding experimental data,

$$I'_{\lambda R} = P_{\lambda} e^{(\mu_{\alpha} - \mu_{\lambda})V^2/b\sin\theta} (A_{\lambda R}/A_{\alpha R}) \quad (6_R)$$

$$I'_{\lambda W} = P_{\lambda} (V_{0\lambda}/V_{0\alpha}) e^{(\mu_{\alpha} - \mu_{\lambda})V^2/b\sin\theta} (A_{\lambda W}/A_{\alpha W}) \quad (6_W)$$

where

$$P_{\lambda} = c_{\lambda}k_{\lambda}/c_{\alpha}k_{\alpha}.$$

Geometric, etc., factors in c_{λ} and c_{α} cancel, so there remains in P_{λ} only the ratio of probabilities of transitions which will produce particular lines when electrons have been removed from the proper inner shells, times the probabilities of these particular electrons being removed. The purpose of the preceding intensity measurements and the subsequent calculations was to evaluate P_{λ} , called the transition probability.

For numerical evaluation it is more convenient to have Eq. (6) in logarithmic form.

$$\log I'_{\lambda R} = \log P_{\lambda} + 0.4343(\mu_{\alpha} - \mu_{\lambda})V^2/b\sin\theta + \log A_{\lambda R} + \log A_{\alpha R}$$

$$\log I'_{\lambda W} = \log P_{\lambda} + \log V_{0\lambda} - \log V_{0\alpha} + 0.4343(\mu_{\alpha} - \mu_{\lambda})V^2/b\sin\theta + \log A_{\lambda W} - \log A_{\alpha W}.$$

The factor 0.4343 changes from a logarithm to the base e to a logarithm to the base 10. The correction factor F_t is the expression which must be multiplied by, or in the logarithmic form, added to, I_{λ}' in order to obtain P_{λ} .

$$\log F_{tR} = 0.4343(\mu_{\lambda} - \mu_{\alpha})V^2/b\sin\theta + \log A_{\alpha R} - \log A_{\lambda R} \quad (7_R)$$

$$\log F_{tW} = \log V_{0\alpha} - \log V_{0\lambda} + 0.4343(\mu_{\lambda} - \mu_{\alpha})V^2/b\sin\theta + \log A_{\alpha W} - \log A_{\lambda W}. \quad (7_W)$$

The definite integrals in Eq. (5) are not readily obtained. It is sometimes more convenient to divide $\log F_t$ into two parts, such that

$$\log F_t = \log F_v + \log F_u. \quad (8)$$

$\log F_v$ is defined as the value of $\log F_t$ when $1/\sin \theta = 0$ (an imaginary value of θ). $\log F_u$ is then defined by Eq. (8). The advantage of this separation is that $\log F_v$ can be evaluated by integration, and $\log F_u$ is so small that an approximate estimate of its magnitude is sufficient. By calculation, F_u was found to vary not more than 0.003 per unit of atomic number, for the elements from tantalum to platinum, with $V=30$ and $1/\sin \theta = 1$.

Setting $1/\sin \theta = 0$ in Eq. (5) and integrating, we get

$$A_{\lambda R0} = V/V_0 - (1/0.4343)(\log V - \log V_0) - 1 \quad (9_R)$$

$$A_{\lambda W0} = V - V_0 - (4V_0/0.4343) \log (V/4V_0 + \frac{3}{4}). \quad (9_W)$$

Using Eqs. (7) and (9), we find that

$$\begin{aligned} \log F_{vR} = \log \left\{ \frac{V}{V_{0\alpha}} - \frac{1}{0.4343}(\log V - \log V_{0\alpha}) - 1 \right\} \\ - \log \left\{ \frac{V}{V_{0\lambda}} - \frac{1}{0.4343}(\log V - \log V_{0\lambda}) - 1 \right\} \end{aligned} \quad (10_R)$$

$$\begin{aligned} \log F_{vW} = \log V_{0\alpha} - \log V_{0\lambda} \\ + \log \left\{ V - V_{0\alpha} - \frac{4V_0}{0.4343} \log (V/4V_{0\alpha} + \frac{3}{4}) \right\} \\ - \log \left\{ V - V_{0\lambda} - \frac{4V_{0\lambda}}{0.4343} \log (V/4V_{0\lambda} + \frac{3}{4}) \right\}. \end{aligned} \quad (10_W)$$

At least qualitatively we may call F_v the correction for tube voltage (replacing the correction to infinite voltage which has been used heretofore). Then F_u may be called the correction for absorption within the target (which has usually been neglected heretofore). As $\log F_u$ approaches zero the application of the foregoing names to F_v and F_u becomes more nearly correct. When $\log F_u$ becomes numerically large, due to considerable absorption within the target, the effects of tube voltage and of absorption within the target become interrelated due to the greater absorption of x-rays from greater depth, and thus the fraction of the beam produced by electrons of one velocity is not the same as the fraction which escapes from the target.

EXPERIMENTAL VERIFICATION OF THE CORRECTION WITHIN THE TARGET

In order to test the validity of the preceding theory, experimental measurements pertaining to the correction within the target were made with a platinum target and are shown in comparison with the theoretical calculations in Fig. 2. The curves represent the theoretical values of $\log F_u$ and the points show experimental values. The theoretical values were obtained by

evaluating Eq. (7). The integration was accomplished graphically, by drawing the curve of the function and measuring the area below it. $1/\sin \theta$ is used instead of θ as the abscissa since the thickness through which the x-rays from a given point are absorbed before leaving the target is proportional to $1/\sin \theta$, and the curves with this abscissa are more nearly linear. Table VIII gives the data for the theoretical curves.

TABLE VIII. Calculated values of F_u for platinum at different angles.

$1/\sin \theta$	$\log F_{uR\beta_1}$	$\log F_{uW\beta_1}$	$\log F_{uR\gamma_1}$	$\log F_{uW\gamma_1}$
1	-0.020	-0.013	-0.004	0
4	-0.071	-0.056	-0.006	0
8	-0.120	-0.102	-0.010	0
16	-0.183	-0.161	-0.008	-0.025
32	-0.254	-0.225	-0.026	-0.018

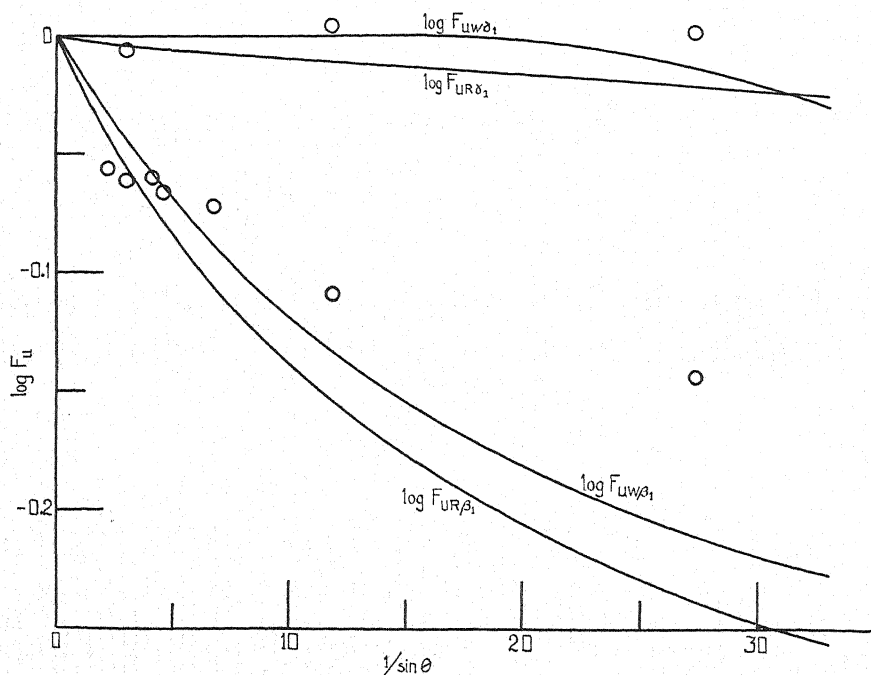


Fig. 2. Calculated curves and experimental points for the logarithm of the reciprocal of the relative intensity as observed at different angles from the surface of a polished platinum target.

The apparatus used for the experimental measurements was the same as described previously for relative intensity measurements, with the exception of the x-ray tube and its mounting. The electron beam was perpendicular to the face of the target. The tube was mounted so that it could be rotated about a vertical axis through its focal spot, and the window of the tube was made large enough to permit the beam to be observed at angles from 0 to 30° with the surface of the target.

TABLE IX. Experimental data for $I(\beta_1)$.

	Trial	$I(\beta_1)$	$I(W\alpha_1)$
$\theta = 28^\circ 08'$ $1/\sin \theta = 2.19$ $I'(\beta_1) = 37.6$ $\log I'(\beta_1) = 1.575$	1	37.0	10
	2	36.8	10
	3	38.2	15
	4	36.0	40
	5	36.0	39
	6	37.0	13
	7	37.0	15
	8	37.5	3
$\theta = 19^\circ 22'$ $1/\sin \theta = 3.02$ $I'(\beta_1) = 38.0$ $\log I'(\beta_1) = 1.580$	1	37.0	3
	2	38.9	3
	3	38.0	3
$\theta = 14^\circ 13'$ $1/\sin \theta = 4.07$ $I'(\beta_1) = 37.9$ $\log I'(\beta_1) = 1.579$	1	37.9	3
	2	37.9	3
$\theta = 12^\circ 40'$ $1/\sin \theta = 4.56$ $I'(\beta_1) = 38.5$ $\log I'(\beta_1) = 1.585$	1	35.7	37
	2	39.9	3
	3	39.5	3
	4	38.8	7
	5	38.8	8
	6	38.3	8
$\theta = 8^\circ 31'$ $1/\sin \theta = 6.75$ $I'(\beta_1) = 39.0$ $\log I'(\beta_1) = 1.591$	1	38.6	16
	2	39.8 ²²	3
	3	38.8 ²²	3
$\theta = 4^\circ 52'$ $1/\sin \theta = 11.78$ $I'(\beta_1) = 42.5$ $\log I'(\beta_1) = 1.628$	1	43.4 ²²	5
	2	42.6 ²²	5
	3	42.4 ²²	5
$\theta = 2^\circ 06'$ $1/\sin \theta = 27.3$ $I'(\beta_1) = 46.0$ $\log I'(\beta_1) = 1.663$	1	48.5 ²²	8
	2	46.2 ²²	8
	3	46.6 ²²	9
	4	46.6 ²²	10

TABLE X. Experimental data for $I(\gamma_1)$.

	Trial	$I(\gamma_1)$	$I(W\alpha_1)$	Weight
$\theta = 19^\circ 22'$ $1/\sin \theta = 3.02$ $I' = 12.6$ $\log I' = 1.100$	1	11.9	6	3
	2	11.9	8	1
	3	12.0	8	2
	4	11.6	8	2
	5	12.0	8	2
$\theta = 4^\circ 52'$ $1/\sin \theta = 11.78$ $I' = 12.3$ $\log I' = 1.090$	1	10.7	15	2
	2	10.9	15	1
	3	10.8	16	2
	4	11.8	6	2
	5	11.7	6	3
$\theta = 2^\circ 06'$ $1/\sin \theta = 27.3$ $I' = 12.4$ $\log I' = 1.093$	1	12.1	10	1
	2	11.3	10	3
	3	11.0	12	3
	4	11.4	13	3

²² A 0.0033 cm mica window was used on the x-ray tube. The observed $I(\beta_1)$ has been corrected to be comparable with the values observed with the 0.0020 cm window used elsewhere.

TABLE XI. Experimental values for F_u of platinum at different angles.

$1/\sin \theta$	$\log I'(\beta_1)$	$\log F_{u\beta_1}$	$\log I'(\gamma_1)$	$\log F_{u\gamma_1}$
2.19	1.575	-0.056	1.100	-0.006
3.02	1.580	-0.061		
4.07	1.579	-0.060		
4.56	1.585	-0.066		
6.75	1.591	-0.072	1.090	0.004
11.78	1.628	-0.109		
27.3	1.663	-0.144	1.093	0.001

The measurement procedure and base corrections were the same as those used in the intensity measurements. In Tables IX and X are shown measurements of I_λ at different angles, and Table XI summarizes these data. The $I(\beta_1)$ and $I(\gamma_1)$ measurements were made under different conditions of the tube window and ionization chamber pressure. They were not corrected to the same conditions, since it is unnecessary. Since many of the measurements were made with an appreciable tungsten film on the target, the corrected average I_λ' is obtained by plotting I_λ versus $I(W\alpha_1)$, the intensity of tungsten $L\alpha_1$, and extrapolating to $I(W\alpha_1) = 0$.

When θ is varied the transition probability and the corrections other than F_u do not vary, so the observed variation in I_λ' must be inversely proportional to the variation in F_u . Since the transition probability is an unknown factor in the proportionality constant, the experimental points are adjusted (by an arbitrary additive constant when expressed in logarithmic form) to fit the calculated curves as well as possible.

It is seen in Fig. 2 that there is a qualitative agreement between the two different theoretical and the experimental results. In each of the three cases $F_{u\beta_1}$ decreases sharply and $F_{u\gamma_1}$ remains nearly constant with $1/\sin \theta$.

The difference between the Rosseland and the Webster calculations consists of a slight separation of the curves. The difference between the shape of the two theoretical curves is less than the separation between them and the experimental points. Consequently no information is gained concerning the relative accuracy of the Rosseland and the Webster functions. In the calculations it is assumed that the surface of the target is a perfect plane. The average depth of production is approximately 4000A. It is believed that the irregularities on the surface of the target were small compared to this depth. The calculations do not take any account of ionization in the target produced by indirect means, such as reabsorption of x-rays. Presuming that one of the theories is correct, both irregularities on the surface and indirect ionization may contribute to the disagreement of the experimental points.

The approximate average depth of production is determined by observing that when $1/\sin \theta = 1$ all the curves of Eq. (5) (the curves which were drawn for graphical integration) were roughly linear, touching zero at $V_x = V_0$. The abscissa is V_x and the ordinate is the intensity contributed at the depth x corresponding to V_x . Therefore the center of gravity has the V_x of the average depth of production. The center of gravity of the triangle is $\frac{1}{3}$ of the way from $V = 30$ to $V_0 \approx 12$, or $V_x \approx 24$. With the use of the Thomson-Whiddington equation, the corresponding $x \approx 4 \times 10^{-5} = 4000A$.

APPLICATION OF THE CORRECTION WITHIN THE TARGET

Log F_{IR} and log F_{IW} were calculated for the preceding intensity measurements, with graphical integration, and are shown in Table V. Since the incident beam of electrons and the emergent x-ray beam each make a 45° angle with the face of the target, the depth of the penetration of an electron before ionizing an atom is equal to the thickness of target material which the x-rays must pass through to reach the surface. This is the same condition as $1/\sin \theta = 1$ when the electron beam is perpendicular to the face of the target.

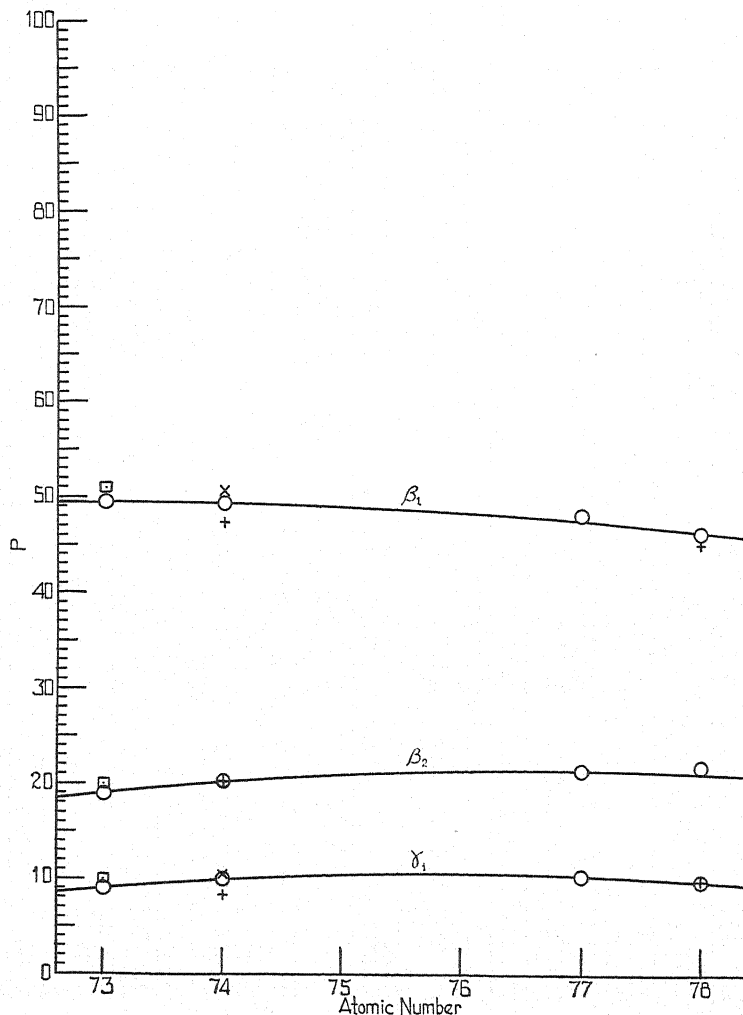


Fig. 3. Intensity relative to $L\alpha_1=100$ at 30 k.v. without correction for partial reflection by the crystal. Plus signs, Jönsson; squares with dots, Hicks; crosses, Allison and Andrew; circles, Andrew.

CONCLUSION

In Table V the corrected intensities are given in three forms, P' , P_R , and P_W . The first is the intensity with all corrections except for partial reflection

at the crystal and for effects within the target. In this form the data are comparable to those of previous investigators, which are also shown in Table V. The published data of Jönsson at 20 k.v. were corrected to 30 k.v. by the assumption that the intensity of a line is proportional to $(V - V_0)^2$. The published data of Allison and Andrew were corrected for absorption in air and in the tube and ionization chamber windows. P_R and P_W are the transition

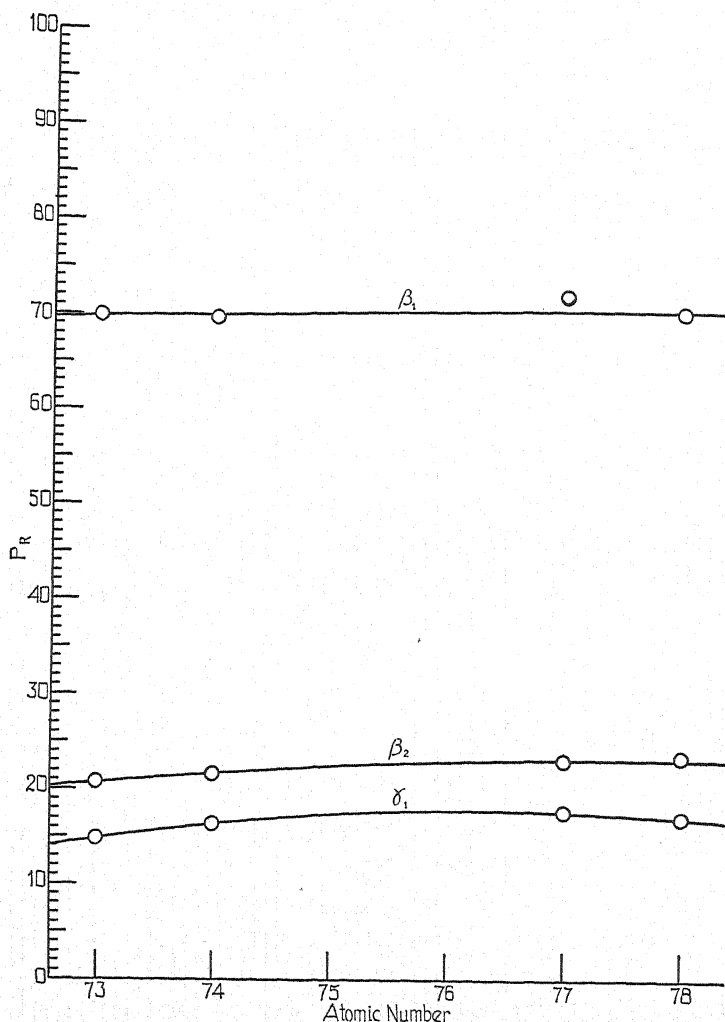


Fig. 4. Transition probability relative to $L\alpha_1=100$ calculated with the Rosseland function, probabilities according to the Rosseland expression and according to the Webster expression, respectively. In Figs. 3, 4 and 5 the results in the three forms mentioned are plotted against the atomic number. In Fig. 3 the measurements of other investigators are shown for comparison. It is seen that the results reported here are in good agreement with former work, and are quite consistent from element to element.

The Webster expression gives transition probability ratios which agree much better than those from the Rosseland expression with the theoretical predictions of the sum rule of Burger and Dorgelo.²³ The predictions are

$$P(\alpha_1):P(\beta_1) = P(\beta_2):P(\gamma_1) = 9:5.$$

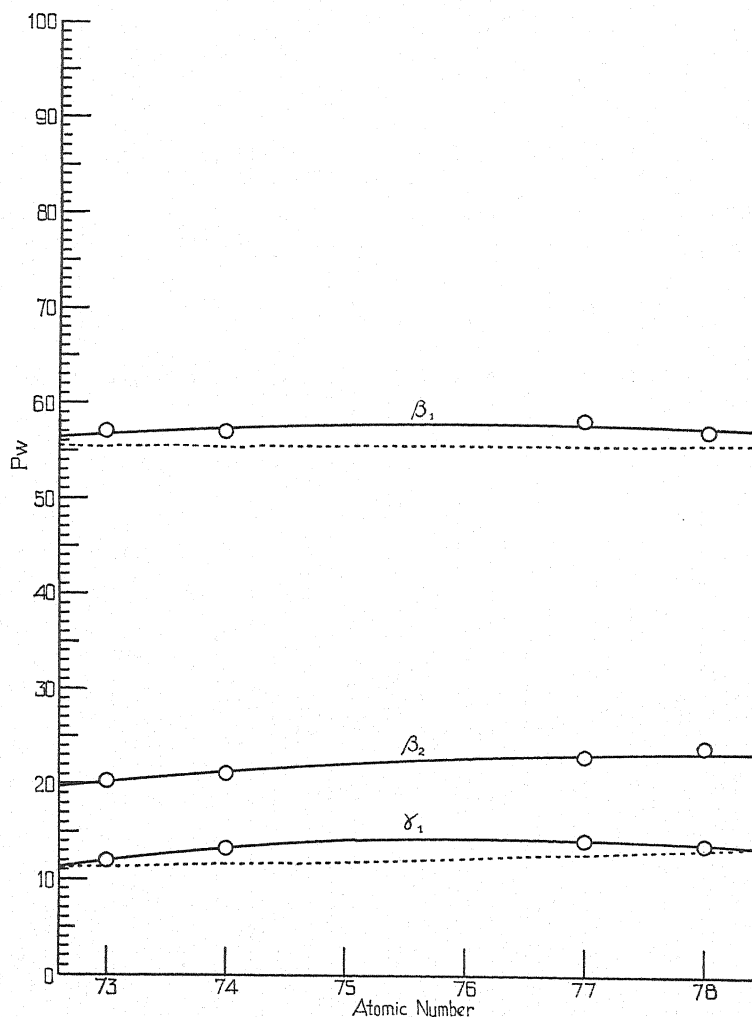


Fig. 5. Transition probability relative to $L\alpha_1=100$ calculated with the Webster, Clark, Yeatman, and Hansen function. Full curve, experimental; broken curve, sum rule.

The dotted curves in Fig. 5 show the predictions for $P(\beta_1)$ ($(5/9)P(\alpha_1)$, $P(\alpha_1)=100$) and $P(\gamma_1)$ ($(5/9)P(\beta_2)$, experimental values of $P(\beta_2)$).

It should be observed that the empirical origin of Eq. (4_W), which may be written

²³ Burger and Dorgelo, *Zeits. f. Physik* **23**, 258 (1924).

$$F_W(x) = k_\lambda V_0 \frac{1}{V_x} \frac{V_x - V_0}{V_x + 3V_0} \quad (4_W')$$

permits changing V_0 in the coefficient to any other power without invalidating the agreement of the function with the experimental data for which it was originated (the variation of intensity of one line with V_x , hence V_0 was a constant). The first power of V_0 is apparently a fortuitous circumstance which results in making the observed intensities agree so closely with the sum rule. Inserting a V_0 in the coefficient of the Rosseland function would make the observed intensities with the corresponding correction fall much closer to the sum rule predictions. However, the theoretical derivation of the Rosseland function shows that such a constant cannot be arbitrarily inserted.

The writer wishes to take this opportunity to express his thanks for the use of the x-ray spectrometer and his appreciation to Professor S. K. Allison for the suggestion of the problem and guidance during the investigation.

The Band Spectra of MgO, CaO and SrO

By P. C. MAHANTI

University College of Science and Technology, Calcutta

(Received September 9, 1932)

New measurements of the wave-lengths of the band heads attributed to the oxides of Mg, Ca and Sr have been made from moderate dispersion spectrograms. For each of these molecules the bands have been classified into two systems. The equations of the band heads in terms of half-quantum numbers for the different systems are as follows:

MgO, red bands:

$$\nu = 16,418.06 + \left\{ 821.95(v' + \tfrac{1}{2}) - 4.05(v' + \tfrac{1}{2})^2 \right\} \\ - \left\{ 665.74(v'' + \tfrac{1}{2}) - 4.41(v'' + \tfrac{1}{2})^2 \right\}$$

MgO, green bands:

$$\nu = 19,944.82 + \left\{ 811.67(v' + \tfrac{1}{2}) - 3.74(v' + \tfrac{1}{2})^2 \right\} \\ - \left\{ 771.42(v'' + \tfrac{1}{2}) - 4.81(v'' + \tfrac{1}{2})^2 \right\}$$

CaO, blue bands:

$$\nu = 23,817.62 + \left\{ 726.53(v' + \tfrac{1}{2}) - 11.66(v' + \tfrac{1}{2})^2 \right\} \\ - \left\{ 811.28(v'' + \tfrac{1}{2}) - 6.60(v'' + \tfrac{1}{2})^2 \right\}$$

CaO, ultraviolet bands:

$$\nu = 28,849.13 + \left\{ 565.06(v' + \tfrac{1}{2}) - 4.48(v' + \tfrac{1}{2})^2 \right\} \\ - \left\{ 725.37(v'' + \tfrac{1}{2}) - 3.56(v'' + \tfrac{1}{2})^2 \right\}$$

SrO, blue bands:

$$\nu = 24,702.81 + \left\{ 519.09(v' + \tfrac{1}{2}) - 3.50(v' + \tfrac{1}{2})^2 \right\} \\ - \left\{ 653.47(v'' + \tfrac{1}{2}) - 4.02(v'' + \tfrac{1}{2})^2 \right\}$$

SrO, ultraviolet bands:

$$\nu = 28,622.18 + \left\{ 497.81(v' + \tfrac{1}{2}) - 5.97(v' + \tfrac{1}{2})^2 \right\} \\ - \left\{ 679.13(v'' + \tfrac{1}{2}) - 9.13(v'' + \tfrac{1}{2})^2 \right\}.$$

INTRODUCTION

THE earliest spectroscopic workers¹ noticed in the spectrum of Mg, Ca and Sr or their salts subjected to a variety of conditions of excitation, a class of bands, which were ascribed by them either to the metals or to their oxides. Kayser was, however, of opinion that both types of bands are present in the spectrum. He has collected the old measurements of wave-lengths of the band heads but no satisfactory agreement is to be found among the various data. With the improvement of the experimental technique, it has however been found that some of these bands, although they appear in the ordinary arc or flame spectrum of Mg, Ca and Sr or their salts, fail to show themselves if the arcing is conducted in vacuum or in a dry hydrogen or nitrogen atmosphere

¹ Kayser, *Handbuch der Spectroscopie* 5, 252, 717 (1910); 7, 172 (1924); 6, 551 (1912).

but increase in their intensity depending on the amount of oxygen present. It is these bands which have been ascribed to the oxides and they form the subject of the present investigation.

In 1927, Mecke and Guillery² analyzed one system in the case of CaO and SrO from the old data then available. The present analysis however discloses that they have used parts of two different systems for CaO. For SrO they have not published any data of band heads analyzed by them. More recently a vibrational quantum analysis³ of the well-known green bands of MgO from measurements on low dispersion spectrograms (about 23A/mm at $\lambda 5000$) has been published.

The present paper deals with the vibrational quantum analysis of the bands of MgO, CaO and SrO from new measurements of the wave-lengths of band heads, believed to be more accurate than existing data. For each of these molecules, the spectrum has been investigated between the region $\lambda 7500$ – $\lambda 2300$, and the bands have been found to form two different systems. Only the bands of MgO lying in the red region appear to offer the best possibilities for a fine structure analysis. Such an analysis is being undertaken and will be reported in a subsequent paper.

EXPERIMENTAL

The spectra herein described, except that of magnesium, were produced in electric arcs between carbon electrodes with some salt of the element under investigation. In the case of magnesium the lower electrode (+) was drilled to hold magnesium rods about $\frac{1}{8}$ inch in diameter. During a single exposure several rods had to be used. The salts employed were pure anhydrous calcium chloride and strontium chloride. The arc was operated on a 220 volt d.c. circuit with the current varying from six to seven amperes but in the case of magnesium, the current was about an ampere.

Spectrograms were taken with the Hilger-Littrow-mounted E.1 prism spectrograph, having a dispersion with the glass optical system of approximately 35A/mm at $\lambda 7500$ to 6A/mm at $\lambda 4400$, and with the quartz system of 17A/mm at $\lambda 4500$ to 2A/mm at $\lambda 2300$ as well as in the first and second orders of a 15 ft. Rowland concave grating set up in a Paschen mounting. The dispersion in the first order is about 3.52A per mm. Ilford Empress and green sensitive orthochromatic plates as well as special rapid panchromatic plates freshly dyed with pinacyanol were used.

The heads are apparently single and fairly sharp except where they are greatly superposed by the structure lines of the preceding bands. With a Gaertner comparator (MI201a), the intense band heads were measured on grating plates while prism spectrograms of moderate dispersion were used for the measurement of the weaker ones. For standards, iron and neon lines were taken.

Eye estimates of the intensities of the heads were made from the plates taken with the prism spectrographs.

² Mecke and Guillery, *Phys. Zeits.* **28**, 514 (1927).

³ Ghosh, Mahanti and Mukherjee, *Phys. Rev.* **35**, 1491 (1930).

The band head data and their vibrational quantum assignments are given in Tables I-VI. λ is the wave-length in air in international angstroms, I the visual estimate of the relative photographic intensity of the band heads, and ν the vacuum wave-number in cm^{-1} . $O-C$ is the difference between the wave-number observed and that calculated from the empirical equation for each system.

Magnified reproductions of typical sequences in the band systems of MgO, CaO and SrO are given in Figs. 1, 2 and 3.

MAGNESIUM OXIDE

In the spectrum of magnesium arc in air the band groups lying between $\lambda 7000$ – $\lambda 5250$ and also extending as far as $\lambda 4700$ as well as those at $\lambda 5205$ and $\lambda 5007$, which are given in the excellent reproduction of Eder and Valenta,⁴ have been attributed to the oxide of magnesium while the ultraviolet bands and a number of visible bands at $\lambda 5125$ and $\lambda 4819$ have been ascribed to the metal. The bands at $\lambda 5007$ were observed by each one of the earliest spectroscopic workers⁵ in the spectrum of magnesium or its salts under various modes of excitation. Lockyer⁶ found them also present in the spectrum of nebulae. The band group at $\lambda 5205$ was obtained only by Eder⁷ in the flame and spark spectra of magnesium and by Brooks⁸ in the anode spectrum in oxygen when a high voltage unidirectional but pulsating discharge was passed between magnesium electrodes. In addition to the above two groups of bands, the latter also observed a number of bands at the red end of the same spectrum and gave approximate measurements of seven band heads between $\lambda 6600$ – $\lambda 5250$. In the present investigation as many as twenty-five heads have been measured in this region and the measurements extended on both sides thus bringing the total number of heads measured to forty-seven for the red bands. Spectrograms taken with the glass spectrograph as well as in the first order of the 15 ft. concave grating were used for measurements which are correct to $\pm 0.05\text{\AA}$. The two band groups at $\lambda 5205$ and $\lambda 5007$ were also measured from the glass prism spectrograms as well as from those taken in the second order of the same grating. They form, respectively, $\Delta\nu = +1$, and 0 sequences of the green system, which includes twenty-three band heads.

The red bands are not of perceptible intensity in the usual flame surrounding the magnesium arc in air. But they are fairly intense if the arc bursts out into a vigorous flame. With an exposure for about an hour with this type of flame, they are well developed on the plates taken with the glass spectrograph, but the band heads lying below $\lambda 5210$ are very much superposed by the green bands.

So far as the writer is aware, no new measurements or vibrational quantum analysis of the red bands have yet been published, while for the green

⁴ Eder and Valenta, *Atlas Typischer Spektren*, Wien (1924).

⁵ Kayser, *Handbuch der Spectroscopie* 5, 717 (1910).

⁶ Lockyer, *Proc. Roy. Soc.* 48, 167 (1890).

⁷ Eder, *Denkschr. Wien. Akad.* 74, 45 (1903).

⁸ Brooks, *Astrophys. J.* 29, 177 (1909).

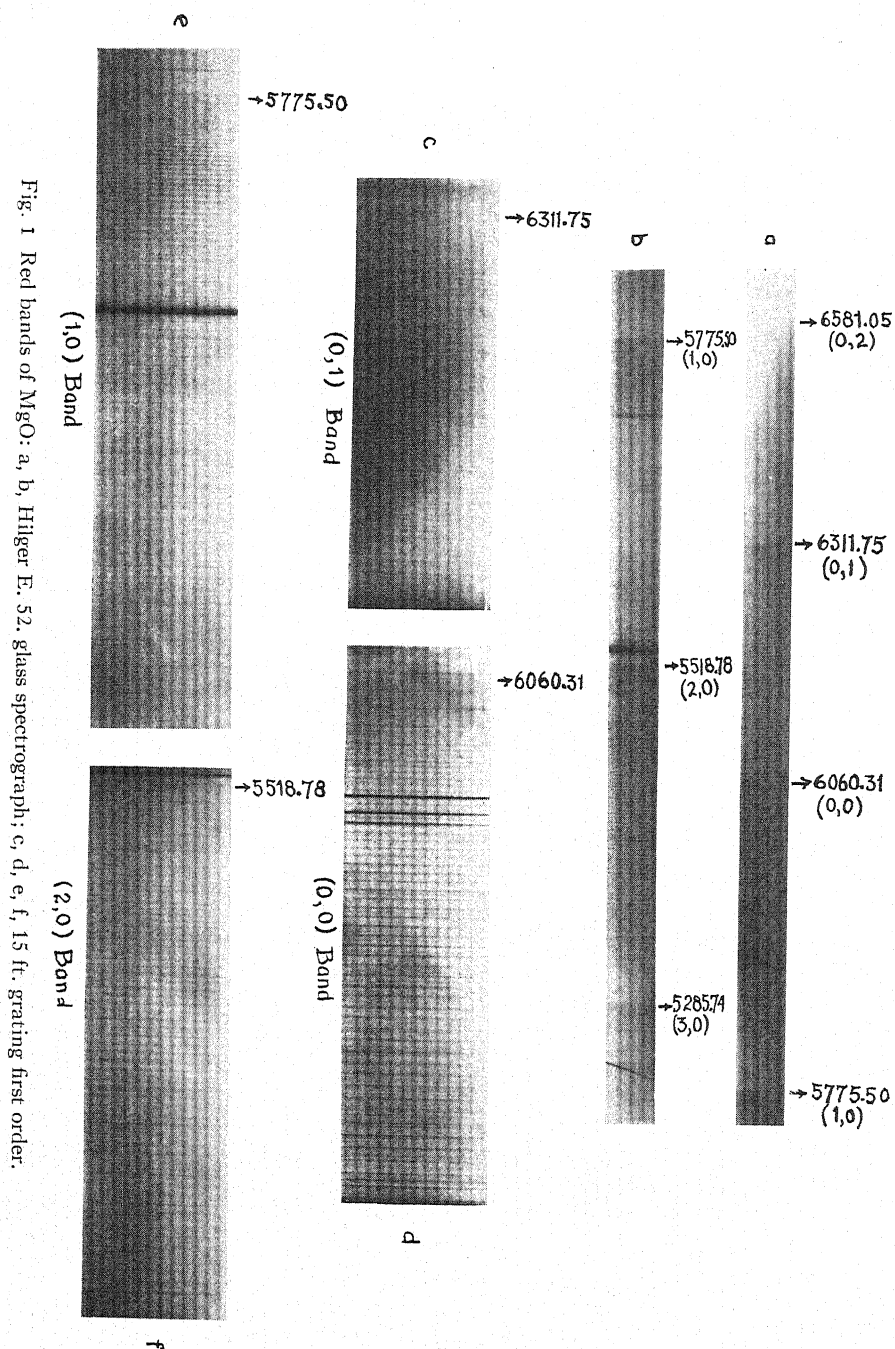
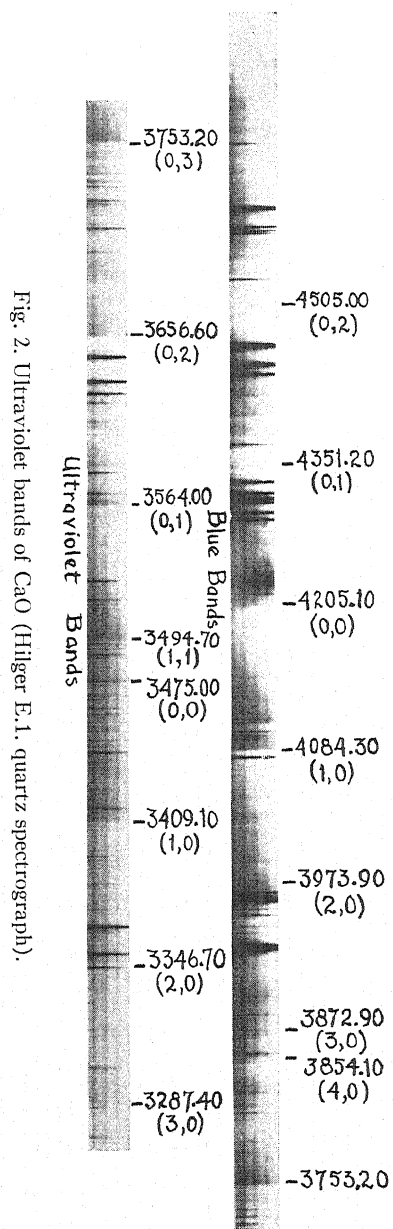


Fig. 1 Red bands of MgO: a, b, Hilger E. 52. glass spectrograph; c, d, e, f, 15 ft. grating first order.



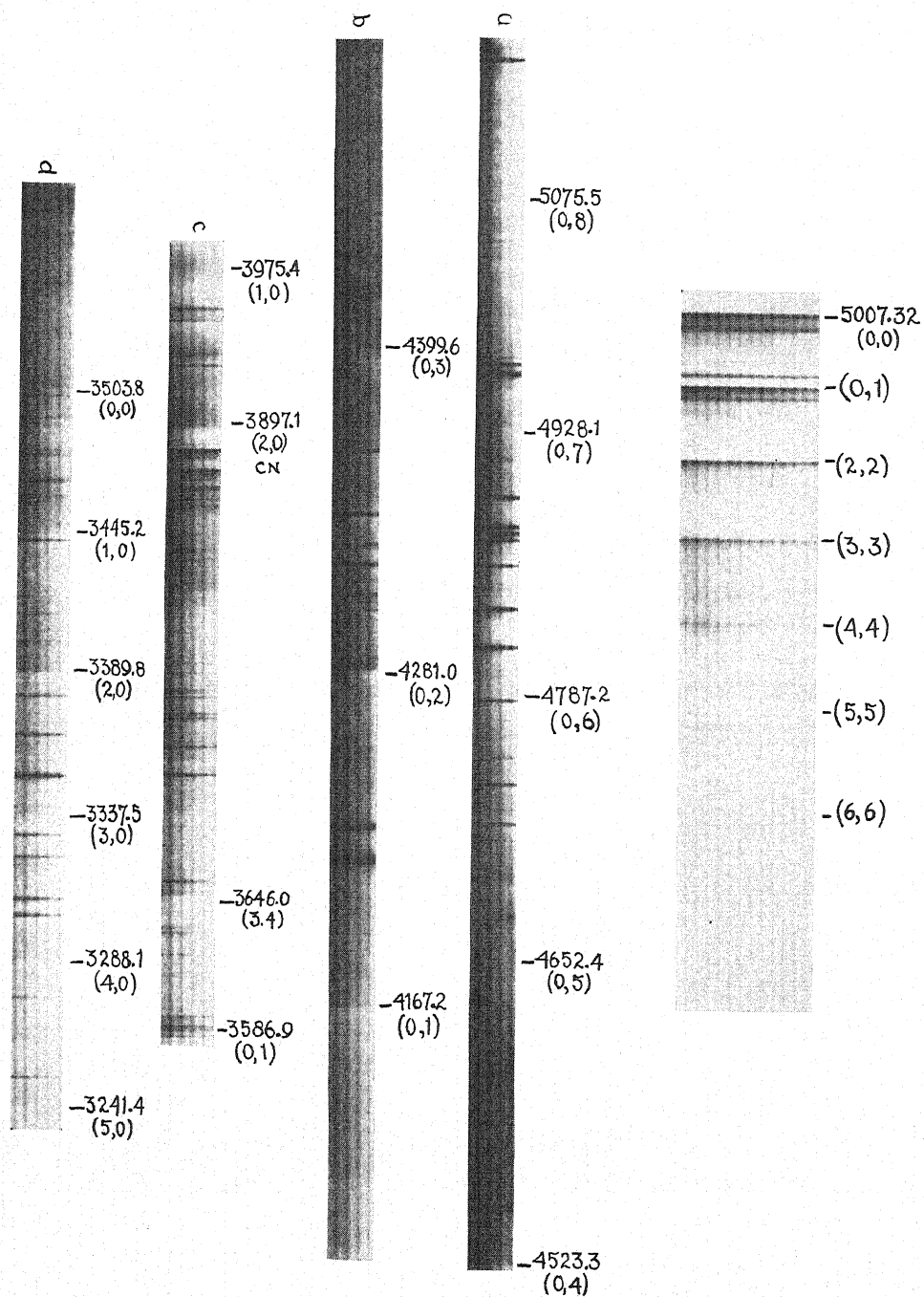


Fig. 3. Right half of figure, green bands of MgO (15 ft. grating second order). Left half, bands of SrO; a, b, Hilger E. 52. glass spectrograph; c, d, Hilger E.1. quartz spectrograph.

bands the analysis has only been done from measurements on low dispersion spectrograms. New measurements of band heads as well as their vibrational assignments are given in Tables I and II.

TABLE I. *The red bands. New data and vibrational quantum analysis.*

v'	v''	$\lambda_{\text{Hd.}} (\text{\AA.})$	I	$\nu \text{ (cm}^{-1}\text{)}$	$O-C \text{ (cm}^{-1}\text{)}$
0	3	6870.19	2	14,551.63	-0.35
1	4	6783.61	1	14,737.35	+1.97
2	5	6699.97	1	14,921.33	+1.83
3	6	6617.78	0	15,106.64	+2.29
0	2	6581.05	3	15,190.95	-0.29
4	7	6537.37	0	15,292.46	+2.56
1	3	6506.26	2	15,365.58	-0.25
2	4	6432.12	1	15,542.69	+1.57
3	5	6359.64	1	15,719.82	+2.68
0	1	6311.75	4	15,839.35	+0.01
4	6	6289.93	0	15,894.04	+0.16
1	2	6246.38	3	16,004.95	-0.14
5	7	6220.59	0	16,071.21	+0.12
2	3	6181.84	2	16,171.95	+0.38
3	4	6118.47	1	16,339.45	+0.69
0	0	6060.31	6	16,496.25	+0.00
1	1	6003.26	2	16,552.99	-0.20
2	2	5947.18	1	16,810.05	-0.78
1	0	5775.50	5	17,309.73	-0.37
2	1	5726.34	3	17,458.33	-0.60
3	2	5677.03	2	17,609.97	+1.50
4	3	5629.06	1	17,760.04	+1.30
2	0	5518.78	4	18,114.93	-0.91
3	1	5475.94	3	18,256.65	+0.08
4	2	5433.39	2	18,399.61	+1.61
5	3	5391.74	1	18,541.74	+1.57
6	4	5349.78	0	18,687.17	+4.12
3	0	5285.74	3	18,913.58	+0.10
4	1	5249.58	2	19,043.86	-2.24
5	2	5212.44	1	19,179.55	+0.12
4	0	5073.95	2	19,703.03	+0.02
5	1	5041.44	1	19,830.09	+2.56
10	7	5034.12	0	19,858.92	+2.00
6	2	5010.39	1	19,952.98	+0.22
10	6	4887.09	1	20,456.38	-4.52
11	7	4855.54	1	20,589.30	-0.43
6	1	4851.49	1	20,606.49	+5.63
7	2	4825.94	1	20,715.58	-2.40
12	8	4824.39	1	20,722.23	+2.94
8	3	4797.98	0	20,836.30	+0.46
13	9	4794.59	1	20,851.03	+1.47
9	4	4772.07	1	20,949.42	-4.98
14	10	4764.61	1	20,982.23	+1.68
10	5	4744.02	1	21,073.06	-0.63
15	11	4736.21	1	21,108.04	-4.22
11	6	4717.73	1	21,190.72	-2.99

The equations of the band heads in terms of half-quantum numbers for the two systems are as follows.
For the red system:

$$\begin{aligned} \nu = & 16,418.06 + \left\{ 821.95(v' + \tfrac{1}{2}) - 4.05(v' + \tfrac{1}{2})^2 \right\} \\ & - \left\{ 665.74(v'' + \tfrac{1}{2}) - 4.41(v'' + \tfrac{1}{2})^2 \right\} \end{aligned} \quad (1)$$

TABLE II. *The green bands. New data and vibrational quantum analysis.*

v'	v''	$\lambda_{\text{Hd.}}(\text{\AA.})$	I	$\nu(\text{cm}^{-1})$	$O-C(\text{cm}^{-1})$
0	1	5205.96	4	19,203.42	+0.03
1	2	5191.98	4	19,255.13	+0.00
2	3	5177.37	3	19,309.46	+0.01
3	4	5162.50	3	19,365.50	-0.16
4	5	5146.85	3	19,423.96	-0.03
5	6	5130.58	2	19,485.56	+1.12
6	7	5113.75	1	19,549.69	+2.68
7	8	5097.04	1	19,613.74	+2.04
8	9	5081.45	0	19,673.95	-4.56
0	0	5007.32	10	19,965.21	0.00
1	1	4996.71	9	20,007.60	+0.02
2	2	4985.92	8	20,050.90	-1.17
3	3	4974.47	7	20,097.06	-1.62
4	4	4962.10	6	20,147.15	-0.26
5	5	4949.53	5	20,198.32	+0.06
6	6	4935.30	4	20,256.56	+5.53
7	7	4923.87	3	20,303.58	-2.74
8	8	4908.61	2	20,366.70	+3.17
9	9	4895.20	2	20,422.49	-0.37
10	10	4880.69	2	20,483.20	-1.11
11	11	4865.41	1	20,547.53	-0.35
12	12	4849.63	0	20,614.39	+0.82
13	13	4834.05	0	20,680.82	-0.56

and for the green system:

$$\begin{aligned} \nu = 19,944.82 + \left\{ 811.67(v' + \tfrac{1}{2}) - 3.74(v' + \tfrac{1}{2})^2 \right\} \\ - \left\{ 771.42(v'' + \tfrac{1}{2}) - 4.81(v'' + \tfrac{1}{2})^2 \right\}. \end{aligned} \quad (2)$$

The intensity distribution among the band heads of the red system follows a typical wide Condon⁹ parabola as is usual for high temperature emission spectra. The bands associated with either $v'=0$ or $v''=0$ are developed strongly but those associated with $v'=0$ are more intense than those with $v''=0$. On the other hand, for the green system, the intensity distribution lies on a very narrow Condon parabola. The distribution of the bands in a $\Delta v=0$ sequence with only weaker $\Delta v=+1$ sequence is in theoretical accordance with the very small change in vibrational frequency as is indicated by Eq. (2), and with correspondingly small change in moment of inertia which it accompanies. In fact, in the extreme case, the small percentage change in moment of inertia is indicative of a very narrow Condon parabola in the v', v'' array of bands and only the $\Delta v=0$ sequence is to be expected. Probably for the green bands, the sequence $\Delta v=-1$ is present but the bands are too weak to be measured under the high magnification of the comparator.

It is evident from Eqs. (1) and (2) that while $\omega_e' > \omega_e''$, $\omega_e' \chi_e' < \omega_e'' \chi_e''$. As a result of this, the successive heads in a sequence diverge with increasing quantum number. The heats of dissociation calculated for the lower levels of the two systems are, respectively, 3.06 and 3.76 volts.

CALCIUM OXIDE

In 1906 Olmsted,¹⁰ during the course of his investigation of the spectra of the flame of the oxy-hydrogen blow-pipe fed with calcium salts, measured

⁹ Condon, Phys. Rev. **28**, 1182 (1926).

¹⁰ Olmsted, Zeits. f. Wiss. Photo. **4**, 255 (1906).

thirty-two heads between the region $\lambda 4400$ – $\lambda 3300$ and attributed them to the metal. Later on Eder and Valenta¹¹ photographed the spectra of the flame of the arc as also of the oxy-coal gas with different salts of calcium introduced into it and published measurements of a number of band heads lying between $\lambda 6650$ – 5300 and also between $\lambda 4600$ – $\lambda 3400$. They, however, ascribed all these bands to the oxide. In 1914 Harnack¹² was led to the same view from a systematic investigation into the spectra of the flame arc in the atmosphere of oxygen and hydrogen as also of the flame formed by spraying finely powdered salts of calcium across an uncondensed spark. In the present investigation only the bands lying between $\lambda 4600$ – $\lambda 3200$ have been definitely ascribed to the oxide while those between $\lambda 6750$ – $\lambda 5300$ are probably emitted by the metal. They are very much superposed by the well-known CaCl bands lying in this region. Seventy-seven heads have been measured on prism spectrograms for the oxide bands and the wave-lengths are correct to $\pm 0.1\text{\AA}$. Their analysis is presented in Tables III and IV. In 1927, Mecke and Guillery² classified twenty-eight heads from the measurements of Olmsted into a single system but it now appears that they used parts of two different systems.

TABLE III. The blue bands. New data and vibrational quantum analysis.

v'	v''	$\lambda_{\text{Hd.}}$ (I. A.)	I	ν (cm ⁻¹)	$O - C$ (cm ⁻¹)
5	7	4597.0	0	21,747.24	-0.23
4	6	4573.9	0	21,857.07	+0.65
3	5	4553.4	1	21,955.48	+0.23
2	4	4535.1	2	22,044.07	+0.10
1	3	4519.1	3	22,122.12	-0.43
0	2	4505.0	4	22,191.35	+0.33
5	6	4449.9	2	22,466.13	-0.22
4	5	4425.8	3	22,588.46	-0.04
3	4	4403.9	6	22,700.79	+0.26
2	3	4384.3	6	22,802.27	-0.17
1	2	4366.7	5	22,894.18	-0.05
0	1	4351.2	5	22,975.73	-0.17
6	6	4336.7	0	23,052.55	-0.41
5	5	4309.5	1	23,198.04	-0.39
4	4	4284.6	1	23,332.86	-0.92
3	3	4261.8	2	23,457.68	-1.33
2	2	4240.8	3	23,573.84	-0.28
1	1	4221.9	5	23,679.37	+0.26
0	0	4205.1	6	23,773.97	-0.01
5	4	4175.4	1	23,943.08	-0.63
4	3	4149.8	2	24,090.77	-1.49
3	2	4126.0	3	24,229.74	-0.95
2	1	4104.1	4	24,359.03	+0.03
1	0	4084.3	5	24,477.11	-0.08
6	4	4075.5	0	24,529.96	-0.36
5	3	4047.3	1	24,700.88	-1.31
4	2	4020.9	1	24,863.05	-0.89
3	1	3996.5	2	25,014.85	-0.72
2	0	3973.9	3	25,157.11	+0.03
6	3	3953.4	0	25,287.55	-1.25
5	2	3924.6	1	25,473.12	-0.75
4	1	3897.8	1	25,648.26	-0.56
3	0	3872.9	2	25,813.15	-0.50

¹¹ Eder and Valenta, *Atlas typischer Spektren*, Wien (1924).¹² Harnack, *Phys. Zeits.* 15, 578 (1914).

TABLE IV. *The ultraviolet bands. New data and vibrational quantum analysis.*

v'	v''	$\lambda_{\text{Hd.}} (\text{\AA.})$	I	$\nu (\text{cm}^{-1})$	$O-C (\text{cm}^{-1})$
2	7	4000.0	1	24,992.96	-0.79
1	6	3979.5	1	25,121.71	-0.44
0	5	3959.4	2	25,249.23	+0.53
4	8	3937.3	0	25,390.95	-1.80
3	7	3915.7	1	25,531.01	-0.93
2	6	3894.7	2	25,668.67	-0.62
1	5	3874.2	2	25,804.49	-0.31
5	8	3858.3	1	25,910.83	-2.18
0	4	3854.1	2	25,939.07	+0.60
4	7	3836.2	1	26,060.10	-1.06
3	6	3814.7	1	26,206.97	-0.49
2	5	3793.7	2	26,352.04	+0.11
1	4	3773.2	2	26,495.20	+0.64
5	7	3761.2	0	26,579.73	-1.68
0	3	3753.2	3	26,636.39	+1.04
4	6	3739.2	1	26,736.12	-0.56
3	5	3717.8	1	26,890.01	-0.10
2	4	3696.9	2	27,042.02	+0.32
1	3	3676.5	3	27,192.07	+0.62
5	6	3667.9	0	27,255.82	-1.12
0	2	3656.6	4	27,340.05	+0.69
4	5	3646.1	1	27,418.78	-0.55
3	4	3624.8	2	27,579.90	+0.02
2	3	3604.0	2	27,739.06	+0.47
1	2	3583.7	3	27,996.19	+0.73
0	1	3564.0	5	28,050.38	-0.11
4	4	3556.6	0	28,108.74	-0.36
3	3	3535.4	1	28,277.29	+0.52
2	2	3514.8	2	28,443.02	+0.42
1	1	3494.7	3	28,606.60	+0.01
0	0	3475.0	6	28,768.77	+0.03
4	3	3470.5	0	28,806.07	+0.08
3	2	3449.6	1	28,980.59	-0.19
2	1	3429.1	2	29,153.84	+0.11
1	0	3409.1	4	29,324.87	+0.03
4	2	3387.7	0	29,510.11	+0.11
3	1	3366.9	1	29,692.41	+0.50
2	0	3346.7	3	29,872.52	+0.53
5	2	3329.0	1	30,030.44	+0.18
4	1	3308.0	2	30,221.08	-0.05
3	0	3287.4	3	30,410.45	+0.29
6	2	3273.3	0	30,541.44	-0.12
5	1	3252.0	1	30,741.47	+0.08
4	0	3231.2	2	30,939.35	-0.03

The equations of the band heads in terms of half-quantum numbers for the two systems are as follows. Blue bands:

$$\begin{aligned} \nu = 23,817.62 + \{726.53(v' + \tfrac{1}{2}) - 11.66(v' + \tfrac{1}{2})^2\} \\ - \{811.28(v'' + \tfrac{1}{2}) - 6.60(v'' + \tfrac{1}{2})^2\} \end{aligned} \quad (3)$$

and ultraviolet bands:

$$\begin{aligned} \nu = 28,849.13 + \{565.06(v' + \tfrac{1}{2}) - 4.48(v' + \tfrac{1}{2})^2\} \\ - \{725.37(v'' + \tfrac{1}{2}) - 3.56(v'' + \tfrac{1}{2})^2\}. \end{aligned} \quad (4)$$

As in the case of MgO band systems, the bands of CaO forming a sequence diverge with increasing quantum number. This is evident from Eqs. (3) and (4) that while $\omega_e' < \omega_e''$, $\omega_e' \chi_e' > \omega_e'' \chi_e''$.

The relative intensities of the bands in each system lie on a wide Condon parabola as in the case of the red bands of MgO.

The heats of dissociation calculated for the lower levels of the two systems are respectively 3.03 and 4.56 volts.

STRONTIUM OXIDE

The earliest spectroscopists¹³ noticed a class of bands between $\lambda 7000$ – $\lambda 5800$ in the flame and spark spectra of strontium salts and attributed them to the oxide. In 1905 Hagenbach and Konen,¹⁴ in addition to these, measured another class of bands between $\lambda 4500$ – $\lambda 3600$ and attributed them both to the metal as their emitter. Later on, Olmsted¹⁵ pointed out that the bands lying below $\lambda 3800$ were due to the oxide. He photographed the spectrum of the oxy-coal gas flame fed with different salts of strontium and published measurements of sixty-six heads between $\lambda 4800$ – $\lambda 3600$ with a concave grating of one meter radius. Afterwards Hartley¹⁶ noticed these bands in the spark spectrum of $\text{Sr}(\text{NO}_3)_2$ in solution as well as in that of oxy-hydrogen flame fed with SrCl_2 and ascribed a part of the spectrum to the oxide. The bands were also measured by Auerbach,¹⁷ Eder and Valenta,¹⁸ and by Harnack,¹⁹ who extended the measurements up to $\lambda 3200$. These authors ascribed all the bands to the oxide. Kayser²⁰ was, however, of opinion that the bands in the long wave-length region might be due to the metal. In the present investigation the bands lying between $\lambda 7100$ – $\lambda 5300$ have been definitely attributed to the metal and those between $\lambda 5300$ – $\lambda 3200$ to the oxide. In the latter region as many as 108 heads have been measured from prism spectrograms and analyzed into two systems (Tables V and VI). The analysis of Mecke and Guillery² is essentially correct for the blue system. It may here be pointed out that the metal bands in the long wave-length region are very much superposed by the well-known SrCl band systems as in the case of calcium.

TABLE V. The blue bands. New data and vibrational quantum analysis.

v'	v''	$\lambda_{\text{Ed.}} (\text{\AA.})$	I	$\nu (\text{cm}^{-1})$	$O-C (\text{cm}^{-1})$
3	12	5279.5	0	18,935.93	-0.57
2	11	5263.0	0	18,995.30	-0.10
1	10	5246.5	1	19,055.04	-0.30
0	9	5229.8	1	19,115.88	-0.44
4	12	5146.0	0	19,427.17	-0.42
3	11	5128.6	0	19,493.08	-0.41
2	10	5111.0	1	19,560.21	-0.22
1	9	5093.3	1	19,628.18	-0.23
0	8	5075.5	1	19,697.02	-0.41
5	12	5021.0	0	19,910.81	-0.87
4	11	5002.6	0	19,984.05	-0.53

¹³ Kayser, *Handbuch der Spectroscopie* 6, 544 (1912).

¹⁴ Hagenbach and Konen, *Atlas der Emission Spectra*, Jena, bei Fischer (1905).

¹⁵ Olmsted, *Zeits. f. Wiss. Photo.* 4, 255 (1906).

¹⁶ Hartley, *Trans. Roy. Soc. Dublin* 9, (2), 85 (1908).

¹⁷ Auerbach, *Zeits. f. Wiss. Photo.* 7, 30 (1909).

¹⁸ Eder and Valenta, *Atlas Typischer Spektren*, Wien (1924).

¹⁹ Harnack, *Zeits. f. Wiss. Photo.* 10, 281 (1912).

²⁰ Kayser, *Handbuch der Spectroscopie* 6, 551 (1912).

TABLE V. (Continued).

v'	v''	$\lambda_{\text{hd.}}(\text{\AA.})$	I	ν (cm^{-1})	$O-C$ (cm^{-1})
3	10	4983.9	0	20,059.03	+0.51
2	9	4965.6	0	20,132.95	-1.55
1	8	4946.9	1	20,209.06	-0.46
0	7	4928.1	1	20,286.15	-0.43
6	12	4903.5	0	20,387.92	+0.15
5	11	4884.3	0	20,468.06	-0.61
4	10	4864.8	0	20,550.11	+0.50
3	9	4845.5	1	20,631.96	+0.37
2	8	4826.1	1	20,714.89	+0.28
1	7	4806.7	1	20,798.50	-0.17
0	6	4787.2	2	20,883.22	-0.55
6	11	4773.1	0	20,944.91	-0.85
5	10	4752.8	0	21,034.36	+0.66
4	9	4732.9	1	21,122.81	+0.13
3	8	4712.8	2	21,212.89	+0.19
2	7	4692.7	5	21,303.75	-0.01
1	6	4672.6	4	21,395.39	-0.47
0	5	4652.4	3	21,488.28	-0.72
6	10	4647.4	0	21,511.40	+0.61
5	9	4626.9	1	21,606.71	-0.06
4	8	4606.2	2	21,703.81	+0.02
3	7	4585.5	3	21,801.78	-0.07
2	6	4564.8	5	21,900.65	-0.30
1	5	4544.1	5	22,000.41	-0.68
6	9	4526.9	1	22,084.00	+0.14
0	4	4523.3	4	22,101.58	-0.69
5	8	4505.7	1	22,187.91	+0.03
4	7	4484.5	3	22,292.80	-0.14
3	6	4463.3	4	22,398.68	-0.36
2	5	4442.1	3	22,505.58	-0.60
1	4	4420.9	5	22,613.50	-0.86
6	8	4410.9	0	22,664.77	-0.20
0	3	4399.6	6	22,722.98	-0.60
5	7	4389.2	1	22,776.72	-0.31
4	6	4367.6	2	22,889.46	-0.67
3	5	4345.9	3	23,003.75	-0.52
2	4	4324.3	3	23,118.65	-0.80
1	3	4302.7	4	23,234.71	-0.96
6	7	4299.2	0	23,253.62	-0.50
0	2	4281.0	5	23,352.48	-0.45
5	6	4277.2	0	23,373.23	-0.99
4	5	4255.1	1	23,494.62	+0.26
3	4	4233.2	2	23,616.16	-1.38
2	3	4211.2	3	23,739.54	-1.22
1	2	4189.1	4	23,864.77	-0.25
0	1	4167.2	5	23,990.19	-0.13
4	4	4147.0	1	24,107.04	-1.59
3	3	4124.7	2	24,237.37	-1.48
7	6	4110.6	0	24,320.51	+0.11
2	2	4102.3	2	24,369.72	-0.39
6	5	4087.9	0	24,455.56	+0.02
1	1	4080.1	2	24,502.31	-0.10
5	4	4065.4	0	24,590.91	-1.81
0	0	4058.0	3	24,635.75	0.00
4	3	4042.8	1	24,728.37	-1.57
3	2	4020.1	2	24,868.00	-0.20
7	5	4010.8	0	24,925.66	-0.97
2	1	3997.7	2	25,007.34	-0.16
6	4	3988.0	0	25,068.16	-0.65
1	0	3975.4	3	25,147.61	-0.23
5	3	3965.2	1	25,212.30	-0.73
4	2	3942.3	1	25,358.75	-0.54
3	1	3919.6	2	25,505.61	+0.02
7	4	3914.6	0	25,538.19	-1.71

TABLE V. (Continued).

v'	v''	$\lambda_{\text{Hd.}}(\text{\AA.})$	I	ν (cm ⁻¹)	O—C (cm ⁻¹)
2	0	3897.1	3	25,652.86	-0.07
6	3	3891.6	0	25,689.12	-2.00
5	2	3868.5	0	25,842.51	-0.87
4	1	3845.6	1	25,996.40	-0.28
3	0	3822.4	2	26,150.76	-0.26
6	2	3798.4	0	26,319.43	-1.04
5	1	3775.3	0	26,480.47	-0.30
4	0	3752.4	1	26,642.07	-0.04

TABLE VI. The ultraviolet bands. New data and vibrational quantum analysis.

v'	v''	$\lambda_{\text{Hd.}}(\text{\AA.})$	I	ν (cm ⁻¹)	O—C (cm ⁻¹)
2	4	3708.5	0	26,957.44	-0.72
1	3	3690.2	1	27,091.12	+0.79
0	2	3671.5	2	27,229.10	+0.28
3	4	3646.0	2	27,419.53	-0.63
2	3	3627.0	1	27,563.17	-1.10
1	2	3607.1	2	27,715.22	+0.53
0	1	3586.9	3	27,871.30	-0.14
3	3	3567.1	1	28,026.00	-0.27
2	2	3546.6	2	28,187.99	-0.64
1	1	3525.4	3	28,357.50	+0.19
0	0	3503.8	6	28,532.31	0.00
3	2	3489.3	1	28,650.87	-0.39
2	1	3467.5	2	28,830.99	-0.89
1	0	3445.2	4	29,017.61	-1.20
4	2	3435.3	1	29,101.23	-0.10
3	1	3412.8	2	29,293.08	-0.85
2	0	3389.8	4	29,491.83	-0.92
4	1	3361.2	1	29,742.76	-0.56
3	0	3337.5	3	29,953.96	-0.16
5	1	3312.4	0	30,180.93	-0.52
4	0	3288.1	2	30,403.97	-0.22
5	0	3241.4	1	30,842.00	-0.32

Besides the bands included in the two systems, there are a few unidentified heads. These were also measured by Olmsted and others, strongest of these are $\lambda 4135.0$ (4), 4113.6 (5) and 4092.6 (4).

The equations representing the band heads of the two systems are as follows.

For the blue bands:

$$\begin{aligned} \nu = & 24,702.81 + \left\{ 519.09(v' + \tfrac{1}{2}) - 3.50(v' + \tfrac{1}{2})^2 \right\} \\ & - \left\{ 653.47(v'' + \tfrac{1}{2}) - 4.02(v'' + \tfrac{1}{2})^2 \right\} \end{aligned} \quad (5)$$

and for the ultraviolet bands:

$$\begin{aligned} \nu = & 28,622.18 + \left\{ 497.81(v' + \tfrac{1}{2}) - 5.97(v' + \tfrac{1}{2})^2 \right\} \\ & - \left\{ 679.13(v'' + \tfrac{1}{2}) - 9.13(v'' + \tfrac{1}{2})^2 \right\}. \end{aligned} \quad (6)$$

Unlike the band systems of MgO and CaO, the bands of SrO in a sequence converge with increasing quantum number as is to be expected from the coefficients of ω_e' , $\omega_e'\chi_e'$, ω_e'' and $\omega_e''\chi_e''$ in Eqs. (5) and (6). On the other hand, the distribution of intensity among the various heads of the two band systems is very much similar to that of CaO. The heats of dissociation calculated for the lower levels of the two systems are, respectively, 3.24 and 1.52 volts.

My best thanks are due to Professor P. N. Ghosh for offering me all the facilities to carry out this investigation.

The Infrared Absorption Spectrum and the Molecular Structure of Ozone

By SHERMAN L. GERHARD
University of Michigan

(Received October 13, 1932)

Of the seven known infrared absorption bands of ozone, four (4.7μ , 7.39μ , 9.6μ , and 11.38μ) have been investigated for the first time with a grating spectrometer. The band at 4.7μ shows three branches, not very sharply defined, while the one at 7.39μ shows only a single peak. The strongest band, at 9.6μ , has been resolved into two main branches which probably belong to two different vibrations. The band at 11.38μ has been tentatively ascribed to nitrogen pentoxide, which often occurs as an impurity in ozone. Three fundamental vibrational frequencies, *viz.*, 528 cm^{-1} , 1033 cm^{-1} , and 1355 cm^{-1} , have been selected from the observational data. The rotational fine structure could not be completely resolved; it appears to have the irregularity characteristic of an asymmetrical rotator. The envelopes of the four observed bands have been completely mapped out. The infrared absorption spectrum of ozone is discussed and it is shown that the molecule cannot have the form of a straight line nor an equilateral triangle but it is probably represented by an isosceles triangle where the angle at the apex is less than 60° . By making use of these assumptions it was possible to order the observed frequencies in a fashion consistent with their envelopes. This general shape of isosceles triangle is the only one allowed by the observational data; the other shape of isosceles triangle, with apex angle greater than 60° , is ruled out.

DURING the past ten years ozone has attracted considerable interest and many attempts have been made to determine its structure. It is one of the few triatomic molecules whose infrared absorption spectrum has not heretofore been investigated with the high dispersion of a grating spectrometer. It is true that very many data have been collected on its absorption bands in the photographic region of the spectrum, but from these it has not been possible as yet to give a satisfactory description of its molecular structure.

John Tyndall¹ in 1872 discovered that ozone absorbs infrared radiation and, in 1904, K. Angstrom² first measured its infrared absorption spectrum. With low concentrations of ozone he found bands at 4.8μ , 5.8μ , 6.7μ and 9.6μ .

A more thorough investigation of the ozone absorption in this region was carried out by E. Ladenburg and E. Lehmann³ in 1906. By using a more efficient method of preparation they were able to observe it in higher concentrations and consequently found some weaker bands which Angstrom had missed. They found bands at 1.1μ , 3.7μ , 4.8μ , 5.9μ , 6.6μ , 7.6μ , 9.9μ and 11.35μ . Of these, the one at 5.9μ was later shown by E. Warburg and G. Leithauser⁴ to be due to nitrogen pentoxide.

¹ John Tyndall, *Contributions to Physics in the Domain of Radiant Heat*, London (1872).

² K. Angstrom, *Arch. f. Mat., Astron., och Physik* 1, 347, 395 (1904).

³ E. Ladenburg and E. Lehmann, *Ann. d. Physik* 21, 305 (1906).

⁴ E. Warburg and G. Leithauser, *Ann. d. Physik* 23, 209 (1907). See also another paper by these same two investigators, *Ann. d. Physik* 28, 313 (1909).

Quite recently A. Jakowlewa and V. Kondratjew⁵ made measurements on some of the ultraviolet electronic bands of ozone. They concluded from the results of their own measurements and those of others that ozone is a linear molecule, but this is not in agreement with our conclusions, as will be shown later.

EXPERIMENTAL

The classical and most common method of preparing ozone is one using a Siemens' ozonizer, in which a silent electric discharge is passed through air or oxygen. This gives only a low yield; the exit gases contain at best only about 10 percent of ozone.

A more efficient method of preparing ozone, described by A. K. Brewer and J. W. Westhaver⁶ was used in the present investigation. In this method a glow discharge is maintained in oxygen while the discharge tube is immersed in liquid air. Under these conditions liquid ozone condenses out on the walls of the discharge tube. Practically pure ozone gas may be obtained by distilling the liquid ozone thus formed. This last procedure, the distillation of the liquid ozone, was a hazardous one in spite of the fact that all organic matter was excluded from the entire system. On four different occasions the discharge tube exploded violently during the course of the distillation.

The absorption cells were glass tubes 4.5 cm in internal diameter and 25 cm and 1 m in length, respectively. Rocksalt windows were fastened on the ends by means of a thin, quick-drying lacquer. This method of fastening the windows had the advantage of enabling one to remove them when necessary by merely soaking in acetone or wood alcohol, thus avoiding the application of heat. The ozone was kept in the cells at atmospheric pressure by means of traps filled with phosphoric acid.

The spectrometer was of the usual type employing a rocksalt prism as a monochromator for the radiation falling on the grating. The thermocouples were very kindly supplied by Dr. J. D. Hardy. They were of the Pfund design and were connected to the familiar type of Moll relay, where the deflections of the first galvanometer were amplified. The aperture throughout the spectrometer was f5. A 25 cm parabolic mirror of 120 cm focal length was used in front of the grating. The slit widths used for each band are indicated in Fig. 1. With 0.88 ampere passing through the Nernst glower, which was used as a source, and the lamp in the Moll relay operating at 2.83 volts a deflection of about 70 mm was obtained at 9.6μ through the empty cell, and with a slit width of 0.3 cm^{-1} . Two gratings were used, with 1440 and 1200 lines per inch, respectively. The calibrations were obtained from charts previously prepared for them by means of standard infrared lines.

On account of the difficulty and hazard involved in handling highly concentrated ozone no attempt was made to perform a quantitative analysis of the contents of the absorption cell. It was, however, possible to make a

⁵ A. Jakowlewa and V. Kondratjew, *Phys. Zeits. d. Sowjetunion* **1**, 471 (1932).

⁶ A. K. Brewer and J. W. Westhaver, *J. Phys. Chem.* **34**, 1280 (1930).

rough estimate of the amount of ozone in the cell from considerations of the general behavior of the preparation.

The results of the investigation are shown in Fig. 1 as a group of curves giving the envelopes of the four different absorption bands studied. Most of the envelopes shows persistent irregularities, which indicate that the resolving power of the spectrometer was almost great enough to reveal the fine structure. It seems probable not only that the fine structure lines observed are real but also that they are distributed in the irregular manner which is characteristic of the asymmetrical rotator. This point will be discussed later.

The 9.6μ band was investigated with both the meter cell and the 25 cm cell. Curve I was taken with practically pure ozone gas at atmospheric pres-

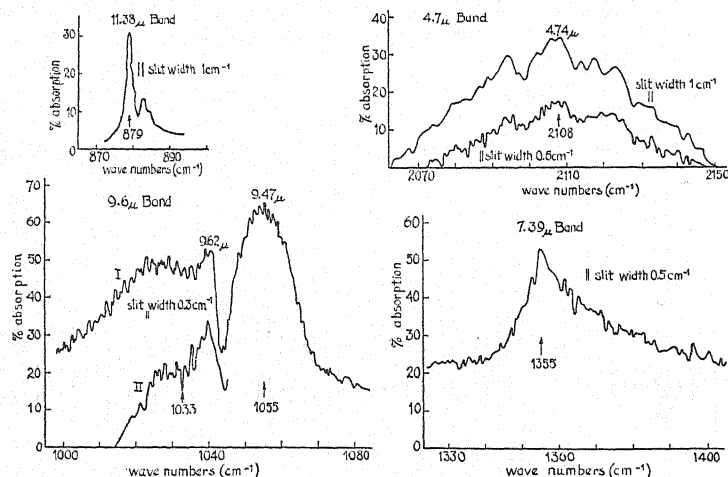


Fig. 1.

sure in the shorter cell, and curve II with a very low concentration in the meter cell. This band has apparently three branches. The one on the high-frequency side of the center (9.62μ) is the strongest, and the one on the low-frequency is the weakest of the three. The low-frequency branch becomes weaker than the other two at low concentration. The high-frequency branch was not studied in detail at low concentrations but a few readings taken at 9.47μ at the same time curve II was taken showed an absorption of about 48 percent, showing that this branch remained the strongest of the three. This behavior indicates that the high-frequency branch may be associated with one fundamental frequency, and the rest of the band with another.

The 7.39μ band lies in a region where the absorption due to water vapor is very noticeable. It also was observed with the same high concentration of ozone in the 25 cm cell that was used in obtaining curve I for the 9.6μ band. The curve shown for this 7.39μ band represents the average of two separate and consistent sets of data taken under the same conditions. The high background on each side of the strong single branch might be fictitious on account of the uncertainty in calculating the percentage absorption in a region where

water vapor absorbs as strongly as it does here. However, it is stronger than the 4.7μ band, which could not be detected under the same conditions.

The bands at 9.6μ and at 7.39μ are the two strongest ones; the others were looked for but could not be detected with the same concentration of ozone in the 25 cm cell.

The two curves shown for the 4.7μ band were obtained with two slightly different ozone concentrations in the meter cell, and also with different slit widths, as indicated in Fig. 1.

The small single peak of absorption at 11.38μ was observable only with very high concentrations of ozone in the meter cell. The curve shown for it was obtained with a higher concentration of ozone in the meter cell than was used to obtain the 4.7μ band, in fact it was not observable under the conditions which yielded the curves for the 4.7μ band.

In the first two columns of Table I is a summary of the wave-lengths and relative intensities of the absorption maxima of ozone obtained in this in-

TABLE I.

Wave-lengths	Relative intensities	Ladenburg and Lehmann	
		Wave-lengths	Relative intensities
—	—	1.1μ	1
—	—	3.7	2
4.74μ	5	4.7	5
—	—	6.6	2
7.39	7	7.7	3
9.47	10		
9.62	8	9.9	10
11.38	2	11.3	3

vestigation. In the last two columns are given the values reported by Ladenburg and Lehmann,³ it is seen that there is very satisfactory agreement between these two sets of results, considering the fact that Ladenburg and Lehmann used a prism spectrometer.

The weak band at 11.38μ does not fit with the other observed bands into any scheme of frequencies. It may possibly be due to nitrogen pentoxide, which has a very strong band at 5.75μ , for the band at 5.75μ may be the first overtone of a fundamental at 11.38μ .

Several attempts were made to find the Raman spectrum of liquid ozone, using pure ozone as well as solutions of ozone in liquid oxygen. The details of these attempts have already been published.⁷ The extreme faintness of the doublet observed, corresponding to a mean frequency shift of 1280 cm^{-1} (7.81μ), and the fact that this frequency does not fit in with the infrared frequencies makes it doubtful whether it is real.

THEORETICAL

§1

The data obtained in this investigation of the infrared absorption bands of ozone are not as complete as might be desired. In the first place its insta-

⁷ G. B. B. M. Sutherland and S. L. Gerhard, *Nature* 130, 241 (1932).

bility caused several explosions and made the gathering of data expensive and difficult, and in the second place the rotational fine structure is so closely spaced that it was not possible to resolve it. It is therefore necessary in the interpretation of the data to approach the subject from a rather general point of view and this requires the discussion of all the possible models for its structure. It will be shown that the data are consistent with only one model, and that furthermore this model has certain other properties similar to the known properties of ozone.

The frequencies observed for ozone have been satisfactorily correlated in the following way. The single band at 1355 cm^{-1} is taken as the first fundamental frequency, ν_1 , then the band at 2710 cm^{-1} , reported by Ladenburg and Lehmann, is its first harmonic, $2\nu_1$. The strong band at 1055 cm^{-1} is assigned to the first overtone of a fundamental ν_2 , at 528 cm^{-1} , which could not be observed because of the high absorption of the rocksalt windows in this region. The minimum at 1033 cm^{-1} is taken as the center of a doublet type band representing the third fundamental frequency, ν_3 . The 2108 cm^{-1} band may be called $2\nu_3$; it is apparently multiple and contains other combinations as well. The weak band reported by Ladenburg and Lehmann at 1515 cm^{-1} may very well be the combination $\nu_2 + \nu_3$. Except for the 11.38μ band, which is ascribed to nitrogen pentoxide, all the known bands of ozone are thus accounted for. There are three fundamental frequencies represented. The fundamental of two of them and the first harmonics of all three have been observed, as well as several combinations.

These bands display different kinds of envelopes. The fundamental, ν_1 at 1355 cm^{-1} , has certainly a zero branch type of envelope, with the zero branch very strong in comparison with the positive and negative branches. The $2\nu_2$ band, at 1055 cm^{-1} , has also a zero branch type of envelope, while that for ν_3 , at 1033 cm^{-1} , is of the doublet type. The envelope for $2\nu_3$, at 2108 cm^{-1} , is apparently of the zero branch type. Unfortunately the envelopes of the remaining bands of ozone have not been observed, however, it will be possible to gather from the data in hand sufficient information to decide on the shape of the molecule.

For a triatomic molecule, such as ozone, there are three plausible shapes, *viz.*, linear, equilateral triangle and isosceles triangle. The three atoms of oxygen making up the ozone molecule need not all be alike; the force fields and electron configurations may not be the same for all the atoms. The possibilities of these three types of structure will now be discussed in connection with the data obtained and with the aid of the results of the wave mechanical analysis of infrared spectra given in a recent paper by D. M. Dennison.⁸

§2

There are two possible linear models for ozone, a symmetrical one, with the three atoms symmetrically arranged along a line, as is the case in carbon

⁸ D. M. Dennison, *Rev. Mod. Phys.* **3**, 280 (1931).

dioxide, and an unsymmetrical one. The symmetrical type of linear molecule would display absorption bands resembling those of carbon dioxide. It would have similar vibrational properties and would obey the same selection rules, namely, that combinations or overtone frequencies which are the sum of any two observed frequencies cannot occur.⁸ These conditions are not met by the frequencies observed for ozone, *viz.*, the band at 2108 cm^{-1} has twice the frequency of the 1033 cm^{-1} band, and the one reported at 2710 cm^{-1} has twice the frequency of the 1355 cm^{-1} band. With 528 cm^{-1} as a fundamental the band reported at 1515 cm^{-1} is assigned to the combination $1033 + 528$. The occurrence of these overtones and combinations is definitely in disagreement with the requirements for a linear symmetrical model and is sufficient to rule it out as a possible structure for ozone.

The other possible linear model would resemble the molecule of nitrous oxide, NNO. The selection rules for this model allow three active fundamental frequencies and all possible combinations and overtones. The vibration-rotation bands consist of fine structure lines regularly spaced in frequency.⁹ There are two types of bands, both having essentially similar positive and negative branches, the one having a strong zero branch and the other none. When the ozone bands are examined it is found that none of them have regularly spaced fine structure lines. The positive and negative branches of the several bands do not stand out distinctly as they do in the case of nitrous oxide. There is no similarity between even the general outlines of the envelopes of any two bands. If ozone were this unsymmetrical linear type of molecule, then the positive and negative branches of the 1033 cm^{-1} and 1355 cm^{-1} (fundamental) bands should be similar and should have almost equal doublet spacings, but this is obviously not the case. These fundamental differences between the observed bands of ozone and those to be expected from linear molecules make it evident that the ozone molecule cannot be a linear one.

§3

In the isosceles triangle model for ozone the oxygen atom at the apex is taken to be different from the two at the base. The general solution of the vibrational problem has already been given by several investigators.^{10,11} Three fundamental frequencies are to be expected for the general isosceles triangle. According to the conventions adopted in labelling these frequencies the electric moment vibrates along the Y axis (*i.e.*, the bisector of the apex angle) for the frequencies ν_1 and ν_2 , where $\nu_1 \geq \nu_2$, and along the X axis (which is perpendicular to the Y axis) for the frequency ν_3 .

In specializing to the equilateral triangle all three atoms become identical. In this case the frequency ν_1 is certainly inactive, since it corresponds to a motion in which all the atoms vibrate along the bisectors of their respective (apex) angles with the same amplitude and in the same phase with respect

⁹ E. K. Plyler and E. F. Barker, *Phys. Rev.* **38**, 1827 (1931).

¹⁰ N. Bjerrum, *Verh. d. Deut. Phys. Ges.* **16**, 640, 737 (1914).

¹¹ D. M. Dennison, *Phil. Mag.* **1**, 195 (1926).

to the center of gravity of the molecule. The two frequencies ν_2 and ν_3 become equal, thus forming degenerate states. Whether or not the frequency ν_2 would also be inactive depends upon the interaction of the electron clouds surrounding the three nuclei when they execute this normal vibration. It is conceivable that at one extreme displacement in this vibration the electrons surrounding the two lower nuclei could so repel those surrounding the upper nucleus that the center of the negative charges would lie above the center of the positive charges, thus producing a change in the electric moment of the molecule. Even if it were active it is very likely that it would be comparatively weak because of the relatively small amplitude of the oscillating electric doublet.

If ozone were this type of molecule it should be possible to correlate all the observed bands with only two fundamental frequencies, and one of these should be inactive. On the contrary the bands observed for ozone cannot be arranged in any scheme with only two fundamental frequencies unless very low frequencies are chosen and the observed bands ascribed to combinations and high multiples of them. This sort of procedure is evidently unreasonable in view of the simple relations existing between the frequencies observed for substances heretofore investigated. It takes three fundamental frequencies to account for all the ozone bands, and these three all appear to be active. This is very strong evidence against the equilateral triangle as the correct model for ozone.

Another source of evidence which is equally important is the almost complete absence of the Raman spectrum of ozone. Up to the present it has been observed that molecules possessing a highly symmetrical configuration, which results in an inactive vibrational frequency, have fairly strong Raman spectra, as in the cases of carbon dioxide and carbon tetrachloride. On the other hand it has also been found true that molecules lacking an inactive frequency, such as water, have a weak Raman spectrum.¹²

§4

The solution of the vibration problem for the isosceles triangle model has already been described. There are three different and active fundamental frequencies. The question of the overtones of these frequencies has been discussed by Dennison,⁸ who showed that in general they would all be active. If the overtone is represented by $\nu = n_1\nu_1 + n_2\nu_2 + n_3\nu_3$ the change of the electric moment is along the Y axis for even values of n_3 and along the X axis for odd values.

The shapes of the envelopes of the bands at these various vibrational frequencies will depend upon the direction of the change of the electric moment with respect to the principal axes of inertia. If in the case of ozone the apex angle is less than 60° , then the axis of least moment of inertia, A , will be along the Y axis, and the axis of middle moment of inertia, B , will be along the X axis.

¹² These results have recently been justified and explained on a theoretical basis by Placzek, *Zeits. f. Physik* 70, 84 (1931).

The axis of greatest moment of inertia, C , is perpendicular to the plane of the figure. No changes of electric moment can ever lie along this axis because no vibrations can take place outside the plane of the triangle. Thus in the general overtone $n_1\nu_1 + n_2\nu_2 + n_3\nu_3$ the change of electric moment will lie along the A axis for even values of n_3 and along the B axis for odd values.

On the other hand, if the apex angle in the case of ozone were greater than 60° the inertial axes A and B would be interchanged, and then in the general overtone the change of electric moment would be along the B axis for even values of n_3 and along the A axis for odd values.

According to Dennison⁸ the envelopes of the bands produced by vibrations of the electric moment along the least axis of inertia should show a decided zero branch, while those produced by vibrations along the middle axis of inertia should show a doublet structure.

Whatever the disposition of the axes of inertia may be in the molecule the two frequencies ν_1 and ν_2 will have the same kind of envelopes, and ν_3 will have a different kind. If only one fundamental frequency displays the doublet type of envelope, then the apex angle is less than 60° , whereas if only one of the fundamental frequencies displays a zero branch, then the apex angle is greater than 60° .

When the envelopes of the ozone bands are examined it becomes evident that they can be very nicely arranged to fit the requirements for an isosceles triangle with the apex angle less than 60° . In Table II is given a comparison

TABLE II.

Wave-lengths	ν_i	Frequencies		Type of envelope	
		observed	Calculated	Observed	Predicted
(18.9 μ)*	ν_2	—	528 cm ⁻¹	—	Z
9.67	ν_3	1033 cm ⁻¹	—	D	D
9.47	$2\nu_2$	1055	—	Z	Z
7.39	ν_1	1355	—	Z	Z
6.6†	$\nu_2 + \nu_3$	1515	{ 1561	—	D
	$3\nu_2$		{ 1584		Z
	$2\nu_3$		{ 2066		Z
4.7	$2\nu_2 + \nu_3$	2108	{ 2088	{ Z	D
	$4\nu_2$		{ 2110		Z
3.7†	$2\nu_1$	2710	2710	—	Z

* This band was not looked for, because it is in a region where the absorption due to the rocksalt windows on the cell made observations impossible.

† Reported by Ladenburg and Lehmann. The wave-lengths are not known as accurately as those of the other bands and nothing is known about the envelopes.

of the observed envelopes and those predicated for ozone on the basis of the isosceles triangle model. In the last two columns D stands for doublet type and Z for zero branch type of envelope.

The fundamental ν_1 displays a zero branch type of envelope, with very weak positive and negative branches; the same holds true for $2\nu_2$. The envelope for ν_3 is of the doublet type, while that for $2\nu_3$ is of the zero branch type, as it should be for even values of n_3 if the apex angle is less than 60° . The observed envelope for the combination $2\nu_2 + \nu_3$ is somewhat obscured by the envelopes of the overtone bands in its immediate vicinity, but the shape

of the whole envelope does not rule out the possibility of a doublet type envelope for this particular combination frequency.

The types of the envelopes of the bands observed show that ozone has the shape of an isosceles triangle with the apex angle less than 60° . This is proven by the occurrence of the zero branch type of envelope for ν_1 and $2\nu_2$. If the molecule were to be represented by an isosceles triangle with an apex angle greater than 60° , then ν_1 and $2\nu_2$ would have the doublet type of envelope and ν_3 would have the zero branch type of envelope. The preponderance of zero branch type over doublet type envelopes in the bands observed for ozone indicates that it has the shape of an isosceles triangle with the apex angle less than 60° . Except for the unknown envelopes of other combinations and overtones the observed data for ozone agree very well with the predictions for this model. The ordering of the ozone data under this scheme may not be unique, but it is a self-consistent one. Other ways of allotting the observed frequencies are possible, but they must all fulfill the requirements of the types of envelopes for the various frequencies.¹³

CONCLUSIONS

The experimental data for ozone have been critically compared with the theoretical predictions for various possible models and also with the data for certain molecules of known structure.

The combination and overtone frequencies observed in the ozone spectrum do not obey the selection rules for a linear symmetrical molecule. The envelopes of the bands and the lack of regularly spaced rotational fine structure lines are not in agreement with those to be expected of a linear unsymmetrical molecule. The equilateral triangle is very definitely ruled out because the frequencies observed for ozone do not obey the requirements that for an equilateral triangle there should be only one active fundamental frequency, and only two fundamental frequencies in all. In addition to this, ozone displays a very weak Raman spectrum, while a highly symmetrical molecule in the form of an equilateral triangle should certainly have a strong Raman spectrum.

The data for ozone do meet the requirements for the isosceles triangle model. There is the correct number of active fundamental frequencies, *viz.*, ν_1 at 1355 cm^{-1} , ν_2 at 528 cm^{-1} , and ν_3 at 1033 cm^{-1} . Overtones and combinations of these fundamental frequencies are also observed. Each fundamental shows its first overtone, and ν_2 apparently displays its second and third overtones. The assignments given the fundamental frequencies thus form a self-consistent scheme, and the calculated frequencies are in fairly good agreement with the observed frequencies. The types of envelopes, zero branch or doublet type, predicted for the fundamental frequencies and the various combinations and overtones appear in the observed bands for the proper fre-

¹³ The case of the oblique triangle has not been discussed since it appears to be so improbable on general grounds. Such a model would, however, have much the same vibrational and rotational properties as an isosceles triangle, except that the direction of change of electric moment would no longer be so simply related to the orientation of the principal axes of inertia.

quencies. On the whole, the observed data for ozone fulfill the requirements for an isosceles triangle with the apex angle less than 60° .

The writer gratefully acknowledges Professor D. M. Dennison's many helpful suggestions in the interpretation of the experimental data, and the generous cooperation of the various members of the Physics Department who made possible the completion of this work.

The Dispersion and Absorption of Helium

By J. P. VINTI

Massachusetts Institute of Technology

(Received September 29, 1932)

An investigation is made of the relative importance of singly-excited, doubly-excited, and continuous states in the dispersion and absorption spectrum of helium. The f -values of the lines due to singly-excited and doubly-excited states are calculated by using wave functions of a screening-constant type, the most important of them having been obtained by variational methods. The f -sum of the continuous spectrum is then obtained by difference, from the Kuhn-Reiche sum rule. It is shown that the role of the singly-excited states is moderate, of the doubly-excited states small, and of the continuous spectrum very large. A table is given of relative intensities in the principal series absorption spectrum. Incidentally, a variational calculation of a wave function for the doubly-excited state $(2s)(2p)^1P$ places this level $302,000\text{ cm}^{-1}$ above the limit of single ionization. The corresponding absorption line comes out about one-thirtieth as strong as the first absorption line of the principal series or about as strong as the fifth line of this series.

IT IS our purpose to investigate the relative importance of the discrete and continuous energy states of atomic helium in dispersion and absorption.

The refractive index of a gas is given by $\mu^2 = 1 + 4\pi L\alpha$, where μ is the refractive index, L the number of atoms per unit volume, and α the polarizability of the atom. The polarizability of an N -electron atom is given by an expression of the form:

$$\alpha = \frac{2}{3} \frac{e^2}{h} \sum_{k \neq 0} \frac{\nu_{k0} (|x_{0k}|^2 + |y_{0k}|^2 + |z_{0k}|^2)}{\nu_{k0}^2 - \nu^2}.$$

Here e and h have their usual meanings, ν_{k0} is the frequency difference between the excited state k and the normal state 0, ν is the frequency of the incident radiation, and ez_{0k} , e.g., is the matrix element between the states 0 and k of the z -component of electric moment, so that:

$$z_{0k} = \int \bar{\psi}_0 \left(\sum_{\mu=1}^N z_{\mu} \right) \psi_k d\tau_1 \cdots d\tau_N,$$

where ψ_0 and ψ_k are the wave functions of the state 0 and k . The summation is to be extended over all the excited states of the atom, continuous included, which have dipole combinations with the normal state.

We can most easily investigate the role of the various parts of the energy spectrum by writing the above formula for α in atomic units, expressing lengths in terms of a_0 (Bohr radius) as unit, and energies in terms of $e^2/(2a_0)$:

$$\alpha = 4a_0^3 \sum_{k \neq 0} \frac{(\frac{1}{3})(W_k - W_0)(|x_{0k}|^2 + |y_{0k}|^2 + |z_{0k}|^2)}{(W_k - W_0)^2 - W^2}.$$

Here W , is the energy in atomic units of a quantum of the incident radiation. If the applied frequency ν is not too large (not greater than that correspond-

ing to 600A), we have $W_v \leq 1.5$. For any state beyond the limit of single ionization (i.e., any doubly-excited or continuous state), $W_k \geq -4$. Then, since $W_0 = -5.81$, we have $W_k - W_0 \geq 1.81$, and $(W_k - W_0)^2 - W_v^2 \geq 1$. Thus the numerator for such a state gives an upper limit to its contribution to the dispersion formula; this numerator is called an f -value. The sum of the f -values of all the doubly-excited and continuous states thus gives an upper limit to their dispersion contribution.

The only singly-excited states which have dipole combinations with the normal state are the "principal series" $(1s)(np)^1P$. One can show that their f -sum gives a lower limit to their dispersion contribution, since for most of them (the lower and thus more important ones) the denominator is less than unity.

These f -values satisfy a simple sum rule by means of which we can estimate the role of the continuous spectrum without handling any continuous spectrum wave functions. Using atomic units, let

$$z = \sum_{\mu=1}^N z_{\mu}, \quad z_{0k} = \int \bar{\psi}_0 z \psi_k d\tau_1 \cdots d\tau_N, \text{ etc.,}$$

and

$$f_{k0} = \left(\frac{1}{3}\right)(W_k - W_0)(|x_{0k}|^2 + |y_{0k}|^2 + |z_{0k}|^2).$$

Then

$$\sum_k f_{k0} = N.$$

For atomic helium, $N=2$, so that

$$\sum_k f_{k0} = 2. \quad (1)$$

(The summation sign is used for all the states, but is understood to include an integral over the continuous spectrum.) We obtain the form pertinent to our problem by splitting the sum into the parts: f' , referring to the states $(1s)(np)^1P$; f'' , referring to doubly excited states arising from the configurations sp , pd , df , etc.;¹ and f_c , referring to the mixed and purely continuous states lumped together.

Then

$$f' + f'' + f_c = 2. \quad (2)$$

We proceed to calculate f' . Now

$$z_{n0} = \int \bar{\psi}_n (r_1 \cos \theta_1 + r_2 \cos \theta_2) \psi_0 d\tau_1 d\tau_2,$$

where ψ_0 refers to the normal state, ψ_n to the state $(1s)(np)^1P$, and the in-

¹ By the Laporte rule no other configurations have dipole combinations with the normal state.

tegration is extended over the coordinates of both electrons. For ψ_0 we use a function due to Eckart:²

$$\psi_0 = [u(\gamma 1)u(\delta 2) + u(\gamma 2)u(\delta 1)]/[2(1 + c^2)]^{1/2} \quad (3)$$

where the u 's are hydrogenic functions for $1s$, with parameters $\gamma = 2.14$ and $\delta = 1.19$ in place of $Z = 2$.

This function has the property of giving slightly too large a value for the diamagnetic susceptibility $|\chi|$; the calculation of $|\chi|$, involving as it does $(\Sigma_i r_i^2)_{00}$, weights comparatively heavily the values of the wave function for large values of r . This means that ψ_0 is likely to be too large rather than too small at large distances; any error in $|z_{n0}|^2$ due to ψ_0 is thus likely to be positive (since z_{n0} contains r_1, r_2 in the integrand). The error in ψ_0 is thus such as to make the calculated f' slightly too large, so that if in spite of this, we find a large value for f_c from the sum rule, we know that such a result is not due to error in ψ_0 .

Letting ψ_2 refer to $(1s)(2p)^1P$, we use the function of Eckart:³

$$\psi_2 = [u(\alpha 1)v(\beta 2) + u(\alpha 2)v(\beta 1)]/2^{1/2}, \quad (4)$$

where u and v are hydrogenic functions of $1s$ and $2p$, and $\alpha = 2.003, \beta = 0.965$, are parameters replacing $Z = 2$. For ψ_n we take the hint from ψ_2 and use a function with zero screening for $1s$, and unit screening for np , since the p electron is now at least two shells farther out than the s -electron:

$$\psi_n = [u(Z1)v_n(\beta 2) + u(Z2)v_n(\beta 1)]/2^{1/2}, \quad (5)$$

where u and v_n refer to the hydrogenic functions for $1s$ and np , Z now replacing α , which in ψ_2 differed negligibly from Z , and $\beta = Z - 1 = 1$. Because of this slight difference we treat z_{20} and z_{n0} separately. By integration,

$$|z_{20}|^2 = [A(\delta)B(\gamma) + A(\gamma)B(\delta)]^2/(1 + c^2),$$

where

$$c^2 = 64(\gamma\delta)^3(\gamma + \delta)^{-6} = 0.775$$

$$A(\epsilon) = 4(2\beta^3\epsilon^3)^{1/2}(\epsilon + \beta/2)^{-5}$$

$$B(\epsilon) = 8(\alpha\epsilon)^{3/2}(\alpha + \epsilon)^{-3}.$$

Inserting the values of α, β, γ , and δ , $|z_{20}|^2 = 0.224$. Similarly, for $n > 2$:

$$|z_{n0}|^2 = [E(\delta)F(\gamma) + E(\gamma)F(\delta)]^2/1.775 \quad (6)$$

where

$$E(\epsilon) = \int u(Z1)u(\epsilon 1)d\tau_1 = 8(Z\epsilon)^{3/2}(Z + \epsilon)^{-3}$$

$$F(\epsilon) = \int r_1 \cos \theta_1 u(\epsilon 1)\bar{v}(\beta 1)d\tau_1$$

² C. Eckart, Phys. Rev. **36**, 883, Eq. (17) (1930).

³ C. Eckart, Phys. Rev. **36**, 883, Eq. (18) (1930).

$$= 16\beta^{-4}(\epsilon^3\beta^3/3)^{1/2}(2\epsilon/\beta-1)n^3[(n+1)n(n-1)]^{1/2} \\ (\epsilon n/\beta-1)^{n-3}(\epsilon n/\beta+1)^{-(n+3)}. \quad (7)$$

By using $E(\gamma)=0.998$, $E(\delta)=0.905$, we get the Table I:

TABLE I. (Energies and lengths are in atomic units.)

n	$ z_{n0} ^2$	$(W_n - W_0)$ obs.	$f_{n0} = (W_n - W_0) z_{n0} ^2$
2	0.224	1.5593	0.349
3	0.0547	1.6966	0.0928
4	0.0204	1.7448	0.0357
5	0.0100	1.7671	0.0177
6	0.00588	1.7792	0.0105
7	0.00351	1.7866	0.0063

We find $\sum_{n=2}^7 f_{n0} = 0.512$, and we get an upper limit to $f_{8,0} + f_{9,0} + f_{10,0}$ by taking $3f_{7,0} = 3 \times 0.0063 = 0.0189$. Thus $\sum_{n=2}^{10} f_{n0} = 0.53$, and by using asymptotic values of $W_n - W_0$ and $F(\epsilon, n)$ for large n , we find that the sum from 11 to ∞ is of the order 0.0095. Thus essentially,

$$f' \equiv \sum_{n=2}^{\infty} f_{n0} = 0.54. \quad (8)$$

Since $h\nu_{0n}B_{0n}$ (where B_{0n} is the usual probability of induced transition) is proportional to f_{0n} , the relative intensities of the lines of the absorption spectrum are given by the last column of Table I. Taking the intensity of the first absorption line $(1s)^2\ ^1S \rightarrow (1s)(2p)^1P$ arbitrarily as 100, the relative intensities of absorption are given by Table II.

TABLE II. Relative intensities of absorption per unit intensity of incident radiation.

2^1P	3^1P	4^1P	5^1P	6^1P	7^1P
100	26.6	10.2	5.07	3.01	1.80

Table II can be continued by means of formulas (6) and (7). For $n > 10$, the asymptotic calculations previously referred to show that $|z_{0n}|^2$ and thus f_{0n} and the entries in Table II fall off inversely as n^3 .

We now consider the doubly-excited states. From the Laporte rule,⁴ or directly from the angular parts of the wave functions, we see that such states as $(2s)^2\ ^1S$, etc., do not combine with the normal state, and that the only doubly-excited states which do so are the singlet states arising from the configurations $(ms)(np)$, $(mp)(nd)$, $(md)(nf)$, etc. In order to obtain an idea of the order of magnitude of the transition probabilities involved, we next investigate in detail that state from this group which is expected to be the most important, namely $(2s)(2p)^1P$.

If u_2 and v are hydrogenic functions of $2s$ and $2p$, respectively, the "unperturbed" wave function of $(2s)(2p)^1P$ is:

$$[u_2(Z1)v(Z2) + u_2(Z2)v(Z1)]/2^{1/2}.$$

⁴ L. Pauling and S. Goudsmit, *Structure of Line Spectra*, McGraw-Hill, 1930, p. 94.

Suppose we should introduce a parameter β in place of Z in the function v , leaving u_2 unchanged. Then

$$\phi = [u_2(Z1)v(\beta 2) + u_2(Z2)v(\beta 1)]/2^{1/2}. \quad (9)$$

Now Eckart's function for $(1s)(2p)^1P$, which is presumably good because of the close check which it gives for the energy, has the form (4), where α is very closely equal to Z , and $\beta = 0.965$. For $(1s)(np)^1P$, where $n > 2$, we have used (5). We see then that the above trial function ϕ for $(2s)(2p)^1P$ is orthogonal to the wave functions of all the states $(1s)(np)^1P$; this statement follows from the presence of the function $u_2(Z)$ without parameters. Because of the angle functions it is orthogonal to the wave functions of all singly-excited singlet states not included in $(1s)(np)^1P$, and to the wave function of $(2s)^2^1S$. Finally, because of its symmetry in electrons 1 and 2, it is orthogonal to the functions of all the triplet states. It is thus a function with the proper symmetry to represent $(2s)(2p)^1P$, possessing the property of orthogonality to the wave functions of all lower states. The minimum of the integral $E \equiv \int \phi H \phi d\tau$ with respect to the parameter β is thus expected to furnish a value of the energy better than the usual first approximation, and higher than the true energy.⁵

This trial function leads to the variational integral: $-E = Z^2/4 + [2(Z - \sigma) - \beta]\beta/4$, where $\sigma = 1 + J$, and $I = (4/\beta) \int (u^2(Z1)|v(\beta 2)|^2/r_{12})d\tau_1d\tau_2$

$$\begin{aligned} \text{or } I = & \frac{x}{(1+x)^5} \left[1 + \frac{5x}{1+x} - \frac{15x^2}{(1+x)^2} + \frac{105x^3}{(1+x)^3} \right] \\ & + \frac{x^3}{(1+x)^3} \left[1 + \frac{3(1-x)}{1+x} + \frac{3(x^2 - 4x + 2)}{(1+x)^2} \right. \\ & \left. + \frac{5(3x^2 - 6x + 2)}{(1+x)^3} + \frac{15x(3x - 4)}{(1+x)^4} + \frac{105x^2}{(1+x)^5} \right] \end{aligned}$$

$$\begin{aligned} J = & (4/\beta) \int u(Z1)u(Z2)v(\beta 1)\bar{v}(\beta 2)/r_{12}d\tau_1d\tau_2 \\ = & \frac{4x^3}{3(1+x)^7} \left[14 - \frac{98x}{1+x} + \frac{185x^3}{(1+x)^2} \right], \quad x = Z/\beta. \end{aligned}$$

The minimum of E occurs at $\beta = 1.58$ and has the value -1.25 atomic units, thus placing the level $3.02 \times 10^5 \text{ cm}^{-1}$ above the limit of single ionization. This value can be checked against the value of 2^1P extrapolated from BII. The nucleus of boron plus its K shell we take as equivalent to a nucleus of charge Z^* , and treat BII as a helium-like atom of nuclear charge Z^* . Expressing the term value in atomic units as $(Z^* - s)^2/2^2$, the assumption of perfect shielding by the K shell leads to $Z^* = 3$ and $s = 0.90$; the assumption of 85 percent shielding by each K electron (from Slater's rules) leads to $Z^* = 3.30$ and $s = 1.20$. These values of s applied to $(2s)(2p)^1P$ of helium lead

⁵ C. Eckart, Phys. Rev. 36, 880, 881 (1930).

to -1.30 and -1.16 , respectively, for the total energy, so that our value -1.25 lies in the correct range.

A direct application of Slater's⁶ shielding rules to $(2s) (2p)$ of helium gives the value -1.36 . Majorana⁷ also has computed this energy, using a variational method due to Fock,⁸ and obtains the value -1.31 ; this value, however, is apt to be lower than the correct value, because the variational method of Fock does not make the trial function orthogonal to the wave functions of the lower states.

With our wave function for $j \equiv (2s) (2p)^1P$ and Eq. (1) for the normal state 0, we find:

$$|z_{0j}|^2 = [M(\delta)N(\gamma) + M(\gamma)N(\delta)]^2/1.775,$$

where

$$M(\epsilon) = 4(2\beta^5\epsilon^3)^{1/2}(\epsilon + \beta/2)^{-5}$$

$$N(\epsilon) = 2(2Z^3\epsilon^3)^{1/2}(\epsilon - Z)(\epsilon + Z/2)^{-4}.$$

By inserting $\gamma = 2.14$, $\delta = 1.19$, $\beta = 1.58$, $Z = 2$, we find that $|z_{0j}|^2 = 0.00251$. Since $W_j - W_0 = 4.56$, we obtain $f_{0j} = 4.56 \times 0.00251 = 0.0114$. By comparing with Table I, we see that the absorption line due to $(2s) (2p)^1P$ comes out about one-thirtieth as strong as the first absorption line of the principal series, or about as strong as the fifth line of the principal series.

We have now the problem of finding a wave function valid in the general case $(ms) (np)^1P$, where $m \geq 2$, $n \geq 2$, computing the matrix elements, and summing f_{0j} over the whole square array of such states. We picture the array as follows:

$$\begin{array}{ccccccc} (2s)(2p) & (2s)(3p) & \cdots & (2s)(10p) & \cdots & (2s)(np) & \cdots \\ (3s)(2p) & (3s)(3p) & \cdots & (3s)(10p) & \cdots & (3s)(np) & \cdots \\ \cdots & \cdots & \cdots & \cdots & \cdots & \cdots & \cdots \\ (10s)(2p) & \cdots & \cdots & (10s)(10p) & \cdots & (10s)(np) & \cdots \\ \cdots & \cdots & \cdots & \cdots & \cdots & \cdots & \cdots \\ (ms)(2p) & \cdots & \cdots & (ms)(10p) & \cdots & (ms)(np) & \cdots \\ \cdots & \cdots & \cdots & \cdots & \cdots & \cdots & \cdots \end{array}$$

We must consider separately the upper right half, the lower left half, and the main diagonal of this array. To treat the upper right half, we can write the unperturbed wave function for $(ms) (np)^1P$:

$$[u_{ms}(Z1)v_{np}(\beta2) + u_{ms}(Z2)v_{np}(\beta1)]/2^{1/2} \quad (10)$$

replacing in v_{np} , however, Z by the parameter $\beta = Z - 1 = 1$. That is, we consider the ms electron to be a perfect shield when $n > m$; this procedure is suggested by the similar one for $(1s) (np)^1P$.

⁶ J. C. Slater, Phys. Rev. **36**, 57 (1930).

⁷ E. Majorana, Nuovo Cimento VIII, (2) 78 (1931).

⁸ V. Fock, Zeits. f. Physik **63**, 855 (1930).

To treat the main diagonal $(ns) (np)^1P$, we use the same form of wave function, taking for β the value 1.58 found by actual calculation in the case $(2s) (2p)^1P$ (justification later).

The lower left half is not amenable to treatment in this way, since we cannot expect a p electron to be as complete a shield as an s electron, because of the non-spherical symmetry. Since, however, we have no reason to believe that its f -sum would be greater than that of the upper right half, we take its f -sum equal to that of the upper right half. This procedure gives us an upper limit, which is all that we need.

The total f -sum of all the doubly-excited sp states can then be expressed as $2R + D$, where R is the f -sum of the upper right half and D that of the main diagonal.

To obtain R , we first calculate $|z_{0j}|^2$ between the normal state 0 and the excited state j , using Eq. (1) for ψ_0 and Eq. (9) for ψ_j . We find:

$$|z_{0j}|^2 = [F(\delta)G(\gamma) + F(\gamma)G(\delta)]^2/1.775, \quad (11)$$

where $F(\epsilon)$ is given by Eq. (7) with $\beta = 1$, and

$$G(\epsilon) = 8(m/Z)^3(Z\epsilon)^{3/2}m^{-1/2}[(\epsilon m/Z - 1)/(\epsilon m/Z + 1)]^{m-2}(\epsilon/Z - 1)(1 + \epsilon m/Z)^{-4}. \quad (12)$$

By using the asymptotic values of $F(\epsilon)$ and $G(\epsilon)$ for large m and n , and replacing the double summation by a double integral which can be shown to be larger, one can show that $\sum_{\infty} \sum_{n>m>10f_{0j}}$ is of the order 10^{-7} , so that the infinite "tail" of R is negligible.

R thus consists essentially of the sum of the f -values of the finite half-array:

$$\begin{array}{ccccccc} (2s)(3p) & (2s)(4p) & \cdots & \cdots & \cdots & (2s)(10p) \\ & (3s)(4p) & \cdots & \cdots & \cdots & (3s)(10p) \\ & (4s)(5p) & \cdots & \cdots & \cdots & (4s)(10p) \\ & & \cdots & \cdots & \cdots & \\ & & & \cdots & \cdots & \\ & & & & \cdots & (9s)(10p) \end{array}$$

Using formulas (11) and (12), we obtain for the sum of $|z_{0j}|^2$ for the first row the value $0.000568/1.775$, and since $W_j - W_0$ is of the order $5.807 - 1 - 1/n^2$, we have $W_j - W_0 < 4.807$; thus the f -sum of the first row is less than $4.807 \times 0.000568/1.775$ or 0.00154 . There are eight rows in all, each row containing one less member than the preceding, and each member lies higher in the diagram of energy levels than the one immediately above, so that its f -value must be less. We thus arrive at an upper limit for R by multiplying 0.00154 by the factor 8, so that $R < 0.0123$, and $2R < 0.0246$. That is, 0.0246 is an upper limit to the f -sum of all the doubly-excited sp states in which the two electrons have different principal quantum numbers.

We now turn to D , the diagonal f -sum. We must obtain a wave function for $(ns) (np)^1P$. We have already found a function for $(2s) (2p)^1P$ of the form (9), where $\beta = 1.58$. As the best improvement that we can make over the

unperturbed zeroth approximation (without encountering prohibitive labor), we can write down such a function for $(ns) (np)^1P$, where u and v now refer to the states ns and np ; we take $\beta = 1.58$. The argument for such a procedure is this: Such a function with $\beta = 2$ is the zeroth approximation, in which the interaction of the electrons is entirely neglected; we know, however, that the deviation from "hydrogenness" can be expressed in most cases sufficiently well by considering that the interaction of the electrons results in a screening effect. If the screening were perfect, we should have $\beta = 1$; no screening means $\beta = 2$. β thus lies between 1 and 2, and since it equals 1.58 for $n = 2$, 1.58 is our only possible estimate for the general case $(ns) (np)^1P$.

With this function, the squared matrix element $|z_{n0}|^2$ is given by Eq. (11), where now $G(\epsilon)$ is given by Eq. (12) with m replaced by n , and $F(\epsilon)$ is given by Eq. (7) with $\beta = 1.58$.

By using the asymptotic values of $F(\epsilon)$ and $G(\epsilon)$ for large n , we can then show that the diagonal f -sum from $n = 11$ to $n = \infty$ is less than an integral of the order 2×10^{-7} , so that it is negligible.

To obtain the diagonal f -sum from $n = 3$ to $n = 10$, we use the formula just found for $|z_{n0}|^2$ and estimate W_n by means of Slater's shielding rules, obtaining $W_n \sim -2(Z - 0.35)^2/n^2 = -5.44/n^2$. Thus $W_n - W_0 \sim 5.807 - 5.44/n^2$. The f -value of $(3s) (3p)^1P$ turns out to be 7.55×10^{-4} , and we can obtain an upper limit to the f -sum from $n = 3$ to $n = 10$ by applying to this the factor 8; this limit is 0.006. On adding 0.0114, the f -value of $(2s) (2p)^1P$, the diagonal f -sum D becomes ≤ 0.017 . Since

$$2R \leq 0.0025, \text{ and } D \leq 0.017, \text{ we have } f'' \equiv 2R + D \leq 0.042. \quad (13)$$

Using Eqs. (2), (8) and (13), we have:

$$f_c = 2 - 0.54 - 0.04 = 1.42. \quad (14)$$

We wish now to investigate the question as to whether allowance for all the other doubly-excited states which combine with the normal state would affect appreciably the value of f'' . We have to consider the states $(ml_1) (nl_2)^1P$, where $1_1 + 1_2$ is odd (by the Laporte rule). In our screening constant functions, the function of $(ml_1) (nl_2)$ differs from that of $(ms) (np)^1P$ only in the angle functions. Since the latter contribute a factor to $|z_{n0}|^2$ which is less than unity, we can obtain an upper limit for each $(ml_1) (nl_2)$ by taking it to be equal to that of $(ms) (np)$. $W_n - W_0$ for a state $(ml_1) (nl_2)$ is of the same order as for the state $(ms) (np)$, since the principal quantum numbers play the principal role in the determination of the energy. We can thus obtain an upper limit to the f -contribution of a given part of the array which gives f'' , when all these other states are included, by applying to the f -value of each $(ms) (np)$ a factor g_{mn} denoting the number of configurations which have values of m and n in common. Neglect of the Laporte rule leads to $g_{mn} \leq mn$; recognition of the rule leads to a smaller value. If, accordingly, a portion of f which was negligible before is found still to be so when the factor mn is applied to each part, we know that it will still be negligible when the Laporte rule is used. In this way it is found that the infinite tails that we met before

are still negligible. On applying the factor mn to the other parts, we find that $f'' \leq 0.043$. Thus Eqs. (13) and (14) remain essentially unchanged by this correction.

It is interesting to compare these figures with some obtained by Margenau.⁹ He finds by a semi-empirical method $f' = 0.18$, and $f'' + f_0 = 1.82$. From the large value of the latter he concludes that the neglect of "double jumps" is responsible for the inaccurate value found in the simple theory of London for van der Waals forces in helium. The present work makes it appear very probable that the inclusion of states beyond the ordinary series limit is essential, but it indicates that of these states, the continuous ones are by far the most important; namely, that part of the continuous spectrum which lies at the limit of the principal series. Stated in another way, the principal series lines in the absorption spectrum of helium are of moderate intensity, the lines due to jumps from the normal state to doubly-excited states are very weak, and the continuous absorption spectrum is very strong. These results are certainly in qualitative agreement with experiment, as evidenced by the measurements of Herzfeld and Wolf on the dispersion of helium.¹⁰ Quantitative comparison can be made only after the absorption spectrum, which lies in the far ultraviolet (around 700A) has been photographed and measured.

The author wishes to acknowledge his indebtedness to Professors J. C. Slater and P. M. Morse for interesting discussions and suggestions during the course of this work.

⁹ H. Margenau, Phys. Rev. 37, 1425 (1931).

¹⁰ K. F. Herzfeld and K. L. Wolf, Ann. d. Physik 76, 71 (1925); 76, 567 (1925).

Radiation from Slow Electrons

By LEO NEDELSKY
University of California

(Received October 4, 1932)

We have developed expressions describing radiation emitted by an electron in the field of a neutral atom, using as a model for the latter a point charge Ze surrounded by a spherical shell of radius a carrying a charge $-Ze$. In the introduction we formulate the physical foundations of the problem. In section I we set up expressions for the matrix components of acceleration and give methods for evaluating the integrals involved. In section II we use results of section I to compute the intensity of radiation J , and the polarization P . For low velocity electrons ($Va^2 < 1$, where V is the energy in volt-electrons and a is in angstrom units) we give simple formulas for both J , and P . For heavier elements J , is independent of Z and is nearly proportional to Va^2 , while for lighter elements J , as a function of Za exhibits a series of striking maxima and minima. For higher velocities we give our results for the most part graphically. We find that the criterion of applicability of bare nucleus model to neutral atoms is $(Z^2/2v)^2 \ll 1$. Except for high voltages however Z should be less than the nuclear charge of the actual atom. We also show that the radiation from protons in the field of our model is simply related to the radiation from electrons in the field of an unscreened nucleus. In section III we discuss how Z and a should be chosen in order that our model, or a nuclear model, may represent an actual atom, and make comparison with experiment finding agreement in the order of magnitude. The last part of the paper is a summary containing all the formulas of importance.

INTRODUCTION

THE first quantum-theoretical treatment of the problem of continuous radiation emitted by an accelerated electron was done by Kramers.¹ On the basis of the correspondence principle Kramers computed the intensity of radiation from an electron which passes through the coulomb field of a point charge Ze . He obtained the following well-known formula

$$J_{kr}' = J_{kr} g'(\gamma_0)$$

with

$$J_{kr} = 32\pi^2 Z^2 e^6 / 3^{3/2} c^3 m^2 v^2 \text{ and } \gamma_0 = 2\pi v Ze^2 / mv^3 \quad (1)$$

where v is the initial velocity of the electron. The value of the factor $g'(\gamma_0)$ does not differ greatly from unity except for small values of γ_0 where it becomes logarithmically infinite. Kramer extended this result to the case of a thick target by using the Thomson-Whiddington law for the loss of velocity of a charged particle in its passage through matter. The resulting expression for J has been found in very good agreement with experimental values for Bremsstrahlung generated by electrons with energies corresponding to several kilovolts.

¹ Kramers, *Phil. Mag.* **46**, 836 (1923).

The more recent quantum-mechanical investigations of the same problem by Oppenheimer,² Gaunt,³ Sugiura,⁴ and finally by Sommerfeld,⁵ confirmed substantially Kramers' formula. The agreement between the results obtained by the two methods has been shown by Gaunt to be especially good for the cases in which the energy of the electrons is not too great. However, even for fast electrons, Oppenheimer and Sommerfeld obtained formulas which confirm Kramers' results in the region of relatively soft radiation.

Agreement between the results predicted by Eq. (1) and the experimental values in the x-ray region is indicative of the fact that for the range of voltages there used the neutral atoms of the target are sufficiently well represented by the nuclear model. This representation fails, however, in the following two cases: (1) low voltages; (2) long wave-length end of the spectrum. In the first place, we notice that the total amount of radiation

$$R = \int_0^{\nu_0} J_\nu d\nu$$

is independent of the voltage and therefore remains finite and large as the voltage goes to zero. In the second place, the intensity of radiation is infinite for vanishing frequencies; i.e., $J_\nu \rightarrow \infty$ as $\nu \rightarrow 0$.

Both the finiteness of the total amount of radiation for zero voltages and the infinite value of the intensity for zero frequency are explainable by the fact that the field of an unscreened nucleus falls off very slowly. We therefore thought it desirable to investigate the effect on the intensity and on the amount of radiation of the screening by the electrons of the atom. We shall give later a criterion for the approximate validity of calculations based on the nuclear model; but we know on physical grounds that screening becomes important chiefly for slow electrons. The case of fast electrons and low frequencies is of no physical interest since the soft radiation emitted is of finite total intensity, hard to observe and of small practical importance.

Of several simple approximate models of the atom we have chosen that of a positive point charge surrounded by a negatively charged spherical shell, the whole system being neutral. We have also made a few computations with a model having two charged concentric shells and obtained results of the same order of magnitude as those for the single shell model. We believe that this qualitative agreement indicates that our model with its sharply defined boundaries is not unsuitable for representing an actual atom.

I

We first consider a system of an electron and an atom—in our case an electron moving in the screened field of force of a nucleus—and find the stationary states of this system with the neglect of radiative forces. Transitions between these states will occur in which the energy of the system diminishes

² Oppenheimer, *Zeits. f. Physik* **41**, 268 (1927); **55**, 725 (1929).

³ Gaunt, *Proc. Roy. Soc. A* **126**, 654 (1930).

⁴ Sugiura, *Phys. Rev.* **34**, 858 (1929).

⁵ Sommerfeld, *Ann. d. Physik* **11**, 257 (1931).

by an amount $E - E'$ and appears in the form of radiation of frequency $\nu = (E - E')/h$. The intensity per unit frequency range of this radiation is given by the well-known formula

$$J_\nu = (4e^2/3c^3) |\alpha_{E,E'}|^2$$

where $\alpha_{E,E'}$ is the matrix component of acceleration of the radiating electron corresponding to the transition $E \rightarrow E'$. This classical formula may of course be justified quantum-mechanically on Dirac's radiation theory. In order to find $\alpha_{E,E'}$ we must know the wave functions corresponding to the initial and to the final states of the system. We shall suppose the former to consist of a uniform stream of electrons incident on the atom together with electrons moving radially away from the atom with velocities equal to those of the incident beam. Since with our model of the atom but a few discrete states are allowable we shall carry out calculations for the continuous radiation only. Then to a transition involving emission of radiation of frequency ν we have an infinite multitude of possible final states corresponding to various directions of ejection of the electron. Various choices of orthogonal functions to represent the final states have been made by different authors. In our case we shall choose those final states which are characterized by the values of the energy, the angular momentum, and the component of the angular momentum in the direction of the incident beam, i.e., by the quantum numbers n , l , and m . These final states present themselves when we separate the wave equation in polar coordinates.

We have chosen polar coordinates because due to the spherical symmetry of our model it is only in these coordinates that the boundary conditions are simple. A further advantage of this choice can be seen as follows. In order to obtain the total transition probability of emission of radiation of a given frequency we must perform a summation over l and m . Now, classically, an electron possessing an angular momentum greater than the product of its linear momentum and the radius of the screening shell would not enter the field of our model and therefore would not radiate. By analogy, we should expect that in quantum mechanics most of the radiation from a slow electron would be produced in transitions between states characterized by small values of l , and that the sum over l would therefore be strongly convergent.

1-1. Wave functions

The wave functions are the solutions of the Schrödinger equation

$$\Delta\psi + (8\pi^2m/h^2)(E - V)\psi = 0. \quad (2)$$

If we call the screening radius, i.e., the radius of the negatively charged shell, a , we must take for our potential function

$$V = Ze^2/a - Ze^2/r \text{ for } r \leq a, \quad (3a)$$

$$V = 0 \quad \text{for } r \geq a. \quad (3b)$$

In polar coordinates the Eq. (2) is separable, and the normalized solution can be written in the form

$$\Psi = \xi_l^m P_l^m(\theta, \phi) u(E, l, r) \quad (4)$$

where

$$P_l^m(\theta, \phi) = (l-m)! \sin^m \theta \left(\frac{d}{d \cos \theta} \right)^{l+m} \frac{(\cos^2 \theta - 1)^l}{2^l l!} e^{im\phi}$$

$$(\xi_l^m)^{-2} = \frac{4\pi}{2l+1} (l-m)! (l+m)!$$

ξ_l^m is the normalizing factor for the angular function P_l^m . $u(E, l, r)$ is the normalized radial function; for the two cases (3a) and (3b) it is known to be

$$\begin{aligned} u(E, l, r) = \psi(n, l, r) &= 4(mb/h)^{1/2} |\delta_l| x^l e^{-x/2} F(\alpha, \rho, x) \\ &= 4(mb/h)^{1/2} |\delta_l| (M_{n,l}(x)/x) \end{aligned} \quad (r \leq a) \quad (4a)$$

$$u(E, l, r) = \phi(b, l, r) = (|N|/(br)^{1/2}) \{J_{l+1/2}(br) + \beta_l J_{-l-1/2}(br)\} \quad (r \geq a) \quad (4b)$$

with the following notation.

$$\left. \begin{aligned} J_p(br) &\text{ is the Bessel function of the order } p \\ F(\alpha, \rho, x) &\text{ is the confluent hypergeometric function}^6 \\ \alpha &= l+1-n \quad k = (2\pi/h)[2m(Ze^2/a - E)]^{1/2} \\ \rho &= 2l+2 \quad b = (2\pi/h)mv \\ x &= 2kr \quad n = 4\pi^2 mZe^2/h^2 k \end{aligned} \right\} \quad (5)$$

$|N|$, $|\delta_l|$ and β_l are constants which are to be determined by the requirement that the radial function $u(E, l, r)$ be normalized with respect to the frequency E/h and be continuous and possess continuous derivatives at the boundary $r=a$.

Following Oppenheimer we normalize $u(E, l, r)$ by the condition

$$\int_0^\infty r^2 dr \left\{ u^*(E', l, r) \int_E^{E+\Delta E} u(E, l, r) dE/h \right\} \rightarrow 1 \text{ as } \Delta E \rightarrow 0$$

$$\text{and } E < E' < E + \Delta E.$$

The integral with respect to r , if taken over a finite range, vanishes as $\Delta E \rightarrow 0$. We shall therefore use the asymptotic expansion of $\phi(b, l, r)$ in place of $u(E, l, r)$. This condition determines the value of N

$$|N|^2 = 4\pi^2 mb/h(1 + \beta_l^2). \quad (6)$$

We determine the remaining two constant δ_l and β_l by imposing the boundary conditions

$$\left. \begin{aligned} \phi(b, l, a) &= \psi(n, l, a) \\ (d/dr)\phi(b, l, a) &= (d/dr)\psi(n, l, a) \end{aligned} \right\}. \quad (7)$$

We thus obtain

⁶ A very complete account of the properties of this function is given by Barnes, Cambr. Phil. Soc. Trans. 20, 253 (1907). He uses the notation ${}_1F_1(\alpha, \rho, x)$.

$$\left. \begin{aligned} \beta_l &= \frac{y^{1/2} J_{l+1/2}(y) M'_{n,l}(z) - (y/z) M_{n,l}(z) (y^{1/2} J_{l+1/2}(y))'}{(y/z) M_{n,l}(z) (y^{1/2} J_{-l-1/2}(y))' - y^{1/2} J_{-l-1/2}(y) M'_{n,l}(z)} \\ \delta_l &= (-1)^{l+1} [M'_{n,l}(z) H_l(y) - (y/z) M_{n,l}(z) H'_l(y)] \end{aligned} \right\} \quad (8)$$

where⁷

$$\begin{aligned} H_l(y) &= \{ y^{1/2} e^{(l+1/2)\pi i} J_{l+1/2}(y) - J_{-l-1/2}(y) \} \\ &= \left(\frac{2}{\pi} \right)^{1/2} e^{-iy} \sum_{\nu=0}^l \frac{(-i)^{l+\nu} (l+\nu)!}{\nu! (l-\nu)! (2y)^\nu} \end{aligned} \quad (9)$$

$$y = ba \text{ and } \tilde{z} = 2ka.$$

1-2. Form of solution

We shall now proceed to form the wave functions corresponding to the initial and to the final states of our system. The wave functions for the final states are given by the complete orthogonal normalized set (4). According to our plan we wish the wave function for the initial state to represent a uniform stream of electrons together with a stream moving radially away from the atom with velocity equal to that of the incident beam. Following Gordon⁸ we take as the wave function for the initial state

$$\Phi_0 = \left(\frac{\pi}{2v} \right)^{1/2} \sum_{l=0}^{\infty} i^l (2l+1) P_l(\cos \theta) \alpha_l \left(\frac{J_{l+1/2}(br)}{(br)^{1/2}} + \beta_l \frac{J_{-l-1/2}(br)}{(br)^{1/2}} \right) \quad (r \geq a). \quad (10)$$

α_l is the normalizing factor to be used for determining the intensity of the electronic beam. It can be found in the following way. At large distances from the atom Φ_0 should be a plane wave; its amplitude is determined by the requirement that it represent a stream of one electron crossing unit area per unit time. The expression for such a plane wave is known to be

$$(\pi/2v)^{1/2} \sum_{l=v}^{\infty} i^l (2l+1) P_l(\cos \theta) [J_{l+1/2}(br)/(br)^{1/2}]. \quad (11)$$

Asymptotically we have

$$\begin{aligned} \frac{J_{l+1/2}(br)}{(br)^{1/2}} &= \left(\frac{2}{\pi} \right)^{1/2} \frac{1}{br} \{ e^{-\pi i(l+1)/2} e^{ibr} + e^{\pi i(l+1)/2} e^{-ibr} \} \\ \frac{J_{-l-1/2}(br)}{(br)^{1/2}} &= \left(\frac{2}{\pi} \right)^{1/2} \frac{1}{br} \{ e^{\pi i l/2} e^{ibr} + e^{-\pi i l/2} e^{-ibr} \}. \end{aligned}$$

Substituting these values in the expressions for Φ_0 (10) and for the plane wave (11) and equating the coefficients of e^{-ibr}/br (representing the ingoing wave) we arrive at the desired result of having a plane wave of the correct amplitude as a part of the wave function for the initial state. We thus obtain

⁷ $H_l(y) = i \sin(l + \frac{1}{2})\pi \cdot y^{1/2} H_{l+1/2}^{(2)}(y)$, where $H_{l+1/2}^{(2)}(y)$ is Hankel's function of the second kind. See Jahnke-Emde, *Funktionstafeln*, p. 95.

⁸ Gordon, *Zeits. f. Physik* **48**, 180 (1928).

$$\alpha_l = [1 + \beta_l e^{\pi i(l+1/2)}]^{-1}. \quad (12)$$

The remainder of Φ_0 , namely the terms containing e^{ibr}/br , when we have subtracted from it the similar terms of the plane wave (11) can be shown for any field of force which vanishes faster than $1/r^2$ as $r \rightarrow \infty$, to give a spherical scattered wave.

To obtain the wave function for the initial state for $r < a$ we apply the boundary conditions (7) to (10). Our result is

$$\Psi_0 = (2/\pi v)^{1/2} \sum_{l=0}^{\infty} i^l (2l+1) P_l(\cos \theta) \delta_l \frac{M_{n,l}(x)}{x} \quad (r \leq a). \quad (13)$$

1-3. Matrix components of acceleration

The matrix component of acceleration corresponding to the transition

$$E \rightarrow E' \quad l \rightarrow l' \quad m \rightarrow m'$$

is defined by the integral

$$(E, l, m | \alpha | E', l', m') = \int \Psi^*(E', l', m', r, \theta, \phi) \alpha \Psi(E, l, m, r, \theta, \phi) d\tau \quad (14)$$

the integration being over all space. α is the vector acceleration which in our case is given by

$$\left. \begin{aligned} \alpha &= - (ze^2/r^2)(1/m)j & (r < a) \\ \alpha &= 0 & (r > a) \end{aligned} \right\} \quad (15)$$

where j is a unit vector with components $(\sin \theta \cos \phi, \sin \theta \sin \phi, \cos \theta)$. Consequently, the integration with respect to r is from 0 to a . We notice further that the initial state of our system (13) is characterized by a single parameter n, l being absent, and m being equal to zero. The final state (4), on the other hand, is specified by n', l', m' . We shall accordingly denote the matrix component of acceleration corresponding to the transition from the initial to the final state by $(n | \alpha | n' l' m')$. We find its value by substituting for $\Psi(Elm r \theta \phi)$ and $\Psi(E'l'm' r \theta \phi)$ in (14) the wave functions given by (13) and (4), respectively, and for α expression (15).

$$(n | \alpha | n' l' m') = - \frac{4ze^2}{\hbar k} \left(\frac{v'}{v} \right)^{1/2} \sum_{l=0}^{\infty} i^l (2l+1) \delta_l | \delta_{l'} | (l0 | j | l' m') I_{l,l'}(n, n') \quad (16)$$

with the abbreviations

$$(l0 | j | l' m') = \int_0^\pi \int_0^{2\pi} \xi_{l', m'}^* P_{l', m'}^* j P_l \sin \theta d\theta d\phi \quad (17)$$

$$I_{l,l'}(n, n') = \int_0^a \frac{M_{n', l'}^*(x') M_{n, l}(x)}{x^2} dx. \quad (18)$$

Finally, in order to obtain the total transition probability corresponding to the emission of radiation of a given frequency ν , i.e., corresponding to a

transition in which only the initial and the final energies are specified, we must square the matrix components (16) and sum over all the possible values of l' and m' . We thus obtain

$$J_\nu = (4e^2/3c^3) |\alpha_{n,n'}|^2 \text{ where } |\alpha_{n,n'}|^2 = \sum_{l'} \sum_{m'} |(n|\alpha|n'l'm')|^2. \quad (19)$$

1-4. Evaluation of $(l_0|j|l'm')$ and summation with respect to m'

We first observe that the integrals (17) vanish unless

$$l = l' \pm 1 \quad m' = \pm 1 \text{ or } 0. \quad (20)$$

Consequently the summation in (16) reduces to two terms $l = l' \pm 1$.

The transition corresponding to $m' = 0$ gives rise to radiation with its electric vector polarized in the direction of the incident beam of electrons; we shall call the intensity of this radiation J_{\parallel} . The other two transitions, i.e., to $m' = \pm 1$ give rise to radiation polarized in the plane at right angles to the direction of the incident beam; we shall denote the corresponding intensity by J_{\perp} . We thus have

$$\begin{aligned} J_{\parallel} &= (4e^2/3c^3) \sum_{l'} |(n|\alpha|n', l', 0)|^2 \\ J_{\perp} &= (4e^2/3c^3) \sum_{l'} \sum_{m'=\pm 1} |(n|\alpha|n', l', m')|^2. \end{aligned} \quad (21)$$

We shall define the degree of polarization of the emitted radiation as observed in the direction at right angles to the incident beam by the usual formula

$$P = (J_{\parallel} - \frac{1}{2}J_{\perp})/(J_{\parallel} + \frac{1}{2}J_{\perp}). \quad (22)$$

When the selection rules (20) are satisfied the integration in (17) can be carried out giving the following easily verifiable results

$$\begin{aligned} |(l-1, 0|j|l, 0)|^2 &= 4\pi l^2/(2l+1)(2l-1)^2 \\ |(l-1, 0|j|l, \pm 1)|^2 &= 2\pi l(l+1)/(2l+1)(2l-1)^2 \\ |(l+1, 0|j|l, 0)|^2 &= 4\pi(l+1)^2/(2l+1)(2l+3)^2 \\ |(l+1, 0|j|l, \pm 1)|^2 &= 2\pi l(l+1)/(2l+1)(2l+3)^2 \\ (l-1, 0|j|l, 0)(l+1, 0|j|l, 0)^* &= 4\pi l(l+1)/(2l-1)(2l+3)(2l+1) \\ (l-1, 0|j|l, \pm 1)(l+1, 0|j|l, \pm 1)^* &= -2\pi l(l+1)/(2l-1)(2l+1)(2l+3). \end{aligned} \quad (23a)$$

It follows immediately that

$$\begin{aligned} \sum_{m'=0, \pm 1} |(l-1, 0|j|l, m')|^2 &= 4\pi l/(2l-1)^2 \\ \sum_{m'=0, \pm 1} |(l+1, 0|j|l, m')|^2 &= 4\pi(l+1)/(2l+3)^2 \\ \sum_{m'=0, \pm 1} (l-1, 0|j|l, m')(l+1, 0|j|l, m')^* &= 0. \end{aligned} \quad (23b)$$

Substituting (23b) into (16) and (19) we obtain an expression for J_ν in which only δ_l and $I_{l,l'}(n, n')$ remain to be evaluated.

$$J_\nu = \frac{16e^3 h^2 n'^2}{3c^3 \pi^3 m^2} \frac{y'}{y} \sum_{l=0}^{\infty} |\delta_{l'}|^2 \{ l |\delta_{l-1}|^2 |I_{l-1,l}(n, n')|^2 + (l+1) |\delta_{l+1}|^2 |I_{l+1,l}(n, n')|^2 \}. \quad (24)$$

1-5. Evaluation of $I_{l,l'}(n, n')$

We must now evaluate the radial integrals

$$I_{l,l'}(n, n') = \int_0^z M_{n,l'}^*(x') M_{n,l}(x) / x^2 dx.$$

First we express $M_{n,l}(x)$ in terms of the confluent hypergeometric functions $F(\alpha, \rho, x)$ by (4a)

$$M_{n,l}(x) = x^{l+1} e^{-x/2} F(\alpha, \rho, x).$$

From (5) we see that either both x and n are real or both purely imaginary. Using the identity

$$F(\alpha, \rho, x) = e^x F(\rho - \alpha, \rho, -x) \quad (25)$$

or in our case $F(l+1-n, 2l+2, x) = e^x F(l+1+n, 2l+2, -x)$ we conclude that $e^{-x/2} F(\alpha, \rho, x)$ is always real since it is equal to its own complex conjugate. Except for a constant factor, which is unity if x is real and $(-1)^{l+1}$ if x is imaginary, we may thus write

$$I_{l,l'}(n, n') = \epsilon^{l'+1} \int_0^z x^{l+l'} e^{-bx} F(\alpha, \rho, x) F(\alpha', \rho', \epsilon x) dx \quad (26)$$

where

$$\epsilon = x'/x \quad b = (x' + x)/2x = (\epsilon + 1)/2. \quad (27)$$

Definite integrals of the type (26) and with the upper limit $\pm i\infty$ occur whenever one deals with wave functions in a Coulomb field of force. In our case, however, the integral is indefinite and requires different methods of treatment. The evaluation of this integral is much more difficult than that of the definite one and we have not been able to obtain a closed form except in certain special cases. Thus we have computed numerical values of I only for real values of the parameters involved. Fortunately it is for the real parameters that our results differ appreciably from those obtained with the nuclear model.

Since in most cases which we shall treat, the value of z is not very large, the most convenient method is to use expansions in small powers of x

$$\begin{aligned} F(\alpha, \rho, x) &= \frac{\Gamma(\rho)}{\Gamma(\alpha)} \sum_{n=0}^{\infty} \frac{\Gamma(\alpha + n) x^n}{\Gamma(\rho + n) \Gamma(n + 1)} \\ F(\alpha', \rho', \epsilon x) &= \frac{\Gamma(\rho')}{\Gamma(\alpha')} \sum_{\nu=0}^{\infty} \frac{\Gamma(\alpha' + \nu) (\epsilon x)^\nu}{\Gamma(\rho' + \nu) \Gamma(\nu + 1)}. \end{aligned} \quad (28)$$

Integrating term by term and using symbol $\gamma(\mu, z)$ for the incomplete gamma-function defined by

$$\gamma(\mu, z) = \int_0^z x^{\mu-1} e^{-x} dx \quad (29)$$

we obtain

$$I_{l,l'}(n, n') = \frac{\Gamma(\rho)\Gamma(\rho')}{\Gamma(\alpha)\Gamma(\alpha')} \frac{\epsilon^{l'+1}}{b^{l+l'+1}} \sum_{\nu=0}^{\infty} \frac{\Gamma(\alpha' + \nu)(\epsilon/b)^{\nu}}{\Gamma(\rho' + \nu)\Gamma(\nu + 1)} \sum_{n=0}^{\infty} \frac{b^{-n}\Gamma(\alpha + n)\gamma(l + l' + 1 + \nu + n, bz)}{\Gamma(\rho + n)\Gamma(n + 1)}. \quad (30)$$

The value of $\gamma(\mu, z)$, since μ is always an integer can be computed from the terminating series

$$\gamma(\mu, z) = \Gamma(\mu) \left\{ 1 - e^{-z} z^{\mu-1} \sum_{s=0}^{\mu-1} \frac{z^{-s}}{\Gamma(\mu - s)} \right\}. \quad (31)$$

Substituting (31) into (30) we obtain $I = I' + I''$, where

$$I' = \frac{\Gamma(\rho')}{\Gamma(\alpha')} \frac{\epsilon^{l'+1}}{b^{l+l'+1}} \sum_{\nu=0}^{\infty} \frac{\Gamma(\alpha' + \nu)\Gamma(l + l' + 1 + \nu)(\epsilon/b)^{\nu} F(\alpha, l + l' + 1 + \nu; \rho; b^{-1})}{\Gamma(\rho' + \nu)\Gamma(\nu + 1)} \quad (32a)$$

and

$$\begin{aligned} I'' &= \frac{\Gamma(\rho)\Gamma(\rho')\epsilon^{l'+1}e^{-bz}}{\Gamma(\alpha)\Gamma(\alpha')b} \sum_{s=0}^{\infty} (bz)^{-s} \sum_{\nu=0}^{\infty} \frac{\Gamma(\alpha' + \nu)(\epsilon z)^{\nu}}{\Gamma(\rho' + \nu)\Gamma(\nu + 1)} \\ &\quad \sum_{n=0}^{\infty} \frac{\Gamma(\alpha + n)\Gamma(l + l' + 1 + \nu + n)z^n}{\Gamma(\rho + n)\Gamma(l + l' + 1 + \nu - s + n)\Gamma(n + 1)} \\ &= \frac{\epsilon^{l'+1}}{b} e^{-bz} \sum_{s=0}^{\infty} \left(\frac{d}{dbz} \right)^s \left\{ z^{l+l'} F(\alpha, \rho, z) F(\alpha', \rho', \epsilon z) \right\}. \end{aligned} \quad (32b)$$

The above method is especially convenient in two special cases. (1) α and α' are negative integers. In this case both series of (30) terminate. (2) z is large and imaginary. This case corresponds to very high voltages, or large radii of the model. ($z \rightarrow +\infty$ corresponds to infinite nuclear charge and the integral diverges.) We can now use the asymptotic expansions

$$F(\alpha, \rho, z) \sim \Gamma(\rho) \left\{ \frac{e^z z^{\alpha-\rho}}{\Gamma(\alpha)} + \frac{(-z)^{-\alpha}}{\Gamma(\rho - \alpha)} \right\} \quad (33)$$

and conclude that all the terms in the summation of I'' are small of the order $1/z^2$, remembering that $\alpha = (\rho/2) + n$ where n is now imaginary.

Another simple case is that of very small z . Provided $\alpha z/\rho$ and $\alpha' z\epsilon/\rho'$ are much smaller than unity, we can take only the first term in the expansion (28). Hence

$$F(\alpha, \rho, x) = F(\alpha', \rho', \epsilon x) \cong 1$$

and the integral (26) becomes

$$I_{l,l'}(n, n') = \frac{\epsilon^{l'+1}}{b^{l+l'+1}} \gamma(l+l'+1, bz). \quad (34)$$

For certain values of the parameters the integral (26) can be evaluated in terms of Bessel functions. Thus for $n=n'=\frac{1}{2}$ we have

$$e^{-z/2} F(\alpha, \rho, x) = e^{-x/2} F(l + \frac{1}{2}, 2l + 2, x) = \frac{2^l \Gamma(l+1)}{y^l} \{J_l(y) + iJ_{l+1}(y)\}$$

where $y = ix/2$. We now have

$$I_{l,l+1}(\frac{1}{2}, \frac{1}{2}) = 2^{4l+3} \Gamma(l+1) \Gamma(l+2) (-1)^{l+1} \int_0^{iz/2} \{J_l + iJ_{l+1}\} \{J_{l+1} + iJ_{l+2}\} dy$$

which with the aid of

$$\int_0^y \{J_l J_{l+2} + J_{l+1}^2\} dy = y \{J_{l+1}^2 - J_l J_{l+2}\}$$

and

$$\int_0^y J_{l+1} \{J_l - J_{l+2}\} dy = \int_0^y 2J_{l+1} J'_{l+1} dy = J_{l+1}^2(y)$$

becomes

$$I_{l,l+1}(\frac{1}{2}, \frac{1}{2}) = 2^{4l+3} \Gamma(l+1) \Gamma(l+2) (-1)^{l+1} \{ (z/2) [J_l(iz/2) J_{l+2}(iz/2) - J_{l+1}^2(iz/2)] + J_{l+1}^2(iz/2) \}. \quad (35)$$

II

2-1. Parametric analysis of J_v

In the preceding section we have given methods for evaluating $I_{l,l'}(n, n')$. J_v could now be computed by assigning definite values to the parameters involved; namely Z, a, v and v' . Before doing this, however, we shall find out in what combinations these parameters enter, for the purpose of reducing, if possible, the number of cases to be considered. On inspecting the expressions (24), (8), and (26) we notice that J_v is a function of

$$z, z', n, n', y, y'$$

if we neglect for the moment the factor e^2/m^2 . Now

$$\begin{aligned} z &= 2ka = 4\pi(2mZae^2/\hbar^2 - m^2v^2a^2/\hbar^2)^{1/2} = z(mZae^2/\hbar^2, mva/\hbar) \\ n &= 4\pi^2mZe^2/\hbar^2k = 8\pi^2mZae^2/\hbar^2z = n(mZae^2/\hbar^2, mva/\hbar) \\ y &= (2\pi/\hbar)mva = y(mva/\hbar). \end{aligned}$$

It follows therefore that

$$J_\nu = \frac{h^2 e^2}{c^3 m^2} f(mZae^2/h^2, mva/h, mv'a/h). \quad (36)$$

We notice that (1) m enters only in the form of the product ma except for the factor $1/m^2$; (2) Z enters only in the form of the product Za .

The first of these conditions we shall utilize in estimating the radiation emitted by a particle of large mass in the field of a screened nucleus. The second condition will allow us to limit our investigations to the relevant range of values of the product Za without specifying the values of the two factors Z and a . We shall use throughout the parameters Za , Va^2 and ν/ν_0 .

2-2. Low voltages

2-21. *Intensity of radiation.* We shall consider the case of low voltages first. As is seen from (9) $|\delta_l|^2$ given by (8) diminishes roughly as y^{2l} for small value of y , i.e., for slow electrons. Hence provided $y \ll 1$ we need consider only two transitions $l=0 \rightarrow 1$ and $1 \rightarrow 0$, contribution to the sum (24) from higher values of l being negligible. Further if y is sufficiently small for the inequality, $mv^2/2 \ll Ze^2/a$, to be true, we have approximately $n=n'$, $Z=Z'=4n$, and therefore $I_{l',l}(n, n') = I_{l,l}(n, n')$. (24) now simplifies to

$$J_\nu = \frac{16e^2 h^2 n'^2}{3c^3 \pi^3 m^2} \frac{y}{y'} |I_{0,1}(n, n)|^2 \{ |\delta_0|^2 |\delta_1'|^2 + |\delta_1|^2 |\delta_0'|^2 \}.$$

Substituting for δ_l their values and neglecting y^2 in comparison with unity we further reduce (24)

$$J_\nu = \frac{4e^2 h^2 n^2}{3c^3 \pi^3 m^2} \frac{|I_{0,1}(n, n)|^2}{|M'_{n,0}|^2 |M'_{n,1} + M_{n,1}/z|^2} \frac{y'}{y} (y^2 + y'^2).$$

We can write J_ν in terms of the frequency ν of radiation emitted and the energy V of the incident electron in electron-volts. Thus defining ν_0 by $h\nu_0 = \frac{1}{2}mv^2$ and using $Va^2 = 300h^2 y^2 / 8\pi^2 em = 3.8y^2$, we obtain the following expression

$$J_\nu = \frac{4e^2}{3c^3} f(n) Va^2 (1 - \nu/\nu_0)^{1/2} (2 - \nu/\nu_0) \quad (Va^2 < 1) \quad (37)$$

where

$$f(n) = \frac{8\pi e}{300m} n^2 \frac{|I_{0,1}(n, n)|^2}{|M'_{n,0}|^2 |M'_{n,1} + M_{n,1}/z|^2} \times 10^{-16} \quad (38)$$

and is a function of the parameters of the model only. We have also found by numerical computation that the two inequalities limiting the region of applicability of (37) can be replaced by a single one $Va^2 < 1$, where V is in volts and a in angstrom units. In its dependence on the frequency, J_ν of (37) is a monotonically decreasing function of ν having a negatively infinite derivative at the Duane-Hunt limit.

2-22. *The total amount of radiation.* To obtain the total amount of radiation R we integrate (37) with respect to the frequency

$$R = \int_0^{v_0} J_r d\nu = (64e/45c^3)(e/300h)V^2 a^2 f(n). \quad (39)$$

We notice especially that R vanishes rapidly as the voltage goes to zero instead of remaining constant as was the case with the nuclear model.

2-23. *Dependence on the parameters of the model.* The dependence of J_r and R on the central charge Z and the screening radius a is given by $a^2 f(n)$. For

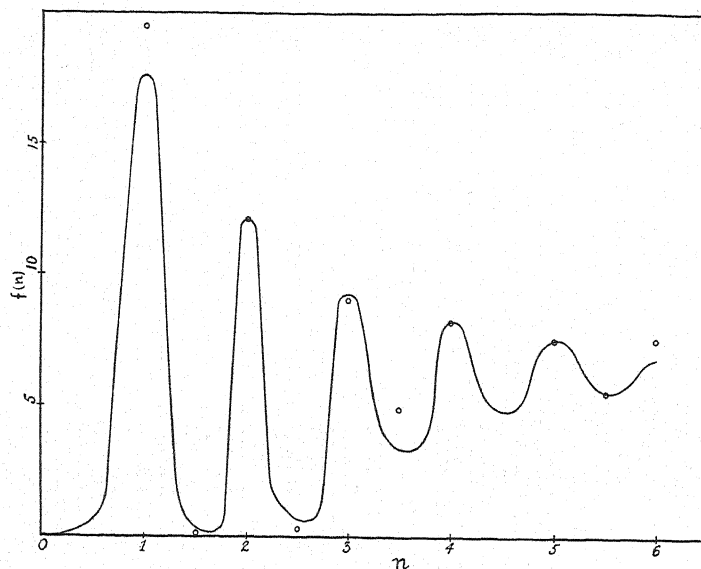


Fig. 1. Variation of $f(n)$ with respect to n . (Circles indicate points computed from the approximate Eq. (38b).)

very small values of n we can use (34) to evaluate $I_{0,1}(n, n)$; to the same approximation we obtain

$$f(n) = (8\pi en^4/300m)10^{-16}. \quad (n \ll 1). \quad (38a)$$

For larger values of n we have used Eq. (38) to calculate $f(n)$ and found that for the range $1 < n < 6$ the calculated points lie rather accurately on the curve represented by an "empirical-theoretical" formula

$$f(n) = 6.5 \left| 1 + (2/n^{3/2}) \cos 2\pi n \right|, \quad (1 < n < 6). \quad (38b)$$

In Fig. 1 we show $f(n)$ as a function of n indicating by means of circles values computed from (38b). We observe that $f(n)$ exhibits a series of maxima corresponding to integral values of n . For large values of n , $f(n)$ has a nearly constant value of about 7. In this region therefore J_r is independent of the central charge and is proportional to the cross-sectional area of the atom.

In order to find a physical explanation of the oscillatory character of $f(n)$ we have computed the values of the integral $I_{n,l} = \int_0^a |\psi_{n,l}|^2 dr$ for several

values of n . We have found that $I_{n,l}$ exhibits even more pronounced maxima for integral values of n than does $f(n)$. Now, since $|\psi(r_1)|^2$ is equal to the probability of finding the electron at $r=r_1$, the integral $I_{n,l}$ is a measure of the time spent by the electron in the region $0 < r < a$, i.e., inside the screening shell. We may suppose therefore that for certain values of Za the electron stays in the field of the model for a very long time, executing several revolutions about the nucleus before escaping.

A similar phenomenon has been found by Allis and Morse⁹ in their study of the cross section for elastic scattering. These authors used a model which is identical with ours. The variation of the cross section q_0 for slow electrons with respect to parameters n and y is shown in their Fig. 3. Their β is our n and their x is our y . For small values of x , i.e., for slow electrons, q_0 exhibits maxima near integral values of n .

2-24. *Polarization.* Using relations

$$I_{0,1}(n, n) = I_{1,0}(n, n)$$

$$|\delta_0'|^2 |\delta_1|^2 / |\delta_0|^2 |\delta_1'|^2 = y'^2 / y^2 = 1 - \nu / \nu_0$$

and considering as before only the two transitions $l1 \rightarrow 0$ and $l0 \rightarrow 1$, we obtain for the degree of polarization P defined by (22)

$$P = 3 / (5 - 2\nu / \nu_0). \quad (40)$$

2-3. Moderate voltages

In this section we shall consider radiation from electrons whose velocity is limited by the relation

$$mv^2/2 < Ze^2/a. \quad (41)$$

For this range of velocities both z and n are real with the result that the evaluation of the radial integrals (18) is simplified.

In contradistinction to the analysis of the preceding sections, now we may no longer assume that $y \ll 1$ and must therefore take into consideration contribution from several values of l . In carrying out the summation over l we have noticed some interesting analogies to classical mechanics. Just as was the case for low voltages the contributions from terms with $(h/2\pi) \cdot l > mva$, i.e., $l > y$ is negligible. Further, for a given voltage, the most important values of l are $l \cong y$ for relatively soft radiation, and smaller values for higher frequencies. As we increase the voltage, thus increasing y , the value of l contributing the most also increases but not as rapidly as does y . These facts seem to indicate that—as was to be expected—most of the radiation from fast electrons and relatively hard radiation from all electrons is emitted in the intense field in the neighborhood of the nucleus, while softer radiation is more likely to be produced with weaker fields and larger paths, the time spent in the field being here the dominant factor. We have also noticed that for the important values of l the transitions $l \rightarrow l-1$ are much more probable than the transitions $l \rightarrow l+1$.

⁹ Allis and Morse, Zeits. f. Physik 20, 567 (1931).

We have carried out calculations for three different values of Za , namely 37, 25.7, 12.6. The range of the parameter Va^2 was from 140 to 350, where V is in volts and a in angstroms. Except for a few control computations, we have chosen the values of Va^2 and ν/ν_0 in such a way as to make both α and α' negative integers. For these values of α and α' formula (30) takes an especially simple form. The range of ν for which this is possible is $\nu/\nu_0 < 0.6$ and $\nu/\nu_0 = 1$ for $Za = 37$ or 25.7, and $\nu/\nu_0 < 0.7$ for $Za = 12.6$. For frequencies other than these we have estimated the values of $I_{l,l'}(n, n')$ by interpolation. Although $I_{l,l'}(n, n')$ is in most cases a monotonic function of ν , because of rapid changes of the slope of this function the interpolation is extremely difficult and therefore the values of $I_{l,l'}(n, n')$ unreliable. In this region the more exact methods such as direct application of the formula (30) proved to be exceedingly laborious, and we have not used them in view of the doubtful importance of precise values of J_ν .

The results of these calculations in their dependence on the various parameters involved are given below.

2-31. *Duane-Hunt limit.* Near the Duane-Hunt limit $y' \ll 1$ and practically all of the radiation is emitted during the transition $l1 \rightarrow 0$. Proceeding as in section 2-21 we obtain

$$J_\nu = G(Va^2, Za)(1 - \nu/\nu_0)^{1/2} \quad (1 - \nu/\nu_0 \ll 1) \quad (42)$$

valid for all voltages, where

$$G(Va^2, Za) = \frac{8e^2 h^2 n'^2}{3c^3 \pi^2 m^2} \frac{|\delta_1|^2}{|M'_{n',0}|^2} |I_{1,0}(n, n')|^2. \quad (43)$$

Of special interest is the behavior of J_ν with respect to the frequency ν , given by $(1 - \nu/\nu_0)^{1/2}$. We see that at the high-frequency limit J_ν vanishes for all finite values of V and a , and that $dJ_\nu/d\nu = -\infty$. The physical reason for the vanishing of J_ν can be seen as follows. On the one hand J_ν is known to be continuous at the limit $\nu = \nu_0$; on the other hand a spectral line of frequency $\nu = \nu_0$ would correspond to an orbit of infinite radius and is therefore disallowed as long as we keep the value of a finite.

We shall now investigate the case of $a = \infty$, i.e., the case of an unscreened nucleus. In this case we can use formula (32). We now have $|z| = \infty$ and therefore $I'' = 0$. Limiting ourselves to high voltages and hard radiation, i.e., $|n| \ll 1$ and $|n/n'| \ll 1$, we shall take only the first two terms in the summation of I' . We thus obtain on neglecting $|n|^2$ and $|n/n'|^2$ in comparison with unity $|I_{1,0}|^2 = 144 |n/n'|^2$ and $|I_{0,1}|^2 = 16 |n/n'|^2$. The normalizing factors δ_i can be easily evaluated by using the asymptotic expansions (33) and (9).

$$\begin{aligned} |\delta_0|^2 &= \pi^2 |n| / (1 - e^{-2\pi|n|}) \\ |\delta_1|^2 &= \pi^2 |n| / 36(1 - e^{-2\pi|n|}). \end{aligned}$$

Contribution from values of l and l' greater than unity can be safely neglected to the approximations which we are using. Substituting the above values of δ_i and I into (24) we finally obtain

$$J_\nu = \frac{2^8 \pi^3 Z^2 e^6}{3 c^3 m^2 v} |n|^2 \frac{1 + |n/n'|^2 (1 + |n'|^2)/9}{(1 - e^{-2\pi|n|})(1 - e^{-2\pi|n'|})}$$

$$\cong \frac{2^8 \pi^3 Z^2 e^6}{3 c^3 m^2 v^2} \frac{|n|^2}{(1 - e^{-2\pi|n|})(1 - e^{-2\pi|n'|})} \quad (44)$$

In the limit of small $|n|$ and $|n/n'|$ Eq. (44) agrees both with the Sommerfeld's⁵ Eq. (99b) and with Oppenheimer's² equation for I^z on p. 733.

Since in either formula, (42) or (44), only one transition $l1 \rightarrow 0$ is important the radiation at the Duane-Hunt limit is always plane polarized in the direction of the incident beam of electrons; i.e., $P=1$.

2-32. J_ν as a function of the frequency. Fig. 2 below shows the variation of J_ν with respect to ν/ν_0 for various values of parameters Va^2 and Za . In each

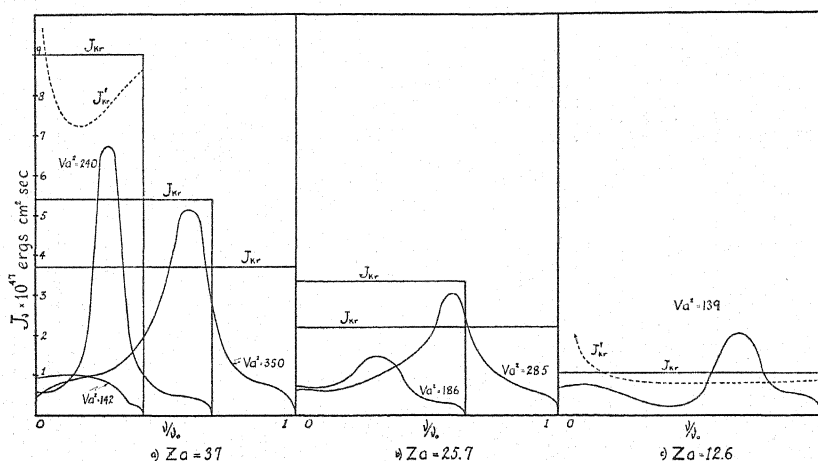


Fig. 2. Intensity of radiation as a function of the frequency.
(V is in volts and a in angstroms.)

of the three parts a, b and c of the figure, ν_0 represents the frequency of the Duane-Hunt limit for the highest value of Va^2 indicated. The straight line curves give the values of J_{kr} and the dotted curves values of J_{kr}' computed from Eq. (1) for the appropriate values of the ratio $Z^2 a^2 / Va^2$.

We notice that the general shape of the curves is approximately the same for all the values of Za and Va^2 . At $\nu=0$ all the curves start with a small slope from a value of J_ν near 0.6×10^{-47} ergs cm^2 sec.; they reach a maximum near the middle of the spectrum and come to zero at the Duane-Hunt limit with an infinite slope. The maximum corresponds approximately to the smallest integral value of n' . As stated in the beginning of section 2-3, *beyond the maximum the curves are definitely unreliable*. They have been determined from the known fact that the slope is infinite at the Duane-Hunt limit and by the use of a few points obtained by difficult graphical interpolation.

2-33. *Dependence of average intensity on V , Z , a .* Despite the uncertainties in values of J_ν for the high-frequency range we can obtain the average values

of J , fairly accurately by computing the areas under the curves of Fig. 2. For convenience of interpolation and extrapolation we shall give a "theoretical-empirical" formula which gives within 10 percent the six values of \bar{J} computable from Fig. 2 and which agrees with Kramers' value J_{kr} as either V or a becomes large, or Z becomes small.

$$\bar{J} = \frac{J_{kr}(Z, V)}{\left[1 + \left(\frac{Z^2}{2V} \right)^2 \frac{1}{1 + (Za/22)^4} \right]^2}. \quad (45)$$

As always, V is in volts and a in angstrom units. It must be remembered that this formula can be relied upon only within the range of values investigated. We know that it is wrong in the region of very small V or a where Eq. (37) should be used. We feel, however, that (45) could be safely used for large V or a , for then it differs from $J_{kr}(Z, V)$ only by a small quantity the exact value of which is not very important.

The region in which \bar{J} is nearly equal to $J_{kr}(Z, V)$ is defined for all values of a by the inequality

$$(Z^2/2V)^2 \ll 1. \quad (46)$$

This inequality may thus be used to define the region of applicability of a nuclear model to a neutral atom. We must remember, however, that even in the region (46) the equality $\bar{J} \cong J_{kr}(Z, V)$ is true only provided the central charge Z is the same for either model. It is clear that Z should always be less than the nuclear charge of the actual atom. We shall discuss the choice of Z in section III.

2-4. Double shell model

Since the model consisting of a point charge surrounded by a negatively charged shell is but a crude approximation to the actual atom it is of interest to find what changes are introduced when the model is varied. For this purpose we modified our model by adding a second negatively charged shell concentric with the first one, the whole system as before being neutral; and carried out calculations only as far as it was necessary in order to ascertain the order of magnitude of J_v .

The procedure for setting up an expression for J_v is essentially the same as in the case of a single shell. We shall consider a point charge Ze , surrounded by an inner shell of radius a and an outer shell of radius R , the latter carrying a charge $-Z_1e$. In order to make the whole system neutral the charge on the inner shell must be $-(Z - Z_1)e$. The potential V in the Schrödinger Eq. (2) must now have 3 different values

$$\begin{aligned} V &= 0 & (r \geq R) \\ V &= Z_1e^2/R - Z_1e^2/r & (a \leq r \leq R) \\ V &= Ze^2/a - Ze^2/r + Z_1e^2/R - Z_1e^2/a. & (r \leq a) \end{aligned}$$

Proceeding as before it is easy to show that

$$J_\nu = \frac{16e^2\hbar^2 p^2}{3c^3\pi^3 m^2} \frac{\gamma'}{\gamma} \sum_{l=0}^{\infty} |\delta_{l'}|^2 \left\{ l |\delta_{l-1}|^2 \left| \epsilon_{l'}^* \epsilon_{l-1} \frac{k}{s} \frac{Z}{Z_1} I_{l-1,l}^{(1)} \right. \right. \\ \left. \left. + I_{l-1,l}^{(2)} \right|^2 + (l+1) |\delta_{l+1}|^2 \left| \epsilon_{l'}^* \epsilon_{l+1} \frac{k}{s} \frac{Z}{Z_1} I_{l+1,l}^{(1)} + I_{l+1,l}^{(2)} \right|^2 \right\}$$

where

$$I_{l,l'}^{(1)} = \int_0^a \frac{M_{n,l'}^*(2k'r) M_{n,l}(2kr)}{(2kr)^2} 2kdr$$

$$I_{l,l'}^{(2)} = \int_a^R \frac{\psi_{p,l'}^*(2s'r) \psi_{p,l}(2sr)}{(2sr)^2} 2sdr$$

$$\psi_{p,l}(2sr) = \frac{1}{2sr} \{ W_{p,l+1/2}(2sr) + \lambda_l W_{-p,l+1/2}(-2sr) \}^{10}$$

$$\lambda_l = \frac{M_{n,l}(2ka) W'_{p,l}(2sa) - (k/s) M'_{n,l}(2ka) W_{p,l}(2sa)}{(k/s) M'_{n,l}(2ka) W_{-p,l+1/2}(2sa) - M_{n,l}(2ka) W'_{-p,l+1/2}(2sa)} \\ (-1)^{l+1}$$

$$\delta_l = \frac{\psi'_{p,l}(2kR) H_l(y) - (b/2s) \psi_{p,l}(2kR) H_l'(y)}{\psi'_{p,l}(2sa) / M_{n,l}(2ka)}$$

$$\epsilon_l = \psi_{p,l}(2sa) / M_{n,l}(2ka)$$

$$s = (2\pi/\hbar) [2m \{ Z_1 e^2 / R - E \}]^{1/2}$$

$$k = (2\pi/\hbar) [2m \{ Z_1 e^2 / R + (Z - Z_1) e^2 / a - E \}]^{1/2}$$

$$p = 4\pi^2 m Z_1 e^2 / \hbar^2 s.$$

The result of the few calculations carried out seems to show that J_ν has the same order of magnitude whether we represent an atomic field as given by Slater¹¹ by a single shell model or by a double-shell one. This is very satisfactory, for since a charged shell model is not very sensitive even to such radical changes as increasing the number of shells, we may hope that our crude model represents fairly accurately the actual atom with its diffuse boundaries.

2-5. Radiation from protons

In this section we shall use the results of the parametric analysis of section 2-1 to estimate the intensity of radiation emitted by a proton in the field of our model. In section 2-1 we have shown that the mass of the incident particle, m , and the radius of the shell, a , enter only in the form of the product ma , except for the factor $1/m^2$. Let us now consider two particles of equal initial velocities, v , and of masses M and m passing through fields limited by radii a and R , respectively. Further, let the values of the radii and masses be so chosen as to satisfy the relation $Ma = mR$. We shall consider transitions in which the final velocity, v' , has the same value for both particles. The frequency ν_1 of radiation emitted by the particle of mass M is then given by

¹⁰ See *Modern Analysis*, Whittaker and Watson, section 16.12 of the 4th edition.

¹¹ Slater, *Phys. Rev.* **36**, 57 (1930).

$$h\nu_1 = \frac{1}{2}(v^2 - v'^2)M.$$

The other particle emits radiation of frequency ν_2

$$h\nu_2 = \frac{1}{2}(v^2 - v'^2)m.$$

It therefore follows from (36) that the intensities of radiation for the two particles per unit ranges of the respective frequencies are connected by the relation

$$J_{\nu_1}(M, a) = (m^2/M^2)J_{\nu_2}(m, R) \quad (47)$$

where $\nu_1/\nu_2 = R/a = M/m$.

We shall apply (47) to the case of a proton of mass M in the field of an atom whose field may be considered limited by a radius, a , of the order of magnitude of $1A$. We shall compare the intensity of radiation emitted by the proton to that of an electron of mass m in the field limited by the radius $R = (M/m)a$. From the known ratio of the masses $M/m = 1850$ we conclude that R is of the order of magnitude of $2000A$. Now it is obvious that a model with a radius of $2000A$ is very nearly equivalent to an unscreened nucleus. We therefore obtain quite generally, provided the velocities of the two particles are equal

$$J_{\nu_1}(\text{proton, atom}) = (m^2/M^2)J_{\nu_2}(\text{electron, nucleus}) \quad (48)$$

where as before $\nu_1/\nu_2 = M/m = 1850$.

If we use Kramers' formula (1) for J_{ν_2} in (48), the resulting expression for J_{ν_1} is identical with Kramers' formula for a proton radiating in the field of an unscreened nucleus. It is perhaps not surprising, however, that a proton radiates nearly as much in a limited field as it does in the field of an unscreened nucleus, for the mass of the proton is so large that its acceleration is negligible except in very intense fields.

III.

3-1. Choice of Z and a

In the preceding section we have given formulas describing the radiation emitted by an electron in the field of a model consisting of a central charge Z surrounded by a negatively charged shell of radius a . Before comparing our results with experimental data we must give methods for the proper choice of Z and a in order that our model may correctly represent an actual atom. We shall see that this choice can be made unambiguously in two limiting cases: (1) high voltages and (2) low voltages. In the intermediate region Z and a must be found by interpolation.

3-11. *High voltages.* In section 2-33 we saw that there exists a region, $(Z^2/2V)^2 \ll 1$, in which the radiation is independent of a and depends only on Z . In this region therefore the nuclear model should give correct results provided Z is properly chosen. In order to determine Z we shall proceed as follows. We shall assume that in the actual atom the effective charge Z at a distance r from the nucleus is given by an expression

$$Z = N(1 - r/R)^s \quad (49)$$

where N is the nuclear charge, and R and s are constants at our disposal to be determined for each atom by investigating its field, for example by Slater's¹¹ method. We shall now determine the region of the field, say near $r=r_{\text{eff}}$, in which most of the radiation is produced when a stream of electrons is incident upon the atom, and take the corresponding charge $Z_{\text{eff}} = N(1 - r_{\text{eff}}/R)^s$ for the central charge of our model. Now for each electron of the incident beam characterized by the distance p of the original path from the nucleus there is a region of the field say about $r=r_p$ in which this particular electron radiates most. We shall assume further then that the radiation of this electron does not differ greatly from that emitted in a coulomb field of central charge $Z_p = N(1 - r_p/R)^s$. The difference is the smaller, the closer the path of the electron approaches a circular orbit of radius r_p .

We may now use Kramers'¹ expression (Eq. (70)) for the intensity of radiation

$$i_\nu dp d\nu = \frac{8\pi^3 Z_p^2 e^6}{c^3 m^2 v^2} \frac{P(\gamma)}{p} dp d\nu \quad (50)$$

where

$$\left. \begin{aligned} P(\gamma) &= \frac{1}{3} \{ [\gamma i^{4/3} 3^{-1/2} H_{1/3}^{(1)}(i\gamma/3)]^2 + [\gamma i^{5/3} 3^{-1/2} H_{2/3}^{(1)}(i\gamma/3)]^2 \} \\ \text{and } \gamma &= 2\pi\nu p^3 v^3 m^3 / Z_p^2 e^4, \end{aligned} \right\} \quad (51)$$

and find the value of p corresponding to the maximum of i_ν . This will give us r_p of the electron which radiates more than any other electron of the beam, i.e., it will give us the value of r_{eff} . Before doing this however we must postulate some functional relation between r_p and p . We shall take it to be

$$r_p = kp \quad (52)$$

where k is independent of p .

Letting

$$\gamma = x^3; kp/R = w; s = 3m/2; \epsilon^3 = N^2 e^4 k^3 / 2\pi\nu v^3 m^2 R^3 \quad (53)$$

we obtain

$$\epsilon x = w/(1 - w)^m \quad (54)$$

and

$$i_\nu = cv^2 P(x^3)/x^3. \quad (55)$$

Since we have to deal only with small values of $i\gamma/3$ we have used expansions about the origin of the Hankel's functions in the expression (51) for $P(x^3)$ and retained only the first two terms for each $H^{(1)}$. The maximum of i_ν can now be found in the usual way by equating the derivative of i_ν to zero.

We carried out our calculations for three special cases: (a) small ϵ ; (b) large ϵ ; (c) $s=3/2$.

(a) When ϵ is small, ϵx and hence w are also small. Thus to the first approximation we have from (54) $\epsilon x = w$. Going to the second approximation we let $w = \epsilon x + g$ where g is small of the order w^2 . Putting this value of w into (54) we obtain

$$\epsilon x = \frac{\epsilon x + g}{(1 - \epsilon x)^m} \frac{1}{(1 - g/1 - \epsilon x)^m} = \frac{\epsilon x + g}{(1 - \epsilon x)^m} \left\{ 1 + \frac{mg}{1 - \epsilon x} + \dots \right\}$$

whence on neglecting g^2

$$w = \frac{\epsilon x}{1 + \epsilon x(m-1)} [(1 - \epsilon x)^{m+1} + m\epsilon x]. \quad (56)$$

Substituting (56) into $di_v/dx=0$ we obtain an equation in x . By using special values for m we found that the maximum lies near $x=0.7$. We have therefore introduced a new variable $y=x-0.7$ and neglecting y^3 we have obtained a quadratic equation in y which we have solved. Our result is

$$\text{and } \left. \begin{aligned} Z_{\text{eff}} &= \frac{N}{(1 + 0.75\epsilon)^s} \\ r_{\text{eff}}/R &= \frac{0.75\epsilon}{(1 + 0.75\epsilon)^{2s/3}} \end{aligned} \right\} \begin{aligned} &\text{provided } \epsilon^2 \ll \left| \frac{8}{s(2s-3)} \right| \\ &\text{or if } s = 3/2, 0.75\epsilon < 1 \end{aligned} \quad (57)$$

(b) When $\epsilon \gg 1$, we have $\gamma \ll 1$, and may take only the lowest power of γ in the expansion of $P(\gamma)$, namely $\gamma^{2/3}$. We thus have

$$i_v = C_1 Z_p^{2/3} p$$

and without further approximations

$$Z_{\text{eff}} = N/(1 + 3/2s)^s; \quad r_{\text{eff}}/R = 3/(3 + 2s). \quad (58)$$

(c) $s=3/2$.

Locating the maximum of i_v is especially easy when $s=3/2$, for then $w = \epsilon x/(1 + \epsilon x)$. Using the method outlined in (a) we have determined the maxima for all values of ϵ . The resulting ratios Z_{eff}/N and r_{eff}/R are plotted against ϵ in Fig. 3.

In all the above formulas we have three adjustable parameters s , R and k . The first two are determined by the field of the atom; the third parameter, k , is some function of N , V , ν and R . The following considerations seem to show, however, that k should not differ greatly from unity; i.e., $r_p \cong p$.

In the first place the path of the incident electron is certain to traverse both regions $r > p$ and $r < p$. For very fast electrons the closest distance of approach to the nucleus, r_m , which is certainly the most important region for these electrons, is nearly equal to p . As we go to slower electrons r_m becomes smaller than p but at the same time the strength of the field becomes less important in comparison with the time spent in the field with the result that the relation between r_p and p tends to remain constant.

We may also arrive at a rough estimate of r_p in the following way. We shall assume that the total radiation from an electron which is deflected through an angle less than 90° is equal to the radiation which would be emitted if the path of the electron consisted of a quarter of a circle of radius r_p . For the latter case we have

$$R = \frac{2e^2}{3c^3} \int \left(\frac{Ne^2}{mr_p} \right)^2 dt = \frac{\pi N^2 e^6}{3c^3 m^2 v r_p}.$$

On the other hand for such deflections, Kramers¹ gives a formula

$$R = \pi N^2 e^6 / 3c^3 m^2 v \phi.$$

Hence if the two R 's are to be equal we must have $r_p = \phi$.

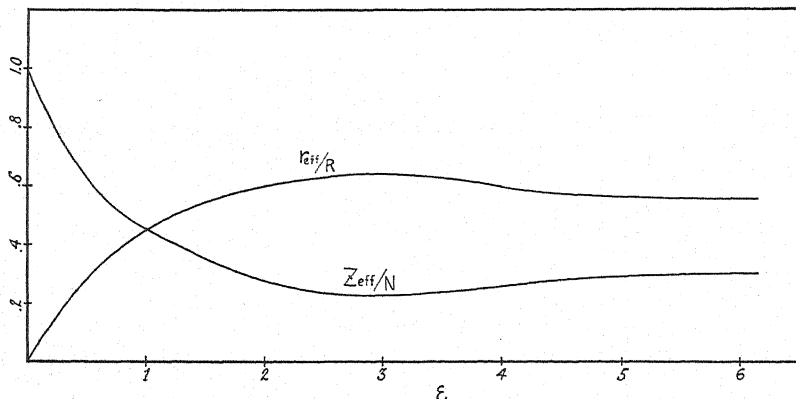


Fig. 3.

Having obtained an estimate of k we may now determine the regions of applicability of Eqs. (57) and (58). For this purpose we shall take $s=3/2$, and $R=2A$, i.e., equal roughly to the radius of an atom. Eq. (57) then becomes:

$$Z_{\text{eff}} = N / [1 + 4.4(N^{2/3}/V^{5/6})(v_0/v)^{1/3}]^{3/2} \quad (57a)$$

with the condition for its validity

$$(4.4N^{2/3}/V^{5/6})(v_0/v)^{1/3} < 1. \quad (59)$$

It is clear that (59) is satisfied in all cases of physical interest, especially in the region in which the nuclear model could be used, i.e., in the region defined by $(Z^2/2V)^2 \ll 1$. Hence Eq. (58) need be used only for the long wave-length end of the spectrum.

3-12. *Low voltages.* We have seen that in the region $Va^2 < 1$ where our Eq. (37) should be used J_s is nearly independent of Z (at least for larger values of n) and is proportional to a^2 . Hence in this region a must be taken somewhat larger than the radius of the atom while Z may be equated to some sort of average of the effective charge inside the atom, the exact value of Z being of little importance.

3-13. *Moderate voltages.* In the region intermediate between the two discussed above, i.e., where Eq. (45) is to be used, the proper choice of Z and a is difficult to determine. For want of better criterion we may suggest that provided $(Z^2/2V)^2$ is not too large or Va^2 too small, Eq. (57) be used, and Z taken to be equal to Z_{eff} and a equal to, say, twice the value of r_{eff} . In the other limiting case the method of section 3-12 may be used with the modification that a should be given a value which is the smaller (and therefore the average value of Z the larger) the harder the radiation.

3-2. Comparison with experiment

Perhaps the greatest applicability of our results and the test of their correctness should be sought in the field of astro-physics, for it is known that certain portions of stellar atmospheres contain a great many neutral atoms. Comparison with terrestrial experiments is made difficult by the fact that our calculations apply only to infinitely thin targets, while the only available data, for the region of voltages in which we are interested, are on radiation from thick targets. On the other hand, we cannot use the Thomson-Whiddington law—as was done by Kramers—to extend our results to the case of thick targets for the following reasons. As we have seen, for slow electrons the cross section for radiation of an atom is small in comparison to its gas-kinetic cross section; as a consequence only a small part of the energy lost by the incident electron appears as radiation, the rest being consumed in increasing the thermal agitations of the lattice. Further it is known that for such electrons the cross section of an atom for inelastic collisions and its gas-kinetic cross section are of the same order of magnitude. Thus only a very few atomic layers contribute appreciably to the radiation since the range in matter of low velocity electrons is extremely short. It is clear therefore that the Thomson-Whiddington which implies continuous loss of energy while applicable to fast electrons with their longer paths and small losses in a single collision, must be replaced in our case by much more detailed and less general calculation. Moreover in the case of metal targets it is questionable whether our spherically symmetrical model is a good approximation to the field about each lattice point of the metal crystal. The problem is simpler in its astrophysical applications since there we have to deal with a gas and the velocity distribution of electrons may be supposed known.

In view of these difficulties and the further difficulty that in the case of thick targets and soft radiation a large part of the radiation may fail to escape due to internal reflection and to absorption we can hope to obtain agreement with experimental results in the order of magnitude only. The only available data in the region of low voltages are to be found in the work of Mohler and Boeckner.¹² These authors, using a small metal probe, measured the absolute intensity of continuous radiation emitted by electrons of energies below 30 volts.

We have made the comparison with their values on the assumption that the amount of radiation emitted by an electron is proportional to the number

¹² Mohler and Boeckner, Bur. Standards J. Research 6, 673 (1931); 7, 751 (1931).

of atoms it encounters. Knowing the number of atoms per unit volume of target and calling the depth of penetration of the electron l we can compute the intensity J of radiation per atom per unit intensity of the electronic beam. Thus for the case of a copper probe, 9.1 volts and 3700A we have

$$J = (3.87 \times 10^{-56})/l \text{ ergs cm}^2 \text{ sec.} \quad (60)$$

We may now evaluate l by equating the experimental and the theoretical values of J . Thus if we use Kramers' formula (1) we obtain $l_{Kr} = 0.0045A$. This absurdly small value of l indicates that the nuclear model cannot be used for very low voltages.

Mohler and Boeckner tentatively used a formula, which Kramers derived for the case of a thick target by using the Thomson-Whiddington law, and found agreement within a factor of 2. We have seen however that neither the nuclear model nor the Thomson-Whiddington law can be applied to the case of very slow electrons; the agreement must therefore be considered accidental.

Before comparing (60) with the equations derived with the aid of our model we must decide upon the values of Z and a corresponding to a neutral copper atom. Using methods of section 3-12 and Slater's atomic fields we obtain $a = 1.73A$ and $Z = 9$. We notice that (58) with $s = 3/2$ gives nearly identical results; namely $Z_{\text{eff}} = 10.3$ and $A = 2r_{\text{eff}} = R = 1.73A$. By using the former values of a and Z in Eq. (45) we obtain in conjunction with (60), $l = 18A$, a value which corresponds to the penetration of 7 or 8 atomic layers. This value of l seems altogether reasonable for very slow electrons and thus provides us with a partial experimental verification of the validity of our formulas at least as to the order to magnitude.

SUMMARY

We have developed expressions describing the radiation emitted by a stream of electrons in the field of a model consisting of a point charge Ze surrounded by a negatively charged spherical shell of radius a , the whole system being neutral. In all the formulas below, a is in angstrom units and V , the energy content of the incident electrons, in electron-volts. We have labeled (emp) formulas which have not been theoretically derived but merely set up to give approximately the same values as those obtained from exact expressions.

We have divided our field of investigation into three regions: (1) low voltages, (2) moderate voltages and (3) high voltages.

(1) Low voltages ($Va^2 < 1$)

$$J_\nu = \frac{4e^2}{3c^3} f(n) Va^2 (1 - \nu/\nu_0)^{1/2} (2 - \nu/\nu_0) \quad (37)$$

where $f(n)$ is given by the graph of Fig. 1, or approximately by

$$f(n) = \frac{8\pi en^4}{300m} 10^{-16} \quad (n \ll 1) \quad (38a)$$

$$f(n) = 6.5 \left| 1 + \frac{2}{n^{3/2}} \cos 2\pi n \right| \quad (n > 1)(\text{emp}) \quad (38b)$$

$$P = 3/(5 - 2\nu/\nu_0). \quad (40)$$

(2) Moderate voltages ($Va^2 < 3 \times 10^{10} eZa$)

$$\bar{J} = \frac{J_{kr}(Z, V)}{\left[1 + \left(\frac{Z^2}{2V} \right)^2 \frac{1}{1 + (Za/22)^4} \right]^2} (\text{emp}) \quad (45)$$

where

$$J_{kr}(Z, V) = (1600\pi^2 e^5 / 3^{1/2} c^3 m) (Z^2/V). \quad (1)$$

(3) High voltages ($(Z^2/2V)^2 \ll 1$)

$$J_\nu = J_{kr}(Z_{\text{eff}}, V)$$

where

$$Z_{\text{eff}} = N/(1 + 0.75\epsilon)^s \quad \left(\begin{array}{l} \epsilon^2 \ll |8/s(2s-3)| \\ \text{or if } s = 3/2, 0.75\epsilon < 1 \end{array} \right) \quad (57)$$

$$Z_{\text{eff}} = N/(1 + 3/2s)^s \quad (\epsilon \gg 1) \quad (58)$$

and

$$\epsilon^3 = N^2 e^4 / 2\pi\nu m^2 \nu^3 R^3 \quad (53)$$

$$P = 1 \text{ for } \nu = \nu_0.$$

We have also carried out a few calculations using a model having two concentric spherical shells of different radii and obtained results of the same order of magnitude with those for the single shell model.

From the fact that the mass of the particle m and the radius of the screening shell a enter into the expression for J_ν only in the form of the product ma we have derived an expression connecting the intensities of radiation from a proton in the field of our model and from an electron of the same velocity in the field of an unscreened nucleus.

$$J_{\nu_1}(\text{proton, atom}) = (m/M^2) J_{\nu_2}(\text{electron, nucleus}) \quad (48)$$

where

$$\nu_1/\nu_2 = M/m \cong 1850$$

and J 's are the intensities per unit range of the respective frequencies.

In section III we have discussed the proper choice of Z and a in order that our model may represent an actual atom. There we have also compared our results with the experimental data of Mohler and Boeckner¹² and found agreement in the order of magnitude.

The writer wishes to thank Dr. H. A. Kramers for suggesting the problem and Dr. J. R. Oppenheimer for his friendly and helpful supervision of this work.

Influence of Crystalline Fields on the Susceptibilities of Salts of Paramagnetic Ions. II. The Iron Group, Especially Ni, Cr and Co

By ROBERT SCHLAPP AND WILLIAM G. PENNEY*
Department of Physics, University of Wisconsin

(Received October 13, 1932)

The present paper is concerned with the calculation of the paramagnetic susceptibility of highly hydrated crystals of the iron group elements Ni, Cr and Co. On the assumption that the metallic ion is subject to a crystalline electric field, predominantly cubic but also with a smaller rhombic term, the Hamiltonian function in a magnetic field H is given by

$$D(x^4 + y^4 + z^4) + Ax^2 + By^2 - (A + B)z^2 + \lambda(L \cdot S) + \beta H \cdot (L + 2S)$$

the numerical value of λ being known from the work of Laporte but the other constants yet to be determined. It actually proves possible to formulate and solve approximately the resulting secular equations and so obtain the first and second order Zeeman effects and hence the susceptibility. For all three ions $L=3$, so that the orbital problem is the same for all. This problem is exactly soluble, the energy levels consisting of two triplets and a singlet, the singlet not lying between the triplets. The effect of the introduction of the spin and its coupling to the orbit then leads to a determinant of order 21 for Ni and of order 28 for Cr and Co. That for Ni factors into one of order 10 and one of order 11, while those for Cr and Co factor into two determinants, identical except for the sign of the coefficient of H . On the assumption of a cubic field of the same sign and of approximately the same magnitude for all three ions the orbit-spin, together with the rhombic field, is able to remove the degeneracy of the lowest level in Ni and Cr only in a high approximation, while with Co the degeneracy is removed in first approximation. This difference accounts for the isotropy of Ni and Cr compared with the anisotropy of Co. In order to obtain agreement with experiment it is necessary to assume that in Ni the singlet of the orbital problem lies lowest. It then follows from the work of Van Vleck that the singlet also lies lowest for Cr but that for Co the singlet lies highest. When the singlet lies lowest, the square of the magneton number is given by the "spin only" value $4S(S+1)$, together with a small orbital contribution of order λ/D , whose sign can be either positive or negative. Actually it is positive for Ni and negative for Cr. In order to fit the results on the principal susceptibilities of Ni, it is necessary to take $D=1260 \text{ cm}^{-1}$, $A=176 \text{ cm}^{-1}$, $B=352 \text{ cm}^{-1}$, the magnitude of λ being -335 cm^{-1} . For Ni and Cr the theory requires that for the mean susceptibility $\chi = Q + P/T$, where P and Q are constants, Q being uniquely determined when P is fixed. Choosing P so that χT passes through the experimental point at 170°K we find that good agreement is obtained over the whole temperature range. For Cr $\lambda=87 \text{ cm}^{-1}$ and we find $D=3730 \text{ cm}^{-1}$, but we cannot determine A or B since there are no data on the principal susceptibilities.

Computational difficulties prevent the accurate solution of the Co problem. The situation is complicated by the experimental data not being complete. It proves necessary to consider a sextet which is soluble only numerically in the general case but perturbation theory can be applied when either the orbit-spin is large compared with the rhombic field or *vice-versa*. We obtain fair agreement with experiment and our calculations indicate that good agreement would be obtained in an intermediate case.

* Commonwealth Fund Fellow.

INTRODUCTION

IN THE following paper the idea of crystal fields of definite symmetry, developed by Van Vleck and others,¹ and already used in a previous article by the authors,² is applied to calculate the susceptibilities of salts of the elements Ni, Co and Cr. There are two respects in which the present problem differs from that of susceptibilities in the rare earth group. In the first place, the incomplete shell which is responsible for the paramagnetism of the iron elements consists of $3d$ electrons, which are much more strongly affected by the crystal fields than the more sheltered $4f$ shell of the rare earths. In the second place the orbit-spin coupling, which determines the multiplet width, is usually smaller in the iron group than in the rare earths. For the latter it was allowable to suppose that each multiplet component underwent a "Stark effect" due to the crystal field, without distortion on account of the other multiplet components. In the iron group, however, the electric field of the crystal is able to break down the relatively weak coupling between orbit and spin, producing an electric Paschen-Back effect; the orbit-spin coupling may be treated hence as a perturbation on an unperturbed problem which neglects the spin. This unperturbed, or orbital problem, as we shall call it, is the same for all three ions Ni^{++} Co^{++} Cr^{++} , since they all have an F state ($L=3$) as ground state.

We assume that the crystal field has no more than rhombic symmetry.³ The high degree of isotropy of Ni salts suggests that in this case the departure from cubic symmetry is small. Now it is known that a field which is nearly cubic decomposes the seven coincident levels of the F state (without spin) into a single level and two triplets, the single level lying outside the triplets and the triplet widths being small compared with the singlet-triplet or the triplet-triplet separations. If the spin and its coupling to the orbit be included, further decompositions of these levels occur. The general theory of susceptibilities shows that Curie's law will cease to be obeyed at low temperatures if kT becomes comparable with the separation of the lowest group of levels. The close conformity of Ni salts to Curie's law over a range of temperature from $300^\circ K$ down to $14^\circ K$ thus requires that a very narrow group of levels must lie considerably below all others. These conditions are satisfied if the single level of the orbital problem lies below the others, and on this assumption it is possible to account qualitatively for both the small anisotropy and the conformity to Curie's law. This arrangement of levels, however, appears to preclude an explanation on the same lines of the much greater anisotropy of the very similar and sometimes isomorphous salts of Co, and of the considerable departures from Curie's law which they exhibit. To ac-

¹ J. H. Van Vleck, *Theory of Electric and Magnetic Susceptibilities*, Oxford (1932).

² W. G. Penney and R. Schlapp, *Phys. Rev.* **41**, 194 (1932). Attention may be called here to a printers error in this paper. Minus signs were omitted in Eqs. (8) and (9) which should read $q = -I/10395$ for (8) and $q = -I/32670$ for (9). Moreover, in the secular determinant for Pr $a = \frac{1}{2}pD$ (not pD) and similarly for Nd $A = 6ap(14)^{1/2}$.

³ The assumption of a rhombic field not predominantly cubic was found to lead to very large asymmetry, in contradiction with experiment.

count for the behavior of Co salts it is necessary to suppose that the levels of the orbital problem in Co are inverted relatively to those in Ni. That such an inversion is actually to be expected in passing from Ni and Cr to Co has been neatly demonstrated by Van Vleck.⁴

EXPERIMENTAL DATA

It is useful at this stage to review the experimental data available on the hydrated salts of Ni, Cr and Co. We restrict ourselves to salts of large magnetic dilution, so that exchange effects may be neglected. Determinations of the three principal susceptibilities of the double sulphates of Co with ammonium, potassium and rubidium, have been made by Rabi⁵ at 300°K. Jackson⁶ has measured the susceptibility of powdered $\text{Ni}(\text{NH}_4)_2(\text{SO}_4)_2 \cdot 6\text{H}_2\text{O}$ and Gorter, de Haas and v. d. Handel⁷ that of powdered $\text{NiSO}_4 \cdot 7\text{H}_2\text{O}$ over a range of temperature between 14°K and 290°K. The graph of $1/\chi$ against T is approximately a straight line through the origin in both cases. Jackson⁶ has measured the three principal susceptibilities of $\text{Co}(\text{NH}_4)_2(\text{SO}_4)_2 \cdot 6\text{H}_2\text{O}$ at various temperatures down to 14°K. His values of the susceptibility extrapolated to a temperature of 300°K differ considerably from Rabi's, and there is only one determination between 20° and 290°K. As far as one can judge, however, the graph of $1/\chi$ against T is a straight line for each of the three principal susceptibilities, down to a temperature of about 50°K, below which the curve bends downwards slightly, so that the susceptibilities are higher than those predicted by the relation $\chi = C/(T + \Delta)$ of Weiss.

Very recently determinations over a temperature range from 250°K to 360°K have been made by Bartlett⁸ for crystalline cobalt ammonium sulphate and certain other crystals. They seem to be the most reliable measurements yet taken, being consistent and in agreement with Rabi's at the single temperature used by him. We are indebted to Dr. Bartlett for communicating these results to us in advance of publication.

The susceptibility of potassium chrome alum in powder form has been measured by de Haas and Gorter⁹ at various temperatures between 290°K and 14°K. They find that the law $\chi = C/T$ is closely obeyed over the whole range. Chrome alum forms crystals in the cubic system so that it may be expected to be magnetically isotropic.¹⁰

⁴ J. H. Van Vleck, *Phys. Rev.* **41**, 208 (1932).

⁵ I. I. Rabi, *Phys. Rev.* **29**, 184 (1927).

⁶ L. C. Jackson, *Phil. Trans. Roy. Soc. London*, **224**, 1 (1922), Leiden Com. 163.

⁷ C. J. Gorter, W. J. de Haas and v. d. Handel, *Proc. Amst. Acad.* **34**, 1 (1931), Leiden Com. 218d.

⁸ B. W. Bartlett, *Phys. Rev.* **41**, 818 (1932).

⁹ W. J. de Haas and C. J. Gorter, Leiden Com. 208d.

¹⁰ Measurements of the susceptibilities of the paramagnetic cubic crystal pyrite were made long ago by Voigt and Kinoshita (*Ann. d. Physik* **24**, 492 (1907)) who found it to be magnetically isotropic. There does not, however, seem to be any reason why magnetic dissymmetry should not exist in cubic crystals, as the electric field acting on the ion may have a lower symmetry than the lattice. See also reference 18.

THE ION IN A PERFECTLY CUBIC FIELD

Before considering the secular determinant explicitly, it is instructive to look at the problem from a more general point of view. The analysis of Bethe¹¹ shows that the cubic field breaks up the F level into three, corresponding to the irreducible representations $\Gamma_2, \Gamma_4, \Gamma_5$, of the cubic group, in his notation. The level Γ_5 lies between Γ_2 and Γ_4 ; Γ_2 is single, while Γ_4 and Γ_5 are each triply degenerate. We shall see later that the intervals between $\Gamma_2, \Gamma_4, \Gamma_5$ are of the order 10^4 cm^{-1} . The reader is referred to Van Vleck's⁴ paper for the demonstration of the fact that in Ni and Cr Γ_2 lies lowest and in Co Γ_4 lies lowest, for a given sign of D in the Hamiltonian. The level Γ_2 is non-magnetic; that is to say an atom in this state has no average orbital magnetic moment. The level Γ_4 is magnetic. Hence if Γ_2 is lowest the orbit is "quenched", i.e., contributes nothing to the susceptibility except a term independent of temperature. If, however, Γ_4 is lowest a certain portion survives.

We have now to consider the influence of the spin. Inclusion of the spin S ($=1$ for Ni and $3/2$ for Co and Cr) without interaction with the orbit makes each level of the orbital problem have an additional $(2S+1)$ -fold degeneracy, which is partially removed by the interaction. By the methods of Bethe's paper the decomposition of the levels is found by reducing the six direct products $\Gamma_i D_k$, ($i=2, 4, 5$; $k=1, 3/2$) to represent the cubic group. Here D_k is the representation group for the rotation of the spin k alone. The result is, in Bethe's notation,

$$\begin{aligned}\Gamma_2 D_1 &= \Gamma_5, & \Gamma_2 D_{3/2} &= \Gamma_8 \\ \Gamma_4 D_1 &= \Gamma_2 + \Gamma_3 + \Gamma_4 + \Gamma_5, & \Gamma_4 D_{3/2} &= \Gamma_6 + \Gamma_7 + 2\Gamma_8, \\ \Gamma_5 D_1 &= \Gamma_1 + \Gamma_3 + \Gamma_4 + \Gamma_5, & \Gamma_5 D_{3/2} &= \Gamma_6 + \Gamma_7 + 2\Gamma_8.\end{aligned}\tag{1}$$

Here $\Gamma_6, \Gamma_7, \Gamma_8$ are the "zweideutig" representations of the cubic group, of dimensions 2, 2, 4, respectively, which always arise with half-integral quantum numbers. These equations state that for Ni, Cr and Co the orbit-spin-interaction does not split the cubic level Γ_2 but splits each of the levels Γ_4, Γ_5 into four components.

Let us suppose that the level Γ_2 of the orbital problem lies lowest. The above reductions show that under the orbit-spin interaction this level does not break up, but remains triply degenerate (in Ni) or quadruply degenerate (in Co and Cr); no energy differences arise in consequence of different orientations of the spin, which therefore remains entirely free at all temperatures to orientate itself along the magnetic field. If the orbital contribution to the moment be neglected, the magneton number would be the Bose-Stoner or "spin only" value $[4S(S+1)]^{1/2}$. A further deduction is that the orbit-spin interaction causes the state Γ_2 to interact with components of Γ_4 and Γ_5 as is seen from the threefold occurrence of Γ_6 or Γ_8 on the right-hand side of (1). This produces a sharing of properties, and in particular gives rise to an orbital contribution to the magnetic moment in the state Γ_2 which is of order

¹¹ H. Bethe, Ann. d. Physik 3, 133 (1929).

λ/D . Thus the orbit-spin coupling produces, in an ion in a cubic field, departures from the Bose-Stoner value which may be either positive or negative according to the sign of λ/D .

The circumstances are not quite so simple if the state Γ_4 lies lowest. Here the orbit-spin coupling partially removes the degeneracy, so that different orientations of the spin have different energies, although, of course, it is not possible to associate a definite axial quantization of the spin with each of the levels. Thus the spin is only partially free and the orbital contribution will also be modified.

THE CONSTANT Δ

In a cubic field the quantity Δ of the Curie-Weiss formula $\chi = C/(T + \Delta)$ is given to a first approximation by the ratio of the coefficients of $1/T$ and $1/T^2$ in the expansion of the susceptibility in inverse powers of T . If we make the usual assumption that the magnetic moment in the absence of the magnetic field contains, besides low-frequency elements $M(n, n')$, only high-frequency elements, and none of intermediate frequency, it is easily shown¹² that

$$k\Delta = \left\{ \sum_{nn'} W_n |M(n, n')|^2 / \sum |M(n, n')|^2 \right\} - \bar{W}$$

the summation being over the group of levels connected by low-frequency elements, and \bar{W} being their mean energy. When the level Γ_2 of the orbital problem, which is not split up by the orbit-spin interaction, lies lowest, the magnetic mean center and the energetic mean center, whose difference gives $k\Delta$ according to the last equation, necessarily coincide. Hence in this case the susceptibility is of the form $\chi = C/T$, correct to terms in $1/T^2$. To this approximation the ion in a cubic field behaves as if it were in the gaseous state.

If the level Γ_4 lies lowest, the magnetic mean center and the energetic mean center do not necessarily coincide, so that the susceptibility will in general have a term in $1/T^2$. Thus leaving aside the question of asymmetry produced by a rhombic field, which is considered in the next section, we should expect Ni and Cr to conform much more closely to Curie's law than Co, as is indeed found to be the case.

ASYMMETRY DUE TO A RHOMBIC FIELD

Let us for the moment neglect the spin. The effect of superposing a rhombic field on the cubic field is, as shown by Bethe,¹¹ to remove all the degeneracy in the orbital problem, the appropriate reduction being

$$\Gamma_2 = G_1, \Gamma_4 = G_2 + G_3 + G_4, \Gamma_5 = G_2 + G_3 + G_4, \quad (2)$$

where G_1, G_2, G_3, G_4 are the four one-dimensional representations of the rhombic group. Fig. 1 shows diagrammatically the decomposition of the levels under the various fields. The level Γ_2 is seen to be completely isolated

¹² C. J. Gorter, Arch. Musee Teyler, 7 (3), 183 (1932). This formula can readily be obtained from the equation for $k\Delta$ on page 197, reference 2, \bar{W} in this case having been chosen to be zero.

from the others. The rhombic field alone, unlike the orbit-spin coupling, does not lead to a sharing of properties between Γ_2 and the other states. If Γ_2 is lowest the rhombic field does not give rise to any orbital contribution to the part of the susceptibility depending on the temperature. The part independent of the temperature is rendered slightly asymmetrical. Although no asymmetry is introduced directly by the rhombic field, the orbit-spin interaction, as we have seen, evokes an orbital contribution to the susceptibility, and this will be rendered anisotropic by the rhombic field. The anisotropy is thus a second order effect; the rhombic field may be comparatively large without producing much anisotropy. Neither the rhombic field alone nor the orbit-

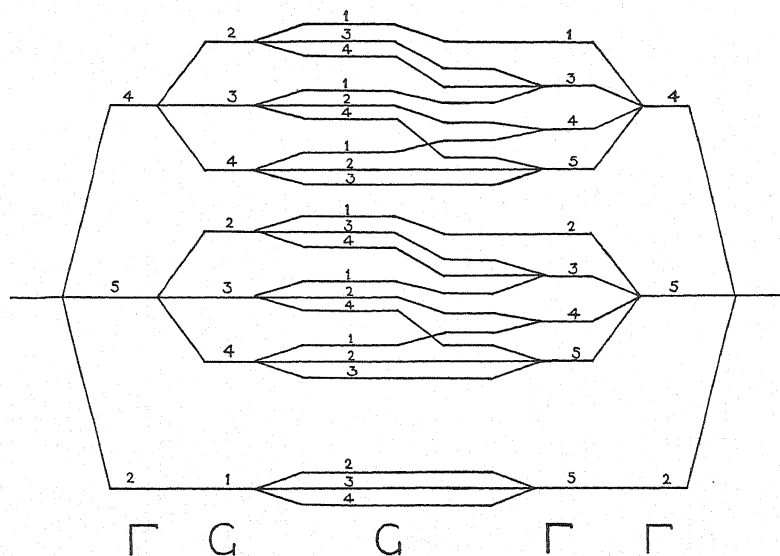


Fig. 1. Fig. 1 shows how the 3F state in nickel is affected by the cubic field, the rhombic field and the orbit-spin coupling. By starting at the left with the free ion, the cubic field splits the single level into three, the numbers and symbols underneath denoting to which representation, in Bethe's notation, the levels belong. The application of the rhombic field splits Γ_4 and Γ_5 each into three, leaving Γ_2 single. The addition of the orbit-spin then removes all the remaining degeneracy. Making the rhombic field zero leaves only orbit-spin and cubic, the way the levels come together being shown. Removal of the orbit-spin leaves only the cubic field, and making this shrink to zero gives once again the free ion.

spin interaction alone can split the level Γ_2 of the cubic field. Both acting together will remove all degeneracy, but the separation produced will depend on a cross term and in addition is a second order effect in λ owing to the vanishing of the mean orbital angular momentum. If the level Γ_4 is lowest, these conclusions do not hold, both the anisotropy and Δ being first order effects of the rhombic field.

If Γ_2 lies lowest, as in Ni and Cr, it is possible to prove a result very similar to that which was shown to hold for the rare earths, namely that the expansion of χ for a crystal powder should contain no term in $1/T^2$. The Hamiltonian inclusive of the magnetic field is invariant for a half turn about the magnetic field. The group consisting of this operation and the identical

operation has two one-dimensional (eindeutig) representations, associated respectively with the odd and even series of values of the quantum number M . (M is not a good quantum number when the electric field and $(L \cdot S)$ are diagonalized.) It is clear that of the three constituent levels $\epsilon_1, \epsilon_2, \epsilon_3$ of Γ_2 , two, (ϵ_1, ϵ_2) belong to one representation, and the third (ϵ_3) to the other. The third level has therefore no magnetic or other connection with the other two, which are linked to each other. In the presence of the magnetic field, the level ϵ_3 is unaltered, while ϵ_1, ϵ_2 undergo equal and opposite displacements away from each other. This neglects the high-frequency shift, which is practically the same for all three levels. The value of $k\Delta$ is therefore $(\epsilon_1 + \epsilon_2 + \epsilon_3)/3 - (\epsilon_1 + \epsilon_2)/2 = (2\epsilon_3 - \epsilon_1 - \epsilon_2)/6$, an expression which is of course invariant of the origin of energy. On permuting the axes the "field free" levels $\epsilon_1, \epsilon_2, \epsilon_3$ undergo a corresponding permutation; if we average the above expressions for $k\Delta$ over three cyclic permutations, which corresponds to finding the value of $k\Delta$ for a crystal powder, the result is seen to vanish.

We now turn our attention to the secular determinant of the problem in order to give the considerations of the foregoing sections a more quantitative form.

THE SECULAR DETERMINANT

The Hamiltonian

We assume a Hamiltonian function

$$\sum_i [D(x_i^4 + y_i^4 + z_i^4) + Ax_i^2 + By_i^2 - (A+B)z_i^2] + \lambda(L \cdot S) + \beta H \cdot (L + 2S) \quad (3)$$

where A, B, D are constants specifying the crystal field, λ is the constant of the orbit-spin interaction, β is the Bohr magneton $eh/4\pi mc$ and H is the magnetic field.

In the Hamiltonian (3) the dominant term is the term in D . The most general field of rhombic symmetry which is nearly cubic would give a Hamiltonian containing other terms in addition to those written down. These would be of higher order and no greater generality would be obtained by their inclusion. The rhombic term and the orbit-spin coupling are of comparable magnitude. The magnetic energy may always be regarded as a small perturbation in calculating the susceptibility, even though the field is strong enough to produce a Paschen-Back effect, always provided that the magnetic separations do not become comparable with kT so that saturation effects occur. This follows from an application of the principle of spectroscopic stability due to Van Vleck.¹³

The matrix elements

The following matrix elements in the (M_L, M_S) system of quantization are required. They have been obtained by the method used in the previous paper.²

$$\begin{aligned} D \sum_i (x_i^4 + y_i^4 + z_i^4) (M_L, M_L) \\ = \text{const.} + q'DM_L^2 [7M_L^2 + 5 - 6L(L+1)], \\ D \sum_i (x_i^4 + y_i^4 + z_i^4) (M_L, M_L \pm 4) \\ = \frac{1}{2} q'D [(L \mp M_L)! (L \pm M_L + 4)! / (L \pm M_L)! (L \mp M_L - 4)!]^{1/2}, \end{aligned}$$

¹³ Reference 1, page 231.

$$\begin{aligned}
& \sum [Ax_i^2 + By_i^2 - (A+B)z_i^2](M_L, M_L) \\
& = \text{const.} + \frac{1}{2}a(A+B)[3M_L^2 - L(L+1)], \\
& \sum [Ax_i^2 + By_i^2 - (A+B)z_i^2](M_L, M_L \pm 2) \\
& = -a(A-B)[(L \mp M_L)!(L \pm M_L + 2)!/(L \mp M_L - 2)!(L \pm M_L)!]^{1/2}/4.
\end{aligned}$$

Here q and a are the ratios of the matrix elements calculated for a system of n electrons to those for a one-electron system; the sign of q has been discussed by Van Vleck.⁴ The summation is over all the electrons of the incomplete group. The two additive constants, as well as q and a , are independent of M_L . These matrix elements are all diagonal in L . The elements non-diagonal in L are not required, since the crystal field is assumed not to destroy the Russell-Saunders coupling of the vectors I_i, s_i . Since the elements do not involve the spin, they may be regarded as diagonal in M_S . We also require

$$\begin{aligned}
(L \cdot S)(M_L, M_S; M_L, M_S) &= M_L M_S, \\
(L \cdot S)(M_L, M_S; M_L \pm 1, M_S \mp 1) \\
&= \frac{1}{2}[(S \pm M_S)(S \mp M_S + 1)(L \mp M_L)(L \pm M_L + 1)]^{1/2}.
\end{aligned}$$

The secular determinant

The orbital problem, being common to all three ions Ni, Co, Cr, may be treated first. The orbital terms of the Hamiltonian are all of type $\Delta M_L = 0, \pm 2, \pm 4$, so that the secular determinant

$$\mathfrak{C}(M_L, M_S; M_L', M_S') - \delta(M_L, M_S; M_L', M_S')W = 0,$$

breaks up into two factors, one of the fourth order involving $M_L = \pm 3, \pm 1$, and one of the third order involving $M_L = 0, \pm 2$. These factors are symmetrical about the principal and secondary diagonals, so that it is necessary to write down only the first row and central elements of the second row of each

$$\begin{vmatrix} -3Dq + 15\sigma & -15^{1/2}\delta & 15^{1/2}Dq & 0 \\ & -5Dq - 9\sigma & -6\delta & \end{vmatrix}, \quad \begin{vmatrix} -13Dq & -30^{1/2}\delta & 5Dq \\ & -12\sigma & \end{vmatrix}$$

Here σ, δ have been written for $a(A \pm B)/2$ and $q = 12q'$. The terms in D can be diagonalized¹⁴ by means of unitary transformations SS^{-1}, TT^{-1} with

$$S = \left(\frac{1}{4}\right) \begin{pmatrix} h & k & -k & -h \\ -k & h & -h & k \\ k & h & h & k \\ h & -k & -k & h \end{pmatrix} \quad \begin{matrix} h = 5^{1/2} \\ k = 3^{1/2} \end{matrix} \quad T = \left(\frac{1}{2}\right)^{1/2} \begin{pmatrix} 1 & 0 & 1 \\ 0 & 2^{1/2} & 0 \\ -1 & 0 & 1 \end{pmatrix}$$

We may denote the matrices S, T by $S(N, M_L), T(N, M_L)$. The columns are numbered by M_L having values $-3, -1, 1, 3$, for S and $-2, 0, 2$ for T . The

¹⁴ The wave functions $S\psi, T\psi$ which the transformations S, T introduce are precisely those given by Bethe (reference 11, page 166). They diagonalize the cubic and rhombic fields except for matrix elements of the rhombic field between different cubic levels.

rows are numbered by a new "cubic" quantum number N which may be supposed to take on the same set of values as M_L . N has no obvious physical meaning, but served to identify the roots W_N in the cubic field according to the scheme

$$W_{-3} = W_0 = W_3 = 0, W_{-2} = W_{-1} = W_1 = -8Dq, W_2 = -18Dq.$$

The relations (2) show that the transformation which diagonalizes the terms in D will factorize the orbital problem into three quadratics and a singlet. These are

$$\begin{vmatrix} 6(\sigma - \delta) & - (15)^{1/2}(3\sigma + \delta) \\ - (15)^{1/2}(3\sigma + \delta) & - 8Dq \end{vmatrix} \begin{vmatrix} - 8Dq & (15)^{1/2}(3\sigma - \delta) \\ (15)^{1/2}(3\sigma - \delta) & 6(\sigma + \delta) \end{vmatrix}$$

$$\begin{vmatrix} - 8Dq & - 2(15)^{1/2}\delta \\ - 2(15)^{1/2}\delta & - 12\sigma \end{vmatrix} \quad - 18Dq$$

We denote the roots of these by (r_{-3}, r_{-1}) , (r_1, r_3) , (r_{-2}, r_0) and r_2 , where the suffix is a new "rhombic" quantum number taking on the same values as N or M_L . This set of roots is, of course, invariant if the coefficients of the rhombic field be permuted cyclically, $A \rightarrow B \rightarrow -(A+B)$ but they undergo the cyclic permutation $r_{-1} \rightarrow r_{-2} \rightarrow r_1$, $r_{-3} \rightarrow r_0 \rightarrow r_3$, while r_2 is invariant. Let the transformation matrices which diagonalize these quadratics for given values of D , A and B be

$$\begin{matrix} & \begin{matrix} -3 & -1 \end{matrix} \\ \begin{matrix} -3 \\ -1 \end{matrix} & \begin{vmatrix} r & s \\ -s & r \end{vmatrix} \end{matrix} \quad \begin{matrix} & \begin{matrix} 1 & 3 \end{matrix} \\ \begin{matrix} 1 \\ 3 \end{matrix} & \begin{vmatrix} t & u \\ -u & t \end{vmatrix} \end{matrix} \quad \begin{matrix} & \begin{matrix} -2 & 0 \end{matrix} \\ \begin{matrix} -2 \\ 0 \end{matrix} & \begin{vmatrix} p & q \\ -q & p \end{vmatrix} \end{matrix} \quad \begin{matrix} & \begin{matrix} 2 \end{matrix} \\ \begin{matrix} 2 \end{matrix} & \begin{vmatrix} 1 \end{vmatrix} \end{matrix} \quad (4)$$

The values of the elements can be calculated for any given values of D , A and B . The columns are numbered by the "cubic" quantum number N and the rows by the "rhombic" quantum number Q . We now introduce the spin and have to differentiate between Ni, Cr and Co.

NICKEL

Mathematical theory

For nickel $S=1$, so that $M_S = -1, 0, 1$. The secular determinant, of order 21, breaks up into one of the tenth and one of the eleventh order, involving, respectively, even and odd values of $M = M_L + M_S$. This follows since the complete Hamiltonian contains only terms of the type $\Delta M = 0, \pm 2, \pm 4$. We are interested primarily in the root $-18Dq$ which lies below the others. It occurs once (with $M_S=0$) in the eleventh order determinant, and twice ($M_S = \pm 1$) in the tenth order determinant. Transforming the eleventh order determinant to the (N, M_S) representation, we require the element

$$\mathcal{H}(2, 0; N', M_S') = T(2, 0; M_L, 0) \mathcal{H}(M_L, 0; M_L', M_S') R^{-1}(M_L', M_S'; N', M_S'),$$

where R stands for S if $M_S' = \pm 1$, and for T if $M_S' = 0$. We have included the quantum number M_S in T and R as though they were diagonal in M_S . They are indeed independent of M_S . In the N, M_S representation the only nonvanishing elements of the orbit-spin and magnetic energies are found to be

$$\mathcal{H}(2, 0; 1, 1) = \mathcal{H}(2, 0; -1, 1) = \mathcal{H}(2, 0; 1, -1) = -\mathcal{H}(2, 0; -1, -1) = (2)^{1/2}\lambda$$

$$\mathcal{H}(2, 0; -2, 0) = 2\omega.$$

We know from (1) that the diagonalization of the orbit-spin terms involves the solution of cubic equations, so that it is simpler to diagonalize rhombic field terms instead. This is accomplished by the matrices (4). The relevant matrix elements in the (Q, M_S) system of representation are

$$\mathcal{H}(2, 0; -3, -1) = \mathcal{H}(2, 0; -3, 1) = (2)^{1/2}\lambda S,$$

$$\mathcal{H}(2, 0; -1, -1) = \mathcal{H}(2, 0; -1, 1) = (2)^{1/2}\lambda r,$$

$$\mathcal{H}(2, 0; 1, -1) = \mathcal{H}(2, 0; 1, 1) = (2)^{1/2}\lambda t,$$

$$\mathcal{H}(2, 0; 3, -1) = \mathcal{H}(2, 0; 3, 1) = -(2)^{1/2}\lambda\omega,$$

$$\mathcal{H}(2, 0; -2, 0) = 2\omega p, \mathcal{H}(2, 0; 0, 0) = -2\omega q,$$

from which the first approximation to the energy can be found. The tenth order determinant is not quite so simple, for the root $-18Dq$ occurs twice, with $M_S = \pm 1$, the degeneracy not being removed by the rhombic field. Suppose the Hamiltonian has been transformed to the (Q, M_S) system, i.e., to the form $\mathcal{H}_0 + \lambda_0 \mathcal{H}_1 + \omega_0 \mathcal{H}_2$, where \mathcal{H}_0 is diagonal and \mathcal{H}_1 has no diagonal terms. Apply the transformation

$$(1 + \lambda S)(\mathcal{H}_0 + \lambda \mathcal{H}_1 + \omega \mathcal{H}_2)(1 - \lambda S + \lambda^2 S^2 + \dots)$$

and choose S so as to make the coefficient of λ vanish in this expression. Then the Hamiltonian becomes

$$\mathcal{H}(n, m) = \mathcal{H}_0(n, m) + \lambda^2 \sum \mathcal{H}_1(n, i) \mathcal{H}_1(i, m) / h\nu(n, i) + \omega \mathcal{H}_2(n, m)$$

$$+ \lambda\omega \sum [\mathcal{H}_1(n, i) \mathcal{H}_2(i, m) / h\nu(n, i) - \mathcal{H}_2(n, i) \mathcal{H}_1(i, m) / h\nu(i, m)]$$

$$+ \dots$$

There are now terms in λ^2 on the diagonal which remove the degeneracy¹⁵ and the coefficient of ω is altered by a term of order $\lambda |D$. We can now set up the quadratic secular problem connected with the two coincident roots, and solve it on the assumption that the magnetic field is small. The two resulting values of W ,¹⁶ together with that obtained from the eleventh order determinant, are given below.

$$-18Dq + 4\lambda^2(\alpha_1 + \alpha_2) + \omega^2(1 + 8\lambda\alpha_1)/\lambda^2(\alpha_2 - \alpha_3) + 4\omega^2\alpha_1,$$

$$-18Dq + 4\lambda^2(\alpha_1 + \alpha_3) - \omega^2(1 + 8\lambda\alpha_1)/\lambda^2(\alpha_2 - \alpha_3) + 4\omega^2\alpha_1,$$

$$-18Dq + 4\lambda^2(\alpha_2 + \alpha_3) + 4\omega^2\alpha_1.$$

Here

$$\alpha_1 = p^2/(r_2 - r_{-2}) + q^2/(r_2 - r_0),$$

$$\alpha_2 = r^2/(r_2 - r_{-1}) + s^2/(r_2 - r_3),$$

$$\alpha_3 = t^2/(r_2 - r_1) + u^2/(r_2 - r_3).$$

¹⁵ J. H. Van Vleck, Phys. Rev. **33**, 467 (1929).

¹⁶ There are actually first order terms in the magnetic field of order $(\lambda^2/\text{cubic sepn.})^2$ but the contribution of these to the susceptibility is so small that they can be completely neglected.

If the axes undergo a permutation represented by $A \rightarrow B \rightarrow -(A+B)$ it is readily verified that the roots r undergo a corresponding permutation, and $\alpha_1 \rightarrow \alpha_2 \rightarrow \alpha_3$. The susceptibility along the z axis is found from the general formula

$$\chi = -(N/H) \sum (\partial W / \partial H) e^{-W/kT} / \sum e^{-W/kT}.$$

On the assumption that the exponentials can be expanded, this gives

$$\chi_1 = (8N\beta^2/3kT)[1 + 8\lambda\alpha_1 + \theta_1/kT + \dots] - 8N\beta^2\alpha_1, \quad (5A)$$

where terms in $1/T^3$ and above have been discarded, and

$$\theta_1 = 2\lambda^2(\alpha_2 + \alpha_3 - 2\alpha_1)/3.$$

The term independent of temperature arises as usual from the term in H^2 in the energy. The other two principal susceptibilities are obtained by permuting the axes cyclically, so that the mean of the three principal susceptibilities is

$$\bar{\chi} = (8N\beta^2/3kT)[1 + (8\lambda/3 - kT)(\alpha_1 + \alpha_2 + \alpha_3)], \quad (5B)$$

in which there is rigorously no term in $1/T^2$.

If the crystal field is assumed to have cubic symmetry, the lowest level has a first order effect, and the susceptibility is

$$\chi = (8N\beta^2/3kT)(1 - 4\lambda/5D) + 4N\beta^2/5D. \quad (5C)$$

Comparison with experiment

In the Hamiltonian the constant λ of the orbit-spin coupling is known, while Aa , Ba , Dq are to be determined from the observed susceptibilities. A measurement of the mean susceptibility at one temperature will enable us to determine the one parameter D if we assume as an approximation that Aa and Ba vanish. The assumption of a purely cubic field is a convenient approximation in estimating the order of magnitude of D . We shall consider later the effect of the rhombic field.

In Ni the multiplet is inverted; its over-all width is given by $|\Delta\nu| = \lambda S(2L+1)$. By using the value 2347 cm^{-1} given by Laporte¹⁷ for $\Delta\nu$ we obtain $\lambda = -335 \text{ cm}^{-1}$. The observed value 26.56×10^{-6} of the susceptibility at 170°K ,⁷ giving $\chi T = 45.15 \times 10^{-4}$, then leads to a value of Dq from Eq. (5) equal to 1485 cm^{-1} , which corresponds to an over-all separation due to the cubic field of the order of 3 volts. Thus according to (5) the graph of χT against T is a straight line which we have chosen to pass through the experimental point at 170°K , and which cuts the χT axis at $\chi T = 43.64 \times 10^{-4}$. If we had calculated Dq from experimental points at different temperatures, slightly different values would have been obtained. In Fig. 2 we have plotted the experimental values of χT obtained by Gorter, de Haas, and van den Handel,⁷ using T as abscissa. It is seen that the experimental points, with the

¹⁷ O. Laporte, Zeits. f. Physik 47, 761 (1928).

exception of those at low temperatures, lie fairly close to the theoretical curve. The relation proposed by Gorter, de Haas, and van den Handel is $\chi(T+3)=\text{const.}$ In Fig. 2 we have also plotted the experimental values of $\Delta(T+3)$ as a function of T ; the approximation of this function to a constant is seen to be very poor indeed. We conclude that the observations are represented much more closely by $\chi T = \text{const.}$ than by $\chi(T+3) = \text{const.}$ It should be remembered that this method of plotting the experimental data, which is equivalent to plotting the square of the effective magneton number as a function of T , is a much more severe test than plotting $1/\chi$ against T , as is usually done.

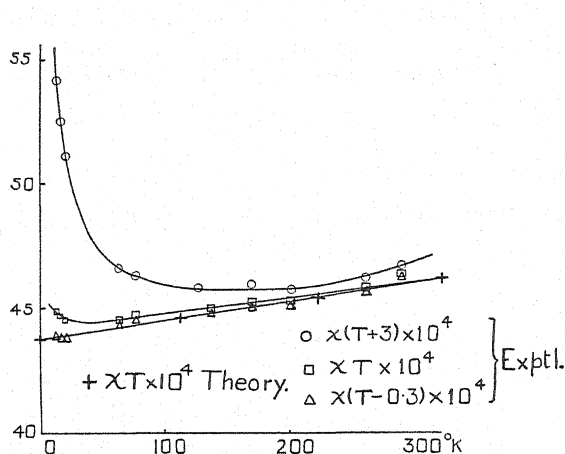


Fig. 2A.

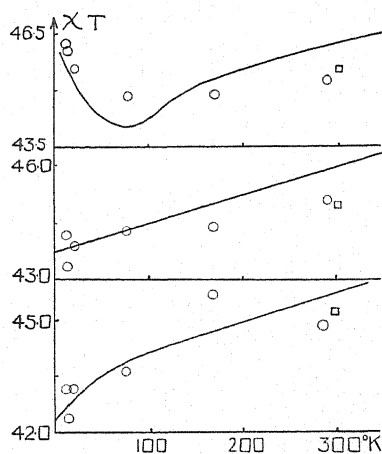


Fig. 2B.

Fig. 2. The curves in Fig. 2A serve a double purpose. In the first place they show that a formula of the type $\chi T = A + BT$ demanded by theory for Ni, represents the experimental points better than the curve $\chi(T+3.0) = \text{const.}$ given by Gorter, de Haas and v. d. Handel.⁷ In the second place it is seen that the experimental values of $\chi(T-0.3) = \text{const.}$ fit the theoretical curve for χT exactly. The addition of -0.3 to T is a minor effect and perhaps represents the result of exchange forces not envisaged in the crystalline potential we have assumed. The one arbitrary parameter in the theory has been chosen to fit the observed magneton number at 170°K . The slope of the χT curve is then uniquely determined and its agreement with experiment is a good confirmation of the theory. Fig. 2B shows the theoretical principal susceptibilities χT of Ni plotted against T , and the experimental points of Jackson corrected by Gorter, de Haas and v. d. Handel,⁷ which are marked in circles (see text).

There still remains the deviation of the three low temperature points from the theoretical curve. The present calculation takes no account of inter-molecular actions, such as exchange effects, which are not describable by an electric field of definite symmetry. These effects are known to be capable of giving rise to a term Δ which will however be small on account of the high dilution of the salt. This correction will be important at low temperatures. If we plot $\chi(T-0.3)$ against T , the experimental points are brought to lie much more nearly on a straight line. It may be that the term $\Delta = 0.3^\circ$ is a measure of inter-molecular actions other than the crystal fields here contemplated,

We must now consider the effect of the rhombic field in producing asymmetry in the principal susceptibilities. Using Rabi's⁵ values for $\text{NiSO}_4(\text{NH}_4)_2\text{SO}_4 \cdot 6\text{H}_2\text{O}$ and equating them to the three expressions obtained by permuting cyclically the indices in (5A), we obtain three simultaneous equations for $\alpha_1, \alpha_2, \alpha_3$, whose solution is

$$\alpha_1 = -7.94 \times 10^{-5}, \alpha_2 = -8.12 \times 10^{-5}, \alpha_3 = -8.29 \times 10^{-5}.$$

From these we have to determine the three parameters Dq, Aa and Ba which specify the crystal field. To set up and solve the algebraic equations connecting these parameters with the α 's would be very lengthy, so we have to recourse to the method of trial and error. Thus we find that a crystal field having the Hamiltonian

$$1260(x^4 + y^4 + z^4) + 176(x^2 + 2y^2 - 3z^2)$$

gives

$$\alpha_1 = -7.96 \times 10^{-5}, \alpha_2 = -8.13 \times 10^{-5}, \alpha_3 = -8.24 \times 10^{-5}.$$

Better agreement could be obtained by using a slightly larger value of the constant of the rhombic field and by changing the ratios of the coefficients of the rhombic field, but it is not, perhaps, worth while pursuing numerical accuracy when the experimental precision is not very high. It is instructive, particularly for comparison with cobalt, to observe how little dissymmetry is produced by a comparatively large rhombic term. Thus the field given above produces an over-all separation of the cubic level Γ_4 amounting to about one-half the interval separating this cubic level from the level Γ_5 . The separation produced in the level Γ_2 has an over-all width of 1.5 cm^{-1} so that the individual values of Δ for the three axes are almost negligible, and the expansions of the exponentials which we have used is legitimate even at liquid hydrogen temperatures. At extremely low temperatures Δ is relatively important and it is this fact that accounts for the different behavior of the principal χT for small values of T , shown in Fig. 2B.

Gorter, de Haas and v. d. Handel⁷ have given values of the principal susceptibilities of $\text{Ni}(\text{SO}_4) \cdot 7\text{H}_2\text{O}$ using their own values of the mean susceptibility together with the differences in the principal susceptibilities found by Jackson.⁶ The exactitude of these values is open to question, but to illustrate how they check with the theory we have plotted the experimental values (shown by circles) and the theoretical curves *using for the constants of the crystal field those values found for* $\text{Ni}(\text{SO}_4)_2(\text{NH}_4)_2 \cdot 6\text{H}_2\text{O}$. The agreement is very good, considering the sensitivity of the method of plotting the results, and the experimental results confirm the existence of a $1/T^2$ term for the individual axes although there is none in the mean. The values found by Rabi⁵ on the ammonium salt are marked by squares. Since, as far as we can tell, the constants of the crystal field acting on the Ni ion are exactly equal in the two salts, it seems likely that the ions surrounding the Ni ions are the same and in the same relative positions in the two salts.

CHROMIUM

Chrome alum, whose susceptibility at temperatures down to that of liquid helium has been measured by de Haas and Gorter,⁹ forms cubic crystals, so that no differences in the principal susceptibilities are to be expected.¹⁸ It will be sufficient to suppose the crystal field to have cubic symmetry. Van Vleck¹⁴ has shown that for Cr, whose ground state is 4F , the matrix elements of $\sum_i (x_i^4 + y_i^4 + z_i^4)$ have the same sign as those of $(x^4 + y^4 + z^4)$ calculated for a single electron system; that is the coefficient q is positive. The root $-18Dq$ (Γ_2) is accordingly lowest. The secular problem inclusive of spin is of order 28; but on account of the selection rule $\Delta M = 0, \pm 2, \pm 4$, obeyed by the Hamiltonian ($\Delta M = 0, \pm 4$ if the rhombic field is absent) the secular determinant breaks up into the product of two, which are identical except as regards the sign of the terms in H . This is, of course, an example of the Kramers degeneracy.¹⁹ Reference to the diagram in Bethe¹¹ shows that the orbit-spin interaction is incapable of removing the degeneracy of Γ_2 in any approximation, so that we need consider only the terms in H , which give rise to first and second order Zeeman effects. Fixing our attention on one of the two secular determinants of order 14, we observe first of all that the root Γ_2 occurs twice ($N=2$, with $M_s = -\frac{1}{2}, \frac{3}{2}$, say). In passing from the original M_L, M_s representation to that in which the cubic field is diagonal, the spin terms $2M_s$ will of course remain on the diagonal, so that the two occurrences of the root Γ_2 have first order moments 3ω and $-\omega$ from this determinant and -3ω and ω from the other. If this were all, the magneton number would have the "spin only" value $(15)^{1/2}$, verifying that the spin is free. But we have still to consider the off-diagonal terms involving ω , which represent the contribution of the orbit, and which are diagonal in M_s . We readily find for the elements satisfying this condition

$$\mathcal{H}(2, -\frac{1}{2}; -2, -\frac{1}{2}) = -\lambda + 2\omega$$

$$\mathcal{H}(2, 3/2; -2, 3/2) = 3\lambda + 2\omega$$

which gives for the levels in the presence of the field

$$\begin{aligned} &= \omega(1 - 2\lambda/5Dq) - 2\omega^2/5Dq, \\ &\pm 3\omega(1 - 2\lambda/5Dq) - 2\omega^2/5Dq. \end{aligned}$$

Disregarding the high-frequency term for the moment, we obtain for the susceptibility

$$\chi = (15N\beta^2/3kT)(1 - 2\lambda/5Dq)^2.$$

¹⁸ The chrome alum $\text{KCr}(\text{SeO}_4)_2 \cdot 12\text{H}_2\text{O}$, which forms cubic crystals has in its absorption spectrum a narrow doublet whose separation is roughly 4 cm^{-1} (cf. K. Schnetzler, *Ann. d. Physik* **10**, 373 (1931)). If this doublet is due to the doubling of the basic level Γ_2 , the Hamiltonian must contain non-cubic terms, besides the predominant cubic terms. This follows since the orbit-spin coupling does not decompose Γ_2 . If this is so, this alum should exhibit slight asymmetry in its principal susceptibilities.

¹⁹ H. A. Kramers, *Proc. Amst. Acad.* **33**, 959 (1930).

Here λ is positive, so that the magneton number should be less than the "spin-only" value, which is actually found to be the case. From the value 912 cm^{-1} given by Laporte¹⁷ for the over-all separation of the 4F multiplet in chromium, we deduce $\lambda = 87 \text{ cm}^{-1}$ and taking de Haas and Gorter's⁹ value 19.02 for the Weiss magneton number of Cr, we obtain $Dq = 3730 \text{ cm}^{-1}$. This justifies our neglect of the high-frequency term, which is proportional to λ/D . The experimental results do not show any trace of high-frequency effects. It is not possible to place much reliance on the above estimate of the magnitude of the separation due to the cubic field, since a small change in the experimental magneton number would produce a very considerable change in the calculated value of Dq . It need scarcely be pointed out that for Cr, as for Ni, the introduction of even a large rhombic field will not appreciably affect the isotropy of the susceptibility. As yet, however, no measurements have been made on the principal susceptibilities of Cr salts.

COBALT

Mathematical theory

It may be stated here that our calculations on Co are not as complete as those on Ni and Cr, but the difficulties are only in the numerical computation. There seems to be no doubt, however, that good agreement with experiment could be obtained by a more exhaustive trial-and-error procedure. The ground state of cobalt is 4F , and the secular determinant is of order 28. On account of the Kramer's degeneracy, it breaks up into two determinants of order 14, identical except for the sign of the terms in the magnetic field. The orbital part of the problem is the same as for nickel, where the ground state was also an F state, so that in a cubic field the roots are 0, $-8Dq$, $-18Dq$. On account of the inversion discussed above, the level 0 (denoted Γ_4 above) is now lowest, and occurs six times in each secular determinant of order 14, namely, with $N = -3, 0, 3$ and $M_s = \frac{3}{2}, \frac{1}{2}$ or $-\frac{3}{2}, -\frac{1}{2}$. The portion of the determinant involving these roots, which coincide in the absence of a rhombic field and orbit-spin coupling, is

$$\begin{array}{cccccc}
 6B - 3l\omega & -3m + 3\omega/2 & 0 & 0 & n & 0 \\
 -3m + 3\omega/2 & 6A - 3l\omega & 0 & 0 & -n & 0 \\
 0 & 0 & 6B + l\omega & m + 3\omega/2 & 2m & n \\
 0 & 0 & m + 3\omega/2 & 6A + l\omega & 2m & -n \\
 n & -n & 2m & 2m & 6C - \omega & 0 \\
 0 & 0 & n & -n & 0 & 6C + 3\omega
 \end{array} \quad (6)$$

Here $l = 1 + 15\lambda/32D$, $m = 3\lambda/4$, $n = 3(3)^{1/2}\lambda/4$. Interaction between the levels 0, $-8Dq$, $-18Dq$ has been taken account of with sufficient accuracy by the diagonal terms in $\omega\lambda/D$. This amounts to discarding the high-frequency part of the susceptibility; if we do this we may restrict ourselves to this sixth order determinant in calculating the levels. As the sextic secular equation is not soluble when the rhombic field is comparable with the orbit-spin coupling,

we must assume that the former is much smaller than the latter or *vice-versa*. Our calculations indicate that the two influences are in fact of comparable magnitude, which makes close numerical agreement difficult to obtain without more elaborate computations. Here we deal with the two extreme cases only.

Orbit-spin greater than rhombic field

Consider first the case where the orbit-spin coupling is greater than the rhombic field. The orbit-spin interaction alone is capable of partially removing the degeneracy in (6). When we do not restrict ourselves to interactions within the sextet the degeneracy which survives the cubic field and the orbit-spin interaction is given by the resolution $\Gamma_4 D_{3/2} = \Gamma_6 + \Gamma_7 + 2\Gamma_8$, i.e., two singlets and a quadratic occurring twice. When we restrict ourselves to interactions within the sextet the degeneracy must at least be as great as this, which ensures that the sextet will have simple roots when σ , δ , ω all vanish. These are readily found to be $15\lambda/4$, $3\lambda/2$ (twice), $-9\lambda/4$ (three times), and the corresponding form of the sextet, with these roots on the diagonal, can easily be written down. The energy levels in the presence of the magnetic field have now to be found on the assumption that the rhombic field is small compared with the orbit-spin interaction. In cobalt $\lambda = -180 \text{ cm}^{-1}$ so that the triply degenerate level $-9\lambda/4$ will have such a small Boltzmann factor that its contribution to the susceptibility may be neglected even at room temperatures; this level does not affect the moment of the level $15\lambda/4$, and in calculating its influence on the moment of the levels $3\lambda/2$, which is relatively less important in any case, we may suppose it to remain undecomposed by the rhombic field. But in obtaining the moments of the two levels $3\lambda/2$, it is necessary to allow the rhombic field to remove this degeneracy. We have calculated the level $15\lambda/4$ correct to a third order approximation and the two levels $3\lambda/2$ to a second order approximation.²⁰ The calculation is straightforward but too elaborate to be given here. To illustrate the type of result obtained, we give the energy levels in the presence of the magnetic field only for the lowest level, correct to a second order perturbation calculation. For brevity the third order terms have been omitted. We find

$$W = 15\lambda/4 - \omega(13/6 + 5\lambda/8D) + [(36\sigma - 35\omega - 165\lambda\omega/16D)^2 + 432\delta^2]/405\lambda + \dots$$

The expressions for the other levels are of the same type.

At sufficiently low temperatures the square of the effective Bohr magneton number $n_B^2 = 3\chi kT/N\beta^2$ is given by three times the square of the coefficient of the term in H . Hence, if we extrapolate the experimental values of χT to $T=0$, we obtain three equations which theoretically enable us to determine σ , δ and D . The values obtained in this way are however so sensitive to variations in χT at $T=0$ within the range of possible error that it is

²⁰ The details of the inclusion of the third order terms in the perturbation problem will be considered by Mr. Jordahl in his paper on Cu.

preferable to proceed differently. The argument of Van Vleck⁴ shows that if the cubic field acting on the metallic ion be the same in nickel ammonium sulphate as in cobalt ammonium sulphate the constant Dq has the same value numerically. We accordingly assume $Dq = -1200 \text{ cm}^{-1}$, thereby giving up the possibility of obtaining values of σ and δ for arbitrarily given values of $(\chi T)_0$; instead we assume values for σ and δ and calculate the susceptibilities at various temperatures. The values which have been chosen for illustration are $\sigma = \delta = 20$, corresponding to a term $40(x^2 - z^2)$ in the Hamiltonian, which gives roughly the right degree of asymmetry. It is of course possible to choose different values for the individual coefficients of x^2 , y^2 , z^2 , but the computations are laborious and do not give any new information. Two points deserve mention. In the first place, a much smaller rhombic field is required in cobalt salts to produce the observed asymmetry than is needed for nickel salts despite the much greater isotropy of the latter. In the second place the calculated mean susceptibility for the three orientations is consistently greater than that observed. Fig. 3A shows the calculated values of $n_B^2 = 3kT\chi/N\beta^2$ plotted against T for the three magnetic axes of $\text{Co}(\text{NH}_4)_2(\text{SO}_4)_2 \cdot 6\text{H}_2\text{O}$. The trend of these curves may readily be understood in a qualitative way. At low temperatures the only level contributing to the susceptibility is the lowest. Since this has both a first and a second order Zeeman effect $\chi T = a + bT$, a and b being constants. At higher temperatures the two states $3\lambda/2$ begin to contribute to the susceptibility, but this is counteracted by the depopulation of the lowest level; these higher levels have smaller Zeeman effects than the levels $15\lambda/4$ so that the curve of χT against T rises less steeply and tends to an almost constant value. At still higher temperatures the three levels $-9\lambda/4$ would also contribute to the susceptibility but these temperatures are not reached experimentally.

The value of n_B^2 is plotted also for the case where there is no rhombic field and this curve is shown dotted in Fig. 3A. It should be noticed that the effect of the rhombic field is to produce asymmetry and also to lower the mean value of the three principal susceptibilities.²¹ Unfortunately, it is not within the limits of the present approximation to make the rhombic field sufficiently large to give agreement with experiment, as then the convergence would be poor. It is very reasonable, however, to suppose that a larger

²¹ Let us imagine the magnitude of the rhombic field is varied from a very large value down to zero. The behavior of the three principal susceptibilities is as follows. Orientation (3) starts at the "spin only" value, decreases and then starts to increase again, finally ending on the curve for zero rhombic field shown in Fig. 3A. Orientation (2) starts slightly above the "spin only" value due to the introduction by the orbit spin coupling of small diagonal elements in the orbital angular momentum, representing the contribution of the higher cubic levels, and then decreases at low temperatures but increases at higher temperatures, ending finally with (3). Orientation (1) is rather complicated. It starts with (2) but the susceptibility increases rapidly with decreasing rhombic field, and develops a hump at low temperatures. This is because for this orientation the lowest level has a large first order Zeeman effect. The susceptibility then begins to fall again, passing through a representative curve shown in Fig. 3B. The hump fades out, the susceptibility decreasing at low and increasing at high temperatures, finally ending with (2) and (3).

rhombic field would give good agreement with experiment, except possibly at low temperatures. Since the only measurements at low temperatures are those of Jackson,⁶ made as long ago as 1922, and which at other temperatures are known to be greatly in error, this discrepancy is not worth considering. When better experimental data are available another effort will be made to obtain a better solution of this troublesome sextet.

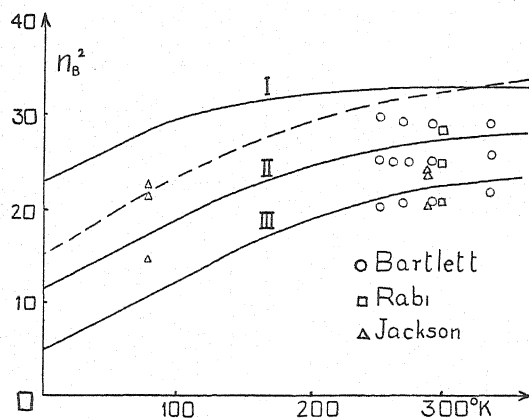


Fig. 3A.

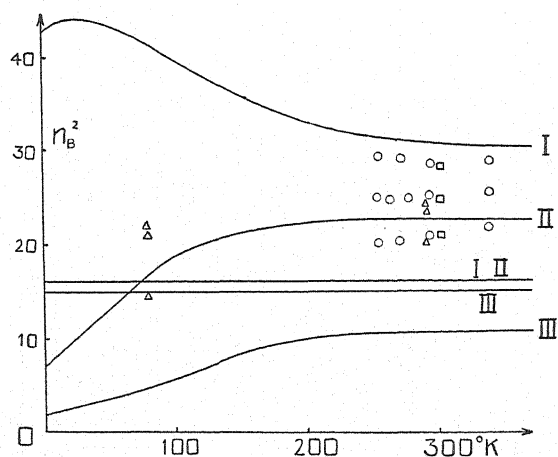


Fig. 3B.

Fig. 3. The heavy lines in Figs. 3 show the calculated values of n_B^2 for $\text{Co}(\text{NH}_4)_2(\text{SO}_4)_2 \cdot 6\text{H}_2\text{O}$ for the two rhombic fields (3A) $40(x^2 - z^2)$ (3B) $200(x^2 - z^2)$, while for comparison, the experimental points obtained by different observers are given. The numbers on the curves denote the axes to which the curves refer. The dotted lines in Fig. 3A is for zero rhombic field; the horizontal straight lines in Fig. 3B are for extremely large rhombic fields. It is reasonable to suppose that a rhombic field intermediate to the values we have taken would give agreement with experiment. It is significant that the results of Bartlett⁸ along axis (1) do actually seem to be falling with increasing T , as would be the case for an intermediate field. The agreement at low temperatures is not good but the experimental values are those of Jackson⁶ and may easily be in error.

Rhombic field greater than orbit-spin

In the hope that a perturbation calculation from the other limiting case would be more effective, calculations were also made from this end. Here the orbit spin is subsidiary to the rhombic field. The rhombic field can be seen to decompose the sextuply degenerate level into three doubly degenerate ones, with separations proportional to the coefficients of the rhombic field. The orbit-spin interaction does not remove the remaining degeneracy in the first approximation, but only in the second. Expressions for the energy levels and their first and second order Zeeman effects can be written down, and the susceptibility calculated for given values of the constants D , A , B , C of the crystal field, such that the rhombic field alone produces a separation which is small compared with that due to the orbit-spin alone. In the absence of the spin the energy levels are $6Aa$, $6Ba$, $-6a(A+B)$. We suppose that $-6a(A+B)$ lies below $6Aa$ and $6Ba$ and calculate the Zeeman effects of the two lowest roots correct to a third approximation, retaining terms in the magnetic field up to H^2 , in the usual way. The Zeeman effects are different according as the magnetic field acts along the x , y , or z axes. The exact expressions are long, but for illustration we give the two lowest roots, when the magnetic field acts along the x , y and z axes, correct only up to a second order perturbation calculation. For brevity the third order terms have been omitted.

$$\left. \begin{aligned} W_{\pm}(x) &= W_{\pm} - \omega_{+}[1 \pm (\alpha + 2\beta)\theta] \pm 2\omega_{+}^2\alpha^2\theta^3/3\lambda^2, \\ W_{\pm}(y) &= W_{\pm} - \omega_{-}[1 \mp (2\alpha + \beta)\theta] \pm 2\omega_{-}^2\beta^2\theta^3/3\lambda^2, \\ W_{\pm}(z) &= W_{\pm} + \omega[1 \pm (\alpha - \beta)\theta] \pm 2\omega^2\theta^3(\alpha + \beta)^2/3\lambda^2 \end{aligned} \right\}$$

where

$$\begin{aligned} W_{\pm} &= -6a(A+B) + 45\lambda^2(\beta - \alpha)/16 \pm 9\lambda^2\theta/4, \\ \theta &= (\alpha^2 + \beta^2 + \alpha\beta), \quad \omega_{+} = \omega(1 + 9\lambda/128D + 9\lambda\beta/4), \\ \omega_{-} &= \omega(1 + 9\lambda/128D - 9\lambda\alpha/4). \end{aligned}$$

We have written $\alpha = 1/6a(B-C)$ and β, γ for the cyclic permutations. From these expressions the principal susceptibilities may be calculated. For illustration, a rhombic field represented by $200(x^2 - z^2)$ in the Hamiltonian has been taken. The result is shown by the curves in Fig. 3B. It is readily verified that the curves correspond with those in Fig. 3A as shown by the numbering. The values of n_B^2 for a very large rhombic field are also shown by the horizontal straight lines. These are only limiting curves, however, since we have assumed the cubic field to predominate and therefore we cannot make the rhombic field as large as we please.

We have now calculated the susceptibilities (*i*) for a rhombic field $40(x^2 - z^2)$ (*ii*) for a rhombic field $200(x^2 - z^2)$, inclusive of orbit-spin coupling in both cases. The latter alone produces an over-all splitting of the level Γ_4 of the cubic field amounting to roughly 1000 cm^{-1} , while the separations produced by fields (*i*) and (*ii*) are respectively 480 cm^{-1} and 2400 cm^{-1} . The principal susceptibilities calculated on the basis of field (*i*) show roughly the

right degree of asymmetry, but are too high. Interpolating between (i) and (ii), it seems that a rhombic field of magnitude intermediate between (i) and (ii), but much nearer (i), will give good agreement with experimental values, except possibly at low temperatures, where however, the experimental values are in considerable doubt. Neither of the two methods of approximation used above are applicable in this intermediate region and the calculation would consist in the numerical solution of the original sextic secular equation.

It is interesting to notice that there would have been no gain in generality if we had added to the Hamiltonian terms representing a field of tetragonal symmetry or terms of rhombic symmetry of higher degree, provided the field of cubic symmetry always predominates. In order to see this we need only observe that in the orbital problem the lowest level Γ_4 of the cubic field is split by the rhombic field into the three levels G_2, G_3, G_4 , no two of which belong to the same representation of the rhombic group. Consequently it is not possible to change the moments of these levels by changing the type of rhombic field nor can this be accomplished even by the superposition of a tetragonal field, since this is only a particular form of rhombic field. Because the moments are fixed, the susceptibility can be changed only through the relative position of the energy levels and as there are three levels, it needs only two parameters to specify them. The two parameters A and B are capable of doing this.

CONCLUSION

In the present paper no account has been taken of the variation with temperature of the constants of the crystal field. The very small changes in interatomic distances caused by thermal expansion may possibly affect these constants quite appreciably because the force between ions in a crystal is known to vary very rapidly with the distance. We have moreover assumed that the principal axes of the various types of crystalline fields all coincide. Perhaps a better approximation to the actual state of affairs would be to assume fields of different symmetry, whose principal axes were inclined to each other, the relative orientations depending on temperature in some complicated way. There would then arise the possibility of an explanation of the results of Bartlett,⁸ who finds that the orientation of the principal susceptibilities relative to the crystallographic axes depend on temperature, the total variation being of the order of 5 degrees in a range of temperature 100°C.

From the considerations developed in this and the preceding paper, it should be evident that it is only rarely that the constant Δ of the experimenters has any theoretical interpretation. In order that it may have, it is necessary that the expansion $\chi = C/T - C\Delta/T^2 + \dots$, should converge very rapidly. This condition may be expressed in another form, that the Stark separations of the levels contributing to the susceptibility should be small compared with kT . This is not satisfied in the rare earths nor with Co but our calculations have shown that it is satisfied with Ni and Cr. That the susceptibility of the rare earths can be represented by the Curie-Weiss law

is merely fortuitous. Even here the value of Δ obtained depends on the temperature at which the measurements are made and in this sense Δ has no theoretical significance.

One of the most surprising facts revealed by our calculations of the susceptibilities in crystals is that a field of cubic symmetry should be capable of allowing such excellent agreement to be obtained with experiment. At first sight there seems to be no reason whatever for the field to possess cubic, or even nearly cubic, symmetry. In the case of Ni it was definitely established that a field predominantly rhombic and of the form $Ax^2 + By^2 - (A+B)z^2$, was incapable of giving the observed principal susceptibilities. The next assumption is naturally a field of cubic symmetry together with a much smaller rhombic term, an assumption which has proved completely successful with Ni, Cr and Co. For the rare earths, where measurements of the principal susceptibilities are lacking, and only the variation with temperature of the mean susceptibility has been observed, good agreement with experiment is obtained on the assumption of a cubic field alone. Without understanding why complicated crystals should have such simple crystalline fields, it must at least be conceded that the evidence in favor of a predominant field of cubic symmetry is strong. Whether or not there are other types of field which will give equally as good agreement with experiment remains to be seen.

In our calculations of paramagnetic susceptibilities, both of the rare earths and of the elements of the iron group, the sign of D in Eq. (3) has been consistently positive. In a Letter to the Editor²² Gorter finds that this choice of the sign of D agrees with there being water molecules (or else oxygen ions) arranged at the corners of an octahedron around the paramagnetic ion.

The writers wish to place on record their thanks to Professor J. H. Van Vleck, to whose constructive and stimulating criticisms the present work owes a great deal.

²² C. J. Gorter, *Phys. Rev.* **42**, 437 (1932).

Diamagnetism of Water at Different Temperatures

By A. P. WILLS AND G. F. BOEKER
Department of Physics, Columbia University

(Received October 10, 1932)

Attention is called to the discordant results found by different observers for the diamagnetism of water at different temperatures. A new and very sensitive device called a manometric balance is described. The device was designed for the purpose of investigating the variation of the specific susceptibility of water with varying temperature. Experiments with water which had just been boiled in order to get rid of dissolved air indicated less diamagnetism at temperatures higher than 23.5°C; and experiments upon water which was boiled and left standing for several days in contact with helium gas indicated greater diamagnetism at temperatures higher than 23.5°C; the change in the specific susceptibility was less than one percent in each case.

THE subject of the present communication has already received considerable attention from various experimentalists. The results obtained by different investigators,¹ using different methods, are not in agreement; in fact, the variations found for the specific susceptibility of water do not always agree as regards sign; for example, Piccard, using a modified Quincke method, found that the diamagnetism of water is greater at higher temperatures, while Cabrera and Duperier, using a torsion method, found it to be less. The magnitudes of the variations found were in all cases less than 3 percent of the specific susceptibility (susceptibility per unit mass) of water at 20°C, which from previous absolute measurements is known to have a numerical value of -0.72×10^{-6} , approximately, in c.g.s. units.

At a recent meeting² of the French Academy a summary of the results obtained by the various investigators referred to above was presented in the form of a diagram. This diagram on a somewhat different scale is reproduced in Fig. 1, a curve representing the results of Mathur, obtained in 1931, being added. The lack of agreement in the results obtained by these investigators for the diamagnetism of water at different temperatures is very remarkable, and the reasons therefore seem very obscure.

The purpose of the present paper is to describe a new method for the investigation of the phenomena in question, and to present the results of some preliminary experiments which may serve to throw some light upon the anomalous results previously obtained.

The device which we employ is called a manometric balance and operates on the principle of balancing the actions of two magnetic fields, one acting upon water at some specified temperature and the other upon water at a

¹ Du Bois, Wied. Ann. 95, 167 (1888); Jager and Meyer, Wied. Ann. 67, 427, 707 (1899); Piaggese, Phys. Zeits. 4, 347 (1905); Piccard, C. R. 155, 1497 (1912); Marke, Bull. Acad. Danemark p. 395 (1916); Cabrera and Duperier, Jour. d. Physique et le Radium 6, 121 (1925); Mathur, Ind. Jour. Phys. 15, part 3, 207 (1931).

² See Comptes Rendus 191, 589 (1930).

standard temperature. The theory of the balance will be given after the apparatus itself has been described.

THE MANOMETRIC BALANCE

In Fig. 2 the letter M designates one of the two coaxial cores of an electromagnet, each core being about 10 cm in diameter, and M_1, M_2 designate two of four equal pole-tips in the forms of truncated cones, cemented on M ; the smaller circular faces of these pole-tips were about 1.5 cm in diameter. The second core M' (not shown in the figure) is also provided with two pole tips M_1', M_2' (not shown in the figure) facing M_1, M_2 ; the gaps between M_1, M_1' and M_2, M_2' were approximately 1 cm in length.

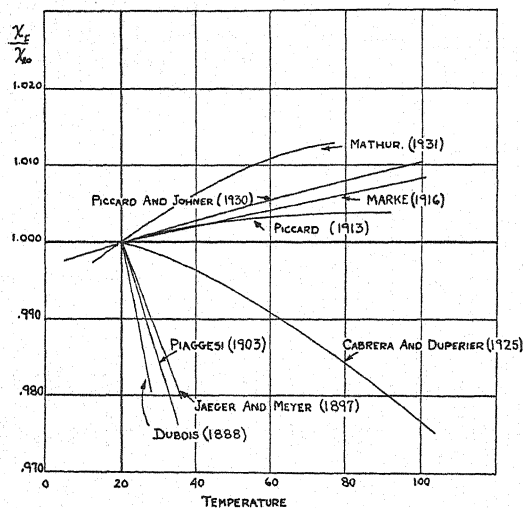


Fig. 1. Summary of results obtained for χ_1/χ_{20} .

The manometric balance itself is made of Pyrex glass throughout, and consists of two branches, a left branch and a right branch. Its essential features are represented in Fig. 2 with designations whose significance is given in the legend below the figure.

The procedure of filling and adjusting the balance is as follows. After mercury has been introduced to the same level in the bulbs E_1, E_2 , the stopcock connecting these bulbs is closed, and liquids are then admitted to the two branches through the filling-funnels A_1, A_2 . After the liquids have reached the tubes t_1, t_2 at the bottom, the 3-way stopcocks B_1, B_2 are so set as to connect each branch with a corresponding mercury cup which, by a vertical adjusting screw C_1 , or C_2 , can be raised or lowered so as to bring the corresponding meniscus m_1 , or m_2 , to approximately the desired position in the meniscus tube t_1 , or t_2 , between the pole-tips M_1, M_1' , or M_2, M_2' . The stopcocks B_1, B_2 are then closed and further adjustments of the menisci m_1, m_2 are made by varying the currents through the resistance coils designated in the figure as coil 1 and coil 2, whereby expansion or contraction of the portions of the liquid columns which they enclose is produced.

The liquid used in the right branch was water at the standard temperature T_0 , (23.5°C), and in the left branch water at some temperature T , or a calibrating solution of nickel chloride at the standard temperature.

The positions of the menisci with respect to their respective pole-tips are determined by two telescopes (not shown in the figure) provided with micrometer eyepieces.

The right branch of the balance is connected with a funnel F through which water containing suspended particles of anise oil can be admitted when desired, the motion of which in the capillary tube designated Cap

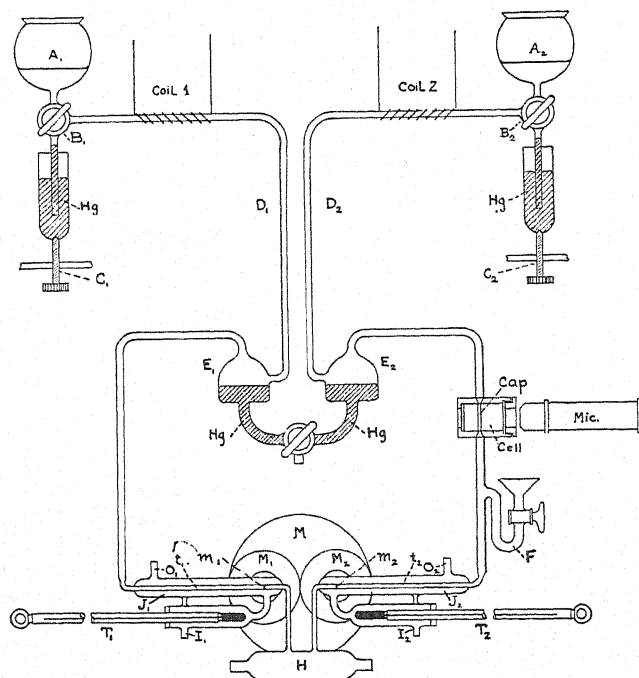


Fig. 2. Manometric balance.

A_1, A_2 —Filling funnels
 B_1, B_2 —3-way stopcocks
 C_1, C_2 —Adjusting screws
 Cap —Capillary tube
 $Cell$ —Canada balsam container
 $Coil\ 1$ —Resistance coil
 $Coil\ 2$ —Resistance coil
 D_1, D_2 —Auxiliary tubes
 E_1, E_2 —Equilibration bulbs
 F —Inlet funnel

H —Helium container
 Hg —Mercury
 I_1, I_2 —Inlets for water jackets
 J_1, J_2 —Water jackets
 M —Core of electromagnet
 M_1, M_2 —Pole tips of electromagnet
 m_1, m_2 —Menisci of liquids
 O_1, O_2 —Outlets for water jackets
 t_1, t_2 —Menisci tubes
 T_1, T_2 —Thermometers

could be observed through the microscope designated Mic . The device designated $Cell$ through which the capillary tube passes is essentially a tube of brass provided with glass ends and filled with Canada balsam.

The letter J_1 designates a jacket enclosing the meniscus tube t_1 , provided with an inlet tube I_1 and an outlet tube O_1 , through which liquid at any de-

sired temperature can be passed for the purpose of regulating the temperature of the water or other liquid in the meniscus tube t_1 . The letters J_2 , I_2 , O_2 have a similar significance with respect to the meniscus tube t_2 . The letters T_1 , T_2 designate thermometers which serve to indicate the temperatures of the liquids in the menisci tubes t_1 , t_2 .

The manometer is mounted on a slate frame which is supported in a vertical plane perpendicular to the axis of the magnet by a suitable cast-iron structure, the latter being bolted to the cement base upon which the magnet rests.

The method of operation of the balance is exemplified by the procedure followed when pure water is under experimentation. While the temperatures of the water in the menisci tubes t_1 , t_2 are maintained at the standard temperature T_0 , the positions of the menisci m_1 , m_2 are varied until a balance is obtained as estimated by the lack of motion, upon throwing on and off the magnetic fields, of the suspended particles in the capillary tube, observed through the microscope *Mic*. The two magnetic fields acting upon the menisci m_1 , m_2 are then the same, H_0 , say. These positions of the menisci are called their zero-positions. Upon changing the temperature of the water in the meniscus tube t_1 , the balance is destroyed; a new balance is obtained upon moving the meniscus m_2 (by varying the currents through coil 1 and coil 2) through a distance D , say, into a slightly stronger or weaker field H , say, as required. During this procedure the meniscus m_1 is kept in its fixed zero-position. The distance D through which the meniscus m_2 is moved in order to effect a balance is measured by the micrometer telescope focussed upon it.

The field H relative to H_0 is derived from a calibration curve, obtained by substituting for the water in the left-branch dilute solutions of nickel chloride at the temperature T_0 and of different known concentrations.³

SENSITIVITY OF BALANCE

In calculating the sensitivity of the balance, we suppose that the water columns in the menisci tubes have the same cross sections, a ; that the mercury columns in the bulbs E_1 , E_2 , have the same cross sections b ; and that the water column in the capillary tube *Cap* has a cross section c . Furthermore, we suppose that the menisci tubes are each inclined downwards at an angle θ to a horizontal plane.

Assuming an initial state of equilibrium, if we let Δl denote the apparent displacement, observed in the microscope *Mic*, of a suspended particle in the capillary tube *Cap* due to a difference of pressure Δp on the menisci m_1 , m_2 , then the sensitivity S , say, of the balance will be proportional to $\Delta l / \Delta p$. A simple calculation shows that:

$$S = \frac{\alpha}{g} \frac{a}{c} \left[\rho_m \frac{a}{b} - \rho_w \left(\frac{a}{b} + \sin \theta \right) \right]^{-1} M, \quad (1)$$

³ The method does not require a knowledge of the absolute values of H and H_0 ; in our experiments these values were probably in the neighborhood of 18,000 c.g.s. units.

where α is the factor of proportionality, g the acceleration due to gravity, ρ_m, ρ_w the densities of mercury and water, respectively, and M the magnifying power of the microscope. It can also easily be shown that the condition for stable equilibrium is:

$$\sin \theta < (a/b)(\rho_m/\rho_w - 1).$$

For the special case in which the menisci tubes are horizontal we have $\sin \theta = 0$, and hence:

$$S = \alpha(b/c)(\rho_m - \rho_w)^{-1}M. \quad (2)$$

For the balance used in our experiments: $\theta = 0$, and $a = 0.070$, $b = 34.0$, $c = 0.0064$, $M = 400$, $\rho_m = 13$, $\rho_w = 1$, approximately, in c.g.s. units. The proportionality factor α could be determined without great trouble if desired.

The sensitivity of the balance used by us is such that changes in the susceptibility of water as small as one ten-thousandth part can easily be detected.

We estimate, with the aid of Eq. (2), that the sensitivity of our balance could easily be increased one thousand times but, owing to vibrational disturbances, this would not be feasible.

THEORY OF THE METHOD

Let κ, κ_0 designate volume susceptibilities of water at the temperatures T, T_0 . When balance obtains:

$$\frac{1}{2}\kappa H_0^2 = \frac{1}{2}\kappa_0 H^2.$$

If χ, χ_0 denote specific susceptibilities and ρ, ρ_0 densities of water at the temperatures T, T_0 , then $\kappa = \rho\chi$ and $\kappa_0 = \rho_0\chi_0$; and hence:

$$\chi/\chi_0 = (\rho_0/\rho)(H^2/H_0^2). \quad (3)$$

We now recall that H_0 represents strength of the magnetic field at the meniscus m_1 in its zero-position, while H represents the strength of the magnetic field acting on the meniscus m_2 when it has been displaced from its zero-position by the amount D , say, necessary to obtain the balance. When the quantity $\rho_0 H^2/H_0^2$ as a function of D is known, formula (3) can be used to calculate the ratio χ/χ_0 , the density ρ being taken from a table for water. A calibration curve giving this quantity as a function of D is obtained as follows:—

A water solution of nickel chloride is prepared which is neutral at the standard temperature T_0 (23.5°C). From this neutral solution several diamagnetic solutions are made, each of which is prepared by adding to a mass m of the neutral solution a mass μ of water, so that the total mass of the diamagnetic solution is $m + \mu$. If χ_n denote the specific susceptibility of such a diamagnetic solution at the standard temperature T_0 and χ_0 that of pure water, then by Wiedemann's law:

$$(m + \mu)\chi_n = \mu\chi_0.$$

Hence:

$$\chi_n/\chi_0 = 1/(1 + \delta), \text{ where: } \delta = m/\mu. \quad (4)$$

If such a diamagnetic solution be introduced in the left branch of the balance with its meniscus m_1 in the field H_0 , and if the right branch contain water with its meniscus m_2 in a field H which is such as to give a balance when the two liquids are at the standard temperature T_0 , then it is evident from Eq. (3) that:

$$\chi_n/\chi_0 = (\rho_0/\rho_\delta)(H^2/H_0^2), \quad (5)$$

where ρ_δ denotes the density of the diamagnetic solution at the standard temperature T_0 . Hence from Eqs. (4) and (5):

$$\frac{\rho_0 H^2}{H_0^2} = \frac{\rho_\delta}{1 + \delta}. \quad (6)$$

Now, supposing the values of δ and ρ_δ to be known, if D denote the necessary displacement of the meniscus m_2 from its zero-position in order to obtain a balance, and if the values of D for several diamagnetic nickel-chloride solutions are known by experiment, a calibration curve can be constructed with the quantity $\rho_0 H^2/H_0^2$ plotted against D .

From the calibration curve the values of the quantity $\rho_0 H/H_0^2$ can be taken for use in Eq. (1), after the value of D has been found for the case in which water at temperature T is balanced against water at the standard temperature T_0 .

CALIBRATION OF THE BALANCE

The data used in the construction of a typical calibration curve are given in Table I. The quantity δ represents the ratio of a mass m of neutral solution to the mass of water μ added to it in forming the diamagnetic solutions numbered 1, 2, . . . 6; ρ_δ represents the density of a diamagnetic solution at the standard temperature T_0 (23.5°C); and D represents the displacement of the meniscus m_2 from its zero-position, expressed in terms of head divisions of the micrometer telescope focussed upon it, in order to produce a balance of a diamagnetic solution against water at the standard temperature T_0 .

TABLE I.

Solution number	δ	ρ_δ	D	$\rho_\delta/(1+\delta)$
1	0	0.99742	0	0.99742
2	0.003749	0.99750	65	0.99377
3	0.007516	0.99758	119	0.99014
4	0.011241	0.99767	175	0.98658
5	0.014999	0.99775	236	0.98301
6	0.018767	0.99783	316	0.97945
7	0.026858	0.99800	413	0.97190
8	0.031305	0.99806	484	0.96776

A calibration curve constructed with the aid of these data is shown in Fig. 3. It is the one used in the construction of curve 2 shown in Fig. 4.

RESULTS

In Fig. 4 there are shown two curves, one labelled curve 1 and the other curve 2. In the case of each curve the ratio of the specific susceptibility of

water at temperature T to that at 20°C , is plotted against the temperature, the temperature 20°C being chosen instead of 23.5°C as the standard temperature in order to facilitate comparisons with the curves of Fig. 1.

The figures associated with the observation points on each curve indicate the corresponding observation times reckoned in minutes from the time at which the zero adjustment of the manometric balance was made. The significance of these annotations will presently become apparent.

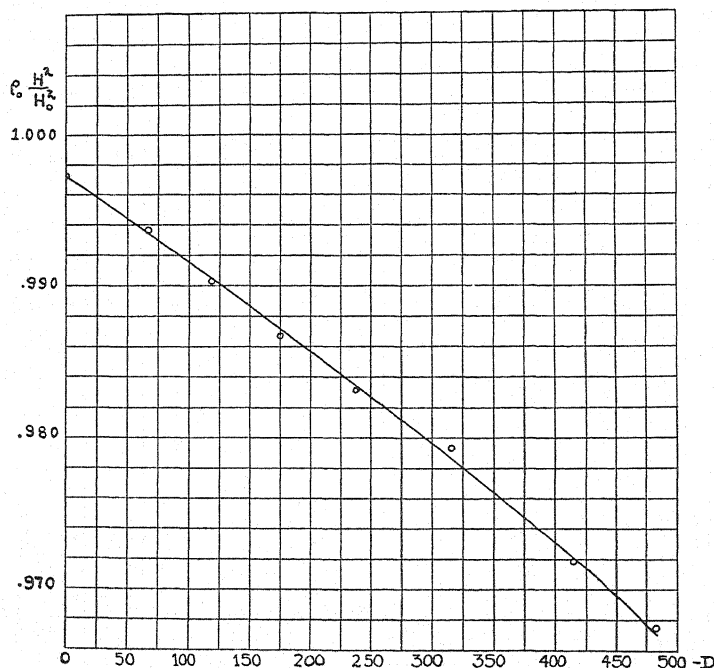


Fig. 3. Calibration curve.

The two curves have certain characteristic features in common, notably the correspondence of maxima and minima points. They differ essentially, however, in that curve 1 indicates that at higher temperatures the diamagnetism of water is *less* than at our standard temperature 23.5°C , while curve 2 indicates that it is *greater*. Each curve was satisfactorily checked by an independent run under corresponding conditions.

The results represented by curve 1 might be cited in support of those found by Cabrera and Duperier (1925), while the results represented by curve 2 might be cited in support of those found by Piccard and Johner (1930); in fact, for temperatures up to 40°C the agreement of curve 2 with the corresponding curve of Piccard and Johner (see Fig. 1) is rather good.

Since the sensitivity of the manometric balance is such as to permit easy detection of changes in relative susceptibility of the order 10^{-4} , the differences between curve 1 and curve 2 must be looked for elsewhere than in the errors of observation.

Various experiments led us finally to the conclusion that these differences have their origin in differences in the procedures followed in preparing the samples of water used in the two sets of experiments.

The water used in both sets of experiments was distilled in the apparatus of the Department of Chemistry, Columbia University. That used in the first set was afterwards boiled vigorously for about 15 minutes in a Pyrex container just before the experiments whose results are represented by curve 1 were begun. The water used in the second set of experiments was similarly prepared, except that after boiling it was sealed in its container after the air

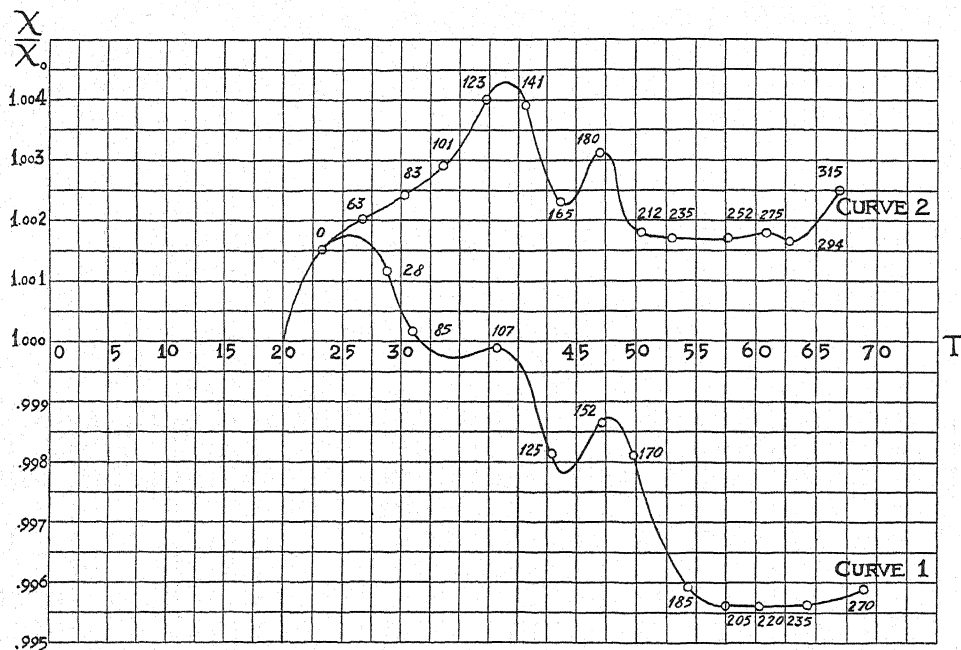


Fig. 4.

therein had been displaced by helium gas and then left to stand for 3 days before using. Throughout each set of experiments the water was kept in contact with helium gas with no air present.

The calibration curve used in the construction of curve 1 was obtained by balancing diamagnetic nickel chloride solutions which had stood for several days in contact with helium gas against recently boiled water at the standard temperature 23.5°C, and the calibration curve used in the construction of curve 2 was obtained in the same way, except that the water used had stood for several days in contact with helium gas.

We are now of the opinion that curve 2 approximates fairly closely a true equilibrium curve, but further rather lengthy experiments will have to be carried out before this opinion can be fully substantiated.

The observations upon which curve 2 was constructed are recorded in the

first three columns of Table II, captioned respectively T , $H \cdot D$, and $T \cdot E$; the first column contains the values of the temperatures at which the observations were made expressed on the centigrade scale; the second column contains the values of the displacements of the meniscus m_2 from its zero position expressed in terms of head divisions on the micrometer telescope focussed upon it; the third column contains the values of the times elapsed expressed in minutes reckoned from the time at which zero adjustment of the manometric balance was made. In the fourth column are found the values in c.g.s. measure of the quantity which captions it, taken from a calibration curve whose derivation is explained above. The fifth column contains the values for the densities of water at the corresponding temperatures. In the sixth column

TABLE II.

T	$H \cdot D$	$T \cdot E$	$\rho_0 H^2 / H_0^2$	ρ	χ / χ_0
23.50	0	0	0.99742	0.99742	1.0000
26.80	6	63	0.99710	0.99660	1.0005
30.45	18	83	0.99640	0.99554	1.0008
33.90	28	101	0.99579	0.99443	1.0013
37.45	30	123	0.99565	0.99318	1.0024
40.60	51	141	0.99440	0.99201	1.0024
43.85	98	165	0.99145	0.99070	1.0007
46.90	106	180	0.99100	0.98944	1.0015
50.50	145	212	0.98860	0.98784	1.0007
53.50	176	235	0.98670	0.98646	1.0002
57.60	210	252	0.98480	0.98455	1.0002
61.00	238	275	0.98300	0.98272	1.0002
63.00	260	294	0.98180	0.98167	1.0001
66.70	280	315	0.98060	0.97966	1.0009

As regards the numbers in the last column of this table, we estimate that, as far as our actual observations are concerned, they may be in error one way or the other by 1 or 2 units in their last places.

are found the ratios of the specific susceptibilities of water at temperatures T to its specific susceptibility at the temperature 23.5°C.

The curve shown in Fig. 5 represents the results of a cyclic run on water which, after boiling, was left for several days in contact with helium gas. The figures associated with the observation points have the same significance as with curve 1 and curve 2, Fig. 4.

An entirely reliable interpretation of the anomalies in the results represented by the curves in Fig. 4 and Fig. 5 cannot, we believe, be given at present. We are confident, however, that the apparently anomalous behavior of water as indicated by these curves cannot be ascribed to errors of observation or to peculiarities of the apparatus; for the susceptibility-temperature curves for benzene and for toluene show no such anomalies.

Questions arise, of course, as to whether the curves for water represent reliable values for the diamagnetism of water or values vitiated by the action (catalytic, perhaps) of unknown impurities or, possibly, by some unsuspected action of a magnetic field upon the surface tension of water, although action of this sort has been fruitlessly sought by various investigators.

If, however, it be granted that the results represented by the curves in Fig. 4 and Fig. 5 are trustworthy, they might, we believe, be explained on the assumption that polymerization changes in water produced by variation in temperature required for their completion a considerable time; but such an assumption is difficult to justify on theoretical grounds.

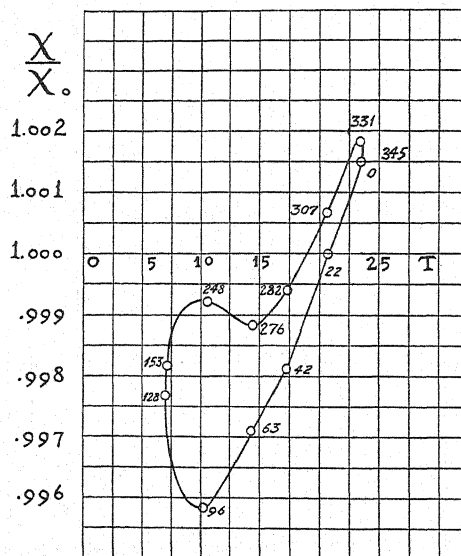


Fig. 5. Cyclic run for water.

A more exhaustive investigation, suggested by the results of our preliminary investigation, will be undertaken in the near future.

We wish to express our appreciation of the very helpful collaboration of Mr. Donald Woodbridge during the later stages of the present investigation.

Some Properties of Homogeneously Distorted Cubic Ferromagnetic Lattices

By FRANCIS BITTER

Westinghouse Research Laboratories, East Pittsburgh, Pennsylvania

(Received September 9, 1932)

The work of Becker and Kersten is amplified in that, starting with a convenient expression for the energy of a magnetically saturated and homogeneously distorted cubic ferromagnetic lattice, the problem is treated with especial reference to the crystallographic symmetry, rather than with the assumption of an isotropic medium, as was done by the above named authors. Application is made of the foregoing to the magnetostriction and magnetization of samples of iron, nickel, and their alloys under tension and compression. The agreement with experiment is qualitatively satisfactory. Further experimental data are needed for a quantitative check. Finally, there is a brief discussion of the effect of magnetization on elastic properties and of hysteresis, and a few important problems are listed.

IN TWO very interesting papers by Becker,¹ and Becker and Kersten,² the magnetic properties of distorted lattices are discussed. These authors assume an expression for the energy of the lattice that is a linear function of the tensor components representing the distortion, and a quadratic function of the direction cosines of the direction of magnetization. In applying this expression, however, they use an approximation which eliminates the symmetry of the crystal present in the original expression for the energy. It is the purpose of this paper to carry out the various calculations without making such simplifying approximations.

ASSUMPTIONS

Although the models of Ewing and Honda have been very useful in the development of ideas about ferromagnetism, recent advances indicate that it is time to examine them critically. It seems desirable, to a certain extent, to get away from such unobservable quantities as the individual magnetic moments of the various atoms in a crystal. Indeed, since wave mechanics has taught us to treat the electric charge surrounding an atom as a continuum, it is only logical to treat the magnetization of a solid as a property of the electric density which occupies the entire space surrounding the nuclei. This indicates that we have to deal, not with an aggregate of dipoles, but with a vector field. We may expect to derive the laws governing the behavior of this vector field from general quantum-mechanical principles, but since the attempts so far made have not been entirely successful, it may be worth trying to formulate them independently, with reference to experimental results only. The first of these laws relates to saturation phenomena. It gives the energy of

¹ R. Becker, *Zeits. f. Physik* **62**, 253 (1930).

² R. Becker and M. Kersten, *Zeits. f. Physik* **64**, 660 (1930).

a saturated ferromagnetic lattice as a function of the direction of magnetization. This part of the problem has been attacked from an atomic point of view by Heisenberg,³ who discusses the existence of magnetization of the type under discussion, and Bloch and Gentile⁴ who take up the orientation in the crystal lattice. An attempt to establish a corrective term applicable to distorted lattices forms the body of this paper. In addition to these laws governing the orientation of the vector I , we need to know how I changes in magnitude. The most generally accepted suggestion is that I does not change in magnitude at all, if we measure it in sufficiently small volumes, but is always equal to I_w , the Weiss spontaneous magnetization. These small volumes must, nevertheless, contain a large number of atoms. In other words, a crystal is divided into small regions whose directions of magnetization are determined by a probability function. This model surely contains some truth, but has not been very useful in explaining the detail of demagnetization, perhaps because other phenomena, such as a periodic reversal of the direction of magnetization,⁵ for instance, obscure its implications. An interesting alternative possibility is to assume that in this problem, as in the case of other vector fields, two separate treatments are called for, corresponding to geometrical optics on the one hand and wave optics on the other. In fact, in view of the general orderliness of nature on a small scale, as contrasted with the general disorder found on a large scale, one might almost suspect that all polarization and diffusion vector fields, when examined in detail, would reveal a wave structure rather than random fluctuations. However that may be, experimental evidence has recently been found, which shows that the magnetization of a single crystal is not uniform, that inhomogeneities exist, and are arranged according to well-defined geometrical patterns.⁶ Therefore on purely empirical grounds we may expect a wave equation to govern the intensity of magnetization, that is, one whose solutions are some sort of oscillating functions. The existence of such an equation will then somehow have to be reconciled to the existence of spontaneous magnetization as postulated by Weiss and Heisenberg.

The above discussion has been introduced in order to emphasize two points. (1) The magnetic properties of a saturated lattice are representable by a function derivable from symmetry considerations and containing a few constants which it is the business of atomic theory to interpret. (2) Whenever other than saturated lattices are discussed, further assumptions must be made. The simplest and most convenient for our purposes are given below.

We shall assume that when the energy of a saturated lattice is less for magnetization along some one direction than for any other direction, then the lattice will actually be magnetically saturated in this one direction of minimum energy. Further, when the energy of a saturated lattice is less for magnetization in n specified directions than in any other directions, then the

³ W. Heisenberg, *Zeits. f. Physik* 49, 619 (1928).

⁴ F. Bloch and G. Gentile, *Zeits. f. Physik* 70, 395 (1931).

⁵ P. S. Epstein, *Phys. Rev.* 41, 91 (1932).

⁶ F. Bitter, *Phys. Rev.* 38, 1903 (1931); 41, 507 (1932).

lattice behaves as if a fraction $1/n$ of its total volume were magnetized to saturation in each of the n directions. The justification for these assumptions is that they are very simple to handle, and that to a first approximation they have been found to represent certain facts very well,⁷ and seem to be adequate here also. As a rule, however, they fall down when applied to problems in which two or more directions have almost equal energies, or when hysteresis is important.

We shall further assume that the energy E_θ' of a *perfect* cubic lattice insofar as it depends on the direction of magnetization may be written

$$E_\theta' = E_1' + E_2' + E_3 \quad (1)$$

$$E_1' = \text{const.} + c' \sum' \alpha_i^2 \alpha_j^2 \quad (2)$$

$$E_2' = \text{const.} + K_1 \sum B_{ii} \alpha_i^2 + K_2 \sum' B_{ij} \alpha_i \alpha_j \quad (3)$$

$$E_3 = -I_w \cdot H. \quad (4)$$

Here E_1' refers to the undistorted cubic lattice, and results from the spin-orbit coupling.⁴ The tensor components B_{ij} give the position x', y', z' of a point after distortion in terms of its coordinates before the distortion.

$$x' = (B_{ii} + 1)x + B_{ij}y + B_{ik}z, \text{ etc.} \quad (5)$$

The quantities α_i are the direction cosines of the magnetization along the i, j, k axes which are assumed parallel to the tetragonal axes of the crystal. E_3 is the energy component due to the external field H . The summations extend over all values of i, j, k , the primed summation indicating $i \neq j$, etc. The constants include all terms independent of α_i , etc.

These equations are inconvenient because they refer to an ideal cubic lattice which is not experimentally available. In order to correct this we must calculate the equilibrium configuration of the lattice under no external forces, and use this as our starting point.

LATTICE UNDER NO EXTERNAL FORCES

Let us write $B_{ij} = A_{ij} + C_{ij}$, where the quantities B_{ij} refer to total distortions measured from the original cubic form of the lattice, C_{ij} are the distortions produced in the lattice by internal forces, and A_{ij} are the distortions produced by external forces alone, measured from the equilibrium configuration of the lattice. We can write

$$E_2' = \text{const.} + K_1 \sum A_{ii} \alpha_i^2 + K_2 \sum' A_{ij} \alpha_i \alpha_j \\ + K_1 \sum C_{ii} \alpha_i^2 + K_2 \sum' C_{ij} \alpha_i \alpha_j.$$

In addition we put for the elastic energy of distortion⁸

⁷ A review is contained in F. Bitter, Phys. Rev. 39, 337, 371 (1932).

⁸ This is the expression used by Becker¹ and is correct for isotropic media. In general, three elastic constants are required to describe cubic crystals. The energy is (Love, *Math. Theory of Elasticity*, page 158)

$$E_4 = (c_{11}/2) \sum C_{ii}^2 + (c_{12}/2) \sum' C_{ii} C_{jj} + c_{44} \sum' C_{ij}^2$$

which reduces to the above for $2c_{44} = c_{11} - c_{12}$. The use of this complete expression does not alter the form of Eqs. (7) or (11), but does alter the relationships 10 and 12 to

$$c = c' + K_1^2/2(c_{11} - c_{12}) - K_2^2/4c_{44}; \chi_1 = -K_1/(c_{11} - c_{12}); \chi_2 = -K_2/2c_{44}.$$

$$E_4 = \frac{1}{2}\lambda [\sum C_{ii}]^2 + G \sum C_{ij}^2,$$

G being the modulus of shear, or rigidity, and $(\lambda + 2G/3)$ the modulus of compression of the (non-magnetic) cubic lattice. The quantities C_{ij} are then so determined that in the absence of external forces ($A_{ij} = 0$)

$$(\partial/\partial C_{ij})(E_2' + E_4) = 0.$$

Carrying this out, we obtain

$$\sum C_{ii} = \text{const.}$$

$$C_{ii} = \text{const.} - (K_1/2G)\alpha_i^2$$

$$C_{ij} = \text{const.} - (K_2/2G)\alpha_i\alpha_j$$

and, remembering that

$$\sum \alpha_i^4 = [\sum \alpha_i^2]^2 - \sum' \alpha_i^2 \alpha_j^2$$

we obtain

$$E_4 = \text{const.} + [(K_2^2 - K_1^2)/4G] \sum' \alpha_i^2 \alpha_j^2$$

$$E_2' = f(A_{ij}) + [(K_1^2 - K_2^2)/2G] \sum' \alpha_i^2 \alpha_j^2.$$

Consequently, putting $E_\theta = E_\theta' + E_4$ and lumping all the terms independent of the direction of magnetization into a single constant, we obtain

$$E_\theta = E_1 + E_2 + E_3 + \text{const.} \quad (6)$$

where

$$E_1 = c \sum' \alpha_i^2 \alpha_j^2 \quad (7)$$

$$E_2 = K_1 \sum A_{ii} \alpha_i^2 + K_2 \sum' A_{ij} \alpha_i \alpha_j \quad (8)$$

$$E_3 = I_w \cdot H \quad (9)$$

$$c = c' + (K_1^2 - K_2^2)/4G \quad (10)$$

where E_1 is the energy of the lattice including magnetostrictive strains, and where the A_{ij} are measured from that configuration of the lattice in which it is in equilibrium with itself. Further, the magnetostriction given by the tensor C_{ij} is more conveniently expressed by the formula for the change in length per unit length in the direction $\beta_i, \beta_j, \beta_k$

$$\delta l/l = \chi_0 + \chi_1 \sum \alpha_i^2 \beta_i^2 + \chi_2 \sum' \alpha_i \alpha_j \beta_i \beta_j \quad (11)$$

which can be derived by noticing that

$$\delta l/l = \sum C_{ii} \beta_i^2 + \sum' C_{ij} \beta_i \beta_j + \text{const.}$$

and substituting the values of C_{ij} found above. On doing this, one obtains Eq. (11) with

$$\chi_1 = -K_1/2G; \chi_2 = -K_2/2G. \quad (12)$$

The expression for $\delta l/l$ gives the difference in length between the final magnetically saturated state and the initial cubic state. Since this initial condition

cannot be realized experimentally, we must choose some other cubic condition as our starting point and correct the above expression by choosing χ_0 to fit experimental observations, instead of using for it that function of λ , G , etc., which results from the foregoing calculation. It is convenient to use as our reference configuration one with no applied field H , in which the sample is completely demagnetized. For the present we need not specify further what this demagnetized condition is. It should be noticed that formula (11) may be checked without any special assumptions regarding χ_0 by measuring the difference in magnetostriction between various directions of magnetization and observation. χ_0 will then drop out.

Insofar as the foregoing considerations are correct, Eqs. (6) to (12) should describe the behavior of saturated crystals. There appear five constants, I_w , c' , K_1 , K_2 , and G which are to be interpreted by quantum theory. This has been attempted for the first two only.

EVALUATION OF E_2

In the following we shall not be concerned with the elastic properties of crystals, but confine ourselves to the description of strains, and moreover to extensions with transverse contractions. The tensor components have been calculated for the following cases.

Extension parallel to $[100]$ axis

$$A_{ii} = A; A_{jj} = A_{kk} = -\mu A; A_{ij} = A_{jk} = \dots = 0.$$

Extension parallel to $[110]$ axis

$$\begin{aligned} A_{ii} = A_{jj} &= [(1 - \mu)/2]A; A_{kk} = -\mu A; \\ A_{ij} = A_{ji} &= [(1 + \mu)/2]A; A_{jk} = A_{ik} = 0. \end{aligned}$$

Extension parallel to $[111]$ axis

$$A_{ii} = A_{jj} = A_{kk} = [(1 - 2\mu)/3]A; A_{ij} = A_{jk} = \dots = [(1 + \mu)/3]A.$$

A measures the extension, and μ determines the extent of the accompanying change in volume. In the ensuing formulae additive constants are neglected.

E_2 for extension parallel to $[100]$ axis

Substituting the values found above into Eq. (8) and putting $\alpha_i = \cos \theta$; $\alpha_j = \sin \theta \sin \phi$; $\alpha_k = \sin \theta \cos \phi$ one obtains

$$E_2 = [(1 + \mu)/2]K_1 A \cos 2\theta, \quad (13)$$

indicating that the energy is independent of the orientation of I_w in the plane normal to the extension, and is a maximum in the direction of extension if $K_1 > 0$.

E_2 for extension parallel to $[110]$ axis

Substituting the appropriate values of A_{ij} into Eq. (8) and putting $\alpha_i = \sin \theta \sin \phi$; $\alpha_j = \sin \theta \cos \phi$; $\alpha_k = \cos \theta$ we obtain

$$E_2 = K_1 A [(1 - \mu)/2] [\sin^2 \theta - \mu \cos^2 \theta] + K_2 A (1 + \mu) \sin^2 \theta \sin \phi \cos \phi. \quad (14)$$

Putting $\theta = \pi/2$, this gives for the (001) plane, which contains the direction of extension

$$E_2 = [(1 + \mu)/2] K_2 A \sin 2\phi$$

which expression has a maximum for $\phi = \pi/4$, or in the direction of extension, if $K_2 > 0$. However, by putting $\phi = \pi/4$, this gives for the (110) plane which also contains the direction of extension,

$$E_2 = - [(1 + \mu)/4] (K_1 + K_2) A \cos 2\theta$$

or for the (110) plane perpendicular to the direction of extension, for which $\phi = -\pi/4$

$$E_2 = - [(1 + \mu)/4] (K_1 - K_2) A \cos 2\theta$$

which shows that the energy is not independent of the orientation of I_w in the plane normal to the extension unless $K_1 = K_2$. Further, E_2 will have its maximum or minimum value in the direction of extension as long as $K_1 + K_2$ has the same sign as K_2 . But if $K_1 + K_2$ has the opposite sign of K_2 , then both maximum and minimum of E_2 will lie in a plane perpendicular to the extension. This latter case is of considerable importance in describing the Villari reversal in iron, as discussed further on.

E_2 for extension parallel to [111] axis

Substituting the appropriate values of A_{ij} into Eq. (8), and writing for the angle θ between the direction $\alpha_i, \alpha_j, \alpha_k$ and the [111] axis whose direction cosines are $3^{-1/2}$,

$$\cos \theta = 3^{-1/2} (\alpha_i + \alpha_j + \alpha_k)$$

we obtain

$$E_2 = [(1 + \mu)/2] K_2 A \cos 2\theta,$$

an expression similar to that for extension along the tetragonal axes, except that K_2 replaces K_1 .

MAGNETOSTRICTION

The formula given in Eq. (11) expresses a complicated relationship between the parallel and transverse components of magnetostriction in their dependence on the direction of magnetization in the crystal. Existing data are not sufficiently reliable for a satisfactory quantitative check, but are perhaps sufficient for a rough estimate of χ_1 and χ_2 for iron and nickel. From Eq. (11) we find the following values of $\delta l/l$. We shall evaluate these con-

TABLE I. Table of theoretical magnetostrictions.

Case	Direction of magnetization	Direction of observation	$\delta l/l$
a	[100] axis; $\alpha_i = 1, \alpha_j = 0, \alpha_k = 0$	$\beta_i = 1, \beta_j = 0, \beta_k = 0$	$\chi_0 + \chi_1$
b	" " " "	$\beta_i = 0, \beta_j = 1, \beta_k = 0$	χ_0
c	" " " "	$\beta_i = 0, \beta_j = 2^{-1/2}, \beta_k = 2^{-1/2}$	χ_0
d	[110] axis; $\alpha_i = 2^{-1/2}, \alpha_j = 2^{-1/2}, \alpha_k = 0$	$\beta_i = 2^{-1/2}, \beta_j = 2^{-1/2}, \beta_k = 0$	$\chi_0 + \frac{1}{2}(\chi_1 + \chi_2)$
e	" " " "	$\beta_i = 2^{-1/2}, \beta_j = -2^{-1/2}, \beta_k = 0$	$\chi_0 + \frac{1}{2}(\chi_1 - \chi_2)$
f	" " " "	$\beta_i = 0, \beta_j = 0, \beta_k = 1$	χ_0
g	[111] axis; $\alpha_i = 3^{-1/2}, \alpha_j = 3^{-1/2}, \alpha_k = 3^{-1/2}$	$\beta_i = 3^{-1/2}, \beta_j = 3^{-1/2}, \beta_k = 3^{-1/2}$	$\chi_0 + \frac{1}{3}(\chi_1 + 2\chi_2)$
h	" " " "	$\beta_i = 2^{-1/2}, \beta_j = -2^{-1/2}, \beta_k = 0$	$\chi_0 + \frac{1}{3}(\chi_1 - \chi_2)$

stants for iron and nickel, assuming that in the experiment the zero reading corresponds to the length for perfect demagnetization. The observations on iron are taken from Honda and Masiyama,⁹ and those on nickel from Masiyama.¹⁰ The observations are tabulated in Table II.

TABLE II. Comparison of theoretical and experimental magnetostrictions.

Case	Theoretical value	Experimental value $\times 10^6$	
		Iron	Nickel
<i>a</i>	$\chi_0 + \chi_1$	$\begin{cases} 17.1 \\ 15.3 \end{cases}$	$\begin{cases} -54.4 \\ -50.7 \end{cases}$
<i>b</i>	χ_0	-15.7	21.1
<i>c</i>	χ_0	-15.4	24.0
<i>d</i>	$\chi_0 + \frac{1}{2}(\chi_1 + \chi_2)$	$\begin{cases} -7.2 \\ -2.7 \end{cases}$	$\begin{cases} -31.3 \\ -33.9 \end{cases}$
<i>e</i>	$\chi_0 + \frac{1}{2}(\chi_1 - \chi_2)$	14.0	14.5
<i>f</i>	χ_0	-9.1	18.3
<i>g</i>	$\chi_0 + \frac{1}{3}(\chi_1 + 2\chi_2)$	-12.9	-27.1
<i>h</i>	$\chi_0 + \frac{1}{3}(\chi_1 - \chi_2)$	20.6	7.2

In order to fit these values we have chosen the constants shown in Table III.

 TABLE III. Magnetostriction constants $\times 10^6$.

	Iron	Nickel
χ_0	-15.5	21.0
χ_1	32.0	-73.5
χ_2	-12.3	-23.5

These values fit the observations in Table II fairly well, except case *h* in iron, which becomes 0 instead of 20.6, and case *e* in nickel, which becomes -4 instead of 14.5. A better all-around fit might be attempted, but this is hardly worth while, since the observations were made on disks cut perpendicular to tetragonal and digonal axes in which the demagnetization is probably structurally different. The constants as evaluated in Table III are therefore only roughly reliable.

As to the dependence of the volume on the direction of magnetization, we have¹¹ $\delta v/v = \sum C_{ii} = \text{constant}$, a relation which holds independently of the choice of constants K_1 and K_2 .

In order to calculate the change in magnetostriction produced by tension we shall make use of the assumption regarding the nature of demagnetization—the material behaves as if a fraction $1/n$ of the total volume is magnetized in each of the n directions of easy magnetization. This assumption requires that the observed longitudinal magnetostriction, or the total change in length from a demagnetized state to saturation can be written:

⁹ K. Honda and Y. Masiyama, Sci. Rep., Tohoku Imp. Univ. 15, 755 (1926).

¹⁰ Y. Masiyama, Sci. Rep., Tohoku Imp. Univ. 17, 945 (1928).

¹¹ $\sum C_{ii}$ is invariant to a rotation of axes, and is therefore equal to the sum of the principal axes of the tensor ellipsoid.

For iron

$$\begin{aligned} \frac{\delta l}{l} \left[\begin{pmatrix} \alpha_i & \alpha_j & \alpha_k \\ \beta_i & \beta_j & \beta_k \end{pmatrix} \right] &= \frac{1}{3} \frac{\delta l}{l} \left[\begin{pmatrix} 1 & 0 & 0 \\ \beta_i & \beta_j & \beta_k \end{pmatrix} \right] - \frac{1}{3} \frac{\delta l}{l} \left[\begin{pmatrix} 0 & 1 & 0 \\ \beta_i & \beta_j & \beta_k \end{pmatrix} \right] \\ &\quad - \frac{1}{3} \frac{\delta l}{l} \left[\begin{pmatrix} 0 & 0 & 1 \\ \beta_i & \beta_j & \beta_k \end{pmatrix} \right]. \end{aligned}$$

For nickel

$$\begin{aligned} \frac{\delta l}{l} \left[\begin{pmatrix} \alpha_i & \alpha_j & \alpha_k \\ \beta_i & \beta_j & \beta_k \end{pmatrix} \right] &= \frac{1}{4} \frac{\delta l}{l} \left[\begin{pmatrix} 3^{-1/2} & 3^{-1/2} & 3^{-1/2} \\ \beta_i & \beta_j & \beta_k \end{pmatrix} \right] - \frac{1}{4} \frac{\delta l}{l} \left[\begin{pmatrix} -3^{-1/2} & 3^{-1/2} & 3^{-1/2} \\ \beta_i & \beta_j & \beta_k \end{pmatrix} \right] \\ &\quad - \frac{1}{4} \frac{\delta l}{l} \left[\begin{pmatrix} 3^{-1/2} & -3^{-1/2} & 3^{-1/2} \\ \beta_i & \beta_j & \beta_k \end{pmatrix} \right] - \frac{1}{4} \frac{\delta l}{l} \left[\begin{pmatrix} 3^{-1/2} & 3^{-1/2} & -3^{-1/2} \\ \beta_i & \beta_j & \beta_k \end{pmatrix} \right] \end{aligned}$$

where the quantities in brackets indicate the directions of magnetization and observation, respectively. Both of these expressions reduce to

$$-\chi_1/3 + \chi_1 \sum \alpha_i^2 \beta_i^2 + \chi_2 \sum' \alpha_i \alpha_j \beta_i \beta_j,$$

which is equivalent to our original expression (11) provided $\chi_0 = -\chi_1/3$. The values in Table III are not quite consistent with this result, so that we may expect discrepancies when making use of the above assumption concerning demagnetization.

We proceed to discuss the longitudinal magnetostriction in crystals under tension and compression in the direction of magnetization. This tension or compression, whenever it is referred to in this article, means tension or compression so large that E_1 may be neglected in Eq. (6). The procedure is here outlined, by way of illustration, for nickel under tension along a trigonal axis. Tension along a trigonal axis in nickel makes the energy a minimum for magnetization in the plane perpendicular to the tension. Therefore the magnetostriction under tension will be that observed without tension plus the change due to the new configuration for demagnetization, which change is given by

$$-\frac{\delta l}{l} \left[\begin{pmatrix} 2^{-1/2} & -2^{-1/2} & 0 \\ 3^{-1/2} & 3^{-1/2} & 3^{-1/2} \end{pmatrix} \right] = -[\chi_0 + \frac{1}{3}(\chi_1 - \chi_2)]$$

or for the total magnetostriction under tension

$$\chi_0 + \frac{1}{3}(\chi_1 + 2\chi_2) - [\chi_0 + \frac{1}{3}(\chi_1 - \chi_2)] = \chi_2.$$

In this case, as in all others, the magnetostriction under tension does not involve χ_0 , and is therefore independent of our special assumptions about demagnetization. Various other cases have been calculated and are tabulated in Table IV. Here χ_0 has been put equal to $-\chi_1/3$ to show in which cases the relation

$$\left. \frac{\delta l}{l} \right]_{\text{tension}} = \frac{3}{2} \left. \frac{\delta l}{l} \right]_{\text{no tension}}$$

which was found by Becker for nickel, holds. In Table IV the values of $\delta l/l$ only are affected by the special choice of χ_0 .

TABLE IV. Longitudinal magnetostriction in crystals with and without tension or compression in the direction of magnetization, assuming a special mechanism for demagnetization which requires that $\chi_0 = -\chi_1/3$.

Material	K_1	K_2	$K_1 + K_2$	Direction of magnetization	$\delta l/l$	$\delta l/l$ with tension	$\delta l/l$ with compression
Fe	-	+	-	[100]	$2\chi_1/3$	0	χ_1
				[110]	$\frac{1}{2}(\chi_1/3 + \chi_2)$	χ_2	$\frac{1}{2}(\chi_1 + \chi_2)$
				[111]	$2\chi_2/3$	χ_2	0
Ni	+	+	+	[100]	$2\chi_1/3$	χ_1	0
				[110]	$\frac{1}{2}(\chi_1/3 + \chi_2)$	$\frac{1}{2}(\chi_1 + \chi_2)$	0
				[111]	$2\chi_2/3$	χ_2	0
80% Ni	?	0	?	[111]	0	0	0
20% Fe							
45% Ni							
55% Fe	?	-	?	[111]	$2\chi_2/3$	0	?

The sign of K_2 for the alloys containing 80 percent Ni and 45 percent Ni is taken from data by Buckley and McKeehan.¹² Further, McKeehan and Cioffi¹³ found that the magnetostriction of a wire of the 80 percent Ni alloy with and without tension is zero, while Honda and Shimizu¹⁴ found that for a wire of the alloy containing 45 percent Ni the magnetostriction under tension is zero. In nickel and iron wires, the last named authors find the magnetostriction with and without tension as shown in Table V.

TABLE V. Magnetostriction of wires.

Without tension	With tension
-4×10^{-6}	in iron $< -9 \times 10^{-6}$
-30×10^{-6}	in nickel $\sim -42 \times 10^{-6}$

All these results are in general agreement with the predictions of Table IV provided we assume the iron wires to be fibered with a digonal axis parallel to the wire axis, and all the other wires to be fibered with a trigonal axis parallel to the wire axis.

The calculation of magnetostriction under tension as a function of H is of course quite possible in accordance with the above. We shall here be content with pointing out that both for iron and nickel wires under sufficient tension, I is proportional to H up to saturation, and the magnetostriction is proportional to I^2 . This is of especial interest for iron, in that it predicts the disappearance of the change in sign in the magnetostriction which has often been observed in wires¹⁴ and single crystals¹⁵ magnetized in a [110] direction. The

¹² O. E. Buckley and L. W. McKeehan, Phys. Rev. **26**, 261 (1925).

¹³ L. W. McKeehan and P. P. Cioffi, Phys. Rev. **28**, 146 (1926).

¹⁴ K. Honda and S. Shimizu, Phil. Mag. **4**, 338 (1902).

¹⁵ W. L. Webster, Proc. Roy. Soc. A109, 570 (1925).

change in sign, or Villari reversal, is discussed from a theoretical point of view by Heisenberg¹⁶ and Akulov.¹⁷ Its disappearance has been observed by Honda and Shimizu.¹⁴

MAGNETIZATION¹⁸

The magnetization curves for crystals under tension may be calculated with the help of Eq. (6) by finding the minima of E_θ . If tension produces a maximum in the direction of magnetization, the material will be more difficult to magnetize under tension, and conversely. Since E_θ has a maximum in the direction of extension for extension in nickel along the tetragonal, digonal and trigonal axes, and in iron along the trigonal axes, these conditions will give rise to properties similar to those found in nickel wires, and discussed at length by Becker and Kersten.¹⁹ On the other hand, iron under tension along a tetragonal axis has a minimum of E_θ in the direction of extension. The four minima at right angles to the direction of extension have been bulged out. In other words, suppose an iron crystal is placed with its tetragonal axes parallel to the axes of a cartesian system of coordinates. E_θ has a minimum along the $\pm x$, $\pm y$, and $\pm z$ axes due to the fact that $C > 0$ in Eq. (7). Extension along the z axis changes E_θ so that it has a minimum in the $\pm z$ directions but a maximum in any direction in the x - y plane. In order to see the effect of extension on magnetization let us assume a small field in the direction of the $+z$ axis. We shall here give up the simple assumption that this small field produces saturation, and assume instead merely that there is a slightly greater probability of finding a volume element magnetized in the $+z$ direction than in any other direction. If, now, we apply tension along the z axis, we effectively dump the contents of the minima along the $\pm x$ and $\pm y$ axes into the minima along the $\pm z$ axis, which, because of the small magnetic field in the $+z$ direction, will fall more into the $+z$ than $-z$ direction, and so increase the magnetization. Iron under tension along a digonal axis is more complicated. Let us assume that extension is along the $[110]$ axis in the model just discussed. This extension will produce maxima of E_θ along the $\pm z$ axes, and minima along the $[1\bar{1}0]$ directions, as may be seen by substituting the values for K_1 and K_2 as given by Table III and Eq. (12) into Eq. (14). A small field in the $[110]$ direction will make the minima of E_θ in the x and y directions less than the minima in the $-x$, $-y$, and $\pm z$ directions. If tension is gradually applied along the $[110]$ axis, the minima in the $\pm z$ directions are first emptied, producing an increase in magnetization. Further extension shifts the minima along the x and y directions into the $(1\bar{1}0)$ directions, producing a decrease in magnetization. This is in accordance with the observations of Honda and Terada²⁰ and others. In general, if a substance is easier

¹⁶ W. Heisenberg, *Zeits. f. Physik* **69**, 287 (1931).

¹⁷ N. Akulov, *Zeits. f. Physik* **69**, 78 (1931).

¹⁸ A further discussion of magnetization with illustrations of the function E_θ will be published in a further paper.

¹⁹ See references 1 and 2, and M. Kersten, *Zeits. f. Physik* **76**, 505 (1932).

²⁰ K. Honda and T. Terada, *Jour. Col. Sci., Tokyo* **21**, Art. 7 (1906).

to magnetize under tension, it is more difficult to magnetize under linear compression. This, however, is not true of iron along a $[110]$ axis. Changing from extension to compression changes the sign of A in Eqs. (13) through (15), and consequently reverses the positions of the maxima and minima of E_θ . But iron under tension along a $[110]$ axis has both maxima and minima of E_θ at right angles to the extension. Compression will reverse these, and so will not produce a minimum in the direction of compression.

ELASTIC PROPERTIES

Since the energy of distortion E_2 as given in Eq. (9) is a linear function of the distortion, we may say that the atomic interactions responsible for E_2 give rise to forces that are independent of the distortion, and dependent only on the direction of magnetization. Consequently, in order to discover any change in the elastic properties of iron due to a change in magnetization from a $[100]$ axis to a $[010]$ axis, for instance, it would be necessary to use methods that were capable of detecting the change in elastic properties due to the application of a constant force.²¹

Finally, it follows from Eq. (12) that the modulus of shear G may be written

$$G = -K_1/2\chi_1 = -K_2/2\chi_2.$$

Since χ_1 or χ_2 can be determined by measurements on magnetostriction, and K_1 or K_2 by measurements on the change in magnetization or magnetostriction under tension, it follows that we can determine G , an elastic constant, by purely magnetic measurements.⁸

HYSTERESIS

Whether or not homogeneous strains are important in determining hysteresis depends entirely on the mechanism by which magnetization changes from one direction, say A , to another B . If this is essentially a rotation, so that the nature of E_θ between A and B actually enters into the problem, then homogeneous distortions certainly will be important. Such a condition is to be expected in rotating fields. It may very well be, on the other hand, that the values of E_θ between A and B are in some cases quite irrelevant. In such cases homogeneous strains would not be important.²²

PROBLEMS

The following problems appear to be among the most interesting and important ones confronting students of ferromagnetism today: (1) The inter-

²¹ If the direction of magnetization depends on distortion the elastic behavior will be modified in a complicated way which will be discussed elsewhere.

²² F. Bloch discusses a mechanism for such changes in direction of magnetization, *Zeits. f. Physik* **74**, 295 (1932).

pretation of the constants c , K_1 , and K_2 in Eqs. (7) and (8). (2) The effect of alloying on these constants, both from an experimental and theoretical point of view. (3) The establishing of Eq. (8) for the energy of distortion and its derivative Eq. (11) for magnetostriction on a firm experimental basis. (4) A determination of the law stating how magnetization changes from one direction to another, together with the related but perhaps more difficult problem of describing demagnetization.

Hall e.m.f. and Intensity of Magnetization

By E. M. PUGH AND T. W. LIPPERT
Carnegie Institute of Technology

(Received October 3, 1932)

Previous experiments have indicated that the Hall e.m.f. depends on intensity of magnetization rather than upon applied field or magnetic induction. Additional evidence is offered, the most important being that provided by a material in which H and B - H are of the same order of magnitude.

IT HAS been shown by one of us¹ that in certain ferromagnetic materials the Hall e.m.f. E is a linear single-valued function of the intensity of magnetization B - H , but is neither a linear nor single-valued function of either the induction B or the applied field H .

The nature of the apparatus used at that time was such that it was possible to obtain accurate results on only two substances, namely, K.S. magnet steel and high carbon steel, and only after they had been hardened by proper heat treatment.

Whether the above rule is general or is merely characteristic of the two materials tested, should be thoroughly investigated on account of its theoretical importance. This is especially true since these two substances had somewhat similar magnetic properties. It was therefore decided so to modify and improve the apparatus that accurate measurements of E , B and H could be made on a great variety of materials.

APPARATUS

In the old apparatus¹ the method of measuring the Hall e.m.f. with a Kohlrausch slide wire made the sensitivity proportional to the resistance of the test bar, forstalling the testing of low resistance bars. The Kohlrausch slide wire was replaced with a Wolff potentiometer which, together with decided improvements in the storage battery current supply, reduced the uncertainty in the e.m.f. measurements on all materials to $\pm 10^{-8}$ volts—less than half the uncertainty previously obtained in high-resistance materials.

The magnetic measurements were also considerably improved by the use of a high-sensitivity galvanometer shunted with a very low resistance which gave it excellent fluxmeter characteristics. Such a well-damped fluxmeter is essential for the accurate measurements of the slow magnetic changes occurring in the bars.

PROCEDURE

The bar under test was first heat treated in an atmosphere of hydrogen, and then placed in the apparatus where it was measured by the step-by-step method described in the former paper.¹ The quantities E , B , and H were ob-

¹ E. M. Pugh, *Phys. Rev.* **36**, 1503 (1930).

tained over the virgin curve and over several succeeding hysteresis loops. These same quantities were then measured over the normal magnetization curve by the method of reversals.

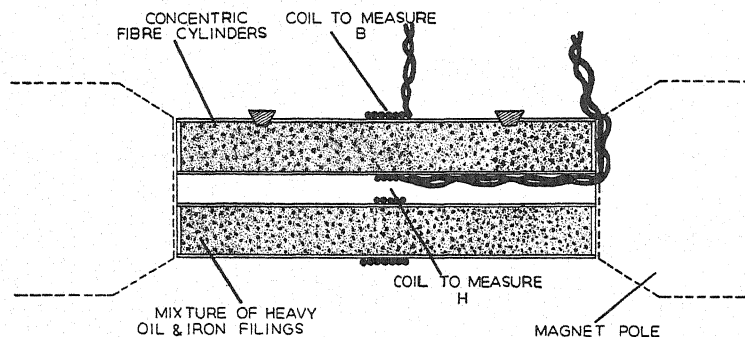


Fig. 1. Variable permeability cylinder to find value of H for samples of low permeability.

The following materials were tested after they had been carefully annealed and also after they had been quenched from a suitably high temperature,—electrolytic iron, high carbon steel, K.S. magnet steel, an iron-cobalt

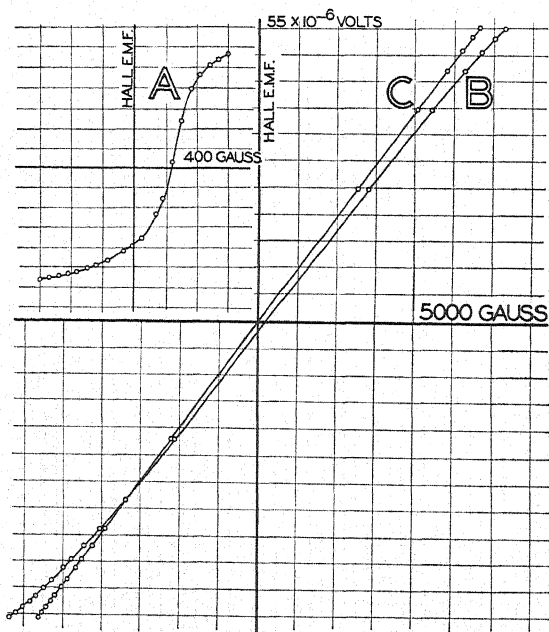


Fig. 2. Hall e.m.f. E in annealed K.S. magnet steel taken along the ascending branch of the first hysteresis loop. Plotted (A) against H , (B) against B , (C) against $B-H$. Current density 40 amperes per cm^2 .

alloy (Fe 50 percent, Co 50 percent), and an iron-nickel alloy (Fe 70 percent, Ni 30 percent). The iron-nickel alloy is only slightly magnetic at room temperature, having a maximum permeability between 3 and 4. It loses its ferromagnetic properties at about 140°C .

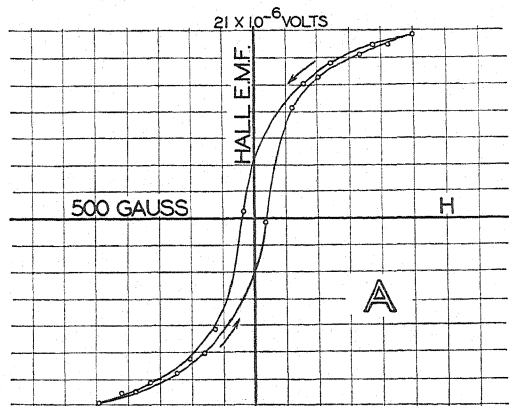


Fig. 3A.

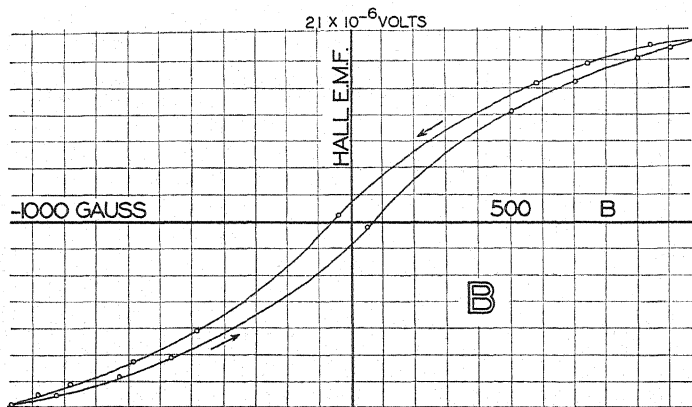


Fig. 3B.

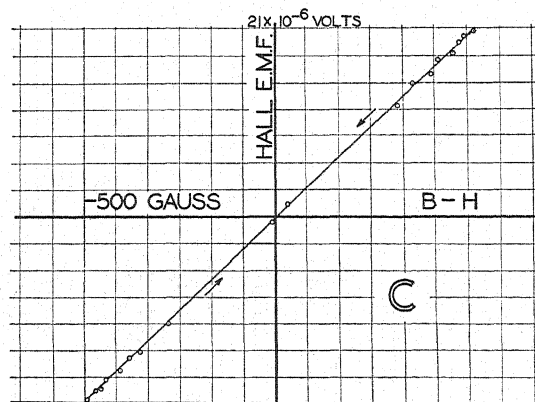


Fig. 3C.

Fig. 3. Hall e.m.f. in quenched iron-nickel alloy (Fe 70 percent, Ni 30 percent). (A) and (B) show the multiple-valued character of the curves with H or B as abscissae; (C) shows the single-valued character of E with $B-H$ as abscissae. Current density 40 amp. per cm^2 .

The tests on this slightly magnetic bar were far more conclusive than on any other specimen because in it the quantities H and $B-H$ were of the same order of magnitude whereas in the other bars H was never more than 5 percent of $B-H$.

The saddle coil method¹ of measuring H was inapplicable to this slightly magnetic alloy and was discarded. Instead H was measured by substituting in place of the bar two concentric cylinders (Fig. 1) between the pole pieces of the electromagnet. The space between the cylinders was filled with a mixture of heavy oil and iron filings in such a proportion that the additional flux due to the iron filings was the same as the additional flux previously due to the test bar. Under these conditions the search coil around the inner cylinder enclosing air only measured the desired value of H .

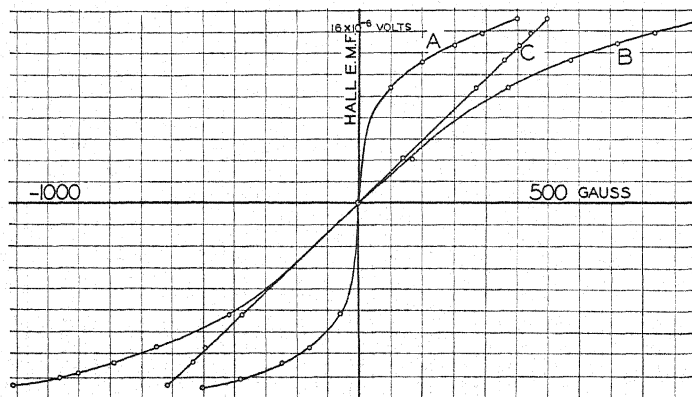


Fig. 4. Hall e.m.f. in baked iron-nickel alloy taken along the normal magnetization curve, where greatest accuracy is obtainable. Current density 40 amp. per cm^2 . (A) and (B) show definite curvature of E with H or B as abscissae; (C) shows the linear character of E with $B-H$ as abscissae.

RESULTS

Figs. 2, 3 and 4 are good examples of the results obtained. Fig. 2 shows the results obtained on the ascending branch of the first hysteresis loop following the annealing of K.S. magnet steel. While the intensity of magnetization was different on the different successive hysteresis loops, no change was found in the ratio of E to $B-H$. *In each material tested the ratio $E/(B-H)$ remained constant, dependent on temperature and previous heat treatment only, for all of the magnetic changes to which it was subjected.*

The best results were obtained with the iron-nickel alloy (Figs. 3 and 4) which, because of its low permeability, furnished a very exacting test of this relationship. It is here obvious that the graph of E is curved and multiple valued (Figs. 3A and 3B) when plotted against either H or B but is straight and single valued against $B-H$, Fig. 3C. The greatest accuracy is attained in taking a normal magnetization curve because the method of reversals eliminates the cumulative errors of the step-by-step method. Fig. 4 shows the Hall

e.m.f. curve taken along the normal magnetization curve of the iron-nickel alloy.

It was not possible to make measurements over a large range of temperatures with the apparatus but the variation of the ratio $E/(B-H)$ in electrolytic iron and in the iron-nickel alloy was investigated over the range available (Fig. 5). In this region the ratio $E/(B-H)$ varies linearly with temperature whereas both E/B and E/H plotted against temperature give curves.

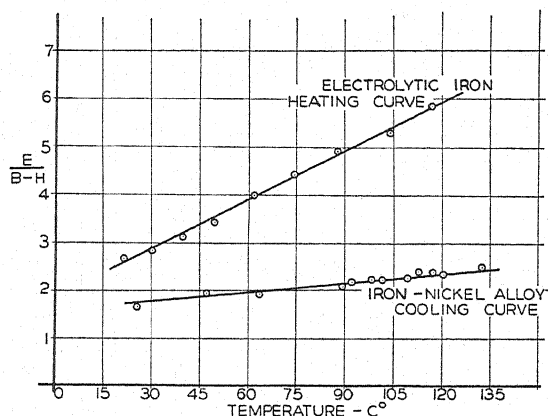


Fig. 5. Variation of ratio $E/(B-H)$ with temperature in electrolytic iron and in the iron-nickel alloy.

These and previous results furnish convincing evidence that the Hall e.m.f. should be considered as a function of the intensity of magnetization alone.

The authors wish to thank Professor Honda of Japan for the K.S. magnet steel and Dr. Elmen of the Bell Telephone Laboratories for other alloys used in this work.

Mono-Crystal Barkhausen Effects in Rotating Fields

By FRED J. BECK, JR.* AND L. W. MCKEEHAN
Sloane Physics Laboratory, Yale University

(Received October 10, 1932)

The directions of Barkhausen effects in a single crystal disk of silicon steel, held stationary in a magnetic field rotating slowly in the plane of the disk, have been determined. Search coils at right angles picked up impulses proportional to selected rectangular components of the changes in magnetization. Measurements on an oscillographic record were made at two values of magnetization, 190 and 100. Values of the angle ϕ between the change in magnetization ΔI and the corresponding variation in the applied field, $(dH/dt)\Delta t$ were determined for various positions of the applied field relative to the crystallographic axes. The normal to the disk made angles of 30° , 60° , 90° with these axes. For these low values of magnetization the effects are mainly transverse with respect to H (and therefore nearly parallel to dH/dt) and are more nearly transverse for the greater value of magnetization. The average value of ϕ is about 20° (ΔI lagging dH/dt) for the lower value of I and is less than 5° for the higher value. The average magnetization apparently lags the applied field and makes a small angle with it. The direction and frequency of effects seemed unaffected by changing the direction of H in the plane of the disk, so that no dependence upon the crystallographic directions of I , H or dH/dt have been established.

INTRODUCTION

A GREAT deal of experimental evidence relating to discontinuous changes in magnetization has been presented since the discovery of the Barkhausen effect.¹ Data have been obtained concerning the effect in various materials, the size of the volume element, or rather the magnitude of the change in magnetic moment, the relation between mechanical strain and effect and the relation between the effect and the slope of the magnetization curve or hysteresis loop. Various methods have been employed for the detection of the discontinuities principal among which are, the measurement of the noise from a telephone receiver, the measurement of the average current output from an amplifier by means of a galvanometer, and the measurement of the instantaneous current output from an amplifier by means of an oscillograph. All but the most recent studies have concerned themselves wholly with the changes in magnetization which take place in the direction of the applied field. Recently Bozorth and Dillinger² and Bozorth³ have studied in addition the change in magnetization occurring in a direction at right angles to the applied field. It is recognized that a knowledge of this so-called transverse effect may give additional information as to the nature of processes occurring in the elementary domains.

* Part of a dissertation presented for the degree of Doctor of Philosophy at Yale University.

¹ H. Barkhausen, *Phys. Zeits.* 20, 401 (1919).

² R. M. Bozorth, and J. F. Dillinger, *Phys. Rev.* [2] 38, 192 (1931); 41, 345 (1932).

³ R. M. Bozorth, *Phys. Rev.* [2] 39, 353 (1932).

In the present investigation a single crystal of silicon steel was employed as a test specimen. An apparatus was devised so that an indication of the longitudinal and transverse components of the change in magnetization arising from one and the same discontinuity could be obtained. As a means of causing the effect a uniformly rotating field was employed, the specimen being held stationary. It was felt that an investigation along these lines would give some insight as to the transverse effect, relate the direction of the change in magnetization with the position of the exciting field and disclose any dependence of the direction of the change in magnetization upon the crystallographic directions of I , H and dH/dt . It seemed likely that a better indication of the actual phenomena taking place could be had by obtaining the ratio of the change in magnetization along the field and at right angles to the field corresponding to each individual discontinuity and then averaging this ratio, rather than considering the ratio of the average longitudinal component to the average transverse component.

THE APPARATUS

The apparatus devised to give the information desired consists essentially of the main exciting field and the search coils, the amplifiers, and the oscillograph. Fig. 1 illustrates the essential features of the effect producing me-

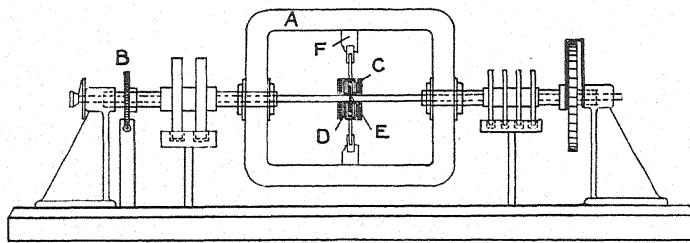


Fig. 1. Side view of mechanism.

chanism. Here A is the field-producing coil consisting of 65 turns of 9 A. W. gauge (diameter 0.289 cm) double cotton covered wire. The winding is excited from a storage battery source of supply and produces a field of strength 4.8 gauss per ampere directed in the plane of the crystal. The main field is electrically driven through reduction pulleys and the worm and wheel B . Throughout the course of the investigation the rate of rotation of the field was 1 revolution in 5.63 minutes. This low rate was found to be necessary in order to secure sufficient resolution between successive discontinuities. To pick up two mutually perpendicular components of magnetization due to a single discontinuity it was necessary to employ two search coils mounted at right angles to each other. These coils are indicated in the diagram as C and D , referred to herein as the outer and inner coils, respectively. The outer coil consists of 12,000 turns of 44 A. W. gauge (diameter 0.0051 cm) enameled wire wound in two sections. The inner coil consists of 11,000 turns of 44 A. W. gauge enameled wire also wound in two sections. The sections of each individual coil are connected in series so that the induced e.m.f.'s will be ad-

ditive. The coils were wound on specially constructed Bakelite forms so arranged that the inner coil could be slipped out of the outer coil and the crystal disk *E* inserted. The coil holder *F* maintains the coils with 90° between their axes and permits shifting of the arrangement relative to the field coil.

In order to obtain measurable impulses it was necessary to amplify the outputs from each search coil. Fig. 2 is a wiring diagram of the amplifiers employed. It was found advisable to use an output transformer in the last

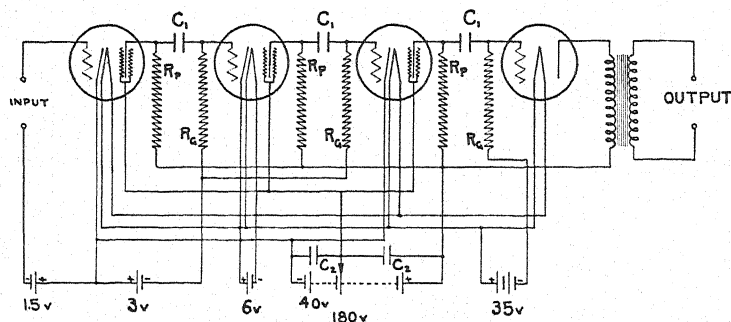


Fig. 2. Wiring diagram of one amplifier.

stage to increase the output current to a value which would actuate the oscillograph. The value of the coupling resistances, coupling condensers and by pass condensers are given below in Table I. Considerable difficulty was met

TABLE I.

	1st	2nd	3rd	4th
R_g	—	50,000	750,000	250,000
R_p	25,000	100,000	50,000	—
C_1	—	0.1	0.1	0.1
$C_2 = 4 \text{ mfd}$				

with in securing the high amplification necessary, consistent with good stability. In order to eliminate feed back, extreme care was taken in the wiring of the amplifiers. Each individual stage of both amplifiers was separately shielded. The input leads from the search coils and the output leads to the oscillograph were also separately shielded. Further, to eliminate disturbances of an electromagnetic origin, the entire apparatus was placed in a large copper box. The search coils and main field were, in addition, separately shielded. The effect of sound vibration was almost wholly eliminated by using non-microphonic tubes and by suspending the amplifiers from rubber tubing which served to damp out the vibrations.

The oscillograph used was a G. E. Type PM-12-A 1 two element instrument. The sensitivity of the elements was 0.7 m.a. per millimeter.

The specimen employed in the experiments was a disk one inch (2.54 cm) in diameter and 0.018 inch (0.0457 cm) thick cut from a single crystal of silicon steel grown by W. E. Ruder of the General Electric Laboratories. Precautions were taken in the cutting to minimize the effect of strain as much as possible. The analysis of the steel used is as follows:

C	Mn	P	S	Si
0.05	0.15	0.038	0.026	3.24.

X-ray analyses showed the specimen to be a single crystal and determined the direction of the cubic axes relative to an indicating mark ruled on the crystal. These directions are indicated in the diagram of Fig. 3.

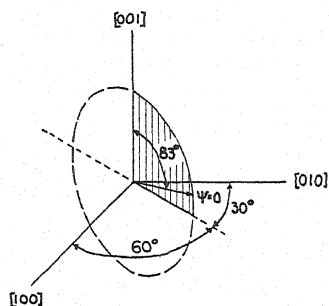


Fig. 3. Relation of cubic crystal axes to plane of disk and fiducial line thereon.

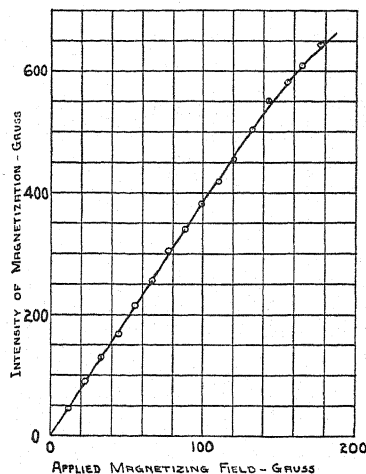


Fig. 4. Relation between magnetization and applied magnetizing field.

A curve showing the relation between the field strength of the main field and the intensity of magnetization is plotted as Fig. 4. The curve was obtained by suspending the disk by means of a fiber in a uniform magnetic field. The disk was then set into oscillation and the period of the system determined at various field strengths. Measurements of the effect were made at two values of I , 190 and 100, corresponding to a main field current of 10 amperes and 5 amperes, respectively.

METHOD OF PROCEDURE

In taking observations the crystal was placed in position in the apparatus so that the indicating mark on it was perpendicular to the base of the apparatus. The main field was then excited from a storage battery source of supply. With the amplifiers in operation the field was slowly rotated at a uniform rate. The rotation of the field caused the appearance of Barkhausen discontinuities, the effect of which could be viewed or photographed by means of the oscillograph. The crystal position was maintained fixed during the course of the measurements. The positions of the field are designated by the angle ψ which is the angle between the field vector and the mark on the crystal. The positions of the search coils relative to the field are designated by means of the angle θ which is the angle between the field vector and the axis of the inner coil.

With the field is a given position, e.g., $\psi=0$ and the search coils at the position $\theta=0$, a photograph is taken of the discontinuities affecting each coil. With the field in the same position, i.e., $\psi=0$ photographs are taken for values of θ from $\theta=0^\circ$ to $\theta=90^\circ$ at 10° intervals. The above process is repeated for values of ψ from $\psi=0$ to $\psi=180^\circ$. Photographs have been taken in the manner outlined above for a main field current of 10 amperes corresponding to an intensity of magnetization of 190 gauss. Another run was taken at a field current of 5 amperes corresponding to an induction of 100 gauss. Here the search coils were always maintained at a position $\theta=45^\circ$ with respect to the field.

The change in magnetization taking place when a discontinuity occurs is proportional to the area under the corresponding curve traced out by the oscillograph. The areas corresponding to each discontinuity were obtained by considering the impulse to be triangular in shape and measuring the base and altitude of the triangle. From these measurements the ratio of the change in magnetization in the outer coil to the change in magnetization in the inner coil can be obtained for the various values of ψ and θ . Curves of this ratio plotted as a function of θ are then obtained corresponding to various values of ψ . In order that these curves have any significance it is necessary that the over-all amplification of both the outer and inner coil circuits be the same in magnitude. The amplifiers employed were matched as closely as possible and the outer coil wound with more turns than the inner coil in order to compensate for the relatively smaller efficiency of the outer coil. Adjustment of the over-all amplification of both circuits was then made by comparing the ratio of the impulses at $\theta=0^\circ$ and $\theta=90^\circ$. If the over-all amplification is f_o for the outer coil circuit and f_i for the inner coil circuit we have

$$f_i/f_o = [(A_o/A_i)_{90}/(A_o/A_i)_0]^{1/2}.$$

Here $(A_o/A_i)_0$ is the ratio of the impulses in the outer and inner coil circuits at $\theta=0^\circ$ and $(A_o/A_i)_{90}$ is the same ratio at $\theta=90^\circ$.

From the data obtained in the manner outlined above the ratio of the change in magnetization along the field and perpendicular to the field may be determined. From this information the angle ϕ which the change in magnetization makes with $(d\mathbf{H}/dt)$ may be determined. These data can be averaged for the various positions of the field and a curve of average ϕ plotted as a function of ψ .

RESULTS AND DISCUSSION

The results of the investigation are contained in curves of which Fig. 5 is typical and in the curves of Fig. 6. In Fig. 6, curve 1 is for a field current of 10 amperes while curve 2 is for a field current of 5 amperes.

The data indicate that changes in magnetization sometimes occur which give a component in a direction opposite to the applied field. This result is in apparent contradiction with expectation in that it seemingly involves a change in magnetization for which there is an increase of the potential energy. However, Bozorth³ points out that in all probability the volume element

undergoing a change is exceedingly small, approximating 10^{-9} cm³. It seems reasonable to suppose that the actuating field causing a Barkhausen discontinuity is the field in the immediate vicinity of the volume element which subsequently undergoes a change. This field is the resultant of the externally applied field and the field due to all other surrounding elements. With this

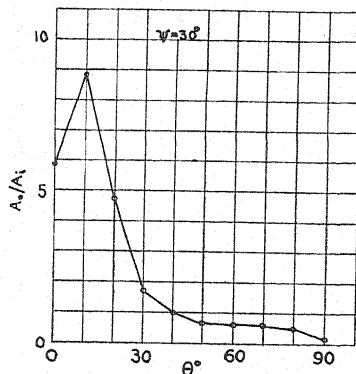


Fig. 5. Relation between ratio (A_o/A_i) of impulses in outer and inner search coils to the search coil setting θ for a single value of ψ . Magnetizing current 10 amperes; A_o/A_i has been corrected for inequality of amplifiers.

supposition the discontinuity may give a longitudinal component in an opposite direction to the applied field and still give a component in the direction of the actuating field in its immediate vicinity. From the curves of average ϕ -vs.- ψ we see that the average change in magnetization involves a transverse component which has a direction always in the direction of the incre-

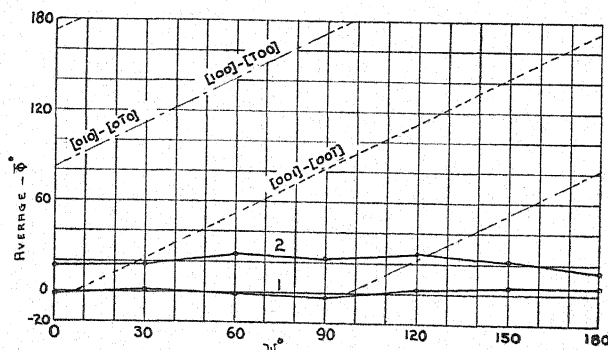


Fig. 6. Relation between mean ϕ and ψ for two magnetizing currents. Curve marked 1 for 10 amperes, curve marked 2 for 5 amperes.

ment of the applied field. Changes in magnetization involving a transverse impulse opposite to this would give values of ϕ greater than 90° . One is led to the conclusion from these results that the average direction of magnetization always lags the direction of the applied field. The data indicate that, for these low values of magnetization and for the particular crystal in question, the change in magnetization has a large component transverse to the

applied field. The average angle ϕ appears to decrease as the field strength is increased. This apparently indicates that the angle between the average magnetization and the applied field is small at large values of magnetization. When saturation is reached the average intensity of magnetization should be directed along the applied field.

It will be interesting to consider the data in light of the possible modes of change in magnetization as indicated by the recent theoretical considerations of Akulov.⁴ On the basis of energies involved Akulov concludes that the changes in magnetization which occur are most probable when these changes occur between pairs of the six [100] directions in a crystal. The theory further indicates that two possible modes of change must be considered in attempting to explain experimental results. The first is the so-called *Umklaupungsprozess* in which the magnetization vector of a small single magnetized region reverses its direction but retains its absolute value unchanged. A change of this type is that in which the change is from the [100] direction to the $[\bar{1}00]$ direction. The second mode of change is the so-called *Drehprozess* in which the magnetization vector turns through 90° but again suffers no change in absolute value. An example of this type would be a change from the [100] direction to the [010] direction. The first type of change involves smaller energies than the second and occurs for lower values of magnetization. At the low values of magnetization at which our experiment was performed it is more probable that changes of the first type would occur. Changes of this type are illustrated by the diagonal lines of Fig. 6. As is seen, there occur regions in the interval $\psi = 0$ to $\psi = 180^\circ$ for which the expected impulses are of the longitudinal type. The actually observed curves indicate that impulses occur which are transverse in character.

If one considers the distortion of the lattice due to mechanical strains as the guiding factor a similar variation of ϕ with ψ would result as was found in connection with Akulov's theory. On Becker's theory⁵ one would have to conclude from the experimental data that the distorted regions travel with the applied field in order to account for the small deviations in the average angle ϕ between $\psi = 0$ and $\psi = 180^\circ$. This is contrary to Becker's postulate that the strains are nearly independent of the condition of magnetization.

⁴ N. S. Akulov, Zeits. f. Physik 67, 794 (1931).

⁵ R. Becker, Zeits. f. Physik 62, 253 (1930).

The Velocity of Sound in an Absorptive Gas

By D. G. BOURGIN

Dept. of Mathematics, University of Illinois

(Received June 13, 1932)

The theory of velocity propagation in a gas as conditioned by internal energy exchanges is considered in detail for the simplest case in which the "lags" may be different—namely, the model with three sets of states. This "second order" theory is required for the interpretation of experimental results where the wave period is of the order of the lag for some states. Assuming the first vibration state of CO_2 to have the largest lag in accordance with Kneser's interpretation of his recent experiments, the necessary approximations are given explicitly and the results are directly applicable to CO_2 . The apparent lag as measured in sound velocity experiments is not the simple stationary state mean "collision life" nor the mean life of the energy quantum except under special conditions and then for only one of the states. The velocity increment in the "resonance" region is given more accurately in terms of transition probabilities and is not described completely by the specific heats as might be expected from the "first order" theory. Contrary to the indications of the simple theory with an empirical constant the external energy is always merely the translation term. The status of the assumed lag assignment in CO_2 is discussed in the light of the results and underlying theory of this paper.

IN TWO earlier papers¹ the author has presented a theory of the propagation of sound in a gas and gas mixtures which deals directly with the fundamental kinetic and atomic qualities of the system. The problem of a gas whose rate of adjustment to fluctuation in translational energy is the same for all internal states was taken up as a special case, or first approximation, under this theory. It was pointed out that this special case corresponded to the macroscopic theory of Herzfeld and Rice.² Recently O. Kneser³ in discussing his important experimental results has used essentially this macroscopic theory and has tried to utilize the ideas of transition probabilities, etc., in connection with it. Such a procedure is artificial and seems limited to "first order" approximations—any more thorough investigation must proceed on some such lines as those pursued in I and II and the present paper.

Because of the highly suggestive nature of Kneser's data and the increasing interest in the field of supersonics, it was felt desirable to refine the pertinent formulae in the same measure as the increase in experimental technique. In the interest of the general reader that part of the theory of I and II germane to the present discussion is briefly reviewed in section I. In section II the problem of a gas model with three internal states is taken up in some detail and the calculations are developed with special reference to Kneser's⁴ research on CO_2 .

¹ D. G. Bourgin, *Nature* 122, 133 (1928); *Phil. Mag.* 7, 821 (1929); *Phys. Rev.* 34, 521 (1929). (These last will be referred to as I and II, respectively.)

² K. F. Herzfeld and F. O. Rice, *Phys. Rev.* 31, 691 (1928).

³ O. Kneser, *Ann. d. Physik* 11, 761, 779 (1931).

⁴ Kneser's remark in a footnote that the writer's developments "nicht zu experimentalle

SECTION I

The principle of detailed balancing yields at equilibrium⁵

$$(\Delta N_i)_T = 0 = \{N_i^2(\bar{f}_{ij} - f_{ij}) + NN_{ij}f_{ij}\} - \{N_j^2(\bar{f}_{ji} - f_{ji}) + NN_{ji}f_{ji}\}. \quad (1.00)$$

If we disturb equilibrium

$$\begin{aligned} \Delta N_i = & - \sum \delta N \{N_{ij}f_{ij} - N_{ji}f_{ji}\} + \delta N_i \{2N_i(\bar{f}_{ij} - f_{ij}) + Nf_{ij}\} \\ & - \delta N_j \{2N_j(f_{ji} - \bar{f}_{ji}) + Nf_{ji}\} + N_i^2 \{\delta(\bar{f}_{ij} + f_{ij})\} + NN_{ij}\delta f_{ij} + \dots \end{aligned} \quad (1.01)$$

We introduce

$$R_{ij} = [2N_i(\bar{f}_{ij} - f_{ij}) + Nf_{ij}]/N. \quad (1.02)$$

Suppose the effective temperature for the state i is $\omega_i \delta T + T_0$, i.e., the number of molecules in state i may be considered to be that corresponding to this temperature at equilibrium, then the change in N_i due to increase of the temperature of this state to $\omega_i \delta T$ is

$$\delta N_i = (\delta N N_i + N \dot{N}_i \omega_i \delta K)/N \quad (1.03)$$

where $K = (3/2)kT$ and $\dot{N}_i = dN_i/dK$ and the first term corresponds to a density increase.

We now observe that if $\omega_r \equiv 1$ then the ΔN_i of Eq. (1.01) is the difference between the number of molecules leaving state i at temperatures T_0 and $T_0 + \delta T$ because of collisions. Since for each fixed temperature $(\Delta N_i)_T = 0$, therefore ΔN_i for $\omega_r \equiv 1$.

If the first term of Eq. (1.03) were alone active we should have (neglecting the effect of variation of N on f_{ij} for the moment)

$$(\Delta N_i)_T, f = (\delta N/N) [(\Delta N_i)_T] = 0. \quad (1.011)$$

Accordingly we may neglect all terms in Eq. (1.01) with δN . Collecting the remaining terms and bearing in mind

$$\begin{aligned} (\Delta N_i)_{\omega_r=1} = 0 = & \sum_j N(\delta N_i R_{ij} - \delta N_j R_{ji}) \\ & + (NN_i - N_i^2)\delta f_{ji} + N_i^2\delta f_{ij} - \dots \end{aligned} \quad (1.012)$$

We may therefore replace the sum of the terms in δf (where δf_{ij} involves δN and δK) by

$$- N[\delta N_i R_{ij} - \delta N_j R_{ji}]_{N, \omega_r=1}.$$

Prüfung dürften" must be ascribed to insufficient acquaintance with the contents of I and II. In fact on adopting the expression for ω given in I, p. 831 footnote, the resulting formula for V^2 , cf. Eq. (2.02) and reference 6 of this paper, is (except for one important point of difference taken up in section II) Kneser's main equation. Even the present paper which provides a more solid basis for interpretation of Kneser's experiments is again only a special case of I.

⁵ If $N^2\gamma/2$ be the number of collisions per unit time in a gas at temperature T then the number involving $N_i - N_j$ meetings is $N_i^2\gamma/2$ (where N_i is the number of molecules per unit volume in state i). The number involving $N_i - N_j$ meetings is $N_i(N - N_i)\gamma$. If \bar{f}_{ij}^1 and f_{ij}^1 are the probabilities of $i \rightarrow j$ transition correlated with each type of collision and if $\bar{f}_{ij} = \bar{f}_{ij}^1\gamma/2$ and $f_{ij} = f_{ij}^1\gamma$, then there results Eq. (1.00).

Eq. (1.01) becomes

$$\Delta N_i = - \left\{ N \sum_j \dot{N}_i R_{ij} (\omega_i - 1) - \dot{N}_j R_{ji} (\omega_j - 1) \right\} \delta K. \quad (1.013)$$

The change of energy due to collision is defined as

$$\Delta K = - \sum \Delta N_i \epsilon_i. \quad (1.04)$$

The equation of continuity is

$$\partial N / \partial t = - (\partial / \partial x) N v \quad (1.05)$$

where v equals the x component of the mass velocity.

Also

$$(\partial \dot{N}_i / \partial t) = - (\partial / \partial x) N_i v + \Delta N_i \quad (1.06)$$

$$(\partial / \partial t) m N v = - (2/3) (\partial K / \partial x) N \quad (1.07)$$

$$(\partial K / \partial t) N = - (5/3) (\partial / \partial x) K N v + \Delta K. \quad (1.08)$$

Assume a plane wave in the gas then

$$\delta N = |\delta N| e^{-j(\nu t - x/\lambda)}$$

where ν is frequency and λ is wave-length, and $j = (-1)^{1/2}$

$$\delta T = |\delta T| e^{-j(\nu t - x/\lambda)}$$

$$\delta v = |v| e^{-j(\nu t - x/\lambda)}.$$

In the undisturbed gas clearly v is 0.

For small amplitude waves v is so small that $v\delta N$ and $v\delta T$ may be neglected. From Eq. (1.05) we have

$$j\nu |\delta N| = jN |v| / \lambda. \quad (1.051)$$

From Eq. (1.06) we get, on referring to Eq. (1.02),

$$j\nu \{ \dot{N}_i \omega_i \delta K + |\delta N| N_i / N \} = jv N_i / \lambda + \Delta N_i. \quad (1.061)$$

Eq. (1.061) yields

$$j\nu \dot{N}_i \omega_i = - N \sum_j \dot{N}_i R_{ij} (\omega_i - 1) - \dot{N}_j (\omega_j - 1). \quad (1.062)$$

These are a set of n non-homogeneous equations in the n quantities ω_i with a unique solution for, because of the presence of $j\nu$ on the diagonal, the determinant will not vanish, i.e., the coefficient of the ii term is $j\nu N_i + N \sum_j \dot{N}_i R_{ij}$ and is the only term in the i th row containing ν .

The elimination of the moduli of K , N and v , leads to one of the key formulae of I and II, namely:

$$j\nu \left[\frac{3mV^2 - 10K/3}{3mV^2 - 2K} \right] = \sum_i (\omega_i - 1) (\Delta K)_i \quad (1.10)$$

where $(\Delta K)_i$ is $N_i A_i \epsilon_i$; V is the complex velocity of sound, and

$$A_i = \sum_j (\dot{N}_i R_{ij} - \dot{N}_j R_{ji}) / \dot{N}_i. \quad (1.11)$$

SECTION II

Before taking up the second order calculation which is the primary object of this paper it seems appropriate to make some preliminary remarks having a direct bearing on Kneser's paper. First we exhibit in slightly more detail than given in I the special case

$$\omega \equiv \omega_i.$$

It follows immediately from Eq. (1.062) that

$$\omega \equiv N A_i / j\nu + N A_i. \quad (2.00)$$

We remark that, with E the internal energy,

$$\begin{aligned} \sum_i \dot{N}_i \epsilon_i &= dE/dK \\ &= N C_i / (3/2)k \end{aligned} \quad (2.01)$$

where C_i is the internal specific heat pro molecule.

Thus

$$V^2 = \frac{K}{3m} \left[\frac{(5/2)k + C_i + j\nu(5k/2)A_i N}{(3/2)k + C_i + j\nu(3k/2)A_i N} \right]. \quad (2.02)$$

This is essentially the equation derived in I expressed in experimentally meaningful terms.⁶ It is the same as Kneser's except in the one respect that the external energy (Kneser's notation C_a) is here given explicitly as $3k/2$ while it is left undetermined in Kneser's formula and is indeed finally given a value greater than that corresponding to the translational energy.

It will be shown in this paper, however, that it is physically inaccurate to assume that the external energy differs from $3/2k$ —the apparent departure is due to the deficiency of the simple $\omega \equiv \omega_i$ theory. In order to avoid repetition the $\omega \equiv \omega_i$, or Herzfeld-Rice, Kneser theory will be referred to under the properly descriptive head, first order theory, to distinguish it from the second order theory of this section.

Kneser has shown by straightforward, detailed computations that the dispersion formula used by him as well as that of Lorentz and Herzfeld-Rice, yields an inflection point with respect to $\log \nu$. Since Eq. (2.02) is, with the exception mentioned, the precise analogue of Kneser's formula, it is clear that properties of this sort hold for Eq. (2.02) also. However, the existence of an inflection point is immediately evident without calculation for a wide class of formulae including the extremely general case taken up in I on the basis of the most simple considerations. One observes merely that for all natural dispersion formulae $r.p. V^2$ is a function of ν^2 finite together with its first derivatives at the end points of the interval $0 \leq \nu \leq \infty$ and continuously differ-

⁶ The only difference is that Eq. (2.02) involves the full expression for ω whereas I employs the first terms only of the series expansion.

entiable twice on this range. Rolle's theorem is all else that is needed (for with these restrictions $r.p. dV^2/d\nu = 0$ for $\nu = 0$ and $\nu = \infty$).

For a very general case $r.p. V^2$ is a rational function of ν^2 with poles not on the real axis. Since the poles of the derivatives of a rational function are at the same points as the poles of the function and all the derivatives of V^2 are rational functions, it follows that this satisfies the conditions stated. For exhibiting the data, it may be convenient to introduce $z=f(\nu)$ which, generally, will be some simple⁷ functional relation. Accordingly the conditions just stated in terms of ν are as easily applied with z .

It is worth while to point out that if $n-1$ states have the same ω then $\omega_n = \omega$ also. Hence one cannot talk about a two state gas model having different ω values.⁸ The proof is immediate and involves the assumption that ν is very small.

From Eq. (1.061) we derive:

$$j\nu \sum_i \dot{N}_i \omega_i = \sum_i (\Delta N_i) = \Delta N. \quad (2.03)$$

Manifestly, ΔN the change in N due to collisions is 0. We observe next that

$$\sum_i \dot{N}_i = dN/dK = 0. \quad (2.04)$$

Therefore if $\omega_i = \omega$ for $i = n, \dots, 1$, we have

$$\begin{aligned} \dot{N}_{1\omega_1} &= -\omega \sum_2^n \dot{N}_i \\ &= \omega \dot{N}_i \end{aligned}$$

or

$$\omega_1 = \omega.$$

Accordingly the next simplest gas model consists of three states (or classes of states) correlated with different ω values.

In order to maintain symmetry, Eqs. (2.03) and (2.04) are not used in what follows now.

Eq. (1.061) yields:

$$\begin{aligned} \dot{N}_i(j\nu + Ns_1)\omega_1 - N\dot{N}_2R_{21}\omega_2 - N\dot{N}_3R_{31}\omega_3 &= N\dot{N}_1A_1 \\ &+ \dot{N}_2(j\nu + Ns_2)\omega_2 - \quad = N\dot{N}_2A_2 \\ &\quad \quad \quad = N\dot{N}_3A_3 \end{aligned} \quad (2.031)$$

where $s_i = \sum_j R_{ij}$. The constant term in the determinant of the equations vanishes and there results

$$\omega_i = \frac{j\nu NA_i + N^2S}{(j\nu)^2 + j\nu N \sum s_i + N^2S} \quad (2.05)$$

⁷ It is therefore of perfunctory interest only to state sufficient conditions on $z=f(\nu)$ to insure finite inflection points in z and dependent on the parameters of $V(\nu)$ when there are inflection points in ν .

⁸ This is not clear in some recent papers.

and accordingly

$$\omega_i - 1 = - \frac{j\nu[j\nu - N(A_i - \sum s_i)]}{(j\nu)^2 + j\nu N \sum s_i + N^2 S} \quad (2.051)$$

where

$$2S = \sum_i^3 \sum_j^3 s_i s_j - R_{ij} R_{ji}, \quad i \neq j.$$

Eq. (2.051) allows of direct physical interpretation. $NA_i \dot{N}_i \delta K$ expresses the change in N_i due to collisions in unit time. The difference in value of N_i for T_0 and $T_0 + \delta T$ is $\dot{N}_i \delta K$. Hence the fictitious time required at constant rate to attain the new equilibrium value would be the ratio of these two quantities or $(A_i N)^{-1}$. This is the "static" lag.⁹ Since increase of the *K.E.* changes N_i and ΔN_i in the same direction it follows from Eq. (1.013) that $A_i > 0$. Although for the first order theory the important low-frequency term for $\omega_i - 1$ is just this static lag the corresponding lag term in the second order theory is $N(A_i - \sum s_j)/N^2 S$. The important point to notice is that the order of the states according to lags is the same as that given by this last formula. This follows from the fact that $\sum s_j > A_i$. While in some instances, because of the approximation that may be made, the lag for state i is closely the mean life of the i th quantum of energy, nevertheless the strict value of this latter life¹⁰ is, of course, $(s_i N)^{-1}$.

In order to make close contact with Kneser's experimental work let us make assumption *A*

$$(a) \quad A_2, A_3 \gg A_1 \quad (b) \quad \epsilon_1 \gg \epsilon_2, \epsilon_3.$$

Furthermore we assume that $(c) \dot{N}_2 R_{21} + \dot{N}_3 R_{31} / \dot{N}_1$ is negligible. The implication of this last condition will perhaps be better apprehended by writing

$$\dot{N}_2 R_{21} + \dot{N}_3 R_{31} \sim (N_1 \dot{N}_2 / N_2) R_{12} + (N_1 \dot{N}_3 / N_3) R_{13}. \quad (2.06)$$

From

$$N_i = N e^{-\epsilon_i / kT} / \sum_j e^{-\epsilon_j / kT} \quad (2.07)$$

(where possible degeneracy has been remotod by the familiar artifice of a small electrostatic field) one finds $N_1 \dot{N}_2 / \dot{N}_1 N_2 = (\bar{\epsilon} - \epsilon_2) / (\bar{\epsilon} - \epsilon_1)$ with $\bar{\epsilon}$ the average internal energy (c) at temperature T_0 . Assumption (c) is satisfied if

⁹ As pointed out in II, the $j\nu$ term is the in the "phase" term and hence the word lag is here used with a different connotation from that employed in II where it characterizes the $(\nu)^2$ term. We remark also that it is the combination $A_i N$, and likewise $s_i N$ and $N^2 S$ that is independent of N . In the notation of I our present A_i is A_i / N_i and $B = \sum_i \dot{N}_i A_i \epsilon_i$. For the $\omega = \omega_i$ case, $(A N)^{-1}$ corresponds to $2\beta/3B$ of I.

¹⁰ The impression seems to persist that radiation "lives" generally are of the order of the atomic ones, namely, 10^{-8} to 10^{-10} seconds and that the collision lives are much longer. (Cf. Kneser, p. 779, *ibid.* and Henry, *Nature*, Feb. 6, 1932). Actually the radiation "lives" will most likely be the longest. In the case of HCl for instance, both theory and experiment indicate a life for the first vibration state as long as 10^{-2} seconds. D. G. Bourgin, *Phys. Rev.* **29**, 794 (1927) and *Phys. Rev.* **32**, 237 (1928).

$$\left| \bar{\epsilon} - \frac{\epsilon_2}{\epsilon_3} \right| \ll \left| \bar{\epsilon} - \epsilon_1 \right| \quad (2.08)$$

which carries with it $N_1 < N_2$, N_3 . With these assumptions $S = s_1(s_2 + s_3)$, $A_1 = s_1$ and as may easily be verified,

$$\omega_1 - 1 = -j\nu/j\nu + Ns_1. \quad (2.052)$$

We remark now that

$$N \sum_i \left(A_i - \sum_j s_j \right) (\Delta K)_i = NS \sum_i \dot{N}_i \epsilon_i.$$

Hence on substituting Eq. (2.051) in Eq. (1.10) and using A one finds:

$$V^2 = \frac{2K}{3m} \left[1 + \frac{\frac{2}{3}}{1 + \left\{ \sum_i \dot{N}_i A_i \epsilon_i j\nu + NS \sum_i \dot{N}_i \epsilon_i (j\nu)^2 + j\nu N \sum s_i + N^2 S \right\}} \right] \quad (2.09)$$

for determining the inflection point we need only the second term in the bracket. The real part is expressible as

$$\frac{\nu^4 + \nu^2 \left\{ N^2 \left[\sum s_i \left(\sum s_i + \sum \dot{N}_i A_i \epsilon_i / N \right) - S - S \left[1 + (C_i / (3k/2)) \right] + N^4 S^2 (1 + C_i / (3k/2)) \right] \right\}}{\nu^4 + N^2 \nu^2 \left[\left(\sum s_i + \sum \dot{N}_i A_i \epsilon_i / N \right)^2 - 2S \left[1 + (C_i / (3k/2)) \right] + N^4 S^2 (1 + C_i / (3k/2))^2 \right]} \quad (2.091)$$

For comparison with Kneser's result we find the inflection point with reference to $\log \nu = z$. To a fair approximation¹¹ the abscissa of the lowest inflection point is:

$$\nu_0 = \frac{Ns_1(3k/2 + C_i)}{(3/2)k - (4s_1/s_2 + s_3)((3k/2) + C_i)}. \quad (2.10)$$

The first order theory yields in this notation:

$$\nu_0 = [Ns_1(3k/2 + C_i)] / (3/2)k. \quad (2.101)$$

The subsequent discussion uses V^2 with the sense of the real part of the squared velocity and the subscripts $0, \mu$ distinguish between the low and the intermediate frequency velocities. Our immediate concern is the magnitude of the increment $V_\mu^2 - V_0^2 = \Delta V^2$ through the resonance region. Kneser obtains numerical agreement with his experimental data by assuming that the external energy is not simply the translational energy but includes¹² the rotational energy as well while the total specific heat remains unaltered. This statement is not correct physically. In fact for the "first approximation" theory involved in Kneser's formulae, one may reason on altogether general grounds as follows. Under assumption A it is clear that at high frequencies

¹¹ In this approximation the next higher order terms are retained till the end.

¹² It is again to be pointed out that we are assuming tentatively with Kneser that the vibration states are the large lag states but the substance of the discussion is independent of this special circumstance.

the vibrational transitions will play a negligible role because of their large lags. Hence one would expect as an approach to the truth that the apparent total specific heat would omit these terms though C_a as always remains the translational energy. Kneser's mistake arises from the fact that his presentation of the simple theory is not really descriptive in that first the shorter lag states are neglected and then the resulting formula is analyzed with respect to behavior in a range where just these states are dominant.

On going to the second approximation it develops that the statements just made are in need of modification and it is evident how a more precise estimate of ΔV^2 is to be arrived at; namely, one needs to determine the value of V_μ^2 for $s_2^2, s_3^2 > (\nu/N)^2 \gg s_1^2$. We shall use Eq. (2.091) for this purpose. Neglecting ν^4 terms restricts the validity of this equation to the low-frequency region. For high frequencies the constant term in the quotient may be omitted and there is obtained thus a sort of asymptotic approximation. In both these extreme cases V^2 (real) is a quotient of monomials in ν^2 in formal analogy with the first approximation problem. The low-frequency equation corresponds to Eq. (2.02) with the important difference that the coefficient of ν^2 is no longer C_a . V_μ^2 lies in the intermediate region of validity of both subsidiary equations. Unless $1 \gg s_1/s_i$ $i=2, 3$ a good approximation will not¹³ be obtained if either the constant or ν^4 terms are neglected. However, in the interest of analytic simplicity we shall consider the ν^2 term as alone being of consequence.

This implies

$$S^2/(s_2 + s_3)\nu^2 \doteq 0$$

$$\omega_i - 1 \doteq + (-j\nu + N(A_i - \sum_j s_j)/j\nu + N \sum_j s_j) \quad i = 2, 3. \quad (2.11)$$

If, besides, terms in S are dropped then

$$V_\mu^2 = \frac{2K}{3m} \left[1 + \frac{k}{(3k/2 + \sum A_i \epsilon_i dN_i/dT/N(s_2 + s_3))} \right]. \quad (2.092)$$

The first order approximation discussed above indicated a relationship of the form

$$V_\mu^2 = \frac{2K}{3m} \left[1 + \frac{k}{3k/2 + C_i - \left(\frac{dN_1}{dT} \epsilon_1/N \right)} \right]. \quad (2.021)$$

Eq. (2.092) and Eq. (2.021) differ except under special supplementary conditions. (For instance if $(dN_1/dT)A_1\epsilon_1/s_2 + s_3$ is negligible then we should require the special relation $A_1 = A_2 = s_2 + s_3$.)

We now turn to the question of deriving transition probabilities information from sound velocity and absorption experiments. All our approximations in this paper have been on the assumption that the vibrational energy has, associated, the larger lag. The assumption is, however, not altogether certain even in the case of CO_2 . The correct argument for such an assignment as a

¹³ This remark is to be kept in mind in any comparison of Eq. (2.091) with the experimental data.

working hypothesis is the agreement of Eq. (2.021) with Kneser's experimental data. The fortunate coincidence that his assumption leads to the same numerical value here is explained by the fact that there are only two terms of importance in C_i (the two rotational states are lumped in the symbol $C_R = k$). With additional terms in C_i the Kneser postulate yields a result at variance with Eq. (2.021). In order to maintain the agreement one should be led to the bizarre conclusion that all the internal energies, save the one vibrational term, are included in the external energy. More explicitly, for the model considered in this paper Eq. (2.02) yields the rigorous value

$$V_\mu^2 = (1 + k/(3/2)k)2K/3m.$$

Kneser's procedure amounts to arbitrarily replacing the $(3/2)k$ term by $(3/2)k + C_R$. This modified V_μ^2 has just the value given by Eq. (2.021) as is evident on observing that the vibrational energy denoted by

$$C_S = dN_1/dT \epsilon_1/N \quad \text{and} \quad C_i = C_R + C_S.$$

For confirmation¹⁴ it is necessary now to use the more accurate Eq. (2.092) and then the analogous second order formula that would result from the supposition that the low energy states¹⁵ (2, 3) have the large lags.¹⁶ The assumption that all rotation states have one type of lag and all vibrational states another may be wide of the truth, in which case a theory is required in which both rotational and rotation-vibrational states exist characterized by the same lag value. Such modifications in the hypothesis may be taken account of by suitably varying the approximations in a treatment like the present one. Then too it may be remarked that the data points in Kneser's figure do not continue into the critical intermediate region, and besides, the experimental accuracy is least here. It seems desirable to supplement and extend the experimental results to higher frequencies by varying the CO₂ percentage in a mixture with a non-masking gas.¹⁷

¹⁴ Conversely if the lag assignment be adopted the experimental data yield estimates of the A_i and C_i combinations occurring in Eqs. (2.10) and (2.092).

¹⁵ Kneser's use of the ratio of the squared velocities in CO₂ and Ar may be expected to minimize viscosity, conductivity, etc., corrections.

¹⁶ Without going into details here, Kneser's attempted "a posteriori" justification for expecting larger lags for the vibration state is inadequate in the writer's opinion if only for the reason of the lack of satisfactoriness in the present day treatments of the circumstances of energy transfer in collision.

¹⁷ The theory of gas mixtures may be developed along lines similar to that presented in this paper. Cf. the footnote in a forthcoming publication of the writer in the Jour. Acoust. Soc. where an error in Eq. (1.2) of II is corrected. The work in II is what I have called here a first order theory—incidentally Eq. (7) of II is the theoretical basis for computing humidity effects, etc., and provides the validation for Reid's empirical formula. Reid, Phys. Rev. 35, 814 (1930). A form of Eq. (7) more convenient to use is

$$\frac{\delta V}{V} = \frac{1}{2} \sum_w \frac{\delta N_w}{N} \left[\frac{C_{nw}}{\bar{C}_n} - \frac{C_{vw}}{\bar{C}_v} - \frac{m_w}{m} \right]$$

where the notation is self-explanatory.

The second order treatment of the absorption may be made to parallel the development of this section by taking the imaginary part of V^2 in Eq. (2.09) and very likely other than lag influences may probably be neglected if the ratio with a rare gas is taken (in accordance with Kneser's suggestion).

An experimental study of the temperature effect seems likely to yield important evidence—the theoretical aspect is clearly outlined, namely, the dependence of R_{ij} (and \dot{N}_j) on T in connection with the variation in collision frequency and average collision energy. In a way this provides a means for isolating the effects of various groups of states; for instance, the inequalities of (cf. Eq. (2.08)) c valid for sufficiently low temperatures but may actually be reversed if the gas be raised to a very high temperature.

In order to make a close contact with Kneser's experimental work let us make assumption A

$$(a) A_2, A_3 \gg A_1; \quad (b) \epsilon_1 \gg \epsilon_2, \epsilon_3.$$

Furthermore we assume that (C) $\dot{N}_2 R_{21} + \dot{N}_3 R_{31} / \dot{N}_1$ is negligible. The conditions implied in this last assumption are indicated clearly on writing

$$\dot{N}_2 R_{21} + \dot{N}_3 R_{31} = N_1 \dot{N}_2 R_{12} / N_2 + \dot{N}_1 N_3 R_{13} / N_3. \quad (2.06)$$

From

$$N_i = N e^{-\epsilon_i / kT} / \sum_j e^{-\epsilon_j / kT} \quad (2.07)$$

one finds

$$N_1 \dot{N}_2 / \dot{N}_1 N_2 = (\bar{\epsilon} - \epsilon_2) / (\bar{\epsilon} - \epsilon_1) \quad (2.08)$$

with $\bar{\epsilon}$ the average internal energy at temperature T_0 .

LETTERS TO THE EDITOR

Prompt publication of brief reports of important discoveries in physics may be secured by addressing them to this department. Closing dates for this department are, for the first issue of the month, the twenty-eighth of the preceding month; for the second issue, the thirteenth of the month. The Board of Editors does not hold itself responsible for the opinions expressed by the correspondents.

The Tropism of Crystals

A crystal is generally described in terms of the positions of its constituent atoms. These are regarded as points, and consequently the energy of the crystal is expressed in terms of the positional coordinates of the atoms. This model may be amplified by giving up the assumption that the atoms are points, or spherically symmetrical centers of force, and by introducing angular coordinates to specify the orientation of each atom. In the language of the quantum theory, the state of an atom or molecule is specified by a variety of quantum numbers that may be interpreted geometrically as specifying an orientation. The orientation of an atom in empty space is, of course, quite arbitrary, as its energy is independent of orientation. In a crystal lattice this is no longer true. Because of the anisotropy of the atomic arrangements in a crystal, certain orientations of the atoms will be energetically preferable to others. We have, thus, besides the anisotropy of the crystallographic planes themselves, other directional properties associated with the various vectors specifying atomic states. If, for instance, all the electronic spins are coupled, we have what might be called spintropism, or *s*-tropism. Likewise, coupled orbits would give rise to *l*-tropism, etc.

To illustrate the significance of the above, let us consider two special cases. The first is that of a cubic lattice in which each atom has a magnetic moment resulting from the electronic spins. The spins are so coupled to each other that the energy is least when neighboring spins are parallel. The crystal exhibits spontaneous magnetization. The spins are further so coupled to the lattice (or to orbits fixed in the lattice) that, if $\alpha_i, \alpha_j, \alpha_k$ represent the direction cosines of the spins with respect to the tetragonal axes of the crystal, the energy of the crystal depends on the orientation of the spins according to the formula

$$c \sum_{i,j,k} \alpha_i^2 \alpha_j^2.$$

If the crystal is distorted by external forces, the energy is increased, first, by the work done against the elastic forces, and secondly, by an amount depending on the orientation of the spins

$$k_1 \sum_{i,j,k} A_{ij} \alpha_i^2 + k_2 \sum_{i,j,k} A_{ij} \alpha_i \alpha_j$$

where A_{ij} , etc., are the components of the tensor describing the distortion, and finally, if the crystal is subjected to the action of a magnetic field, there is a further term in the energy $-(I \cdot H)$.

If the distortion A_{ij} , etc., and the field H are given, it is possible to calculate the energy of the crystal for any orientation of the spins. If this energy has a single minimum, we assume that this minimum gives the direction of actual magnetization, and hence uniquely determines the actual energy of the crystal. If the energy has minima for more than one orientation of the spins, the direction of actual magnetization is not uniquely determined. Changes in the relative position of two or more minima will in general give rise to irreversible changes in the orientation of the spins, and therefore to a dissipation of energy, or hysteresis. This procedure, based on the work of N. Akulov and R. Becker, is shown, in a paper appearing in this journal, to describe the properties of ferromagnetic crystals fairly well.

The second model we shall assume identical with the first, except that the spins are so coupled that the energy is least when the spins cancel each other in pairs. Although there is no resultant magnetization, one may still refer to an orientation of the spins, given again by the quantities $\alpha_i, \alpha_j, \alpha_k$. The orientation of the spins is in this case unaffected by a magnetic field. In general, we may refer to that condition of a crystal in which at least one

aspect of its constituent atoms is unchanged throughout a group of atoms as spontaneous alignment, just as we speak of spontaneous magnetization in a ferromagnetic crystal. A crystal showing spintropism as above would be very similar to a ferromagnetic crystal except in its reaction to a magnetic field. What, then, is peculiar about a ferromagnetic crystal in the absence of a magnetic field? We shall consider here only mechanical and thermal properties. There are others, such as electrical, optical, etc. Four such peculiarities are listed below. These peculiarities may be thought of as defining certain kinds of tropism in crystals of which spintropism is one. Ferromagnetism is then a special kind of spintropism.

(1) There is a critical temperature, or "Curie point," above which ferromagnetism, or more generally spintropism, etc., disappears. In general, a substance may have more than one such critical temperature.

(2) Just as there is a magneto-caloric effect, or reversible change of temperature with magnetization, there should be a reversible change of temperature accompanying elastic distortion, having a maximum at the critical temperature.

(3) There should also exist an elastic hysteresis, or dissipation of energy resulting from elastic distortion. This is caused by irreversible changes in spin orientation. These irreversible processes should occur only when the distortion produces the above-mentioned ambiguity of two or more energetically possible spin orientations. Magnetic hysteresis is most pronounced in distorted or hardened materials, and becomes very slight in single crystals at ordinary temperatures. The same should be true of elastic hysteresis. If a single crystal is rotated in a magnetic field, hysteresis is particularly pronounced in the neighborhood of certain orientations of the crystal in the field. Similarly, if a single crystal is rolled between plates exerting a compressive force, elastic hysteresis should also be more pronounced in the neighborhood of certain orientations of the crystal.

(4) When distortion produces only a single possible orientation of the spins, the elastic properties are uniquely defined. They differ from those of normal cubic crystals because of

the dissymmetry introduced by the spin interactions, or because of the energy expression above involving both the distortion and the spin orientation. In other words, the spin interactions produce strains in the crystal. In the case of ferromagnetic crystals we call these strains magnetostrictive strains. Since any tropism of the kind here under discussion will tend to distort a crystal, we may refer to this distortion as troprostriction. In distorting a cubic crystal, we do work not only against the cubically symmetrical elastic forces, but also against the troprostrictive forces which vary as the direction of spontaneous alignment in the crystal varies. In a paper that is to appear shortly, the effect of spontaneous alignment on the elastic properties of cubic crystals will be investigated mathematically.

Do any crystals aside from ferromagnetic crystals, show tropism of the kind discussed in this note? Many peculiarities, such as elastic hysteresis, unexplained critical temperatures,¹ etc., have been observed, but until the subject is quantitatively formulated and checked it is not possible to determine to what extent such ideas as the above may be useful in explaining the behavior of actual materials. It seems likely, however, that there is something to orient in most crystals. Few atoms are spherically symmetrical, and such spherical symmetry would probably be destroyed by the interatomic forces and fields in a crystal. It is, therefore, to be expected that at sufficiently low temperatures the atoms in a crystal will either be spontaneously aligned, or if the atomic interaction is such that neighboring atoms are not parallel, the crystal will exhibit a complicated tropism and probably periodic structural peculiarities.

F. BITTER

Research Laboratories,
Westinghouse Electric & Mfg. Co.,
East Pittsburgh, Pennsylvania,
October 25, 1932.

¹ Is the transition to the supra-conducting state perhaps the lowest of these critical points below which all the constituents of a crystal are spontaneously aligned and the atomic planes have lost their "thermal roughness"?

X-Ray Reflections from a Quartz Piezoelectric Oscillator in a Bragg Spectrograph

Recently G. W. Fox and P. H. Carr¹ found that the intensity of Laue spots, obtained by passing an x-ray beam through quartz, were increased when the quartz plate was oscillating electrically. However, in a later paper² Fox and Cork failed to obtain any changes in intensity of oscillating quartz lines produced by a Bragg spectrograph. C. S. Barrett and C. E. Howe³ suggested that this failure to get increased intensity was probably due to the existence of an imperfect surface layer in which the extinction had already been reduced to a minimum by the preparation of the crystal. The mode of oscillation of the quartz plate used by Fox and Cork² was such that there existed a node of pressure at the surface of the plate from which the x-ray beam was reflected. Hence, even if elastic deformations of the atomic plane spacings were taking place, no widening of the line obtained could be expected from this experiment.

From experiments performed in this laboratory a widening and an increase in intensity for lines reflected from oscillating quartz were obtained. The quartz crystal used in the experiments was prepared in the following manner. Let EE^1 (Fig. 1) represent the electric

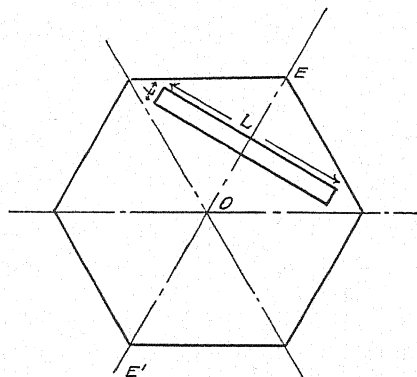


Fig. 1.

axis of a quartz crystal, and let the optic axis pass through O perpendicular to the plane of the paper. The specimen was cut from the crystal as is shown in Fig. 1 with the following dimensions: $L=100$ mm, $t=2$ mm, $w=6$ mm. The dimension L is mutually perpendicular to the electric axis EE^1 and to the optic axis which is perpendicular to the plane of the

drawing. The dimension t is parallel to the axis EE^1 and perpendicular to the optic axis. The dimension w (not shown in Fig. 1) is parallel to the optic axis and perpendicular to the electric axis EE^1 .

The oscillating quartz plate was placed in a Bragg spectrograph between two brass plates which were connected in parallel with the condenser of a resonating circuit. The crystal-to-film distance of the spectrograph was 20 cm. The top brass plate had a window cut so as to allow the x-ray beam to fall on the surface of the quartz which had dimensions 100×6 mm. The crystal was made to oscillate in such a manner that there existed a loop of motion at each end and a node of motion in the center; consequently there was a loop of pressure in the center, and nodes of pressure at the ends. The x-ray beam was reflected from the center of the oscillator. The crystal oscillated at a frequency of 27,400 cycles per second, which result agreed with the calculated value. The source of power was the output of an audio-oscillator connected to an amplifier and inductively coupled with the resonating circuit containing the quartz plate. A shield enabled only half of the film to be exposed at a time. One side of the film was exposed with the crystal not oscillating and the other half with the crystal oscillating. The crystal was kept oscillating at such an amplitude that dL/L was 0.0003 in the L direction. This quantity was measured by means of a calibrated eye piece. The doublet used in the experiment was the $K\alpha_1$ and $K\alpha_2$ lines of molybdenum obtained by the sixth order reflection from the $(1\ 1\ 0)$ set of planes. The crystal was rocked through an angle of 5° during the exposures. It was necessary to expose each side of the film for 40 hours. A careful watch was kept on the power input of the x-ray tube so that accurate intensity comparisons might be made.

The curves shown in Fig. 2 were obtained by examining the photographic record with a microphotometer. The film was passed over a photoelectric cell in steps of 0.02 mm each by means of a ruling machine mechanism. A slit of light 0.02 mm wide and 0.05 inches long was placed above the film in such a position as to be directly over the photoelectric cell. This cell was connected to the grid of a vacuum tube which composed one arm of a Wynn Williams bridge. The deflections of the galvanometer were proportional to the amount of light

¹ Fox and Carr, Phys. Rev. **37**, 1622 (1931).

² Fox and Cork, Phys. Rev. **38**, 1420 (1931).

³ C. E. Howe, Phys. Rev. **39**, 889 (1932).

falling on the cell.

Curve A (Fig. 2) was the curve obtained for the oscillating lines, while curve B was the curve obtained for the non-oscillating lines. At half maximum amplitudes the width of the oscillating $K\alpha_1$ line was found to be 0.600 mm, while the width of the non-oscillating $K\alpha_1$ line was found to be 0.540 mm. The values for the widths of the $K\alpha_2$ lines were practically the same at half amplitudes as those of the $K\alpha_1$ lines. If we take the area under the loops as proportional to the intensity

the relation: $dS = 2r(\Delta D/D) \tan \theta$, where r is the crystal-to-film distance, and θ is in our case 60.3° , we have for dS the following: $dS = 0.0525$ mm. The oscillating lines were found to be 0.060 mm wider at half maximum amplitudes than the non-oscillating lines.

It is not at present known whether this effect obtained is due to extinction reduction solely or whether it is a combination of extinction reduction and elastic deformations of the plane spacings. Experiments are now in progress in which an attempt will be made to

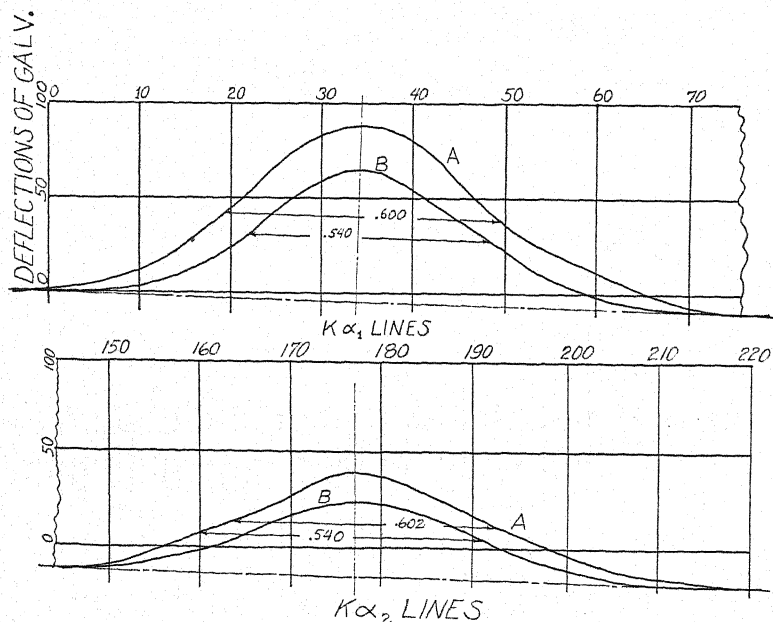


Fig. 2. Settings of ruling machine. One setting = 0.02 mm.

of the lines, we find that the $K\alpha_1$ oscillating line is about 1.5 times as intense as the $K\alpha_1$ non-oscillating line, and that the $K\alpha_2$ oscillating line is about 1.5 times as intense as the $K\alpha_2$ non-oscillating line.

It is interesting to note that if we take $\Delta D/D$ to be $\frac{1}{4}$ the magnitude of dL/L where $\Delta D/D$ is to represent the elastic deformations of the plane spacings for the (1 1 0) set which is at right angles to the elastic deformations of magnitude dL/L ; and substitute the value in

take Bragg reflections from quartz plates which are deformed mechanically and in a homogeneous fashion. A detailed account of the experiments performed in this laboratory and further conclusions will be given at an early date.

M. Y. COLBY
SIDON HARRIS

Physical Laboratories,
University of Texas,
November 8, 1932.

Determination of e/m for an Electron by a New Deflection Method

In spite of the many measurements which have been made of the specific charge of the electron, there is still some uncertainty especially in connection with the value obtained from free electron measurements. Although

two recent measurements^{1,2} on free electrons

¹ C. T. Perry and E. L. Chaffee, *Phys. Rev.* 36, 904 (1930).

² F. Kirchner, *Ann. d. Physik* [5] 8, 975 (1931) and [5] 12, 503 (1932).

in which linear acceleration was used have yielded "low" values of e/m in fair agreement with the spectroscopic value $(1.761 \pm 0.001) \times 10^7$ em units, there remains the fact that the apparently very precise work of Wolf³ using a deflection method gave a high value $(1.7689 \pm 0.0018) \times 10^7$ em units. Hence, it is important that a new deflection determination be made with an accuracy sufficient to determine if the discrepancy is real or due to some unknown sources of error. Secondly, an accurate value of e/m is needed in the very important method that has been developed by Bond⁴ and Birge⁵ of obtaining the most probable values of the physical constants e , h , e/m and α . Not only does the value of e/m influence the values obtained for the other constants but also the major portion of the uncertainty of the results is due to the uncertainty in e/m .

The new deflection method being used was conceived by Professor Ernest O. Lawrence and was most kindly offered to the author as a means of obtaining the results mentioned above. The success of this new determination was made possible by the important advantages of this method over previous ones. The method is essentially as follows. An evacuated brass box B contains six slits labeled A , S and D which are on a circle of radius r . The slits S and the outer slits at A and D are integral parts of the box, while the inner slits at A and D are separate from it and are connected to the output of a radio-frequency oscillator. The box is connected to the grounded side of the output. During the half of each cycle in which the box is positive, electrons are accelerated across the slits at A and leave the outer slit with velocities ranging from zero to that corresponding to the peak voltage of the oscillator. These electrons are bent in circles of various radii by a magnetic field having a direction into the plane of the sketch and produced by a pair of Helmholtz coils. For any given magnetic field H , electrons having a velocity v given by the radial force equation $mv^2/r = Hev$ (em units) will be bent around through the slits S and arrive at D where they will experience a further acceleration or deceleration depending on the time of arrival

relative to the radio-frequency cycle. If a magnetic field is chosen with a related electron velocity such that the time required for the electrons to travel from A to D is one period, then the electrons in traversing the slits at D experience a deceleration exactly equal to the acceleration they received at A and consequently are stopped and fail to reach the collector C . For any other magnetic field a simple analysis shows that half of the electrons passing through the slits S will reach the collector. Hence e/m is determined by the conditions existing when the current to the collector is zero (in reality when it is a minimum). The electron velocity necessary to travel from A to D in one cycle is given by $v = r\theta/T$, where T is the period of the oscillator and θ the angle subtended by the path; or since the frequency $\nu = 1/T$ the velocity is given by $v = r\theta\nu$. Eliminating the velocity by combining this equation with that given above for the radial forces gives the relation

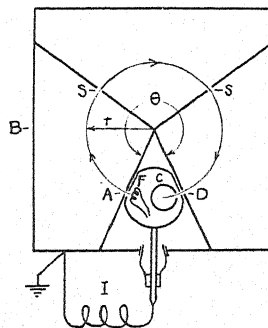


Fig. 1.

for obtaining e/m , namely $e/m = \theta\nu/H$ em units. Here θ is in radians and H is in gauss.

A most important advantage of this method over other free electron methods is that no accelerating voltage need be measured since it is not necessary to know the electron voltage. This feature combined with a modification in the method not described above (due to space limitations) *practically eliminates all errors due to contact potentials* except those due to stray electric fields in the deflecting regions of the box. Due to the construction the latter are necessarily small. Further, the observational precision which the method gives is very good. For example, fifty magnetic field readings (the frequency being held constant) were of such constancy that the observational probable error in e/m was only one part in 100,000.

³ Fritz Wolf, Ann. d. Physik [4] 83, 849 (1927).

⁴ W. N. Bond, Phil. Mag. 10, 994 (1930) and 12, 632 (1931).

⁵ R. T. Birge, Phys. Rev. 40, 228 (1932).

The present results, although still of a preliminary nature, are of an accuracy comparable with present published values. Observations have been taken at two frequencies since constancy of results with change in frequency is of primary importance. With a change in frequency of about 30 percent two frequency runs made up of about 90 observations each gave results differing by only two parts in 10,000. The weighted value of e/m obtained from these two groups of observations with the calculated probable error is $e/m_0 = (1.7592 \pm 0.0006) \times 10^7$ *em* units. The major part of this probable error is due to allowance for possible errors in the magnetic field measurement. However, to allow for still other pos-

sible errors in the experiment the present result may be stated as $e/m_0 = (1.7592 \pm 0.0015) \times 10^7$ *em* units. This result is somewhat lower but not in disagreement with the accepted spectroscopic value. It is in good agreement with Kirchner's results.² A more detailed description of the method and results will be published soon.

The writer is indebted to Professor Ernest O. Lawrence not only for the method, as mentioned above, but also for many helpful discussions during the development of the method.

FRANK G. DUNNINGTON

University of California,
November 12, 1932.

The Value of e/m

During the past two years there have appeared four direct determinations of e/m , each of high accuracy. These results are:¹ (1) C. T. Perry and E. L. Chaffee,² $e/m = 1.761 \pm 0.001$, from electrostatic acceleration of free electrons. (2) F. Kirchner,³ $e/m = 1.7585 \pm 0.0012$ and 1.7590 ± 0.0015 , from two different investigations, by the same method as (1). The weighted average is 1.7587 ± 0.0009 , with the probable error based on internal consistency. The probable error from external consistency is, by chance, only ± 0.00016 . (3) J. S. Campbell and W. V. Houston,⁴ $e/m = 1.7579 \pm 0.0025$, from Zeeman effect measurements. (4) F. G. Dunnington,⁵ $e/m = 1.7592 \pm 0.0015$, from magnetic deflection of free electrons.

The weighted average of these four results, based on three radically different methods, is $e/m = 1.75953 \pm 0.00043$, from external consistency, or ± 0.00059 from internal consistency. This is a very satisfactory agreement and tends to indicate that the probable error assumed by each investigator is a reasonable estimate. In each case, however, this assumed

error is essentially a personal estimate by the investigator, and includes an arbitrary allowance for possible systematic errors of various kinds. Each of the four investigations seems, from superficial examination, to be of essentially the same accuracy. With this new assumption one obtains for the (unweighted) average, $e/m = 1.75920 \pm 0.00044$. This happens to be identical with Dunnington's value. I think that $(1.759 \pm 0.001) \times 10^7$ *em* units may be taken as a conservative estimate of the present most probable direct evaluation of e/m .

I should like to take this occasion to call attention to a numerical error in my recent paper⁶ on certain general constants. On page 257 the correct value of $e_3/4$, resulting from $h_4/3 = 6.5431 \pm 0.0042$, is 4.7721 ± 0.0023 , and not 4.7738 ± 0.0041 as given. This makes the results of solutions *k* and *l* incorrect. The correct results of solution *k* are $h = 6.5432 \pm 0.0083$, $e = 4.7683 \pm 0.0038$, $e/m = 1.7611 \pm 0.0011$, $1/\alpha = 137.310 \pm 0.048$. Solution *l* is based on $e/m = 1.759 \pm 0.001$, as now adopted for the best direct value. The resulting values of e , h , etc., in solution *l*, corrected for the above error, may accordingly be considered the present most probable values. These corrected results are,

$$\begin{aligned} -h &= (6.5420 \pm 0.0083) \times 10^{-27} \text{ erg} \cdot \text{sec.}, \\ e &= (4.7668 \pm 0.0038) \times 10^{-10} \text{ es units}, \\ e/m &= (1.7592 \pm 0.0011) \times 10^7 \text{ em units}, \\ 1/\alpha &= 137.374 \pm 0.048. \end{aligned}$$

RAYMOND T. BIRGE

University of California,
November 12, 1932.

⁶ R. T. Birge, Phys. Rev. 40, 228 and 319 (1932).

¹ This list does not include a very recent value by G. G. Kretschmar (Chicago, November, 1932 meeting of the American Physical Society) of 1.7555 ± 0.0026 , since his method requires a knowledge of other fundamental constants.

² C. T. Perry and E. L. Chaffee, Phys. Rev. 36, 904 (1930).

³ F. Kirchner, Ann. d. Physik 12, 503 (1932).

⁴ J. S. Campbell and W. V. Houston, Phys. Rev. 38, 581 (1931).

⁵ F. G. Dunnington, Phys. Rev. 42, 739 (1932).

Structure of Atomic Nuclei
Errata

(Phys. Rev. 41, 370 (1932))

I have noticed certain errata in my letter to the Physical Review 41, 370 (1932). They are as follows:

P. 370, column 1, line 10 should read "consists of $2(2l+1)$ protons and $2(2l+1)$ neutrons" instead of "consists of $2l+1$ protons and $2l+1$ neutrons."

P. 371, column 2, line 8 should read "neutrons to be" instead of "electrons to be"

JAMES H. BARTLETT, JR.

University of Illinois,
November 9, 1932.

BOOK REVIEWS

Molekulstruktur. Edited by P. Debye. Pp. 197+vii. Figs. 44, Tables 5. S. Hirzel, Leipzig, 1931. Price 10 R.M.

The real benefit from the annual Leipzig lectures is to be had by sitting around the table in the cafe of the Ipabad in Leipzig in between talks. The publisher makes no attempt to collect the discussion which is the most valuable feature of such a scientific gathering. The lectures themselves are usually limited to matters already published and well known to workers in the general field. In some cases new material presented is likely to require immediate modification. But the reader is left to guess what happened after the lectures.

The present series is devoted to chemistry. The speakers are, however, all physicists. K. L. Wolf presents interesting experimental results on the free rotation of the carbon bond. In the second talk R. Mecke provides a masterly exposition of the problems of the spectroscopy of polyatomic molecules. He calls attention to some important regularities in the behavior of simple chemical compounds which are not discussed at all in the fashionable quantum theories of valence. He also shows how these matters can be treated with some success from a classical point of view. Next is a description by F. Rasetti of his experiments on Raman effect in gases and solids. It seems rather strange that he should here repeat his suggestion that the lines he found in calcite and fluorite are due to scattering with large ($\sim 7000 \text{ cm}^{-1}$) frequency shifts. No comment is made of the very convincing explanation furnished by R. Tomaschek (*Nature*, **128**, 495 (1931)) that these lines are due to known fluorescence of common impurities in these minerals.

G. Placzek has a useful paper on his very important method of treating the Smekal-Raman effect. This effect is of interest chiefly in the study of molecular structure and it is therefore appropriate instead of describing it by the roundabout method of general dispersion theory to treat it as an interaction between the electron motions and the motions of the nuclei. Placzek's presentation is not complete but he furnishes references and an extensive table of tensor components.

H. Spooner and R. de L. Kronig have papers on dissociation—especially predissociation. Their discussions are perhaps carefully stated but do not advance the subject beyond innumerable papers which have discussed it in the past. They do not even refer to the experimental results which V. Henri announces in his talk and leave the subject of polyatomic molecules entirely untouched. Henri finds the phenomenon of predissociation to be very widespread among polyatomic molecules which usually have several regions of predissociation. A most remarkable observation which he reports is that the predissociation limit shifts toward longer wave-lengths as the temperature of the absorbing gas is increased.

G. Herzberg contributes the last talk. It is an unusually clear and concise presentation of the newer methods of discussing the electronic structure and valence characteristics of molecules. Herzberg as well as Mullikan and Hund has contributed much to this subject. The methods advocated are still approximate but have important advantages over that due to Heitler and London. The unsatisfactoriness of the latter has been brought out on many hands, especially during the past two years. It is one great advantage of the newer methods that they lead to their wrong results without any stupendous amount of calculating.

R. M. LANGER

California Institute of Technology

The Theory of Electric and Magnetic Susceptibilities. J. H. VAN VLECK. Pp. 384+xi, Figs. 15. Clarendon Press, Oxford. Price \$7.50.

In this book Van Vleck has given with his own characteristic thoroughness and care for details, an excellent survey of the quantum theory of electric and magnetic susceptibilities. In a certain respect the purpose of the book is the same as that of Stoner, which was written in

1926, namely to correlate and explain the great amount of experimental results from the standpoint of the quantum theory. But Van Vleck had the great advantage that he could use the quantum mechanics. Especially in magnetism, since the classical work of Curie, Langevin and Weiss, there has been a great accumulation of experimental material, but I think one may say that a real advance in the understanding first came with the penetration of the ideas and methods of the new mechanics, partly without doubt because of the clarification it brought in the theory of line and band spectra. In dielectrics the advance since Debye is perhaps less striking. The quantum mechanics has, however, here removed, by restoring the classical factor $\frac{1}{3}$, several difficulties, which the application of the old quantum theory had brought.

Chapter I gives the classical foundations. It shows carefully how the macroscopic field equation of Maxwell can be obtained by averaging the microscopic equations of the electron theory. It is perhaps a pity, that the author has not gone into the criticism of the usual expression (34) of the local field, from which the Lorentz-Lorenz formula follows. To the reviewer the validity seems doubtful, especially for polar substances. This point is of interest because of the recent measurements of ϵ for gases at high pressures. Chapter II gives a very complete classical derivation of the Langevin-Debye formula for dielectrics. The reviewer objects though to calling the ordinary simple derivation a rudimentary proof. It follows strictly from the general Boltzmann theorem:

$$dN_1/dN_2 = (dN_1/dN_2)_{T \rightarrow \infty} e^{-V/kT}$$

for the ratio dN_1/dN_2 of the numbers in two elements of the q -space. Of special interest in this chapter is the derivation in §13 for quite general molecular models in close analogy with the quantum mechanical derivation of chapter VII. Chapter III gives then a discussion of the experimental material. Though there is here some overlapping with the book of Debye, the remarks of Van Vleck on the "atomic polarization" are very interesting.

All this was perhaps more or less known. But in chapter IV Van Vleck gives a very striking discussion of the classical theory of magnetism. He throws the proper light and puts the proper stress on the main result of the Leidener thesis of Miss van Leeuwen, namely, that in classical statistics we get strictly always *zero* susceptibility. The well-known result, that the translatory motion of free electrons in a metal gives no diamagnetism with classical statistics, is a special case of the theorem of Miss van Leeuwen. Perhaps the author could have stressed still more the very artificial assumptions one must make in the classical theory to obtain para- or diamagnetism. The assumptions required are: (1) that each molecule has an electronic motion (or current) which is so shielded that the collisions have no effect on it; (2) that when the gas is formed, each molecule is born with the same value for the angular momentum of that electronic motion. Assuming this, one can derive quite generally the Langevin-Pauli formulas for the para- and diamagnetism. Miss van Leeuwen has given several examples; in her terminology, there must exist besides the energy (or function of Routh) other "interesting" additive integrals of the motion.

In chapter V the many difficulties and paradoxes of the old quantum theory with regard especially to electric susceptibilities (i.e., the Glaser effect) are very clearly discussed. And so we are led to the quantum mechanical chapters. Chapter VI gives all that is necessary from the general theory; in addition to the perturbation theory, it contains a very useful treatment of the angular momentum matrices and of the anomalous Zeeman effect. In Chapter VII we are then given the general quantum mechanical derivation of the Langevin-Debye formula, which is due to Van Vleck himself. It is hardly necessary to stress its importance. Besides containing all earlier derivations for special models it has shown clearly the essential assumptions, which are necessary and sufficient. By a witty application of the theorem of spectroscopic stability the author rehabilitates the classical factor $\frac{1}{3}$. Also because of this theorem all the difficulties of the old quantum theory (i.e., with regard to "weak" and "strong" quantization) disappear. Essential in the derivation, and I think already for qualitative discussions of importance, is the distinction between the (compared to kT) high- and low-frequency non-diagonal matrix elements of the magnetic moment. The first contribute to the temperature independent part of χ ; the second, because of the second order Zeeman and Stark effects, which are so often forgotten, *together* with the diagonal elements give the term inversely proportional to T . That it is *not* the diagonal elements alone is perhaps simplest seen in the example of NH_3 . The two

lowest levels, considering only the vibrational states, corresponding to the symmetric and anti-symmetric wave functions of the N-nucleus, have no diagonal element of the electric moment at all. The observed temperature dependence of ϵ is here due only to the second order Stark effect.

The chapters VIII, IX and X give the applications. Chapter VIII discusses the diamagnetic susceptibilities of atoms and monatomic ions; chapter IX the paramagnetism of free atoms and especially of the rare earth ions. The success of Hund's prediction of the magneton numbers had already shown here that these ions even in the solid salts can be considered as being nearly free. Europium and samarium were the only two apparent exceptions. Van Vleck (with Miss A. Frank) has been able to explain these cases also by taking into account the finite multiplet width and the second order Zeeman effect. Also the temperature dependence of χ then agrees beautifully with experiment. Chapter X gives the application to the paramagnetic gases, especially O_2 and NO. The experimental confirmation of Van Vleck's prediction of χ as a function of T in the case of NO is one of the most beautiful successes of his theory.

In chapter XI a new idea enters, namely the crystal field. The author shows how this is able to quench the orbital magnetic moment, and he gives in this way an explanation of the Bose-Stoner hypothesis, which had thrown the first light on the difficult question of the magneton numbers of the iron group. How successful this idea is, Van Vleck and his students have since then shown. It explains beautifully the Curie-Weiss law and its deviations (see Penney and Schlapp, *Phys. Rev.* 41, July 15, 1932). The book closes with a short and clear discussion of the Heisenberg theory of ferromagnetism (chapter XII) and of some related optical phenomena (chapter XIII).

I hope that this review, which, although rather long, could touch only the main points, has given sufficient impression of the rich contents of the book. Because it is written completely from the theoretical standpoint, a beginner will not find it always easy. But for one who has already sufficient background and who wants to acquire a thorough knowledge of the subject, Van Vleck's book is indispensable. I am sure that it will be the starting point for many investigations.

G. E. UHLENBECK
University of Michigan

The Adsorption of Gases by Solids. A general discussion held by the Faraday Society, January, 1932. Pp. 320+iv. Gurney and Jackson, London 1932. Figs. 109. Price, 15/-.

In his introduction to the general meeting of the Faraday Society at Oxford, Professor H. S. Taylor stated that "it is eminently fitting at a time when so much attention is being paid to the fundamental contributions of Faraday to electrical science that the society which bears his name should also devote some thought and discussion to a field of knowledge in which Faraday displayed the same qualities of genius and pre-vision that have given him so preeminent a position among the leaders of scientific thought." With this motivating idea Professor Taylor initiated this important meeting of the Faraday Society at which forty papers were presented and later published as this volume.

Three section meetings were held and at each of these a definite subject was chosen for discussion. The section subjects together with the authors of the introductory papers were as follows: Section I. Experimental methods. Introductory paper by Eric K. Rideal. Section II. Kinetics and energetics of gas adsorption. Introductory paper by Professor Herbert Freundlich. Section III. Theories of the adsorption of gases. Introductory paper by Professor M. Polanyi.

Leading investigators throughout the world presented papers and entered into the discussions which followed. Most of the modern work on the adsorption of gases was covered and many important points of view were given in the general discussion which followed the presentation of the papers. This general discussion fills about forty pages of the book and follows the last paper presented. To those interested in the adsorption of gases by solids, this volume constitutes an important summary of the work in progress, as well as giving the modern point of

view with regard to the theories on the subject. There are a few typographical errors which do not seriously harm the usefulness of the book.

L. H. REVERSON
University of Minnesota

Les Principes de la Mécanique Quantique. P. A. M. DIRAC. Translated by A. Proca and J. Ullmo. Pp. 314+viii. Les Presses Universitaires de France, Paris, 1931. Price 95 Fr.

As is indicated by its title this book is a literal translation of Dirac's work into French, except for the addition of an appendix by Proca on Poisson bracket expressions in classical analytical dynamics. As the English original has been reviewed previously in this journal (Phys. Rev. 37, 97 (1931)) further comment seems unnecessary except that one might have expected some indication in the very last pages of the book that Dirac no longer supports his original interpretation of the negative energy states of relativistic electron theory, (e.g., Proc. Roy. Soc. A133, 60 (1931)). However, those who succeed in getting through to the last page will undoubtedly also succeed in correcting this for themselves.

E. L. HILL
University of Minnesota

Gmelin's Handbuch der anorganischen Chemie 8 Auflage, Herausgegeben von der Deutschen Chemischen Gesellschaft. System Nummer 59, Eisen, Teil A, Lieferung 4. Pp. 260, Figs. 180. Verlag Chemie G.m.b.H. Berlin, 1932, R.M. 41; (subscription price R.M. 35.50).

The volume preceding the present one was published in 1930 and has been reviewed in these columns. Volume 4 of the series on the technology of iron deals with the manufacture, properties, and testing of wrought, bar, cast, and pig iron, of open hearth and Bessemer steel and of slags. One of the outstanding features is the truly international bibliography at the end of each chapter. The great practical importance of iron and steel justifies the extensive technological treatment of the subject in the Gmelin series.

I. M. KOLTHOFF
University of Minnesota

THE PHYSICAL REVIEW

The Measurement of X-Ray Emission Wave-Lengths by Means of the Ruled Grating

By R. B. WITMER AND J. M. CORK
Department of Physics, University of Michigan

(Received September 27, 1932)

With a plane ruled grating, measurements have been made of the emission wave-lengths in the *L* series for the elements Va (23) to Zn (30) and in the *K* series for the elements C (6) to Si (14). With the exception of the *K α* lines of carbon, fluorine and oxygen, the method of the ruled grating yields a longer wave-length in every case than that found for the corresponding lines by the crystal method. The Moseley diagrams representing the observed results are found to be smooth curves. The possible variation of apparent wave-length with a variation in the grazing angle of incidence has been investigated. For angles such that the diffracted lines were not too diffuse, the computed wave-lengths were independent of the incident angle.

INTRODUCTION

SEVERAL investigations have now been carried out to determine the wave-lengths of x-ray spectral lines by means of ruled gratings. In certain of these investigations measurements have been made relative to some particular emission line whose wave-length assumed as a standard has been measured by the Bragg method with a crystal. In other experiments^{1,2,3,4} the wave-lengths have been determined directly from the measurable constants of the apparatus. The results for the wave-lengths so far obtained by this latter method are found in every case to be greater than the corresponding values found by means of the usual crystal method. Disagreement exists only in the magnitude of the discrepancy.

The apparent existence of this difference raises a very important question. If the measurements by means of crystals are correct then there is some defect in applying to the ruled grating in the case of x-rays the same theory that is found satisfactory in the visible and the ultraviolet spectral regions. If the measurements by means of the ruled grating are correct then there is something in error in calculations involving the Bragg law, other than the effect due to the ordinary refraction of x-rays in the crystal, which can be accounted for. If this error exists in the lattice constant *d* then it reflects upon our knowledge of certain other more fundamental constants, namely

¹ E. Bäcklin, *Dissertation*, Upsala, 1928.

² J. A. Bearden, *Proc. Nat. Acad. Sci.* **15**, 528 (1929); *Phys. Rev.* **37**, 1210 (1931).

³ J. M. Cork, *Phys. Rev.* **35**, 1456 (1930).

⁴ C. E. Howe, *Phys. Rev.* **35**, 717 (1930).

The following changes in the apparatus were made. The glass grating employed in this investigation was ruled in the laboratory of Professor M. Siegbahn and obtained through his kindness. The active surface was 3 mm wide and the lines were 2 cm long. Nominally having 600 lines per mm a calibration with known wave-lengths in the arc spectrum of mercury gave for the distance d between lines ($d = 0.00166309$ mm). The glass surface between the rulings and the outside of the plate was etched down on one side so that the direct beam going to the photographic plate was limited on one side by the edge of the ruled surface. The collimating system consisted of parallel slits 0.05 mm wide spaced 20 cm apart. A water-cooled x-ray tube of metal was used in place of the glass tube. A very fine knife edge was placed parallel and close to the rulings of the grating at the center. This reduced materially the stray radiation and general blackening on the photographic plate.

The procedure in taking exposures with the photographic plate at different distances from the grating was followed as previously described. For any particular substance on the target at least five exposures were taken with the photographic plate in a position a close to the grating and then in the position d at a maximum distance from the grating. Reproductions of some typical spectrograms are given in Fig. 1. At least six and sometimes as many as twelve measurable orders were obtained on each photogram.

RESULTS

A summary of the results obtained for the wave-lengths in the K series for the elements investigated is given in Table I. Similarly in Table II are given the values obtained for the wave-lengths in the L series. Along with the results of this investigation are shown the corresponding values from experiments using the crystal method as well as those of other experimenters

TABLE I. Summary of wave-lengths in the K series.

Element		Crystal	Söderman ⁵	Thibaud ⁶	Witmer and Cork
Si	β	6.754	—	—	6.764
	α	7.110	—	—	7.121
Al	β	7.965	—	—	7.967
	α	8.320	—	—	8.334
Mg	β	9.539	—	—	9.558
	α	9.869	—	—	9.898
Na	α	11.885	11.88	—	11.910
F	α	18.37	18.275	—	18.354
O	α	23.73	23.567	23.80	23.644
C	α	45.50	44.54	44.90	44.448

with the ruled grating. In the L series for the elements mentioned here, measurements by the crystal method have been carried out by Siegbahn and Thoriaeus^{7,8} and by Karlsson.⁹ The values from these investigations are

⁵ M. Söderman, *Phil. Mag.* **10**, 600 (1930).

⁶ J. Thibaud, *J. Opt. Soc. Am.* **17**, 145 (1928).

⁷ M. Siegbahn and R. Thoriaeus, *Ark. Mat. Astr. O. Fys.* **18**, 24 (1924).

⁸ R. Thoriaeus, *Phil. Mag.* **1**, 312 (1926); **2**, 1007 (1926).

TABLE II. *Summary of wave-lengths of emission lines in the L series.*

Element	$\beta_{3,4}$	β_1	$\alpha_{1,2}$	η	l	Investigation
Zn 30	11.163	11.96	12.23	13.61	13.97	Ka Crystal
	11.16	11.96	12.23	13.61	13.95	S Crystal
	—	11.96	12.25	—	14.02	Ho
	11.202	11.974	12.252	13.670	14.038	Present
Cu 29	12.07	13.027	13.306	14.87	15.26	Ka Crystal
	12.10	13.03	13.316	14.83	15.19	S Crystal
	—	—	13.60	—	—	Hu
	—	—	13.32	—	15.26	K
	—	—	13.37	14.95	15.33	Ho
	12.091	13.048	13.339	14.910	15.266	Present
Ni 28	13.14	14.25	14.53	16.28	16.66	Ka Crystal
	13.12	14.24	14.53	16.17	16.55	S Crystal
	—	—	14.51	—	—	K
	—	14.28	14.62	16.36	16.73	Ho
	—	14.255	14.556	16.271	16.660	Present
Co 27	14.24	15.63	15.94	17.86	18.25	Ka Crystal
	—	15.62	15.94	17.77	18.20	S Crystal
	—	—	15.94	—	18.28	K
	—	15.64	15.99	—	18.34	Ho
	—	15.690	15.990	—	18.321	Present
Fe 26	15.71	17.23	17.58	19.76	20.09	Ka Crystal
	15.61	17.22	17.58	19.65	20.12	S Crystal
	—	—	17.70	19.60	20.10	Th
	—	—	18.00	—	—	Hu
	—	—	17.61	—	—	B
	—	—	17.54	—	20.15	K
	—	17.29	17.66	—	20.25	Ho
	—	17.281	17.602	—	20.161	Present
Mn 25	—	19.04	19.40	—	—	Ka Crystal
	—	19.04	19.39	—	—	S Crystal
	—	19.17	19.55	—	22.34	Ho
	—	19.136	19.454	—	22.296	Present
Cr 24	—	21.19	21.53	23.28	23.84	Ka Crystal
	—	21.19	21.53	—	—	S Crystal
	—	—	21.74	—	24.73	K
	—	—	21.73	—	—	Ho
	—	21.279	21.670	—	24.788	Present
Va 23	—	—	24.20	—	—	Ka Crystal
	—	—	24.31	—	27.70	Ho
	—	—	24.215	—	27.78	Present

Ka, Karlsson, reference 9; S, Siegbahn and Thoriaeus, references 7 and 8; Ho, Howe, reference 4; Hu, E. L. Hunt, Phys. Rev. 30, 227 (1927); K, G. Kellstrom, Zeits. f. Physik 58, 511 (1929); Th, Thibaud, reference 6.

recorded in Table II. For the wave-lengths of certain η and l lines the agreement between the two crystal determinations is rather unsatisfactory. It is, however, apparent that in every case with the exception of the $K\alpha$ lines for fluorine, oxygen and carbon the value of a particular wave-length by the grating method is greater than the corresponding value found by the crystal method. The discrepancy for the lines in the L series is with few exceptions found to be not as great as was observed by Howe.⁴

⁴ A. Karlsson, Ark. Mat. Ast. O. Fys. 22, 9 (1930).

The Moseley diagrams for the various spectral lines observed, in which the square root of the frequency $(\nu/R)^{1/2}$ is plotted against the atomic number, are remarkably smooth curves. No positions are observed at which the slope of a line changes abruptly as might have been expected from the consideration of the origin of the spectral lines.

Hanawalt and Prins¹⁰ have reported an apparent variation in the wavelength of a particular line with a change in the incident angle θ . The existence of such an effect would render uncertain any measurements made by the grating method and this effect was therefore investigated with considerable care. A complete series of spectrograms (i.e., five plates in each of the *a* and *d* positions) were obtained for the copper *L* lines with each of the following values for the grazing angle of incidence θ :—26'33'', 30'26'', 39'36'', 51'20'' and 1°16'15''. Reproductions of three of these spectrograms are shown in Fig. 1. For any particular wave-length the smaller the value of the grazing angle of incidence θ , the greater is the angular dispersion. This variation is not great. One very apparent effect of using a large incident angle is a broadening of any diffracted line.

TABLE III. *The wave-length of the Cu $K\alpha_{1,2}$ line for different incident angles.*

Grazing angle θ	λ in angstrom units
26'33''	13.339
30'26''	13.339
39'36''	13.335
51'20''	13.342
1°16' 5''	13.368

The wave-length of the $L\alpha_{1,2}$ spectral line of copper as computed for the various values of θ is shown in Table III. For the first four angles the agreement is well within the experimental error. It is believed that the discordant value for the maximum θ is due to an inaccuracy in the calculation caused by the increased width of the diffracted lines.

Measurements by the crystal method of long wave-lengths are necessarily subject to inaccuracies due to the refraction of x-rays in the crystal. In the region of an absorption frequency characteristic of the atoms of the crystal there is an anomalous refractive effect which influences substantially results obtained from the Bragg law. Thus in crystals of gypsum, lauric acid or palmitic acid as used in investigating wave-lengths mentioned in this paper the calculation is complicated by the *K* absorption frequencies for carbon, oxygen, sulphur and calcium. Failure to consider this effect for the longer wave-length *K* series lines together with the uncertainty in the lattice constant of crystals of the fatty acids may account for the unsystematic discrepancy between measurements by the ruled grating and the crystal.

Influenced by calculations of wave-lengths from measurements of the index of refraction of a quartz crystal, Bearden¹¹ has indicated a lack of faith

¹⁰ J. D. Hanawalt and J. A. Prins, *Physica* 12, 1 (1932).

¹¹ J. A. Bearden, *Phys. Rev.* 39, 1 (1932); 40, 471 (1932).

in measurements made by the ruled grating. These calculations with the index of refraction demand a knowledge of: (a) the density of the crystal; (b) the absolute value of e/m for the electron; (c) a factor characteristic of the refracting crystal which is constant for a particular wave-length but which itself demands a knowledge of the wave-length in its determination and (d) an exact evaluation of the index of refraction exhibited by the crystal for the particular wave-length being investigated. If the evident uncertainties in (b) and (c) be overlooked it would still seem that the very short distances to be measured between the relatively diffuse lines on the photographic plates in the experimental procedure of (d) must render this method impotent in expressing a preference between the other two methods.

Laue Patterns from Thick Crystals at Rest and Oscillating Piezoelectrically

By J. M. CORK
University of Michigan

(Received October 26, 1932)

Laue patterns have been observed for thick crystals of quartz and Rochelle salt oscillating piezoelectrically and for the same crystals as well as for calcite, rock-salt and other materials at rest. Patterns have been obtained when the crystalline faces were the natural cleavage surfaces and when they were polished and when etched by suitable solvents. Regular Bragg reflections have been observed and compared for a quartz crystal with polished face and for the same crystal with the face etched with hydrofluoric acid. In the Laue patterns, the individual spots show a multiple structure in every case. The inner spots are double in nature. For the crystal oscillating piezoelectrically or at rest with polished faces the doubling of each spot is radially symmetrical. For the crystal with etched faces and at rest the inner component of the double spot is the stronger particularly for those spots near the center. The Bragg reflection from a quartz crystal with etched face shows the absence of any layer with reduced extinction at the surface. Further elaboration of the Laue diffraction theory seems necessary to account for the multiple structure of the spots formed by an ideally perfect crystal.

THE reflection of x-rays from quartz crystals oscillating piezoelectrically and at rest have been observed by means of the Bragg method and the Laue method in many investigations.^{1,2,3,4} In the transmission method the piezoelectric oscillation leads to an intensity of the reflected x-ray beams much greater than that found for the crystals at rest. Moreover Barrett and Howe have observed that each Laue spot for the oscillating crystal appears to have a fine structure. To observe this fine structure the present investigation employing a more finely collimated beam of x-rays and crystals of greater thickness was undertaken.

APPARATUS AND RESULTS

Two Laue cameras were constructed. In one the distance from the crystal to the photographic plate was 20 cm while in the other the corresponding distance was only 7 cm. It was thus possible to observe the complete pattern or only the central spots in greater detail. In both cases the x-ray beam was collimated by a fine slit system formed by two pinholes each 0.05 cm in diameter and spaced 12 cm apart. The first pinhole was 30 cms from the focal spot of the x-ray tube. A standard 200 kv Coolidge tube with a target of tungsten was employed. It was operated continuously at only 110 kv with a current of 2 milliamperes.

¹ Y. Sakisaka, *Jap. Jour. Phys.* **4**, 171 (1927).

² G. W. Fox and P. H. Carr, *Phys. Rev.* **37**, 1622 (1931).

³ G. W. Fox and J. M. Cork, *Phys. Rev.* **38**, 1420 (1931).

⁴ C. S. Barrett and C. E. Howe, *Phys. Rev.* **38**, 2290 (1931); **39**, 889 (1932).

Exposures were first taken with crystals of quartz ranging in thickness from 4 mm to 7 mm. In the beginning considerable difficulty was experienced in maintaining these thick crystals in the vibrating state continuously. A vacuum tube oscillator with two tubes having capacitive feed-back was arranged which accomplished this result satisfactorily.

Typical patterns obtained with the longer camera are shown in Fig. 1, A, B and C. For the quartz crystal with polished faces the spots were symmetrically double as were also the spots for the oscillating crystal regardless of the nature of the faces. When the crystal with polished faces was etched by immersion in hydrofluoric acid so that the thickness was reduced by not over 0.005 mm a pattern as shown in C, Fig. 1 was obtained. It is apparent that although the spots are now double the component parts are not of equal intensity. The inner part (i.e., that portion usually associated with reflection

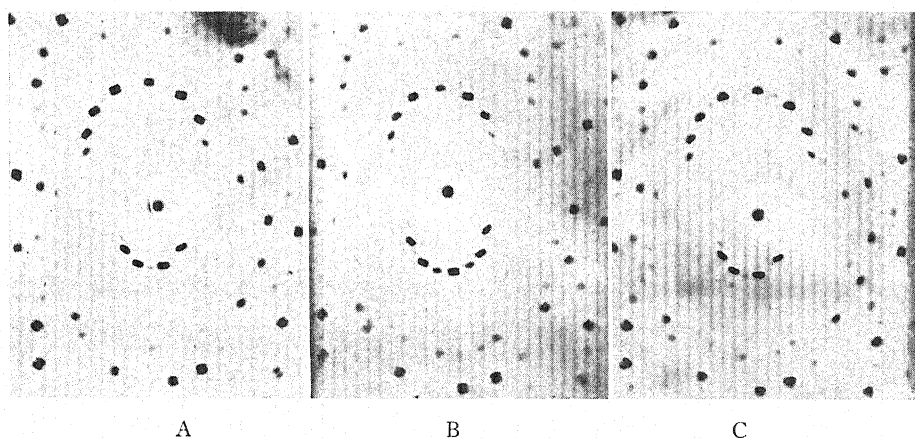
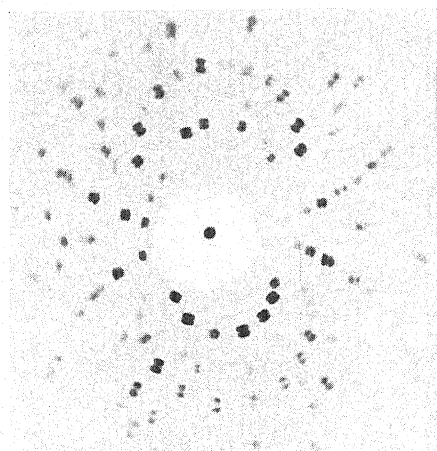


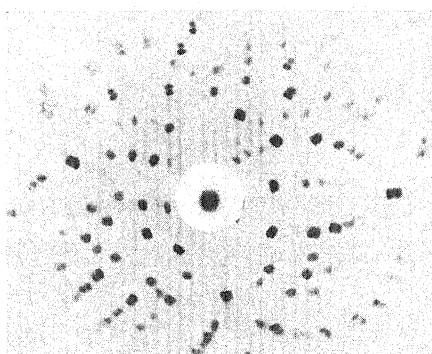
Fig. 1. Laue patterns obtained with quartz. A, etched faces oscillating 12 hr. exposure; B, polished faces non-oscillating 20 hr. exposure; C, etched faces non-oscillating 20 hr. exposure.

from the side of the crystal nearest the photographic plate) is much blacker than the outer component. This dissymmetry is not so apparent in the outer spots of the pattern as shown in the photograms obtained with the shorter camera.

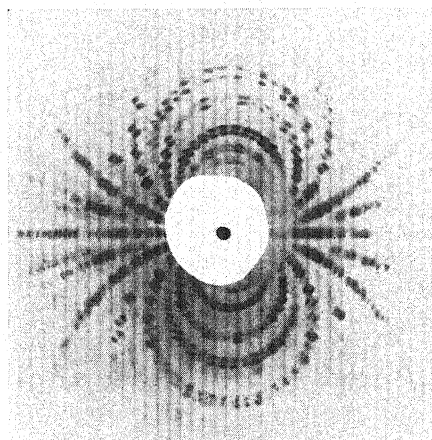
To observe the effect of this etching upon the surface of the crystal the following test was carried out. The quartz crystal was mounted in a Siegbahn vacuum spectrograph and employed to measure the wave-length of the $K\alpha_1$ line of molybdenum ($\lambda = 5.41\text{\AA}$). The crystal was adjusted so that the desired radiation fell on the photographic plate in one position and then both crystal and plate were rotated through predetermined angles so that the same line was reflected to the photographic plate on the opposite side of the direct beam. One should obtain therefore upon the plate the segments of two inverted circles overlapping exactly at the center if the angle of displacement were chosen correctly. With the use of the quartz crystal with polished faces these lines are very diffuse so that the two segments are indistinguish-



A



B



C

Fig. 3. Laue patterns from thick crystals at rest, A, quartz, B, calcite, C, Rochelle salt.

able as shown in Fig. 2A. Upon lightly etching the face of the quartz crystal with hydrofluoric acid these two lines become very sharp and are clearly distinguishable in Fig. 2B. For radiation of this wave-length the penetration into the crystal is exceedingly small and the sharpness of the photographic lines might safely be interpreted as indicating the almost complete absence of any disarranged particles on the surface.

It would appear therefore that the doubling of the spots was not due to a lack of extinction at the surfaces as has been generally assumed. To investigate this phenomenon further, Laue patterns were obtained with freshly cleaved slabs of several other materials. For some exposures the faces were etched by appropriate solvents while for others the specimen was left with its natural cleavage faces. Only in the case of a very bad specimen of rocksalt was a pattern obtained in which the Laue spots were not clearly multiple in structure. The spots toward the center of the pattern were double while those farthest removed from the central position were often triple in nature. Typical photograms of this sort are shown in Fig. 3 A, B and C which are for quartz, calcite and Rochelle salt, respectively.

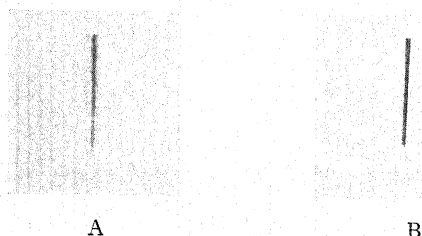


Fig. 2. Double exposures of molybdenum $L\alpha_1$ line, A, polished face, B, etched face.

This doubling or tripling of the Laue spots was undoubtedly first observed by M. de Broglie⁵ when he passed a beam of x-rays through thin slips of crystal (rocksalt and fluorite) at an angle of incidence of 80° or a grazing angle of 10° . In this way he had effectively a thick crystal. The result was explained by assuming that the crystal traversed by the x-ray beam was composed of as many granules separated by accidental parallel cleavage planes as there were components in the spots. This would of course not account for the regularity and radial symmetry always observed in the reflected beams.

Freshly cleaved surfaces of calcite have been found⁶ to give by Bragg surface reflection, spectral lines of width approximating that to be expected for an ideally perfect crystal. From photograms such as Fig. 2B it may be concluded that at least certain specimens of quartz are also very regular. Yet these same crystals give Laue patterns in which the spots have a multiple structure. It would appear that further elaboration of the usual Laue theory introducing interference between non-parallel radiation and perhaps with reference to a secondary structure as proposed by Zwicky,⁷ is necessary.

⁵ M. de Broglie, *Comptes Rendus* **156**, 1153, also 1461 (1913).

⁶ B. Davis and W. Stempel, *Phys. Rev.* **17**, 698 (1921).

⁷ F. Zwicky, *Phys. Rev.* **41**, 400 (1932).

Neutralization and Ionization of High-Velocity Ions of Neon, Argon and Krypton by Collision with Similar Atoms

By HAROLD F. BATHO

Ryerson Physical Laboratory, University of Chicago

(Received October 19, 1932)

Rudnick's work on the measurement of the free path L_0 for the ionization of a helium atom and the free path L_1 for neutralization of a helium ion in helium, has been extended to the gases neon, argon, and krypton for the velocity range corresponding to accelerating potentials of 10,000 to 22,000 volts. With neon, the work has covered the pressure range from 0.75×10^{-2} mm to 4×10^{-2} mm; with argon, from 0.30×10^{-2} mm to 1.6×10^{-2} mm; and with krypton, from 0.30×10^{-2} mm to 1.4×10^{-2} mm. In all cases, the free path for ionization, reduced to 760 mm pressure, is found to be approximately 6.5×10^{-4} cm. For neon, the free path for neutralization is 0.95×10^{-4} cm; for argon, 0.45×10^{-4} cm; and for krypton, 0.35×10^{-4} cm. Both free paths decrease with increasing velocity. The fraction F_∞ of neutral atoms in the beam when the equilibrium condition is reached is approximately 0.86 for neon, 0.93 for argon, and 0.95 for krypton. This fraction decreases with increasing velocity for neon and argon but appears to increase slightly for krypton. The observed dependence of the free paths on pressure is compared with the theoretical dependence. The results obtained are compared with the low-velocity measurements of other workers and the differences discussed. The relationship of this work to Doppler effect experiments with neon and argon is considered.

THE free paths of the positive ions of hydrogen,¹ helium,^{1,2} neon,¹ and argon^{1,3,4} have been measured by several investigators for velocities corresponding to accelerating potentials of less than 1000 volts. In the cases of hydrogen^{5,6,7,8,9,10} and helium¹¹ the measurements have been extended to the voltage range from 5000 to 25,000 volts. The high-velocity work has included measurements of the free paths of the neutral atoms and determination of the fraction of neutral particles in the total beam when an equilibrium is established between the neutral and charged particles. Similar measurements with neon, argon, and krypton for high velocities (10,000 to 22,000 volts) have seemed of interest for comparison with the low-voltage measurements, and of importance in view of the unexpected absence of displaced arc lines in Doppler effect observations of the positive rays of neon^{12,13} and argon^{13,14}.

¹ H. Kallmann and B. Rosen, *Zeits. f. Physik* **61**, 61 (1930).

² A. J. Dempster, *Phil. Mag.* **3**, 115 (1927).

³ Penning and Veenemans, *Zeits. f. Physik* **62**, 746 (1930).

⁴ F. Wolf, *Phys. Zeits.* **32**, 897 (1931).

⁵ W. Wien, *Sitz. d. K. P. Akad. d. Wiss.*, July, 1911, p. 773.

⁶ J. Koenigsberger and J. Kutschewski, *Ann. d. Physik* **37**, 161 (1912).

⁷ A. Rüttenauer, *Zeits. f. Physik* **4**, 267 (1921).

⁸ E. Rüchardt, *Ann. d. Physik* **71**, 377 (1923).

⁹ H. Bartels, *Ann. d. Physik* **6**, 957 (1930).

¹⁰ F. Goldmann, *Ann. d. Physik* **10**, 460 (1931).

¹¹ P. Rudnick, *Phys. Rev.* **38**, 1342 (1931).

Wien⁵ and R  chardt¹⁵ have shown that if F represents the fraction of neutral particles in the total beam, assuming a simple exchange of electrons between moving and rest particles without appreciable change of velocity or direction of the moving particles, the value of F at a distance x from the point of origin of the beam is

$$F = F_{\infty} + (F_0 - F_{\infty})e^{-(1/L_0 + 1/L_1)xp} \quad (1)$$

where F_0 is the neutral fraction at the point of origin, F_{∞} the neutral fraction when an equilibrium is established between neutral and charged particles, $p dx/L_0$ the probability of ionization of a neutral atom in a distance dx , and $p dx/L_1$ the probability of neutralization of an ion in the same distance. L_0 may be interpreted as the mean free path for ionization of an atom and L_1 the free path for neutralization of an ion for unit pressure. Since the ratio

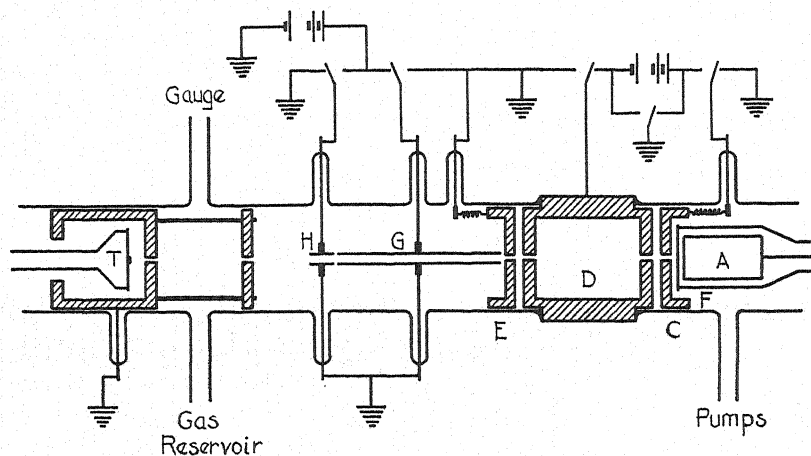


Fig. 1. Diagram of apparatus. A, anode; C, D, and E, accelerating electrodes; F, hot cathode; G, and H, deflecting condensers. T, thermocouple.

of the number of neutral to the number of charged particles in the equilibrium condition of the beam is inversely proportional to the probability of change,

$$F_{\infty} = L_0/(L_0 + L_1). \quad (2)$$

From Eqs. (1) and (2) it is seen that, provided F_0 , p , and x are known, two measurements of F are sufficient for the determination of L_0 , L_1 , and F_{∞} . In practice, to observe F , the total intensity of the beam is measured; then, a transverse electric field is applied at the point x to remove the positive ions, allowing a measurement of the intensity of the remaining neutral atoms. In order to obtain the true value of F , the ratio of neutral intensity to total intensity thus obtained must be corrected for the finite length of the field since the field not only removes all ions already present at the point chosen

¹² W. Romig, Phys. Rev. **38**, 1709 (1931).

¹³ A. I. McPherson, Phys. Rev. **41**, 686 (1932).

¹⁴ K. Friedersdorff, Ann. d. Physik **47**, 737 (1915).

¹⁵ R. R  chardt, Handb. d. Physik **XXIV**, p. 90.

but also removes all ions formed along its length before they have time to return to the neutral state. If the field is applied along a length y of the path of the beam, there will be a simple exponential decay of intensity due to neutrals becoming positive given by

$$I = I_0 e^{-py/L_0} \quad (3)$$

where I_0 is the intensity of the neutrals at the beginning of the field, and I the intensity of the neutrals actually observed. Therefore, the measured ratio must be corrected by the factor e^{py/L_0} to give the true value of F at the beginning of the field.

EXPERIMENTAL ARRANGEMENT

The experimental arrangement used, shown in Fig. 1, was almost identical with that used by Rudnick.¹¹ Ions of the desired gas were formed in a low-voltage arc, by maintaining a small potential difference between the hot filament F and the hollow anode A . The heating current for the filament and the arc potential were supplied by storage batteries. For reasons to be mentioned shortly these batteries were insulated from ground. The filament F and electrode C were maintained at the same potential so that some of the ions formed were drawn through the circular opening in C where they were accelerated by the desired potential difference between C and D . Thus, a beam of high velocity particles proceeded to the thermocouple T . In Doppler effect experiments using this method of producing positive rays, it has been found that very sharp, displaced lines are obtained,^{13,16} indicating that the ions are quite homogeneous in velocity.

For some of the measurements, a beam of particles, which were initially all positive, was required. In this case A , F , and C were raised to a high positive potential with D and E grounded. For other measurements a beam initially neutral was obtained by grounding F , C , and E , and raising D to a high negative potential. With this arrangement the ions were accelerated between C and D . In D they changed charge by collision with gas atoms. All ions remaining in the beam at the end of D were stopped by the retarding field between D and E , allowing only neutral atoms to proceed beyond E . In either case, deflecting fields could be applied along either G or H to remove all ions formed, allowing the measurement of the ratio (uncorrected) of the neutral intensity to the total intensity of the beam.

All cross-hatched parts in Fig. 1 were turned from rolled brass; the anode A was made of nickel; the plates of the condensers G and H of nickel gauze. The electrode D was 5.7 cm in length; G , 7.4 cm; and H , 1.1 cm. The total distance from C to the thermocouple was 24 cm. The thermocouple and the filament and anode were carried on ground joints to facilitate the alignment of the couple and the replacement of the filament. Wax joints were used between the two glass ends of the tube and the center electrode D to permit the easy adjustment and replacement of the electrodes C , D and E .

In all cases it was desirable to have only singly charged ions present. In order to ensure this the arc potential used to form the ions was always less

¹⁶ H. F. Batho and A. J. Dempster, *Astrophys. J.* **75**, 34 (1932).

than the second ionizing potential of the gas in which the measurements were being taken. Doubly charged ions might be formed by collision in passage through the gas but the absence of any displaced lines due to doubly charged particles in Doppler effect experiments with neon and argon,¹⁸ even though no precautions are taken regarding the arc voltage, seems to indicate that the number of doubly charged ions present in the beam is negligible for the pressures and velocities used.

The retarding field used to stop the positive ions, in measurements with an initially neutral beam, accelerated electrons toward the thermocouple. To avoid rather large errors due to this cause, it was necessary to use a transverse magnetic field of sufficient intensity to deflect the electrons, but small enough not to deflect the positive ions appreciably.

It was found that, above 1600 volts, increasing the potential difference across the deflecting condenser did not change appreciably the intensity as measured by the thermocouple; accordingly, this deflecting potential was used to remove all ions from the beam.

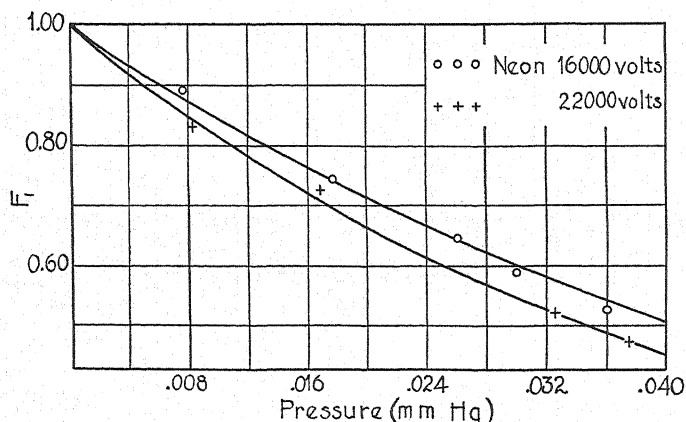


Fig. 2. Relationship between F_1 and pressure. Points shown are experimental values, curves are values plotted from Eq. (4).

The thermocouple was a junction formed by spot-welding 3 mil platinum wire and 10 mil extruded bismuth wire to a platinum foil target 1 mm² in area. The other ends of the wires were joined to nickel lead wires, also by means of platinum foil. The thermoelectric current was indicated by a low-resistance galvanometer of sensitivity 168 megohms. To avoid errors in the measurement of intensity it was found necessary to shield the thermocouple rather carefully. The hot filament was placed slightly off the axis of the tube and the anode was made hollow, thus reducing the amount of radiation reaching the thermocouple directly from the arc in which the ions were formed. The considerable thickness of brass between filament and thermocouple also served the same purpose. Fluctuations in room temperature caused irregular changes in the zero reading of the galvanometer, i.e., in the reading of the galvanometer when no particles were striking the target of the thermocouple. This difficulty was eliminated by enclosing the entire thermocouple end of

the tube in a large asbestos cylinder. After this precaution had been taken, it was found that the zero reading shifted only very slowly.

On account of the wax seals it was not possible to bake out the tube before admitting the gas to be used. However, the exhausting pumps were run at intervals over a period of two or three days before gas was admitted in an attempt to eliminate occluded vapors and gases. With the gases used it was not considered feasible to maintain a steady flow of gas. The neon was admitted to the tube through an adjustable lavite valve,¹⁷ and, after entering the tube, was circulated over charcoal immersed in liquid air. The circulating pump was shut off while readings were being taken to avoid pressure differences along the path of the beam but the gas was circulated at frequent intervals between runs. This appeared sufficient to maintain the purity of the gas. The argon and krypton were purified in the reservoir before entering the tube, by evaporating magnesium in a side tube by means of a high-frequency induction heater. In all cases, a liquid air trap was placed in close connection

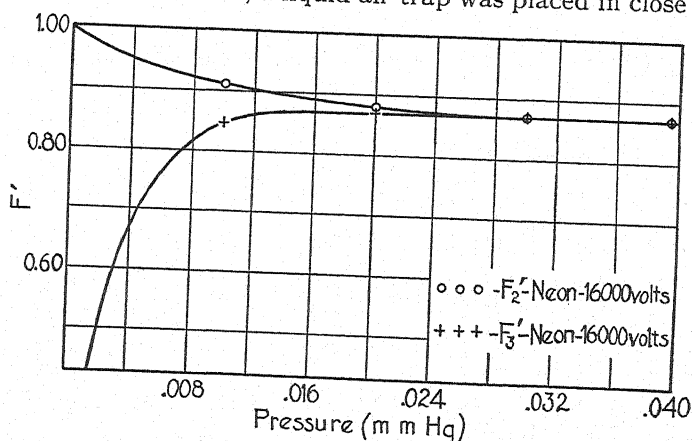


Fig. 3. Relationship between F' and pressure.

with the main tube to eliminate, if possible, vapors of mercury, stopcock grease, and wax. The leads from the reservoir, to the McLeod gauge on which pressures were read, and to the exhausting pump, passed through liquid air traps. During the period in which readings were taken, liquid air was kept on these traps continuously to prevent diffusion of mercury vapor into the tube. These precautions having been taken, the spectrum of the gas in the tube, as examined with a small hand spectroscope, failed to show any mercury lines. As will be seen later, however, there is reason to doubt that these precautions were sufficient to eliminate vapors entirely.

MEASUREMENTS AND RESULTS

For each pressure and voltage three ratios were determined. The first two measurements were made with an initially neutral beam (C and E grounded,

¹⁷ This valve consisted of a lavite cone partially covered with mercury so arranged that the rate of leak could be controlled by changing the mercury level by means of a magnetically operated soft iron plunger. The valve worked very satisfactorily for the purpose for which it was used. The lavite cone was very kindly furnished by the American Lava Corporation.

D at a high negative potential). The first, F_1 , was the ratio of the number of particles reaching the thermocouple, when a deflecting field was applied to the long condenser G only, to the number of particles reaching T with no field applied; the second, F_2 , was a similar ratio with the deflecting field applied to the short condenser H instead of G . The third measurement, F_3 , differed from the second only in the fact that an initially positive beam was used. For each voltage the three ratios were measured at a series of pressures so that curves could be plotted showing the dependence of each ratio on pressure. With all three gases, the measurements covered the voltage range from 7000 to 22,000 volts. With neon, the pressure range was from 0.75×10^{-2} to 4.0×10^{-2} mm of mercury; with argon, from 0.30×10^{-2} to 1.6×10^{-2} mm; with krypton, from 0.30×10^{-2} to 1.4×10^{-2} mm. The lower limits for both velocity

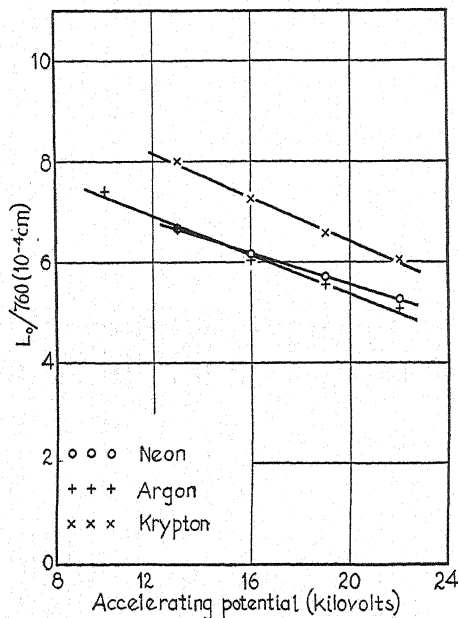


Fig. 4. Relationship between free path for ionization corrected to atmospheric pressure and accelerating potential for neon, argon, and krypton.

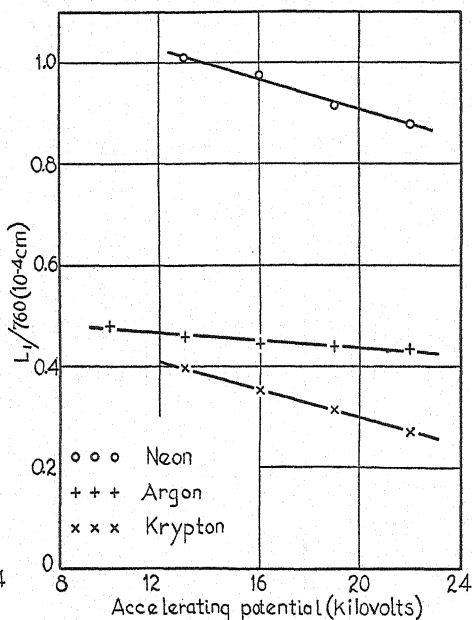


Fig. 5. Relationship between free path for neutralization corrected to atmospheric pressure and accelerating potential for neon, argon, and krypton.

and pressure were set by diminishing intensity; the upper limit of pressure was also set by diminishing intensity, apparently due to scattering; the upper velocity limit was determined by the voltage at which sparking began to occur inside the tube.

From Eqs. (1) and (3) it is seen that the equations expressing the dependence of the various measured quantities on pressure are

$$F_1 \text{ or } F_2 = e^{-p\psi/L_0} [F_\infty + (1 - F_\infty)e^{-(1/L_0 + 1/L_1)pz}], \quad (4)$$

$$F_3 = F_\infty e^{-p\psi/L_0} [1 - e^{-(1/L_0 + 1/L_1)pz}] \quad (5)$$

where x is the distance from the point of origin of the beam to the beginning of the deflecting field and y the length of the field. The expressions for F_1 and F_2 differ only in the values of x and y . For F_1 , $y = y_1 = 7.4$ cm, $x = x_1 = 0.75$ cm; for F_2 , $y = y_2 = 1.1$ cm, $x = x_2 = 8.25$ cm; for F_3 , $y = y_3 = y_2 = 1.1$ cm, $x = x_3 = 14.55$ cm.

Since x_1 is small (0.75 cm) and y_1 relatively large (7.4 cm), the value of F_1 is almost completely independent of L_1 and F_∞ . Therefore, a single measurement of F_1 is sufficient for the determination of L_0 . In Fig. 2, the experimental points obtained in neon for two different voltages, 16,000 and 22,000 volts, are plotted. The curves shown are plotted from Eq. (4) with $L_0 = 0.470$ cm for 1 mm pressure for 16,000 volts, and $L_0 = 0.400$ cm for 22,000 volts. These curves show good agreement with the experimental points for all pressures. They show, also, the dependence of F_1 on voltage, the curve falling as the voltage was increased in all cases.

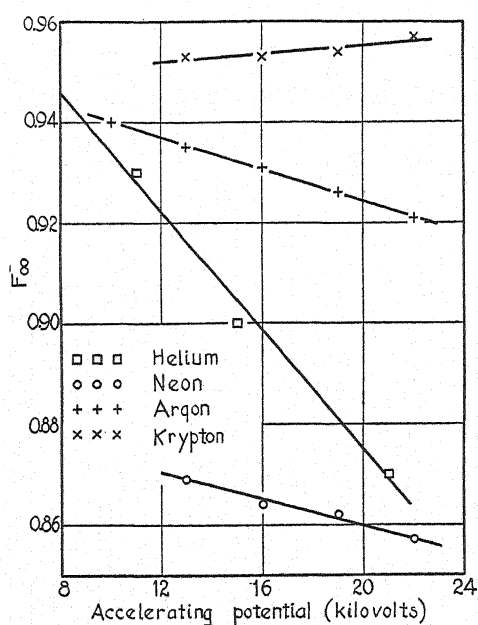


Fig. 6. Relationship between F_∞ and accelerating potential for helium, neon, argon, and krypton.

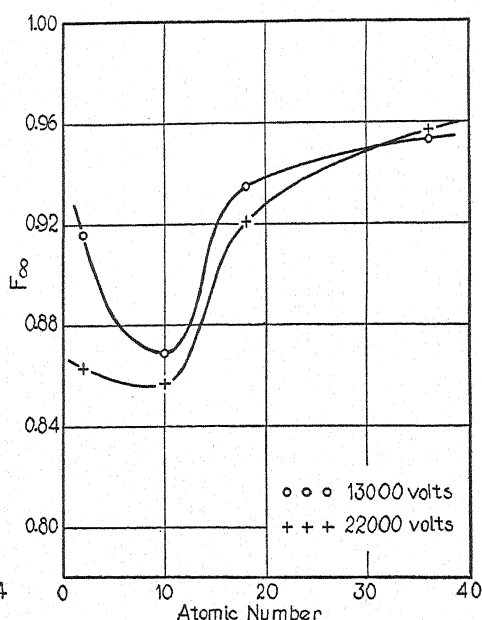


Fig. 7. Relationship between F_∞ and atomic number.

Having obtained the value of L_0 for a particular voltage, we find it possible to calculate the coefficient in front of the brackets in Eqs. (4) and (5) which arises from the decay of intensity in the short condenser. If we multiply the experimentally observed values F_2 and F_3 by e^{pv_2/L_0} and denote the result by F_2' , F_3' , then the corrected experimental values should be connected with the free paths by the relations

$$F_2' = F_\infty + (1 - F_\infty)e^{-(1/L_0 + 1/L_1)px} \quad (6)$$

$$F_3' = F_\infty[1 - e^{-(1/L_0 + 1/L_1)px}]. \quad (7)$$

From these equations, it is seen that both F_2' and F_3' become equal to F_∞ for large pressures. In Fig. 3, the corrected experimental values at different pressures for 16,000 volts for neon have been plotted against pressure. The graph shows that F_2' and F_3' do approach the same constant value at high pressures as indicated by the equations. Thus, the value of F_∞ is obtained. L_1 may be determined from Eq. (2) with the values of L_0 and F_∞ already found.

This process was repeated to find the values of L_0 , L_1 , and F_∞ for each voltage used. The results are given in Table I. Column 3 gives the velocity corresponding to the accelerating potential given in column 2. Columns 4 and 5 show the mean free paths in centimeters corrected to atmospheric pressure of the neutral atoms and positive ions respectively. Column 6 contains the values of F_∞ . The results of other observers and the kinetic theory values of the free paths are included for purposes of comparison. Figs. 4, 5, and 6

TABLE I.

1 Gas	2 Accelerating potential in volts	3 Velocity in cm per sec.	4 $L_0/760$ in cm	5 $L_1/760$ in cm	6 F_∞	7 Observer
Neon	22,000	4.58×10^7	5.3×10^{-4}	0.88×10^{-4}	0.86	Kallmann and Rosen ¹ Kinetic theory value for 20°C and 760 mm
	19,000	4.16	5.7	0.91	0.86	
	16,000	3.91	6.2	0.98	0.86	
	13,000	3.52	6.7	1.01	0.87	
	400	0.62		0.34		
			0.21			
Argon	22,000	3.24×10^7	5.1×10^{-4}	0.44×10^{-4}	0.92	Kallmann and Rosen ¹ Penning and Vennemans ³ Wolf ⁴ Wolf ⁴ Kinetic theory value for 20°C and 760 mm
	19,000	3.03	5.6	0.44	0.93	
	16,000	2.78	6.0	0.44	0.93	
	13,000	2.51	6.7	0.46	0.94	
	10,000	2.20	7.4	0.48	0.94	
	400	0.44		0.15		
	200	0.31		0.13		
	837 20 to 520	0.64 0.38	0.11	0.067 0.11		
Krypton	22,000	2.26×10^7	6.0×10^{-4}	0.27×10^{-4}	0.96	Kinetic theory value for 20°C and 760 mm
	19,000	2.10	6.6	0.32	0.95	
	16,000	1.93	7.3	0.35	0.95	
	13,000	1.74	8.0	0.40	0.95	
			0.10			

show the dependence of L_0 , L_1 , and F_∞ , respectively, on accelerating potential. In Fig. 7, F_∞ is plotted as a function of atomic number for 13,000 and for 22,000 volts. The values for helium are taken from Rudnick's data.¹¹ The measurements at lowest voltages have been omitted from the table and graphs, since all measurements below 13,000 volts were difficult on account of small intensity. Particularly was this true at high pressures as scattering also decreased the intensity. Since the determination of F_∞ and L_1 depends on high-pressure measurements no reliable values could be obtained for low velocities. However, the readings made at lower pressures indicated no large changes in L_0 , L_1 , or F_∞ at these velocities.

DISCUSSION OF RESULTS

The results of the preceding paragraph have been deduced from the observation of F_1 which gives L_0 , the free path for ionization, and of F_∞ , the equilibrium condition reached by the beam. L_1 has been deduced from the equilibrium value and not observed directly. The observations, however,

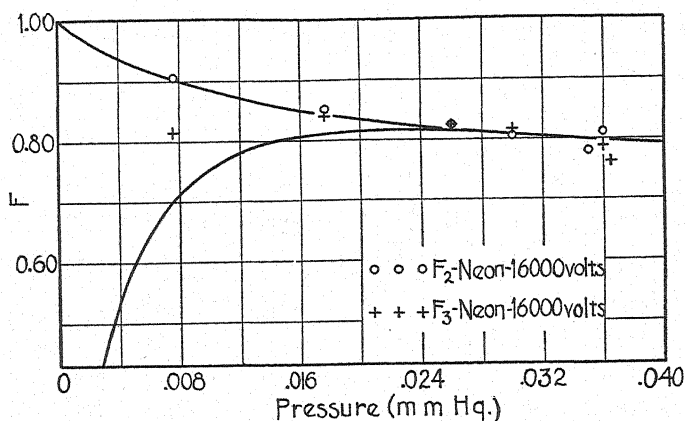


Fig. 8. Relationships between F_2 and pressure, and F_3 and pressure. Points shown are experimental values, curved are values plotted from Eqs. (4) and (5), respectively.

including the dependence of F_2 and F_3 on pressure, contain more data than are required to deduce L_0 and L_1 , and may be used to check the adequacy of the theory to account for the dependence on pressure observed in the case of F_2 and F_3 .

Having determined L_0 , L_1 , and F_∞ for any particular velocity, it is possible to plot complete curves for F_1 , F_2 , and F_3 from Eqs. (4) and (5) for comparison with the experimentally determined points. This has been done already for F_1 in Fig. 2. Fig. 8 is a similar comparison for F_2 and F_3 . As in Fig. 2, the points shown are the observed values, the curves the theoretical values. Since L_0 , L_1 , and F_∞ were determined from the high-pressure data the agreement is necessarily good for these values of the pressure. It is seen that the agreement is good for F_1 and F_2 for all pressures, but that for F_3 , for pressures less than 2×10^{-2} mm, the experimental points lie considerably above the curve plotted from Eq. (5). For argon and krypton the experimental

points for F_1 and F_2 also lie above the curves, but in no case is the deviation as great as for F_3 . With increasing velocity the deviation decreases, being small for the highest velocities.

This deviation from the theoretical curves may be shown in another way. Given a set of values of F_1 , F_2 , and F_3 for a particular pressure and velocity, it is possible to solve Eqs. (4) and (5) for L_0 , L_1 , and F_∞ , i.e., for each velocity it is possible to determine the required constants for a series of pressures. This has been done; the results are shown in Figs. 9 and 10. In Fig. 9, p/L_0 and in Fig. 10, p/L_1 are plotted against pressure. The graphs for neon for accelerating potentials of 16,000 and 22,000 volts are shown in each case. Since L_0 and L_1 are constants,—the free paths for 1 mm pressure—as expressed in the equations, p/L_0 vs. p and p/L_1 vs. p should both give straight lines through the origin. Actually the graphs are approximately straight lines but

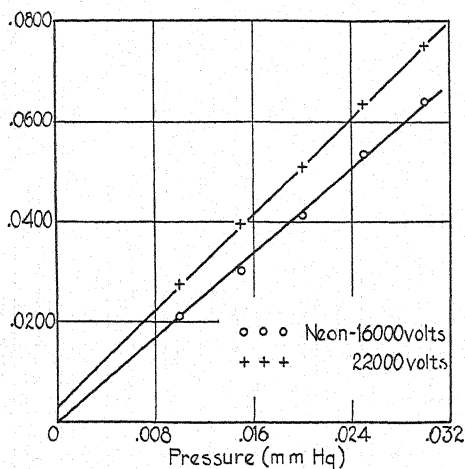


Fig. 9. Relationship between free path for ionization and pressure. Abscissa, p/L_0 .

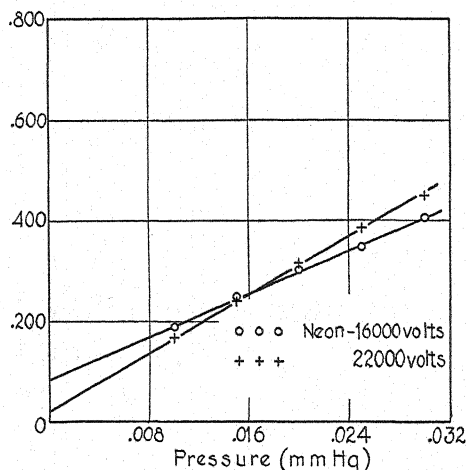


Fig. 10. Relationship between free path for neutralization and pressure. Abscissa, p/L_1 .

do not pass through the origin. In Fig. 9 the displacement is small in both cases—probably less than experimental error. In Fig. 10, however, the displacement is much greater. The fact that it is smaller for 22,000 volts than for 16,000 volts corresponds to the fact that the agreement between experimental and theoretical values, shown in Fig. 8, is much better for the higher velocities. For argon and krypton, the straight lines of Fig. 9 are also displaced from the origin, since for these gases, the experimental values of F_1 and F_2 do not fall on the theoretical curves as they do in the case of neon, but here again the displacement decreases with increasing velocity.

Two arguments may be advanced to justify the calculation of the desired constants from the high-pressure data. First, the corrected curves for F_2 and F_3 , shown in Fig. 3, do exhibit the properties expected at high pressures. Also, it is possible to obtain much better agreement between experimental and theoretical values by using the values of L_0 and L_1 determined for high rather than low pressures. The second is found in Rüchardt's work⁸ with

hydrogen. His data also gave displaced straight lines like those shown in Figs. 9 and 10 when the reciprocals of the free paths were plotted against pressure. However, when the work was repeated, taking great precautions to eliminate all vapors, he obtained straight lines through the origin. He found that the lines obtained in the first case, were displaced considerably from the lines in the second case for low pressures, but that the displacement decreased with increasing pressure, i.e., the values for the free paths, as determined at high pressures, were the same in the two cases. In view of this work, it seems probable that the errors in the values given in Table I are not great.

Several explanations may be suggested for the disagreement between experimental and theoretical curves at low pressures. The fact that the discrepancy increases with decreasing velocity, and is greater for argon and krypton than for neon, suggests that scattering may have influenced the results since a comparison of total beam intensities at different velocities indicated that scattering increases with decreasing velocity and with increasing atomic number. This explanation is further supported by the fact that in some cases the corrected curves F_2' and F_3' of Fig. 3, do not reach a constant value, but appear to continue to decrease with increasing pressure. This can be explained by assuming that the neutral particles were scattered more than the ions. This decrease, however, is scarcely greater than experimental error in any case. An investigation of the effect of scattering shows that the results would depend only on the difference between the scattering coefficients of the atoms and ions, i.e., if they were scattered equally the results would be unaffected. Assuming a difference in scattering, we find that good agreement can be obtained between experimental and theoretical curves, but only when an unreasonably large difference in scattering coefficients is assumed—a difference so large that the intensity of the beam reaching the thermocouple would have been so small as to be quite undetectable. For this reason the scattering explanation seems to be ruled out. However, it should be pointed out that, while a small difference in the scattering of atoms and ions would not change appreciably the measured values of F_1 , F_2 , and F_3 , the values of L_0 , L_1 , and F_∞ , as calculated, might be very considerably in error if such a phenomenon were present.

It has been suggested that three rather than two types of particles may have been present in the beam, e.g., normal atoms, metastable atoms, and positive ions. An investigation of this possibility, with the necessary introduction of rather arbitrary assumptions about the processes involved, gives only slightly better agreement than the simple theory with the experimental values. This better agreement may, perhaps, be explained merely by the fact that another parameter is introduced into the equations; at least, the agreement obtained does not warrant any conclusions as to the correctness of the assumptions made.

In his work on hydrogen, Rüchardt⁸ concluded that the observed discrepancies could be accounted for completely by the presence of vapors in the tube. In the present work, it does not seem unlikely that vapors were

present, despite the precautions taken, since a continuous flow of gas was not used. Further, Bartels¹⁸ found that the fraction of neutral particles increased when the beam passed through a slit. This may be accounted for, probably, by the evolution of vapors due to bombardment of the edges of the slit. In the present work, vapors might be expected to be present for this reason also, since the beam passed through several circular diaphragms. The pressure of such vapors would be independent of the gas pressure in the tube. However, the number of collisions with vapor molecules relative to the number of collisions with gas atoms, would be greater at low pressures; therefore, the discrepancies introduced would be greater at these pressures. The observed deviations would be accounted for if the ions in the beam were more readily neutralized by collisions with the vapor molecules than with the gas atoms, since, in all cases, the fraction of neutral atoms in the beam at low pressures is greater than that expected from high-pressure measurements. On the whole, the presence of vapors seems to be the most reasonable explanation of the observed discrepancies, although it is quite probable that all the suggested phenomena and other more complex ones influence the measurements in some degree. If the discrepancies are accounted for by the presence of vapors, it seems likely that the values given in Table I, determined from the high-pressure measurements, are reasonably accurate. It may seem that the measurements for argon and krypton are much less reliable than for neon since the pressure range investigated was considerably lower, but in this connection, it should be noted that F_2 and F_3 became equal at much lower pressures with these gases than with neon and that the discrepancies observed were only slightly greater than with neon.

It will be seen from Figs. 4 and 5 that, for all the gases investigated in the present work, both free paths decrease slowly with increasing velocity. The behavior of helium differs in two respects; first, the rate of decrease of L_0 with increasing accelerating potential is much greater than for neon, argon, or krypton; secondly, for helium, L_1 increases rather than decreases as the velocity becomes greater. Fig. 7 shows a minimum value of F_∞ as a function of atomic number for both 13,000 and 22,000 volts, although it appears that for higher velocities this minimum would disappear. With reference to the dependence of F_∞ on atomic number, it may be noted further from Fig. 6 that the rate of change of F_∞ with velocity increases with atomic number from a relatively large negative value for helium to a small positive value for krypton. The increase of F_∞ with velocity for krypton, however, is small enough to be rather uncertain.

It is interesting to compare the measured values of the free paths with the kinetic theory values. A comparison shows that for neon the kinetic theory free path is about one-thirtieth of the free path for ionization of a high-velocity atom and about one-fifth of the free path for the neutralization of a fast ion, i.e., a moving atom is ionized at about every thirtieth collision with a rest atom and a moving ion is neutralized at about every fifth collision.

¹⁸ H. Bartels, reference 9, p. 969.

In argon, the probability of ionization is less, occurring for approximately one collision in sixty, but the probability of neutralization is about the same. With krypton, ionization takes place at every seventieth collision, approximately, while neutralization occurs for one collision in four.

A comparison of the free paths of the ions in the present work, with those obtained from the low-velocity measurements of Kallmann and Rosen¹ and others^{3,4} shows that the values for high velocities are approximately three times those for the slow ions in all cases. Since Fig. 5 shows a decrease of L_1 with increasing velocity, for neon, argon, and krypton, the comparison might suggest that the free path for neutralization for these gases, has a maximum for some accelerating potential intermediate between 800 and 7000 volts. This is not a necessary conclusion, however, as the difference in the method of measurement makes the comparison doubtful. In the present work only a difference in the scattering of the atoms and ions would affect the results, whereas with the method used in the low-velocity measurements, any scattering of ions would result in a decrease of the intensity of the ionic beam, and, therefore, in a decrease of the measured free path. It seems probable that scattering would be relatively large for the slow ions, particularly in view of the conclusion of Kallmann, Lasareff, and Rosen in a recent article¹⁹ that slow neutral atoms are scattered at every kinetic theory collision. The difference in the values obtained may, perhaps, be completely explained by the effect of scattering in the low-velocity measurements.

Doppler effect observations of positive rays of neon^{12,13} and argon^{13,14} of velocities similar to those used in the present work show a surprising absence of displaced arc lines. This fact might be interpreted as proof that the particles in the beam are predominantly positive, the absence of neutral atoms accounting for the absence of displaced arc lines. This suggestion is supported by the work of Rutherford²⁰ and Henderson²¹ in which they found that neutral atoms are present in an α -ray beam only at lower velocities. The present experiments show, however, that in neon 86 percent of the particles in the beam are neutral, while in argon 93 percent and in krypton 95 percent are neutral. This seems to rule out the suggested interpretation. The alternative interpretation appears to be that, for some reason, after a collision a moving particle is seldom, if ever, left in an excited neutral state.

The writer desires to acknowledge the assistance given by Professor A. J. Dempster in suggesting the problem, and to thank him for much valuable advice and criticism which have aided in avoiding many of the difficulties of the problem and in solving others when encountered.

¹⁹ H. Kallmann, W. Lasareff and B. Rosen, *Zeits. f. Physik* **76**, 213 (1932).

²⁰ E. Rutherford, *Phil. Mag.* **47**, 277 (1924).

²¹ G. H. Henderson, *Proc. Roy. Soc. A* **109**, 157 (1925).

Extension of the First Spark Spectrum of Caesium (Cs II)

By J. OLTHOFF AND R. A. SAWYER

University of Michigan

(Received September 1, 1932)

With an electrodeless discharge in caesium vapor as a light source, the spark spectrum of caesium has been completely rephotographed in the region $\lambda 2300$ – $\lambda 10,000$ in the first order of 21 ft. concave grating and with a Hilger E1 quartz spectrograph. The observations of Sommer in the region $\lambda 3268$ – $\lambda 7280$ were confirmed and extended and many new lines were photographed outside Sommer's range. These data were used to extend the classifications of Laporte, Miller and Sawyer, based on Sommer's data supplemented by vacuum spectrograph measurements, in which practically only terms belonging to the $5p^5\ ^2P_{1/2}$ limit were identified. In the present work most of the terms of the $5p^5\ (^2P_{3/2})\ 5d, 6d, 6s, 7s,$ and $6p$ configurations were located as well as a few new terms belonging to the $5p^5\ ^2P_{1/2}$ limit, and about 100 additional lines were classified in the Cs II spectrum.

I. INTRODUCTION

IN A recent publication Laporte, Miller¹ and Sawyer presented an interpretation of the first spark spectrum of caesium on the basis of the material of Sommer² who photographed the caesium spark spectrum in the region $\lambda 3267$ – 7280 and arranged 51 lines in a scheme involving transitions between a middle group of five terms and an upper and a lower group of eight and five terms, respectively. Sommer pointed out the similarity to the neon spectrum but was unable to correlate the two spectra unambiguously. Laporte, Miller and Sawyer photographed the caesium spectrum from a hollow cathode discharge in helium with a 1 meter vacuum spectrograph and discovered eight new lines in the region between 962A and 612A. Identification of these ultraviolet lines as transitions between the lowest term $5p^5\ ^1S_0$, and terms of the configurations $5p^5\ (6s, 7s, 5d, 6d)$ having $j=1$, made possible the interpretation of Sommer's scheme since five of the eight ultraviolet lines proved to involve terms in Sommer's scheme.

It was found that Sommer's middle set of terms belonged to the $5p^5\ 6p$ configuration and his upper and lower sets, respectively, to a blend of $5p^5\ 5d$ and $6s$, and $5p^5\ 6d$ and $7s$. However, from the table of electron configurations and expected terms in a rare gas spectrum given in Table I, it may be seen that these three term groups should contain respectively 10, 16 and 16 terms, divided in each case for (jj) coupling, into two sets having as limits, one $5p^5\ ^2P_{1/2}$ and the other $5p^5\ ^2P_{3/2}$ of the Cs II spectrum. The two sets will be completely and widely separated in Cs II as indeed they are for the preceding spectrum of Xe I. Sommer's terms were shown to belong entirely to lower series limit $^2P_{1/2}$, while the remaining three resonance lines which did not fit into his scheme were believed to arise from configurations built upon $^2P_{3/2}$.

¹ Laporte, Miller, Sawyer, *Phys. Rev.* **39**, 458 (1932).

² Sommer, *Ann. d. Physik* **75**, 163 (1924).

TABLE I. *Electron configurations and theoretical terms of the Cs II spectrum.*

Electron configuration	Russell-Saunders	(jj)		Number of levels
		$^2P_{1\frac{1}{2}}$	$^2P_{\frac{3}{2}}$	
$5p^5$	2P			(2)
$5p^6$	1S_0	0		(1)
$5p^6 6s$	1P_1 $^3P_{210}$	21	10	(4)
$5p^6 7s$				
$5p^6 8s$				
...				
$5p^6 6p$	1S_0 1P_1 1D_2 3S_1 $^3P_{210}$ $^3D_{321}$	12 0123	01 12	(10)
$5p^6 7p$				
$5p^6 8p$				
...				
$5p^6 5d$	1P_1 1D_2 1F_3 $^3P_{210}$ $^3D_{321}$ $^3F_{432}$	0123 1234	12 23	(12)
$5p^6 6d$				
$5p^6 7d$				
...				
$5p^6 4f$	1D_2 1F_3 1S_4 $^3D_{321}$ $^3F_{432}$ $^3G_{543}$	1234 2345	23 34	(12)
$5p^6 5f$				
$5p^6 6f$				
...				

An attempt was made in the previous work to locate more terms built on the $^2P_{\frac{3}{2}}$ limit but except for a tentative group of three terms, which combined with the three terms indicated by the three resonance lines mentioned above, none were found. The data of Sommer seemed insufficient in range for the purpose. The present study has been undertaken to extend the experimental data on the spark spectrum of caesium with the hope of locating more terms and especially those based on the $^2P_{\frac{1}{2}}$ limit.

II. EXPERIMENTAL

In the work of Laporte, Miller and Sawyer, the light source used was a hollow cathode discharge in helium. Since, however, the available excitation which can be given to caesium ions by metastable helium atoms is about $163,000 \text{ cm}^{-1}$ and the ionization potential of Cs II was determined to be about $189,000$, this source is not suitable for the excitation of the complete Cs II spectrum.³ The electrodeless discharge was chosen for the present work because of its economy of material and easily controllable conditions.

The discharge tube was a Corex bulb about 4 cm in diameter and 15 cm long, and was originally blown with a side arm in which several seal-off constrictions separated small bulbs, as well as with a side arm for evacuating. In an atmosphere of nitrogen in a manipulation box, a small fraction of a gram of caesium was washed in anhydrous ether and placed in the side arm. The bulb was evacuated by a mercury vapor pump, the first side arm sealed off and the caesium distilled by stages through the small bulbs into the main bulb and the main bulb, after thorough heating while still on the pumps to drive off adsorbed gases and vapors, was sealed off while still hot. The bulb was suspended inside the exciting coil of eight turns of hollow copper tubing wound in a solenoid about 10 cm in diameter and 8 cm long and the whole

³ Cf. for example, Sawyer, Phys. Rev. 36, 44 (1930).

TABLE II.

$5p^5(^2P_{1/2})5d, 6s$			$5p^5$	$5p^5(^2P_{1/2})6p$		
	J		1S_0	1_1	2_2	3_2
		Relative term value	0	1	2	3
			00.00	*126,518.54	*128,089.83	*129,107.65
4_1^0	3	105,949.74			22,139.77 (2) 0.32	23,157.78 (0) 0.13
5_1^0	1	106,222.77		20,295.73 (1) 0.04	21,867.31 (3) -0.25	
$^3P_2^0$	2	*107,392.33		*19,126.12 (8) 0.09	*20,697.48 (6) 0.02	*21,715.33 (10) -0.01
6_2^0	2	107,563.14		18,955.52 (4) -0.08		21,544.16 (1) 0.35
$^3P_1^0$	1	*107,905.01	*107,905 (20) 0.01	*18,613.42 (6) 0.11	*20,184.84 (6) -0.02	
7_0^0	0	108,245.86				
1_1^0	1	*110,945.18	*110,946 (20) -0.72	*15,573.14 (2) 0.18	*17,144.51 (6) 0.10	
2_2^0	2	*112,795.08			*15,294.63 (4) 0.12	*16,312.38 (4) 0.19
3_2^0	3	*113,716.01			*14,373.12 (4) 0.10	*15,390.96 (3) 0.08
$5p^5(^2P_{1/2})5d, 6s$						
1_0^0	0	119,465.28				
2_2^0	2	119,665.41				
3_2^0	2	120,404.87				
4_1^0	1	122,866.03	*122,872 (20) -5.97			
5_1^0	1	123,636.44	*123,645 (20) -8.56			
$5p^5(^2P_{1/2})6d, 7s$						
$^3P_2^0$	2	*149,212.25		*22,693.82 (7) -0.11	*21,122.47 (4) -0.05	*20,104.64 (5) -0.04
$^3P_1^0$	1	*149,605.33	*149,604 (12)	*23,086.95 (4) -0.16	*21,515.53 (5) -0.03	
1_1^0	1	*152,172.11	*152,172 (5) 0.11	*25,653.67 (7) -0.10	*24,082.27 (4) 0.01	
2_2^0	2	*152,791.49		*26,273.12 (6) -0.17	*24,701.59 (4) 0.07	*23,683.75 (3) 0.09
3_2^0	2	*153,302.27		*26,783.83 (2) -0.10	*25,212.38 (6) 0.06	*24,194.54 (2) 0.08
4_2^0	3	*153,556.54			*25,466.74 (6) -0.03	
5_2^0	3	*153,678.17			*25,588.30 (4) 0.04	*24,570.52 (6) -0.04
6_1^0	1	*156,399.31	*156,392 (12) 7.31		*28,309.51 (0) -0.03	
$5p^5(^2P_{1/2})7d, 8s; 5p^5(^2P_{1/2})6d, 7s$						
1_2^0	2	158,717.91			30,628.61 (1) -0.53	29,610.16 (0) 0.10
2_0^0	0	162,352.92		35,834.32 (3p) 0.06		
3_2^0	3	162,388.96			34,299.37 (3) -0.24	
4_1^0	1	163,180.20	*163,180 (7) 0.20	36,662.16 (0p) -0.50	35,090.18 (1p) 0.09	
5_2^0	2	164,444.88		37,926.67 (0p) -0.33	36,355.02 (1p) 0.03	35,337.24 (2) -0.01
6_1^0	1	164,656.77	*164,655 (3) 1.77		36,567.26 (2p) -0.32	
	1	165,813.70				
	2 or 1	165,899.95		39,371.06 (2p) 0.35		
9^0	2 or 1	166,131.11			38,041.11 (2p) 0.17	
10_2^0	3	166,600.74			38,510.97 (1p) -0.06	37,493.20 (0p) -0.11

* Terms and transitions discovered by Laporte, Miller and Sawyer.

TABLE II. (Continued).

$5p^5(^2P_{1/2})6p$			$5p^5(^2P_{1/2})6p$			
4_1	5_2	6_0	1_1	2_1	3_2	4_0
1	2	0	1	1	2	0
*129,989.72	*130,766.00	*133,153.54	141,555.59	143,352.12	143,394.19	144,523.45
	24,816.59 (0) -0.33 24,542.83 (1) 0.40 -0.11		35,332.52 (2p) 0.30 34,163.16 (0) -0.10 33,992.66 (7) -0.21	35,959.78 (1) 0.01 35,789.21 (2) -0.23	37,444.50 (1) -0.05 37,171.83 (2p) -0.41	38,300.69 (0p) -0.01
*22,597.42 (2) -0.03 22,426.92 (3) -0.34	*23,373.78 (9) -0.11		33,650.61 (5) -0.03 33,309.52 (2) 0.21	35,447.19 (2p) -0.08 35,106.30 (0p) -0.04	35,489.04 (4p) 0.14	36,618.32 (1p) 0.12
*22,084.85 (7) -0.14 21,744.06 (2) -0.20	*22,861.10 (6) -0.11	*25,248.63 (5) -0.10	30,610.40 (7) -0.01 28,760.70 (0) -0.19	32,406.84 (1) 0.10 30,557.09 (5) -0.05	32,448.92 (2) 0.09 30,599.05 (7) 0.06 29,677.65 (7) -0.07	33,578.17 (1) 0.10
*19,044.61 (6) -0.11 *17,194.57 (3) 0.07	*19,820.81 (6) -0.03 *17,970.87 (7) 0.05 *17,049.36 (1) 0.03	*22,208.49 (7) -0.17				
			22,090.41 (0) -0.10 21,890.25 (3) -0.07 21,150.58 (1) 0.14 *18,689.34 (3) 0.22 *17,919.29 (0) -0.14	23,886.73 (1) 0.11 23,686.83 (0) -0.12 22,947.39 (0) -0.14 20,486.32 (0) -0.23 19,715.72 (0) -0.04	23,728.67 (6) 0.11 22,989.36 (0) -0.14 *20,528.06 (6) 0.10 *19,757.88 (3) -0.13	*21,657.19 (3) 0.23 *20,886.87 (3) 0.14
*19,615.46 (4) 0.15 *22,182.32 (2) 0.07 *22,801.61 (5) 0.16 *23,312.46 (7) 0.09	*18,446.14 (5) 0.11 *18,839.20 (3) 0.13 *21,406.02 (4) 0.09 *22,025.41 (6) 0.08 *22,536.21 (0) 0.06 *22,790.50 (0) 0.04 *22,912.15 (9) 0.02 *25,633.22 (0) 0.09	*16,451.65 (2) 0.14 19,018.53 (0) 0.04				
*26,409.65 (5) -0.06	*25,633.22 (0) 0.09	*23,245.86 (6) -0.09				
32,363.01 (1) 0.19	27,951.81 (0) 0.10 31,623.10 (0p) -0.14		20,797.53 (1) -0.20	15,365.59 (1) 0.20	18,994.53 (0) 0.24 *19,785.91 (3) 0.10 21,050.61 (2) 0.10 21,262.55 (5) 0.03 22,419.35 (3) 0.16 22,495.94 (2) -0.18 22,736.88 (3) 0.04 23,206.44 (1) 23,206.44 (1) 0.11	*18,656.65 (0) 0.10
33,190.44 (2) 0.04	33,678.55 (2) 0.33 33,890.73 (5) 0.04 35,047.74 (0) -0.04 35,124.31 (4) -0.36 35,365.28 (0p) -0.17	30,026.58 (2) 0.08 31,503.30 (1) -0.07 32,659.85 (1) 0.31	*21,624.51 (4) 0.10 23,101.13 (2) 0.05 24,257.90 (4) 0.21 24,334.53 (0) -0.17 24,575.44 (6) 0.08	19,828.56 (1) 0.48 21,092.66 (5) 0.10 21,304.73 (1) -0.08 22,461.66 (1) 0.08 22,538.01 (4) -0.18 22,779.08 (2) -0.09		
34,666.98 (2) 0.07						
35,900.36 (1p) -0.13 36,141.39 (2p) 0.00						21,290.55 (1) -0.30

* Terms and transitions discovered by Laporte, Miller and Sawyer.

placed in a transite box or oven provided with nichrome heating wires on its inner walls and with a quartz window for end-on observation of the tube. The exciting current was provided by a large commercial induction furnace of quenched gap type operating on 220-volt a.c. The exciting coil was cooled when in operation by water circulation. To attain the requisite vapor pressure of caesium it was necessary to heat the bulb by the oven to a temperature in the range 120°–200°C. Once the discharge had started, the heat from the exciting coil in the luminous vapor and especially from the dielectric losses in the glass was sufficient so that no auxiliary heating was needed. In fact the dielectric loss in the glass heated it to so great an extent that it was found safe to operate the discharge only 15 seconds in each minute. The discharge was bluish-white in color, filling the entire bulb apparently uniformly, and of tremendous brilliancy.

The discharge was photographed in the region $\lambda 2300$ – $\lambda 3300\text{\AA}$ with a Hilger E1 quartz spectrograph and from $\lambda 2300$ – $\lambda 10,000\text{\AA}$ in the first order of a 21 ft, 15,000 line grating. Exposure times, i.e., actual operation of the discharge, varied from 45 sec. with contrast plates on the quartz spectrograph in the region near $\lambda 3000$ to as long as $1\frac{1}{2}$ hours on some of the grating exposures in the less sensitive regions. Few lines were measured on the grating below $\lambda 2700$. The longest wave-length measured was $\lambda 8194$ and the shortest $\lambda 2315$. The short wave-length limit was doubtless due to the absorption of the Corex glass. All wave-lengths were measured against standards from an iron arc and determinations are believed to be accurate in most cases to ± 0.01 or 0.02\AA . Practically all the lines given by Sommer (about 380) were verified and 200 additional lines were measured in his region. The coarse hyperfine structure reported by Sommer for most of the strong lines was not observed. About 300 new lines were found below Sommer's limit in the ultra-violet and a few in the red.

III. ANALYSIS OF DATA

In Table II are given the results of the classification of the spectrum of Cs II. In the first column are given the electronic configurations of the odd terms and spectroscopic notations of the levels where known. Numbers have

TABLE III. Wave-length list of Cs II lines classified.

Int.	λ in air	ν (vac)	Classification
3	vac. 607.31	164,655	$5p^6\ ^1S_0 - (^2P_{1/2}\ 7d, 8s; ^2P_{3/2}\ 6d, 7s)6_1^0$
7	" 612.82	163,180	$5p^6\ ^1S_0 - (^2P_{3/2}\ 6d, 7s)4_1^0$
12	" 639.42	156,392	$5p^6\ ^1S_0 - (^2P_{1/2}\ 6d)6_1^0$
5	" 657.15	152,172	$5p^6\ ^1S_0 - (^2P_{1/2}\ 6d)1_1^0$
12	" 668.43	149,604	$5p^6\ ^1S_0 - (^2P_{1/2}\ 7s\ ^3P_1^0)$
20	" 808.77	123,645	$5p^6\ ^1S_0 - (^2P_{1/2}\ 5d, 6s)5_1^0$
20	" 813.85	122,872	$5p^6\ ^1S_0 - (^2P_{3/2}\ 5d, 6s)4_1^0$
20	" 901.34	110,946	$5p^6\ ^1S_0 - (^2P_{1/2}\ 5d)1_1^0$
20	" 926.75	107,905	$5p^6\ ^1S_0 - (^2P_{1/2}\ 6s)\ ^3P_1^0$
2p	2539.174	39,371.06	$(^2P_{1/2}\ 6p)1_1 - (^2P_{1/2}\ 7d, 8s; ^2P_{3/2}\ 6d, 7s)8^0$
1p	2595.886	38,510.97	$(^2P_{1/2}\ 6p)2_2 - (^2P_{1/2}\ 7d, 8s; ^2P_{3/2}\ 6d, 7s)10_3^0$
0p	2610.140	38,300.69	$(^2P_{3/2}\ 6p)4_0 - (^2P_{1/2}\ 5d, 6s)5_1^0$
2p	2627.952	38,041.11	$(^2P_{1/2}\ 6p)2_2 - (^2P_{1/2}\ 7d, 8s; ^2P_{3/2}\ 6d, 7s)9^0$
0p	2635.882	37,926.67	$(^2P_{1/2}\ 6p)1_1 - (^2P_{1/2}\ 7d, 8s; ^2P_{3/2}\ 6d, 7s)5_2^0$
0p	2666.358	37,493.20	$(^2P_{1/2}\ 6p)3_3 - (^2P_{1/2}\ 7d, 8s; ^2P_{3/2}\ 6d, 7s)10_3^0$

TABLE III. (Continued).

Int.	λ in air	ν (vac)	Classification
1p	2669.792	37,444.50	$(^2P_{1/2} 6p)3_2 - (^2P_{1/2} 5d, 6s)4_0$
2p	2689.412	37,171.83	$(^2P_{1/2} 6p)3_2 - (^2P_{1/2} 5d)5_0$
0p	2726.802	36,662.16	$(^2P_{1/2} 6p)1_1 - (^2P_{1/2} 7d, 8s; ^2P_{1/2} 6d, 7s)4_1^0$
1p	2730.065	36,618.32	$(^2P_{1/2} 6p)4_0 - (^2P_{1/2} 6s)^3P_1^0$
2p	2733.879	36,567.26	$(^2P_{1/2} 6p)2_2 - (^2P_{1/2} 7d, 8s; ^2P_{1/2} 6d, 7s)6_1^0$
1p	2749.839	36,355.02	$(^2P_{1/2} 6p)2_2 - (^2P_{1/2} 7d, 8s; ^2P_{1/2} 6d, 7s)5_2^0$
2p	2766.095	36,141.39	$(^2P_{1/2} 6p)4_1 - (^2P_{1/2} 7d, 8s; ^2P_{1/2} 6d, 7s)9^0$
1p	2780.065	35,959.78	$(^2P_{1/2} 6p)2_1 - (^2P_{1/2} 6s)^2P_2^0$
1p	2784.666	35,900.36	$(^2P_{1/2} 6p)4_1 - (^2P_{1/2} 7d, 8s; (^2P_{1/2} 6d, 7s)8^0$
3p	2789.797	35,834.32	$(^2P_{1/2} 6p)1_1 - (^2P_{1/2} 7d, 8s; ^2P_{1/2} 6d, 7s)2_0^0$
2p	2793.316	35,789.21	$(^2P_{1/2} 6p)2_1 - (^2P_{1/2} 5d, 6s)6_2^0$
4p	2816.943	35,489.04	$(^2P_{1/2} 6p)3_2 - (^2P_{1/2} 6s)^3P_1^0$
2p	2820.268	35,447.19	$(^2P_{1/2} 6p)2_1 - (^2P_{1/2} 6s)^3P_1^0$
0p	2826.802	35,365.28	$(^2P_{1/2} 6p)5_2 - (^2P_{1/2} 7d, 8s; (^2P_{1/2} 6d, 7s)9^0$
2	2829.045	35,337.24	$(^2P_{1/2} 6p)3_3 - (^2P_{1/2} 7d, 8s; ^2P_{1/2} 6d, 7s)5_2^0$
2p	2829.423	35,332.52	$(^2P_{1/2} 6p)1_1 - (^2P_{1/2} 5d)5_1^0$
5	2846.193	35,124.31	$(^2P_{1/2} 6p)5_2 - (^2P_{1/2} 7d, 8s; ^2P_{1/2} 6d, 7s)8^0$
0p	2847.655	35,106.30	$(^2P_{1/2} 6p)2_1 - (^2P_{1/2} 5d)7_0^0$
1p	2848.955	35,090.18	$(^2P_{1/2} 6p)2_2 - (^2P_{1/2} 7d, 8s; ^2P_{1/2} 6d, 7s)4_1^0$
0	2852.415	35,047.74	$(^2P_{1/2} 6p)5_2 - (^2P_{1/2} 7d, 8s; ^2P_{1/2} 6d, 7s)7_1^0$
2	2883.745	34,666.98	$(^2P_{1/2} 6p)4_1 - (^2P_{1/2} 7d, 8s; ^2P_{1/2} 6d, 7s)6_1^0$
3	2914.652	34,299.37	$(^2P_{1/2} 6p)2_2 - (^2P_{1/2} 7d, 8s; (^2P_{1/2} 6d, 7s)3_3^0$
0	2926.274	34,163.16	$(^2P_{1/2} 6p)1_1 - (^2P_{1/2} 6s)^3P_2^0$
7	2940.953	33,992.66	$(^2P_{1/2} 6p)1_1 - (^2P_{1/2} 5d)6_0^0$
5	2949.800	33,890.73	$(^2P_{1/2} 6p)5_2 - (^2P_{1/2} 7d, 8s; ^2P_{1/2} 6d, 7s)6_1^0$
2	2968.383	33,678.55	$(^2P_{1/2} 6p)5_2 - (^2P_{1/2} 7d, 8s; ^2P_{1/2} 6d, 7s)5_2^0$
5	2970.851	33,650.61	$(^2P_{1/2} 6p)1_1 - (^2P_{1/2} 6s)^3P_1^0$
1	2977.258	33,578.17	$(^2P_{1/2} 6p)4_0 - (^2P_{1/2} 5d)1_1^0$
2	3001.271	33,309.52	$(^2P_{1/2} 6p)1_1 - (^2P_{1/2} 5d)7_0^0$
2p	3012.041	33,190.44	$(^2P_{1/2} 6p)4_1 - (^2P_{1/2} 7d, 8s; ^2P_{1/2} 6d, 7s)4_1^0$
1	3060.976	32,659.85	$(^2P_{1/2} 6p)6_0 - (^2P_{1/2} 7d, 8s; ^2P_{1/2} 6d, 7s)7_1^0$
2	3080.874	32,448.92	$(^2P_{1/2} 6p)3_2 - (^2P_{1/2} 5d)1_1^0$
1	3084.875	32,406.84	$(^2P_{1/2} 6p)2_1 - (^2P_{1/2} 5d)1_1^0$
1p	3089.053	32,363.01	$(^2P_{1/2} 6p)4_1 - (^2P_{1/2} 7d, 8s; ^2P_{1/2} 6d, 7s)2_0^0$
0p	3161.333	31,623.10	$(^2P_{1/2} 6p)5_2 - (^2P_{1/2} 7d, 8s; ^2P_{1/2} 6d, 7s)3_3^0$
1	3173.355	31,503.30	$(^2P_{1/2} 6p)6_0 - (^2P_{1/2} 7d, 8s; ^2P_{1/2} 6d, 7s)6_1^0$
1	3263.982	30,628.61	$(^2P_{1/2} 6p)2_2 - (^2P_{1/2} 7d, 8s; ^2P_{1/2} 6d, 7s)1_2^0$
7	3265.924	30,610.40	$(^2P_{1/2} 6p)1_1 - (^2P_{1/2} 5d)1_1^0$
7	3267.135	30,599.05	$(^2P_{1/2} 6p)3_2 - (^2P_{1/2} 5d)2_0^0$
5	3271.626	30,557.09	$(^2P_{1/2} 6p)2_1 - (^2P_{1/2} 5d)2_0^0$
2	3329.428	30,026.58	$(^2P_{1/2} 6p)6_0 - (^2P_{1/2} 7d, 8s; (^2P_{1/2} 6d, 7s)4_1^0$
7	3368.575	29,677.65	$(^2P_{1/2} 6p)3_2 - (^2P_{1/2} 5d)3_0^0$
0	3376.261	29,610.16	$(^2P_{1/2} 6p)3_3 - (^2P_{1/2} 7d, 8s; ^2P_{1/2} 6d, 7s)1_2^0$
0	3475.973	28,760.70	$(^2P_{1/2} 6p)1_1 - (^2P_{1/2} 5d)2_2^0$
0	3531.376	28,309.51	$(^2P_{1/2} 6p)2_2 - (^2P_{1/2} 6d)6_1^0$
0	3576.570	27,951.81	$(^2P_{1/2} 6p)5_2 - (^2P_{1/2} 7d, 8s; ^2P_{1/2} 6d, 7s)1_2^0$
2	3732.539	26,783.83	$(^2P_{1/2} 6p)1_1 - (^2P_{1/2} 6d)3_2^0$
5	3785.424	26,409.65	$(^2P_{1/2} 6p)4_1 - (^2P_{1/2} 6d)6_1^0$
6	3805.096	26,273.12	$(^2P_{1/2} 6p)1_1 - (^2P_{1/2} 6d)2_2^0$
7	3896.978	25,653.67	$(^2P_{1/2} 6p)1_1 - (^2P_{1/2} 6d)1_1^0$
0	3900.09	25,633.22	$(^2P_{1/2} 6p)5_2 - (^2P_{1/2} 6d)6_1^0$
4	3906.939	25,588.30	$(^2P_{1/2} 6p)2_2 - (^2P_{1/2} 6d)5_3^0$
6	3925.583	25,466.74	$(^2P_{1/2} 6p)2_2 - (^2P_{1/2} 6d)4_3^0$
5	3959.495	25,248.63	$(^2P_{1/2} 6p)6_0 - (^2P_{1/2} 6s)^3P_1^0$
6	3965.187	25,212.38	$(^2P_{1/2} 6p)2_2 - (^2P_{1/2} 6d)3_2^0$
0	4028.43	24,816.59	$(^2P_{1/2} 6p)5_2 - (^2P_{1/2} 5d)4_3^0$
4	4047.184	24,701.59	$(^2P_{1/2} 6p)2_2 - (^2P_{1/2} 6d)2_2^0$
6	4067.958	24,575.44	$(^2P_{1/2} 6p)1_1 - (^2P_{1/2} 7d, 8s; ^2P_{1/2} 6d, 7s)9^0$
6	4068.773	24,570.52	$(^2P_{1/2} 6p)3_3 - (^2P_{1/2} 6d)5_3^0$
1	4073.364	24,542.83	$(^2P_{1/2} 6p)5_2 - (^2P_{1/2} 5d)5_1^0$
0	4108.232	24,334.53	$(^2P_{1/2} 6p)1_1 - (^2P_{1/2} 7d, 8s; ^2P_{1/2} 6d, 7s)8^0$
4	4121.210	24,257.90	$(^2P_{1/2} 6p)1_1 - (^2P_{1/2} 7d, 8s; ^2P_{1/2} 6d, 7s)7_1^0$
2	4132.003	24,194.54	$(^2P_{1/2} 6p)3_3 - (^2P_{1/2} 6d)3_2^0$
4	4151.267	24,082.27	$(^2P_{1/2} 6p)2_2 - (^2P_{1/2} 6d)1_1^0$

TABLE III. (Continued).

Int.	λ in air	ν (vac)	Classification
1	4186.249	23,886.73	$(^2P_{1/2} 6p)2_1 - (^2P_{3/2} 5d, 6s)1_0^0$
6	4213.129	23,728.67	$(^2P_{3/2} 6p)3_2 - (^2P_{3/2} 5d, 6s)2_0^0$
0	4220.571	23,686.83	$(^2P_{3/2} 6p)2_1 - (^2P_{3/2} 5d, 6s)2_0^0$
3	4221.119	23,683.75	$(^2P_{1/2} 6p)3_3 - (^2P_{1/2} 6d)2_0^0$
9	4227.100	23,373.78	$(^2P_{1/2} 6p)5_2 - (^2P_{1/2} 6s)^3P_2^0$
7	4228.350	23,312.46	$(^2P_{1/2} 6p)4_1 - (^2P_{1/2} 6d)3_0^0$
1	4307.942	23,206.44	$(^2P_{1/2} 6p)3_2 - (^2P_{1/2} 7d, 8s; ^2P_{1/2} 6d, 7s)10_3^0$
6	4330.636	23,245.86	$(^2P_{1/2} 6p)6_0 - (^2P_{1/2} 6d)6_1^0$
0	4316.992	23,157.78	$(^2P_{1/2} 6p)3_3 - (^2P_{1/2} 5d)4_0^0$
2	4327.580	23,101.13	$(^2P_{1/2} 6p)1_1 - (^2P_{1/2} 7d, 8s; ^2P_{1/2} 6d, 7s)6_1^0$
4	4330.239	23,086.95	$(^2P_{1/2} 6p)1_1 - (^2P_{1/2} 7s)^3P_1^0$
0	4348.620	22,989.36	$(^2P_{3/2} 6p)3_2 - (^2P_{3/2} 5d, 6s)3_0^0$
0	4356.575	22,947.39	$(^2P_{3/2} 6p)2_1 - (^2P_{3/2} 5d, 6s)3_0^0$
9	4363.375	22,912.15	$(^2P_{1/2} 6p)5_2 - (^2P_{1/2} 6d)5_3^0$
6	4373.018	22,861.10	$(^2P_{1/2} 6p)5_2 - (^2P_{1/2} 6s)^3P_1^0$
5	4384.428	22,801.61	$(^2P_{1/2} 6p)4_1 - (^2P_{1/2} 6d)2_0^0$
0	4386.566	22,790.50	$(^2P_{1/2} 6p)5_2 - (^2P_{1/2} 6d)4_0^0$
2	4388.764	22,779.08	$(^2P_{1/2} 6p)2_1 - (^2P_{1/2} 7d, 8s; ^2P_{1/2} 6d, 7s)9_0^0$
3	4396.909	22,736.88	$(^2P_{3/2} 6p)3_2 - (^2P_{3/2} 7d, 8s; ^2P_{3/2} 6d, 7s)9_0^0$
7	4405.253	22,693.82	$(^2P_{1/2} 6p)1_1 - (^2P_{1/2} 7s)^3P_2^0$
2	4424.046	22,597.42	$(^2P_{1/2} 6p)4_1 - (^2P_{1/2} 6s)^3P_2^0$
4	4435.708	22,538.01	$(^2P_{3/2} 6p)2_1 - (^2P_{3/2} 7d, 8s; ^2P_{3/2} 6d, 7s)8_0^0$
0	4436.06	22,536.21	$(^2P_{1/2} 6p)5_2 - (^2P_{1/2} 6d)3_0^0$
2	4444.004	22,495.94	$(^2P_{3/2} 6p)3_2 - (^2P_{3/2} 7d, 8s; ^2P_{3/2} 6d, 7s)8_0^0$
1	4450.785	22,461.66	$(^2P_{3/2} 6p)2_1 - (^2P_{3/2} 7d, 8s; ^2P_{3/2} 6d, 7s)7_1^0$
3	4457.680	22,426.92	$(^2P_{1/2} 6p)4_1 - (^2P_{1/2} 5d)6_2^0$
3	3459.185	22,419.35	$(^2P_{3/2} 6p)3_2 - (^2P_{3/2} 7d, 8s; ^2P_{3/2} 6d, 7s)7_1^0$
7	4501.525	22,208.49	$(^2P_{1/2} 6p)6_0 - (^2P_{1/2} 5d)1_1^0$
2	4506.834	22,182.32	$(^2P_{1/2} 6p)4_1 - (^2P_{1/2} 6d)1_1^0$
2	4515.495	22,139.77	$(^2P_{1/2} 6p)2_2 - (^2P_{1/2} 5d)4_0^0$
0	4525.59	22,090.41	$(^2P_{3/2} 6p)1_1 - (^2P_{3/2} 5d, 6s)1_0^0$
7	4526.725	22,084.85	$(^2P_{1/2} 6p)4_1 - (^2P_{1/2} 6s)^3P_1^0$
6	4538.942	22,025.41	$(^2P_{1/2} 6p)5_2 - (^2P_{1/2} 6d)2_0^0$
3	4566.983	21,890.25	$(^2P_{3/2} 6p)1_1 - (^2P_{3/2} 5d, 6s)2_0^0$
3	4571.786	21,867.31	$(^2P_{1/2} 6p)2_2 - (^2P_{1/2} 5d)5_1^0$
2	4497.673	21,744.06	$(^2P_{1/2} 6p)4_1 - (^2P_{1/2} 6d)7_0^0$
10	4603.755	21,715.33	$(^2P_{3/2} 6p)3_3 - (^2P_{3/2} 6s)^3P_2^0$
3	4616.13	21,657.19	$(^2P_{3/2} 6p)4_0 - (^2P_{3/2} 5d, 6s)4_1^0$
4	4623.091	21,624.51	$(^2P_{3/2} 6p)1_1 - (^2P_{3/2} 7d, 8s; (^2P_{3/2} 5d, 7s)4_1^0$
1	4640.333	21,544.16	$(^2P_{1/2} 6p)3_3 - (^2P_{1/2} 5d)6_2^0$
5	4646.508	21,515.53	$(^2P_{1/2} 6p)2_2 - (^2P_{1/2} 7s)^3P_1^0$
4	4670.280	21,406.02	$(^2P_{1/2} 6p)5_2 - (^2P_{1/2} 6d)1_1^0$
1	4692.482	21,304.73	$(^2P_{3/2} 6p)2_1 - (^2P_{3/2} 7d, 8s; ^2P_{3/2} 6d, 7s)6_1^0$
1	4695.610	21,290.55	$(^2P_{3/2} 6p)4_0 - (^2P_{3/2} 7d, 8s; (^2P_{3/2} 6d, 7s)7_1^0$
5	4701.793	21,262.55	$(^2P_{3/2} 6p)3_2 - (^2P_{3/2} 7d, 8s; (^2P_{3/2} 6d, 7s)6_1^0$
1	4726.684	21,150.58	$(^2P_{3/2} 6p)1_1 - (^2P_{3/2} 6d, 6s)3_0^0$
4	4732.975	21,122.47	$(^2P_{1/2} 6p)2_2 - (^2P_{1/2} 7s)^3P_2^0$
5	4739.665	21,092.66	$(^2P_{3/2} 6p)2_1 - (^2P_{3/2} 7d, 8s; ^2P_{3/2} 6d, 7s)5_2^0$
2	4749.132	21,050.61	$(^2P_{3/2} 6p)3_2 - (^2P_{3/2} 7d, 8s; ^2P_{3/2} 6d, 7s)5_2^0$
3	4786.363	20,886.87	$(^2P_{3/2} 6p)4_0 - (^2P_{3/2} 5d, 6s)5_1^0$
1	4806.924	20,797.53	$(^2P_{3/2} 6p)1_1 - (^2P_{3/2} 7d, 8s; ^2P_{3/2} 6d, 7s)2_0^0$
6	4830.161	20,697.48	$(^2P_{1/2} 6p)2_2 - (^2P_{1/2} 6s)^3P_2^0$
6	4870.024	20,528.06	$(^2P_{3/2} 6p)3_2 - (^2P_{3/2} 5d, 6s)4_1^0$
0	4879.95	20,486.32	$(^2P_{3/2} 6p)2_1 - (^2P_{3/2} 5d, 6s)4_1^0$
1	4925.744	20,295.73	$(^2P_{1/2} 6p)1_1 - (^2P_{1/2} 5d)5_1^0$
6	4952.835	20,184.84	$(^2P_{1/2} 6p)2_2 - (^2P_{1/2} 6s)^3P_1^0$
5	4972.593	20,104.64	$(^2P_{1/2} 6p)3_3 - (^2P_{1/2} 7s)^3P_2^0$
1	5041.828	19,828.56	$(^2P_{3/2} 6p)2_1 - (^2P_{3/2} 7d, 8s; ^2P_{3/2} 6d, 7s)4_1^0$
6	5043.800	19,820.81	$(^2P_{1/2} 6p)5_2 - (^2P_{1/2} 5d)1_1^0$
3	5052.696	19,785.91	$(^2P_{3/2} 6p)3_2 - (^2P_{3/2} 7d, 8s; ^2P_{3/2} 6d, 7s)4_1^0$
3	5059.866	19,757.88	$(^2P_{3/2} 6p)3_2 - (^2P_{3/2} 5d, 6s)5_1^0$
0	5070.684	19,715.72	$(^2P_{3/2} 6p)2_1 - (^2P_{3/2} 5d, 6s)5_1^0$
4	5096.604	19,615.46	$(^2P_{1/2} 6p)4_1 - (^2P_{1/2} 7s)^3P_1^0$
8	5227.002	19,126.12	$(^2P_{1/2} 6p)1_1 - (^2P_{1/2} 6s)^3P_2^0$

TABLE III. (Continued).

Int.	λ in air	ν (vac.)	Classification
6	5249.373	19,044.61	$(^2P_{1\frac{1}{2}} 6p)4_1 - (^2P_{1\frac{1}{2}} 5d)1_1^0$
0	5256.572	19,018.53	$(^2P_{1\frac{1}{2}} 6p)6_0 - (^2P_{1\frac{1}{2}} 6d)1_1^0$
0	5263.21	18,994.53	$(^2P_{1\frac{1}{2}} 6p)3_2 - (^2P_{1\frac{1}{2}} 7d, 8s; ^2P_{\frac{1}{2}} 6d, 7s)3_3^0$
4	5274.044	18,955.52	$(^2P_{1\frac{1}{2}} 6p)1_1 - (^2P_{1\frac{1}{2}} 5d)6_2^0$
3	5306.609	18,839.20	$(^2P_{1\frac{1}{2}} 6p)5_2 - (^2P_{1\frac{1}{2}} 7s)^3P_1^0$
3	5349.10	18,689.34	$(^2P_{1\frac{1}{2}} 6p)1_1 - (^2P_{1\frac{1}{2}} 5d, 6s)4_1^0$
10	5358.53	18,656.65	$(^2P_{1\frac{1}{2}} 6p)4_0 - (^2P_{1\frac{1}{2}} 7d, 8s; ^2P_{\frac{1}{2}} 6d, 7s)4_1^0$
6	5370.979	18,613.42	$(^2P_{1\frac{1}{2}} 6p)1_1 - (^2P_{1\frac{1}{2}} 6s)^3P_1^0$
5	5419.687	18,446.14	$(^2P_{1\frac{1}{2}} 6p)5_2 - (^2P_{1\frac{1}{2}} 7s)^3P_2^0$
7	5563.019	17,970.87	$(^2P_{1\frac{1}{2}} 6p)5_2 - (^2P_{1\frac{1}{2}} 5d)2_2^0$
0	5579.033	17,919.29	$(^2P_{1\frac{1}{2}} 6p)1_1 - (^2P_{1\frac{1}{2}} 5d, 6s)5_1^0$
3	5814.181	17,194.57	$(^2P_{1\frac{1}{2}} 6p)4_1 - (^2P_{1\frac{1}{2}} 5d)2_2^0$
5	5831.159	17,144.51	$(^2P_{1\frac{1}{2}} 6p)2_2 - (^2P_{1\frac{1}{2}} 5d)1_1^0$
1	5863.701	17,049.36	$(^2P_{1\frac{1}{2}} 6p)5_2 - (^2P_{1\frac{1}{2}} 5d)3_3^0$
2	6076.738	16,451.65	$(^2P_{1\frac{1}{2}} 6p)6_0 - (^2P_{1\frac{1}{2}} 7s)^3P_1^0$
4	6128.619	16,312.38	$(^2P_{1\frac{1}{2}} 6p)3_3 - (^2P_{1\frac{1}{2}} 5d)2_2^0$
2	6419.541	15,573.14	$(^2P_{1\frac{1}{2}} 6p)1_1 - (^2P_{1\frac{1}{2}} 5d)1_1^0$
3	6495.528	15,390.96	$(^2P_{1\frac{1}{2}} 6p)3_3 - (^2P_{1\frac{1}{2}} 5d, 6s)3_3^0$
1	6506.254	15,365.59	$(^2P_{1\frac{1}{2}} 6p)2_1 - (^2P_{1\frac{1}{2}} 7d, 8s; ^2P_{\frac{1}{2}} 6d, 7s)1_2^0$
3	6536.440	15,294.63	$(^2P_{1\frac{1}{2}} 6p)2_2 - (^2P_{1\frac{1}{2}} 5d)2_2^0$
4	6955.519	14,373.12	$(^2P_{1\frac{1}{2}} 6p)2_2 - (^2P_{1\frac{1}{2}} 5d)3_3^0$

been assigned to those levels whose L and S values are not fixed. The second column contains the J values of the odd levels, and the third the relative term values referred to $5p^5\ ^1S_0$. The headings of the remaining columns give the electron configurations, spectroscopic notations, J values, and relative term values of the even terms to which are assigned numbers in order of their magnitude in lieu of their undetermined L and S values. In the body of the table are the wave numbers of the classified lines, followed in the parenthesis by their intensities. Except in the case of intensities followed by p (prism) these intensities are from grating measurements. Below each wave number is the discrepancy (calculated value minus observed value) between the observed wave numbers and the wave number calculated from the values assigned to the terms. The terms and transitions established in the previous paper are preceded by asterisks. It will be observed that the only transitions in that work involving terms of the $^2P_{\frac{1}{2}}$ limit were fixed in relation to the rest of the system only by the three resonance lines $\nu\nu$ 122,872, 123,645 and 163,180 and were thus uncertain by as much as $\pm 5\text{ cm}^{-1}$ because of the limited accuracy of the extreme ultraviolet measures. In the present work the first attempt was to remove this uncertainty by finding intercombinations between the $5p^5\ (^2P_{\frac{1}{2}}) 6p$ terms thus established and the terms of the $^2P_{1\frac{1}{2}}$ limit. The lack of precision in the values of the $^2P_{\frac{1}{2}}$ terms, however, made it more feasible to approach the task by searching in the region indicated by these approximate terms for lines having the accurately known differences of the established terms of the $5p^5\ (^2P_{1\frac{1}{2}}) 5d, 6s$ configuration. This procedure in fact not only located the three known terms of $5p^5\ (^2P_{\frac{1}{2}}) 6p$ with precision as 141,555.59, 143,394.19 and 144,523.45 cm^{-1} , but located also one new term of this configuration as 143,352.12 cm^{-1} . The ν differences thus established were used in looking for new odd terms. Sixteen such terms were definitely established, and in addition the three terms involving the three resonance

lines discussed above were accurately fixed as $\nu\nu 122,866.03$, $123,636.44$ and $163,180.20$. It will be noted that in the case of most of the new terms one or two expected transitions are missing. However, each terms seems established beyond doubt by several close coincidences and by expected positions. A few less definitely established terms have been omitted.

Table III contains a list of the Cs II lines classified both in this and in the preceding investigation. In the first column are the intensities from the present grating measurements or in a few cases, where the intensity is followed by p , from the prism measurement; in the second and third columns are the λ 's in air, and the wave numbers in vacuum; the last column contains the classification, with $5p^5$ omitted from all configurations above the ground state.

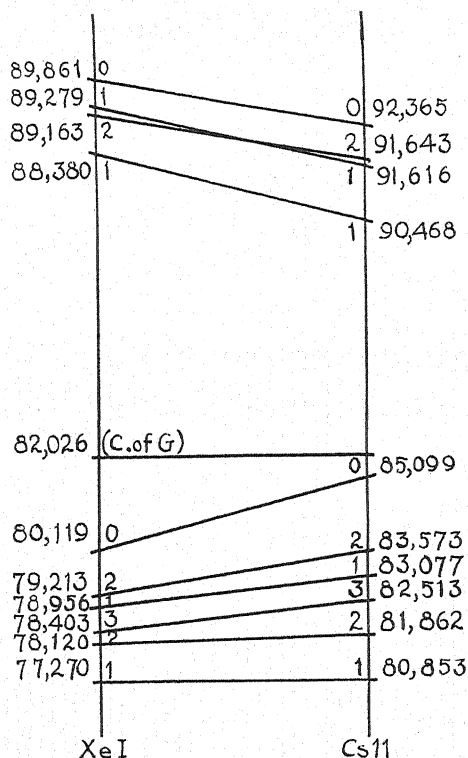


Fig. 1. The $5p^5 6p$ terms of Xe I and Cs II referred to their centers of gravity and reduced in the case of Cs II by multiplying with $9,120/14,270$, the ratio of the relativistic doublets $5p^5$.

It is now of interest to compare the terms as found with those expected as shown in Table I and to consider them in relation to the terms of Xe I.⁴ In Fig. 1 the relative term values of the ten p ($5p^5 6p$) terms of Xe I are drawn referred to their center of gravity, and beside them the ten p terms of Cs II likewise referred to their center of gravity but reduced by multiplication with $9,120/14,270$, the ratio of the relativistic doublets in the two cases. The correspondence is very good. The only crossing over is in two levels which

⁴ Meggers, deBruin and Humphreys, Bureau Standards J. Research 3, 731 (1929).

are very close together. The same crossing occurred in the Kr I-Rb II sequence.⁵ The close correlation of the Xe I terms with those of Cs II is a convincing argument for the correctness of the Cs II analysis.

We may next consider the odd terms. Of the low group around 110,000 cm^{-1} , five terms come from Sommer's work. Four more terms were added in this work. The group was ascribed by Laporte, Miller and Sawyer to a mixture of $5p^5(^2P_{1/2})5d$ and $6s$. Inspection of Table I shows that $6s$ should contribute two terms of $J=1, 2$; and $5d$, eight terms of $J=0, 1, 1, 2, 2, 3, 3, 4$. The group is then completely identified with the exception of the term with $J=4$, which it is impossible to locate since only one even term with $J=3$ is known with which this term could combine. In the previous work $\nu\nu 107,392$, $107,905$ were identified as $6s^3P_2$ and 3P_1 . The present work adds a new term with $J=2$ between these terms but the much greater intensities of the transitions to $107,392$ make it almost certain that this assignment is correct. The remaining terms should arise from $5d$ and may be compared with the corresponding Xe I terms. Since two of the $5d$ terms in Xe I, and one ($J=3$) in Cs II are unknown, a graphical representation as made for the p -terms in Fig. 1 is not useful. The most interesting anomaly is the term with $J=0$. In Xe I as in Ne I this term is the lowest of the $^2P_{1/2}d$ group. In Rb II, however, it is the highest while in Cs II it is in the middle of the group. The remaining $5d$ and $6s$ terms, having $^2P_{1/2}$ as limit form a group of five terms near 120,000 cm^{-1} . As mentioned above two of these terms were located approximately in the work of Laporte, Miller and Sawyer by two extreme ultraviolet lines. They are now definitely fixed in position through the intercombinations of the $(^2P_{1/2})6p$ group, with which they combine, with $(^2P_{1/2})6d, 7s$. Except for the $J=0$ term which must belong to $6s$ it is not possible to assign these terms definitely to $6s$ or $5d$.

The remaining ten odd terms form a group near 160,000 cm^{-1} . These terms are probably a mixture of terms arising from $5p^5(^2P_{1/2})6d, 7s$ and $5p^5(^2P_{1/2})7d, 8s$. Laporte, Miller and Sawyer estimated $5p^5^1S_0$ to be about 189,000 cm^{-1} . On this basis the assumption of a simple Rydberg formula would predict $5p^5(^2P_{1/2})7d, 8s$, from the known positions of $5p^5(^2P_{1/2})5d, 6s$ and $5p^5(^2P_{1/2})6d, 7s$, as a group centered about approximately 165,000 cm^{-1} . Also, on the assumption that the group $5p^5(^2P_{1/2})5d, 6s$ centered about 120,000 cm^{-1} is the first member of a sequence which approaches a limit about 150,000 cm^{-1} (estimated from the relativistic doublet) higher than 189,000 cm^{-1} , the second member would center around approximately 162,000 cm^{-1} . The only basis upon which these terms could be assigned to one group or the other would be a careful determination of the relative intensities of transitions of each term with the $(^2P_{1/2})6p$ group and with the $(^2P_{1/2})6p$ group. Transitions between terms having the same series limit should of course be stronger than between terms having different limits. On the basis of the present eye estimates of lines, which also for the two p -groups lie in quite different spectral regions, little can be said on this basis.

⁵ Laporte, Miller and Sawyer, Phys. Rev. **38**, 843 (1931).

All the terms in this group around $160,000\text{ cm}^{-1}$ are new with the exception of $163,180.20\text{ cm}^{-1}$ which was fixed by a resonance line and three other transitions in the earlier paper. One of the new terms, $164,656.77\text{ cm}^{-1}$ is also confirmed by a vacuum spectrograph line, $\lambda 607.31$, $\nu 164,655$, intensity 3, which was not previously reported.

Transitions involving terms arising from $5p^5nf$ configurations and also from higher members of the s , p , and d configurations might be expected in our data. Although the position of such terms can be predicted with a fair degree of approximation, no certain evidence of transitions involving them has as yet been obtained. The present extension of the Cs II spectrum, however, completes the essential outlines of a scheme analogous in all essentials to the Xe I spectrum, with the terms of each electron configuration divided into two completely separated groups having as series limits in the Cs II spectrum, $5p^5\ ^2P_{1/2}$ and $5p^5\ ^2P_{3/2}$.

Infrared Absorption Spectrum of Hydrogen Cyanide

By KYU NAM CHOI AND E. F. BARKER
University of Michigan

(Received October 24, 1932)

The absorption spectrum of HCN in the gas phase has been investigated by a grating spectrometer with high resolution in the region 3μ – 15μ . Five of the infrared bands were studied, and of these the very intense fundamental at 14μ has been resolved into individual lines forming *P*, *R* and *Q* branches. The first harmonic of the band at 7μ has two maxima, very nearly symmetrical and equal in intensity, and no *Q* branch. Although fine structure is indicated, it is not possible to determine the position of successive individual lines. Three other maxima, less intense and unsymmetrical are found at 4.728μ , 4.760μ , and 4.794μ forming the second harmonic of the same vibration. There is a sharp single maximum at 3.57μ with another very strong double band at 3.04μ .

Form of the HCN molecule. The HCN molecule is linear with fundamental frequencies $\nu_2 = 712\text{ cm}^{-1}$, $\nu_3 = 3289\text{ cm}^{-1}$ and ν_1 approximately 2100 cm^{-1} . The latter has not been observed directly since the band associated with it is of extremely low intensity, but the combination $\nu_1 + \nu_2$ explains the band at 3.57μ . The moment of inertia determined from the fine structure of the 14μ band is $18.68 \times 10^{-40}\text{ g cm}^2$.

INTRODUCTION

RECENT improvements in the apparatus available for measuring infrared absorption have made possible the detailed study of spectra of much greater complexity than could be observed only a few years ago. As a consequence, the infrared absorption spectra have furnished decisive information for determining the molecular configurations of a number of molecules, especially when the fine structure of the bands is observable. The purpose of the present investigation is to examine both the fundamental and harmonic bands of HCN; especially to determine the fine structure of the low-frequency bands which have never been studied before with high resolution.

In 1912, Burmeister¹ investigated the absorption spectrum of gaseous HCN in the region from 3μ to 14μ , finding four bands. Of these, the one having the shortest wave-length 3.04μ is very narrow and intense, apparently corresponding to the fundamental of one of the characteristic vibrations of the molecule. The two bands of greatest wave-length near 7μ and 14μ , are also intense, but appear as broad double maxima. The absorption at the two intermediate-maxima, 4.77μ and 3.57μ , is relatively weak and Burmeister was in doubt as to whether these bands should be attributed to HCN.

In 1923, Barker² investigated some of the absorption bands of HCN with special gratings ruled by himself, giving higher dispersion than was previously employed. He found two maxima, very nearly symmetrical and of equal

¹ Burmeister, D. Ges. Verh. 15, 589 (1913).

² Barker, Phys. Rev. 23, 200 (1924).

intensity, appearing at 6.94μ and 7.32μ . Three others, less intense and unsymmetrical, were observed at 4.756μ , 4.723μ and 4.79μ . Observation at that time did not extend beyond 12μ . From the envelope of the 7μ band he estimated the moment of inertia to be about $13.2 \times 10^{-40} \text{ g cm}^2$.

In 1930, Badger and Binder³ investigated photographically the absorption spectrum in the region $\lambda\lambda 7000\text{--}9200$ using HCN gas in a 280 cm absorption cell. They observed two weak bands of very simple structure occurring at $\lambda 8563$ and $\lambda 7912$ which are interpreted as $3\nu_3 + \nu_1$ and $4\nu_3$ respectively. In these bands they have been able to resolve the rotational structure, and compute the moment of inertia as $18.79 \times 10^{-40} \text{ g cm}^2$.

Very recently, Brackett and Liddel⁴ examined the absorption spectrum of HCN both in liquid and vapor phase mostly in the region from 1μ to 2μ . The instrument used in their investigation was an automatic recording apparatus yielding high resolution. Three bands were observed at 1.5μ , 1.1μ and 1.0μ in the gas absorption. They were interpreted as second and third harmonics of 3.04μ (ν_3) and the combination $2\nu_3 + \nu_1$. All these bands are doublets but the rotational structure was not resolved. The moment of inertia as computed from the envelope of the third harmonic band was $18 \pm 2 \times 10^{-40} \text{ g cm}^2$.

APPARATUS

The grating spectrometer used in this work is of a type similar to that employed by Barker and Meyer⁵ and therefore will not be described here in detail. Modifications of an important nature, however, lead to a high degree of sensitivity of the recording apparatus and hence allow investigation with a grating to a greater wave-length than has been previously reached. As a further consequence of the increased sensitivity, it has been possible to reduce the slit widths considerably and thus obtain improved definition. A grating ruled with 1200 lines per inch was found to be most effective for the region between 7μ and 15μ . From 3μ to the neighborhood of 5μ , the best results were obtained with a grating having 4800 lines per inch. The detecting system consists of a vacuum thermocouple, a Moll thermal relay with a Kipp and Sons high-sensitivity galvanometer of the D'Arsonval type. The calibration is in terms of the mercury line at 1.014μ .

The absorption cells have potassium bromide (K Br) windows and can be used effectively throughout the entire spectral region from 3μ to 15μ . Two absorption cells were used whose lengths are 25 cm and 2.5 cm respectively.

The HCN gas was generated by introducing below the surface of H_2SO_4 a nearly saturated solution of NaCN in water. The gas was frozen in a liquid air trap provided with two stopcocks, and each sample to be examined was distilled over to the absorption cell by warming the trap to 30°C . In order to eliminate the water vapor in the gas, two U tubes were used, the first containing CaCl_2 and the second P_2O_5 .

³ Badger and Binder, *Phys. Rev.* **37**, 800 (1931).

⁴ Brackett and Liddel, *Smithsonian Institution* **85**, No. 5 (1931).

⁵ Barker and Meyer, *Trans. Faraday Soc.* **25**, 12 (1929).

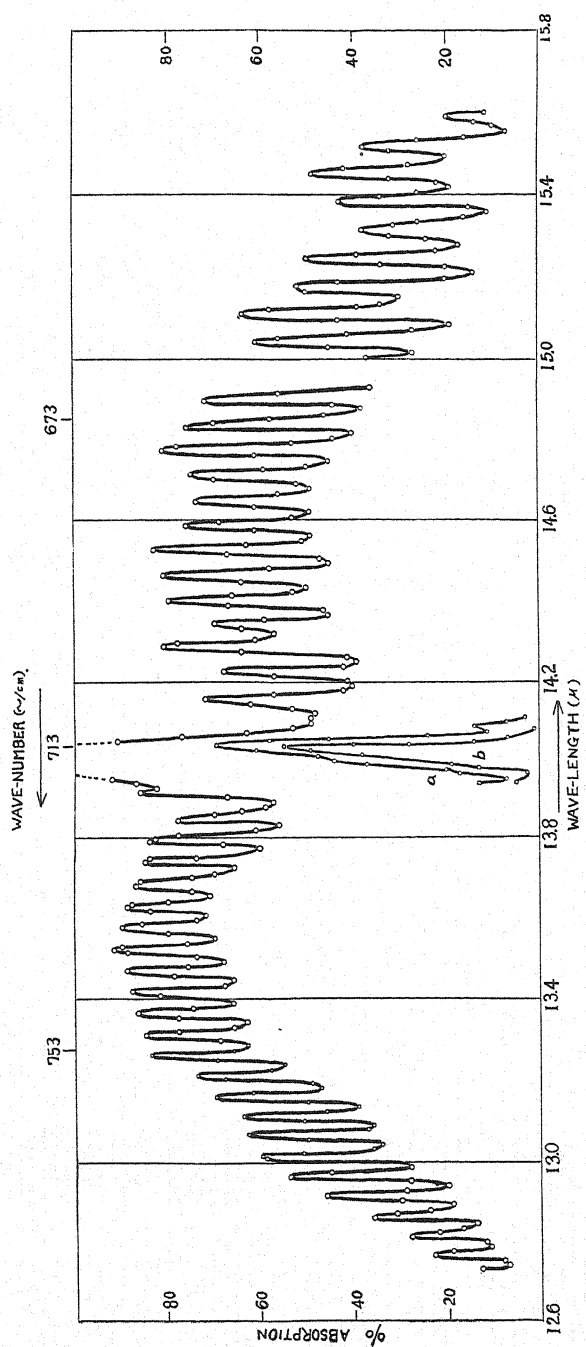


Fig. 1. Fine structure of the 14μ band of HCN.

DISCUSSION OF RESULTS

Region of 14μ

The wide and intense absorption previously observed with two maxima, was resolved into a band consisting of *R*, *Q* and *P* branches as shown in Fig. 1. Repeated observations were taken over this region, using the point by point method, with different pressures of gas and different slits. An extremely small cell, 2.5 cm long with KBr windows, was used, and the figure represents observations made with 35 cm pressure and 0.5 mm slit width. The *Q* branch is so strong that it was impossible to observe it satisfactorily even with 4 or 5 cm of pressure. In order to locate its maximum, the pressure was considerably reduced. The detached portion of curves *a* and *b* shown in Fig. 1 represent observations taken with pressures of 3 mm and 1 mm respectively. The irregularities of the lines which are apparent at the right end of the *P* branch may be attributed to the CO_2 band at 14.8μ . The energy falls off very rapidly in this region due to absorption by the carbon dioxide of the atmosphere. As shown in Fig. 1 there is a small gap near 14.8μ region where the *Q* branch of CO_2 falls and observations could not be made. No convergence is apparent in either the *R* or the *P* branch, the average spacing

TABLE I. Rotation lines in the 14μ band. *Q* branch at 14.0392μ or 712.28 cm^{-1} .

R branch: $\Delta J = +1$			Initial <i>J</i>	P branch: $\Delta J = -1$		
λ	ν	$\Delta\nu$		λ	ν	$\Delta\nu$
13.9780	715.40	3.12	0	—	—	—
13.9200	718.40	3.00	1	—	—	—
13.8544	721.68	3.28	2	14.1554	706.44	—
13.8016	724.55	2.87	3	14.2256	702.95	3.49
13.7489	727.33	2.78	4	14.2841	700.00	2.95
13.6962	730.11	2.78	5	14.3426	697.21	2.79
13.6477	732.72	2.61	6	14.4011	694.39	2.82
13.5909	735.80	3.08	7	14.4654	691.30	3.09
13.5340	738.87	3.07	8	14.5298	688.24	3.06
13.4798	741.85	2.98	9	14.5853	685.62	2.74
13.4299	744.60	2.75	10	14.6438	682.88	2.74
13.3780	747.49	2.89	11	14.7140	679.62	3.26
13.3240	750.72	3.03	12	14.7725	676.92	2.70
13.2711	753.52	3.00	13	14.8310	674.26	2.66
13.2181	756.52	3.00	14	14.8953	671.42	2.84
13.1653	759.57	3.05	15	—	—	—
13.1183	762.27	2.70	16	15.0320	665.24	—
13.0693	765.15	2.88	17	15.1010	662.20	3.04
13.0166	768.24	3.04	18	15.1720	659.10	3.10
12.9640	771.36	3.08	19	15.2410	656.12	2.98
12.9113	774.51	3.15	20	15.3100	653.16	2.96
12.8593	777.65	3.14	21	15.3790	650.23	2.93
12.8203	780.50	1.85	22	15.4480	647.33	2.91
12.7650	783.38	2.88	23	15.5170	644.45	2.88
—	—	—	24	15.5860	641.40	2.85

of the lines being 2.98 cm^{-1} . The small deviations from this value shown in the Table I are partly due to experimental error but also indicate the effect of superposition of bands due to absorption by excited molecules and disturbances from the CO_2 bands. If the above value of the average spacing is applied to the central portion of the band, it is apparent that there are just

3 intervals between the innermost lines as would be expected for a linear molecule. The positions of maximum absorption of the *R*, *Q* and *P* branches fall, approximately, at 737.89, 712.29 and 688.00 cm^{-1} respectively. The most probable frequency of rotation $\bar{\nu}_r$ is thus found to be about 24.9 cm^{-1} .

Region of 7μ

This band is unquestionably the first harmonic of the 14μ band, although it has no *Q* branch since ΔL is even. It was examined with the 2.5 cm cell

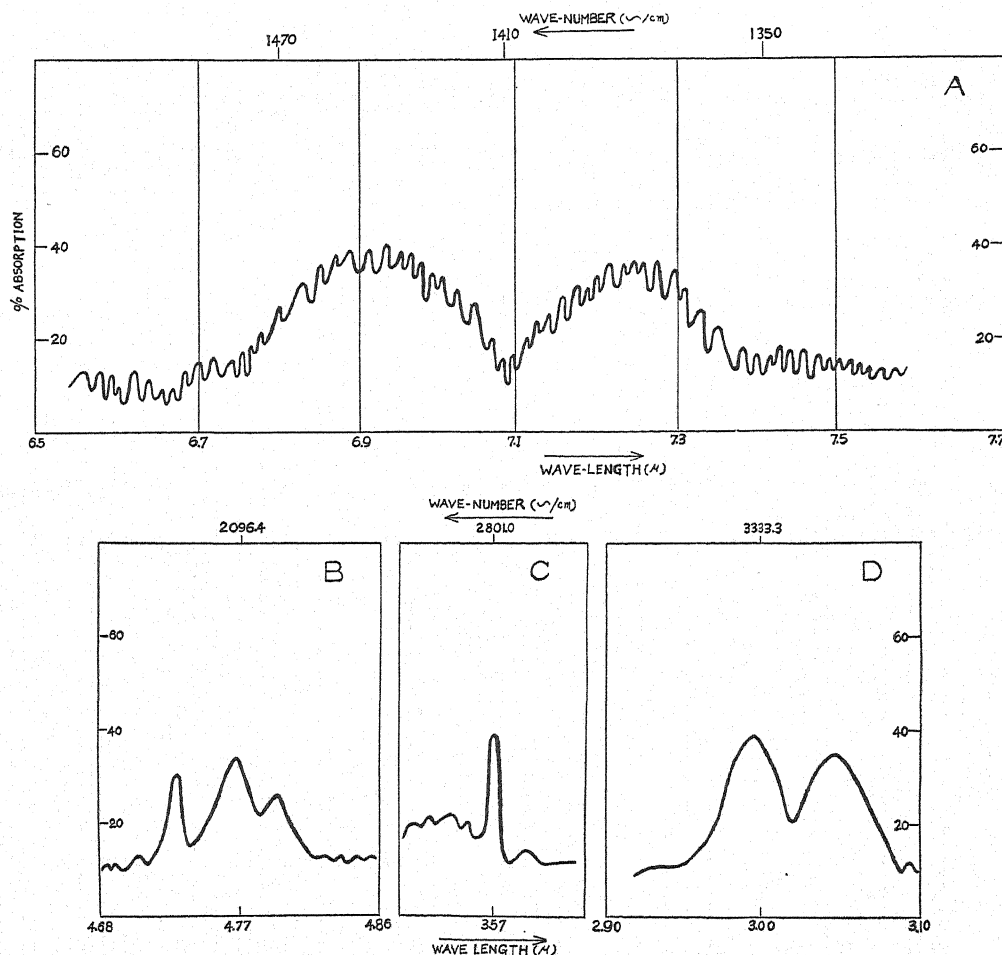


Fig. 2. Near infrared absorption bands of HCN.

A: $2\nu_2$. B: $3\nu_2$. C: $\nu_1 + \nu_2$. D: ν_3 .

and 35 cm pressure, and with a grating having 1200 lines per inch, using the second order. Observations in this region are rendered difficult by the absorption of atmospheric water vapor which presents many sharp maxima where deflections taken either with or without the absorbing cell are reduced below the limit permissible for precise measurement. Several efforts have been made to resolve the individual lines of this band, but the curve shown

in the Fig. 2A represents the best definition obtained. The irregularities of the rotational lines are to a great extent attributable to the water vapor in the atmosphere but there may also be appreciable absorption here by molecules already excited to the level 1. There are two maxima, very nearly symmetrical, with almost equal intensities, separated by a sharp minimum. The position of the missing line is about 1412.4 cm^{-1} . Measurements have been extended in either direction to the region of very low absorption, with some loss in precision, because on the long wave-length side, the energy of the beam falls off rapidly and on the short wave-length side, the intensity of the water vapor absorption increases. Although fine structure is indicated, it is not possible to determine the positions of successive individual lines.

Region of 4.7μ

This region was examined with a grating having 4800 lines per inch and with 0.3 of mm slit. The absorption was very much less intense and could scarcely be located with the 2.5 cm cell. The third curve Fig. 2B represents the absorption, using the 25 cm cell of saturated vapor at about 25°C and atmospheric pressure. The cell was moved alternately in and out of the beam as before. The principle maximum appears at 4.760μ with a second narrow one at 4.728μ and with a third at 4.794μ . These peaks have the appearance of Q branches. From this curve it would be difficult to make an estimate of the value of the moment of inertia in the usual way, but obviously the wave-number differences are not of the same magnitude as those exhibited at 14μ .

Region of 3.6μ

The absorption band near 3.6μ Fig. 2C is also weak, although it was observed with 2.5 cm cell and with the pressure of 65 cm. A single narrow and fairly intense maximum was found at 3.57μ , with a low background on either side. Some indications of fine structure appear in the R branch but further resolution could not be obtained.

Region of 3μ

The single intense absorption band shown by Burmeister was resolved into a doublet Fig. 2D. It was examined with the 2.5 cm cell and with almost atmospheric pressure. The maxima appear at 2.996μ and 3.045μ . Several unsuccessful efforts have been made to resolve the individual lines with the 7200 line grating and different amounts of absorbing gas. The spacing of the maxima is about 53.7 cm^{-1} which is much greater than that observed at 14μ , but nearly the same as at 7μ . This fact combined with the difficulty in resolving the rotation lines, indicates that the absorption by excited molecules must be appreciable.

MECHANICAL INTERPRETATION OF THE VIBRATION-ROTATION BAND

Assuming that the rotation of this molecule may be represented by the equation for the symmetrical top rotator, the total energy in any stationary state is

$$E = E_p + \frac{h^2}{8\pi^2} \left\{ \frac{J(J+1)}{A} + l^2 \left(\frac{1}{C} - \frac{1}{A} \right) \right\},$$

where E_p is the potential energy of deformation and C and A are the moments of inertia about the axis of figure and any axis normal to it.

If $C=0$, as in the unexcited molecule, then E will be finite only if $l=0$, and E_p will also vanish, so that the equation passes over into the expression for the energy of a simple rotator,

$$E_r = J(J+1)h^2/8\pi^2A$$

or $E_r/h = BJ(J+1)$ where $B = h^2/8\pi^2A$ and J may assume all integral values.

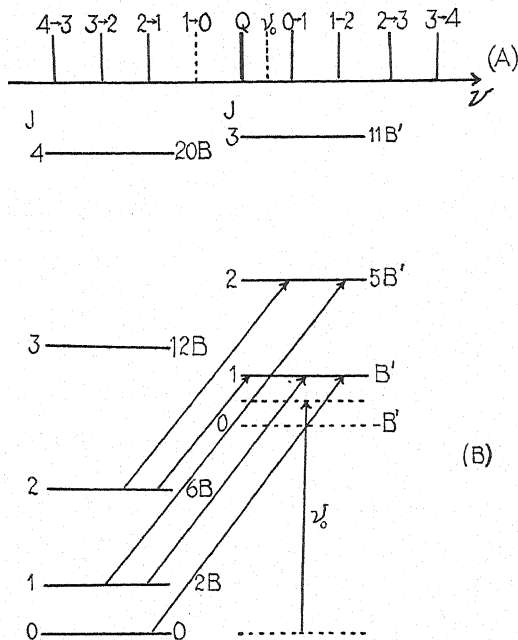


Fig. 3. Band pattern and scheme of energy levels for the transition $0 \rightarrow 1$ in l .

For the special case of an excited molecule in which $l=1$ the equation becomes

$$E' = E_p' + \frac{h^2}{8\pi^2} \left\{ \frac{J(J+1)}{A'} + \left(\frac{1}{C'} - \frac{1}{A'} \right) \right\}$$

or $E'/h = B' (J^2 + J - 1) + \nu_0$ where $\nu_0 = E_p'/h + h/8\pi^2C'$ and $B' = h^2/8\pi^2A'$. J may assume all values except 0, since $J \geq l$.

Fig. 3 shows the energy diagrams for both normal and excited states, with permitted transitions indicated by arrows. Those lines in a band which are due to $\Delta J=0$ belong to the Q branch, those with $\Delta J = \pm 1$ lead to P and R branches respectively. In other words, the absorption $0 \rightarrow 1$ corresponds to the first line of the R branch and the absorption $2 \rightarrow 1$ to the first line of the P branch. There is no transition $1 \rightarrow 0$ since in the excited state, J cannot be

zero. For levels in which $l=0$, J will of course assume all values including 0, while for a level in which $l=2$, J cannot be either 0 or 1.

Fig. 3A represents a system of lines corresponding to a change in l from 0 to 1. ν_0 lies between the Q branch and the first line of the P branch.

THE SCHEME OF VIBRATION LEVELS AND INTERPRETATION OF THE OBSERVED BANDS

Fig. 4 represents the energy levels for the deformation vibration ν_2 following Dennison's analysis. The principal quantum number is the value of ν_2 while the subscript is the value of l associated with it. When $\Delta\nu$ is odd,

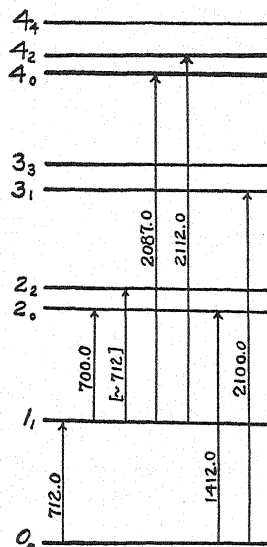


Fig. 4. Vibrational levels for ν_2 .

Δl is restricted to ± 1 and the change in electric moment is normal to the axis of figure, giving rise to bands with Q branches. When $\Delta\nu$ is even, $\Delta l=0$ and there are no Q branches. The most intense absorption bands originate in the level 0_0 but even at room temperature some molecules are excited to higher states. The population of any upper state is determined by the Boltzmann factor and by the statistical weight, the latter being 1 when $l=0$, and 2 when $l \neq 0$. Thus in the state 1_1 there are about 0.06 times as many, in the state 2_0 about 0.0009 times as many, and in 2_2 about 0.0018 times as many as in the state 0_0 .

In addition to the three fundamental vibrations and their harmonics, all of which we should expect to be active, combination bands should appear. There is no restriction upon the values of $\Delta\nu_1$, $\Delta\nu_2$ and $\Delta\nu_3$ in combinations. Although ν_1 has not been observed directly, its value is apparently very close to 2100 cm^{-1} . ν_2 and ν_3 have been identified, their values being 712 cm^{-1} and 3289 cm^{-1} respectively. The rest of the observed bands may now be classified. The band at 4.7μ is apparently the second harmonic of ν_2 , $\Delta\nu_2=3$, for which zero branches should appear. It cannot be ν_1 since the latter would be a doublet. The three maxima may be interpreted as indicated in the dia-

TABLE II. Observed band centers and their assigned quantum transitions.

ν_1	ν_2	ν_3	Band center		Approximate relative intensity
			Wave No. (cm. ⁻¹)	Wave-length (μ)	
0-1(ν_1)	0 ₀ -1 ₁ (ν_2)	0-1(ν_3)	(2100)	(4.76)	?
			712	14.00	1000
			700	14.30	12.0
			712	14.00	
			2100	4.76	0.12
			2087	4.79	0.095
			2112	4.73	0.105
			1412.0	7.00	1.33
			3289	3.04	4.4
0-1	0 ₀ -1 ₁		2801	3.57	1.30

gram, 0₀→3₁ being the most intense peak at 4.76 μ , 1₁→4₀, the weakest one at 4.79 μ and 1₁→4₂ the intermediate one at 4.73 μ . Table II shows the observed band centers and their assigned quantum transitions.

The fact that ν_1 has not been observed is somewhat surprising, and must indicate that for this motion the electric moment has a very small amplitude. The resulting weak band might have been observed if the three components of $3\nu_2$ had not been so intense. That ν_1 actually lies in this region is indicated by the Raman spectrum in which it appears as the most intense line. Kastler⁶ finds the Raman displacement to be 2089 in the gas and 2098 in the liquid. Bhagavantam⁷ gives measurements for liquid HCN only. He finds ν_1 at 2094 for normal molecules, with a weaker line at 2062 doubtless corresponding to absorption by molecules in the excited state 1₁, the intensity ratio being estimated as 24:1. The frequency ν_3 as indicated by his measurements is 3213.

ON THE SHAPE OF THE MOLECULE

All of the bands observed, as well as those reported by Badger and by Brackett are consistent with the hypothesis that the molecule is linear. Only for the linear configuration can the simple structure of the 14 μ band be understood. From the frequencies given in Table I a value of the moment of inertia may be obtained, since

$$\nu(J' \rightarrow J'') - \nu(J' + 2 \rightarrow J'') = 2B'(2J' + 1)$$

the primes referring to the normal state. Computing in this fashion for each pair of lines, we find an average value $I' = 18.68 \times 10^{-40}$ g cm², which compares very well with Badger's value, 18.79×10^{-40} g cm². The same order of magnitude is indicated by the frequency interval between the maxima of the *P* and *R* branches in the 14 μ band, but not in the bands at 7 μ and 3 μ . For the former with $\Delta\nu = 24.9$ cm⁻¹, the classical formula gives $I = 18.32 \times 10^{-40}$ g cm².

It is not possible at present to determine the interatomic distances from the moment of inertia, nor to decide between the two possible configurations designated as hydrogen cyanide HCN or iso-cyanide HNC. However, the simplicity of the rotational structure suggests that probably only one type of molecule is present.

⁶ C. R. Kastler, *Comptes Rendus* **194**, 858 (1932).

⁷ Bhagavantam, *Nature* **126**, 995 (1930).

The Positive Ion Current at the Cathode in the Glow Discharge

By A. KEITH BREWER AND R. R. MILLER

*Fertilizer and Fixed Nitrogen Investigations, U. S. Bureau of Chemistry
and Soils, Washington, D. C.*

(Received August 29, 1932)

The positive ion current passing through a perforation in the cathode of a glow discharge tube has been measured with various types of collectors and the factors influencing the ratio of positive ions to total current studied. At pressures above 0.5 mm the positive ion current constitutes but a small fraction of the total current, while at lower pressures it increases inversely with the pressure, reaching approximately half the total current below 0.01 mm. The fraction of the current carried by positive ions is independent of the size and shape of the perforation, of the current passing through the discharge, and of the position of the anode provided it is not within a certain critical distance from the edge of the Crookes dark space; it does, however, vary with the gas, increasing for decreasing molecular weight.

The possible sources of current to the collector are discussed. The method by which the current due to positive ions is separated from that due to metastable molecules is described. The energy of the positive ions passing through the cathode is shown to correspond to an appreciable fraction of the cathode fall of potential.

IN A series of recent experiments on chemical action in the glow discharge (I-X)¹ it has been shown that the rate of reaction in the discharge can be expressed by a simple electrochemical equivalence law somewhat analogous to Faraday's law for electrolytes and also that the molecules formed in the negative glow are carried to the walls largely as positive ions; little or no reaction occurs in the dark spaces. An estimation of the M/N ratio for the positive ions formed in the discharge necessitates a knowledge of the rate of positive ion formation. Two separate methods used for evaluating the rate of ion formation yield M/N ratios similar to those found by Lind² for α -particles, provided the positive ion current to the cathode is small compared to the electron current.³ The present research was undertaken, therefore, to measure the fraction of the current carried to the cathode by positive ions.

Many attempts have been made to analyze the current at the cathode. Aston⁴ using a perforated cathode measured the current received by a collector immediately behind the perforation. He concluded that as much as half the current might be carried by positive ions, but felt that this conclusion must be accepted with considerable caution, since a negative ion rather than a positive ion current was received by the collector when an appreciable positive charge was applied to it. Guntherschulze⁵ from measurements of the power appearing as heat at the cathode infers that the positive ion cur-

¹ A. Keith Brewer, et al., *J. Phys. Chem.* **33**, 883 (1929) to **36**, 2133 (1932).

² S. C. Lind, *Chemical Effect of α -Rays*, A.C.S. Monograph.

³ A. K. Brewer and P. D. Kueck, *J. Phys. Chem.* (1932).

⁴ F. W. Aston, *Proc. Roy. Soc. A* **96**, 200 (1919).

⁵ Guntherschulze, *Zeits. f. Physik* **37**, 828 (1926).

rent may exceed the electron current by a factor of ten. Uyterhoeven and Harrington⁶ have shown that metastable molecules formed in the discharge exert a prepondering effect over positive ions in the emission of electrons from the cathode. It is now felt that these metastable molecules have largely been responsible for the difficulties involved in measuring the current carried to the cathode by positive ions.

METHOD

The method adopted for this study was a modification of that used by Aston; it consisted of measuring the current passing through a hole pierced in the cathode. There are many difficulties involved in using this method of measurement, most of which can be overcome by a current collector of the proper design. These difficulties are: (1) the discharge is not distributed uniformly over the cathode; (2) the cathode field may be distorted at the perforation; (3) metastable molecules and atoms as well as positive ions will

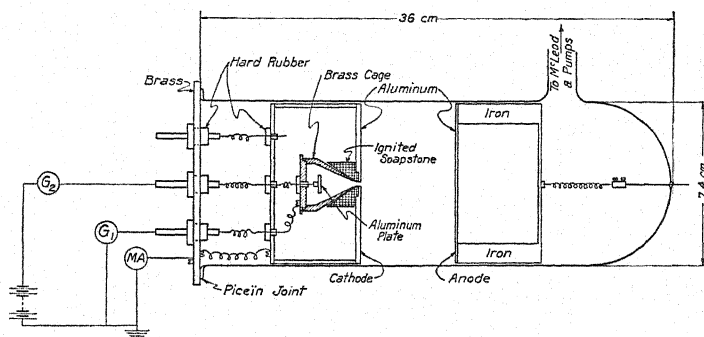


Fig. 1. Apparatus for measuring the positive ion current passing through a perforation in the cathode.

pass through the opening; all are capable of giving off electrons from the collector; (4) the high positive space charge at the opening causes an appreciable electron current to flow from the collecting plate to the cathode even in the absence of applied fields. It is believed that the apparatus as designed overcomes most of these difficulties and that the results give a fair estimation of the positive ion current.

THE APPARATUS

Many types of collectors were tried, including flat plates and a duplicate of that used by Aston. The currents received at the collector varied considerably, depending on the design and dimensions. The apparatus illustrated in Fig. 1 was finally chosen as giving the most reliable results.

The dimensions of the tube are given in the illustrations. The anode was an aluminum plate backed by iron, so its position could be changed by a magnet. The cathode was an aluminum disk covering one end of an enclosed aluminum cylinder 5 cm long and 7.3 cm in diameter. The perforation was a hole 2 mm in diameter placed in the center of the cathode, the cathode wall

⁶ Uyterhoeven and Harrington, *Phys. Rev.* **36**, 709 (1930).

being about 0.5 mm in thickness at this point. The collecting cage was insulated from the cathode by an ignited soapstone block. It was found necessary to have a 5 mm opening in the cage with the soapstone shadowing the cage from the perforation to minimize space charge induced currents between the cage and the cathode. All parts were made tightly fitting to prevent metastable molecules from drifting between the cathode and the cage, thus giving rise to abnormal currents between these points.

The cone shaped cage was superior to the cylindrical type in practice, since it tended to screen the cathode perforation from fields applied to the collecting plate. This prevented a spurious discharge current between the collecting plate and the cathode when a potential was applied to the plate, and also it prevented the number of positive ions entering the cage from being influenced by the plate field.

RESULTS

The effect of pressure

The effect of the pressure in the discharge tube on the positive ion current entering the cage is shown for various gases in Fig. 2.

These data were obtained with no potential applied to either the cage or the plate. In the case of nitrogen the currents to both the cage and the plate are shown. The measured positive ion current in every instance is the sum of these two currents. The corrected positive ion current is the measured current corrected for the fraction of the cathode covered by the discharge at the various pressures. The voltage is the difference in potential between the anode and the cathode; the electrodes were so placed that the positive column was absent.

The currents to the cage and plate are similar for all gases, the only appreciable difference being in magnitude. The cage current, which is larger than the plate current for the higher pressures passes through a maximum and reaches a comparatively small value at low pressures; the current to the plate, however, increased rapidly at the point where the cage current passes through a maximum.

The fraction of the total current carried by the positive ions passing through the perforation is given by the right-hand ordinates. The positive ion current appears to increase with decreasing pressures, the relation between pressure and current being very nearly hyperbolic for every gas except hydrogen. It is of interest to note that when the observed current is corrected for the fraction of the surface covered by the discharge, the positive ion current approaches 50 percent at the lowest pressures for which reliable readings can be taken, about 0.01 mm. At pressures above 0.5 mm the fraction of the total current carried by positive ions in argon, oxygen, and nitrogen is very small, being less than 5 percent. In helium and hydrogen, however, the positive ion current is materially larger.

The effect of pressure on the distribution over the cathode

The positive ion current arriving at various points on the cathode surface as affected by the gas pressure is shown in Fig. 3a. These values given are

for nitrogen and are typical of all gases. The currents passing through holes 2 mm in diameter were measured with plane plate collectors at the cathode center and at 1, 2 and 3 cm from the center. It will be observed that at

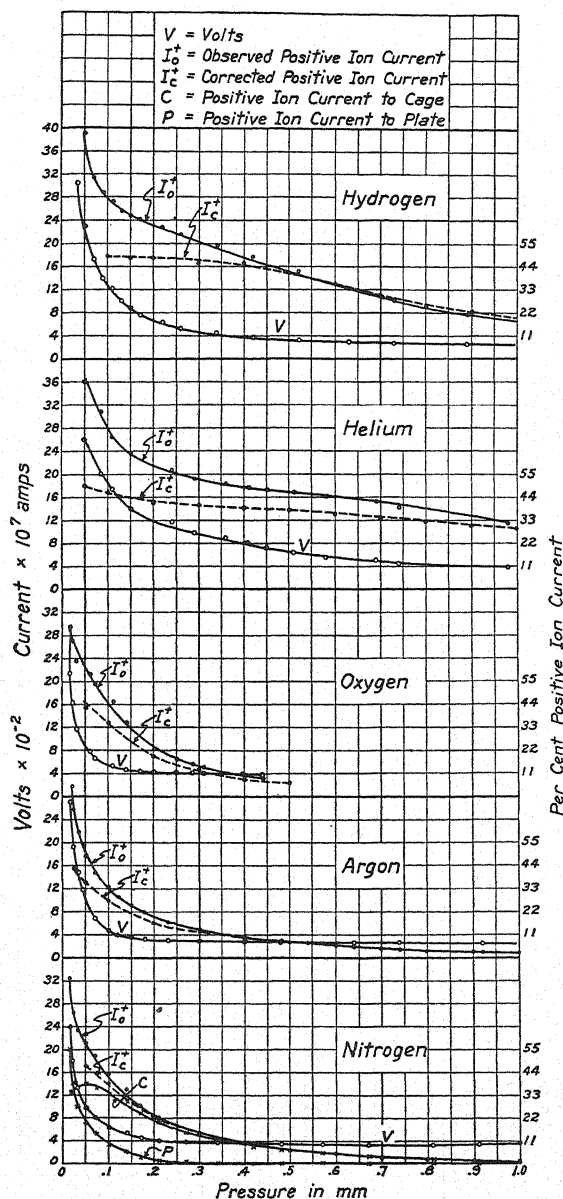


Fig. 2. Curves showing the positive ion current through the cathode perforation and the fraction of the total current carried to the cathode by positive ions.

pressures above 0.3 mm the discharge is quite uniformly distributed over the surface, while at pressures below this point the discharge creeps away from the edge of the cathode and tends to concentrate in two bright sections, one

at the center and the other in the form of a ring at the outer edge of the glowing area.

The effect of the discharge current

The variation of the positive ion current with the current passing the discharge is shown in Fig. 3b. These data are for the current passing through the center perforation in the cathode used in Fig. 3a. The results show the positive ion current to be proportional to the discharge current.

The effect of the cathode potential drop

The correlation between the cathode fall of potential and the positive ion current is illustrated in Fig. 2. In the region where the voltage change with pressure is appreciable, the change is approximately inversely proportional

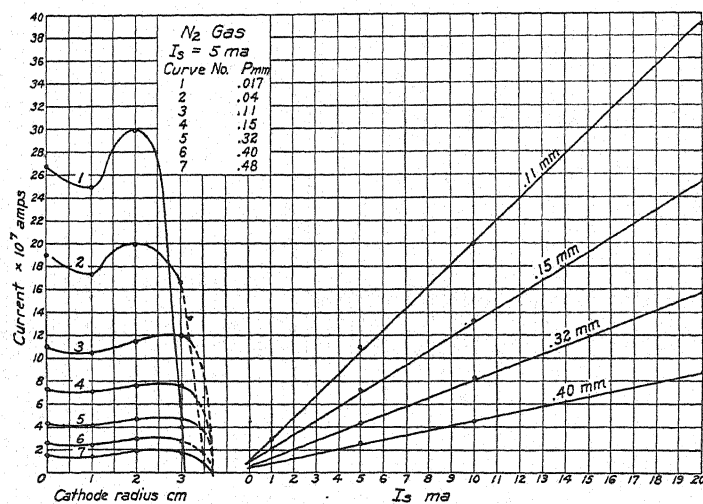


Fig. 3a. The distribution of the positive ion current over the cathode at various discharge pressures.

3b. The dependence of the positive ion current on the total current through the system.

to the pressure. With the possible exception of hydrogen, the positive ion current depends on the pressure in a similar manner.

The effect of area and shape of the perforation

A cathode with an adjustable slit passing through the center was used to test the effect of size of the opening on the positive ion current. The slit was 2.2 cm in length; the areas were varied from 0.007 sq. cm to 0.07 sq. cm, and the pressures from 0.2 mm to 0.5 mm. Over this entire range the positive ion current at each pressure was proportional to the slit area.

The shape of the perforation appears to have little effect on the positive ion current when the distribution of the discharge over the cathode was uniform. Thus round holes gave practically the same current values as did long narrow slits for equivalent areas.

The effect of the anode

The effect of the distance between the anode and cathode on the positive ion current is shown in Fig. 4.

The edge of the dark space is represented by the dotted line at 1 cm. The voltage is the difference in potential between the electrodes. The data show that the position of the anode in the negative glow has no effect on the cathode potential fall, on the current through the system, I_s , or on the positive ion current, I_p , until it approaches within a very short distance from the edge of the dark space. This effective region which determines the characteristics of the discharge is referred to as the vital segment.

The effect of collector potential

The effect of various voltages applied to the plate of the collector illustrated in Fig. 1 is given in Fig. 5.

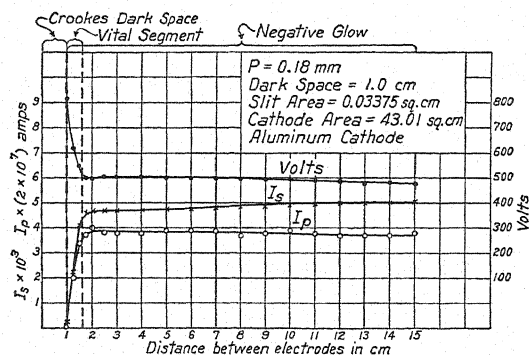


Fig. 4. The effect of the position of the anode on the positive ion current arriving at the cathode.

The results were all very similar in nature so only representative curves are shown. Line 1 shows the effect of potential on the current received by the plate, while line 2 is the current simultaneously received by the cage. Line 3 is the sum of these two currents. It will be seen that the sum of the currents received by the plate and cage is very nearly constant, irrespective of the plate potential. Lines 4, 5, and 6 represent the sums of curves similar to lines 1 and 2 for the pressures indicated.

Line 7 for hydrogen is distinct from those obtained for argon, nitrogen, and oxygen in that it shows a pronounced hump for low applied voltages. The size of the hump decreases with increasing pressure. Similar humps were obtained with helium at the lower pressures.

Line 1 for the current received by the plate is similar to that obtained with a simple plate collector or with a collector of the type used by Aston, the sudden drop for small applied potentials and the negative current for large positive potentials are characteristic of all simple collectors.

The results obtained with a collector of the same type as that shown in Fig. 1, but with a cylindrical rather than a cone shaped cage, were different from those given in Fig. 5 when various accelerating and retarding voltages

were applied to the plate. Two cylinders were used, one with an opening into the cylinder, 2 mm in diameter, the same as the cathode perforation and the other with a 6 mm opening placed symmetrically over the cathode perforation. The walls of the cylinders were machined to a knife edge at the opening in both cases and were insulated from the cathode by a thin sheet of mica. The cylinder with the smaller opening gave unsatisfactory results as the positive space charge due to the ions entering the perforation induced an appreciable electron current from the cage to the cathode. This effect was materially minimized by the 6 mm cage opening. With the larger opening the plate current corresponded exactly to line 1 of Fig. 5. The cage current, however, is illustrated by the dotted line 8, and differs materially from line 2 for the cone shaped cage in that many of the positive ions and metastable molecules that were caught by the cone now go to the cathode and also the number of

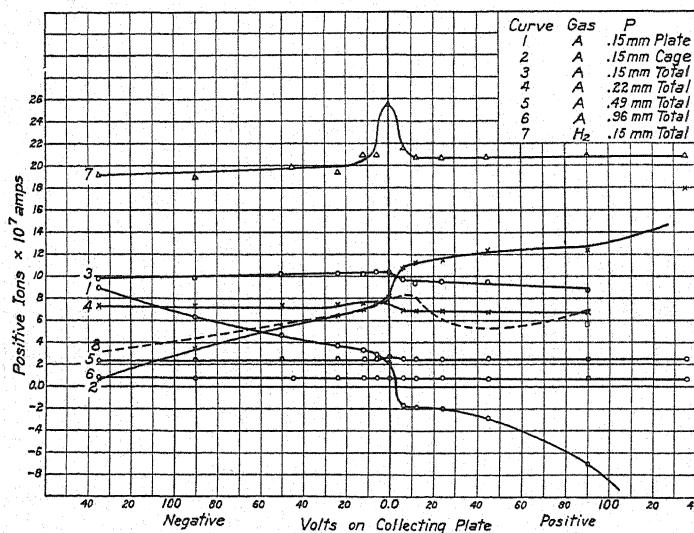


Fig. 5. The effect of plate potentials on the current to the plate and to the cage, and on the total positive ion current passing through the perforation.

positive ions passing through the cathode is doubtlessly materially reduced by the positively charged plate placed immediately over the perforation. Decreasing the distance between the plate and the perforation increased the current from the plate to the cathode, and decreased the current to the cage.

DISCUSSION OF RESULTS

The results just presented may be better understood by a consideration of the possible sources of the currents received by the collector cage and plate. The currents received by the collector may be divided into two types; (1) the primary current entering from the discharge, and (2) secondary current arising within the collector. These types may be subdivided as follows:

- (1) Primary current
 1. Positive ions from discharge (I^+)
 2. Electrons from discharge (e_c)
 - (Dragged in by I^+ or by charge on plate)

(2) Secondary current

1. Secondary electrons ejected by ions (e_{I^+})
2. Secondary electrons ejected by metastable molecules and atoms (e_m)
3. Photoelectrons (e_λ)
4. Ionization by mutual impact of 2 metastables.

The components of the currents received by the plate and cage may now be analyzed as follows:

When plate is negative

Current at the plate

1. I^+
2. e_m from plate
3. e_{I^+} from plate
4. e_λ from plate

Current at cage

1. e_m from plate
2. e_{I^+} from plate
3. e_λ from plate
4. e_c from discharge

When plate is positive

Current at the plate

1. e_m from cage
2. e_λ from cage
3. e_{I^+} from cage
4. e_c from discharge

Current at cage

1. I^+
2. e_m from cage
3. e_λ from cage
4. e_{I^+} from cage

In addition to the above there are two other sources of current that might be registered by the collecting electrodes, namely, an electron current from the plate to the cathode perforation, and an electron current from the cage to the cathode. An example of the plate to cathode current is shown by line 8 in Fig. 5; this did not occur for the cone collector. A cage to cathode current is difficult to avoid but can be reduced by making the cage opening materially larger than the cathode perforation, and also by screening the cage opening from the cathode with some insulating material; a potential on the plate also decreases this current.

A survey of the various currents received by the plate and cage shows that the currents of secondary origin neutralize one another, in that what is lost by one electrode is gained by the other. The sum of the currents to the cage and plate, therefore, represents only the primary currents passing through the cathode perforation, provided no spurious discharges to the cathode occur. Thus it follows that the lines 3, 4, 5, 6, 7, of Fig. 5 represent the current due to the positive ions passing through the orifice minus that due to any electrons that might be dragged along by the intruding positive ions.

An accurate estimation of the primary electron current passing through the cathode perforation cannot be made from the present data; nevertheless the results indicate it to be small compared with the positive ion current. Since the primary electrons necessarily enter the cage with very low initial energy they should be easily stopped by a negative plate potential; the fact that the total current passing through the perforation remains almost constant irrespective of the potential on the plate indicates a negligible electron current. It may be, however, that the small break in line 7 near zero plate voltage is due to the primary electron current.

The hump in curve 7 is characteristic of all the sum curves, although it is negligible for argon, nitrogen, and oxygen, and small for helium. The presence of the hump results from an abnormal electron current from the cage to the cathode that is apparently due to electrons liberated from the edge of the cage by metastable molecules and atoms and drawn to the cathode by the positive space charge set up by the intruding ions. This type of discharge is readily checked by a charge on the plate and ordinarily breaks off more readily for positive than for negative potentials.

It is impossible to obtain an accurate estimation of the energy of the positive ions since the data do not distinguish between electrons liberated by the ions and by metastable molecules. The energy of the ions must be an appreciable fraction of the cathode potential drop, however, since the point of crossing of lines similar to 1 and 2 in Fig. 5 moves toward the positive voltages for decreasing pressure, as well as the positive potential at which the plate current became zero increased with a decrease in pressure. In the case of helium the plate did not register a negative current until a stopping potential of one-quarter the cathode potential was reached. This does not mean that the energy of the ions is but one-quarter of the cathode potential drop but rather that at this retarding voltage the positive ion current to the plate is just balanced by the electron current from the cage to the plate. When there is no charge on the plate the positive ions strike the plate at the lower pressures in a well-defined spot about twice the size of the cathode perforation; this is an indication of a fairly homogeneous beam of ions. It seems probable from a survey of the results as a whole that the ions striking the cathode possess an energy near that of the cathode fall. Such an interpretation is not surprising since it has been shown previously that the length of the Crookes dark space is approximately equal to one mean free path for an electron between ionizing collisions.

These results indicate that the current carried to the cathode by positive ions constitutes but a small fraction of the total current passing through the discharge for all pressures above a few millimeters of mercury. The positive ion current, however, is greater in gases of low molecular weight, the currents being roughly proportional to the relative rate of diffusion of ions in the various gases. Since the potential gradient at the junction of the Crookes dark space and the vital segment is small it is not surprising that the cathode potential drop has little or no effect on the values of the positive ion currents; diffusion is evidently the important thing in determining the movement of ions from the negative glow to the cathode. Even in this vital segment of the negative glow the natural tendency is for the ions to be driven further into the glow rather than towards the cathode, since the average electron producing the ionization has an energy component equal to the cathode potential.⁷ The studies of chemical action in the discharge show clearly that a majority of the ions formed in the negative glow are neutralized on the walls of the discharge tube⁸ rather than at the cathode.

⁷ A. K. Brewer and P. D. Kueck, *J. Phys. Chem.* (1932).

⁸ A. K. Brewer and P. D. Kueck, *J. Phys. Chem.* **35**, 1281 (1931).

On the Nature of Active Nitrogen

By J. OKUBO AND H. HAMADA

Physical Laboratory, Tohoku Imperial University, Sendai, Japan

(Received July 15, 1932)

Since active nitrogen is essentially atomic nitrogen, the following two assumptions (without assuming the existence of the metastable atoms as Cario and Kaplan did) accounts for all the observed results as reasonable consequences of the Franck-Condon principle and the general properties of molecular spectra. The assumptions are: (1) In the vibrational states with $v'' = \sim 8$ in the metastable $A^3\Sigma$ state, and also in those with $v' = \sim 6$ in the upper $B^3\Pi$ state, the near-nuclear turning points of the vibration have the same or nearly equal nuclear separations as those in the equilibrium position of nuclei in the normal molecular state; (2) With the exception of the neutral unexcited molecules and atoms in active nitrogen, the metastable $A^3\Sigma$ molecules in the vibrational state with $v'' = 7$ or 8 are most concentrated.

DURING the past few years, considerable progress has been made in our knowledge of the true nature of active nitrogen. From the results of the exhaustive experiments of Herzberg,¹ Kneser,² Wrede,³ Bay and Steiner,⁴ and others, it is at present generally accepted that active nitrogen is composed of nitrogen atoms and that its main properties are natural consequences of its atomic nature. It seems, however, that some further assumptions are required to account for the emission of the visible afterglow itself.

Assuming the existence of the metastable molecules and metastable atoms, Cario and Kaplan⁵ have made good the defectiveness of Sponer's view⁶ with regard to the nature of active nitrogen, and they have succeeded in explaining the emission of the visible afterglow as well as its other properties. Though their view is very helpful in explaining the special enhancements and energies of the bands emitted by the transitions from the initial levels corresponding to the vibrational quantum numbers ~ 11 and ~ 6 in the $B^3\Pi$ state, we have shown, on the one hand, that the "dark modification," does not exist,⁷ (at least in the sense which they have mentioned) and that active nitrogen has an energy, content independent of its temperature ($-190^\circ \rightarrow 650^\circ\text{C}$). On the other hand, we have shown that the enhanced appearance of the bands above described is not confined to the case of the afterglow bands of active nitrogen, but is also observable in the case of the first-positive bands excited by passing a very weak electrical discharge through nitrogen,⁸ the only difference in the two cases being that in the latter case in comparison with the former, the relative intensities of the bands with $v' = \sim 6$ are greater

¹ G. Herzberg, *Zeits. f. Physik* **49**, 512 (1928).

² H. O. Kneser, *Ann. d. Physik* **87**, 717 (1928).

³ E. Wrede, *Zeits. f. Physik* **54**, 53 (1929).

⁴ Z. Bay and W. Steiner, *Zeits. f. phys. Chemie* **B3**, 149 (1929).

⁵ G. Cario and J. Kaplan, *Zeits. f. Physik* **58**, 769 (1929).

⁶ H. Spomer, *Zeits. f. Physik* **34**, 622 (1925).

^{7,8,9} Detailed statements will be shortly published elsewhere.

than those with $v' \approx 11$. Moreover, from the investigations of metallic spectra excited by active nitrogen, contrary to expectation, no resonance enhancements of the lines due to the metastable atoms (2.37 and 3.56 volts) and metastable molecules (8.2 volts) were found. It seems that the concentrations of these metastable entities should not be so high as Cario and Kaplan expected, even if they exist in active nitrogen.⁹ To explain the observed results, *viz.*, that the maximum of the intensity distribution of the bands in the group, or that of the groups in the band system, is displaced in the direction of the longer wave-lengths by the increase of the pressure,¹⁰ the introduction of inert gases,¹¹ the raising of the temperature,^{7,10} and by the lapse of time directly after the exciting discharge of the active nitrogen has been cut off,¹⁰ some further assumptions are required.

From the result that the selective enhancements of the bands with $v' \approx 11$, $v' \approx 6$, and $v' \approx 2$ in the upper state $B^3\Pi$ are observable not only in the α -bands of active nitrogen, but also in the first-positive bands emitted from nitrogen, especially at the temperature of liquid air. When very weakly excited by the electrons of various velocities, it will be very natural to consider that the appearance of these bands is entirely due to the transitions between the energy levels of nitrogen molecules, and has no direct connection at all with atoms of any kind. Of course, the true nature of active nitrogen will be brought out clearly only after the results of further observations regarding its various properties have been reported, but the following consideration is a means of explaining the excitations of the bands with $v' \approx 11$, ~ 6 , and ~ 2 above described, the displacements of the maximum of intensity in the band group, or in the band system, accompanying the changes of excitational conditions, as well as other properties of active nitrogen, without assuming the existence of metastable atoms.

It seems that the main observed results of the afterglow of active nitrogen will follow very well as consequences of the following two assumptions coupled with the Franck-Condon principle. It is assumed that, (1) in the vibrational states with $v'' \approx 8$ in the metastable $A^3\Sigma$ state, and also in those with $v' \approx 6$ in the upper $B^3\Pi$ state, the near-nuclear turning points of the vibration have the same or nearly equal nuclear separations as those in the equilibrium position of nuclei in the normal $X^1\Sigma$ molecular state; and that (2) with the exception of the neutral unexcited molecules and atoms in active nitrogen, the metastable $A^3\Sigma$ molecules in the vibrational states corresponding to the quantum numbers $v'' \approx 7$ or 8 are most numerous. The approximate potential energy of the molecular states $A^3\Sigma$ and $B^3\Pi$, calculated by the ordinary method with the molecular constants known from the vibrational and rotational analysis,¹² or simply by Morse's function, are plotted in Fig. 1. The equilibrium distance r_e of nuclei in the normal molecular state can be calculated, approximately, by means of the formula $r_e^2\omega_e = \text{constant}$ or $r_e^3\omega_e = \text{constant}$, and it is fairly certain that its value is in the vicinity of

¹⁰ G. Herzberg, *Zeits. f. Physik* **49**, 512 (1928).

¹¹ Lord Rayleigh, *Proc. Roy. Soc. A* **102**, 453 (1923).

¹² S. M. Naudé, *Phys. Rev.* **38**, 372 (1931).

1.09Å, and also that it is nearly equal to the values of the nuclear distance of near-nuclear turning points of the vibration in the $A^3\Sigma$ state corresponding to the vibrational quantum numbers ~ 8 , and approximately to those in the $B^3\Pi$ state corresponding to the vibrational quantum numbers ~ 6 . Therefore assumption (1) may be reasonably accepted. As the energy of the $v'' = 8$ level in the $A^3\Sigma$ state is in the range between 9.5 and 7.5 volts¹³ the excitation of the $A^3\Sigma^{(\sim 8)}$ levels (and so the assumption (2)) is also conceivable from the observed results of the metallic spectra excited by active nitrogen, taking into consideration the Franck-Condon principle.

Certainly, the excitation of these $A^3\Sigma^{(\sim 8)}$ levels may be due to the triple collisions. Here it is only necessary that the energy of the $A^3\Sigma^{(\sim 8)}$ state be not greater than the dissociation energy of the nitrogen molecule. It is not necessary to assume that the former is equal to the latter. Therefore, no modification of this consideration is necessary even though we take the latter as 9.0 or 9.1 volts, so long as the former is not greater than the latter. It is regretted that we have now no reliable data to determine the energies of triplet levels

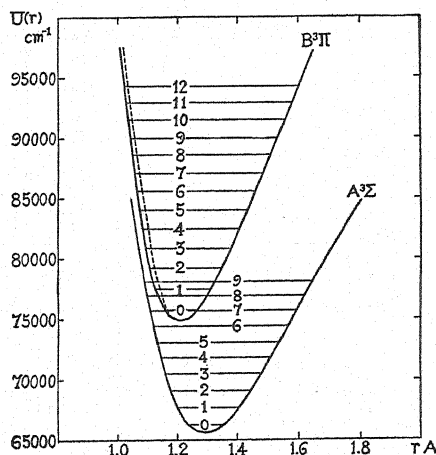


Fig. 1. Approximate potential energy curves for $A^3\Sigma$ and $B^3\Pi$ of N_2 .

of a nitrogen molecule. If it were certain that the energy of the $A^3\Sigma^{(\sim 8)}$ state is greater than the energy of dissociation, a slight modification with regard to the explanation of high concentration of the metastable $A^3\Sigma^{(7 \text{ or } 8)}$ molecules will be necessary, but no alternation of the above assumptions.

From the general nature of triple collisions, i.e., that the metallic lines of the lower excitational energy are excited much more intensely than those of the higher energy in comparison with other cases of excitation, and from the already recognized fact that the only known excited state of the nitrogen molecule directly combined with the $A^3\Sigma$ state is the $B^3\Pi$ state, it is certain that, in the triple collisions between two nitrogen atoms and the metastable molecule in the $A^3\Sigma^{(7 \text{ or } 8)}$ state, the transitions to the $B^3\Pi$ state from the $A^3\Sigma$ state will be most probable in comparison with the transitions to other states. According to the general property above mentioned, the $B^3\Pi$ mole-

¹³ R. S. Mulliken, Rev. Mod. Phys. 4, 54 (1932).

cules in the vibrational level corresponding to the quantum number 11 or 12 will predominate over those corresponding to the quantum number 6 or 7. Consequently, it will be expected that, in the visible afterglow, the bands which are emitted by the transitions from the vibrational level with $v'=11$ or 12 in the $B^3\Pi$ state will appear more enhanced than those from the level with $v'=6$ or 7 in the same state. It will also be easily understood why the bands with smaller v' , especially those with $v'=2$ or v' thereabout, are selectively enhanced in the α -bands of active nitrogen, (of in the spectrum of ordinary nitrogen excited by a very weak electric current at low temperature), as some little concentration of the $A^3\Sigma$ molecules with smaller v'' or $v''=0$ will result from the vibrating metastable molecules $A^3\Sigma^{(\sim 3)}$ etc. In this manner it is possible to understand the special enhancements of the bands in the α -bands of active nitrogen.

As the lifetime of the $A^3\Sigma$ metastable state is believed to be sufficiently long, in the case where a suitable quantity of the inert gas is mixed with nitrogen, or where the pressure of nitrogen is relatively high, the $A^3\Sigma^{(7 \text{ or } 8)}$ molecules will collide more frequently with other neutral unexcited molecules or atoms before the former are again excited to the $B^3\Pi$ state, and the vibrational levels of the former will descend to lower levels ($^3\Sigma^6$, $^3\Sigma^5$, $^3\Sigma^4$, \dots) than those before the collisions. As a result the $B^3\Pi$ molecules having vibrational quantum numbers less than ~ 11 or ~ 6 will predominate. Therefore, the maximum of intensity in the band system or in each group will be displaced towards longer wave-lengths, and the greater the number of collisions, i.e., the higher the pressure of the nitrogen or the inert gas, the greater will be this effect.

At a high temperature on account of the greater relative velocities of molecules and atoms, the probability of triple collisions will naturally be reduced, and in addition there will be required two-stepped excitations for the visible afterglow (α -bands) and a one-stepped excitation for the metallic spectra. The former will appear weaker and weaker in comparison with the latter.¹⁴ This is conceivably the reason the intensity of the visible afterglow is markedly reduced at a high temperature, independent of its energy content (9.51 volts). It is also to be expected that, at high temperature, the vibrational energies of the $A^3\Sigma^{(7 \text{ or } 8)}$ states will be reduced before they undergo the second excitation because triple collisions between molecules and other atoms take place relatively less frequently. The maximum of intensity in the group or band system of the visible afterglow will be naturally displaced towards the longer wave-lengths. On the other hand, where, owing to the smaller relative velocities of molecules and atoms at a low temperature, triple collisions take place frequently, the probability that the $A^3\Sigma^{(7 \text{ or } 8)}$ molecules will be excited again to the $B^3\Pi$ state is considerably increased. There are then observed enhanced intensities and a rapid decay of the after-

¹⁴ In the case where the active nitrogen is flowing through the heated (or cooled) portion of the tube, the decrease (or increase) of intensity of the glow due to the local reduction (or increase) of density of normal atoms and molecules must be taken into consideration.

glow bands, while there is no displacement of the maximum of intensity towards the longer wave-lengths.¹⁴

The reason the intensity of the visible afterglow is considerably reduced in the case where a weak electric discharge is being passed through the active nitrogen, may be that a recombination of the atoms which take part in the triple collisions⁸ is taking place.

It is probable that in the case where a very weak current is passed through ordinary nitrogen, there is a concentration of electrons which has sufficient energy to produce the $B^3\Pi$ molecules with vibrational quantum number ~ 6 by the single collision with the nonvibrating normal $X'\Sigma$ molecules, so that the molecules in that vibrational level will be more concentrated than those in the level with $v' = \sim 11$, because the latter are excited from the $A^3\Sigma^{(7 \text{ or } 8)}$ level indirectly. For this reason the bands emitted from the former, as the initial level of transition, will appear more enhanced than those from the latter, as the results of observations show.

As explained above, considering that the active nitrogen is essentially atomic nitrogen, and, making the two assumptions above stated, it seems, (without assuming the existence of the metastable atoms as Cario and Kaplan did) that all the observed results will follow as reasonable consequences of the Franck-Condon principle, as well as from the general properties of molecular spectra.

Jackson and Broadway¹⁵ consider that they have obtained from their experiment evidence of the presence of metastable nitrogen atoms in the $^2P_{1/2}$ state, but not of the normal 4S atoms. As triple collisions may possibly take place between three normal atoms, it is not unreasonable that such metastable atoms will be present in very small quantity. However, if there were only metastable molecules (8.2 volts) and metastable atoms in active nitrogen, it would be very hard to explain the main properties of it, for example, very long persistence of afterglow, the absence of resonance enhancements of the metallic lines due to these metastable molecules and metastable atoms, and the temperature effect, etc.

¹⁵ L. C. Jackson and L. F. Broadway, Proc. Roy. Soc. A127, 678 (1930).

The Origin of the Mercury Bands at 2480A

By J. GIBSON WINANS
University of Wisconsin

(Received October 19, 1932)

The group of eight mercury bands near 2480A was photographed under varied excitation conditions with the purpose of determining their origin. The source was a discharge through mercury vapor produced in a quartz tube through external electrodes by a low-voltage Tesla coil. Five tubes containing distilled mercury and commercial mercury arc lamp showed this group of bands. These bands were weakened by heat along with known mercury bands. The origin is undoubtedly some form of mercury molecule. The most probable forms are Hg_2^+ and Hg_2 . Five observations favor Hg_2^+ over Hg_2 . (1) These bands have never been observed in fluorescence. (2) The 2476 band is more intense than the 2345 Hg_2 band under strong field excitation but weaker than 2345 under low field excitation. (3) No other bands with properties like those of the 2480 group have been observed in the mercury spectrum and Rayleigh has shown that these bands do not occur in absorption. (4) The bands in this group may be classified as sequences $v'-v''=0 \pm 1 \pm 2 \pm 3$, and a lower limit for D of 0.3 volts estimated. (5) In the $v'-v''=0$ sequence, emission is observed from state $v'=41$ indicating molecules with very high vibrational energy. This energy may be supplied by the electric field if the emitter is an ion but not if it is a neutral molecule.

INTRODUCTION

THE spectrum of a discharge through mercury vapor shows a group of eight bands near 2480A whose origin has been uncertain. These bands are shown in Fig. 1. The most intense band of the group with sharp limits at 2476 and 2482 and a fainter one between 2470 and 2476 were discovered

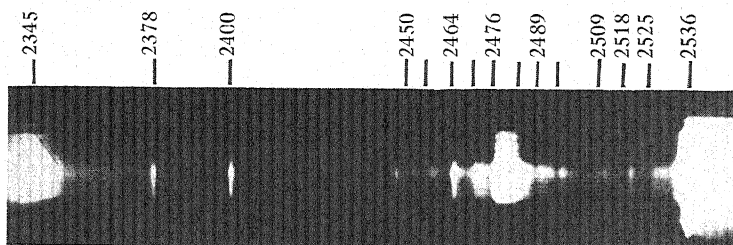


Fig. 1. Mercury bands near 2480A.

by Stark and Wendt¹ who described them as continuous. These bands were observed also by Nagaoka² in the light from a special type of mercury arc. Bands will be referred to by their short wave edges. Pienkowski³ observed some flutings in the 2476 band and Rayleigh⁴ showed that the flutings con-

¹ J. Stark and G. Wendt, *Phys. Zeits.* **14**, 562 (1913).

² H. Nagaoka, *Japanese Jour. Phys.* **1**, 1 (1922).

³ St. Pienkowski, *Bull. de l. Acad. Pol.* **171** (1928).

⁴ Rayleigh, *Proc. Roy. Soc. A* **782**, 349 (1928).

verged toward shorter wave-lengths. Rayleigh also observed that neither 2476 nor 2470 were absorption bands and that 2470 was either continuous or had flutings much more closely spaced than 2476. Condon⁵ suggested that 2476 might be a "diffraction band" of Hg_2 and showed that the frequencies of the flutings followed the law of convergence calculated for diffraction bands. The intensities, however, did not decrease exponentially as predicted. Miss Brozowska⁶ obtained photographs using a spectrograph of 14/mm dispersion and showed that the flutings of 2476 converged according to the equation

$$\nu = A + Cm(m + 1)$$

like the lines in the Q branch of a single band. From her photometer record, reproduced in Fig. 2, it is seen that the flutings are broad in the center and double near the long wave side. Miss Brozowska observed three bands in addition to 2476 and 2470 with short wave edges at 2458, 2450, and 2464. The short wave limit for the 2464 band was hidden by a mercury arc line. She suggested HgH as a possible emitter.

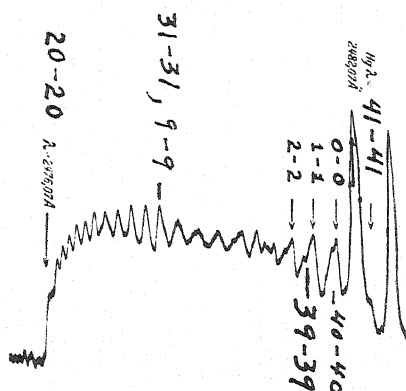


Fig. 2. Flutings of 2476.

These five bands and three new ones were observed by the writer⁷ in the spectrum of an electrodeless discharge through mercury vapor. The new bands have short wave edges at 2495.6, 2489.2, and 2482. They are shown in Fig. 1. The edge of the 2482 band was covered by a mercury arc line.

The entire group of eight bands was observed independently by Hamada⁸ in the spectrum emitted from the hollow cathode of a discharge tube filled with mercury vapor. He found in addition two new bands whose wave-lengths at the maxima he gives as 2504 and 2513.

In the following experiments this group of bands has been studied under varied excitation conditions with the purpose of determining their origin.

⁵ E. U. Condon, *Phys. Rev.* **32**, 858 (1928).

⁶ Miss J. Brozowska, *Zeits. f. Physik* **63**, 577 (1930).

⁷ J. G. Winans, *Phys. Rev.* **38**, 583 (1931).

⁸ H. Hamada, *Phil. Mag.* **22**, 50 (1931).

APPARATUS

The apparatus for these experiments consisted simply of an evacuated quartz tube containing mercury, a low power Tesla coil, and small quartz spectrograph (Hilger E31). Wires were wrapped about each end of the quartz tube, one was grounded and the other was connected to the Tesla coil. The optimum vapor pressure for band emission was maintained by a furnace or by Bunsen burners. In all, five tubes were used, two of which had plane windows and could be viewed end on. Each tube was baked out in a vacuum, a drop of mercury was distilled into it and it was sealed off. The tubes were prepared at different times from different samples of mercury. Sufficient intensity was obtained to photograph the 2476 band in the third order of a 21 foot grating with slit width 0.03 mm and exposure of one week. Exposures with the small quartz spectrograph were made with a very small image of the discharge tube focussed for $\lambda 2480$ on the slit. In this way the light from different parts of the discharge could be compared with a single exposure.

All five tubes gave the bands shown in Fig. 1 and listed in Table I. The wave-lengths agree with those given by Hamada⁸ with the exception of 2518

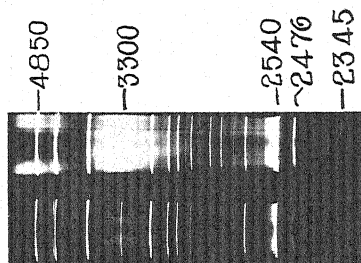


Fig. 3. Effect of heat on mercury bands.

and 2509. Hamada gives 2513 and 2504. He does not list any corresponding to 2525. The discharges also showed a continuous spectrum from 2536 to 2345 with a minimum at 2410. This may be seen in Fig. 1. Some of the tubes gave the HgH bands at 4219, 4017, and 3728 and others did not. The HgH bands when present were emitted only in the neighborhood of the electrodes.

The effect of heat without change in pressure on these bands is shown in Fig. 3 taken while a section of the discharge tube near the center was heated with a blow torch. The central part of the spectrum shows the light emitted by the heated part. Heat was found to weaken the bands at 2495, 2489, 2482, 2476, 2470, 2456 of the 2480 group in addition to the Hg₂ bands with maxima at 4850, 3300, 2650, 2540, and 2345. The others listed in Table I were too weak to be studied in this way. The effect on the 4850 and 3300 bands is the same as that observed in fluorescence.⁹ This assures that the weakening is due to heat and not to a change in discharge conditions.¹⁰

A photometer record of the plate taken on the 21 foot grating verified the structure of 2476 observed by Miss Brozowska and shown in Fig. 2.

⁹ H. Niewodniczanski, *Zeits. f. Physik* **49**, 59 (1928).

¹⁰ J. G. Winans, *Phys. Rev.* **39**, 745 (1932).

TABLE I.

	Short wave limits		$\Delta\nu$	$\nu' - \nu''$	Intensity
	λ	$\nu \text{ cm}^{-1}$			
1	2525.4	39,586			3
2	2518.0	39,702	116		3
3	2509.4	39,838	136		2
4	2495.6	40,059	221	-3	3
5	2489.5	40,157	98	-2	4
6	2482	40,278	121	-1	5
7	2476.07	40,375	97	0	10
8	2469.5	40,482	107	1	5
9	2464	40,572	110	2	3
10	2458.0	40,671	99	3	3
11	2449.5	40,812	141		1

To observe these bands under excitation fields of different strength, one set of photographs was made with the Tesla coil disconnected from the discharge tube and operated at different distances from the tube in air. Excitation of the discharge by strong or weak fields could be obtained by changing the distance between the Tesla coil and the discharge tube. Fig. 4, No. 1 shows that for weak fields the 2345 Hg_2 band and the 2536 line are much stronger than the 2476 band. Fig. 4, No. 2 shows that for strong fields 2476 was more intense than 2345.

Fig. 4, Nos. 3 and 4 give a comparison of the spectra from an ordinary mercury arc with that from a high-frequency discharge. Fig. 4, No. 3 is the spectrum of the mercury arc. Fig. 4, No. 4 is the spectrum obtained by shutting off the arc and operating a high-frequency discharge through the arc chamber while it was cooling. No. 4 shows bands while No. 3 does not, although the vapor pressure for No. 3 was greater than that for No. 4. The exposure for No. 3 was about 0.01 that for No. 4.

DISCUSSION

The origin of the group of bands near 2480 can be definitely taken as some form of mercury molecule, since it was observed in six different tubes containing pure mercury in the present experiments and by other experimenters in previous experiments. This is indicated also by the fact that heat, which is known from the experiments of Koernicke,¹¹ and Kuhn and Freudenberg¹² to reduce the number of mercury molecules causes a weakening of this group of bands along with the mercury bands at 4800, 3300 and 2345. HgH is very unlikely to be the emitter since known HgH bands were found to

¹¹ E. Koernicke, *Zeits. f. Physik* **33**, 219 (1925).

¹² H. Kuhn and K. Freudenberg, *Zeits. f. Physik* **76**, 38 (1932).

differ greatly in intensity relative to the 2476 band in different tubes and at different parts of the discharge. The most probable forms of mercury molecule are Hg_2 and ionized Hg_2 (Hg_2^+). Five observations favor Hg_2^+ over Hg_2 as the emitter.

(1) The 2476 mercury band has never been observed in fluorescence. All of the known Hg_2 bands from $\lambda 7000$ – 2000 as well as most of the mercury arc lines have been observed in fluorescence with no trace of 2476.^{13,14} This indicates that 2476 requires more energy than is available in a fluorescence tube in air, i.e., more energy than that needed for Hg_2 bands and Hg arc lines. This favors Hg_2^+ over Hg_2 as the emitter.

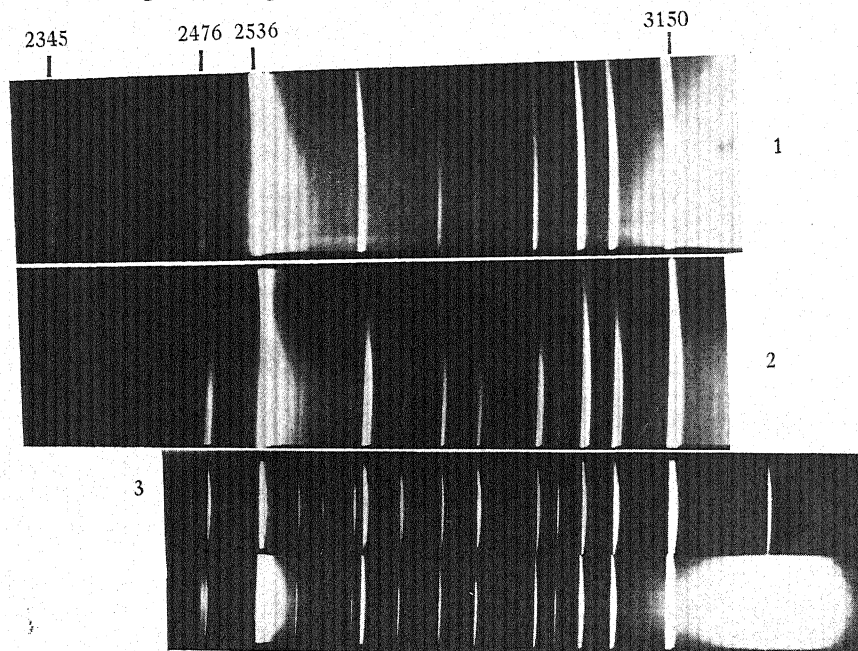


Fig. 4. No. 1 discharge under weak field, No. 2 discharge under strong field, No. 3 mercury arc, No. 4 discharge through mercury arc lamp.

(2) The comparison of intensities of the 2345 Hg_2 band and 2476 under strong and weak field excitation showed that 2476 although of longer wavelength required more energy for excitation than 2345. This also indicates Hg_2^+ instead of Hg_2 as the emitter of 2476.

(3) Rayleigh observed that 2476 is not an absorption band, and no other groups of bands similar to the 2480 group have been observed in the mercury spectrum. If 2476 were due to Hg_2 and not to Hg_2^+ it must be emitted by a transition to a final state which dissociates into one mercury atom in the normal state and one excited to 2^3P_0 or some state of greater energy. The initial molecular state for 2476 would dissociate into one 1^1S atom and an

¹³ R. W. Wood and V. Voss, Proc. Roy. Soc. A119, 698 (1928).

¹⁴ Rayleigh, Proc. Roy. Soc. A137, 101 (1932).

excited atom of 9.7 or more volts energy if D' is approximately equal to D'' . The ionization potential of mercury is 10.4 volts. An atomic state of energy greater than 9.7 volts would lie near the series limit and be one of a large number of similar states. Each of these atomic states would be associated with molecular states and we should observe many bands of character like 2476 instead of only one. Since only one is observed, its origin is very unlikely to be Hg_2 or $D'' \ll D'$ for 2476.

(4) The flutings in the 2476 band are too widely spaced to be rotational lines of Hg_2 or Hg_2^+ .¹⁵ Each fluting must then represent an unresolved band and each member of the 2480 group a sequence of bands. To account for the sharp short wave edge, 2476 must be a sequence which turns back on itself forming a head of bands like those observed in sodium vapor by Loomis and Nile.¹⁶ This point of view explains the intensity distribution, diffuseness, and doubling of flutings shown in Fig. 2. Near the head of the sequence two bands coincide to give sharp intense flutings, near the center they are separated enough to cause diffuseness, and near the long wave edge they are resolved into one strong and one weak component. If the strongest fluting is taken as band 0-0, the weakest is 41-41. If 2476 is taken as the $v'-v''=0$ sequence, the other bands in the 2480 group may be classified as the sequences $v'-v'' = \pm 1 \pm 2 \pm 3$ as shown in Table I. The narrow wave-length range of these sequences indicates that $r_e' - r_e''$ and, if Bates and Andrews relation holds,¹⁷ $D' - D''$ are small. This strengthens the conclusion from observation (3).

Assuming this classification, a lower limit for D may be estimated. Band $v'-v''=3-0$ falls in the narrow sequence 2458 with wave number about 40670. By subtracting from this, the wave number of $v'-v''=0-0$ gives the energy of the third vibration level of the excited molecule as about 380 cm^{-1} . From this $\omega_e' > 125 \text{ cm}^{-1}$. If ω converges linearly with v' the average separation of vibration levels is $> 60 \text{ cm}^{-1}$. Since emission is observed from $v'=41$, D must be $> 2460 \text{ cm}^{-1}$ or 0.3 volts.

(5) On the basis of the classification given above, emission by molecules in state $v'=41$ (vibration energy greater than 0.3 volts) is observed. This favors Hg_2^+ over Hg_2 as the emitter since a charged molecule may acquire high vibration energy from its motion in the electric field. A neutral molecule will possess vibration energy more nearly corresponding to the temperature of the vapor. If $r_e' - r_e''$ is large a neutral molecule might possess high vibrational energy immediately after excitation and emit radiation from that state, but when $r_e' - r_e''$ is small as for 2476, this possibility does not exist.

Each of the five observations discussed indicates that the emitter of the 2480 group of mercury bands is Hg_2^+ .

There are several other observations of interest which remain to be explained. They are (1) The 2470 band sequence has no flutings. This may mean that the flutings do not coincide sufficiently well for resolution. (2) The clas-

¹⁵ Assume $r_e=4.4$ and the energy difference between the first two rotational states is 0.005 cm^{-1} . The smallest separation between flutings is 1.5 cm^{-1} .

¹⁶ F. W. Loomis and S. W. Nile, *Phys. Rev.* **32**, 873 (1928).

¹⁷ J. R. Bates and D. H. Andrews, *Proc. Nat. Acad. Sci.* **14**, 124 (1928).

sification given above accounts for only seven of the eleven bands listed in Table I. Bands 1, 2, and 3 in Table I resemble somewhat bands 7, 8, and 9 and may be another group of sequences of Hg_2^+ . (3) There is a continuous spectrum between 2536 and 2345 with a minimum near 2410. The regions between 2536 and 2410 and between 2400 and 2345 fall just beyond the limits for the 2^3P_2 and 2^3P_1 sharp and diffuse series of Hg. The continuous spectrum is probably the recombination spectra associated with these series. (4) The high-frequency discharge gave greater intensity of bands relative to lines than the mercury arc operated at greater pressure. A possible explanation is that collisions with high-velocity ions destroyed Hg_2 molecules in the arc more than in the discharge because of the greater concentration of ions in the arc.

The explanations suggested here for these last four observations need verification by further experiments.

The writer wishes to thank Professor R. S. Mulliken for suggesting the interpretation of the spectrum as a set of band sequences.

The Auroral Spectrum

By JOSEPH KAPLAN
University of California at Los Angeles

(Received October 24, 1932)

The first-negative bands of nitrogen, which comprise most of the nitrogen radiation in the auroral spectrum, have been excited under conditions which suggest those in the aurora very closely. Active nitrogen is produced in uncondensed discharges in concentrations sufficient to give a strong visible glow. A very strong flash is observed at the beginning of the afterglow, and this flash indicates a high concentration of active material in the exciting discharge itself. Under the best conditions for the production of the afterglow the spectrum of the exciting discharge consists almost entirely of the first-negative bands. The most important characteristic of these bands, as excited under the present conditions, is the absence of lines due to N^+ . The usual excitation of the N_2^+ bands in discharges at low pressures produces these lines, whereas they are almost entirely absent in the auroral spectrum. The excitation of N_2^+ bands in the present experiments is thought to be due to the large concentration of metastable nitrogen molecules in the $A(^3\Sigma)$ state, and this experiment is presented as a proof of their presence in both the aurora and in nitrogen afterglows.

I. INTRODUCTION

RECENT discussions of the origin of the Aurora Borealis have aroused considerable interest in the problems associated with this beautiful and startling phenomenon. Of special interest is the ultraviolet light theory which was proposed by E. O. Hulburt and H. B. Maris¹ in 1929. According to that theory, the auroral displays are caused by blasts of ultraviolet light from the sun which ionize the atoms of the upper atmosphere. These ions are carried to the polar regions where they recombine and emit the auroral radiations. The earlier theories of Birkeland, Störmer and Vegard suggested that the aurora was due to charged particles from the sun which are diverted to polar regions by the earth's magnetic field, and then their energy is given to the atmosphere and converted into auroral radiation. In their paper on auroras and magnetic storms Maris and Hulburt suggested that a complete theory of auroras "will require, among other things, complete knowledge of the energy levels, metastable states and transition probabilities of the atmospheric atoms and molecules, as well as of the exact processes which give rise to the aurora light." It is the purpose of this short paper to make a contribution to that phase of the problem.

The spectrum of the aurora consists in most part of the green aurora line, due to atomic oxygen, and of the first-negative bands, due to N_2^+ . Other bands have been reported in the auroral spectrum, which are members of the second-positive and the first-positive groups of N_2 , but in general these radiations are very weak in comparison with the green line and the negative bands.

¹ Maris and Hulburt, *Phys. Rev.* **33**, 412 (1929).

The green aurora line has been studied with great success in recent years, and much has been written about it. In the present paper we will describe experiments in which the negative nitrogen bands have been studied. Because of the enormous interest shown in the green line, not much work has been done on the study of the conditions of excitation of the negative bands. We have succeeded in exciting them under conditions which suggest the actual auroral conditions so closely that it will be tempting to conclude that we have reproduced the auroral conditions.

II. EXPERIMENTAL METHOD

The experimental method used in this work was a rather unusual one. Active nitrogen was produced by passing an electrical discharge through nitrogen at pressures ranging from 5 to 10 mm, not from the condensed discharge source usually employed in active nitrogen experiments, but from an ordinary uncondensed discharge from two 1-kw, 25,000-volt Thordarssen transformers. In all other experiments of which the writer is aware active nitrogen has been produced by passing a condensed discharge through nitrogen at a pressure of about 0.5 mm or by using an electrodeless discharge at pressures around 0.01 mm. An uncondensed discharge through a tube containing nitrogen will in general not produce active nitrogen in quantities sufficient to show a visible glow. In the present experiment this was not the case. It was possible to produce a strong visible glow in nitrogen even with an uncondensed discharge.

In the present experiments the tube was filled with nitrogen, and a small amount of oxygen was added. Then the tube was run steadily for several days during which the oxygen was gradually cleaned up. At first, the afterglow was the green continuous glow which is so readily produced by an uncondensed discharge in oxygen-nitrogen mixtures. As the oxygen was cleaned up this glow disappeared, and the afterglow due to active nitrogen appeared with increasing intensity. It is interesting to note the continuous transition between the two types of glow. The long running of the tube undoubtedly conditioned the surface of the tube in such a way as to allow it to adsorb nitrogen atoms. These adsorbed atoms react with other nitrogen atoms which collide with the wall, and the production of the visible afterglow is made possible. More will be said about this in a forthcoming paper on active nitrogen. The novelty of the present experiment is in the extremely long treatment of the tube, which finally resulted in walls which were more favorable for the production of the visible glow than those in previously reported experiments. It is difficult to account for the production of the afterglow in an uncondensed discharge in any other way. The strong afterglow in uncondensed discharges has probably been missed by others because of insufficient treatment of the discharge tubes. A condensed discharge will produce a strong afterglow in tubes in which an uncondensed discharge produces a very weak glow, hence experimenters have resorted in general to condensed discharges for the production of active nitrogen. So much, however, for the preparation of the tube. We will now discuss the actual aurora experiments.

The spectra in which we are interested were photographed in the bulb part of a discharge tube consisting of a 500 cc Pyrex bulb and a short length of 1 mm capillary tubing, and the usual large internal aluminum electrodes. The afterglow in the bulb showed a peculiar behavior which the present writer has never observed before. For a very short time after the exciting discharge was interrupted, the glow consisted of an extremely intense flash, much more intense than the afterglow which followed the flash. The writer has seen this "flash glow" hundreds of times, and there is absolutely no question of its existence. The flash was followed by the usual type of steadily decaying afterglow.

It was observed that when the afterglow in the bulb showed the short-lived flash (and this occurred only at the end of a very long treatment of the tube), the spectrum of the exciting discharge consisted of the first-positive bands of nitrogen, the negative bands of N_2^+ and the second-positive bands of N_2 . The more intense the afterglow became, the more thoroughly were the second-positive bands quenched. By not running the tube steadily, but by making and breaking the current about once a second, it was possible to almost completely quench the second-positive group and to weaken the first-positive bands relative to the negative bands. Under the best conditions, the spectrum of the discharge in the bulb part of the tube consisted almost entirely of the negative bands. The plate was exposed to the light from the bulb during the entire "make," and for that reason the spectrum contained more of the second-positive group than if the exposures had been limited to the later part of the make. This could readily be seen by noticing that the second-positive bands flashed up and then died down during the first part of the make. Evidently the condition, which is responsible for the presence of the negative bands, is being produced during the first part of the discharge, and hence is not as steady as it is during the rest of the discharge time.

The spectra which are reproduced will show that some very striking changes have taken place in the nature of the electric discharge as the intensity of the afterglow increases. The spectrum of a discharge in N_2 in which no afterglow is produced consists of the first-positive and the second-positive bands. There is practically no sign of the negative bands. As a rule, the negative bands are produced with high intensity in discharges at pressures of 10^{-2} to 10^{-3} mm, and then they are accompanied by lines due to N^+ . The presence of a strong afterglow changes the spectrum entirely. The spectrum of N_2^+ is now produced at a relatively high pressure and it is not associated with the strong line spectrum of N^+ which is present at low pressures. The first negative bands of the auroral spectrum are also excited without the strong excitation of the N^+ line spectrum. A comparison of the results of the present experiments with actual auroral spectra will show the remarkable resemblance between the two. The absence of the line spectrum of N^+ in the present experiment and in the auroral spectra is probably the most important point of resemblance between the two. These results are shown in Fig. 1.

When the current in the tube is diminished to about one-third of the value

at which the negative bands are produced, the afterglow is of course a very weak one, the negative bands are weak, and the first-positive bands appear with definite maxima in bands arising on B_{10} and B_6 . The 6323 band, corresponding to $B_{10}-A_7$, has been reported in auroral displays, and considerable discussion has taken place recently regarding Vegard's² observations of infrared bands in the aurora which are identified as transitions $B_7 \rightarrow A_6$. The B_6 maximum is quite strong in the negative glow of a discharge tube, and is often prominent in very red nitrogen discharges. The strong excitation of the B_{10} level in the same tube in which the N_2^+ bands appear is a very significant result for an understanding of the auroral spectrum.

III. DISCUSSION

The most significant characteristic of a nitrogen afterglow, for our present discussion, is the presence in it of molecules in the metastable $A(^3\Sigma)$ state. The reader will be referred to papers on active nitrogen for evidence regard-

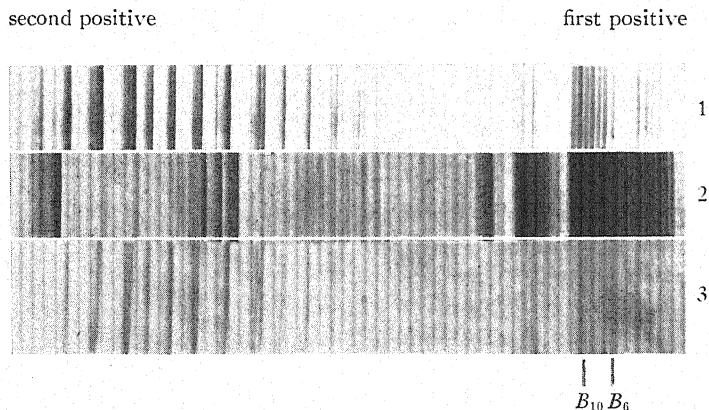


Fig. 1. Spectrum 1, normal excitation of N_2 ; spectrum 2, excitation in an active nitrogen producing discharge; spectrum 3, enhancement of bands which originate on B_6 and B_{10} .

ing the existence of metastable nitrogen molecules in the afterglow. In auroral displays metastable molecules will accumulate as a result of the excitation processes which are responsible for the aurora. The only mechanism for the destruction of metastable molecules in the upper atmosphere is collision with some other particle, whereas in laboratory discharges there is undoubtedly considerable destruction of metastable molecules at the walls. In a tube in which the afterglow is very strong there is a rapid production of metastable molecules, and hence a comparison between the upper atmosphere and such a tube is a reasonable one.

The excitation of the negative bands in these experiments can be explained in a very simple manner. It is only necessary to postulate that the light, emitted in a discharge in which there is a relatively high concentration of metastable molecules, is due to the direct excitation of these molecules by

² Vegard, *Nature* **129**, 468 (1932). Jevons, *Nature* **129**, 754 (1932).

electron impact in the discharge rather than to the excitation of normal nitrogen molecules. Thus, a process which in ordinary tubes is a secondary process, and hence very rare, now becomes quite frequent. The present experiment can be presented as a new proof of the existence of metastable molecules in active nitrogen. The metastable nitrogen molecules in the aurora are probably produced in the same way as in an active nitrogen tube; i.e., during the recombination of atomic nitrogen.

The unusual excitation of the levels B_{10} and B_6 in the same tube as the negative bands, but with weaker currents, gives us a very complete reproduction of the nitrogen part of the auroral spectrum. The existence of streamers and curtains in auroral displays, and their rapid motion, are indications of the unsteady nature of the phenomenon, and they may well be due to variations in an electrical current which is responsible for the excitation of the auroral display. That idea would fit in well with the present results.

This hasty account of the present experiments will be extended in the near future. The role of metastable nitrogen molecules will be discussed both for the aurora and for the light of the night sky. As a result of the present work we are tempted to conclude that the auroral display is really an electrical discharge in a nitrogen-oxygen mixture in which metastable molecules abound. There is, however, a better time for such a conclusion, namely, after more experiments have been performed.

Theory of Vibrational Isotope Effects in Polyatomic Molecules

By E. O. SALANT AND JENNY E. ROSENTHAL
New York University

(Received October 28, 1932)

Following Dennison's general, noncentral force treatment of the normal modes of vibration of symmetrical triatomic and tetratomic molecules, we derive expressions for the effects of isotopy on the normal frequencies. The isotope effect of any particular normal frequency depends on and may serve to evaluate the force constants of the molecule, but sums of certain isotope effects are independent of the constants. For triatomic molecules, the isotope effect of the vibration perpendicular to the symmetry axis depends on the value of the apex angle of the molecule. The sum of the isotope effects of the parallel vibrations is calculable from the masses alone. Definite criteria of collinearity of the molecule from isotope effects are given. For tetratomic molecules, the sum of isotope effects of vibrations parallel to the altitude of the molecular pyramid is calculable from the masses alone, the sum of isotope effects perpendicular to the altitude from the masses and from the ratio of the altitude to the length of side of the triangular base. Whereas the molecule YX_3 has four distant normal frequencies of vibration, it is shown that replacement of one of the X atoms of mass m by an atom of mass $m + \Delta m$ removes the degeneracy of the motion, the resulting molecule having six normal frequencies of vibration. Special relations between the various isotope effects serve as criteria for co-planar molecules.

INTRODUCTION

THERE have been few investigations, experimental or theoretical, of isotope effects in band spectra of polyatomic molecules, the most outstanding being the studies of the vibrational effects in the electronic bands of chlorine dioxide, made by Goodeve and Stein¹ and by Urey and Johnston.² Besides the interest of the isotope effects themselves, Urey and Johnston showed them to be of value as an aid in the assignment of certain spectral frequencies to particular modes of vibration of the ClO_2 molecule.

This they accomplished by comparing the measured isotope effects with those calculated from their expressions for the effects of isotopy of the Y atoms on the normal vibrations of symmetrical triatomic molecules YX_2 ; the expressions were derived from equations of Bjerrum³ for the normal vibrations of symmetrical triatomic molecules, Bjerrum's equations having been based upon the special assumption of valence forces.

It is our purpose here to begin with the more general noncentral force equations of Dennison⁴ for the vibrations of polyatomic molecules and to derive therefrom expressions for the isotope effects of the normal frequencies. We shall obtain equations for the effects of isotopy of the Y atoms, and also of the X atoms, in symmetrical triatomic molecules YX_2 and symmetrical

¹ C. F. Goodeve and C. P. Stein, *Trans. Faraday Soc.* **25**, 736 (1929).

² H. C. Urey and H. Johnston, *Phys. Rev.* **38**, 2131 (1931).

³ N. Bjerrum, *Verh. d. deutsch. phys. Ges.* **16**, 737 (1914).

⁴ D. M. Dennison, *Rev. Mod. Phys.* **3**, 280 (1931).

tetratomic molecules YX_3 ; we have already referred briefly to some of the results of this study.⁵ In Dennison's treatment, it may be recalled, knowledge of the quantitative values of the force constants is quite unnecessary to determine the directions of the displacements with respect to the molecular axis of symmetry, the character of the vibrations following from the basic postulate that the potential energy follows the geometrical symmetry of the molecule.

Besides the assumptions of Dennison's theory, we assume also that, as for diatomic molecules, the forces involved are invariant for an isotopic change of mass. We shall denote the mass of the Y atom by M and the mass of an X atom by m and shall call effects due to isotopes of Y atoms "central isotope effects" and effects due to isotopes of X atoms "end isotope effects." We treat the ratios $\Delta m/m$ and $\Delta M/M$ as small, consequently our results do not apply to isotopes of H atoms.

The general method outlined by Dennison for describing the potential energies T and V will be followed, the normal frequencies ω_i being given by the roots λ_i of the determinantal equation

$$\text{and} \quad \left. \begin{aligned} |\lambda T - V| &= 0 \\ 4\pi^2\omega_i^2 &= \lambda_i \end{aligned} \right\}. \quad (\text{I})$$

The roots and frequencies of molecules $Y^{(M)}X_2^{(m)}$ and $Y^{(M)}X_3^{(m)}$ will be denoted by λ_i and ω_i , the roots and frequencies of molecules having one or more atoms $Y^{(M+\Delta M)}$ or $X^{(m+\Delta m)}$ will be denoted by λ_i^* and ω_i^* . The isotope shift $\Delta\omega_i$ of the normal frequency of vibration ω_i will then be given by

$$\Delta\omega_i/\omega_i = \frac{1}{2}(\lambda_i^*/\lambda_i - 1). \quad (\text{II})$$

Since, as has been shown by Dennison,⁶ the expressions for the transition probabilities of the normal vibrations involve the masses, an isotopic change of mass will affect the Einstein coefficients as well as the frequencies. We regard such effects as small, however, and certainly inextricable from the tangle of polyatomic band lines.

The relative intensities of bands due to the same vibration in molecules differing only in their isotopes will, of course, be determined principally by the relative abundance of the isotopes. Relative abundance of molecules $Y^{(M)}X_n$ and $Y^{(M+\Delta M)}X_n$ will be the same as the relative abundance of the isotopes of the Y atoms. Relative abundances in the cases of isotopes of X atoms are, if the relative abundance of $X^{(m)}$ to $X^{(m+\Delta m)}$ is b/a

$$YX_2^{(m)}:YX^{(m)}X^{(m+\Delta m)}:YX_2^{(m+\Delta m)} = 1:b/a:b^2/a^2$$

$$YX_3^{(m)}:YX_2^{(m)}X^{(m+\Delta m)}:YX^{(m)}X_2^{(m+\Delta m)}:YX_3^{(m+\Delta m)} = 1:b/a:b^2/a^2:b^3/a^3.$$

I. TRIATOMIC MOLECULES

We consider a molecule composed of three particles denoted 1, 2, 3, forming at equilibrium the corners of an isosceles triangle of apex angle 2α and

⁵ E. O. Salant and J. E. Rosenthal, *Phys. Rev.* **39**, 161 (1932).

⁶ D. M. Dennison, *Phil. Mag.* **1**, 195 (1926).

base $2a$, with particle 1 at the apex. Let q_1 be the change in relative displacement of the base particles 2 and 3, q_2 and q_3 the changes in relative displacements of the particles 1 and 2 and of the particles 2 and 3, respectively. The potential energy is then written:

$$V = \frac{1}{2} [K_1(q_2^2 + q_3^2) + K_2q_1^2 + K_3q_1(q_2 + q_3) + K_4q_2q_3] \quad (1)$$

where K_1, K_2, K_3, K_4 are constants (which may involve the angle).

We choose moving coordinates x, y with origin at the center of gravity of the molecule, and x -axis parallel to the direction 2→3, and define new variables q_1, u, v in this system (q_1 unchanged):

$$\left. \begin{aligned} q_1 &= \delta x_3 - \delta x_2 \\ u &= \delta x_1 - \frac{1}{2}(\delta x_2 + \delta x_3) = (q_3 - q_2)/2 \sin \alpha \\ v &= \delta y_1 - \frac{1}{2}(\delta y_2 + \delta y_3) = (q_2 + q_3 - q_1 \sin \alpha)/2 \cos \alpha \end{aligned} \right\} \quad (2)$$

δx_j and δy_j obviously referring to the displacements of the j -th particle. In these variables, the potential energy becomes

$$\left. \begin{aligned} V &= \frac{1}{2}(Aq_1^2 + Bu^2 + Cv^2 + 2Dvq_1), \\ \text{where } A &= (K_1/2) \sin^2 \alpha + K_2 + K_3 \sin^2 \alpha + (K_4/4) \sin^2 \alpha \\ B &= (2K_1 - K_4) \sin^2 \alpha \\ C &= (2K_1 + K_4) \cos^2 \alpha \\ D &= (K_1 + K_3/\sin \alpha + K_4/2) \sin \alpha \cos \alpha \end{aligned} \right\} \quad (3)$$

To obtain the expression for the kinetic energy of the vibrating molecule, we first transform to a fixed coordinate system X, Y in the same plane and with the same origin as the moving system,

$$X = x + \theta y; \quad Y = -\theta x + y$$

where θ denotes a small angle in the X, Y plane.

For the molecule $YX^{(m)}X^{(m+\Delta m)}$, let the Y atom be particle 1, $X^{(m+\Delta m)}$ particle 2, $X^{(m)}$ particle 3. Let

$$\mu = \frac{M}{2m + M}, \quad \mu^* = \frac{M}{2(m + \Delta m) + M}, \quad \rho = \frac{M}{2m + \Delta m + M}.$$

Then the transformation from Eq. (2) to the fixed coordinates and the expressions for the conservation of linear momentum lead to the following relations for the displacements $\delta X_j, \delta Y_j$ in the fixed system:

⁷ It is assumed that when $\cos \alpha = 0$; $C \neq 0$; hence $(2K_1 + K_4)$ involves α .

$$\left. \begin{aligned} \delta X_1 &= \left(\frac{2m + \Delta m}{M} \right) \rho(u + a\theta \cot \alpha) + \frac{\Delta m \rho}{2M} q_1; \\ \delta Y_1 &= \left(\frac{2m + \Delta m}{M} \right) \rho v - \frac{\Delta m \rho}{M} a\theta \\ \delta X_2 &= -\rho(u + a\theta \cot \alpha) - \frac{q_1}{2} \frac{\rho}{\mu}; & \delta Y_2 &= -\rho v + \alpha\theta \frac{\rho}{\mu} \\ \delta X_3 &= -\rho(u + a\theta \cot \alpha) + \frac{q_1}{2} \frac{\rho}{\mu^*}; & \delta Y_3 &= -\rho v + \frac{a\theta \rho}{\mu^*} \end{aligned} \right\}. \quad (4)$$

Writing down the expression for the kinetic energy and substituting for θ its value obtained from the condition $\partial T / \partial \dot{\theta} = 0$ (conservation of angular momentum), we may then write the kinetic energy letting $\epsilon = \Delta m / (2m + \Delta m)$

$$T = \left(\frac{2m + \Delta m}{4} \right) \left[2\rho(\dot{u}^2 + \dot{v}^2) + \dot{q}_1^2 + 2\rho\epsilon\dot{u}\dot{q}_1 - \frac{2\rho^2}{1 + \rho \cot^2 \alpha} \left(\dot{u} \cot \alpha + \frac{\epsilon \dot{q}_1}{2} \cot \alpha - \dot{v} \right)^2 \right]. \quad (5)$$

Neglecting all terms in ϵ^2 , none of whose coefficients are large, we then have

$$T = \left(\frac{2m + \Delta m}{4} \right) \left[2\rho \left(\frac{\dot{u}^2}{1 + \rho \cot^2 \alpha} + \dot{v}^2 \right) + \frac{\dot{q}_1^2}{2} + \frac{2\rho\dot{u}\epsilon}{1 + \rho \cot^2 \alpha} (\dot{q}_1 - 2\rho\dot{v} \cot \alpha) \right]. \quad (6)$$

From Eq. (I), (3) and (6), the vibrations λ_1^* , λ_2^* , parallel to the symmetry axis of the molecule, and the vibration λ_3^* perpendicular to the symmetry axis, are given by

$$\left. \begin{aligned} \left(\frac{2m + \Delta m}{2} \right)^2 \lambda^{*2} - \left(2A + \frac{C}{2\rho} \right) \left(\frac{2m + \Delta m}{2} \right) \lambda^* \\ + \frac{1}{\rho} \left(AC - \frac{D^2}{4} \right) &= 0 & (a) \\ \lambda_3^* &= \frac{B(1/\rho + \cot^2 \alpha)}{2m + \Delta m} & (b) \end{aligned} \right\}. \quad (7)$$

By setting $\Delta m = 0$, Eqs. (7) reduce to the known expressions for the normal frequencies of the molecule $YX_2^{(m)}$

$$\left. \begin{aligned} m^2 \lambda^2 - (2A + C/2\mu)m\lambda + (1/\mu)(AC - D^2/4) &= 0 & (a) \\ \lambda_3 &= B(1/\mu + \cot^2 \alpha)/2m & (b) \end{aligned} \right\}. \quad (8)$$

For a collinear molecule, $D=0$ and $\cot \alpha=0$, Eqs. (7) reducing to

$$\left. \begin{aligned} \lambda_1^* &= \frac{4A}{(2m + \Delta m)}; \lambda_2^* = \frac{C}{\rho(2m + \Delta m)} & (a) \\ \lambda_3^* &= B/(2m + \Delta m)\rho & (b) \end{aligned} \right\} \quad (7')$$

(a) Central isotope effects, molecules $Y^{(M)}X_2^{(m)}$ and $Y^{(M+\Delta M)}X_2^{(m)}$

The vibrations of molecules $Y^{(M+\Delta M)}X_2^{(m)}$ will be described by relations obtained by substituting $M+\Delta M$ for M in Eqs. (8). With these equations and with Eqs. (I), (II), and (8), we have the following relations for central isotope effects:

$$\frac{\Delta\omega_1}{\omega_1} = \frac{(8\pi^2 m \mu \omega_2^2 - C)\Delta M}{8\pi^2(\omega_1^2 - \omega_2^2)M^2} \quad (9)$$

$$\omega_1\Delta\omega_1 + \omega_2\Delta\omega_2 = -C\Delta M/8\pi^2 M(M + \Delta M) \quad (10)$$

$$\frac{\Delta\omega_1}{\omega_1} + \frac{\Delta\omega_2}{\omega_2} = \frac{-m\Delta M}{(M + \Delta M)(2m + M)} \quad (11)$$

$$\frac{\Delta\omega_3}{\omega_3} = \frac{-m\Delta M}{M(M + \Delta M)(1/\mu + \cot^2 \alpha)} \quad (12)$$

Thus, whereas the isotope effect $\Delta\omega_1/\omega_1$ or $\Delta\omega_2/\omega_2$ of either parallel vibration depends on the force constants of the molecule and may have different values in the different electronic states, their sum has a constant value, calculable from the masses alone, for all electronic states. Obviously this relation, Eq. (11), provides a means of assigning bands to particular modes of vibration.

The isotope effect of the perpendicular vibration, $\Delta\omega_3/\omega_3$, may be used to evaluate the molecular angle 2α ; before this can be done, however, it must be known that the frequency being so used is actually the perpendicular frequency, information which will have to come from other data, such as intensities.

For a collinear molecule ($2\alpha=180^\circ$, $D=0$), we have

$$\left. \begin{aligned} \Delta\omega_1 &= 0 \\ \frac{\Delta\omega_2}{\omega_2} &= \frac{\Delta\omega_3}{\omega_3} = \frac{-m\Delta M}{(M + \Delta M)(2m + M)} \end{aligned} \right\} \quad (13)$$

a relation that may be used to determine whether or not a given molecule is collinear.

Since change in electronic state may be accompanied by change in the molecular angle, it is of interest to consider how this will affect the isotope effects. Consider $\Delta M > 0$. When the molecule is collinear, the inactive frequency ω_1 shows no isotope effect, the isotope effect $\Delta\omega/\omega$ of each active frequency is the same and negative. As the molecule bends away from a straight line, the perpendicular isotope effect takes on smaller absolute values, ap-

proaching zero as the equilibrium positions of the two X atoms approach each other. The absolute value $|\Delta\omega_1/\omega_1|$ increases, but without knowledge of the force constants, it cannot be predicted whether $\Delta\omega_1/\omega_1$ will be positive or negative; the change in $\Delta\omega_1/\omega_1$ will be in the opposite direction to the change in $\Delta\omega_2/\omega_2$, of course, in virtue of (11) and (13).

TABLE I. Triatomic molecules. Calculated values of some central isotope effects.

2α	ClO_2	MgI_2	SO_2	H_2S
	$m=16$	127	16	1
	$M=35$	24	32	32
	$\Delta M=2$	1	1	1
180°	$10^2(\Delta\omega_1/\omega_1 + \Delta\omega_2/\omega_2) - 1.293$	-1.82	-0.76	-0.089
150°	$10^2(\Delta\omega_3/\omega_3) - 1.293$	-1.82	-0.76	-0.089
120°	" -1.245	-1.81	-0.73	-0.083
90°	" -1.01	-1.77	-0.65	-0.068
60°	" -0.849	-1.68	-0.51	-0.046
	" -0.502	-1.43	-0.30	-0.023

In Table I are some values of $\Delta\omega_3/\omega_3$ as a function of the molecular angle, calculated for several different molecules, and also values of $\Delta\omega_1/\omega_1 + \Delta\omega_2/\omega_2$ for the same molecules. For $2\alpha = 180^\circ$, Eq. (13) holds.

A relatively heavy end (X) atom renders the perpendicular isotope effect comparatively insensitive to changes in the molecular angle, as may be seen by comparing the values of this effect for MgI_2 and any of the other molecules in the table. Consequently, the isotope effect will not be so reliable in following changes in the angle of molecules with a large m/M .

(b) End isotope effects

The isotope effects for molecules $Y^{(M)}X_2^{(m)}$ and $Y^{(M)}X^{(m)}X^{(m+\Delta m)}$ are easily obtained from Eqs. (I), (II), (7) and (8). Each parallel effect $\Delta\omega_1/\omega_1$ and $\Delta\omega_2/\omega_2$ depends on the force constants, but the sum of the parallel effects is independent of the interatomic forces:

$$\frac{\Delta\omega_1}{\omega_1} + \frac{\Delta\omega_2}{\omega_2} = \frac{-(\mu + 1)\Delta m}{2(2m + \Delta m)}. \quad (14)$$

The perpendicular isotope effect depends upon the molecular angle:

$$\frac{\Delta\omega_3}{\omega_3} = \frac{-(1 + \cot^2 \alpha)\Delta m}{2(1/\mu + \cot^2 \alpha)(2m + \Delta m)}. \quad (15)$$

For a collinear molecule

$$\mu \frac{\Delta\omega_1}{\omega_1} = \frac{\Delta\omega_2}{\omega_2} = \frac{\Delta\omega_3}{\omega_3} = \frac{-\mu\Delta m}{2(2m + \Delta m)}. \quad (16)$$

In Table II are calculated values of the perpendicular isotope effect for a few molecules and several angles.

It is seen that, contrary to the behavior of the central isotope effect, the end isotope effect of the perpendicular vibration increases as the angle di-

TABLE II. Calculated values of perpendicular end isotope effects.

2α , degrees	180	120	$10^2(\Delta\omega_3/\omega_3)$ 90	60	0
$\text{CS}_2^{(32)}, \text{CS}^{(32)}\text{S}^{(33)}$	-0.121	-0.154	-0.210	-0.340	-0.769
$\text{MgCl}_2^{(35)}, \text{MgCl}^{(35)}\text{Cl}^{(37)}$	-0.354	-0.436	-0.565	-0.802	-1.40
$\text{HgCl}_2^{(35)}, \text{HgCl}^{(35)}\text{Cl}^{(37)}$	-1.01	-1.08	-1.17	-1.27	-1.40

minishes, attaining its maximum value, for $\alpha = 0$ of

$$(\Delta\omega_3/\omega_3)_{\max.} = -\Delta m/2(2m + \Delta m).$$

The observation of the perpendicular isotope effect will be favored by a molecule with a small angle and heavy central atom.

By replacing m by $m + \Delta m$ in Eqs. (8), the normal vibrations of molecules $Y^{(M)}X_2^{(m+\Delta m)}$ are obtained. The isotope effects $\Delta\omega_i/\omega_i$ between these molecules and molecules $Y^{(M)}X_2^{(m)}$ are, to the first approximation, twice the value of the corresponding effects between molecules $Y^{(M)}X^{(m)}X^{(m+\Delta m)}$ and $Y^{(M)}X_2^{(m)}$.

II. TETRATOMIC MOLECULES

We consider a molecule composed of four atoms occupying, at equilibrium the corners of a regular pyramid of altitude c and length of side of triangular base a . We consider the Y atom, of mass M , at the apex, and denote its positions by subscript 4; we consider atoms X^* , X , X , with masses $m + \Delta m$, m , m , at the base, denoting their positions by subscripts 1, 2, 3, respectively.

Let $p_1, p_2, p_3, q_1, q_2, q_3$ be the changes in relative displacements of the respective particles, assumed small quantities of the first order, and write $f = (c^2 + a^2/3)^{1/2}$. Then, assuming that the potential energy has the geometrical configuration of the system, we have

$$V = \frac{1}{2} \{ K_1(q_1^2 + q_2^2 + q_3^2) + K_2(q_1q_2 + q_1q_3 + q_2q_3) + K_3(f^2/a^2)(p_1^2 + p_2^2 + p_3^2) + K_4(f^2/a^2)(p_1p_2 + p_1p_3 + p_2p_3) + K_5(f/a)(p_1q_1 + p_2q_2 + p_3q_3) + K_6(f/a)[p_1(q_2 + q_3) + p_2(q_1 + q_3) + p_3(q_1 + q_2)] \} \quad (17)$$

where the K 's are undetermined constants.

We now choose a system of axes, x, y, z with origin at the molecular center of mass and moving with the molecule, with x axis parallel to the 2-3 axis and x, y plane parallel to the 1, 2, 3 plane.

Then let

$$\left. \begin{aligned} \delta x_4 - \frac{1}{3}(\delta x_1 + \delta x_2 + \delta x_3) &= x; \delta x_1 - \frac{1}{2}(\delta x_2 + \delta x_3) = u; \delta x_3 - \delta x_2 = q_1 \\ \delta y_4 - \frac{1}{3}(\delta y_1 + \delta y_2 + \delta y_3) &= y; \delta y_1 - \frac{1}{2}(\delta y_2 + \delta y_3) = v; \delta y_3 - \delta y_2 = 0 \\ \delta z_4 - \frac{1}{3}(\delta z_1 + \delta z_2 + \delta z_3) &= z; \delta z_1 - \frac{1}{2}(\delta z_2 + \delta z_3) = 0; \delta z_3 - \delta z_2 = 0 \end{aligned} \right\} \quad (18)$$

and at equilibrium, we have

$$\left. \begin{aligned} x_4^0 - \frac{1}{3}(x_3^0 + x_2^0 + x_1^0) &= 0; x_1^0 - \frac{1}{2}(x_2^0 + x_3^0) = 0; x_3^0 - x_2^0 = a \\ y_4^0 - \frac{1}{3}(y_3^0 + y_2^0 + y_1^0) &= 0; y_1^0 - \frac{1}{2}(y_2^0 + y_3^0) = a(3)^{1/2}/2; \\ y_3^0 - y_2^0 &= 0 \\ z_4^0 - \frac{1}{3}(z_3^0 + z_2^0 + z_1^0) &= c; z_1^0 - \frac{1}{2}(z_2^0 + z_3^0) = 0; z_3^0 - z_2^0 = 0 \end{aligned} \right\} \quad (19)$$

where, of course, the superscript zero refers to the equilibrium positions. Then writing:

$$\begin{aligned} A &= \frac{1}{2}(K_3 - K_4/2) \\ B &= 3(c^2/a^2)(K_3 + K_4)^8 \\ C &= \frac{1}{4}\left(3K_1 + \frac{3}{2}K_2 + \frac{K_3}{3} + \frac{K_4}{6} + \frac{K_5}{3} + \frac{5K_6}{3}\right) \\ D &= \frac{1}{2}\left(K_1 - \frac{K_2}{2} + \frac{K_3}{9} - \frac{K_4}{18} - \frac{K_5}{3} - \frac{K_6}{3}\right) \\ E &= \frac{K_3}{6} - \frac{K_4}{12} - \frac{K_5}{4} + \frac{K_6}{4} \\ F &= (c/a)3^{-1/2}(K_3 + K_4 + (3/2)K_5 + 3K_6) \end{aligned}$$

the potential energy in these variables become

$$\begin{aligned} V &= \frac{1}{2}\{A(x^2 + y^2) + Bz^2 + (3/2)Cq_1^2 + Du^2 + 2Cv^2 \\ &\quad + 2[E(ux + (3^{1/2}/2)yq_1 - yv) \\ &\quad + Fz((3^{1/2}/2)q_1 + v) + 3^{1/2}(C - D)vq_1]\}. \end{aligned} \quad (20)$$

To obtain the kinetic energy, we first refer to fixed axes X, Y, Z , with same origin as the x, y, z system, and connected by:

$$X = x + \psi y + \theta z; \quad Y = -\psi x + y + \phi z; \quad Z = -\theta x - \phi y + z \quad (21)$$

where ψ, θ, ϕ , are cosines of (X, y) , (X, z) , and (Y, z) , respectively, and the rotation in space is understood to be small.

Neglecting small quantities of the second order, we have

$$\begin{aligned} \delta X_j &= \delta x_j + \psi y_j^0 + \theta z_j^0 \\ \delta Y_j &= -\psi x_j^0 + \delta y_j + \phi z_j^0 \\ \delta Z_j &= -\theta x_j^0 - \phi y_j^0 + \delta z_j. \end{aligned}$$

With these relations and Eqs. (18) and (19) and applying the condition for conservation of linear momentum, the kinetic energy becomes

$$\begin{aligned} T &= \frac{1}{2}\left(m + \frac{\Delta m}{3}\right)\left\{3\rho(\dot{x}^2 + \dot{y}^2 + \dot{z}^2) + \frac{2}{3}(1 + \epsilon)(\dot{u}^2 + \dot{v}^2) + \frac{1}{2}(1 - \epsilon)\dot{q}_1^2\right. \\ &\quad - 4\rho\epsilon(\dot{u}\dot{x} + \dot{v}\dot{y}) + (\beta - \epsilon)\frac{a^2}{2}\dot{\theta}^2 + \frac{a^2}{2}(\beta + \epsilon)\dot{\phi}^2 + a^2\dot{\psi}^2 \\ &\quad + 2\dot{\theta}c\rho(3\dot{x} - 2\epsilon\dot{u}) + 2\dot{\phi}c\rho\left(3\dot{y} - 2\epsilon\dot{v} + 3^{1/2}\epsilon\frac{a}{c}\dot{z}\right) \\ &\quad \left.+ 2\dot{\psi}a\left[-\rho\epsilon(3^{1/2})\dot{x} + \left(\frac{1 + \epsilon}{3^{1/2}}\right)\dot{u}\right] - 2\rho(3^{1/2})ac\epsilon\dot{\psi}\dot{\theta}\right\} \end{aligned} \quad (22)$$

⁸ It is assumed that for $c=0$, $B \neq 0$.

where

$$\left. \begin{aligned} \mu &= \frac{M}{3m + M}, \quad \rho = \frac{M}{3m + \Delta m + M}, \quad \epsilon = \frac{\Delta M}{3m + \Delta m} \\ b &= 6\mu(c^2/a^2) + 1, \quad \beta = 6\rho(c^2/a^2) + 1 \end{aligned} \right\}. \quad (23)$$

From the conservation of angular momentum

$$(\partial T/\partial \dot{\phi} = 0, \partial T/\partial \dot{\theta} = 0, \partial T/\partial \dot{\psi} = 0)$$

and dropping terms in ϵ^2 , we have

$$\begin{aligned} T &= \frac{1}{2} \left(m + \frac{\Delta m}{3} \right) \left\{ \frac{3\rho}{\beta} \left[1 - \epsilon \left(1 - \frac{1}{\beta} \right) \right] \dot{x}^2 + \frac{3\rho}{\beta} \left[1 + \epsilon \left(1 - \frac{1}{\beta} \right) \right] \dot{y}^2 \right. \\ &\quad + 3\rho \dot{z}^2 + \frac{1}{2} (1 - \epsilon) \dot{q}_1^2 + \frac{1}{3} \dot{u}^2 + \frac{2}{3} (1 + \epsilon) \dot{v}^2 \\ &\quad \left. - 2\rho \frac{\epsilon}{\beta} \left(\dot{u}\dot{x} + 2\dot{y}\dot{v} + 6\rho \frac{c}{a} (3^{1/2}) \dot{y}\dot{z} \right) \right\}. \end{aligned} \quad (24)$$

Eqs. (I), (20), and (24) then yield the following equations for the vibrations of the molecule $Y^{(M)}X_2^{(m)}X^{(m+\Delta m)}$:

$$\begin{aligned} \left(m + \frac{\Delta m}{3} \right) \lambda^{*2} - \left(m + \frac{\Delta m}{3} \right) \left(\frac{B}{3\rho} + 6C - 3D \right) \lambda^* \\ + \frac{2BC - BD - F^2}{\rho} = 0 \end{aligned} \quad (25)$$

$$\begin{aligned} \left(m + \frac{\Delta m}{3} \right) \lambda^{*2} - \left(m + \frac{\Delta m}{3} \right) \left\{ \frac{\beta A [1 - \epsilon(1 - 1/\beta)]}{3\rho} + 3D - 2\epsilon E \right\} \lambda^* \\ + \frac{\beta}{\rho} (AD - E^2) [1 - \epsilon(1 - 1/\beta)] = 0 \end{aligned} \quad (26)$$

$$\begin{aligned} \left(m + \frac{\Delta m}{3} \right) \lambda^{*2} - \left(m + \frac{\Delta m}{3} \right) \left\{ \frac{\beta A [1 + \epsilon(1 - 1/\beta)]}{3\rho} + 3D + 2\epsilon E \right\} \lambda^* \\ + \frac{\beta}{\rho} (AD - E^2) [1 + \epsilon(1 - 1/\beta)] = 0. \end{aligned} \quad (27)$$

We denote the roots of (25) by λ_1^*, λ_3^* , of (26) by λ_2^*, λ_4^* of (27) by λ_5^*, λ_6^* . Each of the roots is distinct, so that the molecule $Y^{(M)}X_2^{(m)}X^{(m+\Delta m)}$ has six normal frequencies of vibration. By setting $\Delta m = 0$, these equations reduce to those of the molecule $Y^{(M)}X_3^{(m)}$, Eq. (25) becoming

$$m^2 \lambda^2 - m(B/3\mu + 6C - 3D)\lambda + (2BC - BD - F^2)/\mu = 0 \quad (28)$$

and Eqs. (26) and (27) giving

$$[m^2 \lambda^2 - m(bA/3\mu + 3D)\lambda + (b/\mu)(AD - E^2)]^2 = 0. \quad (29)$$

Dennison has shown that the vibrations represented by (28) are parallel to the altitude c of the molecular pyramid, that the vibrations represented

by (29) are perpendicular to the altitude and that whereas the perpendicular vibrations are four in number, only two are distinct, or, calling the roots of (29) $\lambda_2, \lambda_5, \lambda_4, \lambda_6$, then

$$\lambda_2 = \lambda_5, \lambda_4 = \lambda_6 \quad (30)$$

the molecule $Y^{(M)}X_3^{(m)}$ having four distinct normal frequencies of vibration. Thus the substitution of an atom of mass $(m + \Delta m)$ for one of the base atoms of mass m removes the degeneracy of the parallel mode of vibration, and a gas composed of molecules of $Y^{(M)}X_3^{(m)}$ and $Y^{(M)}X_2^{(m)}X^{(m+\Delta m)}$ will show ten fundamental infrared bands (disregarding, of course, the possibility of one or more being inactive in absorption).

Just as in the triatomic case, any particular isotope shift $\Delta\omega_i/\omega_i$ can be calculated only if the force constants are known, but the sum of the relative isotope effects of the parallel frequencies can be calculated from the masses alone, and the sum of the isotope effects of the perpendicular frequencies from the masses and the ratio of the altitude to the length of side of the base. As it must now be obvious, from the triatomic case, how each individual $\Delta\omega_i/\omega_i$ may be written down, merely by applying Eq. (II), we shall not state these, but shall state only the more interesting and useful expressions for the sums of isotope effects.

(a) Central isotope effects, molecules $Y^{(M)}X_3^{(m)}$ and $Y^{(M+\Delta M)}X_3^{(m)}$

These relationships apply to molecules such as $\text{Cl}^{(35)}\text{O}_3$ and $\text{Cl}^{(37)}\text{O}_3$, $\text{B}^{(10)}\text{I}_3$ and $\text{B}^{(11)}\text{I}_3$.

The normal vibrations of molecules $Y^{(M+\Delta M)}X_3^{(m)}$ are obtained simply by substituting $M + \Delta M$ for M in Eqs. (28) and (29). Then for the parallel vibrations we have

$$\frac{\Delta\omega_1}{\omega_1} + \frac{\Delta\omega_3}{\omega_3} = \frac{(\mu - 1)\Delta M}{2(M + \Delta M)} \quad (31)$$

and for the perpendicular vibrations:

$$\frac{\Delta\omega_2}{\omega_2} + \frac{\Delta\omega_4}{\omega_4} = \frac{(\mu - 1)\Delta M}{2b(M + \Delta M)}. \quad (32)$$

For a co-planar molecule, that is, for one where $c = 0$, $b = 1$ and hence

$$\frac{\Delta\omega_1}{\omega_1} + \frac{\Delta\omega_3}{\omega_3} = \frac{\Delta\omega_2}{\omega_2} + \frac{\Delta\omega_4}{\omega_4} = \frac{(\mu - 1)\Delta M}{2(M + \Delta M)}. \quad (33)$$

(b) End isotope effects, molecules $Y^{(M)}X_3^{(m)}$ and $Y^{(M)}X_2^{(m)}X^{(m+\Delta m)}$

These relationships apply to molecules such as $\text{PCl}_3^{(35)}$ and $\text{PCl}_2^{(35)}\text{Cl}^{(37)}$. From Eqs. (II), (25) and (28) we get, for the parallel vibrations

$$\frac{\Delta\omega_1}{\omega_1} + \frac{\Delta\omega_3}{\omega_3} = -\frac{(\mu + 1)\Delta m}{2(3m + \Delta m)} \approx -\frac{(\mu + 1)\Delta m}{6m}. \quad (34)$$

From (II), (26), (27) and (29) the isotope effects of the perpendicular vibrations are related by:

$$\frac{\Delta\omega_2}{\omega_2} + \frac{\Delta\omega_4}{\omega_4} = -\frac{\Delta m}{6m} \left(\frac{\mu - 2}{b} + 3 \right) \quad (35)$$

$$\frac{\Delta\omega_5}{\omega_5} + \frac{\Delta\omega_6}{\omega_6} = -\frac{\Delta m}{6m} \left(\frac{\mu}{b} + 1 \right) \quad (36)$$

where, it must be recalled, $\omega_2 = \omega_5$, $\omega_4 = \omega_6$, but

$$\Delta\omega_2 \neq \Delta\omega_5 \text{ and } \Delta\omega_4 \neq \Delta\omega_6.$$

For co-planar molecules, $b=1$ and hence

$$\frac{\Delta\omega_1}{\omega_1} + \frac{\Delta\omega_3}{\omega_3} = \frac{\Delta\omega_2}{\omega_2} + \frac{\Delta\omega_4}{\omega_4} = \frac{\Delta\omega_5}{\omega_5} + \frac{\Delta\omega_6}{\omega_6} = -\frac{(\mu + 1)\Delta m}{6m}. \quad (37)$$

To the first order, the isotope effects of $Y^{(M)}X^{(m)}X_2^{(m+\Delta m)}$ are approximately twice the corresponding effects of $Y^{(M)}X_2^{(m)}X^{(m+\Delta m)}$ and isotope effects of $Y^{(M)}X_3^{(m+\Delta m)}$ approximately three times the corresponding effects of the latter.

It is hoped that the above relations for isotope effects may be of use in the analysis of bands of tetratomic molecules.

It may be superfluous to emphasize that the expressions here refer to the frequencies of small vibration and not *exactly* to the (0, 1) bands, but it is expected that the difference in those values may be neglected and our results applied to the (0, 1) bands themselves.

We take this opportunity of thanking Professor D. M. Dennison of the University of Michigan for his interest and advice in this work. This work was begun while one of us (J.E.R.) was a National Research Fellow.

On Radiation Diffusion and the Rapidity of Escape of Resonance Radiation from a Gas

By CARL KENTY

General Electric Vapor Lamp Company, Hoboken, N. J.

(Received August 25, 1932)

The radiation diffusion process is considered from the standpoint of the free paths of the diffusing resonance quanta as influenced by the Doppler and other line broadening effects. Abnormally long free paths are found to be of such importance as to enable resonance radiation to escape from a body of gas faster than has usually been supposed. It is assumed that a large concentration of diffusing resonance quanta will, on the basis of Doppler broadening only, give rise to a characteristic excitation of atoms, as dependent on their speeds, which can be represented by a distribution function which will lie between two limiting distribution functions, namely (1) Maxwell's distribution function and (2) a distribution function expressing a lower relative excitation of the high speed atoms than that of Maxwell, based on the excitation of all atoms as if by absorption of the core of the line. On the basis of (1) and (2), limiting expressions are derived for: (a) the fraction of emitted quanta traversing at least a given distance before absorption, (b) the diffusion coefficient, (c) the average square free path, (d) the average free path. A fundamental difference between radiation diffusion and molecular diffusion appears in that whereas (a) decreases exponentially with the distance in the latter case it is found to decrease only linearly (roughly) with the distance in the former case. For this reason very long free paths are found to be of relatively great importance in radiation diffusion. It is found that, for a gas container of infinite size, (b), (c), and (d) are all infinite. For a gas container of finite size, estimates of the order of magnitude of the apparent or effective values of (b), (c), and (d) are made on the basis of special assumptions. It is found that (b) = $(\frac{1}{2})\bar{p}^2/\tau$ where \bar{p}^2 is the average square free path and τ is the mean life of the excited atom. The same formula is found to hold for the coefficient of molecular diffusion if \bar{p}^2 is used to denote the average square molecular free path and τ is used to represent the mean time between collisions. It is pointed out that coupling and other line broadening effects will still further increase the importance of extremely long free paths and hence also the rapidity of escape of resonance radiation from a gas. The results of the Hg resonance radiation imprisonment experiments of Zemansky and of Webb and Messenger are discussed and are shown to be in accord with the conclusions arrived at above that resonance radiation escapes from a gas faster than according to classical theories of radiation diffusion, the effect being the greater the larger the gas volume or density. The rapidity of escape of $\lambda 2537$ at the lower gas densities ($N=10^{15}$ cm $^{-3}$ or less) in these experiments can be largely accounted for by the Doppler effect on the basis of a diffusion coefficient proportional to the effective average square free path as calculated by the methods of the present paper; at the higher gas densities ($N=30 \times 10^{15}$ cm $^{-3}$) the escape is more rapid than can be accounted for by these methods and this is attributed to coupling or other pressure broadening.

I. INTRODUCTION

THE THEORY of resonance radiation imprisonment and diffusion was first worked out by K. T. Compton¹ on the basis of analogy with mole-

¹ K. T. Compton, Phys. Rev. 20, 283 (1922); Phil. Mag. 45, 752 (1923). See also R. W. Wood, Phil. Mag. 23, 689 (1912).

cular diffusion. Milne² later, using Einstein's theory of radiation, arrived at a very general theory of the passage of resonance radiation through a gas.³ He developed an equation describing this process which at appreciable gas densities, such as are usually met with in practice, reduces to the standard diffusion equation of Compton (except for a slight difference in the numerical factor appearing in the expression for the diffusion coefficient). At very low gas densities, however, where the radiation has a considerable chance of escaping completely from the gas without absorption (mean free path of the radiation greater than the dimensions of the gas container), and where, therefore, diffusion in the usual sense of the term can no longer be thought of, Milne's equation is still applicable, by virtue of an additional term appearing in it, and expresses the fact that the radiation cannot escape from the body of gas faster than according to the exponential constant $1/\tau$ where τ is the mean life of the excited (resonance) state of the atom.

The expression for the diffusion coefficient appearing in these theories is⁴ $1/(3\alpha^2\tau)$ where α is the absorption coefficient of the gas for the resonance radiation. Since because of the Doppler effect or other causes of line broadening a resonance quantum may be absorbed at one frequency by an atom and given out at another,⁵ the question arises as to what value of α should be used in this expression. Compton (in effect) and Milne have assumed an average value of α taken over the breadth of the line (the breadth of the line in emission being taken to be the same as that in absorption) and treated the diffusing resonance quanta as if they had at all times a frequency corresponding to this average value of α . Zemansky⁵ pointed out that, where the line breadth is greater than given by the Doppler effect, as is found to be the case at appreciable gas densities, the diffusion process is probably more complicated; he was, however, led to believe from his experiments in mercury vapor that the resonance radiation diffused as a whole through the gas with a "mean or equivalent" absorption coefficient the numerical value of which was to be found by experiment. According to his measurements, the atomic absorption coefficient calculated from this mean or equivalent absorption coefficient decreased greatly with increasing vapor density (see below). Essentially similar results were obtained by Webb and Messenger⁶ who ascribed the lessening of the apparent atomic absorption coefficient at higher vapor densities to line broadening caused by absorption or other effects.

Later the writer,⁷ and Langmuir and Found⁸ have carried out experiments which indicate that in Ne at a pressure of the order of 1 mm the mean free paths of the scattered resonance radiations are much greater than those

² E. A. Milne, *Jour. Lond. Math. Soc.* 1, 40 (1926).

³ A number of applications of Milne's theory have been made by M. W. Zemansky, *Phys. Rev.* 36, 919 (1930) and a number of preceding papers.

⁴ In Milne's theory the numerical factor is $\frac{1}{2}$ instead of $\frac{1}{3}$.

⁵ M. W. Zemansky, *Phys. Rev.* 29, 513 (1927); see p. 521.

⁶ H. W. Webb and Helen A. Messenger, *Phys. Rev.* 33, 319 (1929). See particularly p. 325.

⁷ Carl Kenty, *Phys. Rev.* 40, 633L (1932). A more complete account of these experiments will be given in a later paper.

⁸ I. Langmuir and Clifton G. Found, unpublished work.

usually thought of for resonance lines⁹ at such gas pressures. The cause of these abnormally long mean free paths has been tentatively attributed to Holtsmark coupling broadening¹⁰ of the resonance lines or to broadening caused by the formation of loosely bound molecules.¹¹ That there is probably some cause of broadening of these lines more important than the Doppler effect, in the case of Ne at pressures of the order of 1 mm, appears from heating experiments to be described in a later paper. But even at low gas densities where the Doppler effect is known to be the main cause of broadening closer scrutiny of the diffusion process* has revealed that very abnormally long free paths will be developed by this process and that under certain circumstances these will be of great importance in aiding the escape of resonance radiation from a gas.¹²

II. AN ATTEMPT TO CALCULATE MORE ACCURATELY THE DIFFUSION COEFFICIENT

Let it be assumed that the only cause of line broadening in the case to be considered is the Doppler effect. Then in Fig. 1 suppose that a quantum of

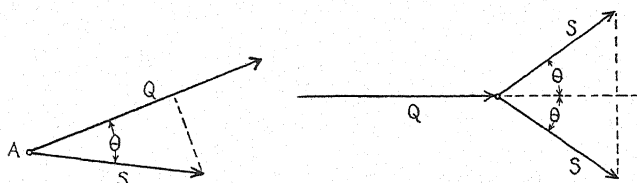


Fig. 1. *S*: direction of motion of emitting atom. *Q*: direction of emitted radiation quantum.

Fig. 2. *Q*: direction of radiation quantum; *S*: direction of absorbing atoms.

resonance radiation is emitted at *A* by an atom of speed *S* in a direction making an angle between θ and $\theta + d\theta$ with the direction of *S*. The component of *S* in the direction of the quantum is $S \cos \theta$. We desire to calculate first the absorption coefficient α of the gas for such a quantum (or for such quanta). In order to be capable of absorbing such a quantum, an atom must have a component of velocity in the direction of the quantum which lies between *U* and $U + \Delta U$ where $U = S \cos \theta$ and ΔU may be regarded as a "limit of tolerance." Now the fraction of all atoms which have components of velocity in a given direction between *U* and $U + \Delta U$ is by kinetic theory equal to $(m/2\pi kT)^{1/2} [\exp - U^2/w^2] \Delta U$ where *m* is the mass of an atom, *k* is Boltzmann's gas constant, *T* is the absolute temperature and $w = (2kT/m)^{1/2}$ is the most probable speed. Clearly α will be proportional to this fraction so

⁹ It has been pointed out to the writer that in the case of the longer wave-length resonance line of Ne ($^1S_0 - ^3P_1$), a relatively long mean free path would be expected in view of the fact that this line is an intercombination line, such lines being usually found relatively weak in absorption in elements of low atomic number.

¹⁰ J. Frenckel, *Zeits. f. Physik* **59**, 198 (1930). See also the original and later papers by J. Holtsmark and L. Mensing.

¹¹ W. Weizel, *Phys. Rev.* **38**, 642 (1931).

* For a recent theory of resonance radiation diffusion which takes into account the Doppler effect see E. W. Samson, *Phys. Rev.* **40**, 940 (1932) and the following note by M. W. Zemansky.

¹² Carl Kenty, *Phys. Rev.* **41**, 390A (1932).

that $\alpha = A(m/2\pi kT)^{1/2} [\exp - U^2/w^2] \Delta U$ where A is a constant of proportionality. By substituting $U=0$ in this expression it is evident that the absorption coefficient for the core of the line, α_0 , will be obtained. Thus $\alpha_0 = A(m/2\pi kT)^{1/2} \Delta U$.

By division of the two expressions, and replacing U by $S \cos \theta$ it is found that

$$\alpha = \alpha_0 \exp - [S^2 \cos^2 \theta / w^2]. \quad (1)$$

The fraction of all such emitted quanta which travel at least a distance r , say, before absorption, will be given by

$$\exp(-r\alpha) = \exp(-r\alpha_0 e^{-(S^2 \cos^2 \theta / w^2)}).$$

On the consideration that all angles of emission are equally likely, the fraction of all quanta emitted by atoms of speed S , say, in directions making angles between θ and $\theta + d\theta$ with the directions of motion of the emitting atoms is simply the fractional solid angle denoted by $\frac{1}{2} \sin \theta d\theta$. Since, as far as the absorption coefficient is concerned, θ is not distinguished from $\pi - \theta$, it will be convenient to treat θ as varying only from 0 to $\pi/2$ and hence to take twice the above fractional solid angle, namely $\sin \theta d\theta$, as the fraction of all quanta emitted at angles between θ and $\theta + d\theta$. The fraction of all quanta emitted by atoms of speed S , which traverse at least a distance r before absorption is then given by

$$f(S, r) = \int_0^{\pi/2} \exp(-r\alpha_0 e^{-(S^2 \cos^2 \theta / w^2)}) \sin \theta d\theta = \frac{w}{S} \int_0^{S/w} \exp(-r\alpha_0 e^{-x^2}) dx$$

where $x = S(\cos \theta)/w$.

Let it first be considered that all atoms are equally likely to be excited and to emit a resonance quantum regardless of their speed—the condition under which a thin emitting layer of gas would emit a line the intensity distribution of which would be the commonly assumed Gauss error curve. Then the fraction of all emitted quanta which are emitted by atoms having speeds between S and $S + dS$ is given by Maxwell's distribution law, namely

$$f_1(S) dS = (4S^2/\pi^{1/2} w^3) e^{-S^2/w^2} dS \quad (2)$$

and as we have just seen the fraction of these which go at least a distance r before absorption is given by $f(S, r)$. The total fraction of *all* emitted quanta which go at least a distance r before absorption is then given by

$$f_1(r) = \frac{4}{\pi^{1/2} w^3} \int_0^\infty S^2 \exp(-S^2/w^2) dS \cdot \frac{w}{S} \int_0^{S/w} \exp(-r\alpha_0 e^{-x^2}) dx. \quad (3)$$

By writing $S/w = y$ and $r\alpha_0 = R$, this may be written

$$f_1(R) = \frac{4}{\pi^{1/2}} \int_0^\infty \int_0^y y \exp(-y^2) \exp(-R e^{-x^2}) dx dy. \quad (4)$$

Here $f_1(R)$ is the fraction of all emitted quanta which traverse at least a distance R times the mean free path, $1/\alpha_0$, of the core of the line. The values of

$f_1(R)$ for several numerical values of R , as calculated from Eq. (4) by graphical integration, are given in Table I.

TABLE I. $f_1(R)$: fraction of all emitted quantal traversing at least a distance R/α_0 assuming all atoms equally likely to emit. $f_2(R)$: the same assuming "weighted distribution function."

R	$f_1(R)$	$f_2(R)$	$Rf_1(R)$	$Rf_2(R)$
10^2	2.73×10^{-3}	9.2×10^{-4}	0.273	0.092
10^3	2.10×10^{-4}	6.5×10^{-5}	0.21	0.065
10^4	1.7×10^{-5}	4.7×10^{-6}	0.17	0.047
10^5	1.6×10^{-6}	3.96×10^{-7}	0.16	0.039

The question may be raised as to whether or not the above assumption is correct that the diffusion process results in a concentration of excited atoms in which one atom is as likely to be excited as another regardless of speed. In order to obtain at least a partial answer to this question consider the hypothetical case in which all atoms are excited through the absorption of radiation which has been emitted by atoms of speed S_0 in the direction of their motion. Let the direction of this radiation be denoted by Q in Fig. 2. Then an atom of speed S , in order to be able to absorb such radiation, must be moving in a direction, making an angle between θ and $\theta + d\theta$ with Q such that, within a certain "limit of tolerance," $S \cos \theta = S_0$. Let it be supposed that this limit of tolerance is ϵw , for convenience. Then $d(S \cos \theta) = \epsilon w = -S \sin \theta d\theta$, or $d\theta = \epsilon w / S \sin \theta$, neglecting the minus sign. Now the probability that an atom will be moving in a direction making an angle between θ and $\theta + d\theta$ with Q is $\frac{1}{2} \sin \theta d\theta$. By substituting the value of $d\theta$, above, it is evident that the relative probability that an atom of speed S , $S > S_0$, will be able to absorb the given radiation will be $\epsilon w / 2S$. Since the fraction of all atoms having speeds between S and $S + dS$ is given by Maxwell's distribution law, Eq. (2) the chance that a quantum of the given radiation will be absorbed by an atom of speed between S and $S + dS$ is proportional to the product of this fraction and the above probability, namely

$$\frac{2K\epsilon S}{(\pi)^{1/2}w^2} e^{-S^2/w^2} dS = f_2(S) dS, \quad f_2(S) = 0 \text{ for } S < S_0$$

where K is a constant of proportionality. Since the quantum is certain to be absorbed by one atom or another (assuming a sufficiently large volume of gas)

$$\int_{S_0}^{\infty} f_2(S) dS = 1. \quad (4a)$$

By choosing $S_0 \ll w$, the fraction of atoms whose speeds are so low as to preclude their being able to absorb the radiation can be made negligibly small. For convenience, suppose $S_0 = 0$, corresponding to excitation by the core of the resonance line. Then Eq. (4a) gives the result that $K\epsilon = (\pi)^{1/2}$ so that

$$f_2(S) dS = (2/w^2) S e^{-S^2/w^2} dS. \quad (5)$$

This may be called the "weighted distribution" function, for the purpose of this paper, in order to distinguish it from the normal distribution function

$f_1(S)dS$ of Maxwell.¹³ It follows from the above that $f_2(S)dS$ represents the fraction of all excited atoms which have speeds between S and $S+dS$ under the assumptions considered. With this weighted distribution function the fraction of all emitted quanta which traverse at least a distance R times the mean free path, $1/\alpha_0$, of the core of the line is found to be given by

$$f_2(R) = 2 \int_0^\infty \int_0^y \exp(-y^2) \exp(-Re^{-x^2}) dx dy \quad (6)$$

as follows by the method of deriving Eq. (4). Values of $f_2(R)$, calculated by graphical integration, for a number of values of R , are given in Table I.

Let us now consider the two functions $f_1(S)dS$ and $f_2(S)dS$ as limiting distribution functions. In view of the appearance of S in the denominator of the expression $\epsilon w/2S$, above, for the relative probability of excitation of an atom of speed S , and the fact that the *bulk* of the diffusing resonance radiation will not have an abnormally large displacement from the core of the line, it is evident that $f_1(S)dS$ expresses a relative excitation of the high speed atoms which is too great to be characteristic of the average excitation by the diffusion process (only if the exciting radiation density were uniform with respect to frequency would $f_1(S)dS$ be attained). On the other hand, since $f_2(S)dS$ was derived on the assumption of excitation by the core of the line ($S_0=0$) this function expresses a relative excitation of the very low speed atoms which is too high (since the actual diffusing radiation has a line breadth which is greater than zero). The true distribution function characteristic of the diffusion process must therefore lie somewhere between these two limiting functions; its actual form would be very difficult to calculate. Further, as will be seen below, it will probably vary from one point to another in a body of gas, depending on geometry and other factors.

The diffusion coefficient of resonance radiation may now be calculated on the basis of Eqs. (3) and (5) as limiting cases.¹⁴ In Fig. 3 let $(N+zdN/dz)$ represent the concentration of excited atoms at any point distant z from the XY plane. Then the number of excited atoms in the element of volume dv , at a distance r from the origin is $(N+r \cos \theta dN/dz)dv$ where θ is the angle between r and the Z axis. If the average life of the excited atoms is τ , then $(N+r \cos \theta dN/dz)dv/\tau$ quanta will be emitted per second from this volume element and of these a fraction $(d\sigma \cos \theta)/4\pi r^2$ will be emitted in directions passing through the surface element $d\sigma$ in the XY plane at the origin. Of all such quanta, a fraction $f_1(r)$ will, by Eq. (3) (to take, first, the case of the normal distribution function), traverse a distance at least as great as r and will hence pass through $d\sigma$. By expressing the volume element in terms of polar coordinates, $dv=r^2 \sin \theta dr d\theta d\phi$ and the total number of quanta passing downward through $d\sigma$ per second is

¹³ It is to be noted that gaseous collisions during the lifetime of the excited state, as at the higher pressures, will tend to bring about the normal distribution function $f_1(S)dS$.

¹⁴ The method used is somewhat analogous to a well-known method for finding molecular diffusion coefficients. See for example, L. B. Loeb, *Kinetic Theory of Gases*, pp. 224, 225. The method indeed seems to be more naturally applicable to radiation diffusion than to molecular diffusion.

$$\iiint (d\sigma/4\pi\tau) \left(N + r \cos \theta \frac{dN}{dz} \right) \cos \theta \sin \theta d\theta d\phi f_1(r) dr$$

where ϕ must be integrated from 0 to 2π , θ from 0 to $\pi/2$ and r from 0 to ∞ . Similarly, the total number of quanta passing per sec. upward through $d\sigma$ is

$$\iiint (d\sigma/4\pi\tau) \left(N - r \cos \theta \frac{dN}{dz} \right) \cos \theta \sin \theta d\theta d\phi f_1(r) dr.$$

The resultant flux of quanta passing through $d\sigma$ is the difference between the above two expressions, namely

$$\frac{\sigma}{2\pi\tau} \frac{dN}{dz} \iiint r f_1(r) \cos^2 \theta \sin \theta d\theta d\phi dr$$

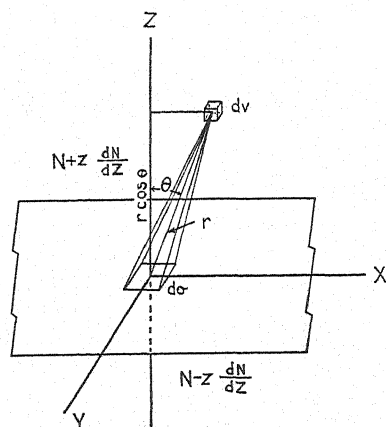


Fig. 3.

and this flux is by definition equal to $Dd\sigma dN/dz$ where D is the diffusion coefficient. By carrying out the integrations for θ and ϕ and writing $r = R/\alpha_0$ as above it follows that

$$D = (1/3\alpha_0^2\tau) \int_0^\infty R f_1(R) dR. \quad (7)$$

Here it may be noted that on the view that all diffusing resonance quanta have the same absorption coefficient α_0 we may write $f_1(R) = \exp(-R)$, simply, $f_1(R)$ denoting the fraction of all emitted quanta which traverse at least a distance $r = R/\alpha_0$ before absorption and this fraction, on the present assumption, being denoted by $\exp - r\alpha_0 = \exp(-R)$, in which case Eq. (7), would give $D = 1/(3\alpha_0^2\tau)$ which is the standard expression for the diffusion coefficient already referred to.

In the actual case considered, however, $Rf_1(R)$ has values some examples of which are given in Table I and it is found that graphical integration of Eq. (7) will yield a value of D which is indefinitely large compared with the standard expression.

On the basis of the weighted distribution function, the diffusion coefficient may be similarly found to be given by

$$D = (1/3\alpha_0^2\tau) \int_0^\infty Rf_2(R)dR. \quad (8)$$

Some examples of the values of $Rf_2(R)$ are given in Table I. It will be observed that these values are falling off with increasing R more rapidly than is the case with $Rf_1(R)$; nevertheless it appears that D as given by Eq. (8) will also be indefinitely large compared with the standard expression. Now $f_2(R)$, being based on $f_2(S)dS$, represents a lower limit for the fraction of emitted quanta traversing at least a distance R/α_0 before being absorbed; since the actual fraction must be greater than this, we may safely regard the diffusion coefficient as indefinitely large compared with $1/(3\alpha_0^2\tau)$.

Essentially, the same result may also be obtained in the following manner. A quantum for which the absorption coefficient is α will have a mean free path, $1/\alpha$. Representing individual free paths by p , we may denote by \bar{p} the average free path taking into account all values of α . The effective average speed of the quantum through the gas¹ will then be \bar{p}/τ . By analogy with molecular diffusion,¹ where the diffusion coefficient is given by $D = \frac{1}{3}v_m L$ where v_m is the average molecular speed and L is the mean free path, one might write for the diffusion coefficient of radiation $D = \frac{1}{3}(\bar{p}/\tau) \cdot \bar{p}$. If the analogy with molecular diffusion were complete and the speed p/τ did not depend on p (in the molecular diffusion case v does not depend on L , at least to a first approximation) it would be justifiable to multiply the average speed \bar{p}/τ by the average free path \bar{p} and so obtain for the diffusion coefficient $\frac{1}{3}(\bar{p})^2/\tau = \frac{1}{3}(1/\alpha)^2/\tau$. But in the case of radiation diffusion a high value of p is *always accompanied by* a high value of $v = \bar{p}/\tau$ (in contradistinction to the molecular diffusion case) and it is clear that the *average square* free path must be taken, that is¹⁵

$$D \sim \frac{1}{3}\bar{p}^2/\tau \quad (9)$$

where, in view of the method of obtaining the result, no significance is to be placed on the factor $(\frac{1}{3})$ (see below).

The average square free path on the present assumptions may be found as follows. The average free path of the quantum represented by Q in Fig. 1, which is supposed to be emitted from an atom of speed S in a direction making an angle between θ and $\theta + d\theta$ with the director of S is $1/\alpha = (1/\alpha_0) \exp S^2 \cos^2 \theta / w^2$ and the average square free path of such a quantum is¹⁶ $(2/\alpha_0^2) \exp 2S^2 \cos^2 \theta / w^2$. Averaging over all values of θ and all values of S , using the one or the other of the two distribution functions $f_1(S)dS$ or $f_2(S)dS$, one obtains for the average square free path, respectively

¹⁵ Although expression (9) may appear like the usual form of the diffusion coefficient, it is really very different because the average of p^2 , is an enormously larger quantity than the reciprocal of the square of the average α . The latter quantity has been evaluated on the basis of either $f_1(S)dS$ or $f_2(S)dS$ and found to be only slightly greater than $1/\alpha_0^2$.

¹⁶ This follows on integration of $x^2 f(x)dx$ from $x=0$ to $x=\infty$ where $f(x)dx = \alpha(\exp -\alpha x)dx$ is the fraction of all free paths lying between x and $x+dx$.

$$\overline{p_1^2} = \frac{4(2)^{1/2}}{(\pi)^{1/2}\alpha_0^2} \int_0^\infty \int_0^{(2)^{1/2}y} ye^{-y^2}e^{x^2}dxdy \quad (10)$$

$$\overline{p_2^2} = \frac{2(2)^{1/2}}{\alpha_0^2} \int_0^\infty \int_0^{(2)^{1/2}y} e^{-y^2}e^{x^2}dxdy \quad (11)$$

where $y=S/w$ as before and $x=(2)^{1/2}(S \cos \theta)/w$. Graphical integration of Eqs. (10) and (11) indicates that both expressions for the average square free path are infinite and hence by Eq. (9) that the diffusion coefficient must be infinite, in agreement with the result already obtained. Indeed the expressions for D obtained by the two methods are mathematically identical if the numerical factor in Eq. (9) is taken as $\frac{1}{6}$ instead of $\frac{1}{3}$, as may be shown as follows. Assume $f(R)$ is the true function representing the fraction of all free paths which are greater than R times the "core mean free path" $1/\alpha_0$. Then the fraction of all free paths which are of length between R/α_0 and $(R+dR)/\alpha_0$ will be $df(R)$ and the average square free path may be written as

$$\overline{p^2} = \frac{1}{\alpha_0^2} \int_{f(R)=0}^1 R^2 df(R).$$

But from the standpoint of the area under a curve this is numerically equivalent to

$$\frac{1}{\alpha_0^2} \int_{R^2=0}^\infty f(R)d(R^2) = \frac{2}{\alpha_0^2} \int_{R=0}^\infty Rf(R)dR$$

so that, referring to Eqs. (7) or (8), we have¹⁷

$$D = (1/6)\overline{p^2}/\tau. \quad (12)$$

The fact that the coefficient of radiation diffusion is infinite has been seen to depend on the importance of extremely long free paths. The result will evidently not apply to most cases met with in practice where such free paths would be greater than the dimensions of the gas container. Hence for practical purposes, it appears that there is no quantity which can properly be defined as the diffusion coefficient of resonance radiation; as the dimensions of the gas container are made larger, (or the density of the gas larger) the apparent diffusion coefficient will increase beyond the value $\frac{1}{3}/\alpha_0^2\tau$ without limit.

¹⁷ It is a curious fact that in a familiar method of finding the coefficient of molecular diffusion (see reference 14) there appears an expression of the form $\int_0^\infty re^{-r/L}dr$, where L is the mean molecular free path, which is equivalent to $(1/\alpha_0^2)\int_0^\infty Rf(R)dR$, above, and that the ordinary coefficient of molecular diffusion, $(1/3)v_m L$, where v_m is the mean thermal speed, may be written as $(1/6)\overline{p^2}v_m/L$ or as $(1/6)\overline{p^2}/t$ where $t=L/v_m$ is the mean time between collisions. (Compare Eq. (12) above.) This follows at once of course from $D=(1/3)v_m L$ since in the case of molecular free paths $\overline{p^2}=2L^2$ (see reference 16). From the present point of view it would appear to be the average square free path, which is of fundamental importance for the coefficient of molecular diffusion as well as for the coefficient of radiation diffusion, and that formula (12) may be of rather general significance.

In dealing with actual cases, for example in attempting to calculate the rate of decay of the resonance radiation emerging from a resonance cell with plane parallel sides after the exciting radiation is cut off (see § IV), the method that has been adopted is to assume that the diffusing radiation can be treated as if it had an apparent or effective diffusion coefficient limiting expressions for which are given by

$$D_1 = (\frac{1}{6})\overline{p_1^2}(y_1)/\tau \quad (13)$$

$$D_2 = (\frac{1}{6})\overline{p_2^2}(y_1)/\tau \quad (14)$$

where $\overline{p_1^2}(y_1)$ and $\overline{p_2^2}(y_1)$ are supposed to be the limiting expressions for the effective average square free path as found by the integrating y in Eqs. (10) and (11), respectively, from 0 to y_1 (instead of from 0 to ∞) and y_1 is defined by

$$(1/\alpha_0) \exp y_1^2 = l \quad (15)$$

where l is the thickness of the cell. By choosing y_1 in this way we disregard those excited atoms whose speeds are such that the mean free paths of the quanta emitted by them in their directions of motion would be greater than l .¹⁸ This procedure is an approximate method of taking into account the fact that free paths greater than the dimensions of the cell are meaningless. The method is roughly justified only in cases where $l \gg 1/\alpha_0$; under these circumstances the fraction of free paths which would be much greater than l will be so small that they can approximately be neglected—only when there are no walls to limit them will such free paths make their really important contribution to the average square free path.

With the above assumptions we may write

$$\overline{p_1^2}(y_1) = \frac{4(2)^{1/2}}{(\pi)^{1/2}\alpha_0^2} \int_0^{y_1} \int_0^{(2)^{1/2}y} ye^{-y} e^x dx dy \quad (16)$$

$$\overline{p_2^2}(y_1) = \frac{2(2)^{1/2}}{\alpha_0^2} \int_0^{y_1} \int_0^{(2)^{1/2}y} e^{-y^2} e^{x^2} dx dy. \quad (17)$$

As pointed out by Dr. Zemansky Eqs. (13) and (14), on substitution from Eqs. (16) and (17), are mathematically identical with Eqs. (7) and (8), respectively, if the complete expressions for $f_1(R)$ and $f_2(R)$ from Eqs. (4) and (6) are substituted in Eqs (7) and (8) and the integrations first performed for R , R varying from 0 to ∞ and the upper limit of integration for y being y_1 in all cases. The integration of R from 0 to ∞ here is approximately justified on account of the limitation placed on y_1 .

Considering the very approximate nature of the assumptions involved we could scarcely expect the present method to yield more than an order of magnitude, for example, for the rate of decay of the radiation emerging from a resonance cell. Further, as discussed above, the method will only be ap-

¹⁸ This follows since the absorption coefficient of quanta emitted by atoms of speed S_1 in their direction of motion will be $\alpha_0 \exp -S_1^2/w^2$ (see above) and the mean free path of such quanta will be $(1/\alpha_0) \exp S_1^2/w^2 = (1/\alpha_0) \exp y_1^2$.

plicable to cases where $l \gg 1/\alpha_0$ i.e., to cases where the great majority of quanta undergo a large number of absorptions and reemissions before escape.

Using the one or the other of the two distribution functions $f_1(S)dS$ or $f_2(S)dS$, we obtain, in a manner similar to the manner of obtaining Eqs. (10) and (11) the following expressions, respectively, for the average free path

$$\bar{p}_1 = \frac{4}{(\pi)^{1/2}\alpha_0} \int_0^\infty \int_0^y y e^{-y^2} e^{x^2} dx dy = \frac{4}{(\pi)^{1/2}\alpha_0} \int_0^\infty \phi_1(y) dy \quad (18)$$

$$\bar{p}_2 = \frac{2}{\alpha_0} \int_0^\infty \int_0^y e^{-y^2} e^{x^2} dx dy = \frac{2}{\alpha_0} \int_0^\infty \phi_2(y) dy \quad (19)$$

for the case of a resonance cell of infinite size, where $y = S/w$ and $x = S(\cos \theta)/w$. The functions $\phi_1(y)$ and $\phi_2(y)$ are plotted in Fig. 4. Graphical integra-

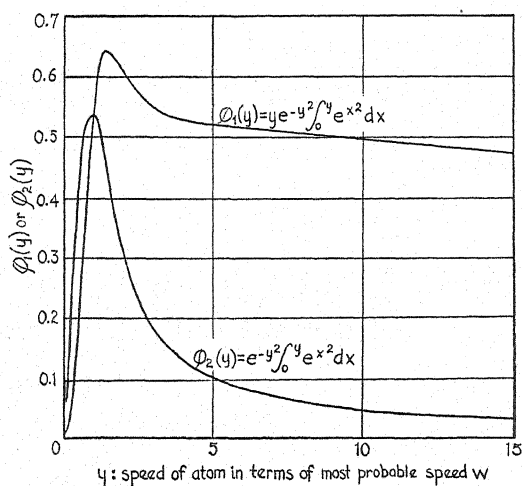


Fig. 4. Plot of functions $\phi_1(y)$ and $\phi_2(y)$ as occurring in Eqs. (18) and (19), respectively.

tion of Eq. (18) from $y=0$ to $y=15$ has yielded the result that $\bar{p}_1 > 16.8/\alpha_0$, 16.8 being the value of $[4/(\pi)^{1/2}] \phi_1(y) dy$ integrated from $y=0$ to $y=15$. In the same way $2\phi_2(y) dy$ integrated from 0 to 15 gave $\bar{p}_2 > 3.6/\alpha_0$. Integration from $y=0$ to $y=\infty$ would evidently yield values of \bar{p}_1 and \bar{p}_2 indefinitely larger than the above. In the case of a cell of finite size an estimate of the order of magnitude of the effective average free path can be obtained through the integration of Eq. (18) or (19) from $y=0$ to $y=y_1$ where y_1 is to be determined by Eq. (15).

Let us consider the case where resonance quanta are liberated at the center of a large spherical mass of gas of radius r . Suppose that the effective average free path inside this sphere is λ and that λ will increase only very slowly with r (as indeed it is found to do according to the method of defining the effective average free path discussed above, l in Eq. (15) being replaced by r). The number of free paths which a quantum will execute before escaping

from the surface of the sphere will on the average be of the order of n where¹⁹

$$n \sim (r/\lambda)^2. \quad (20)$$

Let us consider the chance that a free path will be produced which is greater than r (in which case the quantum will escape directly from the gas) and the dependence of this chance on r . Table I shows that the fraction of all free paths greater than $r = R/\alpha_0$ is decreasing roughly in proportion as R (i.e., r) increases. But the chance of such a free path being produced will be proportional to the average number of free paths made by the quantum before escaping and will therefore increase according to r^2 . Hence the chance that the quantum may escape by making a free path at least of the order of r would appear to increase approximately in proportion to r . But this will not strictly be the case because, as discussed above, the value of λ which can be used in Eq. (14) will increase slowly with r . Nevertheless it seems justifiable to infer that the larger r becomes, the greater will be the line breadth of the emerging radiation. The problem of calculating the actual line breadth, or structure, in any given such case would appear to be one of great difficulty. The case is different from that of absorption broadening as usually considered because the absorbed radiation cannot be neglected—all the radiation must emerge from the sphere, it being assumed here, as elsewhere, above, that there are no losses of quanta in the gas phase as a result of dissipative collisions or otherwise.

Since, as has been seen above, the apparent values of the diffusion coefficient, average square free path, etc., will all increase with the volume of the gas, it is reasonable to suppose that the distribution function itself will vary from one point to another and depend on the geometry of the boundaries of the gas and the point of entry (or production) of the resonance quanta. For example, in the spherical case above it would be reasonable to infer a relative excitation of the high speed atoms which would be higher near the surface than at the center; for near the surface the outward flux of radiation will be preponderantly of frequencies which can only be absorbed by the high speed atoms.

III. THE EFFECT OF PRESSURE BROADENING

It is well known that at appreciable gas densities the breadth of the resonance line, in the case of the alkali metals, Hg, etc., is much greater than that characteristic of the Doppler effect.²⁰ According to Waibel's²⁰ measurements the half breadth in absorption of the $1s-6p(1^2S_{1/2}-6^2P_{3/2})$ line of Cs, for example, at a vapor pressure of 17.5 mm (403°C) is about 2.2×10^{11} sec.⁻¹. This is calculated to be about 150 times the Doppler breadth for Cs at this temperature. Since the broadening was found by Waibel to increase

¹⁹ See the treatment of the analogous problem of electron diffusion by W. Harries and G. Hertz, *Zeits. f. Physik* **46**, 177 (1927).

²⁰ W. Schütz, *Zeits. f. Physik* **35**, 260 (1925); **45**, 30 (1927); R. Minkowski, *Zeits. f. Physik* **36**, 839 (1926); F. Waibel, *Zeits. f. Physik* **53**, 459 (1929). See also B. Trumpp, *Zeits. f. Physik* **34**, 715 (1925) and others. Most studies have been made on the breadth in absorption.

towards lower series members, it is to be inferred that the breadth of the resonance line would be much greater than this. Hopfield²¹ found the He resonance line ($\lambda 584\text{\AA}$) in emission at about 1 mm pressure to be greatly broadened asymmetrically toward the short wave side. Weizel²² states that the broadening on Hopfield's plates is about 500 cm^{-1} . This is calculated to be about 1000 times the Doppler broadening. Weizel has discussed this broadening in He on the basis of forces of the molecular type between the excited He atom and the normal He atom.

Foreign atoms (as in the case of an added gas) do not have nearly the same broadening effect as atoms of the same kind. These effects are commonly referred to as Lorentz collision broadening and Holtsmark coupling broadening,²³ respectively. As an example of the relative magnitude of the two effects, the result of Waibel²⁰ may be cited that the broadening in Cs vapor is about 200 times as great as the broadening due to the same pressure (of the order of 10 mm) of foreign gases.

In cases where such broadening exists, the reasoning used in §II can, of course, have no significance since there only Doppler broadening was assumed.²⁴ Such broadening as is here considered may be inferred to greatly accentuate the effects described above, namely the abnormally rapid escape of resonance radiation from a body of gas and an apparent diffusion coefficient increasing indefinitely, with the size of the vessel and with the gas density, beyond the value usually assumed.

§IV. THE RESONANCE RADIATION IMPRISONMENT EXPERIMENTS OF ZEMANSKY

Zemansky,⁵ repeating an experiment of Miss Hayner,²⁵ excited the mercury vapor in a quartz cell by irradiating it with light from a quartz mercury vapor lamp and studied the rate of falling off of the resonance radiation emerging from the far side of the cell after the exciting radiation was cut off. Extending Milne's theory of radiation diffusion² to take into account the diffusion of excited atoms and the effect of dissipative collisions, Zemansky arrived at the following expression for the exponential constant of decay, I/T , of this radiation

$$\frac{1}{T} = \frac{\pi^2}{4\tau l^2 \beta^2 N^2} + \frac{\pi c}{3(2)^{1/2} l^2 s^2 N} + (2)^{1/2} \pi b s^2 c N. \quad (21)$$

Where τ is the mean life of the excited state, l is the thickness of the cell, β is the "mean or equivalent" atomic absorption coefficient for the radiation,

²¹ J. J. Hopfield, *Astrophys. J.* **72**, 133 (1930).

²² W. Weizel, *Phys. Rev.* **38**, 642 (1931).

²³ L. Mensing, *Zeits. f. Physik* **34**, 611 (1925); J. Holtsmark, *Zeits. f. Physik* **34**, 722 (1925); **54**, 761 (1929); J. Frenckel, *Zeits. f. Physik* **59**, 198 (1930); Lucy Schutz-Mensing, *Zeits. f. Physik* **61**, 655 (1930).

²⁴ R. Minkowski, see reference 20, found that the coupling broadening in Na vapor began to be of relative importance at about 0.02 mm and to increase progressively thereafter with increasing pressure.

²⁵ L. J. Hayner, *Phys. Rev.* **26**, 364 (1925).

supposed by Zemansky to be characteristic of the radiation diffusion process, N is the number of Hg atoms per cm^3 , c is the root mean square speed, s is the distance between centers at impact and b is the probability that a collision between a normal Hg atom and an excited Hg atom will be of the second kind (quenching efficiency; such collisions will in this case presumably result in the production of 2^3P_0 atoms). In this expression the first term represents the rate of decay of the radiation due to the radiation diffusion process, the second the rate of decay due to the diffusion of excited atoms to the walls and the third the rate of decay due to quenching collisions. The experimental values of the exponential constant of decay as obtained by Zemansky for a number of different vapor pressures and for two different cells are represented graphically in Fig. 5. By numerical substitution it was

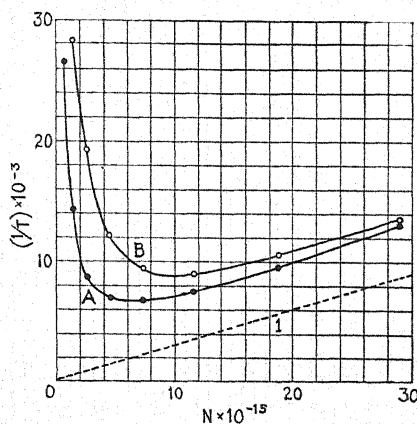


Fig. 5. Exponential constant of decay ($1/T$) of $\lambda 2537$ found by Zemansky (see reference 5). A, 1.95 cm cell; B, 1.3 cm cell; N , number of Hg atoms per cm^3 .

concluded that the second term on the right-hand side of Eq. (21) was negligibly small compared with the others and therefore that the exponential constant should be capable of representation by an equation of the form $1/T = A/N^2 + BN$. Since the experimental curves could not be represented by such an equation, it was inferred that β was not a constant, but decreased as N increased. This inference, which is in agreement with conclusions drawn by Webb and Messenger,⁶ from essentially similar experiments, is in accord with the views arrived at in §§II and III, and will be discussed further below. The line 1 of Fig. 5 was chosen to represent the last term on the right-hand side of Eq. (21). The slope of this line was 3×10^{-13} from which, by substituting the values of $c = 2.2 \times 10^4$ cm/sec., and $s = 6 \times 10^{-8}$ cm,²⁶ the quenching efficiency b , was calculated to be about 10^{-3} . In the more recent notation we may call $bs^2 = \sigma_1^2$, the effective cross section for quenching, from which it follows that σ_1^2 is about 0.0025 times the normal cross section $(3.6 \times 10^{-8})^2$. This is in sufficient accord with the known small quenching cross sections of other monatomic gases for Hg resonance radiation (see below).

²⁶ The kinetic theory radius of the normal mercury atom being about 1.8×10^{-8} cm, it is evident that the radius of the excited atom was taken as 4.2×10^{-8} cm.

Zemansky²⁷ later interpreted his results in a completely different manner. (The two theories will hereinafter be referred to as the first and second theories.) He assumed that the emerging radiation was produced entirely as a result of the raising of 2^3P_0 atoms to the 2^3P_1 state by collisions of the first kind with normal atoms. He assumed further that the resulting resonance radiation escaped from the gas without a new metastable atom being formed and also that the time of imprisonment of this radiation, was small compared with (or at least shorter than) the mean life of the 2^3P_0 atoms, so that the rate of decay of the emerging radiation should be the same as the rate of decay of the 2^3P_0 atoms. On the basis of these assumptions, it was found that the concentration of 2^3P_0 atoms decayed exponentially with the time, with an exponential constant given by the expression

$$1/T = c'/\sigma_d^2 N + 9.04 \times 10^4 \gamma \sigma_d^2 N \quad (22)$$

where c' is a numerical constant, depending on the geometry of the cell and the thermal speed of the atoms, having the value 3.4×10^3 for the large cell (1.95 cm thick) and 6.8×10^3 for the small cell (1.3 cm thick), σ_d is the distance between the center of the 2^3P_0 atom and center of the normal atom at impact, N is the concentration of normal atoms, and γ is the probability that, on collision with a normal atom, a 2^3P_0 atom will be raised to the 2^3P_1 state. The first term on the right-hand side of this equation represents the exponential constant of decay due to diffusion to the walls; it is the important term at the lower pressures. The second term represents the exponential constant of decay due to collisions of the first kind; it is the important term at the higher pressures.

Zemansky found that the experimental curves of Fig. 5 were well represented by Eq. (22) provided σ_d were taken as 2.3×10^{-8} cm and γ as 0.0096. Subtracting from the above value of σ_d the radius of the normal Hg atom, 1.8×10^{-8} cm, a radius of 0.5×10^{-8} cm for the metastable atom was obtained, or 0.3 times the normal radius (diffusion cross section about 0.4—i.e., $(2.3/3.6)^2$ —times the normal cross section). We may write $\gamma \sigma_d^2 = (1 + \epsilon/kT) (\exp - \epsilon/kT) \sigma_0^2$,²⁸ where $\epsilon = 0.218$ volt is the energy difference between the 2^3P_0 and 2^3P_1 states of Hg, k is Boltzmann's constant, T is the absolute temperature and σ_0^2 is the effective cross section for collisions of the first kind between normal and metastable Hg atoms raising the latter to the 2^3P_1 state. (Here $(1 + \epsilon/kT) (\exp - \epsilon/kT)$ is the fraction of all collisions within a distance σ_0 in which the kinetic energy of relative motion is $\geq \epsilon$. This fraction is of the order of 0.01 at the upper temperatures in Zemansky's experiments.) It follows from Zemansky's results that $\sigma_0^2 \sim 5 \times 10^{-16}$ cm² which is again of the order of 0.4 the normal cross section $(3.6 \times 10^{-8})^2$.

In regard to these consequences of the second theory it is unusual to find a diffusion cross section (σ_d^2) for the metastable atom which is so much

²⁷ M. W. Zemansky, Phys. Rev. **34**, 213 (1929).

²⁸ See for example E. W. Samson, Phys. Rev. **40**, 940 (1932).

smaller than the normal cross section. Webb and Messenger²⁹ and Samson²⁸ have found for 2^3P_0 Hg atom diffusing in N_2 cross sections slightly greater than the normal cross section. However in the case of 2^3P_0 Hg atoms diffusing in Hg *vapor* the possible frequent exchange of the energy of these atoms with normal atoms at collisions (exchange of identity) might, as has been pointed out to the writer, account for an apparent abnormally small σ_d^2 . In view of this possibility undue emphasis should probably not be placed on the smallness of σ_d^2 resulting from the second theory.

Of more significance, it is believed, is the value of σ_0^2 of 0.4 times the normal cross section to which the second theory leads. Such a large value of σ_0^2 does not accord with the results of Orthmann and Pringsheim.³⁰ These authors studied the resonance of $\lambda 2537$ and the fluorescence of certain Tl lines as a function of Hg vapor pressure when a quartz Hg vapor resonance cell containing Tl at a fixed vapor pressure of 0.02 mm (610°C) was illuminated with light from a water-cooled quartz mercury arc. As the vapor pressure of the Hg was raised from a few millimeters to 760 mm the resonance of $\lambda 2537$ decreased to almost zero; but the fluorescence of the Tl lines, caused by collisions of the second kind of Tl atoms with metastable Hg atoms, lost practically none of their brilliancy. Since at 760 mm there were roughly 30,000 times as many Hg atoms as Tl atoms present, it follows that a 2^3P_0 Hg atom made roughly this many collisions with normal Hg atoms before colliding with a Tl atom. At the temperature in question, somewhat greater than 610°C, roughly $\frac{1}{4}$ of these collisions, or about 7000, involved relative kinetic energy $\geq \epsilon$ and hence it seems that a 2^3P_0 Hg atom must have been able to withstand at least many hundreds and possibly thousands³¹ of kinetic theory collisions with normal Hg atoms energetically capable of raising it to the 2^3P_1 state. Thus the experiments of Orthmann and Pringsheim indicate σ_0^2 to be at most hundreds of times less than the normal cross section, a result, which is in accord with other evidence now to be discussed.

In all cases known to the writer where there is an appreciable energy exchange (e.g., as great as the 0.218 volts here considered) between the kinetic energy of relative motion of the colliding atoms or molecules and the potential energy of one of them the effective cross sections for these collisions are very small compared with the normal cross sections. As examples there may be mentioned the well-known very small quenching cross sections ($2^3P_1 \rightarrow 2^3P_0$) of monatomic gases for Hg resonance radiation. According to the results of

²⁹ H. W. Webb and Helen A. Messenger, Phys. Rev. 40, 466L (1932).

³⁰ W. Orthmann and P. Pringsheim, Zeits. f. Physik 35, 626 (1926).

³¹ We cannot use the number 7000 here because, when a 2^3P_0 atom is raised to the 2^3P_1 state, this 2^3P_1 atom, or another produced by the absorption of $\lambda 2537$ emitted from it, may be returned to the 2^3P_0 state by a quenching collision. This process probably did not take place very many times, however, for otherwise $\lambda 2537$ would not have been completely quenched. This follows since the average free path of the diffusing $\lambda 2537$ in the resonance cell was probably not less (on account of large coupling or other pressure broadening) than the original average depth of penetration of the exciting light (water-cooled source) and since the cross section for quenching is probably very small.

Zemansky³² the quenching cross sections in the case of He and A are < 0.001 times the normal cross section.³³ Finally may be cited the observed long lives of metastable Ne atoms in Ne at pressures of a few millimeters. From these lives Penning³⁴ has calculated that the s_5 metastable state is able to withstand some 10^5 kinetic theory collisions with normal Ne atoms at room temperature without being raised to the s_4 state. ϵ being only about 0.05 volt in this case nearly half of these collisions are energetically capable of causing the transfer in question.³⁵

It appears therefore that the value of σ_0^2 of 0.4 times the normal cross section which follows from the second theory is higher than any known similar cross sections in cases involving other gases by a factor of at least 100 (and possibly by a factor of 1000 or more).³⁶

Insofar as the conclusions resulting from the second theory (especially the conclusion regarding σ_0^2) are unusual they are deserving of special attention. It is believed, however, that they require further confirmation, not only in view of the discussion already given, but because the experimental results can be sufficiently accounted for, as will be shown below, on the basis of the first theory and §§II and III of the present paper.

Undoubtedly all the processes treated in both theories take place; and a more comprehensive treatment, along the lines of the treatment of Samson,²⁸ would include them all. But it seems highly probable that the collisions of the first kind postulated in the second theory take place only so slowly that this process can, to a first approximation, be disregarded. On this view, the production of $\lambda 2537$ as a result of these collisions was probably so faint as not to have been observed in the experiments, and most of the energy of the 2^3P_0 atoms was probably lost at the walls.

³² M. W. Zemansky, Phys. Rev. **36**, 919 (1930).

³³ The apparent small quenching effects of He and A observed by Stuart, (Zeits. f. Physik **32**, 262 (1925)), which have been discussed by many writers, are probably largely explicable in terms of pressure line broadening (see the recent work of v. Hámos, Zeits. f. Physik **74**, 631 (1932)) and the effects of traces of impurities.

³⁴ F. M. Penning, Zeits. f. Physik **46**, 335 (1928) see also some remarks in this connection by Kenty, Phys. Rev. **40**, 633L (1932).

³⁵ It is to be noted that when the kinetic energy of relative motion is exactly equal to ϵ the cross section for collisions of the first kind is zero because of the infinitely small chance that angular momentum can be conserved in such collisions (see for example Ruark and Urey, *Atoms Molecules and Quanta*, p. 475). When the kinetic energy of relative motion is but very little in excess of ϵ the cross section for such collisions will presumably be small for the same reason. The condition for the conservation of angular momentum should be easier of fulfillment in the case where one of the colliding partners is a molecule for this can take on angular momentum in varying amounts, (see reference 36).

³⁶ M. L. Pool, Phys. Rev. **38**, 955 (1931) has suggested that collisions of the first kind in the case of 2^3P_0 Hg atoms in N_2 may be associated with resonance transfers of energy between N_2 molecules in the first vibration state and 2^3P_0 Hg atoms. Such an explanation might account for the fact that while Cario and Franck (Zeits. f. Physik **37**, 619 (1926)) found that $\lambda 2537$ of Hg was not quenched by N_2 at 750°C , Oldenburg (Zeits. f. Physik **49**, 609 (1928)) found that this radiation was quenched by A at this temperature. Compare also the results of Orthmann and Pringsheim above for Hg at high pressures.

V. APPLICATION OF THE FIRST THEORY WITH THE AID OF §§II AND III

Whether or not collisions of the first kind as postulated in the second theory were of appreciable importance in the experiments it will be evident that the rate of escape of resonance radiation through the Hg vapor must have been at least as rapid as that following from the first theory. As has been discussed above this rate of escape is considerably greater than can be accounted for on the basis of classical theories of resonance radiation diffusion; let us see if it can be accounted for by means of the developments of the present paper.

Having chosen the line 1 of Fig. 5 to represent the last term on the right-hand side of Eq. (21), Zemansky found that in order to account for the decay curves *A* and *B* of Fig. 5, the quantity β , defined by him as the mean or equivalent atomic absorption coefficient, would have to decrease as *N* increased. The values of β for $N = 1.4 \times 10^{15}$ Hg atoms per cm^3 are found to be $0.131 \alpha_0^{-1}$ and $0.124 \alpha_0^{-1}$ for the small (1.3 cm) and large (1.95 cm) cells, respectively, α_0^{-1} being the atomic absorption coefficient for the core of the line, for the appropriate temperature, as calculated from the mean life of the 2^3P_1 Hg atom according to the method used by Zemansky.³⁷ Similarly for $N = 29 \times 10^{15} \text{ cm}^{-3}$ the values found for β are $0.0169 \alpha_0^{-1}$ and $0.0116 \alpha_0^{-1}$ for the small and large cells, respectively.

It will be more in line with the reasoning of §II to study the quantity $(1/\beta)^2$ appearing in Eq. (21) rather than β . In the derivation of Eq. (21) the quantity $1/(4\tau N^2 \beta^2)$ occurs as the diffusion coefficient of the resonance radiation, which may be equated to D_1 or D_2 in Eqs. (13) and (14), respectively. If this is done, it is found that $3/(2N^2 \beta^2) = \overline{p_1^2}(y_1)$ or $\overline{p_2^2}(y_1)$, respectively, and we may regard the quantity $3/(2N^2 \beta^2) = \overline{p_E^2}$ as the experimentally determined effective average square free path, as calculated from the experimental results.

Table II shows the comparison, for two values of *N*, and for the two cells used, of the quantity $\overline{p_E^2}$ with the values of $\overline{p_1^2}(y_1)$ and $\overline{p_2^2}(y_1)$ as calculated by Eqs. (16) and (17), respectively, (with the help of Eq. (15)). All values for

TABLE II. $\overline{p_1^2}(y_1)$, $\overline{p_2^2}(y_1)$: limiting values for the effective average square free path as calculated by Eqs. (16) and (17), respectively. $\overline{p_E^2} = 3/(2N^2 \beta^2)$: effective average square free path as calculated from Zemansky's experimental results. All these quantities are expressed in terms of p_0^2 , the square of the mean free path of the core of the line.

N $\times 10^{-15}$	1.3 cm cell			1.95 cm cell		
	$\overline{p_1^2}(y_1)/p_0^2$	$\overline{p_2^2}(y_1)/p_0^2$	$\overline{p_E^2}/p_0^2$	$\overline{p_1^2}(y_1)/p_0^2$	$\overline{p_2^2}(y_1)/p_0^2$	$\overline{p_E^2}/p_0^2$
1.4	66	28	88	94	38	99
29	910	300	5300	1330	490	11200

³⁷ M. W. Zemansky, Phys. Rev. 36, 219 (1930). See particularly pp. 228, 229. In making the calculations used in the present paper the value of τ of 1.08 and 10^{-7} sec. as found by P. M. Garrett, Phys. Rev. 40, 779 (1932) has been used in place of the value 1.0×10^{-7} sec. used by Zemansky. The values found for α_0' are 1.21×10^{-13} and 1.11×10^{-13} for $T = 70^\circ\text{C}$ and 130°C , respectively, ($N = 1.4 \times 10^{15}$ and 29×10^{15} , respectively).

average square free paths are expressed in terms of p_0^2 where $p_0 = 1/N\alpha_0^1$ is the mean free path of the core of the line, (α_0^1 being the atomic absorption coefficient for the core of the line as calculated in each case for the temperature in question). From Table II it is seen that the observed effective average square free path increases with the thickness of the cell. The theoretical calculations are in agreement with this in that they also predict an increase in the effect average square free path with the size of the cell. Theoretically and experimentally also the effective average square free path (expressed as a multiple of p_0^2) is seen to increase with the gas density. Regarding the actual magnitude of the observed effective average square free path, the near agreement of the order of magnitude of this quantity and the corresponding calculated limiting values in the case of the lower gas density (especially as regards $\bar{p}_1^2(y_1)$) indicates that this quantity could probably be accounted for, with a more rigorous theory, largely on the basis of Doppler broadening only. At the higher gas density ($N = 29 \times 10^{15} \text{ cm}^{-3}$) however, this does not appear to be within the range of possibility in view of the great discrepancies between the observed and calculated values of the average square free path. This is taken to indicate that at the higher gas densities in Zemansky's experiments coupling or other broadening was already of great importance in increasing the rate of escape of the radiation.^{7,38}

The reasoning so far has been based on the assumption that the line 1 of Fig. 5, of slope 3×10^{-13} , is the true line representing the effect of quenching collisions (i.e., the last term on the right-hand side of Eq. (21)). However, the experimental results admit of the assumption of any line of slope between 0 and about 4.5×10^{-13} , to represent the term in question, the variation of β with N being supposed to be such as to enable the experimental curves to be accounted for in any case. It appears, however, that a slope as great as 4.1×10^{-13} cannot be assumed because it is found that a line of this slope would require that $(1/N\beta)^2$ be the same for both cells whereas theory requires, as has been seen above, that this quantity be greater for the larger cell. About all that can be said is that the line, 1, chosen by Zemansky seems to represent a reasonable upper limit for the slope and hence, by Eq. (21) for the quenching efficiency, b (or the quenching cross section, see §IV). The effect of choosing a line of smaller slope than this line would be to increase the observed values of the average square free path and hence to increase the discrepancy between the observed and calculated values of this quantity; but the effect of coupling or other broadening can always be supposed (at least until further data are available) to make up for this discrepancy.

The experiments of Webb and Messenger⁶ on the imprisonment of $\lambda 2537$ of Hg are essentially similar to those of Zemansky. They cover, for the most part, a lower range of vapor densities; but, insofar as the density ranges overlap, the results are in sufficient quantitative agreement; and in general they are in agreement in that both sets of results show that resonance radiation

³⁸ At $N = 29 \times 10^{15}$ atoms per cm the pressure is of the order of 1 mm and Minkowski found the coupling broadening in Na vapor to begin to be of relative importance at 0.02 mm. See reference 24.

escapes from a gas progressively faster than can be accounted for on classical theories of radiation diffusion the higher the gas density. The conclusions arrived at in the present paper are thus also in qualitative agreement with these results of Webb and Messenger. It would appear in view of the near agreement of the orders of magnitude of the observed and calculated average square free paths at the lower densities in Zemansky's experiments (see the first row of Table II), that the exponential constants of decay in Webb and Messenger's experiments, except possibly at the highest densities, could be accounted for on the basis of the Doppler effect alone. Webb and Messenger concluded that their experiments had to do mainly with radiation diffusion (rather than with metastable atoms, at least for all but the higher densities), and that existing theories of radiation diffusion would have to be revised to account for their results; the results of the present paper are in accord with these conclusions.

Since the main body of this paper was written, a paper by Samson²⁸ has appeared in which the effect of Doppler (or other) broadening on the radiation diffusion problem is considered from a different aspect. In the following note, Dr. Zemansky discusses the relationship (particularly as regards the results obtained) of Samson's theory to the present one.

My best thanks are due to Dr. M. W. Zemansky who has read the manuscript and made a number of important suggestions.

Note on the Equivalent Absorption Coefficient for Diffused Resonance Radiation

By M. W. ZEMANSKY
College of the City of New York

(Received August 25, 1932)

It is shown that the ideas expressed in the preceding theoretical paper by Kenty when applied to the diffusion of resonance radiation in a layer of gas of finite thickness provide a method of calculating an equivalent absorption coefficient of the gas for all the frequencies due to the Doppler effect that are present in the diffusing radiation. This average absorption coefficient is calculated and compared with a similar quantity calculated on the basis of a different point of view by Samson. Both average absorption coefficients are discussed in connection with the author's experiments (1927) on the rapidity of escape of resonance radiation emitted from a slab of mercury vapor after the cut-off of the excitation.

IN THE preceding theoretical paper, Kenty gives a treatment of the emission and absorption of quanta by moving atoms, in which it is pointed out that, owing to the Doppler effect, the group of frequencies comprising a Doppler line can pass from one part of a gas to another much more readily than an infinitesimal frequency band at the center of the line when no Doppler effect is present. According to Kenty, his equations are strictly applicable only to a gas of infinite volume, in which case both the diffusion coefficient and the mean free path of the radiation are found to be infinite. An approximate method is given, however, of treating the case of a finite layer of gas. It is not the purpose of this note to scrutinize Kenty's ideas carefully, but instead to examine the consequences of his method of handling the finite case. It will be seen that this method is essentially a device for obtaining an equivalent absorption coefficient of a gas for the group of frequencies generated by the Doppler effect.

According to Kenty, the diffusion coefficient of Doppler radiation in a gas is given by his Eq. (7).

$$D = (1/3\tau k_0^2) \int_0^\infty R f_1(R) dR \quad (1)$$

where k_0 is the absorption coefficient of the gas for the center of the line, τ the lifetime of the excited state to which the atoms are raised by the radiation, and $f_1(R)$ is a distribution function corresponding to a situation in which the atoms are originally excited by a continuous spectrum (in practice by a line much broader than the Doppler line). Of the two distribution functions, $f_1(R)$ and $f_2(R)$, given by Kenty, $f_1(R)$ has been chosen because it is believed that it approximates more closely the actual conditions of an experiment. $f_1(R)$ is given by his Eq. (4), namely

$$f_1(R) = (4/\pi^{1/2}) \int_0^\infty \int_0^y y e^{-y^2} e^{-R} e^{-x^2} dx dy. \quad (2)$$

Substituting Eq. (2) in Eq. (1) and integrating R from 0 to ∞ , we obtain

$$D = [2(2)^{1/2}/3\pi^{1/2}\tau k_0^2] \int_0^\infty y e^{-y^2} dy \int_0^{2^{1/2}y} e^{x^2} dx. \quad (3)$$

The integration over y is an integration over the velocities of the emitting atoms. If all velocities are taken into account D becomes infinite. Kenty's approximate method of handling a practical situation is to integrate y from 0 to an upper limit y_1 , where y_1 is given by the formula

$$k_0 e^{-y_1^2} = 1/l, \quad (4)$$

l being the thickness of the layer of gas. Eq. (3) then becomes

$$\begin{aligned} D &= [2(2)^{1/2}/3\pi^{1/2}\tau k_0^2] \int_0^{y_1} y e^{-y^2} dy \int_0^{2^{1/2}y} e^{x^2} dx \\ &= [2^{1/2}/3\pi^{1/2}\tau k_0^2] \int_0^{y_1} 2ye^{y^2} F(2^{1/2}y) dy \end{aligned} \quad (5)$$

where

$$F(t) = e^{-t^2} \int_0^t e^{x^2} dx. \quad (6)$$

The integral in Eq. (5) can be expressed in terms of the F function defined by Eq. (6) as follows: Integrating by parts,

$$\int_0^{y_1} 2ye^{y^2} F(2^{1/2}y) dy = [e^{y^2} F(2^{1/2}y)]_0^{y_1} - \int_0^{y_1} e^{y^2} dF(2^{1/2}y)$$

and, in virtue of the relation $(d/dt)F(t) = 1 - 2tF(t)$,

$$\begin{aligned} \int_0^{y_1} 2ye^{y^2} F(2^{1/2}y) dy &= e^{y_1^2} F(2^{1/2}y_1) - 2^{1/2} \int_0^{y_1} e^{y^2} [1 - 2(2)^{1/2} F(2^{1/2}y)] dy \\ &= e^{y_1^2} F(2^{1/2}y_1) - 2^{1/2} e^{y_1^2} F(y_1) + 2 \int_0^{y_1} 2ye^{y^2} F(2^{1/2}y) dy \end{aligned}$$

whence, finally

$$\int_0^{y_1} 2ye^{y^2} F(2^{1/2}y) dy = e^{y_1^2} [2^{1/2} F(y_1) - F(2^{1/2}y_1)]. \quad (7)$$

From Eqs. (4), (5) and (7) the diffusion coefficient is found to be

$$D = [(2)^{1/2}l/3\pi^{1/2}\tau k_0] [2^{1/2} F(\ln k_0 l)^{1/2} - F(2 \ln k_0 l)^{1/2}]. \quad (8)$$

On the basis of the Einstein theory of radiation, without appeal to the analogy with molecular diffusion, and neglecting Doppler effect, Milne

showed that radiation of infinitesimal spectral width diffused through a gas with a diffusion coefficient equal to

$$D' = 1/4\alpha^2\tau \quad (9)$$

where α stands for the absorption coefficient of the gas for the radiation in question. In the case of the diffusion of a band of frequencies comprising a line we may define an *equivalent absorption coefficient* as a quantity, \bar{k} which, when substituted for α in Eq. (9), will give the correct diffusion coefficient to be used when the diffusing radiation is not of infinitesimal spectral width.

Kenty's expression for the diffusion coefficient, Eq. (8), enables us to compute \bar{k} when the Doppler effect is present. For, by definition of \bar{k} ,

$$1/4\bar{k}^2\tau = [2^{1/2}l/3\pi^{1/2}\tau k_0] [2^{1/2}F(\ln k_0 l)^{1/2} - F(2 \ln k_0 l)^{1/2}]$$

and

$$\bar{k}l = \left[\frac{3}{4} \left(\frac{\pi}{2} \right)^{1/2} \right]^{1/2} \left[\frac{k_0 l}{2^{1/2}F(\ln k_0 l)^{1/2} - F(2 \ln k_0 l)^{1/2}} \right]^{1/2}. \quad (10)$$

From the splendid table of values of the F function given by Miller and Gordon,¹ $\bar{k}l$ was evaluated for various values of $k_0 l$ and the result is shown in Table I and curve A of Fig. 1. It is seen from the curve that Kenty's method breaks down for small values of $k_0 l$, which is to be expected in view of the approximations made.

TABLE I. Kenty's equivalent absorption coefficient.

$k_0 l$	$\bar{k}l$	$k_0 l$	$\bar{k}l$
1.5	3.05	100	21.2
2	2.76	200	31.4
3	2.97	500	54.2
4	3.31	1000	77.8
5	3.70	2000	114
10	5.39	3000	142
15	6.85	4000	166
20	8.10	5000	186
30	10.4	6000	205
40	12.3	7000	223
50	14.1	8000	240

The problem of calculating an equivalent absorption coefficient for Doppler radiation to be used in conjunction with Milne's radiation diffusion equation was attacked in a different way by Samson² without considering the motions of individual atoms or the free paths of individual groups of quanta. Samson defined an equivalent absorption coefficient \bar{k} as the absorption coefficient that a gas would have for that infinitesimal frequency band which would show the same percentage transmission that is shown by a Doppler line.

The transmission of an infinitesimal frequency band by a gas whose absorption coefficient is \bar{k} is $e^{-\bar{k}l}$, whereas the transmission of a line of the form

¹ W. L. Miller and A. R. Gordon, Phys. Chem. **35**, 2878 (1931).

² E. W. Samson, Phys. Rev. **40**, 940 (1932).

$I_0 e^{-\omega^2}$ by a gas whose absorption coefficient has the form $k_0 e^{-\omega^2}$ is

$$\frac{\int_{-\infty}^{\infty} \exp(-\omega^2) \exp(k_0 l e^{-\omega^2}) d\omega}{\int_{-\infty}^{\infty} \exp(-\omega^2) d\omega}$$

whence Samson's $\bar{k}l$ is given by the relation

$$\exp(-\bar{k}l) = \frac{\int_{-\infty}^{\infty} \exp(-\omega^2) \exp(-k_0 l e^{-\omega^2}) d\omega}{\int_{-\infty}^{\infty} \exp(-\omega^2) d\omega} \quad (11)$$

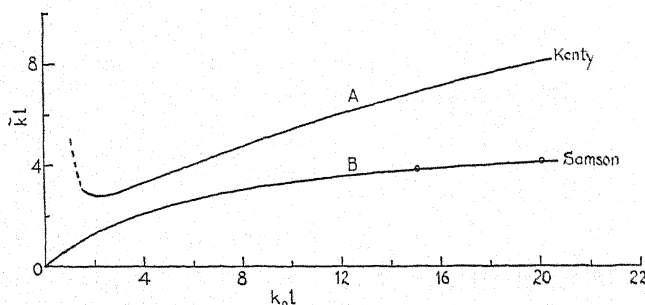


Fig. 1.

Samson's equivalent absorption coefficient is given for a number of values of $k_0 l$ in Table II, and is shown as curve B in Fig. 1. The curve shows that

TABLE II. Samson's equivalent absorption coefficient.

$k_0 l$	$\bar{k}l$	$k_0 l$	$\bar{k}l$
0	0	4	2.104
1	0.665	9.7	3.29
2	1.241	14.4	3.76
3	1.715	19.9	4.15

for small values of $k_0 l$, $\bar{k}l$ behaves as it should, becoming zero when $k_0 l$ is zero. For large values of $k_0 l$ however, judging from the very slow rate at which the curve is rising, it appears that $\bar{k}l$ is too small. One might hazard the guess that Samson's method is valid at low opacities (small values of $k_0 l$) and Kenty's method at high opacities.

In Kenty's experimental paper, the author's experiments on the escape of resonance radiation³ from mercury vapor after the cut-off of the excitation, are interpreted as being due entirely to radiation diffusion rather than to metastable atoms. A complete discussion of the relative merits of these two interpretations is beyond the scope of this note. It should be pointed out,

³ M. W. Zemansky, Phys. Rev. 29, 513 (1927).

however, that, since the two theories are not mutually exclusive, it is quite possible that the correct explanation involves both radiation diffusion and metastable atoms, in a manner similar to Samson's treatment of the after-glow of mercury resonance radiation from a mixture of mercury vapor and nitrogen.

With the assumption that radiation diffusion takes place in these experiments it is instructive to calculate the equivalent absorption coefficient by both Kenty's and Samson's method, and with the aid of Milne's equation for the exponential constant of decay of the escaping radiation, calculate the exponential constant to be expected. This is done as follows:

With the equation⁴

$$5\left(\frac{\pi}{4 \ln 2}\right)^{1/2} k_0 \Delta \nu_D = \frac{\lambda_0^2}{8\pi\tau} \frac{g_2}{g_1} N, \quad (12)$$

it is possible to compute $k_0 l$ at a given vapor pressure (which determines N), a given temperature (which determines $\Delta \nu_D$), and with the most reliable value of $\tau^5 (1.08 \times 10^{-7} \text{ sec.})$. Knowing $k_0 l$, $\bar{k}l$ is obtained either by Kenty's or by Samson's method. Then making use of Milne's equation for the decay constant neglecting impacts,

$$\beta = (1/\tau) / [1 + (\bar{k}l/\lambda_1)^2] \quad (13)$$

where λ_1 is approximately $\pi/2$, β is calculated and compared with the experimental values of β at low vapor pressures before impacts begin to play an important role.

With Kenty's method of calculating $\bar{k}l$, the results are shown in Table III, where it is seen that there is agreement in order of magnitude. With

TABLE III.

$T^\circ K$	$l = 1.95 \text{ cm}$		$l = 1.30 \text{ cm}$	
	Exp. β	β from Eq. (13)	Exp. β	β from Eq. (13)
333	26600	29500		
343	14200	15000	28100	24500
353	8810	7940	19300	12000
363	7070	4380	12100	6750

Samson's equivalent absorption coefficient, the results show a disagreement by a factor of at least 10. This is in line with the statement made previously, namely, that Samson's equivalent absorption coefficient is too small at large values of $k_0 l$.

⁴ M. W. Zemansky, Phys. Rev. **36**, 219 (1930).

⁵ P. H. Garrett, Phys. Rev. **40**, 779 (1932).

The Effect of Tension on the Electrical Resistance of Single Bismuth Crystals

By MILDRED ALLEN

Research Laboratory of Physics, Harvard University

(Received October 19, 1932)

The compensated potentiometer method of measuring minute variations in small resistances which was developed by P. W. Bridgman has been used in the study of the effect of tension, applied parallel to the direction of current flow, on the resistance of single bismuth crystals. The tension coefficient of resistance at 30°C has been found to depend on the orientations both of the principal (111) and secondary (11 $\bar{1}$) cleavage planes with respect to the tension. For the limiting case of the principal cleavage plane perpendicular to the tension, the coefficient is independent of the orientation of the secondary cleavage planes; in that of the principal cleavage plane parallel to the tension, the coefficient varies very little and is very probably independent of the secondary orientation. In the case where the normal to the principal cleavage plane makes an angle of about 60° with the tension, the variation of the coefficient with the orientation of the secondary cleavage plane seems to be a maximum. This variation involves a change in sign as well as in magnitude, so that for certain orientations the coefficient becomes positive instead of remaining negative. The coefficient shows trigonal symmetry, as it must do if it is to be consistent with the known corporeal trigonal symmetry of the bismuth crystal. The paper presents only these empirical results.

THE EFFECT on the resistance of single crystals of various elements produced by hydrostatic pressure¹ has previously been studied, but not the effect of tension.² It is to be expected that the effect of tension will be more complicated than that of hydrostatic pressure, since in the case of the latter the symmetry of the crystal is unchanged. As a result the pressure coefficient of resistance is a function only of a single parameter, the orientation of the main cleavage plane with respect to the direction of the electric current, and, as Professor Bridgman has shown, may be expressed in terms of but two constants, one associated with the current flowing perpendicular to the normal to the principal cleavage plane and the other with a current parallel to it. In the case of tension, on the other hand, the applied force must cause a change in the symmetry of the crystal, a change which depends not only on the orientation of the principal cleavage plane with respect to the tension, but also on the orientation of the secondary cleavage planes. The problem is thus a more complicated one, since the effect may very possibly depend on more than the change of symmetry. Experimentally, however, it has been found that the coefficient may be represented within experimental error as a function of only two parameters which may be taken to

¹ P. W. Bridgman, *Proc. Amer. Acad.* **60**, 305 (1925); **63**, 351 (1929).

² Trapeznikowa (*K. Akad. Amsterdam* **34**, 840 (1931)) finds no effect of tension or of unidirectional pressure on the resistance of bismuth crystals. However, the sensitiveness of his apparatus was such that he could not detect changes of less than 1 percent whereas the changes to be reported in this paper are at most 0.2 percent of the initial resistance.

be the primary and secondary orientations of the crystal with respect to the tension. At the present time, it is only possible to arrange these experimental results of the effect of tension on the resistance of single bismuth crystals in a consistent set of curves without, however, giving any theoretical basis for the curves.

EXPERIMENTAL ARRANGEMENT

To measure the small changes in resistance involved, the compensated potentiometer method developed by Professor Bridgman,³ was used. Fig. 1 gives the electrical connections of this method. The potential difference V_{AB} across the potential leads to the crystal AB is balanced against the potential fall V_{CD} of the supplementary compensating circuit Q , and, when the effect of the tension on the resistance is large enough, this in turn is balanced

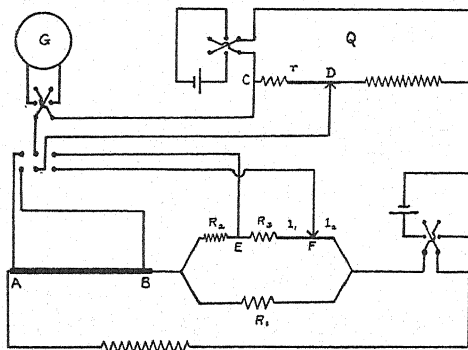


Fig. 1.

against the fall V_{EF} , so that the unknown resistance R_{AB} is calculable in terms of the known resistances R_1 , R_2 , R_3 , l_1 and l_2 . The fractional change in resistance is then

$$\Delta R/R = \Delta R_{AB}/R_{AB} = \Delta l/(l_1 + R_3) \quad (1)$$

where the slide wire lengths are reduced to ohms. As Professor Bridgman has pointed out, the advantage of this method is that the result is independent of the current flowing through the crystal provided that that remains constant during a single reading. This is cared for by using a large and heavy 6-volt storage battery as the source of the current which was usually kept at about 0.45 amp. The largest value of the fraction $\Delta R/R$ actually measured was 22×10^{-4} . Inasmuch as the bismuth resistances themselves were less than 0.01 ohm, the precision of the method is very high. When the effect was too small to be measured by this *null* method, the average change in reading of the galvanometer due to the application of the tension was determined by reading the galvanometer alternately with and without the tension, plotting the observed readings against the time scale and finding the average distance between the two curves. Ideally, both curves should be straight horizontal lines, but the zero drift of the galvanometer, small changes in the voltage

³ P. W. Bridgman, Proc. Amer. Acad. 56, 61 (1921).

of the compensating circuit, and slight variations in temperature which produce in addition to small changes in resistance small thermal e.m.f.'s give rise to small drifts, as in Fig. 2, which is representative of the type of curve obtained in this way. The deflections in most cases were much greater than the drifts observed. These changes in galvanometer readings with tension are proportional to the changes in potential difference and thus to the resistance changes of the crystal, the constants of proportionality⁴ depending in an easily ascertainable manner on the known e.m.f.'s and resistances of the circuit. This *deflection* method was used in each determination of the tension coefficient to check the linearity of the change of resistance with tension and was checked in the case of the greatest tension against the *null* method for absolute value.

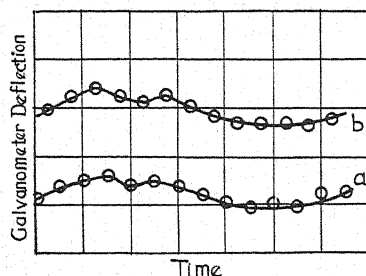


Fig. 2. *a* without tension; *b* with tension.

Since temperature fluctuations produce undesirable changes in the resistance to be measured, the crystal was mounted in a constant temperature bath of kerosene. This was thoroughly stirred and was kept at the constant temperature of approximately 30°C by means of a metal thermostat which, although it drifted slightly, prevented any large sudden change in temperature. In Fig. 3 is sketched the general arrangement of the crystal mounting and constant temperature bath. The heating coil is not shown in the figure, but is wound on a square frame larger than the brass box *mmmm* so that the heat source is not concentrated in one spot. The crystal itself *AB* is mounted on a brass support inside a heavy copper cylinder *pp* 5/32 inch thick, and this

⁴ The voltage sensitivity of the galvanometer, which was made as great as possible by placing the scale about five meters from the galvanometer, varied with each value of the total crystal resistance. The reason for this is obvious. For, applying Kirchhoff's laws to the network, we have, where ΔE is the increase in V_{AB} , Δi_{CD} the change in current in CD produced by the lack of balance, and I_G the current through the galvanometer,

$$\Delta i_{CD} = I_G \quad (a)$$

a relation arising from the condition on current at the junction C , and

$$I_G R_G = (V_{AB})_0 + \Delta E - (V_{CD})_0 - \Delta i_{CD} r \quad (b)$$

arising from the condition on potential falls in the closed circuit $ABCD$. But $(V_{AB})_0$ and $(V_{CD})_0$ are the values of the potential falls for the balanced case and so are equal; hence

$$I_G R_G = \Delta E - I_G r. \quad (c)$$

The voltage sensitivity is consequently

$$\Delta E / I_G = R_G + r. \quad (d)$$

This method will then function with the maximum of ease, if r has approximately the value of the critical damping resistance of the galvanometer.

whole mounting is placed in air inside the brass box. The addition of the brass box seemed advisable, since in its absence it seemed impossible to stir the kerosene sufficiently inside the copper cylinder to insure constancy of temperature. With the addition of the brass box, erratic fluctuations in temperature were no longer observed.

The crystals used which were from $1\frac{1}{2}$ to 3 inches long and had a diameter of approximately $\frac{1}{8}$ inch, had all been made by Professor Bridgman from bismuth furnished by Kahlbaum, and were most generously put by him at the writer's disposal. He had previously used these same crystals in his determination of the specific resistance of bismuth crystals and of their

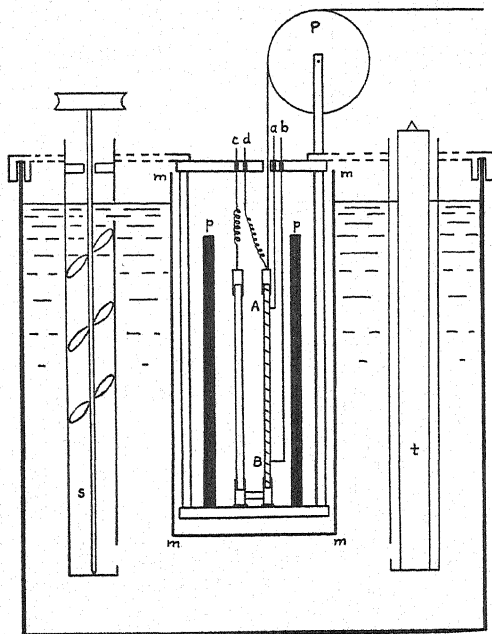


Fig. 3. *AB* crystal; *a, b* potential leads; *c, d* current leads; *pp*, copper cylinder; *mmmm* brass box; *s* stirrer; *t* metal thermostat (shown without amplifying levers); *P* pulley.

hydrostatic pressure coefficient of resistance.¹ These crystals were soft-soldered into brass holders at either end, one of which holders was fastened firmly to the large brass support which held the Bakelite pulley *P* over which the string carrying the tension passed. Fine copper wires of 0.01 inch diameter were soft-soldered to the crystal a few millimeters from each end for potential leads and a thermocouple was soldered close to one end. The other end of this thermocouple was inserted in the kerosene and so enabled one to know when the crystal temperature had come to that of the kerosene; with the air layer between the brass box and the crystal, coming to equilibrium was a slow process and at least an hour was required before equilibrium was obtained. The string carrying the tension passed over another pulley near the galvanometer telescope; weights were hung on a steel spring attached to this end. The steel spring prevented the sudden application of the whole tension

to the crystal. In view of the low elastic limit (22.1 kg/cm² shearing stress across the principal cleavage plane)⁵ of single bismuth crystals, 1200 grams was the greatest force applied with crystals of the given cross section, or about 15–20 kg/cm².

RESULTS

Forty-five single bismuth crystals of different orientations were studied, the adiabatic tension coefficient of resistance β at 30°C being determined in each case. This coefficient is defined as the ratio of the change in resistance produced by a tension of 1 kg/cm² to the total resistance. It is adiabatic in that the time intervals between consecutive applications of the tension were about one minute, so that each reading was taken within half a minute of the establishment of the new state. This short interval would not allow for the establishment of thermal equilibrium. On the basis of an adiabatic process

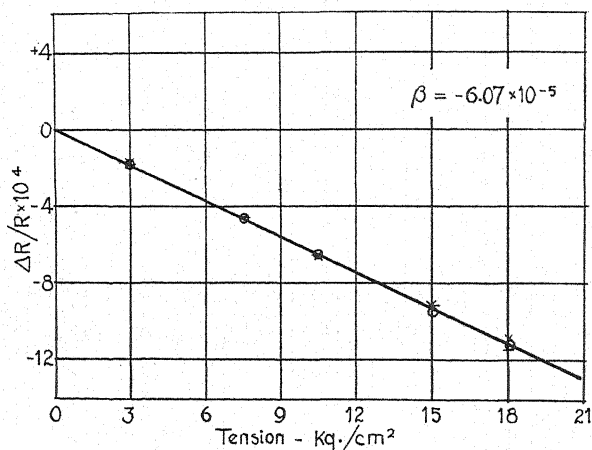


Fig. 4. Circles, plus signs and crosses signify different days' readings.

taking place, the change of temperature arising from the sudden application of the maximum tension comes out by computation to be about -0.006°C . Since the temperature coefficient of resistance of bismuth crystals is 0.00445, this change of temperature produces a relative change in the resistance of -0.27×10^{-4} which corresponds to a change in the computed value of the coefficient β of about -0.18×10^{-5} in each case, the correction to be subtracted in passing from the adiabatic to the isothermal case. Furthermore, no correction was made for the change in resistance arising from the change in dimensions caused by the application of the tension. This varies with the orientation of the crystal, but the correction of the tension coefficient β was always less than -0.4×10^{-5} . Both these corrections were usually negligible with respect to the values of the coefficient actually found and were always of the same order of magnitude as the experimental errors to be expected.

Fig. 4 shows the value of $\Delta R/R$ for a given crystal taken on different days with different tensions and with different distances between the potential

⁵ Georgieff and Schmid, *Zeits. f. Physik* **36**, 759 (1926).

leads. The linearity of the relation between $\Delta R/R$ and the tension applied is clearly in evidence as well as the fact that the experiments under different conditions gave entirely consistent results. It was further checked that the value of the coefficient was independent of the direction and magnitude of the current through the crystal. The specific resistance was determined roughly in every case and with a few exceptions came within 1 percent of Professor Bridgman's value for the given orientation; the dimensions of the crystals, particularly the distance between the potential leads, were not found with sufficient accuracy to warrant any better check.

The tension coefficient of resistance of a given single bismuth crystal was thus shown to be independent of the experimental variables, and so to be a constant characteristic of the given crystal; but in different crystals it varied with the orientation of the cleavage planes of the crystal with respect to the direction of the electric current. In these experiments the crystals were all cylindrical in shape with a diameter much smaller than the linear length; the direction of the electric current coincided with that of the axis of this cylinder and with the direction of the tension. The orientation of the crystal with respect to the axis of the cylinder can be defined in terms of two angles, θ and ϕ . The angle θ determines the orientation of the principal cleavage plane (111) which is perpendicular to the trigonal axis of the crystal and is defined as the angle between the normal to the principal cleavage plane and the longitudinal cylindrical axis of the crystal. The angle ϕ determines the orientation of a secondary cleavage plane with respect to the principal cleavage plane and the cylindrical axis. If the crystal is split along a principal cleavage plane, the section obtained is elliptical in shape. The major axis of this ellipse is the intersection of the plane through the normal to the principal cleavage plane and the cylindrical axis of the crystal with the principal cleavage plane. On the surface of this ellipse are found fine lines making angles of 60° with each other; these are the intersections of secondary cleavage planes with the principal cleavage plane. If the crystal be cleaved along one of these lines, the normal to the new cleavage plane will be found to make either an angle of 71° with that of the principal cleavage plane, or an angle considerably greater than 90° .⁶ Those planes making angles of 71° are the ones to be considered. The angle ϕ is then to be defined as the angle between the projection on the principal cleavage plane of the normal to this secondary cleavage plane and the major axis of the elliptical section of the principal cleavage plane. Since bismuth has trigonal symmetry, these secondary planes will recur every 120° ; and if the change in resistance depends on the orientation of these secondary planes, it should show a periodicity of 120° . It is to be noted that the angle ϕ as measured at one end of the crystal is, because of the known symmetry of the bismuth crystal, the negative of that measured at the other end, and hence it is impossible to differentiate between ϕ and $-\phi$, or between ϕ and $120 - \phi$, since the tension is double-headed and always

⁶ The writer is indebted to Professor Charles Palache of the Department of Mineralogy and Petrography of Harvard University for pointing out to her the characteristics of bismuth crystals here described.

involves two forces which are opposite in direction but equal in magnitude and act on the two ends of the crystal. Thus if the values of the tension coefficient are found between 0° and 60° , those between 60° and 120° are immediately known. With these definitions of the angle determining the orientation of the crystal with respect to the direction of the electric current, crystals having approximately the same orientations gave consistent values for β ;

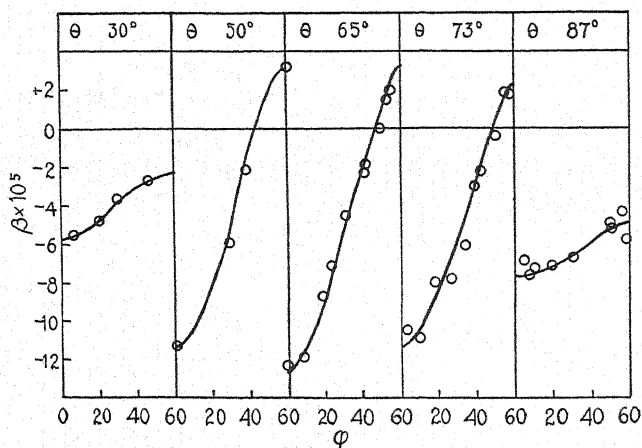


Fig. 5.

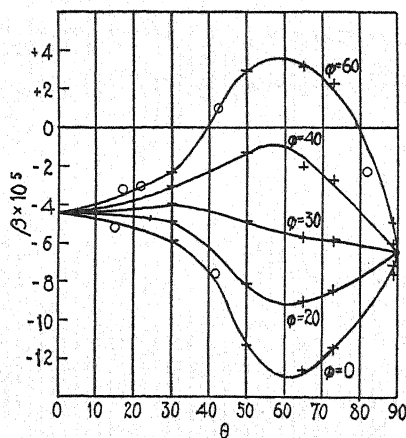


Fig. 6. Plus signs indicate points interpolated from Fig. 5; circles indicate additional points given directly by experiment.

e.g., one crystal defined by $\theta = 63^\circ$ and $\phi = 9^\circ$ gave β as -11.82×10^{-5} while another with $\theta = 69^\circ$ and $\phi = 9^\circ$ gave -11.83×10^{-5} . The angle ϕ was not determined to better than 5° and θ was uncertain to half that amount; hence this agreement is satisfactory.

The dependence of the tension coefficient β on θ and ϕ may be plotted in two ways: (1) giving β as a function of ϕ with θ constant, Fig. 5; and (2) giving β as a function of θ with ϕ constant, Fig. 6. In Fig. 5, thirty-eight of the forty-five experimental points were plotted in five groups, each group

containing the points for which θ was approximately that of the group. The 50° group, for instance, was composed of four observations, for $\theta = 50^\circ, 54^\circ, 50^\circ$ and 50° . There was an even greater divergence in values for the other groups, which gives one good reason why the points do not lie directly on a smooth curve; the 65° group, for instance, includes orientations of 60° to 69° , although the greater number of observations are nearer the mean value. Seven observations lay too far from any one of the group values to be included in Fig. 5, but six of these, indicated by circles, fell readily into Fig. 6. Except for these points, Fig. 6 was plotted by interpolation from Fig. 5. One point for $\theta = 41^\circ$ and $\phi = 47^\circ$ could not be fitted into either figure, but when its value of $+0.35 \times 10^{-5}$ is considered in the light of Fig. 6 it is seen to be fairly

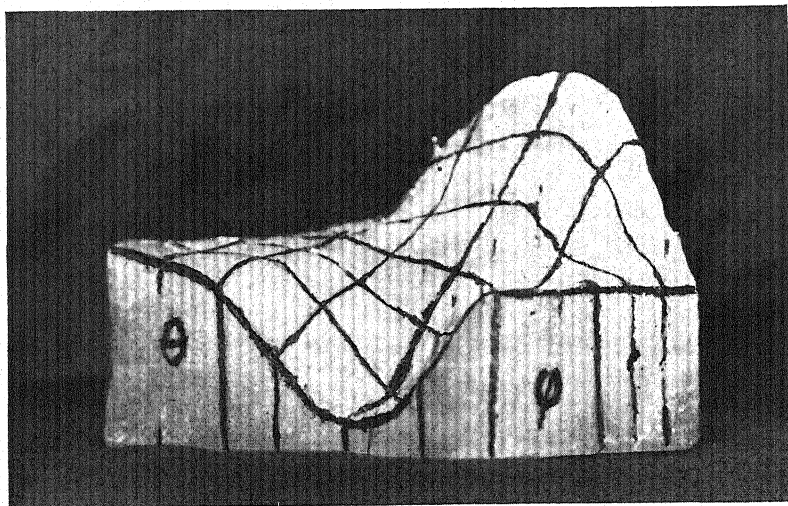


Fig. 7. Three-dimensional model of the variation of β with θ and ϕ . θ increases from left to right from 0° to 90° , intermediate lines being drawn every 15° . ϕ increases from front to back from 0° to 60° , intermediate lines being drawn every 10° . It is to be noted that the intersection of the surface with the plane $\theta = 90^\circ$ gives a very nearly horizontal line and so leads to the conclusion that β (represented by the vertical heights of the model) is independent of ϕ for $\theta = 90^\circ$.

consistent with the curves shown there. Since in plotting the results separately with respect to θ and ϕ , only approximate orientations could be used for each point, it was deemed desirable to plot the coefficient directly as a function of the two variables in the form of a solid model, Fig. 7. This showed nothing very different from the information given by Figs. 5 and 6, although it seemed to point more clearly to the probability that the coefficient is completely independent of the secondary orientation for $\theta = 90^\circ$.

In studying Fig. 5, which gives the dependence on ϕ of the tension coefficient of resistance for crystals with θ constant, it is immediately seen that the coefficient β has trigonal symmetry since, with ϕ and $120 - \phi$ indistinguishable, the curves must be symmetrical about 60° and return to the 0° values at 120° . Furthermore, β depends very markedly on the secondary

orientation ϕ . For instance in the case of $\theta = 65^\circ$, it varies from -12.6×10^{-5} at $\phi = 0^\circ$ to $+3.5 \times 10^{-5}$ at $\phi = 60^\circ$. This variation is interesting, both as regards magnitude and sign. Bismuth is abnormal in that the tension coefficient for the polycrystalline form is negative, but as shown in Fig. 5 for certain orientations of single crystals it becomes positive. It is further to be noted that when θ is close to 0° or to 90° , β varies less with the orientation of the secondary cleavage plane. At small angles of θ , this is to be expected, for in the limiting case of $\theta = 0$, the elliptical cross section becomes circular so that ϕ is entirely indeterminate. Or considering it from a physical point of view, in this case the tension is applied perpendicular to the principal cleavage plane and so does not deform the elementary triangles or hexagons formed on the surface by the intersections of the secondary with the principal cleavage planes; thus the same change of symmetry will occur irrespective of the orientation of the secondary planes. Thus symmetry demands that for $\theta = 0^\circ$ β be independent of ϕ . For $\theta = 90^\circ$ it is more difficult to understand why the effect should not depend on the angle ϕ , since symmetry does not here demand any such independence of ϕ . In this case the elliptical cross section has become indefinitely elongated and consequently has the well-defined direction of the axis of the cylinder. It would appear that the tension would change the symmetry of the elementary triangles or hexagons differently depending on their position relative to the axis of the cylinder. Experimentally, however, there is found little or no variation of the coefficient with ϕ when the principal cleavage plane is parallel to the axis of the crystal. The evidence, although not conclusive, is in the direction that the coefficient is independent of ϕ at $\theta = 90^\circ$. This appears more clearly in Figs. 6 and 7. The points are not sufficiently numerous at either $\theta = 0^\circ$ or 90° to determine the limiting values with a high degree of accuracy. However, there seems to be little doubt that at $\theta = 0$, β is somewhat less negative than it is at $\theta = 90^\circ$. There is some evidence from these curves that the tangent to these curves becomes horizontal at $\theta = 60^\circ$; in most cases this means a minimum or maximum, but for $\phi = 30^\circ$ it would seem to indicate a point of inflection only. The rapid variation of β with θ near 90° explains the comparatively wide scattering of the points in Fig. 5 for $\theta = 87^\circ$.

The fact that the tension coefficient varies so much with the orientation of the crystal may explain the discordance of the various values of β found for polycrystalline bismuth by different observers. Table I gives the various

TABLE I.

Williams ⁷	-5.35×10^{-5} per kg/cm ²
Zavattiero ⁸	-4.25 "
	-3.30 "
Bridgman ⁹	-4.66 "
	-2.92 "
Rolnick ¹⁰	-2.81 "

⁷ W. Ellis Williams, *Phil. Mag.* **13**, 635 (1907).

⁸ E. Zavattiero, *Rend. Accad. Lincei* **29**, (1), 48 (1920).

⁹ P. W. Bridgman, *Proc. Amer. Acad.* **57**, 41 (1922).

¹⁰ Harry Rolnick, *Phys. Rev.* **35**, 506 (1930).

values found. The discrepancies are far greater than can be accounted for by experimental error. It is reasonable to assume that the procedure of each of these observers in producing the specimen of bismuth was such as to emphasize different crystalline orientations in the polycrystalline pieces; such an assumption would be sufficient to explain the differences observed.

The hydrostatic pressure coefficient for bismuth single crystals¹ is for $\theta = 0^\circ + 2.45 \times 10^{-5}$ and for $\theta = 90^\circ + 7.5 \times 10^{-5}$; these are of the same order of magnitude as the tension coefficients found here. The sign of the pressure coefficient is positive and hence abnormal for pressure, in the same way that a negative coefficient is abnormal for a tension effect.

CONCLUSION

In this study of the tension coefficient of resistance in single bismuth crystals at 30°C , where the tension has been applied parallel to the axis of the cylinder in which the crystal is cast and along which the current flows, the coefficient has been found to depend both on the orientation of the principal cleavage plane and of the secondary cleavage planes with respect to the axis of this cylinder. For $\theta = 0^\circ$ and $\theta = 90^\circ$, this coefficient is apparently very little dependent on the orientation of the secondary cleavage planes, whereas for θ close to 60° its dependence on the orientation of the secondary cleavage planes becomes a maximum. This variation involves a change in sign as well as in magnitude, so that for certain orientations the coefficient becomes positive instead of remaining negative. The coefficient shows trigonal symmetry, as it must if it is to be consistent with the corporeal trigonal symmetry of the bismuth crystal.

This paper has been successful, therefore, in finding empirical relations between the tension coefficient of resistance and the orientations of the principal and secondary cleavage planes. To make the solution of the problem complete, a physical theory should be formulated to predict the relations found. However, progress would be made if a formal geometrical theory could be established which would permit the results to be expressed in terms of the parameters θ and ϕ and of three or more unknown but determinable constants. Further experimental work is planned in this field with other crystals of the same type of symmetry, of different types of symmetry, and possibly at radically different temperatures.

It is a pleasure to thank the Director of the laboratory and the authorities of Harvard University for the privilege of working in the Research Laboratory of Physics, and Professor P. W. Bridgman for the suggestion of the problem itself and also of practical details involved in carrying the work to completion.

The Effect of Homogeneous Mechanical Stress on the Electrical Resistance of Crystals

By P. W. BRIDGMAN
Harvard University

(Received October 24, 1932)

It is shown from general considerations of symmetry that the effect of homogeneous mechanical stress on the electrical resistance of a conducting crystal can be expressed in terms of a set of constants, the number of which is equal to the number of elastic moduli, and which connect the resistance with stress by equations very much like the equations connecting strain with stress, except for the difference of a factor 2 in some of the terms. The results are explicitly applied to the case of bismuth, and formulas developed for the change of resistance of a rod cut from the crystal in any direction when subjected to a longitudinal tension. The formulas are checked against the recent experimental results of Miss Allen for bismuth, and agreement found within the limits of error. It is shown that tension measurements alone do not permit an evaluation of all the constants, but if the tension measurements are supplemented by measurements of the effect of hydrostatic pressure in two independent directions, the six constants are then completely determined. Numerical values of the six constants are given for bismuth. Finally the geometrical meaning of the coefficients is briefly discussed and attention called to an effect produced by stress in crystals which is the analogue of the Hall effect produced by a magnetic field in isotropic materials.

IN SPITE of the great amount of work published on the necessary formal geometrical symmetry of all sorts of physical phenomena in crystals, as, for example, most extensively set forth in W. Voigt's *Lehrbuch der Kristallphysik*, the question of the effect of general mechanical stress on the electrical resistance of crystals has not yet been examined. Doubtless the reason for this is that up till now the only such effects which have been studied experimentally are the effects of hydrostatic pressure, and here the symmetry relations are so simple as to be almost intuitively evident. The first experimental attack on the general question has now been made, however, by Miss Allen,¹ who has measured the effect of mechanical tension on the resistance of single crystal rods of bismuth of different orientations. The time is therefore ripe for an examination of the formal symmetry relations, and in particular the number of physical constants necessary to completely characterize the current flow in a conducting crystal subjected to the most general sort of homogeneous mechanical stress. It is obviously not necessary to complicate the problem by considering non-homogeneous stress, for the solution in any such case may be obtained by an integration of the effects in infinitesimal homogeneous elements.

It is natural to attempt to construct a general geometrical theory along the lines suggested in Voigt's book, but a slavish following of pattern is not quite possible because this problem is more complicated than any treated

¹ Mildred Allen, Phys. Rev. 42, 848 (1932).

by Voigt. Here we are concerned with the cooperation of four factors; within the crystal the three factors, current vector, potential gradient vector (in general not in the same direction as the current vector), and stress tensor must be connected with the fourth factor, the physical constitution of the crystal, which is to be represented by an array of coefficients, in such a way as to be consistent with the symmetry of vectors, tensor, and crystal.

By splitting the problem into two parts, the methods of Voigt may be applied. Consider first the relation between current vector, q , and potential gradient, E . The most general linear relation (we assume of course Ohm's law), expresses E as a linear vector function of q . This involves nine coefficients. Experimentally, however, these nine coefficients are always found to reduce to six, the so-called rotary terms being absent. Since there is no reason to suppose that mechanical stress will so essentially modify the constitution of the crystal as to call into existence rotary terms, six coefficients will be assumed to suffice for this analysis. Further experimental justification of this assumption will be afforded by the agreement with experiment in the case of bismuth. We shall have then:

$$\left. \begin{aligned} E_x &= r_{11}q_x + r_{12}q_y + r_{13}q_z \\ E_y &= r_{12}q_x + r_{22}q_y + r_{23}q_z \\ E_z &= r_{13}q_x + r_{23}q_y + r_{33}q_z \end{aligned} \right\} \quad (A)$$

A relation of this form holds in general, whether or not there is a stress acting. Now specialize the coefficients above, defining them as those valid in the absence of stress. If a stress is allowed to act, the effect will be to somewhat change the coefficients, so that when the stress is acting we shall have:

$$\left. \begin{aligned} E_x &= (r_{11} + \delta r_{11})q_x + (r_{12} + \delta r_{12})q_y + (r_{13} + \delta r_{13})q_z \\ E_y &= (r_{12} + \delta r_{12})q_x + \text{etc.} \\ E_z &= (r_{13} + \delta r_{13})q_x + \text{etc.} \end{aligned} \right\} \quad (B)$$

The problem is now to determine the most general form allowable for the δr 's as a function of the stress (restricting ourselves to the linear terms), which shall be consistent with all the symmetry requirements. It is proved in Voigt that the coefficients above have the geometrical nature of the components of a tensor (understanding by tensor the sort of thing of which an ordinary mechanical stress is the simplest example). It follows that the δr 's must also be tensor components. The problem reduces, therefore, to finding the most general tensor a linear function of the applied stress which shall be consistent with the symmetry of the crystal. The strain produced by the stress at once springs to mind. But the actual strain is not quite a tensor, and so does not answer the requirements. It is proved in Voigt, however, that a slightly modified strain is in character a tensor, that is, the aggregate of six quantities obtained by leaving unchanged the three strain components with equal indices, and by dividing by 2 the three shearing components of strain with unlike indices.

The solution, therefore, is now in our hands. Build up from the stress a set of quantities involving coefficients entering in the same way as the coefficients which determine the ordinary elastic strains as a function of stress, except that the constants in the terms analogous to the shearing strains must be divided by 2. This completes the formal solution, since, given the stress, we can now compute the δr 's, and then the equations determine E completely as a function of q , so that the particular connections between E and q which may be expressed in terms of resistance may also be computed under any desired conditions. In particular, we have found that the number of constants necessary to completely define resistance is equal to the number of ordinary elastic constants, 21 at a maximum.

As an illustration of this general analysis I now apply it to the case of bismuth, eventually coming out with the numerical values of the coefficients. The starting point is the relation between strain and stress. The necessary information is on page 585 of Voigt's book, 1928 printing, noticing, however, that our scheme calls for the use of the elastic moduli as distinguished from the elastic constants, which Voigt tabulates, and that this change of itself introduces a factor 2 in certain places. Following the instructions above we now obtain:

$$\left. \begin{aligned} \delta r_{11} &= \rho_{11}X_x + \rho_{12}Y_y + \rho_{13}Z_z + \rho_{14}Y_z & 0 & & 0 \\ \delta r_{12} &= \rho_{12}X_x + \rho_{11}Y_y + \rho_{13}Z_z - \rho_{14}Y_z & 0 & & 0 \\ \delta r_{33} &= \rho_{13}X_x + \rho_{13}Y_y + \rho_{33}Z_z & 0 & 0 & 0 \\ \delta r_{23} &= \frac{1}{2}\rho_{14}X_x + \frac{1}{2}\rho_{14}Y_y & 0 & + \frac{1}{2}\rho_{44}Y_z & 0 \\ \delta r_{31} &= 0 & 0 & 0 & 0 & \frac{1}{2}\rho_{44}Z_x + \rho_{14}X_y \\ \delta r_{12} &= 0 & 0 & 0 & 0 & \rho_{14}Z_x + (\rho_{11} - \rho_{12})X_y \end{aligned} \right\} \quad (C)$$

in which 6 stress-resistance coefficients appear, which, of course, have no numerical relation to the elastic coefficients, but only a formal relation. In this scheme the Z axis is the axis of trigonal symmetry, and the X axis is the axis of two-fold rotational symmetry in the basal plane.

Furthermore it is known that with this choice of axes the resistance coefficients of equations (A) reduce to 2 only, r_{11} and r_{33} . The connection between E and q therefore becomes:

$$\left. \begin{aligned} E_x &= (r_{11} + \delta r_{11})q_x + \delta r_{12}q_y + \delta r_{13}q_z \\ E_y &= \delta r_{12}q_x + (r_{11} + \delta r_{22})q_y + \delta r_{23}q_z \\ E_z &= \delta r_{13}q_x + \delta r_{23}q_y + (r_{33} + \delta r_{33})q_z. \end{aligned} \right\} \quad (D)$$

This solution is now to be applied to the case of a slender cylindrical rod cut from the crystal in any direction, making angles α , β , and γ with the X , Y , Z axes. The cross section of the rod may be of any shape. The current q has access to the rod only through electrodes at the two ends, so that within the rod the current flow is entirely along the rod, with no transverse components. This gives $q_x = q \cos \alpha$ etc., and hence:

$$\left. \begin{aligned} E_x &= q[(r_{11} + \delta r_{11}) \cos \alpha + \delta r_{12} \cos \beta + \delta r_{13} \cos \gamma] \\ E_y &= q[\delta r_{12} \cos \alpha \quad \text{etc.} \\ E_z &= q[\delta r_{13} \cos \alpha \quad \text{etc.} \end{aligned} \right\} \quad (E)$$

In general, E has components transverse to the rod, but it is only the component along the rod which determines the measured resistance. The resistance is obviously $R = (E_x \cos \alpha + E_y \cos \beta + E_z \cos \gamma)/q$, or:

$$R = (r_{11} + \delta r_{11}) \cos^2 \alpha + (r_{11} + \delta r_{22}) \cos^2 \beta + (r_{33} + \delta r_{33}) \cos^2 \gamma + 2\delta r_{23} \cos \beta \cos \gamma + 2\delta r_{31} \cos \gamma \cos \alpha + 2\delta r_{12} \cos \alpha \cos \beta. \quad (F)$$

Next consider the effect of a mechanical tension T applied along the rod. The stress system thereby produced within the rod must satisfy the following conditions:

$$\left. \begin{aligned} X_x \cos \alpha + X_y \cos \beta + X_z \cos \gamma &= T \cos \alpha \\ X_y \cos \alpha + Y_y \cos \beta + Y_z \cos \gamma &= T \cos \beta \\ X_z \cos \alpha + Y_z \cos \beta + Z_z \cos \gamma &= T \cos \gamma \end{aligned} \right\} \quad (G)$$

and

$$\left. \begin{aligned} X_x \cos \alpha' + X_y \cos \beta' + X_z \cos \gamma' &= 0 \\ X_y \cos \alpha' \quad \quad \quad + \text{etc.} &= 0 \\ X_z \cos \alpha' \quad \quad \quad + \text{etc.} &= 0 \end{aligned} \right\} \quad (H)$$

where α' , β' , and γ' are any direction angles satisfying the condition

$$\cos \alpha' \cos \alpha + \cos \beta' \cos \beta + \cos \gamma' \cos \gamma = 0. \quad (I)$$

The conditions (G) come from the requirement that the force across any plane perpendicular to the length of the rod must be T , perpendicular to this plane, and the conditions (H) from the requirement that there is no external force acting across any lateral surface of the rod. By reflecting that the stress quadric in this case reduces to a couple of planes, the solution may be found almost by inspection, and is:

$$\left. \begin{aligned} X_x &= T \cos^2 \alpha, & Y_y &= T \cos^2 \beta, & Z_z &= T \cos^2 \gamma, \\ Y_z &= T \cos \beta \cos \gamma, & Z_x &= T \cos \gamma \cos \alpha, & X_y &= T \cos \alpha \cos \beta. \end{aligned} \right\} \quad (J)$$

The δr 's now assume the values:

$$\left. \begin{aligned} \delta r_{11} &= T[\rho_{11} \cos^2 \alpha + \rho_{12} \cos^2 \beta + \rho_{13} \cos^2 \gamma + \rho_{14} \cos \beta \cos \gamma] \\ \delta r_{22} &= T[\rho_{12} \cos^2 \alpha + \rho_{11} \cos^2 \beta + \rho_{13} \cos^2 \gamma - \rho_{14} \cos \beta \cos \gamma] \\ \delta r_{33} &= T[\rho_{13} \cos^2 \alpha + \rho_{13} \cos^2 \beta + \rho_{33} \cos^2 \gamma] \\ \delta r_{23} &= T[\frac{1}{2}\rho_{14}(\cos^2 \alpha - \cos^2 \beta) + \frac{1}{2}\rho_{44} \cos \beta \cos \gamma] \\ \delta r_{31} &= T[\frac{1}{2}\rho_{44} \cos \alpha \cos \gamma + \rho_{14} \cos \alpha \cos \beta] \\ \delta r_{12} &= T[\rho_{14} \cos \alpha \cos \gamma + (\rho_{11} - \rho_{12}) \cos \alpha \cos \beta] \end{aligned} \right\} \quad (K)$$

The material is now at hand for substituting in the expression (F) for R . Comparison with experiment will be simplified by introducing two new

angles. Project the length of the rod on the basal plane and denote the angles between this projection and the X and Y axes by α'' and β'' , where $\cos \alpha'' = \cos \alpha / (\cos^2 \alpha + \cos^2 \beta)^{1/2}$, and $\cos \beta'' = \cos \beta / (\cos^2 \alpha + \cos^2 \beta)^{1/2}$. Substitution gives, after some simple reductions, for the tension coefficient of resistance:

$$K_T \equiv \frac{1}{T} \frac{\Delta R}{R_0} = \frac{\rho_{11} \sin^4 \gamma + (\rho_{44} + 2\rho_{13}) \cos^2 \gamma \sin^2 \gamma + \rho_{33} \cos^4 \gamma - 2\rho_{14} \cos \gamma \sin^3 \gamma \cos 3\beta''}{r_{11} \sin^2 \gamma + r_{33} \cos^2 \gamma}. \quad (L)$$

Notice that the constant ρ_{12} has cancelled, and ρ_{44} and ρ_{13} enter only through the combination $\rho_{44} + 2\rho_{13}$. Tension measurements are, therefore, not sufficient to exhaustively determine the coefficients, but at most only four relations between the six coefficients can be fixed by such measurements. Explicitly, by appropriately varying the orientation, the constants ρ_{11} , ρ_{33} , and ρ_{14} may be determined, and the combination $\rho_{44} + 2\rho_{13}$. Furthermore, K_T is seen to have three-fold symmetry about the Z axis, as insured by the term in $\cos 3\beta''$. This, of course, is necessary, and constitutes one check on the correctness of the analysis. Another important feature is that K_T has complete rotational symmetry (that is, the term in β'' vanishes) both when the rod is parallel to the trigonal axis and when it is in the basal plane. That this must be the case when the length is along the trigonal axis is evident from most elementary symmetry considerations, but it is not so easily obvious that the coefficient should be independent of orientation in the basal plane. This latter fact was found experimentally by Miss Allen, and was looked on as one of the important results of the paper, although at the time it did not appear whether this was general, or only a fortuitous result for bismuth. The relation now appears necessary for any crystal of the same symmetry as bismuth.

The two remaining relations necessary to completely determine the six constants must be determined by the imposition of other kinds of stress. The simplest is a hydrostatic pressure, and the calculations can be made at once for this case. The stress system is $X_x = Y_y = Z_z = -P$, $Y_z = Z_x = X_y = 0$.

If the rod is cut parallel to the Z axis:

$$\left(\frac{1}{P} \frac{\Delta R}{R_0} \right)_{||} = - \frac{2\rho_{13} + \rho_{33}}{r_{33}}, \quad (M)$$

and when the rod is perpendicular to the Z axis, parallel to the basal plane:

$$\left(\frac{1}{P} \frac{\Delta R}{R_0} \right)_{\perp} = - \frac{\rho_{11} + \rho_{12} + \rho_{13}}{r_{11}}. \quad (N)$$

Examination shows at once that these two additional relations permit explicit solution for the remaining coefficients, so that the six coefficients may be completely determined in terms of tension measurements on four orientations and hydrostatic pressure measurements on two orientations.

The detailed data of Miss Allen permit further check of the above expression for K_T . Such a check may be made in various ways. For example, at constant γ the variation of K_T with β'' may be studied. The formula demands that the variable part of K_T be proportional to $\cos 3\beta''$. Miss Allen's Fig. 5 exhibits the coefficients in this way, and inspection will show that within the limits of experimental error each of the curves of Fig. 5 has the shape of a cosine curve. (Her ϕ and θ are the β'' and γ of this paper respectively.) It may be taken, therefore, that the geometrical theory checks sufficiently well against experiment.

The numerical coefficients may now be computed. The tension coefficients are given in Miss Allen's paper. The pressure coefficients I have found² to be 1.05×10^{-5} for $\gamma = 90^\circ$, and 2.03×10^{-5} for $\gamma = 0^\circ$. The specific resistance I have also found to be $r_{11} = 114.0 \times 10^{-6}$ and $r_{33} = 144.2 \times 10^{-6}$. All these values are at 30°C . The numerical coefficients are now found:

$$\begin{aligned}\rho_{11} &= -7.7 \times 10^{-9}, \quad \rho_{33} = -6.6 \times 10^{-9}, \quad \rho_{12} = +5.6 \times 10^{-9} \\ \rho_{13} &= +1.8 \times 10^{-9}, \quad \rho_{14} = +31.3 \times 10^{-9}, \quad \rho_{44} = -12.3 \times 10^{-9}.\end{aligned}$$

The stress unit is 1 kg/cm^2 . In this computation the corrections for change of dimensions and of angle with stress are neglected. These corrections are just about on the margin of experimental error.

Finally, it is interesting to go back and examine the geometrical significance of the various coefficients by determining what sort of simple measurement would give the isolated coefficient. ρ_{33} and ρ_{11} have already been dealt with, and are directly determined in terms of the tension coefficient of rods parallel and perpendicular to the trigonal axis. The coefficients ρ_{12} and ρ_{13} determine transverse components of e.m.f. when current flows lengthwise in a rod subjected to tension acting lengthwise. For example, if a rod is cut parallel to the Y (or X) axis, and a current passed lengthwise of the rod, then when a tension is applied along the rod, a transverse component of e.m.f. will appear along the X (or Y) axis which determines ρ_{12} . The other cross coefficient ρ_{13} has similar significance with a proper change of letters. The term ρ_{14} points to a formal analogy in crystals to the Hall effect in isotropic metals, the magnetic field being replaced by a compressional force. If a rod of rectangular section is cut with its length along the Z axis and with the X and Y axes along the sides of the rectangular section, and if a current is passed lengthwise of the rod, then a transverse e.m.f. along the Y axis will appear if a compression along the X axis is applied between the opposite faces of the section. Finally, if a bar of rectangular section is cut along the X axis and a shearing stress Y_z is applied to the sides of the bar distorting the cross section, and if a transverse current is led between opposite faces along the Z axis, an e.m.f. between the other two faces is produced by the shearing stress, the magnitude of the effect being determined solely by ρ_{44} .

² P. W. Bridgman, Proc. Amer. Acad. 63, 351 (1929).

Reflection of Metallic Atoms from Alkali Halide Crystals*

By ROBERT REX HANCOX

Department of Physics, Olivet College, Olivet, Michigan

(Received October 26, 1932)

The scattering of molecular beams of mercury from crystals of lithium fluoride, lithium chloride, sodium fluoride, and potassium iodide has been studied as a function of crystal and beam temperatures. A similar study has been made of the scattering of a molecular beam of cadmium from sodium chloride crystals. In all cases a quasi-specular beam of the type reported by Zahl and Ellett (Phys. Rev. **38**, 977 (1931)) for other alkali halide crystals was observed, with the same characteristic temperature changes. Former failures to detect a directed beam in the case of mercury scattered from potassium iodide were shown to have been due to moisture on the crystal surface. The relative number of atoms in the directed beam has been found to decrease with time at low crystal temperatures.

INTRODUCTION

BEAMS of heavy atoms and molecules whose de Broglie wave-lengths, at ordinary thermal velocities, are small compared to crystal spacings do nevertheless when incident upon certain crystals give rise to an apparently coherent scattering.^{1,2,3,4} A beam of cadmium atoms incident upon a rock-salt crystal is not simply absorbed and more or less quickly reevaporated, for this would result in a random distribution of atoms leaving the crystal surface. Only in the case of mercury and certain alkali halide crystals has this scattering been studied in detail. The use of the ionization gauge to determine the spacial distribution of mercury atoms scattered from alkali halide crystals revealed a dependence of the relative probabilities of random and directed scattering and of the direction of maximum intensity in the directed beam upon crystal and beam temperatures. This had not been observed in earlier studies carried out by the condensation method.

The only obstacle to the application of the ionization gauge with other heavy atoms, such as cadmium, is their lower vapor pressure which makes condensation in the gauge more likely. However as it is never necessary to build up a pressure in the ionization gauge greater than say 10^{-5} mm of mercury this obstacle is not a very serious one. The gauge has been used to study the scattering of cadmium from sodium chloride crystals. The phenomena observed in the scattering of mercury from these crystals are observed with cadmium also. The anomalous behavior of potassium iodide re-

* A thesis submitted in partial fulfillment of the requirements for the degree of doctor of philosophy in the department of physics in the graduate college of the State University of Iowa, August, 1932.

¹ A. Ellett and H. Olson, Phys. Rev. **31**, 645 (1928).

² A. Ellett, H. Olson and H. Zahl, Phys. Rev. **34**, 493 (1929).

³ H. A. Zahl, Phys. Rev. **36**, 893 (1930).

⁴ H. A. Zahl and A. Ellett, Phys. Rev. **38**, 977 (1931).

ported by Zahl and Ellett has been found to be due to the effect of moisture upon the crystal surface. Crystals of lithium fluoride, sodium fluoride, and lithium chloride, not previously available have been used with an incident beam of mercury atoms. Lithium fluoride is found to indicate especially clearly the existence of both directed and random scattering.

APPARATUS

The apparatus, shown in Figs. 1 and 2, is essentially the same as that used by Zahl and Ellett,⁴ the only major modification being that the gauge and crystal are mounted on the same rigid metal support. This change was made

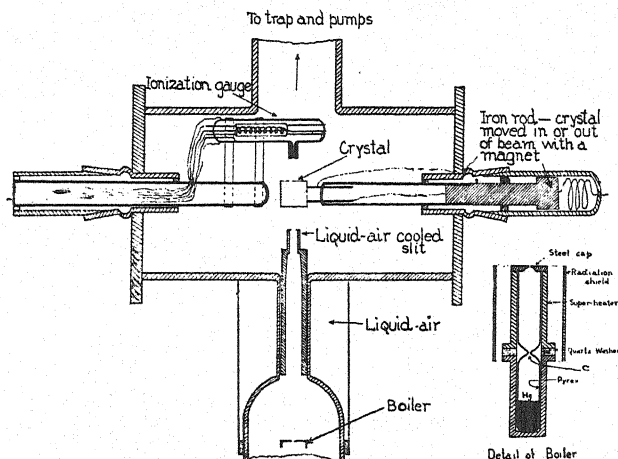


Fig. 1. Diagram of apparatus.

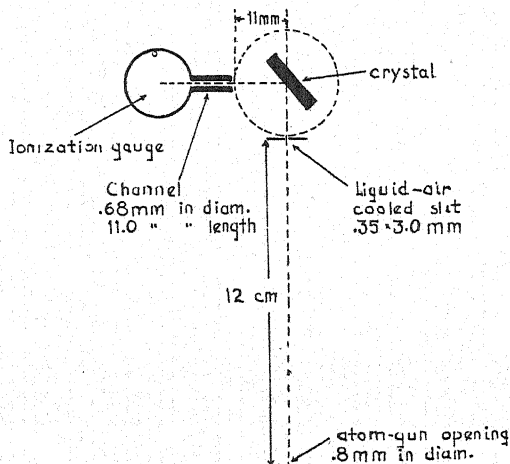


Fig. 2. Essential details of beam system.

to avert the possibility of the gauge and crystal changing their positions after being lined up. The dimensions of the slit defining the incident beam, and the gauge opening were also changed somewhat in order to obtain greater resolving power.

In the use of the apparatus it is necessary that the area on the face of the crystal which is illuminated by the incident beam shall remain stationary as the crystal is rotated, and that the gauge opening shall point directly at this illuminated spot for all positions of the gauge. In order for these conditions to obtain, the axes of rotation of the gauge holder and the crystal holder must be co-linear, and the illuminated area on the crystal face must lie on this common axis of rotation. The proper relative positions of the gauge and crystal were found by placing a closely fitting needle, equal in length to the radius of the circle about which the gauge rotates, into the cylindrical gauge opening and adjusting the relative positions of the gauge and crystal until the point of the needle remained stationary on the crystal face for all positions of the gauge and crystal. Once fixed, this adjustment was permanent since both gauge and crystal were mounted on the same support. The proper positions of the boiler opening and the slit relative to the crystal were found by placing a source of light 1 mm in diameter directly below the slit, the support on which the gauge and crystal were mounted was moved until a beam of light from this source reflected from the crystal face passed into the gauge for all positions of the crystal and the proper relative position of the gauge. Marks were then made on the walls of the glass tube by means of which the boiler opening was mounted at exactly the position of the light source.

In order that the readings of the ionization gauge may represent the actual distribution of atoms scattered by the crystal it is necessary that atoms from all portions of the illuminated area on the crystal face should be able to pass through the gauge opening without collision with the walls. With the incident beam making an angle of 18° with the crystal face the dimensions of the beam system shown in Fig. 2 allow a width of 1.52 mm on the crystal face to be struck by the incident beam. The gauge will admit atoms from a width on the crystal face of 2.04 mm. It is believed that this allows for more error in alignment than was present at any time.

The gauge was of the same type used by Zahl and Ellett,⁴ and was of approximately the same dimensions except for the capillary tube forming the opening into the gauge which was 11 mm long and 0.68 mm in diameter. With a galvanometer of sensitivity 4.5×10^{-9} A/mm (ampere per millimeter) and a filament to grid current of 16 m.A. (milliamperes) in the gauge it is estimated that a galvanometer deflection of 1 mm corresponds to a pressure change in the gauge of 2.1×10^{-8} mm of mercury.

For the experiments with an incident beam of cadmium and with mercury at very low boiler pressures, a galvanometer of sensitivity 4.2×10^{-10} A/mm was used. This, coupled with a filament to grid current of 36 m.A. increased the sensitivity of the gauge by a factor of 21.

The calculation of the gauge sensitivity is based upon the fact that at the equilibrium condition as many atoms leave the gauge per second as enter it. The gauge opening offers no impedance to the incident beam provided the divergence of the beam is negligible. However, to atoms leaving the gauge the impedance is that characteristic of a tube of the dimensions of the gauge opening. This means that a pressure will be built up in the gauge by the

incident beam. If we know the number of atoms entering the gauge per second we can calculate the pressure which they produce and by observing the galvanometer deflection can calculate the sensitivity of the gauge.

By using the galvanometer of sensitivity of 4.4×10^{-9} A/mm it is found that a pressure of 0.708 mm in the boiler and a filament to grid current of 1 m.A. give a galvanometer deflection of 10 cm when placed in the main beam. With kinetic theory formula⁵ for the mass of a gas striking the walls of a container per unit area per second, and for the number of molecules striking unit area per second,

$$n = 3.53 \times 10^{22} \times P/MT^{1/2}$$

and the dimensions of the beam system given in Fig. 2 we find that the number of atoms entering the gauge per second is 11.8×10^{11} . Since this is also the number of atoms leaving the gauge per second we can now make use of Knudsen's⁶ formula for the pressure difference necessary to produce the flow of a quantity of gas, Q measured in cm^3 at 1 bar through a cylindrical tube of length L and radius r , per second.

$$Q = \frac{1}{\rho_1} \frac{P_1 - P_2}{W_1 - W_2}$$

where ρ_1 is the density of the gas at 1 bar pressure and the temperature of the apparatus, and W_1 and W_2 the partial impedance of the tube are given by,

$$W_1 = (2\pi)^{1/2}/S$$

$$W_2 = 3L/4(2\pi)^{1/2}r^3.$$

A thermocouple placed in contact with the glass walls of the gauge read 220°C . Since the temperature of the gauge varies somewhat over different parts of the gauge and the point at which the thermocouple junction was placed was in a cooler part of the gauge. 250°C will be used as the mean temperature of the gauge.

Using the ordinary gas laws we find that the density of mercury vapor at 1 bar pressure and 250°C is 4.26×10^{-10} g/cm³. Substituting these in Knudsen's equation we find for the pressure difference,

$$\begin{aligned} P_1 - P_2 &= 4.53 \times 10^{-2} \text{ dynes/cm}^2 \\ &= 3.4 \times 10^{-5} \text{ mm of mercury.} \end{aligned}$$

This is the pressure produced in the gauge by the incident beam of mercury atoms. Since this pressure produced a galvanometer deflection of 10 cm with a filament to grid current of 1 m.A. it is easily calculated that with a current of 16 m.A. the sensitivity is 2.1×10^{-8} mm pressure change per mm galvanometer deflection.

If care was taken to maintain the liquid air about the slit at the same level, the drift of the low sensitivity galvanometer could be kept less than 2

⁵ Saul Dushman, *High Vacuum*, pp. 234.

⁶ M. Knudsen, *Ann. d. Physik* **28**, 75 and **28**, 999 (1909).

mm per half hour. However, when taking readings of the scattered beam, no attempt was made to keep this level constant. A period of about ten minutes was required to sweep the gauge across the crystal face and during this interval the liquid air level lowered sufficiently to allow a drift of 2 to 4 mm. This is probably due to the liberation of gas from the walls of the apparatus and since it appeared quite uniform could be corrected for.

With the crystal heater at 350°C the residual pressure in the gauge gave a galvanometer deflection of 20 to 30 cm corresponding to a pressure, in mercury vapor, of approximately 5.75×10^{-6} mm. The actual pressure in the gauge was probably greater than this since the gases present would give a lower ionization current than mercury vapor. On the other hand, the pressure in the gauge was probably greater than the pressure in the experimental chamber, due to the continuous liberation of gas from the walls of the gauge. With the crystal heater at 50°C the residual pressure was approximately half the above figure. The residual deflection was balanced out by an opposing potential across the galvanometer.

The system was ordinarily kept evacuated and dry nitrogen admitted for a few minutes while the crystal was being placed in the apparatus. Under these conditions it was only necessary to run the pumps for the period required to outgas the gauge before readings could be taken. The gauge was superheated at a filament current sufficient to give a grid current of 50 m.A. for a period of 4 to 6 hours before readings were taken.

When the high-sensitivity galvanometer was used and the grid current run at 36 m.A., longer outgassing periods were required and an unsteadiness in the residual deflection of the order of a millimeter was usually present. This unsteadiness was approximately one percent of the maximum reading in the scattered beam.

All the crystals used in this work, with the exception of those noted in the table, were grown in this laboratory by R. M. Zabel and the writer. The method used was similar to that used by Strong.⁷

EXPERIMENTAL RESULTS

Data obtained by Zahl and Ellett⁴ on the scattering of mercury from several alkali halide crystals indicated the following points: (1) The existence of a directed beam; (2) the deviation of the direction of maximum intensity in this beam from the direction of specular reflection; (3) the decrease of this deviation with higher beam and lower crystal temperatures and with lighter atoms; (4) better definition of the directed beam (narrowing of the beam) at low crystal temperatures, accompanied by an increase in the relative amount of random scattering.

The results of the present investigation agree with all except the third of these points. The shift in the position of the directed beam with a decrease in crystal temperature or an increase in beam temperature is found to be toward lower grazing angles. At sufficiently large angles of incidence the directed beam lies below the specular position and the shift in its position

⁷ John Strong, *Phys. Rev.* **35**, 1663 (1930).

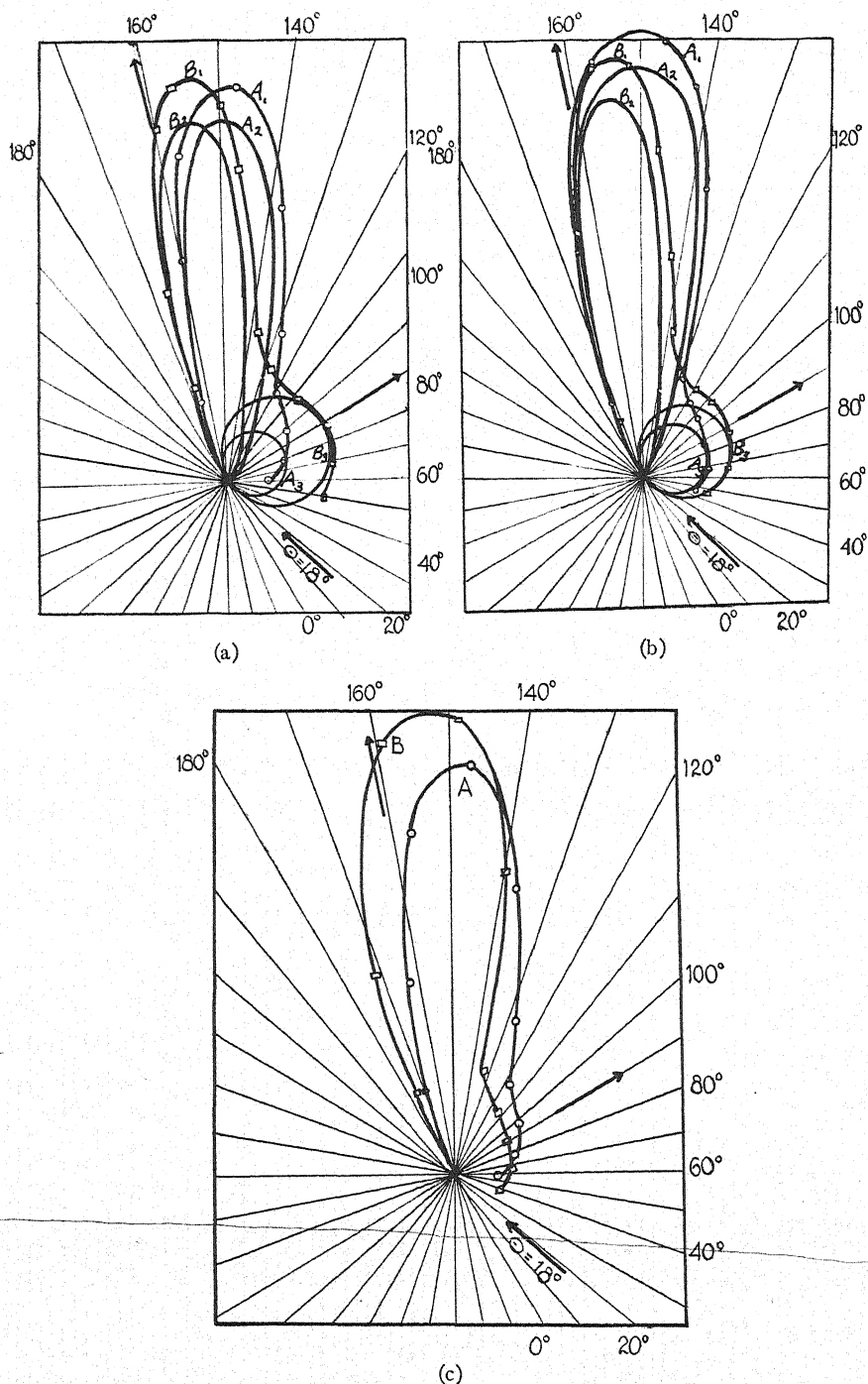


Fig. 3. Distribution of mercury atoms from lithium fluoride as a function of the crystal temperature and the temperature of the incident beam. Table I.^{*}

^{*} The detailed analysis of all curves is given in the appropriate table.

which accompanies a decrease in crystal temperature is away from the specular. Data were not taken by Zahl and Ellett at sufficiently large angles of incidence to bring out this fact.

The observations made by Zahl and Ellett⁴ led them to conclude that the increase in random scattering which accompanied a decrease in crystal temperature was not due to the formation of a gas layer on the crystal surface. The data obtained in this work indicate that the formation of a gas layer on the crystal surface is an important factor when the temperature of the crystal is below that at which occluded gas atoms are driven off the crystal.

I. Reflection of mercury from lithium fluoride

Fig. 3 shows typical sets of curves obtained for mercury beams scattered from a lithium fluoride crystal. Fig. 3a shows the distribution in the scattered beam with a beam temperature of 375°C and an angle of incidence of 18°. Curves A_1 and B_1 are obtained experimentally, A_1 being taken with a crystal temperature of 470°C, and B_1 with the crystal at 50°C. These curves, as Zahl and Ellett pointed out, appear to be the result of superimposing two curves of very simple type, one a circle and the other a symmetrical curve represented approximately by an equation of the form $r = C \cos M\theta$. It appears reasonable to suppose that these curves represent distinct processes one resulting in random scattering, the other giving rise to a directed or coherently scattered beam.

The analysis in this manner of the experimental curves A_1 and B_1 is given in the figure, A_1 being broken up into the circle A_2 and the symmetrical curve A_3 , B_1 into B_2 and B_3 . A similar notation is used throughout. The directed beams, A_2 and B_2 , lie between the specular position and the normal. Comparison of the directed beams shows that the beam from the cold crystal has been shifted away from the normal by 6.3°. The beam from the crystal at 50°C has also been narrowed, and the relative number of atoms scattered at random has been increased as evinced by the larger circle necessary to represent these atoms.

Fig. 3b shows curves taken with a beam temperature of 525°C. Fig. 3c shows the distribution for different beam temperatures, the crystal being at 470°C in both cases. Curve A is taken with the incident beam at 375°C and B with the beam at 525°C. An increase in beam temperature causes the quasi-specular beam to shift in the same direction as a decrease in crystal temperature.

Fig. 4a shows the distribution with an angle of incidence of 57°. The beam in this case has crossed over the specular position and lies closer to the crystal face than a regularly reflected beam. This change in the position of the beam relative to the specular position for varying angles of incidence was consistently observed as an inspection of the table will show. The cosine correction is somewhat uncertain in this case since the larger angle of incidence does not allow the gauge to be rotated over as large an angle. However, the beam is below the specular position whether a cosine correction is made or

not. Also the shift of the quasi-specular beam for a decrease in crystal temperature is definitely away from the specular position. Fig. 9 of the paper by Zahl and Ellett⁴ shows evidence of a similar shift.

The above curves were taken with the crystal oriented so that alternate positive and negative ions were parallel and perpendicular to the plane of the

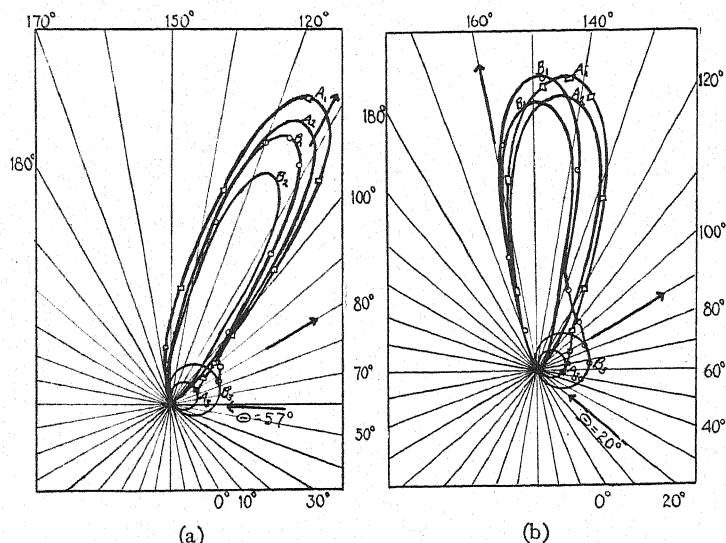


Fig. 4. Distribution of mercury atoms from lithium fluoride as a function of the crystal temperature and the temperature of the incident beam. Table I.

incident beam. Fig. 4b shows a set of curves taken with the crystal rotated 45° about an axis perpendicular to the plane of the incident beam. No change in the scattered beam is observed.

II. Reflection of mercury from sodium fluoride

Fig. 5 (a, b, c) shows the distribution obtained for mercury reflected from sodium fluoride. 5a was taken with a beam temperature of 280°C and crystal temperatures of 550°C and 50°C. 5b was taken with a beam temperature of 475°C and the same crystal temperature as 5a. 5c shows two curves taken at same crystal temperatures but different beam temperatures, A₁ being taken at a beam temperature of 280°C and B₁ at a temperature of 475°C. The curves are somewhat broader than for lithium fluoride but show the same behavior for changes in relative temperature of beam and crystal, and for changes in angle of incidence. The unusually large amount of cosine scattering in 5b is believed to be due to the fact that the crystal had been cold for approximately an hour.

III. Reflection of mercury from lithium chloride

Fig. 6 (a, b) shows curves obtained from lithium chloride. 6a was taken at a beam temperature of 260°C and crystal temperatures of 500°C and 50°C. 6b shows curves taken at a crystal temperature of 500°C, but different beam temperatures, A₁ being taken at a beam temperature of 260°C and B₁ at a

temperature of 500°C. They show the same behavior as the cases discussed above. Crystals of lithium chloride are very deliquescent and it was necessary to adopt some means of getting the crystal in the apparatus without exposure

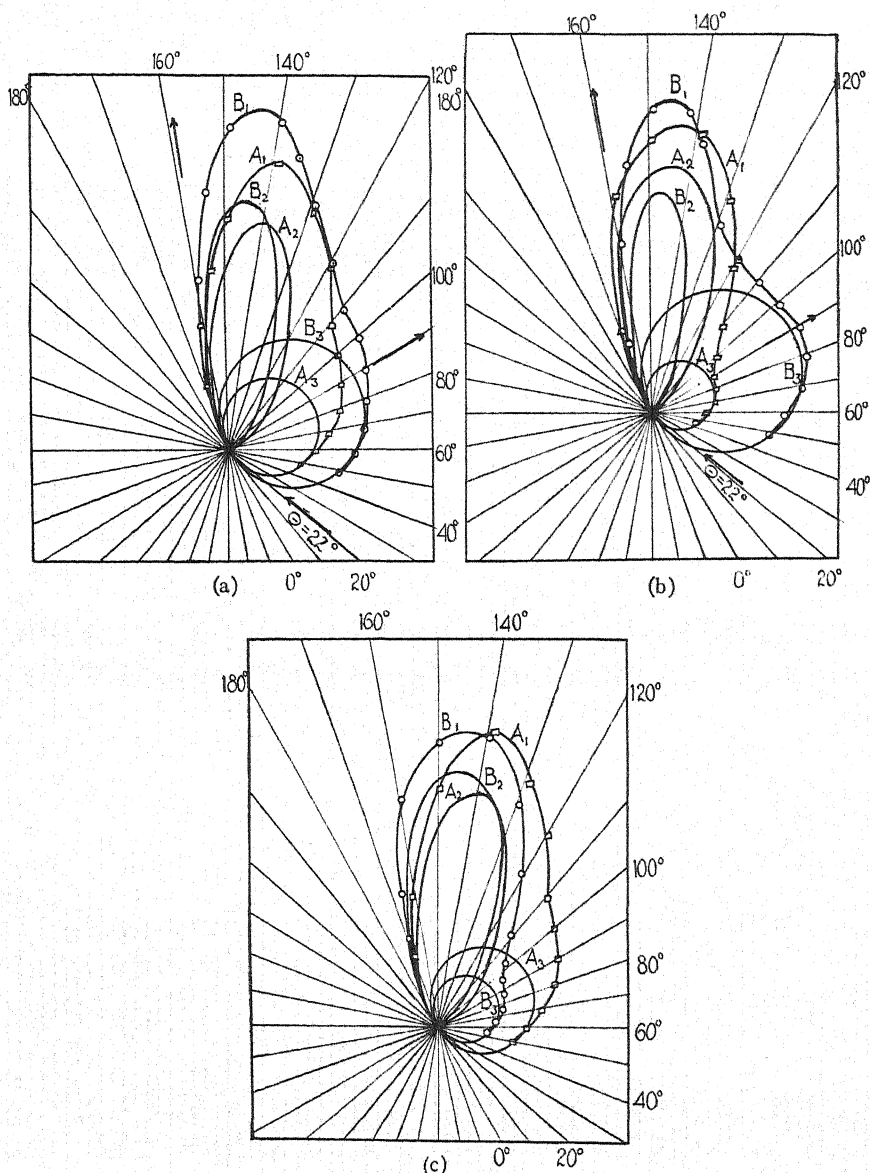


Fig. 5. Distribution of mercury atoms from sodium fluoride crystals as a function of the crystal temperature and the temperature of the incident beam. Table I.

to air. This was done by mounting a tin box with glass windows above the experimental chamber and filling both the box and the entire vacuum system with dry nitrogen at a pressure somewhat above atmospheric, all work on the crystal being done inside this tin box. The connection between the box

and the experimental chamber was made by a short length of tubing made of rubber dam. Long sleeved rubber gloves were attached to the openings in the box through which one worked, so that the crystal could be handled without exposing it to moisture from the hands. The box was thoroughly dried by leaving a dish of phosphorus pentoxide in it for about twelve hours before it was used. The crystal of lithium chloride from which a surface was to be

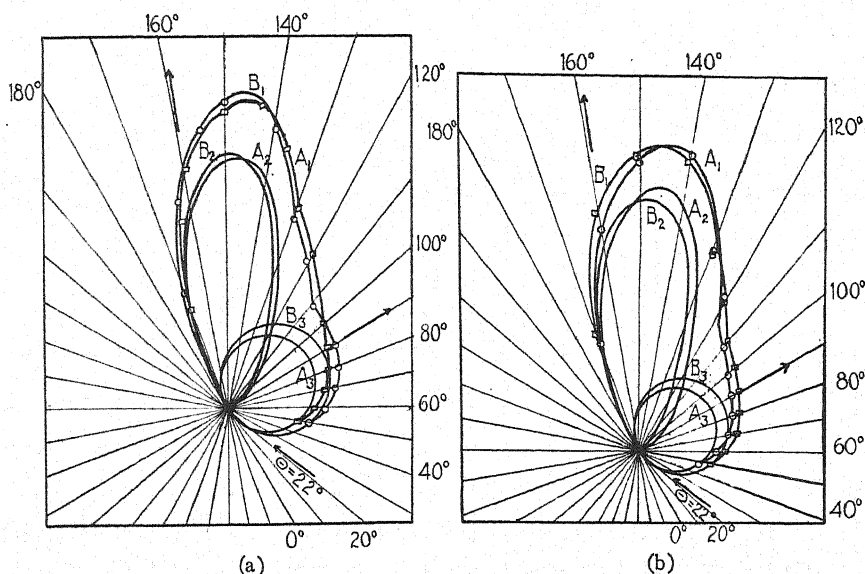


Fig. 6. Distribution of mercury atoms from lithium chloride crystals as a function of the crystal temperature and the temperature of the incident beam. Table I.

split was heated in a vacuum to a temperature of 400°C for four or five hours and then a small glass bomb containing the crystal was sealed off. The glass bomb was broken in the atmosphere of dry nitrogen inside the tin box, the crystal split, mounted on the crystal holder, placed in position and the pumps started immediately. About one minute elapsed from the time the crystal was split until the pumps were started. After taking these precautions in mounting, lithium chloride crystals were found to reflect as well as other non-deliquescent crystals used.

IV. Reflection of mercury from potassium iodide

Other experiments carried out in this laboratory had indicated that in certain cases, exposure to air had an action on the crystal surface which was not reversed by heating in a vacuum. In view of the success attained with lithium chloride it was decided to try the same method of mounting with potassium iodide. It was found that under these conditions a crystal of potassium iodide did give a directed beam. Fig. 7a shows the type of curves obtained. They were taken at a beam temperature of 170°C and crystal temperatures of 400°C and 50°C . In order to determine the effect of air on the reflecting power of the crystal, air was admitted to the system for a period of twenty minutes. This air flowed through a liquid air trap before reaching

the experimental chamber and although the trap was at room temperature within a few minutes after the air was admitted it is doubtful whether much water vapor had diffused into the experimental chamber by the end of the twenty minutes. After outgassing the system and heating the crystal at 400°C for several hours it was found to reflect as well as before. The curves obtained were practically identical with these shown in 7a. The system was then opened again and moist air from the room was driven past the crystal for several minutes by running oil pumps. The pumps were then shut off and the system left open for a period of eighty minutes. Fig. 7b shows the

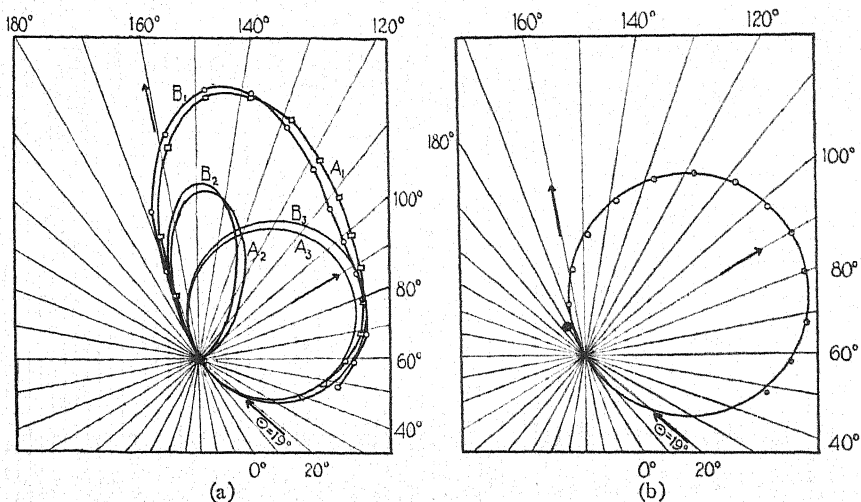


Fig. 7. Distribution of mercury atoms from potassium iodide as a function of the crystal temperature. Table I.

distribution obtained after this exposure. After prolonged heating at a temperature of 450°C the crystal still failed to show any indication of a directed beam. The crystal surface had apparently been completely and permanently ruined as far as its reflecting power was concerned.

V. Reflection of cadmium from NaCl

Since cadmium has a much lower vapor pressure than mercury it appeared that in order to prevent condensation in the gauge, two things were necessary, (1) the sensitivity of the gauge should be increased as much as possible so as to use low vapor pressures, and (2) the gauge should be kept at as high a temperature as possible. Several runs with different galvanometer sensitivities and with different ionization gauges were made before it was found possible to prevent condensation in the gauge. Condensation was always indicated by an unsteady drift of the galvanometer off the scale, and if the condensation became very great, by a marked decrease in the filament to grid current.

By using the gauge at a filament to grid current of 36 m.A. in conjunction with the more sensitive galvanometer, which increased the sensitivity of the gauge by a factor of approximately 21 and allowed the use of much lower vapor pressures, this difficulty was overcome.

Fig. 8 shows a set of curves obtained for cadmium reflected from sodium chloride. They were taken at a beam temperature of 480°C and crystal temperatures of 350°C and 50°C . The deviation from the specular position is not as large as usually observed for mercury incident at the same angle. However, individual crystals of sodium chloride show such a deviation in the angle of the reflected beam that one cannot be certain of this point.

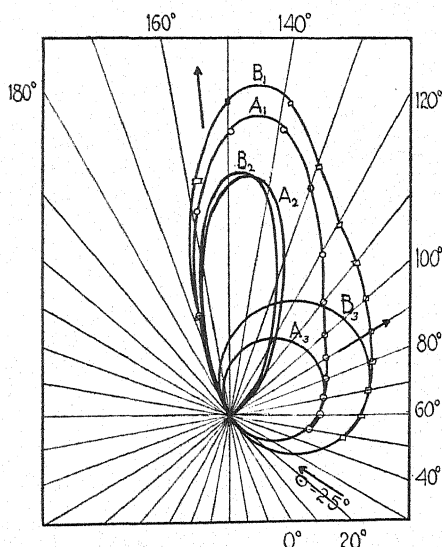


Fig. 8. Distribution of cadmium atoms from sodium chloride as a function of the crystal temperature. Table I.

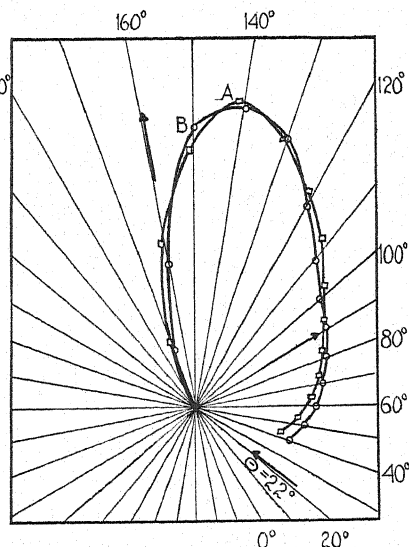


Fig. 9. Distribution of mercury atoms from sodium chloride as a function of the vapor pressure at the gun opening.

VI. Effect of varying pressure in atom-gun on the reflected beam

Fig. 9 shows two curves for mercury reflected from sodium chloride at different boiler pressures. Curve *A* was taken at a pressure of 0.35 mm corresponding to a mean free path of approximately 0.6 mm. Curve *B* was taken at a pressure of 3 mm corresponding to a mean free path of approximately 0.075 mm. The two curves show no appreciable difference. Other curves (not shown) and the data obtained by Zahl and Ellett⁴ show very little difference up to a boiler pressure of 10 mm. This indicates that the deviations from a Maxwell distribution which occur in this range of pressure are not significant as far as these experiments are concerned.

VII. Variation in random scattering from a cold crystal with time

Fig. 10a shows the scattering of a beam of mercury atoms from a sodium fluoride crystal at 50°C as a function of time. The crystal was heated at a temperature of 550°C for several hours while outgassing the system. Curve *A* was taken immediately after the crystal had been cooled to 50°C . Curve *B* after remaining at this temperature for 20 minutes and curve *C* after 60 minutes. The curves show an increase in the random scattering with time, the

positions of the quasi-specular beam apparently remaining unchanged. Fig. 10b shows the distribution as the crystal was reheated. The crystal was heated to 275°C and curve *B* taken. The temperature was then increased to 400°C and curve *C* taken.

These curves show the peak shifted toward the normal from its position with the crystal at 50°C but very little change in the amount of random scattering. Curve *D* taken at 600°C shows the peak still farther shifted toward the normal and the amount of cosine scattering very greatly reduced.

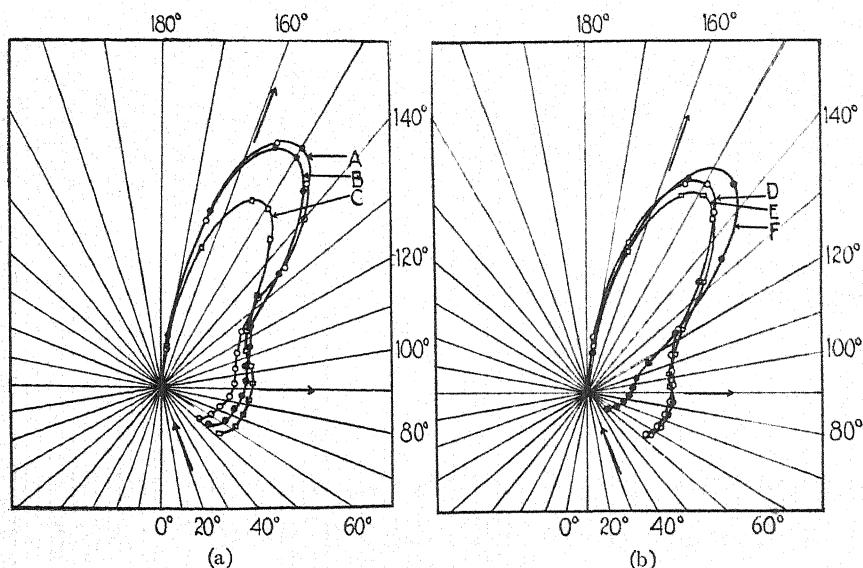


Fig. 10. Distribution of mercury atoms from a sodium fluoride crystal as a function of time and temperature of crystal.

It should be noted that when a crystal of sodium fluoride was exposed to air when placed in the apparatus it was always necessary to heat it at a temperature of at least 550°C for approximately an hour before a directed beam could be obtained.

The tables show the results obtained for the various cases discussed above. The relative number of atoms in the directed beam and in the random scattering were computed by the method described by Zahl and Ellett.⁴

CONCLUSION

A directed beam has been obtained for all the cases investigated. The former unsuccessful attempts to detect a directed beam from crystals of potassium iodide are shown to have been due to contamination of the crystal surface by overexposure to air, particularly to moist air, when it was placed in the apparatus. (The writer found no evidence of a directed beam in several attempts before the method of mounting in an atmosphere of dry nitrogen was developed.)

When a crystal surface was exposed to air, even for periods as short as two or three minutes, it was necessary to heat the crystal to drive off the

TABLE I. *Reflection of mercury from alkali-halide crystals.*

Crystal	Figure identification number	Angle of incidence	Angle of reflection	Temperature of crystal	Change in angle of reflection due to change in crystal temperature	Temperature of mercury beam	Curve describing directed beam	Intensity of directed beam	Intensity of cosine scattering	Total intensity	Percent of atoms contributing to directed beam
(1) LiF*		18°	32°	470°C		285°C	cos 3.3°	23.34	75	98.34	23.8
(1) LiF		18	26	50	6	285	cos 4.°	16.90	68	84.90	19.9
(1) LiF	3(a), A	18	32	470		375	cos 3.8°	31.5	75.3	106.8	25.9
(1) LiF	3a, B	18	25.7	50	6.3	375	cos 5.5°	20	81.6	101.6	19.7
(1) LiF	3b, A	18	29	470		525	cos 3.8°	25.5	67.8	93.3	33.2
(1) LiF	3b, B	18	25	50	4	525	cos 5.°	15.8	88.3	104.1	15.4
(1) LiF		36	40.6	470		285	cos 3.6°	26.52	70.8	97.32	27.2
(1) LiF		36	34.7	50	5.9	285	cos 4.°	30.36	92.4	122.76	24.4
(1) LiF		35	39	470		375	cos 3.8°	47.1	75.6	122.7	38.3
(1) LiF		35	33	50	6	375	cos 4.8°	27.9	94.0	121.9	23
(1) LiF		34	35	470		525	cos 4.4°	25.87	75.3	101.17	25.6
(1) LiF		34	31	50	4	525	cos 4.6°	25.05	77.85	103.9	24.3
(1) LiF		56	52	470		285	cos 3.6°	26.1	42.4	68.5	38.1
(1) LiF		56	48	50	4	285	cos 4.8°	24.01	70.2	94.21	23
(1) LiF		56	55	470		375	cos 4.4°	28.4	64.4	92.8	30.7
(1) LiF		56	53	50	2	375	cos 4.6°	26.9	72	98.9	27.8
(1) LiF		57	55	470		525	cos 4.7°	30.51	56.62	87.13	34.6
(1) LiF	4a, A	57	53	50	2	525	cos 5.5°	18.8	89.6	108.4	17.7
(2) LiF	4a, B	39	48	700		500	cos 4.°	12	17.3	29.3	41
(2) LiF		39	43	50	5	500	cos 5.7°	8.77	25.1	33.87	26
(2) LiF		39	45	50	3	360	cos 5.2°	7.97	22	29.97	26.6

TABLE I. (Continued).

Crystal	Figure identification number	Angle of incidence	Angle of reflection	Temperature of crystal	Change in angle of reflection due to change in crystal temperature	Temperature of mercury beam	Curve describing directed beam	Intensity of directed beam	Intensity of cosine scattering	Total intensity	Percent of atoms contributing to directed beam
(3) NaF	5c, A	22	37	550		475	$\cos 2.8^\circ$	39.75	46.9	86.65	45.7
(3) NaF	5b, A	22	33	50	4	475	$\cos 4.4^\circ$	6.14	77	83.14	7.4
(3) NaF	5b, B										
(3) NaF		37	42.5	550		475	$\cos 3.2^\circ$	15.4	42.6	58	22.7
(3) NaF		37	38	50	4.5	475	$\cos 3.6^\circ$	12.6	53.5	66.1	19.2
(3) NaF		52	49	550		475	$\cos 2.8^\circ$	43.5	42.5	86	50.6
(3) NaF		52	47	50	2	475	$\cos 3.6^\circ$	14	54.5	66.5	25.7
(3) NaF	5c, A	22	40.5	550		280	$\cos 3.2^\circ$	12.2	49	61.2	19.8
(3) NaF	5a, A	22	35.5	50	4.7	280	$\cos 3.6^\circ$	10.6	72	82.6	12.9
(3) NaF	5a, B										
(3) NaF		37	45.5	550		280	$\cos 3.2^\circ$	17.4	62.8	80.2	21.7
(3) NaF		37	43	50	2.5	280	$\cos 3.6^\circ$	11	76	87	12.3
(3) NaF		52	53	550		280	$\cos 3.2^\circ$	19.7	45.7	65.4	30
(3) NaF		52	51	50	2	280	$\cos 4^\circ$	9.8	52	61.8	15.8
(4) NaF		21	32.5	700		500	$\cos 2.8^\circ$	15	18.9	33.9	43.3
(4) NaF		46	45	700		500	$\cos 3^\circ$	11.2	18.9	30.1	37.5
(5) LiCl	6b, B	22	33	500		500	$\cos 3.2^\circ$	8.82	29.8	38.62	22.9
(5) LiCl	6a, A	22	31	50	2	500	$\cos 3.4^\circ$	7.4	32.6	40	18.5
(5) LiCl	6a, B	22	35	500		260	$\cos 3.2^\circ$	8.48	25.2	33.68	25.1
(5) LiCl	6b, A										
(5) LiCl		50	54**	500		500					
(5) LiCl		50	52**	50	2	500					
(5) LiCl		50	55**	500		260					

TABLE I. (Continued)

Crystal	Figure identification number	Angle of incidence	Angle of reflection	Temperature of crystal	Change in angle of reflection due to change in crystal temperature	Curve describing directed beam	Intensity of directed beam	Intensity of cosine scattering	Total intensity	Percent of atoms contributing to directed beam
(6) KI	7a, A	19	34	400		cos 2.6°	7.8	47.8	55.6	14.8
(6) KI	7a, B	19	31	50	3	cos 2.8°	6.9	50.5	57.4	12
(6) KI		27	35	400		cos 2.2°	11.6	53.7	65.3	17.8
(6) KI***		27	35	400		cos 2.4°	13.2	55.6	68.8	19.1
(6) KI***		27	35	50	2	cos 2.6°	9.9	55	64.9	15.2
(6) KI		41	50	400						
(6) KI		41	46	50	4					
(7) NaCl****	8A	25	36	350		cos 3.2°	8.2	31.6	39.8	21
(7) NaCl	8B	25	34	70	2	cos 3.4°	4.2	25.1	29.3	14.4
(7) NaCl		34	40	350		cos 2.6°	10.2	17.1	27.3	37.3
(7) NaCl		34	37	70	3	cos 3.2°	6.1	19.5	25.6	23.8

* The numbers in column one denote different individual crystals. All data for which the number in this column is the same, were taken in a single run.

** These angles represent the peak of the uncorrected beam.

*** After crystal had been exposed to air for 20 minutes.

**** The remainder of the data in this table is for cadmium reflected from natural crystals of sodium chloride.

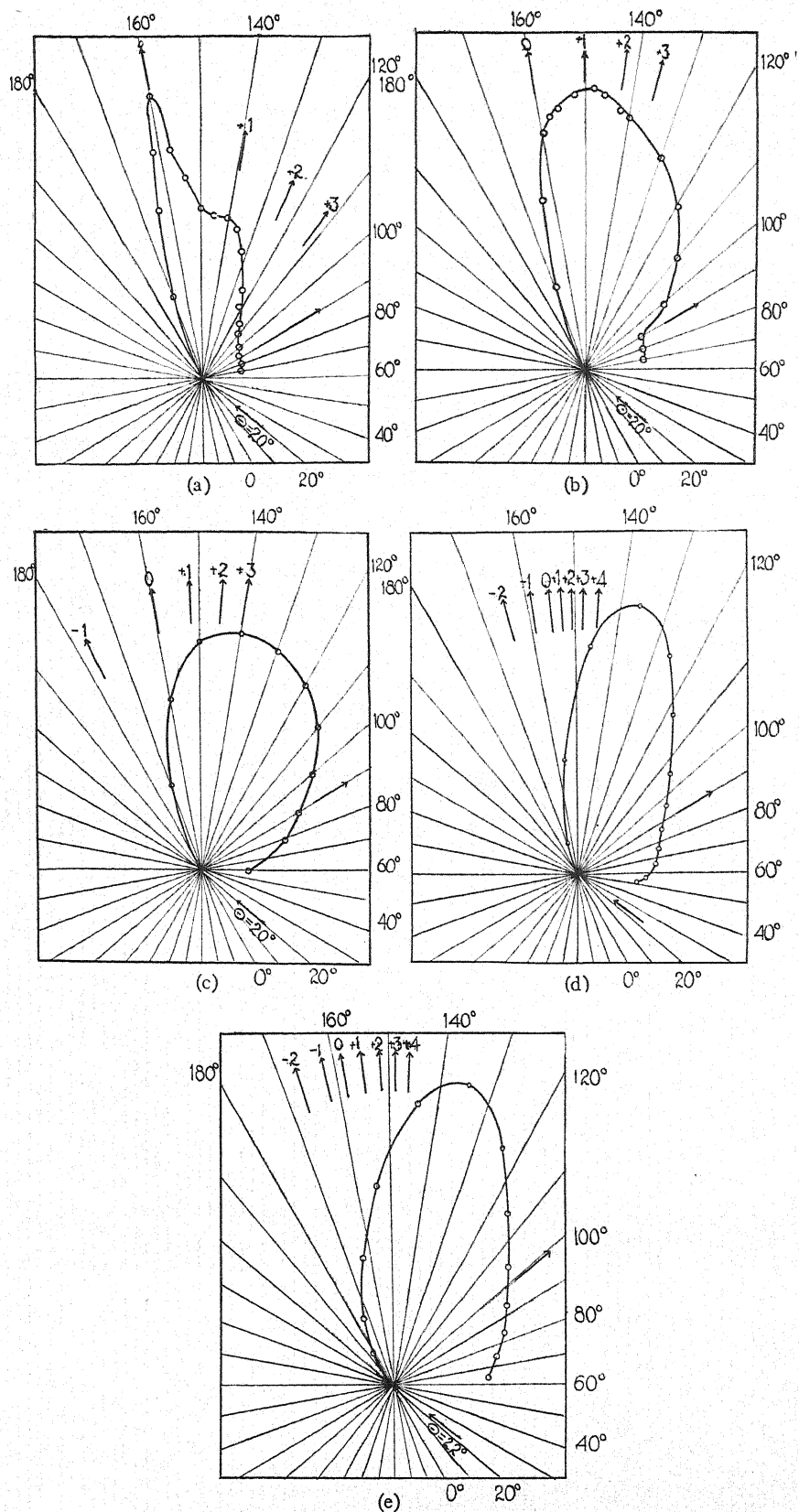


Fig. 11. Distribution of various atomic and molecular beams from sodium chloride crystals; (a) helium, (b) neon, (c) argon, (d) cadmium, and (e) mercury.

adsorbed gas before a directed beam could be obtained. The temperature necessary to accomplish this varied with different crystals, 350°C being sufficient in the case of sodium chloride, for lithium fluoride a temperature of 450°C was necessary and for sodium fluoride a temperature of 550°C was required.

It seems reasonable, as suggested by Zahl and Ellett,⁴ that the better definition of the reflected beam at low crystal temperature is due to the decrease in thermal agitation of the crystal and the consequent increased resolving power. The increase in random scattering at low crystal temperatures is evidently largely due to the formation of a gas layer on the crystal surface.

Fig. 11 shows the distribution in the plane of incidence of helium, neon, argon, cadmium, and mercury⁹ scattered from sodium chloride. That the asymmetry in the helium curve is due to the presence of a surface grating spectrum incompletely resolved is scarcely to be doubted. It is tempting to infer that the other curves are to be accounted for in the same manner. The maxima of the plus or minus first, the plus or minus second, and the plus third and fourth order spectra of the several beams incident upon sodium chloride would lie at the positions indicated by the arrows. If we take this point of view we will then attempt to account for the temperature shift in the direction of maximum scattering by supposing that it is due to a change in the force field at the surface of the crystal of such a character as to make spectra of positive orders relatively more intense at higher crystal temperatures. Thus the observed phenomena may be interpreted qualitatively at least in terms of surface grating diffraction. However, it is difficult to see, if this interpretation is correct, why rotation of the crystal in its own plane produces so little change in the scattering of mercury. With helium quite radical changes occur while no data are available on neon and argon.

In conclusion the writer wishes to express his appreciation to Professor A. Ellett under whose direction the work was done.

⁹ The curves of helium, neon and argon were very kindly loaned to the writer by R. M. Zabel.

The Theory of the Ferromagnetic Anisotropy of Single Crystals

By RICHARD M. BOZORTH
Bell Telephone Laboratories

(Received October 27, 1932)

It is well known that in single crystals of iron and nickel the direction of magnetization is not generally parallel to the direction of the magnetic field, although these crystals belong to the cubic system. When the magnetization in a crystal has a certain value as measured in the direction of the field, there will be also, in general, a component of magnetization measured in the direction at right angles. This paper describes the calculation according to the domain theory, of the normal component of magnetization, using certain assumptions which are almost identical with those used by Heisenberg in his calculation of the magnetostriction of iron crystals. Theoretical curves are shown for a variety of crystallographic directions. Each of these curves shows all of the possible positions and magnitudes of the vector representing the magnetization in iron crystals as the magnetic field parallel to any given direction in the crystal increases in strength from zero to a high value. The theoretical curves are compared with the experimental curves of Honda and Kaya, and show good agreement with them.

INTRODUCTION

RECENTLY Heisenberg¹ has calculated the magnetostriction of a single crystal of iron as dependent upon magnetization, for the three principal directions in the crystal. Restated in my own words, the assumptions used by Heisenberg are as follows:

1. The crystal is composed of a large number of domains, considered for convenience to be equal in size.
2. When the crystal as a whole is in the unmagnetized state, each domain is magnetized to saturation in the direction of a cubic axis, $\langle 100 \rangle$, the directions of the magnetizations of the domains being equally distributed among the six possible directions.
3. When magnetization of the crystal as a whole has a value chosen between zero and a certain limit, the directions of magnetizations in the domains are distributed by chance among the six possible $\langle 100 \rangle$ directions, and that distribution will occur which is the most probable one, subject to the condition that the vector sum of the magnetizations of the domains shall be equal to the previously specified magnetization of the crystal. The precise meaning of the term probability of a distribution is stated in Eq. (2) below.
4. After magnetization of the crystal has increased so that the directions of magnetizations of the domains have become parallel to that cubic axis (or axes) most nearly aligned with the direction of the magnetic field, as-

¹ W. Heisenberg, *Zeits. f. Physik* **69**, 287-297 (1931). Similar assumptions were previously stated by W. L. Webster, *Proc. Phys. Soc. London* **42**, 431-440 (1930), but no quantitative treatment was given nor were calculations made. For a discussion of the domain theory, see E. C. Stover, *Magnetism*, E. P. Dutton and Co., 65-66 (1929), and R. M. Bozorth and J. F. Dillinger, *Phys. Rev.* **41**, 345 (1932).

sumption (3) no longer applies and they leave the cubic axes and approach the field direction continuously until saturation is attained.

5. Associated with each domain is a measurable "magnetostriction," i.e., a deformation of the domain which increases its length in the direction of its magnetization. The magnetostriction of the crystal is the sum of the separate magnetostrictions of the domains, added according to the method of Akulov.²

The magnetostriction curves so calculated for progressive magnetization along the crystallographic directions $\langle 100 \rangle$, $\langle 110 \rangle$ and $\langle 111 \rangle$ have been compared by Heisenberg with the data of Webster³ and show good agreement with them.

Heisenberg limited himself to the calculation of the *magnetostriction*. On the other hand, by using similar but somewhat different assumptions, and extending his general mathematical procedure, it is possible to predict the *direction of magnetization* in a single crystal subjected to a magnetic field having any chosen direction and magnetized to any fraction of saturation.

It is known experimentally that when the crystal is more than about half saturated the direction of magnetization is different from the direction of the field unless the field lies in one of the three principal crystallographic directions (cube edge, face diagonal, and body diagonal) considered by Heisenberg. As the field increases in strength, remaining always constant in direction, the magnetization changes in direction as well as in magnitude.

We now have a satisfactory theory which predicts correctly in all cases the direction of deviation of magnetization from field, and predicts also within the experimental error the magnitude of the deviation observed by Honda and Kaya, whose experimental data are as yet the most complete.

Specifically, the quantities which are calculated for the first time in this paper are the magnitude and direction of the magnetization in a single crystal corresponding to selected values of the component of magnetization in the field direction. These may be calculated for any direction of the field with respect to the crystal axes.

The assumptions made are assumptions (1) to (4) above, with a slight change in assumption (3): the distribution of the directions of magnetization in the domains is now subject to the condition that the vector sum of these magnetizations shall have a component in the direction of the magnetic field equal to the observed value of the magnetization along that direction.

The simplest way to express the results of the calculations seems to be to plot I_H , the component of magnetization parallel to the field, along one axis; and I_n , the component normal to the field, along an axis at right angles. The line joining the origin to any point on the curve so plotted is then a vector representing the total magnetization of the crystal, and the curve is the locus of the end of the vector as the strength of the field directed along the I_H axis increases from a very small to a very large value. Typical curves are shown in Figs. 4 to 6, where the several directions of the field are shown by the arrows.

² N. S. Akulov, *Zeits. f. Physik* 59, 254-264 (1930).

³ W. L. Webster, *Proc. Roy. Soc. London* 109A, 570-584 (1925).

It should be understood that the theory gives no information regarding the *strength* of the magnetic field which is associated with a given magnetization of the crystal, but does define completely all of the magnetic states of the crystal which must occur as the field, acting in any direction, increases indefinitely from zero.

CALCULATIONS

Following Heisenberg's procedure, let N denote the number of domains per unit volume of the crystal. We employ a right-handed set of rectangular coordinate axes which coincide with the crystallographic axes. We consider "distributions" of the elementary domains, each distribution being defined by the numbers, N_1, N_3, N_5 , of elementary regions per unit volume having their magnetic moments in the directions of the positive x, y and z axes, respectively, and by the numbers N_2, N_4, N_6 , of regions having their magnetic moments in the directions of the negative x, y and z axes, respectively. Thus a distribution is represented by a set of positive numbers (N_1, N_2, \dots, N_6) with $N_1 + N_2 + \dots + N_6 = N$. The components of the magnetization along the x, y and z axes are then given by

$$\begin{aligned} I_x/I_\infty &= (N_1 - N_2)/N, \\ I_y/I_\infty &= (N_3 - N_4)/N, \\ I_z/I_\infty &= (N_5 - N_6)/N, \end{aligned} \quad (1)$$

respectively, where I_∞ is the saturation value of magnetization. With Heisenberg we write the probability of the distribution (N_1, N_2, \dots, N_6)

$$P(N_1, N_2, \dots, N_6) = \frac{N!}{(N_1!)(N_2!) \dots (N_6!)} \left(\frac{1}{6}\right)^N. \quad (2)$$

Imposing the condition that the component of magnetization in the direction defined by direction cosines (λ, μ, ν) has a given value I_H , let us seek the most probable distribution consistent with this condition. We have

$$\lambda(N_1 - N_2) + \mu(N_3 - N_4) + \nu(N_5 - N_6) = NI_H/I_\infty. \quad (3)$$

We also have

$$N_1 + N_2 + \dots + N_6 = N. \quad (4)$$

Introducing Lagrangian multipliers, α' and β , we construct the function

$$F = \log P + \alpha' [N_1 + N_2 + \dots + N_6 - N] + \beta [\lambda(N_1 - N_2) + \mu(N_3 - N_4) + \nu(N_5 - N_6) - NI_H/I_\infty]. \quad (5)$$

For the most probable distribution we must have

$$\partial F / \partial N_i = 0, \quad i = 1, 2, \dots, 6. \quad (6)$$

Making use of the approximation

$$\log n! = (n + \frac{1}{2}) \log n - n + \frac{1}{2} \log (2\pi),$$

we obtain from (6) the set of approximate equations

$$\begin{aligned}\log N_1 &= \alpha' + \log (N/6) + \beta\lambda, \\ \log N_2 &= \alpha' + \log (N/6) - \beta\lambda, \\ \log N_3 &= \alpha' + \log (N/6) + \beta\mu, \\ \log N_4 &= \alpha' + \log (N/6) - \beta\mu, \\ \log N_5 &= \alpha' + \log (N/6) + \beta\nu, \\ \log N_6 &= \alpha' + \log (N/6) - \beta\nu.\end{aligned}$$

Write $\alpha' + \log (N/6) = \alpha$. Then we have

$$\left. \begin{aligned}N_1 &= e^{\alpha+\beta\lambda}, N_3 = e^{\alpha+\beta\mu}, N_5 = e^{\alpha+\beta\nu}, \\ N_2 &= e^{\alpha-\beta\lambda}, N_4 = e^{\alpha-\beta\mu}, N_6 = e^{\alpha-\beta\nu}.\end{aligned} \right\} \quad (7)$$

On substituting from (7) in (3) and (4), we obtain the following equations for the determination of α and β :

$$\frac{\lambda sh(\lambda\beta) + \mu sh(\mu\beta) + \nu sh(\nu\beta)}{ch(\lambda\beta) + ch(\mu\beta) + ch(\nu\beta)} = \frac{I_H}{I_\infty}, \quad (8)$$

$$2e^\alpha [ch(\lambda\beta) + ch(\mu\beta) + ch(\nu\beta)] = N. \quad (9)$$

Eq. (8) gives β in terms of λ, μ, ν, I_H ; then (9) gives α in terms of $\lambda, \mu, \nu, I_H, N$. Eqs. (7) then give the most probable distribution (N_1, N_2, \dots, N_6) from which the figures have been plotted.

In Figs. 1 and 2 there are shown the most probable distributions as functions of I_H/I_∞ for two directions (λ, μ, ν). It is to be understood that the preceding theory cannot apply if the value of I_H/I_∞ is greater than that for which one of the N_i 's vanishes. In extending the results into the range of these higher values of I_H we make use of assumption (4) of the introduction.

For purposes of comparison with certain experiments it is necessary to discuss cases in which the magnetization I lies always in a given plane. Accordingly, let us impose the conditions that: (1) the component of magnetization in a given direction (λ', μ', ν') be zero, (2) the component in another direction (λ, μ, ν) have a given value I_H ; and let us seek the most probable distribution consistent with these conditions.

We have Eqs. (3) and (4) and the additional equation

$$\lambda'(N_1 - N_2) + \mu'(N_3 - N_4) + \nu'(N_5 - N_6) = 0. \quad (10)$$

Proceeding as before, we find the values

$$\begin{aligned}N_1 &= e^{\alpha+\lambda\beta+\lambda'\gamma}, N_3 = e^{\alpha+\mu\beta+\mu'\gamma}, N_5 = e^{\alpha+\nu\beta+\nu'\gamma}, \\ N_2 &= e^{\alpha-\lambda\beta-\lambda'\gamma}, N_4 = e^{\alpha-\mu\beta-\mu'\gamma}, N_6 = e^{\alpha-\nu\beta-\nu'\gamma},\end{aligned} \quad (11)$$

where the Lagrangian multipliers α, β, γ , are determined by the equations

$$\lambda' sh(\lambda\beta + \lambda'\gamma) + \mu' sh(\mu\beta + \mu'\gamma) + \nu' sh(\nu\beta + \nu'\gamma) = 0, \quad (12)$$

$$\frac{\lambda sh(\lambda\beta + \lambda'\gamma) + \mu sh(\mu\beta + \mu'\gamma) + \nu sh(\nu\beta + \nu'\gamma)}{ch(\lambda\beta + \lambda'\gamma) + ch(\mu\beta + \mu'\gamma) + ch(\nu\beta + \nu'\gamma)} = \frac{I_H}{I_\infty}, \quad (13)$$

$$2e^\alpha [ch(\lambda\beta + \lambda'\gamma) + ch(\mu\beta + \mu'\gamma) + ch(\nu\beta + \nu'\gamma)] = N. \quad (14)$$

Eq. (12) determines γ in terms of β and the direction cosines; then (13) determines β , and so also γ , in terms of the direction cosines and I_H , then (14) gives α in terms of the direction cosines, I_H , and N . Finally the Eqs. (11) give the required most probable distribution.

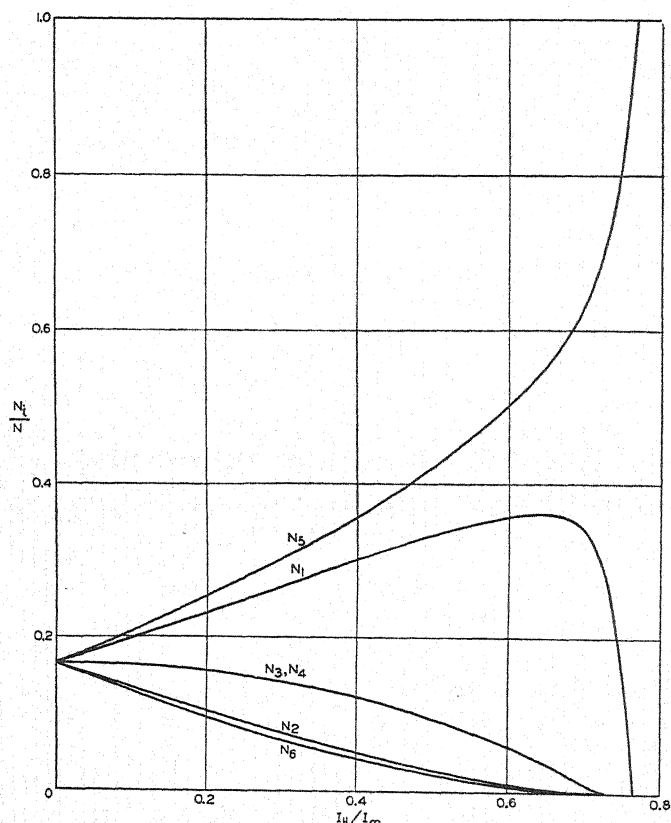


Fig. 1. Curves showing the distribution of directions of magnetizations of the domains among the six $\langle 001 \rangle$ directions. For these curves the direction of the field is defined by the direction cosines $\lambda=0.643$, $\mu=0$, $\nu=0.766$, and is therefore inclined at 40° to a $\langle 001 \rangle$ direction in a $\{001\}$ plane.

The curves in Figs. 2 and 3 show the most probable distributions as functions of I_H/I_∞ for one set of values of λ , μ and ν ; in the case of Fig. 2 the magnetization is not restricted to a plane, in Fig. 3 it is confined to the $(11\bar{1})$ plane ($\lambda'=\mu'=-\nu'=1/3^{1/2}$).

The results may also be expressed in a different way. From the most probable distributions may be determined I_n , the component of magnetization perpendicular to the direction defined by λ , μ and ν ; and therefore knowing

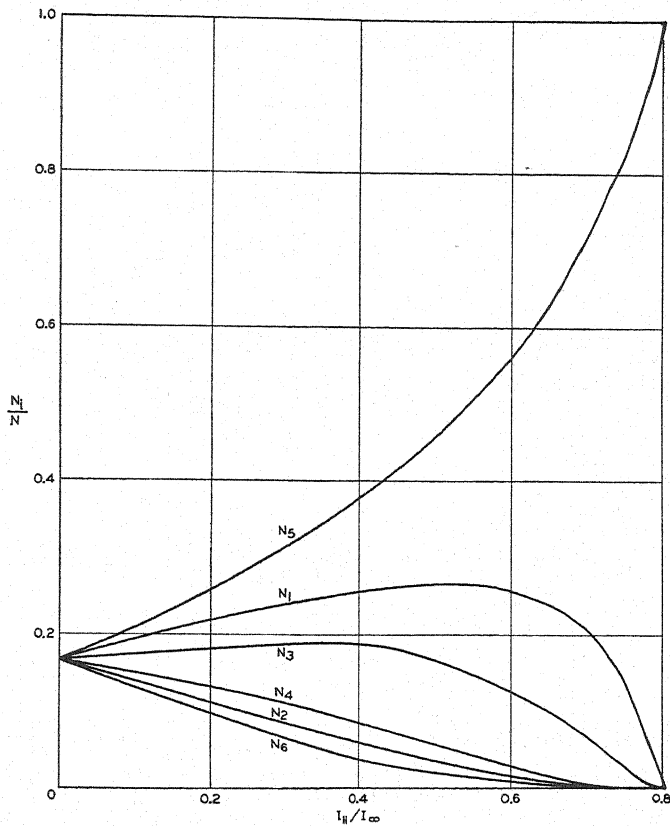


Fig. 2. Distribution curves when the direction of the field has the direction cosines $\lambda = 0.525$, $\mu = 0.279$, $\nu = 0.804$, and therefore lies in the $(11\bar{1})$ plane 10° from the $[112]$ direction. The magnetization is not constrained to lie in the $(11\bar{1})$ plane.

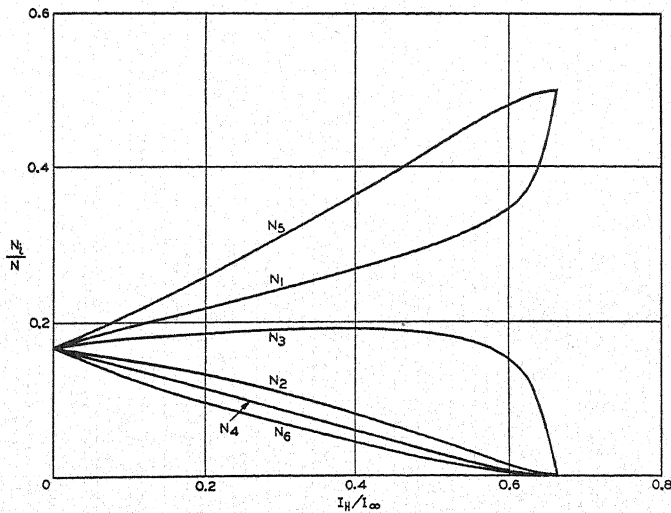


Fig. 3. Distribution curves when the direction of the field is the same as for Fig. 2. The magnetization for this case, however, is confined to the $(11\bar{1})$ plane by the additional condition $N_1 - N_2 + N_3 - N_4 - N_5 + N_6 = 0$.

I_H which lies in the latter direction, I may be determined in magnitude and direction. In the polar diagram of Fig. 4, referring to the (001) plane, each curve marked "CALC." is the locus of the end of the vector representing I ,

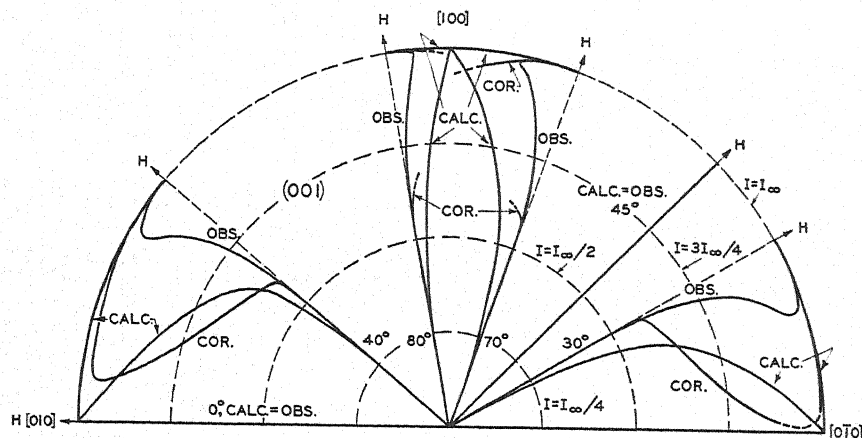


Fig. 4. Polar diagram of magnetization in a {001} plane of iron. Each curve is the path traced from the center of the semi-circle by the end of the vector representing I as I increases in magnitude from zero to I_∞ (the limit of the figure). The direction of the field is that indicated by the arrow, and is the same as the direction of the curve at the origin.

as it passes from the center of the circle to its circumference, while I increases in magnitude from 0 to I_∞ . When I_H becomes so large that one of the N_i 's

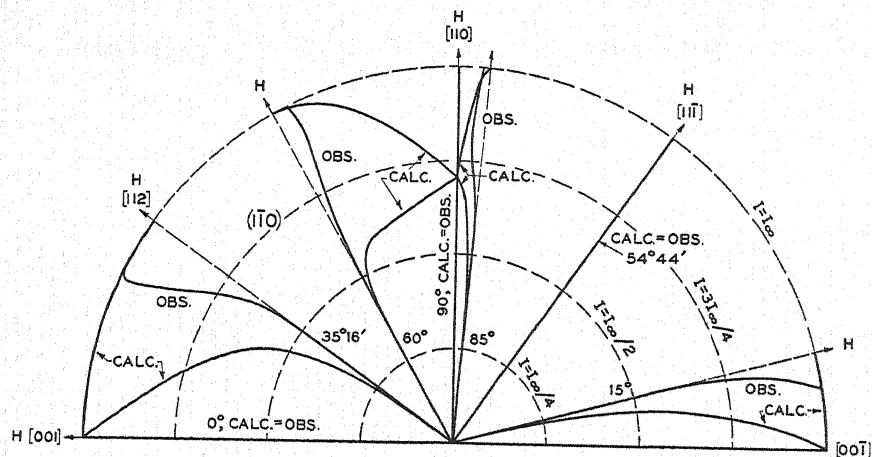


Fig. 5. Polar diagram of magnetization in a {110} plane. The observed curves have not been corrected for the demagnetizing effect of the normal component of magnetization. vanishes (generally when $I = I_\infty$) it is assumed that I turns in a plane into the direction defined by λ , μ and ν .⁴

The calculated curves shown in Figs. 5 and 6 are similarly determined but

⁴ In the special cases where the direction defined by λ , μ and ν makes the same angle with two (or three) of the axes, this last stage begins when $I = I_\infty/2^{1/2}$, (or $I = I_\infty/3^{1/2}$) and it is assumed that each of the two (or three) vectors then directed along the axes turns in a plane into the direction of the field.

are complicated by the fact that I may not equal I_∞ when the redistribution process is complete. In Fig. 6 I does not always lie in the plane of the figure, $(11\bar{1})$. In the latter figure the curve marked "CALC. (1)" is obtained without confining I to the plane, while for curves "CALC. (2)" I is so confined. In Figs. 4 and 5, I is automatically confined to the plane by symmetry.

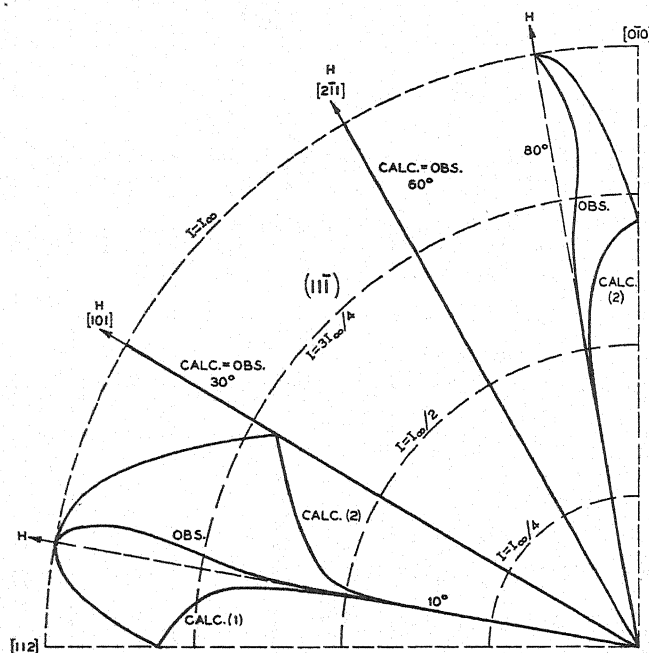


Fig. 6. Polar diagram of magnetization in a $\{111\}$ plane. Curves marked (2) are derived with the magnetization confined to the plane of the figure, corresponding to the experimental data. The observed curves are uncorrected for the demagnetizing effect of the normal component of magnetization.

COMPARISON WITH EXPERIMENT

The most complete data with which to compare the theoretical results are those of Honda and Kaya,⁵ who measured the magnetization parallel and perpendicular to the applied field in an oblate ellipsoid having axes 0.4 mm, 20 mm and 20 mm. From the applied field, they subtract the demagnetizing field acting anti-parallel to the applied field. Considering the resultant field, acting in the same direction as the applied field, to be the effective field, the data are plotted in Figs. 4 to 6 as curves marked "OBS."

These effective fields, however, are not the true magnetic fields acting on the crystal, because no account has yet been taken of the demagnetizing field due to the perpendicular component of the induced magnetization. Proper consideration of this additional field changes considerably the direction of the field which is effective, as shown in Fig. 7. Here the solid arrows are vectors measured from the common point; H' represents the applied field; H_H , the field parallel to H' corrected for the demagnetizing field due to the parallel

⁵ K. Honda and S. Kaya, Sci. Rep. Tohoku Imp. Univ. (1) 15, 721 (1926).

component of magnetization I_H , shown on a different scale by the dotted line; H_n represents the field due to I_n and equal to I_n multiplied by the demagnetizing factor 0.189, and H represents the (true) field equal to the vector sum of $H_{H'}$ and H_n . This correction has been made to all of the data referring to the (001) plane, and the corresponding curves marked "COR." are shown in Fig. 4. These curves lie much nearer to the calculated curves than the "OBS." curves do, and it is obvious that this correction accounts for most of the original difference between the calculated and experimental results.

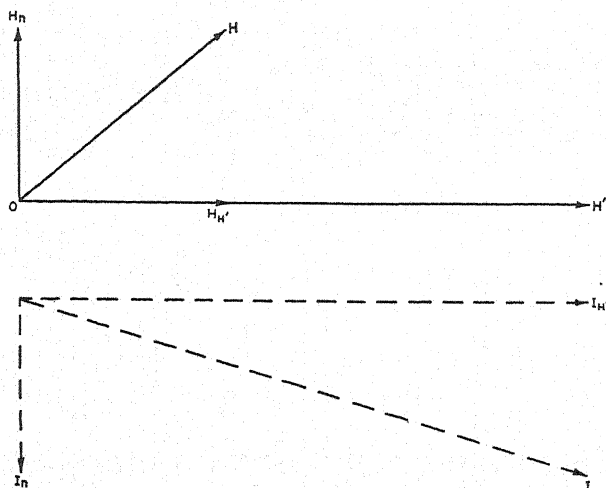


Fig. 7. Vector diagram showing the direction of the (true) field, H , as determined from the applied field, H' , and the demagnetizing fields due to the components of magnetization parallel ($I_{H'}$) and perpendicular (I_n) to the applied field.

The corrected curves were derived from the data in the following way. For a given direction of the applied field H' , and a certain value of the magnetization $I_{H'}$ parallel to the applied field as taken from the tables of Honda and Kaya, the direction of the field H was determined as indicated in Fig. 7 and the component of I parallel to H , I_H was calculated. This was done for all of the data relating to one direction of the applied field and curves plotted relating both θ_I (the angle between I and a particular $\langle 100 \rangle$ axis) and θ_H (the angle between H and the same $\langle 100 \rangle$ axis) with I_H . Similar curves were plotted for each of the four directions of the applied field in the (001) plane for which data exist. Selecting a definite value of I_H , these curves were used to obtain values of θ_H and θ_I by interpolation, one pair of values of the latter being obtained for each of the four directions of the applied field for which measurements were made. With the four points so obtained, a curve was plotted relating θ_H and θ_I , with I_H constant. Other curves were similarly plotted with I_H as parameter, and values of θ_I were read from these as a function of I_H for definite values of θ_H and the results plotted as in Fig. 4. This process naturally was subject to inaccuracies due to interpolation, and the final curves are not to be considered as representing the data exactly. Extrapolations of the curves were avoided, and sometimes no values of θ_I could be

assigned for certain values of θ_H and I_H , the curves in this case being dotted or omitted entirely.

Because these calculations were rather laborious, they were made only for the (001) plane, but since they show that the curves so corrected lie very much closer to the calculated curves it follows that a similar effect would be noted in the other planes. The correction is always in the right direction.

There is still another limitation in comparing the calculations with experiment. The perpendicular component of magnetization was determined by rotation of the single crystal specimen, so that rotational hysteresis is present. These two factors, hysteresis and the inaccuracy in the determination of the direction of the field on account of the large demagnetizing factor, are sufficient to account for the discrepancies between the corrected and calculated curves. The limitations of the data can easily be noticed when the corrected curve is plotted for $\theta_H = 45^\circ$. Although this curve is not reproduced here it swings to within 20° of the cubic axis when I is about 0.8 of saturation. This deviation of I from the direction of H is known to be in error since the "OBS." curve is a straight line, i.e., there is no perpendicular component when the applied field is in this direction.

The results for the (11 $\bar{1}$) plane are particularly interesting, for if H lies in this plane I will generally not do so. When H is inclined 10° to the [211] direction, curve marked "CALC. (1)" in Fig. 6 indicates that the theory predicts an effect in the direction opposite to that observed. In the extremely oblate ellipsoid used in the experiments, however, the magnetization is constrained to lie almost completely in the plane. When this condition is added to the others in the mathematical expression of the theory as described in the preceding section (Eqs. (10) et seq.), the direction of the perpendicular component is the same as that observed, as shown in curve "CALC. (2)."

The agreement between theory and experiment seems to be within the experimental error.

DISCUSSION

In making the calculations and plotting the results in the figures, nothing has been said explicitly about the magnitude of the magnetic field H which in the actual experiment induces the magnetization. The energy associated with each of the six directions of easy magnetization is supposed to be the same irrespective of the magnitude or direction of the field. The field is influential only in producing a magnetization having a component of given magnitude parallel to the field, the component at right angles being determined by probability considerations. There is little question but that this supposition is justified when the magnetization is small, perhaps even when it is as large as one-half of its saturation value, for then the corresponding field-strength is known to be small compared to the internal or molecular fields and cannot change the distribution function appreciably. On the other hand, when I becomes equal to I_∞ the probability considerations no longer apply and the vector representing I_∞ is assumed to turn slowly into the direction of the field, remaining always in the same plane.⁶

⁶ R. Gans, following a proposal of Heisenberg's, has recently indicated how to calculate the position of this vector as dependent upon the field strength. *Phys. Zeits.* **33**, 15 (1932).

The transition between these two situations is undoubtedly not perfectly sharp, and it may be expected that a more complete calculation, taking account of the magnitude of the field, would show the curves to be rounded at the point of contact with a $\langle 100 \rangle$ axis instead of sharp as shown in the figures.

Akulov² has made an extended theoretical study of the ferromagnetic properties of crystals, and has based many of his conclusions on the assumption that the magnetization in a domain may have any direction with respect to the crystal axes—that the domain is magnetically isotropic—as long as the magnetization is less than half of the saturation value. This assumption was made because experiments have shown the magnetization perpendicular to the field to be small or zero when the total magnetization of the crystal is less than half of saturation. Our theory accounts for this experimental fact but is based on the contrary assumption that the domains are saturated in a $\langle 100 \rangle$ direction even for the smallest values of the crystal magnetization. Thus it is unnecessary to accept Akulov's rather artificial picture of isotropic domains suddenly becoming anisotropic when the magnetization of the crystal exceeds a critical value. The curves of Figs. 4 to 6 show how slight is the difference between the directions of H and I when $I < I_s/2$. The difference between the calculated and observed curves in this region may well be due to the inaccuracy of the data, for it is in this region of small field strengths that the demagnetizing action of the perpendicular component, discussed at length above, is a maximum. Rotational hysteresis also would tend to make the observed perpendicular component too small.

Powell⁷ has proposed a theory of the magnetic anisotropy of crystals which expresses the direction of the magnetization as a function of the magnitude and direction of the field. When the field is applied in a $\{111\}$ plane of iron or nickel, however, and the magnetization is constrained also to lie in that plane, his theory requires that I should be parallel to H . The data show that the degree of anisotropy is smaller than in the other planes, but still it appears quite definite, especially for iron. On the other hand, my theory indicates that in this plane and under this condition there should be a deviation of I from H in the observed direction and approximately of the observed amount. This casts considerable doubt on the validity of Powell's theory. Mahajani's⁸ theory is also open to the same objection. It may be mentioned that in comparing his theory with experiment, Powell considered the field H to coincide in direction with the applied field, whereas in general their directions are different as remarked above.

The theory may obviously be applied to nickel, in which the directions of easy magnetization are $\langle 111 \rangle$ instead of $\langle 100 \rangle$ as in iron.

I take pleasure in expressing my indebtedness to L. A. MacColl for the mathematical work of the second section.

⁷ F. C. Powell, Proc. Roy. Soc. London **130A**, 167–181 (1930).

⁸ G. S. Mahajani, Phil. Trans. Roy. Soc. London **228**, 63–114 (1929).

An Empirical Equation of State

By HENRY S. FRANK AND FOO-SONG LEI

Department of Chemistry, Lingnan University, Canton, China

(Received August 22, 1932)

The law of Ramsay and Young, $P = \psi T - \Phi$, is shown to hold for diethyl ether both as a gas and as a highly compressed liquid. A single expression for ψ , $\psi = (R/V)e^{a/V^b}$ is shown to reproduce the experimental data for both conditions, with the same values of the constants a and b . Similar relations exist for carbon dioxide. Hildebrand's expression for Φ for ether is shown to require alteration in order to fit the accurate values for Φ here obtained. His value of about 79 cc for V_0 , the molal volume at the absolute zero of temperature and zero external pressure is verified with a more precise calculation of 79.46 cc. It is suggested that the close fit of Φ to a simple formula at high pressures and the deviations at lower pressures may be due to the existence of a more pronouncedly microcrystalline structure (Andrade Stewart) in the liquid at the higher pressures. The combination of expression for Ψ and Φ is shown to produce an equation of state which is accurate for the dilute gas and the highly compressed liquid, but which fails for intermediate pressures.

A NUMBER of important advances have been made recently in the discussion of the equation-of-state problem. On the theoretical side it has been shown¹ how the quantum mechanics can be applied to the calculation of constants for gases of simple molecular structure, thus for the first time enabling a purely theoretical calculation to be made for a real gas, yielding values for the pressure in substantial agreement with experiment. Of more immediate practical importance is the equation of Beattie and Bridgeman² which represents with great precision the PVT relationships for real gases over wide ranges of temperature and pressure, and has been successful in reproducing pressure and temperature changes of Joule-Thomson coefficients³ and of the ammonia equilibrium.⁴

Neither of the treatments referred to touches on the problem of the continuity of states, nor the possibility of a single equation representing accurately both gaseous and liquid phases. A contribution in this direction has been made by Hildebrand,⁵ who gives an equation for the "internal pressure" $(\partial E/\partial V)_T$ of diethyl ether in both gaseous and liquid states. Whether it is logical to expect a single equation to fit both phases has become questionable, however, in view of recent theories based on x-ray diffraction⁶ and the inter-

¹ (a) J. C. Kirkwood and F. G. Keyes, *Phys. Rev.* **37**, 832 (1931); (b) J. C. Slater, *ibid* **38**, 237 (1931); (c) H. Margenau, *ibid* **38**, 1785 (1931); (d) J. G. Kirkwood, *Phys. Zeits.* **33**, 39 (1932).

² J. A. Beattie and O. C. Bridgeman, *Proc. Am. Acad. Arts and Sci.* **63**, 229 (1928).

³ J. A. Beattie, *Phys. Rev.* **35**, 643 (1930).

⁴ L. J. Gillespie and J. A. Beattie, *Phys. Rev.* **36**, 743 (1930); **36**, 1008 (1930); also *J. Am. Chem. Soc.* **52**, 4239 (1930).

⁵ J. H. Hildebrand, *Phys. Rev.* **34**, 984 (1929). Cf. also R. K. Schofield, *Phil. Mag.* **5**, 1171 (1928).

⁶ G. W. Stewart, *Phys. Rev.* **35**, 726 (1930) and later papers.

pretation of viscosity in liquids.⁷ If liquids are actually microcrystalline in structure, as these theories postulate, then they are less similar to gases than has been supposed, and the "continuity of states" expressed in the equations of van der Waals and Dieterici may require a new interpretation.

In view of the complexity of the subject not only of the structure of liquids but even of collision processes in only moderately compressed gases, we feel that it is still profitable to discuss empirical relationships connecting P , V and T , particularly where these touch liquids. At worst such relationships, if substantiated, will serve as numerical checks upon theoretical equations which may later be worked out.

The equation of Ramsay and Young, $P = \Psi T - \Phi$ where Ψ and Φ are volume functions, has been verified for dilute gases by a number of workers. The van der Waals equation is simply a more explicit form of it, as is also the Keyes equation, $P = RT/V - \delta - a/(V+b)^2$ where $\delta = \alpha V^2$. The Beattie-Bridgeman equation is a further development of the Keyes equation correcting for deviations from the Ramsay-Young law on the assumption that these are due to association.

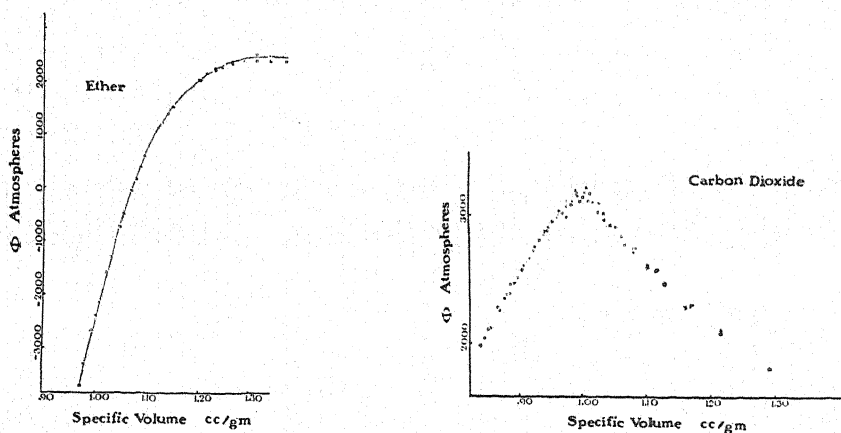


Fig. 1. Measurements at 20°C represented by squares; 40° by crosses; 60° by circles; 80° by triangles.

Fig. 2. Measurements at 0°C represented by squares; 10° by crosses; 20° by circles; 30° by triangles.

We have found empirically that for diethyl ether and carbon dioxide the function Ψ of Ramsay and Young is well represented by $(R/V)e^{a/V^b}$ for specific volumes which are not too small. What interests us particularly is the fact that the same expression with the same numerical constants seems to fit the data for the compressed liquids with great accuracy. The test of this is to assume $P = (RT/V)e^{a/V^b} - \Phi$ and calculate Φ from experimental data. If data for different values of T give calculated Φ 's which fall on the same curve when plotted against volume, it is clear that not only $(\partial P/\partial T)_V$ but also its volume coefficient $\partial^2 P/\partial V \partial T$ is correctly represented. Such curves for ether and CO_2 are reproduced in Fig. 1 and Fig. 2. The data are those of

⁷ E. N. DaC. Andrade, *Nature* **125**, 580 (1930); S. E. Sheppard and R. C. Houck, *J. Rheology* **1**, 349-71 (1930).

Bridgeman and Amagat, and are shown in Tables I and II together with the calculated Φ values. The constants a and b were obtained from the accurate values for Ψ given by Beattie⁸ for gaseous ether and by Bridgeman⁹ for gaseous CO₂. Log log ($\Psi V/R$) was plotted against log V , and the slope and intercept determined for the straight line obtained. The slope is b and the intercept a .

TABLE I. $V-\Phi$ curve for ether. $P = (RT/V)e^{a/V^b} - \Phi$, where $a = 3.153$, $b = 0.844$ and $R = 1.1078$

Volume (cc/g)	Pressure (atm.)	ψT (atm.)	Φ (atm.)	Temperature (°C)
0.9748	12,000	8287	-3713	20
0.9812	12,000	8707	-3293	40
0.9949	12,000	9330	-2670	80
1.0018	11,000	8612	-2388	60
1.0021	10,000	7525	-2475	20
1.0092	10,000	7853	-2147	40
1.0232	10,000	8422	-1578	80
1.0314	9000	7710	-1290	60
1.0416	8000	7006	-994	40
1.0491	8000	7263	-737	60
1.0564	8000	7515	-485	80
1.0705	6000	5951	-49	20
1.0801	6000	6164	+164	40
1.0887	6000	6390	+390	60
1.0960	6000	6607	+607	80
1.1311	4000	5257	1257	40
1.1417	4000	5416	1416	60
1.1517	4000	5547	1547	80
1.2018	2000	4029	2029	20
1.2032	2500	4529	2029	60
1.2157	2000	4136	2136	40
1.2316	1500	3709	2209	20
1.2316	2000	4214	2214	60
1.2479	2000	4286	2286	80
1.2680	1000	3381	2381	20
1.2680	1500	4842	2342	60

TABLE II. $V-\Phi$ curve for CO₂. $P = (RT/V)e^{a/V^b} - \Phi$, where $a = 18749$, $b = 0.9210$ and $R = 1.8652$.

Volume (cc/g)	Pressure (atm.)	ψT (atm.)	Φ (atm.)	Temperature (°C)
0.8377	1000	2990	+1990	0
0.8430	950	3001	+2051	0
0.8483	900	3026	2126	0
0.8525	1000	3127	2127	10
0.8645	750	3039	2289	0
0.8682	1000	3268	2268	20
0.8771	800	3173	2373	10
0.8817	900	3295	2395	20
0.8843	1000	3398	2398	30
0.8850	600	3075	2475	0
0.8915	950	3427	2477	30
0.8961	800	3324	2524	20
0.9036	750	3339	2589	20
0.9048	600	3227	2627	10
0.9154	800	3480	2680	30
0.9208	400	3145	2745	0
0.9238	500	3267	2767	10

⁸ J. A. Beattie, J. A. C. S. **46**, 350 (1924).

⁹ O. C. Bridgeman, J. A. C. S. **49**, 1130 (1927).

TABLE II. (Continued).

Volume (cc/g)	Pressure (atm.)	ψT (atm.)	Φ (atm.)	Temperature (°C)
0.9316	700	3516	2816	30
0.9382	550	3415	2865	20
0.9401	650	3536	2886	30
0.9435	300	3193	2893	0
0.9454	400	3314	2914	10
0.9507	600	3561	2961	30
0.9598	350	3346	2996	10
0.9613	450	3468	3018	20
0.9626	550	3590	3040	30
0.9680	225	3246	3021	0
0.9739	200	3198	2993	0
0.9739	300	3376	3076	10
0.9744	500	3620	3120	30
0.9752	400	3501	3101	20
0.9824	275	3399	3124	10
0.9844	175	3283	3108	0
0.9893	450	3657	3207	30
0.9902	350	3539	3189	20
0.9916	250	3422	3172	10
0.9950	150	3275	3125	0
1.0020	225	3426	3201	10
1.0050	400	3631	3231	30
1.0080	125	3252	3127	0
1.0090	300	3476	3176	20
1.0140	200	3312	3112	10
1.0220	100	3131	3031	0
1.0250	350	3450	3100	30
1.0320	75	3050	2975	0
1.0320	250	3274	3024	20
1.0420	150	3080	2930	10
1.0500	300	3222	2922	30
1.0600	200	3050	2850	20
1.0620	50	2824	2774	0
1.0770	175	2925	2750	20
1.0780	100	2820	2720	10
1.0800	250	3005	2755	30
1.1000	75	2676	2606	10
1.1000	150	2771	2621	20
1.1130	200	2783	2583	30
1.1270	125	2606	2481	20
1.1590	50	2343	2293	10
1.1680	150	2456	2306	30
1.2140	75	2159	2084	29
1.2140	125	2233	2108	30
1.2900	100	1927	1827	30
1.4770	75	1250	1175	30

In the regions where Ramsay and Young's law holds, $\Phi = (\partial E / \partial V)_T$ the so-called "internal pressure" of the substance. Hildebrand has represented this for ether by the equation

$$\Phi = \frac{3180 \times 10^4}{V^2} \left[1 - \left(\frac{79}{V} \right)^8 \right]^{10},$$

verifying his equation against Bridgeman's data. He obtained the form of Φ by analogy with the Born-Landé theory of compressibility of crystal lattices,

¹⁰ Φ is in atmospheres and V in cc per mol. Changing V to cc per gram so as to compare with our figures, Hildebrand's equation becomes

$$\Phi = 5794/V^2 - 9692/V^{10}.$$

and considers its agreement with experiment to speak for the existence of rather simple relations in the structure of liquids. Hildebrand's method of calculating Φ from Bridgeman's data does not give results of high accuracy, and the points do not fit his curve very perfectly. Using our calculated Φ 's for liquid ether, and the accurate values of Beattie⁸ for Φ for gaseous ether, we have modified the constants in Hildebrand's equation, and obtained the following:¹¹

$$\Phi = 3834/V^{1.892} - 6295/V^{7.94}.$$

Taking this equation for Φ , and our Ψ , we obtain for an equation of state for ether:

$$P = (RT/V)e^{a/V^b} - K/V^n + C/V^d,$$

where P is in atmospheres, V is in cc/g. $R=1.1078$, $a=3.153$, $b=0.844$, $k=3834$, $n=1.892$, $c=6295$, and $d=7.94$. Values for P calculated from this equation are compared with experimental ones in Table III.

TABLE III. Ether. A comparison of pressures observed by others and those calculated from our equation of state. Pressure in atmospheres; temperature in °C; $T=t+273.13$.

$V(\text{cc/g})$	$P(\text{calc.})$	$P(\text{obs.})$	$t(^{\circ}\text{C})$	Observer
0.9812	12,044	12,000	40	Bridgeman
1.0092	9942	10,000	50	"
1.0416	8012	8000	40	"
1.0801	6266	6000	40	"
1.1311	4587	4000	40	"
0.9949	12,016	12,000	80	"
1.0232	9997	10,000	80	"
1.0564	8073	8000	80	"
1.0960	6425	6000	80	"
20	16.89	16.88	150	Beattie
25	14.40	14.48	150	"
35	11.08	11.19	150	"
100	4.37	4.32	150	Ramsay & Young
15	25.32	25.04	200	Beattie
20	20.25	20.47	200	"
25	17.13	17.23	200	"
35	12.93	13.05	200	"
15	38.06	37.71	325	"
20	29.34	29.39	325	"
25	23.96	24.05	325	"
35	17.56	17.66	325	"
100	4.90	4.88	195	Ramsay & Young
200	2.52	2.50	195	"
250	1.98	2.01	195	"
300	1.71	1.80	195	"

¹¹ Born and Mayer have recently (M. Born and J. E. Mayer, *Zeits. f. Physik* **75**, 1 (1932); J. E. Mayer and L. Helmholtz, *ibid.* **75**, 19 (1932); J. E. Mayer and M. C. Maltbie, *ibid.* **75**, 748 (1932)) shown that an exponential law is better able to express the repulsive potential in a crystal lattice than is a simple inverse power. We find that their form, $be^{-r/p}$, for repulsive potential, or $C_1V^{-2/3}e^{-C_2V^{1/3}}$ for the repulsive part of Φ does not fit our data as well as the form, C/V^a , which we have used.

It will be observed that the representation of Φ as the algebraic sum of an attractive and a repulsive term each varying as an inverse power of the volume holds with good accuracy in the dilute gas and the highly compressed liquid, but fails for the liquid at lower pressures, and for the compressed gas. It is not clear that the agreement for the highly compressed liquid would persist at still higher pressures, but there seems to be no reason to doubt this. It may be mentioned that the critical constants calculated from this equation by writing $(\partial P/\partial V)_T = 0$ and $(\partial^2 P/\partial V^2)_T = 0$ do not agree with the experimental ones, that is, the critical region lies in the middle range for which the equation does not hold.

The range of pressures covered by the data for CO_2 is not extended enough for this method to furnish any interesting information concerning the form of Φ . As an indication of the limits of accuracy of our values of Ψ , however, we have used our Ψ and Bridgeman's Φ to obtain the results shown in Table IV.

TABLE IV.¹⁰ CO_2 . A comparison of pressures observed by Amagat and those calculated from our equation of state. Pressure in atmospheres; temperatures in $^{\circ}\text{C}$; $T = t + 273.15$.

V cc/g		0	10	20	30	40	50
40	obs.	11.16	12.15	12.67	13.17	13.69	14.19
	calc.	11.70	12.20	12.69	13.19	13.69	14.18
	Δ	0.54	0.05	0.02	0.02	0.00	-0.01
30	obs.	15.08	15.76	16.47	17.15	17.86	18.54
	calc.	15.15	15.82	16.50	17.17	17.85	18.52
	Δ	0.07	0.06	0.03	0.02	-0.01	-0.02
25	obs.	17.66	18.48	19.35	20.19	21.06	21.90
	calc.	17.76	18.58	19.40	20.22	21.05	21.87
	Δ	0.10	0.10	0.05	0.03	-0.01	-0.03

It is not required of an empirical equation that it conform to preconceived ideas of functional form, nor that it lend itself to simple interpretation. If an interpretation is to be given, however, we are inclined to correlate the good agreement of Hildebrand's form of Φ at higher pressures, as well as the poorer agreement at lower pressures, with the cybotactic, or microcrystalline theories of the liquid state already referred to. It seems likely that the orderly arrangement of molecules in the liquid would become more marked at higher pressures, and one might predict that in the pressure region where our equation fits Bridgeman's data the x-ray diffraction rings of ether would be found to be sharper than has yet been observed, and that the fluidity of the liquid would be found to be greatly diminished. Another possibility is that the simpler relations at high pressures correspond to a pressure-inhibition of molecular rotation in the liquid somewhat along the lines suggested for temperature effects in Meyer's¹² interpretation of the transitions observed by Wolfke and Mazur.¹³

In the matter of functional form, it has been customary to express the attractive and repulsive terms in crystals by inverse integral powers of the volume. On the other hand, until the quantum mechanical theory is further

¹² L. Meyer, *Zeits. f. Physik* **75**, 421 (1932).

¹³ M. Wolfke and J. Mazur, *Zeits. f. Physik* **74**, 110 (1932).

developed than at present it will not be certain whether the powers for liquids and compressed gases have to be integral. We have therefore taken the powers empirically as slopes of logarithmic plots. The failure of the equation for liquid ether at lower pressures can be corrected by adding other terms to Φ , but this only serves up to a specific volume of 1.15 cc/g. Beyond this point ΨT fails to represent the effect of temperature, either because Ψ is no longer of the right form, or, more probably, because Ramsay and Young's law no longer holds. The $\Phi - V$ plots for both ether and CO_2 make it seem likely that in the intermediate region the dependence of P upon T becomes more complicated, as is demonstrated for gases under high pressures by the success of the Beattie-Bridgeman equation.

As to the form of Ψ , in searching the literature available to us we have failed to find the form $(R/V)e^{a/V^b}$ used by any previous author, though other forms involving exponentials are not rare. So far as we can tell none of the other forms that have been proposed has the property of representing the liquid phase of ether or of CO_2 . In our form, since the liquids give volumes near 1 cc/g, and b is not far from unity, the fit for the liquid is not very sensitive to changes in b , though such changes are important in the gas phase. There is thus possibly something fortuitous in the fit for the liquid so far as concerns the constant b . This is hardly the case with the constant a , however, and it would be very desirable to learn whether this form of equation applies also to other substances. Unfortunately, the number of substances for which data over considerable temperature and pressure ranges are available for both liquid and gas is small. Even in the case of CO_2 , as has been mentioned, the range of measured pressures is not so great as is desirable.

Hildebrand has assumed that at the absolute zero of temperature and under no external pressure the volume V_0 of any substance is that at which $\Phi = 0$. His value of V_0 for ether, about 79 cc/mol., is verified by our calculation, which gives 1.0727 cc/g, or 79.46 cc/mol.

PROCEEDINGS
of the
AMERICAN PHYSICAL SOCIETY

MINUTES OF THE CHICAGO MEETING, NOVEMBER 25-26, 1932

The 180th regular meeting of the American Physical Society was held in Chicago, Illinois at the Ryerson Physical Laboratory and Eckhart Hall of the University of Chicago on Friday and Saturday, November 25 and 26, 1932. The presiding officers were W. F. G. Swann, President of the Society, Paul D. Foote, Vice-President, Arthur H. Compton, A. J. Dempster and H. A. Erikson.

Judson Court, one of the University dormitories, was the Society headquarters and the Society dinner was held there on Friday evening. About ninety guests were present. President Swann presided and the after dinner speakers were Arthur H. Compton, who related some of his experiences in his cosmic-ray expedition, Editor John T. Tate, who reviewed the returns on the publication questionnaire and pointed out the probable savings to be secured by the new program under the American Institute of Physics, and Karl K. Darrow who recalled numerous interesting features of past meetings of the Society.

The new College Physics Museum in Belfield Hall was kept open both days for inspection by the members of the Society.

Meeting of the Council. At its meeting on Friday, November 25th, the Council approved the transfer of four members to the grade of fellowship. Thirty-nine candidates were elected to membership. *Transferred from membership to fellowship:* Richard M. Badger, Kenneth T. Bainbridge, Weldon G. Brown and G. B. Kistiakowsky. *Elected to membership:* Hollis S. Baird, Victor W. Cohen, William T. Cooke, Edward M. Cratty, W. P. Cunningham, Robert W. Ditchburn, John Dropkin, P. O. Ewald, Guy Forman, G. Norris Glasoe, G. G. Harvey, Clarence D. Hause, Laurence B. Heilprin, Banesh Hoffman, Joseph Joffe, Joseph S. Knapper, Homer C. Knauss, Walter H. Mais, H. E. Malstrom, J. Carlisle Mouzon, Elton M. Palmer, Anna W. Pearsall, John M. Pearson, Fred G. Person, H. S. Polin, Seymour Rosin, Angus S. Roy, Harold L. Saxton, George K. Schoepfle, Sidney L. Siegel, Selby M. Skinner, Frank M. Sparks, Alexander W. Stern, Herbert M. Strong, B. J. Thompson, Clinton E. Trimble, Louis R. Weber, George W. Wheelwright, and Henry L. Yeagley.

The regular scientific session consisted of fifty-five papers, six of which, numbers 10, 11, 20, 40, 41 and 44, were read by title. A complete list of authors and abstracts will be found in the following pages.

W. L. SEVERINGHAUS, *Secretary*

ABSTRACTS

1. The magnetic susceptibilities of some common gases. G. G. HAVENS, *University of Wisconsin*.—In view of the large differences among the results of various observers for the magnetic susceptibilities of common gases, it seemed desirable to apply to some of these gases the method described in a previous article. (Phys. Rev. **41**, 339 (1932)). Being a comparison method, the values obtained are relative to a provisional value of $X_{O_2} = 3335 \times 10^{-6}$ for the molecular susceptibility of oxygen at 20°C. If the value for oxygen should later prove to be different, the values for these gases will be changed proportionally. The results obtained are: $X_{H_2} = -4.014 \times 10^{-6}$, $X_{He} = -1.925 \times 10^{-6}$, $X_{N_2} = -11.94 \times 10^{-6}$, $X_{CO_2} = -20.81 \times 10^{-6}$. The results for H_2 , He and N_2 are in good agreement with those obtained by Wills and Hector. (Phys. Rev. **23**, 209 (1924).) The value of the temperature presented the largest uncertainty in the measurement of susceptibilities at liquid air temperatures; however it was found that the molecular susceptibilities of H_2 and He at liquid air temperatures vary less than 4 percent from those obtained at room temperatures. This result disagrees with that of Bitter (Phys. Rev. **36**, 1648 (1930)) which indicates a decrease of more than 40 percent in the molecular susceptibility of H_2 in going from room to liquid air temperatures. Preliminary observations indicate that the susceptibilities of ortho- and para-hydrogen are the same within 1 percent.

2. The paramagnetic susceptibility of Cu^{++} . O. M. JORDAHL, *University of Wisconsin*.—Calculations have been made for the susceptibility of the Cu^{++} ion subject to a crystal potential field of predominantly cubic symmetry with a small rhombic field superposed. The Hamiltonian is

$$Ax^2 + By^2 - (A+B)z^2 + E(x^4 + y^4 + z^4) + \lambda(L \cdot S) + \beta H(L + 2S)$$

By proper choice of the parameters, the resulting expressions for the principal susceptibilities are capable of agreement with the known experimental data. To a good approximation, the expression for the mean (i.e. powder) susceptibility X_m is independent of both the magnitude and the asymmetry of the rhombic field, and gives a linear dependence on temperature for the quantity $(X_m k T / N \beta^2)$. This agrees with the Leiden data of de Haas and Gorter on $CuSO_4 \cdot 5H_2O$ from 14°K to 290°K. In order to fit the data of Bartlett on the principal susceptibilities of $Cu(NH_4)_2(SO_4)_2 \cdot 6H_2O$ and $CuK_2(SO_4)_2 \cdot 6H_2O$ (Phys. Rev. **41**, 818 (1932)) it is necessary to choose the parameters so that the cubic field produces a splitting of approximately 20,000 cm^{-1} and the splitting of the lower cubic level by the rhombic field is about 300 cm^{-1} . These values agree approximately with those found for Co, Ni and Cr by R. Schlapp and W. G. Penney. (Phys. Rev., in press.)

3. A compact high potential electrostatic generator. HENRY A. BARTON, *American Institute of Physics*, D. W. MUELLER, *Princeton University* and L. C. VAN ATTA, *Massachusetts Institute of Technology*.—An inexpensive and compact continuous high-potential source was desired for nuclear research. A Van de Graaff, belt-type, electrostatic generator has been built. To overcome the corona limitation due to high potentials and small dimensions, the entire apparatus is mounted in a cylindrical steel drum and the insulating air raised to a pressure of several atmospheres. A cylindrical electrode is supported in the center of the drum by two textolite cylindrical tubes of the same diameter. In one of these runs a silk charging belt similar to that in the original Van de Graaff generator. The other supporting tube can be evacuated and it will be used in applying high potentials to the acceleration of charged particles. At a pressure of seven atmospheres, a potential of about one million volts was generated. High pressures also permit greater charge to be carried on the belt. In a separate test, also at seven atmospheres pressure, the belt transported charge at the rate of 0.1 m.a. It will be possible to operate at twice the pressure so far used. The belt can be driven twice as fast as now and a parallel belt added. It is hoped to generate a kilowatt at about two million volts.

4. The production of high-velocity protons by repeated accelerations. A. J. DEMPSTER, *University of Chicago*.—The principle of a simple method for repeated acceleration of canal rays has been tested. The positive rays from a high potential hydrogen discharge tube pass into hydrogen at higher pressure where some of the atoms become neutral and the equilibrium

ratio between positive and neutral particles is approached. The neutral rays then cross a high retarding field into a positively charged metallic chamber 32 mm long connected to the anode. During their passage through this chamber, at a pressure of 0.2 mm Hg, a number of the neutral atoms revert to the positively charged state. On leaving the positively charged metallic chamber, these positively charged atoms are accelerated and attain twice their original energy. The process may be repeated indefinitely with a loss of intensity at each passage through an accelerating chamber. An experiment was carried out with one accelerator in which the energy of the rays was deduced from the deflection, by a short transverse electric field, of the spot produced by the rays on a fluorescent screen. With the accelerator grounded a maximum energy of 22,500 volts was observed, and with the accelerator joined to the anode of the discharge tube a new spot appeared with half the deflection, corresponding to an energy of 45,000 volts.

5. Polarization of collecting electrodes in high vacua. A. E. SHAW, *University of Chicago*—

In an experiment to determine e/m by electron deflection in superimposed electrostatic and magnetic fields, it was found possible to determine accurately the value of the surface charges that form on the plates to which the electric potential is applied and which must be corrected for. These surface layers have been found to vary with the material of the plates, the gas pressure and the intensity of the electron beam. They are independent of the intensity of the electrostatic field. With bronze at pressures of 5×10^{-7} mm Hg and an electron current of 3×10^{-12} ampere, the surface potential was 0.263 volt. With a current of 10^{-9} ampere the pressure remaining the same, the potential increased to 0.998 volt. With gold the surface potential was less than 0.005 volt, at pressures of 5×10^{-7} mm Hg and an electron current of 3×10^{-12} ampere.

6. Ionization of He by electron impact. W. W. WETZEL, *University of Minnesota*.—The Born collision theory (neglecting exchange effects) is applied to the ionization of He by electron impact. The distributions in angle and energy of the scattered electrons have been calculated for initial electron energies of 50, 100, 200, and 500 volts. The curves are in qualitative agreement with the experiments of Van Atta in He for the distribution in energy and with those of Tate and Palmer in Hg for the angular distribution. The most probable mode of ionization is for scattering in the forward direction with a loss of about one volt energy, the probability dropping rapidly to zero just at the ionization potential. The theoretical curves show, however, a continually increasing total probability of ionization due to excessive scattering in the forward direction. To obviate this difficulty the distortion of the wave forms of the incident and scattered electrons is being studied. Preliminary considerations indicate also a reasonably good probability for ionization and simultaneous excitation in He.

7. Ionization by electron impact in water vapor and sulphur dioxide. H. D. SMYTH AND D. W. MUELLER, *Princeton University*.—Ionization in water vapor and sulphur dioxide has been studied with the mass-spectrograph previously used by Smyth and Stueckelberg. In water vapor the results of previous investigators have been confirmed and extended. Two I.P.'s for H_2O^+ were found, 12.7 ± 0.3 and 16.0 ± 0.6 volts. Other positive ions in much smaller numbers appeared as follows: H^+ at 18.9, OH^+ at 18.9, H_2O^+ with H_2O^+ , O^+ at 18.5, H_2^+ at 33.5 and O_2^+ (very weak). In sulphur dioxide which has apparently never before been studied, SO_2^+ ions appeared at 13.1 ± 0.3 volts. SO^+ ions at 16.5 ± 0.5 and ions of mass 32, either S^+ or O_2^+ , at 16.0 ± 0.7 , increasing sharply at 22.3 ± 1.0 . No O^+ ions were observed. The existence of a strong second I.P. for H_2O^+ had been suggested by Smyth and Stueckelberg on experimental grounds and by Mulliken for theoretical reasons. Consideration of the probable ionization processes corresponding to the other results shows one point of special interest. Evidently the processes $\text{H}_2\text{O} \rightarrow \text{H}_2 + \text{O}^+$ and $\text{SO}_2 \rightarrow \text{S}^+ + \text{O}_2$ both occur and at very nearly the minimum energy calculated. This means that in the process of ionization not only are the chemical bonds between the O (or S) and H (or O) atoms broken but new bonds are established between the H (or O) atoms themselves which did not exist in the normal state.

8. Radiation excited by canal ray impact. F. L. VERWIEBE, *University of Chicago*.—Hydrogen canal rays accelerated in a field up to 50 kv were allowed to impinge on a metal

target, and the beam of particles and radiation emitted from the target was investigated. Pin-hole images of the focal spot were obtained on Schumann plates and plates coated with molybdenum tri-oxide. The tri-oxide indicates the presence of atomic hydrogen. By means of a deflecting magnetic field it was found that the beam coming from the target consisted mainly of neutral particles or of radiation, and also of a fainter beam of protons which had a velocity practically equal to that of the protons in the incident canal rays. The presence of uncharged hydrogen atoms in the neutral beam was shown by the image of characteristic light blue color formed on a molybdenum tri-oxide plate. A grating was used to determine whether the undeflected beam also contained electromagnetic radiation. A diffraction pattern was obtained and the value of the wave-length was found to agree within the limits of the accuracy of the measurements with that of the first Lyman line, 1216A'. No wave-lengths shorter than this of observable intensity were found.

9. Radiation from positive ions in argon, neon, helium. A. I. MCPHERSON, *University of Chicago (Introduced by A. J. Dempster)*.—Light excitation was produced by a stream of high speed—20,000 volt—positive ions of argon, neon, helium in passage through rarefied argon, neon, helium respectively. The spectra observed in the direction of motion show groups of doublets, whose separation varies with the velocity of the positive ions, a sharply marked Doppler displacement. In argon and neon, the first spark lines are strongly excited in both the gas at rest and in the moving particles, the intensity of the displaced line in each doublet being only slightly less than that of the undisplaced line. The arc lines appear relatively weak, and in the very few cases where an arc line has an accompanying Doppler line, it is very faint indeed. In helium many of the lines of both arc and spark spectra show the effect clearly but the intensity of the displaced line is usually much less than that of the rest line, and the relative intensity varies greatly from line to line.

10. The actinium branching ratio. FORREST WESTERN AND ARTHUR RUARK, *University of Pittsburgh*.—The actinium branching ratio is $\lambda_{Ac}N_{Ac}/E$; $\lambda_{Ac}N_{Ac}$ is the activity of the actinium in equilibrium with a sample of uranium of activity $2E$. Assuming one or two actino-uranium isotopes, the ratio $B = \lambda_{Ac}N_{Ac}/\lambda_1N_1$ is more useful. (Subscripts 1, 2, 3, 4 refer to isotopes 238, 234, 239, 235.) B is determined from the saturation currents i_U and i_{Pa} , from a sample of uranium and its associated protoactinium, and the alpha particle ion numbers k_{Pa} , k_1 , \dots , k_4 . Ziegert's determinations of ion numbers and the above actinouranium hypothesis, necessitate revision of branching ratios given by Widdowson-Russell and Hahn-Meitner. Assuming two actinouranium isotopes of masses 235 and 239, we find that

$$B = [(k_1 + k_2)i_{Pa}] / [k_{Pa}i_U - (k_3 + k_4)i_{Pa}].$$

If U_3 does not exist, put $k_3 = 0$. k_1 , k_2 and k_{Pa} are known. It seems probable from work of Ziegert and of Wilkins-Rayton that $k_3 \leq k_4 \leq k_2$. If so, data of Widdowson-Russell and Hahn-Meitner yield $B = 0.0281$ or 0.0320 if U_3 is non-existent; and $B = 0.0285$ or 0.0325 , if U_3 exists. Data of Wildish are not appreciably affected; von Grosse, details unpublished, obtained 0.04 .

11. The atomic weights of radioactive substances. FORREST WESTERN AND ARTHUR RUARK, *University of Pittsburgh*.—Given the isotopic weights of Ra G, Ac D, and Th D, that of any other radioactive substance can be obtained by adding the masses of the particles emitted and the mass equivalent of the energy lost, in the intervening disintegrations. Such computations were made by St. Meyer but we do not agree with all his conclusions. Using Aston's analyses of leads, chemically-determined atomic weights, and the packing fraction curve, one finds in three ways that the weight of Pb^{216} is 205.984 ± 0.03 on the chemical scale. The weights of Pb^{207} and Pb^{208} are assumed to differ from this by integers, by analogy with the behaviors of Hg and Kr. We then obtain the following isotopic weights.

	Calculated	Accepted chemical value
Radium	226.027	225.967 \pm 0.012
Protoactinium	231.039	
U^{234}	234.040	238.137 \pm 0.013 (U mixture)
U^{235}	235.045	
U^{238}	238.046	
U^{239}	239.051	
Thorium	232.035	232.120 \pm 0.014

Any reasonable assumption as to half-lives of possible actinouranium isotopes yields an atomic weight for U unreconcilable with that obtained chemically. The calculated atomic weights of Ra, Th, and U should be used in preference to currently accepted values.

12. Argon in the ionization method of measuring cosmic rays and γ -rays. JOHN J. HOPFIELD, *Basic Science Division, A Century of Progress, Chicago. (Introduced by H. G. Gale.)*—Ionization current-voltage curves of argon at 31 atm. and 71 atm. and at four γ -ray intensities of ratios 1, 10, 100 and 1000 were not convertible into one another by constant factors. The superiority of argon over air for ionization chambers, and the slower recombination of its ions is shown in the following:

Pressure in atm.	10	20	30	40	50	60	70	80	90	100
I , ions/cc. sec. per atm. (argon)	3.75×10^2	3.45	3.09	2.80	2.57	2.36	2.19	2.03	1.89	1.77
I , ions/cc. sec. per atm. (air)	1.80×10^2	1.44	1.18	1.02	0.90	0.80	0.71	0.65	0.59	0.55
$I_{\text{argon.}}/I_{\text{air.}}$	2.08	2.40	2.61	2.73	2.84	2.95	3.05	3.12	3.18	3.23

It is seen from these data that the argon ionization-pressure curve is more nearly linear than that of air; furthermore the argon curve is rising rapidly even at the end pressure. Preliminary results indicate that the ratio of intensity of cosmic rays to γ -rays is a function of the argon pressure. At 36 atm. it was 0.117, and at 74 atm., 0.139. This change could be accounted for by insufficient voltage for saturation. A smaller ratio of cosmic rays to γ -rays was measured in argon (0.117) than in air (0.149), at the same pressure. This seems to be the first direct comparison of the action of cosmic rays on monatomic and diatomic gases. This smaller ratio accords with the suggestion that the primary attack of cosmic rays is on atomic nuclei, since argon has half as many as air. Other explanations are tenable. These experiments were carried out through the courtesy of the University of Chicago.

13. Sea level intensity of cosmic rays in certain localities from 46° south to 68° north latitude. ARTHUR H. COMPTON, *University of Chicago.*—Measurements have been made, with the help of many cooperating physicists, of the cosmic rays at typical stations in Hawaii, New Zealand, Australia, east and west equatorial Pacific ocean, Panama, Peru, Mexico, United States, Canada and Switzerland. When reduced to normal barometric pressure, or sea level, these data show nearly uniform intensity for latitudes north of 34° in United States and south of 34° in Australasia. Between these latitudes the intensity drops sharply to a value about 87 percent as great as that in the temperate zones. As compared with northern North America, northern Europe has sensibly the same intensity of cosmic rays, while the data indicate that in temperate Australasia the intensity is 2 or 3 percent greater. These data are probably in error by about 1 percent. A comparison of the data taken in Peru and Mexico shows a much closer correlation of the intensity of the cosmic rays with the dip of the magnetic needle than with the geographic latitude. The differences in intensity thus seem to be due to the earth's magnetic field, which would seem to imply that the cosmic rays are electrical in character.

14. Diffraction of low-speed electrons by a tungsten single crystal. WAYNE T. SPROULL, *University of Wisconsin.*—The (1-1-2) and (1-0-0) planes of a tungsten crystal were bombarded at normal incidence with primary electrons and the intensity of the full-velocity secondary beams measured as a function of azimuth, co-latitude (θ), and primary voltage. A new magnetic deflection method of analyzing the secondaries permitted observations at co-latitudes down to zero. The crystal was outgassed 1550 hours at temperatures up to 1600°C at pressures of 10^{-7} mm of Hg or less. Beams fitting the usual theory were found for the (1-1-2) plane in the azimuth parallel to the diagonals of the lattice cubes, but in the azimuth (A) perpendicular at the cube diagonals strong sharp beams were found at every primary voltage tried, their positions accurately obeying the volume law $n\lambda = d/\sqrt{b} + 2d/\sqrt{b} \sin(30^\circ - \theta)$ after making the usual allowance for the work function W_a . Beams found in the (1-0-0) plane obeyed the usual theory, except that during growth and decay they also obeyed the volume law and not the surface law. Consistent values were obtained for W_a , the average being 4.82 volts. The effect of variation of angle of incidence was briefly studied. A possible explanation of the peculiar behavior of the beams in the A azimuth of the (1-1-2) plane is outlined.

15. **Intensity distribution in electron diffraction patterns of ZnO.** H. J. YEARIAN AND K. LARK-HOROVITZ, *Purdue University*.—A well-defined electron beam from a hot filament has been used in the range between 3.3 and 25 kv for the production of diffraction patterns of ZnO powder. Purest ZnO has been prepared directly on the slit using a zinc arc, or has been deposited chemically. The geometry of the diffraction pattern is identical with the corresponding x-ray pattern, giving $C_{\text{ZnO}}^{\text{th}}$, $a=3.22 \text{ \AA}$, $c/a=1.61$; there appear however also forbidden lines (fractional orders). The intensity distribution shows marked deviations from the intensity distribution of the x-ray patterns. It has been shown that these deviations are not due to pre-

hkl	10 $\bar{1}$ 0	0002	10 $\bar{1}$ 1	10 $\bar{1}$ 2	1120 . . .	11 $\bar{2}$ 4	1232
Elec. int.	St.	V.V.St.	V.St.	V.St.	St.	F	V.St.
X-ray int.	St.	Med.	St.	Med.	St.	F	F

ferred orientation, differences in structure due to methods of preparation, or coincidences with another form of ZnO. The theoretical explanation of the F curves thus obtained is discussed on the basis of additional surface reflection, dynamic reflection, and finally under the assumption that nuclear parameter is slightly greater than the electronic parameter. A partial explanation of the intensity distribution on this basis is possible.

16. **Deflection of a beam of HCl molecules by a non-homogeneous electric field.** EDWIN MCMILLAN, *Princeton University*.—It was found possible to use a film of ammonia frozen on to a polished metal surface by liquid air as a quantitative detector for a beam of HCl; this was done by putting a number of exposures on the target during each run to serve as intensity marks, and photographing and photometering the resulting deposits of NH_4Cl . The intensity distribution in a beam broadened by passage through a nonhomogeneous electric field was measured by this means, and found to agree with the theory. An attempt was made to resolve the deflected beam into components by the use of a mechanical velocity filter. This failed because of lack of intensity of the beam after filtration.

17. **A determination of e/m by means of photoelectrons excited by x-rays.** G. G. KRET-SCHMAR, *University of Chicago*.—A value of e/m has been obtained by a magnetic deflection method making use of x-ray photoelectrons and the magnetic spectrograph. Electrons were ejected from thin evaporated or sputtered films of gold, silver, copper and platinum by the x-radiation from a molybdenum target metal tube placed close to the film and working at an input of 1.5 kilowatts. The velocity of ejection of the photoelectrons was computed from the difference between the energies associated with Mo K radiation and the various absorption limits of the sputtered films. Relativity corrections were made since these velocities correspond to 8000 to 15,000 equivalent volts. The α_1 and α_2 components of the molybdenum $K\alpha$ line were clearly resolved since the magnetic field was kept very constant by the use of a potentiometer and continuous hand control. The weighted mean value of e/m_0 obtained from five plates is $1.7555 \pm 0.0026 \times 10^7 \text{ e.m.u. per gram}$. It is to be noted however, that the absolute accuracy of this result is dependent upon the values of x-ray wave-lengths from crystal measurements.

18. **Theory of the energy distribution of photoelectrons.** LEE A. DUBRIDGE, *Washington University, St. Louis, Mo.*—The success of Fowler's theory in predicting the form of photoelectric spectral distribution curves at various temperatures leads one to expect that similar methods would yield expressions for the energy distribution and voltage-current curves. Considering first only the energies normal to the surface (plane parallel electrodes) and using the Fermi statistics, an expression has been derived for the voltage-current curve which is identical with Fowler's equation for the total emission, except that the surface potential jump W_a is replaced by $(W_a + Ve)$ where V is the retarding potential. The theoretical curve is in good agreement with preliminary experimental results, and yields a method of determining the maximum emission energy at 0°K . At all higher temperatures the voltage-current curves should approach the axis asymptotically. This has an important bearing on the photoelectric determination of h . When the total energies of the emitted electrons are considered a more complex expression results, which can, however, be put in a form for comparison with experiment. The predicted curve is widely different from those usually observed experimentally, and experiments are under way to determine the cause of the discrepancy.

19. Energy distribution of secondary electrons from molybdenum. L. J. HAWORTH, *University of Wisconsin*.—A careful study has been made of the distribution in energy of secondary electrons emitted by a thoroughly outgassed Mo target when bombarded with a narrow, homogeneous beam of primary electrons. As observed by Farnsworth, Soller, and others, two groups of secondary electrons predominate; the usual large group of "full velocity" secondaries of energy equal to that of the primaries, and an equally large group of very slow secondaries of energy from zero to 15 volts. In addition to the general distribution several small groups of secondaries may be distinguished. These may be divided into two classes: (1) groups similar to those reported by Rudberg (P.R.S. 127, 111 (1930)) consisting of electrons of energies certain fixed amounts less than that of the primary electrons; (2) groups of electrons of fixed energy relative to the absolute scale, independent of the energy of the primary electrons. A study was also made of the number of "full velocity" secondaries as a function of primary energy. An attempt has been made to explain the results obtained on the basis of theory developed by Kronig, Penney, and others, relative to allowed energy levels for electrons in a metallic lattice.

20. Scattering of slow electrons by caesium ions. C. BOECKNER AND F. L. MOHLER, *Bureau of Standards, Washington, D.C.*—Measurements were made of the gradient and the temperature and concentration of the electrons in the positive column of a caesium vapor discharge. From such measurements the electron mobility and the effective cross section of the caesium atoms for electron scattering can be deduced. (T. J. Killian, *Phys. Rev.* 35, 1238 (1930).) It is found that the scattering cross section increases linearly with electron concentration, the increase being very rapid for low pressures. The variation at all caesium pressures can be explained by the assumption that scattering is due to the sum of the effects of the ions and neutral caesium atoms. The cross section of ions for the interception of slow electrons (0.3 volts) obtained by means of this assumption is very large, 80×10^{-14} cm². The cross section of the neutral atoms is 3.8×10^{-14} , a value in fair agreement with that obtained from more direct measurements. The large cross section of the ions can be explained by the ordinary electrostatic attraction between particles of opposite charge. A 0.3 volt electron, for example, whose original direction of motion passes 40A from an ion is deflected through 60° by the action of the electrostatic forces.

21. The scattering of lithium ions from a nickel surface. ANDREW LONGACRE, *Princeton University*.—The velocity and intensity of lithium ions scattered from a metal surface have been measured by allowing the ions scattered to pass through openings into a Faraday collector. The source (heated spodumene) and collimating apertures could be rotated around the target so that the latter could be bombarded from any arbitrary angle. The Faraday collector was supported rigidly in order to obtain satisfactory insulation and the angle of scattering varied by rotating the source and target together. With a homogeneous initial beam the ions are scattered in the general direction corresponding to the specular reflection of light. There is no evidence of a general scattering obeying a cosine law. In the immediate neighborhood of maximum intensity the scattering obeys a form of cosine law. By means of retarding potentials the energies of the scattered ions was measured and the scattered beam was found to have a more homogeneous distribution the greater the angle of scattering. The most probable energy, E , of the scattered ions varies with the angle of scattering, θ , and may be expressed by the following relation, $E = a\theta + b$, where a is a constant depending only upon the angle of incidence and b is a constant depending upon the incident energy as well as upon the angle of incidence.

22. The behavior of crystalline test bodies in streaming solutions. T. W. MOORE, *Purdue University*, (Introduced by K. Lark-Horovitz).—The change in shape of test bodies of rock salt in NaCl solutions of various concentrations and flowing with different velocities has been studied. In dilute solutions the influence of the solubility of the salt is prevalent. In more concentrated solutions the test body assumes the shape determined by the hydrodynamic forces exerted on the material by the streaming liquid. In saturated solutions the test body assumes a shape which is practically determined by the hydrodynamic forces only: hydrodynamic profile. The results are applied to the observations on the erosion of natural rock and technically used material.

23. The electrical properties of surface layers. K. LARK-HOROVITZ AND J. E. FERGUSON, *Purdue University*.—With a polonium electrode as a sounding device, the potential at the interface air-liquid has been investigated for pure water, electrolyte solutions and monomolecular layers of stearic and oleic acid spread on the surface of electrolytic solutions. It has been found that the surface of electrolyte solutions in pure water is not consisting of a pure water layer, but that ions are diffusing into the surface layers (behavior in HCl, NaOH, NaCl solutions). The monomolecular layers of stearic and oleic acid act like solid electrolytes, behaving for a change from acid to alkali similar to a hydrogen electrode on the acid side and similar to a sodium electrode on the alkaline side. The surface of pure water which has not been cleaned as for surface tension experiments appears to be covered with a film of organic substance acting like the fatty acid mentioned above. The phenomena observed with these layers present a striking analogy to the phenomena observed with glass, quartz, and paraffin films.

24. The cybotactic condition of ethyl ether in the region of the critical point. ROSS D. SPANGLER, *The State University of Iowa*.—X-ray diffraction curves of ethyl ether are taken at various temperatures, pressures, and specific volumes with special emphasis in the region of the critical point. With constant pressure and increasing temperature and specific volume, the diffraction curve changes from that typical of a liquid, with a pronounced peak, signifying cybotactic molecular grouping, to that typical of a polyatomic gas with no peak signifying randomly arranged molecules. The peak disappears approximately at the critical volume but not at the critical temperature. At intermediate temperatures and specific volumes, the curve is a composite of a gas and a liquid curve indicating that some of the molecules are in groups and others are randomly arranged. Within the present range of pressures, the type of curve obtained does not change with temperature if the specific volume is held constant. For example, no difference is found between curves taken at ten degrees above and below the critical temperature of 194.6°C. Beyond a certain specific volume, approximately the critical one, no indications of groups are found and the type of curve obtained is independent of temperature pressure, and specific volume within the ranges used.

25. On the process of liquefaction. G. W. STEWART, *University of Iowa*.—The paper at this meeting by Spangler calls attention to a necessary revision in current ideas concerning liquefaction. It has long been thought that liquefaction is dependent upon some type of aggregation of molecules. It is now seen that while well-defined aggregates are essential to liquefaction, yet they exist also under other conditions, for example at a higher temperature and less specific volume than the critical values. The process of liquefaction does not require an increase in the number of molecules per cm³ in the cybotactic groups. It may occur with the number of aggregated molecules either constant or decreasing and pressure and temperature decreasing. The extent of the groups depends most importantly upon the specific volume. Liquefaction depends by definition on the possible existence of a second fluid phase in equilibrium and not as directly upon aggregation as formerly supposed.

26. Diffuse scattering of x-rays from a complicated crystal. G. E. M. JAUNCEY AND PAUL EHRENFEST II, *Washington University, St. Louis*.—Jauncey has recently obtained a formula for the diffuse scattering of x-rays from a crystal consisting of different kinds of atoms and possessing a lattice of any kind. In order to test this formula we have measured the diffuse scattering of x-rays from calcite at various angles. We find that the *S* curve for calcite falls between the *S* curve for sodium fluoride and that for sylvine and close to the *S* curve for rocksalt. This is as it should be according to the theory. Another interesting point is that the intensity of the diffuse scattering from a crystal does not depend upon the perfection of the crystal as is the case for Bragg reflection—calcite being a nearly perfect crystal and rocksalt a very imperfect (or mosaic) crystal.

27. Diffuse scattering of x-rays from an NaF crystal at low temperatures. P. S. WILLIAMS AND G. E. M. JAUNCEY, *Washington University, St. Louis*.—Using the photographic method described by Jauncey and Harvey, we have obtained for each of several scattering angles the ratio of the intensity of x-rays diffusely scattered from a crystal of sodium fluoride at the temperature of dry ice in butyl alcohol (about -70°C in the apparatus used) to that of the rays

scattered from the same crystal at room temperature ($+22^{\circ}\text{C}$). The value of $(\sin \frac{1}{2}\phi)/\lambda$ was found for each angle of scattering. The ratios are as follows, the first of each pair of numbers being the value of $(\sin \frac{1}{2}\phi)/\lambda$: 0.14, 0.932; 0.27, 0.917; 0.41, 0.919; 0.54, 0.931; 0.67, 0.947; 0.80, 0.973; 0.93, 0.980. The experiment is being continued with the crystal cooled to the temperature of liquid air.

28. The relative intensities of the $L\alpha_1$ and $L\beta_2$ lines in the fluorescent x-ray spectrum of uranium. REGINALD J. STEPHENSON, *University of Chicago*. (Introduced by S. K. Allison.)—Radiation from a metal x-ray tube with a molybdenum target fell on a secondary radiator of uranium and excited its fluorescent spectrum. The Mo K lines lie between the L_{II} and L_{III} absorption limits of uranium, hence the lines from the L_{III} limit will be excited strongly while those from L_I and L_{II} are excited comparatively weakly by the general radiation of the primary x-rays. A source of constant high voltage was used and the tube run at constant voltage and current. A single crystal ionization spectrometer served to analyze the radiation emitted by the uranium. In order to compare the fluorescent intensities with those observed in primary x-rays, it was necessary to measure the absorption coefficients of uranium for its L -series lines. The following results were obtained:

Line	Wave-length	Atomic absorption coef.
$L\gamma_1$	0.6163Å	2.8×10^{-20}
$L\beta_3$	0.7088	4.3 "
$L\beta_2$	0.7531	2.2 "
$L\alpha_1$	0.9087	2.8 "

After making all necessary corrections it was found that the relative intensity of the lines $L\alpha_1$ and $L\beta_2$ from the L_{III} level was the same in the fluorescent spectrum as in the primary spectrum observed by Allison (Phys. Rev. 32, 1 (1928)).

29. The dynamic reflection of x-rays from ZnS. I. G. GEIB AND K. LARK-HOROVITZ, *Purdue University*.—It has been suggested by Ewald (Zeits. f. Krist. 65, 251 (1927)) that for absorbing atoms the intensity distribution of an x-ray pattern depends on the direction of the x-ray beam relative to the crystal. ZnS crystals cut normally to the trigonal axis give plane parallel plates, one of which exhibits the 111, the other the $\bar{1}\bar{1}\bar{1}$ plane as has been shown directly by Lark-Horovitz in adsorption experiments with radioactive vapors (Proc. Vienna Acad. 1925). Using two such plates a Seeman slit spectrograph has been constructed with the $+111$ (Zn) and $\bar{1}\bar{1}\bar{1}$ (S) faces adjusted accurately in one plane to reflect gold, tungsten and tungsten-tantalum L radiation. These radiations contain lines on both sides of the Zn absorption limit and should therefore exhibit the effect predicted by theory. The photographic plate shows the L spectrum reflected simultaneously but with different intensity distributions from the Zn and S surfaces, due to absorption in the Zn atoms. The ratios (averages) of reflecting powers are:

Wave-length	1298.8	1285.0	1279.2	1273.8	1259.9	1242.0 x.u.
R_S (first order)						
Ratio						
R_{Zn}	1.00	1.00	1.42	1.38	1.22	1.12
R_{Zn} (third order)						
Ratio						
R_S	1.00	1.00	2.13	1.68		1.36

(in good agreement with the results of Coster (Zeits. f. Physik 63, 345 (1930)).

30. A direct comparison of photographic and ionization methods of measuring x-ray intensities. ELMER DERSHEM, *University of Chicago*.—This investigation was undertaken to determine the relative precision which might practically be obtained by the photographic and ionization methods. The Mo $K\alpha_1$ line was isolated by crystal reflection and the ratio by which the intensity was reduced by passage through aluminum filters was measured by both methods. The photographic density determinations were made with the use of the photoelectric photometer previously described (R.S.I. 3, 43 (1932)) and the ionization intensity measurements were made with an argon filled ionization chamber and Lindemann electrometer. The results show an average probable error for a single observation of 0.52 percent in the case of ionization measure-

ments and of 2.1 percent when the photographic method is used. However, the ionization method is more subject to errors which may not be reduced by repeated measurements. The results show that the errors introduced by assuming the exact validity of the reciprocity law of blackening of a photographic plate by x-rays is not greater than one percent for intensity ratios up to twenty to one, if one assumes the ionization measurements to be correct.

31. Absorption coefficients in optically excited mercury vapor. M. L. POOL AND S. J. SIMMONS, *Ohio State University*.—Mercury vapor at room temperature with various pressures of admixed purified nitrogen was optically excited by the resonance radiation from three quartz mercury arcs. From a fourth arc, magnetically deflected and water cooled, the radiation 4047, 2967 and 2752, all terminating on the 2^3P_0 state, was passed through the resonance tube of excited mercury vapor, and the absorption for each wave-length for various lengths of absorbing vapor was measured photometrically. It was found that the intensity of 2752 decreased nearly exponentially giving a linear absorption coefficient that varied slightly with the nitrogen pressure. However, for the lines 4047 and 2967 it was found that the simple exponential absorption law was not obeyed but that the fractional decrease in intensity per unit length of path decreased rapidly as the total length of the absorbing vapor increased. This peculiar decrease in intensity was further dependent upon the pressure of the admixed nitrogen. No other lines showed measurable absorption. The behavior of the 4047 and 2967 absorption for any given pressure may be adequately described by the sum of two exponentials with two quite different linear absorption coefficients.

32. The Zeeman effect of the spectra of Sb II and Sb III. J. B. GREEN AND R. A. LORING, *Ohio State University*.—The spectra of SbII and SbIII have been investigated at field strengths of about 40000 gauss. Zeeman patterns of the lines of SbII show general agreement with Lang's (in print) classifications in the spectra, and quite general disagreement with D'Lavale's classifications (Proc. Roy. Soc. June, 1931). The spectrum of SbIII shows that the two principle valence electrons have practically $j-j$ coupling, so that, except for a few cases, the assignment of l -values to the levels is not possible. Lang's classification of the s^2p^2 configuration is in good agreement with Goudsmit's theory. The Zeeman patterns of SbIII are also in good agreement with Lang's classification (Phys. Rev. 45, 435 (1930)) of this spectrum. Several of the lines of this spectrum, as well as of SbII show broadening and extra components due to the hyperfine structure. The levels of the s^2ps configuration of Sb II and the s^2s , s^2p and sp^2 of Sb III show this effect most strongly, as is to be expected from the theory.

33. The two vector problem in Pb V and Bi VI. A. T. GOBLE AND J. E. MACK, *University of Wisconsin*.—The configurations $5d^{10}$, $5d^96s$, and $5d^96p$ of Pb V and Bi VI have been identified (except d^9p , $J=0$) from Arvidsson's wave-length list (Ann. d. Physik 12, 787 (1932)). The coupling exhibited is the most nearly pure jj of any known in optical spectra. The d^9p levels lie in four separate groups, and the visually estimated intensities agree roughly with the expectations. The d^9s intervals, like similar intervals in the spectra of other very heavy elements, show some departure from the exact theoretical formulas (Houston, Laporte, Inglis) which can hardly be attributed to neighboring configurations. The exact formulas of Johnson (Phys. Rev. 38, 1628 (1931)) have been applied to d^9p after transformation of the energy matrix to the jj system of representation to give the two coupling coefficients and five electrostatic parameters. These parameters, reapplied in the formulas, give roots in fair agreement with the observed terms, but in view of the inexactness of the d^9s check the approximate success in expressing the ten available intervals in terms of the seven parameters may be considered a significant check upon the theory. The line $d^9_{3/2s} - d^9_{3/2p_{1/2}}$ of Bi VI shows partially resolved hyperfine structure.

34. Dispersion of the Kerr effect in the near infrared. L. R. INGERSOLL AND W. R. WINCH, *University of Wisconsin*.—Measurements of the Kerr electro-optic effect have been made on carbon bisulphide, nitrobenzene, halowax, and a number of other liquids over a spectral region extending from the sodium lines to about 2μ , or some four times the wave-length range investigated by other observers. The method is a spectro-bolometric one, involving effectively the measurement of the minor axis of the ellipse into which the plane polarized light is converted by the electrostatic stress in the Kerr cell. The high potential of 2000 to 40,000

volts, or more, is furnished by a kenotron and condenser equipment. The Havelock formula $B = C(n^2 - 1)^2 / \lambda n$ for the dispersion of the Kerr double refraction fits the measured dispersion fairly well for a short region beyond the visible spectrum—to $\lambda = 0.9\mu$ in some cases—but the discrepancy increases for longer wave-lengths.

35. The theory of refraction shooting. MORRIS MUSKAT, *Gulf Research Laboratory, Pittsburgh, Pa.*—Considerations of geometrical optics indicate that the limiting refracted rays travelling along the interface between two homogeneous elastic media should carry inappreciable amounts of energy. Nevertheless, the "first arrival" waves in refraction shooting processes which give linear time distance curves, can only be interpreted geometrically on assuming that they are due to such limiting rays travelling along the interface with the speed of the high velocity medium. A wave theory analysis of the problem resolves the difficulty. By an extension of Jeffrey's treatment for the case of fluid media to that of general elastic media it was found that four kinds of "refracted" waves of the above type will be produced upon the incidence at a plane interface of either a longitudinal or transverse spherical wave pulse. Two of the waves will be recorded as longitudinal waves and the other two as transverse. One of each pair effectively travels along the interface with the longitudinal velocity of the refracting medium and the other two travel with the transverse velocity. Their amplitudes vary inversely as the square of the distance from the source and correspond to vertical displacements of the same order as those due to the directly reflected waves.

36. Light intensities at different depths in water as determined by means of a quartz spectrograph. HENRY A. ERIKSON, *University of Minnesota.*—A quartz prism dispersing system in a specially designed housing was used for evaluating the intensities of different wave-lengths in the visible spectrum at different depths in water on Gunflint Lake on the northern border of Minnesota. The spectrum was photographed at different points down to 70 ft. and from these the intensities of the different wave-lengths were evaluated from characteristic curves obtained from standard exposures using wire screens. It was found that the variation of the intensity with depth was exponential in the case of some wave-lengths but not in the case of all. From the results obtained absorption constants were obtained for the different wave-lengths.

37. A twenty-one foot grazing incidence vacuum spectrograph. P. GERALD KRUGER AND F. S. COOPER, *University of Illinois.*—A grazing incidence vacuum spectrograph, for a twenty one foot focal length grating, ruled 30,000 lines per inch, has been set up and adjusted. The angle of incidence is 79 degrees. This gives the following dispersions at various wave-lengths between 0 and 500A.

λ	Dispersion
100A	0.332A per mm
150	0.360
200	0.387
300	0.435
400	0.477
500	0.516

Copper electrodes were used in a "hot spark" for the light source during adjustment. The power was supplied at 100,000 volts d.c., by a four kenotron bridge set. The lines obtained were very sharp so that it was possible to measure their wave-lengths more accurately than has been done previously in this region.

38. A high-pressure spectrometer. FRANKLIN E. POINDEXTER AND LOUIS E. JAMES, *St. Louis University.*—A spectrometer has been constructed for the study of the change in the refractive index of liquids with pressure. The pressure on the liquid prism is measured directly by means of a plunger and lever. The index of refraction of water for each of the Hg lines 4359A, 5461A, and 5790A has been obtained at a series of pressures from 1 to 1440 atmospheres. We find that the Lorentz-Lorentz relation, $(n^2 - 1)/(n^2 + 2) \cdot 1/\rho = K$, where n = index of refraction, ρ = density, and K = constant does not hold; i.e., the K 's at the lowest and highest pressures are:

	K 1 atmosphere	K 1440 atmospheres
4359A	0.2106	0.2092
5461A	0.2074	0.2070
5790A	0.2067	0.2062

39. The influence of pressure on the formation of the latent photographic image, particularly its effect on reversal in the region of solarization. KARL A. MARING, S.J., *St. Louis University*. (Introduced by F. E. Poindexter.)—Photographic materials were exposed, so that a central region was under pressure and a rim area without pressure. The pressure area showed a reduction in density over the rim area depending, in amount, on the exposure and the pressure. This reduction in density fell off with increasing exposure, gained with increasing pressure. However, this reduction of the density is not a linear factor of either exposure or pressure. In the region of solarization, a marked acceleration of reversal is noted in the pressure region. This pressure effect seems to call attention again to the photomechanical disintegration theory of the latent image formation.

40. Direct measurement of the gravitational effect of the moon. KENNETH HARTLEY, *Hartley Gravity Balance Corporation, Houston, Tex.*—The sensitivity of the gravity balance described in the March number of Physics is such that a correction must be made for the effect of the attraction of the moon. This lunar effect has been measured by hourly readings over one complete cycle and agrees, within the observational error, with the effect calculated for the vertical component of the pull of the moon without any compensation for the centrifugal effect of the earth's motion around the center of gravity of the system. The effect has a period of 24.8 hours and not 12.4 hours as the tides, there is no trace of the twelve-hour period. Values of gravity plotted against time follow accurately a sine curve which shows a small time lag as compared with the theoretical curve. This does not seem to be accidental but has not been explained.

41. Thermal expansion of antimony. PETER HIDNERT AND H. S. KRIDER, *Bureau of Standards, Washington, D. C.*—Measurements were made on the linear thermal expansion of three samples of cast antimony between room temperature and 560°C and the data were correlated with available results obtained by previous investigators to 300°C. The minimum and maximum values for the coefficients of expansion of the three samples are given in the following table.

Temperature range	Average coefficients of expansion per degree centigrade
20 to 60°C	8.5 to 10.8×10^{-6}
20 to 100	8.4 to 11.0
20 to 200	8.7 to 11.3
20 to 300	9.2 to 11.4
20 to 400	9.2 to 11.5
20 to 500	9.5 to 11.6
20 to 550	9.7 to 11.6

A manuscript giving additional details and indicating the cause of the differences obtained in the expansion of different samples of antimony, is being prepared for publication in the Bureau of Standards Journal of Research.

42. Refractory materials for melting pure metals. H. B. WAHLIN, O. D. FRITSCHÉ AND J. F. OESTERLE, *University of Wisconsin*.—A study of various refractories has shown that porcelain as well as magnesia crucibles volatilize and reduce sufficiently, when heated in a vacuum, to contaminate pure metals contained in them. Crucibles of pure, fused thorium oxide are the most satisfactory and will withstand heating in a vacuum for long periods of time. Special shapes of crucibles may be readily prepared by using moulds made of a fusible alloy which is melted off before firing. The crucibles should be fired to a temperature of 1800°C, care being taken to prevent the formation of thorium carbide which, due to interaction with the moisture of the air, will cause the crucibles to break up.

43. The Joule-Thomson effect in helium. J. R. ROEBUCK AND HAROLD OSTERBERG, *University of Wisconsin*.—Isenthalpic curves have been measured from -190° to $+300^{\circ}\text{C}$. They are straight lines over the 200 atm. range except at the lowest temperature. Their slope, μ is negative over the whole range. At -190°C μ is increasing sharply with falling temperature moving toward the known-positive value at liquid hydrogen temperatures. From -50 to 150° μ decreases slowly and linearly. It goes through a minimum at about 200° and increases slowly thereafter. The free expansion coefficient, η calculated from these data, is negative and decreasing with rising temperature, between -50 and 200°C . This trend of η makes very improbable any prediction that helium will become a perfect gas at any temperature. With falling temperature η apparently becomes positive. These facts are difficult to reconcile with the older conception of the van der Waals forces but they may be explained qualitatively, at least, by restricting the attractive and repulsive forces to a very small fraction of the mean free path. The data are being used to calculate the Kelvin temperature of the ice point from the helium thermometer work.

44. Oscillations produced by beads of corona discharges. J. TYKOCINSKI TYKOCINER, *University of Illinois*.—The investigation of oscillations due to single bead discharges (Phys. Rev. 39, 189 (1932) Abs. 52) has been extended to cases when a number N of beads act simultaneously. If the discharge consists of beads equal in size and brightness and distributed at regular distances along the negatively charged wire, the frequency is N times smaller than that obtained for a single bead, provided that the pressure, P , and the total corona current, I , remain constant. For the frequency f the relation was found $f = cIM/N$ where M is the number indicating the harmonic and c is a constant. For beads differing in size and distributed irregularly along the wire, oscillations of a complex character are obtained which contain as many fundamental frequencies as there are beads on the wire. The linear relation between f and I ceases when the current through a single bead reaches a definite value I_p . With further increase of current the rate of frequency increase diminishes and, from a critical value I_c on, the frequency decreases until, at a current $2I_c$, oscillations stop altogether. These relations were investigated for pressures within 5–60 mm Hg. The appearance of the bead gradually changes with the current, but at the characteristic point when oscillations stop sudden changes in the appearance can be observed.

45. Some experiments on electrets. O. J. JOHNSON AND P. H. CARR, *Iowa State College, Ames, Iowa*.—Electrets have been made after the manner of Eguchi from a mixture of Car-nauba wax and rosin in electric fields as small as a few hundred volts per centimeter. A series of experiments was made in which the electric field was applied to the wax mixture at different temperatures and allowed to remain until the wax cooled to room temperature. Another series was made in which the electric field was applied when the wax was molten but was removed from each successive sample when it had cooled to a temperature lower than that at which the field was removed from the preceding sample. The strength of the electret resulting from each sample was measured. Results indicate that the molecules of the wax mixture become fixed in their polarized positions, so that random reorientation is negligible, at a temperature definitely lower than the temperature at which solidification takes place. Electrets have also been made from molten sulphur, but their properties have not been studied.

46. The measurement of the piezoelectric deformations of quartz and tourmaline plates by means of a modified optical lever. GEORGE A. FINK, *Iowa State College*. (Introduced by G. W. Fox).—The observation of the piezoelectric deformation of quartz or tourmaline plates used for radio frequency oscillators requires a more sensitive measuring scheme than that afforded by direct optical interference or the ordinary type of optical lever. With a potential difference of 500 volts between the crystal electrodes, a deformation of only 10\AA is to be expected. To amplify such small movements, a lever has been built having an amplification ratio of 1866, such that, by interferential observation of a mirror on the long end, a movement of the short end of only 0.15\AA can be detected. Values of the piezoelectric constants for quartz and tourmaline as determined from the inverse effect are in fair agreement with those found by previous

observers from the direct effect. The structure of the quartz crystals was found to be very non-uniform; various crystals and different parts of the same crystal plate giving results differing by more than the experimental error.

47. Modes of vibration of piezoelectric crystals. N. H. WILLIAMS, *University of Michigan*.

—(a) A crystal is made to oscillate by subjecting it to the action of an air wave produced at a considerable distance from the crystal by a jet of air escaping from a small tube. The piezoelectric charge developed on the surface of the crystal as a result of the oscillation is mapped out by means of a tuned amplifier, and the vibration is analyzed into a fundamental and many overtones. The crystals are long in one dimension and the vibrations are along the length. Under these conditions the overtones are approximate harmonics. (b) Exciting the crystal electrically by means of two tubes and especially designed electrodes, any harmonic up to the tenth can be produced. The crystal usually has only one mode of vibration for each pair of electrodes.

48. A nonthermionic amplifier tube. HERBERT J. REICH, *University of Illinois*.—Grid control of a glow discharge is obtained in this tube by so designing and placing the grid that it is out of the direct path of the discharge between anode and cathode. Variation of the grid potential modifies the electric field in such a manner as to control the number of electrons which move through a distance sufficient to produce ionization. By maintaining the static grid potential at such a value that the number of positive ions which strike the grid is equal to or slightly in excess of the number of electrons, the grid current may be limited to less than ten microamperes. The discharge is at all times under control of the grid and may be completely extinguished by it. The gas pressure is found to be very important in obtaining satisfactory operation. The relation of structural parameters to tube constants is being studied, but little attempt has yet been made to improve the amplification characteristics. A conservative average for tubes made during the preliminary investigation gives values of 3 for amplification factor and 100 micromhos for mutual conductance. With proper design and choice of gas pressure, little or no ballast resistance is required.

49. The use of vacuum tube electrometers for measuring the potentials of high-resistance cells. ROBERT E. BURROUGHS AND J. E. FERGUSON, *Purdue University*.—By using the relation between the grid potential and the plate current of a thermionic vacuum tube one is able to construct an electrometer of high sensitivity. Such electrometers have been used in the measurements of electromotive forces of cells whose internal resistances are very high. In these measurements the vacuum tube is operated with its grid at floating potential so the current drawn from the cell will be very small. The cell potential is then measured by applying a compensating potential in series with the cell in the grid circuit of the electrometer. Using a null method, when this compensating potential is adjusted so as to give zero indication on the electrometer it is a measure of the electromotive force of the cell. This method gives satisfactory results for cells whose resistances are below 10^{11} ohms. For resistances higher than this a difficulty is encountered. The current to the grid of the vacuum tube is so small that the time required to change the grid potential, sufficiently to secure a balance with precision, is of such length that lack of circuit stability renders the method useless.

50. Improved burner for singing flames. Overtones in vibrating strings. JOHN J. HOPFIELD, *Basic Science Division, A Century of Progress, Chicago*. (Introduced by H. G. Gale).—By using a suitable double burner with the flames at different heights instead of a single flame, the flames vibrate to the resonance tones of a pipe even when the larger flame was several inches long. It was found that the smaller flame starts the singing and the larger one responds. (Demonstration.)

By using a modified 120 cycle tuning fork operated on 60 cycle current, one can produce not only the 120 cycle fundamental in a Melde string but also the note of frequency 60 and many integral multiples of these tones. These are made evident in the point symmetrical form of the standing waves in the string, and also they can be separately sounded in a tube fitted with a sliding plunger and held near a disc attached to the side of the string. (Demonstration.)

51. **Atomic wave functions.** F. W. BROWN, *University of Illinois*. (Introduced by J. H. Bartlett, Jr.) The writer has found a Hartree field for normal F. The use of this field in conjunction with the one already obtained by Hartree for F^- enables one to test the wave equation of the "hole," given by Heisenberg and Dirac (Heisenberg, *Ann. d. Physik* 10, 888 (1931); Dirac, *Ann. de L'Inst. H. Poincaré*, Vol. 1 Pt. 4, 357). The equation was found to give the wrong sign for the electron affinity of F, the reason being that in its derivation no account is taken of the difference between the electron functions of F and those of F^- . As a check on the accuracy of the work, a self-consistent field for Ne^+ is being obtained. It is also intended to represent these wave functions of the Hartree field by the analytic functions devised by Slater (*Phys. Rev.* 42, 33 (1932)).

52. **On Compton's latitude effect of cosmic radiation.** G. LEMAITRE AND M. S. VALARTA, *University of Louvain and Massachusetts Institute of Technology*. By considering the influence of the earth's magnetic field on the motion of charged particles (electrons, protons, etc.) coming to the earth from all directions in space it is shown that the experimental variation of cosmic-ray intensity with magnetic latitude, as found by Compton and his collaborators, is fully accounted for. The cosmic radiation must contain charged particles of energy between 0.5×10^{10} and 3×10^{10} electron-volts for electrons or protons; 0.7 to 5.5×10^{10} electron-volts for alpha-particles. The experimental curve may be represented by a suitable mixture of rays of these energies, but it is not at all excluded that a part of the radiation may consist of photons or neutrons. For predominantly negative particles there must be in the region of rapidly varying intensity a predominant eastward direction, and conversely for positive rays. Because of the fact that in regions near the magnetic equator there is a predominance of rays coming nearly horizontally, the absorption by the atmosphere may be increased. Finally the fact that Compton's result definitely shows that the cosmic rays contain charged particles gives some support to the theory of super-radioactive origin of these rays advanced by one of the present authors.

53. **Methods of acquirement of cosmic-ray energies.** W. F. G. SWANN, *Bartol Research Foundation of the Franklin Institute*. Consider the growth of a sunspot of diameter ten times that of the earth. The line integral of the electric field around a circuit encircling the magnetic field of this spot is $[\pi H(6.5 \times 10^9)]^2 / (T \times 10^8)$ where H is the magnetic field of the spot, and T the time in which it is created. This line integral amounts to 10^{10} volts if the field of the spot is 2000 gauss and is created in about three days. The details of the electronic motion on the field are complicated; but, it appears that acquirement of high energy by such means should be possible, particularly in the case of larger spots which may exist in stars other than our sun. It is probable that the mean free path is sufficiently long in the regions concerned to ensure that the rate of acquirement of energy would be less than the rate of loss by collision. In connection with the foregoing view, attention is called to the increase of auroral activity during sun spot activity. Another suggestion arises from possible electrostatic fields of the stars. A charge on the sun such as would give a field of no more than one volt per centimeter at the surface would correspond to a potential of 5×10^{10} volts. In the case of a galaxy of stars, the potential at the surface of the galaxy would be of the order $Na^2 X/R$, where N is the number of stars in the galaxy, a the radius of a star, R the radius of the galaxy, and X the surface field of a star. The value of X necessary to result in any assigned value of the potential at the surface of the galaxy decreases with increase of R since N increases more rapidly than R .

54. **The neutron, the element neutron, and a nuclear exclusion principle.** WILLIAM D. HARKINS, *University of Chicago*. The neutron, discovered in the radiations from beryllium, by M. and Mme. Joliot and particularly by Chadwick, represents an element of atomic number zero, which may be called *neutron*. The composition of the beryllium nucleus was indicated by the writer in 1915 to be two alpha-particles united by a condensed nuclear hydrogen atom, or neutron. The general existence of neutrons and their properties were predicted in 1920 by Harkins (April 12) and by Rutherford (June 3). It was also shown by the writer that a second or *isotopic* number (I) is as necessary as the atomic number (Z) to specify an atomic species. The formula of any nucleus is $(p_e)_Z(pe)_I$, in which (pe) represents a neutron (n) (*Physical Review* 19, 139 and 142 (1922)), and (p_e) is the nucleus of hydrogen 2, which is the half-alpha-particle. This

formula may be written either as $(np)Zn_I$ or $(a/2)Zn_I$ or its equivalent $a_{\alpha/2}n_{\alpha/2}(I/2)$ which indicates that the neutrons in the half-alpha-particles are almost always paired, and the extra neutrons (n) are usually paired. Now $Z+I=N$ is the total number of neutrons in the nucleus, and Z the number of extra protons, that is those not in neutrons. The following relations hold: (1) Not more than one proton can combine with a neutron. (2) About 125 of every 126 atoms in the earth's crust contain an even number of neutrons, so the neutrons seem to be paired. (3) The general stability of atomic nuclei is determined by Z and by either N/P or N/Z , in which $P=N+Z$. (4) The hydrogen 2 or half-alpha-particles are paired in about 95 percent of all atoms, and thus exist as alpha-particles. (5) Less than one atom in ten thousand contains an odd half-alpha-particle with no extra neutrons. (6) If both an odd half-alpha-particle and extra neutrons are present, the total number of extra neutrons is always odd, and no atoms exist (except unstable radioactive species whose half lives are smaller than 8 days) in which this number is even. Thus the total number of neutrons in such an atom must be even, so the neutrons are paired. However, a few of these may not have paired spins.

55. A demountable metal x-ray tube. K. LARK-HOROVITZ AND E. M. MILLER, *Purdue University*. With Pyrex and sillimanite tubes of a special form as insulators and chromium plated brass for anode and cathode parts, an x-ray tube has been constructed, free from any wax joints or seals, which will stand 70 m.a. at 75 kv continuous operation. With these tubes, by using a line focus, it was possible to resolve in a photograph taken in 120th of a second the $K\alpha$ doublet of copper reflected from a calcite crystal with a Seeman wedge (distance plate-crystal 55 cm). The exposures have been timed by using a falling slit between spectrograph and plate (d.c.). Imprints have been made on a falling plate which show that the spectra have been registered in less than 1/200 of a second (a.c.). The $K\alpha$ doublet of copper has been photographed at a distance of three meters between spectrograph and plate in 60 seconds. Diffraction patterns from powders can be obtained in a few seconds.

AUTHOR INDEX TO ABSTRACTS OF CHICAGO MEETING

- Barton, Henry A., D. W. Mueller and L. C. Van Atta—No. 3
 Boeckner, C. and F. L. Mohler—No. 20
 Brown, F. W.—No. 51
 Burroughs, Robert E. and J. E. Ferguson—No. 49

 Carr, P. H.—See Johnson
 Compton, Arthur H.—No. 13
 Cooper, F. S.—see Kruger

 Dempster, A. J.—No. 4
 Dershem, Elmer—No. 30
 DuBridge, Lee A.—No. 18

 Ehrenfest II, Paul—see Jauncey
 Erikson, Henry A.—No. 36

 Ferguson, J. E.—see Burroughs
 ——— see Lark-Horovitz
 Fink, George A.—No. 46
 Fritzsche, O. D.—see Wahlin

 Geib, I. G. and K. Lark-Horovitz—No. 29
 Goble, A. T. and J. E. Mack—No. 33
 Green, J. B. and R. A. Loring—No. 32

 Harkins, William D.—No. 54
 Hartley, Kenneth—No. 40
 Havens, G. G.—No. 1
 Haworth, L. J.—No. 19
 Hidnert, Peter and H. S. Krider—No. 41
 Hopfield, John J.—Nos. 12, 50

 Ingersoll, L. R. and W. R. Winch—No. 34

 James, Louis E.—see Poindexter
 Jauncey, G. E. M.—see Williams, P. S.
 ——— and Paul Ehrenfest II—No. 26
 Johnson, O. J. and P. H. Carr—No. 45
 Jordahl, O. M.—No. 2

 Kretschmar, G. G.—No. 17
 Krider, H. S.—see Hidnert
 Kruger, P. Gerald and F. S. Cooper—No. 37

 Lark-Horovitz, K.—see Geib
 ——— see Yearian
 ——— and J. E. Ferguson—No. 23
 ——— and E. M. Miller—No. 55

 Lemaitre, G. and M. S. Vallarta—No. 52
 Longacre, Andrew—No. 21
 Loring, R. A.—see Green

 McMillan, Edwin—No. 16
 McPherson, A. I.—No. 9
 Mack, J. E.—see Goble
 Maring, Karl A.—No. 39
 Miller, E. M.—see Lark-Horovitz
 Mohler, F. L.—see Boeckner
 Moore, T. W.—No. 22
 Mueller, D. W.—see Barton
 ——— see Smyth
 Muskat, Morris—No. 35

 Oesterle, J. F.—see Wahlin
 Osterberg, Harold—see Roebuck

 Poindexter, Franklin E. and Louis E. James—No. 38
 Pool, M. L. and S. J. Simmons—No. 31

 Reich, Herbert J.—No. 48
 Roebuck, J. R. and Harold Osterberg—No. 43

 Shaw, A. E.—No. 5
 Simmons, S. J.—see Pool
 Smyth, H. D. and D. W. Mueller—No. 7
 Spangler, Ross D.—No. 24
 Sproull, Wayne T.—No. 14
 Stephenson, Reginald J.—No. 28
 Stewart, G. W.—No. 25
 Swann, W. F. G.—No. 53

 Tykociner, J. Tykocinski—No. 44

 Vallarta, M. S.—see Lemaitre
 Van Atta, L. C.—see Barton
 Verwiebe, F. L.—No. 8

 Wahlin, H. B., O. D. Fritzsche and J. F. Oesterle—No. 42
 Western, Forrest and Arthur Ruark—Nos. 10, 11
 Wetzel, W. W.—No. 6
 Williams, N. H.—No. 47
 Williams, P. S. and G. E. M. Jauncey—No. 27
 Winch, W. R.—see Ingersoll

 Yearian, H. J. and K. Lark-Horovitz—No. 15

AUTHOR INDEX TO VOLUME 42

References with (A) are to abstracts of papers presented at meetings of the Physical Society and references with (L) are to Letters to the Editor.

- Albertson, Walter. Note on the term system of Ir I—443(L)
- Allen, Mildred. Effect of tension on the electrical resistance of single bismuth crystals—848
- Allen, P. K. (see Bennett, R. D.)—446(L)
- Allis, W. P. (see Morse, Phillip M.)—588(A)
- Almy, G. M. and C. D. Hause. Spectrum of potassium hydride—242
- Andrew, Victor J. Relative intensities of the $L\alpha_1$, β_1 , β_2 and γ_1 lines in tantalum, tungsten, iridium, and platinum—591
- Ashley, Muriel F. and F. A. Jenkins. Possibility of the existence of the chlorine isotope Cl^{32} —438(L)
- Bainbridge, Kenneth T. Isotopic weight of H^2 —1
- Barker, E. F. (see Choi, Kyu Nam)—777
- (see Hardy, J. D.)—279
- Barnes, LeRoy L. Emission of positive ions from heated metals—487
- Temperature variation of the positive ion emission from molybdenum—492
- Barnett, S. J. Gyromagnetic ratios for nickel and cobalt—147(L)
- Bartlett, J. H., Jr. Structure of atomic nuclei. II—145(L)
- Errata: Structure of atomic nuclei—737
- Barton, Henry A., D. W. Mueller and L. C. Van Atta. Compact high potential electrostatic generator—901(A)
- Batho, Harold F. Neutralization and ionization of high-velocity ions of neon, argon and krypton by collision with similar atoms—753
- Bear, Richard S. (see Spedding, Frank H.)—58, 76
- Beck, Fred J., Jr. and L. W. McKeehan. Monocrystal Barkhausen effects in rotating fields—714
- Benade, J. M. Self-recording cosmic-ray electrometer and depth-ionization curve—290
- Bennett, Ralph D. (see Stearns, J. C.)—317(L)
- J. L. Dunham, E. H. Bramhall, and P. K. Allen. Intensity of cosmic-ray ionization in Western North America—446(L)
- Bhagavantam, S. Raman effect in gases: CO and NO—437(L)
- Birge, Raymond T. Value of e/m —736(L)
- Bitter, Francis. Some properties of homogeneously distorted cubic ferromagnetic lattices—697
- Tropism of crystals—731(L)
- Boeckner, C. and F. L. Mohler. Scattering of slow electrons by caesium ions—906(A)
- Boeker, G. F. (see Wills, A. P.)—687
- Bourgin, D. G. Velocity of sound in an absorptive gas—721
- Bozorth, Richard M. Theory of the ferromagnetic anisotropy of single crystals—882
- Bramhall, E. H. (see Bennett, R. D.)—446(L)
- Brasefield, Charles J. Ionization of helium, neon and argon under impact of their own atoms and positive ions—11
- Breazeale, William M. (see Slack, Francis G.)—305
- Breit, G. Isotope displacement in hyperfine structure—348
- Brewer, A. Keith and R. R. Miller. Positive ion current at the cathode in the glow discharge—786
- Bridgman, P. W. Effect of homogeneous mechanical stress on the electrical resistance of crystals—858
- Effect of pressure on the electrical resistance of fifteen metals down to liquid oxygen temperatures—587(A)
- Brown, F. W. Atomic wave functions—914(A)
- Brown, Weldon G. Absorption spectrum of iodine bromide—355
- Broxon, James W. Cosmic-ray ionization as a function of pressure, temperature, and dimensions of the ionization chamber—321
- Burroughs, Robert E. and J. E. Ferguson. Use of vacuum tube electrometers for measuring the potentials of high-resistance cells—913(A)
- Calbick, C. J. (see Davisson, C. J.)—580(L)
- Caldwell, S. Differential analyzer solution for the wave functions of the K -shell—589(A)
- Carr, P. H. (see Johnson, O. J.)—912(A)
- Child, C. D. Luminosity of sodium flames—146(L)
- Choi, Kyu Nam and E. F. Barker. Infrared absorption spectrum of hydrogen cyanide—777
- Chylinski, S. Magnetic spectra of secondary electrons from silver—393
- On the scattering of hard x-rays by solids—153
- Colby, M. Y. and Sidon Harris. X-ray reflection from a quartz piezoelectric oscillator in a Bragg spectrograph—733(L)
- Collins, George (see Wood, R. W.)—386

- Compton, Arthur H. Sea level intensity of cosmic rays in certain localities from 46° south to 68° north latitude—904(A)
- Compton, K. T. and E. S. Lamar. Momentum transfer to cathode surfaces by impacting positive ions in a helium arc—588(A)
- Coolidge, Albert Sprague. Quantum mechanics treatment of the water molecule—189
- Cooper, F. S. (see Kruger, P. Gerald)—910(A)
- Cork, J. M. Laue patterns from thick crystals at rest and oscillating piezoelectrically—749
— (see Witmer, R. B.)—743
- Davisson, C. J. and C. J. Calbick. Electron lenses—580(L)
- Dempster, A. J. Production of high-velocity protons by repeated accelerations—901(A)
- Dennison, D. M. (see Hardy, J. D.)—279
- Dershew, Elmer. Direct comparison of photographic and ionization methods of measuring x-ray intensities—908(A)
- Ditchburn, R. W. Emission probability for a colliding atom—314(L)
- DuBridge, Lee A. Theory of the energy distribution of photoelectrons—905(A)
— and W. W. Roehr. Thermionic and photoelectric work functions of molybdenum—52
- Dunham, J. L. (see Bennett, R. D.)—446(L)
- Dunnington, Frank G. Determination of e/m for an electron by a new deflection method—734(L)
- Duveneck, F. B. (see Webster, D. L.)—141(L)
- Ehrenfest, Paul II (see Jauncey, G. E. M.)—907(A)
- Erikson, Henry A. Light intensities at different depths in water as determined by means of a quartz spectrograph—910(A)
- Farnsworth, H. E. Electron diffraction by a silver film on a gold crystal—588(A)
- Feenberg, Eugene. Scattering of slow electrons. Part II—17
- Ferguson, J. E. (see Burroughs, Robert E.)—913(A)
— (see Lark-Horovitz, K.)—907(A)
- Fink, George A. Measurement of the piezoelectric deformations of quartz and tourmaline plates by means of a modified optical lever—912(A)
- Focken, C. M. Velocities of ions and electrons in pure gases—577(L)
- Frank, Henry S. and Foo-Song Lei. Empirical equation of state—893
- Fritzsche, O. D. (see Wahlin, H. B.)—911(A)
- Geib, I. G. and K. Lark-Horovitz. Dynamic reflection of x-rays from ZnS—908(A)
- Gerhard, Sherman L. Infrared absorption spectrum and the molecular structure of ozone—622
- Goble, A. T. and J. E. Mack. Two vector problem in Pb V and Bi VI—909(A)
- Gorter, C. J. Note on the electric field in paramagnetic crystals—437(L)
- Granath, L. P. Nuclear spin and magnetic moment of Li^7 —44
- Green, J. B. and R. A. Loring. Zeeman effect of the spectra of Sb II and Sb III—909(A)
- Greene, Ernest W. and John Warren Williams. Variation of dielectric constant with temperature. II. Electric moments of the ethylene halides—119
- Gross, E. and J. Khvostikov. Variation of the structure of scattered lines with the frequency of the primary light—579(L)
- Grosse, A. v. On the origin of the actinium series of radioactive elements—565
- Gruner, J. W. Book review—451
- Guillemin, V., Jr. On the possibility of deriving work from statistical fluctuations—589(A)
- Hamada, H. (see Okubo, J.)—795
- Hancox, Robert Rex. Reflection of metallic atoms from alkali halide crystals—864
- Hansen, W. W. (see Webster, D. L.)—141(L)
- Hardy, J. D., E. F. Barker and D. M. Dennison. Infrared spectrum of H^2Cl —279
- Harkins, William D. Neutron, the element neutron, and a nuclear exclusion principle—914(A)
- Harris, Sidon (see Colby, M. Y.)—733(L)
- Hartley, Kenneth. Direct measurement of the gravitational effect of the moon—911(A)
- Hause, C. D. (see Almy, G. M.)—242
- Havens, G. G. Magnetic susceptibilities of some common gases—901(A)
- Haworth, L. J. Energy distribution of secondary electrons from molybdenum—906(A)
- Heaps, C. W. Effect of strain on magnetostriction and magnetization in nickel—108
- Herzfeld, Karl F. Book review—319
- Hidnert, Peter and H. S. Krider. Thermal expansion of antimony—911(A)
- Hill, E. L. Book review—741
- Hoag, J. Barton and Haydn Jones. Permeability of iron at ultra-radio frequencies—571
- Hollaender, Alexander (see Williams, John Warren)—379
- Hopfield, John J. Argon in the ionization method of measuring cosmic rays and γ -rays—904(A)
— Improved burner for singing flames. Overtones in vibrating strings—913(A)
- Howell, L. G. (see Mott-Smith, L. M.)—314(L)
- Hughes, A. L. Angular distribution of electrons scattered in mercury vapor—147(L)
- Hukumoto, Y. On the continuous absorption spectrum of alkyl iodides—313(L)

- Ingersoll, L. R. and W. R. Winch. Dispersion of the Kerr effect in the near infrared—909(A)
- Inglis, D. R. Heisenberg theory of ferromagnetism—442(L)
- James, Louis E. (see Poindexter, Franklin E.)—910(A)
- Jauncey, G. E. M. Remarks on the scattering of x-rays by gases and crystals—453
 — (see Williams, P. S.)—907(A)
 — and Paul Ehrenfest II. Diffuse scattering of x-rays from a complicated crystal—907(A)
- Jen, C. K. Continuous electron affinity spectrum of hydrogen—588(A)
- Jenkins, F. A. (see Ashley, Muriel F.)—438(L)
 — and Andrew McKellar. Mass ratio of the boron isotopes from the spectrum of BO—464
- Johnson, O. J. and P. H. Carr. Some experiments on electrets—912(A)
- Johnson, Thomas H. (see Street, J. C.)—142(L)
- Jones, Haydn (see Hoag, J. Barton)—571
- Jordahl, O. M. Paramagnetic susceptibility of Cu^{++} —901(A)
- Kaplan, Joseph. Auroral spectrum—807
 — Luminescence of solid nitrogen—86
 — Products of dissociation in nitrogen—97
- Kennedy, Roy J. and Edward M. Thorndike. Experimental establishment of the relativity of time—400
- Kenty, Carl. On radiation diffusion and the rapidity of escape of resonance radiation from a gas—823
- Khvostikov, J. (see Gross, E.)—579
- Kolthoff, I. M. Book reviews—451, 741
- Kretschmar, G. G. Determination of e/m by means of photoelectrons excited by x-rays—905(A)
- Krider, H. S. (see Hidnert, Peter)—911(A)
- Kruger, P. Gerald and F. S. Cooper. Twenty-one foot grazing incidence vacuum spectrograph—910(A)
- Kuhn, H. and O. Oldenberg. Errata: Evidence of space quantization of atoms upon impact—312
- Lamar, E. S. (see Compton, K. T.)—588(A)
- Lang, R. J. and E. H. Vestine. First spark spectrum of antimony—233
- Langer, R. M. Book review—738
- Laporte, Otto. Approximation of geometric optics as applied to a Dirac electron moving in a magnetic field—340
- Lark-Horovitz, K. (see Geib, I. G.)—908(A)
 — (see Yearian, H. J.)—905(A)
 — and J. E. Ferguson. Electrical properties of surface layers—907(A)
 — and E. M. Miller. Demountable metal x-ray tube—915(A)
- Lawrence, Ernest O. Book review—451
 —, M. Stanley Livingston and Milton G. White. Disintegration of lithium by swiftly-moving protons—150(L)
- Lei, Foo-Song (see Frank, Henry S.)—893
- Lemaître, G. and M. S. Vallarta. On Compton's latitude effect of cosmic radiation—914(A)
- Libby, W. F. Simple amplifier for Geiger-Müller counters—440(L)
- Lippert, T. W. (see Pugh, E. M.)—709
- Livingston, M. Stanley. High-speed hydrogen ions—441(L)
 — (see Lawrence, Ernest O.)—150(L)
- Locher, Gordon L. Photoelectric quantum counters for visible and ultraviolet light. Part I.—525
- Longacre, Andrew. Scattering of lithium ions from a nickel surface—906(A)
- Loring, R. A. (see Green, J. B.)—909(A)
- Mack, J. E. (see Goble, A. T.)—909(A)
- Mahanti, P. C. Band spectra of MgO , CaO and SrO —609
- Maring, Karl A. Influence of pressure on the formation of the latent photographic image, particularly its effect on reversal in the region of solarization—911(A)
- Matuyama, E. On the lifetime of the metastable 3P_2 neon atom—373
- Maxwell, Louis R. On the radiation originating from a beam of electrons in mercury vapor and the mean life of the 2^3S_1 state—148(L)
- McKeehan, L. W. (see Beck, Fred J., Jr.)—714
- McKellar, Andrew (see Jenkins, F. A.)—464
- McMillan, Edwin. Deflection of a beam of HCl molecules by a non-homogeneous electric field—905(A)
- McPherson, A. I. Radiation from positive ions in argon, neon, helium—903(A)
- Miller, E. M. (see Lark-Horovitz, K.)—915(A)
- Miller, R. R. (see Brewer, A. Keith)—786
- Mohler, F. L. (see Boeckner, C.)—906(A)
- Moore, T. W. Behavior of crystalline test bodies in streaming solutions—906(A)
- Morse, Philip M. (see Rosen, N.)—210
 — and W. P. Allis. Effect of exchange on elastic cross sections—588(A)
- Mott-Smith, L. M. and L. G. Howell. Airplane cosmic-ray intensity measurements—314(L)
- Mueller, D. W. (see Barton, Henry A.)—901(A)
 — (see Smyth, H. D.)—902(A)
- Mulliken, Robert S. On the interpretation of the rotational structure of the CO_2 emission bands—364
- Murphy, George M. and Harold C. Urey. Errata: On the relative abundances of the nitrogen and oxygen isotopes—312
- Muskat, Morris. Theory of refraction shooting—910(A)

- Nedelsky, Leo. Radiation from slow electrons—641
- Noll, F. H. Waldemar. X-ray diffraction in ethyl ether near the critical point—336
- Oesterle, J. F. (see Wahlin, H. B.)—911(A)
- Okubo, J. and H. Hamada. On the nature of active nitrogen—795
- Oldenberg, O. (see Kuhn, H.)—312
- Olthoff, J. and R. A. Sawyer. Extension of the first spark spectrum of caesium (Cs II)—766
- Osterberg, Harold (see Roebuck, J. R.)—912(A)
- Overbeck, Wilcox P. (see Stearns, J. C.)—317(L)
- Page, Leigh. Momentum relations in crossed fields—101
- Patten, C. G. (see Uber, Fred M.)—229
- Penney, W. G. Law of force between two He atoms—585(L)
- (see Schlapp, Robert)—666
- Pfund, A. H. Filter for the study of the Raman effect—581(L)
- Piekara, A. Dielectric constant and electric polarization of mixtures in the neighborhood of the critical point—448(L)
- Electric moment of the molecule of nitrobenzene—449(L)
- Pielemeier, W. H. Erratum: Supersonic dispersion and absorption in CO_2 —436
- Pierce, G. W. Some applications of high-frequency sound effects—589(A)
- Poindexter, Franklin E. and Louis E. James. High-pressure spectrometer—910(A)
- Pool, M. L. and S. J. Simmons. Absorption coefficients in optically excited mercury vapor—909(A)
- Pugh, E. M. and T. W. Lippert. Hall e.m.f. and intensity of magnetization—709
- Rank, David H. Isotope of hydrogen in the atomic spectrum—446(L)
- Reich, Herbert J. Nonthermionic amplifier tube—913(A)
- Reichrudel, E. (see Spiwak, G.)—580(L)
- Reyerson, L. H. Book review—740
- Rieke, Foster F. Anomalous rotational temperature of mercury hydride—587(A)
- Roebuck, J. R. and Harold Osterberg. Joule-Thomson effect in helium—912(A)
- Roehr, W. W. (see DuBridge, Lee A.)—52
- Rosen, N. and Philip M. Morse. On the vibrations of polyatomic molecules—210
- Rosenthal, Jenny E. (see Salant, E. O.)—812
- Ruark, Arthur (see Western, Forrest)—903(A); 903(A)
- Salant, E. O. and Jenny E. Rosenthal. Theory of vibrational isotope effects in polyatomic molecules—812
- Saper, Paul G. Rotational analysis of ultraviolet bands of silicon monoxide—498
- Sawyer, R. A. (see Olthoff, J.)—766
- Schlapp, Robert and William G. Penney. Influence of crystalline fields on the susceptibilities of salts of paramagnetic ions. II. The iron group, especially Ni, Cr and CO—666
- Schmid, R. F. Rotational analysis of the first-negative bands of the CO^+ molecule—182
- Shaw, A. E. Polarization of collecting electrodes in high vacua—902(A)
- Shortley, G. H. (see Ufford, C. W.)—167
- Simmons, S. J. (see Pool, M. L.)—909(A)
- Sixtus, K. J. and L. Tonks. Propagation of large Barkhausen discontinuities. II—419
- Slack, Francis G. and William M. Breazeale. Magneto-optic rotation by condenser discharge—305
- Slater, J. C. Analytic atomic wave functions—33
- Recent developments in the theory of magnetism—589(A)
- Smith, Lloyd P. Calculation of the quantum defect for highly excited *S* states of para- and ortho-helium—176
- Smyth, H. D. and D. W. Mueller. Ionization by electron impact in water vapor and sulphur dioxide—902(A)
- Spangler, Rose D. Cybotactic condition of ethyl ether in the region of the critical point—907(A)
- Spedding, Frank H. and Richard S. Bear. Absorption spectra of the samarium ion in solids. I. Absorption by large single crystals of $\text{SmCl}_3 \cdot 6\text{H}_2\text{O}$ —58
- Absorption spectra of the samarium ion in solids. II. Conglomerate absorption of $\text{SmCl}_3 \cdot 6\text{H}_2\text{O}$ and a partial energy level diagram of the Sm^{+++} ion as it exists in crystalline $\text{SmCl}_3 \cdot 6\text{H}_2\text{O}$ —76
- Spiwak, G. and E. Reichrudel. On the secondary emission from collectors in neon discharge—580(L)
- Sproull, Wayne T. Diffraction of low speed electrons by a tungsten single crystal—904(A)
- Stearns, J. C., Wilcox P. Overbeck and Ralph D. Bennett. Solar component of cosmic rays—317(L)
- Stehn, J. R. Note on perturbation theory of molecules formed from two *2p* atoms—582(L)
- Stephenson, Reginald J. Relative intensities of the $L\alpha_1$ and $L\beta_2$ lines in the fluorescent x-ray spectrum of uranium—908(A)
- Sterne, Theodore E. Vapor pressure constant of methane—556
- Stewart, G. W. On the process of liquefaction—907(A)

- Street, J. C. and Thomas H. Johnson. Concerning the production of groups of secondaries by the cosmic radiation—142(L)
- Strong, John and S. C. Woo. Far infrared spectra of gases—267
- Stueckelberg, E. C. G. Theory of continuous absorption of oxygen at 1450A—518
- Swann, W. F. G. Methods of acquirement of cosmic-ray energies—914(A)
- Thorndike, Edward M. (see Kennedy, Roy J.)—400
- Tonks, L. (see Sixtus, K. J.)—419
- Tykociner, J. Tykocinski. Oscillations produced by beads of corona discharges—912(A)
- Uber, Fred M. and C. G. Patten. Magnitudes of the *L* absorption discontinuities of gold—229
- Ufford, C. W. and G. H. Shortley. Atomic eigenfunctions and energies—167
- Uhlenbeck, G. E. Book review—738
- Urey, Harold C. (see Murphy, George M.)—312
- Valasek, Joseph. Book reviews—152
- Vallarta, M. S. (see Lemaitre, G.)—914(A)
- Van Atta, L. C. (see Barton, Henry A.)—901(A)
- Van Dyke, K. S. Temperature variation of viscosity and of the piezoelectric constant of quartz—587(A)
- Varney, Robert N. Non-existence of ion mobility spectrum in air—547
- Verwiebe, F. L. Radiation excited by canal ray impact—902(A)
- Vestine, E. H. (see Lang, R. J.)—233
- Vinti, J. P. Dispersion and absorption of helium—632
- Vollrath, Richard E. High-voltage direct-current generator—298
- Wahlin, H. B., O. D. Fritsche, and J. F. Oesterle. Refractory materials for melting pure metals—911(A)
- Watson, William W. Zeeman effect of perturbed terms in the CO angstrom bands—509
- Webster, D. L., W. W. Hansen, F. B. Duveneck. Probabilities of *K*-electron ionization of silver by cathode rays—141(L)
- Wensel, H. T. Book review—319
- Western, Forrest and Arthur Ruark. Actinium branching ratio—903(A)
- Atomic weights of radioactive substances—903(A)
- Wetzel, W. W. Ionization of He by electron impact—902(A)
- White, Milton G. (see Lawrence, Ernest O.)—150(L)
- Williams, John Warren (see Greene, Ernest W.)—119
- and Alexander Hollaender. Molecular scattering of light from ammonia solutions. The fine structure of a vibrational Raman band—379
- Williams, N. H. Modes of vibration of piezoelectric crystals—913(A)
- Williams, P. S. and G. E. M. Jauncey. Diffuse scattering of x-rays from an NaF crystal at low temperatures—907(A)
- Williams, S. R. Mechanical hardness as measured by magnetostrictive effects—589(A)
- Wills, A. P. and G. F. Boeker. Diamagnetism of water at different temperatures—687
- Winans, J. Gibson. Origin of the mercury bands at 2480A—800
- Winch, W. R. (see Ingersoll, L. R.)—909(A)
- Witmer, Enos E. Unitary theory, pure number ratios and the masses of atomic nuclei—316(L)
- and J. M. Cork. Measurement of x-ray emission wave-lengths by means of the ruled grating—743
- Woo, S. C. (see Strong, John)—267
- Wood, R. W. and George Collins. Raman spectra of a series of normal alcohols and other compounds—386
- Yearian, H. J. and K. Lark-Horovitz. Intensity distribution in electron diffraction patterns of ZnO—905(A)
- Zabel, R. M. Reflection of atomic beams from sodium chloride crystals—218
- Zemansky, M. W. Note on the equivalent absorption coefficient for diffused resonance radiation—843

ANALYTIC SUBJECT INDEX TO VOLUME 42

References marked (A) are to abstracts of papers presented at meetings of the Physical Society, those marked with (L) are to Letters to the Editor.

Absorption of light (see also Spectra, absorption)

- Absorption coefficient for diffused radiation, M. W. Zemansky—843
- In optically excited Hg, M. L. Pool, S. J. Simmons—909(A)
- Intensities at different depths in water, H. A. Erikson—910(A)

Accommodation coefficient

- For He positive ions, K. T. Compton, E. S. Lamar—588(A)

Acoustics

- Burner for singing flames, overtones in strings, J. J. Hopfield—913(A)
- Erratum: Supersonic dispersion and absorption in CO₂, W. H. Pielemeier—436
- Velocity of sound in an absorptive gas, D. G. Bourgin—721

Activated gases

- Nature of active N, J. Okubo, H. Hamada—795

Affinity

- Continuous electron affinity spectrum of H, C. K. Jen—588(A)

Afterglow

- Auroral spectrum, J. Kaplan—807
- Nature of active N, J. Okubo, H. Hamada—795

Arcs (see Discharge of electricity in gases)**Astrophysics**

- Gunn's theory of double stars, L. Page—101

Atomic and molecular beams

- Deflection of HCl molecules by a non-homogeneous electric field, E. McMillan—905(A)
- Radiation excited by canal ray impact, F. L. Verwiebe—902(A)
- Reflection from alkali halide crystals, R. R. Hancock—864
- Reflection from NaCl crystals, R. M. Zabel—218
- Scattering of Li ions from Ni, A. Longacre—906(A)

Atomic form factors

- Function of temperature, G. E. M. Jauncey—453

Aurora

- Auroral spectrum, J. Kaplan—807
- Luminescence of solid N., J. Kaplan—86

Barkhausen effect (see Magnetic properties)**Book reviews**

- Allen, H. Stanley. *Electrons and Waves*—451
- Chase, C. T. *A History of Experimental Physics*—152
- Debye, P. *Molekulstruktur*—743
- Dirac, P. A. M. *Les Principes de la Mécanique Quantique*—746
- Faraday Society. *The Adsorption of Gases by Solids*—745
- Fleury, Pierre. *Étalon Photométriques*—319
- Gmelin's *Hankbuch der anorganischen Chemie*, 8 auflage, Herausgegeben von der Deutschen chemischen gesellschaft. Teil A. Lieferung 4—746
- Gmelin's *Handbuch der anorganischen Chemie*, 8 auflage, Herausgegeben von der Deutschen chemischen gesellschaft. Teil B. Lieferung 5—451
- Houston, R. A. *Vision and Colour Vision*—152
- Knaggs, I. E. and B. Karlik. *Tables of Cubic Crystal Structure of Elements and Compounds*—451
- Kohlrausch, Friedrich. *Kleiner Leitfaden der Praktischen Physik*—319
- Van Vleck, J. H. *The Theory of Electric and Magnetic Susceptibilities*—743

Constants, physical

- Unitary theory and pure number ratios, E. Wigner—316(L)

Cosmic radiation

- Acquirement of energies, W. F. G. Swann—914(A)
- Airplane intensity measurements, L. M. Mott-Smith, L. G. Howell—314(L)
- A in the ionization method of measuring, J. J. Hopfield—904(A)
- Compton's latitude effect, G. Lemaitre, M. S. Vallarta—914(A)
- Intensity variation with latitude, A. H. Compton—904(A). R. D. Bennett, J. L. Dunham, E. H. Bramhall, P. K. Allen—446(L)
- Ionization as a function of pressure and temperature, J. W. Broxon—321
- Production of groups of secondaries, J. C. Street, T. H. Johnson—142(L)
- Self-recording electrometer; depth-ionization curve, J. M. Benade—290

- Cosmic radiation (continued)**
Solar component, J. C. Stearns, W. P. Overbeck, R. D. Bennett—317(L)
- Crystals and crystal structure**
Crystalline fields and the susceptibilities of salts of Ni, Cr, and Co, R. Schlapp, W. G. Penney—666
Electric field in paramagnetic crystals, C. J. Gorter—437(L)
Ferromagnetic anisotropy of single crystals; theory, R. M. Bozorth—882
Homogeneous mechanical stress and electrical resistance, P. W. Bridgman—858
Reflection of metallic atoms from alkali halide crystals, R. R. Hancox—864
Laue patterns from crystals oscillating piezoelectrically, M. Y. Colby, S. Harris—733(L) J. M. Cork—749
Mono-crystal Barkhausen effects, F. J. Beck, Jr., L. W. McKeehan—714
Piezoelectric deformations of quartz and tourmaline plates, G. A. Fink—912(A)
Tension and electrical resistance of single Bi crystals, M. Allen—848
Tropism of crystals, F. Bitter—731(L)
Vibration of piezoelectric crystals, N. H. Williams—913(A)
- Cybotactic state**
In ethyl ether, F. H. W. Noll—336
Of ethyl ether in the region of the critical point, R. D. Spangler—907(A)
Process of liquefaction, G. W. Stewart—907(A)
- Dielectric constants**
Moment of nitrobenzene, A. Piekara—449(L)
Of organic liquid mixtures, A. Piekara—448(L)
Temperature variation of moments of ethylene halides, E. W. Greene, J. W. Williams—119
- Diffraction of atoms (see Atomic and molecular beams)**
- Diffraction of electrons (see Electron diffraction)**
- Diffusion**
Of resonance radiation in gas, C. Kenty—823
- Discharge of electricity in gases**
Currents carried by electrons, K. T. Compton, E. S. Lamar—588(A)
Diffusion of resonance radiation in a gas, C. Kenty—823
Neutralization and ionization of high-velocity ions by collision, H. F. Batho—753
Positive ion current at cathode, A. K. Brewer, R. R. Miller—786
- Secondary emission from collectors in Ne discharge, G. Spiwak, E. Reichrudel—580(L)
- Disintegration of nucleus**
Of Li by protons, E. O. Lawrence, M. S. Livingston, M. G. White—150(L)
- Dissociation**
In N, J. Kaplan—97
- Efficiency of ionization**
K-electron ionization of Ag, D. L. Webster, W. W. Hansen, F. B. Duveneck—141(L)
- Elasticity**
And magnetic properties, F. Bitter—697
Theory of "refraction shooting," M. Muskat—910(A)
- Electrets**
In wax mixtures and S, O. J. Johnson, P. H. Carr—912(A)
- Electrical conductivity and resistance**
Of fifteen metals down to liquid O temperatures; effect of pressure, P. W. Bridgman—587(A)
Homogeneous mechanical stress and electrical resistance of crystals, P. W. Bridgman—858
Tension and electrical resistance of single Bi crystals, M. Allen—848
- Electrical oscillations and waves**
By beads of corona discharges, J. Tykocinski Tykociner—912(A)
- Electric moment (see Dielectric constant)**
- Electromagnetic theory**
Momentum relations in crossed fields, L. Page—101
- Electron diffraction**
Intensity distribution, H. J. Yearian, K. Lark-Horovitz—905(A)
By an Ag film on an Au crystal, H. E. Farnsworth—588(A)
By a w-single crystal, W. T. Sproull—904(A)
- Electron lenses**
A correction, C. J. Davisson, C. J. Calbick—580(L)
- Electrons**
Dirac electron moving in a magnetic field, O. Laporte—340
- Electrons, scattering of**
Slow electrons by Cs ions, C. Boeckner, F. L. Mohler—906(A)
Theoretical calculations, W. W. Wetzel—902(A)

Electrons, secondary

- From collectors in Ne discharge, G. Spiwak, E. Reichrudel—580(L)
- Energy distribution of electrons from Mo, L. J. Haworth—906(A)
- Magnetic spectra from Ag, S. Chylinski—393

Electro-optical effects (see also Photoelectric effect)

- Kerr effect in infrared, L. R. Ingersoll, W. R. Winch—909(A)

 e/m

- Determination for an electron by a new deflection method, F. G. Dunnington—734(L)
- Determination by means of photoelectrons excited by x-rays, G. G. Kretschmar—905(A)
- Value of, for electron, R. T. Birge—736(L)

Energy states of atoms (see also Spectra, atomic)

- Atomic eigenfunctions and energies, C. W. Ufford, G. H. Shortley—167

Energy states of molecules (see Molecular structure and constants; Spectra, molecular)**Errata**

- Abundances of N and O isotopes, G. M. Murphy, H. C. Urey—312
- Electron lenses, C. J. Davisson, C. J. Calbick—580(L)
- Probable values of e , h , e/m and α , R. T. Birge—736(L)
- Space quantization of atoms upon impact, H. Kuhn, O. Oldenberg—312
- Structure of atomic nuclei, J. W. Bartlett, Jr.—737
- Supersonic dispersion and absorption in CO_2 , W. H. Pielemeier—436

Ferromagnetism (see Magnetic properties)**Flames**

- Luminosity of sodium flames, C. D. Child—146(L)

Gases (see Kinetic theory of gases)**Geophysics**

- Erosion of rock, T. W. Moore—906(A)
- Measurement of the gravitational effect of the moon, K. Hartley—911(A)
- "Refraction shooting," M. Muskat—910(A)

Gyromagnetization (see Magnetic properties)**Hall effect**

- And intensity of magnetization, E. M. Pugh, T. W. Lippert—709

Heat of dissociation (see Dissociation)**High voltage tubes and machines**

- Compact high potential electrostatic generator, H. A. Barton, D. W. Mueller, L. C. Van Atta—901(A)
- For producing H ions, M. S. Livingston—441(L)

Hyperfine structure

- And isotope displacements, G. Breit—348

Instruments (see Methods and instruments)**Ionization by positive ions** (see Ionization potentials)**Ionization potentials**

- Electron impact in water vapor and sulphur dioxide, H. D. Smyth, D. W. Mueller—902(A)
- By impact of atoms and positive ions, C. J. Brasefield—11

Ions, high-speed

- H ions, M. S. Livingston—441(L)
- Neutralization and ionization of high-velocity ions, by collision, H. F. Batho—753
- By repeated accelerations, A. J. Dempster—901(A)

Ions in gases

- Ions in crossed fields, L. Page—101
- Neutralization and ionization of high-velocity ions by collision, H. F. Batho—753
- Radiation from positive ions in A, Ne, He, A. I. McPherson—903(A)

Ions, mobility (see also Ions in gases)

- Mobility spectrum in air, R. N. Varney—547
- In pure gases, C. M. Focken—577(L)

Isotopes

- Abundance of H^2 from spectrum, J. D. Hardy, E. F. Barker, D. M. Dennison—279
- Atomic weights, of radioactive substances, F. Western, A. Ruark—903(A)
- Detection of $\text{H}^2\gamma$ line, D. H. Rank—446(L)
- Erratum: Relative abundance of N and O isotopes, G. M. Murphy, H. C. Urey—312
- Existence of Cl^{39} , M. F. Ashley, F. A. Jenkins—438(L)
- And hyperfine structure, G. Breit—348
- Ratio of masses in B, F. A. Jenkins, A. McKellar—464
- Vibrational isotope effects in polyatomic molecules, E. O. Salant, J. E. Rosenthal—812
- Weight of H^2 , K. T. Bainbridge—1

Joule-Thomson effect

- In He, J. R. Roebuck, H. Osterberg—912(A)

Kinetic theory of gases

- Law of force between two He atoms, W. G. Penney—585(L)

Liquids

- Crystalline test bodies in streaming solutions, T. W. Moore—906(A)
Electrical properties of surface layers, K. Lark-Horovitz, J. E. Ferguson—907(A)
Ethyl ether in the region of the critical point, R. D. Spangler—907(A)
Process of liquefaction, G. W. Stewart—907(A)

Luminescence

- Of solid nitrogen, J. Kaplan—86

Magnetic properties

- Barkhausen effects in rotating fields, F. J. Beck, Jr., L. W. McKeehan—714
Diamagnetism of water at different temperatures, A. P. Wills, G. F. Boeker—687
Of distorted cubic ferromagnetic lattices, F. Bitter—697
Effect of strain in Ni, C. W. Heaps—108
Electric field in paramagnetic crystals, C. J. Gorter—437(L)
Ferromagnetic anisotropy of single crystals; theory, R. M. Bozorth—882
Gyromagnetic ratios for Ni and Co, S. J. Barnett—147(L)
And Hall e.m.f., E. M. Pugh, T. W. Lippert—709
Heisenberg theory of ferromagnetism, D. R. Inglis—442(L)
Magnetic moment of Li^+ , L. P. Granath—44
Paramagnetic susceptibility of Cu^{++} , O. M. Jordahl—901(A)
Permeability of Fe at high frequencies, J. B. Hoag, H. Jones—571
Propagation of Barkhausen discontinuities, K. J. Sixtus, L. Tonks—419
Susceptibilities of common gases, G. G. Havens—901(A)
Susceptibilities of salts of Ni, Cr and Co, R. Schlapp, W. G. Penney—666

Magneto-optical effects

- Rotation by condenser discharge, F. G. Slack, W. M. Breazeale—305

Magnetostriction

- Effect of strain in Ni, C. W. Heaps—108

Mass-spectrograph (see also methods and instruments)

- Ionization by electron impact in water vapor and sulphur dioxide, H. D. Smyth, D. W. Mueller—902(A)

Mean life

- Of $^3\text{P}_2$ Ne atom, E. Matuyama—373
Of 2^3S_1 state of Hg, L. R. Maxwell—148

Measurements (see Methods and instruments)**Mechanics, quantum—atomic structure and spectra**

- Analytic wave functions, J. C. Slater—33
Atomic eigenfunctions and energies, C. W. Ufford, G. H. Shortley—167
Atomic wave functions, F. W. Brown—914(A)
Quantum defect for highly excited S states of para- and orthohelium, L. P. Smith—176

Mechanics, quantum—general

- Continuous electron affinity spectrum of H, C. K. Jen—588(A)
Differential analyzer solution for wave functions, S. Caldwell—589(A)
Dirac electron moving in a magnetic field, O. Laporte—340
Dispersion and absorption of He, J. P. Vinti—632
Effect of exchange on elastic cross sections, P. M. Morse, W. P. Allis—588(A)
Ionization of He by electron impact, W. W. Wetzel—902(A)
Possibility of deriving work from statistical fluctuations, V. Guillemin, Jr.—589(A)
Radiation from slow electrons, L. Nedelsky—641
Scattering of slow electrons, E. Feenberg—17
Susceptibilities of salts of paramagnetic ions, R. Schlapp, W. G. Penney—666
Vapor pressure constant, T. E. Sterne—556

Mechanics, quantum—molecular structure and spectra

- Calculation on the water molecule, A. S. Coolidge—189
Continuous absorption of O_2 ; theory, E. C. G. Stueckelberg—518
Molecules formed from two $2p$ atoms, J. R. Stehn—582(L)
Vibrations of polyatomic molecules; NH_3 , N. Rosen, P. M. Morse—210

Metastable atoms and molecules

- Lifetime $^3\text{P}_2$ Ne atom, E. Matuyama—373

Methods and instruments

- Amplifier for Geiger-Müller counters, W. F. Libby—440(L)
Burner for singing flames, J. J. Hopfield—913(A)
Compact high-potential electrostatic generator, H. A. Barton, D. W. Mueller, L. C. Van Atta—901(A)
Comparison of photographic and ionization methods of measuring x-ray intensities, E. Dershem—908(A)
Determination of dielectric constant of a vapor, E. W. Greene, J. W. Williams—119
Differential analyzer solution for the wave function of the K-shell, S. Caldwell—589(A)
Filter for Raman effect, A. H. Pfund—581(L)

Methods and instruments (continued)

- High-pressure spectrometer, F. E. Poindexter, L. E. James—910(A)
- High-velocity protons by repeated accelerations, A. J. Dempster—901(A)
- High-voltage direct-current generator, R. E. Vollrath—298
- Magneto-optic rotation, F. G. Slack, W. M. Breazeale—305
- Measurement of the gravitational effect of the moon, K. Hartley—911(A)
- Modified optical lever, G. A. Fink—912(A)
- Non-thermionic amplifier, H. J. Reich—913(A)
- Photoelectric quantum counters, G. L. Locher—525
- Polarization of electrodes in vacua, A. E. Shaw—902(A)
- Refractory materials for melting pure metals, H. B. Wahlin, O. D. Fritsche, J. F. Oesterle—911(A)
- Self-recording cosmic-ray electrometer, J. M. Benade—290
- Vacuum spectrograph, P. G. Kruger, F. S. Cooper—910(A)
- Vacuum tube electrometers, R. E. Burroughs, J. E. Ferguson—913(A)
- Vibration of piezoelectric crystals, N. H. Williams—913(A)

Mobility of ions (see Ions, mobility)**Molecular structure and constants** (see also Spectra, molecular and Raman spectra)

- Energy level diagram of the Sm^{+++} ion in solids, F. H. Spedding, R. S. Bear—76
- Of HCN, K. N. Choi, E. F. Barker—777
- Molecules formed from two $2p$ atoms, perturbation theory, J. R. Stehn—582(L)
- Of NH_3 , J. W. Williams, A. Hollaender—379
- Of ozone, S. L. Gerhard—622
- Vibrations of polyatomic molecules; NH_3 , N. Rosen, P. M. Morse—210
- Of water molecule, A. S. Coolidge—189

Nuclear spin (see also Hyperfine structure)

- Of Li^7 , L. P. Granath—44

Nucleus

- Disintegration of Li by protons, E. O. Lawrence, M. S. Livingston, M. G. White—150
- Masses of atomic nuclei, E. E. Witmer—316(L)
- Nuclear exclusion principle, W. D. Harkins—914(A)
- Structure of, J. H. Bartlett, Jr.—145(L)

Neutrons

- And nuclear structure, W. D. Harkins—914(A)

Optical constants and properties

- Change of n with pressure, F. E. Poindexter, L. E. James—910(A)
- Dispersion and absorption of He, J. P. Vinti—632

Packing fraction

- Of H^2 , K. T. Bainbridge—1

Permeability (see Magnetic properties)**Photoelectric effect and properties**

- e/m of photoelectrons, G. G. Kretschmar—905(A)
- Energy distribution of photoelectrons, L. A. DuBridge—905(A)
- Quantum counters for visible and ultraviolet light, G. L. Locher—525

Photography

- Influence of pressure on latent photographic image, K. A. Maring—911(A)

Photometry

- Quantum counters for visible and ultraviolet light, G. L. Locher—525

Piezoelectric effect

- Temperature variation of constant of quartz, K. S. Van Dyke—587(A)
- Work functions of Mo, L. A. DuBridge, W. W. Roehr—52
- X-ray reflection from oscillating crystals, M. Y. Colby, S. Harris—733(L); J. M. Cork—749

Polarization, electrical (see Dielectric constants)**Positive ray analysis** (see also Mass-spectrograph)

- Ions from heated metals, L. L. Barnes—487

Probability of ionization (see Efficiency of ionization)**Quantum defect**

- For highly excited S states of para- and ortho-helium, L. P. Smith—176

Radioactivity

- Ac branching ratio, F. Western, A. Ruark—903(A)
- Atomic weights, Forrest Western, A. Ruark—903(A)
- Origin of the Ac series, A. v. Grosse—565

Raman spectra

- In CO and NO, S. Bhagavantam—437(L)
- Filter for Raman effect, A. H. Pfund—581(L)
- Fine structure of a Raman band, J. W. Williams, A. Hollaender—379
- Of normal alcohols and organic compounds, R. W. Wood, G. Collins—386
- Variation of structure of scattered lines with the frequency, E. Gross, J. Khvostikov—579(L)

- Relativity**
Experimental establishment of the relativity of time, R. J. Kennedy, E. M. Thorndike—400
- Resistance, electrical** (see Electrical conductivity and resistance)
- Resonance radiation**
Absorption coefficient for diffused radiation, M. W. Zemansky—843
Diffusion and escape from a gas, C. Kenty—823
- Scattering of electrons** (see also Electron diffraction)
Angular distribution in Hg vapor, A. L. Hughes—147(L)
Equations for scattering, E. Feenberg—17
- Scattering of light** (see also Raman spectra)
From NH_3 solutions, J. W. Williams, A. Hol-laender—379
- Secondary electrons** (see Electrons, secondary)
- Solutions**
Crystalline test bodies in streaming solutions, T. W. Moore—906(A)
- Sound** (see Acoustics)
- Spectra, absorption** (see also Absorption of light)
Coefficients in optically excited mercury, M. L. Pool, S. J. Simmons—909(A)
Conglomerate of $\text{SmCl}_3 \cdot 6\text{H}_2\text{O}$, F. H. Spedding, R. S. Bear—76
Continuous absorption of O_2 , theory, E. C. G. Stueckelberg—518
Continuous spectrum of alkyl iodides, Y. Hukamoto—313(L)
Of HCN, infrared, K. N. Choi, E. F. Barker—777
Of IBr, W. G. Brown—355
Infrared of ozone, S. L. Gerhard—622
Intensities at different depths in water, H. A. Erikson—910(A)
Of single crystals of $\text{SmCl}_3 \cdot 6\text{H}_2\text{O}$, F. H. Spedding, R. S. Bear—58
- Spectra, atomic**
Detection of $\text{H}^2\gamma$ -line, D. H. Rank—446(L)
Emission probability for a colliding atom, R. W. Ditchburn—314(L)
Extension of spectrum of Cs II, J. Olthoff, R. A. Sawyer—766
Of high speed positive ions in A, Ne and He, A. I. McPherson—903(A)
Of Sb II, R. J. Lang, E. H. Vestine—233
Term system of Ir I, W. Albertson—433(L)
Two vector problem in Pb V and Bi VI, A. T. Goble, J. E. Mack—909(A)
- Spectra, general**
Auroral spectrum, J. Kaplan—807
B isotopes from band spectra, F. A. Jenkins, A. McKellar—464
Lines from Hg vapor in beam of electrons, L. R. Maxwell—148
Radiation excited by canal ray impact, F. L. Verwiebe—902(A)
- Spectra, molecular** (see also molecular structure and constants)
Anomalous rotational temperature of HgH, F. F. Rieke—587(A)
Far infrared of HCl and NH_3 , J. Strong, S. C. Woo—267
First negative bands of the CO^+ , R. F. Schmid—182
Hg bands at 2480A, J. G. Winans—800
Infrared of H^2Cl , J. D. Hardy, E. F. Barker, D. M. Dennison—279
Interpretation of the CO_2 emission bands, R. S. Mulliken—364
Of KH, G. M. Almy, C. D. Hause—242
Of MgO, CaO and SrO, P. C. Mahanti—609
Rotational analysis of ultraviolet bands of SiO , P. G. Saper—498
Vibrational isotope effects in polyatomic molecules, E. O. Salant, J. E. Rosenthal—812
- Spectroscopy, technique**
Grazing incidence vacuum spectrograph, P. G. Kruger, F. S. Cooper—910(A)
- Surface phenomena**
Electrical properties of surface layers, K. Lark-Horovitz, J. E. Ferguson—907(A)
- Susceptibility, magnetic** (see Magnetic properties)
- Thermal expansion**
Of Sb, P. Hidnert, H. S. Krider—911(A)
- Thermionic emission of electrons, emitting surfaces**
Work function of Mo, L. A. DuBridge, W. W. Roehr—52
- Thermionic emission of positive ions**
Of metals from metals, L. L. Barnes—487
Temperature variation of emission from Mo, L. L. Barnes—492
- Thermodynamics**
Possibility of deriving work from statistical fluctuations, V. Guillemin, Jr.—589(A)
Vapor pressure constant, T. E. Sterne—556
- Vacuum tubes**
Non-thermionic amplifier, H. J. Reich—913(A)
Vacuum tube electrometer, R. E. Burroughs, J. E. Ferguson—913(A)

Vapor pressure

Vapor pressure constant from quantum mechanics, T. E. Sterne—556

Virial coefficient

Force between two He atoms, W. G. Penney—585(L)

Viscosity

Temperature variation in quartz, K. S. Van Dyke—587(A)

Wave Mechanics (see Mechanics, quantum, etc.)**X-rays, diffraction scattering, reflection and refraction**

Diffraction in ethyl ether, F. H. W. Noll—336

Diffuse scattering from a complicated crystal, G. E. M. Jauncey, P. Ehrenfest II—907(A)

Dynamic reflection from ZnS, I. G. Geib, K. Lark-Horovitz—908(A)

Laue patterns from crystals oscillating piezoelectrically, M. Y. Colby, S. Harris—733(L), J. M. Cork—749

L discontinuities of Au, Fred M. Uber, C. G. Patten—229

Scattering of from an NaF crystal at low temperatures, P. S. Williams, G. E. M. Jauncey—907(A)

Scattering by gases and crystals, G. E. M. Jauncey—453

Scattering of hard x-rays by solids, S. Chylinski—153

X-rays, emission

Relative intensities of the $L\alpha_1$ and $L\beta_2$ lines in the fluorescent spectrum of U, R. J. Stephenson—908(A)

Relative intensities of the $L\alpha_1$, β_1 , β_2 , and γ_1 in Ta, W, Ir and Pt, V. J. Andrew—591

X-rays, spectra and spectroscopy, wave-length measurements

Comparison of photographic and ionization methods of measuring x-ray intensities, E. Dershem—908(A)

Wave-lengths by means of the ruled grating, R. B. Witmer, J. M. Cork—743

X-rays, tubes, apparatus

Demountable metal tube, K. Lark-Horovitz, E. M. Miller—915(A)

Zeeman effect

Perturbed terms in the CO angstrom bands, W. W. Watson—509

Of Sb II and Sb III, J. B. Green, R. A. Loring—909(A)